

Dec 13.4.90

CUL-4102909-21-P024450

AJR

21

American
Journal of
Roentgenology



January 1989

PercuCut™ Cut-Biopsy Needles from E-Z-EM provide reliable results in virtually all soft-tissue biopsies. Patented, specially designed "keyhole" cutting-edges on the cannula tip precisely core tissue samples. Ultra-thin-wall tubing maximizes sample size while minimizing needle gauge and patient trauma.

Three PercuCut needle designs allow the physician complete flexibility in obtaining a biopsy sample.

Cut-Biopsy Needle—a keyhole cutting-edge cannula with stylet. Includes a unique syringe which creates and maintains negative pressure during the biopsy procedure.

Coaxial Sheath Cut-Biopsy Needle—a three-part sheath/cannula/stylet design for multiple samples through a single puncture. Our unique aspirating syringe system is also included.

Self-Aspirating Cut-Biopsy Needle—a biopsy needle that combines our keyhole-cutting technology with a specially designed self-aspirating diaphragm hub which permits one-hand operation without a syringe.

PercuCut Needles have proven their ability to provide excellent, reliable histological and cytological samples in virtually all soft-tissue biopsies. All use a straight-tracking trocar pointed stylet for precise placement, and are available in gauges and lengths to suit any application.

For additional information on all of the PercuCut products, contact your local representative, or call E-Z-EM toll-free at 1-800-544-4624. In New York call 516-333-8230.

E-Z-EM
More than barium—much more



E-Z-EM, Inc.
7 Portland Avenue
Westbury, N.Y. 11590

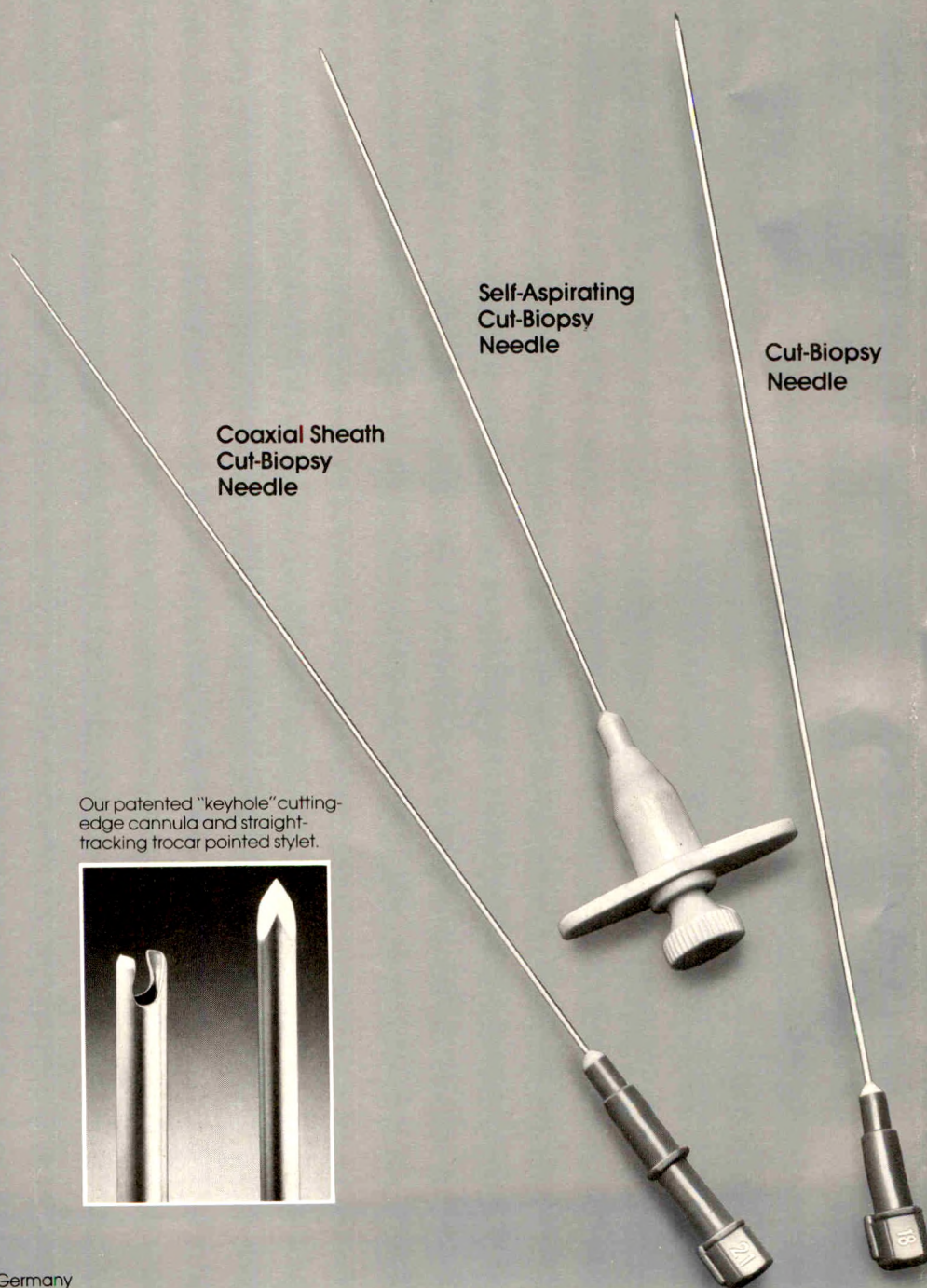
CIRCLE 5 ON READER SERVICE CARD

© 1987 E-Z-EM, Inc.

Manufactured for E-Z-EM by Angiomed®, West Germany

Reliable histological
and cytological
fine needle
aspiration biopsies
...from E-Z-EM

PercuCut™



Coaxial Sheath
Cut-Biopsy
Needle

Self-Aspirating
Cut-Biopsy
Needle

Cut-Biopsy
Needle

Our patented "keyhole" cutting-edge cannula and straight-tracking trocar pointed stylet.

AJR

American Journal of Roentgenology
Diagnostic Imaging and Related Sciences

P24,450

- Editor-In-Chief** Robert N. Berk, *La Jolla, California*
University of California, San Diego
School of Medicine and Medical Center
- Editor Emeritus** Melvin M. Figley, *Seattle, Washington*
- Associate Editor** Saskia von Waldenburg Hilton, *San Diego, California*
- Consulting Editor** Juan M. Taveras, *Boston, Massachusetts*
- Statistician** Charles C. Berry, *San Diego, California*

Editorial Board

- | | | |
|-------------------------|--------------------------|--------------------|
| John R. Amberg | William R. Hendee | Peter M. Ronai |
| Itamar Aviad | John R. Hesselink | Sjef H. J. Ruijs |
| Lawrence W. Bassett | Charles B. Higgins | Carol M. Rumack |
| Gregory P. Borkowski | Melvyn T. Korobkin | Stuart S. Sagel |
| William G. Bradley, Jr. | Thomas L. Lawson | David J. Sartoris |
| Peter L. Cooperberg | Bruce L. McClennan | Stefan C. Schatzki |
| N. Reed Dunnick | Albert A. Moss | Edward A. Sickles |
| David K. Edwards | Jeffrey H. Newhouse | Barry A. Siegel |
| Ronald G. Evens | Donald L. Resnick | David D. Stark |
| David S. Feigin | Stewart R. Reuter | Edward T. Stewart |
| Paul J. Friedman | Charles A. Rohrmann, Jr. | Eric vanSonnenberg |

Editorial Staff: Margaret Levene, *publications supervisor*; Katie L. Spiller, Barbara Rose, Barbara L. Halliburton, and Janine Anderson, *manuscript editors*; Nancy Rydbeck, *office manager*; Sheri Smith, *administrative assistant*; Sandra L. Griffin, *administrative secretary*.

AJR, AMERICAN JOURNAL OF ROENTGENOLOGY (ISSN 0361 803X) is the official journal of the American Roentgen Ray Society and is published monthly by Williams & Wilkins, 428 E. Preston St., Baltimore, MD 21202. Annual dues include \$50 for journal subscription. Second-class postage paid at Baltimore, MD, and at additional mailing offices. Postmaster, send address changes (Form 3579) to AJR, 428 E. Preston St., Baltimore, MD 21202. Subscription rates \$100 (\$135 foreign); institutions \$110 (\$145 foreign); in training \$25 (\$50 foreign); single copy \$16 (\$19 foreign). Japanese rates include airfreight. Japanese yen price is available from our sole agent USACO Corporation, 13-12, Shimbashi 1-Chome, Minato-Ku, Tokyo 105, Japan, telephone 03-502-6471. Airmail rates furnished on request. Indexed by *Current Contents* and *Index Medicus*. Copyright © 1988 by American Roentgen Ray Society.

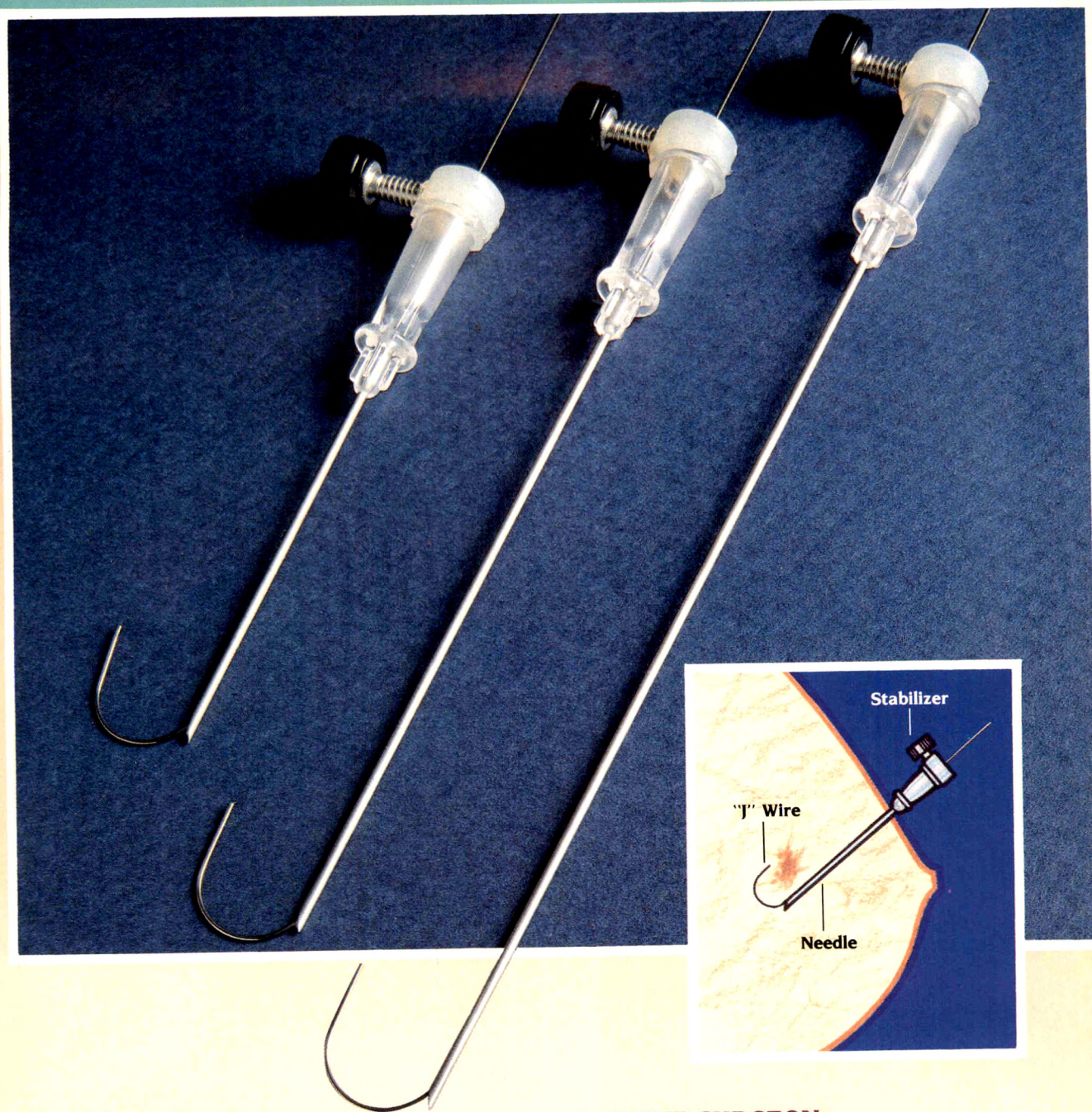
0361-803X/88\$2.00



HOMER MAMMALOK™

NEEDLE/WIRE LOCALIZER

"Designed in conjunction with leading Radiologists and Surgeons"



FOR THE RADIOLOGIST:

- The flexible "J" wire may be retracted and advanced as necessary until accurate placement is achieved.

FOR THE SURGEON:

- When the needle is left in place, the Surgeon has a palpable guide that cannot be transected during surgical dissection.

For More Information, Please Call: 1-800-833-9973; in New York 1-800-424-7171
Telephone (518) 798-0067 • Telex 671198 NAMIC UW • Telefax (518) 798-5437

NAMIC®

ANGIOGRAPHIC SYSTEMS DIVISION
GLENS FALLS, NEW YORK 12801
CIRCLE 41 ON READER SERVICE CARD

Step Up to Excellence

AJR Guidelines for Authors

Address new and revised manuscripts, correspondence, and classified ads to the Editor:

AJR Editorial Office
2223 Avenida de la Playa, Suite 200
La Jolla, CA 92037-3218

Telephone: (619) 459-2229; FAX: (619) 459-8814

Inquiries regarding subscriptions, display advertising, reprints, or permission to republish AJR material should be addressed to the publisher:

The Williams & Wilkins Co.
428 E. Preston St.

Baltimore, MD 21202 Telephone: (301) 528-4133

The AJR publishes original contributions to the advancement of medical diagnosis and treatment. Submitted manuscripts should not contain previously published material and should not be under consideration for publication elsewhere. Papers dealing with neuroradiology should be addressed to: American Journal of Neuroradiology, Dept. of Radiology, Massachusetts General Hospital, Boston, MA 02114. At the discretion of the AJR Editor, AJNR articles that are of interest to the general reader may be republished in the AJR. Neuroradiologic papers sent to the AJR will be forwarded to the Editorial Office of the AJNR.

Manuscript decisions are based on peer review. Reviewers receive manuscripts without title pages to ensure an unbiased review. Statements made in the article, including changes made by the Editor or manuscript editor, are the responsibility of the author and not of the AJR or its publisher. Authors will be sent the edited manuscript, galley proof, and proofs of illustrations. If the corresponding author will be unavailable to review galleys, arrangements should be made for a coauthor or colleague to read and return the proof.

The following guidelines are based on instructions set forth in the **Uniform Requirements for Manuscripts Submitted to Biomedical Journals** (*Ann Intern Med* 1988;108:258-265). Articles will be edited, however, to conform to the individual style of AJR.

General Guidelines for Major Papers

Abstract. Clearly state (in 200 words or less) the purpose, methods, results, and conclusions of the study. Include actual data.

Introduction. Briefly describe the purpose of the investigation, including relevant background information.

Methods. Describe the research plan, the materials (or subjects), and the methods used, in that order. Explain in detail how disease was confirmed and how subjectivity in observations was controlled.

Results. Present results in a clear, logical sequence. If tables are used, do not duplicate tabular data in text, but do describe important trends and points.

Discussion. Describe the limitations of the research plan, materials (or subjects), and methods, considering both the

purpose and the outcome of the study. When results differ from those of previous investigators, explain the discrepancy.

AUTHOR'S CHECKLIST

For priority handling, complete the following checklist, sign the copyright form on the reverse side of this page, and include both with the manuscript.

_____ Two copies of the manuscript (the original and a photocopy) and two complete sets of figures are submitted. One copy has been retained by the author.

_____ If appropriate, AJR Guidelines for case reports, technical notes, pictorial essays, or letters to the Editor have been followed. (See page A5.)

_____ The manuscript, including references, figure legends, and tables, is typed double-spaced on 8½ × 11 in. (21.6 × 27.9 cm) nonerasable paper. Right-hand margins are not justified.

_____ All manuscript pages are numbered consecutively beginning with the abstract. Authors' names do not appear on the manuscript pages.

_____ The manuscript is organized as follows: title page, blind title page (title only), abstract, introduction, methods, results, discussion, acknowledgments, references, tables, figure legends, and figures.

_____ Informed consent has been obtained from patients who participated in clinical investigations. If experiments were performed on animals, authors complied with NIH guidelines for use of laboratory animals.

_____ Use of unfamiliar acronyms and abbreviations is kept to a minimum. When abbreviations are used they are defined at first mention, followed by the abbreviation in parentheses.

_____ Metric measurements are used throughout, or the metric equivalent is given in parentheses.

_____ Names and locations (city and state only) of manufacturers are given for equipment and nongeneric drugs.

Title Page

_____ The following information is given: title of article; names and complete addresses (including zip code) of all authors; current addresses of authors who have moved since study; acknowledgment of grant or other assistance. The corresponding author is clearly identified, and a current address, phone number, and Fax number are given.

_____ Two copies of a blind title page are included giving only the title (without the authors' names) for use in the review process.

Abstract

_____ An abstract of approximately 200 words concisely states the purpose, methods, and results of the study in one paragraph. Actual data are included. Conclusions are stated in a second, summary paragraph.

_____ No abbreviations or reference citations are used.

References

References (not to exceed 35) are typed double-spaced starting on a separate page and are **numbered consecutively in the order in which they appear in the text**.

All references are cited in the text and are enclosed in brackets and typed on line with the text (not superscript).

Unpublished data are not cited in the reference list, but are cited parenthetically in the text, for example, (Smith DJ, personal communication), (Smith DJ, unpublished data). This includes papers submitted, but not yet accepted, for publication.

Inclusive page numbers (e.g., 333–335) are given for all references.

Journal names are abbreviated according to *Index Medicus*.

Style and punctuation of references follow the format illustrated in the following examples (all authors are listed when six or less; when seven or more authors, the first three are listed, followed by "et al."):

Journal article

1. Long RS, Roe EW, Wu EU, et al. Membrane oxygenation: radiographic appearance. *AJR* **1986**;146:1257–1260

Book

2. Smith LW, Cohen AR. *Pathology of tumors*, 6th ed. Baltimore: Williams & Wilkins, **1977**:100–109

Chapter in a book

3. Breon AJ. Serum monitors of bone metastasis. In: Clark SA, ed. *Bone metastases*. Baltimore: Williams & Wilkins, **1983**:165–180

Paper presented at a meeting

4. Lau FS, Kirk AN. MR imaging of the spine. Presented at the annual meeting of the American Roentgen Ray Society, Washington, DC, April **1986**

Tables

Each table is typed double-spaced on a separate page without vertical or horizontal rules; each has a short, descriptive title. Tables do not exceed two pages in length and contain at least four lines of data.

Tables are numbered in the order in which they are cited in the text.

Abbreviations are defined in an explanatory note below each table.

Tables are self-explanatory and do not duplicate data given in the text or figures.

All arithmetic (percentages, totals, differences) has been double checked for accuracy, and tabular data agree with data given in the text.

Figures and Legends

Two complete sets of original figures are submitted unmounted in labeled envelopes.

Figures are clean, unscratched, 5 × 7 in. (13 × 18 cm) glossy prints with **white borders**. A separate print is submitted for each figure *part*.

All figure parts relating to one patient are in one figure.

Each figure is labeled on the back with the figure number and an arrow indicating "top." For black-and-white figures, labeling is done on a gummed label, which is then affixed to the back of the print. *Never* use labels on color figures, but write figure number on the back lightly in pencil. *Never* use ink on front or back of any figures.

Author's names are *not* written on the backs of figures.

Only removable (rub-on) arrows and letters are used on the figures. Symbols are uniform in size and style and are not broken or cracked.

Images are uniform in size and magnification.

Line drawings are done in black ink on a white background. They are professional in quality, and all use the same size type. (Only glossy prints are acceptable.)

Written permission has been obtained for use of all previously published illustrations (and copies of permission letters are included), and an appropriate credit line is given in the legends.

Legends are typed double-spaced, and figure numbers correspond with the order in which the figures are cited in the text.

Transfer of Copyright Agreement, Conflict of Interest Acknowledgment, Certification of Coauthors, and Exclusive Publication Statement

Complete copyright to the article entitled: _____

is hereby transferred to the American Roentgen Ray Society (for United States government employees to the extent transferable), effective if and when the article is accepted for publication in the *American Journal of Roentgenology*. In the case of the authors who are officers or employees of the United States government, the American Roentgen Ray Society recognizes that works prepared by officers or employees of the United States government as part of their official government duties are in the public domain.

Authors reserve all proprietary rights other than copyright, such as patent rights and the right to use all or part of this article in future works of their own. The authors retain the right of replication, subject only to crediting the original source of publication and receiving written permission from the publisher.

Authors guarantee that this manuscript contains no matter that is libelous or otherwise unlawful, invades individual privacy, or infringes any proprietary rights.

Authors understand that they will receive no royalty or other compensation from the American Roentgen Ray Society or the publisher.

Authors guarantee that the editor has been or will be informed of any proprietary or commercial interest or conflicts of interest the authors may have that relate directly or indirectly to the subject of this article.

All authors certify that they have made substantive and specific intellectual contributions to the article and assume public responsibility for its content.

Finally, the authors certify that none of the material in this manuscript has been published previously or is currently under consideration for publication elsewhere.

First author/date

Second author

Third author

Fourth author

Fifth author

Sixth author

This agreement must be signed by all authors in order for the manuscript to be published.

Case Reports

A case report is a brief description of a special case that provides a message that transcends the individual patient.

Format. There is no abstract. The introduction should be a short paragraph giving the general background and the specific interest of the case. No more than one case should be described in detail (similar ones can be mentioned briefly in the discussion). Emphasis should be on the radiologic aspects; clinical information must be limited to that necessary to provide a background for the radiology. The discussion should be succinct and should focus on the specific message and relevance of radiologic methods. A review of the literature is not appropriate.

Length. Maximum of five double-spaced, typewritten pages, including the references but not the title page or figure legends.

References. Maximum of eight.

Figures. Maximum of three or four, unless the text is shortened accordingly. Legends must not repeat the text.

Tables and Acknowledgments. Not appropriate in case reports.

Technical Notes

A technical note is a brief description of a specific technique or procedure, modification of a technique, or equipment of interest to radiologists.

Format. No abstract, headings, or subheadings are required. If headings are used, they should be a combination of "Case Report," "Materials and Methods," "Results," and "Discussion." A brief one-paragraph introduction should be included to give the general background. Discussion should be limited to the specific message, including the uses of the technique or equipment. Literature reviews and lengthy case reports are not appropriate.

Length. Maximum of five double-spaced, typewritten pages, including the references but not the title page or figure legends.

References. Maximum of eight.

Figures. Maximum of two, unless the text is shortened accordingly.

Tables and Acknowledgments. Not appropriate in technical notes.

Pictorial Essays

A pictorial essay is an article that conveys its message through illustrations and their legends. Unlike other AJR articles, which are based on original research, pictorial essays serve primarily as teaching tools, like exhibits at a scientific meeting. They are not encyclopedic book chapters. No abstract is necessary.

Length. Maximum of four double-spaced, typewritten pages, including the references but not the title page or figure legends.

References. Maximum of four.

Figures. Maximum of 30 figure parts. Number should be as few as necessary to convey the message of the paper.

Tables and Acknowledgments. Not appropriate in pictorial essays.

Letters to the Editor and Replies

Letters to the Editor and Replies should offer objective and constructive criticism of published articles. Letters may also discuss matters of general interest to radiologists. Do not end a letter with a hand-written signature.

Format. All letters should be typed double-spaced on nonletterhead paper, with no greeting or salutation. Name and affiliation should appear at the end of the letter. Titles for letters should be short and pertinent. The title for a reply is simply "Reply."

Length. Maximum of two double-spaced, typewritten pages, including references.

References. Maximum of four.

Figures. Maximum of two.

Tables and Acknowledgments. Not appropriate in Letters to the Editor and Replies.

Opinions, Commentaries, and Perspectives

Opinions, commentaries, and perspectives are special articles dealing with controversial topics or issues of special concern to radiologists.

Format. Include a title page but no abstract. Headings may be used to break up the text.

Length. Maximum of five double-spaced, typewritten pages.

References. Maximum of five.

Tables and Figures. Maximum of four.

Computer Page Articles

Articles published on the computer page deal with practical computer applications to radiology.

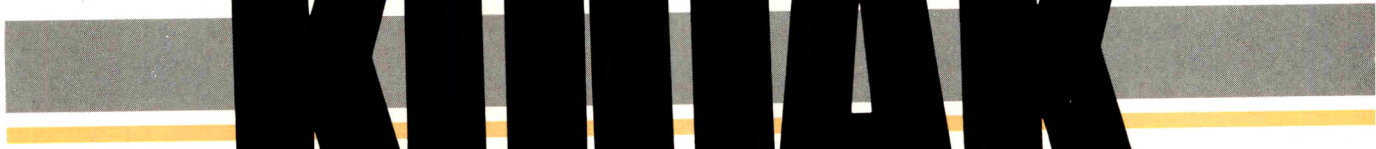
Format. Include a title page but no abstract.

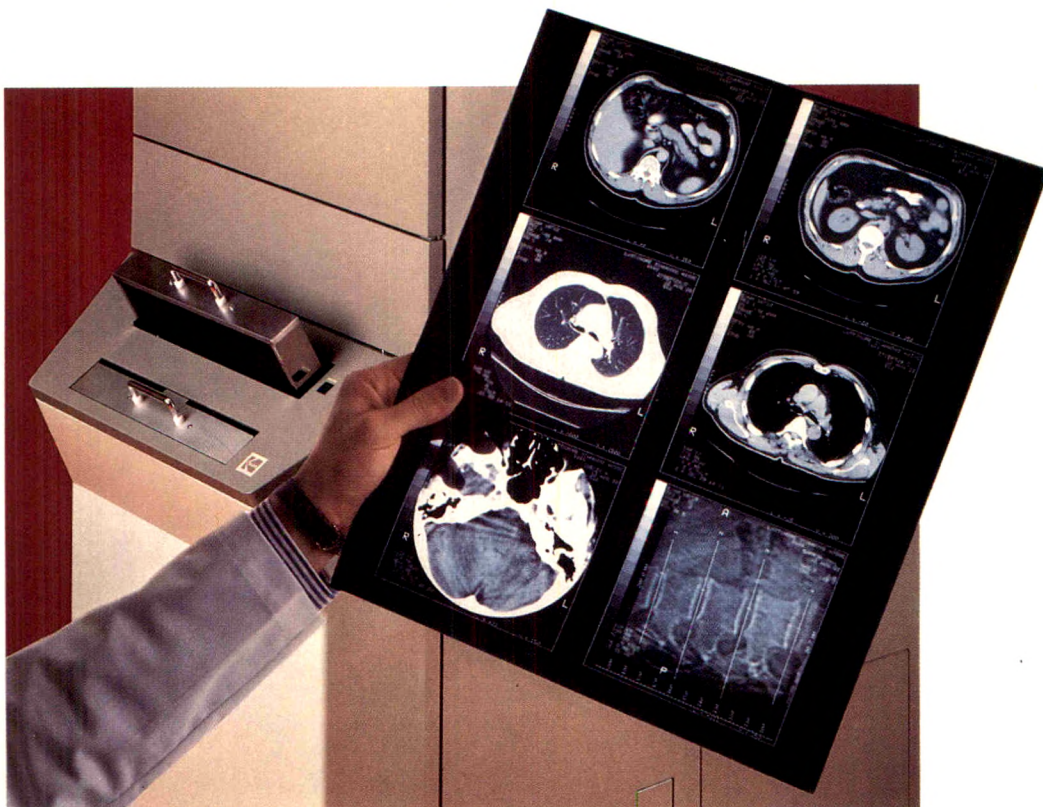
Length. Maximum of eight double-spaced, typewritten pages.

References. Maximum of five.

Figures and Tables. Maximum of five. Computer printouts are not acceptable. Figures must be submitted as 5 × 7 in. glossy prints.

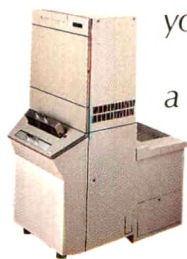
**STEP UP
TO LASER
IMAGING
WITH
KODAK**

A decorative horizontal bar consisting of a thick grey band with a thin yellow line running through its center, positioned behind the word KODAK.



***Introducing the Kodak Ektascan laser printer, model 100.
The quality of digital imaging for today's and tomorrow's
imaging systems.***

Now you can have consistent, artifact-free, high-resolution digital images from current and future imaging systems. The new Kodak Ektascan laser printer, model 100, is available with custom interfaces for CT, MRI and DSA. Flexible tone scaling gives you the look you like on Kodak Ektascan laser imaging film. And a compact 28 x 30-inch footprint makes it ideal for mobile applications. Part of a complete Kodak imaging system, the Ektascan laser printer, docked to a Kodak processor, gives you maximum productivity.



Ask your Kodak representative for details, or specify a Kodak Ektascan laser printer when you order an imaging system.

The digital imaging advantage.

The new vision of Kodak



AJR Business and Subscriber Information

The American Roentgen Ray Society

AJR, *American Journal of Roentgenology*, is published monthly to disseminate research on current developments in the radiologic sciences and commentary on topics related to radiology. It is published by the American Roentgen Ray Society, 1891 Preston White Dr., Reston, VA 22091; (703) 648-8992. Inquiries regarding society business, the annual ARRS meeting, and membership should be addressed to the Society at the above address.

Correspondence Concerning the AJR

Correspondence regarding display (not classified) advertising, subscriptions, address changes, reprints, and permission requests should be addressed to Williams & Wilkins, 428 E. Preston St., Baltimore, MD 21202; (301) 528-4000.

Correspondence regarding editorial matters and classified advertising should be addressed to Editorial Office, *AJR*, 2223 Avenida de la Playa, Ste. 200, La Jolla, CA 92037-3218; telephone (619) 459-2229; FAX (619) 459-8814. For information on manuscript submission, see Guidelines for Authors, pages A3-A5.

Subscriber Information

Subscription requests and inquiries should be sent to Williams & Wilkins, 428 E. Preston St., Baltimore, MD 21202. ARRS annual dues include \$50 for journal subscription. Subscription rates are as follows: nonmembers, \$100/year (\$135 foreign); institutions, \$110 (\$145 foreign); nonmember in-training, \$25 (\$50 foreign). Single copies of the Journal may

be purchased for \$16 (\$19 foreign). Airmail rates will be furnished on request.

Japanese rates include airfreight. Japanese yen price is available from our sole agent, USACO Corporation, 13-12, Shimbashi 1-Chome, Minato-Ku, Tokyo 105, Japan; telephone 03-502-6471.

If a subscriber receives a damaged copy of the *AJR* or fails to receive an issue, the subscriber should notify Williams & Wilkins (428 E. Preston St., Baltimore, MD 21202) within 60 days of publication (90 days for foreign subscribers) and that issue will be replaced.

Change of address information should be sent to Williams & Wilkins, 428 E. Preston St., Baltimore, MD 21202. Allow 90 days for address changes.

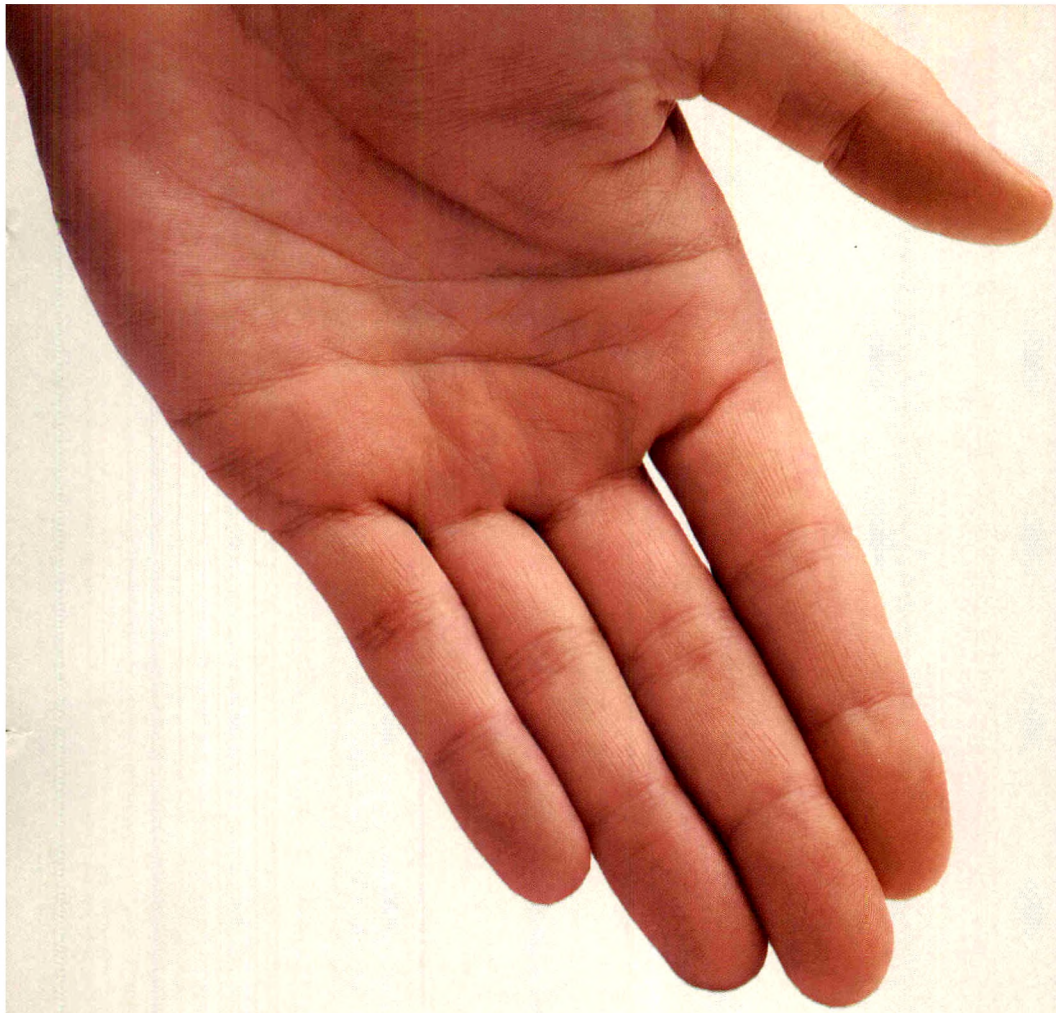
Copyrights, Permissions, and Reprints

The American Roentgen Ray Society holds the copyright for all material published in the *AJR*. No part of this publication may be reproduced without permission from the ARRS. Requests for such permission should be addressed to Williams & Wilkins, 428 E. Preston St., Baltimore, MD 21202.

For reprints of a particular article, please contact the author designated in the footnotes for that article.

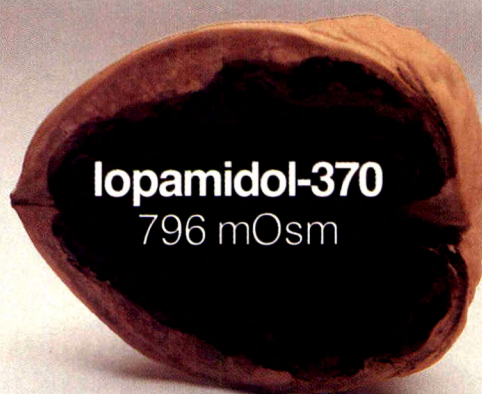
Indexes

The *AJR* provides volume and yearly indexes (subject and author) in the June and December issues each year. *AJR* articles are also indexed in *Current Contents*, *Index Medicus*, and the cumulative index published by *Radiology*.

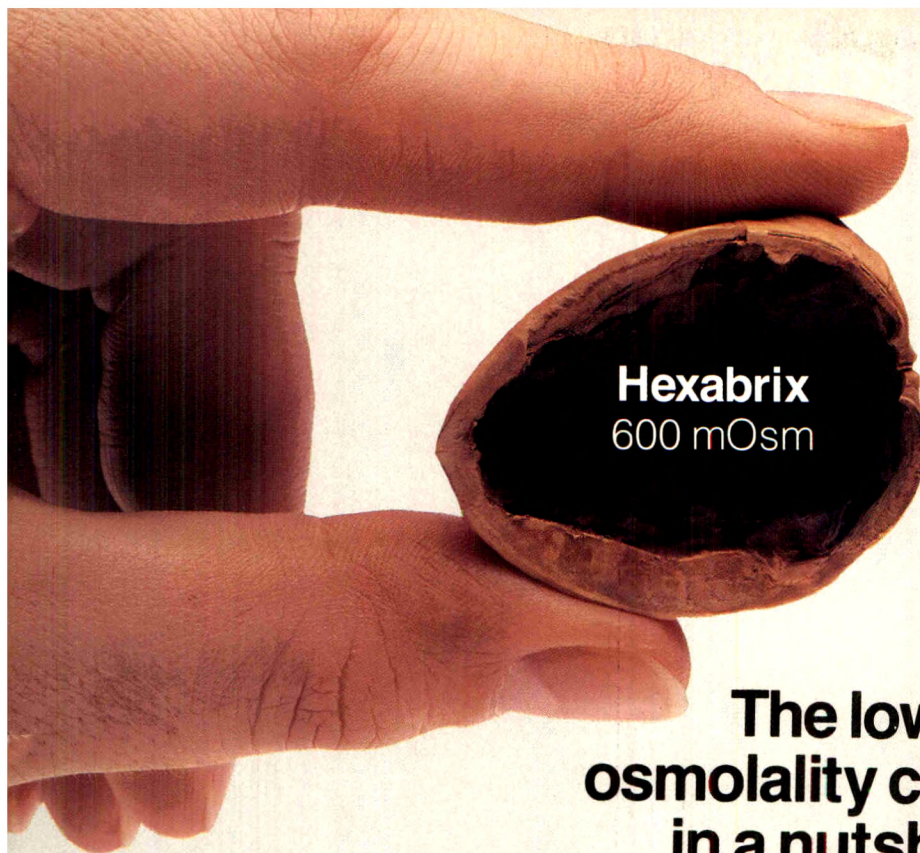


**For greater patient comfort
and the lowest osmolality,
the choice is yours...**





F R O M M A I I



Hexabrix
600 mOsm

The low osmolality choice, in a nutshell

Compare Hexabrix with the nonionics, and you'll find that Hexabrix not only has the lowest osmolality, but also the least amount of patient discomfort in interventional procedures.

Least heat and pain

Recent comparative studies demonstrate that Hexabrix produces significantly less heat¹ and pain¹⁻³ than iopamidol and/or iohexol during arteriography procedures.¹⁻³

Less risk of clotting *in vitro*

Hexabrix has been shown to be a stronger inhibitor of clotting^{4,5} and platelet aggregation^{5,6} *in vitro* than iopamidol or iohexol.

Good angiographic technique should be followed in all procedures involving contrast media. Even when meticulous technique is used, some mixing of blood with contrast media in syringes and catheters is possible. Prolonged contact of blood and contrast media in syringes and catheters can lead to clot formation.

Lowest viscosity

Hexabrix has the lowest viscosity at 37°C (7.5 cps), compared to iohexol-350 (10.4 cps) or iopamidol-370 (9.4 cps).

HEXABRIX[†]

(ioxaglate meglumine 39.3%/
ioxaglate sodium 19.6% injection)

Please see following page for references and brief summary of prescribing information.

N C K B O D T

HEXABRIX[†] (ioxaglate meglumine 39.3%/ioxaglate sodium 19.6% injection)

HEXABRIX[®]
Each milliliter of HEXABRIX contains 393 mg of ioxaglate meglumine, 196 mg of ioxaglate sodium and 0.10 mg edetate calcium disodium as a stabilizer. The solution contains 3.48 mEq (0.15 mEq) sodium in each milliliter and provides 32% (320 mEq/L) organically bound iodine.

CONTRAINDICATIONS

HEXABRIX is contraindicated for use in myelography. Refer to PRECAUTIONS concerning hypersensitivity. Hysterosalpingography should not be performed during the menstrual period, in pregnant patients, in patients with known infection in any portion of the genital tract, or in patients in whom cervical ceratoplasty or ceratoplasty has been performed within 30 days. Arthrography should not be performed if infection is present in or near the joint.

WARNINGS

Serious or fatal reactions have been associated with the administration of iodine containing radiopaque media. It is of utmost importance to be completely prepared to treat any contrast medium reaction.

As with any contrast medium, serious neurologic sequelae, including permanent paralysis, can occur following cerebral arteriography, selective spinal arteriography and arteriography of vessels supplying the spinal cord. The injection of a contrast medium should never be made following the administration of vasopressors, since they strongly potentiate neurologic effects.

In patients with subarachnoid hemorrhage, a rare association between contrast administration and clinical deterioration, including convulsions and death, has been reported. Therefore, administration of intravascular iodinated contrast media in these patients should be undertaken with caution.

A definite risk exists in the use of intravascular contrast agents in patients who are known to have multiple myeloma. In such instances anuria has developed, resulting in progressive uremia, renal failure and eventually death. Although neither the contrast agent nor dehydration has separately proved to be the cause of anuria in myeloma, it has been speculated that the combination of both may be a causative factor. The risk in myelomatous patients is not a contraindication to the procedure; however, partial dehydration in the preparation of these patients for the examination is not recommended since this may predispose to precipitation of myeloma protein in the renal tubules. No form of therapy, including dialysis, has been successful in reversing the effect. Myeloma, which occurs most commonly in persons over 40, should be considered before instituting intravascular administration of contrast agents.

Administration of radiopaque materials to patients known or suspected to have pheochromocytoma should be performed with extreme caution. In the opinion of the physician, the possible benefits of such procedures outweigh the considered risks, the procedures may be performed; however, the amount of radiopaque medium injected should be kept to an absolute minimum. The blood pressure should be assessed throughout the procedure, and measures for treatment of a hypertensive crisis should be available.

Since intravascular administration of contrast media may promote sickling in individuals who are homozygous for sickle cell disease, fluid restriction is not advised.

In patients with advanced renal disease, iodinated contrast media should be used with caution and only when the need for the examination dictates, since excretion of the medium may be impaired. Patients with combined renal and hepatic disease, those with severe hypotension or congestive heart failure and recent renal transplant recipients present an additional risk.

Renal failure has been reported in patients with liver dysfunction who were given an oral cholecystographic agent followed by an intravascular iodinated radiopaque agent and also in patients with occult renal disease, notably diabetes and hypertension. In these classes of patients there should be no fluid restriction and every attempt made to maintain normal hydration prior to contrast medium injection, since dehydration is the single most important factor influencing further renal impairment.

Caution should be exercised in performing contrast medium studies in patients with endotoxemia and/or those with elevated body temperatures.

Reports of thyroid storm occurring following the intravascular use of iodinated radiopaque agents in patients with hyperthyroidism or with an autonomously functioning thyroid nodule, suggest that this additional risk be evaluated before use of this drug. Iodine-containing contrast agents may alter the results of thyroid function tests which depend on iodine estimation, e.g., PBI, and may also affect results of radioactive iodine uptake studies. Such tests, if indicated, should be performed prior to the administration of this preparation.

PRECAUTIONS

Diagnostic procedures which involve the use of iodinated intravascular contrast agents should be carried out under the direction of personnel skilled and experienced in the particular procedure to be performed. All procedures utilizing contrast media carry a definite risk of producing adverse reactions. While most reactions are minor, life-threatening and fatal reactions may occur without warning, and this risk must be weighed against the benefit of the procedure. A fully equipped emergency cart, or equivalent supplies and equipment, and personnel competent in recognizing and treating adverse reactions of all types should always be available. If a serious reaction should occur, immediately discontinue administration. Since severe delayed reactions have been known to occur, emergency facilities and competent personnel should be available for at least 30 to 60 minutes after administration. (See ADVERSE REACTIONS.)

Preparatory dehydration is dangerous and may contribute to acute renal failure in infants, young children, the elderly, patients with pre-existing renal insufficiency, patients with multiple myeloma, patients with advanced vascular disease and diabetic patients.

Acute renal failure has been reported in diabetic patients with diabetic nephropathy and in susceptible non-diabetic patients (often elderly with pre-existing renal disease) following the administration of iodinated contrast agents. Therefore, careful consideration of the potential risks should be given before performing this radiographic procedure in these patients.

Severe reactions to contrast media often resemble allergic responses. This has prompted the use of several provocative pretesting methods, none of which can be relied on to predict severe reactions. No conclusive relationship between severe reactions and antigen-antibody reactions or other manifestations of allergy has been established. The possibility of an

idiosyncratic reaction in patients who have previously received a contrast medium without ill effect should always be considered. Prior to the injection of any contrast medium, the patient should be questioned to obtain a medical history with emphasis on allergy and hypersensitivity. A positive history of bronchial asthma or allergy (including food), a family history of allergy, or a previous reaction of hypersensitivity to a contrast agent may imply a greater than usual risk. Such a history may be more accurate than pre-testing in predicting the potential for reaction, although not necessarily the severity or type of reaction in the individual case. A positive history of this type does not arbitrarily contraindicate the use of a contrast agent when a diagnostic procedure is thought essential, but does call for caution. (See ADVERSE REACTIONS.)

Prophylactic therapy including corticosteroids and antihistamines should be considered for patients who present with a strong allergic history, a previous reaction to a contrast medium, or a positive pre-test since in these patients the incidence of reaction is two to three times that of the general population. Adequate doses of corticosteroids should be started early enough prior to contrast medium injection to be effective and should continue through the time of injection and for 24 hours after injection. Antihistamines should be administered within 30 minutes of the contrast medium injection. Recent reports indicate that such pre-treatment does not prevent serious life-threatening reactions, but may reduce both their incidence and severity. A separate syringe should be used for these injections.

General anesthesia may be indicated in the performance of some procedures in selected patients; however, a higher incidence of adverse reactions has been reported in these patients, and may be attributable to the inability of the patient to identify untoward symptoms or to the hypotensive effect of anesthesia which can prolong the circulation time and increase the duration of contact of the contrast agent.

Angiography should be avoided whenever possible in patients with homocystinuria because of the risk of inducing thrombosis and embolism.

PRECAUTIONS FOR SPECIFIC PROCEDURES

Pediatric Angiography. It is advisable to monitor for ECG and vital signs changes throughout the procedure.

When large individual doses are administered, sufficient time should be allowed for any observed changes to return to or near baseline prior to making the next injection.

Caution should be used when making right heart injections in patients with pulmonary hypertension or incipient heart failure, since this may lead to increased right side pressures with subsequent bradycardia and systemic hypotension. Patients with pulmonary disease present additional risks.

Caution is advised in cyanotic infants since apnea, bradycardia, other arrhythmias and a tendency to acidosis are more likely to occur.

Since infants are more likely to respond with convulsions than are adults, the amount of total dosage is of particular importance. Repeated injections are hazardous in infants weighing less than 7 kg, particularly when these infants have pre-existing compromised right heart function or obliterated pulmonary vascular beds.

Selective Coronary Arteriography with or without left ventriculography. During the administration of large doses of HEXABRIX, continuous monitoring of vital signs is desirable. Caution is advised in the administration of large volumes to patients with incipient heart failure because of the possibility of aggravating the pre-existing condition. Hypotension should be corrected promptly since it may result in serious arrhythmias.

Special care regarding dosage should be observed in patients with right ventricular failure, pulmonary hypertension, or stenotic pulmonary vascular beds because of hemodynamic changes which may occur after injection into the right heart outflow tract.

Peripheral Arteriography. Moderate decreases in blood pressure occur frequently with intra-arterial (brachial) injections. This change is usually transient and requires no treatment; however, the blood pressure should be monitored for approximately ten minutes following injection.

Extreme caution during injection of the contrast agent is necessary to avoid extravasation and fluoroscopy is recommended. This is especially important in patients with severe arterial disease.

Cerebral Arteriography. Cerebral angiography should be performed with special caution in patients with advanced arteriosclerosis, severe hypertension, cardiac decompensation, senile, recent cerebral thrombosis or embolism, and migraine.

Intra-Arterial Digital Subtraction Angiography. The risks associated with IA-DSA are those usually attendant with catheter procedures. Following the procedure, gentle pressure hemostasis is required, followed by observation and immobilization of the limb for several hours to prevent hemorrhage from the site of arterial puncture.

Patient motion, including respiration and swallowing, can result in misregistration leading to image degradation and non-diagnostic studies.

Intravenous Digital Subtraction Angiography. The risks associated with IV-DSA include those usually attendant with catheter procedures and include intraluminal injuries, vessel dissection and tissue extravasation. The potential risk is reduced when small test injections of contrast medium are made under fluoroscopic observation to insure that the catheter tip is properly positioned and, in the case of peripheral placement, that the vein is of adequate size.

Patient motion, including respiration and swallowing, can result in misregistration leading to image degradation and non-diagnostic studies.

Peripheral Venography. Special care is required when venography is performed in patients with suspected thrombosis, phlebitis, severe ischemic disease, local infection or a totally obstructed venous system.

Extreme caution during injection of contrast media is necessary to avoid extravasation and fluoroscopy is recommended. This is especially important in patients with severe arterial or venous disease.

Excretory Urography. Infants and small children should not have any fluid restrictions prior to excretory urography. (See WARNINGS and PRECAUTIONS concerning preparatory dehydration.)

Contrast Enhancement in Body Computed Tomography. Patient cooperation is essential since patient motion, including respiration, can markedly affect image quality. The use of an intravascular contrast medium can obscure tumors in patients undergoing CT evaluation of the liver, resulting in a false negative diagnosis. Dynamic CT scanning is the procedure of choice for malignant tumor enhancement.

Arthrography. Strict aseptic technique is required to prevent the introduction of infection. Fluoroscopic control should be used to insure proper introduction of the needle into the synovial space and prevent extracapsular injection. Aspiration of excessive synovial fluid will reduce the pain on injection and prevent the dilution of the contrast agent. It is important that undue pressure not be exerted during the injection.

Hysterosalpingography. Caution should be exercised in patients suspected of having cervical or tubal carcinoma to avoid possible spread of the lesion by the procedure. Delayed onset of pain and fever (1-2 days) may be indicative of pelvic infection.

Carcinogenesis, Mutagenesis, Impairment of Fertility. No long-term animal studies have been performed to evaluate carcinogenic potential. However, animal studies suggest that this drug is not mutagenic and does not affect fertility in males or females.

Pregnancy Category B. Reproduction studies have been performed in rats and rabbits at doses up to two times the maximum adult human dose and have revealed no evidence of impaired fertility or harm to the fetus due to HEXABRIX. There are, however, no adequate and well-controlled studies in pregnant women. Because animal reproduction studies are not always predictive of human response, this drug should be used during pregnancy only if clearly needed.

Nursing Mothers. Ioxaglate salts are excreted unchanged in human milk. Because of the potential for adverse effects in nursing infants, bottle feedings should be substituted for breast feedings for 24 hours following the administration of this drug.

Pediatric Use. Safety and effectiveness in children has been established in pediatric angiography and intravenous excretory urography. Data have not been submitted to support the safety and effectiveness of HEXABRIX in other indications. (Precautions for specific procedures receive comment under that procedure.)

ADVERSE REACTIONS

Adverse reactions to injectable contrast media fall into two categories: chemotoxic reactions and idiosyncratic reactions.

Chemotoxic reactions result from the physicochemical properties of the contrast media, the dose and the speed of injection. All hemodynamic disturbances and changes to organs or vessels perfused by the contrast medium are included in this category.

Idiosyncratic reactions include all other reactions. They occur more frequently in patients 20 to 40 years old. Idiosyncratic reactions may or may not be dependent on the dose injected, the speed of injection, the mode of injection and the radiographic procedure. Idiosyncratic reactions are subdivided into minor, intermediate and severe. The minor reactions are self-limited and of short duration; the severe reactions are life-threatening and treatment is urgent and mandatory.

NOTE: Not all of the following adverse reactions have been reported with HEXABRIX. Because HEXABRIX is an iodinated intravascular contrast agent, all of the side effects and toxicity associated with agents of this class are theoretically possible, and this should be borne in mind when HEXABRIX is administered.

Severe, life-threatening anaphylactoid reactions, mostly of cardiovascular origin, have occurred following the administration of HEXABRIX as well as other iodine-containing contrast agents. Most deaths occur during injection or 5 to 10 minutes later. The main feature being cardiac arrest with cardiovascular disease as the main aggravating factor. Isolated reports of hypotensive collapse and shock are found in the literature. Based upon clinical literature, reported deaths from the administration of conventional iodinated contrast agents range from 6.6 per 1 million (0.00066 percent) to 1 in 10,000 patients (0.01 percent).

Regardless of the contrast agent employed, the overall estimated incidence of serious adverse reactions is higher with coronary arteriography than with other procedures. Cardiac decompensation, serious arrhythmias, or myocardial ischemia or infarction may occur during coronary arteriography and left ventriculography.

The most frequent adverse reactions are nausea, vomiting, facial flush and a feeling of body warmth. These are usually of brief duration. In double-blind clinical trials, HEXABRIX produced less discomfort upon injection (pain and heat) when compared to various other contrast agents. Other reactions include the following:

Hypersensitivity reactions. Dermal manifestations of urticaria with or without pruritus, erythema and maculopapular rash. Dry mouth, Swallowing. Constitutional symptoms. Facial peripheral and angioneurotic edema. Symptoms related to the respiratory system include sneezing, nasal stuffiness, coughing, choking, dyspnea, chest tightness and wheezing, which may be initial manifestations of more severe and infrequent reactions including asthmatic attack, laryngospasm and bronchospasm with or without edema, pulmonary edema, apnea and cyanosis. Rarely, these allergic-type reactions can progress into anaphylaxis with loss of consciousness, coma, severe cardiovascular disturbances, and death.

Cardiovascular reactions. Generalized vasodilation, flushing and venospasm. Occasionally thrombosis or rarely, thrombophlebitis. Extremely rare cases of disseminated intravascular coagulation resulting in death have been reported. Severe cardiovascular responses include rare cases of hypotensive shock, coronary insufficiency, cardiac arrhythmia, fibrillation and arrest. These severe reactions are usually reversible with prompt and appropriate management, however, fatalities have occurred.

Technique reactions. Extravasation with burning pain, hematomas, ecchymosis and tissue necrosis, vascular constriction due to injection rate, thrombosis and thrombophlebitis.

Neurological reactions. Spasm, convulsions, aphasia, syncope, paresis, paralysis resulting from spinal cord injury and pathology associated with the syndrome of transverse myelitis, visual field losses which are usually transient but may be permanent, coma and death.

Other reactions. Headache, trembling, shaking, chills with or without fever, hyperthermia and lightheadedness. Temporary renal shutdown or other nephropathy.

Pediatric angiography has been complicated by intramural injection with marked adverse effects on cardiac function.

During selective coronary arteriography with or without left ventriculography, patients may have clinically insignificant ECG changes. The following adverse effects have occurred in conjunction with the administration of iodinated intravascular contrast agents for this procedure: hypotension, shock, anginal pain, myocardial infarction, cardiac arrhythmias (bradycardia, ventricular tachycardia, ventricular fibrillation) and cardiac arrest. Fatalities have been reported. Complications to the procedure include dissection of coronary arteries, dislodgement of atheromatous plaques, perforation, hemorrhage and thrombosis.

Following peripheral arteriography hemorrhage and thrombosis have occurred at the puncture site of the percutaneous injection. Brachial plexus injury has been reported following axillary artery injection.

The major causes of cerebral arteriographic adverse reactions appear to be repeated injections of the contrast material, administration of doses higher than those recommended, the presence of occlusive atherosclerotic vascular disease and the method and technique of injection. Adverse reactions are normally mild and transient. A feeling of warmth in the face and neck is frequently experienced. Infrequently, a more severe burning discomfort is observed. Transient visual hallucinations have been reported. Serious neurological reactions that have been associated with cerebral angiography and not listed under Adverse Reactions include stroke, amnesia and respiratory difficulties. Visual field defects with anopia and reversible neurological deficit lasting from 24 hours to 48 hours have been reported. Confusion, disorientation with hallucination, and absence of vision sometimes lasting for one week have also been reported. Cardiovascular reactions that may occur with some frequency are bradycardia and either an increase or decrease in systemic blood pressure. The blood pressure change is transient and usually requires no treatment. Arthrography may induce joint pain or discomfort which is usually mild and transient but occasionally may be severe and persist for 24 to 48 hours following the procedure. Effusion requiring aspiration may occur in patients with rheumatoid arthritis. Fever and pain, cramping and tenderness of the abdomen have been reported following hysterosalpingography.

OVERDOSAGE

Overdosages may occur. The adverse effects of overdoses are life-threatening and affect mainly the pulmonary and cardiovascular systems. The symptoms may include cyanosis, bradycardia, acidosis, pulmonary hemorrhage, convulsions, coma and cardiac arrest. Treatment of an overdose is directed toward the support of all vital functions and prompt institution of symptomatic therapy.

Ioxaglate salts are dialyzable. The intravenous LD₅₀ values of HEXABRIX (in grams of iodine/kilogram body weight) were 11.2 g/kg in mice, >8 g/kg in rats, >6.4 g/kg in rabbits and >10.2 g/kg in dogs.

DOSAGE AND ADMINISTRATION

Details on dosage are provided in the package insert. **CON-SULT FULL PACKAGE INSERT BEFORE USE.**
Rev. Jan 1987

References:

1. Stris MG, Laerum F. Iohexol and ioxaglate in peripheral angiography. *Acta Radiologica* 1987; 28:767-770.
2. Smith DC, Yahiku PY, Maloney MD, et al: Three new low-osmolality contrast agents: A comparative study of patient discomfort. *Am J Neuroradiol* 1988; 9:137-139.
3. Murphy WA, Campbell DR, Fraser DB. Pain in peripheral arteriography: An assessment of conventional versus ionic and non-ionic low-osmolality contrast agents. *J Can Assoc Radiol* 1988; 39:103-106.
4. Engelhart JA, Smith D, Bull BS, et al: Aspiration blood and low-osmolality contrast agents: An embolic hazard? Presented at the 73rd Meeting of the Radiological Society of North America, Chicago, IL, Dec 1, 1987.
5. Mosier LD, Joist JH, Chance D, et al: In vitro effects of ionic and nonionic contrast media on coagulation, platelet function, and fibrinolysis. Presented at the 73rd Meeting of the Radiological Society of North America, Chicago, IL, Nov 30, 1987.
6. Stormorken H, Skape IO, Testart MC: Effect of various contrast media on coagulation, fibrinolysis, and platelet function: An in vitro and in vivo study. *Invest Radiol* 1986; 21:348-354.



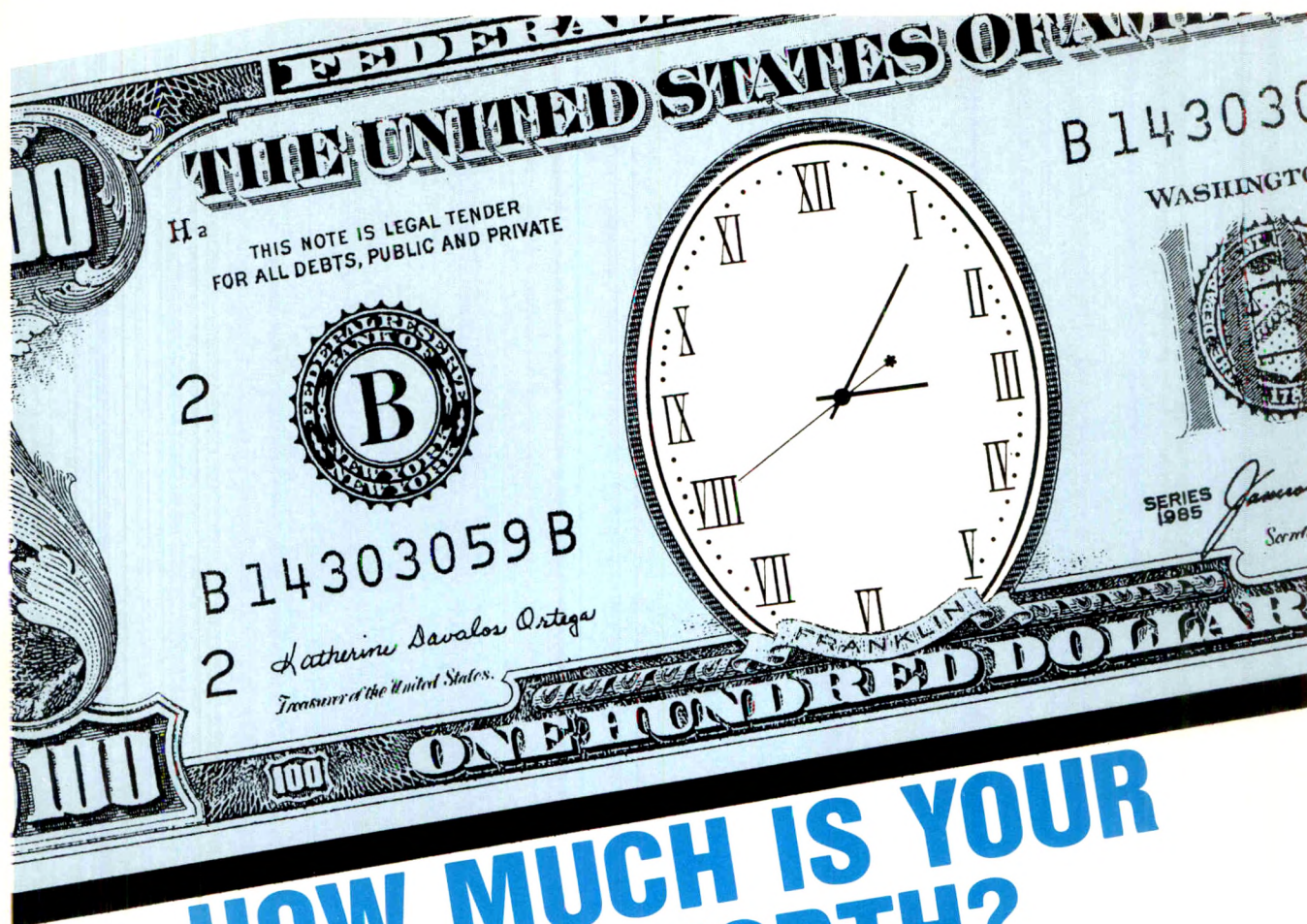
Changing the look of medicine.

Diagnostic Products Division
Mallinckrodt, Inc.

Post Office Box 5840
St. Louis, MO 63134

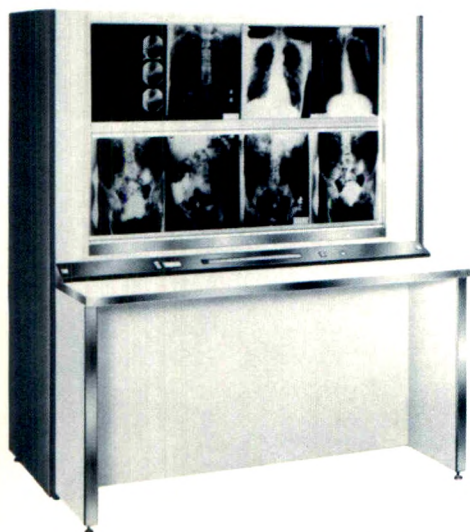
CIRCLE 22 ON READER SERVICE CARD

For orders,
medical and/or
professional assistance
call
(800) 325-3688 TOLL FREE



HOW MUCH IS YOUR TIME WORTH?

If, like most Radiologists, you spend 30% or more of your day **handling** films, let us show you how S & S Motorized Viewers **eliminate** those **COSTLY WASTED HOURS!**



Model MV216

- From 48 up to 324 14" x 17" films can be pre-loaded and stored in proper sequence to be recalled when needed for viewing in as little as 7 seconds—by simply pressing a button!
- All 12 models feature illumination brighter than most other viewers, plus individual panel light controls which promote viewer concentration and increase reading efficiency.
- Some models feature an optional "floating bright spot" which illuminates dense area—at the touch of a button.

- Optional remote controls eliminate need to stand directly in front of viewer to operate it.
- Smaller capacity units on casters provide room-to-room mobility as needed.
- Specially dedicated models are also available for MAMMOGRAPHY, ULTRASOUND, CT and NUCLEAR FILM VIEWING.

Ideal for Teaching, Lecturing or Consultation, S & S Motorized Viewers turn waste into efficiency. **How much is YOUR time worth?** Call S & S or your local x-ray dealer **today.**

CIRCLE 9 ON READER SERVICE CARD

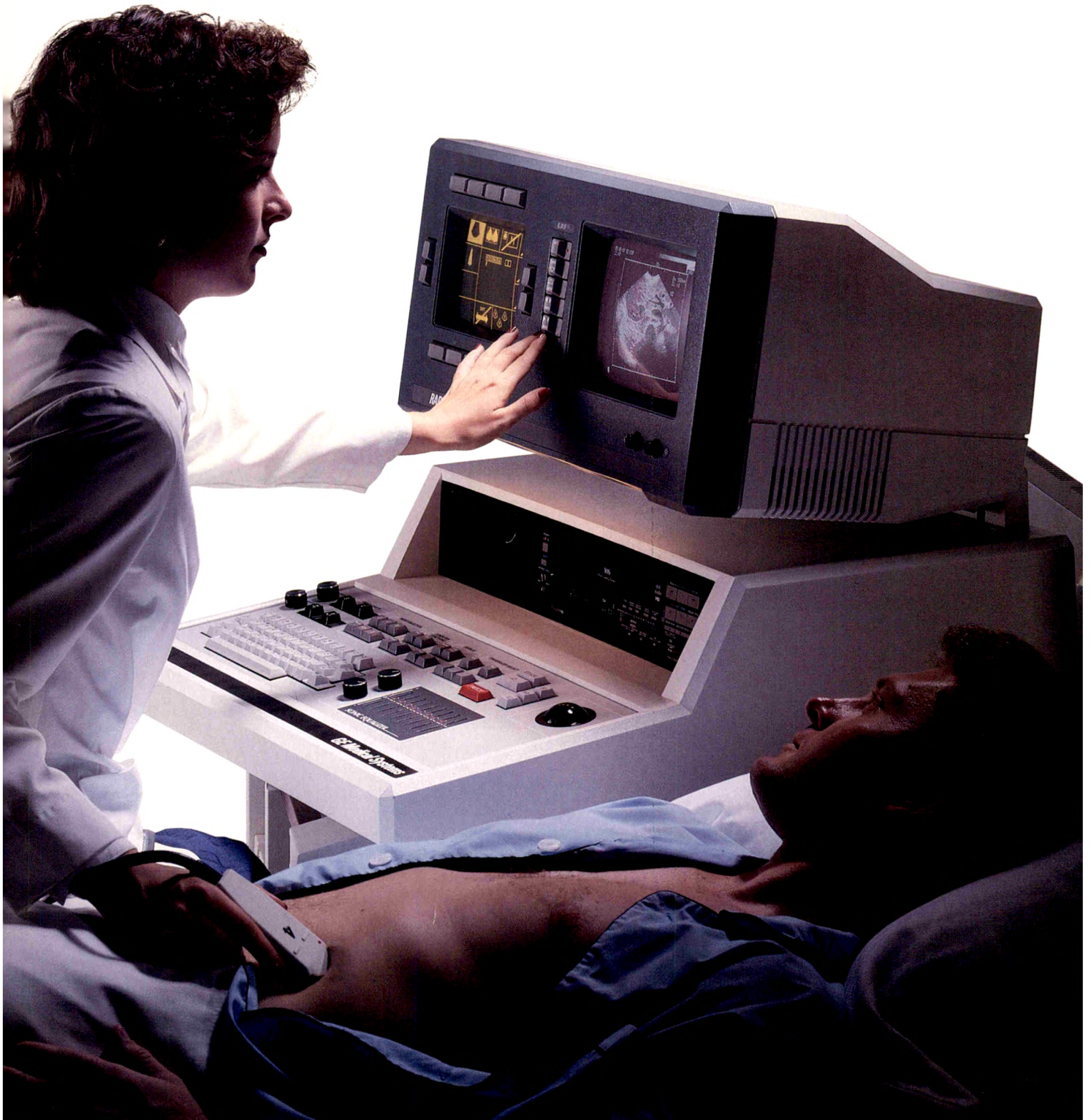
S & S X-RAY PRODUCTS INC.

1101 Linwood Street
Brooklyn, NY 11208
800/347-XRAY
718/649-8500
FAX 718/257-0219



RADIUS

ULTRASOUND



Clearly, a better choice.

Introducing Radius™: the only ultrasound system to offer you complete clinical flexibility *plus* the benefits of radial array technology.

Clearly, superb images

Radius combines the advantages of sophisticated linear arrays with sector's more compact acoustic access... and then further enhances image quality in a number of ways:

- Geometric beam steering keeps the effective aperture constant throughout the field of view. That makes spatial resolution more uniform, and keeps it independent of sector angles—even those exceeding 100°.

- Electronic radial focus maintains the finest focus throughout the image, for clearer border definition.

- Active acoustic aperture maintains an optimal transmit aperture size and apodizes both transmit and receive apertures to minimize side lobes.

The result: Radius provides excellent spatial resolution, contrast discrimination, and uniformity, as well as an extended dynamic range—the major components of image quality.

Clearly, comprehensive

Radius delivers outstanding image quality in general radiology, ob/gyn, peripheral vascular, cardiac and Doppler applications—including PV and abdominal studies.

And to further extend its diagnostic utility, it also provides capabilities ranging from complete quantification software and spectral analysis to integrated floppy disk storage.

What's more, Radius is designed to accommodate new probes, software, and emerging applications—including color flow mapping.

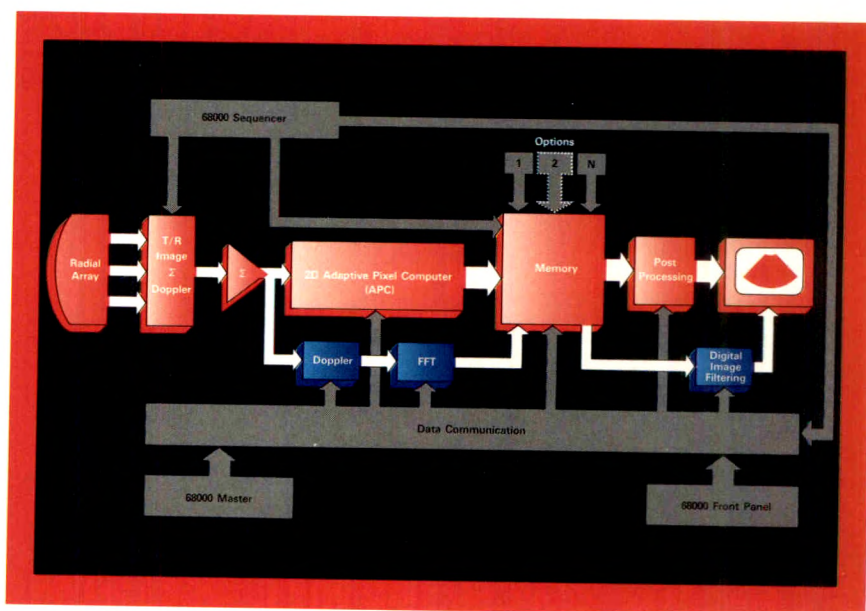
Clearly, GE

Best of all, Radius offers you the security of working with the world's leading diagnostic imaging manufacturer—and of knowing that we'll be here to serve you for many years.

When you weigh *all* the factors, the better choice becomes clear:
Radius ultrasound.

For more information, please contact your GE Representative or call:

(800) 624-5692



CIRCLE 27 ON READER SERVICE CARD

GE Medical Systems

*There's never been a
better time to choose GE*

Radiology unfolded . . .

With the ever-increasing number of subspecialties in radiology, it has been difficult to find a book which offers a comprehensive view of this most important discipline, one that speaks to health care professionals and lay persons alike.

Look no further . . .

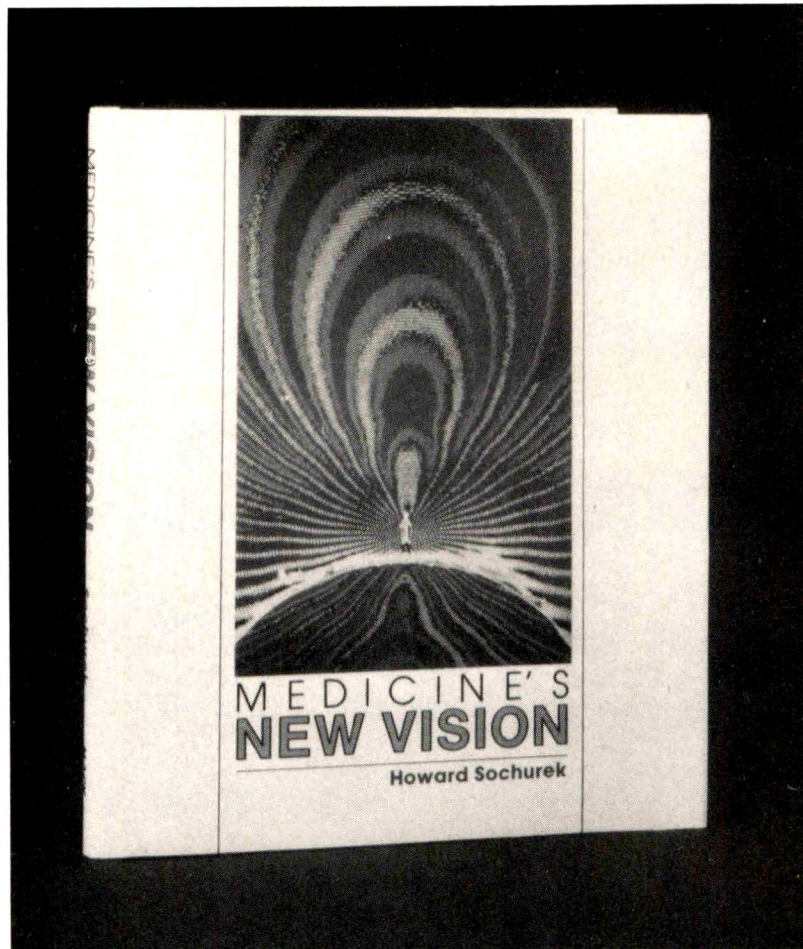
We are proud to introduce *Medicine's New Vision*, a large format book filled with visually stunning, full-color images and accompanied by an exciting, informative text which melds the professionals with the images and with the human beings whose very lives depend on the skillful application of state-of-the-art technology.

Reviewed and approved by the Radiological Society of North America, the world's largest organization dedicated to education in the field of radiology, *Medicine's New Vision* explains the diagnostic role of the radiologist in terms that the lay reader can understand and provides case histories illustrating life-saving techniques. For health care professionals in the field, it also illuminates today's diversity of techniques and applications, and looks to the exciting future of radiology.

192 pages, 9 1/4" X 10 3/4"
148 full color illustrations

Only \$39.95 (postpaid)

100% guaranteed. If for any reason you are not pleased with *Medicine's New Vision*, just return the book within 30 days of receipt and we will refund your money.



ORDER *Medicine's New Vision* TODAY

- for your personal library
- to educate patients and house staff
- as presentations to students, community leaders and media representatives

To Order — complete and mail this order form

Make checks payable to:
MACK PUBLISHING COMPANY

Mail to:
Medicine's New Vision
Mack Publishing Company
20th & Northampton Sts.
Easton, PA 18042

Yes—I wish to order *Medicine's New Vision*

Number of copies _____ @ \$39.95 per copy

Total price \$ _____ postpaid (PA residents please add 6% sales tax)

☐ Payment enclosed

☐ MasterCard ☐ Visa

Account Number

--	--	--	--	--	--	--	--	--	--	--	--	--	--	--	--	--	--	--	--

Signature _____

Exp. date

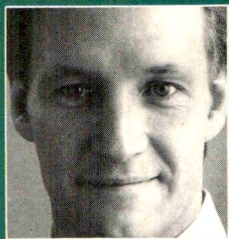
--	--	--	--

Name _____

Address _____

City _____ State _____ Zip _____

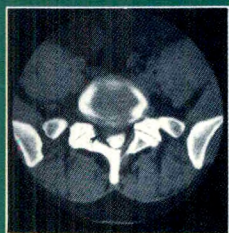
Telephone number (_____) _____



In vascular contrast procedures...

Of commercially available contrast media...

"Iohexol has the lowest chemotoxicity of any contrast agent yet synthesized, and it is the combination of this low chemotoxicity with low osmolality that makes it an agent of such low systemic toxicity."¹



The image of safety.



The OMNI TRIAD
symbolizes the three
factors diagnosticians demand
in contrast-enhanced imaging:
• Safety • Imaging performance
• Patient comfort and tolerance

NONIONIC
OMNIPAQUE[®]
(IOHEXOL)



See next page for important product information concerning contraindications, warnings, adverse reactions, patient selection, and use with...
See next page for important product information concerning contraindications, warnings, adverse reactions, patient selection, and use with...

OMNIPAQUE® 240 300 350

INJECTION (IOHEXOL) INTRAVASCULAR

PLEASE CONSULT FULL PRODUCT INFORMATION BEFORE USING.
A SUMMARY FOLLOWS:

DESCRIPTION: OMNIPAQUE is a sterile, pyrogen- and preservative-free, nonionic, water-soluble radiographic contrast medium for intravascular administration in concentrations of 240, 300, and 350 mgI/mL. OMNIPAQUE 240 contains 518 mg of iohexol equivalent to 240 mg of organic iodine per mL. OMNIPAQUE 300 contains 647 mg of iohexol equivalent to 300 mg of organic iodine per mL, and OMNIPAQUE 350 contains 755 mg of iohexol equivalent to 350 mg of organic iodine per mL. Each milliliter of iohexol solution contains 1.21 mg tromethamine and 0.1 mg edetate calcium disodium with the pH adjusted between 6.8 and 7.7 with hydrochloric acid or sodium hydroxide. Unused portions must be discarded. Iohecol solution is sensitive to light and should be protected from exposure.

CONTRAINDICATIONS: OMNIPAQUE should not be administered to patients with a known hypersensitivity to iohecol.

WARNINGS: OMNIPAQUE should be used with extreme care in patients with severely impaired renal and/or hepatic function; severe thyrotoxicosis; hyperthyroidism; or an autonomously functioning thyroid nodule; diabetes with a serum creatinine level above 3 mg/dL. It is not recommended for use in patients with anuria.

Patients with known or suspected pheochromocytoma should receive a minimum of contrast medium if the benefit of the examination is judged to outweigh its risk; blood pressure should be monitored throughout the procedure, and measures for the treatment of hypertensive crisis should be readily available.

Contrast agents are potentially hazardous in patients with multiple myeloma or other paraproteinemia, particularly those with therapeutically resistant anuria. The combination of contrast agent and dehydration may precipitate myeloma protein in the renal tubules. No form of therapy, including dialysis, has been successful in reversing the effect. Myeloma, which occurs most commonly in persons over age 40, should be considered before instituting intravascular administration of contrast agents.

Ionic contrast media, when injected intravenously or intra-arterially, may promote sickling in individuals who are homozygous for sickle cell disease.

PRECAUTIONS: Diagnostic procedures that involve the use of radiopaque diagnostic agents should be carried out under the direction of personnel with the prerequisite training and with a thorough knowledge of the particular procedure to be performed. Appropriate facilities should be available for coping with any complication of the procedure, as well as for emergency treatment of severe reactions to the contrast agent itself. Competent personnel and emergency facilities should be available for at least 30 to 60 minutes, since severe delayed reactions have occurred (see ADVERSE REACTIONS). The possibility of serious, life-threatening, fatal, anaphylactoid, or cardiovascular reactions should always be considered (see ADVERSE REACTIONS). It is of utmost importance that a course of action be carefully planned in advance for immediate treatment of serious reactions. Preparatory dehydration is dangerous and may contribute to acute renal failure in patients with advanced vascular disease, in diabetic patients, and in susceptible nondiabetic patients (often elderly with preexisting renal disease), infants, and small children. Patients should be well hydrated prior to and following iohecol administration. Careful consideration of the potential risk of acute renal failure should be given before performing excretory urography in diabetic patients with diabetic nephropathy and in susceptible nondiabetic patients (often elderly with preexisting renal disease). Immediately following surgery, excretory urography should be used with caution in renal transplant recipients. The possibility of an idiosyncratic reaction in susceptible patients should always be considered (see ADVERSE REACTIONS). The susceptible population includes, but is not limited to, patients with a history of a previous reaction to contrast media, patients with a known sensitivity to iodine per se, and patients with a known clinical hypersensitivity: bronchial asthma, hay fever, and food allergies. A thorough medical history with emphasis on allergy and hypersensitivity, prior to the injection of any contrast media, may be more accurate than pretesting in predicting potential adverse reactions.

A positive history of allergies or hypersensitivity does not arbitrarily contraindicate the use of a contrast agent where a diagnostic procedure is thought essential, but caution should be exercised (see ADVERSE REACTIONS). Premedication with antihistamines or corticosteroids to avoid or minimize possible allergic reactions in such patients should be considered and administered using separate syringes. Recent reports indicate that such pretreatment does not prevent serious, life-threatening reactions but may reduce both their incidence and severity.

Even though the osmolality of OMNIPAQUE is low compared to diatrizoate- or iohalamate-based ionic agents of comparable iodine concentration, the potential transitory increase in circulatory osmotic load in patients with congestive heart failure requires caution during injection. These patients should be observed for several hours following the procedure to detect delayed hemodynamic disturbances.

General anesthesia may be indicated in the performance of some procedures in selected adult patients, however, a higher incidence of adverse reactions has been reported in these patients and may be attributable to the inability of the patient to identify untoward symptoms or to the hypotensive effect of the anesthesia, which can reduce cardiac output and increase the duration of exposure to the contrast agent.

Angiography should be avoided whenever possible in patients with hemocystinuria, because of the risk of inducing thrombosis and embolism.

In angiographic procedures, the possibility of dislodging plaques or damaging or perforating the vessel wall should be borne in mind during the catheter manipulations and contrast medium injection. Test injections to ensure proper catheter placement are recommended.

Selective coronary arteriography should be performed only in those patients in whom the expected benefits outweigh the potential risk. The inherent risks of angiography in patients with chronic pulmonary emphysema must be weighed against the necessity for performing this procedure.

When OMNIPAQUE is to be injected using plastic disposable syringes, the contrast medium should be drawn into the syringe and used immediately.

The inhibitory effects of nonionic contrast media on mechanisms of hemostasis have been shown, in vitro, to be less than those of ionic contrast media at comparable concentrations. For this reason, standard angiographic procedures should always be followed: angiographic catheters should be flushed frequently, and prolonged contact of blood with contrast media in syringes and catheters should be avoided.

If nondisposable equipment is used, scrupulous care should be taken to prevent residual contamination with traces of cleansing agents.

Parenteral products should be inspected and discarded if particulate matter or discoloration is present.

Drug/Laboratory Test Interaction: If iodine-containing isotopes are to be administered for the diagnosis of thyroid disease, the iodine-binding capacity of thyroid tissue may be reduced for up to 2 weeks after contrast medium administration. Thyroid function tests which do not depend on iodine estimation, eg, T₃ resin uptake or direct thyroxine assays, are not affected. Many radiopaque contrast agents are incompatible in vitro with some antihistamines and many other drugs; therefore, no other pharmaceuticals should be admixed with contrast agents.

Carcinogenesis, Mutagenesis, Impairment of Fertility: No long-term animal studies have been performed to evaluate carcinogenic potential, mutagenesis, or whether OMNIPAQUE can affect fertility in men or women.

Pregnancy Category B: Reproduction studies have been performed in rats and rabbits with up to 100 times the recommended human dose. No evidence of impaired fertility or harm to the fetus has been demonstrated due to OMNIPAQUE. There are, however, no studies in pregnant women. Because animal reproduction studies are not always predictive of human response, this drug should be used during pregnancy only if clearly needed.

Nursing Mothers: It is not known to what extent iohecol is excreted in human milk. However, many injectable contrast agents are excreted unchanged in human milk. Although it has not been established that serious adverse reactions occur in nursing infants, caution should be exercised when intravascular contrast media are administered to nursing women. Bottle feedings may be substituted for breast feedings for 24 hours following administration of OMNIPAQUE.

Pediatric Use (Indicated for Angiocardiology and Urography): Pediatric patients at higher risk of experiencing adverse events during contrast medium administration may include those having asthma, a sensitivity to medication and/or allergens, congestive heart failure, a serum creatinine > 1.5 mg/dL, or those less than 12 months of age.

ADVERSE REACTIONS: Usually mild to moderate in severity. However, serious, life-threatening, and fatal reactions, mostly of cardiovascular origin, have been associated with the administration of iodine-containing contrast media, including OMNIPAQUE. The injection of contrast media is frequently associated with the sensation of warmth and pain, especially in peripheral angiography; pain and warmth are less frequent and less severe with OMNIPAQUE than with many contrast media.

OMNIPAQUE* injection (iohecol)

Cardiovascular System: Arrhythmias including PVCs and PACs (2%), angina/chest pain (1%) and hypotension (0.8%). Others including cardiac failure, asystole, bradycardia, tachycardia, and vasovagal reaction were reported with an individual incidence of less than 0.4%. In controlled clinical trials involving 1,213 patients, one fatality occurred. A cause-and-effect relationship between this death and iohecol has not been established.

Nervous System: Vertigo [including dizziness and lightheadedness] (0.7%), pain (3%), photomas (2%), headache (2%), and taste perversion (1%). Others including anxiety, blurred vision, fever, motor and speech dysfunction, convulsion, paresthesia, somnolence, stiff neck, hemiparesis, and nystagmus were reported, with an individual incidence of less than 0.3%.

Respiratory System: Dyspnea and laryngitis, with an individual incidence of 0.1%.

Gastrointestinal System: Nausea (2%) and vomiting (0.6%). Others including diarrhea, dyspepsia, and dry mouth were reported, with an individual incidence of less than 0.2%.

Skin and Appendages: Urticaria (0.3%) and purpura (0.1%).

Pediatric Angiocardiology and urography: In controlled clinical trials involving 324 patients, adverse reactions following the use of OMNIPAQUE 300 and OMNIPAQUE 350 were generally less frequent than with adults. **Cardiovascular System:** Ventricular tachycardia (0.6%), 2:1 heart block (0.6%), hypertension (0.3%), and anemia (0.3%).

Nervous System: Pain (0.6%), fever (0.6%), and convulsion (0.3%).

Respiratory System: Congestion (0.3%) and apnea (0.3%).

Gastrointestinal System: Nausea (1%), hypoglycemia (0.3%), and vomiting (2%).

Skin and Appendages: Rash (0.3%).

General Adverse Reactions to Contrast Media: The following reactions have been reported after administration of other intravascular iodinated contrast media, and rarely with iohecol. *Reactions due to technique:* hematomas and ecchymoses. *Hemodynamic reactions:* vein cramp and thrombophlebitis following intravenous injection. *Cardiovascular reactions:* rare cases of cardiac arrhythmias, reflex tachycardia, chest pain, cyanosis, hypertension, hypotension, peripheral vasodilatation, shock, and cardiac arrest. *Renal reactions:* occasionally, transient proteinuria, rarely oliguria or anuria. *Allergic reactions:* asthmatic attacks, nasal and conjunctival symptoms, dermal reactions such as urticaria with or without pruritus, as well as pleomorphic rashes, sneezing, and lacrimation, rarely anaphylactoid reactions. Rare fatalities have occurred due to these or unknown causes. *Signs and symptoms related to the respiratory system:* pulmonary or laryngeal edema, bronchospasm, dyspnea, or to the nervous system: restlessness, tremors, convulsions. *Other reactions:* flushing, pain, warmth, metallic taste, nausea, vomiting, anxiety, headache, confusion, pallor, weakness, sweating, localized areas of edema (especially facial cramps), neutropenia, and dizziness. Rarely, immediate or delayed rigors can occur, sometimes accompanied by hyperpyrexia. Infrequently, "iodism" (salivary gland swelling) from organic iodinated compounds appears 2 days after exposure and subsides by the sixth day.

In general, the reactions that are known to occur upon parenteral administration of iodinated contrast agents are possible with any nonionic agent. Approximately 95% of adverse reactions accompanying the use of water-soluble intravascularly administered contrast agents are mild to moderate in degree. However, severe, life-threatening anaphylactoid reactions, mostly of cardiovascular origin, have occurred. Reported incidences of death range from 6.6 per 1 million (0.00066%) to 1 in 10,000 (0.01%). Most deaths occur during injection or 5 to 10 minutes later. The main feature being cardiac arrest, with cardiovascular disease as the main aggravating factor. Isolated reports of hypotensive collapse and shock are found in the literature. The incidence of shock is estimated to be 1 out of 20,000 (0.005%) patients.

Adverse reactions to injectable contrast media fall into two categories: chemotoxic reactions and idiosyncratic reactions.

Chemotoxic reactions result from the physicochemical properties of the contrast media, the dose, and the speed of injection. All hemodynamic disturbances and injuries to organs or vessels perfused by the contrast medium are included in this category.

Idiosyncratic reactions include all other reactions. They occur more frequently in patients 20 to 40 years old. Idiosyncratic reactions may or may not be dependent on the amount of dose injected, the speed of injection, and the radiographic procedure. Idiosyncratic reactions are subdivided into minor, intermediate, and severe. The minor reactions are self-limited and of short duration; the severe reactions are life-threatening and treatment is urgent and mandatory.

The reported incidence of adverse reactions to contrast media in patients with a history of allergy is twice that in the general population. Patients with a history of previous reactions to a contrast medium are three times more susceptible than other patients. However, sensitivity to contrast media does not appear to increase with repeated examinations.

Most adverse reactions to injectable contrast media appear within 1 to 3 minutes after the start of injection, but delayed reactions may occur.

Regardless of the contrast agent employed, the overall estimated incidence of serious adverse reactions is higher with angiocardiology than with other procedures. Cardiac decompensation, serious arrhythmias, angina pectoris, or myocardial ischemia or infarction may occur during angiocardiology and left ventriculography. Electrocardiographic and hemodynamic abnormalities occur less frequently with OMNIPAQUE than with diatrizoate meglumine and diatrizoate sodium injection.

OVERDOSAGE: Overdosage may occur. The adverse effects of overdosage are life-threatening and affect mainly the pulmonary and cardiovascular systems. The symptoms include cyanosis, bradycardia, acidosis, pulmonary hemorrhage, convulsions, coma, and cardiac arrest. Treatment of an overdosage is directed toward the support of all vital functions and prompt institution of symptomatic therapy.

The intravenous LD₅₀ values of OMNIPAQUE (in grams of iodine per kilogram body weight) are 24.2 in mice and 15.0 in rats.

Reference: 1. Dawson P. Chemotoxicity of contrast media and clinical adverse effects: A review. *Invest Radiol* 1985;20(suppl): 84-91.

CIRCLE 24 ON READER SERVICE CARD



Winthrop Pharmaceuticals
Division of Sterling Drug Inc.
New York, NY 10016

SEP-3™... User-Friendly Brain of the PUCK CM™ System



The New SEP-3 Program Control... Expands Filmchanger Capability

The SEP-3 Program Control operates one, two, or (optionally) three PUCK CM and PUCK C Filmchangers in any combination. Exposure rates up to 4 exp./sec. Interfaces with two generators, injector, table stepping device and other auxiliaries. Stores up to twenty user-designed and user-entered programs which can be easily altered by operator. Film marking entered through SEP-3 keyboard. System information is clearly displayed in the SEP-3 console window.

CIRCLE 4 ON READER SERVICE CARD

The capability of SEP-3 is just one of the many important new features from which you will benefit when you choose the new PUCK CM Filmchanger System from Elema-Schonander. Call us for a demonstration.

Elema-Schonander, Inc.

2360 N. Palmer Drive, P.O. Box 94517

Schaumburg, IL 60173-3887

Phone: (312) 397-5900

Teletex 26300143

Telefax (312) 397-5943

88212



How to stay on top of MR



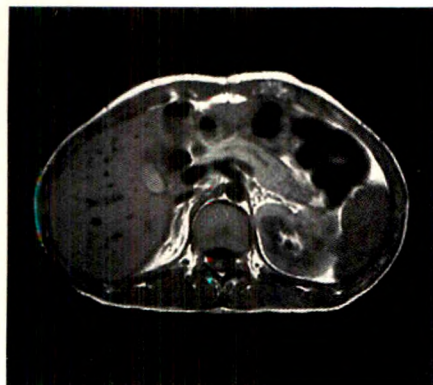
Signa.

Signa... The standard of excellence

It takes a lot to stay on top of MR. You need a high-performance system that offers comprehensive applications and superior images. A system with the flexibility to give you the competitive edge today and tomorrow. That's why more hospitals and imaging centers are using Signa® than any other MR system.

Signa is designed to give you high throughput and reliability. Signa users image an average of more than 13 patients/day. That's well above the typical break-even figure of 8 patients/day.

That's performance.



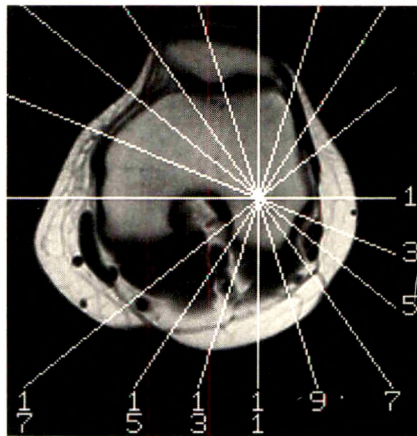
Signa's motion compensation capabilities provide excellent body images.

Superior image quality

Signa image quality gives you a clear advantage throughout the entire body. And that's a distinct edge for generating referrals.

■ Signa's high signal-to-noise ratio allows thin slice, small FOV, single-excitation imaging with superior contrast and resolution.

■ Multi-slice, multi-angle, single acquisition techniques help give you greater diagnostic sensitivity and efficiency.



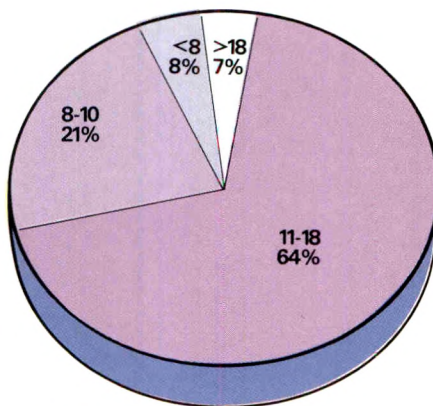
Signa can perform multi-plane/multi-angle techniques in a single acquisition.

■ Three types of motion compensation techniques help minimize motion artifacts.

■ Cine review of fast scan acquisitions helps increase applications by providing a dynamic review of anatomy, such as knees and temporomandibular joints.

■ Off-center FOV imaging with surface coils yields submillimeter resolution of fine anatomy.

■ Shielded gradient coils are designed to help ensure the future performance of your system.



SIGNA SITE STUDIES PER DAY

High study volumes are routine at the majority of Signa sites, based on a 1987 survey.

Options to expand performance

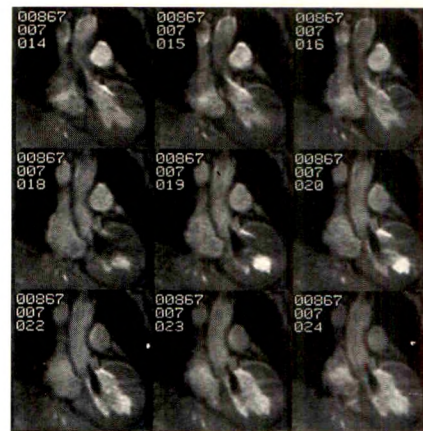
Signa gives you access to a full range of system options.

■ Cine Plus for dynamic heart and cerebrovascular system studies.

■ Peripheral gating for rapid patient preparation and easy acquisition of gated images.

■ Full range of surface coils to increase resolution in small, specific areas.

■ Automatic record-keeping systems to help effectively manage site performance.



Cine Plus gives Signa the ability to acquire and display anatomy dynamically.

Leading-edge capability

Signa is designed to grow with you. From studies that helped establish MR's diagnostic power, to new applications like cine, angiography,* and spectroscopy,* GE's commitment to Signa will help keep you on top of MR.

For more information, please contact your GE Representative or call us toll free at:

(800) 624-5692.

*Some Signa system features are currently classified as investigational and are limited by federal law to investigational use.



CIRCLE 3 ON READER SERVICE CARD

GE Medical Systems

There's never been a better time to choose GE

THE RADIOLOGY REVIEW COURSE

May 28-June 3, 1989 — Louisville

September 27-October 3, 1989 — Chicago

Cosponsored by the Osler Institute and St. Louis University
at times and places most convenient for you

OBJECTIVES

- Improve basic knowledge and clinical skills in radiology
- Assist residents and fellows to organize study
- Prepare recent graduates to meet their next milestones
- Provide practicing radiologists with a review and update

METHODS

- HOME STUDY MATERIALS with syllabus of questions and answers — and assignments
- SEMINAR with projection slides and syllabus
- PRACTICE EXERCISES with oral and written parts

"The faculty was outstanding. The most pleasant thing was learning a tremendous amount, not only from world-famous authorities but from people who are relatively unknown as well."

RADIOLOGIC PHYSICS

Radiation and Radiology
X-rays and Imaging
Fluoroscopy and Tomography
Computed Tomography
Ultrasonography
Magnetic Resonance Imaging
Quality Assurance

NUCLEAR RADIOLOGY

Decay and Detectors
Statistics and Instrumentation
Radiopharmaceuticals
Quality Control and Licensure
Endocrine Scans and Treatment
GI, GU, Bone, and Brain
Liver, Spleen, and Lung
Ga, In, and Heart

CHEST

Infiltrates and Cavities
Nodules and Masses
Mediastinum
Breast

CARDIOVASCULAR

Heart and Aorta
Coronary Arteries
Peripheral Arteries
Echocardiography

GASTROINTESTINAL

Esophagus and Stomach
Small Bowel and Colon
Liver and Gallbladder
Pancreas and Spleen

GENITOURINARY

Kidney and Ureter
Bladder and Pelvis
Abdominal Ultrasound
Ob. and Pelvic Ultrasound

BONE AND JOINTS

Tumors and Trauma
Metabolic and Endocrine
Infection and Dysplasia
Articular Disorders

NEURO., HEAD AND NECK

Skull and Contents
Spine, Disc and Cord
Temporal and Facial Bones
Sinuses, Larynx and Neck

PEDIATRIC

Bones, Joints and Chest
Gastrointestinal Tract
Genitourinary Tract
Central Nervous System
Cardiovascular System

*"Accommodations were comfortable..."**

GOALS AND LOCATION: These courses are designed, scheduled and located to serve the needs of radiology residents and recent graduates. Home study questions are sent upon registration. The courses include both lectures and question sessions — faculty and students both questioning and answering in practice for what will follow. The early fall course is more theoretical and the December and May courses are more clinical. Your best value is to repeat the seminar for half price. The May meeting will be at the Executive West Hotel, Louisville, Kentucky.

*"...and those little extras..."**

LOWEST AIR FARES: Reliable Travel offers you the lowest air fare — often below super-saver rates. Please call toll-free 1-800-645-6504 ext. 10 and identify yourself with this Osler course.

*"...remarkably complete and pleasant..."**

PLACEMENT SERVICE: For a practice opportunity write or call (800) 356-7537.

*"...the most education for the money..."**

FEES AND C.M.E. CREDITS:

- **Physician or Resident:**

	Phy.	Res.	hrs.
• May 28: Rad. Physics	\$135	\$ 90	10
• May 29-June 3: Clin. Rad.	\$630	\$420	60
• May 28-June 3: Full Course	\$720	\$480	70
- Repeating course within 3 years: half price
- Dec. 1989: Small-group, subspecialty reviews \$210 (past participants \$105)/day; 10hr./day
- Add 10% to any payment after May 15, 1989.
- Attendees not in course hotel add \$8/day.
- \$50.00 will reserve your position.
- Most home study materials will be mailed after half the registration fee is received.
- St. Louis University is accredited by the ACCME and designates this program for up to 70 hours in Category 1 of the Physician's Recognition Award of the A.M.A.

*"...home study material was extremely helpful..."**

CANCELLATIONS: Refunds subject to \$50 fee, will be made until the seminar begins.

- Cancellation after mailing home study material requires retention of half of the fee.

*"I feel [the course] helped me pass..."**

INFORMATION:

Joseph H. Selliken, Jr., M.D.
THE OSLER INSTITUTE
1094 Dawn Lane, Terre Haute, IN 47802
(800) 356-7537 or (812) 299-5658

** Comments by past Osler participants*

Limited Enrollment: THE RADIOLOGY REVIEW REGISTRATION

Name _____

Address _____

City/State/Zip _____

Phone _____

For: ☐ May 28-June 3, 1989 — Louisville

☐ Sept. 27-Oct. 3, 1989 — Chicago

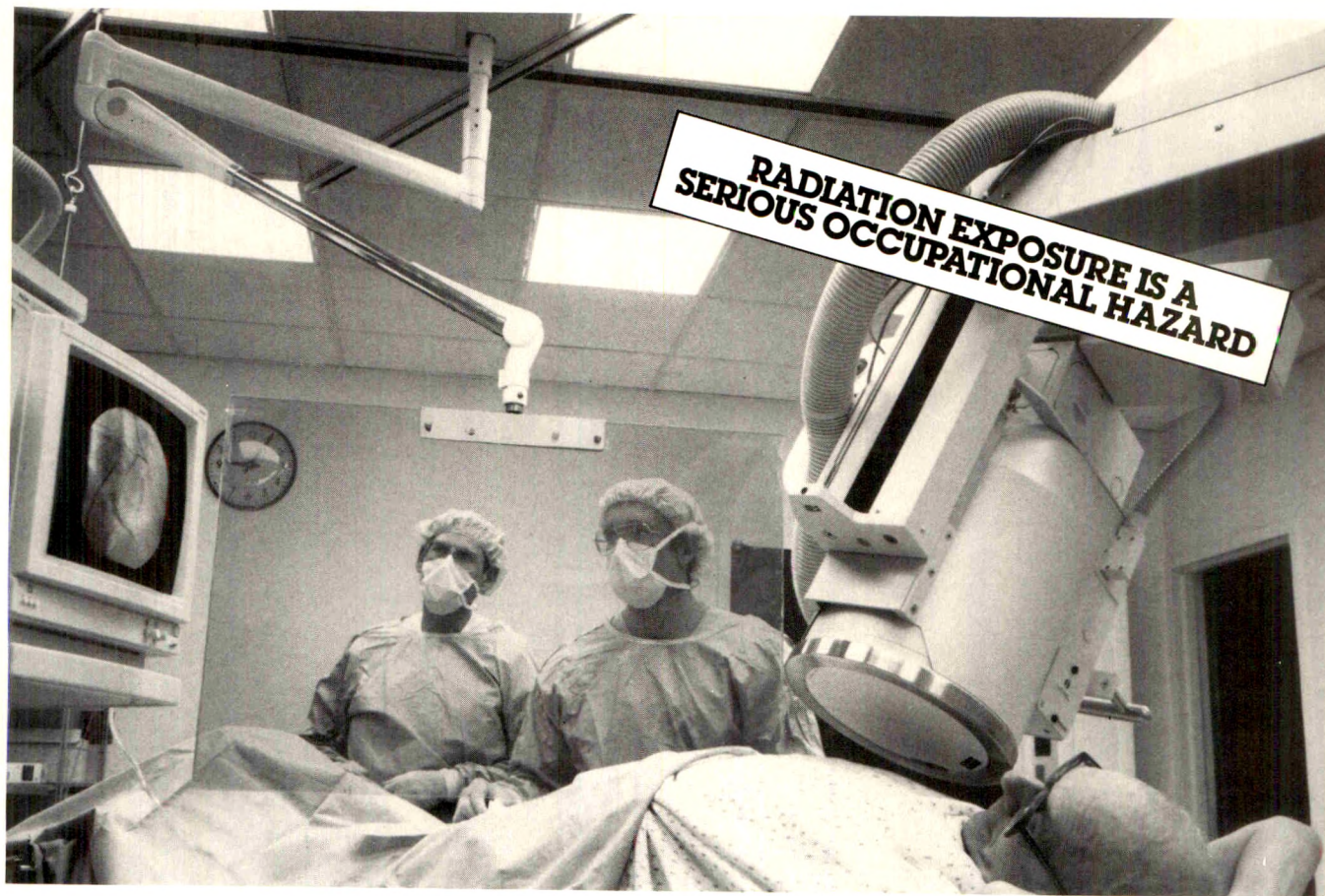
☐ December 1989 — Louisville

☐ Check enclosed for \$ _____

☐ Please send more information

Mail today to:

1094 Dawn Lane, Dept. A1
P.O. Box 2218
Terre Haute, IN 47802



Cardiac Cath and Special Procedures Personnel...

NOW YOU CAN GET GREATER RADIATION PROTECTION WITH CLEAR-Pb® Fixed-Mount Overhead X-Ray Barriers

*In 4 panoramic shield sizes...18" x 24" to 36" x 24"...
at budget-pleasing prices.*

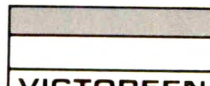
- **Unsurpassed radiation protection;** shatter-resistant, transparent lead-plastic (0.5mm lead equivalency).
- **Bigger shielding area and panoramic visibility;** no need to reposition the barrier during procedure; protects two people, if required.
- **Easy-to-use, adjustable, spring-loaded fixed ceiling mounted suspension system;** pull down to use, push up and out of the way at the end of the procedure

Existing lead-glass overhead barriers (usually 16" x 12" or 20" x 16") are so small that when you move, you must also move the barrier to avoid exposure. Now, depending on your needs and budget, you can select from 4 CLEAR-Pb Overhead Barriers with panoramic shield sizes from 18" x 24" to 36" x 24", and get greater protection from scatter radiation.

For complete details, request Bulletin 423-44

CIRCLE 16 ON READER SERVICE CARD

NUCLEAR ASSOCIATES



A Division of VICTOREEN, INC.
100 VOICE ROAD
CARLE PLACE, NY 11514-1593 U.S.A.
(516) 741-6360



CHALLENGE 89

DECISIONS IN IMAGING

London, England

June 24-30, 1989

This didactic course will afford participants approximately 25 Category I CME credits and be presented through lectures and case discussions. Topics in **Magnetic Resonance Imaging**, **Computed Tomography** and **Ultrasonography** will be offered in a correlative manner discussing the proper uses of each modality and the results that can be obtained. The program is sponsored by **University Imaging Associates**, and will be presented by noted **University of Southern California** faculty members and a renowned faculty from Great Britain. The course immediately precedes the **INTERNATIONAL CONGRESS OF RADIOLOGY IN PARIS** and will allow participants to enjoy the **WIMBLEDON TENNIS TOURNAMENT**, and continue on, if desired, to the International Congress. Course sessions will extend from June 25th-29th. One day's sessions will be held at Addenbrookes Hospital in Cambridge, England and another day will be at the National Heart and Chest Hospital in London.

INVITED FACULTY

William D. Boswell, Jr., M.D.

University of So. California
Los Angeles, California

Graham Bydder, M.D.

Hammersmith Hospital
London, England

Patrick Colletti, M.D.

University of So. California
Los Angeles, California

David Cosgrove, M.D.

Royal Marsden Hospital
London, England

James M. Halls, M.D.

University of So. California
Los Angeles, California

Christine Heron, M.D.

St. George's Hospital
London, England

Andrew Hine, M.D.

Central Middlesex Hospital
London, England

Janet Husband, M.D.

Royal Marsden Hospital
London, England

Donald Longmore, M.D.

National Heart & Chest Hospital
London, England

Dr. Rod Mohiaddin

National Heart & Chest Hospital
London, England

Philip W. Ralls, M.D.

University of So. California
Los Angeles, California

Simon Rees, M.D.

National Heart & Chest Hospital
London, England

Brian Worthington, M.D.

University of Nottingham
Nottingham, England

Richard Underwood, M.D.

National Heart & Chest Hospital
London, England

Ian R. Young, M.D.

Hirst Research Center
Wembley, England

Chi-Shing Zee, M.D.

University of So. California
Los Angeles, California

Meeting Coordinator: Ronald J. Friedman, M.D., University of Southern California

Registration Information: Payable in U.S. Dollars and drawn on a U.S. Bank to **University Imaging Associates**. \$450 to March 31, 1989. Thereafter \$495.
Fellows, Residents, Interns, Technicians, Nurses with letter — Less \$100.

For Registration or Further Meeting Information:

University Imaging Associates
Los Angeles County — USC Medical Center
Box 66, 1200 North State Street
Los Angeles, California 90033
Telephone: (213) 226-7245

Progress in Radiology

Preoperative Imaging-Guided Needle Placement and Localization of Clinically Occult Breast Lesions

Daniel B. Kopans¹ and Cynthia A. Swann²

It is now well established that mammographic screening of asymptomatic women can detect breast cancers earlier and this can result in an absolute mortality reduction of 30–40% [1, 2]. Mammography is the only imaging method with proved efficacy for screening that can effectively detect clinically occult malignancy in asymptomatic women. Cancers that are detected by mammography alone are more likely to be diagnosed at an earlier stage than are clinically evident cancers, and generally the prognosis in these cases is more favorable.

Unfortunately, despite mammography's unsurpassed ability to find clinically occult breast cancer at an earlier stage, benign and malignant lesions may have similar morphology. Patterns of tumor growth and the breast's response frequently are nonspecific. Characteristics such as smooth, well-defined margins are statistically more common with benign lesions, but some cancers are sharply marginated. Even the classic lucent zone or "halo sign" surrounding circumscribed masses does not always guarantee a benign process [3]. At the other end of the spectrum, the spiculated architectural distortion of a radial scar (or area of fat necrosis [4, 5]) is indistinguishable from the characteristic morphologic changes produced by breast cancer. Microcalcifications associated with cancer frequently are identical in morphology to those produced by benign processes. Often, biopsy is the only certain way to distinguish a benign from a malignant finding.

Recent attention has been focused on the number of benign biopsies that can be anticipated if cancers are to be diagnosed at the earliest possible stage. It is difficult to determine

accurately the appropriate ratio of benign to malignant biopsies in the present "screening" environment in the United States [6]. Maintaining a low threshold for intervention has resulted in cancerous lesions being diagnosed when at least 20–30% are less than 1 cm in diameter or when they are still intraductal. As new data become available that more accurately characterize the morphologic differences, and with the increasing use of fine-needle aspiration cytology, it may be possible to avoid many benign biopsies, or at least to give the patient and her physician more specific information on which to base decisions. Currently, however, a positive predictive value for impalpable, mammographically detected lesions ranges between 20% and 30% [7–9]. As a consequence, whether placing a guide for the surgeon or performing a cytologic aspirate, it has become increasingly important for the radiologist to safely and accurately position a needle in the breast. Precise needle placement is mandatory if aspiration cytology is to be reliable; similar accuracy is needed to guide open biopsy and to ensure that the lesion in question is excised and that the cosmetic defect is minimized.

The localization of most clinically occult, mammographically detected lesions is accomplished by using mammographic guidance. Because most of these lesions are in fact benign, quadrant resection is absolutely contraindicated. Attempting to relate the position of a lesion as seen on mammograms in which the breast was vigorously compressed and pulled away from the chest wall to its position when the patient is in the supine position in the operating room can lead to inaccuracies.

Received October 6, 1987; accepted after revision August 15, 1988.

¹ Department of Radiology, Massachusetts General Hospital, Massachusetts General Hospital Cancer Center, and Harvard Medical School, Boston, MA 02114. Address reprint requests to D. B. Kopans, Dept. of Radiology, Massachusetts General Hospital, Boston, MA 02114.

² Holy Cross Hospital of Silver Spring, 1500 Forest Glen Rd., Silver Spring, MD 20910.

AJR 152:1–9, January 1989 0361–803X/89/1521–0001 © American Roentgen Ray Society

Similarly, skin markers are only reliable if the lesion is just beneath the surface of the skin. The internal structures of the breast are too elastic to permit accurate localization by using skin coordinates. Both approaches are inaccurate and will result in resection of an unnecessarily large volume of breast tissue.

To minimize the volume of tissue excised, the goal of accurate preoperative localization should be the positioning of a needle through or alongside the lesion. If cytologic evaluation is to be undertaken, then the needle must be placed in the lesion.

The purpose of this review is to summarize the advantages and disadvantages of some of the approaches used for needle/guide placement and the localization of occult breast lesions. The techniques that ultimately are adopted should take into account the patient's safety, the ease and accuracy of the procedure for the radiologist, and the approach of the surgeon.

Locating an Occult Lesion

The three-dimensional location of a lesion within the breast is usually apparent from standard orthogonal views. Occasionally, a lesion is visible in only one projection. In this situation, before recommending a biopsy, the radiologist should return to the projection on which the area in question was first detected and prove that the lesion is in fact real and not just an overlapping of shadows. This can be accomplished by using coned-down spot compression to mechanically separate the overlapping structures. Alternatively, by rotating the tube and slightly varying the angle of the incident X-ray beam, or by rolling the breast tissue to reorient the overlapping structures, a true lesion can be differentiated from a conglomerate structure [10]. By using these parallax techniques and the apparent shift of a lesion relative to the other breast structures, one can verify the presence of a lesion and also simultaneously determine its location in the breast. Usually, once the general location of a lesion is determined, it can be shown accurately on an orthogonal view.

We recently have described an alternative method of needle placement that uses simple stereotaxis and the plain geometric relationship of similar triangles; this method permits accurate localization from two slightly varying mammographic projections [11], and is particularly useful when a lesion is difficult to project in two orthogonal planes.

If these methods fail, sonography can be used to locate masses [12]; if rotated views and sonograms fail to triangulate a lesion, CT can be used [13]. A mass that is surrounded by fat usually is identifiable by CT. This technique generally is not capable of finding clustered microcalcifications unless there are enough microcalcifications in an isolated volume of breast tissue to avoid attenuation dilution by volume averaging. If the lesion can be located by CT scanning, guides for the surgeon can be positioned by using CT guidance.

Preparation of the Patient

Any time a needle is to be introduced into the breast, the procedure should be explained to the patient so that she is

fully informed. She should be given support throughout the procedure (which generally causes a high level of anxiety) and should be attended at all times. No published data are available on the frequency of vasovagal reactions, but it has been our experience that such reactions can be kept to a minimum by distracting the patient with continuous pleasant conversation and by preventing her from viewing the needle. Syncope episodes should occur in less than 2% of women undergoing needle localization. We have never needed to use medication to treat these rare episodes. Placing the patient supine for several minutes is all that is required and the procedure can then be completed.

The patient must be fully cooperative. Sedation should be avoided. Local anesthesia may be used, but for most women, it is not needed and may be more painful than the localization itself. If the patient experiences discomfort, an anesthetic can be injected at any time through most localization needles.

General Considerations

The surgeon needs to understand that these biopsies require thought and attention to detail. Careful surgical dissection avoids dislodging needles or cutting wires. A close cooperative effort between the radiologist, surgeon, and pathologist is necessary. The radiologist should understand the features of lesions that should arouse concern, and avoid recommending biopsy of lesions that are characteristically benign. Safe, accurate localization techniques permit the aggressive evaluation of indeterminate lesions when they are small, which results in diagnosis at an earlier stage and a commensurate reduction in the overall mortality rate.

Choice of Localization Guide

The actual choice of mechanical guides depends on the direction of insertion and the specific preferences of the radiologist and surgeon. Many systems are available (Fig. 1).

Straight Needle

The simplest guide for preoperative localization is the insertion of a conventional hypodermic needle. If a straight needle is used, it must be long enough to pass through and beyond the lesion; this will prevent the suspected tissue from slipping back off the end.

Advantages.—A straight needle is the simplest guide to place in the breast. Because of its stiffness, the surgeon can easily palpate its course and this can facilitate accurate surgery. It can be removed easily or can be repositioned if its relationship to the lesion is incorrect.

Disadvantages.—The protrusion of the needle hub above the skin may result in the inadvertent snagging of the needle, causing it to be pulled out of the breast prematurely. This possibility can be reduced by carefully taping the needle to the skin or by modifying a standard 22-gauge spinal needle, creating flat-head needles of varying lengths that can be inserted flush with the skin (Fig. 2).

Although many surgeons find a straight needle to be sufficient, it provides only two-dimensional accuracy, which means

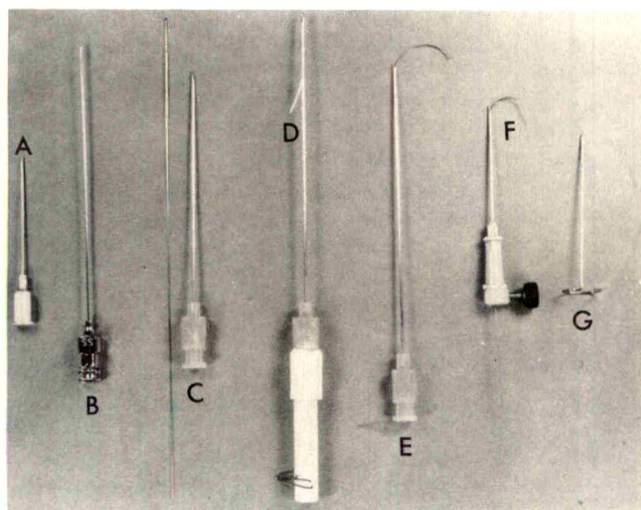


Fig. 1.—Various localization devices.

A, Standard 1.5-in. (3.8-cm) needle.

B, 3.5-in. (8.9-cm) spinal needle.

C, Springhook wire and introducing needle.

D, Springhook wire configured to be extended through a side hole in needle. Needle can be repositioned by pushing wire toward needle tip, retracting hook back into needle.

E, Curved-end wire that can be pushed out through needle tip or pulled back in to reposition needle.

F, Another curved-end retractable wire with immobilization screw for hookwire.

G, Modified needle with flat top to fit flush with skin.

that the surgeon must estimate the distance of the lesion along the needle shaft (Fig. 3). If it is used to localize deep lesions in an anteroposterior approach, it may not penetrate the lesion because of the mammographer's fear of entering the thorax. Furthermore, movement of the breast may cause the lesion to slip off the needle.

Hookwire Systems

Wires have been devised that hook into the tissue to provide a three-dimensionally stable guide for the surgeon. The first such system uses a wire that is bent into the shape of a hook that protrudes out the tip of the introducing needle.

Fig. 2.—A and B, A flat-head needle can be made from a conventional spinal needle by pulling stylette back 1–2 cm (A) and then bending needle at desired length (B).

C, Second bend is perpendicular to first to form a spiral.

D, Then, excess is cut off.

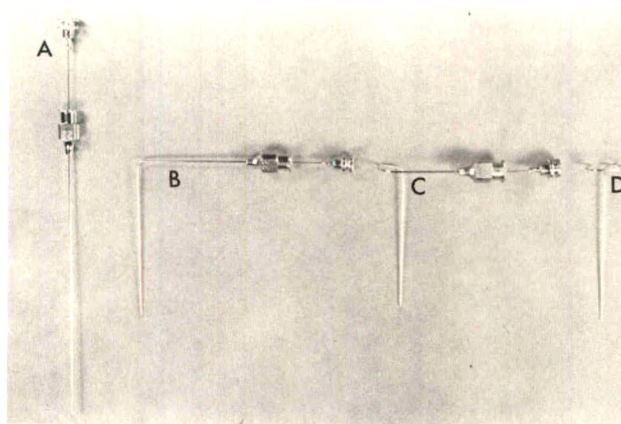


Fig. 3.—A flat-head, modified spinal needle has been passed through a small lesion from bottom of breast. Note that surgeon must estimate distance of lesion along needle.

2

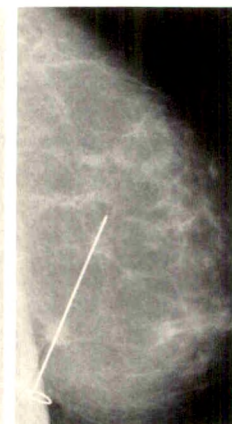
It requires a skin incision, and because the hook is outside the needle tip, it hooks into the tissue immediately and cannot be repositioned [14].

A more accurate guide was devised by bending wire of appropriate composition into a spring hook [15]. This configuration permits the hook to be completely contained in and to pass through the needle lumen, reforming to hook in the tissue when it is released from the needle tip. The introducing needle can thus be optimally positioned before engaging the hook. Lesions can be aspirated through these needles, and then the wire can be afterloaded to anchor in the tissue [16].

Advantages.—Wires afford the most accurate three-dimensional localization. Wires have the additional advantage of flexibility so that nothing projects above the skin, which makes it more difficult for them to become dislodged. They are comfortable for the patient, and the surgeon can apply gentle traction to assist in the dissection.

Disadvantages.—A consequence of their flexibility is the fact that unless the surgeon follows the wire directly from the skin insertion site into the breast, wires may be difficult to locate within the breast. This can be corrected by stiffening them by passing a cannula over them in the operating room [16]. Wires should not be used by the surgeon as retractors because they can, with sufficient traction, be pulled out of the breast. They are stable in fibroglandular tissue; however, because fat is almost liquid at body temperature, wires may be moved in fat if there is no firmer tissue in which to anchor them. The surgeon must also dissect carefully to avoid inadvertently cutting them with scissors or a cautery.

The wire must be long enough so that it will not disappear into the breast when the breast is in its natural position. This is especially important if the wire is being used while the patient is supine. There is the danger that the reexpanded breast will completely envelop the wire when the patient sits up. A safe length for the wire can be estimated from the mammogram so that it exceeds, by several centimeters, the distance from the skin entry site to the lesion. This length is derived by measuring this distance on the mammographic projection where the breast was compressed orthogonal to the direction the needle is to be inserted. The lesion may be closer to the surface of the breast than this measurement indicates, but it cannot be farther. If the length of wire is chosen properly and if insertion is performed parallel to the



3

chest wall, there is no special need to anchor the protruding end of the wire and it may be loosely taped to the skin.

"Anchored" Needles

Attempts have been made to combine hooked wires with needles in an effort to stabilize three-dimensionally a stiff needle in the breast.

Curved wires that protrude from the needle tip.—A curved-end wire that can be retracted into the introducing needle, thereby permitting repositioning, was initially described as uncuttable and as three-dimensionally stable [17]. More recently, however, it has been recommended that the introducing needle be left in the breast, producing a stiff, palpable needle anchored by a curved end wire and protecting the wire from inadvertent transection [18].

Advantages.—A needle that has a protruding wire with a tight curve can be repositioned even after the hook is advanced by permitting retraction of the hook back into the needle. This repositioning capability is useful for accurate positioning, and the stiffer target is helpful for the surgeon.

Disadvantages.—Unfortunately, there are trade-offs with all guides. The ability to straighten out the curve and pull the wire back into the needle weakens its holding power. When the curved hook is engaged at the appropriate depth of the lesion, there may be a considerable length of needle projecting above the skin. To avoid inadvertently pulling the needle out of the breast, it is now recommended that the introducing needle be pushed completely into the breast flush with the skin before advancing the hook [18], thereby losing the third dimension. Use of the system in this fashion may have little advantage over a straight-needle technique because the surgeon must once again estimate the location of the lesion along the needle shaft.

Hookwires that protrude from the side of the needle.—Another method of combining needles and wires permits the hookwire to project out of a hole in the side of the needle. The purpose of this needle is to provide a stiff guide that has three-dimensional stability and that also can be repositioned. The commercially available needle comes with a clamp that is fastened at the surface of the skin to prevent advance of the needle deeper into the breast tissue.

Advantages.—The major advantages of this system are the stiffness of the guide for the surgeon and the ability to reposition the needle. A stable, three-dimensionally accurate localization can result. A recently reported study suggested that a wire protruding from the side of a needle had 1.5 times the holding power of a flexible springhook wire anchor, and six times the holding power of a curved wire protruding from the end of the needle [19].

Disadvantage.—The major drawback of this system is that it is not flexible. Three-dimensional positioning results in variable lengths of needle protruding out of the breast, and this needle must be protected; otherwise, the protruding segment

could be hit inadvertently, damaging the tissues or accidentally dislodging it.

Directing Needle Placement

The Anteroposterior Approach

The introduction of a needle from the front of the breast is the optimal means of guiding a surgeon to a suspected abnormality. Methods have been described that attempt to transpose measurements from the mammogram to the uncompressed breast [20]. By measuring the distance of the lesion from the nipple in the two projections, an estimate of its location can be made. These measurements are transferred to the patient who is either seated or supine. The needle is positioned initially at this point and then directed back toward the lesion. Because of the elasticity of the breast and variable magnification on the mammogram, the initial placement of an anterior guide is an approximation. This is compensated for in part by adding a magnification factor. Orthogonal mammograms are obtained to estimate the relationship and distances of the needle tip from the lesion. The needle is then repositioned to better approximate the location of the lesion, and confirmatory mammograms are obtained [20, 21]. The repositioning sequence is continued until the needle is in the desired relationship to the lesion.

Advantages.—Many breast surgeons prefer that a guide be placed in an anteroposterior direction to facilitate surgery because this parallels their surgical approach. They can dissect directly down the needle or wire to the lesion. If the needle can be inserted at the limbus of the areola, then the surgery can be performed more easily through a periareolar incision, which results in a scar that is more difficult to detect. This also facilitates the inclusion of the surgical track in a mastectomy if this is the ultimate therapeutic choice.

Disadvantages.—Positioning guides from the front of the breast directed back toward the chest wall cannot be done under direct visualization because mammograms can be obtained only orthogonal to this direction. The anteroposterior approach is used by many mammographers with good results, but the neophyte should be aware that this approach is based on successive approximations and requires a degree of skill if accurate localizations are to result. Furthermore, if an anteroposterior needle insertion is used, caution is strongly advised, particularly for lesions close to the chest wall. When a needle is introduced back toward the chest wall, it has the potential of being inserted into the pectoralis muscles or through into the pleural space [22], lung, or mediastinum. There have been cases of pneumothorax caused by introducing needles in this direction, and wires placed in this fashion that were too short for the depth of the lesion have been enveloped by the breast, disappearing into it when the patient sat up. A few of these wires not only have completely retracted into the breast, but some were not retrieved and over a period of time were massaged by body motion into other parts of the body [23]. If an anteroposterior approach is used, it should be done cautiously and is probably best suited for superficial lesions.

Although there is no reason to suspect that breast cancer cells are easily seeded along needle tracks, this remains a theoretical possibility; thus the course of a needle must be considered. Tracking cells into the pleural space probably should be avoided. If an anteroposterior approach seems desirable, the radiologist and surgeon should consult with the radiation therapist. Drawing biopsy tissue containing a breast cancer through a large volume of the breast to remove it through a circumareolar incision may preclude conservation therapy owing to the large volume of tissue that must subsequently receive a high-dose therapeutic radiation "boost."

Guides Introduced Parallel to the Chest Wall

Most localization complications can be avoided if guide placement is accomplished by using appropriate techniques and needle insertions parallel to the chest wall (PCW) [24].

The PCW procedure is accomplished by evaluating the location of the lesion on the basis of the screening mammograms. If it is closest to the medial surface of the breast, initial needle positioning is accomplished in a mediolateral approach and the needle is inserted from the medial skin surface. Similarly, if the lesion is close to the lateral surface of the breast, a lateromedial approach is used. A lesion near the top of the breast is localized by using a craniocaudal projection, whereas one at the bottom of the breast is localized by using a caudocranial projection.

Once the shortest distance has been determined, the breast is compressed within the mammographic unit; a fenestrated compression plate is used so that the preliminary mammogram will project the lesion in the opening in the compression plate (Fig. 4A). The x and y coordinates of the lesion are determined either from marks around the plate opening or from a marker placed on the skin and superimposed on the lesion. Some compression plates contain multiple holes rather than a single opening. These can be used, but the holes must be large enough to permit the needle hub to pass through, and the breast may need to be repositioned if a hole does not overlie the lesion.

After suitable skin preparation, a needle is introduced in the direction of the X-ray beam. Ideally, when the needle is introduced, its hub should be superimposed on the shaft of the needle and on the lesion, as viewed mammographically through the compression plate (Fig. 4B). This will ensure that the needle will pass directly through the lesion or at least that the lesion will be within 5 mm of the needle shaft, as long as the needle tip has been passed beyond the depth of the lesion. This relationship is easily accomplished by aligning the needle under the centering light of the mammography unit. These lights are generally aligned with the X-ray beam, and if the shadow of the hub superimposes on the needle shaft under this light and the tip is directly over the lesion, the needle will be properly aligned on the mammogram. The needle should be advanced so that it passes through and beyond, "impaling" the suspicious lesion.

The procedure requires a film holder that permits removal of film/screen or Xerox cassettes without moving the breast

and so that the breast remains compressed in the mammographic system while a confirmatory mammogram is obtained. As compression is released, the needle tip should be kept beyond the target by pulling the breast up around the needle so that the lesion will remain along its shaft. If the initial placement is suboptimal, it is possible to withdraw the needle partially, change the insertion angle, and reinsert it without repuncturing the skin to achieve a more accurate position.

In the first projection the proximity of the needle to the lesion in the x and y dimensions is accurately accomplished. The breast compression is then released, and the patient is moved back from the system. The gantry is rotated 90° in preparation for the z or depth determination. The fenestrated compression plate is replaced by a small spot compression device. It is no longer necessary to compress the entire breast because the area in question occupies only a small volume, and only the relationship of the needle to the area in question is required. When the spot compression device is used, the breast is recompressed so that the X-ray beam is perpendicular to the shaft of the needle (Fig. 4C). In the initial projection, the needle was passed an arbitrary distance beyond the lesion. In the orthogonal view, this distance can be measured.

If a simple needle technique is used, this orthogonal projection is the final view required because it gives the surgeon the relationship of the lesion along the shaft of the needle. When this technique is used, the needle must be longer than the distance to the lesion because it is necessary to pass the tip of the needle beyond the lesion to ensure that the lesion remains along the needle shaft, regardless of the position of the breast at surgery.

The orthogonal view permits withdrawal of the needle so that the tip can be positioned precisely. If cytologic material is to be obtained, the needle is withdrawn until the tip is in the lesion. If a hookwire system is used for localization, it is withdrawn so that the tip is at the level at which the hook will be placed. In general, it is best to anchor the hook slightly deeper than the lesion so that if there is any movement of the wire with slight traction at surgery, the hook will pull into the lesion and not away from it. When the springhook wire system is used, the best approach is to position the lesion along the thickened distal segment of wire (Fig. 4D). This thickened segment can be used by the surgeon as a marker to indicate that the level of the lesion has been reached and that the hook is 2 cm beyond. The surgeon may then remove a small cylinder of tissue around the thickened segment and hook.

This same guidance technique can be used to aspirate impalpable lesions for cytologic analysis. The mammographic compression helps prevent the target tissue from moving when pushed by the needle tip. Orthogonal projections are the most accurate way of positioning a needle, and the position of the needle tip in the lesion can be confirmed easily.

Advantages.—The PCW approach is the most accurate method of needle positioning because the breast can be held firmly in the mammographic compression system during the procedure with the lesion under direct visualization. Orthogonal views are the most accurate method of precisely positioning a needle for either localization or fine-needle aspiration cytology. The parallel approach is also the safest because there is no danger of hitting any tissue other than breast.

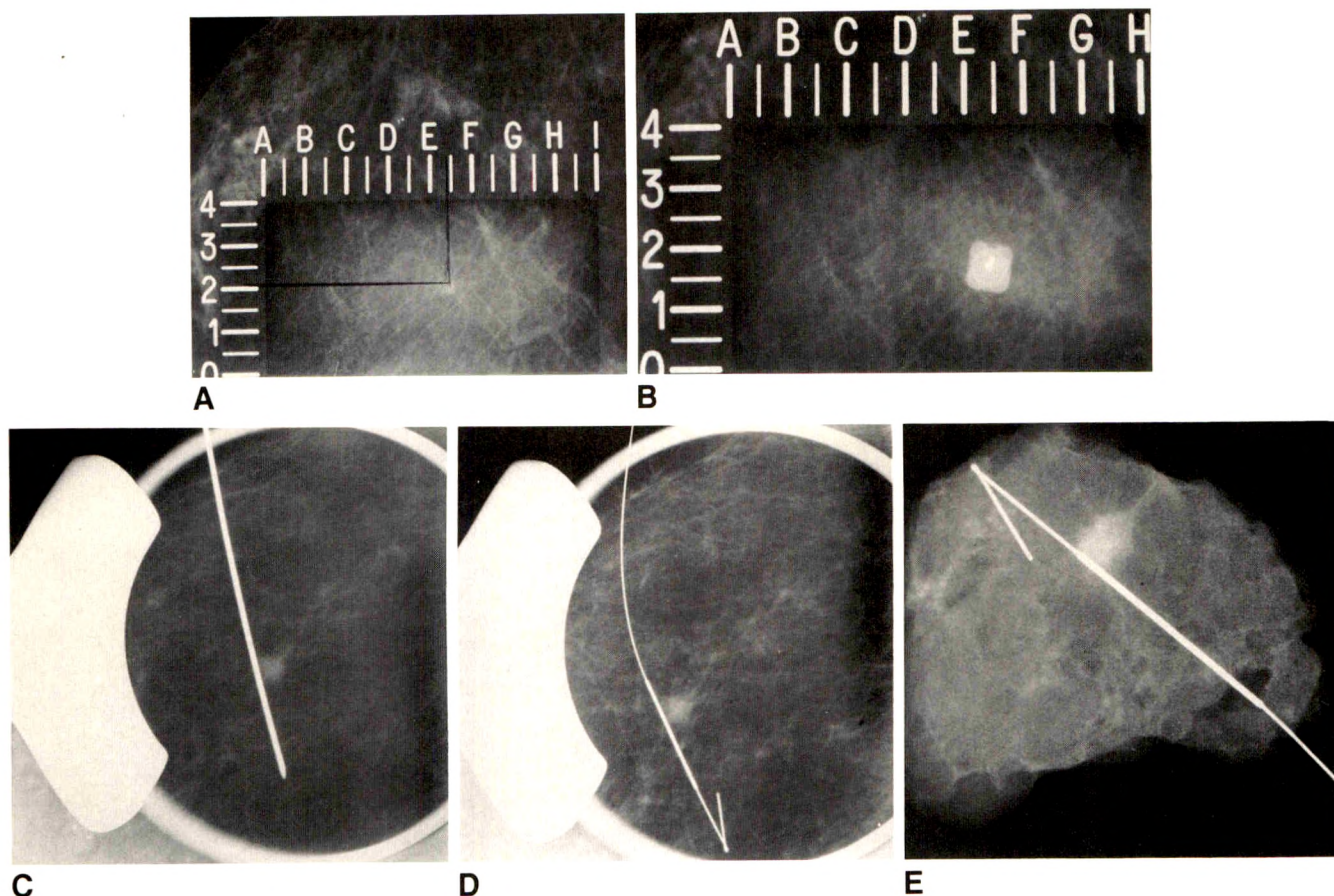


Fig. 4.—A, Lesion is positioned over opening in compression plate, and its coordinates are determined.
 B, If needle hub superimposes on shaft and is centered on lesion, then needle must be within 5 mm of lesion.
 C, Breast is recompressed perpendicular to needle with a spot compression device so that Z distance can be determined and needle can be pulled back if necessary. If a straight needle technique is used, this final picture gives the surgeon an indication of the distance the lesion is along the shaft.
 D, If a hookwire is used, wire should be positioned so that lesion is along thickened segment proximal to hook.
 E, Compressed specimen radiography shows lesion in excised tissue.

Disadvantages.—Needle placement parallel to the chest wall is inherently safer and more accurate, but it may complicate the surgical approach. The surgeon would prefer to dissect down the needle or wire directly back toward the chest wall, often from a circumareolar incision. Some surgeons have expressed their concern that tumor cells may be seeded along the needle track; these surgeons would prefer to excise the localizer track if the chosen therapy is a mastectomy. A parallel approach may make this difficult because the needle may be inserted through a skin surface that may not be included in the elliptical mastectomy incision. We have followed women whose cancers were localized preoperatively and have found that there is no increase in local recurrence rates from the theoretic seeding of the needle track when an approach parallel to the chest wall was used [25]. Because anteroposterior needle positioning carries the risk of needle passage through the relative barrier of the pectoralis fascia or into the pleural space, the theoretical possibility of seeding tumor into significant extramammary locations is greater when the anteroposterior approach is used. So far, no studies have been done to investigate this possibility.

Stereotactic Needle Placement

Modifications of the PCW approach underlie the recent interest in stereotactic needle positioning. With the breast held in a fenestrated compression device, the X-ray tube is shifted to provide pictures of the lesion from two different angles. By calculating the apparent shift of the lesion relative to fixed reference points, one can determine the depth of the lesion beneath the skin, permitting accurate needle positioning through the opening in the compression plate.

Advantages.—The stereotactic method has the same safety advantage as the standard PCW approach. The major difference is that it permits the breast to be maintained in one position throughout the procedure because the tube rather than the patient is shifted. A needle guide that is fixed to the system may be an advantage for accurate needle placement.

Disadvantages.—The major disadvantage of stereotactic needle positioning is the cost of the equipment. Either a dedicated unit [26] or an expensive modification to an existing mammography system is needed. Because the images obtained are less than orthogonal, the inherent accuracy is less

than that available with conventional 90° projections, but theoretically the technique is accurate within 2–3 mm.

Of course, all needle-positioning techniques rely on the needle's staying in the prescribed track; however, the fibrous structures of the breast can cause the needle to deviate, regardless of the aiming method. Furthermore, firm lesions may be pushed aside and not penetrated by the needle as it is introduced.

The Spot Method

The spot method, or injection of a vital dye in the vicinity of the lesion to visibly stain the tissue, has been used successfully to guide surgery [27]. A needle is positioned under imaging guidance so that its tip is at the lesion to be localized; then the dye is injected. The needle is left in place or, as it is withdrawn, additional dye is introduced along the track so that the surgeon can follow the stain to the tissue to be excised. Very small amounts of dye are used to avoid staining too large a volume of breast tissue. The vital dye can be mixed with iodinated contrast material so that the volume of tissue in which the dye is deposited can be seen mammographically.

Advantages.—By staining the tissues, the surgeon is afforded a visual guide to the volume of breast containing the lesion in question. If the needle track is stained, a guide cannot be dislodged inadvertently.

Disadvantages.—The radiologist has no control over the direction in which the dye spreads from the needle tip. Also, sometimes the dye diffuses into a larger volume of tissue than desired if there is a significant delay between dye injection and surgical removal, and this reduces the accuracy of the technique. The use of iodinated contrast material may make it more difficult to see the lesion on specimen radiographs of the excised tissues. When these materials are used, there is also a small risk that the patient will have an adverse reaction to the injected substance.

The Specimen

After surgical excision, specimen radiography should be performed by compressing the specimen within the mammographic system or in special specimen radiography units. Compression of the specimen permits the visualization of masses (Fig. 4E) as well as calcifications in the tissue samples. This is especially necessary if xeroradiography is used to image the specimen.

Placement of a second needle in the specimen through the lesion may assist the pathologist. We routinely obtain two specimen radiographs. One is for the imaging record, and the second accompanies the tissue when it is sent to the pathology laboratory. Ideally, the specimen is sectioned and radiographs are obtained so that the slice containing the lesion can be identified. If this is not possible, the radiologist should be aware that the lesion may be overlooked on routine histologic sections (it takes more than 2000 4- μ m-thick slices to fully examine 1 cm³ of breast tissue); it may be necessary to radiograph the paraffin blocks containing residual tissue to

determine whether the lesion is even deeper in the block, in which case additional histologic sections would be required.

Sonographically Guided Aspiration and Localization

Sonography can be helpful in evaluating lesions that are palpable but difficult to assess clinically, as well as those that are clinically occult but detected mammographically, to determine whether they are simple cysts or indeterminate solid masses. Sonography can be used to guide the aspiration of cysts, when necessary, and to aid in the triangulation and localization of impalpable masses [12].

A biopsy transducer may facilitate the positioning of needles within impalpable lesions [28]. Most breast lesions are relatively superficial, and the use of these transducers may require a very shallow angle for the passage of the needle. The shallow angle may make entry into the lesion difficult, because if the needle pushes the lesion against elastic breast tissue, the target tissue may move.

Sonographically guided localization can be accomplished without special attachments [12]. The patient is positioned supine with her ipsilateral arm comfortably extended behind her head to flatten the breast tissue overlying the lesion against the chest wall. This helps to immobilize the lesion as well as to reduce the amount of tissue that must be traversed by the needle. A 5-mHz (or higher) transducer, focused to the near field, should be used. The tissues from the skin to a depth of 3–4 cm must be in focus. Transverse and sagittal scans are obtained, and the largest portion of the lesion is identified. Triangulation can be facilitated by introducing a thin tube (such as a plastic coffee stirrer) or piece of wire between the transducer and the skin. Introduced perpendicular to the scan plane, the shadow of the straw will first project on the lesion when the tip of the straw is overlying the lesion. This is the location at which the needle is introduced. The skin is marked, providing rapid triangulation of the x and y coordinates of the lesion in a single step. The depth of the lesion is obtained from the sonographic image. This depth may be slightly inaccurate owing to the pressure of the transducer on the skin compressing the tissue through which the needle will pass.

Without permitting the patient to change position, the skin is cleansed, and a plastic drape with a fenestration is placed around the entry site to provide a sterile field. The localization needle is passed to the depth determined by the scan in the direction taken by the sound beam. Caution is advised because the needle is directed toward the chest wall. If firm tissue is encountered and if it cannot be determined whether this is the anterior margin of the lesion or the chest wall, it is wise to lift the breast away from the chest wall before advancing the needle deeper. A hookwire system is preferred for anterior localizations because a plain needle that is advanced to the lesion in the anteroposterior position with the patient supine will not be long enough when the patient sits up and the breast reexpands, assuming its natural position. A straight needle may thus be pulled out of the lesion. If a hookwire is used, it will anchor in the tissue and will pull into the breast with the hook remaining at the depth in which

it has been positioned. Thus, a long wire should be chosen. Confirmatory mammograms show the relationship of a wire to the lesion after sonographically guided introduction (Fig. 5).

CT-Guided Localization

Occasionally, lesions that are difficult to successfully triangulate by mammographic projections or by sonography can be located by CT [13]. If the patient is oriented within the scanner so that the breasts are symmetrically positioned, slices can be compared and asymmetric areas of increased attenuation can be delineated. In general, CT is used when a lesion is visible only in the lateral projection close to the chest wall. The breast is scanned with 1-cm-thick slices at 1-cm intervals covering the portion of the breast in which the lesion

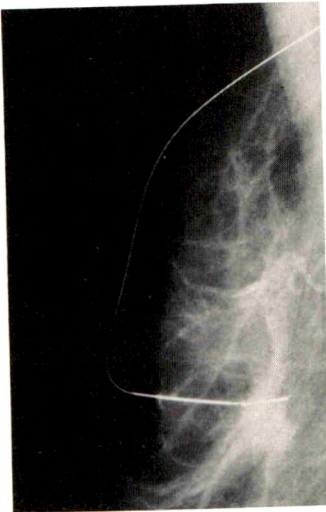


Fig. 5.—After sonographically guided localization, a mammogram should be obtained to confirm relationship of lesion to wire.

is suspected on the basis of mammography. Once located, a guide can be placed at the lesion preoperatively by using the scanner.

The patient should remain within the scanner during the localization procedure so that the position of the breast will not shift on the chest wall with table movement. Thus, a scan plane indicator within the gantry is necessary. The skin is cleansed with an antiseptic solution, and a sterile piece of wire or thin needle (which can be imaged without causing artifacts) is taped to the skin in a sagittal orientation; this is done in the region in which the lesion has been identified so that a cross section of the wire on the skin will appear on the scans (Fig. 6). This provides a constant reference line. The patient is then positioned in the gantry so that a minimum amount of breast tissue overlies the lesion, which is again located by scanning. Once the lesion is identified again, a thinner slice thickness is advisable to place a guide accurately. The location of the lesion is measured relative to the wire reference on the skin, and the depth of the lesion is easily determined from the scan. Once again, a hookwire system is preferable to a straight needle technique because, when the patient sits up, a straight needle will be pulled away from the lesion as the breast reexpands. As the introducing needle is directed back toward the chest wall, care should be taken to avoid entering the pectoralis or thorax. The needle should be carefully aligned within the scan plane so that the hub and tip are in the same plane. Thus, the position of the tip is clearly delineated on the scan and can be safely advanced. A hookwire can be engaged when the needle tip is satisfactorily positioned just deep to the lesion.

As with sonography, the patient is allowed to sit up after the procedure, permitting the wire to draw into the breast to its maximum depth. As always, the wire must be long enough so that it will not be drawn completely into the breast. Then the external wire is taped loosely to the skin, and a sterile gauze is placed over the entry site.

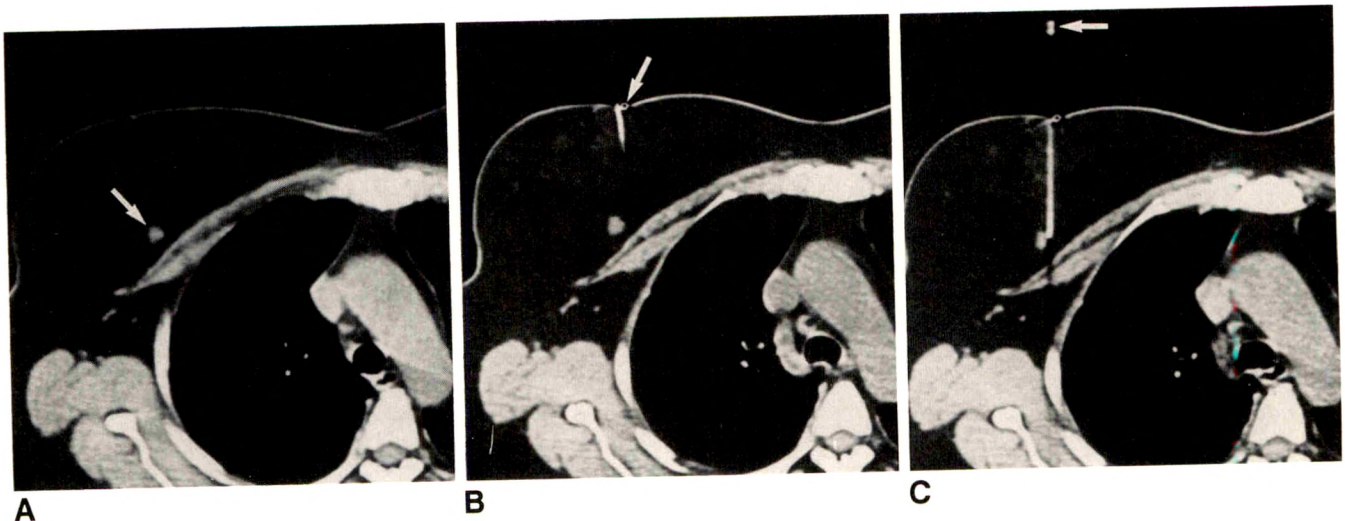


Fig. 6.—CT-guided localization.

A, Lesion (arrow) is located deep in right breast.

B, Cross-section of a wire is visible on skin (arrow) and is taped at top and bottom of breast, providing a constant reference for introduction of needle (whose tip is carefully monitored).

C, Because it was angled incorrectly, needle was repositioned to hit lesion. To avoid misinterpreting true position of needle tip because of angling through slice, hub (arrow) and entire length of needle should be seen in thin slice. A wire is engaged when appropriate depth is reached.

Future Possibilities

Other innovative localization guides probably will be devised. In addition, through the use of stereotaxis, needles may one day be positioned accurately from the front of the breast; this will necessitate the construction of compression plates that will permit access to the front of the breast while it remains compressed. We have used the divergence of the X-ray beam to achieve stereo images to accomplish this. With a movable compression device, an image can be obtained with the breast at one side of the imaging area. While compression is maintained, the patient is moved to the other side of the imaging area and a second image is obtained. The parallax between these two images can be used to determine the height of the lesion above the image plane, and thus all three coordinates can be determined to permit needle positioning from the front of the breast. It remains to be seen whether this method has any practical use given the ease and accuracy by which localization can be achieved currently.

The most likely major advance will be the percutaneous removal of lesions up to 1 cm³ in volume without the need for an operating room or a surgeon. This will help reduce the morbidity from a biopsy and will permit more expeditious diagnosis of mammographically detected lesions with a minimum of cosmetic damage. As the breast is held in the mammographic unit, a large-diameter sheath can be advanced to the lesion under mammographic guidance. By having the breast in the mammographic unit, accurate guide placement can be achieved and confirmation of removal of the lesion is immediate. Although this technique is being explored, hemorrhage is the major obstacle that must be addressed before safe percutaneous excisional biopsy can be achieved. Hematoma formation is, itself, not dangerous, but the spread of cancer cells within a hematoma may compromise therapy and survival, and thus this problem needs to be solved before percutaneous excision can be used clinically.

REFERENCES

- Shapiro S, Venet W, Venet L, Roeser R. Ten to fourteen-year effect of screening on breast cancer mortality. *J Natl Cancer Inst* 1982;69(2):349-355
- Tabar L, Fagerberg CJG, Gad A, et al. Reduction in mortality from breast cancer after mass screening with mammography. *Lancet* 1985;1:829-832
- Swann CA, Kopans DB, Koerner FC, McCarthy KA, White G, Hall DA. The halo sign and malignant breast lesions. *AJR* 1987;149:1145-1147
- Cohen MI, Matthies HJ, Mintzer RA, Keen ME, Murad T. Indurative mastopathy: a cause of false-positive mammograms. *Radiology* 1985;155:69-71
- Bassett LW, Gold RH, Cove HC. Mammographic spectrum of traumatic fat necrosis: the fallibility of "pathognomonic" signs of carcinoma. *AJR* 1978;130:119-122
- Kopans DB, Swann CA. Observations on mammographic screening and false-positive mammograms. *AJR* 1988;150:785-786
- Gisvold JJ, Martin JK. Prebiopsy localization of nonpalpable breast lesions. *AJR* 1984;143:477-481
- Meyer JE, Kopans DB, Stomper PC, Lindfors KK. Occult breast abnormalities: percutaneous preoperative needle localization. *Radiology* 1984;150:335-337
- Rosenberg AL, Schwartz GF, Feig SA, Patchefsky AS. Clinically occult breast lesions: localization and significance. *Radiology* 1987;162:167-170
- Swann CA, Kopans DB, McCarthy KA, White G, Hall DA. Localization of occult breast lesions: practical solutions to problems of triangulation and localization. *Radiology* 1987;163:577-579
- Kopans DB, Waitzkin ED, Linetsky L, et al. Localization of breast lesions identified on only one mammographic view. *AJR* 1987;149:39-41
- Kopans DB, Meyer JE, Lindfors KK, Buccianeri SS. Breast sonography to guide aspiration of cysts and preoperative localization of occult breast lesions. *AJR* 1984;143:489-492
- Kopans DB, Meyer JE. Computed tomography guided localization of clinically occult breast carcinoma—the "N" skin guide. *Radiology* 1982;145:211-212
- Hall FM, Frank HA. Preoperative localization of nonpalpable breast lesions. *AJR* 1979;132:101-105
- Kopans DB, Deluca S. A modified needle-hookwire technique to simplify the preoperative localization of occult breast lesions. *Radiology* 1980;134:781
- Kopans DB, Meyer JE. The versatile spring-hookwire breast lesion localizer. *AJR* 1982;138:586-587
- Homer MJ. Nonpalpable breast lesion localization using a curved-end retractable wire. *Radiology* 1985;157:259-260
- Homer MJ, Pile-Spellman ER. Needle localization of occult breast lesions with a curved-end retractable wire: technique and pitfalls. *Radiology* 1986;161:547-548
- Urrutia EJ, Hawkins IF, Hawkins MC, Kirby IB, Copelan EM. Clinical experience of a new retractable barb needle for breast lesion localization: the first 60 cases. Presented at the annual meeting of the Radiologic Society of North America, Chicago, IL, December 1987
- Becker W. Stereotactic localization of breast lesions. *Radiology* 1979;133:238-240
- Feig SA. Localization of clinically occult breast lesions. *Radiol Clin North Am* 1983;21:155-172
- Bristol JB, Jones PA. Transgression of localizing wire into the pleural cavity prior to mammography. *Br J Radiol* 1981;54:139-140
- Davis PS, Wechsler RJ, Feig SA, March DE. Migration of breast biopsy localization wire. *AJR* 1988;150:787-788
- Kopans DB, Meyer JE, Lindfors KK, McCarthy KA. Spring-hookwire breast lesion localizer: use with rigid compression mammographic systems. *Radiology* 1985;157:505-507
- Kopans DB, Gallagher WJ, Swann CA, et al. Does preoperative needle localization lead to an increase in local cancer recurrence? *Radiology* 1988;167:667-668
- Gent HG, Sprenger E, Dowlatshahi K. Stereotactic needle localization and cytological diagnosis of occult breast lesions. *Ann Surg* 1986;204(5):580-584
- Horns JW, Arndt RD. Percutaneous spot localization of nonpalpable breast lesions. *AJR* 1976;127:253-256
- Rizzatto G, Solbiati L, Croce F, Derchi LE. Aspiration biopsy of superficial lesions: ultrasonic guidance with a linear-array probe. *AJR* 1987;148:623-625

Book Review

Gallenblasensteine. Ihre Morphogenese und Auswahl zur Litholyse. By Carlheinrich Wolpers. Basel: Karger, 202 pp., 1987. DM 190

Formerly, "gallstones" or "no gallstones" was almost the only decision required of the radiologist when viewing an oral cholecystogram. In truth, it was somewhat boring. Alternatives to cholecystectomy are now changing that situation. Among these alternative choices are litholysis with bile acids or lithotripsy followed by treatment with bile acids. Percutaneous cholecystostomy can be followed by infusion of methyl *tert*-butyl ether or by tunable dye laser therapy. Undoubtedly, other methods are already in existence, and still others are contemplated. Success of these methods other than cholecystectomy often depends on accurate pretherapeutic information about the stones. These questions are asked: Are the stones calcified? How many stones are there? What size are the stones? Is there more than one family of stones? Are the stones cholesterol or pigment stones? The venerable oral cholecystogram has been reestablished as an important diagnostic method to answer these questions.

Wolpers not only provides a base for interpreting the oral cholecystogram but also enriches the reader regarding the fundamentals of gallstone disease. The book's origin is interesting. It represents the compilation of his personal experience of more than 30 years in the practice of internal medicine (which included doing cholecystography) and is evidence to support the stereotype of German persistence and compulsiveness. The analysis is of 966 patients with gallstones. Because serial oral cholecystograms were obtained in 429 patients, he had an opportunity to study the natural history of stone growth. In 129 patients, the stones removed were subjected to scanning electron microscopy. This was an excellent method to determine both the major chemical components of the stones and the location of these components. In 184 patients, the results of attempted bile acid litholysis were followed up by performing oral cholecystograms.

Out of this comes a thesis about the formation of solitary and multiple stones, and the writing is supported with 134 multifformat illustrations of the cholecystograms and stone specimens.

What are some of the conclusions of these observations? Wolpers believes that the solitary cholesterol stone first forms a macroscopic, radiologically detectable plaque and then ages into a sphere. Later it becomes an ellipsoid, and, if it is more than 16 mm in its long

diameter, it most probably has been coated with calcium bilirubinate. He thinks that multiple cholesterol stones develop simultaneously and do not become faceted until they are more than 6 years old. Age hinders bile acid litholysis of predominantly cholesterol stones because the stones develop a calcium and pigment coating that is not soluble. For this reason, the radiologic estimation of stone age is important when litholysis is contemplated.

A second family of stones may presage the occurrence of symptoms in a patient who has large silent stones. The new, smaller stones can occlude the cystic duct. Wolpers thinks that treatment of the second family with bile acids may be important even though the older larger stones remain in the gallbladder.

His observations on primary pigment stones seem to me the most important contribution. These stones do not dissolve with bile acid therapy, and lithotripsy may fragment the stones into undesirable sharp, irregular fragments (Sackmann M, personal communication in Munich). Wolpers shows multiple examples of these stones. He was almost always successful in recognizing them because of their characteristic irregular contours as seen on the oral cholecystogram. After viewing the illustrations, the reader will have enhanced confidence in the ability to diagnose pigment stones.

One of Wolpers's cases is unusually provocative: A stone with a calcified rim had developed a calcified center when seen 6 years later. This observation upsets the concept that stones may change only by accretion on their surface.

Dr. Wolpers's monograph is a scholarly work that provides an education in gallstone development, composition, and response to litholysis. With gallstone lithotripsy about to explode on the American horizon, this information is important. Overall this is a remarkable book. All of his conclusions may not stand the test of time, but his data provide a strong base for our current needs in interpretation of the oral cholecystogram. A translation of this book into English is needed.

John R. Amberg
University of California, San Diego
San Diego, CA 92103-1990

Progress in Radiology

Nonsurgical Therapy of Gallstones: Implications for Imaging

Joseph F. Simeone,¹ Peter R. Mueller, and Joseph T. Ferrucci

The year 1988 represents a major landmark in the diagnosis and management of gallstone disease. First and most important is the virtual revolution in treatment as several new nonsurgical modes of therapy are being introduced almost simultaneously to physicians in the United States. These include oral bile acids, extracorporeal shock-wave lithotripsy (ESWL), and contact dissolution with methyl *tert*-butyl ether (MTBE). Paralleling these developments, gallstone imaging is undergoing a similar period of rapid transition. As these new therapeutic techniques become more widely available, diagnostic gallstone imaging will become a more rigorous and demanding exercise. Heretofore, the only therapy available was cholecystectomy, and therefore the only issue for radiologic interpretation was whether gallstones were present. A positive or negative answer sufficed. However, because all the new nonsurgical modes of therapy are predicated on specific, objective, morphologic characteristics of the gallstone, the number of gallstones, and functional status of the gallbladder, there is a new need to quantify, characterize, and measure gallstones and to determine the patency of the cystic duct. Sonographic and cholecystographic techniques will necessarily become more refined. We review some of these new requirements in the imaging diagnosis of gallstones.

Selection of Patients for Treatment by Oral Bile Acid Therapy: The Role of Imaging

The principal morphologic criteria for primary treatment of cholesterol gallstones with the oral bile acid, ursodeoxycholic

acid (URSO), newly approved by the Food and Drug Administration (FDA), are listed in the following paragraphs. These are adapted from the FDA Ciba-Geigy URSO clinical trial protocols. To what extent they may be liberalized in the future remains to be determined.

If the diagnosis of gallstones has been established by some previous imaging technique, the size of the largest gallstone as measured on sonography must not exceed 20 mm in greatest diameter. However, at present there is no practical limit on the number of stones. The rationale for the 20-mm limitation relates to the stone surface area available for dissolution. The smaller the stone, the larger the surface area per unit volume and the more likely and more complete will be the ultimate dissolution.

On plain abdominal radiographs, stones must be nonradioopaque. Calcified stones or stones with a calcific rim will be excluded. However, gallstones with a small calcific nidus less than 3 mm would still be suitable for URSO therapy. As with sonography, radiographic technique must be optimized (Fig. 1). Coned views of the right upper quadrant in the prone position will give best results. Radiographic technique with low kVp and high mAs will maximize calcium detectability.

Oral cholecystography must disclose that there is adequate gallbladder visualization. This ensures that the cystic duct is patent, which is essential if URSO-rich hepatic bile is to flow into the gallbladder lumen to exert its local chemolytic effect. The gallstones also must be radiolucent when visualized during oral cholecystography (Fig. 1). Because overlying bowel gas or stool, or rib calcification, might obscure right

Received July 5, 1988; accepted after revision August 19, 1988.

Presented in part at the annual meeting of the Society of Gastrointestinal Radiologists, Nassau, Bahamas, January 1988.

¹ All authors: Department of Radiology, Massachusetts General Hospital and Harvard Medical School, Boston, MA 02114. Address reprint requests to J. F. Simeone.

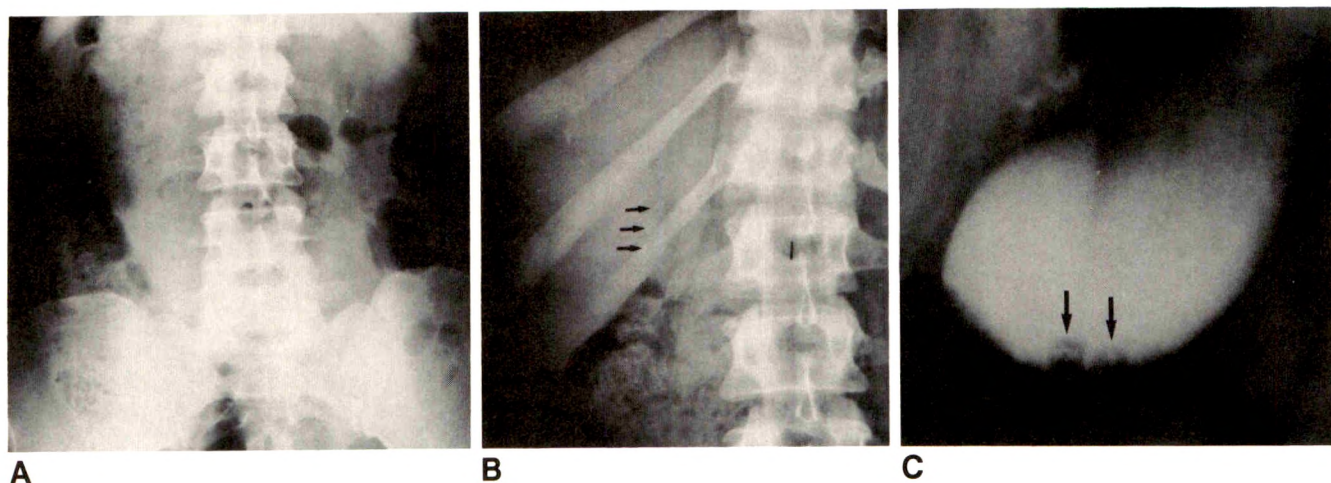


Fig. 1.—Plain film technique: positioning of central ray for detection of gallstone calcification.

A, Initial survey film shows no calcification in right upper quadrant. Note stool in colon and failure to image above 12th rib on supine abdominal view.

B, Film and beam centered to show right upper quadrant above 12th rib show three calculi (arrows).

C, Presence of calcification within gallstones confirmed by oral cholecystogram (arrows).

upper quadrant calcification, a more focused view of the stones provided by coned-down views during oral cholecystography often more precisely localizes stone and nonstone calcifications than do full abdominal films. Small central foci of gallstone calcification may be invisible on the plain abdominal radiograph and may be disclosed only after the gallstone is contrasted against opacified bile in a functioning gallbladder (Fig. 1). Right upper quadrant calcifications may be more specifically identified as being within or not within the gallbladder (Fig. 2). The classic techniques for performing oral cholecystography should be implemented once again [1, 2]. Measurement of stone size by oral cholecystography will assume a new importance because precise determination of stone size by sonography will not always be possible. An optimal oral cholecystographic technique should minimize the effects of radiographic magnification. Therefore, overhead radiographs should be obtained with the patient in the prone oblique position. Magnification factors for each individual radiographic unit should be calculated. Measurements of stone size determined on upright spot films should be corrected individually for magnification. Many younger physicians and radiologists will have to relearn the standard principles of patient preparation, oral cholecystographic contrast excretion pathways, and cholecystographic interpretation.

Selection of Patients for Treatment with ESWL: The Role of Imaging

The two major differences between patient eligibility for URSO therapy and eligibility for ESWL are the number and size of the gallstones [3, 4]. For URSO use, any number of stones may be present as long as each is 2.0 cm or less in diameter. In the FDA-approved clinical trial protocols for ESWL, no more than three stones may be present, and no stone may exceed 3.0 cm. Thus, the criteria for ESWL (at

least with the Dornier and Medstone protocols approved to date) are more limited relative to stone number but more liberal relative to size than are those for treatment with oral bile acids.

Sonography will be used to examine patients after the ESWL procedure to check for stone fragments, sludge, or possible complications of ESWL, such as biliary duct dilatation, focal liver changes, pancreatitis, or gallbladder wall abnormalities. Standard sonographic techniques can be used to look for fragments or sludge. If small, nonshadowing fragments are seen, movement of the fragments with a change in the position of the patient will confirm their presence. If sludge is present, stone fragments lying within the sludge will have to be searched for more carefully so as not to be missed, and then the patient can be declared free of calculi. The highest resolution transducers will be required during post-ESWL scanning to search for these fragments within the sludge.

Selection of Patients for Treatment with MTBE: The Role of Imaging

Eligibility criteria for gallstone dissolution with MTBE are even more liberal than those of URSO or ESWL [4, 5]. No limit on the number or size of stones present currently exists, although stones must be noncalcified or only minimally calcified as determined on plain films and CT scans. CT is also used to determine the access route for catheter passage. Gallbladder function as determined by oral cholecystography is not mandatory, because there is yet no consensus whether cystic duct patency is a desirable or an undesirable precondition. Patency of the cystic duct would be a negative factor in that it could allow excessive spillage of the potentially toxic MTBE into the duodenum.

Fig. 2.—Oral cholecystogram shows right upper quadrant calcification is not in gallbladder.

A, Plain film shows right upper quadrant calcification. Organ of origin not clear.

B, Oral cholecystogram shows that calcification is above gallbladder, probably within calcified hepatic granuloma.

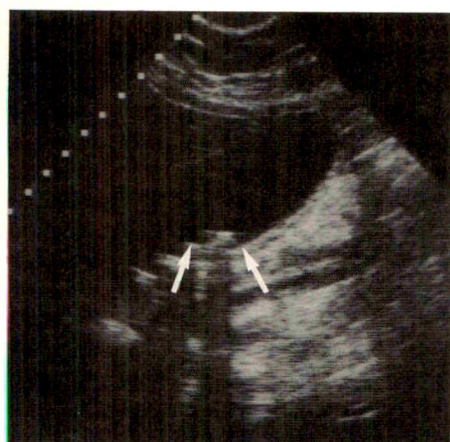
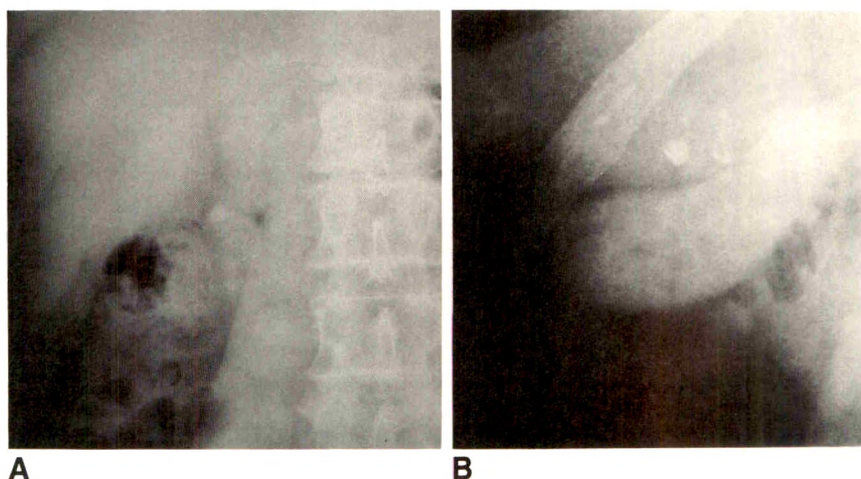


Fig. 3.—Sonographic technique: limitations of lateral resolution. Four gallstones are present. Each stone shows side-lobe artifact in lateral plane (arrow), which makes assessment of lateral diameter difficult. Only axial measurement of stone size would be accurate with this scanner.

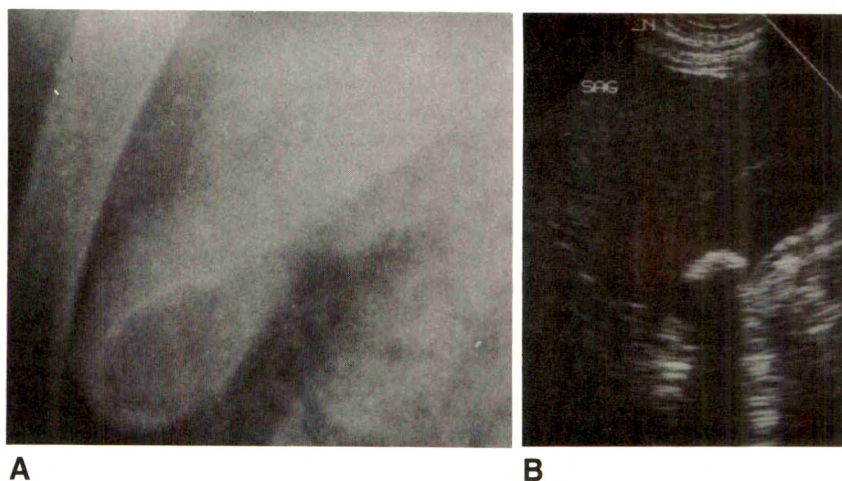


Fig. 4.—Sonographic technique, large stone: limitations of axial resolution.
A, Oral cholecystogram shows 2.5-cm oval stone.
B, Sonogram shows difficulty of assessing axial measurements of stone. Large stone size causes posterior shadowing, which obscures both posterior wall of stone and gallbladder wall.

Sonographic Techniques

Special technical maneuvers for performing sonographic studies of the gallbladder will assume new clinical importance. Sizing artifacts from reflective surfaces, axial vs lateral resolution measurements (Figs. 3 and 4), and magnification of hard-copy images for measurements will now require attention. Optimal stone measurements should be done in the axial (anteroposterior) diameter; a resolution in this dimension is superior to lateral resolution (Figs. 3 and 4). In addition, patient positioning will need to be tailored in order to count and measure stones individually (Fig. 5). Hard copies should be magnified for better depiction of stone details. Also, markers or cursor readouts of stone dimensions should be displayed clearly. Transducer frequencies of at least 5 MHz will be required to obtain ideal image quality. Abdominal radiologists

and sonographers will probably master these new requirements readily.

Although sonography is widely accepted as being approximately 15–20% more sensitive than oral cholecystography is in the detection of gallstones (Fig. 6), emerging correlative experience when the two procedures are performed in conjunction with an imaging workup for nonsurgical gallstone therapy discloses new insights into biliary calculus imaging. A recent prospective study comparing oral cholecystography and sonography determined no statistically significant difference between the two imaging techniques in detecting gallbladder disease (stones, adenomyosis, cholesterosis, and cholecystitis) [6]. Sonography detected calculi more accurately than oral cholecystography did (sensitivities, 93% vs 65%). However, in the detection of acalculous gallbladder diseases, oral cholecystography was as sensitive as sonog-

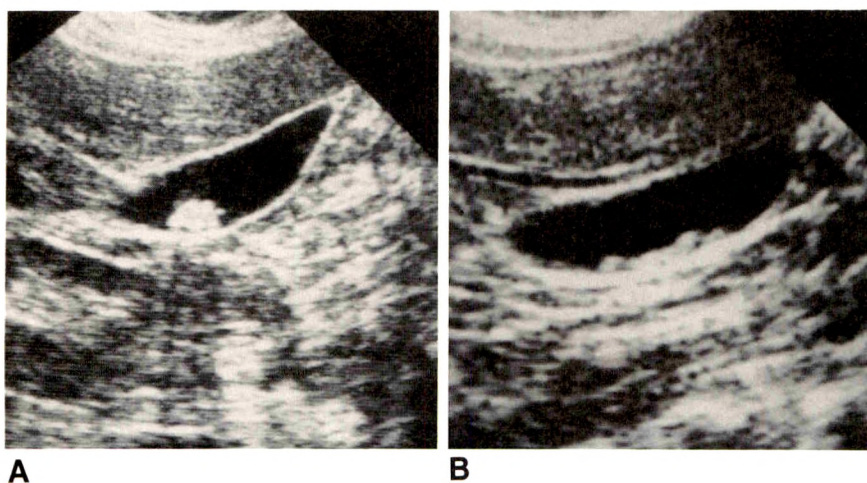


Fig. 5.—Sonographic misrepresentation of stone number.

A, Sonogram of gallbladder appears to show solitary stone.

B, After patient has been turned into left posterior oblique position, multiple small stones separate along dependent gallbladder wall.

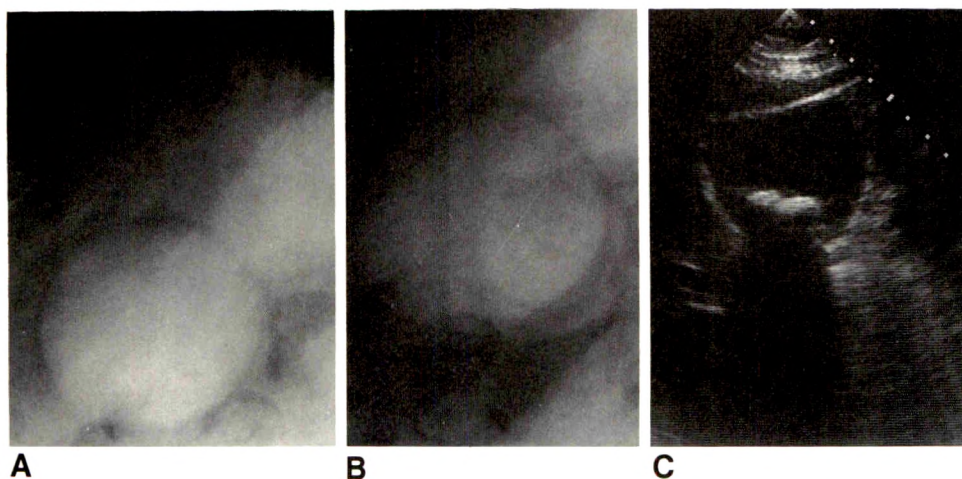


Fig. 6.—False-negative oral cholecystogram.

A and B, Oral cholecystograms show well-opacified gallbladder with no calculi.

C, Sonogram clearly shows at least two stones, the largest of which is almost 2 cm.

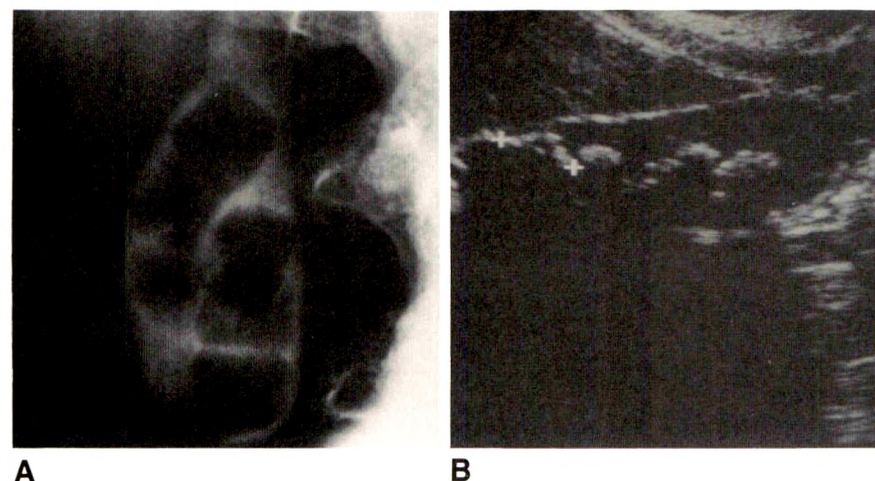


Fig. 7.—Cholecystographic-sonographic correlation. Oral cholecystography better shows size, shape, and number of stones.

A, Oral cholecystogram clearly shows at least six stones, most of which are cuboidal.

B, Sonogram shows maximum of four stones. Cuboidal stone shape is not clear. In addition, size of stones prevents sound beam from clearly delineating back wall of stone and wall of gallbladder, making measurement in axial plane imprecise.

raphy. The authors concluded that neither sonography nor oral cholecystography has a major diagnostic advantage in screening patients for gallbladder disease.

Sonography appears to be less accurate in counting stones, and direct correlation and comparison between sonography and oral cholecystography will be necessary for

precise determination of the number of stones in almost every patient (Fig. 7). Moreover, measurements of gallstone size on sonography are accurate in stones smaller than 2 cm but are not as accurate when stones exceed 2 cm (Figs. 8 and 9). This is due to the acoustic reflection and absorption of the ultrasound beam obscuring the deep and polar surfaces of

the typical large oval calculus. Thus, the larger stones often under consideration for ESWL may attenuate the ultrasound beam. The back wall of the stone may not be visible, and exact measurement in the axial plane will not be possible because all of the stone cannot be seen on sonography. However, if only one or possibly two stones are present, the measurement in the axial plane may be used. Even though the back wall of the stone is not visible, the dependent gallbladder wall can be extrapolated from continuity of the visible gallbladder wall on either side of the stone (Fig. 3). The

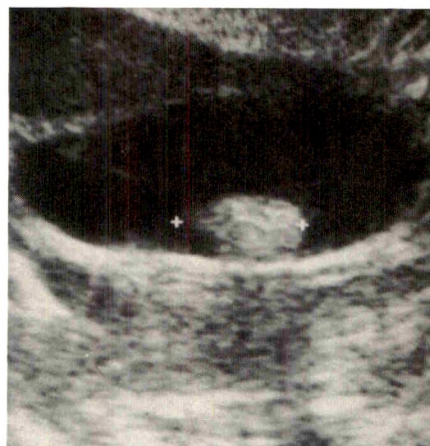
back wall of the stone can then be assumed to be directly in contact with the mucosal surface of the gallbladder wall, and measurement can be made to that point. When more than one stone is present, most of the posterior gallbladder wall may be invisible because of beam attenuation, and axial measurements may again be impossible (Fig. 7). Lateral dimensions will have to suffice in this latter situation.

Further, as stones grow to larger than 1 cm, they tend to become ovoid. The diameters of an oval stone (Fig. 4) are better determined by oral cholecystography than by the lateral

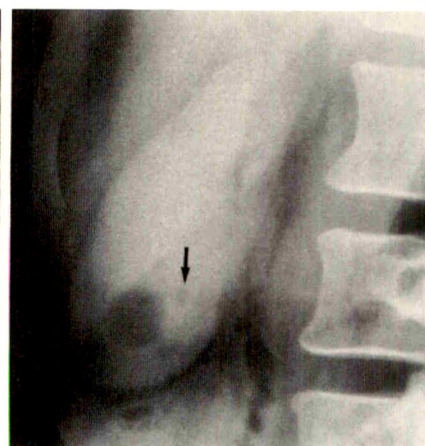
Fig. 8.—Cholecystographic-sonographic correlation. Oral cholecystography shows size and number of stones.

A, Sonogram appears to show single oval stone with maximum diameter of 2.4 cm.

B, Oral cholecystogram shows two stones: large spherical stone 1.9 cm in diameter and smaller 5-mm stone (arrow).



A



B



A



B

Fig. 9.—Cholecystographic-sonographic correlation. A 20-mm gallstone was missed on sonography.

A, Sonograms show multiple small calculi within gallbladder. Several images failed to show any stone larger than 10 mm.

B, Upright oral cholecystogram discloses large, 20-mm stone (arrows) and smaller stones that have gravitated to dependent portion of gallbladder.

resolution of the ultrasound beam (which is the orientation an oval stone presents to the ultrasound beam with the patient in the supine position).

To some radiologists, it may be a new idea that identification of the exact number of gallstones may be misleading on both sonography and oral cholecystography. However, because of overlap and obscuration to the X-ray and/or ultrasound beam, tailored techniques that use decubitus, upright, and prone positions will be used increasingly. Further, a cross-check between findings of oral cholecystography and sonography will be necessary. In general, the imaging studies showing the greatest number and largest stones should be considered correct. A strong revival of the once outmoded oral cholecystogram is a foregone conclusion.

Will CT Play a Role in Gallstone Imaging?

Although CT has shown a moderately high sensitivity of 79% in the detection of gallstones [7], the obvious advantage offered by CT in gallstone imaging is in the detection of stone calcification not seen with conventional plain film radiography. Calcification is visible in 65% of stones detected when optimal CT techniques are used [7]. This is essentially identical to the frequency of stone calcification seen on in vitro specimen radiographs in the study of gallstone morphology recently reported by Brink et al. [4]. Calcification may appear as a densely calcified nidus, a rim of higher density, or an area of somewhat higher attenuation stones that are only slightly calcified (Fig. 10).

The implications for patient eligibility when CT is used to evaluate gallbladder calculi are obvious. With increased detection of calcification, fewer patients would be eligible for USRO, ESWL, and MTBE therapy because of the presumed diminished effectiveness of gallstone dissolution when calcium is present. However, no study has shown any quantitative correlation between the amount of calcium present and the clinical efficacy of these nonsurgical therapies. It may well be that the small amounts of calcium seen on CT do not actually impair clinical success, especially with ESWL. Calcified gallstones (plain film) are already being fragmented in Europe: Sackmann et al. [8] recently reported successful

fragmentation in 29 of 31 patients with symptomatic stones with calcified rims. A combination of ESWL and oral bile acid therapy was used in these patients. Put simply, CT may just be too sensitive to calcification to be clinically relevant.

Another consideration is that, given current examination costs, the widespread use of CT scanning (two to five times more expensive than sonography in most areas of the country) makes the preprocedure workup of gallstone patients far too expensive. Amberg and Leopold [9] pleaded for medical and fiscal sanity in treating gallstone disease. Including CT scans in the imaging workup of gallstones appears economically unfeasible.

Selection of Patients for Nonsurgical Treatment: The Role of Imaging

Although the commonly quoted figure of one million new gallstone patients diagnosed annually in the United States is widely accepted, knowledgeable sonographers have long suspected that the number of gallstone patients that could be found on a careful sonographic population screening survey would be even higher. Indeed, such a study just published from Norway showed that 35% of subjects 40–49 years old had gallstones, and the percentage rose to 39% for subjects 60–69 years old, regardless of symptoms [10].

Nevertheless, little data exist as to the proportion of gallstone patients potentially suitable for the new nonsurgical forms of therapy. Certain generalizations, however, are possible. First, all patients being assessed for the nonsurgical approaches will require a functioning oral cholecystogram except when MTBE is considered. What is the likelihood that oral cholecystography will show visualization in a population of individuals with gallstones? The only available data in the literature pertinent to this question come from the study of the Rome Group for the Epidemiology and Prevention of Cholelithiasis (GREPCO) [3]. In this sonographic population survey of asymptomatic patients in Italy, gallstones shown by sonography were not seen on oral cholecystography in 28% of these patients. Conventional wisdom holds that radiopaque gallstones are present in about 20% of all patients. The GREPCO data show similar figures (18%). Analysis of 100

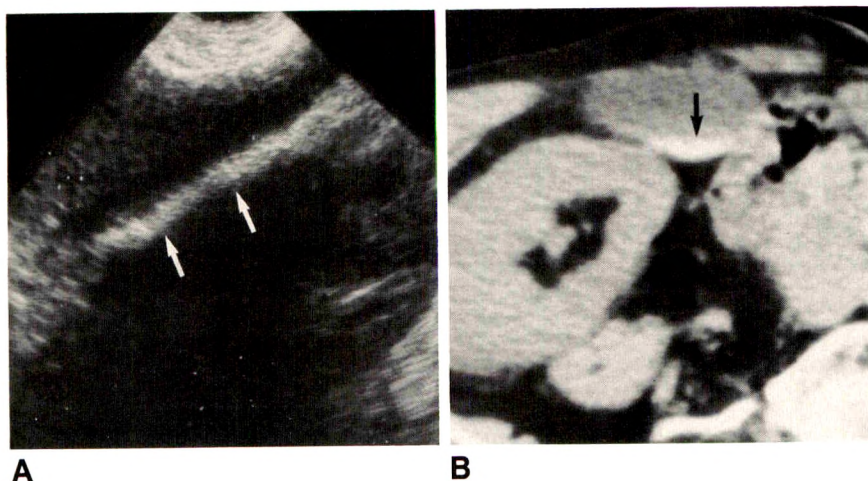


Fig. 10.—CT of cholelithiasis. No plain film calcification was detected.

A, Sonogram shows multiple, layered, small calculi (arrows).

B, CT scan shows layer of calcification (arrow) in dependent portion of gallbladder.

consecutive surgically removed gallstone-containing gallbladders at the Massachusetts General Hospital also showed 17% of patients to have stones that were heavily calcified [4].

Our study at Massachusetts General Hospital and the GREPCO report also carefully analyzed stone size and number. Both studies suggest that about 50% of all gallstone patients currently would be suitable for oral bile acid therapy by using the FDA sanctioned eligibility criteria. By the same token, the criteria currently in effect for ESWL are stricter, allowing no more than an approximately 25% eligibility [11]. MTBE eligibility projects to approximately 75% because a functioning oral cholecystogram is not mandatory and there is no limit on size or number of stones [5, 12]. In the future, the task for gallstone imaging will focus as much on characterization and quantification of gallbladder contents as on the more traditional requirement for distinguishing disease vs no disease.

REFERENCES

1. Berk RN, Leopold G, Ferrucci JT. *Radiology of the gallbladder and bile ducts: diagnosis and intervention*. Philadelphia: Saunders, 1983
2. Berk RN, Ferrucci JT, Fordtran JS, et al. Radiological diagnosis of gallbladder disease: an imaging symposium. *Radiology* 1981; 141:49-52
3. Rome Group for the Epidemiology and Prevention of Cholelithiasis (GREPCO). Radiologic appearance of gallstones and its relationship with biliary symptoms and awareness of having gallstones. Observations during epidemiologic studies. *Dig Dis Sci* 1987; 32(4):349-353
4. Brink JA, Simeone JF, Mueller PR, Richter JM, Prien EL, Ferrucci JT. Physical characteristics of gallstones removed at cholecystectomy: implications for extracorporeal shock-wave lithotripsy. *AJR* 1988; 151:927-931
5. Allen MJ, Borody TJ, Bugliosi N, et al. Rapid dissolution of gallstones by methyl-tert-butyl ether. *N Engl J Med* 1985; 312:217-220
6. Gelfand DW, Wolfman NT, Ott DJ, et al. Oral cholecystography vs gallbladder sonography: a prospective blinded reappraisal. *AJR* 1988; 151:69-72
7. Barakos JA, Ralls PW, Lapin SA. Cholelithiasis: evaluation with CT. *Radiology* 1987; 162:415-418
8. Sackmann M, Delius M, Sauerbruch T, et al. Treatment of gallbladder stones with radiopaque rims by ESWL. Presented at the International Bile Acid meeting, Freiburg, W. Germany, June 1988
9. Amberg JR, Leopold GR. Commentary. Is oral cholecystography still useful? *AJR* 1988; 151:73-74
10. Glambek I, Kvaale G, Arnesjo B, Soreide R. Prevalence of gallstones in a Norwegian population. *Scand J Gastroenterol* 1987; 22:1089-1094
11. Sackmann M, Delius M, Sauerbruch T, et al. Shock-wave lithotripsy of gallbladder stones. *N Engl J Med* 1988; 318:393-397
12. vanSonnenberg E, Hofmann AF, Neoptolemus J, Wittich GR, Princenthal RA, Willson SW. Gallstone dissolution with methyl-tert-butyl ether via percutaneous cholecystostomy: success and caveats. *AJR* 1986; 146:865-867

Book Review

Fundamentals of Radiology, 4th ed. By Lucy Frank Squire and Robert Novelline. Cambridge, MA: Harvard University Press, 355 pp., 1988. \$29.50

Squire and Novelline's *Fundamentals of Radiology* is a new edition of an introductory text for medical students. Most of the book is devoted to a review of radiologic techniques and film findings by organ system, with chest radiology appropriately emphasized. All of the major areas of radiology are covered, including current material on CT and MR. Although the space devoted to CT is large, this is now appropriate in an introductory text. In general, special procedures and techniques other than plain films are especially well covered. However, the section on ventilation-perfusion lung scanning should be more complete, with emphasis on the importance of size and distribution of perfusion defects. The major omission is the lack of a thorough discussion of mammography, which has become more important in the last few years. Careful analysis of the lordotic view and plain-film studies of cardiac disease are of little current interest and are too extensive for an introductory book.

Background material is clear and beautifully describes roentgenographic history and basic principles and techniques. Philosophic discussions on the importance of old films, clinical correlation, order-

ing studies appropriately, and the relationship of clinicians and radiologists are scattered throughout the text. The significance of this material would be better emphasized by a separate chapter at the start of the book.

Fundamentals of Radiology is well written in an informal style. Scattered unknown film cases are used to challenge the reader to use skills taught in the text. The layout of the book is superb, and most illustrations are clear and make the appropriate points.

Medical students over the years have loved this textbook and rightly have made it a widely used introductory text for diagnostic radiology. The fourth edition continues previous high standards and brings the book up-to-date. This large, hard-cover book is printed on good quality paper and is attractive. It is an exceptionally good value for the money, and I recommend it without qualification.

John V. Forrest
University of California, San Diego, Medical Center
San Diego, CA 92103

Progress in Radiology

Visual Fuzzy Cluster Analysis of MR Images

Stuart W. Young,¹ Cristina Ballerio,¹ and Clark L. Carrol²

MR contrast resolution is superior to that of both CT and sonography [1, 2] and has the unique ability to obtain multiple, qualitatively different images of the same anatomic region on the basis of an emphasis of the various MR parameters. However, the gray-scale visual synthesis and conspicuity queuing commonly used in interpreting MR scans is beginning to have significant limitations. Attempting to interpret a routine MR study consisting of 60 to 100 $\times 10^6$ bits of information requires considerable training and discipline. New pulsing sequences, contrast agents, and multinuclear scanning will surely add orders of magnitude to the quantity of data available to the physician for interpretation.

Techniques for data-dimension reduction are needed to handle this large and exploding volume of information. This article describes the use of a fuzzy cluster analysis framework useful in analyzing MR scans by the visual synthesis method and in teaching MR to trainees [3]. We have called this approach visual fuzzy cluster analysis (VFCA). Fuzzy cluster analysis [4, 5] is a computerized postprocessing approach to the data-reduction problem. Briefly, all tissues are categorized by the computer on the basis of data obtained from the multiple scanning sequences used in the MR study, and then tissues are assigned membership to a cluster (fuzzy cluster) of similar tissues. The clusters themselves can be displayed or the distribution of cluster membership can be displayed on the anatomic map of the MR slices. Although computer-based displays that use these methods are not widely available yet, we have found VFCA to be useful in MR interpretation.

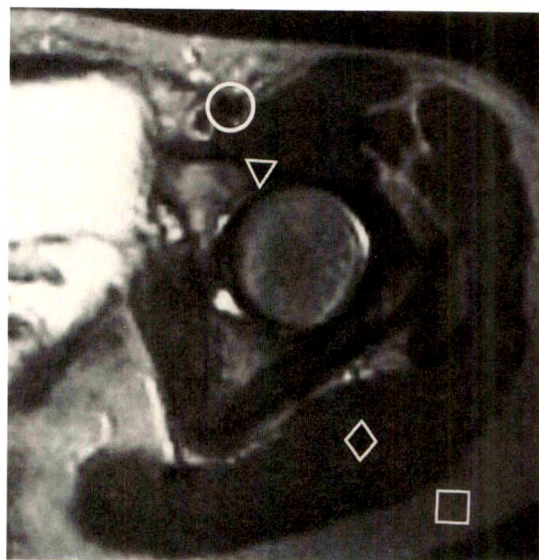


Fig. 1.—Axial MR scan, 2000/70 of pelvis shows visual fuzzy cluster approach for assignment of gray-scale signatures to normal tissue. Iliac artery (circle), cortical bone (triangle), fat (square), muscle (diamond), and fluid within bladder (upper left) are seen. Inspection of femoral head reveals it to be a member of the fat fuzzy cluster set (square) and internally homogeneous and therefore normal. Tissue surrounding femoral head (high intensity at 2 and 8 o'clock positions) belongs to fuzzy cluster set defined by fluid in bladder and thus represents an effusion in left hip. Only one image of this sequence is shown. Tissues were studied with four pulse sequences: partial saturation, 600/20; spin echo, 2000/20, 70; and gradient echo/small tip angle, 25/15/30° tip angle.

Received June 9, 1988; accepted after revision August 9, 1988.

This work was supported in part by a grant from the General Electric Co., Fremont, CA 94539.

¹ Department of Diagnostic Radiology and Nuclear Medicine, S-052, Stanford University School of Medicine, Stanford, CA 94305. Address reprint requests to S. W. Young.

² Department of Radiology, St. Luke's Episcopal Hospital, Texas Medical Center, Houston, TX 77030.

AJR 152:19-25, January 1989 0361-803X/89/1521-0019 © American Roentgen Ray Society

Furthermore, familiarity with the concepts of data-dimension reduction will facilitate the dissemination and use of these approaches to MR interpretation when the computer-based displays are widely available.

VFCA

Computer-based fuzzy cluster analysis, which is valuable in MR interpretation [6, 7], is an off-line process requiring considerable computer expertise and computer time. VFCA is a modification of this approach that can be used by the physician interpreting the MR scan as the scanning sequences are obtained [3].

Use of the conventional visual synthesis approach involves a general understanding of the pulsing sequences used and a knowledge of the relaxation times and the motion effects and artifacts present within the normal and abnormal tissue; the method relies on conspicuity (differences in the displayed gray scale) for visual clues regarding areas of abnormality.

To use the VFCA method in a diagnostic or teaching session requires the assembling of MR scans by similar scanning sequences (i.e., data dimension) and a working knowledge of anatomy previously acquired from CT or sonographic experience. Gray-scale signatures are then assigned for each type of normal tissue included in the anatomic slices. Figure 1 illustrates the gray-scale signature for arterial blood, cortical bone, muscle, fat, and fluid (bladder) included in this example from a four-dimensional feature-space MR series. For simplicity, an axial spin-echo image, 2000/70 (TR/TE), is shown; however, the VFCA method can be applied without any knowledge of the exact pulsing sequences used or their probable effects on the tissues being studied. The interpreter could use any number of parameters while simultaneously improving the characterization of the tissues. Once established, these fuzzy clusters (gray-scale signatures) are used to confirm that all structures tentatively assumed to be a given type of tissue actually match the cluster set through all angles of view. All tissues are inspected sequentially for internal homogeneity and thus appropriate membership in the prescribed fuzzy cluster set (as is commonly done in routine scanning today); areas or tissues considered to be abnormal can be confirmed as abnormal because they do not match any of the normal tissue (i.e., they have a unique gray-scale signature and fuzzy cluster set membership). Structures determined to be abnormal on the basis of their abnormal anatomic profile can be defined further as to the types of tissue constituting the abnormalities, thus affording further delineation of the origin of the abnormality being studied. This approach provides the structure for a thorough and disciplined search pattern for MR scan evaluation as opposed to a general search for conspicuity, which ignores the concept of appropriate fuzzy cluster set membership as an important diagnostic tool. VFCA also provides a method for confirming the accuracy of an interpretation by using an internal standard for each patient in each scan.

VFCA aids tissue characterization of normal and subsequently abnormal tissue on the basis of the particular gray-scale signature of normal and abnormal tissues by using the

scanning sequences and other factors unique to the specific patient being examined under the conditions of the MR evaluation.

VFCA links the concepts of visual synthesis and fuzzy cluster analysis in a usable and potentially advantageous way. One advantage of the VFCA approach is derived from the computer fuzzy cluster method, because the physician does not need extensive prior knowledge of MR. This is an advantage when MR studies are being explained to referring physicians unfamiliar with MR or during the MR training period. It provides a disciplined method for thoroughly assessing and interpreting the large amount of data present on MR scans, and, because it is visual technique, no additional computers or display outputs are needed.

Another advantage of VFCA over unsupervised computer-based fuzzy cluster analysis is the ability to adjust fuzzy cluster set membership with respect to inhomogeneities in the B0 and B1 magnetic fields. This is illustrated in Figure 1, where magnetic inhomogeneity causes an increase in signal intensity from the patient's left to right across the image, causing the signal recorded for the fat in the perineal region and the region anterior to the bladder to be of higher intensity than the signal recorded for the fat in the left buttock. Unsupervised computer analysis would display these tissues as two separate tissue clusters.

Fuzzy cluster analysis is based on fuzzy mathematical set theory, which uses partial or "fuzzy" assignment of members to sets [4, 5]. As applied to MR, fuzzy cluster analysis of the MR images involves the following steps: First, the scan data from multiple pulsing sequences are entered into the computer and tissues are grouped together depending on the similarity of their MR signals. In a given scan series, any number of divisions of the data can be selected by the physician. To a point, the more divisions the greater is the potential for tissue characterization. For example, in Figure 2 the data are separated into five divisions. The computer can be supervised (i.e., a cursor position can direct the classification of tissues) or unsupervised (i.e., the computer makes the tissue assignments based on how closely an unknown tissue matches other tissues within the scan under consideration). In MR, the number of source images (i.e., pulsing sequences) determines the data base within which the cluster analysis is carried out [6, 7]. As illustrated in Figure 2, the three pulsing sequences used in the three source images (600/20, 2000/40, and 2000/80) can be thought of as defining a rectangular cubic coordinate system (referred to as a feature space) within which the tissue clusters are placed to achieve their separation. Any abnormal tissue (the cancer in this illustration) will be displayed as a cluster separate from the normal tissues. In this example, five tissues have been defined as clusters on the basis of the three-dimensional coordinates. Set membership is assigned if a tissue's collective signal characteristic is close to that of the other tissues under consideration. Fuzzy clustering algorithms are superior to boundary-seeking or edge-seeking algorithms because the transition between normal and abnormal tissue is often a continuum with vague boundaries, and fuzzy clustering more accurately models this type of transitional uncertainty [5, 7].

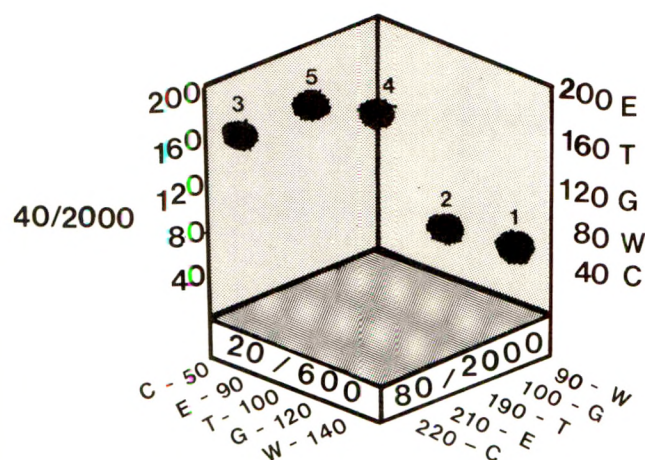


Fig. 2.—Computer-generated three-dimensional fuzzy cluster analysis obtained from axial MR scans shows distribution of cluster centers representing five different tissue types. Axes of feature space are formed by intensity scales of source T1-weighted, 600/20; T2-weighted, 2000/80; and intermediate-weighted, 2000/40, images obtained at 1.5 T. Size of each cluster is approximately a radius of 1 SD, with “fuzzy” margins drawn for purposes of illustration. Each tissue is assigned to a cluster on the basis of the distance of its particular signal characteristics from the cluster’s center. Although the feature space can be as large as the number of scanning parameters used (including multinuclear, chemical shift, magnetic susceptibility, or flow), and any part of the body can be examined in this fashion, the tissues here represent white matter (W, cluster 1); gray matter (G, cluster 2); neoplasm (T, cluster 4); CSF (C, cluster 3); and edema (E, cluster 5). (Reprinted from Young [3], with permission.)

Once the tissues have been grouped (assigned to a fuzzy cluster), each cluster can be assigned a shade of gray, and a cluster distribution can be displayed on anatomically mapped images called classified images. The gray scale is based on the distribution of each cluster within the slice of the MR scan. In these classified image displays, the separation between normal and abnormal tissues and the margins of surrounding edema is often possible even when this distinction cannot be determined from visual inspection of the source images themselves [6, 7]. Any number of source images can be used to generate the classified image [4, 5]. As more qualitatively different source images are used, the likelihood of separating two tissues with a similar signal in one source image by their signal difference in another source image increases. The potential for improving tissue specificity beyond that obtainable with visual analysis is great; also, linking routine visual synthesis interpretations of MR scans and a knowledge of computer-based fuzzy cluster analysis of the selected feature space can be a beneficial aid to the practical clinical logic.

Clinical Applications

Figure 3 illustrates the use of the VFCA method to both rule in and rule out disease. Both the CT and MR scans of this patient with known mediastinal malignant lymphoma were initially interpreted as being positive for malignant lymphoma in the spleen and a paracaval lymph node at the level of the right renal hilus. By using gray-scale conspicuity and conventional visual synthesis as the method of MR interpretation,

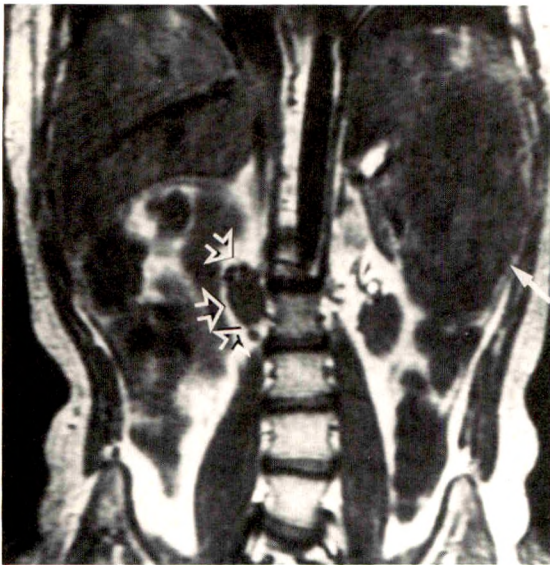
attention is drawn to the spleen because it is enlarged and to the paracaval mass because of the surrounding fat and because normally no mass is present in this area. However, considering the case as a data set consisting of a five-dimensional feature space (defined by the five pulsing sequences) revealed that the spleen did have a unique fuzzy cluster set membership, thus indicating that it was not normal tissue and probably was enlarged because of malignant lymphoma. The paracaval mass belonged to the fuzzy cluster set described by the normal renal tissue and thus was a portion of the lower pole of the right kidney, which was separated from the body of the kidney by a complete fetal lobulation. This impression was confirmed at surgery.

The number of source images determines the dimensionality of the data feature space. Any number of source images can be used to generate the cluster sets, and increasing the number of source images increases the likelihood of separating two tissues with indistinguishable signals on some of the source images by their differing signals on other images. This is illustrated in Figure 4, which was obtained in the workup of a 17-year-old girl with Ewing sarcoma. The Ewing sarcoma is not detectable on two of the images (Figs. 4A and 4B), but is detectable by comparing these two MR scans with another of the source images (Fig. 4D). The diagnosis in this case might have been missed if only two source images (Figs. 4A and 4B) had been used, because the sarcoma had not distorted the normal anatomic outline of the adductor muscles and was isointense relative to the surrounding tissue and contralateral adductor muscles.

The sagittal MR scans from two women evaluated for abdominal masses help to illustrate the use of VFCA in defining the cause of detected abnormalities. The abnormalities shown in Figure 5 are conspicuous by virtue of their large size. However, VFCA of the tissues, by assigning set membership, allowed further classification of the masses. In the first patient (Figs. 5A and 5B), the multiple, well-demarcated, round uterine masses belong in the cluster assigned to normal muscle and thus represent uterine leiomyomas. An additional unique cluster is noted superiorly, and its increased intensity correlated with areas of hemorrhage found in a leiomatous uterus at surgery.

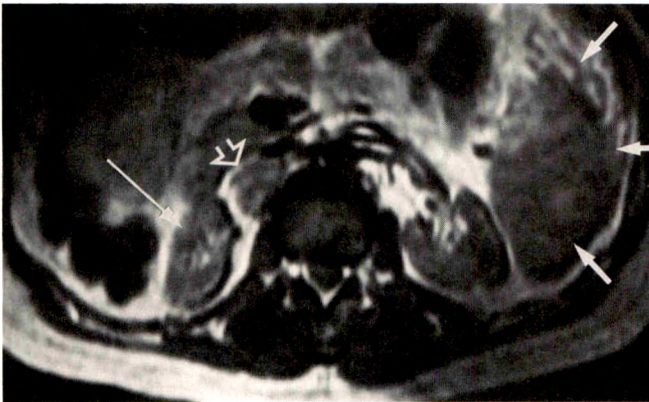
The sagittal scans of the second patient (Figs. 5C and 5D), however, are more complex. One spherical region of the abnormal mass belongs to the cluster set of normal muscle and so, similar to the previous case, probably represents a leiomyoma. However, an inferior region belongs to the cluster set defined by the fluid in the bladder, and therefore probably is an area of cystic fluid. At least two additional unique regions can be seen between the fluid collection and the top of the mass that are not members of any normal tissue defined by this feature space set of primary scans. A region of normal uterine wall surrounded this entire abnormality. This combination of fuzzy cluster set membership strongly suggested a uterine malignant neoplasm because it was circumscribed by normal uterine wall and because of the presence of unique (not normal tissue) cluster sets present within the mass. Because of the presence of a leiomyoma within the mass, a sarcomatous degeneration of a leiomyoma was strongly sug-

P24,450

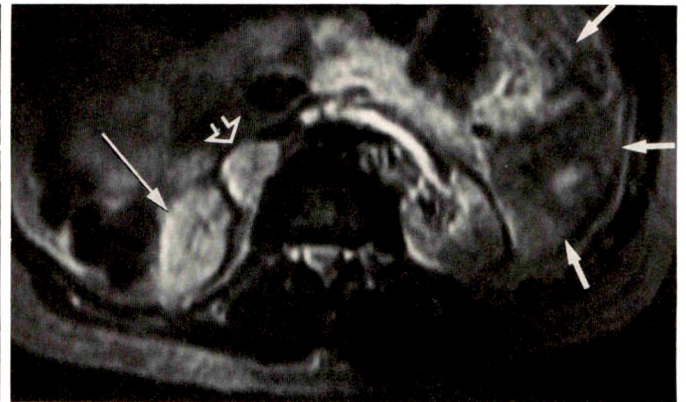


A

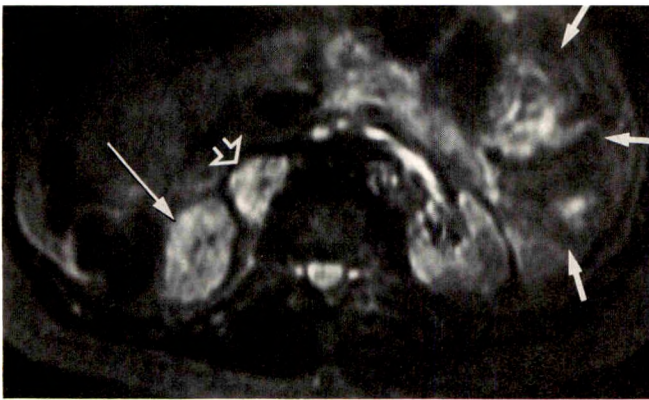
Fig. 3.—Coronal 800/25 (A) and transaxial 2500/25 (B), 2500/50 (C), 2500/75 (D), and 2500/100 (E) MR source images obtained in staging evaluation of patient with known malignant lymphoma who was initially interpreted as having malignancy in an enlarged spleen (short solid white arrows) and paracaval lymph node mass located between kidney and inferior vena cava (open arrows). Commonly used principle of structural conspicuity draws attention to spleen because it is enlarged and to paracaval mass because normally no mass should be present in this region. Visual cluster analysis, however, confirmed that spleen had a unique fuzzy cluster set membership in addition to being enlarged and heterogeneous. However, mass between right kidney and inferior vena cava did not belong to fuzzy cluster set of splenic malignancy, but was a member of fuzzy cluster set describing kidney (long solid white arrows, B–E), indicating that this structure was normal renal tissue separated from body of kidney by a deep fetal lobulation.



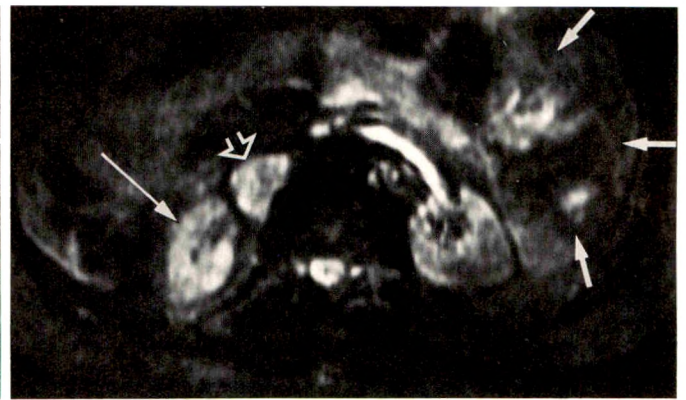
B



C



D



E

gested. At surgery, sarcomatous degeneration of a leiomyoma and mixed müllerian sarcoma were found.

Discussion

On the basis of an emphasis of the various MR parameters of the tissue (nuclear density, T1 and T2 relaxation times, and motion or flow), MR is capable of obtaining multiple, qualita-

tively different images of the same tissue. When multinuclear, multiplane, and chemical-shift scanning are considered, the multiparametric nature of MR provides the potential for greatly improved tissue characterization and the potential for detecting diseases at the biochemical level. However, MR produces an overwhelming volume of image data for the physician to analyze by traditional gray-scale comparison methods. In clinical practice today, a different pulsing sequence often is

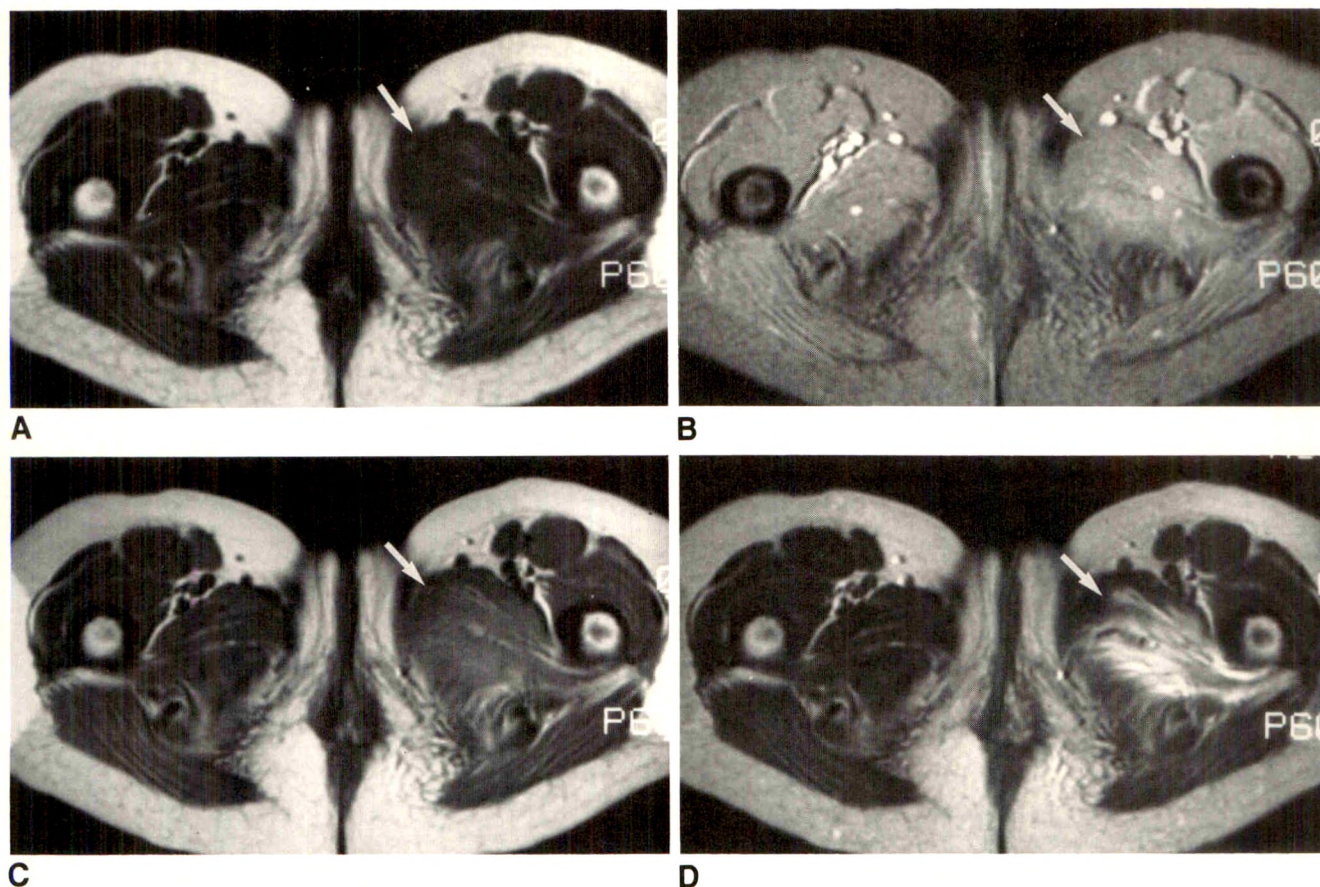


Fig. 4.—Four MR source images, 800/20 (A), 25/10/15° tip angle (B), 2500/20 (C), and 2000/75 (D), in patient being staged for known Ewing sarcoma. Increasing the number of source images increases the likelihood of separating two tissues with indistinguishable signals on some source images by differing signals in other images; the diagnosis in this case might have been missed if only two source images (A and B) were used, because sarcoma (arrows) had invaded but not distorted adductor anatomy. Thus, sarcoma is not detectable on A or B and possibly C (where fuzzy cluster membership, or gray-scale signature, of Ewing sarcoma involving left adductor muscles is identical to that of adductor muscles on right); it is detectable on D (where signal intensities on source images are quite different). Gradient-echo image reveals enlarged and more numerous blood vessels within Ewing sarcoma, which are seen as high-intensity circles within neoplasm.

used with each different orthogonal angle of view. Image interpretation with visual synthesis of multiple pulsing sequences and just three orthogonal views is subject to errors introduced by observer fatigue and observer biases. Failure to perform a disciplined search of the images, and resulting failure to detect inconsistencies in the gray scale from one angle of view and pulsing sequence to another, are common problems in MR training programs.

Gray-scale visual synthesis commonly used in interpreting MR scans has some limitations in practice. The interpretation of an MR study can be a considerable challenge for the physician who has attempted to learn MR from the literature or by attending refresher courses. Often, only one or two views are presented for each case, and the variability of the gray scale due to different MR scanners, different fields, artifacts, or nonstandardized settings of the machines can be confusing. Furthermore, the gray scales in normal and abnormal tissues are variable and can be influenced by the hydration status or temperature of the patient or by the drugs being administered [8–13].

One measure of the diagnostic challenge presented by an MR scan is the sheer quantity of data. For example, in our

institution, a routine examination of the pelvis involves sagittal and coronal partial-saturation studies containing 42 images and first- and second-echo spin-echo sequences usually containing 40 images. Each image usually is obtained with a 256×256 matrix and 12 to 14 bits in the dynamic range, thus providing 64×10^6 bits of information for analysis. In addition, intrinsic inhomogeneities, scan artifacts, or other peculiarities of the study must be accounted for in the interpretation. It takes persistence and discipline to carefully evaluate each tissue and anatomic structure with respect to each of these variables.

Clearly, techniques for data-dimension (i.e., various scanning sequences) reduction are needed for analysis of these image sets of multiparametric data. Several computerized image analysis techniques largely derived from methods developed by the National Aeronautic and Space Administration for multispectral analysis of earth satellite images have been applied to MR. The simplest classification procedure begins with the observer's identification of tissue regions (e.g., tumor, edema, and normal) based on prior knowledge or assumptions about true tissue characteristics. The computer then takes this supervised classification scheme and assigns each

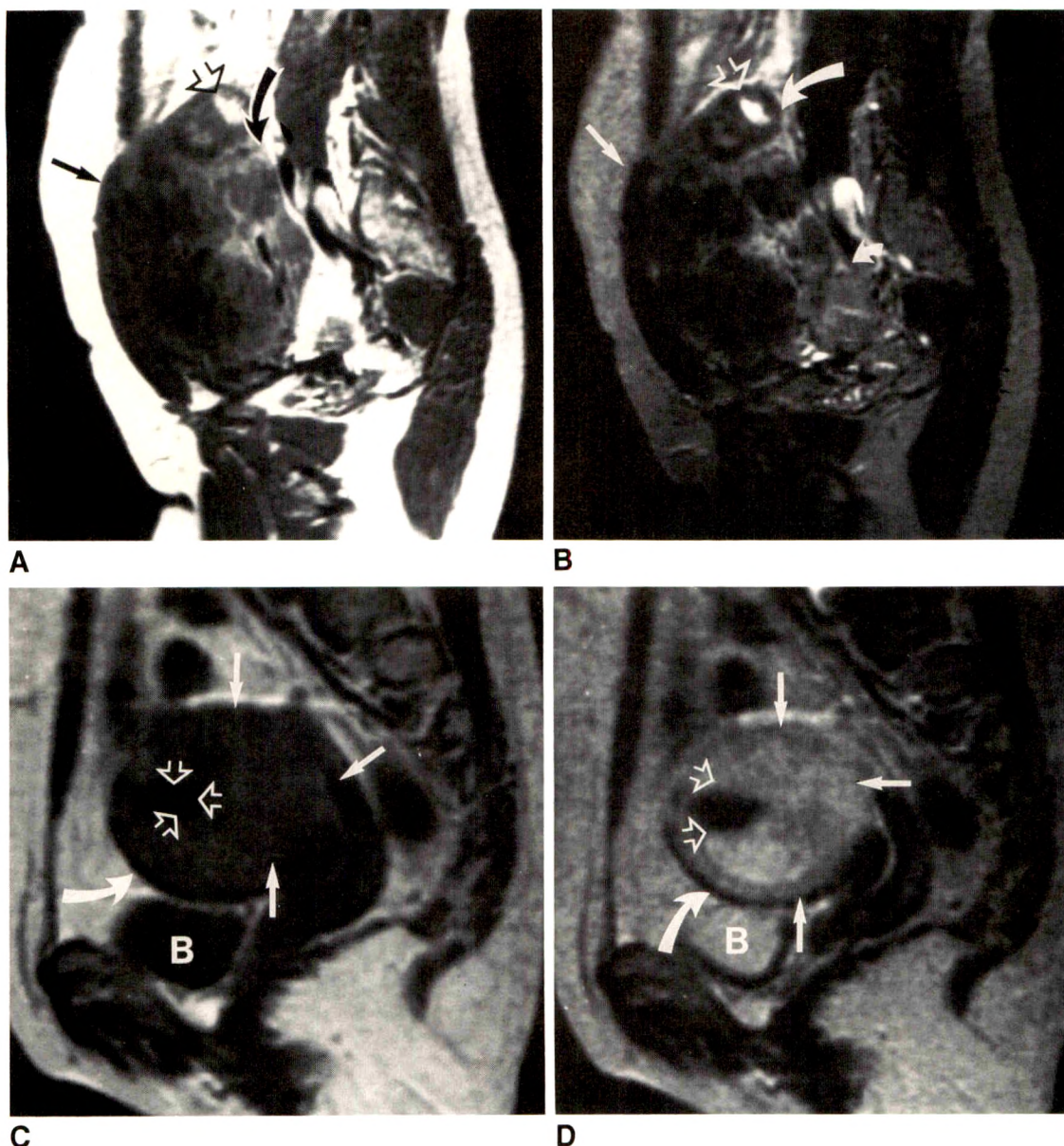


Fig. 5.—Sagittal pelvic MR scans from two women being evaluated for abdominal masses. Abnormalities are conspicuous by virtue of their large size. However, careful analysis of tissues by visual fuzzy cluster set membership allows further classification of masses (not all source images are shown).

A and B, MR source images, 1500/25 (A) and 1500/75 (B). Multiple, well-demarcated, round uterine masses belong in cluster assigned to normal muscle, as illustrated by adjacent rectus (straight solid arrows). Tissue surrounding spherical masses belongs to cluster assigned to normal uterine wall (curved arrows). Normal uterine tissue is seen above cervix in posterior pelvis. Additional unique cluster is noted superiorly (open arrows), and its increased intensity correlated with areas of hemorrhage within large leiomyomas found at surgery.

C and D, Sagittal MR source images, 2000/25 (C) and 2000/75 (D), in second patient are more complex. One spherical region of abnormal mass belongs to cluster set of normal muscle (open arrows). An inferior region (curved arrows) belongs to cluster set defined by fluid in bladder (B). At least two additional unique regions can be seen between fluid collection and top of mass (straight solid arrows) that are not members of any normal tissue defined by this feature space set of primary scans, including a region of normal uterine wall that surrounds entire abnormality. This combination of fuzzy cluster set membership strongly suggests a uterine abnormality because it is largely defined by normal uterine wall; neoplastic, probably malignant degeneration is indicated because of unique cluster sets present within mass; and leiomyoma within the mass suggests sarcomatous degeneration of leiomyoma. At surgery, sarcomatous degeneration of a leiomyoma and mixed müllerian sarcoma were found.

pixel in the image to the appropriate tissue category. More sophisticated approaches allow unsupervised (automated) classification of tissues into categories without observer bias by using multivariate statistical analysis techniques.

As previously discussed, fuzzy cluster analysis is another

computerized postprocessing approach to this problem [3, 4]. VFCA [5] uses the fuzzy cluster analysis framework to analyze MR images by the visual synthesis method, and this approach can be useful in interpreting MR images and in teaching MR.

ACKNOWLEDGMENTS

We thank R. E. DeLaPaz for providing the data used in the fuzzy cluster analysis in Figure 1 and Lisa Pettegrew for manuscript preparation.

REFERENCES

1. Hricak H. MR of the female pelvis: a review. *AJR* **1986**;146:1115-1122
2. Worthington JL, Balfe DM, Lee JKT, et al. Uterine neoplasms: MR imaging. *Radiology* **1986**;159:725-730
3. Young SW. *Magnetic resonance imaging: basic principles*, 2nd ed. New York:Raven, **1987**
4. Bezdek JC. *Pattern recognition with fuzzy objective function algorithms*. New York:Plenum, **1981**
5. Cannon RL, Dave JV, Bezdek JC. Efficient implementation of the fuzzy c-means clustering algorithms. *IEEE Trans Pattern Recognition Machine Intelligence* **1985**; PAMI-8:248-255
6. DeLaPaz RL, Bernstein R, Dave JV, Chang PJ. Tissue characterization with MR using advanced digital processing techniques ("fuzzy clustering"). Presented at the annual meeting of the Society of Magnetic Resonance in Medicine, Montreal, August **1986**:229
7. DeLaPaz RL, Chang PJ, Bernstein R, Dave JV. Approximate fuzzy c-means (AFCM) cluster analysis of medical magnetic resonance image (MR) data. Presented at the IEEE Systems Management and Cybernetics Conference, Alexandria, VA, October **1987**
8. Bottomley PA, Foster TH, Argersinger RE, et al. A review of normal tissue hydrogen NMR relaxation times and relaxation mechanisms from 1-100 MHz: dependence on tissue type, NMR frequency, temperature, species, excision, and age. *Med Phys* **1984**;11:425-448
9. Brown JJ, vanSonnenberg E. MR characterization of biologic tissues and fluids. *Appl Radiol* **1986**;15(3):73-76
10. Brown MS, Gore JC. NMR relaxation in hydrogels: a model for tissues (abstr). *Magn Reson Imaging* **1987**;5[suppl 1]:88
11. Foster MA, Rimmington JE, Mallard JR. Variation in tissue T1 relaxation time with measurement temperature and frequency: an in vitro study of rat tissues (abstr). *Magn Reson Imaging* **1987**;5[suppl 1]:90
12. Wolf GL, Sullenberger PC, Bickerstaff KJ. The effects of temperature upon proton relaxation rates in biological tissues (abstr). *Magn Reson Imaging* **1987**;5[suppl 1]:91
13. Fung BM. Correlation of relaxation times with water content in muscle and brain tissues. *Biochim Biophys Acta* **1977**;497:317-322

The American Roentgen Ray Society is pleased to announce that the Honorable William Bradley, Senator from New Jersey, will give the Caldwell lecture at the 1989 ARRS meeting in New Orleans, LA. The topic of Senator Bradley's lecture will be "Health-Care Choices for the Nineties."

Book Reviews

Computed Tomography of the Chest. A Teaching File. By M. Elon Gale and Joel B. Karlinsky. Chicago: Year Book Medical, 254 pp., 1988. \$54

Radiology residents beginning their training in CT of the body almost uniformly claim that chest CT is the most difficult part to master. This introductory text by Gale and Karlinsky can ease the transition to a basic overview of this complex subject.

The book is divided into chapters based on the major structural systems in the thorax: the pulmonary parenchyma, hila and airways, mediastinum, cardiovascular system, pleura, diaphragm, and chest wall. The introductory chapter illustrates normal anatomy of the mediastinum, bronchi, and lungs; both soft-tissue and lung window settings are used, extending from the thoracic inlet to the diaphragm. A list of cited references, divided according to chapters, and a standard index conclude the volume. Each page is devoted to a single clinical case. One or more CT scans show the pertinent diagnostic features. These features are described and amplified in the accompanying captions, along with a discussion of clinical information about the specific disease entity and its differential diagnosis.

In addition to including examples of most of the commonly encountered diseases encountered in chest CT, the book also illustrates a scattering of interesting but far less common entities. Many of these are instructive, but I question the value of illustrating nonfatty mediastinal liposarcoma—an entity unlikely to be encountered in the lifetime of most radiologists. More importantly, I question the value of illustrating the CT appearance of many of the infectious and diffuse lung diseases described: For most of them, plain chest radiographs provide more information at a fraction of the cost of a CT scan. With the value of CT so well established in the other areas of chest

disease, it is surprising that the authors chose to illustrate cases for which the indications and usefulness of CT are doubtful at best. It is easy to spot these cases: The amount of text devoted to clinical features dwarfs the description and discussion of the CT findings.

The value of using a teaching-file case format depends completely on the quality of the images and the accompanying text. This book excels on both counts. The CT images have been carefully chosen to show clearly and sharply the diagnostic features under discussion. The arrows, letters, and other labeling devices have been carefully selected for size, boldness, location, and shading to optimize their teaching value. Most impressive to me is the quality of the text accompanying each case. The sentences and paragraphs contain a maximum of useful information compacted into simple, lucid statements. The quality of the paper, printing, binding, and hard cover is exemplary. One disappointing feature is the large amount of blank paper: On at least half of the pages, the printed illustrations and accompanying text occupy less than half of the available space.

This book is highly recommended to all radiology residents and to pulmonologists, thoracic surgeons, and other clinicians who are involved in the care of patients with chest diseases. It will be of much less use to the practicing radiologist who is already experienced in the interpretation of chest CT scans.

Melvyn Korobkin
Sinai Hospital of Detroit
Detroit, MI 48235-2899

Progress in Digital Angiocardiology. Edited by P. H. Heintzen and J. H. Bürsch. Boston: Kluwer Academic, 353 pp., 1988. \$145

Progress in Digital Angiocardiology is a compilation of scientific papers presented at a recent symposium. The unifying themes are digital imaging and the heart. This volume has several authors and presents a diverse series of topics, ranging from the mechanics of outpatient digital coronary arteriography to the theoretical basis of reconstruction techniques for three-dimensional coronary arteriography. That is a lot of ground to cover for a 350-page volume!

By and large, the articles are well-written. Some of the chapters, however, are written in an awkward style and may in fact have been written by someone who does not speak English and/or have been poorly translated.

Some of the information in this book is quite interesting and on the cutting edge of cardiology; the discussion of the measurement and quantification of coronary reserve is quite thorough and up-to-date. Additionally, the chapters on the digital quantification of valvular regurgitation are quite thorough and present the mathematical techniques for understanding valvular regurgitation in a clear and concise fashion. An interesting set of articles juxtaposes the technique of

acquiring coronary images in an analog fashion and converting them to a digital format for subsequent analysis (i.e., 35-mm cine acquisition converted to computer-digital memory) vs true digital acquisition and subsequent digital processing and analysis.

The organization of the book is logical and cohesive, and articles are well illustrated. The references are all current and in major journals. Because the book has several authors and is the direct result of a symposium, it has substantial duplication of material in several of the articles. Most of the information presented in each chapter is available in the literature but not as conveniently as in this single volume. The price of \$145 seems high for a text of this nature.

The book would be useful as a general reference in a cardiac catheterization-cardiovascular laboratory or for a radiologist who is interested in cardiac radiology. It would not have broad appeal to the practicing general radiologist.

Barry S. Robbins
San Jose, CA 95112

Superior Mediastinal Widening from Spine Fractures Mimicking Aortic Rupture on Chest Radiographs

Lee N. Dennis^{1,2}
Lee F. Rogers¹

Mediastinal widening on chest radiographs associated with lower cervical and upper thoracic spine fractures can mimic the radiographic findings of aortic rupture. Frontal chest radiographs from 54 patients with traumatic fractures of at least one vertebral body from C6 to T8 were examined for signs suggestive of aortic rupture. These signs included (1) mediastinal width equal to or greater than 8 cm; (2) presence of a left apical cap; (3) a right paratracheal stripe of 5 mm or more; and (4) deviation of the nasogastric tube, when present, to the right of the T4 spinous process. Thirty-seven patients (69%) had radiographic signs suggestive of aortic rupture on the initial anteroposterior chest film. The single patient in this group who actually had an aortic rupture died in the emergency department shortly after admission. The spine fracture could be identified on the initial chest radiograph in 19 (51%) of the 37 patients.

These results show that a widened mediastinum on chest radiographs after trauma is not a specific finding of aortic rupture. In these cases, the upper thoracic spine should be examined closely on the initial frontal chest radiograph for evidence of fracture. If a fracture of the upper thoracic spine is identified, an aortic rupture is unlikely in the absence of clinical signs and symptoms supporting this diagnosis.

Mediastinal widening on chest radiographs in patients with chest trauma has been considered the hallmark of mediastinal hemorrhage [1]. We examined the chest radiographs of patients with traumatic fractures of the upper thoracic and lower cervical spine to determine if widening of the superior mediastinum in these cases mimics the widening seen on chest radiographs in patients with aortic rupture.

Materials and Methods

The initial anteroposterior chest radiographs of 54 patients seen at Northwestern Memorial Hospital between 1975 and 1986 with acute fractures of the lower cervical and upper thoracic spine were reviewed. The vertebrae involved were from C6 to T8 (Table 1). The 46 men and eight women ranged in age from 15 to 72 years. The chest films were portable anteroposterior radiographs obtained with the patient supine and with a standard film-tube distance of 125 cm. Other available imaging studies were reviewed only after a decision was made based on the chest radiographs. These included angiography in six cases, venography in two, tomography in 50, and CT in five.

Each of the 54 chest radiographs was reviewed separately by two radiologists. When a disagreement occurred between the two reviewers, a decision was reached by consensus with a third radiologist. The clinical history revealed to the reviewers was that the patient was from the emergency department and had sustained chest trauma. The exact mechanism of trauma was not disclosed.

In each case the following measurements or observations were made: (1) mediastinal width at the level of the aortic knob; (2) presence or absence of a left apical cap; (3) right paratracheal stripe width; and (4) deviation of the nasogastric tube, when present, to the right. Whether a vertebral body fracture was present or suspected was also noted. Confirmation of the vertebral fractures was made subsequently by lateral radiography, CT, or tomography. This information was not known to the reviewers of the initial chest radiographs.

Received April 4, 1988; accepted after revision August 30, 1988.

¹ Department of Radiology, Northwestern University Medical School, 710 N. Fairbanks Ct., Chicago, IL 60611. Address reprint requests to L. F. Rogers.

² Present address: Department of Radiology, Milwaukee County Medical Complex, 8700 W. Wisconsin Ave., Milwaukee, WI 53226.

AJR 152:27-30, January 1989

0361-803X/89/1521-0027

© American Roentgen Ray Society

Results

Thirty-seven (69%) of the 54 patients with lower cervical or upper thoracic spine fractures had mediastinal widening on their initial chest radiographs. Only one of these patients had an aortic rupture, and he died on admission to the emergency

TABLE 1: Chest Radiographic Findings in 54 Patients with Spine Fractures

Vertebra(e) Involved	No. of Patients
With mediastinal widening:	
C6 facet	1 ^a
C6-C7	2
C7-T1 fracture dislocation	2
C7-T2	1
T1-T2 spinous process	1
T1-T2 fracture dislocation	1
T2-T3 spinous process	1
T2-T3 fracture dislocation	3
T3-T4 fracture dislocation	3
T3-T5	1
T4	2
T4 fracture with C6-T3 spinous process	1
T4-T5 fracture dislocation	7
T5-T6 fracture dislocation	4
T6-T7 fracture dislocation	5
T6-T8 fracture dislocation	1
T7-T8	1
Subtotal	37
Without mediastinal widening:	
T2-T4	1
T3-T4	1
T3-T4 fracture dislocation with C6 spinous process	1
T4-T5	1
T4-T5 fracture dislocation	3
T4-T7	1
T5-T6 fracture dislocation	2
T5-T6	1
T6-T7 fracture dislocation	3
T7-T8 fracture dislocation	2
T8	1
Subtotal	17
Total	54

^a Patient with aortic rupture.

department. Aortography was performed in six cases and CT in another five, and no aortic rupture was seen. In the remaining 25 cases, aortography and/or CT were not immediately performed because aortic rupture was not clinically suspected. We assumed that a traumatic rupture of the aorta was not present in these 25 cases because these patients survived their hospital admission. All 37 patients with mediastinal widening had at least one other radiographic finding suggestive of aortic rupture (Table 2). No specific radiographic sign of aortic rupture was found with greater or less frequency, except for deviation of the nasogastric tube (a nasogastric tube was in place in only four patients when the initial chest radiograph was obtained). The patient who did have aortic rupture had no radiographic findings to distinguish his findings from the remaining 36 patients and permit a specific diagnosis of aortic rupture.

Of the 54 chest radiographs initially reviewed, 17 patients with acute fractures of the upper thoracic spine ranging from T2 to T8 did not have mediastinal widening (Table 1). Rupture of the aorta was not suspected in any of these patients clinically or radiographically.

In 19 of the 37 patients with lower cervical and upper thoracic spine fractures who had mediastinal widening on chest radiographs, the fracture could be identified on the initial chest film. In two of these cases, the fracture was present on the initial chest radiograph but was missed both clinically and radiographically (Figs. 1 and 2). Both of these

TABLE 2: Chest Radiographic Signs of Aortic Rupture in 54 Patients with Spine Fractures

Radiographic Signs of Aortic Rupture	No. of Patients (%)
Mediastinal width ≥ 8 cm	28 (52)
Right paratracheal stripe ≥ 5 mm	32 (59)
Left apical cap	29 (54)
Deviation of the nasogastric tube to the right ^a	1 (2)
Normal mediastinum	17 (31)

^a Four patients had nasogastric tubes in place at the time of the initial chest film.

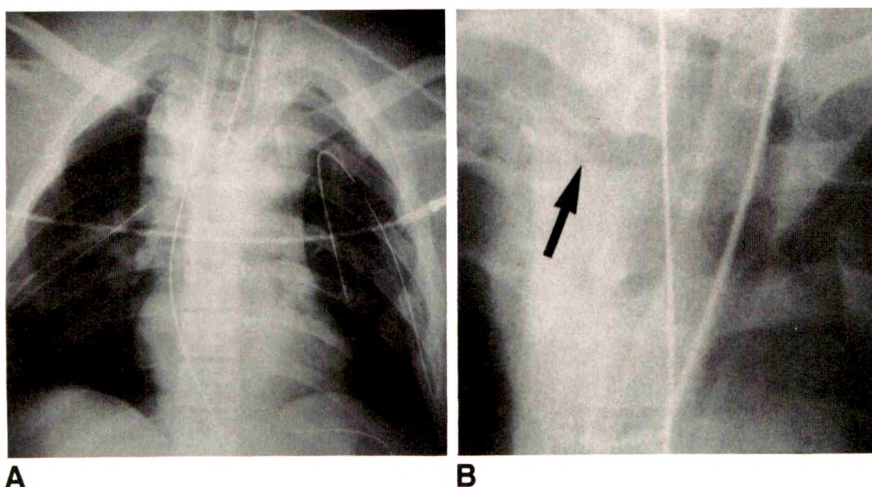


Fig. 1.—22-year-old man involved in motor-vehicle accident.

A, Initial chest film shows mediastinal widening, biapical capping, widening of right paratracheal stripe, and deviation of nasogastric tube to right.

B, Coned-down view of upper thoracic spine shows T2-T3 fracture dislocation with malalignment of lateral margins of vertebral bodies (arrow), which in retrospect was evident on initial chest radiograph.

patients had radiographic signs suggestive of aortic rupture. These included mediastinal widening and widening of the right paratracheal stripe in both patients and biapical capping and deviation of the nasogastric tube to the right of T4 in one of the patients. Both patients underwent aortography, which revealed intact aortas. In the remaining 18 cases, the fracture or fractures were diagnosed by tomography and lateral radiography.

A subtle fracture of T4-T5 was noted on an initial chest radiograph of a patient who was immediately immobilized (Fig. 3). An aortic rupture was not suspected clinically, and the mediastinal widening and apical capping were thought to be caused by bleeding associated with the fracture and/or nonaortic mediastinal hemorrhage.

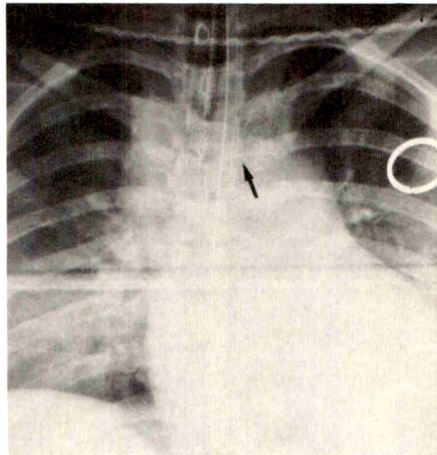
An aortic rupture was clinically and radiographically suspected in an unconscious patient involved in a motor-vehicle accident (Fig. 4). The initial chest radiograph did not include the lower cervical spine, and no disruption of the vertebral

column was noted. The oblique film from the angiogram revealed a C7-T1 dislocation that was subsequently confirmed with tomography. The patient had incomplete quadriplegia with a C6 level. It is not certain if movement during aortography contributed to the neurologic injury.

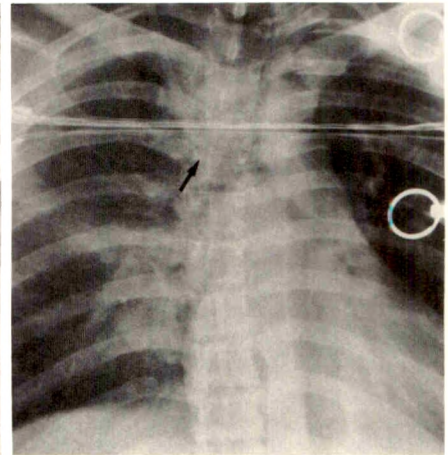
Discussion

The literature is replete with quantitative and descriptive criteria to suggest the diagnosis of aortic rupture in patients who have had chest trauma. Recently described criteria have included (1) mediastinal width equal to or greater than 8 cm [2], (2) the presence of a left apical cap [3], (3) a right paratracheal stripe of 5 mm or more [4], and (4) deviation of the nasogastric tube to the right of the T4 spinous process [5]. Although these criteria can assist in identifying patients with aortic tears, they are nonspecific because mediastinal

Fig. 2.—Chest radiograph in a 15-year-old girl who fell 6 m shows mediastinal widening, widening of right paratracheal stripe, and fracture of right clavicle. Also present is disruption of thoracic spine at T3-T4 with malalignment of spinous processes (arrow), which was not identified on chest film.

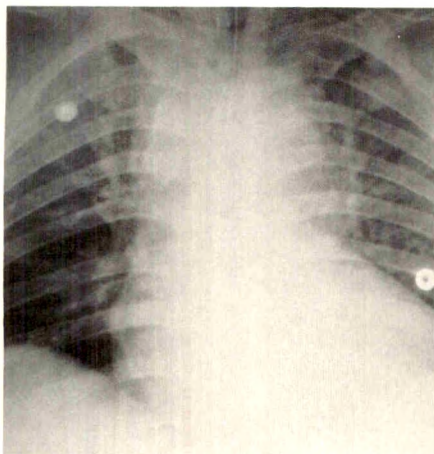


2



3

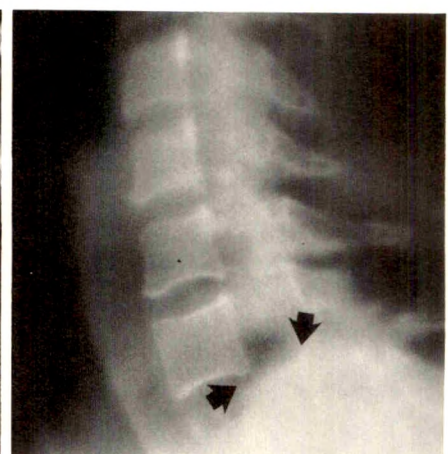
Fig. 3.—Chest radiograph of a 21-year-old man involved in motor-vehicle accident shows mediastinal widening and bilateral apical capping. In addition, subtle disruption of thoracic spine is noted at T4-T5 (arrow).



A



B



C

Fig. 4.—38-year-old motor-vehicle-accident victim.

A, Initial chest radiograph shows mediastinal widening, widening of right paratracheal stripe, and obscuration of aortic knob. Lower cervical spine is not included on film.

B, Aortography showed normal aorta. Oblique film from aortogram shows clinically unrecognized C7-T1 dislocation (arrows).

C, Tomogram confirms C7-T1 dislocation (arrows).

hemorrhage may result from both aortic and nonaortic causes [6]. In a series reported by Sandor [7], 14 (88%) of 16 patients sustaining chest trauma had mediastinal hemorrhage due to nonaortic causes that included vertebral body fractures, rib fractures, venous tears, arterial tears other than great vessels, inferior dissection of blood from the cervical region, and anterior dissection of blood from a paravertebral hematoma.

In our series of 54 patients with fractures of the lower cervical and upper thoracic spine (C6–T8), 37 (69%) had mediastinal widening and at least one other radiographic finding suggestive of aortic rupture. Only one of the 37 patients had an aortic rupture. The remaining 36 had mediastinal hematomas as a result of thoracic spine trauma. Our study shows that an acute fracture of the lower cervical or upper thoracic spine can be a significant cause of mediastinal hemorrhage. The resultant mediastinal widening noted on chest radiographs can mimic widening associated with aortic rupture. Gopalakrishnan and El Masri [8] recently noted that traumatic fractures of the sternum associated with spinal fractures can produce significant mediastinal widening that may be difficult to differentiate from widening caused by aortic rupture.

In two of our cases, the thoracic spine fracture was overlooked on the initial chest radiograph (Figs. 1 and 2). We stress the importance of examining the upper thoracic spine

for fracture in patients who sustain chest trauma. If mediastinal widening is present, both aortic and nonaortic causes of mediastinal hemorrhage must be considered. Our study suggests that if a fracture of the upper thoracic spine can be identified to account for the mediastinal widening, aortic rupture is unlikely in the absence of clinical signs and symptoms that support this diagnosis.

REFERENCES

1. Woodring JH, Loh FK, Kryscio RJ. Mediastinal hemorrhage: an evaluation of radiographic manifestations. *Radiology* **1984**; 151:15–21
2. Marsh DG, Sturm JT. Traumatic aortic rupture: roentgenographic indications for angiography. *Ann Thorac Surg* **1976**; 21:337–340
3. Simeone JF, Minagi H, Putman CE. Traumatic disruption of the thoracic aorta: significance of the left apical extrapleural cap. *Radiology* **1975**; 117:265–268
4. Woodring JH, Pulmano CM, Stevens RK. The right paratracheal stripe in blunt chest trauma. *Radiology* **1982**; 143:605–608
5. Tisnado J, Tsai FY, Als A, Roach JF. A new radiographic sign of acute traumatic rupture of the thoracic aorta: displacement of the nasogastric tube to the right. *Radiology* **1977**; 125:603–608
6. Seltzer SE, D'Orsi C, Kirshner R, DeWeese JA. Traumatic aortic rupture: plain radiographic findings. *AJR* **1981**; 137:1011–1014
7. Sandor F. Incidence and significance of traumatic mediastinal haematoma. *Thorax* **1967**; 22:43–63
8. Gopalakrishnan KC, El Masri WS. Fractures of the sternum associated with spinal injury. *J Bone Joint Surg [Br]* **1986**; 68-B:179–181

Transthoracic Aspiration Needle Biopsy: Value in the Diagnosis of Pulmonary Infections

Dewey J. Conces, Jr.¹
 Steven A. Clark²
 Robert D. Tarver¹
 G. Rudolph Schwenk²

We reviewed 441 transthoracic needle aspiration biopsies to evaluate the use of the procedure in the diagnosis of pulmonary infections. Sixty-seven (15%) of the biopsies were performed because pulmonary infection was suspected. In these 67 cases, a specific diagnosis was made in 45 (67%). In 46 cases in which infection was ultimately found to be present, aspiration biopsy identified the organism in 35 (76%). Overall, clinically useful information was obtained in 54 (81%) of the 67 biopsies performed for pulmonary infection. In 369 biopsies performed for suspected malignant neoplasm, pulmonary infection was diagnosed in 13. The only significant complication was pneumothorax, which occurred in 18% of the biopsies. Chest tube placement was required in 5% of the biopsies.

We conclude that transthoracic aspiration needle biopsy is of value in the diagnosis of suspected pulmonary infections.

Pulmonary infections are a common clinical problem both in persons who have normal immune defenses and in those who are immunocompromised. Ideally, the causative organism should be identified so that antibiotic therapy can be tailored for a specific organism. This is especially true in immunocompromised patients in whom pneumonia develops rapidly and is caused by a wide range of organisms. Noninvasive techniques such as sputum examination and culture may identify the causative organism. When these studies are nondiagnostic, a choice must be made between empiric therapy and an invasive diagnostic test. Although immunocompetent patients with community-acquired pneumonias may be treated empirically, the nature of pneumonias in immunosuppressed individuals frequently dictates that a more aggressive approach be taken in identifying the etiologic agent.

A variety of invasive techniques are available that allow identification of the infectious agent. Bronchoscopic biopsy, bronchoalveolar lavage, percutaneous needle biopsy, and open-lung biopsy have been used to diagnose the cause of pneumonias [1-4]. To evaluate the usefulness of transthoracic needle aspiration biopsy in the diagnosis of pulmonary infections, we reviewed 441 such biopsies.

Materials and Methods

From January 1983 to April 1988, 441 transthoracic needle aspiration biopsies were performed at our institution. In 369 of these, the radiographic abnormality was believed to represent either a primary malignancy or a metastatic lesion. In 13 patients of this group, infection was found to be the sole cause of the radiographic abnormality. Suspected pulmonary infection was the indication for 67 of the biopsies. The results of these 80 biopsies are evaluated in this study.

The 80 biopsies were performed on 76 patients (51 men, 25 women). The age range was 18-94 years (average, 49). Four patients had two biopsies performed. The lesions biopsied included nodule or nodular infiltrate (35), infiltrate (31), cavity (13), and mediastinal fluid collection (one). Two infiltrates were diffuse, and the others were focal. In the patients biopsied because of suspected infection, 20 had no underlying conditions that would predis-

Received July 11, 1988; accepted after revision August 19, 1988.

¹ Department of Radiology, Indiana University Hospital, X-64, 926 W. Michigan St., Indianapolis, IN 46223. Address reprint requests to D. J. Conces, Jr.

² Department of Pathology, Indiana University School of Medicine, Indianapolis, IN 46223.

AJR 152:31-34, January 1989

0361-803X/89/1521-0031

© American Roentgen Ray Society

pose them to infection. In 47 patients, a variety of underlying conditions were present that compromised the immune defenses: renal transplant (20), heart transplant (four), bone marrow transplant (four), lymphatic malignancy (10), myelodysplasia (three), solid malignant neoplasm being treated with chemotherapy (four), and treatment with steroids (two). In the patients with a suspected malignant neoplasm, 10 had no known underlying condition and three had an extrathoracic malignancy with suspected thoracic metastasis.

Seventy-two of the biopsies were performed on hospitalized patients, and eight were performed on outpatients. Platelet count, prothrombin time, and partial thromboplastin time were obtained in 50 of the patients before biopsy. A platelet count alone was obtained in 20 patients, prothrombin time and partial thromboplastin time alone were obtained in five patients, and no clotting studies were obtained in three patients. Two patients had mild elevation of prothrombin time, and two patients had mild elevation of partial thromboplastin time. These abnormalities were mild, so they did not preclude biopsy. Seven patients had severe thrombocytopenia and were given platelet transfusions before biopsy.

The biopsies were performed with fluoroscopic guidance in 72 cases and with CT guidance in eight. For all biopsies, a coaxial system with a 19-gauge outer guide needle and either a 22- or 23-gauge inner Greene biopsy needle (DGBS-1 or DGBS-2, Cook, Bloomington, IN) was used. During suspended respiration, the guide needle with stylet in place was advanced through the pleura. It was then advanced by using either intermittent fluoroscopy or repeat CT scanning for guidance until the tip was either in the lesion or immediately adjacent to it. The stylet was then removed from the guide needle, and the biopsy needle attached to a 10-ml syringe was advanced to the end of the guide needle. The biopsy was then obtained by applying suction and advancing the needle with multiple, rapid, short, reciprocating movements. Suction was released, and the biopsy needle was removed. The stylet was reinserted into the guide needle, which was left in place.

The specimen was then expressed onto a sterile slide. Smears were prepared by a cytopathologist who was in attendance at all biopsies. Paired slides were made of each sample. The initial sample had one slide placed in 95% ethyl alcohol for later staining with Papanicolaou stain. The other was air dried and immediately stained with a modified Wright-Giemsa stain (Hema 3, Curtin Matheson Scientific, Houston, TX). Staining with the modified Wright-Giemsa stain took approximately 1 min. The slide was then reviewed by the cytopathologist who gave a preliminary interpretation. If the sample showed only normal lung elements, the needle was repositioned and another sample was obtained. This was repeated until the biopsied material showed pathologic changes. When inflammatory changes were noted, several additional samples were obtained from which dried slides were made for later staining with microbiologic stains. Samples were also placed in thioglycolate broth for culture. Periodically during the sampling, additional slides were stained and examined to ensure that the samples being obtained remained adequate and representative. The number of biopsy samples obtained ranged from 3 to 20 (average, 9). The guide needle was removed only after sufficient material was obtained.

Chest radiographs were obtained immediately after completion of the biopsy and again 4 hr later to determine if a pneumothorax was present. Any pneumothorax found was either observed or treated with a chest tube, depending on its size and the presence of symptoms.

The laboratory studies performed on the biopsy specimens varied. Cytologic stains (modified Wright-Giemsa and Papanicolaou) were used in 78 biopsies. The following microbiologic stains were used: Gram stain (64), Giemsa stain (64), Gomori's methenamine-silver

stain (64), modified acid-fast stain (64), auramine rhodamine stain (74), acid-fast stain (74), and *Legionella* direct fluorescent antibody stain (23). The thioglycolate broth was plated out onto specific culture materials: aerobic (66), anaerobic (28), fungal (72), acid-fast bacilli (73), *Legionella* (21), viral (15), *Mycoplasma* (11), and *Chlamydia* (three).

Results

The results of the 67 biopsies done because of suspected infection can be divided up into four groups: infectious, specific noninfectious, nonspecific noninfectious, and inadequate. Infectious organisms were found in 35 (52%) of the biopsies. The following organisms were identified: *Aspergillus* (eight), anaerobes (five), *Pseudomonas aeruginosa* (four), *Nocardia asteroides* (three), cytomegalovirus (three), *Legionella* (two), *Cryptococcus neoformans* (two), *Staphylococcus aureus* (one), *Staphylococcus epidermidis* (one), *Rhodococcus* (one), *Propionibacterium acnes* (one), *Mycobacterium tuberculosis* (one), *Mycobacterium kansasii* (one), *Phycomyces* (one), *Histoplasma capsulatum* (one), *Candida* (one), and *Ustilago* (one). With the exception of the infections caused by anaerobes and two of the cytomegalovirus infections, the infections were caused by single organisms. In infections caused by anaerobes, one to nine different organisms were isolated from the lung. In two cases of cytomegalovirus infection, nuclear inclusion bodies characteristic of the infection were identified. In these cases, the cytomegalovirus infection was considered subclinical and not responsible for the radiographic findings, which were attributed to *Nocardia* in one case and *Ustilago* in the other.

In 10 patients, a specific noninfectious diagnosis was made. Benign causes were pulmonary infarct (three), hematoma (one), lipoid pneumonia (one), and radiation change (one). Malignant causes were lymphoma (two), bronchoalveolar carcinoma (one), and chronic lymphocytic leukemia (one). The bronchoalveolar carcinoma was a new diagnosis, but the other neoplasms represented pulmonary involvement of a previously diagnosed malignancy.

Biopsies in 18 patients provided nonspecific results. These revealed varying degrees of inflammatory change with no organism identified. In eight patients, the results of the biopsy were thought to be accurate and to indicate a resolving inflammatory process. These patients were observed, and the radiographic abnormality resolved without therapy. Empiric therapy was used in five patients who were thought to have an infection on the basis of clinical findings. Two patients had positive blood cultures and were treated accordingly. A repeat biopsy was performed in one patient, and *Histoplasma* was identified in the sample from the second biopsy. A nasal biopsy was performed in one patient in which the needle biopsy suggested Wegener granulomatosis. One patient had an open-lung biopsy, which revealed a pulmonary infarct.

In four patients, the material obtained at biopsy was so scant that no diagnosis could be made. These biopsies were considered inadequate. Empiric therapy was used in two of these patients, one was observed, and one had a positive blood culture.

Of the 67 transthoracic needle aspiration biopsies performed because of suspected infection, a specific diagnosis was made in 45 (67%). Ultimately 46 cases were thought to be due to an infectious process. Of these 46 cases, an organism was identified by biopsy in 35 (76%). Clinically useful information (specific result or finding of nonspecific inflammation thought to represent resolving inflammatory process) was obtained in 54 biopsies (81%).

In 13 of the patients biopsied because of suspected malignant neoplasm, a diagnosis of pulmonary infection was made. The following organisms were identified: *Aspergillus* (two), *Hemophilus influenzae* (two), *Nocardia asteroides* (one), *Serratia marcescens* (one), viridans streptococci (one), *Mycobacterium tuberculosis* (one), *Mycobacterium kansasii* (one), *Actinomyces* (one), *Phycomyces* (one), *Blastomyces dermatitidis* (one), degenerate septate hyphae (one), and mixed infection (*Candida*, *Proteus mirabilis*, viridans streptococci, and *Corynebacterium*) (one). In one patient, both *Aspergillus* and *Nocardia* were identified.

In 57 of the 80 biopsies studied, no complications occurred. Contusion occurred in nine, and hemoptysis occurred in two. Pneumothorax developed in 14 patients; 10 of these patients were observed, and four required placement of a chest tube.

The results of the laboratory studies performed on the biopsy material varied. Of the 48 transthoracic needle aspiration biopsies in which infection was identified, both positive microbiologic stain and culture were positive in 23 cases. Positive culture and negative stain occurred in 13 biopsies. Eight biopsies had negative culture and a positive microbiologic stain. Of the 44 biopsies that had organisms identified on microbiologic studies, cytologic stains were positive for organisms in 18 and showed only inflammatory changes in 26. In six cases, cytology identified organisms that were not found on microbiologic studies. In four of these biopsies, the microbiologic studies were negative, and in two, cytology showed changes caused by cytomegalovirus that were not detected on the microbiologic studies.

In 68 of the 80 cases studied, transthoracic needle aspiration biopsy was the only invasive procedure performed. Bronchoscopy, which was performed in five patients, was nondiagnostic in four and yielded the same organism as aspiration biopsy in one. Open-lung biopsy was performed in two patients. In the first case, pulmonary infarct was diagnosed in a patient in whom the aspiration biopsy had shown only inflammatory change. In the second case, in which aspiration biopsy had identified *Mycobacterium kansasii*, the open-lung biopsy was nondiagnostic. In single cases, pleural fluid, CSF, and cutaneous abscess pus were cultured. These grew organisms that were identical to those found on aspiration biopsy of the lung. One patient in whom nuclear inclusion bodies characteristic of cytomegalovirus were shown on aspiration biopsy had positive cytomegalovirus deoxyribonucleic acid probe on an endoscopic biopsy of gastric mucosa. One patient had a sinus biopsy, which resulted in a diagnosis of Wegener granulomatosis. Blood cultures were positive in five patients. In three cases in which the biopsy was either inadequate or nonspecific, blood cultures identified organisms. In two cases

in which organisms were identified on aspiration biopsy, blood cultures were positive for additional organisms.

Discussion

Leyden in 1883 [5] reported the first use of transthoracic needle aspiration biopsy when he diagnosed a case of pneumococcal pneumonia. There was only limited use of the technique until the 1960s and 1970s. At that time, because of the development of thin needles, improved image intensifiers, and sophisticated cytologic techniques, transthoracic needle aspiration biopsy was shown to be useful in the diagnosis of malignant neoplasms. Several reports have described the usefulness of this technique in the diagnosis of pulmonary infections [3, 6–9]. In these studies, the etiologic organism was identified in 64–80% of the patients. Despite this high diagnostic yield, transthoracic needle aspiration biopsy has not been used as frequently in the diagnosis of pulmonary infections as it has been in the diagnosis of pulmonary neoplasms.

The results of our study show that transthoracic needle aspiration biopsy is useful in the diagnosis of pulmonary infections. A specific diagnosis was possible in 67% of the cases of suspected infection. In those cases in which infection was present, biopsy identified the etiologic organism in 76%. Most importantly, it provided clinically useful information on which treatment decisions were based in 80% of the cases.

Like results of any diagnostic procedure or test, the results of transthoracic needle aspiration biopsy must be interpreted in light of the clinical findings. A biopsy that shows nonspecific inflammation may be interpreted as representing a resolving infection in an asymptomatic individual who may then be observed. The same result in an individual whose clinical symptoms indicate an infection should be questioned. Also, the identification of an organism does not necessarily indicate an active infection, as was seen here in two cases in which cytomegalovirus was identified but believed to represent a subclinical infection.

Several factors may contribute to a false-negative transthoracic needle aspiration biopsy in a patient with pulmonary infection. The institution of antibiotic therapy before the biopsy is performed may result in a negative biopsy. Therefore, the biopsy should be performed if possible before antibiotic therapy is started. This may also explain why in some of the biopsies in this series the microbiologic stains were positive but the cultures were negative. Another pitfall is an inadequate volume of biopsy material. This problem can be minimized by obtaining multiple samples. A coaxial needle system allows multiple samples to be obtained rapidly after the initial placement of the guide needle. This additional material may be divided in such a fashion that adequate amounts are available for each of the numerous stains and cultures that are performed. A third potential problem is sampling error with uninfected parenchyma being biopsied. In this study, all biopsies were performed by a radiology-cytology team. This team approach to biopsies improves the reliability and adequacy of the biopsy specimens [10]. By reviewing each sample as it is

obtained, the cytologist can ensure that the samples are from involved parenchyma.

In previous studies, saline has been injected through the needle and then aspirated [3, 6–9]. If bacteriostatic saline is used, the growth of organisms may be inhibited. We also think that samples obtained by using nonbacteriostatic saline are not optimal for the identification of infectious organisms. The saline dilutes the sample obtained. This decreases the number of organisms in a given volume and reduces the chance of their being identified. We think that a "dry" sample of lung that has not been diluted with saline is best.

The results of this series show that multiple laboratory studies should be performed on the biopsy specimen. In only 23 of the 44 patients with positive microbiologic studies were both the stains and culture positive. In the remaining 21 cases, only the stain or only the culture was positive. Because of the wide variety of organisms that may produce pneumonia in the immunocompromised patient, many different stains and culture media should be used. Cytologic examination of the biopsy material also was useful; in six patients, organisms were seen on cytologic stains that were not detected on any of the microbiologic studies. The staff of the cytology laboratory used in this study had extensive experience in handling needle-biopsy specimens. The staff of the microbiology laboratory was accustomed to evaluating samples from patients suspected of having opportunistic infections. To achieve optimal results with transthoracic needle aspiration biopsy, excellent cytology and microbiology laboratories are needed.

The 13 cases of infection found in patients suspected of having a malignant neoplasm support the value of cytologic monitoring of the biopsy specimens as the specimens are obtained. The identification of an inflammatory and not neo-

plastic process while the biopsy was in progress allowed samples to be obtained for the necessary microbiologic studies.

The complication rate in this series is acceptable, in view of the importance of obtaining a specific diagnosis. The overall frequency of pneumothorax was 18%, and in only 5% of the cases was a chest tube required. Only two patients had hemoptysis, which was self-limited.

REFERENCES

1. Lauver GL, Hasan FM, Morgan RB, Campbell SC. The usefulness of fiberoptic bronchoscopy in evaluating new pulmonary lesions in the compromised host. *Am J Med* 1979;66:580–585
2. Stover DE, Zaman MB, Hajdu SI, Lange M, Gold J, Armstrong D. Bronchoalveolar lavage in the diagnosis of diffuse pulmonary infiltrates in the immunosuppressed host. *Ann Intern Med* 1984;101:1–7
3. Bandt PD, Blank N, Castellino RA. Needle diagnosis of pneumonitis: value in high risk patients. *JAMA* 1972;220:1578–1580
4. Cheson BD, Samlowski WE, Tang TT, Spruance SL. Value of open-lung biopsy in 87 immunocompromised patients with pulmonary infiltrates. *Cancer* 1985;55:453–459
5. Leyden T. Über infektiöse Pneumonie. *Dtsch Med Wochenschr* 1883;9:52–54
6. Castellino RA, Blank N. Etiologic diagnosis of focal pulmonary infection in immunocompromised patients by fluoroscopically guided percutaneous needle aspiration. *Radiology* 1979;132:563–567
7. Zavala DC, Schoell JE. Ultrathin needle aspiration on the lung in infectious and malignant disease. *Am Rev Respir Dis* 1981;123:125–131
8. Davidson M, Tempest B, Palmer DL. Bacteriologic diagnosis of acute pneumonia. Comparison of sputum, transtracheal aspirates, and lung aspirates. *JAMA* 1976;235:158–163
9. Palmer DL, Davidson M, Lusk R. Needle aspiration of the lung in complex pneumonias. *Chest* 1980;78:16–21
10. Conces DJ Jr, Schwenk GR, Doering PR, Glant MD. Thoracic needle biopsy: improved results utilizing a team approach. *Chest* 1987;91:813–816

Mammographic Film-Processor Temperature, Development Time, and Chemistry: Effect on Dose, Contrast, and Noise

Carolyn Kimme-Smith¹
 Peter A. Rothschild²
 Lawrence W. Bassett¹
 Richard H. Gold¹
 Charles Moler¹

Six different combinations of film-processor temperature (33.3°C, 35°C), development time (22 sec, 44 sec), and chemistry (Du Pont medium contrast developer [MCD] and Kodak rapid process [RP] developer) were each evaluated by separate analyses with Hurter and Driffield curves, test images of plastic step wedges, noise variance analysis, and phantom images; each combination also was evaluated clinically. Du Pont MCD chemistry produced greater contrast than did Kodak RP chemistry. A change in temperature from 33.3°C (92°F) to 35°C (95°F) had the least effect on dose and image contrast. Temperatures of 36.7°C (98°F) and 38.3°C (101°F) also were tested with extended processing. The speed increased for 36.7°C but decreased at 38.3°C. Base plus fog increased, but contrast decreased for these higher temperatures. Increasing development time had the greatest effect on decreasing the dose required for equivalent film darkening when imaging BR12 breast equivalent test objects; ion chamber measurements showed a 32% reduction in dose when the development time was increased from 22 to 44 sec. Although noise variance doubled in images processed with the extended development time, diagnostic capability was not compromised.

Extending the processing time for mammographic films was an effective method of dose reduction, whereas varying the processing temperature and chemicals had less effect on contrast and dose.

The recent introduction of lower-dose mammographic screen-film combinations [1], coupled with new mammographic X-ray units that produce a low milliamperesecond output (because of small focal spots and/or single-phase generators), have revived interest in further reducing the radiation dose. Film-development temperature and development time are both known to affect film speed, contrast, and base-plus-fog level (the optical density of unexposed portions of the film) [2]. Base plus fog is also affected by potassium bromide and other antifoggants used in present-day developing solutions, particularly at temperatures above 32.2°C (90°F). Because the processor temperature may drift if the temperature regulator is defective, temperature control is a constant concern in film development. However, the amount of time the film is kept in the developing solution does not vary enough from one radiograph to the next to cause changes in image quality. Development time should be sufficient to allow full development of exposed grains of silver halide but should not be so long as to cause an increase in base plus fog [3]. In a 90-sec processor, the nominal time that the film is in the developer is 22 sec. Experiments done in the 1950s with Kodak No-Screen Medical X-ray film processed at 20.5°C (69°F) showed that by simply doubling the time the film was in the developer from 4 to 8 min, both speed and contrast could be increased without significantly increasing the base-plus-fog level [4]. Expert photographers know that film speed can be increased by "push-processing" [5]; that is, by prolonging the time that the film is in the developer. Tabar and Dean [6] have described the successful implementation of longer film-development time for mammography. Although their experience with increased development time was with Kodak RP (rapid process) chemistry, other chemistries could be expected to

Received April 4, 1988; accepted after revision September 19, 1988.

¹ Department of Radiological Sciences, Iris Cantor Mammography Screening Center, UCLA School of Medicine, Los Angeles, CA 90024-1721. Address reprint requests to C. Kimme-Smith.

² Department of Radiology, University of California, San Francisco, San Francisco, CA 94143.

AJR 152:35-40, January 1989

0361-803X/89/1521-0035

© American Roentgen Ray Society

perform equally well. We describe a series of experiments to quantify the effects of temperature change, processor chemistry, and prolonged development time on single-emulsion mammographic film images.

Materials and Methods

To be compatible with all other film processors in our X-ray department, the Kodak M6 RP X-OMAT 90-sec film processor in our mammographic suite had been operating with Du Pont MCD (medium contrast developer) chemical solutions at 33.3°C (92°F). For our experiments, we first changed from Du Pont to Kodak chemistry and then increased the developing temperature to 35°C (95°F). We found that temperatures above 35°C were difficult to control in our processor, so only H and D (Hurter and Driffield) curves, rather than the complete experiments described in the following paragraph, were recorded for these higher temperatures. Next, the gears on the mammographic processor were changed to decrease the transport speed and to extend the standard 90-sec processing time to 3 min. Because of the nature of our processor, we had to lengthen the entire processing time in order to change the film development time from 22 to 44 sec. The replenishment of chemicals was then adjusted for the slower speed. Later, we replaced the Kodak RP chemistry with Du Pont MCD chemistry. Table 1 describes the order of each parameter variation.

For each of the six experiments, we exposed the Kodak Ortho M (OM-SO177) film to a Du Pont Cronex Cine sensitometer with green light so that an H and D curve could be plotted. The OM/MinR film-screen combinations were exposed to four test objects in order to quantify changes in contrast and spatial resolution. Two of the test objects, an acrylic step wedge of 1.58-mm increments and a piece of acrylic coated with particles of aluminum (simulating calcifications) (Fig. 1), were exposed at 28 kVp with a grid and at 25 kVp without a grid at two ranges of optical density: from 0.5 to 2.5 and from 0.3 to 1.5 optical density (OD). The aluminum specks ranged in diameter from 1.2 to 0.7 mm. Both the step wedge and the simulated calcifications were placed on a 4.4-cm-thick block of acrylic, representing a magnification factor of 1.07 for a gridless exposure and 1.08 for an exposure made with a moving grid. The other test objects were a Kodak ITO Pathé lucite phantom and an epoxy-based, tissue-equivalent (BR12) phantom embedded with breast tissue and simulated calcifications. These were exposed with the automatic exposure timer so that an OD of 1.0 predominated. Noise was investigated only in experiments 1 and 5 because these experiments represented the greatest exposure difference. Two 0.73 OD step wedge images from the lower-exposure images (0.3–1.5 OD) and two 0.75 OD step

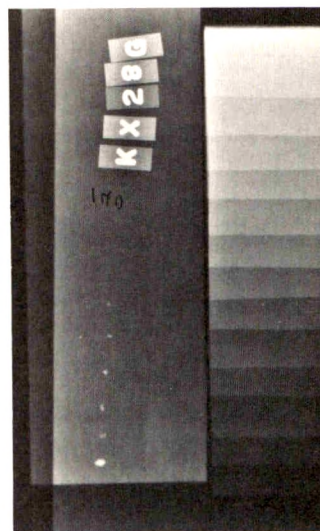


Fig. 1.—Lucite wedge with 1.58-mm steps and high-contrast resolution target containing aluminum specks representing microcalcifications (0.98 mm in their largest dimension); wedge was imaged on top of 4 cm of acrylic at 28 kVp with grid and processed for 3 min.

wedges from the higher-exposure images (0.5–2.5 OD) were scanned with a Joyce Loebel microdensitometer. The four images had been exposed at 25 kVp without a grid; one film in each pair was processed with Du Pont chemical solutions at 33.3°C for 90 sec, and the other film was processed at 35°C for 3 min. The second set of images from the higher-exposure wedge images tested whether the results were independent of the wedge position. A Wiener spectrum was not calculated because of the large number of points needed and because of the small variation in OD in the scanned data when the long, thin aperture required for a Wiener spectrum was used. The microdensitometer aperture consisted of a 0.05 mm × 0.05 mm aperture, and the 5-mm linear scan was magnified 20× and sampled every 0.2 mm. Means and standard deviations were computed from the 25 points on each scan. Four scans from different areas of each image were treated similarly so that variations between standard deviations could be assessed.

Tabar and Dean [6] have suggested that mammograms that are imaged without a grid and developed for 44 sec have as much contrast as mammograms that are imaged with a grid and developed for 22 sec. To test this hypothesis, we imaged an acrylic step wedge with 1.58-mm steps and placed it on top of 3.6 and 4.8 cm of additional acrylic. Two exposures with different techniques were each repeated twice and developed at 22 and 44 sec with Du Pont chemistry at 33.9°C (93°F). The first exposure was made at 28 kVp with a grid, and the second exposure was made at 26 kVp without a grid (our usual clinical techniques). Background OD ranged from 0.93 to 0.8 in the four films. In addition, calibrated calcium chips ranging in size from 0.3 to 1 mm also were imaged for all four techniques. The step-wedge densities were measured with a densitometer and plotted in a manner similar to that shown in Figure 1. The calcifications were subjectively evaluated for visibility and contrast.

For each parameter change, the Kodak and BR12 test objects were evaluated before any clinical images were processed with the new parameter variation. When the test object images were judged to be diagnostic, the processor modifications were used for routine mammography. For those patients who had earlier mammograms and who were now having follow-up studies, comparisons between two or more processing parameter variations were possible.

Dose reduction was measured by imaging a 4-cm-thick BR12 tissue-equivalent test object under automatic exposure control with a calibrated Victoreen ion chamber interposed in the beam. Each exposure was varied by adjustments in the automatic exposure control until optical densities of films developed for 22 sec were within 0.1 OD of films developed for 44 sec.

TABLE 1: Processor Parameter Variations Showing Order of Six Experiments

	22-Sec Development	44-Sec Development
Kodak RP chemistry		
33.3°C (92°F)	2	NT
35°C (95°F)	3	4
Du Pont MCD chemistry		
33.3°C (92°F)	1	6
35°C (95°F)	NT	5

Note.—The numbers in the second column refer to the order in which each combination of parameters was tested. RP = rapid process; MCD = medium contrast developer. NT indicates that these combinations were not tested, because these temperature variations had so little effect on dose and contrast.

Results

Sensitometer strips were processed for all six experiments. Table 2 compares relative film speed, film gamma, average gradient, and base plus fog for each parameter tested. Relative film speed assumes that experiment 1 had a speed of 100. The speed of each experiment was compared with the speed of experiment 1. Film gamma is computed from the maximum slope of the H and D curve (usually between 1.4 and 2.3 OD). The average gradient is the slope of the H and D curve between 0.25 OD plus base plus fog and 2.0 OD plus base plus fog. The largest variations in parameters occurred from experiments 2 to 5, in which chemistry, development time, and temperature were varied (Fig. 2). Although the maximum gradient varied over all three parameters, the average gradient showed a variation of only 0.29.

The exposed step-wedge OD values for the gridless 0.3 to 1.5 OD range best illustrate the contrast changes resulting from these experiments (Fig. 3). The 3-min processing (44-sec developing) required 40 mAs, whereas the 90-sec processing (22-sec developing) required 63 mAs. As seen in Table 2, Du Pont MCD chemistry increased film contrast when combined with extended processing. Both the H and D curves and the step-wedge graph show that temperature variations between 33.3°C and 35°C did not affect contrast or speed significantly. This observation meant that two of the eight possible parameter variations (Table 1) did not need to be tested. Experiment 6 reconfirmed the independence of temperature for the longer development time, as was observed in experiments 2 and 3 for the shorter development time. H and D curves obtained for Du Pont chemistry and 3-min processing at 33.3°C, 34.4°C, 36.7°C, and 38.3°C (i.e., 92°F, 94°F, 98°F, and 101°F) showed increased speed up to 36.7°C but decreased to 34.4°C values when the temperature went to 38.3°C. Table 3 gives the relative speed, gamma, contrast, and base plus fog for these temperature changes. Whereas speed was enhanced at 36.7°C, contrast decreased and the processor thermostat could not keep the temperature at a uniform level. Variations above 36.7°C decreased speed and increased both film artifacts and base plus fog.

The ability to identify simulated calcifications was not significantly affected by changes in temperature, processing time, or chemistry. Eight of nine high-contrast aluminum gran-

ules could be identified in all but the underexposed OD images. A slight increase in target visibility for Du Pont chemistry that occurred when the processing was changed from 33.3°C/90 sec (experiment 1) to 35°C/3 min (experiment 5) was probably due to increased contrast. The Kodak chemistry experiments for the same parameter variations (experiments 2 and 4) did not have as much improvement in contrast.

The noise analysis for experiments 1 and 5 was designed to quantify the increased quantum mottle expected from the lower exposure of the film developed at 44 sec. The step wedges selected for analysis had a diffuse densitometer value of 0.73 and 0.75 OD. The microdensitometer scans of these wedge images had ranges of ± 0.18 OD values around 0.75 OD when the film samples were scanned. The film developed for 44 sec had a 50% greater variation from the mean density

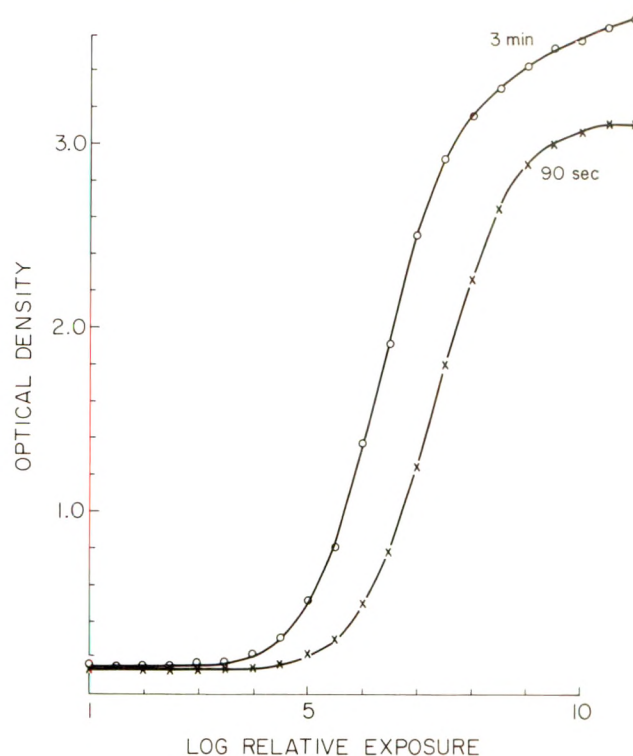


Fig. 2.—Hurter and Driffield curves of a sensitometer strip (green spectrum) processed for 90 sec and for 3 min (experiments 2 and 5).

TABLE 2: Film Changes Due to Processor Parameter Variations

	Kodak RP Chemistry		Du Pont MCD Chemistry	
	33.3°C (92°F)	35°C (95°F)	33.3°C (92°F)	35°C (95°F)
Relative film speed ^a				
22-sec development	115	115	100	NT
44-sec development	NT	145	155	158
Film gamma				
22-sec development	3.81	3.81	4.05	NT
44-sec development	NT	3.88	4.43	4.45
Average film gradient				
22-sec development	2.73	2.73	3.02	NT
44-sec development	NT	2.82	3.02	3.02
Base plus fog				
22-sec development	0.15	0.15	0.15	NT
44-sec development	NT	0.15	0.15	0.16

Note.—RP = rapid process; MCD = medium contrast developer; NT = not tested.

^a With respect to speed used in experiment 1.

of 0.73 OD than the film developed for 22 sec. Specifically, the film processed for 90 sec had a standard deviation of 0.05 OD from a mean of 0.73 OD, whereas the film processed for 3 min had a standard deviation of 0.08 OD from the same

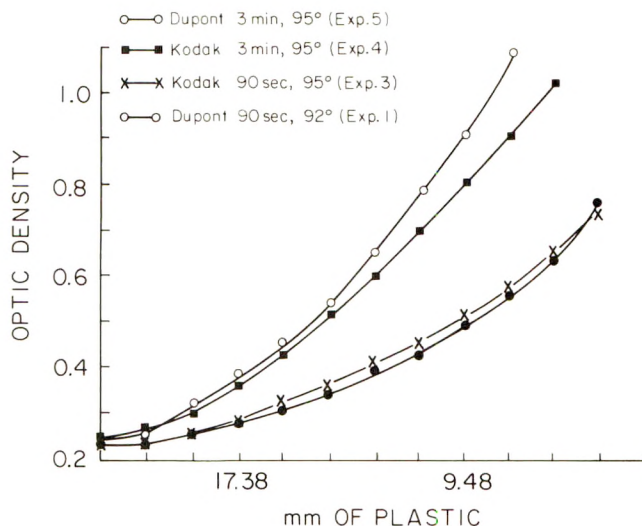


Fig. 3.—Densitometer values read from step wedge in Fig. 1 are plotted for a 25-kVp gridless exposure with a density range of 0.3 to 1.5 optical density.

TABLE 3: Developer Temperature Effects for Du Pont Chemistry with 3-Min Processing Time

Temperature	Relative Film Speed ^a	Film Gamma	Average Gradient	Base Plus Fog
33.3°C (92°F)	125	4.43	3.02	0.15
34.4°C (94°F)	145	4.37	3.02	0.15
36.7°C (98°F)	182	4.14	2.97	0.16
38.3°C (101°F)	138	4.15	3.02	0.17

^a Compared with Du Pont chemistry, 90 sec, 33.3°C (92°F).

mean. Because the film processed for 3 min required less radiation to acquire 0.73 OD values, the quantum mottle could be expected to be greater for these samples. The increase in microdensitometer variance for the lower-dose samples is consistent with increased quantum mottle.

The comparison of step-wedge films exposed with a grid and developed for 22 sec and a film exposed without a grid and developed for 44 sec showed increased contrast for the extended-process, gridless exposure. When contrast was measured between 1.0 and 1.9 OD, the slope of the plotted step-wedge OD values was 0.13 for the exposure made with a grid and developed for 22 sec compared with 0.15 for the exposure made without a grid and developed for 44 sec. This contrast difference is similar to contrast differences for exposures obtained with a grid and without a grid and developed for 22 sec. However, the use of a grid made less difference in contrast between the films developed for 44 sec.

Although this wedge experiment would seem to validate the hypothesis that grids are less necessary when films are developed with extended processing, the calcium-speck resolution phantom showed that targets below 0.5 mm in diameter were not as visible in the gridless, push-processed exposures (background density of 0.93) as they were in the exposures developed for 22-sec and made with a grid (background density of 0.80). Scatter was provided by 4.8 cm of acrylic for these images.

Dose measurements showed that images processed with Du Pont chemistry at 33.3°C for 90 sec required 1.36 R (0.35 mC/kg) skin exposure compared with 0.895 R (0.23 mC/kg) for images processed with Du Pont chemistry at 35°C for 3 min. This represents a dose reduction of 34%.

None of the test object images were judged to be so poor as to preclude clinical imaging. Figure 4 illustrates clinical imaging with experiments 1 and 2, in which only the chemistry varied, whereas Figure 5 illustrates clinical imaging with a variation of both chemistry and temperature. Figure 6 illus-

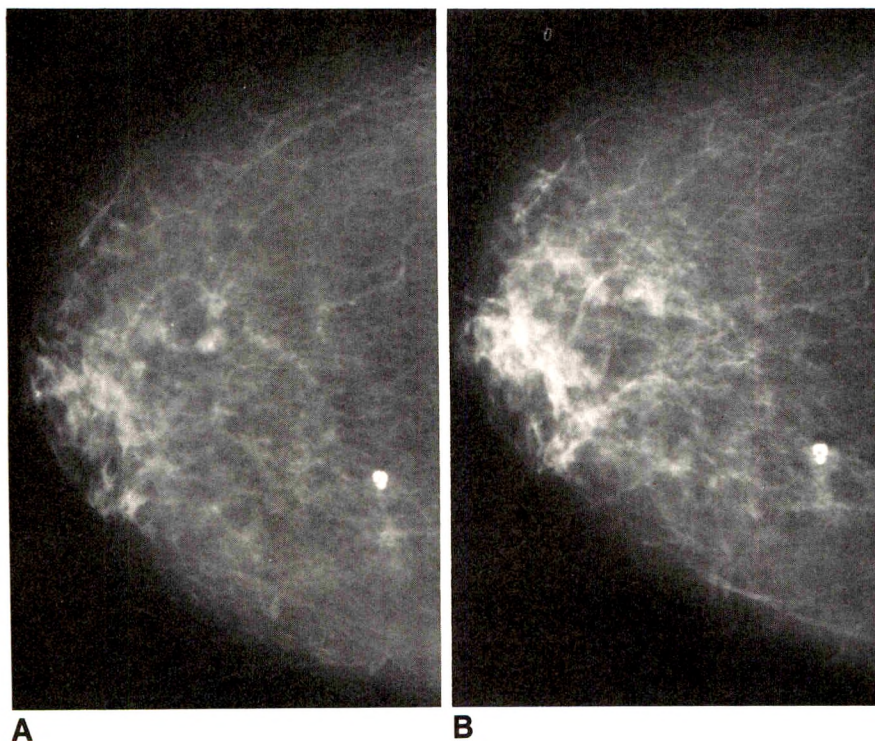


Fig. 4.—A, Breast imaged at 28 kVp, with a grid, at 33.3°C for 90 sec. Du Pont chemistry was used.

B, 1 year later, same breast and same view are imaged with same technique and processor parameters, but with Kodak chemistry.

trates variations of all three parameters for imaging a fatty breast. Figures 7A and 7B represent the same variations in parameter as those illustrated in Figure 6, but for a dense breast with a silicone implant. Figure 7C illustrates the increased contrast that the Du Pont chemistry provides when film is developed for 44 sec.

Discussion

Every effort should be made to decrease the radiation dose without adversely affecting image quality. This can be done

by means of a variety of methods. One method uses the shorter exposures that are possible with faster film-screen combinations such as Tmat-M when used with MinR fast double screens, or when Du Pont Microvision film or Konica CM film is used instead of OM film, or when Kodak MinR medium screens are used with OM film. These imaging techniques can reduce doses from 25% to 55%. Extended processing can also reduce the dose without reducing film image quality.

Most dedicated mammographic units adequately image the

Fig. 5.—A, Breast imaged at 30 kVp with a grid and with Du Pont chemistry at 33.3°C for 90 sec (experiment 1).

B, Image of same breast obtained 1 year later with Kodak chemistry at 35°C for 90 sec (experiment 3). Contrast difference between two images is due to chemistry change, not temperature.

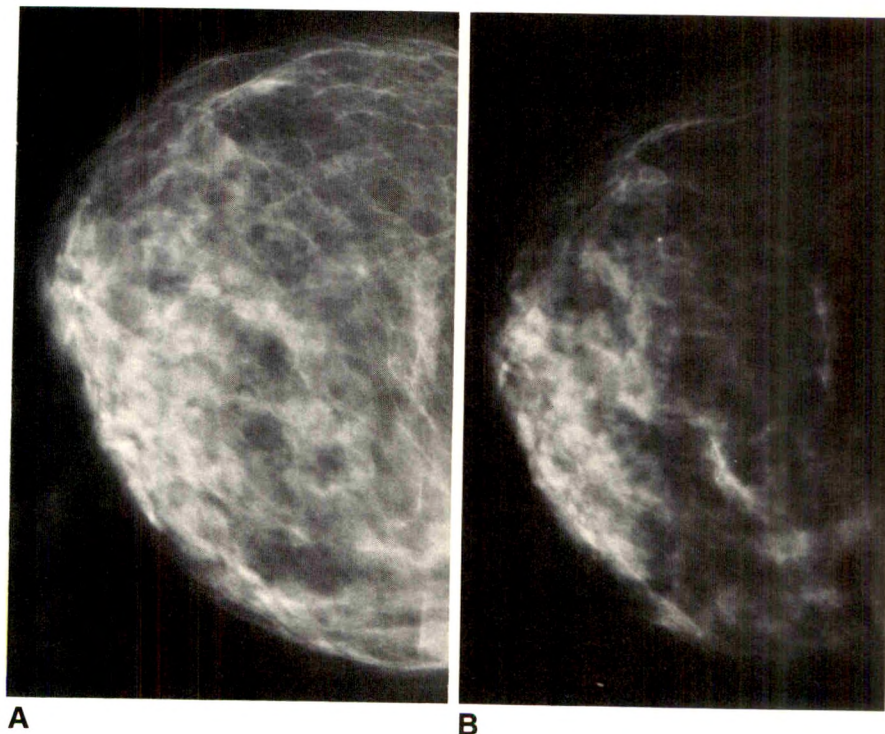
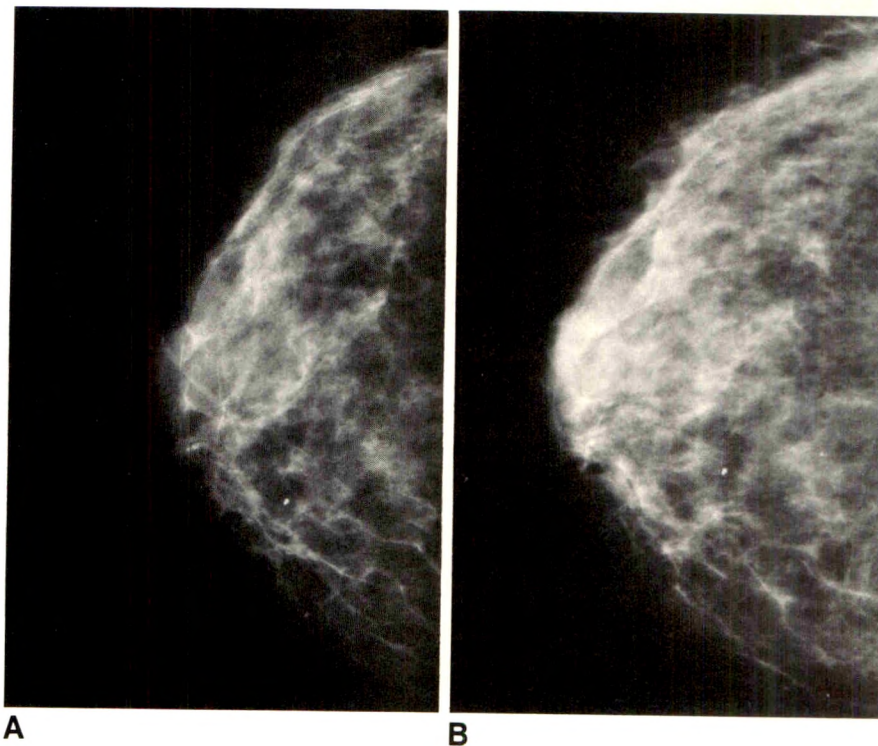


Fig. 6.—A, 7-cm-thick breast imaged with Du Pont chemistry at 33.3°C for 90 sec.

B, Image of same breast obtained 1 year later with Kodak chemistry at 35°C for 3 min (experiment 4). Increased penetration of glandular tissue is possible at a reduced dose.

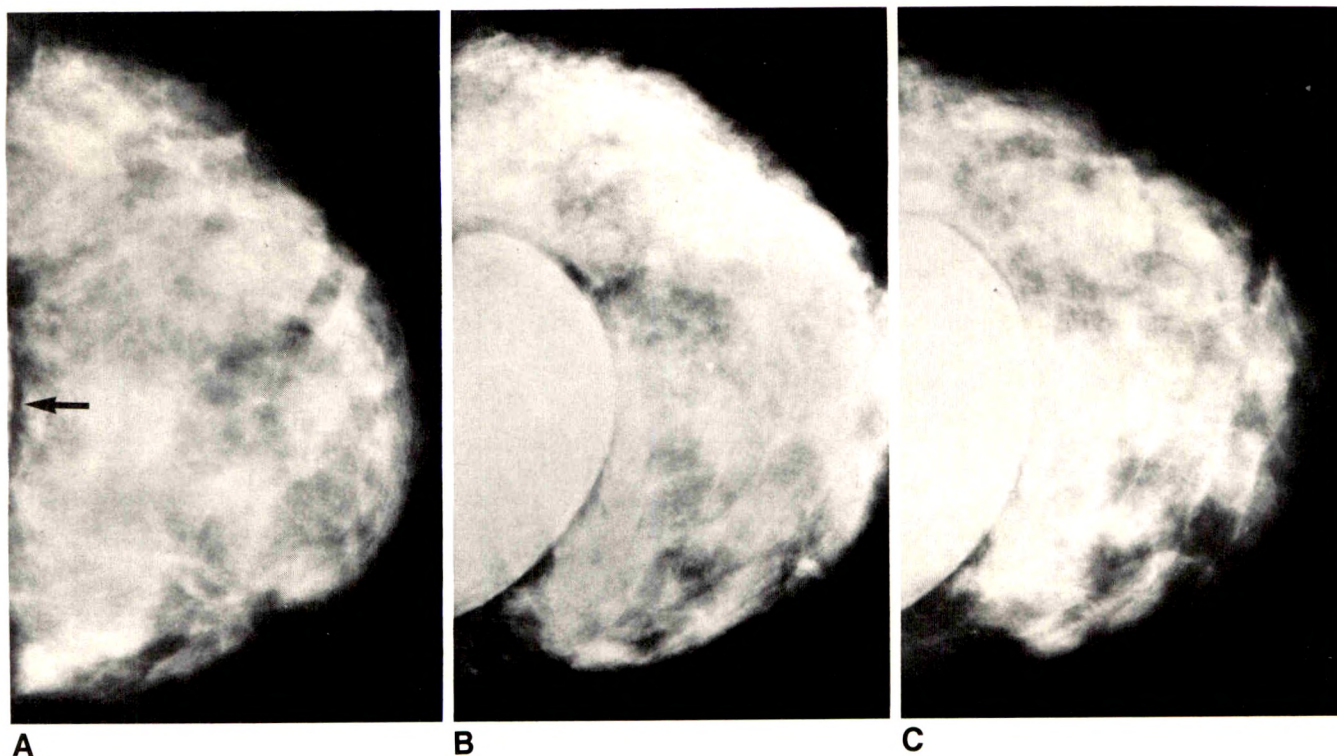


Fig. 7.—A, A dense breast containing a silicone implant (arrow) imaged at 32 kVp with a grid and with Du Pont chemistry at 33.3°C for 90 sec. B, Image of same breast obtained with Kodak chemistry at 35°C for 3 min. C, Image of same breast obtained with Du Pont chemistry at 35°C for 3 min. All three images show poor penetration due to dense glandular tissue.

average breast in less than 1 sec. However, very large breasts, dense breasts, and breasts containing silicone implants sometimes require exposures exceeding 1 sec, particularly for magnified views when small focal spots are used. When exposures exceed 2 sec in duration, reciprocity failure of the film may account for underexposed films or, when film density is correctly maintained, for an increase in dose of over 30% [7]. Thus, dose-reduction techniques are particularly beneficial for those patients who would receive the greatest exposures. Shorter exposures reduce patient motion and may eliminate "timing out" of the automatic exposure control during the exposure.

We have used 3-min processing for 1½ years. The developer is changed every 2 weeks, at which time the processor is thoroughly cleaned. If the processor is used also for films other than mammograms, extended processing may not be the best method for dose reduction unless the other films for which it is used are also single-emulsion film (such as film for extremity radiography) or film used in a multifilm camera whose exposures can be adjusted to compensate for the extended processing.

Prebiopsy needle localization procedures may require periods of sustained breast compression while radiographs are being exposed and processed. Although patients undergoing the localization may complain of longer breast compression

when extended processing is used, all of our patients have been able to complete the localization procedures successfully.

Extended processing is not for everyone. When the processor used for mammography must be shared with other imaging techniques, longer processing times are not possible. However, when mammography has a dedicated processor, extended processing time is an effective method of dose reduction and contrast improvement.

REFERENCES

1. Kimme-Smith C, Bassett LW, Gold RH, Roe D, Orr J. Mammographic dual-screen-dual-emulsion-film combination: visibility of microcalcifications and effect on image contrast. *Radiology* 1987;165:313-318
2. Haus AG. Recent advances in screen-film mammography. *Radiol Clin North Am* 1987;25(5):913-928
3. Curry TS, Dowdey JE, Murry RC. *Christensen's introduction to the physics of diagnostic radiology*, 3rd ed. Philadelphia: Lea & Febiger, 1984:130
4. Johns HE, Cunningham JR. *The physics of radiology*. Springfield, IL: Charles C Thomas, 1974:610
5. Eastman-Kodak. *More joy of photography*. Reading, MA: Addison-Wesley 1981:49
6. Tabar L, Dean PB. Screen/film mammography: quality control. In: Feig SA, McLelland R, eds. *Breast carcinoma: current diagnosis and treatment*. New York: Masson, 1983:161-168
7. Arnold BA, Eisenberg H, Bjarngard BE. Measurement of reciprocity law failure in green-sensitivity X-ray films. *Radiology* 1978;126:493-498

The Value of Non-Contrast-Enhanced CT in Blunt Abdominal Trauma

James Kelly¹
Vassilios Raptopoulos
Ashley Davidoff
Richard Waite
Patricia Norton

The usefulness of noncontrast CT, limited to the upper abdomen, in conjunction with conventional IV contrast-enhanced scanning was studied prospectively in 190 patients who had sustained blunt abdominal trauma. In 78, visceral injuries were confirmed at surgery or at follow-up CT. Of the patients with injuries, 14 (18%) had hyperdense hematomas on the noncontrast studies that became isodense after IV administration of contrast material. These hematomas generally were small and posed an immediate threat to life in only one patient (0.5% of all subjects). In 13% of patients with injury (5% of the total), the additional information did influence treatment planning (surgery in two and intensive conservative treatment in eight). Compared with conventional contrast scanning, the combined noncontrast-contrast technique increased the scanning time only by about 5½ min, but it improved the sensitivity and accuracy of CT in detecting visceral injuries from 74% and 84% to 92% and 91%, respectively ($p \leq .003$ and $p \leq .04$).

Although contrast-enhanced scanning alone accurately depicts visceral injuries requiring surgical treatment, the incorporation of a noncontrast sequence can detect a subgroup of patients who require intensive conservative management with bed rest and close observation. This additional information can be obtained expeditiously, with minimal additional effort or intervention. The use of noncontrast scanning alone is not recommended.

CT is widely used in the evaluation of major blunt abdominal trauma and has largely replaced other imaging methods and diagnostic peritoneal lavage [1]. The conventional scanning technique has been derived from the extensive experience at the San Francisco General Hospital and excludes scanning before IV administration of iodinated contrast material [2-4]. According to these investigators, this saves valuable time, and their experience has shown that, even though a hematoma may appear isodense compared with the intraabdominal structures, it is rarely the sole indicator of visceral injury. These investigators, however, are keenly aware that a hyperdense recent hematoma on nonenhanced scans, reported to occur in 75% of the cases, may appear isodense after enhancement of the abdominal organs with IV contrast medium, especially if inadequate amounts of these agents are administered [4-6]. After observing a hyperdense-isodense sequence in the appearance of hematomas in a number of subjects without trauma, scanned both before and after IV contrast administration, we have been uncomfortable evaluating patients in our regional trauma center with contrast-enhanced scanning only.

With the advent of high-resolution fast scanning, the time limitation imposed by the older scanners has been reduced significantly, while contrast and spatial resolution have improved. This study was undertaken to assess prospectively whether the incorporation of a limited nonenhanced CT scanning sequence in patients with blunt abdominal trauma would provide information beyond that obtained with conventional scanning with IV contrast material.

Received June 24, 1988; accepted after revision August 23, 1988.

¹ All authors: Department of Radiology, Section of Abdominal Imaging, University of Massachusetts Medical Center, 55 Lake Ave. N., Worcester, MA 01655. Address reprint requests to V. Raptopoulos.

AJR 152:41-46, January 1989

0361-803X/89/1521-0041

© American Roentgen Ray Society

Subjects and Methods

A prospective study was started in August 1986. All patients with blunt abdominal trauma who were considered hemodynamically stable enough to undergo CT were scanned both without and with IV contrast material. Over a period of 14 months, 190 patients were studied. All scans were obtained within 4 hr after admission to the emergency ward of a regional trauma center; 73% were performed within 2 hr.

A GE 9800 CT scanner was used (General Electric, Milwaukee, WI). Initially, 1-cm-thick images were obtained every 2 cm over the upper abdomen. This was followed by IV administration of 100–150 ml of a 60% iodinated contrast agent while 1-cm-thick scans were obtained at 1-cm intervals over the abdomen and pelvis. The IV contrast material was administered at a rate of 1–1.5 ml/sec with a power injector (MEDRAD Mark IV CT Injector, MEDRAD, Pittsburgh, PA). Scanning started 20–30 sec after initiation of the injection, and scans were obtained every 10 sec (2 sec for data acquisition and 8 sec for table incrementation). The number of images obtained without IV contrast material and the additional scanning time required for the noncontrast series were recorded.

Both the nonenhanced and the contrast-enhanced scans were viewed with conventional (300–600 H) and narrow (100–200 H) window widths. Attenuation values were obtained to confirm the visual impression of CT density differences. The hard-copy images were reviewed by at least two radiologists, first by one of 14 residents and then by one of four attending physicians assigned to the clinical service at the time of scanning. There was a 1- to 10-hr lapse between the two readings. The data were tabulated at the time of clinical assessment, and the consensus of opinions was taken for data analysis. In cases of disagreement, the opinion of a second attending physician was obtained.

The contrast-enhanced scans were interpreted first, followed by reading of the nonenhanced and combined studies. However, some of the residents may have looked at the nonenhanced scans first because all critically ill patients, including those with trauma, are monitored closely during scanning. Thus, the first readers may have been aware of the results of the companion tests, and such knowledge could have influenced the reading, resulting in interpretation bias [7]. In order to diminish this potential bias, a preliminary report was given after the first reader's interpretations for immediate treatment planning. The attending physician then reviewed the studies according to the protocol. Although blinded independent analysis would have further reduced any potential interpretation bias, it could have also diminished the clinical relevance of the results by eliminating the inevitable pressure that emergency situations play in decision making. In addition, our main goal was not to compare the contrast-enhanced with the nonenhanced scanning techniques separately but to assess whether the incorporation of a short nonenhanced sequence would have an influence in interpreting conventional contrast-enhanced scans.

In 102 patients, confirmation of the CT interpretations was made at surgery ($n = 34$) or with follow-up CT, which showed changes typical of resolving traumatic injury ($n = 44$) [2–4, 6] or confirmed absence of visceral trauma ($n = 24$). The remaining 88 patients, all of whom had a normal abdominal CT scan initially, were followed clinically for at least 3 months. Because the value of CT for blunt abdominal trauma has been established in clinical practice and surgical proof is not always obtained [1–4], we assumed that verification bias and bias from the absence of a separate definitive reference test would be minimized by close CT follow-up and relatively long clinical follow-up [7]. In addition, patients with equivocal initial CT diagnoses were divided into groups of probably positive or probably negative test results, which (results) were considered test-positive or test-

negative. The final assessment of these tests was made by correlating the findings at surgery or repeat CT in 1–3 days and clinical follow-up for at least 3 months. We assumed that this distinction would minimize the bias from uninterpretable tests results [7]. The sensitivity, specificity, and accuracy of the nonenhanced and enhanced scans as well as of the two studies in conjunction were calculated on the basis of the above assumptions. The chi-square test was applied to determine statistically significant differences of these values among the three types of studies.

Results

An average of 10 nonenhanced images were obtained per patient, amounting to 1 min 40 sec of actual scanning. The average delay before the contrast-enhanced scan was 5 min 20 sec.

Of the 190 patients with major blunt abdominal trauma, 78 (41%) proved to have abdominal visceral injuries at surgery ($n = 34$) or by follow-up CT ($n = 44$). Seventy-two of these injuries were identified on the combined unenhanced-enhanced CT scans. Compared with the abdominal organs, the injury appeared hypodense on 55 and hyperdense on three scans obtained with IV contrast agents (Table 1). In the remaining 14 patients (18% of those with visceral trauma, 7.4% of all subjects), the injury was hyperdense on the nonenhanced scans; however, after administration of IV contrast material, the evidence of trauma became isodense and was obscured (Table 1; Fig. 1). In these cases, the density of the hyperdense hematomas was 10–15 H higher than that of the affected organs, and the nonenhanced images had to be viewed with narrow window widths (100–200 H) for expedient identification. Although this resulted in considerably noisy images, at these settings the hematomas were depicted readily (Figs. 2–4).

All the hematomas identified by nonenhanced scanning only were relatively small. These included injuries to the spleen ($n = 3$, Fig. 1), the liver ($n = 4$, Fig. 2), the mesentery and the duodenum ($n = 3$, Fig. 3), the kidney ($n = 2$), and the adrenal gland ($n = 1$). One patient had an immediate life-threatening injury to the aorta, depicted as a periaortic hematoma on the abdominal nonenhanced scan (Fig. 4). Exploratory laparotomy was performed in two other patients, one with a splenic hematoma and another with duodenal hematoma, but these injuries were not considered to pose an immediate threat to life.

TABLE 1: CT Density of Visceral Hematomas vs Parenchymal Density

Nonenhanced Scans	Contrast-Enhanced Scans, True (False) CT Results			
	Hyperdense	Isodense	Hypodense	Total
Hyperdense	3 (2)	14 (1)	21 (2)	38 (5)
Isodense	0	0 (6)	22 (3)	22 (9)
Hypodense	0	0	12 (3)	12 (3)
Total	3 (2)	14 (7)	55 (8)	72 (17)

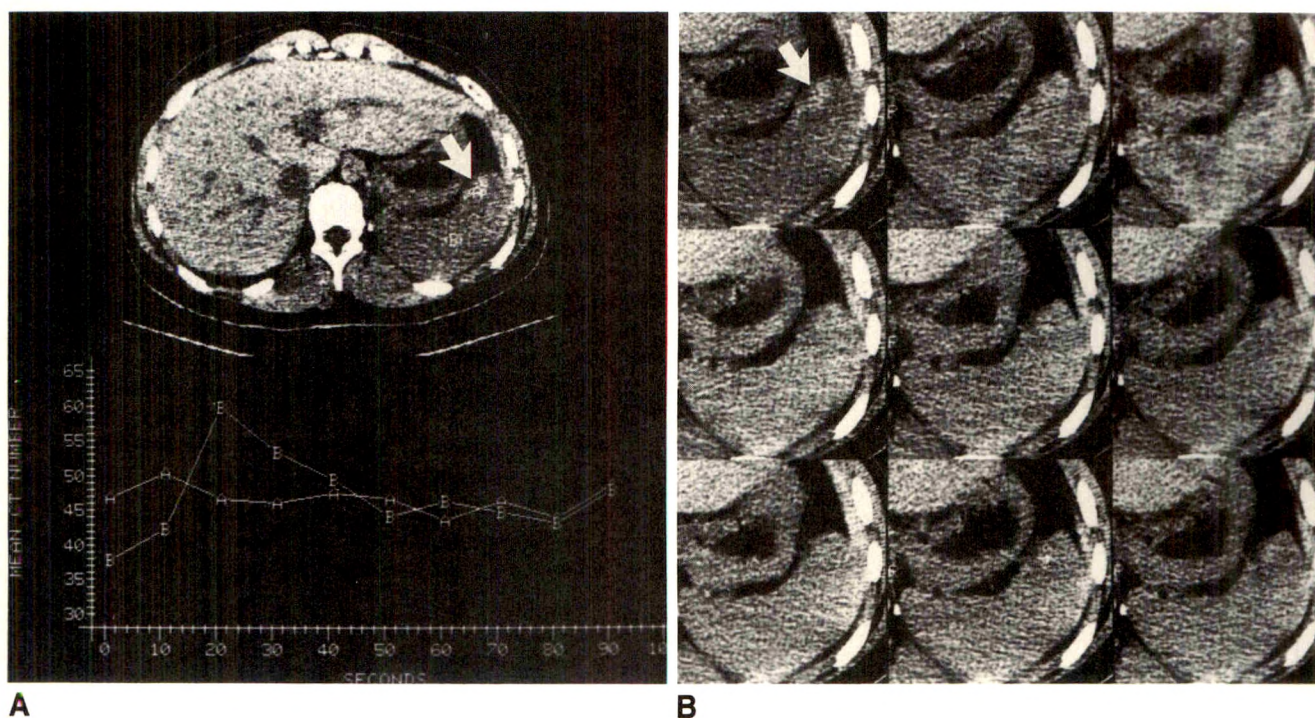
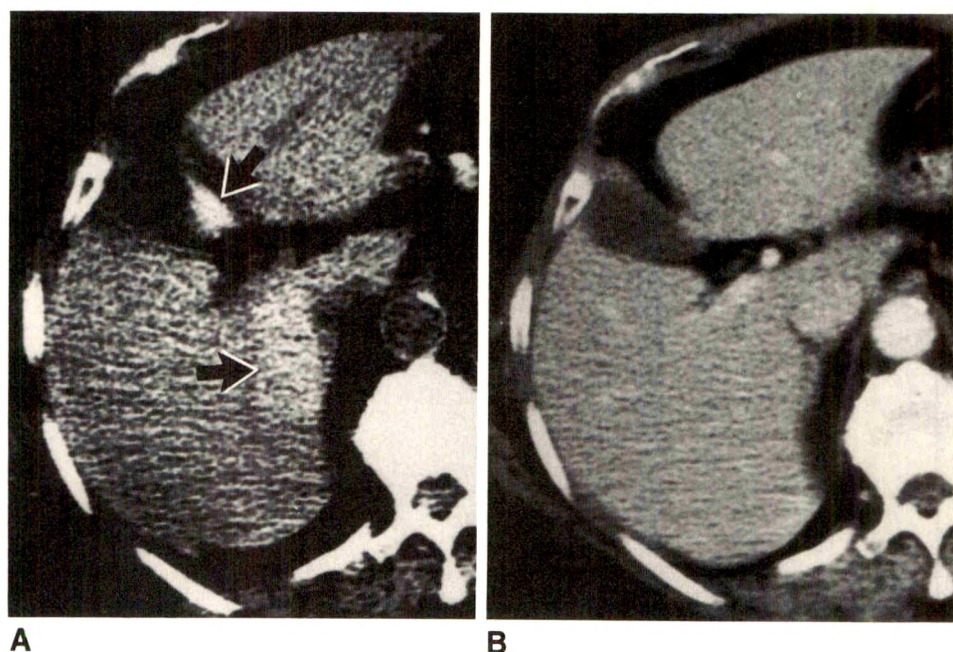


Fig. 1.—Splenic hematoma in patient scanned with dynamic CT.
 A, Precontrast scan shows hyperdense splenic hematoma (arrow). Time-density graphs show no change in density of hematoma (A), while splenic parenchyma (B) changes from hypo- to hyper- to isodense in respect to density of hemorrhage.
 B, Serial images from dynamic sequence show progressive changes in density of spleen, which eventually becomes isodense relative to hematoma (arrow). Note transient inhomogeneity of splenic enhancement pattern (top row) [5].

Fig. 2.—A and B, CT scans show liver hematomas. Precontrast scan (A) shows two hyperdense hematomas (arrows), which became isodense after IV contrast enhancement (B). On follow-up CT, both regions appeared hypodense on contrast-enhanced scans.



In four of 14 patients in whom hematomas were identified on the nonenhanced scans only, there was additional evidence of trauma. These included a small perisplenic fluid collection in a patient with splenic injury, a small perinephric

collection in a patient with renal injury, and a small amount of free peritoneal fluid in a patient with liver injury; none of these patients underwent surgery. The fourth patient, who had a small duodenal hematoma and small amount of peritoneal

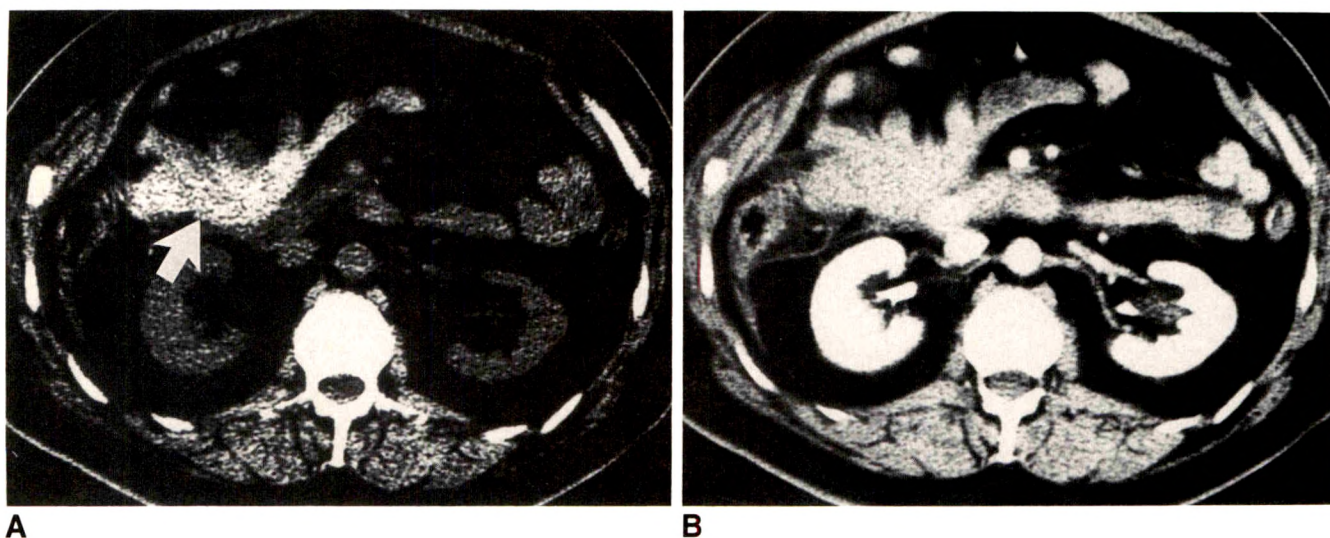


Fig. 3.—A and B, CT scans. Mesenteric hematoma (arrow) on a nonenhanced scan (A) was mistaken for nonopacified bowel on a contrast-enhanced scan (B).

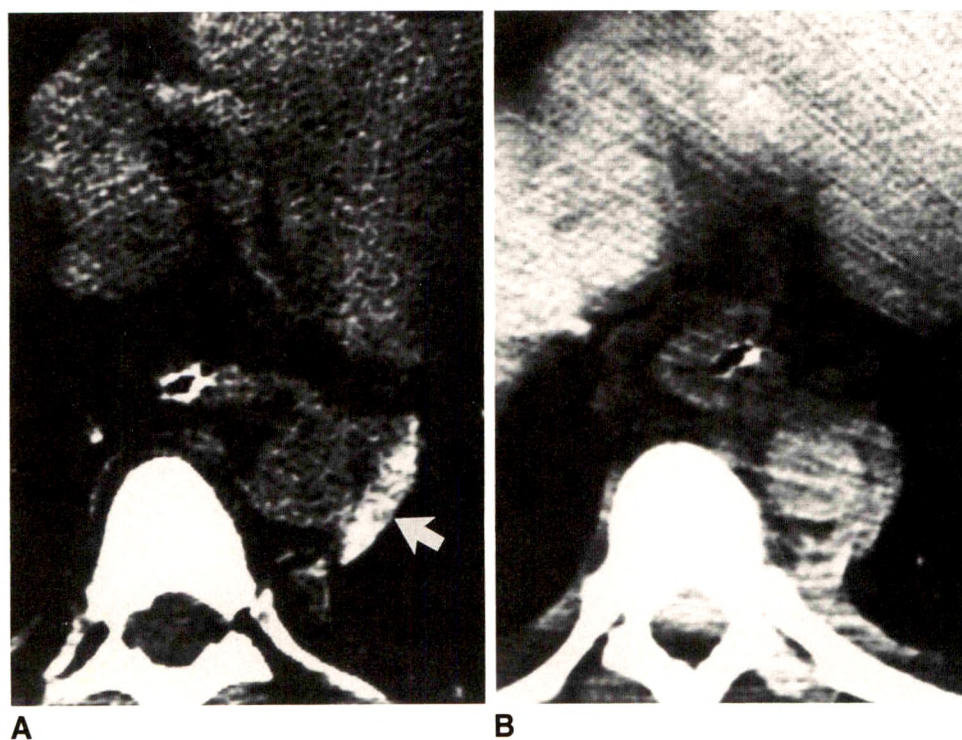


Fig. 4.—A and B, CT scans of abdomen. Periaortic hematoma (arrow), identified by its high density on non-contrast scan (A), became isodense and was misinterpreted as pleural fluid/hematoma on IV contrast-enhanced scan (B). Subsequent aortogram showed thoracic aortic tear, which was repaired surgically.

fluid, was treated surgically. The findings on the noncontrast scan only influenced the treatment planning of 10 patients (13% of those with visceral injury, or 5% of all patients) who otherwise would have been admitted to the hospital for 24-hr observation only or would not have been treated. Two were treated surgically and eight conservatively. Their management included the minimum of a 24-hr stay in the trauma intensive care unit, followed by bed rest and close monitoring of vital signs for an additional 2 days. They also had a minimum of one additional CT scan and were followed periodically for at

least 3 months and until there was marked or complete resolution of the hematomas on CT.

The incorporation of nonenhanced scanning in the CT evaluation of patients with blunt abdominal trauma significantly improved the sensitivity and accuracy of CT in detecting visceral injuries (Table 2). These values increased from 74% and 84% in contrast scanning to 92% and 91% in combined nonenhanced-enhanced studies ($p \leq .003$ and $p \leq .04$). There was no statistically significant difference in specificity among the two studies or with the noncontrast scans alone. Although

TABLE 2: Assessment of Diagnostic CT Techniques in Patients with Blunt Abdominal Trauma

	Scanning Technique			Significance (p)		
	Nonenhanced	Enhanced	Combined	Nonenhanced vs Enhanced	Nonenhanced vs Combined	Enhanced vs Combined
True positive (no.)	50	58	72	NA	NA	NA
False positive (no.)	8	10	11	NA	NA	NA
True negative (no.)	104	102	101	NA	NA	NA
False negative (no.)	28	29	6	NA	NA	NA
Sensitivity (%)	64	74	92	NS	≤.0001	≤.003
Specificity (%)	93	91	90	NS	NS	NS
Accuracy (%)	81	84	91	NS	≤.005	≤.04
Rate (%):						
False positive	7	9	10	NS	NS	NS
False negative	36	26	8	NS	≤.0001	≤.003
Predictive value (%):						
Positive result	86	85	87	NS	NS	NS
Negative result	79	84	94	NS	NS	≤.01

Note.—NA = not applicable; NS = not significant.

this may be attributed to criterion shift of the observers, it may also be due to the importance the detection of a hematoma plays in interpreting CT scans in patients with blunt abdominal trauma. Comparing the nonenhanced and conventional contrast scanning techniques, no statistically significant difference was found in sensitivity, specificity, or accuracy. However, there was a difference in the types of injuries detected. In 22 patients with visceral injuries, the hematomas were isodense on the nonenhanced scan and hypodense with contrast enhancement. These injuries generally were more severe than the ones identified on nonenhanced scans only, and 13 (59%) of these patients were treated surgically.

Discussion

The appearance of recent hemorrhage on abdominal CT images depends on the variables influencing the attenuation of the hematoma and the visceral structures. The density of hemorrhage depends on the hematocrit, on clot formation and retraction, on the sedimentation of cellular elements in blood, and on the time interval between hemorrhage and scanning [6, 8–10]. The attenuation of the abdominal structures depends on the consistency of the soft tissues, including the presence or absence of disease, as well as on the use or nonuse of IV contrast agents [4–6, 11]. IV contrast material introduces additional variables, and the degree of contrast enhancement depends on the amount of contrast material used and the rate of injection, on the vascularity and parenchymal consistency of the abdominal structures, on the underlying cardiovascular state of the subject, and on the amount of extracellular fluid, as well as on the timing of scanning in respect to the administration of contrast material [4–6] (Fig. 1). Finally, window and level settings play important roles in visual contrast resolution [6, 10].

Compared with the abdominal soft tissues, with CT attenuation values of about 30–60 H, recent abdominal hemorrhage (about 30–50 H) may be hyper-, iso-, or hypodense [6, 9, 10]. After IV administration of iodinated contrast material, the parenchymal organ enhancement, to about 40–90 H,

usually renders the hemorrhage hypodense [1–4, 10]. This explains the rationale for scanning patients with blunt abdominal injury with IV contrast material only, together with the need for an expedient diagnosis and the accuracy of contrast-enhanced CT in determining which patients need surgery [1–4]. However, it has been suggested that some hematomas are seen on nonenhanced scans only; false-negative CT diagnoses, especially in splenic trauma, have been reported, and it is not rare to identify more hematomas at surgery than are observed on contrast-enhanced CT [1, 4, 6, 12, 13].

Our data show that a number of injuries (18%) are hyperdense on nonenhanced scans and isodense after administration of IV contrast material. This percentage may be even higher in practice, because in this study we tried using a consistent technique to minimize some of the variables that influence the CT attenuation of hematomas and visceral structures. The difference in density of the hematomas identified by nonenhanced scanning only, as compared with the juxtaposed soft tissues, was approximately equal to the degree of the tissue density enhancement after administration of IV contrast material. Viewed with a narrow window width of 100–200 H, the injuries were depicted readily on the nonenhanced images, and, because the attenuation of recent hemorrhage is nearly diagnostic [6, 8], both their detection and the observers' confidence were facilitated. In our material, this was particularly important because generally the hematomas were small but their detection did influence treatment planning. The specific high attenuation of recent hematomas on nonenhanced scans may also help to differentiate visceral injuries from incidental abnormalities that may appear hypodense on contrast-enhanced studies.

Although the incorporation of nonenhanced scanning influenced treatment planning in 13% of patients with visceral injuries (5% of all patients), it could not be determined whether this had any significant impact on the final outcome. Such a determination would require a much larger population as well as a double-blind study, which, considering the ethical ramifications, may not be justified. The delay in the scanning time posed by the nonenhanced sequence was about 5½ min. Of

this time, an average of 1 min 40 sec was allocated to actual scanning, whereas the remainder was needed for preparing for the IV contrast-enhanced sequence. Within these 4 min, the nonenhanced images can be reconstructed, and if fast reconstruction software and a fast hard-copy imager are available, the nonenhanced study may be available on film before the first contrast-enhanced images appear on the monitor. Although additional time may be required for reviewing, filming, storage, and so forth, this should not add to the patient's time on the CT table. Furthermore, the additional expense of a nonenhanced sequence, as well as the charges for more conservative treatment and additional clinical and CT follow-up, was estimated at \$23,950, or \$135 per patient. We believe that the reasonable additional time required and modest increase in expense are worth the added sensitivity and accuracy achieved with the combined nonenhanced-enhanced test.

Our findings further support the use of IV contrast material when evaluating blunt abdominal trauma with CT. Although no significant difference was found between nonenhanced and contrast-enhanced studies read alone, this probably was due to bias from case mix (spectrum) [7]. In 28% of the patients with visceral injury, the hematomas were isodense on the nonenhanced scans and hypodense on the IV contrast-enhanced scans. These generally were severe injuries, and surgical intervention was required in over one-half of the cases.

Nearly all immediate life-threatening visceral injuries in patients with blunt abdominal trauma were depicted with conventional contrast-enhanced scans, but the incorporation of nonenhanced studies significantly improved the sensitivity and accuracy of CT by identifying smaller injuries that otherwise may have been undetected. It could not be determined from this study whether these injuries require additional man-

agement. However, with appropriate equipment, the added information can be obtained expeditiously and with minimal additional effort or intervention. We conclude that nonenhanced scanning should be incorporated into the routine CT evaluation of blunt abdominal trauma.

REFERENCES

1. Wing VW, Federle MP, Morris JA Jr, Jeffrey RB, Bluth R. The clinical impact of CT for blunt abdominal trauma. *AJR* **1985**;145:1191-1194
2. Federle MP, Goldberg HI, Kaiser JA, Moss AA, Jeffrey RB Jr, Mall JC. Evaluation of abdominal trauma by computed tomography. *Radiology* **1981**;138:637-644
3. Federle MP. Computed tomography of blunt abdominal trauma. *Radiol Clin North Am* **1983**;21:461-475
4. Federle MP. CT of upper abdominal trauma. *Semin Roentgenol* **1984**;19:269-280
5. Glazer GM, Axel L, Goldberg HI, Moss AA. Dynamic CT of the normal spleen. *AJR* **1981**;137:343-346
6. Wolverson MK, Crepps LF, Sundaram M, Heiberg E, Vas WG, Shields JB. Hyperdensity of recent hemorrhage at body computed tomography: incidence and morphologic variation. *Radiology* **1983**;148:779-784
7. Begg CB, McNeil BJ. Assessment of radiologic tests: control of bias and other design considerations. *Radiology* **1988**;167:565-569
8. Norman D, Price D, Boyd D, Fishman R, Newton TH. Quantitative aspects of computed tomography of the blood and cerebrospinal fluid. *Radiology* **1977**;123:335-338
9. Swensen SJ, McLeod RA, Stephens DH. CT of extracranial hemorrhage and hematomas. *AJR* **1984**;143:907-912
10. Federle MP, Jeffrey RB Jr. Hemoperitoneum studied by computed tomography. *Radiology* **1983**;148:187-192
11. Mategrano VC, Petasnick J, Clark J, Bin AC, Weinstein R. Attenuation values in computed tomography of the abdomen. *Radiology* **1977**;125:135-140
12. Pappas D, Mirvis SE, Crepps JT. Splenic trauma: false-negative CT diagnosis in cases of delayed rupture. *AJR* **1987**;149:727-728
13. Fabian TC, Mangiante EC, White TJ, Patterson CR, Boldreghini S, Britt LG. A prospective study of 91 patients undergoing both computed tomography and peritoneal lavage following blunt abdominal trauma. *J Trauma* **1986**;26:602-607

The reader's attention is directed to the commentary on this article, which appears on the following pages.

Commentary

On the Value of Non-Contrast-Enhanced CT in Blunt Abdominal Trauma

Howard J. Mindell¹

In the preceding article, Kelly et al. [1] report on the utility of adding non-contrast-enhanced scans to conventional contrast-enhanced CT for the evaluation of patients with blunt abdominal trauma. These authors prospectively evaluated 190 such patients for whom the noncontrast scans were added. Comparisons were made between the contrast-only and the combination (noncontrast with contrast) sequences. Tabulation of data was done by radiology residents at the time of the examination and then again by staff radiologists several hours later. Findings were validated by surgery in 34, by follow-up CT in 68, and by clinical follow-up of at least 3 months in 88 patients. Sensitivity and accuracy increased from 74% and 84% in contrast-only scanning to 92% and 91% with the combined sequence. In 14 patients (7.4% of all subjects), small hematomas (one life-threatening) were discovered by the added noncontrast scans. The authors suggest that the additional time and cost (5.5 min of scan time and \$135 per patient) are justified, and they recommend altering the conventional protocol to include noncontrast as well as contrast CT for blunt abdominal trauma.

Certain aspects of the data-gathering method are open to question. Both the control (with contrast) and variable (non-contrast or combined sequence) images in the experimental model were analyzed by the same person at nearly the same time. Moreover, the analysis was frequently done under stressful emergency circumstances, in which critical diagnostic judgments were required. What temptation was there for the radiology resident to peek at the noncontrast scans prematurely? The authors concede this potential bias but cite

the mitigating effect of the subsequent staff review protocol and note that a blinded independent analysis of the films could have decreased the clinical relevance of the results. Surgical proof of findings was available in only 34 of the 190 patients. The lack of a definite reference test has been a persistent theme in the literature on this topic. For example, Kaufman et al. [2], in a study of CT for upper abdominal trauma in 100 children, lamented the lack of a gold standard for measuring results. In their series, no imaged patient died, and very few had surgery. In the study by Federle and Jeffrey [3], only 39 of 300 patients had surgical confirmation; even when surgery was done, it was frequently delayed for several hours or resulted in either inadequate or conflicting estimates of the size of traumatic hematomas. In any case, the proof of findings offered by Kelly et al. [1] is concordant with that already accepted in the literature.

Why did Kelly et al. embark on this ambitious project? They noted hematomas seen as hyperdense on precontrast scans became isodense (and invisible) on contrast-enhanced scans in nontrauma patients, and they felt "uncomfortable" with using only contrast scans in abdominal trauma. Wolverson et al. [4] had reported previously that contrast material could mask the hyperdensity of recent hemorrhage; in their retrospective study, scanning had been done with and without contrast material. However, using only contrast-enhanced CT is widely accepted as accurate and reliable for abdominal trauma. Federle and Jeffrey [3] had only one false-negative result and two false-positive results in 300 cases and found that CT "is sensitive and specific for hemoperitoneum." The

This article is a commentary on the preceding article by Kelly et al.

¹ Department of Radiology, University of Vermont College of Medicine, The Medical Center Hospital of Vermont, Burlington, VT 05401. Address reprint requests to H. J. Mindell.

sensitivity and accuracy in the study by Kelly et al. for contrast-only scans at 74% and 84% are lower than other experiences. Wing et al. [5] reported a sensitivity of 100%, a specificity of 96.8%, and an accuracy of 97.6% with contrast-only scans, reporting that in no case did CT miss a significant intraabdominal injury. Nonetheless, the study by Kelly et al. [1] is the first prospective systematic analysis of the yield of adding noncontrast scans to CT protocol for blunt abdominal trauma. Although questions might arise about data-gathering methods or validation of findings, a laudable major effort was expended. The illustrations leave no doubt that some number of additional small hematomas will be found by adding the noncontrast scans. The question is whether the additional findings are worth the additional time and expense.

The additional time for the noncontrast scans (5.5 min added onto a 30-min procedure) represents an 18% increase—"quality time" when fast decisions are needed in critically ill patients who frequently also require other studies. The expense of \$135 more per patient includes charges for "enhanced conservative treatment" and additional clinical and CT follow-up. At our hospital, the actual total charge for abdominal CT with contrast is \$431, and the total charge for both contrast and noncontrast is \$512, an additional cost for the noncontrast scans of \$81 or 19%. What is the necessity for these additional expenditures? Kelly et al. note that "contrast scanning alone accurately depicts visceral injuries requiring surgical treatment," citing an immediate threat to life in only one patient in their series. In a group of 273 patients with small hematomas [3], only 11 needed surgery, always for reasons other than the presence of a small (100–200 ml) hematoma. The moderate (250–500 ml) or large (>500 ml) hematomas requiring surgery were readily seen with contrast

CT. Kaufman et al. [2] noted that a negative CT does not mean that the patient can be discharged. Only clinical circumstances can dictate treatment decisions. Would not the "intensive conservative treatment" by Kelly et al. [1] be required in all nonsurgical patients regardless of whether a small hematoma was found?

A recent popular surgical textbook by Davis [6] lauded diagnostic peritoneal lavage as the "most expedient and reliable method of identifying intraperitoneal hemorrhage," suggesting that CT "may have a complementary role but has some practical limitations in the acutely injured patient." Adding noncontrast scans to the CT protocol for abdominal trauma to find small, probably inconsequential hematomas does not seem warranted and might be construed as another "practical limitation" to the wider use of CT for abdominal trauma. One could argue that cheaper, faster (ultrafast?) CT would be more effective in the larger goal of the complete elimination of the need for diagnostic peritoneal lavage in blunt abdominal trauma.

REFERENCES

1. Kelly J, Raptopoulos V, Davidoff A, Waite R, Norton P. The value of non-contrast-enhanced CT in blunt abdominal trauma. *AJR* 1989;152:41–46
2. Kaufman RA, Tewbin R, Babcock DS, et al. Upper abdominal trauma in children: imaging evaluation. *AJR* 1984;142:449–460
3. Federle MP, Jeffrey RB Jr. Hemoperitoneum studied by computed tomography. *Radiology* 1983;148:187–192
4. Wolverson MK, Crepps LR, Sundaram M, Heiberg E, Vas WG, Shields JB. Hyperdensity of recent hemorrhage at body computed tomography: incidence and morphologic variation. *Radiology* 1983;148:779–784
5. Wing VW, Federle MP, Morris JA, Jeffrey RB, Bluth R. The clinical impact of CT for blunt abdominal trauma. *AJR* 1985;45:1191–1194
6. Davis JH. *Clinical surgery*. St. Louis: Mosby, 1987:2773

Sonography in Patients with Suspected Acute Appendicitis: Value in Establishing Alternative Diagnoses

Erik H. L. Gaensler¹
R. Brooke Jeffrey, Jr.
Faye C. Laing
Ronald R. Townsend

We reviewed the clinical and sonographic findings in 297 patients who had graded compression sonography for suspected acute appendicitis. The purpose of the study was to determine the accuracy of sonography in detecting other diseases in the 174 patients in this group who proved not to have acute appendicitis. Of the 174 patients without acute appendicitis, 93 patients (53%) were ultimately discharged with a diagnosis of abdominal pain of unknown origin. Of the 81 patients in whom specific diagnoses were established, sonography suggested the correct diagnosis in 57 patients (70%). A broad spectrum of diseases was detected, including: gynecologic diseases (35); visceral diseases, including hollow viscera and diseases of liver, pancreas, or spleen (18); and urinary tract abnormalities (four).

This study suggests that sonography is useful in establishing alternative diagnoses in patients undergoing sonography for suspected acute appendicitis.

Graded compression sonography has been useful in diagnosing acute appendi-

the final diagnosis, even if other studies were required to confirm the diagnosis.

Before any sonogram was done, a careful history was obtained. Patients were asked to locate their abdominal pain by pointing with one finger to the site of maximal discomfort. They were questioned specifically about the presence of upper abdominal or flank pain and tenderness. The graded compression technique used to perform the sonograms has been described previously [2-4]. All right lower quadrant scans were performed with a 5-MHz linear-array transducer (Acuson, Mountain View, CA); these scans were considered nondiagnostic if adequate bowel compression could not be obtained because of severe pain, obesity, or ascites. In women in whom no sonographic evidence of appendicitis was detected (111 patients), a sonogram of the pelvis was routinely obtained with a 3.5-MHz sector scanner. If the bladder was empty, or in cases of suspected pelvic diseases (21 patients), endovaginal sonography also was performed with a dedicated 5-MHz transducer. A real-time examination of the upper abdomen also was performed using a 3.5-MHz sector transducer in patients without sonographic evidence of appendicitis, which includes all 174 patients reviewed in this study. Total examination time varied considerably but averaged approximately 20 to 30 min.

Results

Of the 81 patients with true-negative sonograms for appendicitis in whom a specific alternative diagnosis was subsequently established, the proved diagnoses were gynecologic disease (44); visceral diseases, including hollow viscera and diseases of liver, pancreas, or spleen (22); urinary tract abnormalities (12) or extraabdominal abnormalities (three).

In the 44 patients subsequently shown to have gynecologic diseases, the final diagnoses were based on surgical findings in eight patients and on a combination of clinical, imaging, and laboratory findings, as well as on response to therapy, in the remaining 36 patients. The sonographic diagnoses were correct in 21 (75%) of the 28 patients with pelvic inflammatory disease, in 12 (86%) of the 14 patients with ovarian cysts, and in both of the two patients with uterine myomas. Overall, the sensitivity of sonography for detecting gynecologic diseases was 80% (35 correct diagnoses in 44 patients).

In 18 (82%) of the 22 patients with proved visceral abnormalities, diagnoses were suggested by the initial sonograms. The final diagnoses were confirmed by pathologic and/or surgical findings in four patients, and the remaining diagnoses were based on a combination of clinical, radiologic, and laboratory findings, as well as on response to therapy. Three patients had small bowel obstruction diagnosed by sonography on the basis of detection of dilated, fluid-filled loops with hyperperistalsis. Two cases of colonic diverticulitis were diagnosed prospectively by sonography on the basis of mural thickening of the cecum and calcified enteroliths with acoustic shadowing within diverticula. Sonograms in three patients with infectious enteritis showed thickening of the terminal ileum. Two additional cases of mesenteric adenitis were diagnosed by sonography on the basis of visualization of markedly enlarged lymph nodes; one of these cases was confirmed surgically. Three cases of spontaneous bacterial peritonitis were diagnosed by detection of peritoneal fluid collections, which were subsequently aspirated under sonographic guid-

ance. A sonogram in one patient showed a fluid collection and thickened adjacent bowel loops, which proved at surgery to be an interloop abscess. Three patients had lesions of solid viscera detected by sonography: hepatic amebic abscess (one patient), perisplenic hematoma (one patient), and acute pancreatitis (one patient). The sonographic diagnosis of a perforated biliary endoprosthesis was suggested in a patient who had known extrahepatic cholangiocarcinoma and whose sonogram showed free air and free interperitoneal fluid in the right lower quadrant. In four patients with visceral abnormalities, the sonogram failed to detect the precise cause. These included two patients with duodenal ulcers, one patient with colonic diverticulitis, and one patient with *Shigella* gastroenteritis.

In the 12 patients who subsequently proved to have urinary tract disease, the correct diagnoses were suggested by sonography in four patients (33%). The diagnoses included ureterolithiasis (three patients) and a perirenal hematoma (one patient). The eight negative sonograms included those of six patients with pyelonephritis and two patients who were ultimately shown on urography to have mild hydronephrosis, suggestive of a recently passed stone. Surgical procedures were not required in any patient with urinary tract abnormalities, although one patient with a large perirenal hematoma underwent percutaneous drainage.

Three patients with a sonogram negative for appendicitis had alternative diagnoses that were not directly related to abnormalities within the abdomen or pelvis. The final diagnosis in these patients included generalized *Streptococcus viridans* sepsis, left lower lobe pneumonia, and pulmonary infarction associated with a sickle cell crisis.

Discussion

Sonography is necessary to establish the diagnosis of acute appendicitis only when the clinical findings are equivocal. Many of these patients will subsequently be shown to have some other disorder. Fifty-three percent of our 174 patients without acute appendicitis received no specific diagnosis. Their abdominal symptoms were presumably due to viral gastroenteritis, mild cases of mesenteric adenitis, or other self-limiting abnormalities. However, in patients in whom an alternative diagnosis was established, our data show that sonography was of considerable value. An alternative diagnosis was suggested by sonography in 70%.

In our patients, acute gynecologic problems were the most common diseases clinically confused with acute appendicitis. The difficulty in establishing the diagnosis of acute appendicitis in young women has been well documented: Rates of misdiagnosis of appendicitis in women who are 20-40 years old are often excessively high (reported to be approximately 40%) [7]. Of 44 women with gynecologic disease that mimicked acute appendicitis in our study, sonography was able to suggest the correct diagnosis in 35 (80%). Because of the clearly visible sonographic findings, only 18% of patients required laparotomy and/or laparoscopy (eight of 44 patients). In most patients, the diagnosis was established on the basis of the initial sonograms, culture results, cervical motion ten-

derness, response to antibiotics, and follow-up sonographic studies.

The 22 cases of gastrointestinal abnormalities encompassed a broad spectrum of disease, including such diverse entities as hepatic amebic abscesses, small bowel obstruction, colonic diverticulitis, duodenal ulcer, perisplenic hematomas, and pancreatitis. Overall, sonography led to the correct final diagnosis in 18 (82%) of 22 patients in this group. In many cases, the sonographic abnormality, such as thickening of the bowel wall, was relatively nonspecific. Other radiologic or laboratory studies or invasive procedures were needed to pinpoint the cause of the sonographic abnormality. However, sonography did detect the lesion and correctly guided the patient's subsequent evaluation. Four (33%) of 12 patients with urinary tract abnormalities were detected by sonography. Most often, obstructing calculi were detected because of associated hydronephrosis. As previously noted, sonography may produce false-negative findings in patients with nonobstructing stones because of the absence of significant pelvocalyceal dilatation [8].

In this study, sonography was able to suggest a specific alternative diagnosis to appendicitis in 57 (33%) of 174 patients. Furthermore, none of these 57 cases represent false-negative findings for acute appendicitis. When the 97 patients with true-positive sonographic diagnoses for acute appendicitis are added to the 57 patients with alternative diagnoses suggested by sonography, the total number of correct specific

diagnoses suggested by sonography was 154 (52%) of 297 patients.

In summary, most patients who have confusing signs and symptoms of acute appendicitis and who are referred for sonography will not have acute appendicitis. When sonography is negative for appendicitis, routine sonography of the upper abdomen and pelvis also should be performed in an effort to identify other conditions that may be causing the symptoms.

REFERENCES

1. Jeffrey RB, Laing FC, Townsend RR. Acute appendicitis: sonographic criteria based on 250 cases. *Radiology* **1988**;167:327-329
2. Puylaert JBCM. Acute appendicitis: US evaluation using graded compression. *Radiology* **1986**;158:355-360
3. Puylaert JBCM, Rutgers PH, Lalisang RI, et al. A prospective study of ultrasonography in the diagnosis of appendicitis. *N Engl J Med* **1987**;317:666-669
4. Jeffrey RB Jr, Laing FC, Lewis FR. Acute appendicitis: high-resolution real time US findings. *Radiology* **1987**;163:11-14
5. Abu-Yousef MM, Bleicher JJ, Maher JW, Urdaneta LF, Franken EA Jr, Metcalf AM. High-resolution sonography of acute appendicitis. *AJR* **1987**;149:53-58
6. Karstrup S, Torp-Pederson S, Roikjaer A. Ultrasonic visualization of the inflamed appendix. *Br J Radiol* **1986**;59:985-986
7. Lewis FR, Holcroft JW, Boey J, Dunphy JE. Appendicitis: a critical review of diagnosis and treatment in 1000 cases. *Arch Surg* **1975**;110:677-681
8. Laing FC, Jeffrey RB Jr, Wing VW. Ultrasound versus excretory urography in evaluating acute flank pain. *Radiology* **1985**;154:613-616

Book Review

Small Bowel Radiology. Introduction and Atlas. By Günther Antes and Franz Eggemann. New York: Springer-Verlag, 207 pp., 1988. \$110

This slim atlas of 207 pages contains 276 figures, indicating the emphasis on illustrating the radiologic manifestations of small-bowel abnormalities. This book deals only with the double-contrast enteroclysis examination of the small bowel, which, in the opinion of the authors, produces optimal results in the diagnosis of small-bowel abnormalities. After a brief description of the examination technique used by the authors, an excellent chapter presents basic signs and interpretation, with extensive illustration of normal findings and pathologic changes, such as mucosal, submucosal, and serosal involvement. This chapter also emphasizes evaluation of motility disorders, which has not been stressed before in the English literature on enteroclysis.

The second part of the atlas, which occupies about two-thirds of this volume, describes and illustrates most of the known small-bowel abnormalities. This section is divided into inflammatory conditions, tumors, motility disorders, obstructions, and malformations. The opportunistic small-bowel infections that occur in AIDS patients (such as cryptosporidiosis, isosporiosis, *Mycobacterium avium intracellulare* infections, and cytomegalovirus infections) are not mentioned.

Sandwiched between the concluding chapter and the index is the bibliography, which contains representative radiologic and clinical papers on small-bowel examination and disease. Although most of the articles are in English, many cite German-language publications.

The illustrations throughout the text are superb. Unfortunately, the legends are not always placed in the optimal position relative to the illustrations, and the lettered designations are often confusing, sometimes appearing in front of the descriptive sentence and sometimes at the end in parentheses. As is the case in many atlases, the text is often many pages away from the illustrations.

Occasionally, the authors use unfamiliar terms, such as "*subileus*." Some concepts, such as *nonpropulsive hyperperistalsis*, are explained only briefly and are not referenced. In the descriptions of contrast media, unfortunately, the authors refer to commercial preparations rather than to the barium concentration (weight/volume) as is customary.

This small atlas is recommended to radiologists who are interested in the gastrointestinal tract and to gastroenterologists. It certainly belongs in the library of any radiology training program. The concise text and the large number of illustrations make it suitable both for reading in its entirety and for use as a reference. Perhaps the beautiful illustrations will stimulate readers to become proficient in enteroclysis and thus advance the radiologic evaluation of the small bowel.

Herbert F. Gramm
Harvard Medical School
Boston, MA 02215

Rectal Involvement by Prostatic Carcinoma: Barium Enema Findings

Stephen E. Rubesin¹
 Marc S. Levine
 Mario Bezzi
 Howard M. Pollack
 Igor Laufer
 Hans Herlinger
 Gwen Harris

A retrospective study was performed to determine the radiographic features of prostatic carcinoma invading the rectum on double-contrast barium enemas. In 11 such patients, these examinations revealed localized narrowing and/or spiculation of the rectum (four cases); a smooth, extrinsic mass impression on the rectosigmoid colon (two cases); an umbilicated submucosal mass in the rectosigmoid colon (one case); and rectosigmoid narrowing with spiculated, pleated mucosal folds in the narrowed segment of bowel (four cases). Thus, most patients (64%) had localized involvement of the rectosigmoid colon with sparing of the distal rectum. The anatomic-pathologic basis for the localized spread of prostatic carcinoma to the rectosigmoid colon is illustrated on MR scans.

Thus, prostatic carcinoma invading the rectum may be manifested on double-contrast barium enema by a spectrum of radiographic findings, and most patients have localized rectosigmoid involvement with sparing of the distal rectum.

Although the prostate and rectum are contiguous structures, prostatic carcinoma rarely invades the rectum because Denonvillier fascia is an effective barrier in preventing extension of tumor from the prostate posteriorly into the rectum [1-3]. As a result, rectal invasion by prostatic carcinoma occurs in only 0.5-11.5% of patients [4, 5]. Even when prostatic carcinoma does invade the rectum, this possibility may not be suspected clinically, so that rectal involvement often is discovered unexpectedly at surgery or at autopsy [5-7].

The appearance of prostatic carcinoma invading the rectum has been reported previously on single-contrast barium enema examinations [4, 5, 7-12]. The classic findings of rectal narrowing and obstruction have sometimes led to an erroneous diagnosis of rectal carcinoma [4, 5, 8, 9, 13, 14]. However, those reports were published before the widespread use of double-contrast techniques for examining the colon. We therefore reviewed all cases of prostatic carcinoma involving the rectum or rectosigmoid colon on double-contrast barium enema at our hospital during the past decade to determine whether double-contrast radiography has altered our perception of rectal invasion by prostatic cancer.

Materials and Methods

Eleven patients with prostatic adenocarcinoma involving the rectum and/or sigmoid colon were examined by double-contrast barium enema at our hospital between 1978 and 1986. Nine patients had prostatic adenocarcinoma directly invading the rectal or rectosigmoid wall; the remaining two patients had prostatic carcinoma extrinsically compressing, but not invading, the rectosigmoid junction. The average age of the patients was 69 years (range, 55-85 years). All 11 patients had double-contrast barium enemas; the technique described by Laufer [15] was used. The films were reviewed retrospectively to determine the radiographic features of this condition. Confirmation of rectal or rectosigmoid involvement by prostatic carcinoma was obtained by exploratory laparotomy in four cases, by rectal biopsy in six cases, and by CT in one case. The surgical and pathologic reports were correlated with

Received July 29, 1988; accepted after revision September 20, 1988.

¹ All authors: Department of Radiology, Hospital of the University of Pennsylvania, 3400 Spruce St., Philadelphia, PA 19104. Address reprint requests to S. E. Rubesin.

AJR 152:53-57, January 1989

0361-803X/89/1521-0053

© American Roentgen Ray Society

the radiographic findings. Medical records were also reviewed to determine the patients' clinical presentation, treatment, and course.

Results

Clinical Findings

Of 11 patients with prostatic carcinoma involving the colon, five had a known diagnosis of prostatic carcinoma at the time of the barium enema examination. The average interval between the diagnosis of prostatic carcinoma and the barium enema was 1.4 years (range, 1–3 years). In those five patients, a coexisting colonic neoplasm was suspected because of a rectal mass on digital examination (two cases), constipation (one case), weight loss (one case), and a history of previous colon cancer (one case). The remaining six patients did not have a known diagnosis of prostatic carcinoma at the time of the barium enema examination. They underwent barium enemas because of constipation or decreasing stool caliber (three cases) and abnormal digital examination with findings suspicious for rectal carcinoma or intraperitoneal metastases to the rectovesical space (three cases).

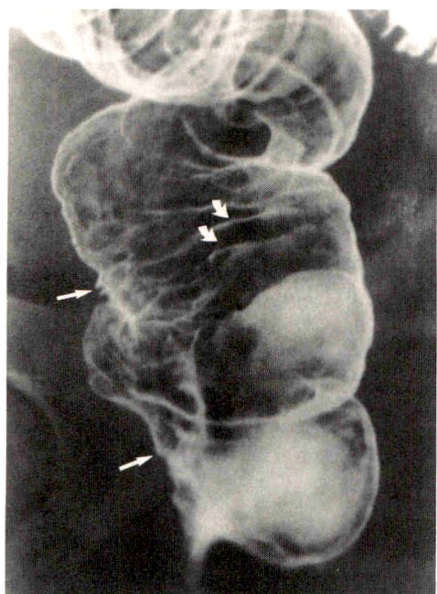
The treatment for these 11 patients included prostatectomy (two cases), transurethral resection of the prostate (six cases), bilateral orchiectomy (five cases), external beam radiation (three cases), and/or estrogen therapy (three cases). Six patients died within 2 years of the barium enema examination, and no autopsies were performed. The remaining five patients were discharged with diffuse disease and pelvic metastases, and all were lost to clinical follow-up.

Radiographic Findings

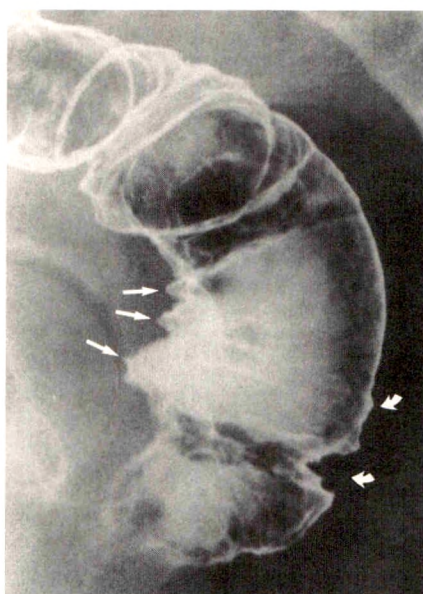
Four patients had disease confined to the rectum, with circumferential mass effect, narrowing, and/or spiculated, tethered mucosal folds (Figs. 1 and 2). The remaining seven patients had localized involvement of the rectosigmoid colon with sparing of the distal rectum. Two of those patients had a smooth, extrinsic, 5-cm mass impression on the anterior wall of the rectosigmoid junction (Fig. 3). Another patient had a discrete, 2-cm, submucosal mass with central umbilication on the left anterolateral wall of the rectosigmoid colon. The remaining four patients had rectosigmoid narrowing, with marked spiculation and pleating of mucosal folds in this region (Figs. 4 and 5). The average length of the narrowed rectosigmoid colon was 11 cm (range, 7–15 cm). Although the degree of mass effect and pleating of the bowel was greatest anteriorly in the region of the rectosigmoid junction, the mass extended circumferentially behind the rectosigmoid colon into the presacral space in all four cases. The average width of the presacral space was 5.5 cm at the S3–S4 level in those four cases (range, 4.5–6.0 cm) (normal presacral space, 0.7 cm; range, 0.2–1.6 cm) [16].

Discussion

Barium enemas may be performed in patients who have gastrointestinal symptoms due to rectal involvement by prostatic carcinoma. In some cases, the referring clinician is unaware of the patient's underlying prostatic cancer. In six of the 11 patients in our study, the diagnosis of prostatic cancer



A



B



Fig. 2.—Distal rectal invasion by prostatic carcinoma. Note distal rectal narrowing with circumferential pleating of mucosa and spiculation of luminal contour (arrows).

Fig. 1.—Rectal invasion by prostatic carcinoma.

A, Anteroposterior spot film shows mass effect and spiculation predominantly along right lateral wall of rectum (straight arrows) and en-face pleating of mucosa (curved arrows).

B, Lateral spot film of rectum shows mass effect along anterior rectal wall and spiculation of mucosal contour (straight arrows). Mild circumferential extension is seen distally (curved arrows). Rectal biopsy showed poorly differentiated prostatic carcinoma in submucosa, with focal microscopic invasion of mucosa.

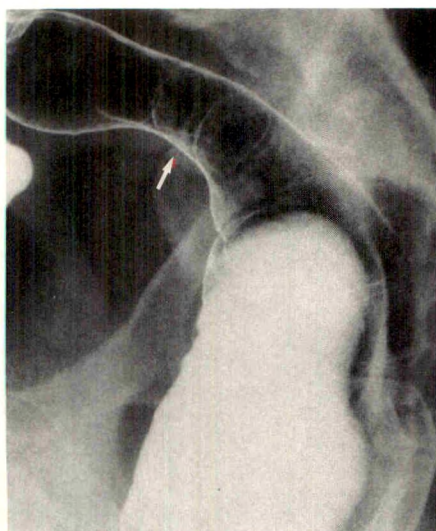
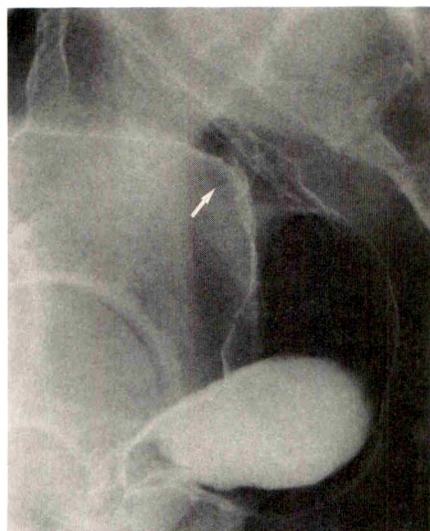
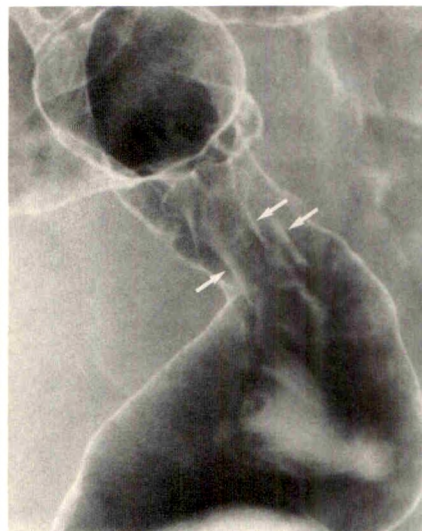


Fig. 3.—Extrinsic mass impression by prostatic carcinoma. Lateral spot film of rectum shows smooth, 5-cm, extrinsic mass indenting anterior wall of rectosigmoid junction (arrow). An extremely large, 207-g prostate gland was removed by suprapubic prostatectomy. No surgical evidence of colonic invasion was found.



A

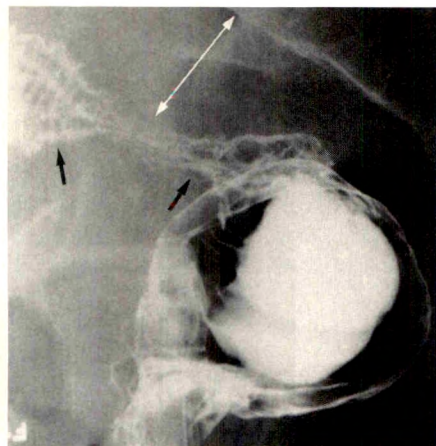


B

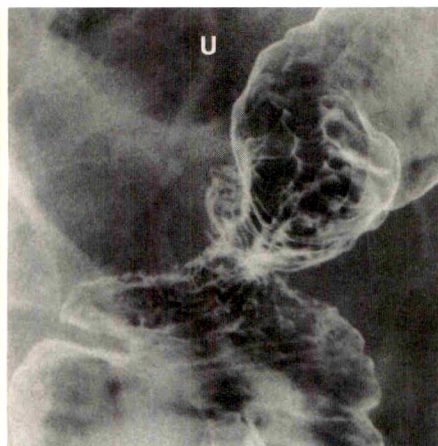
Fig. 4.—Rectosigmoid invasion by prostatic carcinoma.

A, Lateral spot film of rectum shows extrinsic mass effect and slight tethering of anterior rectosigmoid colon with narrowing of lumen (arrow).

B, Close-up oblique view of rectosigmoid junction shows circumferential pleating of mucosa (arrows). Proctoscopy and biopsies revealed prostatic carcinoma invading submucosa. Direct invasion of rectosigmoid colon was confirmed during right hemicolectomy for a coexisting colonic carcinoma.



A



B

Fig. 5.—Direct invasion of rectosigmoid colon by prostatic carcinoma. Lateral (A) and slight left posterior oblique (B) views of rectum show mass effect and markedly spiculated contour along anterior rectosigmoid junction and sigmoid colon (black arrows), and widening of superior presacral space (double white arrow). Note opacification of right ureter (U) from earlier IV urography. At exploratory laparotomy, prostatic carcinoma had directly invaded sigmoid colon. Although intraperitoneal metastases to rectovesical space may produce a similar appearance, circumferential narrowing of rectosigmoid colon and widening of presacral space should suggest correct diagnosis.

was not known at the time of the barium enema. The remaining five patients had known prostatic cancer, but a coexisting colonic neoplasm was suspected because of gastrointestinal symptoms. Thus, it is important to be able to recognize colonic involvement by prostatic carcinoma on barium enema examination.

The normal prostate gland abuts the anterior wall of the middle and distal rectum, extending about 5–6 cm from the anal verge [1]. This anatomic relationship between the prostate and rectum is seen well on sagittal MR scans of the pelvis (Fig. 6). Thus when prostatic carcinoma invades the rectum, one might expect to find mass effect and spiculation along the anterior wall of the middle or distal rectum on barium enema examinations [11]. Surprisingly, however, only

four of our patients (36%) with prostatic carcinoma had distal rectal involvement, whereas seven patients (64%) had localized involvement of the rectosigmoid junction with sparing of the distal rectum. More than two decades ago, Becker [7] similarly found that most patients with rectal invasion by prostatic carcinoma had localized rectosigmoid involvement.

The spread of prostatic carcinoma to the rectosigmoid colon with distal rectal sparing can be explained by the fact that this tumor usually spreads superiorly to the seminal vesicles before it extends posteriorly and laterally to invade the rectum. As a result, prostatic carcinoma may extend as far as 10–12 cm from the anal verge [1], directly abutting the anterior wall of the rectosigmoid junction and displacing the rectovesical space anteriorly and superiorly. Thus, prostatic

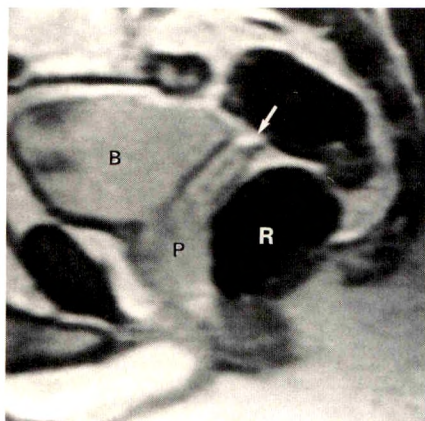


Fig. 6.—T2-weighted sagittal MR scan of pelvis shows that normal prostate gland (P) abuts mid and distal rectum (R) anteriorly. Note region of peritoneal reflection (arrow) overlying midportion of seminal vesicles. Rectum has been distended with air by rectal catheter. B = bladder.

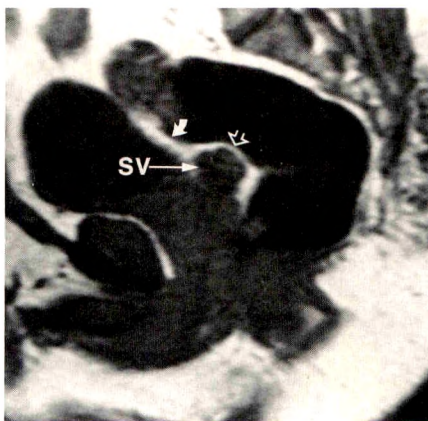


Fig. 7.—T1-weighted sagittal MR scan of pelvis shows mild extrinsic mass effect (open arrow) on air-filled rectosigmoid junction by enlarged seminal vesicle (SV). At surgery, prostatic carcinoma invaded seminal vesicle but not rectum. This sagittal MR scan is the correlate of the smooth extrinsic mass impression on the rectosigmoid junction seen on barium enema in Fig. 3. Note that peritoneal reflection has been lifted cranially and anteriorly (curved arrow) because of prostatic and seminal vesicular enlargement.

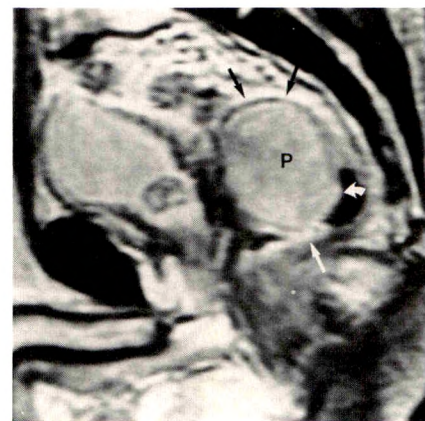


Fig. 8.—T2-weighted sagittal MR scan of pelvis shows huge prostatic carcinoma (P) obliterating lumen of rectosigmoid colon (black arrows) and rectum (straight white arrow). Original rectosigmoid junction is shown (curved arrow). This sagittal view shows marked cranial growth of tumor into region of seminal vesicles with invasion of rectosigmoid colon.

carcinoma may directly invade the rectosigmoid colon while sparing the distal rectum. These features are well illustrated on sagittal MR scans of the pelvis in patients with prostatic carcinoma invading the seminal vesicles and/or rectosigmoid colon (Figs. 7 and 8).

Rectosigmoid involvement by prostatic carcinoma is first manifested radiographically by a smooth, extrinsic mass impression on the anterior wall of the bowel (Fig. 3). This extrinsic mass effect may represent prostatic carcinoma impressing the colon (as, for example, when the malignancy is superimposed on a large, benign hyperplastic prostate) or prostatic carcinoma invading the seminal vesicles (Fig. 7). With direct invasion of the rectosigmoid colon, the luminal contour may have an irregular, spiculated appearance, predominantly along its anterior border (Fig. 4). In advanced cases, posterior spread of tumor between the periprostatic and perirectal layers of Denonvillier fascia may cause circumferential narrowing and spiculation of the bowel with associated widening of the presacral space (Fig. 5) [7]. Thus, the radiographic findings depend on (1) the size of the prostate, (2) the status of the seminal vesicles, (3) the depth of bowel-wall invasion, and (4) the extent of circumferential spread of tumor.

When rectosigmoid invasion by prostatic carcinoma causes narrowing, mass effect, and spiculation of the bowel, predominantly along its anterior border, the differential diagnosis includes intraperitoneal metastases or abscess formation in the rectovesical space [4, 7]. However, prostatic carcinoma usually spreads posteriorly around the bowel, causing circumferential narrowing and widening of the presacral space, whereas neoplastic or inflammatory seeding of the rectovesical space almost always produces abnormalities that are confined to the anterior wall of the rectosigmoid colon [11]. Patients with invasive prostatic carcinoma also have osteo-

blastic metastases or ureteral obstruction more frequently than do patients with intraperitoneal metastases from pancreatic, gastric, or colonic carcinoma, and often will have elevated levels of serum acid phosphatase or prostatic-specific antigen at this stage of the disease. Of course, the correct diagnosis should be suggested by a history of known prostatic carcinoma. Thus, these conditions usually can be differentiated on radiographic and/or clinical grounds.

Invasion of the distal rectum by prostatic carcinoma may produce a spiculated, pleated mucosal contour indistinguishable from that of bladder cancer or other pelvic malignancy invading the bowel [4, 7, 12]. Perirectal inflammatory processes, such as Crohn disease or lymphogranuloma venereum, may produce a similar appearance [4, 7, 10, 12]. Rarely, carcinoid tumor of the rectum may produce narrowing and spiculation mimicking this appearance [17].

In the past, prostatic carcinoma invading the rectum has been misdiagnosed as rectal carcinoma on single-contrast barium enema examinations [4, 5, 8, 9, 13, 14]. In our study, however, rectal involvement by prostatic cancer could be differentiated from rectal carcinoma by the typical mucosal pleating or tethering observed in the rectum or rectosigmoid colon on double-contrast radiographs (Figs. 1, 2, 4, and 5). The latter finding indicates a desmoplastic response to a neoplastic or inflammatory process in the bowel wall [11] and is rarely observed in patients with primary colorectal cancers.

When rectal involvement by prostatic carcinoma is suspected, proctoscopy and rectal biopsy may be performed to confirm the diagnosis. Immunohistochemical stains for prostatic-specific antigen or prostatic acid phosphatase, markers that identify tissue of prostatic origin, may also be helpful in identifying poorly differentiated carcinomas as prostatic in origin [2, 18, 19]. CT, transrectal sonography, and/or MR imaging may then be used to stage the disease [20–25].

REFERENCES

- Goldfarb S, Leiter E. Invasion of the rectum by carcinoma of the prostate. *Arch Surg* **1980**;115:1117-1119
- Huang TY, Yam LT, Li CY. Unusual radiologic features of metastatic prostatic carcinoma confirmed by immunohistochemical study. *Urology* **1984**;23:218-223
- Lazarus JA. Complete rectal occlusion necessitating colostomy due to carcinoma of the prostate. *Am J Surg* **1935**;30:502-505
- Gengler L, Baer J, Finby N. Rectal and sigmoid involvement secondary to carcinoma of the prostate. *AJR* **1975**;125:910-917
- Winter CC. The problem of rectal involvement by prostatic cancer. *Surg Gynecol Obstet* **1957**;105:136-140
- Aigen AB, Schapira HE. Metastatic carcinoma of prostate and bladder causing intestinal obstruction. *Urology* **1983**;21:464-466
- Becker JA. Prostatic carcinoma involving the rectum and sigmoid colon. *AJR* **1965**;94:421-428
- Fry DE, Amin M, Harbrecht PJ. Rectal obstruction secondary to carcinoma of the prostate. *Ann Surg* **1979**;189:488-492
- Lasser A. Adenocarcinoma of the prostate involving the rectum. *Dis Colon Rectum* **1978**;21:23-25
- Shin MS, Witten DM. Unusual involvement of the rectum by carcinoma of the prostate. *Am J Dig Dis* **1975**;20:42-48
- Meyers MA. *Dynamic radiology of the abdomen. Normal and pathologic anatomy*, 2nd ed. New York: Springer-Verlag, **1982**:55-92
- Mir M, Dikranian H, Cogbill CL. Carcinoma of the prostate presenting as obstructive carcinoma of the rectum. *Am Surg* **1973**;39:582-586
- Davis JM. Carcinoma of the prostate presenting as disease of the rectum. *Br J Urol* **1960**;32:197-203
- Laufer I. *Double contrast radiology with endoscopic correlation*. Philadelphia: Saunders, **1979**
- Chrispin AR, Fry IK. The presacral space shown by barium enema. *Br J Radiol* **1963**;36:319-322
- Peskin GW, Orloff MJ. A clinical study of 25 patients with carcinoid tumors of the rectum. *Surg Gynecol Obstet* **1959**;109:673-681
- Fair WR. Carcinoma of the prostate: current thoughts on diagnosis and staging. *Surg Clin North Am* **1982**;62:1085-1098
- Li CY, Lam WKW, Yam LT. Immunohistochemical diagnosis of prostatic cancer with metastasis. *Cancer* **1980**;46:706-712
- Morgan CL, Calkins RF, Cavalcanti EG. Computed tomography in the evaluation, staging and therapy of carcinoma of the bladder and prostate. *Radiology* **1981**;140:751-761
- Rifkin MD, Marks G. Transrectal US as an adjunct in the diagnosis of rectal and extrarectal tumors. *Radiology* **1985**;157:499-502
- Lee F, Gray JM, McLeary RD, et al. Prostatic evaluation by transrectal sonography: criteria for diagnosis of early carcinoma. *Radiology* **1986**;158:91-95
- Rifkin MD, Friedland GW, Shortliffe L. Prostatic evaluation by transrectal endosonography: detection of carcinoma. *Radiology* **1986**;158:85-90
- Biondetti PR, Lee JKT, Ling D, Catalona WJ. Clinical stage B prostate carcinoma: staging with MR imaging. *Radiology* **1987**;162:325-329

Book Review

Gastrointestinal Nuclear Imaging. Edited by Michael G. Velchik and Abass Alavi. (Vol. 7 of Contemporary Issues in Gastroenterology. Edited by Sidney Cohen and Roger D. Soloway.) New York: Churchill Livingstone, 289 pp., 1988. \$65

Of the 12 chapters in this book, three are contributed by the editors and two by their colleagues at the University of Pennsylvania. The first chapter gives a comprehensive coverage on the subject of salivary scintigraphy. A gamut of salivary pathologic changes is presented at the end of it. Techniques for studies of gastrointestinal transit, including esophageal transit, gastric emptying, small and large bowel transit, and gastroesophageal reflux, are presented in the second chapter. Their relative values are also given. Chapter 3 reviews in detail the localization of ectopic gastric mucosa by scintigraphy. Topics included are Meckel diverticulum, duplication of alimentary tract, retained gastric antrum, and Barrett esophagus. Relevant pitfalls are also covered in this chapter. The detection and localization of lower gastrointestinal bleeding site is described in chapter 4. Extensive discussion is presented on the merits and pitfalls of the two methods: ^{99m}Tc -sulfur colloid and labeled RBCs. Their own preference of ^{99m}Tc -sulfur colloid scintigraphy as the initial study is explained.

Chapter 5 covers radiopharmaceuticals and the technique and application of scintigraphy to the diagnosis of focal and diffuse hepatic and splenic disease. Single-photon emission CT of the liver is discussed in chapter 6. Chapter 7 presents the problems in abscess detection with both gallium-67 and ^{111}In -labeled WBCs. Chapter 8 gives a concise coverage of LeVeen shunt patency evaluation. A comprehensive review of hepatobiliary scintigraphy is given in chapter 9, with 231 references. Chapter 10 is on the subject of pediatric applications of liver-spleen imaging and gastroesophageal reflux im-

aging. Chapter 11 deals with imaging with radiolabeled monoclonal antibodies. In the last chapter, miscellaneous studies on the gastrointestinal tract with nuclear medicine methods are covered. Topics include quantification of gastrointestinal blood loss, albumin loss, vitamin B₁₂ absorption, iron absorption, breath assays, carbohydrate absorption, bile-salt breath analysis, xylose absorption, and fat absorption.

There is a similar book by British authors, *Nuclear Gastroenterology*, edited by P. J. A. Robinson (London: Churchill Livingstone, 180 pp. \$59.50). Topics covered in both volumes are similar, except for salivary imaging. Both are written by authors with a great deal of experience. Because the discussions are complementary in many places, I recommend reading both books for an update on nuclear medicine applications in gastroenterology.

I have a minor complaint about this book. The paper is of good quality, but the shiny finish makes it difficult to read under many lighting conditions. In conclusion, this book is highly recommended for general nuclear medicine physicians as a source of reference on the subject of gastrointestinal nuclear imaging.

Hing-Har Lo
University of Virginia
Charlottesville, VA 22908
Montgomery Radiology Associates
Blacksburg, VA 24060

Heterotopic Gastric Mucosa in the Duodenal Bulb: Relationship to Peptic Ulcer

Robin H. M. Smithuis^{1,2}
Colin G. Vos^{1,3}

Heterotopic gastric mucosa in the duodenal bulb causes a characteristic radiologic abnormality consisting of multiple small, well-defined nodules in the mucosa. This finding was identified in 92 (5%) of 1873 consecutive standard biphasic barium examinations of the upper gastrointestinal tract. Of these 92, only one patient (1%) had an associated duodenal ulcer as compared with the other 1781 patients without heterotopic gastric mucosa of whom 225 (13%) had duodenal ulcers or scars ($p = .002$). No gastric ulcers or ulcer scars were identified in the patients with heterotopic gastric mucosa, whereas ulcers or scars were identified in 88 patients (5%) without heterotopic gastric mucosa ($p = .05$).

These data raise the possibility that heterotopic gastric mucosa protects against peptic ulceration.

Heterotopic gastric mucosa (HGM) can be found in all portions of the alimentary tract. It may be either an acquired metaplasia, as in Barrett esophagus, or a true gastric heterotopia of congenital origin, as in Meckel diverticulum [1-5].

In the duodenum, both forms can be found. The gastric metaplasia consists of flat lesions that cannot be identified radiologically. This metaplasia has a positive correlation with duodenal ulceration [6-8]. In its congenital form, HGM consists of nodules that protrude from the surface of the duodenal mucosa and that can be identified radiologically. Usually they appear as multiple sharply margined elevations with an angular form. The individual excrescences range in diameter from one to several millimeters and are located adjacent to the pylorus [9] (Figs. 1 and 2).

The clinical significance of the congenital form of HGM in the duodenal bulb is not known. The purpose of this study was to determine the relationship between HGM and peptic ulceration.

Materials and Methods

This retrospective study included all 1873 consecutive patients with dyspepsia who had radiographic examinations of the upper gastrointestinal tract between January 1984 and June 1985 at St. Elisabeth's of Groote Gasthuis. The patients ranged in age from 12 to 89 years (mean, 49). The contrast study consisted of a standard biphasic barium examination of the stomach and duodenum. IV glucagon was given in all cases.

All studies were reviewed by one of the authors for the presence of HGM and duodenal or gastric ulcers or scars. The findings were compared with the original reports. Any disagreement was discussed until final consensus was achieved. When they interpreted the radiographs, all examiners understood the purpose of the study (i.e., to assess the relation between HGM and peptic ulceration).

The radiologic diagnosis of HGM was made when characteristic elevated nodules were present in the duodenal bulb [9]. Whenever HGM could not be confidently differentiated from other elevated lesions in the duodenum, such as Brunner gland hyperplasia, benign lymphoid hyperplasia, or celiac disease, the diagnosis of HGM was not made. This distinction was

Received April 14, 1988; accepted after revision July 22, 1988.

¹ Department of Radiology, St. Elisabeth's of Groote Gasthuis, POB 417, 2000 AK Haarlem, the Netherlands.

² Present address: Department of Radiology, University Hospital Leiden, P.O. Box 9600, 2300 RC Leiden, the Netherlands. Address reprint requests to R. H. M. Smithuis.

³ Present address: Department of Radiology, University Hospital Utrecht, Catherijnesingel 101, 3511 GV Utrecht, the Netherlands.

AJR 152:59-61, January 1989
0361-803X/89/1521-0059
© American Roentgen Ray Society

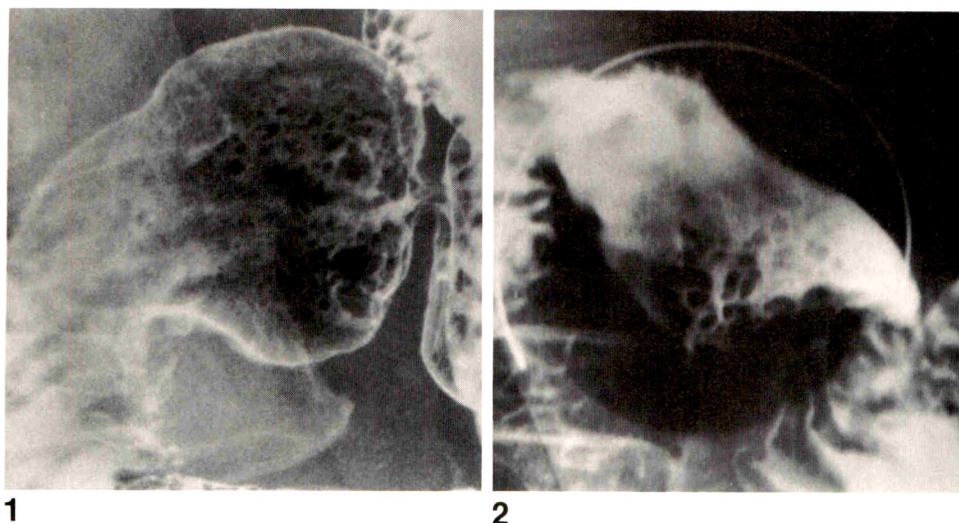


Fig. 1.—Air-contrast radiograph (obtained with patient in supine position) shows multiple abruptly margined excrescences of different size in the duodenal cap, characteristic of heterotopic gastric mucosa. Endoscopy was not performed.

Fig. 2.—Compression radiograph in another patient (obtained with patient in erect position) shows multiple elevated lesions. Lesions range in size from 1 to 6 mm and are located predominantly adjacent to the pylorus. Biopsy showed heterotopic gastric mucosa.

made on the basis of the number, size, location, and type of margin of the nodules.

A persistent focal collection of barium in the gastric or duodenal wall was classified as an ulcer. A pattern of radiating folds in the mucosa of the stomach or duodenum or a characteristic deformity of the duodenal bulb, without a barium collection, was considered an ulcer scar.

The prevalence of ulceration in patients with HGM was compared with that in patients without HGM by using the chi-square test with Yate's correction. Endoscopy was performed in 19 (21%) of 92 patients with the radiologic diagnosis of HGM for reasons not related to the presence of HGM. All the biopsies in these cases showed full-thickness gastric mucosa of the fundic type, consistent with the diagnosis of congenital HGM [1, 4, 6].

Results

In 92 patients (5%), the radiologic examination revealed characteristic elevated nodules in the duodenal bulb, consistent with the diagnosis of HGM. None of these 92 patients had a gastric ulcer, and only one had a duodenal ulcer on the barium study. The ulcer in that case was located at the junction of the apex of the bulb and the second part of the duodenum and was confirmed endoscopically.

In the group of 1781 patients without radiologic evidence of HGM, 225 patients (13%) had an active ulcer (144 patients) or ulcer scar (81 patients) in the duodenum. Eighty-eight patients (5%) had a gastric ulcer (57 cases) or ulcer scar (31 cases). The differences between patients with HGM and patients without HGM in occurrence rates of duodenal and gastric ulcers or scars were statistically significant ($p = .002$ and $p = .05$, respectively).

Discussion

The nodules of congenital HGM consist of gastric mucosa of the fundic type. The ability of HGM to secrete acid has been shown by endoscopic Congo Red test and by the accumulation of ^{14}C -aminopyrine [10, 11]. The radiographic findings of HGM were first described by Mitre and Brodmerkel

in 1974 [12]. In 1980, Langkemper et al. [9] described the radiographic and endoscopic findings in 22 patients with HGM in the duodenal bulb.

The nodules of HGM have a characteristic radiographic appearance and usually can be differentiated from other duodenal lesions. The nodules in Brunner gland hyperplasia are not angular but have smooth margins that reflect their submucosal origin. These nodules are more evenly distributed on the mucosal surface [2]. Benign lymphoid hyperplasia consists of numerous round elevations with a uniform diameter of 1–2 mm that cover the entire surface of the duodenal bulb [2]. In celiac disease, filling defects may occur in the duodenal bulb, causing an unusual mosaic pattern [13]. These lesions usually are accompanied by other mucosal abnormalities. None of the entities that may simulate the appearance of HGM have a predilection for the juxtapyloric region.

Using strict criteria for the radiologic diagnosis of HGM, we found a 100% radiologic-pathologic correlation in the 19 cases that were biopsied. This excellent correlation makes it appropriate to base the study purely on radiologic findings. The 5% prevalence of HGM in our study may seem to be high, but endoscopic reports have found this condition in as many as 12% of cases [14].

The clinical significance of HGM, especially in relation to peptic ulceration, is unknown. In many reports on HGM, however, no mention is made of associated duodenal or gastric ulceration [3, 15–18].

There are only two reports in which peptic ulcers were found in association with HGM [14, 19]. Recently, Agha et al. [19] found erosions in five of 25 cases of biopsy-proved HGM. Two of these patients had associated ulcer craters in the duodenal bulb. These patients had an unusual form of HGM that consisted of coarse, nodular mucosa of the duodenal bulb. To our knowledge, this radiologic pattern of HGM has not been described before and differs from the usual type of HGM, which consists of clusters of 1- to 3-mm plaques raised above the flat duodenal mucosa.

We found a low prevalence of peptic ulceration in patients with HGM. One explanation could be that the presence of a

duodenal ulcer or scar makes it impossible to detect HGM. In our experience, however, glucagon-induced hypotonia allows visualization of the mucosal surface, even when deformation or ulceration of the duodenal bulb is present. Moreover, this explanation would not account for the absence of gastric ulceration in these patients. Another possibility is that HGM, presenting as multiple elevated lesions in the duodenal bulb, provides some protection against peptic ulceration. Negative feedback on gastric acid output, triggered by duodenal acidification, could be a possible mechanism [20].

REFERENCES

1. Taylor AL. The epithelial heterotopias of the alimentary tract. *J Pathol Bacteriol* 1927;30:415-449
2. Op den Orth JO. Duodenum. In: Margulis RA, Burhenne HJ, eds. *Alimentary tract radiology*, 3rd ed. St. Louis, MO: Mosby, 1983:800-831
3. Cynn WS, Rickett RR. Heterotopic gastric mucosal polyp in the duodenal bulb associated with congenital absence of the gallbladder. *Am J Gastroenterol* 1973;60:171-177
4. Wolff M. Heterotopic gastric epithelium in the rectum: a report of three new cases with a review of 81 cases of gastric heterotopia in the alimentary canal. *Am J Clin Pathol* 1971;55:604-616
5. Whitehead R. *Mucosal biopsy of the gastrointestinal tract*. Philadelphia: Saunders, 1985:128-138
6. Johanssen AA, Hansen OH. Heterotopic gastric epithelium in the duodenum and its correlation to gastric disease and acid level. *Acta Pathol Microbiol Immunol Scand [A]* 1973;81,5:676-680
7. James AH. Gastric epithelium in the duodenum. *Gut* 1964;5:285-294
8. Hoedemaeker PJ. Heterotopic gastric mucosa in the duodenum. *Digestion* 1970;3:165-173
9. Langkemper R, Hoek AC, Dekker W, Op den Orth JO. Elevated lesions in the duodenal bulb caused by heterotopic gastric mucosa. *Radiology* 1980;137:621-624
10. Ikeda K, Sannohe Y, Murayama H, Ikeda R, Inutsuha S. Heterotopic gastric mucosa in the duodenum: reaction to Congo red under fiberoscopic observation. *Endoscopy* 1982;4:166-167
11. Haglund U, Rehnberg O, Elander B, Fellenius E, Knutson F, Olbe L. Acid secreting gastric heterotopia in the duodenum. *Acta Chir Scand* 1982;148:693-696
12. Mitre R, Brodmerkel G. Heterotopic parietal cells in the duodenal bulb (abstr). *Gastrointest Endosc* 1974;20:182
13. Jones B, Bayless TM, Hamilton SR, Yardley JH. "Bubbly" duodenal bulb in celiac disease: radiologic-pathologic correlation. *AJR* 1984;142:119-122
14. Weingart J, Seib HJ, Elster K, Ottenjann R. Magenschleimhaut-heterotopien im oberen Gastrointestinaltrakt. *Leber Magen Darm* 1984;14:155-160
15. Franzin G, Musola R, Negri A, Mencarelli R, Fratton A. Heterotopic gastric (fundic) mucosa in the duodenum. *Endoscopy* 1982;4:166-167
16. Johanssen AA, Hansen OH. Macroscopically demonstrable heterotopic gastric mucosa in the duodenum. *Scand J Gastroenterol* 1973;8:59-63
17. Spiller RC, Shousha S, Barrison IG. Heterotopic gastric tissue in the duodenum: a report of eight cases. *Dig Dis Sci* 1982;27:880-883
18. Lessells A, Martin D. Heterotopic gastric mucosa in the duodenum. *J Clin Pathol* 1982;35:591-595
19. Agha FP, Ghahremani GG, Tsang T, Victor TA. Heterotopic gastric mucosa in the duodenum: radiographic findings. *AJR* 1988;150:291-294
20. Andersson S, Nilsson G, Uvnas B. Effect of acid in proximal and distal duodenal pouches on gastric secretory responses to gastrin and histamine. *Acta Physiol Scand* 1967;71:368-378

Gastrointestinal Radiology Update 1989

Focus: New Problems and New Solutions

American Roentgen Ray Society Annual Meeting Friday Symposium

May 12, 1989, New Orleans Hilton, New Orleans, LA

The Immune System and Its Deficiencies

8:00–8:20 a.m.	Immune diseases and the small intestine (<i>Olmsted</i>)
8:20–8:50 a.m.	AIDS and the GI radiologist (<i>Federle</i>)
8:50–9:10 a.m.	Iatrogenic immune suppression (<i>Jones</i>)

The Bile Ducts: Linking Diagnosis and Therapy

9:25–9:45 a.m.	Diagnostic radiology of the bile ducts— 1989 (<i>Balfe</i>)
9:45–10:15 a.m.	Innovative intervention in biliary disease (<i>Teplick</i>)
10:15–10:35 a.m.	Biliary lithotripsy (<i>Ferrucci</i>)

New Horizons in Oncology: Focus on Cancer of the Rectum

10:50–11:10 a.m.	Imaging and immunity: monoclonal antibodies (<i>Wahl</i>)
11:10–11:35 a.m.	Cross-sectional imaging: staging and recurrence (<i>Thompson</i>)
11:35–Noon	Endosonography in the rectosigmoid (<i>Hill</i>)

Primary Liver Tumors: Diagnosis by MR Imaging

Ernst Rummeny^{1,2}
 Ralph Weissleder¹
 David D. Stark¹
 Sanjay Saini¹
 Carolyn C. Compton³
 William Bennett³
 Peter F. Hahn¹
 Jack Wittenberg¹
 Ronald A. Malt⁴
 Joseph T. Ferrucci¹

MR features of 153 proved primary liver tumors (95 malignant, 58 benign) in 55 patients with hepatocellular carcinoma (21), cholangiocarcinoma (seven), carcinosarcoma (one), hepatoblastoma (one), hemangioma (16), hepatic adenoma (four), focal nodular hyperplasia (three), leiomyoma (one), and hemangioendothelioma (one) were studied retrospectively to determine which techniques are most reliable for lesion detection and which criteria are most useful for differential diagnosis. MR data were correlated with histologic features such as fatty degeneration, fibrosis, and peritumoral edema. Unlike metastatic cancer, hepatocellular carcinoma was best detected ($p < .01$) with T2-weighted pulse sequences. The mean tumor-liver T2 difference was 34.4%, while the mean T1 difference was only 21.8%. A tissue-specific diagnosis of hepatocellular carcinoma was possible in 14 of 21 patients by identification of fatty degeneration of the tumor (eight of 17), tumor capsule (five of 21), and/or vascular invasion (six of 21). MR features of peritumoral edema, present in six of 21 patients with hepatocellular carcinoma and in seven of 25 patients with metastases, were exclusively associated with malignant tumors.

The large variation in tissue characteristics (relaxation times and proton density) seen in primary liver tumors necessitates the use of multiple pulse sequences to maximize lesion detection. However, the combined use of T1- and T2-weighted spin-echo and T2-weighted phase-contrast images had the advantage of distinguishing benign from malignant primary liver tumors in 48 of 55 patients in this series.

MR imaging has become an important diagnostic technique in the detection of focal liver lesions. Preliminary studies using a variety of MR imaging techniques have shown promise for detection and differential diagnosis of hepatocellular carcinoma (HCC) [1, 2], cholangiocarcinoma [3], and benign primary liver tumors [4-6]. To identify pulse sequences best suited to detection of primary liver tumors (PLTs) and to establish criteria for differential diagnosis, we evaluated quantitative MR findings and morphologic features in 55 patients with PLT.

Materials and Methods

Subjects

A total of 80 subjects were studied: 43 women and 35 men (23-74 years old), and two children (2 and 7 years old). The study population included 55 consecutive patients with histologically proved or well-documented PLTs referred for MR imaging to the Massachusetts General Hospital. Thirty patients had malignant PLTs and 25 patients had benign PLTs. Of the 30 patients with malignant PLTs, 21 had HCC, seven had cholangiocarcinoma, one had a carcinosarcoma, and one had a hepatoblastoma. Of the 25 patients with benign PLTs, 16 had cavernous hemangiomas, four had hepatic adenomas, three had focal nodular hyperplasia, one had a leiomyoma, and one had a hemangioendothelioma.

To distinguish features specific for PLT from features seen in patients with secondary (metastatic) cancer, we selected a control group of 25 consecutive patients with 105 hepatic lesions, histologic proof of adenocarcinoma metastatic to the liver, and proved primary colon

Received May 31, 1988; accepted after revision August 1, 1988.

E. Rummeny is supported by the Deutsche Forschungsgemeinschaft, Ru-374; D. D. Stark is supported by American Cancer Society grants JFRA-163 and PDT-326; and S. Saini is supported by the Research and Educational Fund of the Radiological Society of North America.

¹ Department of Radiology, Massachusetts General Hospital and Harvard Medical School, Fruit St., Boston, MA 02114. Address reprint requests to D. D. Stark.

² Present address: Department of Clinical Radiology, Westfälische Wilhelms-Universität, Albert-Schweitzer-Str. 33, D-4400 Münster, W. Germany.

³ Department of Pathology, Massachusetts General Hospital and Harvard Medical School, Boston, MA 02114.

⁴ Surgical Services, Massachusetts General Hospital, and Department of Surgery, Harvard Medical School, Boston, MA 02114.

AJR 152:63-72, January 1989

0361-803X/89/1521-0063

© American Roentgen Ray Society

cancer. This histologically homogeneous group, with the most common type of secondary liver cancer, was used as a reference standard. The control patients were scanned during the same period of time (October 1986 through November 1987) with the same techniques, and images were analyzed in the same manner as for the PLT (experimental) group.

Pathology

The diagnosis of malignant PLT was pathologically proved in all 30 cases by resection ($n = 14$), surgical biopsy ($n = 7$), fine-needle biopsy ($n = 4$), or autopsy ($n = 5$). Of the 25 patients with benign PLTs, pathologic proof was obtained by surgical resection ($n = 7$), biopsy ($n = 7$), or autopsy ($n = 1$). In 10 patients with cavernous hemangioma, the diagnosis was established after 12–24 months of clinical observation, including repeated imaging studies. Liver metastases were proved by surgery in 11 patients, by fine-needle biopsy in eight, and by serial imaging studies in six.

Gross and histologic examinations of 20 resected PLTs (14 malignant, six benign) were performed by a liver pathologist within 12–48 hr of the MR examination. All 20 intact tumor specimens were sectioned in the transverse plane to facilitate detailed correlation with MR images. In two of the five autopsy cases, pathologic correlation of the disease with MR images was performed 3 weeks and 2 months after the MR examination.

Tumor size, location, vascular invasion, and presence of intrahepatic or extrahepatic metastases were recorded. Peritumoral edema (correlated with the MR finding of peritumoral hyperintensity) was diagnosed when markedly dilated sinusoids or dilated lymphatic channels were found in nontumorous liver tissue adjacent to a lesion [7]. Morphologic features of the tumor (vascular invasion, capsule, septation, scar, necrosis, and calcification) and adjacent liver tissue (peritumoral edema and bile stasis) were tabulated for each specimen.

Histologic specimens of all 30 malignant PLTs were fixed in formalin and were stained with one or more of the following: hematoxylin-eosin, oil-red-O for fat, Masson trichrome for collagen, periodic acid-Schiff for glycogen, and Hall for bile. Immunohistochemical stains were used to support the diagnosis of HCC by demonstrating intracytoplasmic hyaline globules containing α_1 -antitrypsin or α_1 -fetoprotein [8]. All specimens were reviewed and scored for the degree of necrosis, fibrosis, and fatty degeneration.

MR Imaging

MR images were obtained by using a 0.6-T superconducting imaging system [9]. With a slice thickness of 15 mm and an interslice gap of 25%, 11 sections were obtained in the transverse plane. A field of view of 41 cm and 128×256 image matrix yielded an in-plane resolution of 3.2×1.6 mm.

Multiple pulse sequences (four to eight; mean, five) were performed in each patient. Spin-echo (SE) images were acquired as T1-weighted images with 260/14 (TR/TE) and as multiple T2-weighted images with 2350/60, 120, 180. Inversion-recovery (IR) T1-weighted images were obtained with 1500/450/30 (TR/TI/TE). Phase-contrast (PC) images were acquired by using the method of Dixon and colleagues [10] with 2350/30 or 2350/60. Gradient-echo (GE) T1-weighted images were obtained with 200/11 and a 90° flip angle.

Quantitative Image Analysis

Signal-intensity measurements were obtained from regions of tumor, liver, and background noise by using operator-defined regions of interest [5, 6]. The contrast-to-noise ratio (CNR) is an effective

parameter for quantifying MR pulse sequence performance, because the absolute magnitude of CNR correlates with lesion detectability [11–13]. Tumor-liver CNR was calculated as the tumor-liver signal-intensity difference normalized to noise, the standard deviation of the background pixel signal intensity: $CNR = (S_{\text{tumor}} - S_{\text{liver}})/\text{noise}$.

For quantitative comparison of data obtained from images acquired with different scan times, CNR values for spin-echo and phase-contrast sequences (but not breath-hold gradient-echo sequences) were normalized to reflect a standard 10-min scan time: $CNR_{10 \text{ min}} = \text{measured CNR} \times (10/\text{scan time})^{0.5}$ [11, 14].

Tumor/liver signal-intensity ratios ($S_{\text{tumor}}/S_{\text{liver}}$) have been used for tissue characterization [6, 15] and as a measure of image contrast ($(S_{\text{tumor}} - S_{\text{liver}})/S_{\text{liver}}$ [16]. Unlike the task of lesion detection, tissue characterization does not depend on image noise, and therefore normalization to a fixed scan time is not necessary.

Tissue relaxation times have also been applied to characterize hepatic tumors [5, 17]. Tissue relaxation times (T1 and T2) and proton density were calculated with an iterative three-dimensional computer algorithm based on the Marquard method [18], simultaneously fitting the signal-intensity data measured from three to six images to the signal-intensity formula of spin-echo sequences.

Qualitative Image Analysis

MR images were analyzed independently by three radiologists without the knowledge of pathologic findings. Averaged readings of all three radiologists, rounded to the closest integer, are presented in Table 1. The number of lesions detected with each pulse sequence, compared with the number of lesions found by gross pathologic examination and/or other imaging techniques, is taken as a measure of sensitivity for lesion detection. The inescapable uncertainties in confirmation of individual lesions have been discussed [19].

The following morphologic MR imaging findings were tabulated for comparison with pathologic findings: vascular invasion, peritumoral hyperintensity, tumor capsule, intratumoral septation, central scar, necrosis, or calcification. Peritumoral hyperintensity (correlated with pathologic evidence of peritumoral edema) was diagnosed on T2-weighted images within areas of morphologically intact liver (i.e., liver tissue showing normal hepatic and portal veins). Tumor capsule was demonstrated as a thin circumferential rim, hypointense relative to liver, on T1-weighted images [1]. The MR diagnosis of tumor necrosis was based on demonstration of central regions within the tumor appearing hypointense relative to the tumor periphery on T1-weighted images and/or hyperintense relative to the tumor periphery on T2-weighted images. Intratumoral calcifications were diagnosed when punctate areas of hypointensity on T1-weighted images matched hypointense areas on even-echo T2-weighted images.

Statistical Analysis

To analyze the significance of differences in lesion detection and tumor-liver CNR among pulse sequences and in lesion/liver signal intensity, proton density, and T1 and T2 relaxation times among the different tumor types, we performed an analysis of variance for repeated measures (mixed model [20]) using a commercial software package [21]. Correction for normality, required for the analysis of variance, was achieved by data transformation with arc sine transformation (for number of lesions detected) and square root transformation (for CNR, tumor/liver ratio, proton density, T1, and T2) methods [20, 22]. Analysis of variance was performed for the subsets of HCC, cholangiocarcinoma, hemangioma, and metastases. Pairwise comparisons of all means were performed with the Scheffé multicomparison procedure [20]. For the subsets of adenoma, focal nodular

hyperplasia, and all other less common hepatic neoplasms, analysis of variance was not performed because the number of patients was not sufficient to fit this statistical model.

The Wilcoxon test [23] was used to analyze the significance of differences in proton density and T1 and T2 relaxation times between each tumor type and adjacent uninvolved liver. This statistical test was also applied to compare the signal-intensity ratios of fatty and fibrotic HCC vs nonfatty and nonfibrotic HCC.

Results

Lesion Detection

HCC was best ($p < .01$) detected with conventional T2-weighted spin-echo techniques (Table 1). Although T1-weighted techniques provided greater anatomic resolution, the absolute magnitude of tumor-liver CNR was significantly lower ($p < .05$) as compared with T2-weighted techniques (Table 2), a difference that is consistent with the smaller number of lesions detected by T1-weighted methods (Fig. 1 and Table 1).

No statistically significant difference was seen in detection of cholangiocarcinoma among the different pulse sequences used (Table 1). Individual lesions were often difficult to detect

because of volume-averaging with adjacent portal vessels and dilated bile ducts (Fig. 2). However, the highest lesion-liver CNR ($p < .01$) was found by using the phase-contrast technique (Table 2).

Metastases were best detected and showed the highest CNR with T1-weighted spin-echo and T2-weighted phase-contrast techniques (Tables 1 and 2), as in previous studies with midfield (<1.0-T) systems [10–12, 19]. The gradient-echo (fast scan breath-hold) method consistently detected fewer lesions ($p < .01$) and had lower CNR values ($p < .05$) than did conventional 10-min spin-echo pulse sequences. The T2-weighted phase-contrast technique was better than the T2-weighted spin-echo imaging in detecting liver metastases (Table 1) and showed CNRs significantly higher than those of corresponding in-phase spin-echo pulse sequences (Table 2).

Cavernous hemangioma was reliably detected ($p < .05$) and had large CNR values with either T2-weighted spin-echo or phase-contrast techniques (Tables 1 and 2). The T1-weighted spin-echo technique was inferior to T2-weighted techniques in the detection of small hemangiomas because these hemangiomas are similar in appearance to hepatic vessels. The gradient-echo technique was significantly inferior ($p < .05$) because of its reduced CNR (Table 2), which can

TABLE 1: Detection of Primary and Secondary Liver Tumors by MR Imaging

Tissue Type	No. of Patients	Fraction of Lesions Detected					
		SE 260/14	SE 2350/60	SE 2350/120	SE 2350/180	PC 2350/60	GE 200/11
Hepatocellular carcinoma	21	41/84	75/84 ^a	65/84	57/84	11/22	8/13
Cholangiocarcinoma	7	5/9	3/9	3/9	2/9	3/6	3/5
Hemangioma	16	35/50 ^b	43/50	46/50	47/50	10/12	9/18 ^c
Focal nodular hyperplasia	3	2/3	3/3	3/3	3/3	NA	NA
Hepatic adenoma	4	4/4	4/4	4/4	4/4	NA	1/1
Metastases	25	87/105	85/105	84/105	80/105	67/72 ^d	34/64 ^e

Note.—An analysis of variance (ANOVA) was performed among all pulse sequences for hepatocellular carcinoma, cholangiocarcinoma, hemangioma, and metastases. ANOVA was not applied to focal nodular hyperplasia and hepatic adenoma because the number of samples was not sufficient for this test. Numerators were rounded to the closest integer. SE = spin-echo; PC = phase-contrast; GE = gradient-echo; NA = not available.

^a Significantly larger ($p < .01/6.7$; 5, 272 [p value/F value; degrees of freedom]) fraction than SE 260/14 or SE 2350/180; other comparisons not significant (NS, $p > .05$).

^{b,c} Significantly smaller ($p < .01/8.6$; 5, 208) fraction than SE 2350/60, 120, 180; and PC 2350/60.

^d Significantly larger ($p < .01/12.9$; 5, 374) fraction than GE 200/11 and SE 2350/180; other comparisons NS.

^e Significantly smaller ($p < .01/12.9$, 5, 374) fraction than SE 260/14; SE 2350/60, 120, 180, and PC 2350/60.

TABLE 2: Lesion-Liver Contrast-to-Noise Ratios for Tumors of Varying Histology

Tissue Type	SE 260/14	SE 2350/60	SE 2350/120	SE 2350/180	PC 2350/60	GE 200/11
Hepatocellular carcinoma	-3.1 ± 8.7	7.6 ± 4.3^a	7.0 ± 4.6	5.5 ± 3.6	7.2 ± 4.9	-2.1 ± 2.2
Cholangiocarcinoma	-6.1 ± 2.6	7.5 ± 2.1	6.8 ± 3.3	8.8 ± 3.4	12.6 ± 3.2^b	-3.4 ± 1.4
Hemangioma	-14.0 ± 5.7	15.5 ± 6.5	16.8 ± 6.6	21.3 ± 7.8^c	19.2 ± 6.1	9.9 ± 2.0
Focal nodular hyperplasia	-0.4 ± 0.1	1.5 ± 0.8	1.5 ± 1.1	2.1 ± 0.8	NA	NA
Hepatic adenoma	-0.9 ± 3.6	9.3 ± 0.6	7.1 ± 1.6	10.6 ± 5.1	NA	4.1 ± 3.2
Metastases	-8.3 ± 3.6^d	4.7 ± 2.4	5.5 ± 3.1	4.9 ± 2.6	8.7 ± 4.2^d	-4.8 ± 2.7

Note.—An analysis of variance was performed among all pulse sequences for hepatocellular carcinoma, cholangiocarcinoma, hemangioma, and metastases. SE = spin-echo; PC = phase-contrast; GE = gradient-echo; NA = not available.

^a Contrast-to-noise ratio (CNR) higher ($p < .05/2.8$; 5, 55) [p value/F value; degrees of freedom]) than SE 260/14 and GE 200/11; other comparisons not significant (NS).

^b CNR higher ($p < .05/11.2$; 5, 21) than SE 260/14, SE 2350/120, and GE 200/11; other comparisons NS.

^c CNR higher ($p < .05/5.95$; 5, 69) than SE 260/14 and GE 200/11; other comparisons NS.

^d CNR higher ($p \leq .05/2.74$; 5, 67) than SE 2350/60, SE 2350/120, and GE 200/11. (PC 2350/60 images (opposed phase) showed significantly ($p < .05$, Wilcoxon) higher CNR values than conventional SE 2350/60.)

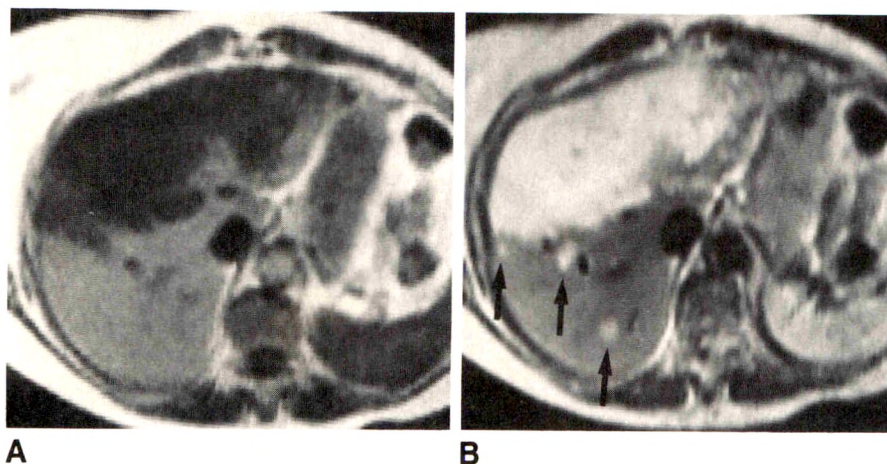


Fig. 1.—Multifocal hepatocellular carcinoma. A, T1-weighted spin-echo image, 260/14, shows large hypointense tumor mass involving both right and left liver.

B, T2-weighted spin-echo image, 2350/60, displays large mass hyperintense relative to liver. Satellite nodules, not detected on T1-weighted image, can be clearly identified (arrows).

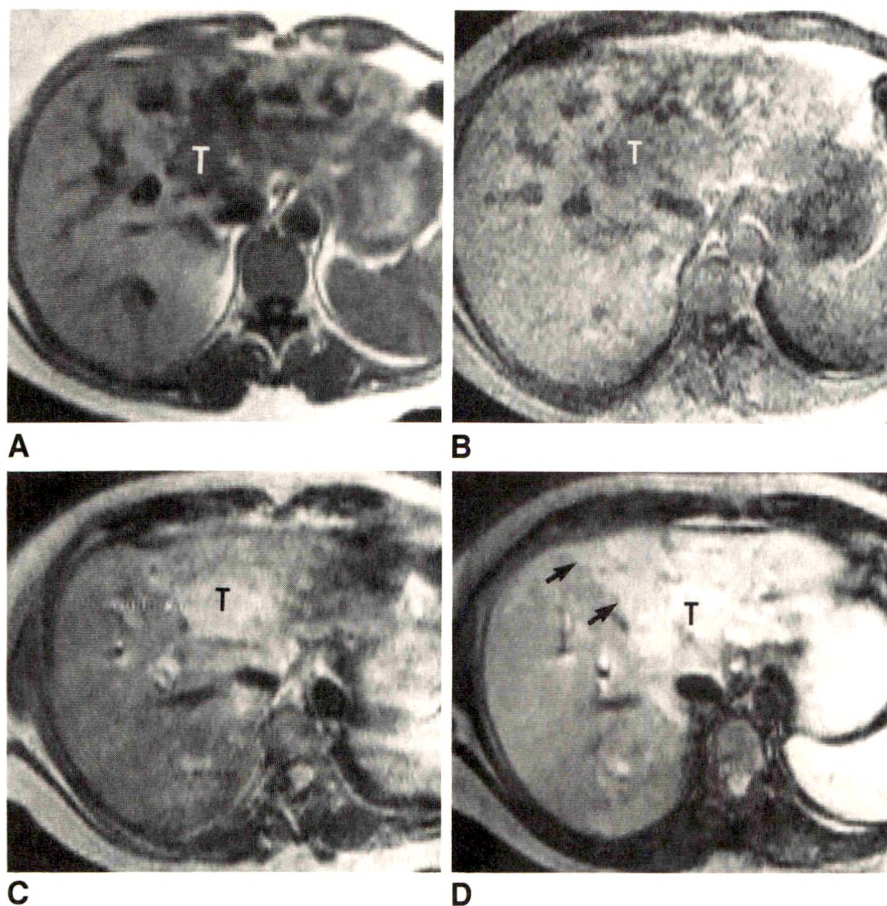


Fig. 2.—Cholangiocarcinoma.

A, Spin-echo image, 260/14, shows massive hepatic infiltration by tumor (T). Tumor is seen as mass lesion slightly hypointense relative to liver.

B, T1-weighted gradient-echo image, 200/11, appears grainy because of lower signal-to-noise ratio and shows tumor (T) as low-contrast lesion.

C and D, Conventional T2-weighted spin-echo image, 2350/60 (C), and phase-contrast image, 2350/60 (D), obtained at same anatomic level as A display tumor (T) as hyperintense relative to liver. Phase-contrast image shows larger geographic zone of hyperintensity (arrows), pathologically proved to correspond to bile stasis and edema.

be attributed to shorter scan time and incomplete suppression of cardiac pulsation and peristaltic motion artifacts [24].

Hepatic adenoma, like HCC, was best detected and showed the highest CNR on T2-weighted images (Table 1, Table 2, and Fig. 3). Focal nodular hyperplasia was nearly isointense relative to adjacent liver (Fig. 4) and showed low CNR values on all pulse sequences, as has been described previously [4]. Indeed, detection of focal nodular hyperplasia

in two of three cases was achieved largely by visualization of the central scar, which had larger CNR values than the remainder of the lesion. The CNR values of the individual cases of carcinosarcoma (SE 260/14, -10.5 ; SE 2350/60, 3.1 ; Fig. 5), leiomyoma (SE 260/14, -8.3 ; SE 2350/60, 8.9), and hemangioendothelioma (SE 260/14, -7.8 ; SE 2350/60, 7.9) showed CNR values comparable with those of metastatic cancer.

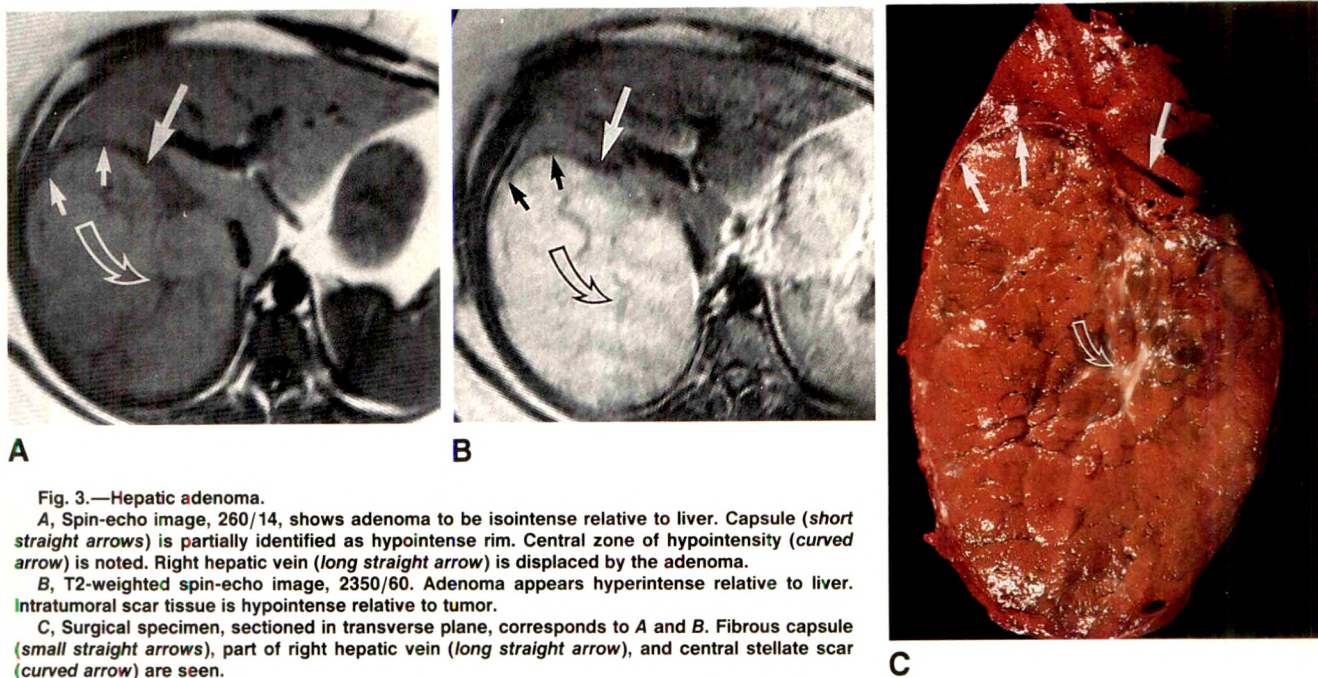


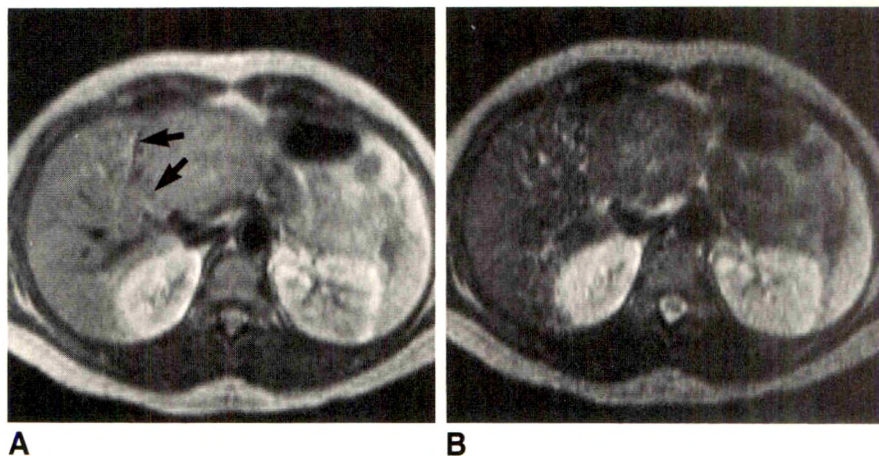
Fig. 3.—Hepatic adenoma.

A, Spin-echo image, 260/14, shows adenoma to be isointense relative to liver. Capsule (short straight arrows) is partially identified as hypointense rim. Central zone of hypointensity (curved arrow) is noted. Right hepatic vein (long straight arrow) is displaced by the adenoma.

B, T2-weighted spin-echo image, 2350/60. Adenoma appears hyperintense relative to liver. Intratumoral scar tissue is hypointense relative to tumor.

C, Surgical specimen, sectioned in transverse plane, corresponds to A and B. Fibrous capsule (small straight arrows), part of right hepatic vein (long straight arrow), and central stellate scar (curved arrow) are seen.

Fig. 4.—Focal nodular hyperplasia. Spin-echo images, 2350/60 (A) and 2350/180 (B), show tumor as mass isointense relative to liver, manifested primarily by its mass effect (arrows).



Tissue Characterization

Quantitative parameters.—To characterize malignant (primary or secondary) and benign liver tumors, we calculated lesion/liver signal-intensity data (Table 3) and tissue relaxation times and proton densities (Table 4) [6, 15, 17].

Fatty degeneration of hepatocellular neoplasms is a common pathologic feature [1] and was analyzed in 17 of 21 HCCs for which histologic material was available for review. Histologically documented fatty degeneration of eight tumors correlated ($p < .05$) with increased (≥ 0.9) lesion/liver signal-intensity ratios (Table 3) on the T1-weighted (short TR/TE) images (Figs. 3, 6, and 7); nonfatty HCCs all had ratios of 0.8 or less. This correlation was confirmed by analysis of the proton density and relaxation time data (Table 4), which show that fatty tumors have a significantly reduced T1 relaxation

time ($p < .05$) and an increased proton density ($p < .05$). These findings were specific; that is, they were not observed in any other tumor. Conversely, no statistically significant differences were observed in tumor/liver signal-intensity ratios of 10 fibrotic HCCs as compared with seven nonfibrotic HCCs.

Chemical-shift (phase-contrast) signal-intensity data also correlated significantly ($p < .05$) with fatty infiltration of hepatocellular tumors. Comparison of conventional spin-echo (in-phase) and phase-contrast (opposed-phase) data showed a significant ($p < .05$) decrease in tumor/liver ratios on phase-contrast images (Fig. 6). This finding also indicates that some HCCs contain more triglyceride than does adjacent liver tissue. Conversely, nonhepatocellular benign and malignant neoplasms do not undergo fatty degeneration and therefore show a significantly increased ($p < .05$) tumor/liver ratio on

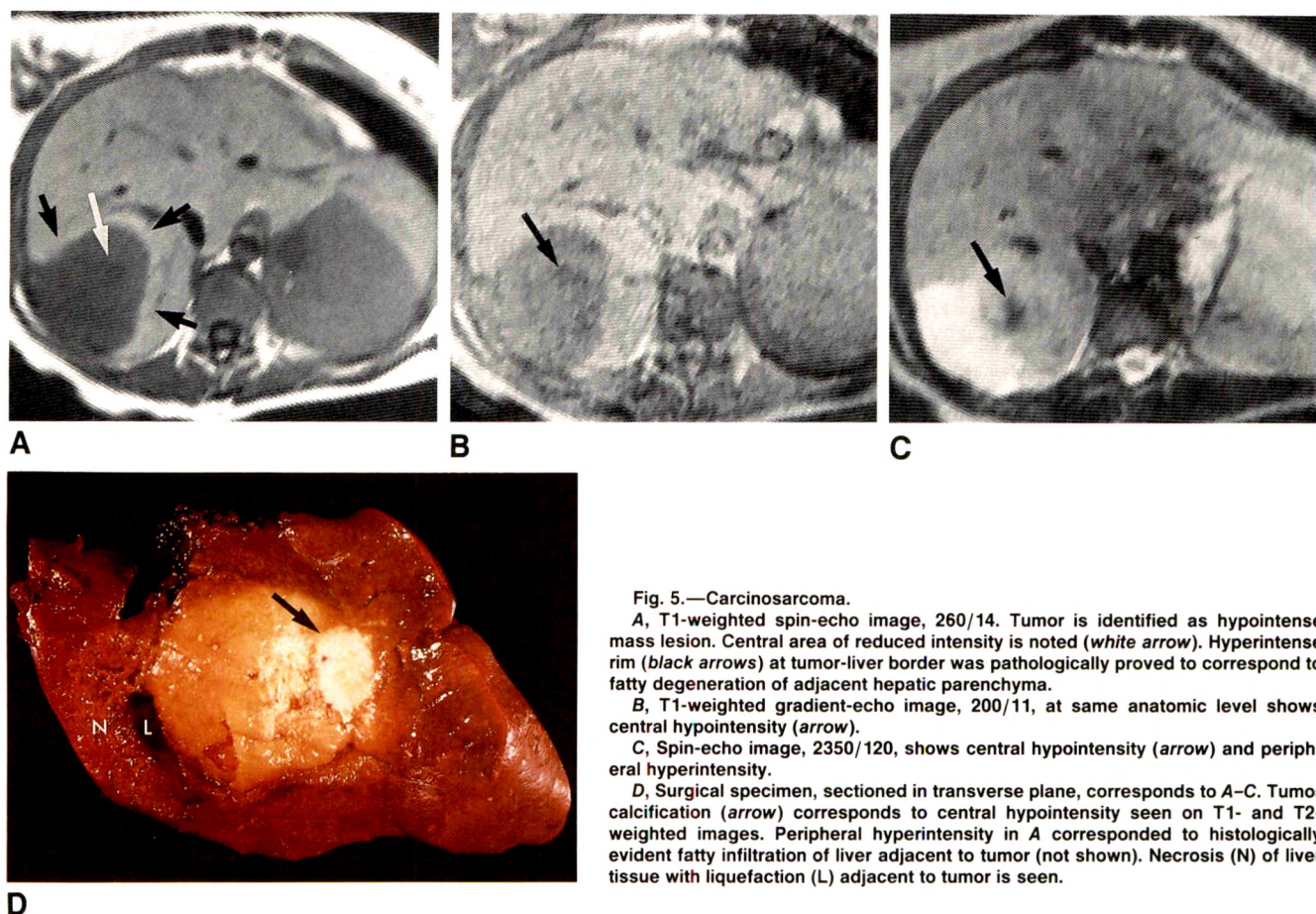


Fig. 5.—Carcinosarcoma.

A, T1-weighted spin-echo image, 260/14. Tumor is identified as hypointense mass lesion. Central area of reduced intensity is noted (white arrow). Hyperintense rim (black arrows) at tumor-liver border was pathologically proved to correspond to fatty degeneration of adjacent hepatic parenchyma.

B, T1-weighted gradient-echo image, 200/11, at same anatomic level shows central hypointensity (arrow).

C, Spin-echo image, 2350/120, shows central hypointensity (arrow) and peripheral hyperintensity.

D, Surgical specimen, sectioned in transverse plane, corresponds to A–C. Tumor calcification (arrow) corresponds to central hypointensity seen on T1- and T2-weighted images. Peripheral hyperintensity in A corresponded to histologically evident fatty infiltration of liver adjacent to tumor (not shown). Necrosis (N) of liver tissue with liquefaction (L) adjacent to tumor is seen.

TABLE 3: Tissue Characterization: Lesion/Liver Signal-Intensity Ratios

Tissue Type	SE 260/14	SE 2350/60	SE 2350/120	SE 2350/180	PC 2350/60	GE 200/11
Hepatocellular carcinoma	0.83 ± 0.22 ^a	1.7 ± 0.6	2.1 ± 0.6	2.1 ± 1.0	1.6 ± 0.5	0.92 ± 0.1
Cholangiocarcinoma	0.72 ± 0.11	1.5 ± 0.1	2.1 ± 0.7	3.2 ± 0.6	2.0 ± 0.3	0.84 ± 0.1
Hemangioma	0.62 ± 0.11	1.8 ± 0.5	3.2 ± 1.0 ^b	4.9 ± 1.7 ^c	3.6 ± 2.3	0.88 ± 0.1
Focal nodular hyperplasia	0.95 ± 0.1	1.0 ± 0.3	1.1 ± 0.2	1.2 ± 0.2	NA	NA
Hepatic adenoma	1.22 ± 0.1	1.7 ± 0.2	2.1 ± 0.7	2.3 ± 0.8	NA	1.2 ± 0.2
Metastases	0.71 ± 0.12	1.3 ± 0.2	1.7 ± 0.4	1.7 ± 0.7	2.2 ± 0.5 ^d	0.76 ± 0.2

Note.—An analysis of variance was performed among hepatocellular carcinoma, cholangiocarcinoma, hemangioma, and metastases for each pulse sequence. SE = spin-echo; PC = phase-contrast; GE = gradient-echo; NA = not available.

^a Significantly higher ($p < .01/6.0; 3, 49$) [p value/F value; degrees of freedom]) than for hemangioma; other comparisons not significant.

^{b,c} Significantly higher ($p < .001/12.8^b, 27.3^c; 3, 51$) than for hepatocellular carcinoma, cholangiocarcinoma, and metastases.

^d PC 2350/60 images (opposed phase) showed significant ($p < .05$, Wilcoxon test) increase relative to conventional SE 2350/60.

phase-contrast images compared with conventional in-phase images. This finding indicates that the triglyceride content of nonhepatocellular neoplasms is less than that of adjacent liver [12].

The mean difference between cancer and adjacent liver and the biologic variation of tissue characteristics (Table 4), quantified as the fraction (standard deviation/mean), were calculated to reveal potential sources of image contrast. For HCC, T2 showed the largest difference (34.4%) between

cancer and adjacent liver, and the variation in T2 was low ($\pm 20.9\%$). Owing to the presence of fat in some HCCs, proton density and T1 showed unusually large variation, as compared with metastases. For metastases, T1 showed the largest mean difference (38.5%) between cancer and adjacent liver, and T1 also showed the lowest variation from tumor to tumor ($\pm 14.5\%$).

Cavernous hemangiomas showed significantly ($p < .001$) greater tumor/liver signal-intensity ratios than did other benign

TABLE 4: Tissue Relaxation Times and Proton Densities Calculated from In Vivo MR Image Data

Diagnosis	No. of Patients	T1	T2	Proton Density
Hepatocellular carcinoma:				
All	21	594 ± 124 ^a	86 ± 18 ^a	556 ± 253
Fatty tumors	7	494 ± 35 ^b	80 ± 17 ^a	742 ± 252 ^{a,b}
Fibrotic tumors	7	668 ± 111 ^a	84 ± 10 ^a	457 ± 74
Uninvolved liver	21	488 ± 122	64 ± 15	501 ± 126
Cholangiocarcinoma:				
All	6	656 ± 172 ^a	98 ± 18 ^a	531 ± 213
Uninvolved liver	6	429 ± 88	60 ± 16	449 ± 198
Hemangioma:				
All	16	1038 ± 556 ^a	166 ± 44 ^{a,b}	507 ± 192
Uninvolved liver	16	450 ± 113	59 ± 5	582 ± 137
Metastases:				
All	15	691 ± 100 ^a	76 ± 22 ^a	583 ± 153
Uninvolved liver	15	499 ± 102	58 ± 10	604 ± 164

Note.—An analysis of variance was performed among hepatocellular carcinoma, cholangiocarcinoma, hemangioma, and metastases for T1, T2, and proton density. F values/degrees of freedom were 6.45/3, 49; 29.1/3, 47; and 2.95/3, 41 for T1, T2, and proton density, respectively.

^aRelaxation time or proton density significantly greater than that of uninvolved liver ($p < .05$).

^bRelaxation time or proton density significantly different for this tumor as compared with all other tumors ($p < .05$).

or malignant neoplasms on both the 120- and 180-msec T2-weighted spin-echo images (Table 3) and the diagnosis of benign PLT was made in all 16 cases. The images obtained using 60-msec T2-weighted spin-echo, phase-contrast, T1-weighted spin-echo, and gradient-echo techniques did not show significant tissue specificity. Of the three calculated tissue parameters (proton density, T1 and T2) only the mean T2 relaxation time of cavernous hemangioma was significantly longer ($p < .05$) than for other hepatic neoplasms. However, owing to the large standard deviation ($\pm 27\%$) of this parameter, T2 relaxation times were not useful in the diagnosis of individual cases.

Qualitative parameters.—The two most useful morphologic features for differential diagnosis of liver tumors were identification of vascular invasion (Fig. 6D) and the presence of a tumor capsule (Fig. 7A). Invasion of portal or hepatic veins, best shown by using the first echo of a T2-weighted pulse sequence, was shown by MR in six (29%) of 21 patients with HCC. With surgical and/or pathologic inspection as the gold standard, there were no false-positive or false-negative MR examinations.

Tumor capsules were shown by MR in five (24%) of 21 HCCs and in one (25%) of four hepatic adenomas (Fig. 3) [25]. Tumor capsules were best seen on the spin-echo 260/14 sequence. All of the patients in this series had tumor

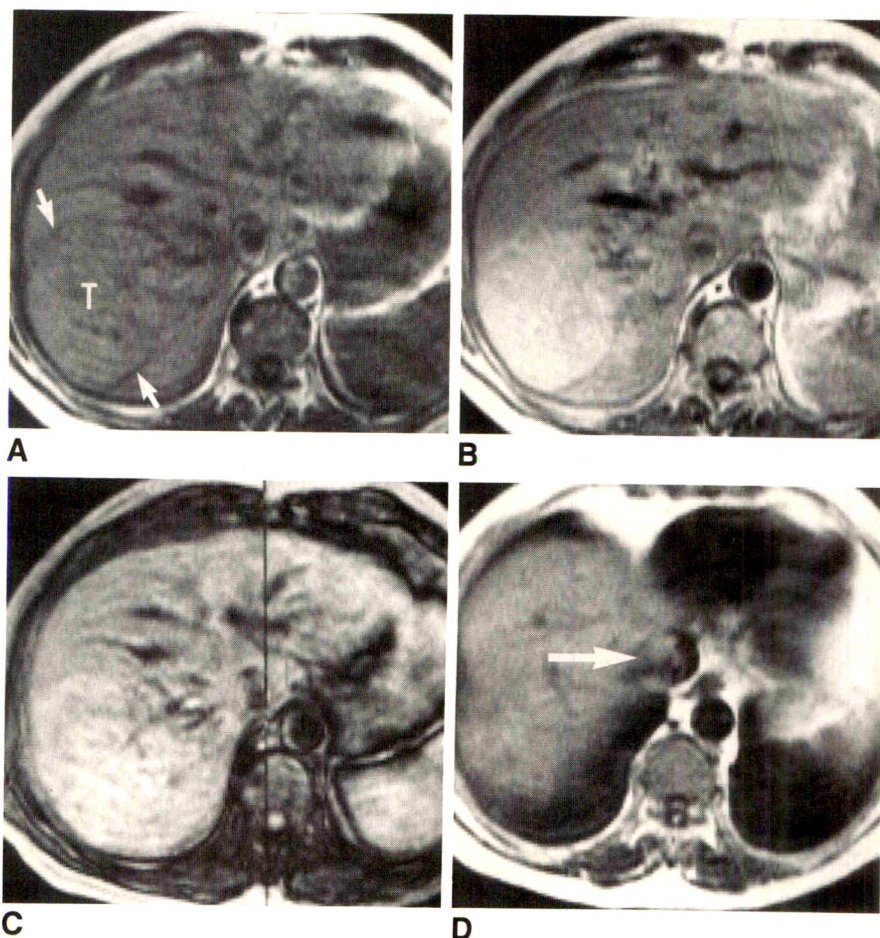


Fig. 6.—Hepatocellular carcinoma with fatty degeneration and vascular invasion.

A, Spin-echo image, 260/14, shows encapsulated (arrows) tumor (T) isointense relative to liver because of fatty degeneration of tumor.

B, Conventional T2-weighted spin-echo image, 2350/60, shows increased tumor-liver contrast.

C, Phase-contrast image, 2350/60, displays lower tumor signal intensity (i.e., lower contrast) because of phase cancellation of signal from fat and water within tumor cells.

D, Spin-echo image, 260/14, shows vascular invasion (arrow) of tumor through right hepatic vein into vena cava.

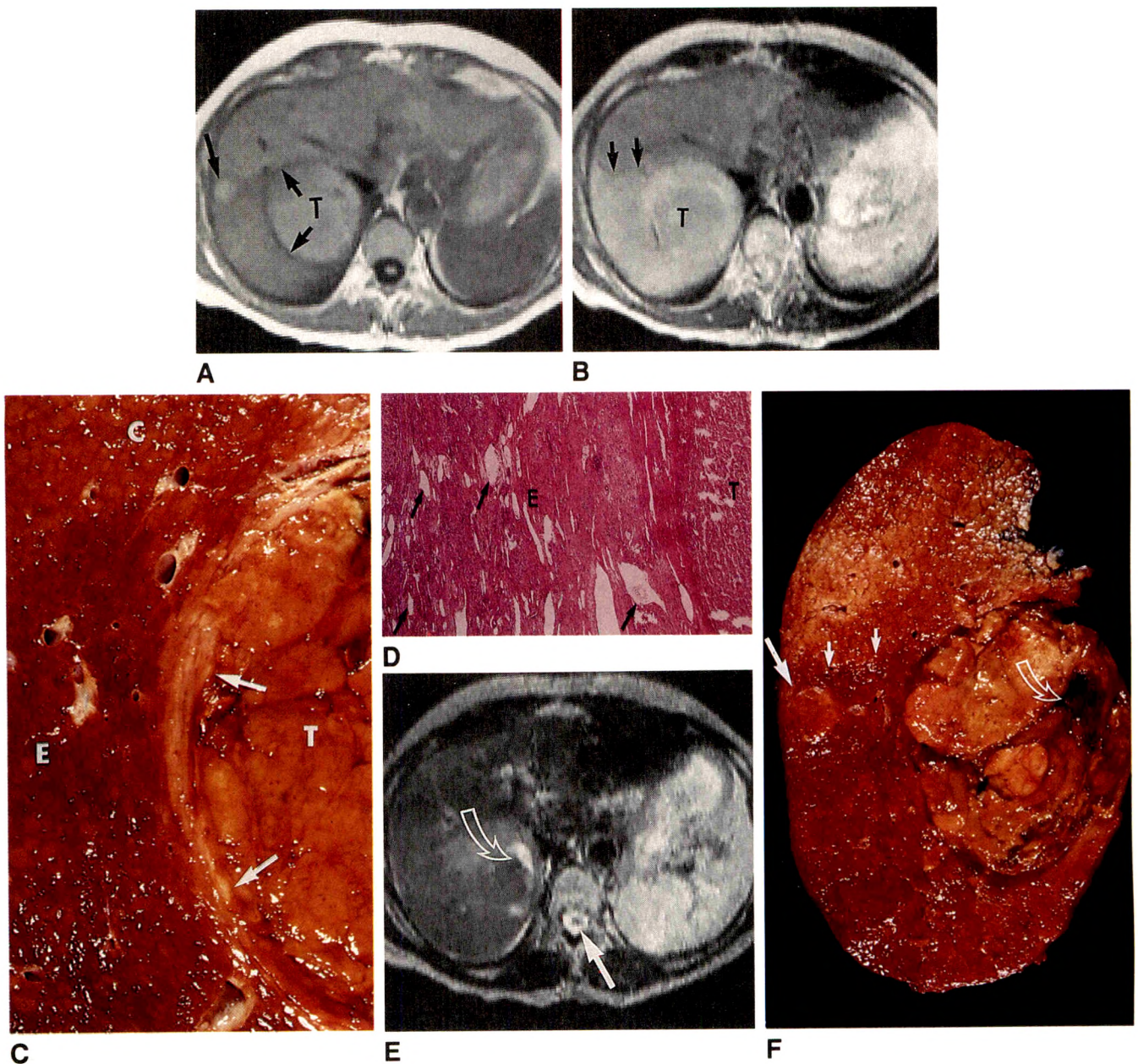


Fig. 7.—Encapsulated hepatocellular carcinoma.

A, Spin-echo image, 260/14, shows tumor (T), hyperintense relative to liver, surrounded by low-signal-intensity capsule (small arrows). Posterior segment of right lobe shows lower signal intensity than does remainder of liver. Hyperintense satellite nodule is seen (longest arrow).

B, T2-weighted spin-echo image, 2350/60, shows edematous liver tissue of right lobe (arrows) as hyperintense zone.

C, Surgical specimen sectioned in transverse plane corresponds to A and B. Tumor (T), fibrous tumor capsule (arrows), edematous parenchyma of right lobe (E), and cirrhotic liver tissue (C) of anterior right hepatic lobe are shown.

D, Histologic specimen (magnification $\times 31$) of edematous hepatic parenchyma (E) of right lobe with dilated lymphatic and venous channels (arrows); adjacent tumor tissue (T).

E, T2-weighted spin-echo image, 2350/120, 2 cm caudal to A-C shows zone of tumor necrosis (curved arrow) as hyperintense area. This image also shows lower signal intensity of hepatocellular carcinoma relative to CSF (straight arrow), which distinguishes solid neoplasms from cavernous hemangiomas.

F, Surgical specimen (same section as E) shows intratumoral necrosis (curved arrow) and satellite nodule (large straight arrow). Border (small straight arrows) between edematous and nonedematous liver tissue is distinct.

capsules more than 1 mm thick. Tumor capsules of benign and malignant lesions were indistinguishable on histology and MR.

Peritumoral edema, visualized by MR and confirmed by histologic examination, was a useful diagnostic feature exclu-

sively associated with malignant hepatic lesions and was seen in six (29%) of 21 patients with HCC and in two of seven patients with cholangiocarcinoma. Edema was typically seen on T2-weighted images as a zone of hyperintensity extending from the tumor margin into adjacent liver tissue (Figs. 2D and

7B). T1-weighted images were normal in zones of edema in five of these cases but showed a subtle hyperintensity (relative to normal liver tissue) in one case (Fig. 7A). Edema frequently showed a geographic distribution on MR images such as a wedge shape extending from an apex at the tumor to a broad base at the liver capsule, reflecting the expected distribution of lymphatic or venous blockage (Fig. 7D) [26]. Cholangiocarcinoma was recognized by periportal infiltration in five of seven cases, but tumor could not be distinguished from associated edema in two cases. Other hyperintense structures, such as the peripheral rim of metastatic cancer [27], may be relatively specific for malignant tumors, as it was seen in five (20%) of 25 patients with metastases but in none of the patients with benign liver lesions.

Other morphologic features, such as the number of lesions or their location, and internal features such as septation, scarring, necrosis, and calcification were less reliable for differential diagnosis. Overall, the diagnosis of benign vs malignant PLT was possible in 48 of 55 cases by using the criteria developed in this series, applied retrospectively. A tissue-specific diagnosis was made in 14 of 21 HCCs, in two of three focal nodular hyperplasias, and in all hemangiomas.

Discussion

Our results show that T2-weighted spin-echo images are more sensitive than T2-weighted phase-contrast, T1-weighted spin-echo, or gradient-echo techniques for detection of HCC, the most common and treatable malignant PLT. Therefore, it is important not to rely on MR techniques designed to screen for hepatic metastases [10–12] in patients at risk for HCC. Because HCC can be treated by surgical excision, staging is critical to treatment planning [28], and T2-weighted images must be obtained to maximize detection of small intrahepatic metastases ("satellite" or "daughter" nodules).

MR can suggest a tissue-specific diagnosis of hepatocellular neoplasm by demonstration of tumor fat, tumor capsule, or vascular invasion. In our series, 47% of HCCs showed evidence of fatty change on MR images. Fatty tumors could be diagnosed on the basis of iso- or hyperintensity on T1-weighted spin-echo images and/or a decrement in the tumor/liver ratio on phase-contrast images. Although the occurrence rate of tumor capsules was lower (24%) in our series than the 42% recently reported in an Asian population [1, 29], this feature was specific for hepatocellular neoplasms (malignant and benign).

Experience with MR imaging of cholangiocarcinoma and other less common malignant PLTs is limited [3]. Our data suggest that these tumors may have no specific tissue characteristics. Both T1-weighted and T2-weighted images should be obtained because they convey complementary diagnostic information. T1-weighted images provide good anatomic resolution because of greater signal-to-noise ratios and can be used to determine exact tumor margins (Fig. 2). T2-weighted images provide good tumor-liver contrast and can detect vascular invasion and peritumoral edema (Fig. 2).

The major differential diagnosis of primary malignant liver tumors is cavernous hemangioma, the most common hepatic

tumor. As HCC is often hypervascular, CT, scintigraphic, and even angiographic findings can be ambiguous. Our results show that MR can reliably ($p < .001$) distinguish HCC from hemangioma on heavily T2-weighted images (Fig. 7E and Table 3). Although hypervascular and cystic metastases such as sarcoma or metastatic islet cell neoplasms occasionally can mimic the appearance of cavernous hemangioma [27], this problem has not yet been encountered with HCC. Conversely, a cavernous hemangioma rarely may be densely calcified or scarred and can mimic the appearance of a necrotic hepatic neoplasm. Cavernous hemangiomas have not shown MR evidence of a capsule, fatty degeneration, or other features diagnostic of HCC.

In summary, our results indicate that T1-weighted pulse sequences, recommended as the principal technique for screening patients at risk for hepatic metastases on low- and mid-field (<1-T) MR systems, are not sufficient for detecting or staging HCC. The combined use of T1- and T2-weighted pulse sequences allows an accurate differential diagnosis of PLT in most cases. The ability of MR imaging to identify features specific for hepatocellular neoplasms such as fatty degeneration of tumor or capsule, or features such as peritumoral edema and vascular invasion, may represent an advantage over CT, sonography, and scintigraphy.

ACKNOWLEDGMENTS

We thank S. Pampallona and J. Orav, Department of Biostatistics, Harvard School of Public Health, for help in the statistical evaluation and Michelle Forrestall and Steve Conley, Pathology Photography Laboratory, Massachusetts General Hospital, for assistance in photography.

REFERENCES

1. Ebara M, Ohto M, Watanabe Y, et al. Diagnosis of small hepatocellular carcinoma: correlation of MR imaging and tumor histologic studies. *Radiology* 1986;159:371–377
2. Vermess M, Leung AW-L, Bydder GM, Steiner RE, Blumgart LH, Young I. MR imaging of the liver in primary hepatocellular carcinoma. *J Comput Assist Tomogr* 1985;9:749–754
3. Doores CG, Kerlan RK, Hricak H, Wall SD, Margulis AR. Cholangiocarcinoma: imaging by MR. *Radiology* 1986;159:89–94
4. Butch RJ, Stark DD, Malt RA. MR imaging of hepatic focal nodular hyperplasia. *J Comput Assist Tomogr* 1986;10:874–877
5. Stark DD, Felder RC, Wittenberg J, et al. Magnetic resonance imaging of cavernous hemangioma of the liver: tissue-specific characterization. *AJR* 1985;145:213–220
6. Glazer GM, Aisen AM, Francis IR, Gyves JW, Lande I, Adler DD. Hepatic cavernous hemangioma: magnetic resonance imaging. *Radiology* 1985;155:417–420
7. Elizondo G, Weissleder R, Stark DD, et al. Amebic liver abscess: diagnosis and treatment evaluation with MR imaging. *Radiology* 1987;165:795–800
8. Cohen C. Intracytoplasmic hyaline globules in hepatocellular carcinomas. *Cancer* 1976;37:1754–1758
9. Kneeland JB, Knowles RJR, Cahill PT. Magnetic resonance imaging systems: optimization in clinical use. *Radiology* 1984;153:473–478
10. Lee JKT, Heiken JP, Dixon WT. Detection of hepatic metastasis by proton spectroscopic imaging. *Radiology* 1985;156:429–433
11. Stark DD, Wittenberg J, Edelman RR, et al. Detection of hepatic metastases: analysis of pulse sequence performance in MR imaging. *Radiology* 1986;159:365–370
12. Stark DD, Wittenberg J, Middleton MS, Ferrucci JT Jr. Liver metastases: detection by phase-contrast MR imaging. *Radiology* 1986;158:327–332
13. Tsang YM, Stark DD, Chia-Mei Chen M, Weissleder R, Wittenberg J,

- Ferrucci JT. Hepatic micrometastases: ferrite-enhanced MR imaging. *Radiology* **1988**;167:21-24
14. Hendrick RE, Nelson TR, Hendee WR. Optimizing tissue contrast in magnetic resonance imaging. *Magn Reson Imaging* **1984**;2:193-204
 15. Chang A, Glazer HS, Lee JKT, Ling D, Heiken JP. Adrenal gland: MR imaging. *Radiology* **1987**;163:123-128
 16. Schmidt HC, Tscholakoff D, Hricak H, Higgins CB. MR image contrast and relaxation times of solid tumors in the chest, abdomen, and pelvis. *J Comput Assist Tomogr* **1985**;9:738-748
 17. Bottomley PA, Hardy CJ, Argersinger RE, Allen-Moore G. A review of ¹H nuclear magnetic resonance relaxation in pathology: are T1 and T2 diagnostic? *Med Phys* **1987**;14:1-37
 18. Press WH, Flannery BP, Teukolsky SA, Vetterling WT. *Numerical recipes: the art of scientific computing*. New York: Cambridge University, **1986**:523-528
 19. Stark DD, Wittenberg J, Butch RJ, Ferrucci JT. Hepatic metastases: randomized, controlled comparison of detection with MR imaging and CT. *Radiology* **1987**;165:399-406
 20. Armitage P, Berry G. *Statistical methods in medical research*, 2nd ed. Oxford, England: Blackwell Scientific, **1987**
 21. SAS Institute Inc. *SAS user's guide: statistics*, 5th ed. Cary, NC: SAS Institute, **1985**
 22. Haseman JK, Kupper LL. Analysis of dichotomous response data from certain toxicological experiments. *Biometrics* **1979**;35:281-293
 23. Zar JH. *Biostatistical analysis*. Englewood Cliffs, NJ: Prentice-Hall, **1974**
 24. Stark DD, Hendrick RE, Hahn PF, Ferrucci JT. Motion artifact reduction with fast spin-echo imaging. *Radiology* **1987**;164:183-191
 25. Stark DD. Liver. Hepatic adenoma. In: Stark DD, Bradley WG, eds. *Magnetic resonance imaging*. St. Louis: Mosby, **1988**:1012-1013
 26. Itai Y, Ohtomo K, Kokubo T, Okada Y, Yamauchi T, Yoshida H. Segmental intensity differences in the liver on MR images: a sign of intrahepatic portal flow stoppage. *Radiology* **1988**;167:17-19
 27. Wittenberg J, Stark DD, Forman B, et al. Differentiation of hepatic metastases from hemangioma and cysts by MR. *AJR* **1988**;151:79-84
 28. Malt RA. Surgery for hepatic neoplasms. *N Engl J Med* **1985**;313:1591-1596
 29. Itoh K, Nishimura K, Togashi K, et al. Hepatocellular carcinoma: MR imaging. *Radiology* **1987**;164:21-25

Technical Note

Percutaneous Transhepatic Oddi-Sphincter Dilatation for Bile Duct Stone Removal

Lanfroi Graziani,¹ Giancarlo Fabrizzi,¹ Ercolano Manfrini,¹ Renato Galeazzi,² and Umberto Freddara²

To date, there have been only a few reports of percutaneous transhepatic dilatation of the sphincter of Oddi with a balloon catheter for treatment of common bile duct calculi [1-4]. We present our experience with this technique in 11 consecutive patients.

Materials and Methods

Eleven patients with bile duct stones were referred for percutaneous transhepatic treatment. All but two had undergone a cholecystectomy, and none had a T tube in place.

Six women and five men (age range, 52-87 years; mean, 71) were studied; all 11 patients had symptomatic biliary duct stones with obstructive jaundice or cholangitis. Previous endoscopic treatment had been unsuccessful in eight patients, and three patients had coexisting stenosis of the bile duct that could not be treated by endoscopy.

The stones ranged in diameter from 3 to 18 mm. Eight patients had stones larger than 10 mm.

Percutaneous transhepatic cholangiography was done with a 22-gauge needle. The anatomy of the intrahepatic bile ducts was evaluated carefully in order to select the best duct for catheterization. After insertion of a polyethylene Ring-type catheter (8.3 French), external drainage was performed for 3-5 days to decompress the biliary tree and create a parenchymal tract. When the Ring catheter was removed, the parenchymal tract was dilated to allow insertion of a 10- to 12-French Desilet-Hoffmann introducer sheath (Cook, Bloomington, IN), enabling us to exchange catheters over a guidewire.

Dilatation of the papilla was done with a Grüntzig-type balloon

catheter (diameter, 10-20 mm). The diameter used depended on the size of the stone; the 15-mm balloon catheter was selected in most cases.

Inflation of the balloon was done gradually, and full distension was maintained for about 3 min. The pain caused by full inflation was controlled with IV administration of fentanyl and diazepam. In a few cases in which multiple stones were present in the distal common duct, we had to move the stones away from the papilla before it could be dilated. In these cases, the lip of the catheter was advanced into the duodenum. The balloon was partially inflated and pulled back, moving the stones in its path.

After distension of the balloon, the stone was pushed into the duodenum with a 13- to 20-mm angiographic occlusion balloon catheter. Balloon size was determined by the diameter of the common bile duct and the size of the stone.

At the end of the procedure, the introducer Teflon sheath was removed, and a polyurethane bile drain (10- to 12-French Cope-type) was positioned with its tip anchored in the duodenum as a transpapillary stent. The large-bore external drain was useful to decompress the distal common bile duct and the confluence of the pancreatic duct and to allow prompt detection of bleeding. All patients were carefully monitored for clinical and laboratory signs of acute pancreatitis, duct perforation, and hemorrhage. A complete blood count and serum amylase and creatinine analyses were done daily for at least 2 days after the procedure.

The parenchymal access tract was allowed to close within 5-8 days by gradually reducing the caliber of the drain catheter. Later, a 5-French pigtail catheter was positioned in the common hepatic duct so that a final cholangiogram could be performed to verify the absence of residual stones.

Received May 13, 1988; accepted after revision July 5, 1988.

¹ Servizio di Radiologia, Ospedale Regionale Umberto I°, Piazza Cappelli 1, 60100 Ancona, Italy. Address reprint requests to L. Graziani.

² Divisione di Gastroenterologia ed Endoscopia Digestiva, Ospedale Regionale Umberto I°, Piazza Cappelli 1, 60100 Ancona, Italy.

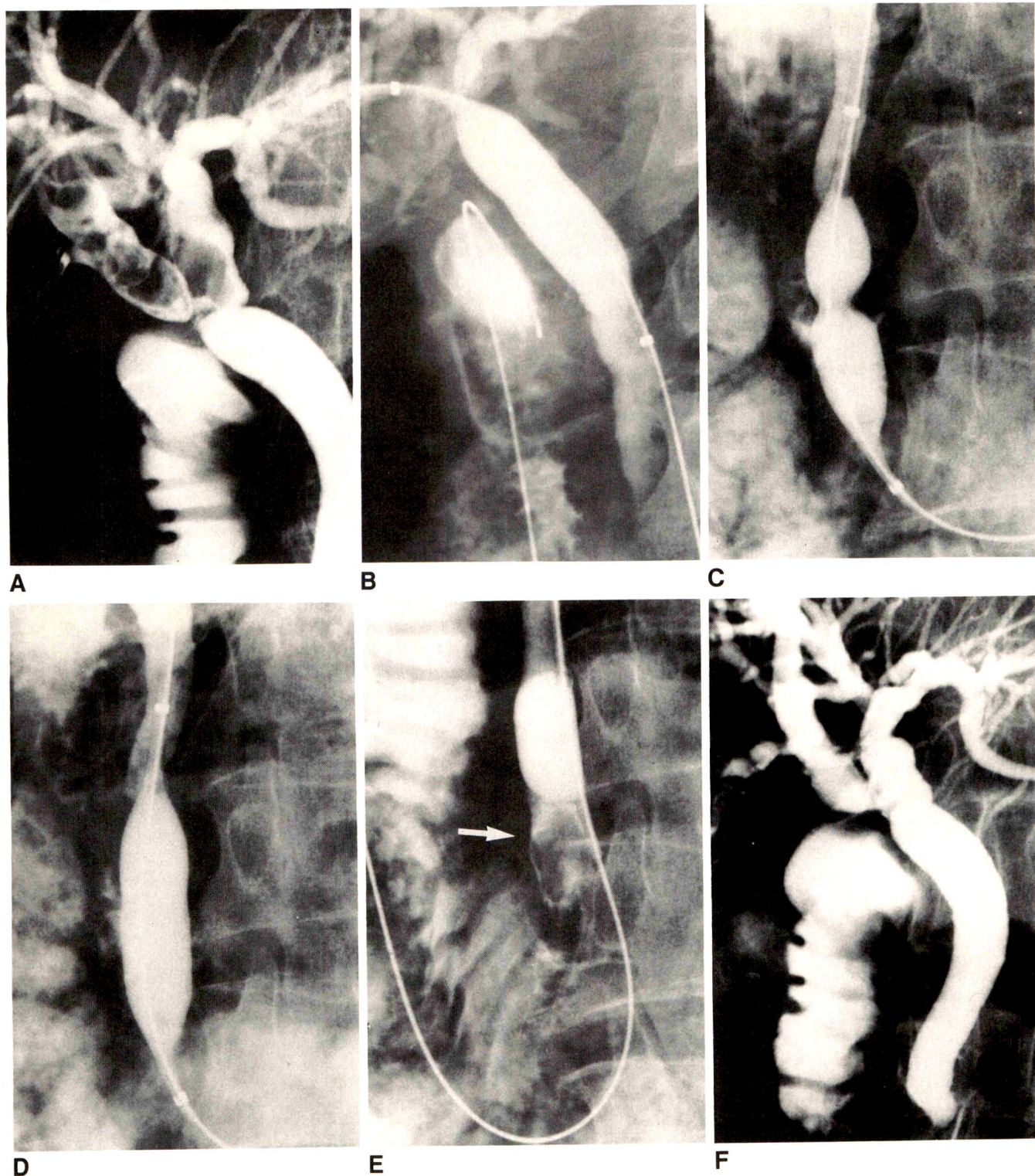


Fig. 1.—A, Cholangiogram shows multiple intrahepatic stones retained above surgical stenosis at origin of common hepatic duct.
B, Cholangiogram shows dilatation of bile duct stenosis.
C and D, Cholangiogram shows balloon dilatation of sphincter of Oddi.
E, Cholangiogram shows stone (arrow) about to be pushed into duodenum by a balloon inflated in bile duct.
F, Final cholangiogram shows no residual calculi.

Results

The stones were successfully pushed into the duodenum in all cases, and the stenoses, present in three patients, were dilated successfully (Fig. 1). In five patients, multiple calculi were removed in two to four successive sessions; in each of the other patients, the stones were removed in one session. In one case, a small stone remained in a long cystic duct remnant with no clinical consequences. In two patients with gallstones, the stones migrated spontaneously into the common bile duct; subsequently, these stones were easily pushed into the duodenum by lavage or with an occlusion balloon. Six patients had fever that disappeared after IV antibiotic therapy. One patient developed a small right pleural effusion. Although three patients had a transient elevation of the serum amylase to twice the upper limits of normal, none had clinical evidence of acute pancreatitis.

All patients remained asymptomatic on follow-up over 3–26 months (mean, 10.7 months).

Discussion

Eight cases of percutaneous transhepatic balloon dilatation of the sphincter of Oddi, to allow common duct stones to pass into the duodenum, have been reported [1–4]. In three of these patients, the dilatation was performed through a T-tube tract [1–4]. In only one patient was the dilatation performed via the transhepatic route [3]. The route was not specified in the other four patients [4].

Staritz et al. [5] reported the use of papillary dilatation in 11 patients; they used a 15-mm diameter balloon to remove biliary calculi that were as large as 12 mm via the duodenum.

Because of the risk of wedging the stone at the sphincter of Oddi, no attempt was made to push a stone into the duodenum without first dilating the papilla. A stone wedged at the sphincter of Oddi could lead to pancreatitis or make stone removal difficult.

Dilatation of the papilla of Vater was accomplished with balloons having diameters 10 mm or larger. Smaller balloons were not used because they cannot produce the dilatation needed for the passing of the stones and because of the risk of papillary stenosis.

REFERENCES

1. Centola CAP, Jander HP, Stauffer A, Russinovich NAE. Balloon dilatation of the papilla of Vater to allow biliary stone passage. *AJR* 1981;136:613–614
2. Fataar S, Bassiony H, Abou-Neema T. The percutaneous "stretch and push" technique for removing retained biliary calculi. *Br J Radiol* 1982;55:456–459
3. Saeed M, Newman GE, Dunnick NR. Use of angioplasty balloons in the percutaneous management of biliary calculi: tandem-balloon method. *AJR* 1987;148:745–746
4. Meranze SG, Stein EJ, Burke DR, Hartz WH, McLean GK. Removal of retained common bile duct stones with angiographic occlusion balloons. *AJR* 1986;146:383–385
5. Staritz M, Ewe K, Meyer zum Buschenfelde KH. Endoscopic papillary dilation (EPD) for the treatment of common bile duct stones and papillary stenosis. *Endoscopy* 1983;15:197–198

Videotape Review

MRI of the Knee. By Murray A. Solomon. (videotape 1 of Murray Solomon's Magnetic Resonance Video Review.) Burlingame, CA: Murray Solomon's MRVR, (415) 692-8230, 1988. Single tape, \$125; series of 6 tapes, \$495

This 2-hr videotape provides valuable insight into the technique and interpretation of MR imaging of the knee, reflecting Dr. Solomon's extensive personal experience with the subject. The scope of material covered is comprehensive, with consideration given to normal anatomy and the complete spectrum of pathologic changes affecting this articulation. Specific areas of discussion include the application of MR to meniscal tears, cruciate and collateral ligament injuries, synovial cysts, osteonecrosis, disorders involving subchondral bone, hyaline cartilage abnormalities, and primary arthritic conditions. Presentation of this information is well organized and is highlighted by the articulate narrating voice of Dr. Solomon, which effectively maintains the viewer's attention.

Specific advantages of the videotape include its tutorial style of presentation; inclusion of numerous supplementary diagrams, tables, and textual summaries of didactic material; and comprehensive coverage of the subject. Considering the rapid pace of advancements in musculoskeletal MR, it is remarkably up-to-date and includes valuable information on fast-gradient echo imaging via partial flip-angles and on three-dimensional data acquisition with nonorthogonal image reconstruction. Although the MR images shown on the tape reflect Dr. Solomon's personal experience from the standpoint of technique, he carefully avoids bias by including frequent oral and visual reference to the literature.

It is extremely difficult to point out negative aspects of this informative videotape. An unavoidable one is the loss of spatial resolution of the MR image that is inherent in conveying view-box material via a television camera and video system. In addition, Dr. Solomon's voice occasionally is momentarily lost, so the viewer must infer missing words or syllables. Finally, it can be anticipated that the videotape will gradually lose its value as a teaching aid as time passes and the field progresses. It could readily be updated by a supplementary volume on the subject prepared at some future date.

When compared with other available information sources on MR imaging of the knee, this videotape ranks high. Many students of MR may find this approach preferable to reading a textbook or journal article, from the standpoint of both time-effectiveness and personal communication of information. The presentation is more current than most available textbooks on the subject, but it does not compete with journals, such as the *AJR*, that feature rapid turnaround time for scientific papers. When compared with the recent *RSNA Today* video digest on MR of the knee, by David J. Sartoris and Gerrold H. Mink (Vol. 2, No. 2, 1988), Dr. Solomon's videotape is longer, more comprehensive and up-to-date, and less biased toward the personal experience of its narrator.

From a practical standpoint, the tape will be valuable to a broad audience, including (1) practicing radiologists who have no formal training in MR, (2) radiology residents and fellows in training, (3) orthopedic surgeons and rheumatologists at all levels of experience, (4) radiologists familiar with musculoskeletal MR who desire a succinct yet comprehensive review on this anatomic area, and (5) MR technologists who seek insight into the interpretation of knee studies. At the present time, the presentation is well worth its moderate cost, and it would be a valuable addition to the videotape library of any radiology department, including both the academic and private-practice settings. In particular, institutions offering visiting fellowship programs in MR would find acquisition of this video review beneficial as a complement to other teaching tools (lectures, case readout sessions, interesting case files). Dr. Solomon is thus to be complimented for synthesizing an extremely complicated subject into a usable and practical instructional aid.

David J. Sartoris
University of California, San Diego, Medical Center
San Diego, CA 92103

Age-Related Changes of the Prostate: Evaluation by MR Imaging

Kenneth S. Allen¹
Herbert Y. Kressel
Peter H. Arger
Howard M. Pollack

The pelvic MR examinations of 40 men without known prostatic disease were reviewed retrospectively. Axial long TR/long TE images were evaluated with respect to prostatic zonal size and signal intensity. Findings were correlated with each patient's age (17-74 years). The central region of the prostate and the peripheral zone enlarged with age; the central gland increased in size by an average of 175% between the second and eighth decades and the peripheral zone increased by an average of 67%. The anterior fibromuscular stroma decreased with increasing age (from an average anteroposterior thickness of 1.2 cm in the second decade to 0.4 cm in the eighth decade) and also became thinner as a function of increasing gland size. The periprostatic venous plexus became less prominent as a function of increasing age, decreasing from 2.5 to 1.5 mm in average maximal diameter, but this venous caliber was not significantly correlated with gland size. The conspicuity of the peripheral zone with respect to the central gland was improved, both as a function of increasing age and increasing gland size, and conspicuity was greatest on long TR/long TE images because of excellent contrast resolution.

We conclude that in older age groups, the zonal anatomy of the prostate is more clearly defined than in young patients, both because of morphologic changes in prostate structure and because of physiologic changes resulting in differing zonal MR signal intensities.

MR imaging of the prostate is a major focus of research because of the high prevalence of prostate disease in an increasingly aged population [1] and because of the shortcomings of other imaging methods. Prostatic zonal anatomy has been well characterized on MR imaging performed at high field strengths [2-5]. Anecdotal reference has been made to the changing MR appearance of the prostate that occurs with age, but no systematic review of these changes has been presented.

The purposes of this study were to review the appearance of the normal prostate on MR images of the pelvis performed for reasons other than prostate disease and to correlate the findings with patients' ages. Particular attention was paid to variations of zonal architecture with respect to size and signal intensity.

Materials and Methods

The zonal anatomy and signal intensity of the prostate were analyzed retrospectively on pelvic MR scans obtained in 40 men, and the findings were correlated with the patients' ages. None of the patients were known to have prostatic disease at the time of examination. Patients with unknown prostate conditions may have been included in the study because exhaustive data regarding the prostate (history, physical examination, chemical studies) were not obtained from these patients. The reasons for examination were avascular necrosis of the hip (18 patients), colon carcinoma (two), bladder carcinoma (three), Hodgkin disease (one), testicular carcinoma (six), anal carcinoma (one), hip osteomyelitis (one), pelvic pain (five), adrenal mass (one), thigh mass (one), and seminal vesicle cyst (one). The patients were 17-74 years old and were grouped by decades: 10-19 (two), 20-29 (eight), 30-39 (eight), 40-49 (eight), 50-59 (five), 60-69 (seven), and 70-79 (two).

Received July 6, 1988; accepted after revision August 30, 1988.

¹ All authors: Radiology Department, Hospital of the University of Pennsylvania, 3400 Spruce St., Philadelphia, PA 19104. Address reprint requests to K. S. Allen.

AJR 152:77-81, January 1989
0361-803X/89/1521-0077
© American Roentgen Ray Society

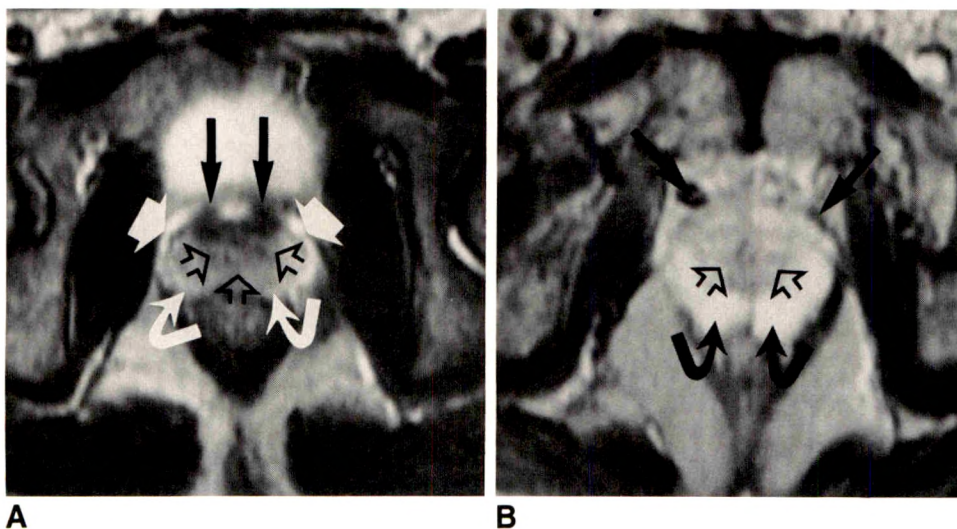


Fig. 1.—Axial images (2500/80) through base of prostate gland.

A, 24-year-old man with testicular carcinoma. Low-signal-intensity central gland (open arrows) is poorly distinguished from higher-signal-intensity peripheral zone (curved arrows). Note thick anterior fibromuscular stroma (solid black arrows) and surrounding periprostatic venous plexus (straight white arrows).

B, 69-year-old man with bladder carcinoma. Central gland (open arrows) and peripheral zone (curved arrows) are enlarged and easily distinguishable. Fibromuscular stroma (straight solid arrows) is poorly identified in this older patient.

Images were obtained with a commercially available 1.5-T magnet (Signa, GE, Milwaukee, WI). Because the examinations were performed for a number of different reasons, a variety of imaging protocols were used. The common denominator for all of these studies was a sequence of axial images through the prostate gland, 5-mm-thick slices with a 1-mm interslice gap, that used a spin-echo multislice technique with long TRs and two TEs, 2000–2500/20–40, 75–100 (TR/TE). The predominantly T2-weighted images allowed satisfactory visualization of the prostatic zonal anatomy for determination of zonal size and signal intensity. Other imaging parameters included a matrix size of 128×256 pixels, field of view ranging from 32 to 44 cm, and two excitations.

On each examination, the overall dimensions of the prostate were measured. All measurements were made by one observer on images displayed on the viewing console. In 35 of the 40 patients, independent measurements by an observer blinded to previous results and blinded to age were repeated at another time on hard-copy images. Because there was no significant difference between the measurements obtained by either method, both techniques appeared to yield valid numeric data. Axial images near the base of the gland were then selected on which the cross-sectional area of the various zones appeared largest (Fig. 1). The perimeters of the central gland and peripheral zones were traced on the viewing console on one image each to calculate relative regional size. The average absolute signal intensity for each of these regions of interest (central gland and peripheral zone) was also displayed. For the purposes of this investigation, the term *central gland* has been applied loosely to include all the zones of the prostate central to the peripheral zone. This central gland includes the prostatic urethra, the periurethral zone, the true central zone, the transitional zones, and probably some elements of fibromuscular stroma. Not all these regions are separately distinguishable with consistency on MR images, especially for the purpose of reliable measurement, so they have been grouped into one measurable zone.

In young patients occasionally it was difficult to distinguish the central gland from the peripheral zone with conventional window and level settings (Fig. 1A). In these cases, a very narrow window (10 signal intensity units) enabled distinction of the two regions. Signal heterogeneity within each zone was approximated by the magnitude of the standard deviation of the average zonal signal intensity. We recorded also the anteroposterior dimension of the anterior fibromuscular stroma. This region is of variable size in any individual patient, so the maximal measurable thickness at any level was tabulated. The periprostatic venous plexus caliber was determined also. This structure is nonuniform in thickness as well. The maximal calibers at any

level of the right and left plexi were averaged to determine this measurement (Fig. 1). Every examination included long TR/TE images with at least two different TEs, so that the described procedure was carried out twice for each patient, once for each pulse sequence.

Calculations were then performed to determine the ratio of the size of the central gland to that of the peripheral zone, the signal intensity ratio, and the signal heterogeneity as a function of patient age. Regression and correlation analyses were used to determine the statistical significance of relationships identified among these parameters.

Results

The prostate gland was visualized satisfactorily on all examinations and on all pulse sequences. The cross-sectional areas of the central gland, peripheral zone, and overall prostate were plotted as a function of age (Fig. 2). The prostate enlarged with age, primarily because of an increase in the size of the central gland (Fig. 1). The correlation between age and zonal area was greatest for the central gland ($r = .95$) and was statistically significant ($p < .01$). A similar relationship between age and peripheral zone size was present; the correlation was less ($r = .94$) but still significant ($p < .01$).

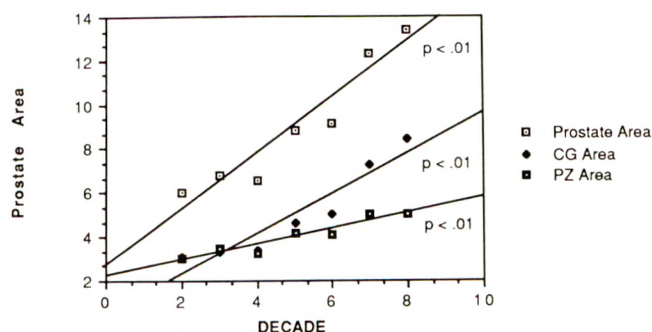


Fig. 2.—Graph of maximal zonal cross-sectional area (cm^2) vs age. Both mean central gland (CG) area and mean peripheral zone (PZ) area enlarge significantly with age.

Fig. 3.—Axial images (2500/80) through base of prostate gland.

A, 25-year-old man with testicular carcinoma. Periprostatic venous plexus (arrows) is prominent and nearly surrounds prostate.

B, 56-year-old man with avascular necrosis of the hip. Peripheral zone (curved arrows) is easily distinguished from central gland (open arrows), but surrounding periprostatic venous plexus (straight solid arrows) is attenuated.

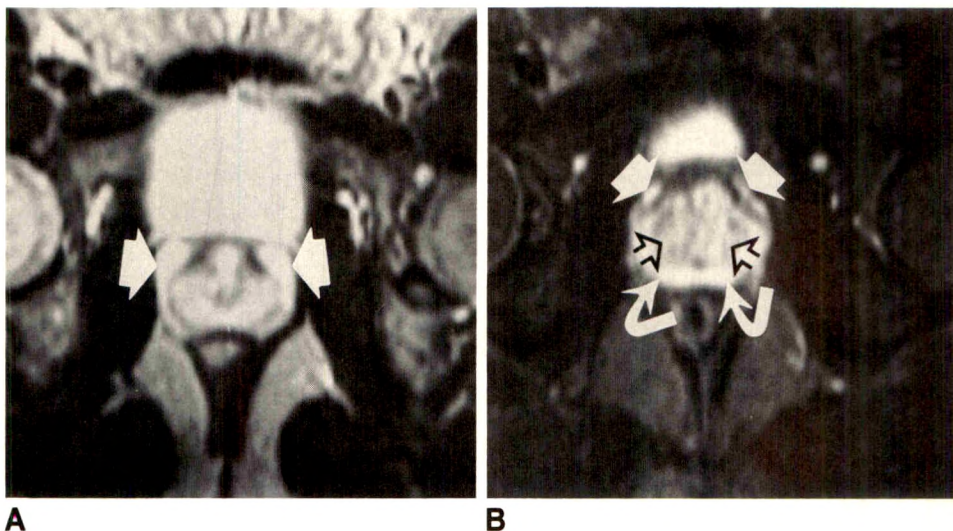


TABLE 1: Prostate Measurements Relative to Age

Age Range (years)	No. of Patients	Mean Measurements			
		Area of Central Gland (cm ²) ± SD (% SD)	Area of Peripheral Zone (cm ²)	Thickness of Fibromuscular Stroma (cm)	Caliber of Periprostatic Venous Plexus (mm)
10-19	2	3.1 ± 0.5 (16)	3.0	1.2	2.5
20-29	8	3.3 ± 0.8 (24)	3.5	1.1	2.5
30-39	8	3.4 ± 0.6 (18)	3.2	1.0	2.7
40-49	8	4.6 ± 1.1 (24)	4.2	0.8	1.9
50-59	5	5.0 ± 2.7 (54)	4.1	0.7	1.3
60-69	7	7.3 ± 2.5 (34)	5.0	0.6	1.6
70+	2	8.4 ± 3.3 (39)	5.0	0.4	1.5

Enlargement of the central gland and peripheral zone occurred in the same patients. With each advancing decade, there was a broader range of central gland and peripheral zone size. In the third decade (ages 20-29), the mean cross-sectional area of the central gland was $3.3 \pm 0.8 \text{ cm}^2$, whereas in the sixth decade the mean area was $5.0 \pm 2.7 \text{ cm}^2$ (Table 1).

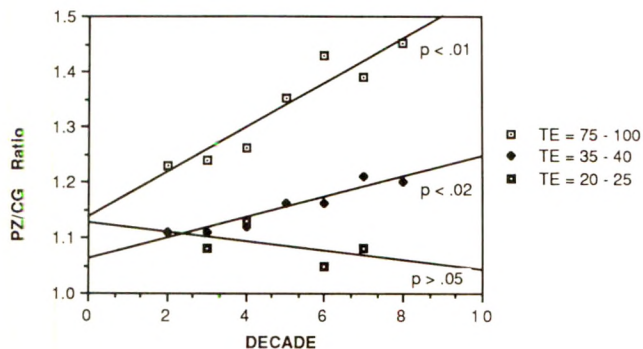


Fig. 4.—Graph of peripheral zone (PZ) to central gland (CG) signal-intensity ratio vs patient age. Peripheral zone becomes brighter with respect to central gland as a function of age. This contrast discrimination is greatest on long TR/long TE images and is not significantly age-related on proton-density images.

The anterior fibromuscular stroma, in contrast to the glandular zones of the prostate, became less prominent with age. The mean anteroposterior thickness of this region measured 1.1 cm in the third decade and decreased to 0.6 cm in the seventh decade (Fig. 1). There was an equivalent correlation of decreasing thickness of fibromuscular stroma with age and with glandular size. Similarly, the periprostatic venous plexus was reduced in caliber with increasing age. The diameter of the periprostatic venous plexus changed from a mean of 2.5 mm in the third decade to 1.3 mm in the sixth decade (Table 1). There was a significant correlation of this decreased venous diameter with patient age ($p < .001$) but not with gland size ($p > .05$) (Fig. 3).

Average zonal signal intensities were determined for the central gland and peripheral zone by outlining regions of interest on the viewing console. The ratio of the signal intensity of the peripheral zone to that of the central gland was greater than unity on all pulse sequences (i.e., the peripheral zone was always brighter than the central gland). On the long TR/TE pulse sequences, a clear relationship was established of peripheral zone to central gland ratio as a function of patient age (Fig. 4): The peripheral zone to central gland ratio increased linearly with age ($p < .01$). This ratio also increased as a function of gland size ($p < .05$). Thus, the discrimination

of central gland from peripheral zone, although not always straightforward, was generally easier in the older age groups than in the younger (Fig. 1). The distinction of central gland from peripheral zone was enhanced with the use of longer TEs, with a mean peripheral zone/central gland signal-intensity ratio at TE = 75–100 msec of 1.32, vs 1.15 at TE = 30–40 msec and 1.08 at TE = 20–25 msec (proton-density image) (Table 2). The linear rise of the peripheral zone/central gland signal-intensity ratio with patient age was demonstrable at TE = 75–100 msec ($p < .01$) and TE = 30–40 msec ($p < .02$), but no relationship between signal-intensity ratio and age was evident on the proton-density images (TE = 20–25 msec) (Fig. 4).

Zonal signal heterogeneity was compared among the different age groups; across the central and peripheral zones; and among the short, intermediate, and long TEs without revelation of any significant trends in zonal homogeneity or inhomogeneity.

Discussion

The outstanding contrast resolution of long TR/long TE images at 1.5 T allows one to visualize prostatic anatomy in a new way [4]. As with other organs, age-related anatomic changes occur in the prostate. By documenting the patterns of change that occur with age, one can show the wide range of normal appearances and perhaps better understand the significance of the variable signal intensities encountered.

The prostate is a coronally oriented organ with left/right symmetry, so optimal visualization of the gland is achieved in the axial plane. The prostate is positioned like an inverted pyramid with the base caudal to the bladder. The central gland is broadest near the prostate base, and the cross-sectional area of the peripheral zone is greatest just caudal to this level. Volumetric measurements of portions of the prostate often are unreliably determined on the basis of axial images because of volume-averaging of small structures, so the zonal-size comparisons made here are simply related to the maximal zonal cross-sectional area identified at any level within the gland.

The central gland is composed of several zones, including the transitional and periurethral zones, which are not always distinguishable on MR images. The latter zones are the sites of origin of benign prostatic hyperplasia [6]. Benign prostatic

hyperplasia is not present invariably, so that even in the older population some glands were not enlarged. On the other hand, the age of onset of benign prostatic hyperplasia may be early; several patients in the fourth and fifth decades had central gland enlargement characteristic of this condition [7–9]. Glandular enlargement similarly occurs within the peripheral zone [6], resulting in a less dramatic but nonetheless significant increase in the size of the peripheral zone with age. The pattern in Figure 1 closely resembles the pattern of surgically obtained prostate specimens, correlating glandular weight with patient age [1]. The number of study patients included in the second and eighth decades is small, so that these groups do not carry statistical significance of their own, but in association with the findings from the other age groups, the trend seen from the second to the eighth decades is valid.

The anterior fibromuscular stroma region of low signal intensity was most prominent in young patients with small prostate glands. With increasing size of the central gland and with increased patient age, a significant tendency toward reduction in thickness of this region was found, possibly due to compression or stretching by the enlarged gland and/or to muscular atrophy associated with age. The factors of age and increasing central gland size appear to contribute equally to this decline in the fibromuscular zone. Likewise, the periprostatic venous plexus, which generally was prominent in young patients with small glands, became less prominent with increasing age. Although this phenomenon in part may be due to venous compression by gland enlargement, the inverse correlation of venous caliber to patient age was much greater than was the inverse correlation of venous caliber to gland size. With increasing gland size competing factors may contribute to changes in venous caliber: The increased blood flow to an enlarged gland causes engorgement of the venous plexus, whereas glandular enlargement also causes compression and stretching of the vessels.

The ratio of the signal intensity of the peripheral zone to that of the central gland is a quantitative marker of the subjective ease with which the central gland can be distinguished from the peripheral zone. This distinction, in general, is made more easily in older men (Fig. 1). Both the central gland and the peripheral zone become relatively higher in signal intensity with respect to the adjacent internal obturator muscles as a function of age, but the peripheral zone does so to a greater extent than does the central gland. The difference in signal intensity that develops with age between central gland and peripheral zone may be related to differences in composition of hyperplastic elements: Perhaps there is more stromal hyperplasia in the central gland (lower signal) and more glandular hyperplasia (higher signal) in the peripheral zone [3]. This hypothesis might also explain the limited signal-intensity differences between the central gland and peripheral zone in young patients in whom there is no prostatic hyperplasia and in whom the glandular tissues of the transition zone and peripheral zone are histologically identical [6].

Inspection of the enlarged central glands of the older patients reveals a nodular pattern of hyperplasia, with varying signal intensities of different nodules. Despite the gross appearance of nodularity and decreased central gland homogeneity, the computed heterogeneity of the central gland was not significantly different in older vs younger patients. Visually,

TABLE 2: Peripheral Zone to Central Gland Signal-Intensity Ratios

Age Range (years)	No. of Patients	Signal-Intensity Ratio (mean \pm SD) by TE		
		20–25 msec	35–40 msec	75–100 msec
10–19	2	NA	1.11	1.23 \pm 0.05
20–29	8	1.08	1.11	1.24 \pm 0.04
30–39	8	1.13	1.12	1.26 \pm 0.06
40–49	8	NA	1.16	1.35 \pm 0.08
50–59	5	1.05	1.16	1.43 \pm 0.06
60–69	7	1.08	1.21	1.39 \pm 0.15
70+	2	NA	1.20	1.45 \pm 0.14

Note.—TR = 2000–2500 msec. NA = not available.

all six glands with a central region exceeding 7.2 cm^2 showed nodularity, and eight of 10 central glands larger than 5.5 cm^2 were nodular. No central glands smaller than 5.5 cm^2 were frankly nodular in appearance.

As expected, the spin-echo sequences with longer TEs provided images with increased contrast discrimination between prostatic zones [4]. Long TR/short TE (spin-density) images showed no relationship between the ratio of the signal intensity of the peripheral zone to that of the central gland and age, whereas long TR/intermediate TE (30–40 msec) images showed a positive linear relationship that was seen even more clearly on long TR/long TE (75–100 msec) images.

REFERENCES

1. Walsh PC. Benign prostatic hyperplasia. In: Walsh PC, Gittes RF, Perlmutter AD, Stamey TA, eds. *Urology*. Philadelphia: Saunders, 1986: 1248–1263
2. Hricak H, Doms GC, McNeal JE, et al. MR imaging of the prostate gland: normal anatomy. *AJR* 1987;248:51–58
3. Sommer FG, McNeal JE, Carrol CL. MR depiction of zonal anatomy of the prostate at 1.5 T. *J Comput Assist Tomogr* 1986;10:983–989
4. Phillips ME, Kressel HY, Spritzer CE, et al. Normal prostate and adjacent structures: MR imaging at 1.5 T. *Radiology* 1987;164:381–386
5. Carrol CL, Sommer FG, McNeal JE, Stamey TA. The abnormal prostate: MR imaging at 1.5 T with histopathologic correlation. *Radiology* 1987;163:521–525
6. McNeal JE. The prostate gland. *Monogr Urol* 1983;4(1):3–33
7. Ling D, Lee JKT, Heiken JP, Balfe DM, Glazer HS, McClennan BL. Prostatic carcinoma and benign prostatic hyperplasia: inability of MR imaging to distinguish between the two diseases. *Radiology* 1986;158:103–107
8. Hruban RH, Zerhouni EA, Dagher AP, Pessar MG, Hutchins GM. Morphologic basis of MR imaging of benign prostatic hyperplasia. *J Comput Assist Tomogr* 1987;11:1035–1041
9. Phillips ME, Kressel HY, Spritzer CE, et al. Prostatic disorders: MR imaging at 1.5 Tesla. *Radiology* 1987;164:386

Book Review

Imaging of the Foot and Ankle. By D. M. Forrester, Morrie E. Kricun, and Roger Kerr. (From the Clinical Diagnostic Imaging Series. Edited by Morrie E. Kricun.) Rockville, MD: Aspen, 325 pp., 1988. \$93

This book is part of the Clinical Diagnostic Imaging Series edited by Morrie E. Kricun. It brings together a myriad of facts about anatomy and pathology of the foot and ankle under one cover, including the newest imaging techniques. The book is divided into three sections: anatomic considerations, conventional foot and ankle disorders, and advanced imaging of foot and ankle disorders. It is extensively illustrated with anatomic sections, drawings, and radiographic images.

The first section of the book compares anatomic sections in coronal, sagittal, and axial planes with corresponding MR images and a few CT scans. A brief description of the positioning of the foot for radiographs is included. Not all of the descriptions are accompanied by radiographic examples. The black-and-white format for the anatomic sections is not optimum for visualization of detail. Also, the legends that accompany the illustrations are gathered together on one page, which is inconvenient. I think it would have been more useful to include fewer anatomic sections, make them in color, and provide clearer labels. For a more complete discussion of foot skeletal anatomy and positioning, the reader might refer to the book *Atlas of Foot Radiology* by Montagne, Chevrot, and Galmiche.

The second part of the book is an extensive atlas of various foot and ankle disorders, some of which are localized to the foot and others that are manifestations of a more generalized disorder. This

section is quite useful because of the large volume of material included and the excellent quality of the radiographs. The material is divided into congenital foot disorders, generalized disease conditions, trauma, sports injuries, arthritis, infection, bone infarction, and tumors.

The third section includes newer imaging methods and more specialized techniques. The topics are tomography, xeroradiography, radionuclide imaging, arthrography, CT, and MR imaging. Everything except the sonographic study of tendons and soft-tissue masses is included. The discussion of these specialized techniques is useful, although some of the MR images are not up to current standards. The explanation of the use of radionuclide scans in infection is especially useful. Because the second section of the book is "disease" oriented and the third section is "technique" oriented, some redundancies occur.

The text has only a few minor discrepancies. The radiographs for posttraumatic flatfoot and clubfoot are reversed. The illustrations for the lateral-medial view of the sesmoid bones of the foot are incorrect.

R. F. Kilcoyne
Audie L. Murphy Memorial Veterans Hospital
San Antonio, TX 78284

Pictorial Essay

Primary Retroperitoneal Neoplasms: CT Findings in 90 Cases with Clinical and Pathologic Correlation

Richard H. Lane,¹ David H. Stephens,¹ and Herbert M. Reiman²

Primary retroperitoneal neoplasms comprise a rare and diverse group of tumors that arise within the retroperitoneum but outside the major organs of that compartment [1]. Currently CT is the preferred imaging technique for their evaluation [2-4]. We reviewed the CT scans obtained at initial presentation in 90 patients with primary retroperitoneal neoplasms. Pathologic specimens and clinical histories were reviewed and correlated with CT findings. The specific diagnoses of the neoplasms in the series are tabulated in Table 1.

Primary Retroperitoneal Neoplasms

Malignant Fibrous Histiocytoma

The average age of patients was 64 years old (the ratio of males to females was 12:4); common clinical presentations were abdominal mass, abdominal pain, and anemia. The average tumor size (greatest cross-sectional diameter) on CT was 12 cm. Nine tumors were seen on CT as muscle-density masses with regions of low density representing necrosis (Figs. 1A and 1C). Seven of the smaller tumors were of homogeneous muscle density (Fig. 1D). One-fourth of the tumors contained areas of dystrophic calcification.

Liposarcoma

The average age (68 years old), male predominance (male:female, 8:3), and clinical presentation were similar to

those of patients with malignant fibrous histiocytoma. Liposarcoma was the largest tumor in our series, with an average CT diameter of 20 cm. The tumors were evenly divided among three histologic types. Four well-differentiated liposarcomas

TABLE 1: Primary Retroperitoneal Neoplasms

Type of Lesion	No. (%)
Malignant	
Malignant fibrous histiocytoma	16
Liposarcoma	11
Leiomyosarcoma	10
Neurofibrosarcoma	5
Neuroblastoma/ganglioneuroblastoma	4
Malignant germ cell	4
Malignant paraganglioma	3
Hemangiopericytoma	2
Undifferentiated sarcoma	2
Fibrosarcoma	1
Rhabdomyosarcoma	1
Subtotal	59 (66)
Benign	
Paraganglioma	9
Neurofibroma	6
Neurilemoma	5
Hemangioma/lymphangioma	4
Lipoma	3
Ganglioneuroma	2
Teratoma	1
Desmoid tumor	1
Subtotal	31 (34)
Total	90 (100)

Received July 18, 1988; accepted after revision August 19, 1988.

Presented in part at the annual meeting of the American Roentgen Ray Society, San Francisco, May 1988.

¹ Department of Radiology, Mayo Clinic, Rochester, MN 55905. Address reprint requests to D. H. Stephens.

² Department of Surgical Pathology, Rochester Methodist Hospital, Mayo Foundation, Rochester, MN 55905.

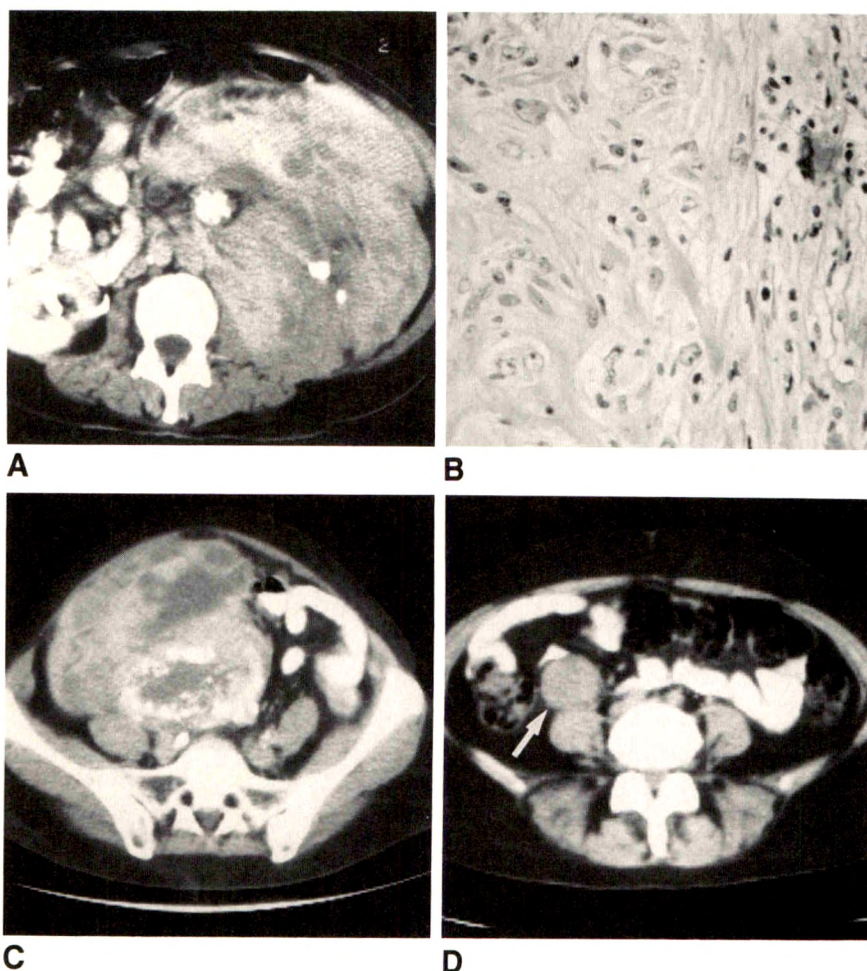


Fig. 1.—Malignant fibrous histiocytoma. A, CT scan shows large retroperitoneal tumor with dystrophic calcification and necrosis.

B, Histologic section shows mixed population of spindling, histiocytelike, and inflammatory cells in fibrous stroma with no particular cellular differentiation, characteristic of malignant fibrous histiocytoma. (H and E, $\times 250$)

C, CT of another patient with large tumor that contains areas of dystrophic calcification and necrosis.

D, In a different patient, CT shows small, malignant fibrous histiocytoma (arrow) of homogeneous, muscle density just anterior to right psoas muscle.

were seen on CT as heterogeneous masses of predominantly fat density with irregular regions of higher density (Fig. 2). Two of four myxoid liposarcomas had an intermediate soft-tissue density on CT (Fig. 3), whereas the other two tumors were seen as muscle-density masses with regions of necrosis. Three pleomorphic liposarcomas were depicted as aggressive muscle-density masses with regions of necrosis (Fig. 4).

Leiomyosarcoma

Except for a more even gender distribution (male:female, 4:6), the clinical presentation of patients with leiomyosarcoma was similar to that of patients with malignant fibrous histiocytoma and liposarcoma. The average tumor diameter on CT was 11 cm. Seven tumors were seen on CT as muscle-density masses with regions of low density representing necrosis (Figs. 5A and 5C). Three of the smaller tumors were of homogeneous muscle density (Fig. 5D). Necrotic regions generally were more extensive than those seen in other tumors in this series. CT showed hepatic metastasis in three patients.

Other Malignant Neoplasms

Other than a slightly younger age of occurrence (average, 57 years old), the clinical presentation of patients with neurofibrosarcoma was similar to that of patients with the previously discussed malignant tumors. The average tumor diameter on CT was 14 cm. Four tumors appeared as muscle-density masses with regions of necrosis (Fig. 6). One tumor was of a homogeneous density, slightly less than that of muscle.

Neuroblastoma and ganglioneuroblastoma occurred in young children with abdominal mass or pain. Two of four tumors were calcified on CT.

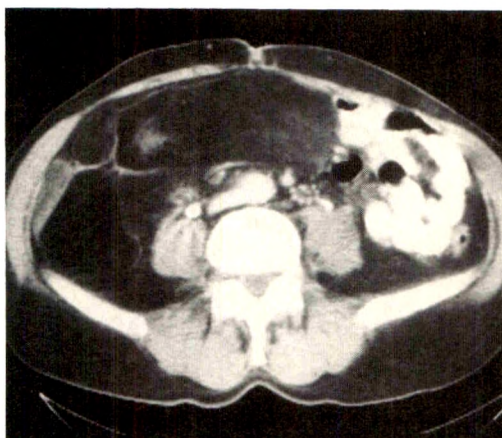
Our two cases of hemangiopericytoma occurred in young adults (19 and 44 years old). CT showed prominent IV contrast enhancement of the tumor in one of these (Fig. 7).

Also occurring in young adults (average age, 33 years old) were malignant germ cell tumors. In these cases, radiologic and/or surgical investigation of the gonads as well as clinical follow-up failed to detect a gonadal primary tumor. On CT, these tumors were seen as inhomogeneous masses of muscle and near-water densities (Fig. 8).

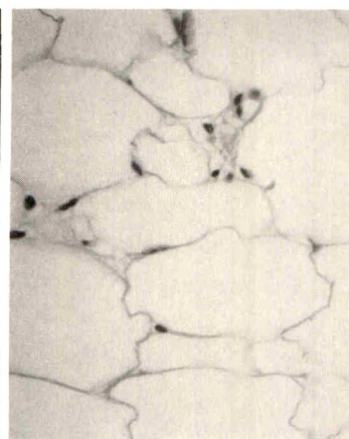
Fig. 2.—Well-differentiated liposarcoma.

A, CT scan shows large retroperitoneal tumor of predominantly fat density. Note irregular wisps and strands of higher density within tumor, characteristic of well-differentiated liposarcoma.

B, Histologic section shows irregular, mature fat cells. (H and E, $\times 250$)



A

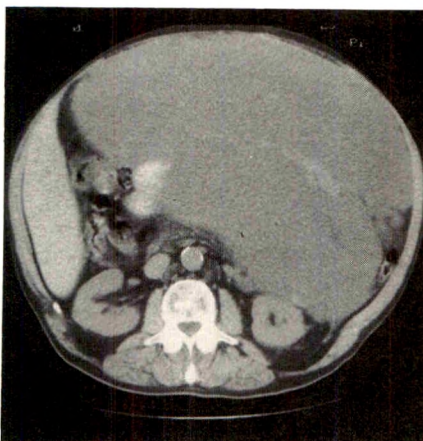


B

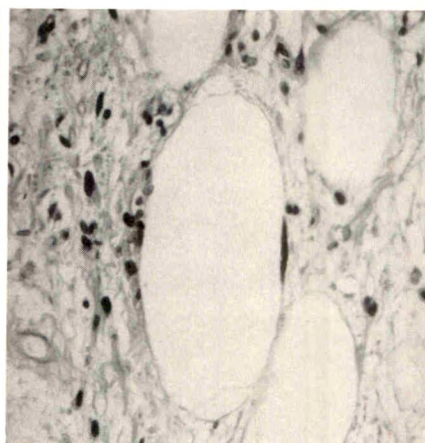
Fig. 3.—Myxoid liposarcoma.

A, CT scan shows large retroperitoneal tumor of intermediate soft-tissue density.

B, Histologic section contains fat cells and lipoblasts within amorphous, myxoid matrix. (H and E, $\times 250$)



A

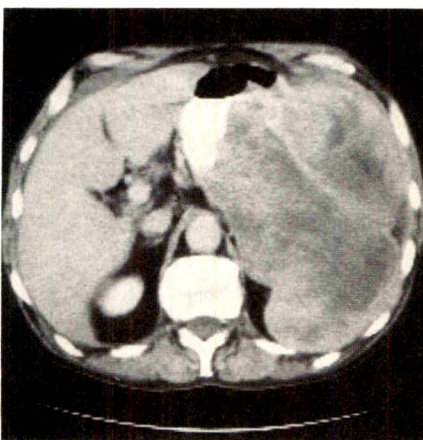


B

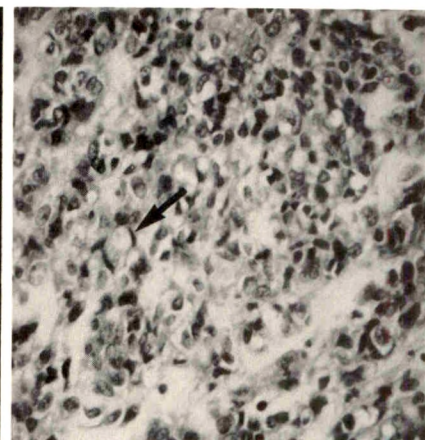
Fig. 4.—Pleomorphic liposarcoma.

A, CT scan shows aggressive retroperitoneal tumor that has regions of necrosis and invades posterior wall of stomach.

B, Histologic section contains field of malignant, dedifferentiated cells with lipoblast (arrow) in center. (H and E, $\times 250$)



A



B

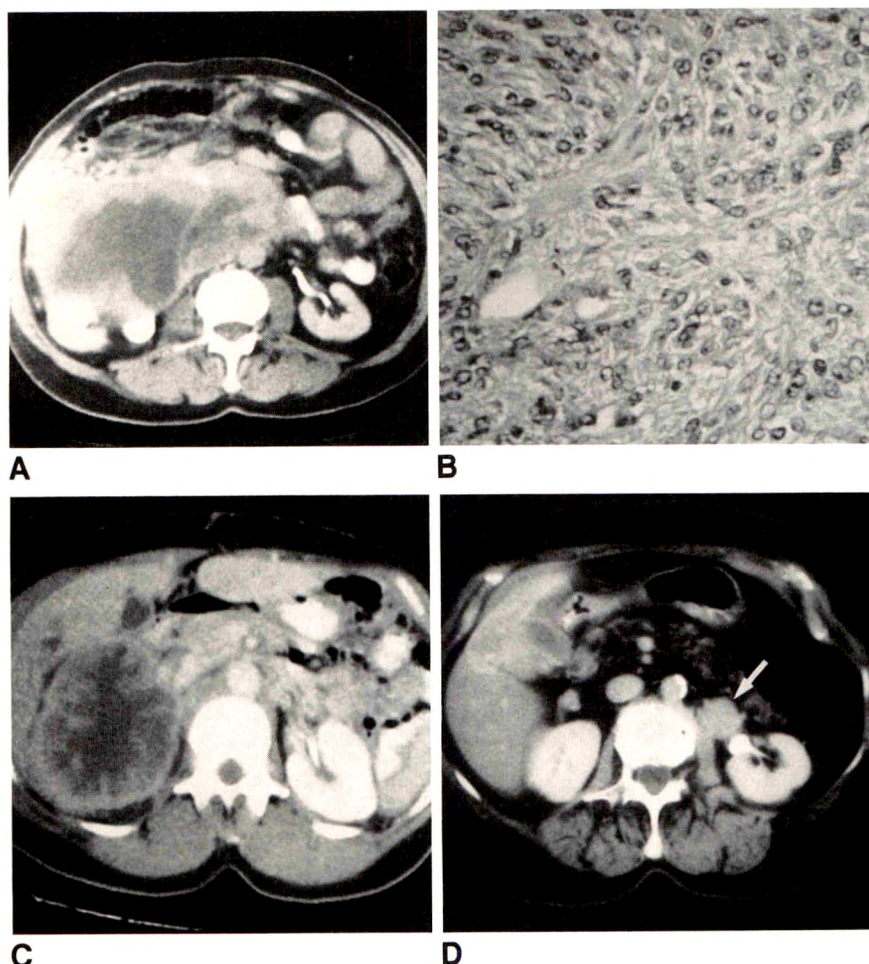


Fig. 5.—Leiomyosarcoma.

A, CT scan shows aggressive retroperitoneal tumor with large central region of necrosis.

B, Histologic section contains typical malignant, spindling cells of leiomyosarcoma. (H and E, $\times 250$)

C, Another large tumor with central necrosis.

D, Example of small leiomyosarcoma (arrow) of homogeneous, muscle density adjacent to left renal hilus. An enlarged retroperitoneal lymph node could also give this appearance.

The undifferentiated sarcomas, fibrosarcoma, and rhabdomyosarcoma appeared on CT as muscle-density masses with regions of necrosis. The rhabdomyosarcoma occurred in a 14-year-old boy (Fig. 9), whereas the other tumor types occurred in older adults.

Paraganglioma

Retroperitoneal paragangliomas are found in a paraaortic location from the renal arteries to the aortic bifurcation. The average age of patients in our series was 38 years old, and there was a male predominance (male:female, 8:4). Eleven patients had evidence of catecholamine excess. Metastasis is the criterion for malignancy. The benign tumors were small (average diameter, 4 cm) and of muscle density (Fig. 10A). The malignant tumors were larger (average diameter, 9 cm) and contained low-density regions representing necrosis (Fig. 10C).

Neurofibroma

The average age of patients was 40 years old, and there was a male-to-female ratio of 2:4. Four of six patients had

neurofibromatosis. The average CT diameter was 5 cm. The tumors had a characteristic CT appearance, which was that of a well-defined, homogeneous mass of near-water-density (Fig. 11).

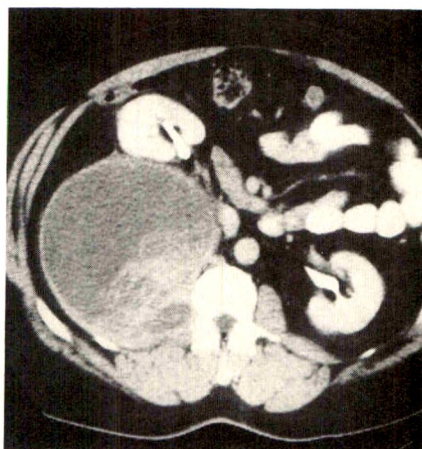
Neurilemoma

The average age of patients was 52 years old; there was a male-to-female ratio of 2:3; and none of the patients had neurofibromatosis. The average diameter was 6 cm. The CT densities of neurilemmomas were more variable than those of neurofibromas. These tumors were seen as well-defined masses with CT densities ranging from near that of water to muscle (Fig. 12).

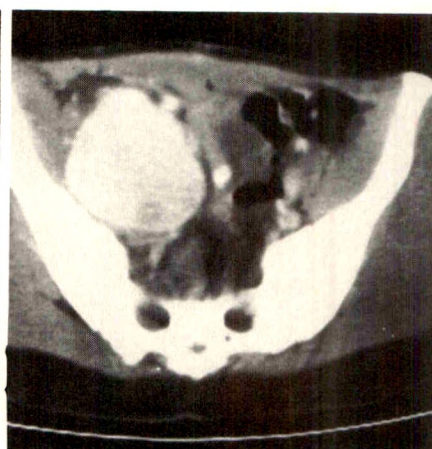
Other Benign Neoplasms

The three hemangiomas occurred in young adults (average age, 25 years old) with abdominal pain. The average CT diameter was 7 cm, and two tumors contained calcification. All three tumors underwent prominent IV contrast enhancement (Fig. 13). A lymphangioma was seen in a 3-year-old girl

Fig. 6.—Neurofibrosarcoma. CT scan shows retroperitoneal tumor with large region of central necrosis. As is true here, these tumors tended to occur in a posterior retroperitoneal location.



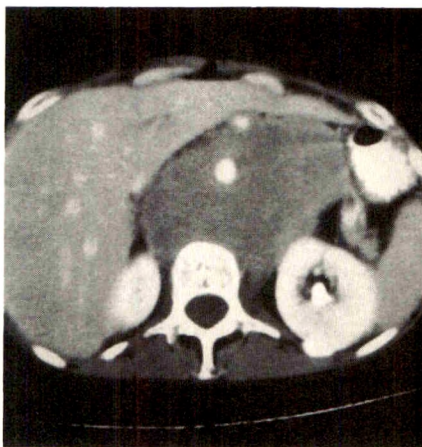
6



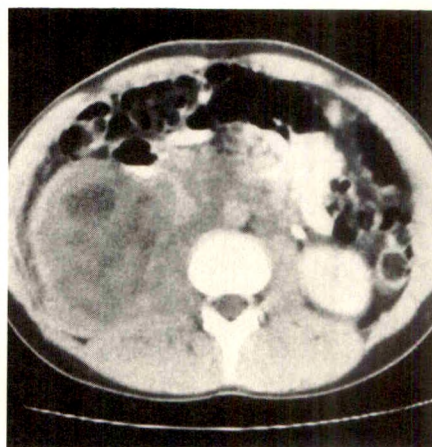
7

Fig. 7.—Hemangiopericytoma. CT scan shows retroperitoneal tumor with prominent IV contrast enhancement, consistent with this vascular neoplasm.

Fig. 8.—Malignant germ cell tumor. CT scan shows low-density mass in paraaortic region of retroperitoneum. Note that tumor encases aorta and displaces superior mesenteric artery anteriorly.



8



9

Fig. 9.—Rhabdomyosarcoma. CT scan shows aggressive retroperitoneal tumor with necrosis.

with an abdominal mass. CT revealed a 28-cm, low-density retroperitoneal mass.

Lipomas were seen in patients of various ages (4, 40, and 58 years old). The tumors had a characteristic CT appearance: homogeneous, fat-density tumor with well-defined borders (Fig. 14). Areas of higher density, as seen in liposarcoma, were not present.

A benign teratoma was found in a 68-year-old woman with abdominal pain. On CT, characteristic mixed components were identified in a predominantly cystic mass (Fig. 15).

Finally, the ganglioneuromas, which occurred in children, and desmoid tumor, which occurred in a 33-year-old woman, had nonspecific CT appearances of inhomogeneous soft-tissue masses in the retroperitoneum.

Conclusions

Primary retroperitoneal neoplasms comprise a rare and diverse group of tumors. The CT appearance of individual tumor types generally correlates with histopathologic findings.

In some cases, clinical correlation can be helpful in formulating a differential diagnosis.

Although CT is nonspecific in many cases, a number of CT features and clinical findings may suggest specific diagnoses when present: (1) presence of calcification in malignant fibrous histiocytoma; (2) presence of fat in a mass lesion of heterogeneous density in liposarcoma; (3) large regions of necrosis in leiomyosarcoma (although this is a relatively nonspecific finding in that other tumor types may contain necrotic regions); (4) calcified tumor in a child in neuroblastoma; (5) hypervascularity of hemangioma and hemangiopericytoma; (6) catecholamine excess and paraaortic location in paraganglioma; (7) homogeneous, low density of neurofibroma; (8) homogeneous, fat density of lipoma; and (9) characteristic mixed components of teratoma.

A knowledge of the range of CT appearances and various clinical settings for this rare group of neoplasms should assist the radiologist in making an appropriate CT interpretation when one of them is encountered.

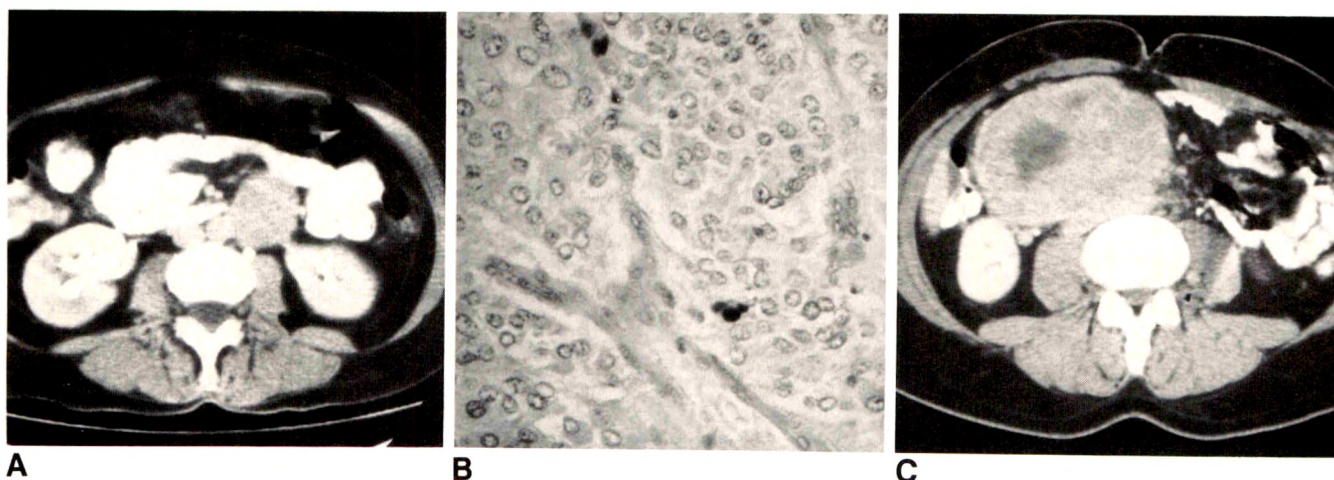


Fig. 10.—Paraganglioma.

A, CT scan of benign paraganglioma shows muscle-density tumor in left paraaortic location.

B, Histologic section contains small, uniform cells arranged in clusters separated by blood vessels, characteristic of paraganglioma. (H and E, $\times 250$)

C, CT scan of malignant paraganglioma shows larger tumor with central necrosis, more typical of the appearance of paragangliomas that have metastasized.

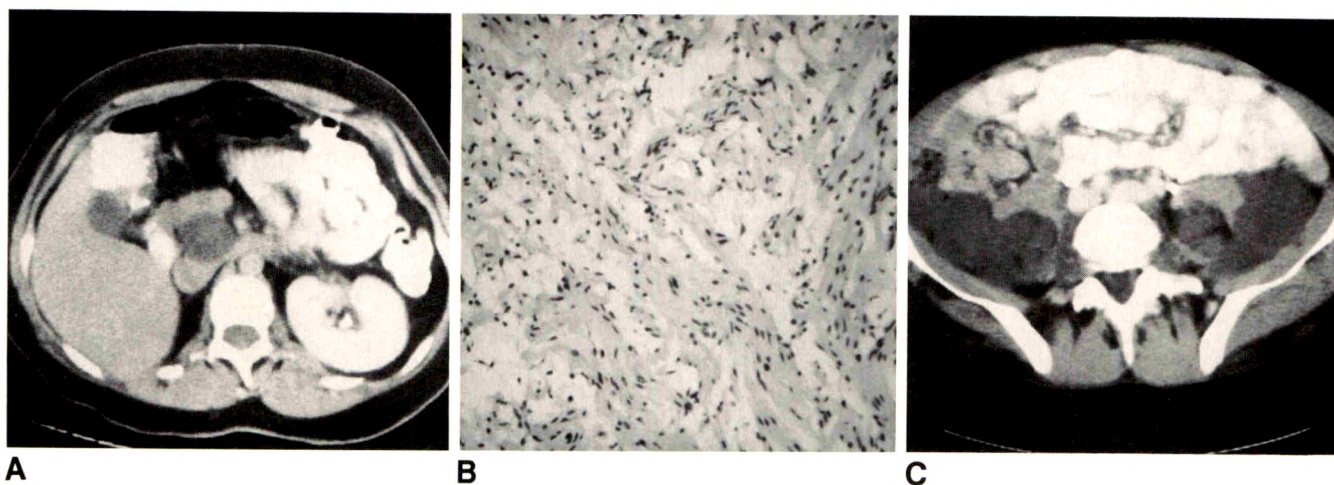


Fig. 11.—Neurofibroma.

A, CT scan shows tumor of homogeneous, near-water density just anterior to inferior vena cava.

B, Histologic section contains spindle cells within loose, edematous matrix, which correlates with low density on CT. (H and E, $\times 100$)

C, CT scan of bilateral plexiform neurofibromas, virtually pathognomonic of neurofibromatosis.

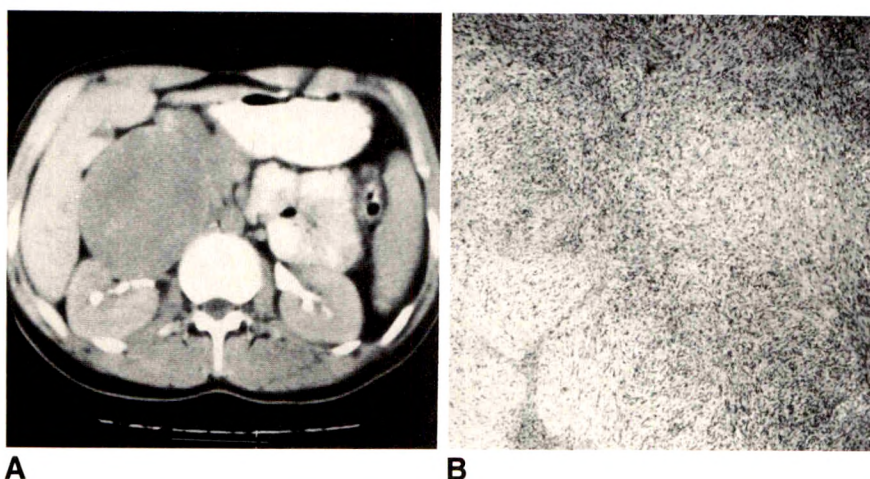


Fig. 12.—Neurilemoma.

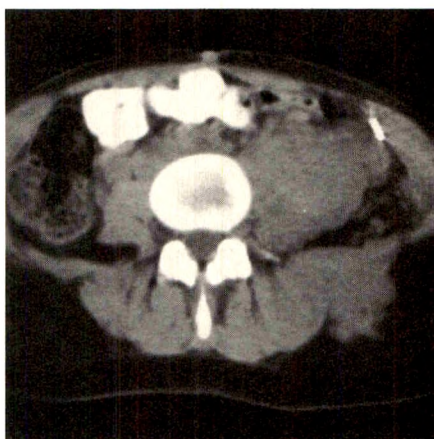
A, CT scan shows homogeneous, muscle-density tumor just anterior to right kidney.

B, Histologic section contains characteristic features of neurilemoma: cellular Antoni A regions are seen on right; less cellular, edematous Antoni B regions are seen on left. Individual tumors vary according to relative content of these two histologic patterns, which may account for variability of CT densities found in these tumors. (H and E, $\times 40$)

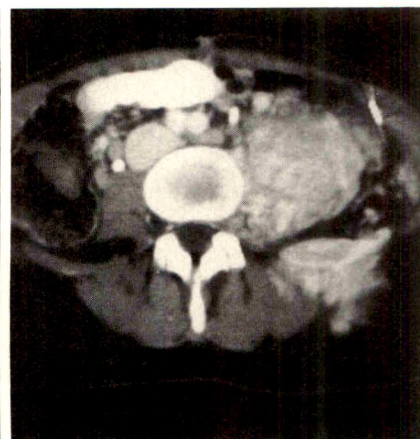
Fig. 13.—Hemangioma.

A, CT scan shows muscle-density tumor in left retroperitoneum.

B, After administration of IV contrast material, CT scan shows prominent enhancement pattern that is characteristic of this vascular neoplasm. Also note infiltration of posterior abdominal wall by tumor.



A



B

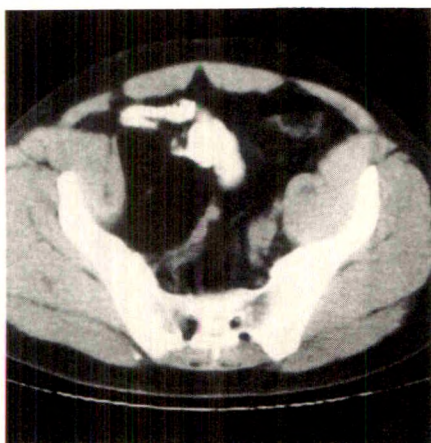
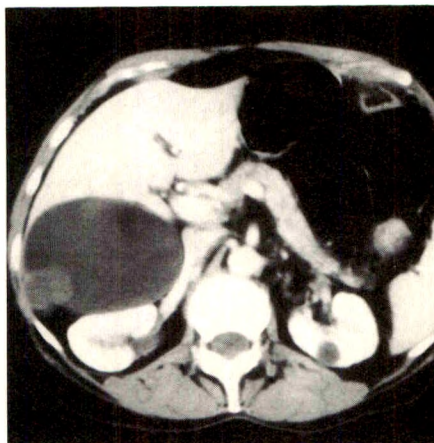
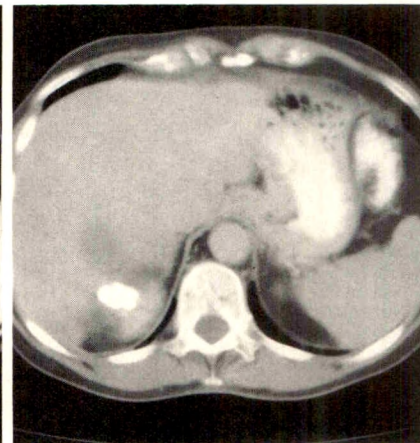


Fig. 14.—Lipoma. CT scan shows homogeneous, fat-density tumor with well-defined borders in lower right retroperitoneum.



A



B

Fig. 15.—Benign teratoma.

A, CT scan shows predominantly water-density mass posterior to liver, with focal area of fat anteromedially.

B, CT scan at another level shows several calcific densities, most likely representing teeth.

REFERENCES

1. Bosniak MA, Siegelman SS, Evans JA. Tumors of the retroperitoneum. In: Hodes PJ, ed. *An atlas of tumor radiology. The adrenal, retroperitoneum, and lower urinary tract*. Chicago: Year Book Medical, 1976:232-237
2. Stephens DH, Sheedy PF, Hattery RR, Williamson B Jr. Diagnosis and evaluation of retroperitoneal tumors by computed tomography. *AJR* 1977;129:395-402
3. Egund N, Ekelund L, Sako M, Persson B. CT of soft tissue tumors. *AJR* 1981;137:725-729
4. Stephens DH. Retroperitoneal masses. In: Taveras JM, Ferrucci JT, eds. *Radiology. Diagnosis-imaging-intervention*, vol. 4. Philadelphia: Lippincott, 1986:3-8

Categorical Course on Uroradiology

American Roentgen Ray Society 89th Annual Meeting

May 7-11, 1989, New Orleans Hilton, New Orleans, LA

Sunday, May 7

10:00-10:10 a.m.

10:10-10:50 a.m.

10:50-11:30 a.m.

11:30-Noon

Break

1:30-2:15 p.m.

2:15-3:00 p.m.

Break

3:30-4:15 p.m.

4:15-5:00 p.m.

Contrast Media/Infection/Renal Masses (Moderators: *Pollack* [a.m.] and *Mellins* [p.m.])

Welcome and Introduction

Contrast media. Comparison of ionic and nonionic agents: pharmacology, physiology, and guidelines for practical usage (*Katzberg*)

Toxicity and reactions to contrast media (*Pfister*)

Evaluation of the azotemic patient (*Talner*)

Acute renal infections (*McClennan*)

Chronic renal infections (*Kenny*)

Cystic diseases of the kidney (*Hartman*)

Neoplasms of the kidney (*Stanley*)

Monday, May 8

1:30-2:15 p.m.

2:15-2:45 p.m.

2:45-3:15 p.m.

Break

3:45-4:15 p.m.

4:15-5:00 p.m.

Prostate/Bladder/Scrotum (Moderator: *Davidson*)

Imaging of the urinary bladder (*Hattery*)

Epidemiology and natural history of carcinoma of the prostate (*Amis*)

Ultrasonography of the prostate (*Rifkin*)

CT and MRI of the prostate (*Hricak*)

Imaging of the scrotum (*Rosenfield*)

Tuesday, May 9

3:30-4:05 p.m.

4:05-4:40 p.m.

4:40-5:15 p.m.

Stone Disease (Moderator: *Newhouse*)

Radiological aspects of urolithiasis (*Bush*)

Extracorporeal stone therapy (ESWL) (*LeRoy*)

Interventional procedures in urolithiasis (*Banner*)

Wednesday, May 10

3:30-4:00 p.m.

4:00-4:45 p.m.

4:45-5:15 p.m.

Impotence and Erectile Insufficiency (Moderator: *Lang*)

Pathology and physiology of impotence (*Goldstein*)

Radiology of impotence (*Bookstein*)

Radiology of penile prostheses (*Cohan*)

Thursday, May 11

3:30-4:05 p.m.

4:05-4:40 p.m.

4:40-5:15 p.m.

Retroperitoneum (Moderator: *Hartman*)

Adrenal imaging (*Dunnick*)

Perinephric disease (*Levine*)

Retroperitoneal disease (*Lee*)

Inability of Sonography to Detect Imminent Ovulation

Debra Zandt-Stastny¹
 M. Kristin Thorsen¹
 William D. Middleton^{1,2}
 James Aiman³
 Ann Zion³
 Mary McAsey³
 Lori Harms³

Sonographic visualization of the cumulus oophorus or of morphologic alterations in the wall of the dominant follicle have been reported to be reliable signs of imminent ovulation when conventional transabdominal sonography is used. To determine if transvaginal sonography could allow a more frequent and confident prediction of imminent ovulation, we prospectively monitored 22 ovulatory menstrual cycles in four women undergoing artificial insemination and in 13 normally menstruating volunteers. Scanning was done on alternate days in the periovulatory period; a 7.5-MHz transvaginal transducer was used. Despite the improved resolution obtained with transvaginal sonography, confident identification of the cumulus oophorus or of mural changes in the follicle was not possible in any of the cycles followed. No other consistent follicular characteristic predicted imminent ovulation.

We conclude that confident prediction of imminent ovulation is not possible with sonographic analysis.

Accurate timing of ovulation is a critical requirement in the management of infertility. This is generally accomplished through close monitoring of biochemical factors such as serum estradiol or luteinizing hormone concentrations. Several sonographic signs have been reported to be reliable indicators of imminent ovulation. Identification of the cumulus oophorus as an echogenic mass protruding into the follicle has been reported by several investigators as an indication that ovulation will occur within the next 36 hr [1-3]. Changes in the follicular wall, including a line of decreased echogenicity surrounding the wall and a crenated appearance within the inner surface of the wall, have been reported as signs indicating ovulation will occur within 24 and 6-10 hr, respectively [4]. These investigators used gray-scale equipment, static B-mode and real-time sonography, with a suprapubic approach and a full-bladder technique to visualize the ovaries.

Improved visualization of ovarian morphology has become possible recently with the use of high-resolution transvaginal transducers. This study was performed to determine if transvaginal sonography could identify these reported signs more consistently than was possible with transabdominal scanning as reported in the literature and to determine if new signs of imminent ovulation could be identified.

Subjects and Methods

The study subjects were four women with normal menstrual cycles who were undergoing artificial insemination because of male infertility and 13 normally menstruating volunteers. Five women were scanned for two cycles. Therefore, a total of 22 cycles were evaluated. The women were 23-38 years old (mean, 31). Ten women had had previous pregnancies. The average menstrual cycle length was 28 days (range, 23-34). Biphasic basal temperature graphs confirmed ovulation in the four women undergoing artificial insemination.

Sonograms were obtained by using a 7.5-MHz mechanical sector transducer designed specifically for transvaginal use (Ausonics Corp., Milwaukee, WI). A single baseline examination was performed between days 5 and 8 of the menstrual cycle. A series of examinations

Received July 1, 1988; accepted after revision September 16, 1988.

Presented at the at the annual meeting of the American Roentgen Ray Society, San Francisco, CA, May 1988.

¹Department of Radiology, Medical College of Wisconsin, Milwaukee County Medical Complex, 8700 W. Wisconsin Ave., Milwaukee, WI 53226. Address reprint requests to M. K. Thorsen.

²Present address: Mallinckrodt Institute of Radiology, 510 S. Kingshighway Blvd., St. Louis, MO 63110.

³Department of Obstetrics and Gynecology, Medical College of Wisconsin, Milwaukee County Medical Complex, Milwaukee, WI 53226.

AJR 152:91-95, January 1989

0361-803X/89/1521-0091

© American Roentgen Ray Society

was then performed on alternate days in the periovulatory period. A final examination was done in the mid to late luteal phase of the menstrual cycle. Specific signs of imminent ovulation were sought prospectively while scanning was being done. These included identification of the cumulus oophorus, a line of decreased echogenicity surrounding the follicle, or a crenated pattern within the follicle. In addition, all sonograms were reviewed retrospectively to determine if there were other consistent findings before ovulation. Follicles were measured with electronic calipers from inner wall to inner wall in sagittal and coronal planes.

Laboratory parameters were followed in all patients to determine the time of ovulation. Each woman collected a urine sample daily in the periovulatory period, and the normal preovulatory surge of luteinizing hormone was detected by using commercial kits with a sensitivity of 25 mIU/ml. Quantitative determination of luteinizing hormone in the urine was made by means of radioimmunoassay. A serum sample was obtained on the day of urinary luteinizing hormone peak for both serum luteinizing hormone and estradiol-17 beta concentrations as indicators of impending ovulation. A second serum sample was obtained in the luteal phase for progesterone to document the occurrence of normal ovulation. A serum progesterone concentration greater than 5 ng/ml was taken as evidence of ovulation.

Results

In all 22 cycles, there was sonographic evidence of the development of a dominant follicle. The average maximal diameter of 22 follicles before rupture was 21.3 mm (range, 17–26). Figure 1 shows a plot of follicle diameter in millimeters vs time in days, with the day of the urinary luteinizing hormone peak being day 0. Usually the follicle reached its maximal diameter on day 0, the day of urinary luteinizing hormone peak.

Two types of follicular changes were observed at ovulation. In 20 cycles, the follicle completely disappeared (Fig. 2). In two cycles, the cyst decreased in size and developed irregular margins (Fig. 3).

In no instance was there convincing evidence of an echogenic mass that could be interpreted as a cumulus oophorus protruding into the lumen of the follicle. A line of decreased echogenicity surrounding the follicle could not be documented in any of these cycles. A crenated appearance to the inner wall was seen only 30–48 hr after the rise in urinary luteinizing

hormone and only when the follicle had decreased significantly in size (Fig. 3).

A retrospective analysis of all sonograms showed no consistent follicular changes that could be used for predicting imminent ovulation. In all instances, the walls of the follicle were smooth and well defined. The follicles were round or oval, and there were no internal echoes. The interface between the wall of the follicle and the remainder of the ovary was not interrupted by any characteristic changes.

Discussion

Sonography plans an integral part in the evaluation and monitoring of infertile women. It has considerable potential value in the prediction of imminent ovulation. Such prediction would aid in precise timing of artificial insemination, oocyte retrieval for in vitro fertilization, and administration of human chorionic gonadotropin.

Previous investigators have found that the size of the follicle before rupture is unreliable as a single index of imminent ovulation [5, 6]. Our results lead us to concur with this finding. Because the size of the follicle varies from 17 to 26 mm before rupture, use of follicular size as a sole predictor of ovulation is unreliable.

Marinho et al. [7] studied 46 normal cycles with transabdominal sonography and described changes that occur in the follicle after ovulation. These included (1) complete disappearance of the follicle (85%), (2) decrease in mean diameter of the follicle (9%), (3) change in the shape of the follicle (2%), and (4) increase in echogenic properties (4%). We found a similar distribution, with complete disappearance of the follicle in 91% of cycles and a decrease in the size of the follicle with irregular margins in two cycles (9%). In most patients, the complete disappearance of the follicle is a reliable indicator of ovulation.

By using static B-mode sonographic equipment in 56 women, Kerin et al. [1] identified an echogenic area projecting into the lumen in 23% of follicles greater than 18 mm in diameter. With conventional real-time equipment, Mendelson et al. [8] identified a linear, curvilinear, or poorly defined echogenic focus adjacent to the wall of a large follicle in eight of 28 women, who were followed over 77 cycles and who ultimately became pregnant. These structures were interpreted as the cumulus oophorus and were considered to be a predictor of imminent ovulation.

Picker et al. [4] described two additional sonographic findings thought to occur immediately before ovulation. Using a static B-mode unit, they retrospectively identified a line of decreased echogenicity around the follicle within 24 hr of ovulation in 12 of 12 patients. This was interpreted to be due to edema within the thecal tissue surrounding the follicle. In addition, they described a crenated pattern within the inner wall of the follicle in four of 12 women that was considered to be separation of the granulosa cell layer immediately (6–10 hr) before ovulation.

In our patients, we searched prospectively for these signs by using a high-resolution transvaginal transducer. We presumed that the superior visualization of follicular morphology

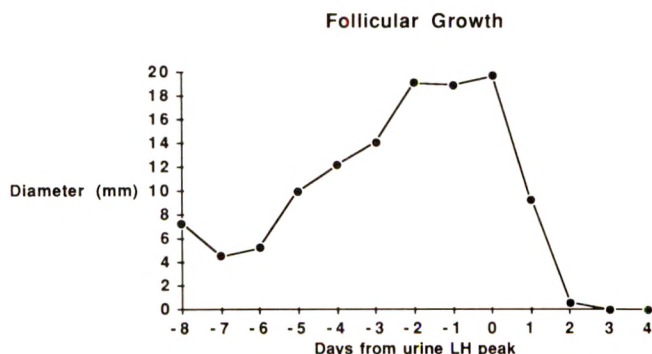


Fig. 1.—Graph of follicular growth shows average maximal follicular size of 22 follicles measured sonographically in relation to days of cycle. Day of urinary luteinizing hormone (LH) peak is day 0.

Fig. 2.—Serial sonograms show most common pattern of follicle growth. Arrows show right ovary.

A, Day 5: Three follicles are seen; largest is 7 mm.

B, Day 12: Dominant follicle is now 17 mm in size.

C, Day 14: Dominant follicle has reached 20 mm in diameter.

D, Day 16: Dominant follicle is not seen.

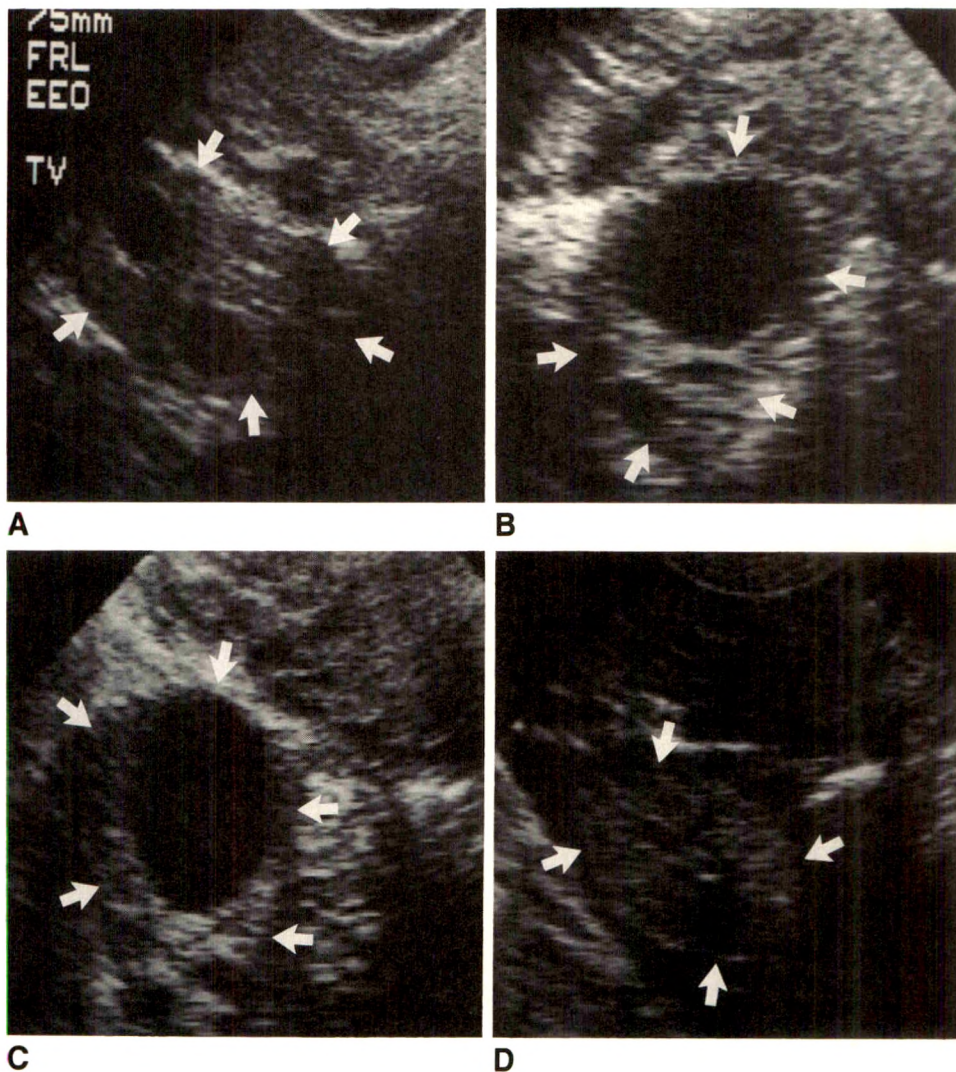
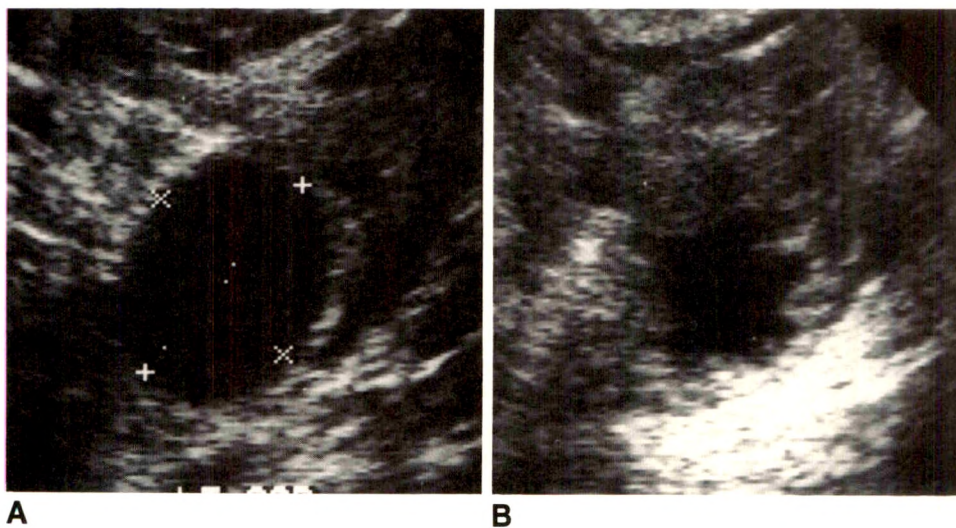


Fig. 3.—Serial sonograms show crenation of dominant follicle after ovulation.

A, Day 14: Dominant follicle is 23 mm.

B, Day 16: Follicle has decreased in size and margins are irregular.



with transvaginal sonography would allow more frequent and confident identification of the signs of imminent ovulation. Unexpectedly, we obtained the opposite result. Despite the improved resolution, it was not possible to identify the cumulus oophorus or changes in the wall of the follicle that predicted imminent ovulation.

One possible explanation for the discrepancy between our study and previous studies might be the differences in study methods. If the theoretical chances of visualizing the cumulus increase as scans are obtained closer to the time of ovulation, then the alternate-day scanning protocol used in this study might account for the decreased frequency of visualization compared with the daily scanning protocol used by Kerin et al. [1]. Fortunately, Kerin et al. calculated their frequency of visualization of the cumulus oophorus in follicles greater than 18 mm in size. Eighteen of our follicles reached this size. Therefore, we think our studies can be compared, despite differences in scanning frequency.

We think that our inability to visualize the cumulus is best explained by known follicular anatomy. Early in the development of the follicle, the cumulus oophorus occupies a rela-

tively large percentage of the follicular lumen. Histologic sections of small follicles reflect this relative prominence of the cumulus [9]. However, as the follicle itself enlarges, the relative prominence of the cumulus with respect to the follicular lumen is not maintained. Therefore, histologic sections of small early follicles do not accurately reflect the expected findings in the large preovulatory follicle. Unfortunately, this has not been well recognized and has led to the erroneous assumption that the cumulus should occupy a significant portion of the lumen of the dominant follicle and should be sonographically visible.

The actual size of the cumulus oophorus is 100–150 μ m (0.1–0.15 mm) [10]. This explains the ability to aspirate the cumulus with needles of internal diameters in the 1-mm range. Certainly, identification of such a small soft-tissue structure with conventional transvaginal transducers would not be expected, and our study suggests also that confident identification is not possible with transvaginal sonography.

Recognizing the discrepancy in the actual size of the cumulus and the size of the structures identified sonographically, Bomsel-Helmreich [11] proposed that reflections from viscous

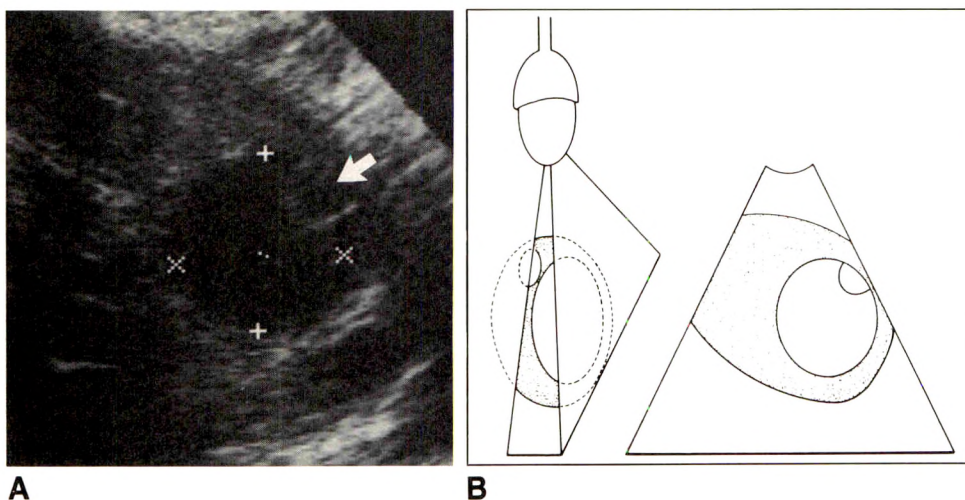


Fig. 4.—Slice-thickness artifact.
A, Sonogram shows adjacent follicle (arrow) protruding into lumen of dominant follicle because of slice-thickness artifact.
B, Schematic drawing shows concept of slice-thickness artifact. Because the ultrasound beam has a finite width, adjacent structures may be "averaged" together.

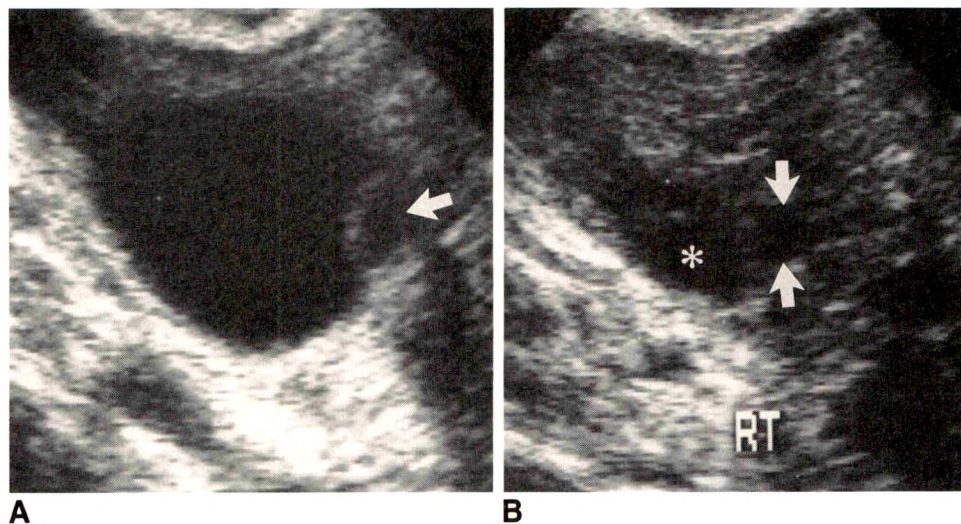


Fig. 5.—Serial sonograms show slice-thickness artifact mimicking a cumulus oophorus. This eccentric adjacent follicle is present before and after ovulation and is clearly not a cumulus.
A, Day 18: Small adjacent follicle (arrow) protrudes into lumen of dominant follicle.
B, Day 20: dominant follicle has ruptured (*), but smaller follicle (arrows) persists after ovulation.

fluid immediately surrounding the cumulus accounted for the structures seen sonographically. Although this is possible, we think it is quite unlikely for two reasons. First, viscous fluid might lead to low-level echoes, but it would not explain the echogenic structures frequently identified as the cumulus. Second, because of the improved ability to detect low-level echoes with transvaginal sonography, it is extremely doubtful that viscous fluid would not have been detected in this sample of patients but would have been detected in other studies that used conventional transabdominal sonography.

We think that artifactual echoes have largely accounted for the structures previously thought to represent the cumulus. It is well known that fluid-filled structures, such as ovarian follicles, are particularly prone to sonographic artifacts. This occurs because these structures are anechoic. Artifactual echoes, which normally are obscured in the echogenic background of soft tissues, are readily apparent in the anechoic background of a cystic structure. Side-lobe artifacts and slice-thickness artifacts could both produce internal echoes that might be misinterpreted as a cumulus oophorus within the follicle [12, 13]. Adjacent small follicles also may be misinterpreted as intrafollicular because of slice-thickness artifacts (Figs. 4 and 5). The fact that these artifacts are more readily apparent in larger follicles could explain their occurrence in the periovulatory period.

The differences between our results and those of Picker et al. [4] with respect to changes in the follicular wall are more difficult to explain. The original study that described the mural changes is difficult to analyze. The number of patients scanned, the number of cycles followed, the actual frequency of visualization of the stated mural changes, and the scanning interval used were not specified. However, we think that our inability to reproduce the original findings, despite a prospective search with a high-resolution transducer, makes it extremely doubtful that their original retrospective study with static B-mode equipment accurately reflects findings that sonographers should expect to visualize in the preovulatory period.

In conclusion, we have been unable to duplicate previous results that suggested that sonography was capable of predicting imminent ovulation. This includes identification of the cumulus oophorus or identification of changes in the wall of the follicle. We think that these previously described findings were probably the result of sonographic artifacts or misidentification of postovulatory changes.

REFERENCES

1. Kerin JF, Edmonds DK, Warnes GM, et al. Morphological and functional relations of graafian follicle growth to ovulation in women using ultrasonic, laparoscopic, and biochemical measurements. *Br J Obstet Gynaecol* **1981**;88:81-90
2. Hackelöer BJ. The role of ultrasound in female infertility management. *Ultrasound Med Biol* **1984**;10:35-50
3. Hackelöer BJ, Fleming R, Robinson HP, Adam AH, Coutts JRT. Correlation of ultrasonic and endocrinologic assessment of human follicular development. *Am J Obstet Gynecol* **1979**;135:122-128
4. Picker RH, Smith DH, Tucker MH, Saunders DM. Ultrasonic signs of imminent ovulation. *JCU* **1983**;11:1-2
5. Ritchie WG. Sonographic evaluation of normal and induced ovulation. *Radiology* **1986**;161:1-10
6. Queenan JT, O'Brien GD, Bains LM, Simpson J, Collins WP, Campbell S. Ultrasonic scanning of ovaries to detect ovulation in women. *Fertil Steril* **1980**;34:99-105
7. Marinho AO, Sallam HN, Goessens LKV, Collins WP, Rodeck CH, Campbell S. Real time pelvic ultrasonography during the peri-ovulatory period of patients attending an artificial insemination clinic. *Fertil Steril* **1982**;37:633-638
8. Mendelson EB, Friedman H, Neiman HL, Calenoff L, Vogelzand RL, Cohen MR. The role of imaging in infertility management. *AJR* **1985**;144:415-420
9. Williams PL, Warwick R. *Gray's anatomy*, 36th ed. Philadelphia: Saunders, **1980**:92
10. Veeck LL. *Atlas of the human oocyte & early conceptus*. Baltimore: Williams & Wilkins, **1986**:5
11. Bomsel-Helmreich O. The pre-ovulatory human oocyte and its microenvironment. In: Beier HM, Lindner HR, eds. *Fertilization of the human egg in vitro*. Berlin: Springer-Verlag, **1983**:19-34
12. Laing FC, Kurtz AB. The importance of ultrasonic side-lobe artifacts. *Radiology* **1982**;145:763-768
13. Goldstein A, Madrazo BL. Slice-thickness artifacts in gray-scale ultrasound. *JCU* **1981**;9:365-375

Book Review

Interventional Radiology. Edited by Wilfrido R. Castañeda-Zuñiga and S. Murthy Tadavarthy. (Part of the series Golden's Diagnostic Radiology. Series editor: John H. Harris, Jr.) Baltimore: Williams & Wilkins, 873 pp., 1988. \$149.95

This textbook, the newest volume in the series Golden's Diagnostic Radiology, deals entirely with interventional radiology. Many of the chapters have as many as 19 authors. The text has an authoritative ring, because most of the authors are from the University of Minnesota, where much of the pioneering technology in this field originated. European and Asian radiologists are also well represented, which brings to this text a description of techniques that are not widely practiced in the United States. The text is liberally interspersed with drawings, high-quality film reproductions, and photographs of various types of catheters and other hardware. When applicable, the available nonradiologic alternatives to the various interventional techniques, as well as ample discussion of the variations in technique that are available, are presented. Extensive references at the end of each chapter and a well-organized index enhance the book's usefulness.

All of the standard procedures of interventional radiology are presented. Similar techniques are discussed in multiple chapters by different authors. This organizational style leads to overlap of material and may be overwhelming to some readers. However, this text is primarily designed for the experienced practitioner, and the wealth of material is invaluable as one reference presents the multiplicity of interventional techniques that have been developed over the past 20 years.

This book contains many excellent chapters. The presentation of percutaneous transluminal angioplasty and fibrinolytic therapy represent the current state of the art. An extensive, highly informative chapter, written by many of the original investigators, highlights much of the experimental background of the mechanism and physiology of angioplasty as well as the physical basis for determining expansion characteristics and dilatation performance of angioplasty balloons. The chapters on peripheral and renal angioplasty are concise and well organized, and contain up-to-date information on selection of patients, techniques, and results.

Discussion of percutaneous and endourologic techniques makes up 25% of the book. In an excellent discussion of the anatomic basis for performing safe percutaneous renal puncture, most of the known

techniques are extensively described. Every conceivable percutaneous endourologic technique is discussed, from simple nephrostomy drainage to percutaneous ureteral clipping. An overlong section deals with percutaneous nephrostolithotomy, although only passing reference is made to extracorporeal shock-wave lithotripsy (ESWL)—a surprising omission, because most renal stones are now treated with ESWL. Comparatively short chapters on the techniques of percutaneous drainage and biopsy of chest and abdominal lesions are a good summary of the available concepts and indications. The chapter on treatment of hepatobiliary disease is well presented and illustrates beautifully all of the known interventional techniques.

A few specific criticisms are warranted. The information contained in the chapter on laser angioplasty is dated. The extremely brief chapter on noninvasive evaluation of peripheral vascular disease contains little useful information. The chapter on the pharmacologic or embolic control of gastrointestinal hemorrhage does not discuss the angiographic diagnosis of determining the bleeding site. A chapter on how to establish, equip, staff, and run an interventional radiology service within the modern community or university hospital would have been most welcome. A chapter dealing with drugs for sedation and anesthesia and ancillary methods of pain control in the interventional suite and monitoring of patients would have been an important addition.

These criticisms aside, this is a well-conceived and well-executed textbook. To the resident, or beginning interventionist, this book can serve as a guide to what is possible to accomplish. For the experienced practitioner, I know of no other single source that contains so much useful information. This text should find its way into every radiology departmental library and should be included in the personal library of anyone who has a more than passing interest in the subject.

Edward M. Druy
George Washington University, Medical Center
Washington, DC 20037

Fluoroscopically Guided Pyeloureteral Interventions by Using a Perurethral Transvesical Approach

Marco A. Amendola¹
 Marc P. Banner¹
 Howard M. Pollack¹
 Roy L. Gordon^{1,2}

Using a perurethral transvesical approach, we attempted a total of 180 varied pyeloureteral urologic interventional procedures during a 20-month period; 168 were successfully accomplished (93% success rate). We used standard interventional equipment, fluoroscopy, and (for access to the upper urinary tract) ureteral catheters that had been partially or completely inserted at cystoscopy by urologists. The successful procedures included insertion of double-pigtail ureteral stents (42 procedures), insertion of single-pigtail ureteral stents (47), advancement of arrested or incompletely inserted retrograde ureteral catheters (42), urothelial biopsy (30), balloon dilatation of ureteral strictures (three), retrograde cannulation of ureteropelvic junction obstructions that could not be negotiated in a percutaneous antegrade fashion (three), and ureteral stone extraction (one). The method was unsuccessful in 12 patients. Failures were due to caudal migration of a ureteral catheter into the bladder in eight patients and to an inability to advance a guidewire beyond an area of ureteral obstruction or perforation in four. Although most commonly used as an adjunct to extracorporeal shock-wave lithotripsy of renal and proximal ureteral calculi, the perurethral approach was extremely valuable for a wide variety of other indications. Significant complications, encountered in 5% of the procedures, included urosepsis (two), ureteral perforations (five), and cannulation of a false ureteral lumen (two). These problems resolved without sequelae with conservative management.

The perurethral transvesical approach represents a relatively simple, safe, and expeditious interventional urologic method. It frequently obviated other more invasive interventions such as percutaneous nephrostomy, ureteroscopy, or surgery.

Traditionally, urologists have almost always gained access to the kidney and ureter in retrograde fashion. In the face of certain technical limitations, however, including inability to pass a catheter beyond an obstruction and lack of fluoroscopic guidance, the endoscopically controlled approach to the kidney or ureter may fall short of its anticipated goals. In such cases, we have found that fluoroscopically guided perurethral intervention performed by radiologists working in close collaboration with urologists can often salvage potentially unsuccessful or incomplete cystoscopic procedures so that they can be satisfactorily completed. Herein, we report using a perurethral transvesical approach in 154 patients in whom 180 interventional radiologic procedures were performed during a 20-month period.

Materials and Methods

From July 1985 to March 1987, a total of 180 interventional procedures in 154 patients were performed in a retrograde perurethral transvesical fashion. The 84 women and 70 men were 14–84 years old. The procedures used standard guidewires, catheters, and sheaths; fluoroscopic guidance; and partially or completely inserted ureteral catheters for access to the upper urinary tract. One hundred sixty-eight procedures were successfully accomplished. The indications for these procedures were advancement of ureteral catheters in which retrograde cystoscopic insertion had been arrested (42 patients), placement of single-pigtail (47) or double-pigtail (42) ureteral stents, urothelial brush biopsies (30), balloon catheter

Received June 30, 1988; accepted after revision August 12, 1988.

Presented at the annual meeting of the American Roentgen Ray Society, Miami Beach, FL, April 1987.

¹ Department of Radiology, Hospital of the University of Pennsylvania, 3400 Spruce St., Philadelphia, PA 19104. Address reprint requests to M. A. Amendola.

² Present address: Department of Radiology, University of California, San Francisco, CA 94143.

AJR 152:97–102, January 1989
 0361–803X/89/1521–0097
 © American Roentgen Ray Society

dilatation of ureteral stenoses (three), retrograde cannulation of ureteropelvic junction obstructions that could not be negotiated in an antegrade fashion (three), and ureteral stone extraction (one). In 12 patients perurethral transvesical manipulations were not successful, usually because of loss of access to the ureter.

Techniques for Perurethral Retrograde Transvesical Manipulation

All patients received topical urethral anesthetic with 2% Xylocaine jelly (lidocaine HCl jelly, Astra Pharmaceutical Products, Westborough, MA). IV sedation under nursing supervision was employed frequently, usually with narcotic analgesics and/or Versed (midazolam, Hoffmann-La Roche, Nutley, NJ). Epidural anesthetic was used in selected cases (e.g., when manipulations immediately preceded extracorporeal shock-wave lithotripsy (ESWL) or when a potentially painful or prolonged procedure was anticipated). Parenteral broad-spectrum antibiotics were routinely administered before retrograde manipulations, which were performed under fully sterile conditions.

Access to the upper urinary tract was provided by prior cystoscopy or ureteroscopy, at which time catheters were partially or completely inserted into the ureters. These catheters were taped securely to a urethral Foley catheter to prevent their caudal migration during transport of the patient to the radiology department.

The ureteral catheters used were usually 5 French in diameter and of one of three types: open-ended, whistle-tip, or Pollack universal (#022105 5-French, Cook Urological, Spencer, IN). Each will accept a 0.038-in. (0.097-cm) guidewire. The advantage of the universal catheter lies in its smooth conical tip and an internal lumen that becomes progressively more peripheral until it terminates at a near-distal side hole. This configuration allows a straight guidewire to pass easily from the catheter tip yet maintains the catheter's round tip, which facilitates its cystoscopic insertion into the ureter. A torque guidewire (#THSF-38-145-THG, Cook, Bloomington, IN) with a tight distal curve usually can be made to exit the side hole of a closed-end whistle-tip catheter. Should this maneuver not allow guidewire egress, an appropriate-size Desilets-Hoffman sheath (#VSVSS 5.5-, 6.3-, and 7.5-French, Cook) can be passed coaxially over the ureteral catheter. These 32-cm-long Teflon sheaths are available in 5.5-, 6.3-, and 7.5-French inner diameters and fit snugly over 5-, 6-, and 7-French retrograde ureteral catheters, respectively. If the length of the ureteral catheter protruding from the urethral meatus is less than that of the sheath, the distal end of the catheter can be secured with a nylon suture while the coaxial sheath is inserted initially. After completely advancing the sheath, the catheter is removed, leaving the sheath as a conduit for further maneuvers.

A potential technical pitfall relates to the presence of an intravesical loop of ureteral catheter at the beginning of the fluoroscopic portion of the procedure. Passage of a standard guidewire may accentuate this loop and cause the catheter to retract from the ureter into the bladder, thereby losing access to the ureter. This problem can be circumvented in several ways. The easiest maneuver is to deflate the balloon of the Foley catheter and straighten the intravesical loop by gently retracting the proximal end of the ureteral catheter before passing a guidewire through that segment of catheter that traverses the bladder. Although this technique usually is successful, we occasionally found it necessary to use a movable-core wire or a glidewire (#46-160, Medi-tech, Watertown, MA). Either of these usually can be passed through coiled catheters without causing the intraureteral end of the catheter to be forced distally in the ureter.

Retrograde perurethral intraureteral manipulations are facilitated considerably by using peel-away and non-peel-away Teflon sheaths with introducers. Of the former, the one we use most often is the Banner sheath (#CPLIW-7.0 (to 11.0)-38-BANNER-012486, Cook Urological), a 65-cm-long peel-away sheath mounted on a gradually

tapered, stiff Teflon introducer of the Van Andel type. These sheaths are available with inner diameters ranging from 7 to 11 French (and corresponding outer diameters of 9–13 French). Less often, we use a 60-cm-long Smith peel-away sheath with a short tapered introducer and an inner diameter of 9 French (#074009, Cook Urological) or a non-peel-away 32-cm-long Desilets-Hoffman sheath with a short tapered introducer and an inner diameter of 8–10 French (#VSSW-8.0 to 10.0-38-32, Cook). Among their many advantages, these sheaths (1) provide a large conduit from urethra to ureter for passage of various instruments up the ureter; (2) prevent catheters and guidewires from looping and buckling in the bladder when attempts are being made to negotiate catheters, wires, and other instruments through areas of ureteral obstruction or tortuosity; and (3) provide ureteral stabilization and straightening. They allow manipulations and instrument exchanges to be performed inside the sheath lumen without the discomfort to the patient that is associated with urethral, bladder neck, or trigonal irritation, and they are particularly helpful in male patients. These sheaths also allow the direct delivery of forward and torque forces to the tip of the guidewire, which is essential when attempting to bypass ureteral obstructions (Fig. 1). A minor disadvantage of the Teflon sheaths is their relatively thin wall. They are easier to kink than are angiographic or urologic catheters.

Indications for Retrograde Perurethral Manipulations

Of 180 perurethral procedures, 102 (57%) were performed as an adjunct to ESWL of renal and proximal ureteral calculi; 78 (43%) procedures were performed for indications unrelated to ESWL. Incompletely inserted retrograde ureteral catheters were advanced farther up the ureter in 42 patients (Fig. 1). In 34 cases, these catheters were used to (1) assist fluoroscopic localization of ureteral calculi during ESWL, (2) facilitate identification of poorly opaque or nonopaque calculi by allowing retrograde pyeloureterography, or (3) relocate ureteral calculi to the renal pelvis in preparation for ESWL. In eight patients, the indications for catheter advancement were not related to ESWL and included short-term stenting of ureteral perforations and advancement of retrograde catheters to facilitate subsequent percutaneous nephrostolithotomy and/or balloon dilatation of ureteral strictures.

Retrograde perurethral placement of single-pigtail ureteral stents was performed in 34 cases as an adjunct to ESWL in order to (1) provide short-term upper urinary tract drainage before or after ESWL, (2) stent ureteral perforations that resulted from pre- or post-ESWL manipulations (Fig. 2), or (3) facilitate chemolysis of fragmented calculi after ESWL. In 13 instances, other indications not related to ESWL included a host of conditions necessitating short-term relief of urinary obstruction, such as bacterial or fungal pyonephrosis and temporary bypass of malignant ureteral obstructions in severely ill patients before the start of more definitive treatment, including longer-term drainage with double-pigtail stents.

Retrograde perurethral placement of double-pigtail ureteral stents (Fig. 3) was used to provide medium- to long-term internal drainage of obstructed renal units as an adjunct to ESWL in 28 patients and for other indications in 14 patients. In the latter group, the most prevalent indication was to achieve palliative internal drainage in nine patients with retroperitoneal malignancies after a cystoscopic attempt at drainage had failed. Fluoroscopically controlled retrograde perurethral brush biopsies of suspected urothelial tumors were performed in 30 patients. This subgroup of patients is the subject of a separate communication [1] and therefore will not be discussed further. Balloon dilatation of ureteral or ureteropelvic junction strictures (Fig. 4) was accomplished successfully via the retrograde perurethral route in three patients who declined percutaneous antegrade dilatation. In one other patient, a proximal ureteral calculus was removed in the

Fig. 1.—Advancement of retrograde ureteral catheter as adjunct to extracorporeal shock-wave lithotripsy (ESWL).

A, Cystoscopic insertion of two ureteral catheters to facilitate ESWL of left proximal ureteral calculus (arrow) resulted in arrested catheter passage at S1 level.

B, Retrograde ureterogram under fluoroscopic guidance shows that both catheters were inadvertently inserted into lumen of unsuspected blind-ending ureteral bud.

C, By using fluoroscopy and with patient in right posterior oblique position (with respect to table top), torque guidewire could be advanced into true ureteral lumen, beyond stone and into kidney.

D, 5-French catheter (arrow) could not be passed coaxially beyond obstructing stone without buckling wire in bladder or causing guidewire to retract into ureter.

E, By placing peel-away Teflon sheath (arrows) to stabilize ureter, 5-French catheter could be advanced easily into kidney. The patient was then ready for ESWL.



A



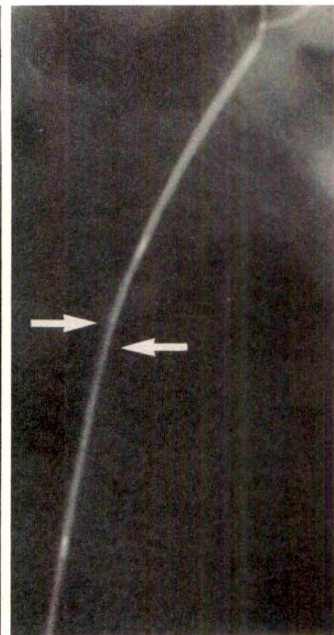
B



C



D

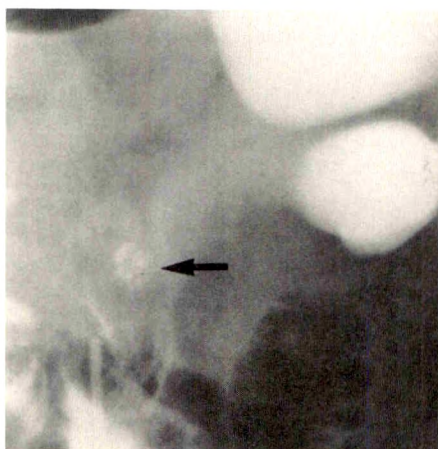


E

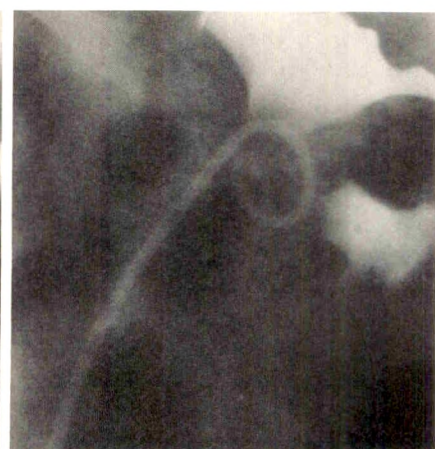
Fig. 2.—Stenting of ureteral perforation.

A, During cystoscopic retrograde manipulation of impacted stone (arrow) in left ureteropelvic junction, ureter was perforated. Note hydronephrosis and extravasated contrast material around ureteral catheter.

B, By using fluoroscopy and intravesical sheath for stabilization, torque guidewire and catheter could be passed beyond stone. Catheter was then exchanged for a single-pigtail ureteral stent. This allowed ureteral perforation to heal and facilitated extracorporeal shock-wave lithotripsy.



A



B

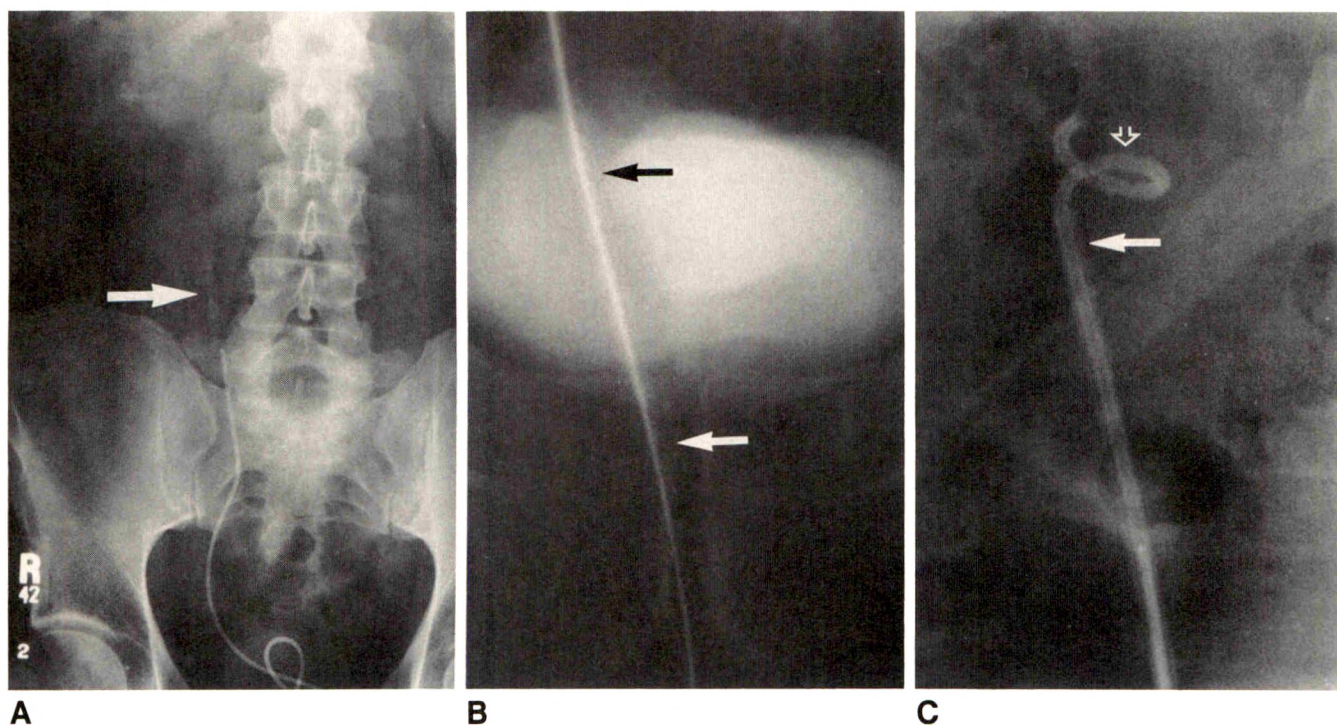


Fig. 3.—Retrograde placement of double-pigtail ureteral stent.

A, After extracorporeal shock-wave lithotripsy, a 5-French ureteral catheter could not be advanced cystoscopically beyond obstructing midureteral column of disintegrated stone fragments (arrow). This manipulation resulted in looping of catheter in bladder.

B, Ureteral catheter was exchanged over guidewire for 9-French Banner peel-away sheath (arrows). Sheath provides straight conduit from bladder neck to ureteral orifice. Sheath facilitated retrograde cannulation of stone-laden ureter by floppy-tip guidewire and ureteral catheter. The sheath was then advanced to renal pelvis.

C, 6-French double-pigtail stent (open arrow) inserted through peel-away sheath (solid arrow) is being positioned in renal pelvis. Sheath was then removed and distal pigtail of stent positioned in bladder.

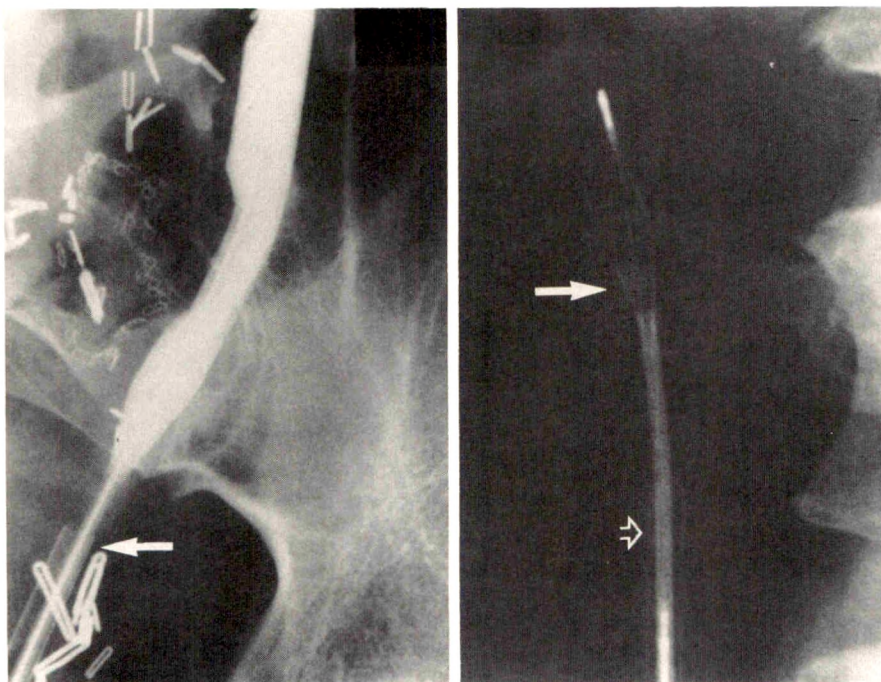


Fig. 4.—Perurethral dilatation of ureteral stricture. Postoperative benign ureteral stricture is being dilated with balloon catheter inserted in retrograde fashion. Waist in partially inflated balloon at site of stricture has not yet been effaced. To facilitate insertion and removal of balloon catheter and minimize patient discomfort, we performed the procedure through a 11-French Banner sheath inserted perurethrally and positioned in distal ureter (arrow).

Fig. 5.—Fluoroscopically guided perurethral ureterolithotomy. Proximal ureteral calculus (solid arrow) at level of L2 transverse process was resistant to extracorporeal shock-wave lithotripsy and percutaneous ureterolithotomy. It could be entrapped in wires of helical stone basket inserted through 11-French Banner sheath (open arrow) and extracted. Sheath prevented potential injury to ureter at level of iliac vessels and intramural ureter.

radiology department after two unsuccessful ESWL treatments and an unsuccessful attempt at percutaneous antegrade ureterolithotomy (Fig. 5). In three patients with stenotic ureteropelvic junctions that could not be negotiated in a percutaneous antegrade fashion, successful retrograde catheterization was possible with the perurethral transvesical approach.

Results

With the perurethral transvesical approach, the attempted procedures were accomplished successfully in 168 (93%) of 180 cases. The method was not successful in 12 patients. Failures were most often attributable to caudal migration of a partially inserted ureteral catheter into the bladder (eight patients). These occurred either during transport of the patient from the cystoscopy suite to the radiology department or during initial radiologic manipulation of a retrograde catheter that had been inserted only a short distance into the distal ureter. In four patients, we were unable to advance a guidewire beyond an area of ureteral obstruction or cystoscopically related ureteral perforation. These four patients were subsequently managed by percutaneous antegrade drainage and stenting.

Nine significant complications were directly related to the retrograde radiologic procedure, for a complication rate of 5%. Two patients developed Gram-negative sepsis within 12 hr of manipulation despite routine antibiotic prophylaxis. Both improved with continued appropriate IV antibiotic therapy and supportive measures. In five patients, the ureter was perforated with a guidewire despite fluoroscopic monitoring. In each case, immediate ureteral stenting (also via the perurethral retrograde approach) for 3–7 days allowed these perforations to heal without sequelae. In two patients, a retrograde catheter was inadvertently advanced through a false ureteral channel that had been created by prior cystoscopic manipulation. The catheters entered what appeared to be the renal collecting system. The false passages were recognized within the ensuing 24 hr because of poor urinary drainage from the affected renal unit as well as a subsequent abnormal retrograde pyelogram. These catheters were withdrawn to a normal area of ureter, and the true lumen was reentered. With appropriate stenting and drainage, both patients improved clinically without sequelae.

Discussion

Access to the kidney and ureter in a patient with an intact urinary tract may be accomplished in a retrograde (perurethral) or antegrade (percutaneous) fashion. The retrograde cystoscopic approach has been the traditional method used by urologists. Radiologists, on the other hand, are more familiar with the antegrade approach, for which a percutaneous nephrostomy is required. More recently, two additional approaches to the upper urinary tract have been added: ureteroscopy [2] and a combined method that uses cystoscopy, retrograde catheter manipulation, and fluoroscopy [3, 4]. The latter method has been used primarily to manage renal calculi, although it was initially described by Fritzsche et

al. [5], who successfully stented four partially obstructed ureters in a retrograde fashion.

On the basis of our experience with the Desilets-Hoffman sheath in performing percutaneous nephrostolithotomy, we modified the sheath in several ways [6]. Lengthening the vascular sheath to 32 cm and diminishing its lumen to 5.5 or 6.3 French allowed the retrograde perurethral exchange of closed-ended whistle-tip ureteral catheters to open-ended catheters that would easily accept standard guidewires. This exchange would then allow for fluoroscopically guided wire/catheter ureteral manipulations, which often could accomplish tasks that cystoscopically inserted ureteral catheters could not. Other modifications resulted in use of 32-cm-long Desilets-Hoffman sheaths with an inner diameter of 8–10 French and 65-cm-long peel-away sheaths with tapered Teflon introducers and inner diameters of 7–11 French. These sheaths considerably expanded the horizons of fluoroscopically guided ureteral manipulations by providing intravesical stabilization for guidewires and catheters. They further facilitated ureteral catheterization and stenting by traversing and simultaneously dilating areas of ureteral narrowing that would have interfered with the passage of soft ureteral stent catheters. These sheaths have, in fact, served to facilitate all of the retrograde perurethral manipulations we are reporting.

The techniques described herein are considerably more versatile than the planned use of the sheathed coaxial ureteral catheter for fluoroscopically guided retrograde procedures described by Lieberman et al. [7]. Although their 8.5-French catheter would have allowed most of our retrograde manipulations, its insertion (through a 22-French cystoscopic sheath) must be planned ahead of time. This is in contradistinction to our procedures, most of which followed the unexpected cystoscopic failure to accomplish a specific goal. A technique more similar to the present technique was used by Bixon et al. [8], who were able to bypass ureteral obstructions in a retrograde fashion by using fluoroscopic guidance in 22 of 24 patients. Five of their patients had experienced a ureteral perforation during the cystoscopic attempt at renal drainage.

Since the foundations for this combined urologic/radiologic approach to the ureter had been laid in the early 1980s, the technique became eminently applicable to managing patients treated with ESWL. The most frequently used manipulation required for successful ESWL is retrograde ureteral catheterization [9], either before ESWL (most commonly to bypass ureteral calculi with a catheter or stent) or after ESWL (to relieve ureteral obstruction by disintegrated stone fragments or to facilitate spontaneous passage of a large number of stone fragments) [9, 10]. In our institution, 2055 patients were treated with ESWL during the same 20-month period of this study. One hundred two perurethral transvesical procedures were performed in the radiology department as an adjunct to ESWL. Thus, 5% of ESWL treatments were assisted by the application of this interventional technique.

During the same 20-month period, 40 percutaneous nephrostomies were obviated by successful perurethral transvesical manipulations. Twenty-seven of these potential nephrostomies were related to ESWL, whereas non-ESWL indications were present in the other 13 patients. Application

of the techniques described herein therefore can be expected to decrease the number of percutaneous nephrostomies performed.

Although the perurethral retrograde approach is equally applicable to all segments of the ureter, the technique is more likely to fail when the patient has distal ureteral disease. As indicated earlier, catheters inserted cystoscopically into only the distal ureter may inadvertently migrate back into the bladder as a result of ureteral peristalsis and/or patient motion during transportation from the cystoscopy suite to the radiology department. Secure fixation of the ureteral catheter to the Foley catheter during transport of the patient is important to prevent this migration. The suture or tape that binds the two should not be loosened until *immediately* before the radiologist is ready to proceed with instrumentation. Also, unless extreme caution is used, when the tip of the catheter is in the distal ureter only, retrograde passage of a guidewire through the catheter may cause that catheter to back out of the ureter. If this happens, several recourses are available. If a urologist is nearby, cystoscopy with a flexible cystoscope can be performed almost immediately on the radiographic table without needing to reposition the patient (the lithotomy position is not necessary for flexible cystoscopy), and the catheter can be reinserted. Alternatively, the patient may have to be returned to the cystoscopy room for repeat cystoscopy and ureteral catheterization with a rigid cystoscope. If these measures fail or cannot be implemented, percutaneous nephrostomy usually is the final option.

Retrograde, fluoroscopically guided, pyeloureteral manipulations are both successful and safe. In this study, 93% of the procedures were completed successfully; five ureters (2.8%) were perforated but healed with simple stenting. When using Lunderquist-Ring torque wires, which we have found indispensable to successful manipulations, one must be mindful that they are inherently stiffer, and, therefore, potentially more traumatic than standard floppy-tipped guidewires. By using care, however, and especially by advancing the wire with a rotary rather than a direct forward motion, ureteral injuries can be held to an acceptable minimum. Although we extracted one ureteral calculus in our series of 180 procedures, we would caution against retrograde removal of calculi from the upper ureter. It is dangerous and easily can lead to ureteral avulsion. It is also unnecessary, because ESWL is the treatment of choice in this setting.

The success of this retrograde approach to the kidney and ureter ultimately is based on the foresight of the urologist to leave a ureteral catheter in situ and send the patient to the radiology department to have the clinically indicated procedure completed. This, in turn, is predicated on the urologist's acceptance that a combined cystoscopic/radiologic/fluoroscopic attempt at retrograde catheterization can be successful even after a cystoscopic attempt at drainage or stent placement has failed.

On the basis of our experience, we conclude that the fluoroscopically guided, perurethral, transvesical retrograde approach represents a relatively simple, safe, and expeditious interventional urologic method. Close cooperation with our urologic colleagues is essential for the application and success of these procedures. Although this approach was used most commonly in our practice as an adjunct to ESWL, it was also extremely valuable for a host of non-stone-related indications. In many instances, it obviated other more invasive interventional procedures, such as percutaneous nephrostomy, ureteroscopy, or surgery.

REFERENCES

1. Sheline M, Amendola MA, Pollack HM, Banner MP, de las Morenas A, Wein AJ. The practical value of fluoroscopically guided brush biopsy of the upper urinary tract. Presented at the annual meeting of the American Roentgen Ray Society, San Francisco, May 1988
2. Bush IM, Guinan P, Lanners J. Ureterorenoscopy. *Urol Clin North Am* 1982;9:131-136
3. Lawson RK, Murphy JB, Taylor AJ, Jacobs SC. Retrograde method for percutaneous access to the kidney. *Urology* 1983;22:580-582
4. Hawkins IF Jr, Hunter P, Leal G, et al. Retrograde nephrostomy for stone removal: combined cystoscopic/percutaneous technique. *AJR* 1984;143:299-304
5. Fritzsche P, Moorhead JD, Axford PD, Torrey RR. Urologic applications of angiographic guide wire and catheter techniques. *J Urol* 1981;125:774-780
6. Banner MP, Bergmann L, Pollack HM. Expanded uses of Teflon sheaths in interventional urology. Presented at the annual meeting of the American Roentgen Ray Society, Washington, DC, April 1986
7. Lieberman RP, Cummings KB, Leslie SW. Sheathed catheter system for fluoroscopically guided retrograde catheterization, and brush and forceps biopsy of the upper urinary tract. *J Urol* 1984;131:450-453
8. Bixon R, Laffey KJ, Benson MC, Martin EC. Retrograde urinary drainage: a combined approach. *J Endourol* 1987;1:153-160
9. Kellum CD, Tegtmeier CJ, Jenkins AD, et al. The role of radiology in extracorporeal shock wave therapy. *Radiology* 1987;165:431-438
10. Fedullo LM, Pollack HM, Banner MP, Amendola MA, Van Arsdalen KN. The development of steinstrassen after ESWL: frequency, natural history, and radiologic management. *AJR* 1988;151:1145-1147

The Laminar Space in the Diagnosis of Rotational Flexion Injuries of the Cervical Spine

Jeremy WR Young¹
Charles S. Resnik¹
Paula DeCandido²
Stuart E. Mirvis¹

We measured the distance between the spinolaminar line and the articular pillars of the cervical spine (the laminar space), identified on lateral radiograph, to determine the diagnostic value of changes in this measurement in cases of unilateral facet dislocation. Twenty-seven cases of unilateral facet dislocation were compared with 70 normal spines and with 29 cases of hyperflexion injuries without unilateral facet dislocation. Abrupt alteration of the laminar space between two adjacent levels was found to be an accurate measure of rotation of the spine at the levels concerned; on the basis of this alteration, we were able to correctly diagnose 23 of 27 cases of unilateral facet dislocation and 22 of 23 cases of unilateral facet dislocation between C2 and C6. In only two of the 70 normal cases was a similar alteration of the laminar space seen, and one of these was due to a previous fracture. In none of the 29 cases of hyperflexion injury without unilateral facet dislocation was there abrupt alteration of the laminar space.

We conclude that abrupt alteration of the laminar space is an accurate determinant for rotational anomalies of the cervical spine and, in particular, for unilateral facet dislocation.

Hyperflexion injuries of the cervical spine occur as a result of either flexion alone or a combination of flexion and rotation. Depending on their severity, pure flexion injuries give rise to hyperflexion sprains, wedge fractures of the vertebral bodies, or bilateral locked facets, and these injuries may also be associated with fractures of the articular pillars [1-4]. Flexion and rotation forces may give rise to unilateral facet lock, with or without fractures of the articular pillars.

We examined 27 cases of hyperflexion/rotation injuries involving unilateral dislocation of the facets (including one case of unilateral perched facet) and compared the lateral radiographs showing these findings with normal radiographs and with those showing other varieties of hyperflexion cervical spine injury. We also describe a new sign that aids in accurate differentiation of these injuries.

Subjects and Methods

Fifty-six patients with hyperflexion injuries (27 with and 29 without unilateral facet dislocation) who presented to the emergency room and the Shock Trauma Center of the University of Maryland Hospital over a 1-year period were included in the study. Those with hyperflexion injuries (but without facet dislocation) included 10 patients with hyperflexion sprain, two with bilateral perched facets, five with bilateral locked facets, five with hyperflexion wedge fracture, and seven with hyperflexion teardrop fracture. The lateral radiographs in these patients and in 70 normal subjects were randomized and presented to three skeletal radiologists for interpretation. The radiologists were given no clinical information and were asked to measure the distance between the spinolaminar line and the most dorsal surface of each paired articular pillar (the laminar space), for each vertebral level, and to offer a diagnosis based on their evaluation of the laminar space measurements (Fig. 1). In addition, at a later date, we reexamined the full series of radiographs of the abnormal cases to determine the radiographic findings attributable to each fracture. The results were then tabulated.

The laminar space was consistently measurable only at the C3, C4, C5, and C6 levels. This was due to difficulties in defining the posterior facet line at C2 in many cases, the

Received May 12, 1988; accepted after revision August 4, 1988.

Presented at the annual meeting of the American Roentgen Ray Society, San Francisco, CA, May 1988.

¹ Department of Diagnostic Radiology, University of Maryland Medical System/Hospital, 22 S. Greene St., Baltimore, MD 21201. Address reprint requests to J. WR Young.

² University of Maryland Medical System/Hospital, Baltimore, MD 21201.

AJR 152:103-107, January 1989

0361-803X/89/1521-0103

© American Roentgen Ray Society



Fig. 1.—Normal spine. Laminar space is shown. In this case, normal mild progressive widening of laminar space is present from C2 to C6 owing to mild progressive rotation of the spine.



Fig. 2.—Bilateral facet lock. Laminar space above and below the dislocation is wide and symmetric.



Fig. 3.—Flexion sprain with widening of posterior intervertebral space, interfacet joint, and spinous processes (asterisks). Laminar space, however, is symmetric and equal above and below injury.

elongation of the facet of C7 that occurs normally, and difficulty in visualizing the spinolaminar line at C7. The C2 laminar space was measurable in only 23 cases.

Finally, a medical student without experience in orthopedic radiology was invited to evaluate the data compiled by the radiologists and to score each spine as positive or negative for rotational injury solely on the basis of the laminar space distances.

Results

Of the 70 normal cases, a gradual and stepwise variation in the laminar space was identified in 47, reflecting a normal mild twisting of the spine (Fig. 1). The results for laminar-space measurements and levels of injury in the abnormal spines are shown in Table 1.

In the cases of hyperflexion injury without unilateral facet dislocation, three of the five cases of bilateral facet lock showed anterior displacement of the vertebral body that was greater than one-half of the anteroposterior diameter with respect to the vertebral body below. However, in two cases, the displacement was only about 45%. In every case, a normal laminar space was present, despite significant forward displacement of the superior vertebra (Fig. 2). In all cases of flexion sprain and bilateral perched facet, the laminar space again followed a normal pattern (Fig. 3).

Unilateral facet dislocation occurred in 26 cases, with one additional case of unilateral perched facet. Unilateral facet dislocation was associated with fractures of the facets in nine cases. In 22 cases, there was anterior displacement (3–7 mm) of the vertebral body with respect to the vertebra below.

TABLE 1: Flexion and Flexion/Rotation Injuries Studied

Injury	No. of Cases				
	C2–C3	C3–C4	C4–C5	C5–C6	C6–C7
Unilateral facet dislocation	2 (1)	3 (3)	11 (11)	8 (7)	2
Unilateral perched facet	0	0	1 (1)	0	0
Flexion sprain	0	1	3	4	1
Flexion teardrop fracture	0	1	3	3	0
Wedge fracture	0	2	2	1	0
Bilateral facet lock	0	1	1	2	1
Bilateral perched facet	0	0	1	1	0

Note.—Figures in parentheses indicate number of cases in which the laminar space alteration was indicative of rotational anomaly injury. In all other cases, laminar space alteration was not indicative of such an injury.

In five cases, anterior displacement of less than 3 mm was seen (Fig. 4).

In all but one case of unilateral facet dislocation between C3 and C6, an abrupt change in the laminar space was obvious at the level of dislocation (Figs. 4 and 5). This was identified either by abrupt narrowing of the laminar space at the levels above a symmetrically wide interspace or vice versa. In the remaining case, the alteration in the laminar space was less marked, with only a mild reversal of the progressive narrowing of the laminar space shown at higher levels above (Fig. 6).

Of the nine cases in which fractures of the facet occurred with dislocation, the fractures were horizontal in five cases and involved the superior facet of the normally positioned

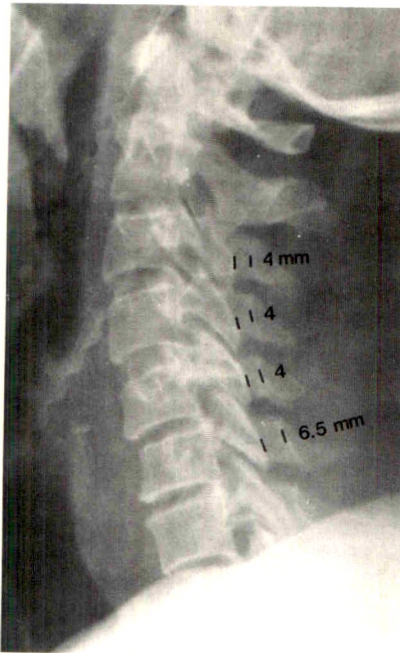


Fig. 4.—Unilateral facet dislocation. Subtle rotation of spine at C5 level is shown by abrupt change in laminar space. There is only minimal anterior subluxation of the vertebral body of C5 on C6.



Fig. 5.—Unilateral facet dislocation. Abrupt narrowing of laminar space at C4 is again shown. Superior and mild anterior displacement of C4 relative to C5 is seen.



Fig. 6.—Apparently normal laminar space, despite mild subluxation of C5 on C6, is seen in this case of unilateral facet dislocation. This injury has only a mild rotational component, with a minimally displaced fracture of the superior facet of C6 (arrow). In practice, progressive narrowing of laminar space from C3 to C5 is reversed at C6, where laminar space is wider than at C5.

Fig. 7.—Unilateral facet dislocation at C6–C7. Laminar space is not helpful in making the diagnosis. Normally overlapping facets are seen at C7 (arrow). A "bow tie" sign is seen.



7

Fig. 8.—Previous facet fracture at C4 has caused indistinctness of articular pillar. Laminar space is narrowed at this level.



8

vertebra with anterior slippage of the superior fragment. In four cases, the fracture involved the inferior facet of the abnormally positioned superior vertebra.

"Fanning" of the spinous process at the level of injury was seen in only 10 of the 27 cases of unilateral facet dislocation, but it was an obvious finding in 24 of the 29 cases of hyperflexion injury without unilateral facet dislocation.

The classical "bow tie" appearance of the vertebra above the level of dislocation with a normal appearance inferiorly was seen in only nine cases of unilateral facet dislocation (Fig. 7). An apparent "bow tie" sign was evident in four normal cases in which a gradual twisting or rotation of the spine was caused by positioning and identified by observation of the progressive narrowing of the laminar space. Angulation of the dislocated vertebral body was present in 10 cases, and widening of the interspinous space was present in 10 cases.

In 22 of the normal cases, there was evidence of unrelated disease. This was always due to degenerative disease, with disk space narrowing, osteophyte formation, and minimal subluxations, usually at the C4–C6 levels. In only four cases was an apparent abnormal "step off" in the laminar space seen by one of the reviewers; the other two reviewers did not make this observation. Further review of these cases indicated that the difficulty in ascertaining the exact posterior margin of the articular facet resulted either from closely overlapping facets (three cases) or from posterior osteophytes (one case). In two cases, an abrupt widening or narrowing of the laminar space occurred at one level only. This was due to a previous facet fracture in one case (Fig. 8). In the second case, no obvious cause for this was found.

The medical student correctly diagnosed 23 out of 27 cases of unilateral facet dislocation on the basis of an abrupt alteration in the laminar space. The only cases missed by the student were two at the C6 level, one at the C2–C3 level, and one in which no apparent gross change in the laminar space occurred (Fig. 6). Of the other cases, she incorrectly suggested rotation in four cases, but the reviewing radiologists had also disagreed about these cases.

Discussion

Unilateral facet dislocation of the cervical spine is caused either by simultaneous excessive flexion and rotation occurring together or by flexion of an already rotated head [2–6]. Several events take place when this injury occurs. With extreme torsion, the interfacet joint on one side of the vertebral column acts as a pivot with the facet of the superior vertebra on the contralateral side moving upward and forward over the articular mass of the vertebral body below, thus "locking" anteriorly [1–3]. The affected joint capsule and interspinous ligaments tear, although the contralateral capsule may be disrupted also [4]. This is considered a stable injury because the superior articular facet is relatively fixed between the inferior articular facet and vertebral body of the subjacent vertebra. This injury has been found in 4–16% [1, 4, 6–9] of patients referred for cervical spine trauma and may be associated with a fracture of the facet of the displaced vertebra [1, 4, 8, 10].

Although relatively rare, unilateral facet dislocation is important because often it is missed on initial examination, and delayed diagnosis results in difficulty in reduction and possible persistent deformity [4, 7]. Braakman and Vinken [4] found that 16 of 33 patients in their series with unilateral facet dislocation initially were diagnosed incorrectly. In six of 26 patients with unilateral facet dislocation studied by Rorabeck et al. [11], the diagnosis was missed for periods of 3 weeks to 3 months.

One of the radiographic signs that has been used to diagnose unilateral facet dislocation and has been documented by previous researchers is displacement of the interfacet joint on lateral films. This rotational deformity may result in a double set of articular facets above the level of injury, the so-called "bow tie" appearance, because one of the articular masses is displaced anteriorly with respect to the contralateral side (Fig. 7). Below the injury site, the facets are parallel, and only one set of facets is seen per vertebra [2–7]. The converse situation may also occur. This "bow tie" sign, however, was seen in only 33% of our cases of unilateral facet dislocation.

In unilateral facet dislocation, the body of the dislocated vertebra may become anteriorly displaced less than or equal to one-half the anteroposterior diameter of the vertebral body [1–4, 6, 12]. In our series, moderate anterior subluxation of the vertebral body was a relatively consistent finding, with displacement of 3–7 mm found in 22 of the 27 cases. However, this was also noted in seven of the 10 cases of flexion sprain, in two of the five cases of wedge fractures, and in four of the seven cases of teardrop flexion fractures. Therefore, this is a nonspecific sign and merely indicates significant posterior ligamentous and capsular disruption. However, when used in conjunction with alteration in the laminar space, this finding provided an accurate indication of unilateral facet dislocation.

Fanning or widening of the interspinous and interlaminar distance may be seen on the lateral projection and again represents rupture of posterior ligaments. In our series, this occurred in only 10 out of 27 cases of unilateral facet dislocation, even though posterior ligamentous disruption is implied in all cases. On the anteroposterior view, a displacement of spinous processes to the side of facet injury superior to the dislocation may be seen [6–8]. However, we did not evaluate this parameter in the present study.

The single case of unilateral facet dislocation in our series in which the laminar space was inconclusive between the C3 and C6 levels involved a fracture of the articular facet (Fig. 6). The reason for the false negative in this case lies in the mild rotational deformity that occurred because of the associated facet fracture. In practice, careful review of the radiograph reveals that there was a reversal of the normal progressive narrowing of the laminar space that was seen above the level of injury.

It is difficult to make an accurate diagnosis on the basis of the radiographic signs of unilateral facet dislocation previously described in the literature because their presence is variable. Our observation of an abrupt alteration in the laminar space at the level of unilateral facet dislocation, however, is highly accurate and correlates with the abrupt rotational deformity at the level of injury. In our series, 23 out of 27 cases showed

this sign, proving that it is the most accurate and most reliable sign for diagnosis of unilateral facet dislocation.

REFERENCES

1. Woodring JM, Goldstein SJ. Fractures of the articular processes of the C-spine. *AJR* 1982;139:341-344
2. Rogers LF. *Radiology of skeletal trauma*. New York: Churchill Livingstone, 1982:299-301
3. Dalinka MK, Dixon L, Verstandig A, Chapter 143. In: Taveras JM, Ferruci JT, eds. *Radiology—diagnosis, imaging, intervention*, vol. 5. Philadelphia: Lippincott, 1987:7-8
4. Braakman R, Vinken PJ. Unilateral facet interlocking in the lower C-spine. *J Bone Joint Surg [Br]* 1967;49-B:249-257
5. Whitley JE, Forsyth HF. The classification of C-spine injuries. *AJR* 1969;107:493-504
6. Harris JH, Edeiken MB, eds. *The radiology of acute cervical spine trauma*, 2nd ed. Baltimore, MD: Williams & Wilkins 1987:119-121
7. Scher AT. Unilateral locked facet in C-spine injuries. *AJR* 1977;129:45-48
8. Bohlman HH. Acute fractures and dislocations of the C-spine: an analysis of 300 patients. *J Bone Joint Surg [Am]* 1979;61-A:1119-1142
9. Rogers WA. Fractures and dislocations of the C-spine. *J Bone Joint Surg [Am]* 1957;39-A:341-376
10. Smith GR, Beckly DE, Abel MS. Articular mass fracture: a neglected cause of post-traumatic neck pain? *Clin Radiol* 1976;27:333-340
11. Rorabeck CH, Bourne RB, Hawkins RJ, Rock M. Unilateral facet dislocation of the C-spine: diagnosis and results of treatment (abstr). *J Bone Joint Surg [Br]* 1982;64-B:641
12. Beatson TR. Fractures and dislocations of the cervical spine. *J Bone Joint Surg [Br]* 1963;45-B:21-35

Book Review

Assessing the Skeletal Maturity of the Hand-Wrist. Fels Method. By Alex F. Roche, William Cameron Chumlea, and David Thissen. Springfield, IL: Charles C Thomas, 339 pp., 1988. \$57.50

Assessment of skeletal maturity is often required in the management of children who have endocrine disorders or other growth abnormalities. This book provides a new twist to the two well-established systems already widely applied: the atlas system of Greulich and Pyle and the scoring system of Tanner and Whitehouse. The authors have developed a computer program to analyze the data obtained by assessment of a single film of the hand and wrist. The system for skeletal age determination is based on extensive research over many years by the Fels Longitudinal Study of Growth and Development at Wright State University.

The book includes a description of bone maturation, an extensive history of the assessment of skeletal maturity, comparison of all methods of assessment of skeletal maturity, and a comprehensive bibliography. The Fels method is described in detail: its materials and methods, applications, and the statistical analyses.

The authors are thorough in every regard, including instructions such as the following: "The radiograph should be assessed in a dimly lit room. The less light the better for viewing radiographs, but if the room is too dark, the assessor will be unable to read the parts of this book to which reference must be made during the assessment process." The Fels method requires scoring maturity indicators in most of the bones of the hand and wrist. Quality reproductions of the radiographs with excellent details and appropriate diagrams are used

to indicate the features necessary for scoring. The descriptive text is sometimes awkwardly worded and a bit difficult to follow. Another problem is the frequent separation of figures from the corresponding text by several pages.

The book has potential value for pediatric radiologists, endocrinologists, and orthopedic surgeons. Although the Fels method is touted as simple, significant time is required to become familiar with the scoring system (test radiographs are available for self-assessment) and access to a computer. (The program costs \$3 and is available from Dr. Alex F. Roche, Fels Research Institute, 1005 Xenia Ave., Yellow Springs, OH 45387.) Compared with the relatively simpler atlas method of skeletal maturity determination, the Fels method is substantially more time-consuming. However, it provides a more accurate and reliable estimate of skeletal maturity. As with other labor-intensive activities that must be evaluated before implementation in the clinical setting, the technique will have to withstand the scrutiny of professionals caught in the cost-benefit squeeze.

Melissa R. Spevak
Paul K. Kleinman
*University of Massachusetts Medical Center
Worcester, MA 01655*

CT of Severe Renal Trauma in Children: Evaluation and Course of Healing with Conservative Therapy

Amy J. Yale-Loehr^{1,2}
 Sandra S. Kramer¹
 David M. Quinlan³
 Norman D. La France¹
 Sally E. Mitchell¹
 John P. Gearhart³

Over a 2-year period, blunt renal injuries were classified on a four-point scale: grade 1, contusions; grade 2, tears limited to the cortex (renal lacerations); grade 3, tears extending to the collecting system (renal fractures); and grade 4, renal vascular pedicle injuries. We report our findings in nine children with grade 2 and grade 3 blunt renal injuries who were evaluated with CT. One patient had a nephrectomy; the other eight were managed nonsurgically. Six patients had follow-up CT scans 5–19 months later to assess healing. Scars were evident in each case, and the extent of deformity paralleled the magnitude of the initial injury. One patient with a grade 2 injury and two patients with grade 3 injuries healed with small focal scars; three patients with grade 3 injuries healed with large polar scars. In five patients, the CT findings were compared with the findings on ^{99m}Tc-DTPA renal imaging. The injured kidneys contributed 30–45% (mean, 38%) of total renal function.

In six patients with renal trauma who were treated conservatively, the involved kidneys healed and significant kidney function was preserved, although early surgical intervention might have been beneficial for one of these patients. Prospective studies are needed to evaluate further the effectiveness of this conservative approach.

CT is an effective, noninvasive method of accurately assessing the extent of renal injury in children who have suffered blunt abdominal trauma [1–3]. Detailed CT evaluation of renal injuries aids in the clinical decision of whether or when to intervene surgically [4–6]. Renal contusions are best managed nonsurgically, and shattered kidneys and injuries to the renal vascular pedicle require early surgery. However, treatment of renal lacerations and fractures is not standardized: some researchers advocate early surgical intervention; others recommend expectant, nonsurgical management [7–13]. The goals are the same with either expectant or surgical management: the preservation of the renal parenchyma and the safety of the patient. We have used CT to evaluate the extent of injury and course of healing in five children who were managed conservatively after grade 3 renal trauma and in one child with grade 2 renal trauma. In the five children with grade 3 injuries, CT scans were correlated with nuclear renal scans to quantify relative renal function.

Subjects and Methods

Between 1984 and 1986, 21 children were admitted to the hospital with the diagnosis of blunt renal trauma. By using IV pyelography and/or CT in conjunction with clinical assessment, renal injuries were categorized on a four-point scale. Grade 1 encompassed minor renal injuries, including normal studies, asymmetric nephrograms or pyelograms, and/or zones of poorly functioning, contused, renal parenchyma. Grade 2 was defined as renal parenchymal tears limited to the cortex (renal laceration). Grade 3 included renal parenchymal tears extending into the collecting system (renal fracture), and grade 4 included renal vascular pedicle injuries. During this period, no children with grade 4 injuries were admitted. Of the 21 children, eight had CT only, nine had IV pyelography only, and three had both CT and IV pyelography. One patient with flank pain and microhematuria clinically had a grade 1 injury;

Received June 13, 1988; accepted after revision September 19, 1988.

Presented at The Inaugural Conjoint Meeting of The Society for International Pediatric Radiology, Toronto, Ontario, Canada, June 1987.

¹ Department of Radiology, The Johns Hopkins Medical Institutions, 600 N. Wolfe St., Baltimore, MD 21205.

² Present address: Department of Diagnostic Radiology, University of Maryland Medical System/Hospital, 22 S. Greene St., Baltimore, MD 21201. Address reprint requests to A. J. Yale-Loehr.

³ Department of Urology, The Johns Hopkins Medical Institutions, 600 N. Wolfe St., Baltimore, MD 21205.

AJR 152:109–113, January 1989
 0361–803X/89/1521–0109
 © American Roentgen Ray Society

his parents refused IV pyelography and CT for him. All children with grade 3 injuries had CT. In the nine children who were studied with IV pyelography alone, subtle grade 2 injuries may have been missed. However, these children were clinically stable, and further imaging evaluation was not indicated.

Nine (42%) of the 21 patients admitted had grade 2 or grade 3 injuries, as defined above. This percentage is not meant to accurately reflect the overall prevalence of grade 2 and/or grade 3 injuries; our population was a select group of children whose injuries necessitated hospital admission. All nine children in this final study group were evaluated with CT within 24 hr of admission. The group included five girls and four boys (age range, 6–14 years; mean, 9). Seven injuries resulted from automobile accidents (five pedestrian and two passenger); the other two injuries resulted from falls. Six of the renal injuries were on the left side; three were on the right side. Associated injuries occurred in the five children involved in pedestrian accidents. These included three CNS injuries, one splenic laceration, one pulmonary contusion with associated rib fractures, and four extremity fractures.

Initial CT examinations were analyzed for presence, site, and extent of renal extravasation of urine; perirenal and/or pararenal hematoma; intraperitoneal fluid; and zones of diminished renal function. Six patients had follow-up CT examinations 5–19 months after the original injury. The kidneys were analyzed for the presence of scarring and deformity, either polar or focal, in correlation with the original injury. In five of these, functional assessment was performed with nuclear renal scanning. Clinical follow-up studies, including evaluation of blood pressure, were done at regular intervals.

CT scans were performed on a Siemens DR 3; a 3-sec scan time was used. All scans were done with IV contrast medium (2 ml/kg) delivered either as a single bolus or as a bolus followed by a rapid drip. Contiguous 8-mm-thick scans at 10-mm increments from the diaphragm through the iliac crest or pelvis were obtained on the initial studies. The follow-up studies were limited to the levels of the kidneys. Coronal and sagittal reformatted images were obtained in the follow-up cases to aid in assessing deformity.

Nuclear renal imaging was performed by using technetium-99m diethylenetriamine pentaacetic acid (^{99m}Tc -DTPA); imaging was done with a large field-of-view gamma camera and a general all-purpose collimator interfaced to a dedicated computer. Dose was calculated as a percentage of the adult dose of 20 mCi (740 MBq) by using the patient's body weight and the West nomogram. Patients were imaged for 30 min, with flow and delayed time-activity curves generated from continuously acquired data. Split relative renal function was obtained

at 1 min. In one case, renal imaging with ^{99m}Tc -DMSA was performed as well.

Results

Of the nine patients in our study, three had grade 2 injuries and six had grade 3 injuries that were clearly depicted on CT. All nine patients had perirenal hematoma, five had pararenal hematoma, and five had intraperitoneal fluid. Solitary parenchymal tears were identified in the three patients with grade 2 injuries and in one patient with a grade 3 injury; the other five patients with grade 3 injuries had multiple tears. In addition, zones of absent or diminished function adjacent to the parenchymal defects were identified in six patients: five with grade 3 injuries and one with a grade 2 injury.

One patient in this group had a severely comminuted left renal fracture (grade 3 injury). The only functioning renal tissue seen on CT were a few fragments in the upper pole. A ^{99m}Tc -DTPA scan obtained 2 days after injury showed greatly diminished flow and function as well as extravasation (Fig. 1). At nephrectomy, the kidney was found to have a stellate fracture with patchy ischemic and necrotic renal tissue. The specimen findings correlated closely with the CT findings.

The remaining eight children were managed with close clinical follow-up and, if appropriate, imaging evaluation. One patient required surgical drainage at 8 days, percutaneous drainage at 40 days, and embolization of a leaking renal pseudoaneurysm at 50 days. Despite his protracted course, he was managed without surgery. One patient died of CNS injuries, but the other seven patients made uneventful recoveries.

On follow-up CT, all five patients with grade 3 injuries and one patient with grade 2 injury had scars at the sites of original injury. Focal scars were present in one patient with a grade 2 injury and in two patients with grade 3 injuries (Fig. 2). Polar scars were noted in three patients with grade 3 injuries. In one patient, the polar scar was subtle and was seen best on the reformatted coronal and sagittal images (Fig. 3). One polar scar was associated with a small subcapsular fluid collection (Fig. 4). The remaining five patients with

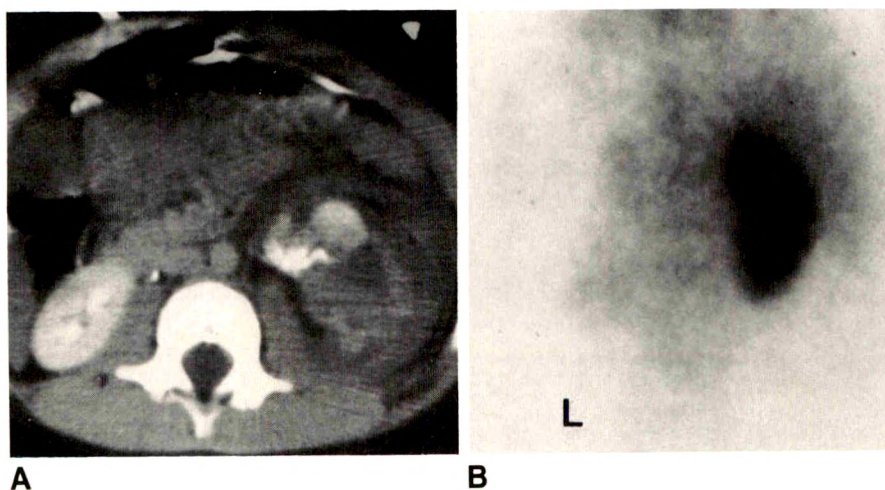


Fig. 1.—7-year-old boy who was struck by a car.

A, CT scan shows a small fragment of functioning renal tissue, perirenal and pararenal hematomas, contrast extravasation, and intraperitoneal fluid.

B, ^{99m}Tc -DTPA scintigram obtained 2 days later shows greatly diminished function on side of injury. Patient had a nephrectomy. L = left.

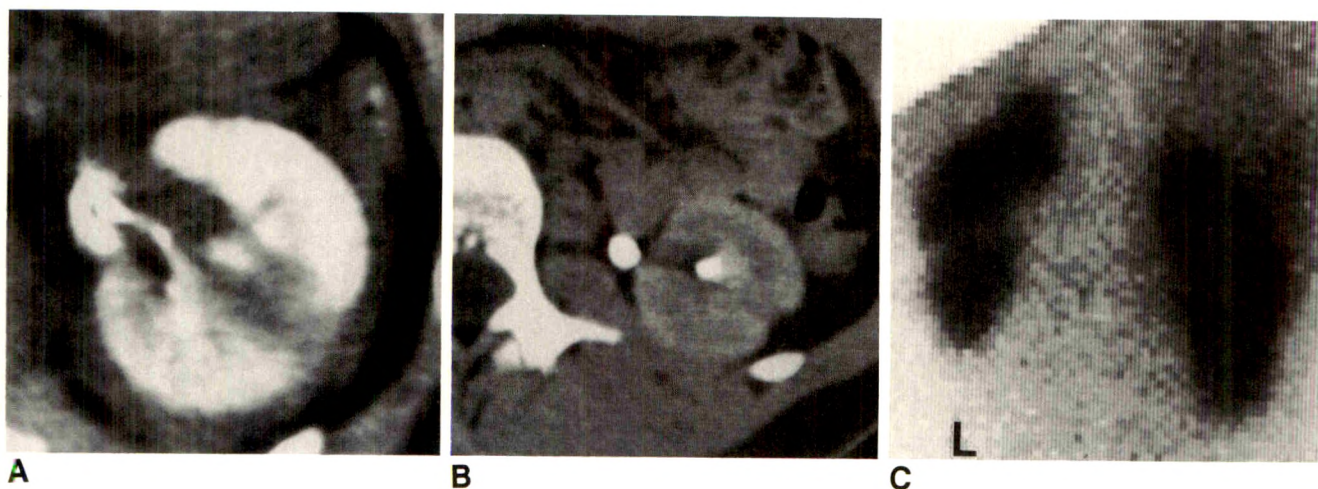


Fig. 2.—12-year-old girl who fell from a seesaw.

A, Initial CT scan shows renal fracture with extravasation and perirenal hematoma.

B, Follow-up CT scan obtained 12 months later shows focal renal scar.

C, ^{99m}Tc -DTPA renal scintigram obtained 12 months later; left kidney contributes 42% of total renal function. L = left.

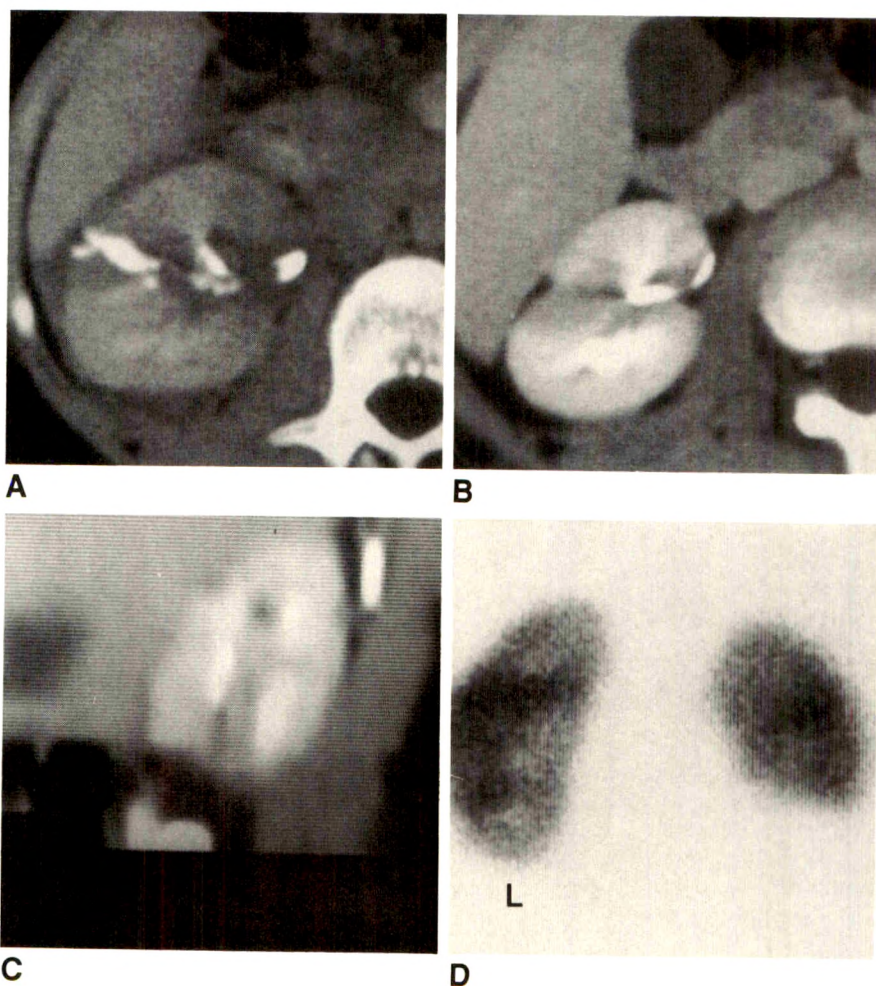


Fig. 3.—11-year-old boy who was a passenger in a motor vehicle accident.

A, Initial CT scan shows renal fracture with extravasation along fracture line and perirenal hematoma.

B and C, CT follow-up scans 5 months later show a coronal scar extending into lower pole.

D, Nonfunctioning lower pole seen on follow-up ^{99m}Tc -DMSA renal scintigram; right kidney contributes 40% of total renal function. L = left.

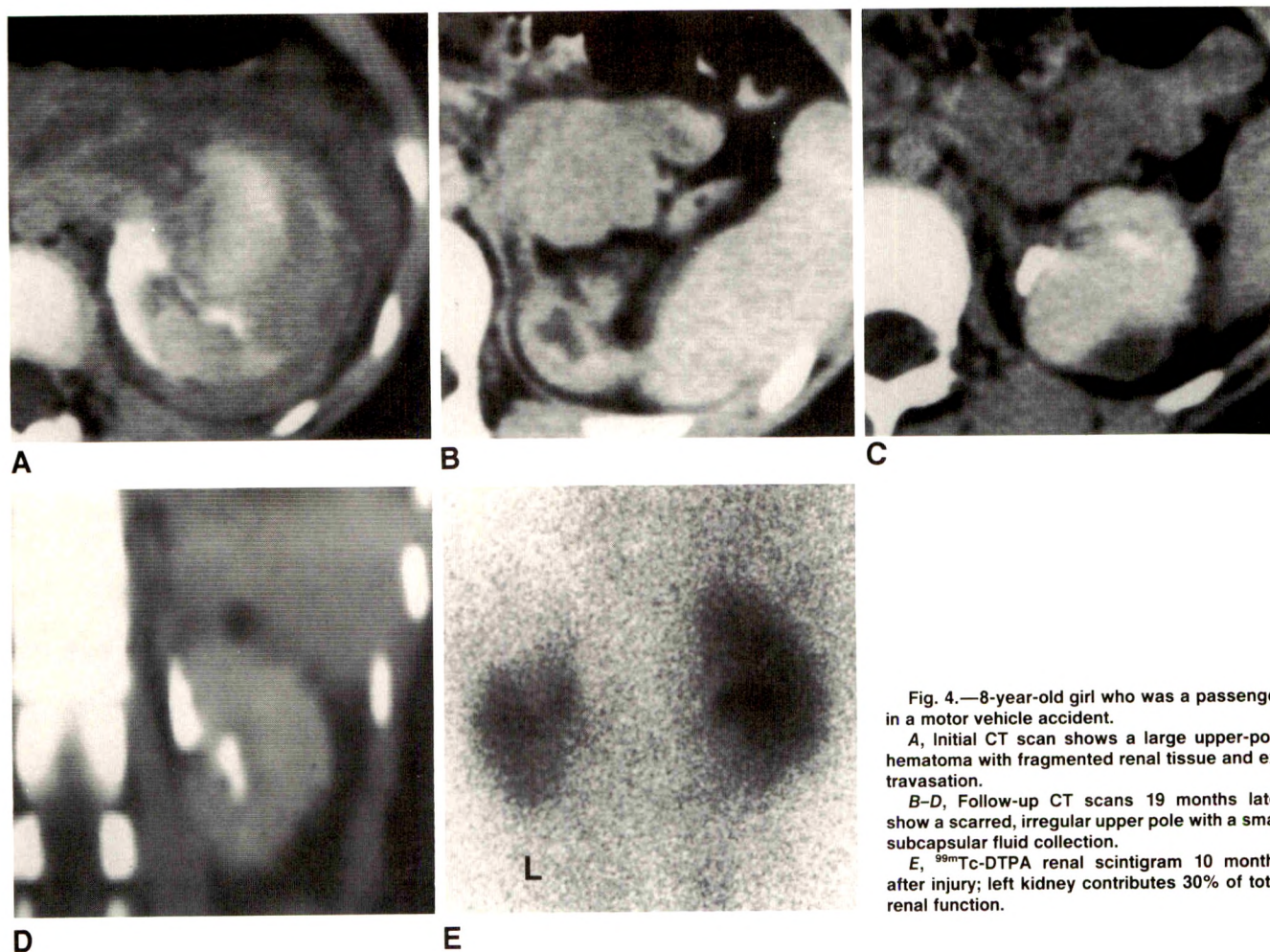


Fig. 4.—8-year-old girl who was a passenger in a motor vehicle accident.

A, Initial CT scan shows a large upper-pole hematoma with fragmented renal tissue and extravasation.

B–D, Follow-up CT scans 19 months later show a scarred, irregular upper pole with a small subcapsular fluid collection.

E, ^{99m}Tc -DTPA renal scintigram 10 months after injury; left kidney contributes 30% of total renal function.

grade 3 injuries had ^{99m}Tc -DTPA renal scintigraphy 5–12 months after injury. The injured kidneys provided 30–45% (mean, 38%) of total renal function. One patient also had a ^{99m}Tc -DMSA scintigram. The split relative renal functions in both types of nuclear tests were the same. The three patients in whom polar scars were identified on CT had greater diminution in function than did the patients with focal scars.

There were no unexpected findings on follow-up imaging. One patient died, one had a nephrectomy, and one was lost to follow-up. In clinical follow-up 18–34 months after the original injury, the six remaining patients stayed normotensive and had normal blood urea nitrogen and creatinine levels.

Discussion

Many studies have shown the usefulness of CT in evaluating pediatric trauma, including blunt trauma to the kidney. Contrast-enhanced CT obviates multiple imaging studies to evaluate the abdominal viscera. In addition to providing detailed information about structural integrity or deformity of the kidney, contrast-enhanced CT allows a qualitative assessment of renal function. The correlation of CT and nuclear

renography in the follow-up assessment of grade 2 and grade 3 renal injuries initially evaluated with CT provides both qualitative and quantitative information about healing.

Because of the noninvasive nature of this study, we do not have a surgical or pathologic gold standard with which to compare our CT findings. However, experimental work has been done to assess the course of healing in traumatized cat and dog kidneys [14–16]. Gerlaugh et al. [14] experimentally traumatized kidneys and examined them histologically as the organs healed. They initially identified hematoma and hemorrhagic extravasation at the site of laceration. One month later, they noted fibrosis at the site of laceration. At 2–8 months, the scarred area had contracted further, but the remainder of the kidney was normal. Their work supports our descriptive CT assessment of healing in injured kidneys.

Previous reports have described follow-up with IV pyelography and nuclear renography in conservatively managed renal trauma cases in children and adults [17–20]. We think that IV pyelography probably underestimates the scarring and deformity that follow severe renal injuries, which would explain the previous reports of patients with severe renal injuries who had normal follow-up IV pyelograms [17–20]. The superior spatial and contrast resolution of CT permitted detec-

tion of scarring in each case we followed. In one case of a grade 2 injury, the change was subtle and probably would not have been detected with IV pyelography. On CT, the undamaged portions of the traumatized kidney appeared to function as well as the normal kidney.

In addition to possible alteration in relative renal function after renal trauma, development of posttraumatic hypertension is a risk. The true prevalence of hypertension as a sequela to trauma is unknown [7, 17, 19, 21, 22]. In our study to date, 18–34 months after injury, the six patients remain normotensive. Continued follow-up into adulthood is important, however, because the onset of hypertension can occur years after the injury.

Jakse et al. [21] have evaluated the outcome in 30 cases of blunt renal injury in children that were managed with early surgery. The nephrectomy rate in their series was low, 7.5%. They used isotope studies to evaluate renal plasma flow and IV pyelography to assess renal growth and found no late complications with their surgical management. Cass et al. [22] compared the long-term results of surgically and conservatively managed renal lacerations and fractures. They concluded that conservative management was more likely to lead to radiographic abnormalities and/or hypertension than was surgical management. However, they did not include nephrectomy or partial nephrectomy as a radiographic abnormality. The study also failed to note specific information about the method of follow-up imaging.

The clinicians at our institution have taken a conservative approach to the treatment of renal trauma in children, with close clinical follow-up and radiographic evaluation of patients. In the patients we studied (five with grade 3 injuries and one with grade 2 injuries), the kidneys healed and significant kidney function was preserved. One patient who had a protracted course of healing might have benefited from early surgical intervention. Prospective studies are needed to further evaluate the validity of our conservative approach.

ACKNOWLEDGMENT

We thank Patricia Thompson for her secretarial assistance in preparing this manuscript.

REFERENCES

1. Kaufman RA, Towbin R, Babcock DS, et al. Upper abdominal trauma in children: imaging evaluation. *AJR* 1984;142:449–460
2. Berger PE, Kuhn JP. CT of blunt abdominal trauma in childhood. *AJR* 1981;136:105–110
3. Karp MP, Cooney DR, Berger PE, Kuhn JP, Jewett TC. The role of computed tomography in the evaluation of blunt abdominal trauma in children. *J Pediatr Surg* 1981;16:316–323
4. Federle MP, Kaiser JA, McAninch JW, Jeffrey RB, Mall JC. The role of computed tomography in renal trauma. *Radiology* 1981;141:455–460
5. McAninch JW, Federle MP. Evaluation of renal injuries with computerized tomography. *J Urol* 1982;128:456–460
6. Erturk E, Sheinfeld J, DiMarco PL, Cockett ATK. Renal trauma: evaluation by computerized tomography. *J Urol* 1985;133:946–949
7. Peterson NE. Intermediate-degree blunt renal trauma. *J Trauma* 1977;17:425–435
8. Peterson NE, Stables D. Blunt renal injuries of intermediate degree. *Urology* 1977;9:11–16
9. Evins SC, Thomason WB, Rosenblum R. Non-operative management of severe renal lacerations. *J Urol* 1986;123:247–249
10. Cass AS. Immediate radiologic and surgical management of renal injuries. *J Trauma* 1982;22:361–363
11. Cass AS, Luxenberg M, Gleich P, Smith C. Type of blunt renal injury rather than associated extravasation should determine treatment. *Urology* 1985;26:249–251
12. Mendez R. Renal trauma. *J Urol* 1977;118:698–703
13. Mandour WA, Lai MK, Linke CA, Frank IN. Blunt renal trauma in the pediatric patient. *J Pediatr Surg* 1981;16:669–676
14. Gerlaugh RL, DeMuth WE, Rattner WH, Murphy JJ. The healing of renal wounds. II. Surgical repair of contusions and lacerations. *J Urol* 1960;83:529–534
15. Trabucco A. Some radiologic findings and anatomic-pathological results of experimental renal trauma. *J Urol* 1943;49:601–617
16. Stirling WC, Lands AM. An experimental study of injuries of the kidney. *J Urol* 1937;37:466–479
17. Hutchison RJ, Nogrady MB. Late sequelae of renal trauma in the pediatric age group. *J Can Assoc Radiol* 1973;24:3–11
18. Ahmed S, Morris LL. Parenchymal injuries secondary to blunt abdominal trauma in childhood: a 10 year review. *Br J Urol* 1982;54:470–477
19. Mogensen P, Agger P, Ostergaard AH. A conservative approach to the management of blunt renal trauma: results of a follow-up study. *Br J Urol* 1980;52:338–341
20. Bergqvist D, Grenabo L, Hedelin H, Lindroth B, Tengstrom B. Long-time follow-up of patients with conservatively treated blunt renal injuries. *Acta Chir Scand* 1980;146:291–294
21. Jakse G, Putz A, Gassner I, Zechman W. Early surgery in the management of pediatric blunt renal trauma. *J Urol* 1984;131:920–924
22. Cass AS, Luxenberg PG, Gleich P, Smith C. Long-term results of conservative and surgical management of blunt renal lacerations. *Br J Urol* 1987;59:17–20

Book Review

Fetal Echocardiography. An Atlas. By Kathryn L. Reed, Caroline F. Anderson, and Lewis Shenker. New York: Alan R. Liss, 146 pp., 1988. \$62.50

The authors state that this book is a basic guide to fetal heart examinations that use echocardiography. It is intended for everyone who is concerned with the fetus as a patient, including those in the fields of obstetrics, pediatrics, cardiology, imaging, physiology, anatomy, and genetics.

The content of the atlas is divided into eight chapters: "Introduction," "Fetal Heart Anatomy and Physiology," "Methods of Examination," "The Abnormal Fetal Heart," "M-Mode Echocardiography," "Doppler Echocardiography," "Fetal Cardiac Arrhythmias," and "Color Flow Mapping" (by David Sahn).

The book is filled with good-quality echocardiographic images acquired with various types of sonographic equipment. The highlights of the book are the excellent anatomic line drawings by the illustrator, Fred Anderson. The authors have correlated representative illustrations of fetal position, anatomic structures, and fetal echocardiographic images in both normal and pathologic conditions. The enlarged echocardiographic images and anatomic correlations are well labeled for easy comparison.

The chapter on fetal anatomy and physiology is quite basic. This could have been expanded to include the embryologic development of the fetal heart so the reader would have a better understanding of complex heart disease and how it develops.

The chapter on Doppler technique is excellent. The authors have had considerable experience in this field of fetal echocardiography and have presented Doppler flow patterns and normal values for

cardiac valves and for shunt flows through the patent ductus and foramen ovale. The flow patterns through the umbilical vessels are also presented with normal values.

The chapter on fetal arrhythmias is well illustrated, with clearly defined legends to help interpret the M-mode tracings. It might have been useful for the authors to mention the occurrence of rhythm variations that the normal fetus can have with increased frequency in the third trimester. This chapter concentrates on fetal arrhythmias that are persistent throughout the echocardiographic examination.

The chapter on the newer technique of color-flow mapping was written by one of the pioneers in the field, David Sahn. He briefly describes some of the physical characteristics of color-flow mapping and problems encountered with present equipment. He describes the shape of vessels and chambers, intercirculatory communications, and variant "turbulent" flow patterns seen with color flow and describes the advantage this technique can offer in complex congenital heart disease.

Overall, this atlas of fetal echocardiography is well documented and illustrated. The book would be an excellent addition to the library of those who perform fetal echocardiography.

Sandra L. Hagen-Ansert
University of California, San Diego, Medical Center
San Diego, CA 92103

Radiographic Evaluation of Subureteric Injection of Teflon to Correct Vesicoureteral Reflux

Margaret D. Gore¹
 Sandra K. Fernbach¹
 James S. Donaldson¹
 Arnold Shkolnik¹
 Mark R. Zaontz²
 William E. Kaplan²

The imaging studies of 83 children (115 ureters) with vesicoureteral reflux who were treated by subureteric injection of Teflon (STING) were reviewed. On plain films, the Teflon rarely may be seen as faintly radiodense. On sonography, it is echogenic and has variable acoustic shadowing. On CT it is dense (160–466 H). Postsurgical cystography showed cessation of reflux in 83 ureters (72%). Complications of STING were uncommon. No granulomatous masses were identified in the region adjacent to the STING. Transient, free peritoneal fluid developed in three children and ureteral dilatation in six, three of whom required intervention. In one child, most of the Teflon disappeared from the original site of injection, as noted on a follow-up CT scan; possibly it had been extruded into the bladder.

The STING procedure probably will become more popular. Knowledge of its radiologic appearance is important for the radiologist in order to effectively evaluate these children postoperatively.

Vesicoureteral reflux is a common disorder of children that, when severe and chronic, or when coexisting with infected urine, can cause significant damage to the renal parenchyma and eventual loss of renal function [1]. Both medical and surgical approaches to the treatment of reflux have been developed. There is disagreement about which therapy is most beneficial in children with intermediate degrees of reflux. Certain situations generally prompt surgical intervention, such as grade V reflux, recurrent urinary tract infection despite appropriate antibiotic treatment, and noncompliance with medical treatment.

Although the overall success rate of the various antireflux procedures is greater than 95% [2–4], they all entail both an abdominal and a bladder incision, several hours of surgery and general anesthesia, and a hospital stay of several days.

In 1981, the STING procedure (subureteric Teflon injection) was developed to treat vesicoureteral reflux [5, 6]. Polytetrafluoroethylene (Teflon, DuPont, Wilmington, DE) mixed with glycerin (Ethicon Polytef, Mentor Division, Codman & Shurteff, Inc., Randolph, MA) is injected into the submucosa inferior to the ureteral orifice. The mass effect of the Teflon elevates and narrows the ureteral orifice and supports the ureter inferiorly. The injection is performed through a special needle inserted through the cystoscope. It is an outpatient procedure, and it takes approximately 15 min.

Most radiographic studies performed after STING are obtained to evaluate the success of the procedure and document cessation of reflux. Recent reports of migration of the Teflon particles and granuloma formation locally and in distant sites prompted us to look critically at STING sites and adjacent soft tissues [7].

The radiologic appearance of the Polytef paste has received scant attention [8]. The real and potential complications of STING have been reviewed only in the urological literature [9–13]. We describe the preliminary results of STING at our institution and the radiographic appearances.

Received May 26, 1988; accepted after revision August 22, 1988.

¹ Departments of Radiology, Northwestern University and The Children's Memorial Hospital, 230 Children's Plaza, Chicago, IL 60614. Address reprint requests to S. K. Fernbach.

² Departments of Urology, Northwestern University and The Children's Memorial Hospital, Chicago, IL 60614.

AJR 152:115–119, January 1989
 0361–803X/89/1521–0115
 © American Roentgen Ray Society

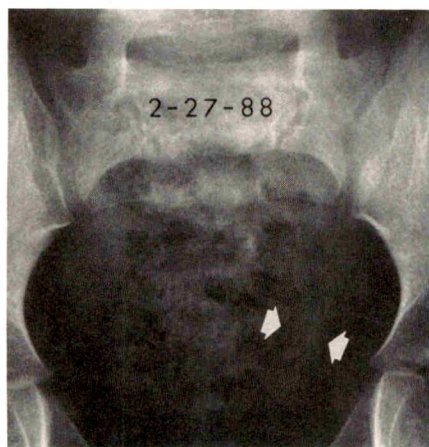
Materials and Methods

From January 1986 through February 1988, 83 children (59 girls, 24 boys) with reflux underwent STING. Informed consent was obtained for all children. All children needed antireflux treatment according to the criteria described in the introduction. The ages at the time of the first STING procedure ranged from 1 year 3 months to 16 years 7 months (median age, 6 years 7 months). The STING procedure was performed once on 115 ureters, twice on 18 ureters, and three times on one ureter. Fifty-two children had idiopathic reflux, and 29 had reflux associated with a neurogenic bladder. Of the two remaining patients, one had ablation of posterior urethral valve and one had repaired bladder exstrophy. The medical records and imaging studies of all the children through March 1988 were reviewed. Imaging studies were done at the discretion of the clinical service and were reviewed retrospectively. Postoperative plain abdominal or pelvic radiographs were available in 57 children. Follow-up cystography was performed in 82, with one child lost to follow-up. Intraoperative (post-STING) cystography was done in seven (eight studies), standard voiding cystourethrography in 16 (21 studies), and nuclear cystography in 73 (95 studies) [14, 15]. Nuclear cystography was performed by using the technique of Conway et al. [15] (Siemens ZLC Series, Des Plaines, IL). Eighteen patients were studied with noncontrast pelvic CT. Axial scans were obtained at 5- or 10-mm intervals on a General Electric 9800 Quick Scanner (Milwaukee, WI). Forty-one patients underwent a total of 73 sonographic examinations of the urinary tract. Sonography was performed with real-time equipment and 3.5- or 5.0-MHz linear-array or sector transducers (Acuson 128, Mountain View, CA). Repeat sonography was performed (1) to exclude the development of upper tract obstruction; (2) to evaluate the appearance of the bladder after STING; or (3) to evaluate routinely the urinary tract in children with meningomyelocele, posterior urethral valve ablation, or repaired bladder exstrophy.

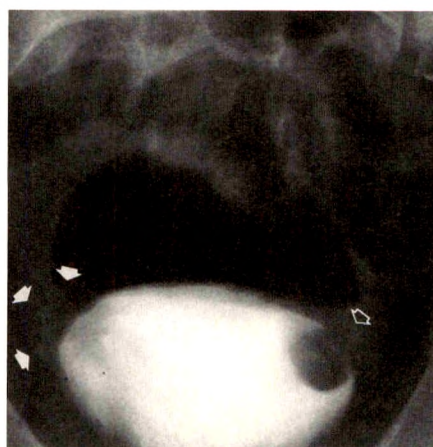
Results

Plain Radiography

On plain radiographs of the pelvis, STING was identified retrospectively in 18 (22%) of 81 ureters. The injection site appeared as an ovoid area of faintly increased density (Fig. 1). The Teflon had never been recognized prospectively or described in the radiographic report.



1



2

Excretory Urography/Cystography

In only four of 66 studies was the bladder contour sufficiently altered by the bulging of the mucosa so that a "filling defect" was visible on fluoroscopic cystography or excretory urography (Fig. 2). This small number may represent a technical bias, because in 21 of the excretory urograms the bladder was drained via catheter to enhance upper tract drainage and to prevent reflux from simulating function. As in routine postreplantation excretory urography, the ureter and pelvicaliceal system were considered to be unobstructed when their caliber did not exceed their caliber on preoperative cystography.

The Teflon could not be identified on nuclear studies. In 12 children (16 ureters), more than one technique was used to evaluate for residual reflux. All of the five children who underwent intraoperative and nuclear cystography and six of the seven who had fluoroscopic cystography and nuclear cystography had congruent results with no residual reflux. One child had mild residual unilateral reflux on nuclear cystography and no reflux on fluoroscopic cystography. After the first injection, reflux ceased in 73% of the ureters. The success rate improved with subsequent STING procedures: 80% after the second STING and 81% after the third. The success rate after the first STING in children with neurogenic bladder was 64%, while in those with idiopathic reflux the success rate was 78%.

Sonography

The Teflon was recognized on 39 of 40 sonograms that were obtained prospectively with knowledge that STING had been performed. Adequate bladder distension was important for visualization of the Teflon. The Teflon was seen as an echogenic mass that cast a variable acoustic shadow (Fig. 3). The location of the Teflon within the bladder wall varied. The Teflon was seen deep in the bladder or bulging into the bladder lumen. In a few cases, the distal ureter was seen to be displaced anteriorly by the bulging Teflon bead (Fig. 4). In the other 33 examinations, the injection site was not seen

Fig. 1.—4½-year-old girl who underwent left subureteric Teflon injection 6 months before. Teflon has produced faint radiodensity (arrows).

Fig. 2.—2-year-old girl who had undergone bilateral subureteric Teflon injection (STING) and a second left STING. Excretory urogram shows filling defects along superolateral aspect of bladder wall bilaterally (open arrow). There is increased density in soft tissues adjacent to smaller bladder defect on right (solid arrows).

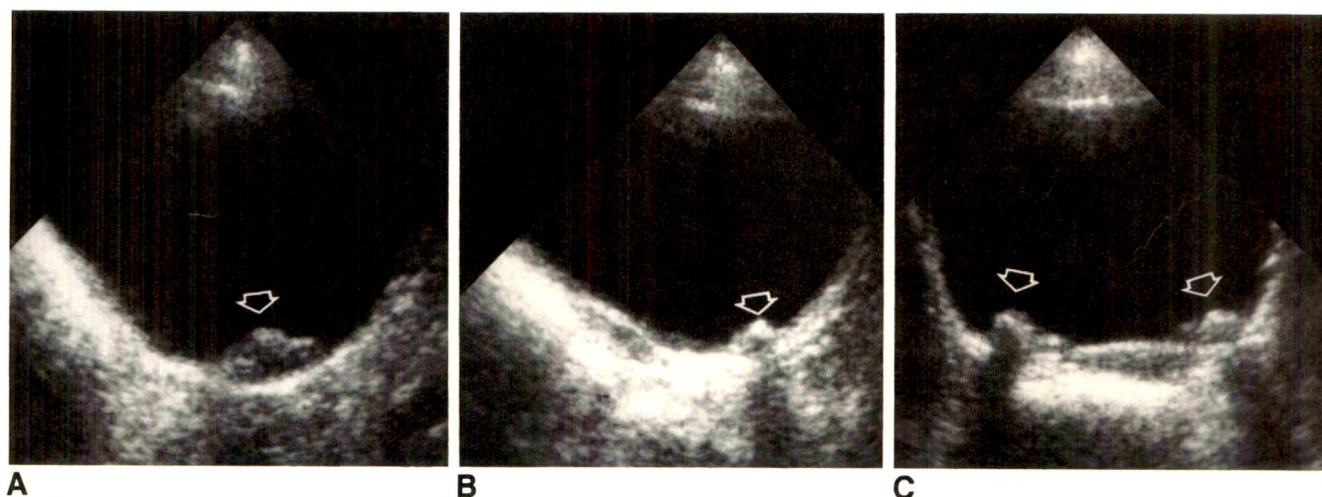


Fig. 3.—5-year-old studied 1 month after bilateral subureteric Teflon injection.

A, Longitudinal sonogram through left of bladder shows that injected material is echogenic and, on this scan, produces almost no shadowing (arrow). B, Longitudinal sonogram through right side of bladder shows injected material as small, intensely echogenic focus (arrow) producing marked shadowing.

C, Transverse sonogram of bladder. Both injection sites are visualized as protruding into bladder lumen (arrows) and as producing acoustic shadowing.

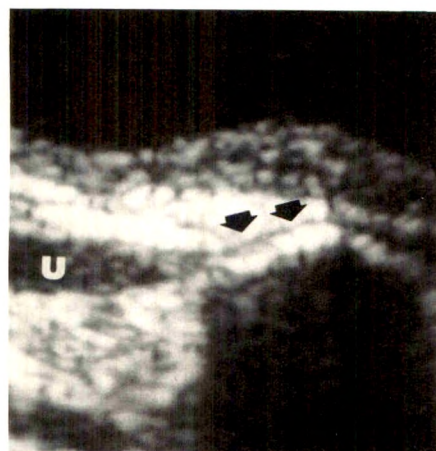


Fig. 4.—Longitudinal sonogram in 4-year-old girl shows distal portion of ureter (u) is lifted up and tapered by Teflon beneath (arrows). There is marked acoustic shadowing.

because of a variety of technical factors: inadequate bladder distension, nonrecognition, and, hence, nonfilming of the injection site.

Computed Tomography

In each of the 18 children who had undergone STING, the Teflon injection site was clearly seen as a dense mass measuring 160–466 H. The Teflon usually appeared homogeneously dense, but in four children the Teflon had central, low-density areas possibly caused by injection of air bubbles or incomplete mixing of the Teflon with the glycerin paste (Fig. 5). No evidence of Teflon was seen elsewhere in the pelvis.

The location of the Teflon was variable. In two patients it was seen in a retrovesical location only, and in two patients in an intramural location only. In 14 patients, the Teflon bulged

from an intramural location into the retrovesical space or anteriorly into the lumen (Fig. 6). The amount of Teflon in an intramural location did not correlate with the success in eliminating reflux. In no child was a soft-tissue mass detected adjacent to the Teflon.

One child had two CT scans, the first 2 days after STING and the second 3 months after STING. The Teflon beads were noted bilaterally on the original CT scans, but one bead was markedly smaller on the follow-up study. It was not found in the remainder of the pelvis.

Complications

In the first 5 postoperative days, nine children had sonography or CT. In three, there was free fluid in the pelvis. One of these three has a ventriculoperitoneal shunt catheter.

Postoperative ureteral dilatation not present on preoperative studies was found in six of 13 children studied within the first 4 weeks with sonography or excretory urography. Three of the six have required intervention, two with temporary ureteral stents and one with reimplantation of the ureter. New ureteral dilatation was not seen on later studies. Acute obstruction in which the preoperative caliber of the ureter did not increase could not be diagnosed.

Twenty-six children had persistent reflux after the first STING. Of these, 10 of 39 refluxing ureters had been successfully treated with the first STING, but 29 ureters continued to reflux. Fifteen children (18 ureters) underwent a second STING. Nine chose ureteral reimplantation after the first or second STING. Seven are currently being followed. At surgery, performed 6–12 months after STING, the injected Teflon easily separated from adjacent soft tissues and produced no local scarring or granulomatous masses. Pathologic sections through the removed tissue showed Teflon particles surrounded by chronic inflammatory cells.

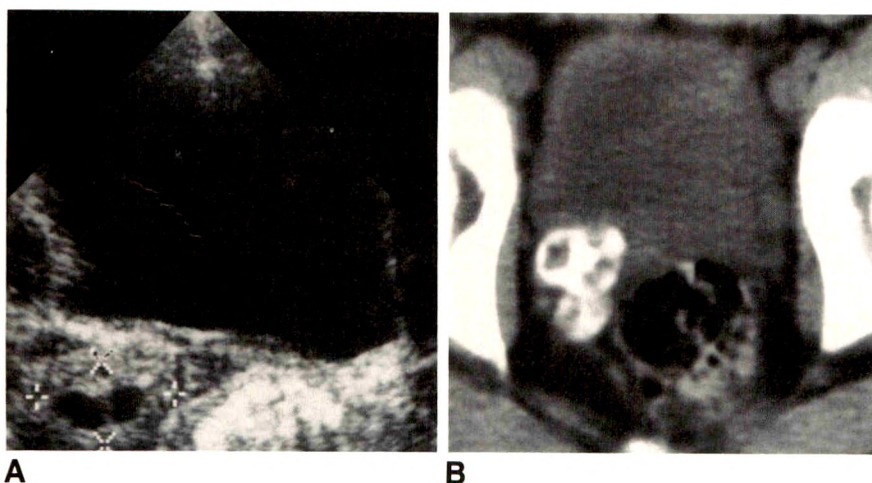


Fig. 5.—7-year-old girl studied 19 months after right-sided subureteric Teflon injection.
A, Transverse sonogram of bladder shows "cystic" regions (cursors) within region of injected Teflon paste; this appearance simulates an ovary.
B, Axial CT scan of bladder at same level.

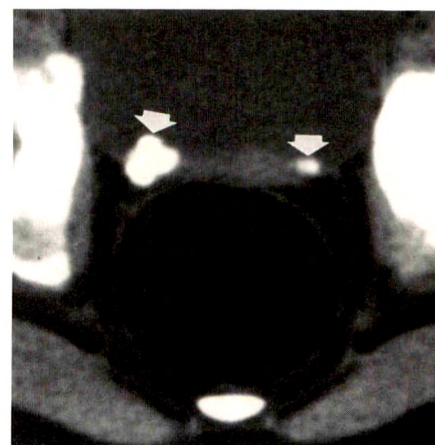


Fig. 6.—Nonenhanced axial CT scan of bladder shows portion of each subureteric Teflon injection (arrows). At this level Teflon appears to be in bladder wall, in contrast to sonogram, where it projected into bladder lumen.

Discussion

The STING procedure has been used since 1981 in children with reflux [5, 6]. It can be used with all grades of reflux. The procedure is well tolerated, can be performed on an outpatient basis, and requires little operating room time compared with the conventional antireflux surgical procedures [5, 6, 9–13]. STING may be performed on the same ureter more than once if necessary. It does not preclude performance of a future open antireflux operation [9–12].

In earlier publications, cessation of reflux after a single STING procedure ranged from 66% to 81% [5, 6, 9–11]. The success rate after the first STING was comparable in the children we studied.

Teflon paste has been injected into the thyroarytenoid muscle by otolaryngologists to treat vocal cord paralysis in adult patients for over two decades [16–20]. Few complications have been documented. In a large series of over 1100 patients with vocal cord injection, the most serious complication, local drifting or misplacement of the Teflon, occurred in only 1.9% of cases [19].

After Matouschek [5, 6] introduced the STING technique for treating reflux, Teflon injections were done in piglets and, later, in a large series of children [9–12]. Recent animal studies have reported the presence of enlarging Polytef granulomas at injection sites and at some sites of distant migration [7]. In the series of Puri and O'Donnell [9–11], the potential long-term complications, migration of Teflon and enlargement of the injected mass (granuloma formation), were not found. Cystoscopy performed by them as late as 3 years after STING showed no enlargement at the injection site [11]; this parallels the findings of our urological colleagues. Complications such as obstruction were nonexistent in their patients, although six children in our series did experience post-STING ureteral obstruction.

Excretory urography has been performed routinely after most antireflux procedures. Sequential sonographic studies (pre- and postoperative) of the kidneys can be used to evaluate the degree of hydronephrosis. From our experience, only a small number of children (six of 83) have developed new or worsening hydronephrosis acutely, and only half of those have required intervention. Careful postoperative evaluation of the kidneys, however, is recommended.

On sonography, the Teflon was found in 39 of 40 children when prospectively sought during the examination. The shadowing produced by the Teflon may be confused with air-filled bowel loops by the inexperienced examiner. Small amounts of Teflon projecting into the bladder lumen also may simulate a redundant bladder wall if the bladder is not distended.

On CT, the Teflon was seen in various locations relative to the bladder wall. The location did not correlate with the success of the STING. Without prior history of the procedure, the location and density of the Teflon may be mistaken for a calculus in a bladder diverticulum.

In three children, free peritoneal fluid was noted in the pelvis on CT or sonography performed within 5 days of the STING. One of these children had a ventriculoperitoneal shunt, which could explain the presence of free fluid. A second child, a girl, may have had fluid because of hormonal, cyclic changes. The third child had transient peritoneal signs prompting the CT evaluation. We suspect that the Teflon or glycerin paste may have caused a chemical peritonitis. In one child, a follow-up CT scan revealed that the original injected Teflon had almost completely disappeared. Teflon was not seen elsewhere in the pelvis, and we postulate that, because of the superficial location, the Teflon may have been extruded into the bladder and passed per urethra.

The radiologist should become familiar with the radiologic appearances of the STING procedure in order to effectively evaluate these children postoperatively, to prevent potential

pitfalls in the interpretation of imaging studies, and to be alert to potential complications. The STING procedure will probably be performed with increasing frequency in the future because of the numerous advantages and a success rate comparable to other antireflux surgery.

ACKNOWLEDGMENT

We thank Sally Caravella for assistance in manuscript preparation.

REFERENCES

- Hodson CJ, Edwards D. Chronic pyelonephritis and vesicoureteric reflux. *Clin Radiol* 1960;11:219
- Politano VA, Leadbetter WF. An operative technique for the correction of ureteric reflux. *J Urol* 1958;79:932
- Marberger M, Altwein JE, Straub E, Wulff HD, Hohenfellner R. The Lich-Gregoir antireflux plasty: experience with 371 children. *J Urol* 1978;120:216
- Cohen SJ. The Cohen reimplantation technique. *Birth Defects* 1977;13:391-395
- Matouschek E. Treatment of vesicorenal reflux by transurethral Teflon injection. *Urologe* 1981;20:263-264
- Matouschek E. New concept for the treatment of vesicourethral reflux: endoscopic injection of Teflon. *Arch Esp Urol* 1981;34:385-388
- Malizia AA, Reiman HM, Myers RP, et al. Migration and granulomatous reaction after periurethral injection of polytetrafluoroethylene (Teflon). *JAMA* 1984;251:3277-3281
- Sweeney LE, Thomas PS. Evaluation of subureteric Teflon injection as an antireflux procedure. *Ann Radiol (Paris)* 1987;30:478-481
- Puri P, O'Donnell B. Correction of experimentally produced vesicoureteric reflux in the piglet by intravesical injection of Teflon. *Br Med J* 1984;289:5-7
- O'Donnell B, Puri P. Treatment of vesicoureteric reflux by endoscopic injection of Teflon. *Br Med J* 1984;289:7-9
- O'Donnell B, Puri P. Endoscopic correction of primary vesicoureteric reflux. *Br J Urol* 1986;58:601-604
- Puri P, O'Donnell B. Endoscopic correction of grades IV and V. Primary vesicoureteric reflux: six to thirty month follow-up in 42 ureters. *J Pediatr Surg* 1986;293:1404-1406
- Kaplan WE, Dalton DP, Firlit CS. The endoscopic correction of reflux by polytetrafluoroethylene injection. *J Urol* 1987;138:953-955
- Leibovic SJ, Lebowitz RL. Reducing patient dose in voiding cystourethrography. *Urol Radiol* 1981;2:103-108
- Conway JJ, King LR, Belman AB, Thorson T Jr. Detection of vesicoureteral reflux with radionuclide cystography. A comparison study with roentgenographic cystography. *AJR* 1972;115:720-727
- Lewy RB. Response of laryngeal tissue to granular Teflon in situ. *Arch Otolaryngol Head Neck Surg* 1966;83:355-359
- Boedts D, Roels H, Kluyskens P. Laryngeal tissue responses to Teflon. *Arch Otolaryngol Head Neck Surg* 1967;86:562-567
- Dedo HH, Urrea RD, Lawson L. Intracordal injection of Teflon in the treatment of 135 patients with dysphonia. *Ann Otol Rhinol Laryngol* 1973;82:661-667
- Lewy RB. Experience with vocal cord injection. *Ann Otol Rhinol Laryngol* 1975;85:440-450
- Lewy RB, Miller D. Immediate local tissue reactions to Teflon vocal cord implants. *Laryngoscope* 1978;88:1339-1342

Delayed Radiologic Appearance of Bilateral Thoracic Ectopic Kidneys

Robert M. Liddell,¹ David M. Rosenbaum,² and Joel D. Blumhagen²

Superior renal ectopia (thoracic kidney) is rare and usually causes no symptoms. It is most often discovered as a posterior mediastinal or juxtadiaphragmatic "mass" by chest radiography. IV urography [1] or sonography [2, 3] allow differentiation from significant lesions, thus avoiding surgery or biopsy. We report an unusual case of an infant with bilateral superior renal ectopia in whom the position of the kidneys appeared to be normal at birth.

Case Report

A 6-month-old boy with Down syndrome and endocardial cushion defect was admitted to the hospital for banding of the pulmonary artery because of increasing congestive heart failure. Significant medical history included duodenal atresia, which was treated by duodenoduodenostomy when the baby was 1 day old. Preoperative chest radiographs (Figs. 1C and 1D) revealed cardiomegaly, pulmonary hyperinflation, enlarged pulmonary vessels, and bilateral basilar masses that were shown to be kidneys by sonography (Figs. 2C and 2D). Review of the patient's neonatal chest radiographs (Figs. 1A and 1B) and abdominal sonograms (Figs. 2A and 2B) showed that the position of the kidneys was normal at that time. Since then, the patient's renal function has remained normal.

Discussion

Unilateral thoracic (or superior) renal ectopia is a rare anomaly, encountered only once in a series of 13,000 autopsies and accounting for less than 5% of all renal ectopies [4].

Unlike pelvic ectopic kidneys, which sometimes are obstructed, have calculi, or are infected, thoracic ectopic kidneys are usually normal otherwise. They are more common on the left side and are usually isolated incidental findings [5]. Three instances of bilateral thoracic kidneys have been reported [6–8]. There is one previous report of delayed appearance of a unilateral thoracic kidney in a 4-year-old boy [9].

Except for the few cases in which thoracic ectopic kidney was thought to be caused by traumatic diaphragmatic disruption [10, 11], most thoracic renal ectopies are assumed to be congenital. In some cases, anomalously superior origin of the renal vessels had been found [4], whereas in others the renal vessels are simply longer than normal [5]. The relationship of the superior ectopic kidney to the diaphragm has been variable in those cases investigated by surgery or autopsy [5, 7, 12]. Occasionally, the kidney resides entirely above the diaphragm, but most often it occupies a posteromedial diaphragmatic defect that may or may not be capped by fibrous tissue [12].

A variety of embryologic causes have been proposed. Superior migration of the metanephros before completion of diaphragmatic development during the eighth week of gestation is common to most of these theories [5, 7, 12]. In our patient, because of the normal position of the kidneys at birth, we postulate that a congenital diaphragmatic defect occurred independent of renal ascent. Delayed appearance of thoracic kidney could be explained by the theory of Fleischner et al. [1], who suggested that the diaphragmatic malformation

Received May 23, 1988; accepted after revision July 7, 1988.

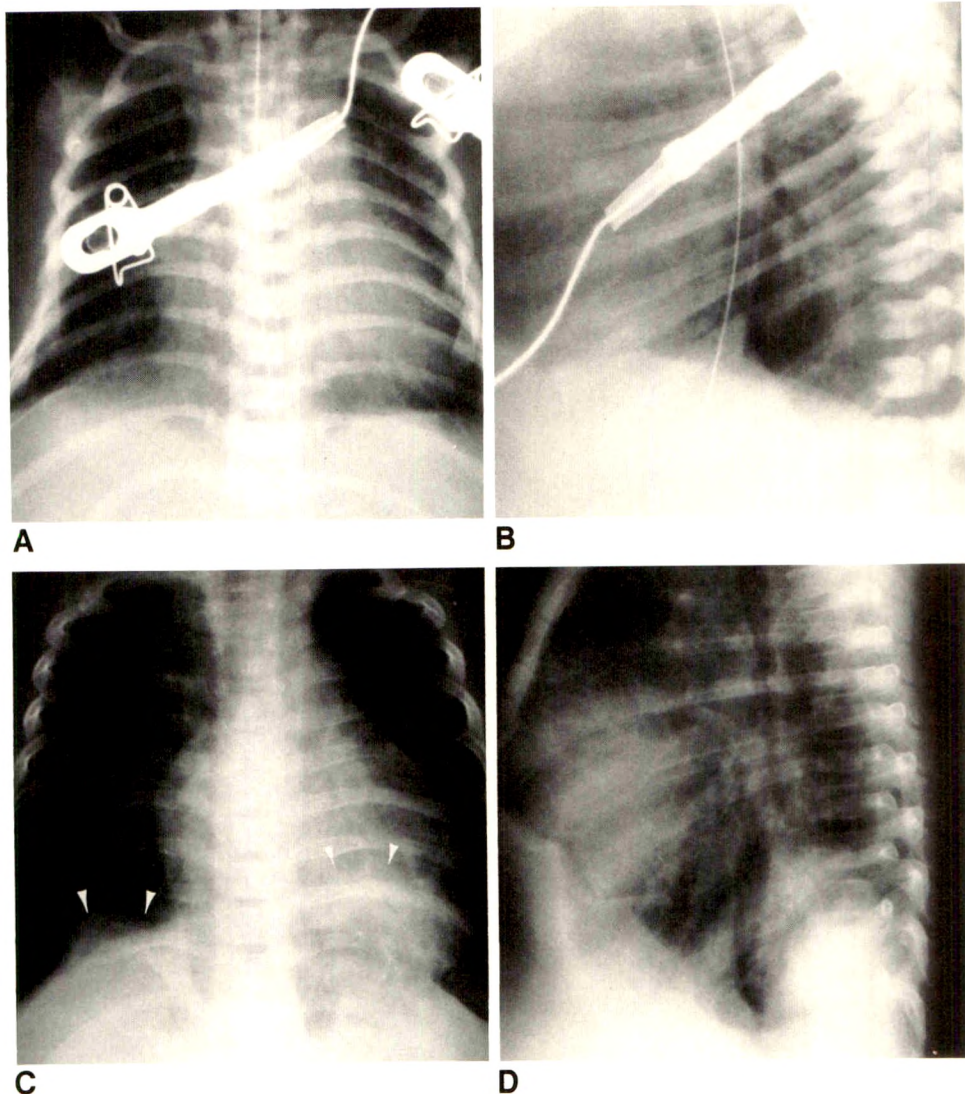
¹ Department of Radiology, University of Washington School of Medicine, Seattle, WA 98195.

² Department of Radiology, Children's Hospital and Medical Center, 4800 Sand Point Way N.E., Seattle, WA 98105. Address reprint requests to D. M. Rosenbaum, Radiology, CHMC, P.O. Box C5371, Seattle, WA 98105.

AJR 152:120–122, January 1989 0361–803X/89/1521–0120 © American Roentgen Ray Society

Fig. 1.—A and B, Frontal (A) and lateral (B) chest radiographs when patient was 1 day old show cardiomegaly and pulmonary vascular prominence. Diaphragmatic contour is normal.

C and D, Frontal (C) and lateral (D) chest radiographs when patient was 6 months old show bilateral posterior basal masses. Despite hyperinflation, the posterior masses extend to level of T9 on right and T8 on left (arrowheads).



might be caused by a delay in the disappearance of the mesonephros during development, leading to a diaphragmatic defect that later could be occupied by the kidney.

A previously normal chest radiograph does not exclude the possibility of superior renal ectopia (thoracic kidney) in the evaluation of a posterior basal mass or masses, as shown by our case. Sonography or urography can confirm the diagnosis easily.

REFERENCES

1. Fleischner FG, Robins SA, Abrams M. High renal ectopia and congenital diaphragmatic hernia. *Radiology* 1950;55:24-26
2. Kangaroo H, Sukov R, Sample WF, Lipson M, Smith L. Ultrasonographic evaluation of juxtadiaphragmatic masses in children. *Radiology* 1977;125:785-787
3. Sumner TE, Volberg FM, Smolen PM. Intrathoracic kidney—diagnosis by ultrasound. *Pediatr Radiol* 1982;12:78-80
4. Campbell MF. Renal ectopy. *J Urol* 1930;24:187-198
5. Malter IJ, Stanley RJ. The intrathoracic kidney: with a review of the literature. *J Urol* 1972;107:538-541
6. Berlin HS, Stein J, Poppel MH. Congenital superior ectopia of the kidney. *AJR* 1957;78:508-517
7. Hertz M, Shahin N. Ectopic thoracic kidney. *Israel J Med Sci* 1969;5:98-101
8. Lundius B. Intrathoracic kidney. *AJR* 1975;125:678-681
9. Usta HY, Rizk F. Delayed appearance of an intra-thoracic kidney. *Pediatr Radiol* 1984;14:449-450
10. Testas P. Desinsertion traumatique du diaphragme et hernie thoracique du rein droit. *Chirurgie* 1983;109:768-771
11. Williams RG, Tillinghast AJ. Diaphragmatic herniation of the kidney. *Radiology* 1949;53:566-568
12. N'Guessen G, Stephens FG, Pick J. Congenital superior ectopic (thoracic) kidney. *Urology* 1984;24:219-228

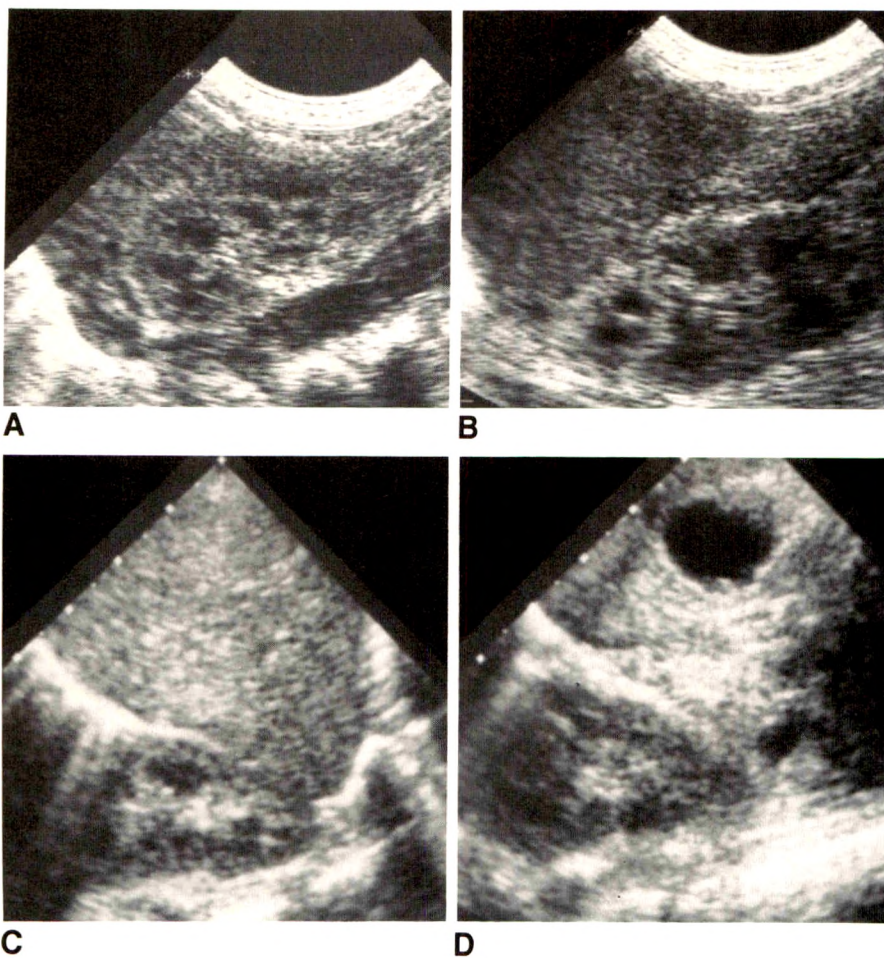


Fig. 2.—A and B, Longitudinal right (A) and left (B) sonograms obtained during neonatal period show kidneys below diaphragm on each side.

C and D, Longitudinal sonograms of kidneys when patient was 6 months old show that right (C) and left (D) kidneys both extend above diaphragmatic contour.

Case Report

Torsion of Normal Uterine Adnexa Before Menarche: CT Appearance

Richard D. Bellah¹ and N. Thorne Griscom

Ovarian torsion is rare and seldom is diagnosed preoperatively. Furthermore, the symptoms of adnexal torsion often mimic those of common maladies such as gastroenteritis and appendicitis. When the sonogram is nondiagnostic and the clinical picture is unclear, as is often the case, a CT examination may yield additional information. We have seen three children with torsion of normal adnexa in whom contrast-enhanced CT studies provided clues to the correct diagnosis.

Case Report

A 6-year-old girl was admitted because of a 2-day history of persistent right lower quadrant pain, nausea, and vomiting. The pain, which initially radiated to the right groin, gradually became periumbilical. Her abdomen was soft but tender in all quadrants without localizing signs or rebound. No mass was palpable by abdominal or rectal examination. A sonogram of the pelvis showed a small amount of free intraperitoneal fluid. A solid mass containing small, anechoic areas lay behind the bladder and to the right of the midline. A contrast-enhanced CT scan of the pelvis obtained the next day (Fig. 1) showed a 4 × 5 cm inhomogeneous pelvic mass anterior to the rectum; it was thought to be ovarian in origin and perhaps to represent infarction caused by torsion.

Later that day, laparotomy showed a large, congested, purple, strangulated right ovary with torsion. The infarcted ovary and adjacent Fallopian tube were removed. Pathologic examination confirmed that the right ovary was totally replaced by hemorrhagic infarction. Scattered follicular cysts also were noted. She was discharged on day 7 and has done well in the succeeding 24 months.

Discussion

Torsion of normal uterine adnexa before menarche is rare; approximately 60 cases have been reported [1–5]. Because many common conditions (e.g., appendicitis, gastroenteritis, and pyelonephritis) mimic adnexal torsion, the correct preoperative diagnosis seldom is made.

Adnexal torsion is more frequent when the ovary is abnormal [6]. Ten postmenarcheal patients with torsion of abnormal adnexa (seven simple ovarian cysts, two paraovarian cysts, one dermoid) have been seen in our hospital in the past 5 years.

Several reports have shown that, in the appropriate clinical setting of severe intermittent abdominal pain, sonography can be helpful in the diagnosis of ovarian torsion [1, 2]. However, the sonographic features are at times nonspecific [5] and consist only of a solid pelvic mass with or without free pelvic fluid. In such instances, CT may be helpful in the diagnostic evaluation. In addition to the case reported, we have seen two other premenarcheal girls (4 and 8 years old) with torsion of normal adnexa in whom CT studies (Figs. 2 and 3) were performed after nondiagnostic sonographic evaluation.

The CT appearance of ovarian torsion parallels the sonographic findings reported by previous authors: a markedly enlarged ovary containing several cystic structures, usually peripheral, which presumably represented dilated follicles [1, 3]. Dynamic scanning after contrast administration provides useful information regarding the vascularity of the mass; the surrounding enhancing vessels (Figs. 1 and 2) reflect congested

Received January 19, 1988; accepted after revision July 7, 1988.

¹ Both authors: Department of Radiology, The Children's Hospital, 300 Longwood Ave., Boston, MA 02115. Address reprint requests to N. T. Griscom.

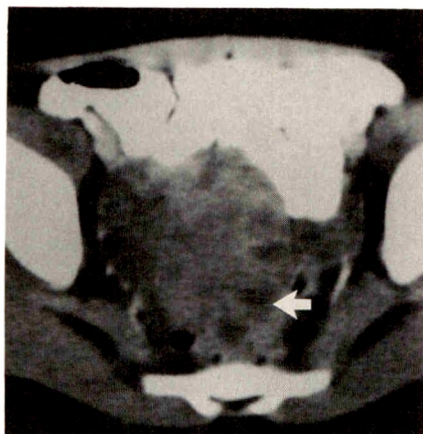


Fig. 1.—Case 1: Contrast-enhanced CT shows a large, complex pelvic mass with multiple peripheral foci (arrow) of low attenuation. Opacified pelvic vessels can be seen draped around mass.



Fig. 2.—Case 2: Contrast-enhanced CT shows a large, midline pelvic mass behind the bladder with peripheral areas (arrow) of low absorption. Surgery revealed a large, congested, and infarcted left ovary with torsion.

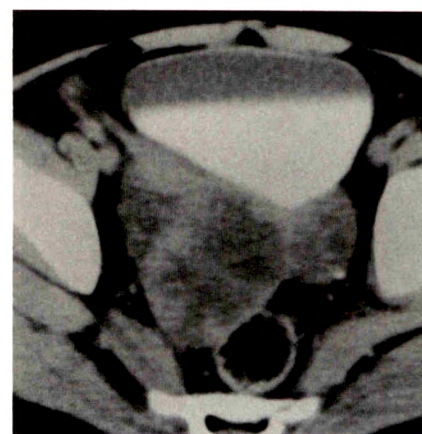


Fig. 3.—Case 3: Contrast-enhanced CT shows a complex mass anterior to the rectum. Exploration showed 720° torsion of the right ovary with hemorrhage and necrosis.

tion, whereas the heterogeneity in attenuation indicates variability in vascularity. The involved ovary may enlarge to such a degree that it assumes a midline position behind the bladder (Fig. 2); the premenarchal uterus may be difficult to identify separately.

Although the CT pattern is not specific, adnexal torsion should be considered in the differential diagnosis of complex (predominantly solid) extrauterine masses in the premenarchal girl. Ovarian germ-cell tumors (dermoids, dysgerminomas, endodermal sinus tumors) may also have a complex appearance [7, 8], sometimes with fat or calcification, and CT is clearly helpful in this regard. Nonovarian conditions within the radiologic differential diagnosis (these might be excluded on clinical grounds) include pelvic abscess, rhabdomyosarcoma, pelvic lymphoma, and leukemia with pelvic adenopathy.

If adnexal torsion is detected promptly, ovarian blood supply may be reestablished with derotation [4], thereby saving the ovary and its hormonal and reproductive function. Furthermore, the surgeon should verify that the contralateral ovary is normal at the time of surgery in order to exclude the

remote possibility of bilateral tumoral involvement. When the sonogram is nondiagnostic, a CT examination may provide additional useful information leading to the correct preoperative diagnosis of adnexal torsion.

REFERENCES

1. Graif M, Itzchak Y. Sonographic evaluation of ovarian torsion in childhood and adolescence. *AJR* 1988;150:647-649
2. Farrell TP, Boal DK, Teele RL, Ballantine T. Acute torsion of normal uterine adnexa in children: sonographic demonstration. *AJR* 1982;139:1223-1225
3. Evans JP. Torsion of the normal uterine adnexa in premenarchal girls. *J Pediatr Surg* 1978;13:195-196
4. James DF, Barber KRK, Graber EA. Torsion of normal uterine adnexa in children: report of three cases. *Obstet Gynecol* 1970;35:226-230
5. Wu A, Siegel M. Sonography of pelvic masses in children: diagnostic predictability. *AJR* 1987;148:1199-1202
6. Golladay ES, Mollitt DL. Ovarian masses in the child and adolescent. *South Med J* 1983;76:954-957
7. Gross B, Moss A, Mihara K, Goldberg H, Glazer G. Computed tomography of gynecologic diseases. *AJR* 1983;141:765-773
8. Walsh JA, Zelenik ME, Maxymiv GW. CT diagnosis of torsion of benign cystic teratoma of the ovary. *South Med J* 1986;79:379-381

Case Report

Mediastinal Bronchogenic Cyst: Prenatal Sonographic Diagnosis

George Young,¹ Philippe R. L'Heureux, Steven T. Krueckeberg, and David A. Swanson

Bronchogenic cyst of the mediastinum in infancy is a well-defined entity characterized by recurrent cough, wheezing, pneumonia, atelectasis, and obstructive emphysema and causing various degrees of respiratory distress [1]. These cysts generally are located near the carina between the trachea and the esophagus and often obstruct the main bronchi, causing respiratory distress [1].

The recognition of thoracic malformations in utero is important because many of these anomalies present with severe respiratory distress in the immediate neonatal period [2]. Early recognition and identification of a pulmonary abnormality can expedite obstetric management and direct effective postpartum treatment. Several conditions, among them congenital cystic adenomatoid malformation, diaphragmatic hernia, bronchopulmonary sequestration, hydrothorax, and intrapulmonary bronchogenic cysts have been reported to have distinct prenatal sonographic characteristics [2, 3]. We report a case in which the prenatal diagnosis of a bronchogenic cyst was made by sonography.

Case Report

A 41-year-old Southeast Asian immigrant, gravida 9, para 8, was admitted with premature dilatation of the cervix. Four of her previous deliveries had been full term, and the infants had been normal. However, all four had died later in childhood of unknown causes.

During her present pregnancy, the patient was seen for routine prenatal care at 23 weeks menstrual age. Sonographic examination at that time showed polyhydramnios, a large and uniformly hyper-

echoic left lung, and displacement of the heart and mediastinum toward the right (Fig. 1A). The stomach was positioned normally in the left upper quadrant of the abdomen (Fig. 1B). The diaphragm was intact. The spinal canal and ventral abdominal wall were normal. A sonogram obtained at 30 weeks menstrual age confirmed this abnormality. Interval fetal growth remained normal. A provisional diagnosis of congenital lobar emphysema, cystic adenomatoid malformation, or obstructive emphysema was considered. Amniocentesis revealed a Lecithin-Sphingomyelin ratio of 1.5. At 36 weeks gestation, labor was induced and the patient delivered a 3210-g girl who was in respiratory distress. Apgar scores were 2 and 5 at 1 and 5 min, respectively.

A chest radiograph obtained when the neonate was 2 hr old showed obstructive emphysema of the left lung with mediastinal shift (Fig. 2A). A barium esophagram showed a mass at the level of the carina between the trachea and esophagus. In order to exclude an anomalous left pulmonary artery (vascular sling), an IV contrast-enhanced CT examination of the chest was performed, revealing a well-defined, 1.5-cm, water-density mass at the carina (Fig. 2B). On the basis of these studies, the diagnosis of bronchogenic cyst was made and was confirmed by subsequent surgical excision and histologic examination.

Discussion

Bronchogenic cysts result from abnormal budding of the ventral diverticulum of the primitive foregut. When abnormal budding occurs early in bronchial development, the cysts occur in the mediastinum (30%); if they occur later, the cysts are pulmonary (70%) [4]. Most pulmonary bronchogenic cysts are asymptomatic and often are incidental findings on routine

Received May 26, 1988; accepted after revision July 7, 1988.

¹ All authors: Department of Medical Imaging, St. Paul-Ramsey Medical Center, Jackson at University, St. Paul, MN 55101, and the University of Minnesota School of Medicine, 420 Delaware St. S.E., Minneapolis, MN 55455. Address reprint requests to G. Young at St. Paul-Ramsey Medical Center.

AJR 152:125-127, January 1989 0361-803X/89/1521-0125 © American Roentgen Ray Society

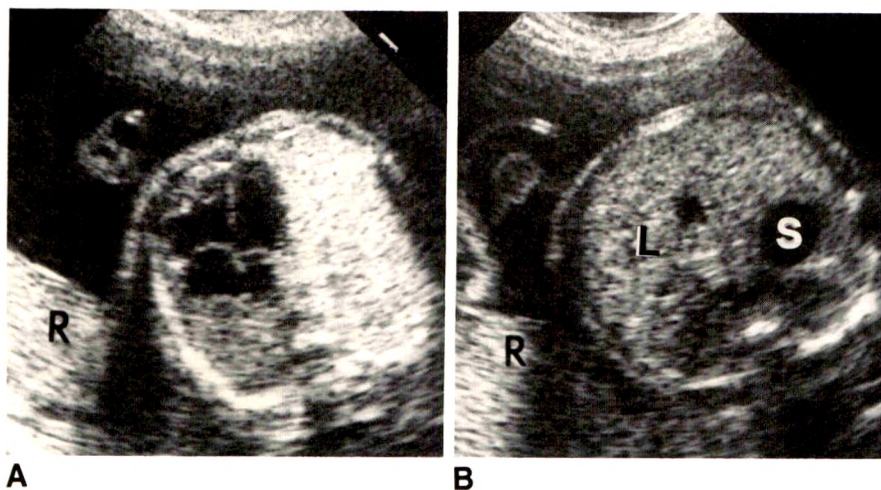


Fig. 1.—A, Transverse scan through thorax shows a hyperechoic and enlarged left lung displacing four-chambered heart toward right side. R = right.

B, Transverse scan through upper abdomen shows stomach bubble (S) and liver (L) to have a normal relationship. R = right.

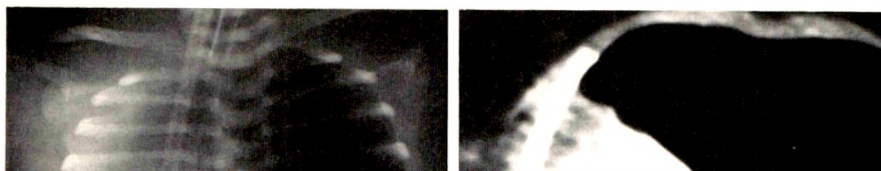


Fig. 2.—A, Left lung shows unilateral hyperaeration and decreased pulmonary vascularity. Severe contralateral mediastinal shift is present.

B, Contrast-enhanced CT scan of chest shows a low-attenuation, water-density mass (asterisk) posterior to carina. Note compression of left main bronchus (curved arrow). R = right.

might be more echopenic or cystic. Esophageal duplications and neuroenteric cysts are often unilocular, echopenic, and extrapulmonary. Cystic adenomatoid malformations are either multilocular (types I and II) or hyperechoic (microcystic, type III), cause mediastinal shift, and often are associated with hydrops and ascites [3, 9]. Congenital diaphragmatic hernia is multicystic or mixed; it is characterized by partial or complete absence of a hemidiaphragm, mediastinal shift, and an absent or abnormally positioned stomach bubble [2]. Congenital hydrothorax may be bilateral, but often is unilateral and characteristically is echopenic; there also may be a collapsed or hypoplastic lung adjacent to the heart [10].

REFERENCES

1. Eraklis AJ, Griscom NT, McGovern JB. Bronchogenic cysts of the mediastinum in infancy. *N Engl J Med* 1969;281:1150-1155
2. Reece EA, Lockwood CJ, Rizzo N, Pilu G, Bovicelli L, Hobbins JC. Intrinsic intrathoracic malformations of the fetus: sonographic detection and clinical presentation. *Obstet Gynecol* 1987;70:627-632
3. Graham D, Winn K, Dex W, Sanders RC. Prenatal diagnosis of cystic adenomatoid malformation of the lung. *J Ultrasound Med* 1982;1:9-12
4. Rogers LF, Osmer JC. Bronchogenic cysts. A review of 46 cases. *AJR* 1964;91:273-283
5. Albright EB, Crane JP, Schackelford GD. Prenatal diagnosis of a bronchogenic cyst. *J Ultrasound Med* 1988;7:91-95
6. Griscom NT, Harris GBC, Wohl MEB, Yawter GF, Eraklis AJ. Fluid-filled lung due to airway obstruction in the newborn. *Pediatrics* 1969;43:383-390
7. Avery ME. *The lung and its disorders in the newborn infant*, 4th ed. Philadelphia: Saunders, 1981:29-36
8. Fagan CJ, Swischuk LE. The opaque lung in lobar emphysema. *AJR* 1972;114:300-304
9. Stocker JT, Madewell JE, Drake RM. Congenital cystic adenomatoid malformation of the lung. *Hum Pathol* 1977;8:155-171
10. Bovicelli L, Rizzo N, Orsini LF, Calderoni P. Ultrasonic real-time diagnosis of fetal hydrothorax and lung hypoplasia. *JCU* 1981;9:253-254

Case Report

MR Imaging of Double-Outlet Right Ventricle

E. William Akins,¹ Tomas D. Martin,² James A. Alexander,² Daniel G. Knauf,² and Benjamin E. Victorica³

In double-outlet right ventricle (DORV), the anatomic relationship between the ventricular septal defect (VSD) and the outlet arteries determines how the patient will be managed surgically [1]. Presently, the standard techniques used to determine this relationship are angiocardiology and two-dimensional echocardiography. In the case reported, MR imaging was used concomitantly with angiocardiology and was found to be capable of providing this information noninvasively. Multiplanar depiction and the wide field of view are the principal advantages of MR imaging in this setting. In the case presented, MR imaging was used to differentiate DORV with aortic-committed VSD from Taussig-Bing anomaly and also from transposition of the great arteries associated with a VSD. MR imaging also has been useful in the postoperative depiction of Rastelli homograft conduits and for internal repair of the VSD.

Case Report

A 9-year-old girl had presented in infancy with cyanotic congenital heart disease. Initial catheterization done when the patient was 1 month old suggested DORV, VSD, and pulmonary outflow-tract obstruction. A right aortic arch was present with mirror-image branching of the brachiocephalic vessels. The left anterior descending coronary artery was shown to arise from the right coronary artery and then to cross in front of the pulmonary outflow tract. Chest radiographs revealed hyperexpansion of the left upper lobe. The patient was managed medically until she was 4 years old, at which time her hematocrit had increased (60%) and her tolerance to exercise had decreased. She underwent an uncomplicated left Blalock-Taussig shunt, resulting in a lessening of symptoms. She was considered for

complete repair when she was 9 years old. Repeat catheterization confirmed the presence of DORV and pulmonic infundibular stenosis and suggested that the VSD was committed to the aorta. In considering surgical correction, MR imaging was used to further evaluate the VSD-aortic relationship. MR imaging was performed with a 0.15-T resistive magnet, conventional gated spin-echo pulse sequences, and a double-loop cardiac surface coil. Oblique imaging planes were obtained by using electronic, gradient-angle rotation to supplement the conventional planes. MR imaging revealed definite evidence of DORV, with a side-by-side relationship of the great vessels at the cardiac base; oblique sections confirmed the angiographic findings of aortic commitment of the large VSD (Fig. 1). The pulmonary infundibulum was markedly narrowed, and the left upper lobe was emphysematous. Thoracotomy was performed to confirm these findings, but repair was aborted because numerous small branches of the anomalous coronary circulation were noted over the pulmonary-outflow tract, precluding placement of a Rastelli conduit. The patient recovered and will be reconsidered for repair at a later date.

Discussion

Congenital cardiac conotruncal abnormalities represent a spectrum that includes truncus arteriosus, complete transposition of the great vessels, DORV, and tetralogy of Fallot. The outlet arteries have various relationships to the commonly occurring VSD, and the position and size of the aorta and pulmonary artery with respect to the ventricles are important for classification and management [1]. In DORV, which accounts for approximately 1.3% of all congenital heart disease [2], both the aorta and the pulmonary artery arise completely or nearly completely from the right ventricle. Classically, the

Received January 25, 1988; accepted after revision July 18, 1988.

¹ Department of Radiology, Box J-374, JHMC, University of Florida, College of Medicine, Gainesville, FL 32610. Address reprint requests to E. W. Atkins.

² Department of Surgery, University of Florida, College of Medicine, Gainesville, FL 32610.

³ Department of Pediatrics, University of Florida, College of Medicine, Gainesville, FL 32610.

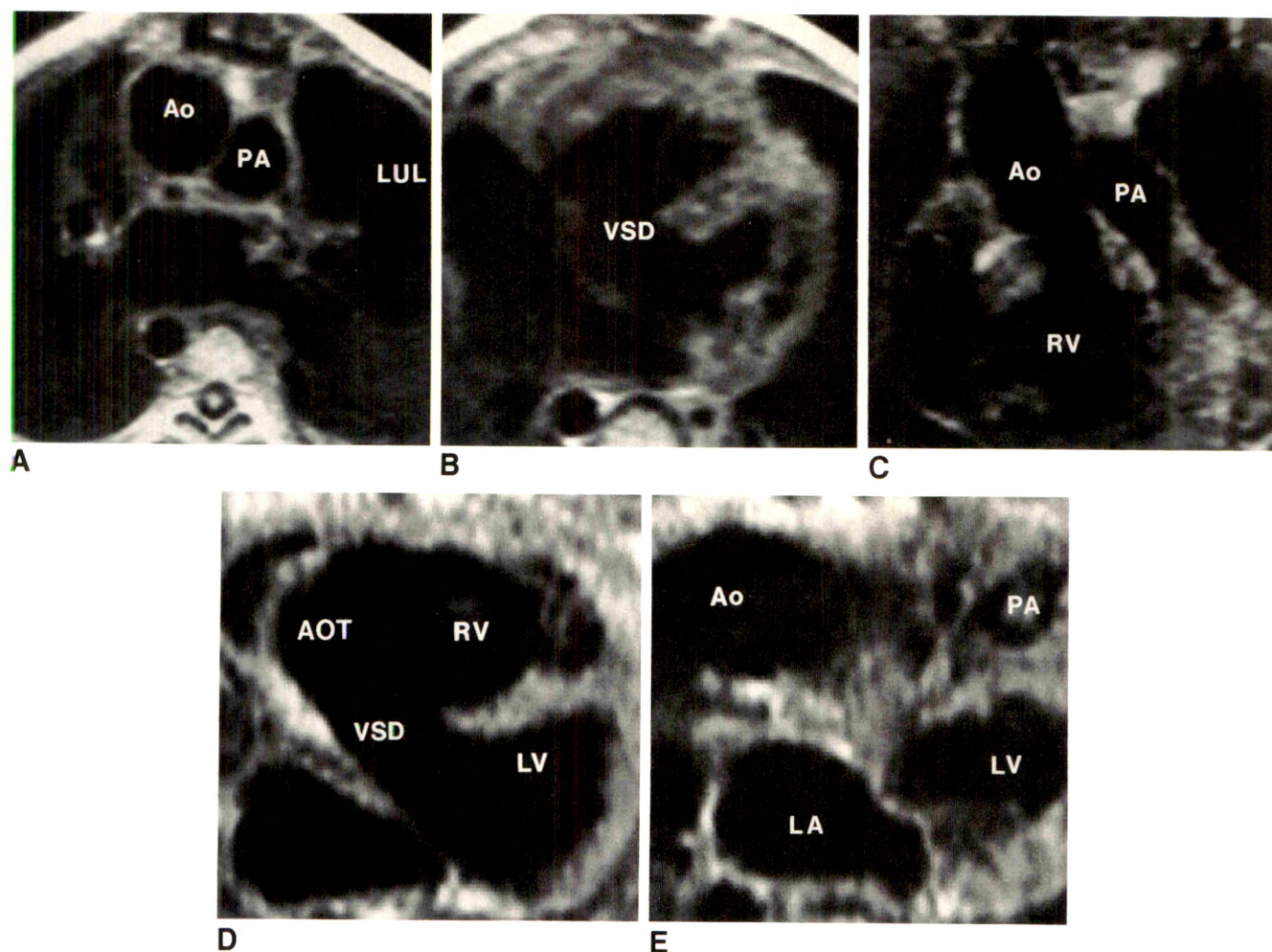


Fig. 1.—Patient with classic double-outlet right ventricle and aortic-committed ventricular septal defect.

A, Transverse section at cardiac base shows nearly side-by-side appearance of great vessels, with aorta (Ao) to right of pulmonary artery (PA). A right aortic arch is present. There is emphysema of left upper lobe (LUL), causing slight dextroposition of heart.

B, Transverse section reveals large ventricular septal defect (VSD) under aortic root and right ventricular hypertrophy. Transverse sections do not clearly reveal commitment of ventricular septal defect.

C, Coronal section reveals classic side-by-side appearance of great vessels, with extensive trabeculation, causing infundibular stenosis of pulmonary artery (PA). An infundibular septum is noted between pulmonary and aortic outflow tracts. Ao = aorta; RV = right ventricle.

D, Long-axis section perpendicular to septum reveals large ventricular septal defect (VSD). Ventricular septal defect leads directly to aortic outflow tract (AOT); this pathway does not compromise pulmonary outflow tract. RV = right ventricle; LV = left ventricle.

E, Long-axis section 1 cm above D shows relationship of aorta (Ao) to stenotic pulmonary artery (PA) at root. Comparing this section with D is helpful for full appreciation of aortic commitment of ventricular septal defect. LA = left atrium, LV = left ventricle.

arteries arise from the base of the heart in a side-by-side relationship with the aorta to the right, but various degrees of transposition may be present in some cases [3].

The relationship of the VSD to the aorta (commitment) should be determined in order to properly plan a complete surgical repair [4, 5]. Aortic commitment of the VSD allows internal repair by intraventricular baffle when pulmonic stenosis is not severe [4]. It is particularly important to differentiate between simple DORV and the Taussig-Bing anomaly in which the VSD is committed to the pulmonary artery, because the surgical approach is markedly different in each case [5].

The angiocardiac appearance of double-outlet right ventricle was first described by Carey and Edwards in 1965 [6]. Cineangiography remains the standard method for diagnosis and classification of these conditions. The angio-

graphic assessment often may be supplemented by two-dimensional echocardiography, which is noninvasive and provides excellent multiplanar, real-time representation of these relationships [7].

Occasionally, however, unsuspected findings are encountered at surgery that change the nature of the surgical management. MR imaging can provide precise cross-sectional cardiac images that can be obtained from unlimited vantage points and that can image the heart and great vessels reliably with respect to the chest cavity. Each MR examination can be individualized by selection of unlimited imaging planes to answer specific questions regarding relationships between the great vessels. Guit et al. [8] described the use of MR imaging for evaluation of levotransposition of the aorta and discussed the importance of multislice depiction for precise

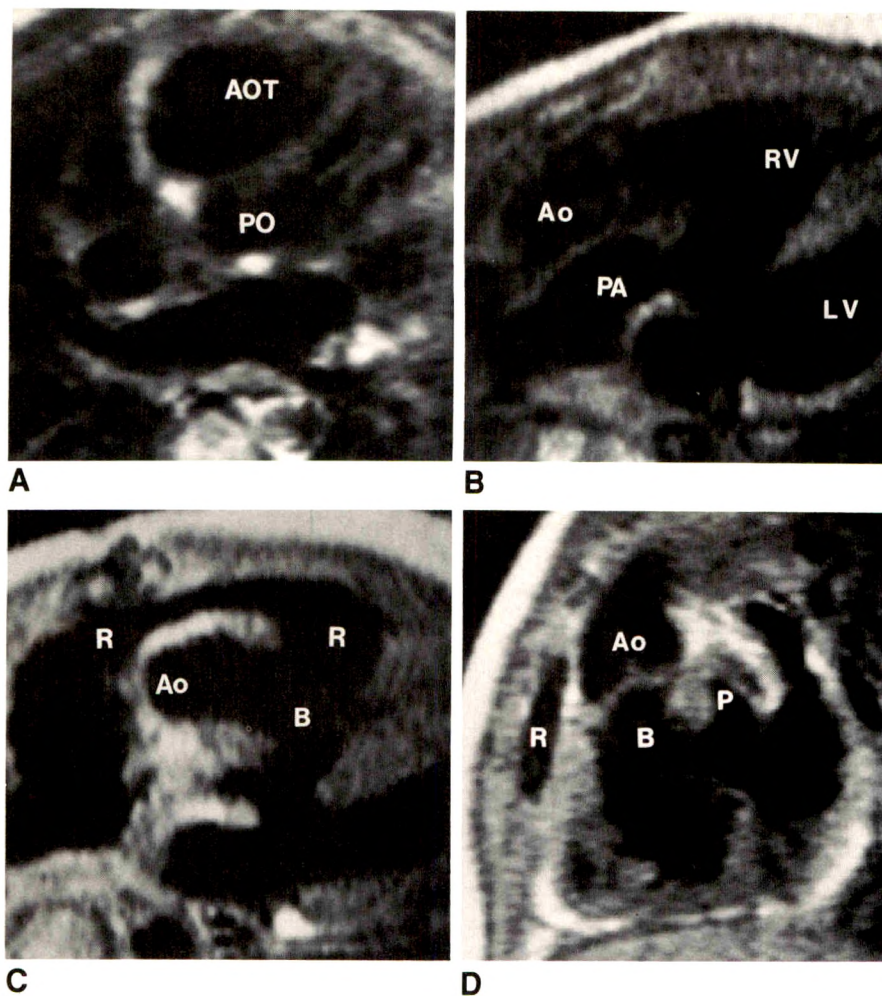


Fig. 2.—Patient with transposition of great arteries with pulmonary-committed ventricular septal defect. A and B are preoperative MR scans. C and D are postoperative MR scans.

A, Axial section reveals anterior position of aortic outflow tract (AOT) with pulmonary outflow tract (PO) emerging posteriorly. A large infundibular septum is present.

B, Long-axis section clearly shows that aorta (Ao) arises from right ventricle (RV). Ventricular septal defect is directly committed to transposed pulmonary artery (PA). LV = left ventricle.

C, Long-axis section reveals ligated pulmonary artery with internal baffle (B) connecting ventricular septal defect to aorta (Ao). A Rastelli conduit (R) has been placed anteriorly and is compressed by sternum.

D, An oblique section angled to relate baffle to aortic root reflects this anatomy to even better advantage. Internal baffle (B) leading to aorta (Ao) is shown clearly. Pulmonary artery (P) has been ligated. Rastelli conduit is compressed anteriorly (R).

evaluation of ventriculoarterial connections. They described a case of DORV that was imaged after surgery. This report documents the first use of MR imaging to precisely depict the ventriculoarterial anatomy in DORV, as compared with that in transposition of the great vessels.

MR imaging was used in another patient with transposition of the great vessels to show pulmonic commitment of the VSD (Fig. 2). The long-axis plane clearly showed the great-vessel relationship in VSD. Postoperative anatomy was also readily assessed by MR imaging. The clear anatomic depiction that is possible with MR imaging and the ease with which this technique can be used (especially in older children) suggests that it may be helpful for preoperative evaluation of selected patients with congenital heart disease. Until MR imaging proves reliable for noninvasive coronary artery imaging, angiography often will be necessary for complete preoperative evaluation. MR imaging may supplement other imaging techniques in difficult cases and can aid the surgeon in planning complete repair of DORV and transposition of the great vessels.

REFERENCES

1. Kinsley RH, Ritter DG, McGoon DC. The surgical repair of positional anomalies of the conotruncus. *J Thorac Cardiovasc Surg* 1974;67:395-403
2. Stellin G, Zuberbuhler JR, Anderson RH, Path MRC, Siewers RD. The surgical anatomy of Taussig-Bing malformation. *J Thorac Cardiovasc Surg* 1987;93:560-569
3. Zamora R, Moller JH, Edwards JE. Double outlet right ventricle: anatomic types and associated anomalies. *Chest* 1975;68:672-677
4. Patrick DL, McGoon DC. An operation for double outlet right ventricle with transposition of the great arteries. *J Cardiovasc Surg* 1968;9:537-542
5. Sridaromont S, Feldt RH, Ritter DG, Davis GD, Edwards JE. Double outlet right ventricle: hemodynamic and anatomic correlations. *Am J Cardiol* 1976;38:85-94
6. Carey LS, Edwards JE. Roentgenographic features in cases with origin of both great arteries from the right ventricle without pulmonary stenosis. *AJR* 1965;93:269-297
7. Hagler DJ, Tajik AJ, Seward JB, Mair DD, Ritter DG. Double outlet right ventricle: wide angle two-dimensional echocardiographic observation. *Circulation* 1981;63:419-428
8. Guit GL, Bluemm R, Rohmer R, et al. Levotransposition of the aorta: identification of segmental cardiac anatomy using MR imaging. *Radiology* 1986;161:673-679

Dyke Award

Gd-DTPA-Enhanced MR Imaging of Experimental Bacterial Meningitis: Evaluation and Comparison with CT

Vincent P. Mathews¹
 Michael A. Kuharik¹
 Mary K. Edwards¹
 Peter G. D'Amour¹
 Biagio Azzarelli²
 R. Gerald Dreesen¹

Gd-DTPA-enhanced MR images of experimental bacterial meningitis were obtained after *Staphylococcus aureus* was inoculated directly into the cisterna magna of four dogs. Each animal was studied with both unenhanced and enhanced MR and CT with Gd-DTPA and meglumine iohalamate, respectively. The enhancement patterns resulting from these techniques were compared and images were correlated with histopathology. All animals demonstrated abnormal leptomeningeal enhancement on MR with Gd-DTPA, but only one of four dogs exhibited abnormal contrast enhancement on CT. In these animals Gd-DTPA-enhanced MR also identified complications of meningitis, such as ventriculitis and cerebritis, more effectively than CT did. Unenhanced MR was not helpful in identifying meningitis. Histologic evaluation demonstrated that the abnormal areas of contrast enhancement on MR and CT correlated with inflammatory cell infiltration. However, some regions of mild leptomeningitis, ependymitis, and cerebritis identified histologically did not demonstrate abnormal enhancement.

Since the animal model used was clinically and pathologically similar to human meningitis, we propose that Gd-DTPA-enhanced MR will subsequently be found more effective than unenhanced MR and IV contrast-enhanced CT for demonstrating meningitis and its complications in humans.

Uncomplicated bacterial meningitis is an infectious process in which organisms and exudate are confined to the CSF spaces and the leptomeninges [1]. The diagnosis of acute bacterial meningitis is based on the clinical presentation and laboratory CSF findings [2]. The development of CT has provided a noninvasive means of imaging the intracranial manifestations of meningitis. More important, CT has been shown effective in evaluating the complications of meningitis such as hydrocephalus, cerebritis, abscess, subdural empyema or effusion, ventriculitis, and infarction [3-9]. Other authors have indicated that CT may be valuable in predicting eventual neurologic outcome in meningitis patients [6, 7]. Contrast-enhanced CT is recommended for these patients since it may reveal areas of involvement not detected with plain CT. Meningeal, cisternal, or parenchymal enhancement may be seen after contrast administration [3, 7, 10].

More recently, MR imaging of meningitis has been described [10, 11]. Although not yet reported, paramagnetic contrast agents have been predicted to demonstrate abnormal MR enhancement in meningitis [12].

The purpose of this study is to evaluate MR of experimental bacterial meningitis and its complications using an established canine model and the paramagnetic agent gadolinium(Gd)-DTPA. The paramagnetic enhancement patterns observed on MR were compared with CT images and correlated with histopathology.

Materials and Methods

Experimental Model

Using a modification of a previously described model [13], we induced bacterial meningitis in four mongrel dogs each weighing between 10 and 22 kg. One milliliter of a saline suspension

This article appears in the November/December 1988 issue of *AJNR* and the January 1989 issue of *AJR*.

Received March 25, 1988; accepted after revision July 7, 1988.

Presented at the annual meeting of the American Society of Neuroradiology, Chicago, May 1988.

¹ Department of Radiology, University Hospital, 926 W. Michigan, Indianapolis, IN 46223. Address reprint requests to M. K. Edwards.

² Department of Pathology, University Hospital, Indianapolis, IN 46223.

AJR 152:131-136, January 1989

0361-803X/89/1521-0131

© American Roentgen Ray Society

of *Staphylococcus aureus* (*S. aureus*), containing approximately 10^9 organisms, was injected into the cisterna magna. Intramuscular ketamine provided sedation for inoculation and imaging. The animals were observed closely for clinical signs of meningitis.

Imaging Techniques

CT (General Electric 9800) was performed both with and without IV contrast (2.2 ml/kg 60% meglumine iohalamate). High-resolution 5-mm axial sections were obtained with the CT scanner operating at 120 kVp and 140 mA. Enhanced scans were acquired 5 min after IV contrast injection.

A 1.5-T superconducting MR imager (Picker International) was used with a 28-cm internal diameter head coil. Images were acquired in the axial and coronal planes using a 5-mm slice thickness, 256×256 matrix, two repetitions, and a 20-cm field of view. The pulse sequences used were a spin-echo format with 600/26 for T1-weighted images and 2000/90 for T2-weighted images. Motion artifact suppression technique (MAST) was used with the T2-weighted sequence and allowed the acquisition of only a single echo. T1- and T2-weighted images were obtained before Gd-DTPA administration and T1-weighted images were acquired 5 min after the IV injection of Gd-DTPA at a dose of 0.2 mmol/kg. MR was performed immediately after CT. CT and MR, with and without iodinated contrast and Gd-DTPA, respectively, were obtained before and at intervals ranging from 13 to 134 hr after the induction of meningitis. Specifically, the animals were imaged after inoculation as follows: dog 1 at 28 hr, dog 2 at 15, 40, and 64 hr, dog 3 at 15 and 134 hr, and dog 4 at 15 hr.

Pathologic Examination

CSF was sampled and analyzed prior to bacterial inoculation. After inoculation, CSF was obtained at the time of imaging and examined for cell count and protein as well as cultured for bacterial growth. Animals were sacrificed at different intervals ranging from 15 to 135 hr after inoculation, immediately following the imaging procedures. The brains were fixed in formalin for a minimum of 2 weeks and then cut at 5-mm intervals either in the axial or coronal plane. Representative sections were obtained for histology. Examination was performed on 10- μ m-thick sections of paraffin-embedded material. The sections were stained with hematoxylin and eosin (H and E).

Results

Experimental Model

Meningitis was confirmed in all four animals by the clinical observation of lethargy, nuchal rigidity, and varying degrees of gait disturbance as well as the development of CSF leukocytosis and protein elevation. CSF cultures were positive for *S. aureus* growth.

CT and MR

CT scans were degraded variably by streak artifacts caused by the relatively thick canine skulls. Because of these artifacts, changes in ventricular size associated with meningitis were not appreciated by CT. Abnormal contrast enhancement was evaluated by comparing scans before and after inoculation. Twenty-eight hours after the induction of meningitis, one of four animals demonstrated abnormal contrast enhancement

by CT. This enhancement was mild in nature and was located in the posterior fossa (Figs. 1A and 1B).

MR images prior to the induction of meningitis were normal in the four animals. Pre-Gd-DTPA T1- and T2-weighted images revealed increased ventricular size in each of the infected animals but did not demonstrate signal abnormality of the leptomeninges or cisterns. On the post-Gd-DTPA T1-weighted images, abnormal enhancement was observed in all four animals between 13 and 29 hr after inoculation. Bright paramagnetic enhancement of the posterior fossa meninges, basal cisterns, and/or superficial cerebellar and brainstem parenchyma developed in all four animals (Figs. 1C and 1D). At the same time, supratentorial leptomeningeal enhancement occurred in only two of four dogs. One of these dogs exhibited diffuse gyriform enhancement suggesting underlying cerebritis (Fig. 2). Another animal (dog 3) demonstrated subependymal paramagnetic enhancement of the third and lateral ventricles on the post-Gd-DTPA T1-weighted image 134 hr after induction of infection, suggesting the development of ventriculitis (Figs. 3A–3C). The pre-Gd-DTPA T2-weighted image of this animal demonstrated abnormal irregular bright signal in the subependymal region of the lateral ventricles (Fig. 3D).

Neuropathology

After necropsy, all four animals were found to have the characteristic inflammatory cell infiltration of the leptomeninges seen in meningitis (Fig. 4). In all dogs the underlying superficial cortex was also mildly inflamed. In each animal, areas of abnormal paramagnetic enhancement observed on the post-Gd-DTPA T1-weighted image correlated with severe inflammatory changes histologically. However, areas of less intense meningeal inflammation at necropsy did not demonstrate abnormal enhancement on MR. In addition, two dogs (1 and 2) had mild ependymitis histologically without associated Gd-DTPA enhancement. However, at necropsy dog 3 demonstrated very severe ependymitis with subependymal cerebritis and choroid plexus inflammation (Fig. 5). These findings correlated well with the pattern of abnormal paramagnetic enhancement on the T1-weighted images (Figs. 3B and 3C).

Discussion

Bacterial meningitis develops in humans when the causative organism reaches the leptomeninges via the bloodstream, by direct extension from an adjacent infection, or by traumatic inoculation [2]. The method of direct inoculation used in this study, although artificial, effectively produced clinical, laboratory, and histologic findings identical to those in naturally acquired disease [2].

CT has been used primarily to detect complications associated with meningitis [3–7, 9]. The actual meningeal involvement by the infection, however, has only been inconsistently demonstrated by CT as areas of contrast enhancement. The proposed mechanisms for enhancement with iodinated contrast include the presence of contrast in dilated and engorged

Fig. 1.—Dog 1.

A, Unenhanced CT scan obtained 27 hr after inoculation is unremarkable.

B, Contrast-enhanced CT scan obtained at the same time as A demonstrates mild posterior fossa enhancement (arrowheads).

C, Unenhanced 600/20 T1-weighted image of the animal imaged in A and B obtained before the induction of meningitis.

D, Post-Gd-DTPA 600/20 T1-weighted image 1 hr after A and B and at a similar level to C shows abnormal enhancement of meninges surrounding cerebellum (arrowheads).

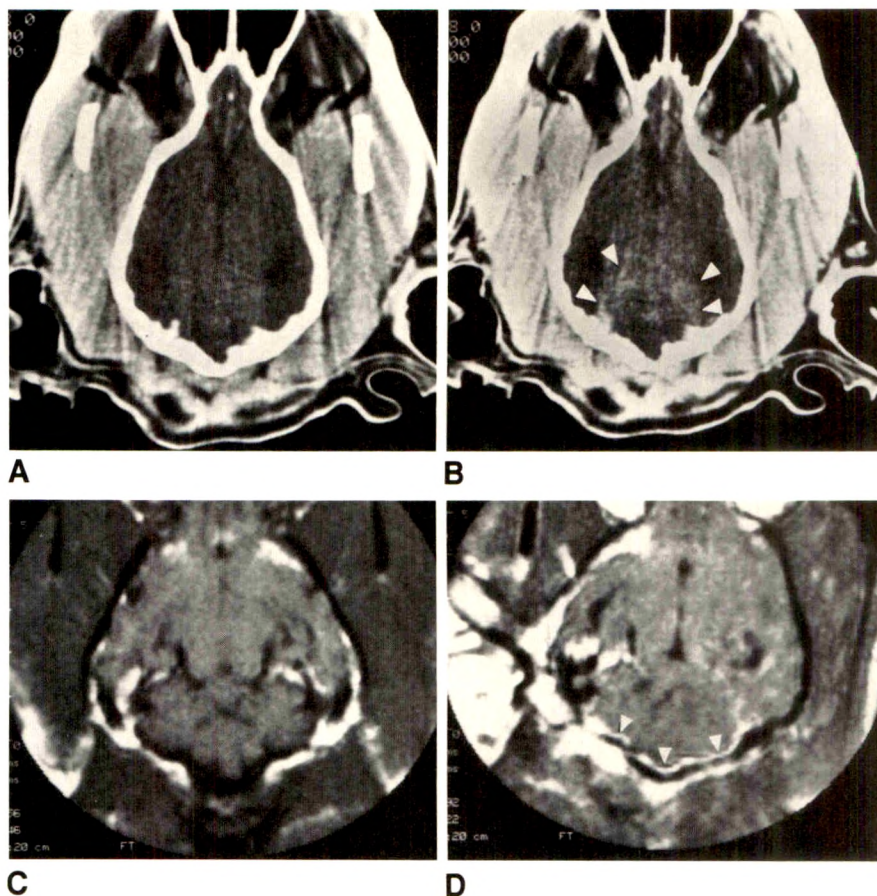
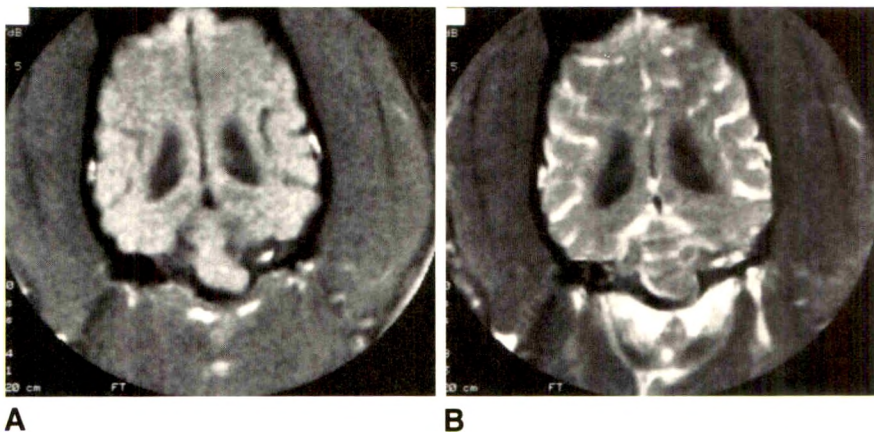


Fig. 2.—Images of dog 2 obtained 15 hr after bacterial inoculation.

A, Pre-Gd-DTPA 600/26 T1-weighted image shows mild hydrocephalus.

B, Post-Gd-DTPA 650/26 T1-weighted image exhibits marked meningeal and cortical enhancement both supratentorially and infratentorially.



leptomeningeal vessels and abnormal function of the blood-meningeal barrier resulting from inflammation near these vessels [3, 6, 14]. The term blood-meningeal barrier refers to that portion of the blood-brain barrier formed by capillaries of the leptomeninges [3].

Gd-DTPA has previously been shown to function similarly to water-soluble, iodinated contrast agents and to produce abnormal enhancement in CNS infections [15–17]. However, while flowing blood reliably enhances with contrast-enhanced CT, the arterial and capillary vascular space inconsistently enhances with Gd-DTPA-enhanced MR [18]. Therefore,

blood-meningeal barrier abnormalities rather than contrast material in vessels are more likely to be responsible for the reproducible leptomeningeal MR contrast enhancement observed in this study.

In our cases of experimental meningitis, post-Gd-DTPA T1-weighted images more consistently exhibited abnormal enhancement than did contrast-enhanced CT. The extent of meningeal inflammation was also more accurately depicted by Gd-DTPA-enhanced MR than by contrast-enhanced CT. In one case of ventriculitis, Gd-DTPA-enhanced T1-weighted images demonstrated marked ependymal enhancement

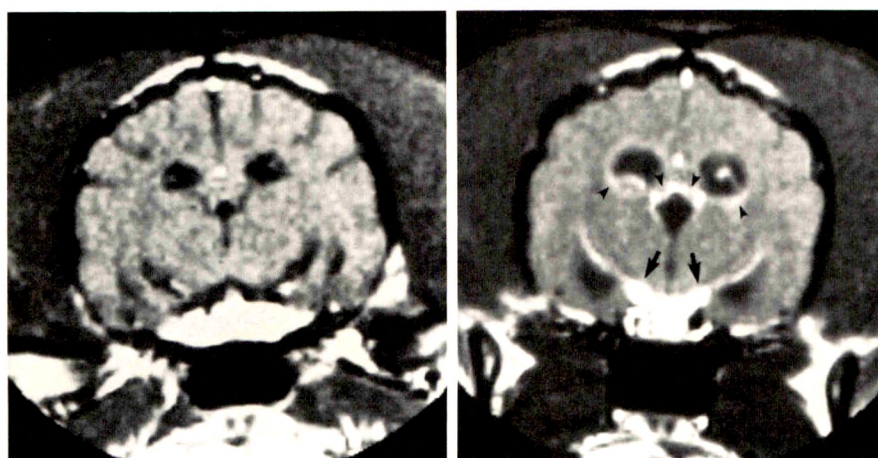


Fig. 3.—Dog 3.

A, Post-Gd-DTPA 500/26 coronal T1-weighted image before induction of meningitis reveals no abnormal areas of enhancement.

B, Post-Gd-DTPA 650/26 coronal T1-weighted image 5 days after onset of meningitis demonstrates dilatation of lateral and third ventricles as well as abnormal contrast enhancement of the ventricular lining (arrowheads) and basal cisterns (arrows).

C, Post-Gd-DTPA 600/26 axial T1-weighted image at same time as B exhibits abnormal ventricular (arrowheads) and posterior fossa (arrows) enhancement.

D, Pre-Gd-DTPA 2000/90 axial T2-weighted image obtained just prior to B and C demonstrates mild contour irregularity (arrowheads) of lateral ventricles posteriorly. Signal in the meningeal region is unchanged from premeningitis images.

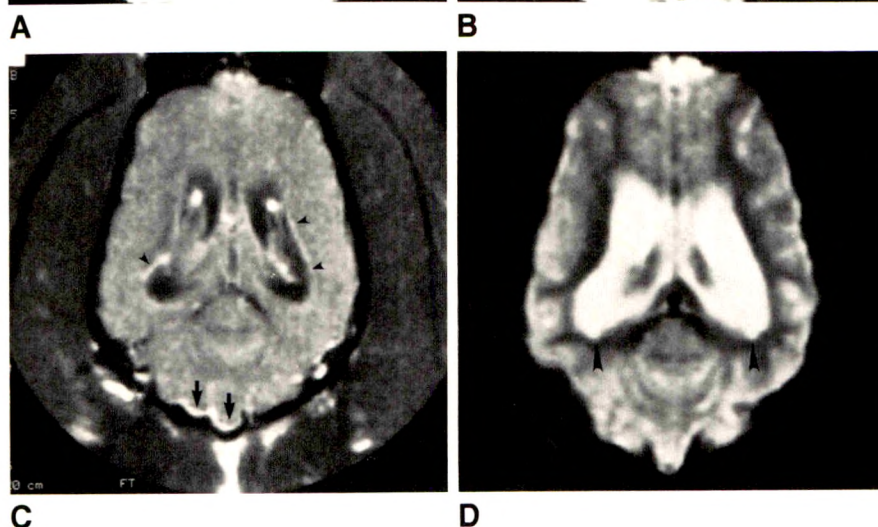


Fig. 4.—Photomicrograph illustrates extensive acute inflammatory infiltrates confined primarily to the leptomeninges (arrows). (H and E, $\times 40$)

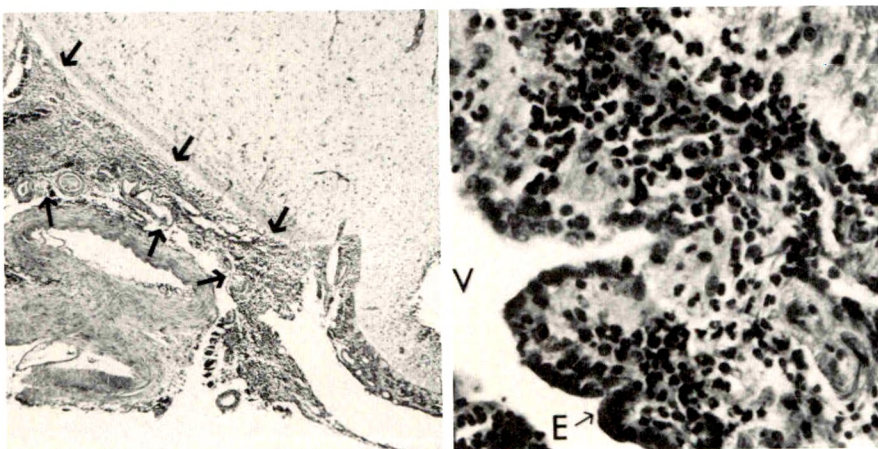


Fig. 5.—Photomicrograph demonstrates extensive acute inflammatory infiltrates in subependymal region. V = lateral ventricle. E = ependyma. (H and E, $\times 400$)

whereas contrast-enhanced CT was unremarkable. These observations are probably the result of the superior anatomic detail and greater tissue contrast afforded by MR relative to CT. These advantages are especially beneficial around the brainstem and areas adjacent to cortical bone where contrast enhancement on CT may be obscured. However, Gd-DTPA may, for as yet undetermined reasons, be more sensitive in

delineating blood-brain barrier abnormalities than iodinated contrast.

Pathologic examination of the animals in this study demonstrated that areas of contrast enhancement on both CT and MR images correlated with inflammatory cell infiltration. This has been assumed to be the case in CT of meningitis, but histologic correlation with CT or MR has not been previ-

ously disclosed. The value of CT in demonstrating the extent of infection in meningitis [6] and ventriculitis [9] has been reported. In our animal model Gd-DTPA-enhanced T1-weighted images revealed inflammatory meningeal and ependymal processes more effectively than did contrast-enhanced CT. However, Gd-DTPA-enhanced MR is not completely accurate in depicting CNS inflammation, as indicated by the histologic demonstration of areas of leptomeningitis, cerebritis, and ventriculitis that did not enhance after Gd-DTPA administration. These areas of inflammation were mild, however, whereas regions of more intense inflammation corresponded more closely to paramagnetic contrast enhancement on MR. This suggests that there may be a threshold of inflammation above which there is enough disruption of the blood-meningeal barrier to permit the visualization of Gd-DTPA enhancement. Nevertheless, as MR is improved, the disparity between diagnostic imaging and histology may further diminish.

The observation that unenhanced T1- and T2-weighted images were not helpful in detecting meningitis is notable. Peripheral extension of white-matter MR signal such that it appeared to merge with marrow signal has been described in meningitis [11] but was not seen in our cases. In the case of severe ventriculitis T2-weighted images revealed irregular contour of the lateral ventricles, which may be a helpful sign in making this diagnosis. Irregularity of ventricular margins has previously been described in some CT cases of ependymitis [20]. Mild degrees of ventriculitis and cerebritis were also not identified with T2-weighted or unenhanced T1-weighted images.

The clinical usefulness of MR in the management of patients with meningitis remains to be determined. The delineation of the extent of meningeal involvement may be important when evaluating patients with delayed response to therapy. Persistent meningeal inflammation or the development of ventriculitis may be illustrated in these patients and, on the basis of our results, will likely be more effectively depicted with Gd-DTPA-enhanced T1-weighted images than with contrast-enhanced CT or unenhanced MR. Previous investigation has indicated that MR may be more effective than CT in detecting the early stages of abscess formation [16, 17], which may also complicate meningitis. Other authors studying brain abscess have suggested that the greater inherent tissue contrast of MR relative to CT as well as the higher therapeutic safety index of Gd-DTPA compared with iohalamate allows one to obtain more information from Gd-DTPA-enhanced MR than from contrast-enhanced CT [21]. This argument can be applied to the imaging of meningitis and its complications as well.

Conclusions

Gd-DTPA-enhanced MR demonstrated abnormalities characteristic of meningitis with far greater frequency than did contrast-enhanced CT. While others have found ventricular dilatation to be the most common CT abnormality in meningitis [20, 22], meningeal and cisternal MR contrast enhancement with Gd-DTPA was just as common as hydrocephalus in our meningitis model. In this study Gd-DTPA-enhanced T1-

weighted images were superior to contrast-enhanced CT scans not only in the detection of meningeal involvement but also in the identification of complications such as cerebritis and ventriculitis. Unenhanced MR was not helpful in identifying meningitis in these animals but it did detect some complications of meningitis such as hydrocephalus and ventriculitis. Since the animal model of meningitis used produced clinical and pathologic responses similar to those in human meningitis, we propose that Gd-DTPA-enhanced MR will prove more effective than contrast-enhanced CT and unenhanced MR for demonstrating meningeal inflammation as well as the complications of meningitis in humans.

ACKNOWLEDGMENTS

We thank Lawrence Wheat of the Department of Medicine and Eugene Klatte of the Department of Radiology for their advice on this project and Erv Herman and Ed Rhodes for technical assistance.

REFERENCES

- Waggener JD. The pathophysiology of bacterial meningitis and cerebral abscesses: an anatomical interpretation. *Adv Neurol* 1974;6:1-17
- Overturf GD, Hoeprich PD. Bacterial meningitis. In: Hoeprich PD, ed. *Infectious diseases: a modern treatise of infectious processes*. Philadelphia: Harper & Row, 1983:1035-1052
- Bilaniuk LT, Zimmerman RA, Brown L, Yoo HJ, Goldberg HI. Computed tomography in meningitis. *Neuroradiology* 1978;16:13-14
- Claveria LE, du Boulay GH, Mosely IF. Intracranial infections: investigation by computerized axial tomography. *Neuroradiology* 1976;12:59-71
- Naidu S, Glista G, Fine M, Brumlik J, Palacios E. Serial CT scans in *Haemophilus influenzae* meningitis of childhood. *Develop Med Child Neurol* 1982;24:69-76
- Centeno RS, Winter J, Bentson JR, Kneeland WF. CT evaluation of *Haemophilus influenzae* meningitis with clinical and pathologic correlation. *Comput Radiol* 1983;7(4):243-249
- Packer RJ, Bilaniuk LT, Zimmerman RA. CT parenchymal abnormalities in bacterial meningitis: clinical significance. *J Comput Assist Tomogr* 1982;6(6):1064-1068
- Zimmerman RA, Patel S, Bilaniuk LT. Demonstration of purulent bacterial intracranial infections by computed tomography. *AJR* 1976;127:155-165
- Cockrill HH, Driesbach J, Lowe B, Yamanchi T. Computed tomography in leptomeningeal infections. *AJR* 1978;130:511-515
- Zimmerman RA, Bilaniuk LT, Sze G. Intracranial infection. In: Brandt-Zawadzki M, Norman D, eds. *Magnetic resonance imaging of the central nervous system*. New York: Raven, 1987:235-257
- Bydder GM, Steiner RE, Young IR, et al. Clinical NMR imaging of the brain: 140 cases. *AJNR* 1982;3:459-480, *AJR* 1982;139:215-236
- Enzmann DR. *Imaging of infections and inflammations of the central nervous system: computed tomography, ultrasound, and nuclear magnetic resonance*. New York: Raven, 1984:188-233
- Vergin H, Bishop-Freudling GB, Foing N, Szelenyi I, Armengaud H, van Tho T. Diffusion of metioprim, tetroxoprim, sulphadiazine in the cerebrospinal fluid of dogs with healthy meninges and dogs with experimental meningitis. *Chemotherapy* 1984;30:297-304
- Enzmann DR, Norman D, Mani J, Newton TH. Computed tomography of granulomatous basal arachnoiditis. *Radiology* 1976;120:341-344
- Davidson HD, Steiner RE. Magnetic resonance imaging in infections of the central nervous system. *AJNR* 1985;6:499-504
- Grossman RI, Joseph PM, Wolf G, et al. Experimental intracranial septic infarction: magnetic resonance enhancement. *Radiology* 1985;155:649-653
- Runge VM, Clanton JA, Price AC, et al. Evaluation of contrast-enhanced MR imaging in a brain-abscess model. *AJNR* 1985;6:139-147
- Kilgore DP, Breger RK, Daniels DL, Pojunas KW, Williams AL, Haughton VM. Cranial tissues: normal MR appearance after intravenous injection of Gd-DTPA. *Radiology* 1986;160:757-761
- Nielsen H, Gyldensted C. Computed tomography in the diagnosis of

- cerebral abscess. *Neuroradiology* **1977**;12:207-217
20. Stovring J, Snyder RD. Computed tomography in childhood bacterial meningitis. *J Pediatr* **1980** 96(5):820-823
21. Runge VM, Clanton JA, Price AC, et al. The use of Gd-DTPA as a perfusion agent and marker of blood-brain barrier disruption. *Magn Reson Imaging* **1985**;3:43-55
22. Snyder RD, Stovring J. The follow-up CT scan in childhood meningitis. *Neuroradiology* **1978**;16:22-23

American Roentgen Ray Society Residents' Award Papers, 1989

The ARRS announces competition for the 1989 President's Award and two Executive Council Awards for the best papers concerning the clinical application of the radiologic sciences.

Awards

The winner of the President's Award will receive a certificate and a \$1000 prize. The winners of the two Executive Council Awards will each be given a certificate and a prize of \$500. The winners will be announced on March 15, 1989. Winning papers will be presented at the ARRS annual meeting at the New Orleans Hilton, New Orleans, LA, May 7-12, 1989. Winning papers will be submitted for early publication in the *American Journal of Roentgenology*. All other papers will be returned to the authors.

Regulations

Eligibility is limited to residents or fellows in radiology who have not yet completed 4 years of approved training in a radiologic discipline. A letter from the resident's department chairman attesting to this status must accompany the manuscript. The resident must be the sole or senior author and be responsible for all or most of the project.

Submitted manuscripts must not exceed 5000 words and have no more than 10 illustrations. Four copies of the manuscript and illustrations are required. Submitted manuscripts should not contain previously presented or published material and should not be under consideration for publication elsewhere.

Deadline for submissions is February 10, 1989. Send papers to

B. G. Brogdon, M.D.
Chairman, Committee on Education & Research
American Roentgen Ray Society
Department of Radiology
University of South Alabama Medical Center
2451 Fillingim Street
Mobile, AL 36617

MR Imaging of Hemorrhagic Intracranial Neoplasms

Sylvie Destian¹
 Gordon Sze²
 George Krol²
 Robert D. Zimmerman¹
 Michael D. F. Deck¹

Thirty patients with intracranial tumors containing hemorrhage of varying stages were examined with high-field-strength MR imaging and CT to determine what differences might exist between hemorrhagic tumor and pure hemorrhage. Pathology was obtained in the six patients with primary tumors and in 14 of the 24 patients with metastases. Similar to evolving intraparenchymal hematomas, hemorrhagic neoplasms undergo changes in their appearance that can be categorized into three distinct intensity patterns, or stages. Stage 1 is characterized as iso- or hypointensity on short TR sequences and as hypointensity on long TR sequences; stage 2 as developing hyperintensity on both short and long TR sequences, without evidence of a well-defined black rim; and stage 3 as a hyperintense lesion with a well-defined black rim on long TR sequences. An additional mixed-intensity pattern was identified, which contained areas corresponding to more than one stage. In all of the cases exhibiting this pattern, pathology confirmed that the appearance was due to recurrent bleeding. We found several characteristics on MR that, when present, suggest an underlying neoplasm. These include delay in evolution between stages, central or eccentric hyperintensity in stage 2, and a mixed-intensity pattern. In addition, the presence of a hemosiderin rim does not exclude an underlying neoplasm.

We found that the MR patterns that characterize hemorrhagic intracranial neoplasms should help to determine the cause of the hemorrhage.

During the past few years MR imaging has emerged as superior to CT in detecting intraparenchymal hemorrhage, particularly in the subacute and chronic phases. In addition, it is an excellent, noninvasive way to screen for, and follow, intracranial neoplasms. In patients who present with a hemorrhage on MR, however, it may be necessary to determine the underlying cause of hemorrhage.

Recently, several reports have described the MR characteristics of intraparenchymal hemorrhage [1-11]. However, only a few studies describing the MR characteristics of hemorrhagic neoplasms have been reported in the literature [11-15]. Therefore, we examined patients with hemorrhagic neoplasms to determine whether there were any differences in the appearance of the lesions on MR that would distinguish them from pure hemorrhage.

Materials and Methods

Thirty patients with hemorrhagic intracranial neoplasms were examined by MR and CT. There were 22 men and eight women, ranging in age from 20 to 72 years old. Six of the patients had primary tumors and 24 had metastatic tumors. Pathology was obtained in all six patients with primary tumors and in 14 of the patients with metastases. The primary tumors included two gliomas, two meningiomas, an ependymoma, and a primary meningeal melanoma. The metastatic tumors included 12 of melanoma, two of lung, two of renal cell, two of colon, and one each of bladder, thyroid, testicular, endometrial, rhabdomyosarcoma, and extragonadal choriocarcinoma.

All patients were examined on a 1.5-T GE superconducting magnet using short TR, 600-800/20-25/2 (TR range/TE range/excitations), and multiecho long TR, 2000/35-80/2, spin-

This article appears in the November/December 1988 issue of *AJNR* and the January 1989 issue of *AJR*.

Received November 30, 1987; accepted after revision March 28, 1988.

¹ Department of Radiology, Cornell University Medical Center and New York Hospital, 525 E. 68th St., New York, NY 10021.

² Department of Medical Imaging, Memorial Sloan-Kettering Cancer Center, 1275 York Ave., New York, NY 10021. Address reprint requests to G. Sze.

AJR 152:137-144, January 1989

0361-803X/89/1521-0137

© American Roentgen Ray Society

echo sequences. The images were acquired on a 256×256 or 256×128 matrix with a 5-mm slice thickness. The interslice gap was 1 mm for the short TR sequences and 2.5 mm for the long TR sequences. In addition, each patient had a noncontrast and a contrast CT scan, which were performed on a fourth-generation scanner with contiguous 5–10-mm-thick slices, either the same day or within 3 days of the MR imaging. The age of the hemorrhage was determined by the clinical history and the CT findings, and then correlated with the appearance on MR.

Six of the patients with metastatic disease had a follow-up examination at least once, and in one case five times. Three of the patients had more than one examination prior to their initial surgery. The other three patients developed new lesions after initial resection and were followed untreated for their new brain metastases, or had resection of a new lesion. The stage of each lesion was determined by its appearance on the first examination.

All of the surgical specimens were subjected to routine gross and microscopic pathologic examination. Five of the seven excised melanoma metastases, however, were found to be heavily pigmented on microscopic examination with hematoxylin and eosin. Therefore, special staining techniques were employed for these five specimens to determine whether the hyperpigmentation was due to melanin, hemosiderin, or both. A Fontana Masson stain was done to detect melanin and an iron stain was done to detect hemosiderin.

Results

We found that hemorrhagic neoplasms undergo changes in their appearance that can be categorized into three distinct intensity patterns. These intensity patterns, however, are only

somewhat time-dependent in that they do not always correlate with the clinical time course of the neoplastic hemorrhage, as they do with pure hemorrhage. The conventional terms used to describe the age-related signal intensity patterns of pure hemorrhage—i.e., acute, subacute and chronic—are not really appropriate when referring to neoplastic hemorrhage, because the time of evolution of the latter is variable. Therefore, rather than using the conventional nomenclature, which may be misleading, we defined the intensity patterns of our lesions as stages 1, 2, and 3. Table 1 is a summary of the findings in 24 of our patients as compared with findings in pure hemorrhage. A stage-1 lesion (Fig. 1) is isointense or mildly hypointense on short TR sequences and hypointense on long TR sequences. Seven of the patients had stage-1 lesions. Included in this group were one patient with a meningioma, two patients with metastatic melanoma, and one patient each with metastatic bladder, metastatic rectal, and metastatic colon carcinoma. Stage-2 lesions (Fig. 2) develop hyperintensity on both short and long TR sequences. Of the six patients in this group, one patient had an astrocytoma, three patients had metastatic melanoma, and the other two patients had metastatic endometrial and metastatic testicular carcinoma. Stage-3 lesions (Fig. 3) are hyperintense on both short and long TR sequences with a well-defined black rim on the long TR sequence. Eleven patients had stage-3 lesions. One of these patients had a meningioma, one had a primary meningeal melanoma, four had metastatic melanoma, two

TABLE 1: Signal Intensity Patterns of Hemorrhagic Neoplasms Compared with Described Evolution of Pure Hemorrhage

Hemorrhagic Neoplasm		Signal Intensity		Pure Hemorrhage	
Stage	Age	Short TR	Long TR	Stage	Age
1	Variable	Iso, Hypo	Hypo	Acute	2–5 days
2	Variable	Iso→Hyper	Iso→Hyper	Subacute	5–14 days
3	Variable	Hyper	Hyper with black rim	Chronic	2 wk–mos
M	Variable	Variable	Variable		

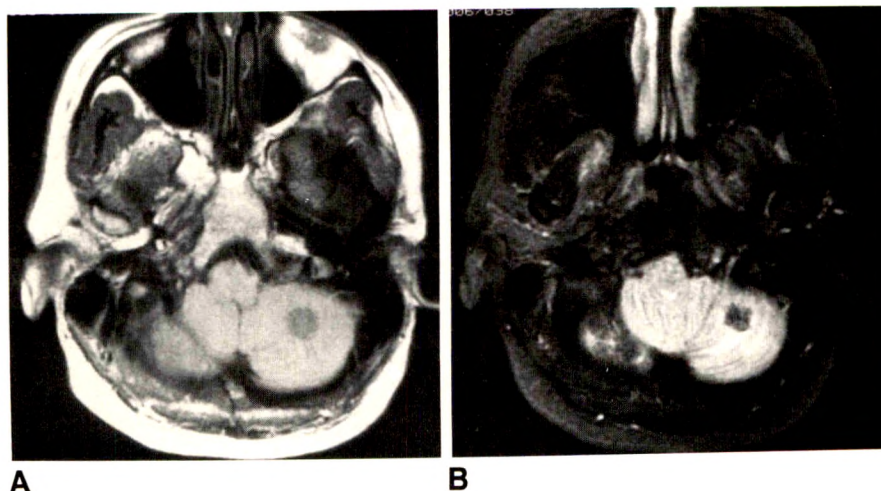


Fig. 1.—A and B, Colon metastases, left cerebellum; stage 1. Lesion is mildly hypointense on short TR sequence (600/20) (A) and markedly hypointense on long TR sequence (2000/70) (B).

Fig. 2.—A and B, Testicular metastasis, right cerebellum; stage 2. Lesion contains eccentric hyperintensity (solid arrows) representing free methemoglobin on both short TR (600/20) (A) and long TR (2000/70) (B) sequences. Isointense area on short TR sequence, which is hypointense on long TR sequence (open arrows), represents residual stage-1 hemorrhage.

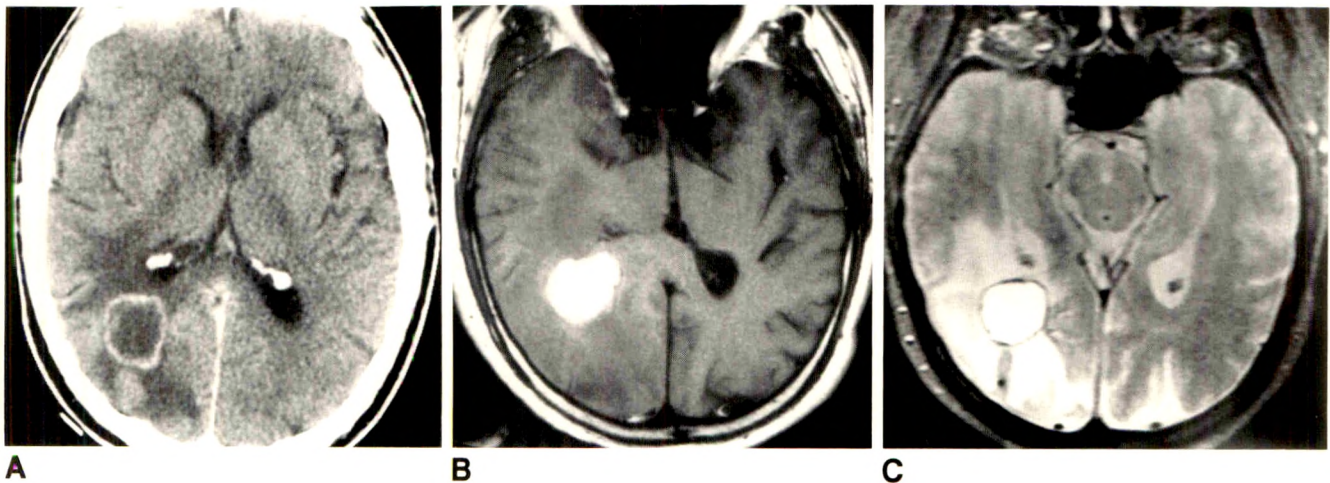
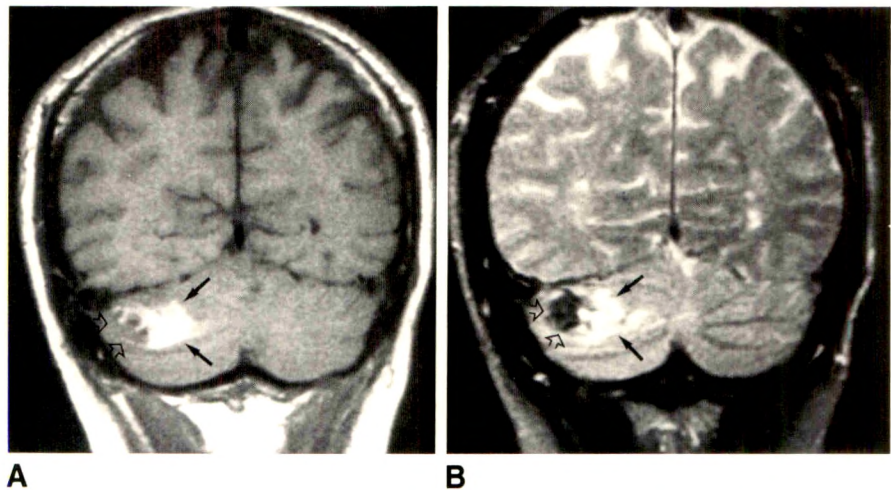


Fig. 3.—A–C, Renal cell metastasis, right occipital lobe; stage 3. Contrast CT scan (A) shows ring-enhancing hypodense mass in right occipital lobe. Lesion is hyperintense on both short TR sequence (600/20) (B) and long TR sequence (2000/70) (C) with a well-defined thin hypointense rim apparent on long TR image.

had metastatic lung, two had metastatic renal cell, and one had metastatic choriocarcinoma. Additionally, six patients exhibited a fourth intensity pattern, which we defined as mixed (Fig. 4). Those lesions demonstrating a mixed-signal-intensity pattern contained areas corresponding to more than one of the three stages described above. Three of the mixed lesions (metastatic melanoma, metastatic rhabdomyosarcoma, and glioblastoma multiforme) contained stage-1 and stage-2 elements. Two of the mixed lesions (ependymoma and metastatic melanoma) contained elements of all three stages, and the sixth mixed lesion (metastatic thyroid) contained stage-2 and stage-3 elements.

On noncontrast CT, five of the stage-1 lesions were hyperdense and two were mildly hyperdense. Two of the stage-2 lesions were isodense, one was mildly hyperdense, and three were hyperdense. Five of the stage-3 lesions were hypodense, four were isodense, and two were mildly hyperdense.

All of the mixed-stage lesions appeared inhomogeneous, containing areas of hypo-, iso-, and hyperdensity (Fig. 4A). After the administration of IV contrast material, the five hyperdense stage-1 lesions did not demonstrate appreciable enhancement, but the two mildly hyperdense stage-1 lesions enhanced homogeneously. The two stage-2 lesions that were isodense on noncontrast CT demonstrated ring enhancement after contrast administration; the other four enhanced homogeneously. Four of the five hypodense stage-3 lesions demonstrated ring enhancement (Fig. 3A), and one did not enhance. The other six stage-3 lesions demonstrated homogeneous enhancement. All of the mixed-stage lesions enhanced inhomogeneously (Fig. 4B).

Histopathology was available in five of the patients with stage-1 lesions, one of the patients with a stage-2 lesion, eight of the patients with stage-3 lesions, and all of the patients with mixed lesions. All of the stage-1 lesions con-

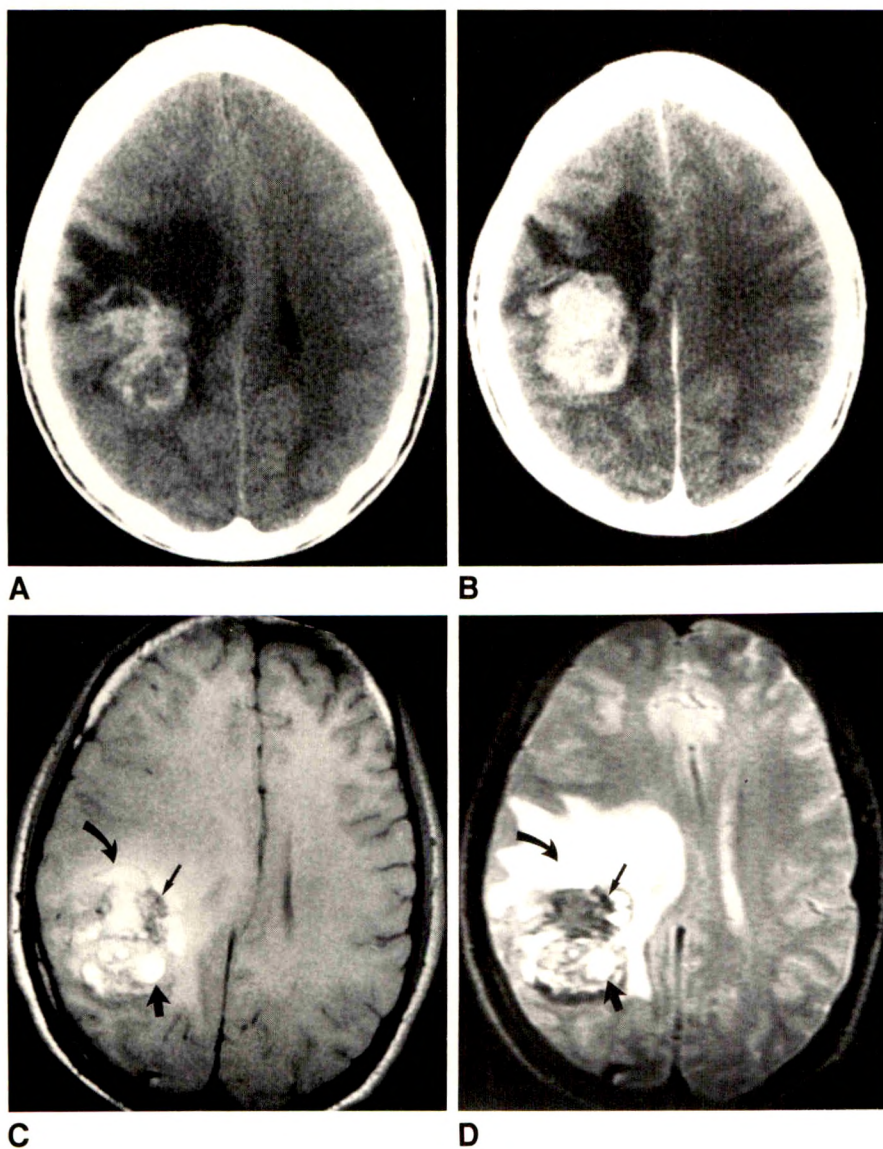


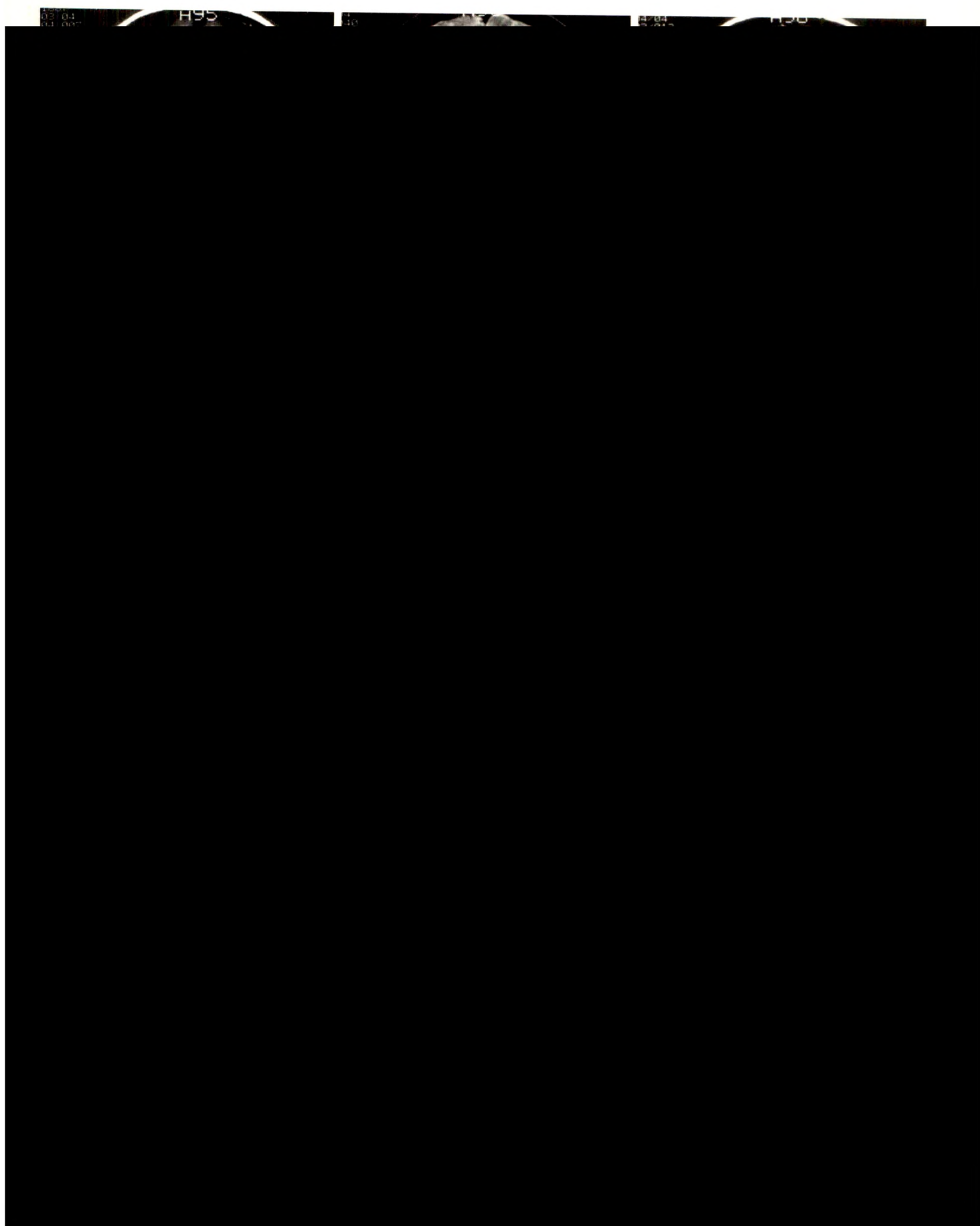
Fig. 4.—A–D, Melanoma metastasis, right frontoparietal region; mixed signal intensity. Noncontrast CT scan (A) shows inhomogeneous mass with areas of hypo- and hyperdensity. Contrast CT scan (B) (obtained at slightly higher level) demonstrates areas of enhancement within lesion. On short TR (800/20) (C) and long TR (2000/70) (D) sequences, lesion contains areas corresponding to stage-1 hemorrhage (small arrows), stage-2 hemorrhage (large arrows), and stage-3 hemorrhage (curved arrows).

tained fresh hemorrhage on histologic examination. The stage-2 lesion contained organizing hemorrhage without evidence of hemosiderin, and the stage-3 lesions contained old hemorrhage and hemosiderin. In each of the mixed lesions pathology demonstrated areas of hemorrhage in different stages of evolution, corresponding to the stages seen on MR. The stages of those lesions without pathology were determined by their appearance on MR and confirmed by the clinical history and the appearance of the lesions on CT.

Although there was direct correlation between the stage of the hemorrhagic component of the lesions on MR and what was seen pathologically, the intensity pattern of the hemorrhagic neoplasms did not necessarily reflect the clinical age of the hemorrhage. While in some cases the time course of evolution was similar to pure hemorrhage, in other cases there was a delay in evolution between stages. Of the four

patients who were examined serially, three had a lesion or lesions that exhibited delayed evolution. The most dramatic example (Fig. 5) occurred in a patient who was followed over several months before treatment was begun for her hemorrhagic supratentorial colon metastases, which developed after resection of three hemorrhagic posterior fossa metastases. On the initial scan the lesion was hypointense on both short and long TR sequences, corresponding to a stage-1 lesion. One month later the lesion was still hypointense on both short and long TR sequences, in contrast to what one would expect to see in a pure hemorrhage. Two months after the initial examination, however, the lesion began to develop some hyperintensity.

Another significant difference in the appearance of hemorrhagic neoplasms is seen in stage-2 lesions. While in pure subacute intraparenchymal hemorrhage the hyperintensity



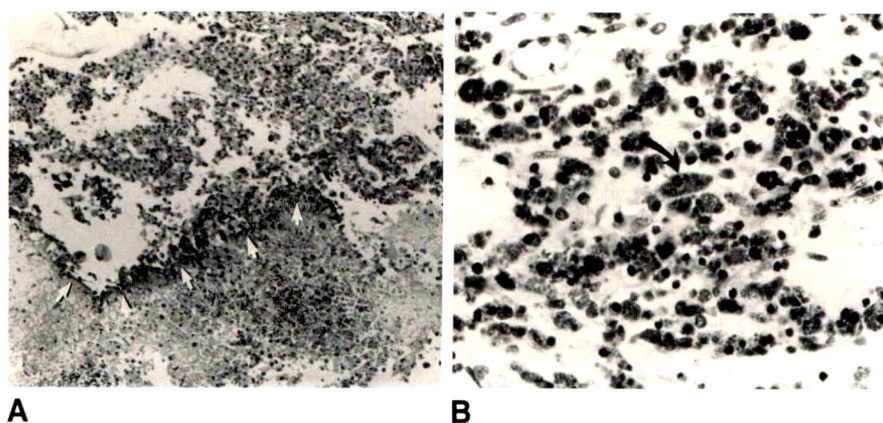


Fig. 6.—A and B, Renal cell metastasis; hemosiderin. Histologic section, obtained from patient whose CT and MR scans are seen in Fig. 3, shows rim of hemosiderin-laden macrophages at low power (small arrows) (A) and hemosiderin granules within a macrophage at high power (curved arrow) (B).

TABLE 2: Histologically Proved Melanomas

Case No.	Age	Gender	Metastases	Stage	Melanin	Hemosiderin	Signal Intensity	
							Short TR	Long TR
1	49	F	3	1	+	—	↓	↓↓
2	50	F	1	1	+	—	↓	↓↓
3	45	M	1	3	+	+	↑↑	↑↑*
4	61	M	2	3	—	+	↑↑	↑↑*
5	54	M	1	3	—	+	↑↑	↑↑*
6	65	M	1	M (1,2)	+	—	M	M
7	35	M	1	M (1,2,3)	+	+	M	M*

Note.—↓ = mildly hypointense, ↓↓ = markedly hypointense, ↑↑ = markedly hyperintense, * = black rim, M = mixed appearance.

is, it was not possible to distinguish between them in the presence of hemorrhage.

We also examined the stage-2, stage-3, and mixed lesions with respect to whether tumor tissue itself was visible within the lesions, and whether this was helpful in differentiating hemorrhagic neoplasms from pure hemorrhage. In 10 of the patients, there were areas within the lesions that were either isointense or slightly hypointense on the short TR images, and hyperintense on long TR images. These signal-intensity differences appeared to correlate with either nonhemorrhagic cystic areas or tumor nodularity within the hemorrhage. By definition, the stage-1 lesions were excluded because they did not contain any hyperintense areas.

Finally, the amount of edema surrounding the lesions in our patients varied. In general, the presence of edema was not helpful in differentiating hemorrhagic neoplasms from pure hemorrhage. In six of our patients, however, the amount of edema was so significant that it made the presence of underlying neoplasm more likely. In the remaining patients, we felt that the small to moderate amount of edema did not allow us to make this distinction.

Discussion

The incidence of intracranial hemorrhage resulting from neoplasm has been reported to range from 1–14% depending

on the series [16–19]. Factors that affect the incidence include the source of the clinical information (surgery vs autopsy), the type of neoplasm (primary vs secondary), and whether the patient is symptomatic [16]. Of the primary intracranial neoplasms, hemorrhage occurs most frequently in relation to pituitary neoplasms [17, 19]. Other primary tumors that have been reported to bleed include glioblastoma multiforme, lower-grade gliomas, ependymomas, choroid plexus papillomas, sarcomas, and meningiomas. The incidence of hemorrhage in metastatic neoplasms is highest in melanoma, hypernephroma, bronchogenic carcinoma, and choriocarcinoma [16, 18, 19]. Other metastatic tumors that bleed are breast and thyroid.

Delayed evolution of hemorrhage within a hemorrhagic neoplasm on MR has been reported [12]. The authors noted a delay of 16 days from the hypointensity associated with acute hemorrhage to the hyperintensity associated with the formation of free methemoglobin. We have noted even longer delays, up to several months. The etiology of this delay is unclear. Methemoglobin formation is maximal at relatively low oxygen tensions, about 20–25 mm [20, 21]. Since oxygen is necessary for the formation of the agents responsible for the oxidation of deoxyhemoglobin to methemoglobin, and oxygen limits the concentration of deoxyhemoglobin available for oxidation to methemoglobin, the formation of methemoglobin

is negligible at zero and at high oxygen tensions. At 20–25 mm, there is enough oxygen to allow formation of the reducing agents, yet not enough to limit the concentration of deoxy-hemoglobin. Therefore, the relative hypoxia within tumors [22] should favor, rather than delay, the formation of methemoglobin. Perhaps a more likely explanation for the delay in evolution is the continued oozing of blood from the lesion and/or the rapid absorption of hemoglobin breakdown products by a very vascular tumor.

Since methemoglobin formation is maximal at relatively low oxygen tensions, this would appear to be the most reasonable explanation for the central hyperintensity commonly seen in our stage-2 hemorrhagic neoplasms. This is not surprising in view of the lower oxygen tension of tumors compared with normal tissue, particularly at the center of the neoplasm [22]. It also follows that in a pure hematoma, where the center has very low oxygen tension, thus inhibiting the formation of the reducing agents necessary for the oxidation of deoxyhemoglobin to methemoglobin, the formation of methemoglobin initially occurs at the periphery. In a few of our cases there were areas of hyperintensity on the short TR images that became hypointense on the long TR images (Fig. 2). This most likely represents the shortening of the T1 relaxation time by methemoglobin, and a magnetic susceptibility effect of intracellular hemoglobin breakdown products on the T2 relaxation time.

In addition to central methemoglobin formation, central hyperintensity in our hemorrhagic neoplasms also appeared to be due, in some cases, to actual visualization of tumor tissue. This could be differentiated from methemoglobin changes because the hyperintensity associated with nonhemorrhagic tumor tissue was visible only on the long TR images. The presence of nonhemorrhagic tumor foci, combined with the frequent central hyperintensity due to methemoglobin on both the short TR and long TR images, proved virtually diagnostic of hemorrhagic neoplasm.

On pathologic examination, all six of the lesions exhibiting mixed signal intensity on MR contained hemorrhage in different stages of evolution. There was a direct correlation between the pathologic and MR findings. Therefore, we believe that the mixed-intensity pattern is consistent with recurrent bleeding within the tumor.

In a report of the MR appearance of hemorrhagic neoplasms [12], the authors stated that the hemosiderin rim was absent, diminished, or irregular. Our findings were slightly different. In 10 of 11 patients with stage-3 lesions (eight of them with pathologic confirmation) the hemosiderin rim, although diminished and not as prominent as in a pure bleed, completely surrounded the hemorrhage. Whether this is a function of the size of the hemorrhage is not clear, but it is important not to exclude an underlying neoplasm if a complete rim of hemosiderin is present.

All the patients with metastatic melanoma had findings consistent with hemorrhage on MR. Although the presence or absence of melanin could not be determined on the basis of the MR appearance, the stage of evolution of the hemorrhage was correctly predicted on the basis of the MR appearance of the lesions. Therefore, it would appear that

hemorrhage exerts a stronger influence on the signal characteristics than melanin. Our findings concur with a prior report [13] in which the authors found differences in the signal-intensity patterns of nonhemorrhagic melanotic melanoma, nonhemorrhagic amelanotic melanoma, and hemorrhagic melanoma, but that hemorrhagic amelanotic melanoma and hemorrhagic melanotic melanoma exhibited similar signal-intensity characteristics.

Obviously, the presence of a hemorrhage in an area not usually associated with trauma or hypertension should suggest an underlying tumor as one of the possible causes. However, tumors can also occur in locations that are more often associated with trauma or hypertension. In our study of hemorrhagic neoplasms we found certain patterns or characteristics on MR that should help the diagnostician determine the cause of a hemorrhage in any location. An underlying neoplasm should be suspected in any hemorrhage that evolves slowly, develops central or eccentric hyperintensity as it evolves, or exhibits a mixed-signal-intensity pattern. In addition, we emphasize the importance of not excluding the possibility of underlying neoplasm if the hemorrhage develops a hemosiderin rim.

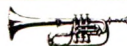
ACKNOWLEDGMENT

We are grateful to Patricia Dudley for her help in the preparation of this manuscript.

REFERENCES

1. Dooms GC, Uske A, Brant-Zawadzki M, et al. Spin-echo MR imaging of intracranial hemorrhage. *Neuroradiology* 1986;28:132–138
2. Di Chiro G, Brooks RA, Girton ME, et al. Sequential MR studies of intracerebral hematomas in monkeys. *AJNR* 1986;7:193–199
3. Sipponen JT, Sepponen RE, Sivula A. Nuclear magnetic resonance (NMR) imaging of intracerebral hemorrhage in the acute and resolving phases. *J Comput Assist Tomogr* 1983;7:954–959
4. Zimmerman RA, Bilaniuk LT, Grossman RI, et al. Resistive NMR of intracranial hematomas. *Neuroradiology* 1985;27:16–20
5. Swensen SJ, Keller PL, Berquist TH, McLeod RA, Stephens DH. Magnetic resonance imaging of hemorrhage. *AJR* 1985;145:921–927
6. Edelman RR, Johnson K, Buxton R, et al. MR of hemorrhage: a new approach. *AJNR* 1986;7:751–756
7. Cohen MD, McGuire W, Cory DA, Smith JA. MR appearance of blood and blood products: an in vitro study. *AJR* 1986;146:1293–1297
8. Bradley WG, Schmidt PG. Effect of methemoglobin formation on the MR appearance of subarachnoid hemorrhage. *Radiology* 1985;156:99–103
9. Gomori JM, Grossman RI, Goldberg HI, Zimmerman RA, Bilaniuk LT. Intracranial hematomas: imaging by high-field MR. *Radiology* 1985;157:87–93
10. Hecht-Leavitt C, Gomori JM, Grossman RI, et al. High-field MRI of hemorrhagic cortical infarction. *AJNR* 1986;7:581–585
11. DeLaPaz RL, New PFJ, Buonanno FS, et al. NMR imaging of intracranial hemorrhage. *J Comput Assist Tomogr* 1984;8:599–607
12. Atlas SW, Grossman RI, Gomori JM, et al. Hemorrhagic intracranial malignant neoplasms: spin-echo MR imaging. *Radiology* 1987;164:71–77
13. Atlas SW, Grossman RI, Gomori JM, et al. MR imaging of intracranial metastatic melanoma. *J Comput Assist Tomogr* 1987;11:577–583
14. Woodruff WW, Djang WT, McLendon RE, Heinz ER, Voorhees DR. Intracerebral malignant melanoma: high-field-strength MR imaging. *Radiology* 1987;165:209–213
15. Sze G, Krol G, Olsen WL, et al. Hemorrhagic neoplasms: MR mimics of

- occult vascular malformations. *AJNR* **1987**;8:795-802
16. Mandybur TI. Intracranial hemorrhage caused by metastatic tumors. *Neurology* **1977**;27:650-655
 17. Weisberg LA. Hemorrhagic primary intracranial neoplasms: clinical-computed tomographic correlations. *Comput Radiol* **1986**;10:131-136
 18. Weisberg LA. Hemorrhagic metastatic intracranial neoplasms: Clinical-computed tomographic correlations. *Comput Radiol* **1985**;9:105-114
 19. Wakai S, Yamakawa K, Manaka S, Takakura K. Spontaneous intracranial hemorrhage caused by brain tumor: its incidence and clinical significance. *Neurosurgery* **1982**;10:437-444
 20. Bodansky O. Methemoglobinemia and methemoglobin-producing compounds. *Pharmacol Rev* **1951**;3:144-196
 21. Neill JM, Hastings AB. The influence of the tension of molecular oxygen upon certain oxidations of hemoglobin. *J Biol Chem* **1925**;63:479-492
 22. Gatenby RA, Coia LR, Richter MP, et al. Oxygen tension in human tumors: in vivo mapping using CT-guided probes. *Radiology* **1985**;156:211-214



Scientific Program (200 papers)

Instructional Courses (60 hours)

Categorical Course on
Genitourinary Radiology

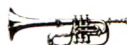
The Caldwell Lecture

Award Papers

Scientific Exhibits

Social, Golf, and Tennis Programs

Guest Programs



Come to the American Roentgen Ray Society

89th

ANNUAL MEETING



New Orleans Hilton

May 7-12, 1989

High-Resolution MR Imaging of Pituitary Microadenomas at 1.5 T: Experience with Cushing Disease

Wallace W. Peck¹
William P. Dillon¹
David Norman¹
T. H. Newton¹
Charles B. Wilson²

The MR images of 27 patients with clinically and biochemically suspected Cushing disease were evaluated retrospectively in a blinded fashion. The MR interpretation was compared with detailed operative diagrams and operative and pathologic reports. The examinations were performed on a 1.5-T MR system with thin-section sagittal and coronal T1-weighted (short TR/TE) images. Each pituitary half was considered separately (54 "halves"). Twenty-one pituitary halves were considered to have glandular abnormalities on MR. Compared with surgical findings, 17 MR findings were true positives and four were false positives (one pars intermedia cyst, three normal tissue). Of the 33 pituitary halves considered normal on MR, 26 were true negatives and seven were false negatives. MR had an overall sensitivity of 71% and a specificity of 87% for these adrenocorticotrophic hormone (ACTH)-secreting pituitary adenomas. A focal glandular hypointensity identified on coronal images was the most sensitive predictor of adenoma location. Sagittal images were not useful in either detection or localization. Upward convexity of the gland and deviation of the stalk were less useful indicators. Abnormalities of the sellar floor were the least reliable.

In comparison with the capabilities of CT detection of microadenomas described in the current literature, it appears that high-field thin-section MR of the sella is the most sensitive imaging method for preoperative localization of ACTH-secreting adenomas in patients with Cushing disease.

Cushing syndrome is characterized by hypercortisolism leading to typical clinical features including, but not limited to, obesity, hypertension, hirsutism, ecchymoses, menstrual irregularities, cutaneous striae, acne, and fatigue. Cushing disease is characterized by hypersecretion of adrenocorticotrophic hormone (ACTH) by the pituitary gland with secondary bilateral adrenal cortical hyperplasia [1]. Pituitary adenomas are estimated to be present in 60–96% of these patients [2–4]. As a rule these adenomas are 10 mm in diameter or smaller (microadenomas) [3, 4]. Previous studies that used thin-section contrast-enhanced CT of the sella for preoperative localization of these tumors have reported disappointing results [5–10]. The value of MR imaging in the evaluation of sellar and parasellar diseases has recently been emphasized [11–15]. Our purpose was to determine the sensitivity and specificity of thin-section high-field MR in Cushing disease.

Materials and Methods

Twenty-seven patients with a clinical diagnosis of Cushing disease were evaluated preoperatively with MR examination of the sella from January 1985 to March 1987. The diagnosis of Cushing disease was established before MR examination by (1) an abnormal response to the dexamethasone suppression test [3, 4] as reflected in nonsuppressibility of steroids in plasma and/or urine by the administration of low-dose dexamethasone, or some suppressability with high-dose dexamethasone, and (2) normal or slightly elevated plasma levels of ACTH as determined by immunoassay techniques in the presence of hypercortisolism. All patients had transsphenoidal surgery, performed by a single neurosurgeon, subsequent to MR examination. When abnormal tissue was evident at the surface of the normal anterior

This article appears in the November/December 1988 issue of *AJNR* and the January 1989 issue of *AJR*.

Received February 17, 1988; accepted after revision June 16, 1988.

¹ Department of Radiology, University of California, San Francisco, 505 Parnassus Ave., San Francisco, CA 94143. Address reprint requests to W. P. Dillon.

² Department of Neurosurgery, University of California, San Francisco, San Francisco, CA 94143.

AJR 152:145–151, January 1989

0361–803X/89/1521–0145

© American Roentgen Ray Society

lobe, this tissue was selectively resected and the tumor bed cauterized with an absorbable gelatin sponge (Gelfoam) soaked in absolute alcohol. When no tumor was evident by direct inspection, the pituitary was explored with a series of horizontal and vertical incisions. When the tumor was located, the margins of the incision were separated, abnormal tissue was resected, and the cavity was cauterized with absolute alcohol. When the margin between adenoma and the adjacent pituitary gland was sharp and distinct, no normal pituitary tissue was removed. When the preoperative MR study correctly localized the tumor, the surgeon would not routinely examine the remaining pituitary tissue, as the incidence of simultaneous pituitary neoplasms is extremely small. When surgical exploration of the pituitary gland revealed no abnormal tissue (nine patients), a total hypophysectomy (six patients) or biopsy (three patients) was performed. All specimens were subject to pathologic review. Adenomas demonstrated a homogeneous cell population and stained selectively for ACTH with immunohistologic techniques. If an adenoma could not be identified, reticulin stains were used to rule out pituitary hyperplasia.

MR images were obtained with a 1.5-T system.* T1-weighted 3-mm-thick sagittal and coronal spin-echo images, 600/20/4 (TR/TE/excitations), were obtained by using a 20-cm field of view, a 256 × 256 matrix, and an interslice gap of 0.3 mm (10%). Five patients had preoperative contrast-enhanced CT and six patients had an inferior petrosal sinus sampling.

The scans were retrospectively reviewed in consensus by four neuroradiologists who were aware that the patients had a diagnosis of Cushing disease with subsequent transsphenoidal surgery. The results of surgery, pathologic examination, and contrast-enhanced CT or venous sampling were not known at the time of the review. The presence or absence of an abnormality was determined for the left and right halves of each pituitary gland. Thus, 54 pituitary halves were evaluated in 27 patients. The MR image was considered positive only if the pituitary gland contained a focal area of low signal and/or focal enlargement. The size of the adenoma, position of the stalk, sloping of the sellar floor, and possible involvement of the cavernous sinus were also recorded. The surgical and pathologic reports were reviewed and correlated with the MR findings. Because a positive or negative score was recorded for each half of the pituitary gland, sensitivity and specificity were calculated. For example, if the consensus was that an adenoma was present on the left, but one was found on the right, then the result of the left side was a false positive and on the right side a false negative.

Results

The group of 27 patients comprised 21 females and six males with a mean age of 35 years (range, 14–56 years). Adenomas were pathologically confirmed in 24 patients (89%) (Table 1). Neither a discrete adenoma nor pituitary hyperplasia was identified in the remaining three patients (two total hypophysectomies, one biopsy). A "white, watery" lesion ranging from 1.5 to 10 mm in diameter (mean, 5 mm) typical of an ACTH-producing adenoma was resected and confirmed pathologically in 18 patients. Six (mean age, 46) of nine patients who had negative explorations had total hypophysectomies. Small (1–2 mm) adenomas were found on histologic analysis in four of these six patients. The remaining two glands were normal. Pituitary glands in the three remaining negative explorations (mean age, 20) were biopsied. In two of the three

TABLE 1: Surgical Results in Patients with Cushing Disease

Finding	No. of Patients (n = 27)
Pathologically proved adenoma	24
Adenoma found at surgery	18
Negative exploration:	
Total hypophysectomy:	
Adenoma	4
Normal	2
Subtotal	6
Biopsy:	
Adenoma	2
Normal	1
Subtotal	3
Total	9

TABLE 2: MR and Surgical Correlation in 27 Patients with Cushing Disease

MR Finding: Surgical Determination	No. of Pituitary Halves
Abnormal (19 patients):	
Adenoma:	
Hypointense	14
Isointense	3
Subtotal (true positive)	17
Pars intermedia cyst	1
Normal	3
Subtotal (false positive)	4
Total	21
Normal (25 patients):	
Normal (true negative)	26
Adenoma (false negative)	7
Total	33

Note.—Sensitivity = true positive/(true positive + false negative) = 17/(17 + 7) = 71%; specificity = true negative/(true negative + false positive) = 26/(26 + 4) = 87%.

TABLE 3: MR Observations in Surgically Verified Cushing Adenoma

Finding	
Mean size (range) of adenoma (in mm):	
MR	6.0 (3.0–10)
Surgery	4.6 (1.5–10)
Stalk deviation:	
Contralateral	12
Midline	8
Ipsilateral	4
Sloped sellar floor:	
Ipsilateral	5
Straight	15
Contralateral	4
Cavernous invasion on MR:	
False negative	4
False positive	1

* General Electric, Milwaukee, WI.

patients, the biopsies were in areas considered to be abnormal on the MR image. On histologic examination an adenoma was identified in both patients. In the third patient (normal MR image), a discolored area within the pituitary gland was biopsied but was histologically normal. These data are summarized in Table 1.

The MR results are summarized and correlated with surgical findings in Table 2. Table 3 summarizes some secondary MR observations. Twenty-one pituitary halves exhibited focal abnormalities on MR images in 19 patients (in two patients focal lesions were identified on each side of the gland) on the coronal images (Tables 2 and 3). The sagittal images were much less useful in detecting abnormalities. Seventeen (81%) of these twenty-one focal abnormalities (14 hypointense and three isointense on MR) were adenomas (Figs. 1–3), one (low intensity) was a pars intermedia cyst, and three (14%) (two

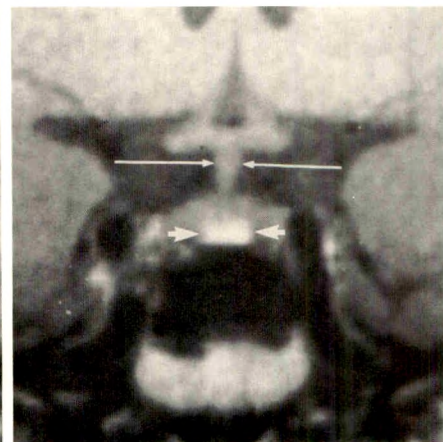
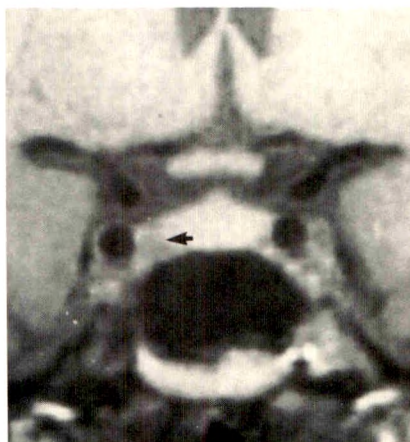
isointense, one hypointense) were normal (Figs. 4 and 5). No signal intensity or morphologic differences were noted among these lesions on T1-weighted studies. Since T2-weighted sequences were not routinely obtained, we do not know if these lesions could have been differentiated further. These results were expressed as 17 (81%) true positives and four (19%) false positives. Thirty-three pituitary halves were considered normal: 16 were from the eight patients with completely normal studies and 17 from the patients considered to have a focal lesion on the contralateral side (Table 2). At surgery and/or pathology, seven (21%) of these 33 halves contained adenomas (seven false negatives) ranging from 1.5 to 6 mm in diameter (mean, 3.5 mm) (Figs. 5 and 6). The remaining 26 halves were all true negatives (Fig. 7). The overall sensitivity of MR in detecting ACTH-secreting adenomas was 71% and the specificity was 87%.

Fig. 1.—17-year-old woman with Cushing disease. T1-weighted coronal images, 600/20.

A, Right-sided 4-mm low signal intensity abuts medial dural reflection of cavernous sinus (arrow). Left half of gland is normal.

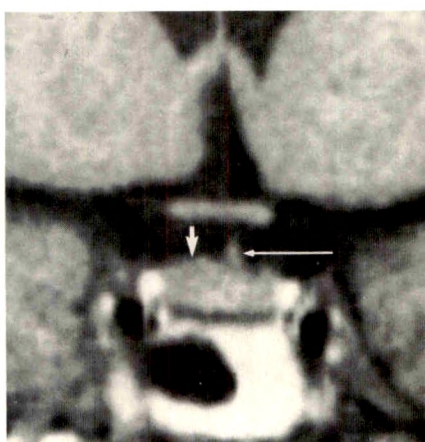
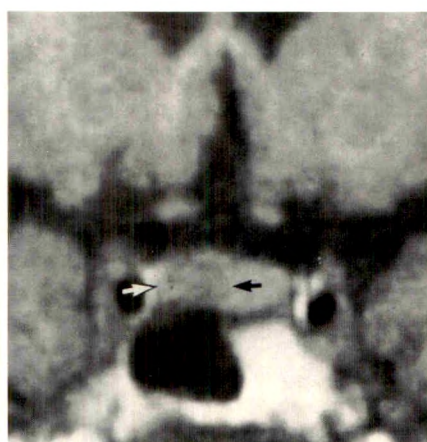
B, More posterior cut. Pituitary stalk is midline (long arrows). High signal intensity (short arrows) of posterior pituitary is a normal finding.

At surgery, low-intensity focus corresponded to 3-mm right-sided ACTH-secreting adenoma (right half = true positive; left half = true negative).



A

B



A

B

Fig. 2.—A and B, 29-year-old woman with Cushing disease. T1-weighted coronal images, 600/20, show right-sided 9-mm hypointense adenoma (short arrows) with slight upward convexity of pituitary gland. B (3 mm posterior to A) also shows slight leftward shift of pituitary stalk (long arrow). At surgery, low-intensity focus corresponded to 8-mm right-sided ACTH-secreting adenoma. (Right half = true positive; left half = true negative.)

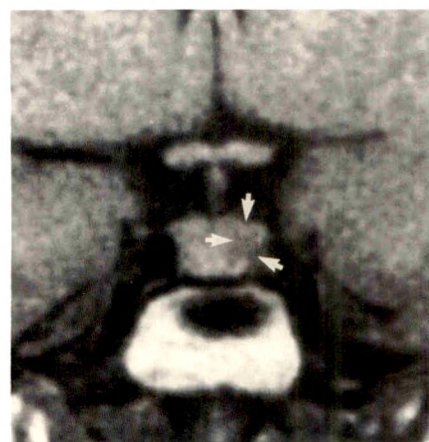


Fig. 3.—30-year-old woman with Cushing disease. T1-weighted coronal image, 600/20, shows poorly margined left-sided hypointensity measuring 8 mm in diameter (arrows) with normal midline stalk. At surgery, low-intensity focus corresponded to left-sided 5-mm ACTH-secreting adenoma. (Left half = true positive; right half = true negative.)

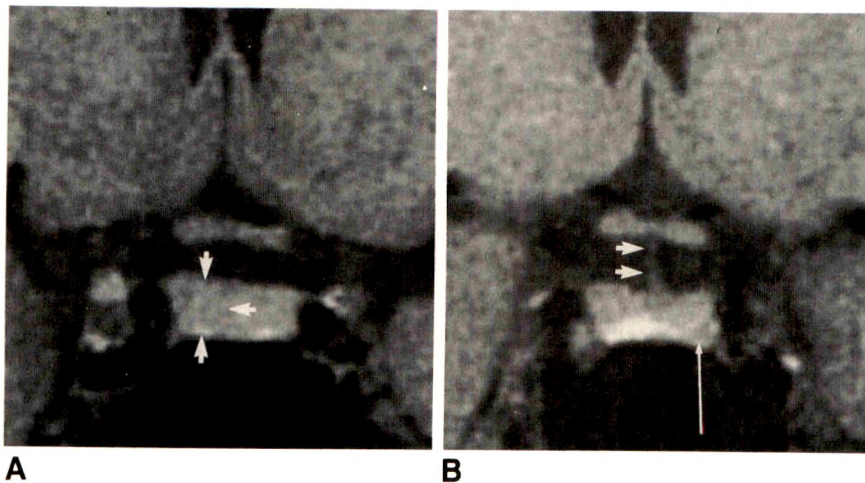


Fig. 4.—27-year-old woman with Cushing disease. T1-weighted coronal images, 600/20.

A, Poorly defined right-sided 5-mm low-intensity area with slight upward convexity of pituitary gland (arrows).

B, Adjacent posterior section shows 3-mm focus of low signal in left posterolateral wing adjacent to medial dural reflection of cavernous sinus (long arrow). Pituitary stalk is shifted slightly to left (short arrows).

At surgery, 3-mm right-sided adenoma was identified corresponding to low-intensity lesion seen on MR. Left side was normal. (Right half = true positive; left half = false positive.)

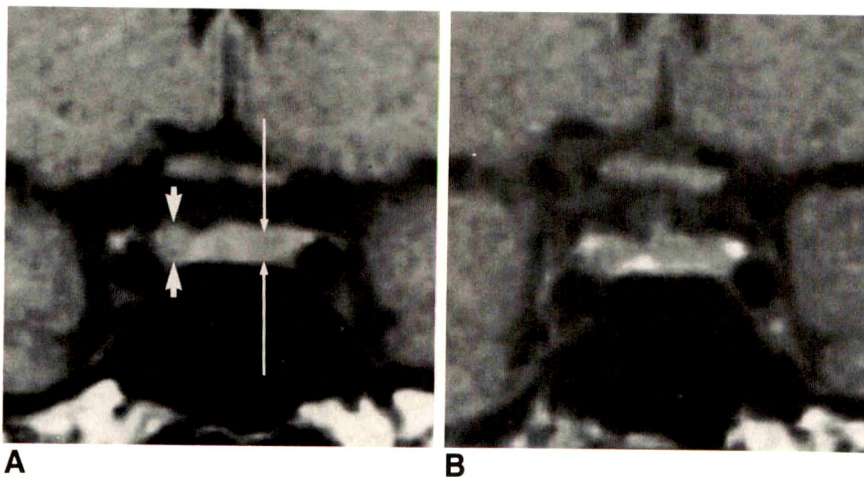


Fig. 5.—A and B, 38-year-old woman with Cushing disease. T1-weighted coronal images, 600/20. Well-defined prospectively identified 4-mm focus of low signal in right lateral wing, adjacent to medial dural reflection of cavernous sinus (short arrows). Less well defined 5-mm region of low signal on left (long arrows) not identified prospectively. Stalk is midline. At surgery, right side was normal, and 6-mm ACTH-secreting adenoma was found in left lateral wing, corresponding to low intensity identified (long arrows). (Right half = false positive; left half = false negative.)

MR tended to overestimate the size of the adenomas as compared with the surgically reported size (Table 3). The average size of the 17 adenomas seen on MR was 6 mm (range, 3–10 mm), whereas the mean reported size at surgery was 4.6 mm (range, 1.5–10 mm). The reason for this discrepancy is uncertain. In the data analysis, the adenomas missed at surgery were all assumed to be smaller than 2 mm.

Secondary findings of mass effect supported the diagnosis in some of the 24 cases of adenoma: The sellar floor sloped ipsilateral to the adenoma in five patients, sloped contralateral to the adenoma in four patients, and was straight in 15 patients. Erosion of the lamina dura could not be identified on MR. The stalk was deviated away from the adenoma in 12 patients (50%), was deviated toward the adenoma in four patients, and was midline in eight patients (Table 3). In two of the three adenomas that were isointense, the stalk was deviated away from the adenoma. In two patients suspicious lesions were identified in both halves of their glands. Stalk deviation to the contralateral side correctly identified the side of the adenoma in both these patients. However, surgical confirmation of the second abnormality was not obtained, because once an adenoma is encountered, the remaining gland is not routinely explored owing to the rarity of simulta-

neous microadenomas. Follow-up prolactin levels diminished to normal in these two patients, and we presume only a single adenoma was present.

Cavernous sinus involvement was suspected in only one patient in whom a small amount of soft tissue of intermediate intensity was found adjacent to the intracavernous carotid artery. This soft tissue was directly contiguous with a focal low-intensity abnormality in the pituitary. At surgery, this side was normal; the adenoma (without cavernous invasion) was found on the contralateral side. In four patients, it was determined at surgery that the adenoma was adherent to the medial dural reflection of the cavernous sinus (Table 3). Total resection of the tumor was possible in only two of these patients. This had not been suspected prospectively, and in retrospect there were no findings to suggest possible invasion.

Sampling of the inferior petrosal sinuses correctly predicted tumor location in five of six patients. In one patient, ACTH levels were slightly higher on the normal side. Thin-section, high-resolution contrast-enhanced CT yielded three true positives, one false negative, and one true negative. The MR findings in these five patients were four true positives and one true negative.

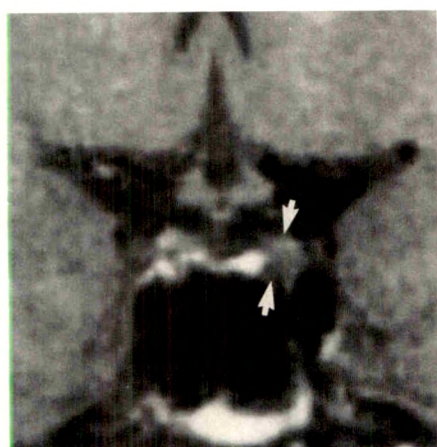


Fig. 6.—32-year-old woman 2 years after transsphenoidal surgery for Cushing disease. Persistent symptoms initiated reevaluation. T1-weighted coronal image, 600/20, was prospectively called normal with a midline stalk. In retrospect, there is a well-defined 4-mm low-intensity focus on left adjacent to cavernous sinus (arrows). Preoperative inferior petrosal sinus sampling showed abnormal ACTH elevation on left. At surgery, low-intensity focus corresponded to 4-mm left-sided ACTH-secreting adenoma. (Right half = true negative; left half = false negative.)

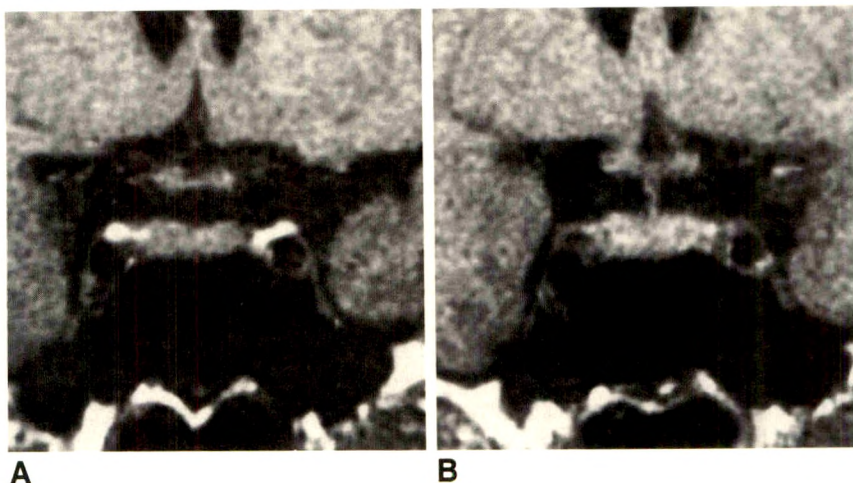


Fig. 7.—A and B, 41-year-old man with Cushing disease. T1-weighted coronal images, 600/20. Normal anterior lobe. Stalk is midline. Total hypophysectomy was performed after negative exploration. At final pathology, only normal pituitary gland was identified. (Left half = true negative; right half = true negative.)

Discussion

Pituitary adenomas constitute approximately 10% of all symptomatic brain tumors [16]. They may be classified as nonsecreting or secreting. The former are always macroadenomas and cause signs or symptoms secondary to either local mass effect or pituitary secretory failure. Secretory adenomas typically are smaller and usually have one of three clinical features: (1) acromegaly (growth hormone-secreting adenomas), (2) amenorrhea and/or galactorrhea in women or decreased libido in men (prolactinomas), or (3) Cushing syndrome (ACTH-secreting adenomas).

Hypersecretion of ACTH in Cushing syndrome originates either in the pituitary (Cushing disease) or in an ectopic ACTH-secreting tumor. ACTH secretion from a pituitary adenoma usually is not suppressed by small doses of dexamethasone but is suppressed by large doses of dexamethasone. By contrast, ACTH secretion from ectopic ACTH-producing tumors usually is autonomous and should lack inhibitory control by plasma cortisol. In one clinical series, however, a large dose of dexamethasone did produce suppression in 19% of patients with ectopic ACTH-producing tumors [17].

Pituitary adenomas (predominantly microadenomas) are reported in 60–96% of patients with Cushing disease [2–4]. Abnormal hypothalamic-pituitary function may be responsible for the hypersecretion of ACTH in the remainder of patients [18, 19]. Transsphenoidal resection of the adenoma currently is believed to be the therapeutic procedure of choice [4, 17]. The fact that most but not all patients with a positive dexamethasone suppression test have a pituitary tumor and that the hypothalamus may be the source of hypersecretion justifies

the need for an imaging technique that accurately localizes a lesion within the sella.

The sensitivity of CT in detecting pituitary adenomas is influenced by the size of the tumor, the quality of equipment, the imaging technique, the amount of iodinated contrast material, and the method of contrast administration. Although somewhat variable, routine rapid-drip-infusion contrast-enhanced CT studies generally demonstrate microadenomas as being lower in density and macroadenomas as being higher in density than the adjacent pituitary gland. The sensitivity of CT in detecting macroadenomas is reported to be as high as 100% [20]. Microadenomas (tumors 10 mm in diameter or smaller) traditionally have been more difficult to detect. This was especially true for lesions smaller than 5 mm [6]. With high-resolution CT, Marcovitz et al. [20, 21] recently reported a sensitivity of 81.2% for growth-hormone microadenomas and a sensitivity of 91.9% for prolactin microadenomas. The vast majority of the growth-hormone microadenomas were larger than 5 mm, whereas the prolactin microadenomas had a broader range of sizes with equal numbers being larger and smaller than 5 mm. The literature would suggest that prolactinomas in general are easier to detect on CT than are most adenomas [22]. False-positive rates vary from 25 to 50% for microadenomas [6, 22]. Focal low densities that can simulate a pituitary microadenoma include pars intermedia cysts or high-spatial-frequency artifacts [23].

About 73–88% of ACTH-secreting tumors are microadenomas [3, 10]. Cushing adenomas traditionally have been very difficult to detect with CT. This may relate to the contrast enhancement characteristics of the tumor. In a series of 14 patients with Cushing disease, Teasdale et al. [6] reported

detection by CT in eight (57%) of 14 patients. A recent investigation of 50 patients with surgically verified Cushing adenomas reported an overall 30% sensitivity with high-resolution thin-section contrast-enhanced CT, but only a 17% sensitivity in the 42 patients with microadenomas [9]. Marcovitz et al. [10] recently reported a sensitivity of 63% and specificity of 62.5% for ACTH-secreting adenomas with direct coronal enhanced CT. However, they reported a sensitivity of only 58% for microadenomas. In our series, all lesions found at surgery were less than 10 mm in diameter.

Early reports indicated a poor sensitivity for MR in the detection of pituitary adenomas [5–10]. Images were acquired early in the evolution of MR instruments. Quality was limited by thick sections (greater than 5 mm), lower field strength, and suboptimal signal-to-noise. More recent studies have shown that microadenomas can be detected with MR [14, 15, 24–26]. Kulkarni et al. [26] recently reported a sensitivity of 83% for MR in detecting microadenomas at 1.5 T. This compared with a sensitivity of 42% for CT. In that particular study, only eight of the 37 patients had surgical confirmation via transsphenoidal surgery. On short TR/TE images (T1-weighted), most microadenomas are of low signal relative to that of the normal gland. On long TR/TE images (T2-weighted), the pattern is more variable, with an approximately equal distribution of hypo-, iso-, and hyperintense adenomas being identified relative to the normal pituitary gland [14]. In addition, our experience suggests that T2-weighted images rarely add any practical information to the T1-weighted studies, yet they take considerably longer to acquire. These findings have led to a recommendation we support that T1-weighted images alone be used for the routine evaluation of pituitary adenomas [24], reserving T2-weighted sequences for postoperative patients or those infrequent cases in which a suspected tumor cannot be detected on T1-weighted images alone.

Dwyer et al. [15] recently reported the findings on contrast-enhanced MR and CT in 12 patients with proved Cushing disease. They used a 0.5-T MR imager with 5-mm-thick contiguous slices and compared it with high-resolution, direct coronal CT with 3-mm slices overlapping 1 mm. Short TR images identified eight (67%) adenomas before enhancement and 10 (83%) after gadolinium-DTPA enhancement; contrast-enhanced CT detected four (33%) of the adenomas. Eight (67%) of these were microadenomas, comparing favorably with the sensitivity of 71% noted in our series.

In our series, MR tended to overestimate the surgically reported size of pituitary microadenomas (Fig. 4). In one patient this discrepancy was explained by hypointense scar tissue (resulting from previous transsphenoidal surgery) with a 2-mm microadenoma embedded within it. The explanation for the discrepancy in the remainder of the cases is less certain, but it may have been due in part to a lack of well-defined margins on MR, to peritumoral edema, or to an underestimation of the size of the tumor by the neurosurgeon.

Secondary signs of mass effect were not as helpful as focal-intensity changes within the pituitary gland (Figs. 1, 3, 6, and 7; Table 4). Changes in the floor of the sella are of little value in predicting the site of an adenoma [22]. Sloping of the sellar floor had no correlation with the location of the tumor.

Pituitary stalk deviation has been shown to be of little value for localizing adenomas [6, 22, 27, 28]. However, a recent MR study suggested that the presence of such deviation was helpful to confirm focal glandular abnormalities [14]. In our series, the pituitary stalk was displaced from its normal midline position in 16 patients. In 12 of these 16 patients the displacement of the stalk correctly predicted the side of the adenoma (Fig. 2). Although we agree with Kucharczyk et al. [14] that deviation of the stalk increases the confidence level, it should be discounted in the presence of a clear focal hypointensity on the side ipsilateral to the deviated stalk (Figs. 1 and 3). Stalk deviation proved very useful in localizing the adenoma in the patients in whom the adenomas were isointense or in whom pituitary MR abnormalities were bilateral (Fig. 4).

The predictability of cavernous sinus invasion with the use of MR is poor [29]. One patient in whom involvement of the cavernous sinus was suspected on MR proved to have no such invasion at surgery. In four other patients with surgically proved invasion of the cavernous sinus, no indication of such involvement was seen on MR. MR's poor sensitivity in the detection of cavernous sinus invasion most likely is due to an inability to visualize the very thin medial dural reflection of the cavernous sinus [29].

Our study was performed on a highly selected group of patients. The sensitivity and specificity of MR in the diagnosis of ACTH-secreting microadenomas may be overstated. The patients' preliminary diagnoses of Cushing disease were supported by clinical evaluations and hormonal assays. The probability of an adenoma was high. Although the patient population was skewed, our retrospective review is a realistic representation of the clinical situation at the time MR imaging is required. However, since 10–20% of patients examined at autopsy have asymptomatic adenomas [30] and 10–20% may have benign pituitary cysts [23], a prospective MR study is necessary to evaluate the appearance of the "normal" gland and to determine the true incidence of false-positive studies.

When our review is compared with the CT series cited herein, high-field, thin-section MR appears to be the preferable imaging method in the evaluation of patients with suspected Cushing disease. The technique has the added advantages of no contrast material and no radiation exposure. The radiologic diagnosis rests on the finding of a focal hypointensity or an isointense focal bulge within the pituitary gland on short TR images. Stalk displacement may support the diagnosis, but in the presence of a focal low intensity it should not be used to support a diagnosis of a lesion contralateral to the focal low-signal-intensity region. Gd-DTPA may prove useful in further increasing sensitivity [15]. Inferior petrosal sinus ACTH sampling should be reserved for patients with small or recurrent adenomas that cannot be accurately or confidently localized with planar imaging techniques.

REFERENCES

1. Gold EM. The Cushing syndromes: changing views of diagnosis and treatment. *Ann Intern Med* 1979;90:829–844
2. Robert F, Pelletier G, Hardy J. Pituitary adenomas in Cushing's disease. A histologic, ultrastructural, and immunochemical study. *Arch Pathol Lab Med* 1978;102:448–455
3. Boggan JE, Tyrrell JB, Wilson CB. Transsphenoidal microsurgical manage-

- ment of Cushing's disease. Report of 100 cases. *J Neurosurg* 1983;59:195-200
4. Tyrrell JB, Brooks RM, Fitzgerald PA, Cofoid PB, Forsham PH, Wilson CB. Cushing's disease. Selective transsphenoidal resection of pituitary microadenomas. *N Engl J Med* 1978;298:753-758
 5. Pojunas KW, Daniels DL, Williams AL, Thorsen MK, Haughton VM. Pituitary and adrenal CT of Cushing's syndrome. *AJR* 1986;146:1235-1238
 6. Teasdale E, Teasdale G, Mohsen F, MacPherson P. High-resolution computed tomography in pituitary microadenoma: is seeing believing? *Clin Radiol* 1986;37:227-232
 7. Valenta LJ, Sostrin RD, Eisenberg H, Tamkin JA, Elias AN. Diagnosis of pituitary tumors by hormone assays and computerized tomography. *Am J Med* 1982;72:861-873
 8. Hemminghytt S, Kalkhoff RK, Daniels DL, Williams AL, Grogan JP, Haughton VM. Computed tomographic study of hormone-secreting microadenomas. *Radiology* 1983;146:65-69
 9. Saris SC, Patronas NJ, Doppman JL, et al. Cushing syndrome: pituitary CT scanning. *Radiology* 1987;162:775-777
 10. Marcovitz S, Wee C, Chan J, Haroy J. The diagnostic accuracy of preoperative CT scanning in the evaluation of pituitary ACTH-secreting adenomas. *AJNR* 1987;8:641-644
 11. Lee BCP, Deck MDF. Sellar and juxtasellar lesion detection with MR. *Radiology* 1985;157:143-147
 12. Bilaniuk LT, Zimmerman RA, Wehrli FW, et al. Magnetic resonance imaging of pituitary lesions using 1.0 to 1.5T field strength. *Radiology* 1984;153:415-418
 13. Glaser B, Sheinfeld M, Benmair J, Kaplan N. Magnetic resonance imaging of the pituitary gland. *Clin Radiol* 1986;37:9-14
 14. Kucharczyk W, Davis DO, Kelly WM, Sze G, Norman D, Newton TH. Pituitary adenomas: high-resolution MR imaging at 1.5T. *Radiology* 1986;161:761-765
 15. Dwyer AJ, Frank JA, Doppman JL, et al. Pituitary adenomas in patients with Cushing's disease: initial experience with Gd-DTPA-enhanced MR imaging. *Radiology* 1987;163:421-426
 16. Sakoda K, Mukada K, Yonezawa M, et al. CT scans of pituitary adenomas. *Neuroradiology* 1981;20:249-253
 17. Salassa RM, Law ER, Carpenter PC, Northcutt RC. Transsphenoidal removal of pituitary microadenoma in Cushing's disease. *Mayo Clin Proc* 1978;53:24-28
 18. Imura H. Ectopic hormone syndromes. *Clin Endocrinol Metab* 1980;9:235-260
 19. Feldman JM. Cushing's disease: a hypothalamic flush? *N Engl J Med* 1975;293:930-931
 20. Marcovitz S, Wee R, Chan S, Hardy J. Diagnostic accuracy of preoperative CT scanning of pituitary somatotroph adenomas. *AJNR* 1988;9:19-22
 21. Marcovitz S, Wee R, Chan J, Hardy J. Diagnostic accuracy of preoperative CT scanning of pituitary prolactinomas. *AJNR* 1988;9:13-17
 22. Davis PC, Hoffman JC, Tindall GT, Braun IF. Prolactin-secreting pituitary microadenomas: inaccuracy of high-resolution CT imaging. *AJNR* 1984;5:721-726
 23. Chambers EF, Turski PA, LeMasters D, Newton TH. Regions of low density in the contrast-enhanced pituitary gland: normal and pathologic processes. *Radiology* 1982;144:109-113
 24. Pojunas KW, Daniels DL, Williams AL, Haughton VM. MR imaging of prolactin-secreting microadenomas. *AJNR* 1986;7:209-213
 25. Davis PC, Hoffman JC, Spencer T, Tindall GT, Braun IF. MR imaging of pituitary adenoma: CT, clinical, and surgical correlation. *AJR* 1987;148:797-802
 26. Kulkarni MV, Lee KF, McArdle C, Yeakley JW, Haar FL. 1.5-T MR imaging of pituitary microadenomas: technical considerations and CT correlation. *AJNR* 1988;9:5-11
 27. Mark L, Pech P, Daniels D, Charles C, Williams A, Haughton V. The pituitary fossa: a correlative anatomic and MR study. *Radiology* 1984;153:453-457
 28. Raji MR, Kishore PRS, Becker DP. Pituitary microadenoma: a radiological-surgical correlative study. *Radiology* 1981;139:95-99
 29. Scotti G, Yu C-Y, Dillon WP, et al. MR imaging of cavernous sinus involvement by pituitary adenomas. *AJNR* 1988;9:657-664, *AJR* 1988;151:799-806
 30. Burrow GN, Wortzman G, Rewcastle NB, Holgate RC, Kovacs K. Microadenomas of the pituitary and abnormal sellar tomograms in an unselected autopsy series. *N Engl J Med* 1981;304:156-158

Book Review

The Radiologic Clinics of North America. Imaging in Neuroradiology. Part 1. Guest editors: S. Howard Lee and Robert A. Zimmerman. Philadelphia: Saunders, July 1988;26(4):701-891. \$22.95; by subscription, 6 issues annually for \$89

This important volume on neuroradiography is devoted entirely to the newly evolved technology of MR imaging and is informative for radiologists, neurologists, neurosurgeons, oncologists, pediatricians, and all physicians who deal with brain and spinal disorders. The contributions of 26 authors are contained in 10 chapters. The illustrations are excellent throughout.

For those interested in the fundamental physics of MR, the first chapter illustrates the basic four steps of preparatory alignment, RF excitation, relaxation and signal measurement, and spatial localization. Various image acquisition approaches are discussed

on the early experiences at the University of Wisconsin on using experimental sodium MR for studies of cerebral blood flow, seizures, cell mitoses, and energy state. MR enhancement with gadolinium-DTPA in normal conditions and in various tumors and vascular lesions is the topic of the last article. The use of this compound makes MR a more complete technique for imaging the brain and spine. It is particularly useful in showing meningioma, which is often isodense without it.

A major strength of this book lies in the clinical disease sections, which illustrate neurofibromatosis, tuberous sclerosis, von Hippel-

Histochemical Characterization and Functional Significance of the Hyperintense Signal on MR Images of the Posterior Pituitary

John Kucharczyk^{1,2}
 Walter Kucharczyk³
 Isabelle Berry^{1,4}
 Jack de Groot⁵
 William Kelly⁶
 David Norman¹
 T. H. Newton¹

MR imaging of the pituitary fossa characteristically shows a well-circumscribed area of high signal intensity in the posterior lobe on T1-weighted images. We used a combination of high-field MR, electron microscopy, and histologic techniques in experimental animals to determine whether the hyperintensity of the posterior lobe might be functionally related to hormone neurosecretory processes, and to attempt to establish its chemical nature. Histologic sections of a dog's pituitary gland processed with lipid-specific markers showed intense staining in the posterior lobe but not in the anterior lobe, thus documenting the location of fat in the posterior pituitary. Administration of vasoactive drugs known to influence vasopressin secretion to anesthetized cats produced changes in the volume of high-intensity signal in the posterior pituitary. Subsequent electron microscopy showed a significant increase in posterior lobe glial cell lipid droplets and neurosecretory granules in dehydration-stimulated cats.

The data suggest that the pituitary hyperintensity represents intracellular lipid signal in the glial cell pituicytes of the posterior lobe or neurosecretory granules containing vasopressin. The volume of the signal may, in turn, reflect the functional state of hormonal release from the neurohypophysis.

While CT and MR imaging can both be used to evaluate patients with suspected pituitary disease, high-field high-resolution MR imaging is increasingly the method of choice [1-3]. The inherently superior contrast provided by MR is especially advantageous in the region of the sella turcica, where numerous biochemically heterogeneous soft-tissue structures and fluid compartments are located in close anatomical association.

Several MR studies of the sella have shown that a well-defined area of high signal intensity on T1-weighted images, located just anterior to the dorsum, corresponds to a variable portion of the posterior lobe [4, 5]. Furthermore, the size, shape, and exact position of this bright signal are influenced by intrasellar and suprasellar lesions [1-5]. In particular, the absence of high signal intensity in the posterior lobe of patients with central diabetes insipidus suggests a possible functional relationship to hypothalamic-pituitary hormone secretory processes [1-3].

The peptide hormones vasopressin and oxytocin are synthesized in the supraoptic and paraventricular nuclei of the hypothalamus and are transported by axoplasmic flow into the posterior lobe for subsequent release into the circulation. Histologically, the posterior pituitary is composed of unmyelinated nerve fibers, axon terminals containing the neurosecretory products, and a variable number of astrocytic glial cells or "pituicytes" [6-10]. The pituicytes are found in close contact with axon terminals containing vasopressin and, in both humans [11] and various experimental animals [12-20], show signs of raised metabolic activity and increased intracellular lipid content under conditions that promote increased hormone release. In the present study, we investigated the possibility that the high-intensity signal in T1-weighted images of the posterior lobe may be due to intracellular lipid in the pituicytes.

This article appears in the November/December 1988 issue of *AJNR* and the January 1989 issue of *AJR*.

Received December 16, 1987; accepted after revision July 18, 1988.

Presented at the annual meeting of the American Society of Neuroradiology, New York, May 1987.

¹ Department of Radiology, L371, University of California, San Francisco, 505 Parnassus, San Francisco, CA 94143. Address reprint requests to J. Kucharczyk.

² Department of Physiology, University of Ottawa, Ottawa, Ontario, Canada K1H 8M5.

³ Department of Radiology, The Toronto Hospital, Toronto, Ontario, Canada M5G 2C4.

⁴ Service de Neuroradiologie, Hopital Purpan, Toulouse, France.

⁵ Department of Anatomy, University of California, San Francisco, CA 94043.

⁶ Department of Radiology, David Grant USAF Hospital, Travis Air Force Base, CA 94535.

AJR 152:153-157, January 1989

0361-803X/89/1521-0153

© American Roentgen Ray Society

Materials and Methods

To establish the location of the high signal intensity seen on T1-weighted images of the sella turcica, the pituitary gland and sella turcica of a dog were examined under light microscopy. After the animal was sacrificed by barbiturate overdose, the sphenoid bone with its intrasellar contents intact was excised and immediately imaged with T1-weighted sagittal and T1-weighted axial sections, 600/20 (TR/TE). The pituitary gland was then removed, fixed, and stained with Oil Red O, a lipid-specific stain, and examined at $\times 100$ magnification. The staining characteristics of the anterior and posterior lobes of the pituitary were compared.

MR studies were then carried out on five 16–24-hr food-deprived adult cats and a single dog tranquilized with acepromazine (2–4 mg/kg, IM), and subsequently anesthetized with sodium pentobarbital (30–35 mg/kg, IV) or halothane. Animals were ventilated through an endotracheal tube in order to maintain normal pO_2 (100–150 torr) and pCO_2 (27–35 torr) levels. A femoral artery and vein were catheterized for blood pressure monitoring and drug administration. The rectal temperature was maintained at $37 \pm 0.5^\circ\text{C}$ with an electronically controlled body heating pad.

Images were acquired on a GE CSI-II imager/spectrometer operating at 2T and an 8.3-cm inner-diameter homebuilt "birdcage" head coil tuned to the proton resonant frequency. T1-weighted (450/20) and T2-weighted (3000/40,80) 2-mm-thick (2DFT) or 1.25-mm-thick (3DFT) contiguous images were obtained in the sagittal and coronal planes in a 3×8 -cm field of view, and 128×256 -pixel acquisition matrix. The scan range was adjusted to ensure that the median eminence was completely within the margins of a single section location. All images were retrospectively reviewed by three or more observers with attention focused on the architectural features and intrinsic signal characteristics of the hypothalamic-pituitary axis.

Subsequently, T1- and T2-weighted midsagittal images were obtained before and after administration of epinephrine (1–10 $\mu\text{g/kg}$,

bolus IV, three injections in three cats), isoproterenol (10–50 $\mu\text{g/kg}$, bolus IV, four injections in three cats) and sodium pentobarbital (10–30 mg/kg, IV, four injections in four cats). Images were produced at 5–10 min intervals for 30–60 min after administration of each drug in order to determine whether the intensity or volume of the pituitary "bright spot" had been altered. Arterial blood pressure was recorded continuously during this period. At the conclusion of each MR study, the animal was sacrificed by IV barbiturate overdose. The pituitary fossa of one intact cat was reimaged 72 hr postmortem.

Ultrastructural features of the pituitary were examined in 24–48-hr water-deprived cats ($n = 2$) and rats ($n = 4$), and in normally hydrated controls (one cat and two rats). Animals were killed by halothane or isoflurane overdose and prepared for electron microscopy in accordance with methods described previously [12, 21]. Briefly, animals were perfused via IV with 0.9% NaCl followed by 4% glutaraldehyde in 0.1 M sodium cacodylate buffer (pH 7.4) containing 0.5% dimethyl sulfoxide. The pituitary gland was removed, separated into anterior and posterior lobes under $\times 40$ magnification, and the two lobes were stored overnight in fixative. Blocks of the neurohypophysis were then removed with a hypodermic needle, treated with Os O₄, and embedded. Uranyl acetate en bloc staining was carried out after osmication.

Sections 1–2 μm thick were cut through the blocks to establish the presence of neural lobe tissue. Thin sections were cut at various levels and stained with lead citrate. Prints of electron micrographs of individual pituicytes were analyzed at a final magnification of $\times 7500$ –26,000.

Results

MR imaging of the dog's excised sella turcica and pituitary gland revealed the typical hyperintense region in the posterior

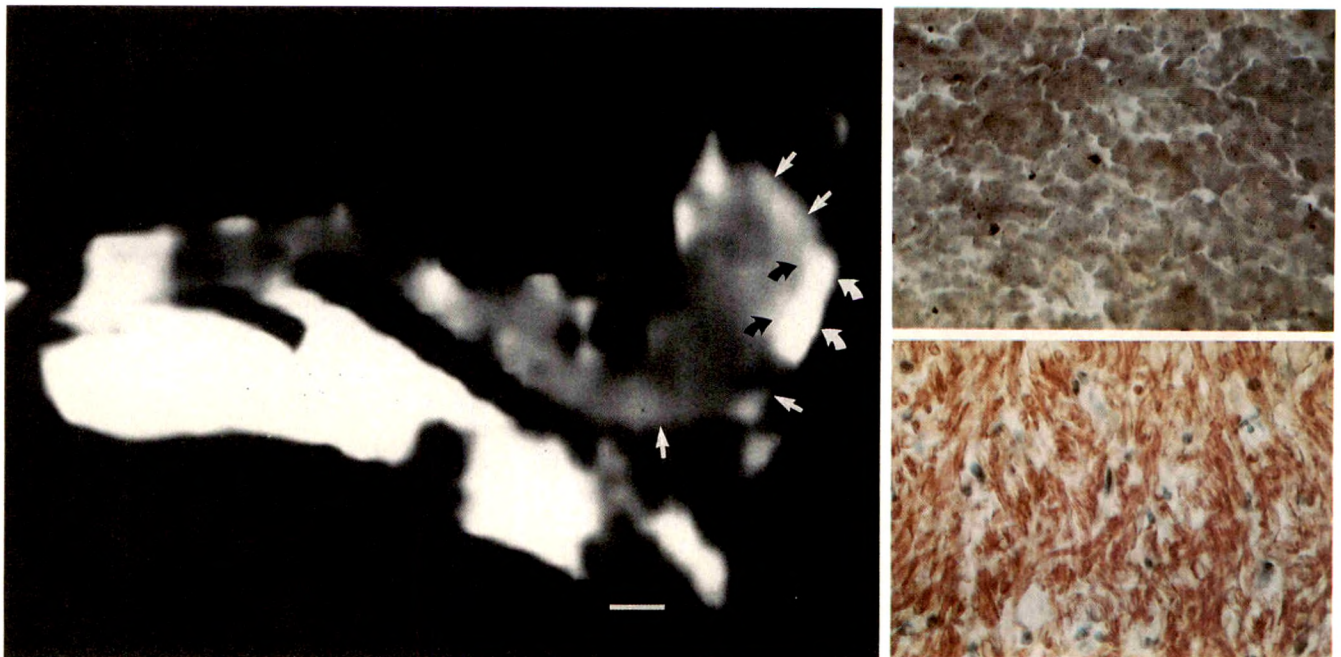


Fig. 1.—A, T1-weighted sagittal MR image of excised sphenoid bone of dog. Large area of high signal intensity represents marrow within sphenoid bone. Low-signal cortical bone of sella floor is identified by straight arrows. Intermediate-intensity tissue superior to floor is the anterior pituitary. High-intensity posterior pituitary is identified by curved arrows. Horizontal bar = 1 mm.

B, Oil Red O stain of anterior (top) and posterior (bottom) lobes at $\times 100$ magnification shows typical architectures. Note relative paucity of fat in anterior lobe compared with abundant red-staining lipid material in posterior pituitary.

sella (Fig. 1A). Histologic sections with Oil Red O staining revealed abundant fat in the posterior lobe (Fig. 1B), which we believe is the source of the bright signal on T1-weighted images. An earlier report [22] had assigned this hyperintensity to the "sellar fat pad," a point with which we disagree.

MR studies of the cats' pituitary fossa also showed areas of hyperintense signal on T1-weighted images in the posterior-inferior part of the sella (Fig. 2A) similar to MR studies of human pituitary [2, 3, 5]. As in the human, this high signal intensity was usually biconvex or semilunar in shape and of variable size between individual animals.

On T2-weighted images, the posterior lobe hyperintensity differed from adjacent areas of high signal. Although the intensity diminished with progressively increased T2 weighting, the degree of signal loss was less than that of marrow in the dorsum and clivus. Thus, the MR signal characteristics of the posterior pituitary lobe of the cat and dog appear to be very similar to those reported in human studies [5].

In the sequential MR studies of drug effects, the observers agreed that an IV dose of epinephrine, which raised mean arterial blood pressure (MAP) by 40–60 mm Hg, produced a slight decrease in the volume of the pituitary "bright spot"

(Fig. 2B). On the other hand, administration of the beta-adrenergic agonist isoproterenol, in doses that reduced MAP by 40–80 mm Hg, increased the volume of the bright signal (Fig. 2C). Qualitatively similar changes were observed in each of the other animals tested with epinephrine and isoproterenol. Changes in MAP of as little as 10 mm Hg are known to influence vasopressin biosynthesis and release by baroreceptor mechanisms [23]. A small segment of the high-intensity signal was still present on a T1-weighted image taken 72 hr postmortem (Fig. 2D). The possible significance of this latter observation is not clear at this time.

In the next series of experiments, we attempted to elucidate the specific location and possible significance of the hyperintense signal by examining the ultrastructural characteristics of the posterior lobe. In electron micrographs of the cats' neurohypophysis, pituicytes were identified by the presence of nuclei, ribosomes, Golgi complexes, and liposomes in their cytoplasm. Neurosecretory axon terminals with their characteristic vesicles were also seen adjacent to or directly opposed to the pituicytes. The major difference observed between the normally hydrated (Fig. 3A) and dehydrated (Fig. 3B) neurohypophysis was a large increase in the number and

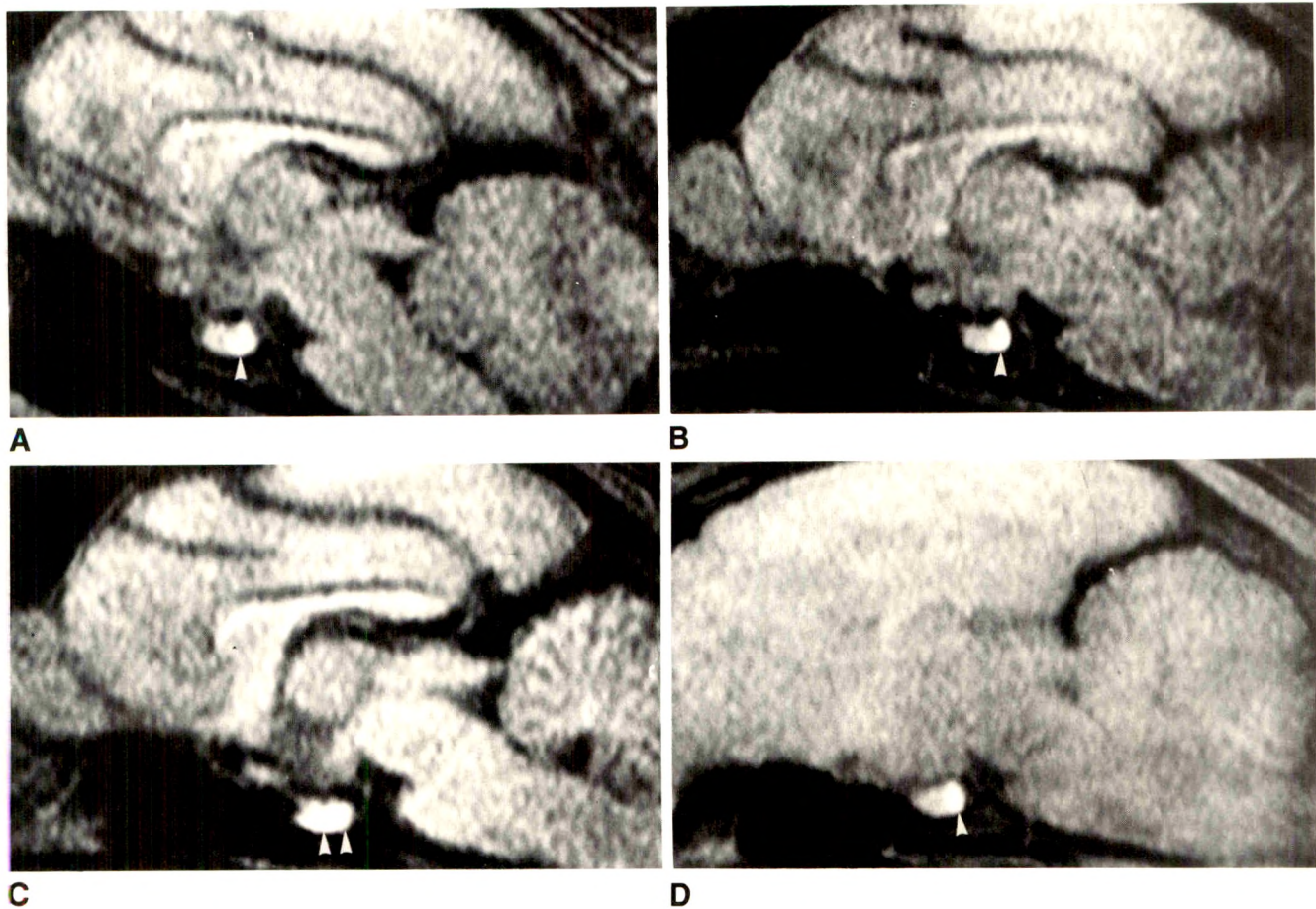


Fig. 2.—Midsagittal MR image of cat brain. T1-weighted spin-echo images (450/15/4) 3-mm slice thickness, 8 × 8-cm field of view, 128 × 256 matrix. A, Preinjection control image; B, 1 min after IV injection of 1 µg/kg epinephrine; C, 5 min after IV injection of 5 µg/kg isoproterenol; D, same cat brain reimaged 72 hr postmortem. Volume of hyperintense signal in posterior pituitary (arrowheads in all images) appears to be slightly decreased after epinephrine injection and increased after isoproterenol administration. Some hyperintensity persisted for 3 days postmortem.

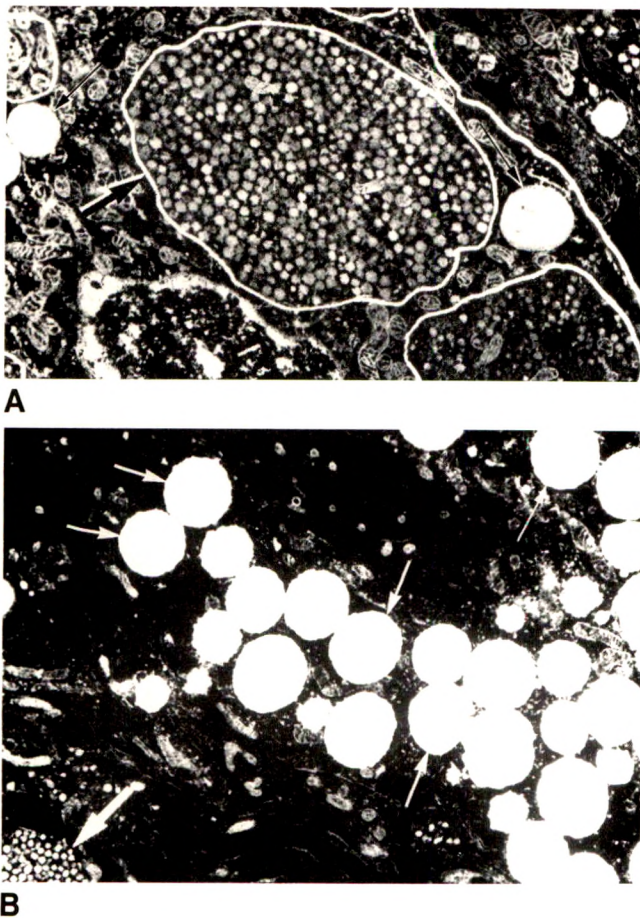


Fig. 3.—Electron micrographs of single pituicytes from posterior pituitary of normally hydrated (A) and 48-hr water-deprived (B) cats. Shown is part of the pituicyte cytoplasm with lipid droplets (*smaller arrows*) and neurosecretory axon terminals (boundaries drawn) containing vasopressin and oxytocin (*larger arrows*). Note that the number of lipid droplets is much increased in the dehydrated animal. Magnification: $\times 26,400$ (A) and $\times 28,700$ (B).

size of lipid droplets interspersed throughout the pituicyte cytoplasm in the dehydrated animals.

Discussion

The neural parenchyma of the mammalian pars nervosa consists of unmyelinated neurosecretory axons and cellular elements termed "pituicytes" [7, 11]. Typical slender axonal fibers, measuring 0.5 to 1 μm in diameter, could be recognized in our electron micrographs of the cats' neurohypophysis by their characteristic parallel rows of neurotubules and filaments. The neurosecretory axons contain the usual axonal organelles as well as 100–200 nm dense core vesicles [24]. The vesicles in effect package the neurohypophysial hormones and carrier proteins that are produced in the perikarya of the supraoptic and paraventricular nuclei of the hypothalamus, and are then transported axonally to the posterior lobe for storage in the axon terminals or release into the perivascular space [8].

Studies in a number of mammalian species, including the human [11], have shown that pituicytes make up 25–30% of the volume of the neural lobe [25] and are closely associated with the neurosecretory process. In electron micrographs in our study, these astrocytic glial cells were frequently seen to have neurosecretory axonal processes indented into their cytoplasm, suggesting the possibility of neuro-glial communication in the process of hormone release [12, 13]. An even more prominent ultrastructural feature was the large increase in lipid droplets in the posterior lobe pituicytes of cats that had been water-deprived for 48-hr prior to electron microscopy. Generalized pituicyte hypertrophy [15], as well as an increase in pituicyte electron-dense cytoplasmic bodies [16] and intracellular lipid droplets [12–15, 17, 26] have previously been noted in animals under conditions in which neurosecretion of vasopressin is stimulated, such as several days of water deprivation or salt loading.

The results of our histologic study with lipid-specific marker confirm that the posterior lobe, unlike the anterior pituitary, has a high lipid content. It thus seems probable that the hyperintense signal observed on T1-weighted images of the posterior sella represents lipids contained in the pituicyte glial cells of the posterior lobe. The finding that the volume of the hyperintense area on MR could be increased by pharmacological manipulations known to increase plasma vasopressin levels further supports the view that the lipid content of the pituicytes is closely related to the state of hormone release from the posterior lobe.

The functional importance of the intracellular lipids present in the posterior pituitary is unknown. There has been speculation that phagocytosis may be a physiological role for pituicytes. After surgical transection of the hypothalamic–pituitary stalk in rats, the axons in the neural lobe degenerate and are phagocytosed by these astroglial cells [25]. On the basis of the results of their ultrastructural study of the human neural lobe, Takei et al. [11] proposed that pituicytes provide a cytoplasmic machinery to catabolize "unused or excess" neurosecretory material. In the human, at least, the large increase in pituitary fat droplets during periods of intense neurosecretory activity is paralleled in the neuronal perikarya by a great increase in the number of lysosomes. Additionally, an increase in the number of hematogenous monocytes and perivascular histiocytes is seen in the posterior pituitary at that time [11]. The increased number of macrophages is thought to reflect an elevated metabolism involving various cellular, especially membrane-bound, constituents [11].

Thus, while the origin of the fat droplet inclusions in pituicytes is not yet fully understood, they may represent an accumulation site for the release or disposal of membrane lipid products. In addition to lysosomal degradation of material in neurosecretory axon endings [20], there is indirect evidence that pituicytes can take part in lipid storage and catabolism [15]. Lipoprotein material resulting from excretory and autophagic activities in axonal endings may therefore be temporarily stored in the form of lipid droplets prior to reutilization in the formation of a new membrane. Although we are not aware of any direct proof for such a transfer of lipid material in the posterior pituitary, membrane phospholipid breakdown,

storage, and reutilization have been demonstrated in several other secretory cells [27]. Such an explanation would account for the increased liposome content of pituicytes observed in electron micrographs of the actively secreting neurohypophysis, and may explain the high signal intensity of the posterior lobe in T1-weighted MR images.

REFERENCES

- Kucharczyk W, Davis DO, Kelly WM, et al. Pituitary adenomas: high resolution MR imaging at 1.5 T. *Radiology* 1986;161:761-765
- Fujisawa I, Nishimura K, Asoto R, et al. Posterior lobe of the pituitary in diabetes insipidus: MR findings. *J Comput Assist Tomogr* 1987;11:221-225
- Fujisawa I, Asato R, Nishimura K, et al. Anterior and posterior lobes of the pituitary gland: assessment by 1.5 T MR imaging. *J Comput Assist Tomogr* 1987;11:214-220
- Kelly WM, Kucharczyk W, Kucharczyk J, et al. Posterior pituitary ectopia: an MR feature of pituitary dwarfism. *AJNR* 1988;9:453-460
- Columbo N, Berry I, Kucharczyk J, et al. Posterior pituitary gland: appearance on magnetic resonance images in normal and pathologic states. *Radiology* 1987;165:481-485
- Decherney A, Naftolin F. Hypothalamic and pituitary development in the fetus. *Clin Obstet Gynecol* 1980;23:749
- Bucy PC. The pars nervosa of the bovine hypophysis. *J Comp Neurol* 1930;50:505-519
- Dreifuss JJ. A review on neurosecretory granules, their contents and mechanisms of release. *Ann NY Acad Sci* 1975;258:184-201
- Okado N, Yokata N. An electron microscopic study of the structural development of the neural lobe in the human fetus. *Am J Anat* 1980;159:261
- Holmes RL, Ball JN. *The pituitary gland, a comparative account*. London: Cambridge University Press, 1974:63-94
- Takei Y, Seyama S, Pearl GS, et al. Ultrastructural study of the human neurohypophysis. II: Cellular elements of the neural parenchyma, the pituicytes. *Cell Tiss Res* 1980;205:273-287
- Tweedle CD, Hatton GI. Evidence for dynamic interactions between pituicytes and neurosecretory axons in the rat. *Neuroscience* 1980;5:661-667
- Tweedle CD. Ultrastructural manifestations of increased hormone release in the neurohypophysis. In: Cross BA, Leng G, eds. *The neurohypophysis: structure, function and control. Progress in brain research*, vol. 60. Amsterdam: Elsevier, 1983
- Tweedle CD, Hatton GI. Ultrastructural changes in rat hypothalamic neurosecretory cells and their associated glia during minimal dehydration and rehydration. *Cell Tiss Res* 1977;181:59-92
- Krsulovic J, Bruckner G. Morphological characteristics of pituicytes in different functional stages. *Z Zellforsch* 1969;99:210-220
- Davis E, Morris JF. Lysosomes and Herring bodies in the neural lobe of saline and pitressin-treated rats. *J Anat* 1973;114:291-292
- Levesque F, Small M. The relationship of the pituicyte to the posterior lobe hormones. *Endocrinology* 1959;65:909-915
- Tweedle CD, Hatton GI. Magnocellular neuropeptidergic terminals in neurohypophysis: rapid glial release of enclosed axons during parturition. *Brain Res Bull* 1982;8:205-209
- Boer GJ, van Rheenen-Verberg CMF. Acid phosphate in rat neurohypophyseal dispersions and its fractions enriched for neurosecretosomes and pituicytes after water deprivation and lactation. *Brain Res* 1976;114:279-292
- Kodama Y, Fujita H. Some findings on the fine structure of the neurohypophysis in dehydrated and pitressin treated mice. *Arch Histol Jap* 1975;38:121-131
- Karnovsky MJ. The ultrastructural basis of capillary permeability studied with peroxide as a tracer. *J Cell Biol* 1967;35:213
- Mark L, Pech MP, Daniels D, et al. Pituitary fossa: a correlative anatomic and MR study. *Radiology* 1984;153:453-457
- Dunn FL, Brennan TJ, Nelson AE, et al. The role of blood osmolality and volume in regulating vasopressin secretion in the rat. *J Clin Invest* 1973;52:3212-3219
- Seyama S, Pearl GS, Takei Y. Ultrastructural study of the human neurohypophysis. I: Neurosecretory axons and their dilatations in the pars nervosa. *Cell Tiss Res* 1980;205:253-271
- Nordmann JJ. Ultrastructural morphometry of the rat neurohypophysis. *J Anat* 1977;123:213-218
- Dellman HD, Stoeckel ME, Porte A, et al. Ultrastructure of neurohypophysial glial cells following stalk transection in the rat. *Experientia* 1974;30:1220-1222
- Hokin LE, Huebner D. Radioautographic localization of the increased synthesis of the phosphatidylinositol in response to pancreozymin of acetylcholine in guinea pig pancreas slices. *J Cell Biol* 1967;33:521-530

Books Received

Receipt of books is acknowledged as a courtesy to the sender. Books considered of sufficient interest are reviewed as space permits. If the book has been reviewed in the *AJR*, the date of its review is given in parentheses.

Radionuclide Bone Imaging and Densitometry. Edited by Fred A. Mettler, Jr. (vol. 4 of Contemporary Issues in Nuclear Imaging.) New York: Churchill Livingstone, 342 pp., 1988. \$72 (10/88)

The Chest. By Isadore Meschan. (vol. 4 in Roentgen Signs in Diagnostic Imaging, 2nd ed.) Philadelphia: Saunders, 1038 pp., 1987. \$125 (10/88)

Essentials of Clinical MRI. Edited by Theo H. M. Falke. Boston: Nijhoff, 235 pp., 1988. \$79 (10/88)

Clinical Applications of Cardiac Digital Angiography. By G. G. John Mancini. New York: Raven, 324 pp., 1987. \$79 (10/88)

Computed Cranial and Spinal Imaging. A Practical Introduction. By John M. Stevens, Alan R. Valentine, and Brian E. Kendall. Baltimore: Williams & Wilkins, 248 pp., 1988. \$44.95 (10/88)

Sectional Fetal Anatomy in Ultrasound. By Alf Staudach. New York: Springer-Verlag, 198 pp., 1987. \$59.50 (10/88)

Magnetic Resonance Imaging. Physical and Biological Principles. By Stewart C. Bushong. St. Louis: Mosby, 382 pp., 1988. \$36.95 (10/88)

Fetal Sectional Anatomy and Ultrasonography. By Lewis H. Nelson III, Walter J. Bo, and George C. Lynch. Baltimore: Williams & Wilkins, 208 pp., 1988. \$65 (10/88)

Cerebral Angio-CT. By Kazuhiko Sadamoto and Keiji Fukui. New York: Raven, 112 pp., 1988. \$49 (10/88)

Techniques and Indications in Radiology. Kidney and Urinary Tract. By Sebastian Lange. (Translated from the German by Chris Hall and Erika Brewer.) New York: Thieme Medical, 430 pp., 1987. \$17 (11/88)

Clinical Efficacy of Positron Emission Tomography. Edited by W. D. Heiss, G. Pawlik, K. Herholz, and K. Wienhard. (11th in the series Developments in Nuclear Medicine; series edited by Peter H. Cox.) Boston: Nijhoff, 421 pp., 1987. \$118.50 (11/88)

Magnetic Resonance Imaging of the Thorax. By Miriam Sperber and Marc C. Kaiser. St. Louis: Warren H. Green, 270 pp., 1987. \$65 (11/88)

The Radiologic Clinics of North America. Recent Advances in Practical Pediatric Radiology. Guest editors: Kook Sang Oh and Thomas M. Bender. Philadelphia: Saunders, March 1988; 26:181-469. \$22.95; by subscription, six issues annually for \$89 (11/88)

Impact of Functional Imaging in Neurology and Psychiatry. Proceedings of the 2nd International rCBF Workshop. Held at Supetar/Brac, Yugoslavia, September 29 to October 4, 1986. Edited by John Wade, Stevo Knežević, V. Alexander Maximilian, Zdenko Muhrin, and Isak Prohovnik. (vol. 5 in the series Current Problems in Neurology.) London: John Libbey, 199 pp., 1987. \$46 (11/88)

Cranial Magnetic Resonance Imaging. By Allen D. Elster. New York: Churchill Livingstone, 423 pp., 1988. \$95 (11/88)

Dissection Manual. Companion to Rohen/Yokochi Color Atlas of Anatomy, 2nd ed. By Jack L. Wilson. New York: Igaku-Shoin, 244 pp., 1988. \$19.50 (11/88)

Color Atlas of Anatomy. A Photographic Study of the Human Body, 2nd ed. By Johannes W. Rohen and Chihiro Yokochi. New York: Igaku-Shoin, 469 pp., 1988. \$45 (11/88)

Computed Tomography of the Head and Neck. Edited by Thomas H. Newton, Anton N. Hasso, and William P. Dillon. (vol. 3 in the series

Modern Neuroradiology.) San Anselmo, CA: Clavadel Press, 480 pp., 1988. \$135 (11/88)

Doppler Echocardiography. 2nd ed. By Stanley J. Goldberg, Hugh D. Allen, Gerald R. Marx, and Richard L. Donnerstein. Philadelphia: Lea & Febiger, 313 pp., 1988. \$45 (11/88)

Radiologic Atlas of Pulmonary Abnormalities in Children, 2nd ed. By Edward B. Singleton, Milton L. Wagner, and Robert V. Dutton. Philadelphia: Saunders, 355 pp., 1988. \$75 (11/88)

Obstetrical Measurement in Ultrasound. A Reference Manual. By Alfred B. Kurtz and Barry B. Goldberg. Chicago: Year Book Medical, 214 pp., 1988. \$45 (11/88)

RSNA Today, Vol. 2, No. 2. Oak Brook, IL: The Radiological Society of North America, 1988. \$75; by subscription, 4 issues annually at \$225 for members and \$275 for nonmembers (VHS videotape) (11/88)

Dynamic Radiology of the Abdomen. Normal and Pathologic Anatomy, 3rd ed. By Morton A. Meyers. New York: Springer-Verlag, 507 pp., 1988. \$110 (11/88)

Radiology-Electromedicine. Physics, Technique, Applications. By Arturo Gilardoni, Marco T. Gilardoni, Andrea A. Orsini, and Luca A. Orsini. Lecco, Italy: Casa Editrice Stefanoni, 432 pp., 1987. \$240 (11/88)

Textbook of Diagnostic Imaging, vols. 1-3. Edited by Charles E. Putman and Carl E. Ravin. Philadelphia: Saunders, 2158 pp., 1988. Vol. 1, \$95; vols. 2 and 3, \$100 each (12/88)

Clinical Neuroimaging. (vol. 4 of Frontiers of Clinical Neuroscience.) Edited by William H. Theodore. New York: Alan R. Liss, 300 pp., 1988. \$62.50 (12/88)

Imaging and Visual Documentation in Medicine. Edited by K. Wamsteker, U. Jonas, G. van der Veen, and P. F. G. M. van Waes. New York: Excerpta Medica, 838 pp., 1987. (12/88)

The Radiologic Clinics of North America. Imaging Strategies in MRI. Guest editor: Marcia C. Fishman-Javitt. Philadelphia: Saunders, May 1988; 26:471-699. \$22.95; by subscription, 6 issues annually for \$89 (12/88)

Arthritis in Black and White. By Anne C. Brower. Philadelphia: Saunders, 365 pp., 1988. \$55 (12/88)

Magnetic Resonance Imaging. Basis for Interpretation. By Robert Sigal, D. Doyan, Ph. Halimi, and H. Atlan. (Translated by S. Assénat and R. Sigal.) New York: Springer-Verlag, 102 pp., 1988. \$39 (12/88)

Computed Tomography of the Pituitary Gland. An Anatomical and Pathological Study. By M. J. Hendriks. Wolfeboro, NH: Van Gorcum, 126 pp., 1988. soft cover (12/88)

Rheumatologic Disorders. By Lawrence F. Layfer, Jerry Petasnick, and Robert S. Katz. (vol. 19 of Advanced Exercises in Diagnostic Radiology.) Philadelphia: Saunders, 186 pp., 1988. \$29.50 (12/88)

Applications of Noninvasive Vascular Techniques. By Amil J. Gerlock, Jr., Vishan L. Giyanani, and Carol Krebs. Philadelphia: Saunders, 541 pp., 1988. \$65 (12/88)

Controversies in Breast Disease. Edited by Sharon Grundfest-Broniatowski and Caldwell B. Esselstyn, Jr. New York: Marcel Dekker, 514 pp., 1988. \$150 (12/88)

Radiology of AIDS. Edited by Michael P. Federle, Alec J. Megibow, and David P. Naidich. New York: Raven, 163 pp., 1988. \$89 (12/88)

Imaging of Vertebral Trauma. By Richard H. Daffner. Rockville, MD: Aspen, 165 pp., 1988. \$78 (12/88)

MR Imaging of Parkinson Disease with Spin-Echo and Gradient-Echo Sequences

Bruce H. Braffman^{1,2}
 Robert I. Grossman¹
 Herbert I. Goldberg¹
 Matthew B. Stern³
 Howard I. Hurtig³
 David B. Hackney¹
 Larissa T. Bilaniuk¹
 Robert A. Zimmerman¹

High-field MR with both spin-echo and gradient-echo sequences was performed in 21 patients with (idiopathic, drug-responsive) Parkinson disease. The use of gradient echoes allowed more sensitive detection than did spin echoes of susceptibility changes in the putamina and substantia nigra. No statistically significant difference in putaminal hypointensity on long TR/long TE spin-echo sequences or on T2*-weighted images using gradient-echo sequences was observed between Parkinson patients and controls. There was also no statistically significant difference in the frequency of restoration of the signal intensity of the substantia nigra between the two groups of patients. The width of the pars compacta of the substantia nigra in patients with Parkinson disease was 2.12 ± 0.82 mm (mean \pm SD). This value in age- and gender-matched controls was 2.67 ± 0.5 . Comparing these two groups with an unpaired t test resulted in a *p* value less than or equal to .005.

Our MR study with spin-echo and gradient-echo images in Parkinson and control patients was able to substantiate and elaborate on previously described MR features of Parkinson disease.

Several investigators have described the MR imaging features of Parkinson disease (i.e., the primary or idiopathic form) and parkinsonian syndromes (i.e., secondary parkinsonism or Parkinson plus) [1-4]. Their pioneering work pointed to the utility of MR as a diagnostic tool in the evaluation of these patients. Drayer et al. [1] and Pastakia et al. [2] described an abnormal decrease in signal intensity of the putamina on long TR/long TE spin-echo sequences in multiple-system atrophy, a parkinsonian syndrome, probably due to iron (or other paramagnetic) deposition. Duguid et al. [3] found a narrowing of the signal from the pars compacta of the substantia nigra in Parkinson patients relative to controls. Rutledge et al. [4] reported a loss of the normal hypointensity on long TR/long TE spin-echo images in the dorsal lateral aspect of the substantia nigra in patients with Parkinson disease and parkinsonian syndromes. They referred to this as restoration of the signal intensity of the putamen on long TR/long TE spin-echo sequences in two patients with unclassified parkinsonism, but not in patients with Parkinson disease.

Our study used a gradient echo to emphasize the susceptibility effects (hypointensity on long TR images) noted by other investigators and prospectively included only those who met the clinical criteria for Parkinson disease. The objective was to identify which of the MR features described above are seen in a group of patients with a relatively homogeneous clinical syndrome.

Subjects and Methods

Patients were selected by three neurologists from among those under their clinical care. Inclusion criteria required classic symptoms (bradykinesia, "resting" tremor, rigidity, and festinating gait [5]) and a good response to medication. All patients meeting these criteria were asked to participate in this study. This selection process yielded 21 MR studies of

This article appears in the November/December 1988 issue of *AJNR* and the January 1989 issue of *AJR*.

Received December 7, 1987; accepted after revision June 8, 1988.

Presented at the annual meeting of the American Society of Neuroradiology, New York City, May 1987.

This work was supported in part by a gift from Bernard Caplan.

¹Department of Radiology, Hospital of the University of Pennsylvania, 3400 Spruce St., Philadelphia, PA 19104. Address reprint requests to R. I. Grossman.

²Present address: Department of Radiology, Memorial Hospital, 3501 Johnson St., Hollywood, FL 33021.

³Department of Neurology, Hospital of the University of Pennsylvania, Philadelphia, PA 19104, and The Graduate Hospital, 18th and Lombard Sts., Philadelphia, PA 19146.

AJR 152:159-165, January 1989
 0361-803X/89/1521-0159
 © American Roentgen Ray Society

Parkinson patients ages 41–76 years old, including 11 men and 10 women. Controls were selected by retrospectively reviewing patients scanned for reasons unrelated to movement disorders. Medical charts of control subjects were reviewed. All had received a neurologic examination. They had various neurologic deficits, but none of these controls had bradykinesia, resting tremor, rigidity, festinating gait, or other symptoms of Parkinson disease. Controls were excluded if there was evidence on MR of a mass in the midbrain distorting the anatomy of the substantia nigra. Controls with a history of radiation injury, Alzheimer disease, and multiple sclerosis (i.e., disorders that may result in abnormal concentrations of brain iron [6]) were excluded. This yielded 24 MR studies of controls.

All patients and controls were examined on a 1.5-T unit* with both spin-echo and gradient-echo sequences. The spin-echo sequences used a short TR, 600/20 (TR/TE), and a long TR, 2500/20,80 (TR/first-echo TE, second-echo TE). Acquisition time was 2.5 min and 10 min 48 sec for the short and long TR sequences, respectively.

Gradient-echo images were obtained in patients and controls by using one of two sequences. The gradient-recalled acquisition in the steady state (GRASS) technique, 200/50, used an RF pulse angle of 10°. The scanning time was approximately 45 sec per slice. The partial-saturation interleave technique, 750/50, also used an RF pulse angle of 10°. These parameters resulted in contrast based mainly on T2* differences [7, 8]. Scanning time was approximately 3 min 48 sec for eight to 12 sections. For both spin-echo and gradient-echo sequences, section thickness was 5 mm with a 2.5-mm interval between sections. The scanning plane was axial, 0–20° degrees positive to the inferior orbitomeatal line.

We analyzed the intensity of the putamina in patients and controls with both the gradient-echo and spin-echo techniques on relatively T2*- and T2-weighted images (i.e., long TR/long TE sequences), respectively. Three neuroradiologists evaluated the MR images of patients and controls in a blinded fashion. Visual analysis was standardized to four discrete ratings. Grades 0–3 were variable patterns of hypointensities of the putamina relative to cortical gray matter. Grade 0 was for no hypointensity (Fig. 1); grade 1 was for hypointensity limited to the lateral margin of the putamen (Fig. 2); grade 2 was for hypointensity extending through part of the body of the putamen (Fig. 3); and grade 3 was for diffuse hypointensity of the entire putamen (Fig. 4).

The signal intensity of the substantia nigra was recorded as normal, restored, or questionably restored (i.e., loss of the normal hypointensity of the dorsal lateral aspect of the substantia nigra), as described by Rutledge et al. [4], on both spin-echo and gradient-echo sequences (Fig. 5).

Duguid et al. [3] described the anatomy of the pars compacta of the substantia nigra on MR. They found no significant change in the width of the pars compacta when the scanning plane was oriented between 0° and 20° positive to the inferior orbitomeatal line. On a long TR spin-echo sequence, the pars compacta is the relatively hyperintense band between the hypointense pars reticulata of the substantia nigra and the hypointense red nucleus (Fig. 6).

The width of the pars compacta signal in patients and controls was measured on the basis of a variation of the method described by Duguid et al. [3]. Intensity values of a straight line perpendicular to the pars compacta through the center of the red nucleus were measured on an image of the midbrain. We drew two additional parallel straight lines 1 mm to either side. At the half-height maximum intensity value between the hypointense red nucleus and relatively hyperintense pars compacta we placed one cursor. At the corresponding half-height maximum intensity value between the pars compacta and relatively hypointense pars reticulata we placed a

second cursor. The distance between the two was taken as the width of the pars compacta. We averaged three values for each pars compacta. The precision of this method was determined by repeating the measurements on three separate occasions in three different subjects. In each subject, a mean width and a standard deviation were determined. The standard deviation divided by the mean width was taken as a measure of the precision [9]. The average precision in these three patients was 3.4%.

Additional observations on MR, such as the presence of punctate hyperintense foci on long TR images in the globus pallidus and substantia nigra and presence of cortical atrophy (none, mild, moderate, and marked), were recorded.

Results

The widths of the pars compacta in both groups are listed in Table 1. Five Parkinson patients were either unable to maintain the head position in order to scan through the midbrain at 0–20° positive to the inferior orbitomeatal line or moved during scanning, and therefore were excluded. (In one of these five patients, the midbrain nuclei were not identified on MR, possibly because of the 2.5-mm gap between 5-mm slices.) The mean width in the Parkinson group was 2.12 mm (SD = 0.82). This value in the age- and gender-matched controls was 2.67 mm (SD = 0.5). There was a significant overlap between the two groups, as reflected in the relatively large standard deviations and as seen in Table 1. Nonetheless, comparing these two groups with an unpaired t test [9] resulted in a *p* value less than or equal to .005. In some (but not all) cases, the smaller width of the pars compacta in Parkinson patients was visibly detectable (Fig. 7A). MR in one Parkinson patient was notable for a width of 0 of the pars compacta; that is, there was complete loss of the hyperintense band between the red nucleus and the pars reticulata (Fig. 7B).

The grades of the intensities of the putamina on the spin-echo and gradient-echo images are listed in Table 2. In one Parkinson patient, putamina were graded 3 bilaterally on the spin-echo sequence (Fig. 4). This same patient and an additional Parkinson patient (whose putamina were graded 1 on the spin-echo sequence) had putamina that were graded 3 bilaterally on gradient-echo sequences. No control subject had putamina that were graded 3 on either gradient-echo or spin-echo sequences. The number of Parkinson patients and controls included in this study is not large enough to determine whether the number of patients with putamina graded 3 is statistically significant. The grades of the two groups of subjects could be compared by using a chi-square test if there were five or more putamina of each grade [9]. To achieve this, we combined grades 2 and 3. A comparison of the grades of the putamina in the Parkinson group with those in the control group by using chi-square revealed no statistically significant difference between the two groups ($\chi^2 = .693$, $p > .05$ on spin-echo sequences and $\chi^2 = .024$, $p > .05$ on gradient-echo sequences).

Restoration of the signal intensity of the substantia nigra was seen in 10 (24%) of 42 Parkinson patients and in seven (15%) of 48 control patients on spin-echo sequences (Table 3). Although restoration was more common in the Parkinson

* General Electric, Milwaukee, WI.

Fig. 1.—MR image (2500/80) of 49-year-old man with Parkinson disease. Globi pallidi (arrows) are hypointense relative to cortical gray matter. Putamina (arrowheads) are isointense. Putamina were graded 0.

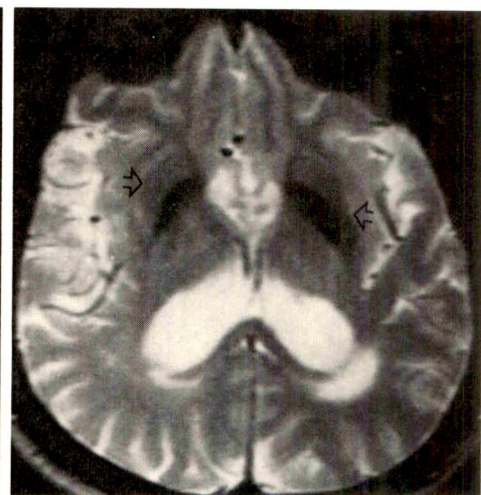


Fig. 2.—MR image (2500/80) of 76-year-old man with Parkinson disease. Hypointensity is limited to lateral aspect of putamina. (arrowheads), left side greater than right. Both were graded 1.

Fig. 3.—MR image (2500/80) of 73-year-old woman with Parkinson disease. Bilateral putaminal hypointensity involves most, but not all, of putamina. They were graded 2. Also note bilateral punctate hyperintense foci (arrowheads) in globi pallidi.

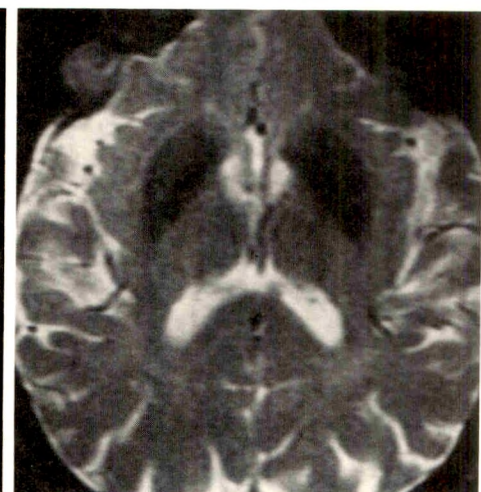


Fig. 4.—MR image (2500/80) of 68-year-old man with Parkinson disease. Hypointensity involves entire putamina diffusely. They were graded 3.

Fig. 5.—MR image (2500/80) of 64-year-old man with Parkinson disease. There is loss of normal hypointensity of dorsal lateral aspect of substantia nigra; that is, there is restoration of signal intensity [4].

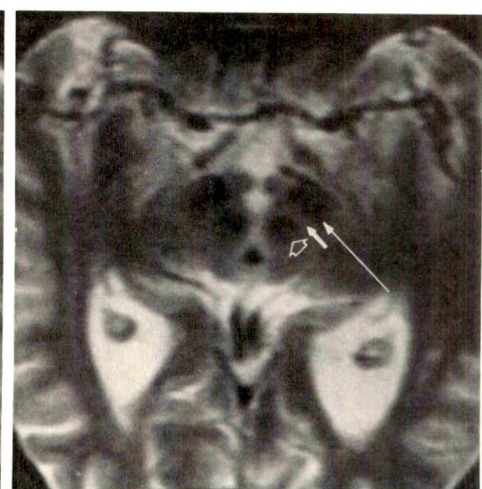


Fig. 6.—MR image (2500/80) of 60-year-old woman scanned for unrelated disorder (control subject). Scanning plane is 0–20° positive to inferior orbitomeatal line. Pars compacta of substantia nigra (short solid arrow) is the relatively hyperintense band between hypointense pars reticulata (long solid arrow) of substantia nigra and hypointense red nucleus (open arrow).

TABLE 1: Measured Widths of the Pars Compacta of Substantia Nigra in Parkinson and Control Subjects

Group: Case No.	Width (mm)	
	Right	Left
Parkinson:		
1	2.53	1.92
2	1.84	2.10
3	2.95	1.77
4	3.36	2.88
5	1.85	1.96
6	1.71	2.50
7	2.14	1.72
8	2.27	1.67
9	2.24	4.10
10	0	0
11	2.99	1.65
12	2.88	2.54
13	2.70	1.97
14	2.32	1.84
15	3.04	0.96
16	1.72	2.13
Control:		
1	1.95	2.56
2	2.78	2.79
3	2.83	4.22
4	2.51	2.61
5	2.88	2.99
6	2.78	2.91
7	2.18	2.43
8	2.20	3.08
9	2.30	2.01
10	3.71	3.50
11	2.13	1.80
12	2.61	2.24
13	3.00	3.36
14	1.86	2.15
15	2.83	2.63
16	3.09	2.67
17	3.05	2.32
18	1.97	1.92
19	3.10	2.61
20	3.31	2.72
21	2.39	2.45
22	3.04	2.98
23	2.66	2.82
24	2.85	2.98

Note.—Five of the 21 Parkinson patients are not included here because they were unable to maintain proper head position for scanning through the midbrain at 0–20° positive to the inferior orbitomeatal line, or moved during scanning.

patients, comparing the two groups with chi-square revealed the difference was not statistically significant ($\chi^2 = 2.86$, $p > .05$). On gradient-echo sequences, the substantia nigra was restored in four (10%) of 40 Parkinson patients and in two (4%) of 46 controls (Table 3). The substantia nigra was in the restored category in too few patients (less than five) on gradient-echo sequences to determine statistical significance.

Atrophy was more common in the Parkinson group than in the control group (Fig. 8) (Table 4). Comparing the two groups with chi-square revealed the difference was not statistically significant ($\chi^2 = 3.285$, $p > .05$). However, in selecting controls, we did not exclude subjects with disorders that may result in atrophy. It is possible that this difference in atrophy

would be statistically significant if it were compared with otherwise normal elderly subjects.

Three patients had bilateral hyperintense foci on the long TR spin-echo sequences in the globi pallidi (Fig. 3). One of these patients was hypertensive; the other two were neither hypertensive nor had other cardiovascular risk factors. No control subject revealed these features.

Four patients had hyperintense foci on the long TR spin-echo sequences in the substantia nigra or in adjacent structures (Fig. 9). None of these patients was hypertensive or had other cardiovascular risk factors. Three control subjects revealed similar findings. One was hypertensive while the others were neither hypertensive nor had other cardiovascular risk factors.

Discussion

Although known since ancient times, Parkinson disease, or paralysis agitans, was first described concisely by James Parkinson in 1817 [10]. The disease is relatively prevalent. Approximately 1% of the population over the age of 50 years in the United States is affected, for a total of approximately a half million people [5]. Its onset is between 40 and 70 years of age.

The neuropathologic hallmark of the disease is loss of neuromelanin-containing neurons in the substantia nigra (most marked in the central part of the pars compacta), the locus ceruleus, and the dorsal vagal nucleus [17–17]. Associated changes of gliosis occur at these sites. The remaining cells contain Lewy bodies, an eosinophilic cytoplasmic inclusion.

Our study corroborated the results described by Duguid et al. [3] regarding a decreased width in the pars compacta of the substantia nigra in Parkinson patients. As those authors commented, this MR appearance probably reflects the atrophy of this structure described in the neuropathologic literature, but possibly may be due to increased iron in this region.

Of interest are the four parkinsonian patients who, in addition to a decreased breadth of the pars compacta, revealed punctate hyperintense foci of the substantia nigra on long TR spin-echo sequences (Fig. 9). This may represent the gliosis that accompanies the cell loss of the pars compacta. Similar punctate hyperintense foci of the substantia nigra in three control subjects, however, illustrate the lack of specificity of this latter observation.

Gradient-echo images are more sensitive than spin-echo images to local magnetic field inhomogeneity [18]. This greater sensitivity accounts for the higher grading of the putamen and lower incidence of restoration of the substantia nigra in both Parkinson patients and controls on gradient-echo compared with spin-echo images (Tables 2 and 3). We were unable to detect a statistically significant difference in the grading of the putamen in the Parkinson group compared with the control group on either spin-echo or gradient-echo sequences. However, we did observe grade 3 in both putamina of one Parkinson patient with the spin-echo technique (Fig. 4) and in an additional patient with the gradient-echo technique, but in no control patient with either technique. Our

Fig. 7.—A, MR image (2500/80) of 76-year-old woman with Parkinson disease (same patient as in Fig. 2). Observe narrowed hyperintense band (pars compacta of left substantia nigra) between hypointense pars reticulata of left substantia nigra and left red nucleus. Right pars compacta is not affected as markedly.

B, MR image (2500/80) of 73-year-old woman with Parkinson disease (same patient as in Fig. 3). Note complete loss of normal hyperintense band between pars reticulata of substantia nigra and red nuclei bilaterally.

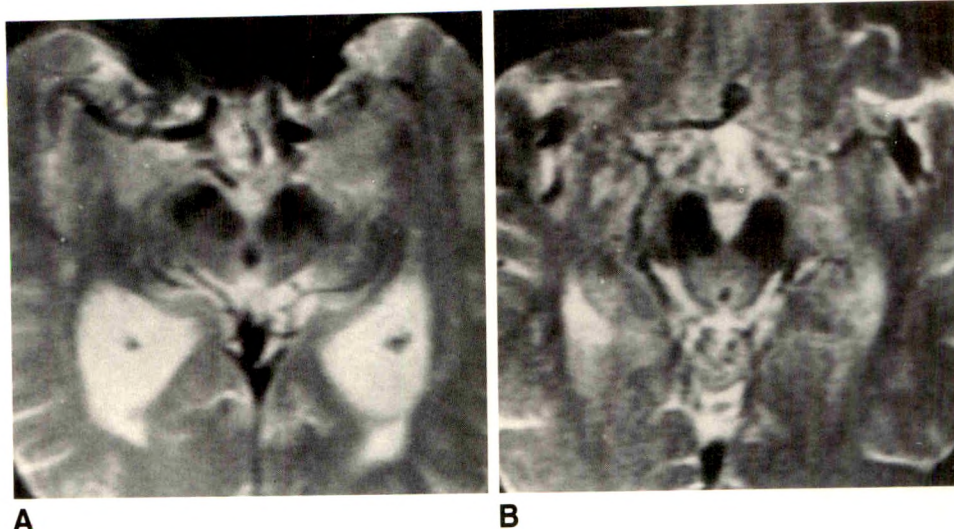


TABLE 2: Putaminal Intensities in Parkinson and Control Patients on Spin-Echo and Gradient-Echo Sequences

Sequence: Intensity Grade	No. (%)	
	Parkinson	Control
Spin-echo 2500/80:		
0	5 (12)	6 (13)
1	30 (71)	36 (75)
2	5 (12)	6 (13)
3	2 (5)	0
Gradient-echo:		
0	6 (15)	3 (7)
1	17 (43)	24 (52)
2	13 (33)	19 (41)
3	4 (10)	0

Note.—Grade 0 = no hypointensity; 1 = hypointensity limited to the lateral margin of the putamen; 2 = hypointensity extending through part of the body of the putamen; 3 = diffuse hypointensity of the entire putamen.

TABLE 3: Restoration of the Signal Intensities [4] of the Substantia Nigra in Parkinson and Control Patients on Spin-Echo and Gradient-Echo Sequences

Sequence: Signal Intensity	No. (%)	
	Parkinson	Control
Spin-echo 2500/80:		
Restored	10 (24)	7 (15)
Normal	32 (76)	41 (85)
Gradient-echo:		
Restored	4 (10)	2 (4)
Normal	36 (90)	44 (96)

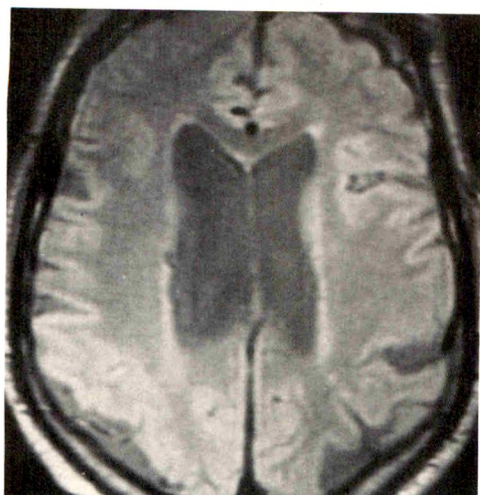
patient and control populations were not large enough to determine whether these one or two patients whose putamina were graded 3 constitute a statistically significant group.

Drayer et al. [1] reviewed the literature regarding brain iron and Parkinson disease. Earle [16] found that measurements of brain tissue iron concentration by X-ray fluorescent spectrographic analysis in 11 formalin-fixed brains of subjects with Parkinson disease were increased by a factor of 2 or more

as compared with normals. Earle noted a generalized shift of this element rather than a focal deposition of this substance. Other authors have reported a localized deposition of iron. Rojas et al. [19] found an increase in glial and neuronal intracytoplasmic iron pigments in the ventrolateral thalamic, lentiform, and caudate nuclei, but not in the cerebral cortex in Parkinson patients (four idiopathic, two "arteriosclerotic," one postencephalitic). Five of these subjects who either had autopsy or had a needle biopsy of the liver also had a systemic siderosis. Unlike the description of Rojas et al. of no iron in the cerebral cortex, Kingo [20] described a positive iron reaction in the frontal cortex and substantia nigra in Parkinson patients. Lhermitte et al. [21] observed increased iron in the globus pallidus in one case of postencephalitic parkinsonism. Barbeau and Boileau [22] demonstrated an increase in urinary iron excretion in Parkinson patients following a single muscular injection of iron chelates, suggesting an increase in body storage of mobile iron in Parkinson disease. In a recent study, Rutledge and Schallert [23] evaluated the effect of administering a catecholaminergic neurotoxin to rats. On MR, these subjects revealed an abnormal hypointensity in the striato-nigral tract. The authors suggested this may be due to ferritin deposition.

The conclusive role of iron or another paramagnetic substance (striatal, nigral, and/or other) in Parkinson patients awaits further investigation. On the basis of our study, however, most patients with Parkinson disease do not demonstrate a pattern of putaminal hypointensity on long TR/long TE spin-echo images or on T2*-weighted images (gradient-echo sequences) that differs from that of controls. Alternatively, patients with the parkinsonian syndromes of multiple-system atrophy, Shy-Drager syndrome, and progressive supranuclear palsy may reveal more marked putaminal hypointensity on these sequences than do either Parkinson patients or normals [1, 2]. Therefore, MR may serve as an adjunct to the clinical examination in differentiating Parkinson disease from certain parkinsonian syndromes.

Although we found restoration of the signal intensity of the substantia nigra to be more frequent in Parkinson patients



8



9

Fig. 8.—MR image (2500/20) of 76-year-old man with Parkinson disease. Observe marked cortical and central parenchymal loss with enlarged subarachnoid spaces, particularly of parietooccipital lobes, and enlarged lateral ventricles.

Fig. 9.—MR image (2500/20) of 67-year-old woman with Parkinson disease. Observe bilateral punctate hyperintense foci (arrows) in substantia nigra. One lesion is at junction of left pars reticulata and pars compacta; the other is in right pars compacta.

TABLE 4: Cortical Atrophy in Parkinson and Control Patients

Degree of Cortical Atrophy	No. (%)	
	Parkinson	Control
Normal	0	3 (13)
Mild	10 (48)	13 (54)
Moderate	6 (28)	6 (25)
Marked	5 (24)	2 (8)

than in controls, it was not a statistically significant difference. Rutledge et al. [4] suggested the restoration of signal intensity may be due to depletion of iron by increased cellular metabolic activity or local cell death resulting in expansion of the extracellular space, which overwhelms the T2* effect and increases the signal.

The significance of pallidal lesions in Parkinson disease is controversial. Pakkenberg [24] described a paleness of the cytoplasm of pallidal cells in Parkinson patients. Denny-Brown [25] observed pallor in myelin-stained preparations of the globus pallidus in these subjects. Lipkin [26] reported atrophy of the globus pallidus in these patients compared with age-matched controls. However, other investigators found no difference in the pallidi of Parkinson patients compared with controls [13, 14, 27–29]. Oppenheimer [17] commented that the above-described pathologic changes of the basal ganglia are seen in elderly people not suffering from parkinsonism. In our study, bilateral pallidal hyperintense foci on long TR spin-echo images were noted in three of the 21 Parkinson patients (Fig. 3) and in none of the 24 controls. This suggests there may be an increased incidence of such lesions in Parkinson patients. Rutledge et al. [4] observed similar findings in four of their seven patients with Shy-Drager syndrome. They suggested that the appearance of the globus pallidus may allow distinction between olivopontocerebellar degeneration and Shy-Drager syndrome on MR. Our observation of this change in three patients with Parkinson disease implies that it may not allow such differentiation.

We found moderate or marked atrophy in 52% of our patients and in 33% of our controls. Although the difference was not statistically significant, in selecting controls we did not exclude those with other processes that may result in atrophy. Alvord [15] stated that atrophy probably is significant and beyond what one would expect for age. Rutledge et al. [4] found generalized atrophy in 86% of patients with parkinsonism and in 56% of age-matched controls.

The progress in our understanding the features of Parkinson disease on MR may parallel the experience of F. H. Lewy, as described and quoted by Alvord [15]. After a lifetime of study of Parkinson disease, Lewy said, "When I had investigated my first two dozen cases, . . . I was convinced that I knew where the cause of tremor and rigidity was located. When I had examined pathologically the seventh dozen, . . . I was completely confused because you seemed to be able to prove just as well one theory as the contrary one."

Our data confirm certain MR features of Parkinson disease:

1. There is a statistically significant decrease in the width of the pars compacta [3]. This probably reflects selective loss of neuromelanin-containing cells of the pars compacta of the substantia nigra, but may also be due to iron deposition. This may be the characteristic feature of the disease on MR. In some cases, accompanying hyperintense foci may be seen that may represent the concomitant gliosis.

2. Most Parkinson patients do not show a pattern of putaminal hypointensity on long TR/long TE spin-echo images or on T2*-weighted images (gradient-echo sequences) that differs from that of controls.

3. Although restoration of the signal intensity of the substantia nigra [4] occurred more often in Parkinson patients than in controls, it was not statistically significant in our study.

4. Moderate and marked cortical atrophy occurred more often in Parkinson patients than in controls; however, the difference was not statistically significant.

5. Pallidal lesions, which may be the same lesions described in elderly patients without the disease, may occur more often in patients with Parkinson disease.

ACKNOWLEDGMENT

We thank Harold Kundel for assistance with the statistical analysis of our data.

REFERENCES

1. Drayer BP, Olanow W, Burger P, et al. Parkinson plus syndrome: diagnosis using high field MR imaging of brain iron. *Radiology* **1986**;159:493-498
2. Pastakia B, Polinsky R, Di Chiro G, et al. Multiple system atrophy (Shy-Drager syndrome): MR imaging. *Radiology* **1986**;159:499-505
3. Duguid JR, De La Paz R, DeGroot J. Magnetic resonance imaging of the midbrain in Parkinson's disease. *Ann Neurol* **1986**;20:744-747
4. Rutledge JN, Hilal SK, Silver AJ, Defendi R, Fahn S. Study of movement disorders and brain iron by MR. *AJNR* **1987**;8:397-411
5. Adams RD, Victor M. Diseases characterized by abnormalities of posture and movement. In: *Principles of neurology*, 2nd ed. New York: McGraw-Hill, **1981**:807-813
6. Drayer BP. Degenerative brain disorders and brain iron. In: Brant-Zawadzki M, Norman D, eds. *Magnetic resonance imaging of the central nervous system*. New York: Raven, **1987**:123-130
7. Wehrli F, Prost JH, Roberts F. The distinguishing properties of gradient-recalled acquisition in the steady state (GRASS). *Magn Reson Imaging* **1987**;5[Suppl 1]:105
8. Buxton RB, Edelman RR, Rosen BR, et al. Contrast in rapid MR imaging: T1- and T2-weighted imaging. *J Comput Assist Tomogr* **1987**;11(1):7-16
9. Fleiss JL. *Statistical methods for rates and proportions*, 2nd ed. New York: Wiley, **1981**
10. Parkinson J. An essay on the shaking palsy. London: Whittingham & Rowland, **1817**. (Reprinted in Critchley M, ed. *James Parkinson*. London: Macmillan, **1955**)
11. Tretiakoff C. Contribution a l'etude de l'anatomie pathologique du locus niger [Thesis]. Paris: University of Paris, **1919**
12. Foix MC. Les lesions anatomiques de la maladie de Parkinson. *Rev Neurol (Paris)* **1921**;28:593-600
13. Hassler R. Zur Pathologie der Paralysis agitans und des postencephalitischen Parkinsonismus. *J Psychol Neurol* **1938**;48:387-476
14. Klaue R. Parkinsonsche Krankheit (paralysis agitans) und postencephalitische Parkinsonismus. *Eur Arch Psychiatry Neurol Sci* **1940**;111:251-321
15. Alvord EC. The pathology of parkinsonism. In: Minckler J, ed. *Pathology of the nervous system*, vol. 1. New York: McGraw-Hill, **1968**:1152-1161
16. Earle KM. Studies on Parkinson's disease including x-ray fluorescent spectroscopy of formalin fixed brain tissue. *J Neuropathol Exp Neurol* **1968**;27:1-14
17. Oppenheimer DR. Diseases of the basal ganglia, cerebellum, and motor neurons. In: Adams JH, Corsellis JAN, Duchon LW, eds. *Greenfield's neuropathology*, 4th ed. New York: Wiley-Medical, **1984**:699-747
18. Edelman RR, Johnson K, Buxton R, et al. MR of hemorrhage: a new approach. *AJNR* **1986**;7:751-756
19. Rojas G, Asenjo A, Chiorino R, Aranda L, Rocamora R, Donso P. Cellular and subcellular structure of the ventrolateral nucleus of the thalamus in Parkinson disease. Deposits of iron. *Appl Neurophysiol* **1965**;26:362-376
20. Kingo S. Sobre la reaccion de fierro en el cerebro en los parkinsonismus postencefalicos. *Fukuoka Ikwaidsigaku Zasshi* **1934**;27:142
21. Lhermitte J, Kraus WM, McAlpine D. Etude des produits de desintegration et des depots du globus pallidus dans un cas de syndrome parkinsonien. *Rev Neurol (Paris)* **1924**;1:356-361
22. Barbeau A, Boileau JL. Mobilizable iron in Parkinson's disease (abstract). *Neurology* **1969**;19:314
23. Rutledge JN, Schallert T. Evaluation of iron distribution by MR T2* effect in unilateral dopamine depleted rats. Presented at the annual meeting of the Society of Magnetic Resonance in Medicine, New York City, August **1987**
24. Pakkenberg H. Globus pallidus in parkinsonism. *Acta Neurol Scand [Suppl]* **1963**;39:139-144
25. Denny-Brown D. *The basal ganglia and their relation to disorders of movement*. London: Oxford University, **1962**
26. Lipkin LE. Cytoplasmic inclusions in ganglion cells associated with parkinsonian states; a neurocellular change studied in 53 cases and 206 controls. *Am J Pathol* **1959**;35:1117-1133
27. Hassler R. Zur pathologischen Anatomie des senilen und des parkinsonistischen Tremor. *J Psychol Neurol* **1939**;49:193
28. Hallevorden J. Zur Pathogenese des postencephalitischen Parkinsonismus. *Klin Wochenschr* **1933**;12:692-695
29. Hallevorden J. Anatomische Untersuchungen zur Pathogenese des postencephalitischen Parkinsonismus. *Dtsch Z Nervenheilk* **1935**;136:68-77

FORTHCOMING ARTICLES

REVIEW ARTICLE

Modern diagnostic imaging in joint disease. *Dalinka MK, Kricun ME, Zlatkin MB, Hibbard C*

PROGRESS IN RADIOLOGY

Dual-energy radiographic absorptiometry for bone densitometry: current status and perspective. *Sartoris DJ, Resnick D*
Perfluorooctylbromide: a new contrast agent for CT, sonography, and MR imaging. *Mattrey RF*

FRONTIERS IN RADIOLOGY

New perspectives in thrombus-specific imaging: radiolabeled monoclonal antibodies. *Oster ZH, Som P*

CARDIOPULMONARY RADIOLOGY

The diagnosis of pulmonary nodules: comparison between standard and inverse digitized images and conventional chest radiographs. *Sheline ME, Brikman I, Epstein DM, Mezrich JL, Kundel HL, Arenson RL*
Case report. Pulmonary edema due to ingestion of organophosphate insecticide. *Li C, Miller WT, Jiang J*

GASTROINTESTINAL RADIOLOGY

Percutaneous transhepatic embolization of gastroesophageal varices: results in 400 patients. *L'Herminé C, Chastanet P, Delemazure O, Bonnière PL, Durieu JP, Paris JC*
CT evaluation of suspected hepatic metastases: comparison of techniques for IV contrast enhancement. *Paushter DM, Zeman RK, Schiebeler ML, Choyke PL, Jaffe MH, Clark LR*
Commentary. Dynamic CT scanning. *Foley WD*
Intrahepatic cholangiographic abnormalities in liver transplants: correlation with biopsy evidence of rejection and other disorders. *Bauman J, Campbell WL, Demetris AJ, Zajko AB*
Periportal low-attenuation areas on CT: value as evidence of liver transplant rejection. *Kaplan SB, Sumkin JH, Campbell WL, Zajko AB, Demetris AJ*
The sonographic diagnosis of acute gangrenous cholecystitis: importance of the Murphy sign. *Simeone JF, Brink JA, Mueller PR, et al.*
Technical note. The use of color-flow Doppler sonography to distinguish between dilated intrahepatic ducts and vascular structures. *Ralls PW, Mayekawa DS, Lee KP, Johnson MB, Halls J*

GENITOURINARY RADIOLOGY

Color Doppler ultrasound of the normal testis. *Middleton WD, Thorne DA, Melson GL*
Wilms tumor (nephroblastoma) in the adult patient: clinical and radiologic manifestations. *Kioumehri F, Cochran ST, Layfield L, Yaghamai I, Ngo C, Smith SR*
Percutaneous, large-bore, suprapubic cystostomy: technique and results. *Papanicolaou N, Pfister RC, Nocks BN*
Case report. Renal lymphangiomyoma—a rare cause of a multiloculated renal mass. *Jacobs JE, Sussman SK, Glickstein MF*

MUSCULOSKELETAL RADIOLOGY

Pictorial essay. The subclavian triangle: CT analysis. *Wechsler RJ, Rao VM, Newman LM*
Flexion teardrop fracture of the cervical spine: radiographic characteristics. *Kim KS, Chen HH, Russell EJ, Rogers LF*
MR imaging of the pars interarticularis. *Johnson DW, Farnum GN, Latchaw RE, Erba SM*
Incidental detection of hematopoietic hyperplasia on routine knee MR imaging. *Deutsch AL, Mink JH, Rosenfelt FP, Waxman AD*
Pictorial essay. Imaging of pigmented villonodular synovitis with emphasis on MR imaging. *Jelinek JS, Kransdorf MJ, Utz JA, et al.*

PEDIATRIC RADIOLOGY

Case report. Cerebellar atrophy caused by high-dose cytosine arabinoside: CT and MR findings. *Miller L, Link MP, Bologna S, Parker BR*
Case report. Aortico-left ventricular tunnel: diagnosis by cine angiocardiology. *Guo D-W*

NEURORADIOLOGY

Efficacy of MR vs CT in epilepsy. *Heinz ER, Heinz TR, Radtke R, et al.*
Absence of the septum pellucidum: a useful sign in the diagnosis of congenital brain malformations. *Barkovich AJ, Norman D*
Intracranial oligodendrogliomas: imaging findings in 35 untreated cases. *Lee Y-Y, Van Tassel P*

VASCULAR AND INTERVENTIONAL RADIOLOGY

Color Doppler ultrasound imaging of lower extremity venous disease. *Foley WD, Middleton WD, Lawson TL, Erickson S, Quiroz FA, Macrander S*
Case report. Fat-shift artifact simulating aortic dissection on MR images. *Lotan CS, Cranney GB, Doyle M, Pohost GM*
Chemotherapy and embolization via the inferior epigastric artery for the treatment of primary and metastatic cancer. *O'Keeffe F, Lorigan JG, Charnsangavej C, Carrasco CH, Richli WR, Wallace S*
Technical note. A technique for pulmonary artery catheterization in patients with right ventricular enlargement. *Waltman AC, Walker TG*
Case report. Embolotherapy of a high-flow false aneurysm by using an occlusion balloon, thrombin, steel coils, and a detachable balloon. *Lammert GK, Merine D, White RI Jr, Fishman EK, Porterfield JK*

CONTRAST MATERIAL

Anticoagulant effects of contrast material: in vitro study of iohexol, ioxaglate, and diatrizoate. *Rasuli P, McLeish WA, Hammond DI*

Superparamagnetic Iron Oxide: Pharmacokinetics and Toxicity

Ralph Weissleder¹
David D. Stark¹
Barry L. Engelstad²
Bruce R. Bacon³
Carolyn C. Compton⁴
David L. White²
Paula Jacobs⁵
Jerome Lewis⁵

The pharmacokinetics (distribution, metabolism, bioavailability, excretion) and toxicity (acute and subacute toxicity, mutagenicity) of a superparamagnetic iron oxide preparation (AMI-25), currently used in clinical trials, were evaluated by ⁵⁹Fe radiotracer studies, measurements of relaxation times, the ability to reverse iron deficiency anemia, histologic examination, and laboratory parameters. One hour after administration of AMI-25 to rats (18 μ mol Fe/kg; 1 mg Fe/kg), $82.6 \pm 0.3\%$ of the administered dose was sequestered in the liver and $6.2 \pm 7.6\%$ in the spleen. Peak concentrations of ⁵⁹Fe were found in liver after 2 hr and in the spleen after 4 hr. ⁵⁹Fe slowly cleared from liver (half-life, 3 days) and spleen (half-life, 4 days) and was incorporated into hemoglobin of erythrocytes in a time-dependent fashion. The half-time of the T2 effect on liver and spleen (24–48 hr) was shorter than the ⁵⁹Fe clearance, indicating metabolism of AMI-25 into other forms of iron. IV administration of AMI-25 (30 mg Fe/kg) corrected iron-deficiency anemia and showed bioavailability similar to that of commercially available IV iron preparations within 7 days. No acute or subacute toxic effects were detected by histologic or serologic studies in rats or beagle dogs who received a total of 3000 μ mol Fe/kg, 150 times the dose proposed for MR imaging of the liver.

Our results indicate that AMI-25 is a fully biocompatible potential contrast agent for MR.

Received July 8, 1988; accepted after revision August 23, 1988.

D. D. Stark is supported by American Cancer Society grants PDT 326 and JFRA-163 and is a member of the Scientific Advisory Board of Advanced Magnetics, Inc.

B. L. Engelstad is supported in part by U. S. Public Health Service grant ROICA 38918.

B. R. Bacon is supported in part by United States Public Health Service grants ROIDK 31505 and R23DK 35469.

J. Lewis is supported in part by National Cancer Institute grant CA 426170-02.

¹ Department of Radiology, Massachusetts General Hospital and Harvard Medical School, 35 Fruit St., Boston, MA 02114. Address reprint requests to R. Weissleder.

² Department of Radiology, Contrast Media Laboratory, University of California, San Francisco, CA 94143.

³ Department of Internal Medicine, Louisiana State University Medical Center, Shreveport, LA 71130.

⁴ Department of Pathology, Massachusetts General Hospital and Harvard Medical School, Boston, MA 02114.

⁵ Advanced Magnetics, Inc., Cambridge, MA 02138.

AJR 152:167–173, January 1989

0361-803X/89/1521-0167

© American Roentgen Ray Society

Magnetic iron oxides are a new class of MR contrast agents that have been shown to significantly increase the detectability of hepatic [1, 2] and splenic tumors [3, 4] by MR. A variety of preparations have been tested in preclinical studies, including ferromagnetic microspheres having a starch [5] or albumin matrix [6], magnetite [7, 8], albumin-coated magnetite [9], and superparamagnetic crystalline iron oxide [10, 11].

In this study, we evaluated AMI-25, the first superparamagnetic iron oxide preparation to be used in clinical trials [12, 13], to determine its distribution, bioavailability, metabolism, excretion, and toxicity. The pharmacokinetic behavior of AMI-25 was determined independently by ⁵⁹Fe radiotracer studies, tissue relaxation time measurements, the ability to reverse iron-deficiency states, and histologic inspection of tissue. Studies of acute and subacute toxicity were performed in rodents and dogs. The Ames test was performed to assess potential mutagenicity.

Materials and Methods

Iron Oxide

Superparamagnetic iron oxide (AMI-25), prepared by modification of the method of Whitehead et al. [11], was synthesized by Advanced Magnetics, Inc., Cambridge, MA. The material was provided as a stable aqueous colloid with a concentration of 200 μ mol Fe/ml (11.2 mg Fe/ml). The volume median diameter of particles was 80 nm as measured by laser light scattering (Brookhaven BI-90 particle sizer, Brookhaven, NY). The relaxivity of this preparation was $3 \times 10^4 \text{ sec}^{-1} \text{ M}^{-1}$ for 1/T1 and $1 \times 10^5 \text{ sec}^{-1} \text{ M}^{-1}$ for 1/T2 in water (20 MHz, 37°C). The magnetic properties of this preparation have been reported in more detail elsewhere [10].

Radioactive AMI-25 was synthesized by incorporating ^{59}Fe into the superparamagnetic iron oxide core. The specific activity was 8460 $\mu\text{Ci}/\mu\text{mol}$ (313,020 $\text{kBq}/\mu\text{mol}$) Fe at calibration. The radiolabeled particles were mixed with unlabeled particles to give a specific activity of 36 $\mu\text{Ci}/\mu\text{mol}$ (1332 $\text{kBq}/\mu\text{mol}$) Fe. Pharmacokinetic studies were performed at a dose of 18 μmol Fe/kg (equivalent to 1 mg Fe/kg), similar to the dose proposed for clinical MR (20 μmol Fe/kg) [13].

Animals

Sprague-Dawley rats (Charles River Laboratories, Wilmington, MA) were anesthetized via intraperitoneal administration of 30–50 mg/kg sodium pentobarbital. Fifty-five male Sprague-Dawley rats (300–350 g) were used for radiotracer studies (four for whole body clearance, 48 for organ biodistribution, and three for erythrocyte incorporation), 39 for relaxation time measurement, and seven for histology. Toxicology studies were performed on 32 male and 32 female Sprague-Dawley rats.

Iron deficiency was produced by feeding 30 weanling (50–70 g) Sprague-Dawley rats (Zivic-Miller, Allison Park, PA) an iron-deficient diet (Low Iron Diet, ICN Nutritional Biochemicals, Cleveland, OH). Eight control animals received a standard diet (Purina Rat Chow, Ralston Purina, St. Louis, MO). Animals were housed in polyethylene cages with stainless steel tops.

A total of 30 beagle dogs (15 male, 15 female, 4 months old) were used for toxicology studies (Hazelton Research Animals, Cumberland, VA).

^{59}Fe Radiotracer Studies

Organ biodistribution was determined by injection of ^{59}Fe -AMI-25 at a dose of 18 μmol Fe/kg (2 $\mu\text{Ci}/\text{kg}$ [74 kBq/kg]). Animals were sacrificed before injection and at several points after injection (7.5, 15, and 30 min; 1, 2, 4, 8, and 16 hr; and 2, 4, 7, 14, 34, 60, and 90 days; three animals at each time point). Liver, spleen, blood, lung, kidney, and brain were obtained, and the radioactivity measured together with an ^{59}Fe standard. Radioactivity was corrected at each time point for ^{59}Fe decay, and results were expressed as the percentage of the injected dose per organ or gram tissue. Values were expressed as mean \pm standard deviation.

RBC incorporation of iron oxide was determined after IV administration of ^{59}Fe -AMI-25 (18 μmol Fe/kg) into three rats. Serial 0.2-ml blood samples were obtained after 1, 2, 4, 7, 14, 21, 28, 35, 42, 49, and 56 days. After blood samples were centrifuged and washed, 0.05 ml of erythrocytes were counted. At day 21, the total blood volume was determined by the ^{51}Cr radioisotope dilution technique. The RBC volume was calculated as total blood volume multiplied by the hematocrit.

Whole-body clearance studies were conducted in four rats injected with ^{59}Fe -AMI-25, at 18 μmol Fe/kg (2 $\mu\text{Ci}/\text{kg}$ [74 kBq/kg]). Counts from each rat were immediately obtained in a chamber counter (Tobor Nuclear, Chicago, IL), and then the rats were placed in a metabolic cage. Serial counting was performed at 2 hr and at 1, 2, 4, 7, 14, and 28 days. Separate fecal and urine samples and a ^{59}Fe standard were counted at identical time points.

Iron-Deficiency Studies

Weanling rats were divided into four groups of five animals each. Group 1 received the standard chow diet (normal controls), and groups 2–4 received the iron-deficient diet. After 4 weeks, rats in

group 1 (normal controls) and group 2 (iron deficiency) were sacrificed to confirm the presence of iron deficiency. Animals in group 3 received a single IV injection of iron-dextran as a positive control (Imferon, Merrel Dow Pharmaceuticals; 30 mg Fe/kg), and group 4 received a single injection of superparamagnetic iron oxide (AMI-25; 537 μmol Fe/kg corresponding to 30 mg Fe/kg). At 1, 3, 5, and 7 days after the administration of Imferon and AMI-25, rats from groups 3 and 4 were sacrificed by exsanguination via cardiac puncture. Hematocrit [14], hemoglobin [14], serum iron [15], and total iron-binding capacity [16] were determined by using standard methods. Liver iron concentrations were determined by using the chemical method of Torrance and Bothwell [17].

To evaluate the effect of dose in the reversal of anemia, we performed a separate study. Varying doses of AMI-25 (18, 89, 179, 357, and 536 μmol Fe/kg corresponding to 1, 5, 10, 20, and 30 mg Fe/kg) were administered to anemic rats ($n = 3$ for each dose). In this group of animals, only hematocrit and liver iron concentrations were determined 7 days after administration.

Relaxation Time Measurements

MR relaxation times of liver, spleen, lung, kidney, and muscle were determined to measure the effect of AMI-25 on each tissue. AMI-25 was injected at a dose of 18 μmol Fe/kg and groups ($n = 3$) of animals were sacrificed at 7.5, 15, 30, 60, 120, and 240 min and at 1, 2, 4, 7, 14, 28, and 91 days after injection. Animals were sacrificed by exsanguination, and organs were removed immediately. Relaxation time measurements were performed at 37°C within 1 hr after sacrifice.

T2 values were obtained by using an NMR spectrometer (PC 20 Minispec, IBM) operating at 0.47 T, corresponding to a proton resonance frequency of 20 MHz. After calibration, T2 was obtained from 10 data points generated with a Carr-Purcell-Meiboom-Gill pulse sequence [18]. T2 values were plotted as reciprocal values ($1/T2$ relaxation rate) over time.

Pathologic Studies

Histologic examinations of liver were performed to document disappearance of stainable iron after administration of AMI-25. Histologic examinations were performed before, at 3 hr, and at 1, 2, 9, 16, and 30 days after injection of AMI-25 (18 μmol Fe/kg; 1 mg Fe/kg). Samples of excised livers were fixed in 10% formalin, embedded in paraffin, and stained for iron with Perls' Prussian blue stain. In this histochemical method, ferric iron is dissolved from organic complexes (hemosiderin, ferritin, iron-dextran, AMI-25, etc.) by hydrochloric acid, and then reacts with potassium ferrocyanide [$\text{K}_4\text{Fe}(\text{CN})_6$] to form the blue precipitate, ferric ferrocyanide [$\text{Fe}_4[\text{Fe}(\text{CN})_6]_3$] [19]. Prussian blue stain sections were randomly coded and scored for iron content by a pathologist.

Toxicity

Studies of acute toxicity were performed in 18 rats and in 12 beagle dogs. Animals were injected with 500 μmol Fe/kg (28 mg Fe/kg) or 3000 μmol Fe/kg (168 mg Fe/kg) of AMI-25. Control animals were handled and injected in a similar way but did not receive AMI-25. Animals were observed for 14 days, sacrificed, and autopsied.

Studies of subacute toxicity were performed in 60 rats and in 18 beagle dogs. Over a period of 3 weeks each animal received a total of nine injections with either 0, 50 μmol Fe/kg (2.8 mg Fe/kg), or 250 μmol Fe/kg (14 mg Fe/kg) of AMI-25 per injection. All animals were

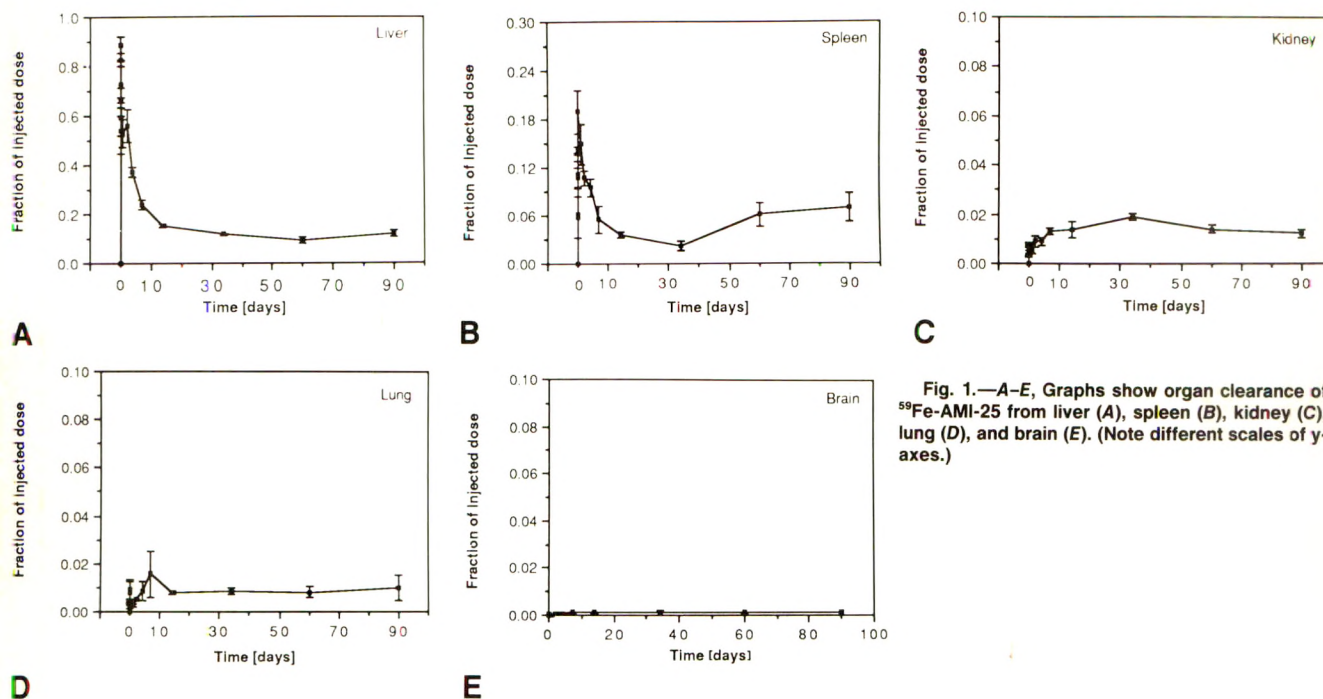


Fig. 1.—A–E, Graphs show organ clearance of ^{59}Fe -AMI-25 from liver (A), spleen (B), kidney (C), lung (D), and brain (E). (Note different scales of y-axes.)

checked twice daily for mortality and morbidity, and detailed physical examinations were performed before the start of the experiment and weekly thereafter. Blood (hematocrit, hemoglobin, erythrocyte count, leukocyte count, differential, and platelets), serum (Na, K, Cl, Ca, albumin, globulin, alkaline phosphatase, bilirubin, urea nitrogen, glucose, lactate dehydrogenase, aspartate aminotransferase, alanine aminotransferase, cholesterol, and serum iron), and urine samples were examined before the study began and on the last day. After 3 weeks the animals were sacrificed and autopsied. Gross examination was performed on 41 tissue samples. Histology was performed on tissue from liver, spleen, lung, bone marrow, lymph nodes, kidneys, brain, spinal cord, heart, aorta, glands, testes, ovaries, uterus, bowel, pancreas, bladder, muscle, and the injection site.

Mutagenicity was studied by the Ames *Salmonella* microsome reverse mutation assay, which measures back mutation to histidine independence of histidine mutants of *Salmonella typhimurium* [20]. This widely used test has been developed for testing chemicals for their ability to interact with DNA or mutagenicity [20, 21]. Five different strains of *Salmonella* (TA-1535, TA-1537, TA-1538, TA-90, and TA-100) were obtained (B. Ames, University of California at Berkeley, Berkeley, CA) and stored as frozen cultures. Different doses of iron oxide, ranging from 0.143 to 214 $\mu\text{mol Fe/plate}$ (0.008–12 mg Fe/plate) of AMI-25, were incubated with colonies (10^9 bacteria) at 37°C for 2 days. Thereafter, the number of revertant colonies was recorded.

Results

Pharmacokinetics

Distribution.—One hour after injection of ^{59}Fe -AMI-25, high concentrations of ^{59}Fe were found in liver ($82.6 \pm 0.26\%$ of the injected dose) and spleen ($6.2 \pm 7.31\%$ of the injected dose). When organ biodistribution was expressed as per-

centage of injected dose per gram of tissue, liver ($6.3 \pm 0.52\%/g$) and spleen ($10.9 \pm 7.56\%/g$) showed the highest concentrations (Fig. 1). Only minimal amounts of ^{59}Fe were detectable in other tissues, such as those of kidney, lung, and brain.

Determinations of T2 relaxation times showed a similar tissue-specific distribution in the reticuloendothelial system (Table 1). One hour after administration, $1/T_2$ of liver increased from $27.1 \pm 1.6 \text{ msec}^{-1}$ to $58.4 \pm 1.7 \text{ msec}^{-1}$ (215%) and that of spleen increased from $16.1 \pm 0.9 \text{ msec}^{-1}$ to $52.6 \pm 7.6 \text{ msec}^{-1}$ (327%). Changes in $1/T_2$ of lung, kidney, and muscle were minimal.

Metabolism.—Organ clearance was determined by measuring organ disappearance of ^{59}Fe (Fig. 1) and by serial determination of T2 relaxation times (Fig. 2). Maximum concentrations of ^{59}Fe were achieved in the liver at 2 hr ($88.6 \pm 3.4\%$ of the injected dose). In the spleen, maximum concentrations ($18.9 \pm 2.8\%$ of the injected dose) were observed 4 hr after the injection, indicating redistribution of iron. The observed half-life of ^{59}Fe was 3 days for liver and 4 days for spleen.

Relaxation time measurements showed a maximum increase in $1/T_2$ of liver and spleen within 4 hr after administration of AMI-25. Thereafter, $1/T_2$ decreased consistently (Fig. 2). Half-time of the liver and spleen $1/T_2$ effect was shorter than the organ clearance as measured by ^{59}Fe studies. In both liver and spleen, half-time of the $1/T_2$ effect occurred within 24–48 hr.

Bioavailability.—Molecular iron of ^{59}Fe -AMI-25 was incorporated into hemoglobin of normal rats in a time-dependent fashion (Fig. 3). One percent of the injected dose was associated with erythrocytes on day 2, 14% by day 7, and 20% by day 49.

TABLE 1: 1/T₂ Relaxation Rates Before and 1 hr After Administration of AMI-25

Organ	Rate (msec ⁻¹)		Ratio ^a
	Before	After	
Liver	27.1 ± 1.6	58.4 ± 1.7	0.54
Spleen	16.1 ± 0.9	52.6 ± 7.6	0.69
Lung	13.2 ± 0.8	14.9 ± 0.9	0.11
Kidney	18.7 ± 1.2	19.4 ± 1.0	0.04
Muscle	23.1 ± 1.8	25.2 ± 1.2	0.08

Note.—AMI-25 was injected at a dose of 18 $\mu\text{mol Fe/kg}$ (20 MHz, 37°C).

^a $(T_{2\text{post}} - T_{2\text{pre}})/T_{2\text{pre}}$. A ratio of zero indicates no uptake. The larger the ratio, the greater the uptake.

A dietary-induced iron-deficiency anemia was confirmed after 4 weeks by reduced levels of hemoglobin (7.9 ± 0.9 g/dl) and serum iron (49 ± 11 $\mu\text{g/dl}$) (Table 2). The total iron-binding capacity was normal (547 ± 25 $\mu\text{g/dl}$), but the saturation with molecular iron was reduced in anemic ($8.9 \pm 1.8\%$) but not in control animals ($36.1 \pm 6.1\%$).

After a single dose of Imferon (30 mg Fe/kg), hemoglobin, serum iron, and saturation of iron-binding capacity gradually returned to normal within 7 days. A single administration of AMI-25 reversed anemia similarly, indicating incorporation of iron from iron oxide into hemoglobin. Serial hematocrit determinations performed after 1 day ($28.6 \pm 2.72\%$), 3 days ($35.7 \pm 3.7\%$), 5 days ($39.4 \pm 1.96\%$), and 7 days ($42.2 \pm 0.42\%$) showed a gradual increase up to normal values ($43.5 \pm 0.83\%$) (Fig. 4).

Administration of variable doses of AMI-25 to anemic animals resulted in similar reversal of anemia (Fig. 5). Liver iron levels were elevated in animals that had received 178 $\mu\text{mol Fe/kg}$ (192 ± 22.2 $\mu\text{g/g}$ liver wet wt.), 357 $\mu\text{mol Fe/kg}$ (391 ± 50.6 $\mu\text{g/g}$ liver wet wt.), or 536 $\mu\text{mol Fe/kg}$ (563 ± 51.6 $\mu\text{g/g}$ liver wet wt.) of AMI-25. Animals receiving 90 $\mu\text{mol Fe/kg}$ (104.8 ± 13.4 $\mu\text{g/g}$ liver wet wt.) had liver iron contents similar to those in control animals (97 ± 10.4 $\mu\text{g/g}$ liver wet wt.).

At 3 hr, Kupffer cells throughout the lobules were filled with large amounts of stainable iron (Fig. 6). By 24 hr, the centrilobular zones were largely depleted of iron, but Kupffer cells in midacinar and periportal zones still contained significant amounts of iron, although the amounts were qualitatively reduced compared with amounts found at 3 hr. At 2 days, iron-containing macrophages began to appear in portal tracts, and the amount of iron seen in midacinar and periportal Kupffer cells was further reduced. By 9 days, only small amounts of iron were seen in scattered periportal and midacinar Kupffer cells, and the number of iron-bearing portal macrophages was increased. At 16 and 30 days, no stainable iron was seen in the liver, and the appearance was indistinguishable from liver specimens from uninjected control animals. No hepatocellular pathologic changes were found in any of the study specimens.

Excretion.—The whole body clearance of ^{59}Fe was 20% after 14 days and 35% after 28 days (Fig. 7). Fitting eight data points to a monoexponential clearance function, clearance (C) can be expressed as $C = 1.002 \times 10^{(-0.0067 \times T)}$, where T is the time after injection in days and -0.0067 is the

elimination constant [22]. The correlation coefficient of data fitted by using the least-squares method was 1.0 (Cricket Graph, Cricket Software, Philadelphia, PA). The extrapolated half-time of whole body clearance of ^{59}Fe was thus 44.9 days; $T_{1/4}$ was 18.7 days and $T_{3/4}$ was 89.9 days. Excretion of ^{59}Fe in urine and feces was 1.1% after 2 days and 10.1% after 7 days.

Toxicity

Acute toxicity.—Studies on acute toxicity revealed that AMI-25 had no lethal effect on animals at the highest dose injected (3000 $\mu\text{mol Fe/kg}$). Immediately after injection, animals showed a reversible discoloration of mucosa that was attributed to the black coloration of the agent. During the 14 days of observation, no adverse effects were seen on body weight or food consumption.

Subacute toxicity.—Studies on subacute toxicity revealed that injection of AMI-25 had no effect on mortality, morbidity, body weight, or food consumption. Laboratory values were all within normal range. Hematocrits and levels of serum iron and hemoglobin were increased but still within normal limits. Histologic studies showed increased amounts of pigment in the reticuloendothelial cells of the liver, spleen, and lymph nodes, and in macrophages at the injection site. No evidence of tissue damage was observed in any of the animals.

Mutagenicity.—The Ames test did not reveal an increased number of histidine revertant colonies after incubation with or without metabolic activation. AMI-25 was nontoxic to all indicator organisms up to the highest concentration of 214 $\mu\text{mol Fe/plate}$ (12 mg Fe/plate).

Discussion

Most paramagnetic MR contrast agents are designed by binding toxic metal ions to low-molecular-weight chelates. This strategy of chelation is a suitable method for agents confined to the extravascular space, but a poor choice for intracellular agents. Intracellular exposure of the chelate to acidic environments (lysosomes, vesicles) can result in dissociation of the metal ion from its chelate. The strategy used in the design of AMI-25 was to use a biodegradable iron oxide as the magnetically active label [10]. Superparamagnetic iron oxides are extremely good enhancers of proton relaxation with R₂ relaxivities an order of magnitude greater than those of paramagnetic ion chelates.

Biodistribution of AMI-25 as measured by ^{59}Fe and relaxation time studies is consistent with a model of initial vascular distribution of the agent and specific uptake in reticuloendothelial cells. Whereas radiotracer studies measure ^{59}Fe in both intact iron oxide crystals and ^{59}Fe degradation products derived from metabolism of the iron oxide, measurements of relaxation times quantify the superparamagnetic effect of intact iron oxide crystals only. Our results with both techniques indicate similar initial distribution of IV administered AMI-25, with 85–95% uptake in the reticuloendothelial system. Particles administered IV are cleared by macrophages and can be identified histologically in Kupffer cells of the liver or in macrophage cells in the splenic red pulp (C. C. Compton, unpublished results). Intracellular particles are found routinely

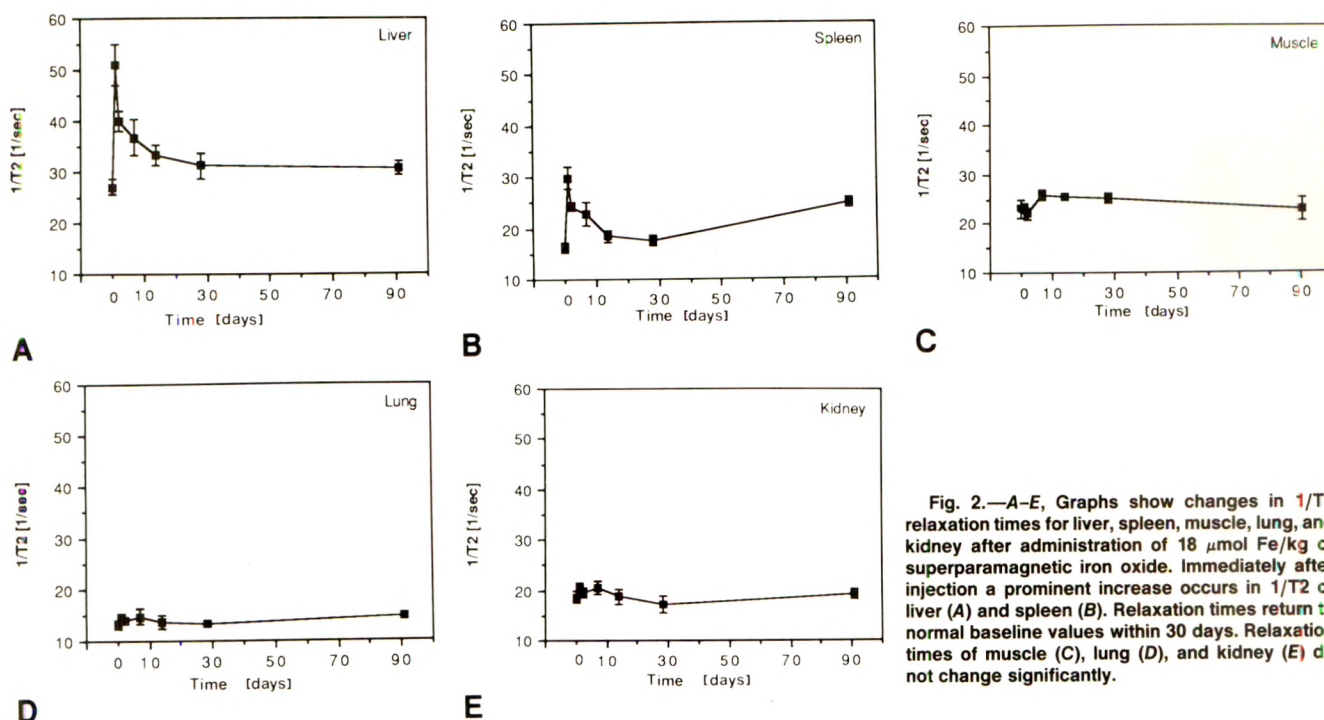


Fig. 2.—A-E, Graphs show changes in $1/T_2$ relaxation times for liver, spleen, muscle, lung, and kidney after administration of $18 \mu\text{mol Fe/kg}$ of superparamagnetic iron oxide. Immediately after injection a prominent increase occurs in $1/T_2$ of liver (A) and spleen (B). Relaxation times return to normal baseline values within 30 days. Relaxation times of muscle (C), lung (D), and kidney (E) do not change significantly.

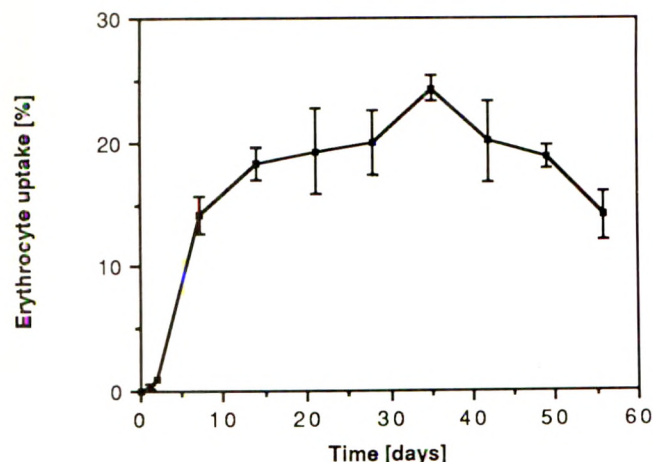


Fig. 3.—Graph shows that incorporation of iron from AMI-25 into hemoglobin in erythrocytes peaks 5–40 days after administration and decreases thereafter.

in lysosomes in which intracellular degradation takes place via a wide variety of hydrolytic enzymes [10].

Metabolism of intravenously administered AMI-25 was studied by measuring ^{59}Fe organ clearance, tissue relaxation times, and histology. After approximately 1 day, increases in T_2 and T_1 values toward the precontrast baseline represent the dissolution of the superparamagnetic particles in liver and spleen. As evidenced by radiotracer studies, iron is still present; however, it is no longer in the crystalline form necessary for superparamagnetic behavior. Interestingly, spleen displays a second peak of radioactivity after 60 days. This lower peak

TABLE 2: Reversal of Anemia After Administration of 30 mg Fe/kg Iron-Dextran (Imferon) and AMI-25

Group	Hemoglobin (g/dl)	Serum Iron ($\mu\text{g/dl}$)	Nonbinding Capacity	
			Total ($\mu\text{g/dl}$)	Saturation (%)
Normal	14.7 ± 0.4	194 ± 24	540 ± 43	36.1 ± 6.1
Iron deficiency anemia	7.9 ± 0.9	49 ± 11	547 ± 25	8.9 ± 1.8
Iron-dextran	13.5 ± 0.4	162 ± 33	544 ± 59	29.9 ± 7.4
AMI-25	13.3 ± 1.0	242 ± 65	545 ± 23	43.3 ± 13.1

is most likely due to secondary ^{59}Fe uptake from senescent erythrocytes. Clinical observation of reversal of liver [13] and spleen [12] signal intensity strengthens experimental evidence and suggests a similar metabolism of iron oxide in humans.

Bioavailability, the incorporation of molecular iron into hemoglobin after administration of ^{59}Fe -AMI-25, was evident from the incorporation of ^{59}Fe into hemoglobin. Twenty percent of the iron was found in hemoglobin 14 days after IV administration. Similar rates of erythrocyte incorporation (21%) have been reported for radiolabeled ferritin [23]. Bioavailability was also shown by the ability of AMI-25 to reverse iron-deficiency anemia to an extent similar to that of hematinic iron-dextran.

Acute toxicity of the superparamagnetic iron oxide preparation evaluated in this study was not evident at doses up to $3000 \mu\text{mol Fe/kg}$ and the LD_{50} would exceed this dose. The safety index (ratio of the acute lethal dose to the effective dose), therefore, is greater than 1:150. For comparison, safety margins for paramagnetic gadolinium-chelates [24] and for

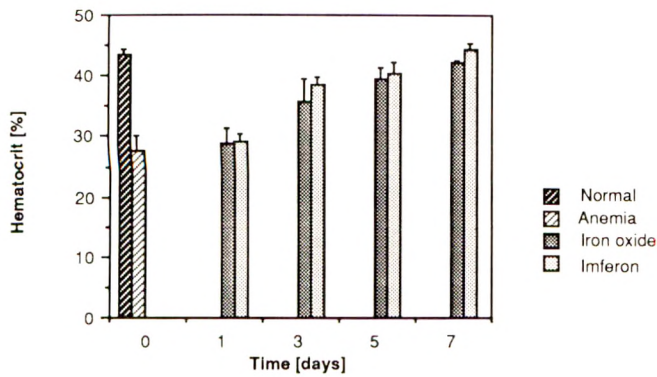


Fig. 4.—Graph shows that administration of AMI-25 reverses anemia in iron-deficient animals. After administration of 30 mg Fe/kg of iron dextran (Imferon) or iron oxide (AMI-25), hematocrit values increase to normal baseline values within 7 days. On days 3 and 7, hematocrits were also repeated from normal control and iron-deficient animals to confirm unchanged baseline values (not shown).

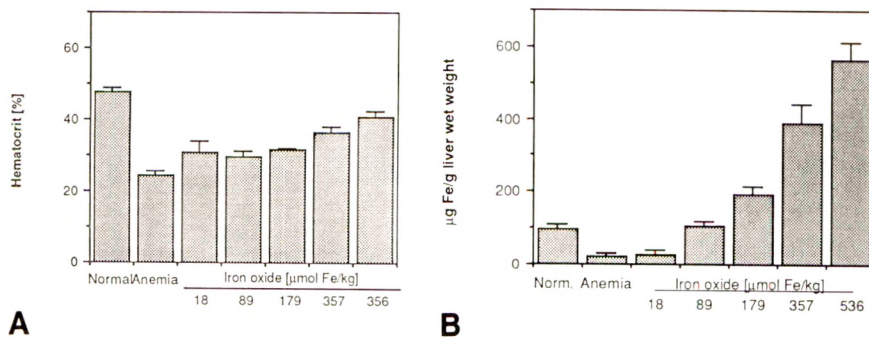


Fig. 5.—A and B, Graphs show effect of AMI-25 on hematocrit and liver iron concentration. AMI-25 was administered to anemic rats at various doses (18, 89, 179, 357, and 536 $\mu\text{mol Fe/kg}$, corresponding to 1, 5, 10, 20, and 30 mg Fe/kg). Hematocrits (A) and liver iron concentrations (B) were obtained 7 days after injection. Increasing doses of iron oxide have only moderate effect on reversal of iron-deficiency anemia. Administration of 18 $\mu\text{mol Fe/kg}$ has effect similar to that of 10 times higher dose (A). Liver iron concentrations increase with increasing doses of AMI-25. Low doses (18 $\mu\text{mol Fe/kg}$), as proposed for clinical imaging, do not significantly increase liver iron concentration (B). Norm. = normal.

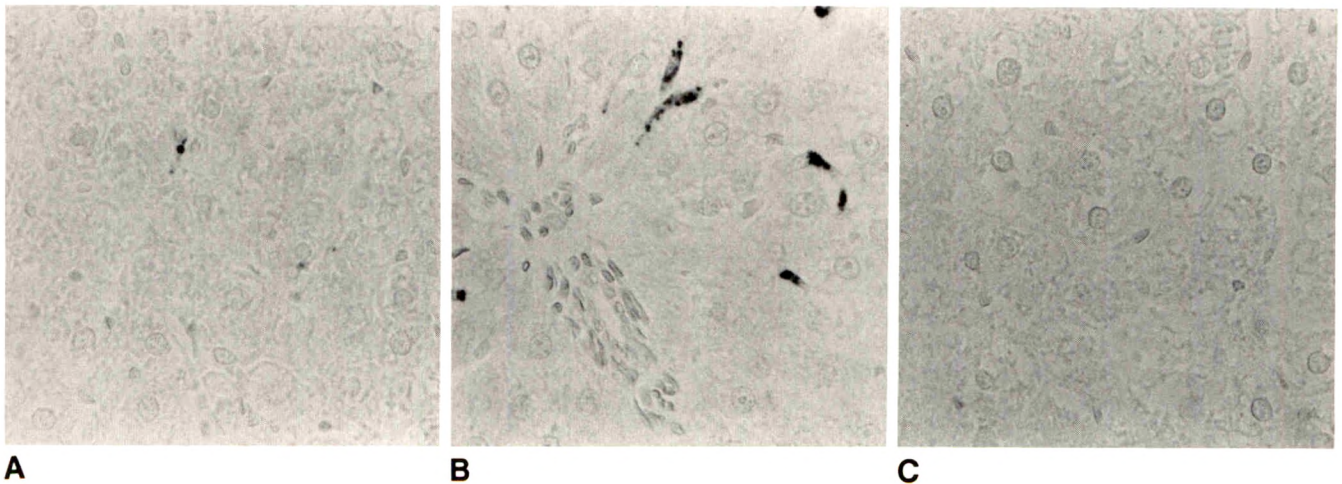


Fig. 6.—Photomicrographs of liver (Perls' Prussian blue stain $\times 700$, photographed with red filter).

A, No significant amounts of stainable iron are seen before injection of AMI-25.

B, 3 hr after administration of 18 $\mu\text{mol Fe/kg}$ of AMI-25. Stainable iron is seen as pigment in reticuloendothelial Kupffer cells.

C, 16 days after administration of 18 $\mu\text{mol Fe/kg}$ of AMI-25, liver parenchyma shows no increased amounts of stainable iron, indicating biodegradation.

conventional diatrizoate contrast agents are considerably lower.

Subacute and chronic toxic effects of iron overload have been documented in hemochromatosis if total body iron exceeds 15 g [25]. Cirrhosis and hepatocellular carcinoma can develop if liver iron concentration exceeds 4000 $\mu\text{g/g}$ wet weight (normal, 200 $\mu\text{g/g}$ wet weight) [26, 27]. The amount of iron in the dose of AMI-25 proposed for diagnostic imaging (20 $\mu\text{mol Fe/kg}$) is small compared with the normal liver iron stores. A 70-kg human would receive 80 mg of iron, and extrapolation of our radiotracer studies indicate that a single injection would transiently increase liver iron from 200 to 212 $\mu\text{g/g}$ wet tissue, far below the limit required for hepatotoxic changes to occur.

In summary, our results indicate that AMI-25 is a biodegradable superparamagnetic iron oxide preparation. Molecular iron is available to normal human iron stores; however, degradation of particles is slow enough to allow a broad

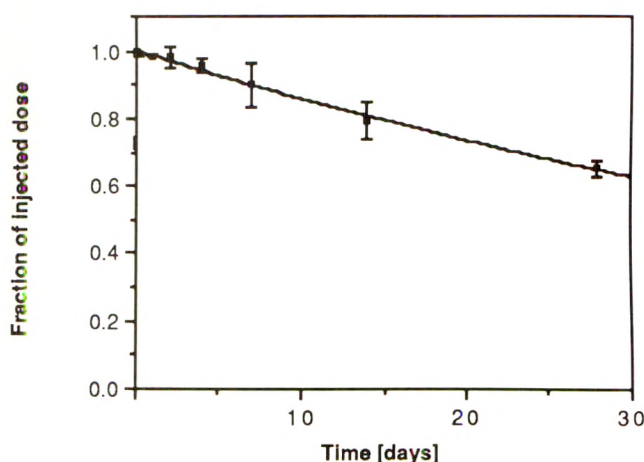


Fig. 7.—Graph shows whole-body clearance of ^{59}Fe , administered as AMI-25, to be 25% after 19 days.

window for effective MR imaging. AMI-25 has a safety margin considerably higher than that of conventional radiopaque and paramagnetic MR contrast agents. Clinical efficacy studies of this prototype MR contrast agent are being conducted currently [12, 13, 28].

REFERENCES

- Weissleder R, Saini S, Stark DD, et al. Dual contrast MR imaging. *AJR* 1988; 150:561-566
- Weissleder R, Stark DD, Compton CC, Ferrucci JT. MRI of hepatic lymphoma: an experimental study in rodents using ferrite. *AJR* 1987; 149:1161-1165
- Weissleder R, Stark DD, Rummeny EJ, Compton CC, Ferrucci JT. Splenic lymphoma: ferrite-enhanced MR imaging in rats. *Radiology* 1988; 166:423-430
- Weissleder R, Hahn PF, Stark DD, et al. MRI of the spleen: ferrite-enhanced detection of splenic metastases. *AJR* 1987; 149:723-726
- Olsson MRE, Persson BRB, Salford LG, Schroder U. Ferromagnetic particles as contrast agent in T2 NMR imaging. *Magn Reson Imaging* 1986; 4:437-440
- Widder DJ, Greif WL, Widder KJ, Edelman RR, Brady TJ. Magnetite albumin microspheres. *AJR* 1987; 148:399-404
- Wolf GL, Burrett KR, Goldstein EJ, Joseph PM. Contrast agents for magnetic resonance imaging. In: Kressel H, ed. *Magnetic resonance annual*. New York: Raven, 1985; 231-265
- Renshaw PF, Owens CS, McLaughlin AC, Frey TG, Leigh JS. Ferromagnetic contrast agents: a new approach. *Magn Reson Med* 1986; 3: 217-255
- Mendonca-Dias MH, Lauterbur PC. Ferromagnetic particles as contrast agents for magnetic resonance imaging of liver and spleen. *Magn Reson Med* 1986; 3:328-330
- Josephson L, Lewis J, Jacobs P, Hahn PF, Stark DD. The effects of iron oxides on proton relaxivity. *Magn Reson Med* (in press)
- Whitehead RA, Chagnon MS, Groman EV, Josephson L, inventors. Magnetic particles for use in preparations. U. S. patent 4,554,088. Washington, DC: U. S. Patent Office, 1985
- Weissleder R, Hahn PF, Stark DD, et al. Superparamagnetic iron oxide: detection of focal splenic tumors by MRI. *Radiology* (in press)
- Stark DD, Weissleder R, Elizondo G, et al. Superparamagnetic iron oxide: clinical application as a contrast agent for magnetic resonance imaging of the liver. *Radiology* 1988; 168:297-301
- Eilers RJ. Notification of final adoption of an international method and standard solution for hemoglobinometry specifications for preparation of standard solution. *Am J Clin Pathol* 1967; 47:212-214
- International Committee for Standardization in Hematology. Recommendations for measurement of serum iron in human blood. *Br J Haematol* 1978; 38:291-294
- International Committee for Standardization in Hematology. The measurement of total and unsaturated iron-binding capacity in serum. *Br J Haematol* 1978; 38:281-290
- Torrance JD, Bothwell TH. Tissue iron stores. In: Cook J, ed. *Iron*. New York: Churchill-Livingstone, 1980: 90-115
- PC100 user's manual. Billerica, MA: USA Bruker Instruments, 1988
- Drury RAB, Wallington EA. *Carleton's histological technique*, 5th ed. New York: Oxford University Press, 1980:264-267
- Ames BN. Identifying environmental chemicals causing mutations and cancer. *Science* 1979; 204:587-593
- Devoret R. Bacterial tests for potential carcinogens. *Sci Am* 1979; 241: 40-50
- Ritschel WA. *Handbook of basic pharmacokinetics*. Hamilton, IL: Drug Intelligence Publications, 1986
- Hershko C, Cook JD, Finch CA. Storage iron kinetics. III. Study of desferrioxamine action by selective radioiron labels of RE and parenchymal cells. *J Lab Clin Med* 1973; 81:876-886
- Brasch RC, Bennett HF. Considerations in the choice of contrast media in MR imaging. *Radiology* 1988; 166:897-899
- Weir MP, Gibson JF, Peters TJ. Haemosiderosis and tissue damage. *Cell Biochem Funct* 1984; 2:186-194
- Bassett ML, Halliday JW, Powell LW. Value of hepatic iron measurements in early hemochromatosis and determination of the critical iron level associated with fibrosis. *Hepatology* 1986; 6:24-29
- Tavill AS, Bacon BR. Hemochromatosis: how much is too much? *Hepatology* 1986; 6:142-145
- Weissleder R, Elizondo G, Stark DD, et al. The diagnosis of splenic lymphoma by MR imaging: value of superparamagnetic iron oxide. *AJR* 1989; 152:175-180

Book Review

Ultrasonography of the Spleen. By Jean-Noël Bruneton, M. Benozio, M. Bléry, H. A. Gharbi, B. Senecail, and V. Tran-Minh. New York: Springer-Verlag, 84 pp., 1988. \$65.50

This monograph on sonography of the spleen is written entirely by French-speaking authors and has been translated into English. Although numerous instances of awkward style and foreign terminology can be found, the authors' meaning is invariably clear.

The book has chapters on normal anatomy and variants, congenital anomalies, trauma, tumors, abscess and infarction, and parasitic disease. It is assumed that the reader has a basic knowledge of physics and scanning techniques. The text is heavily weighted toward sonography; some comparisons with CT and nuclear medicine are made. Clinical and pathologic correlations are brief. The figure quality ranges from excellent to adequate; most of the illustrations are good frozen frames from real-time scans.

The spleen has been referred to as an "orphan organ" because it belongs to no one in particular in the "organ-oriented" academic radiology department (if abdominal imaging is divided into gastrointestinal and genitourinary imaging). The spleen certainly belongs to no one category on the radiology boards. Sonography (indeed all

diagnostic imaging) of the spleen is a difficult subject to write well about because few splenic entities have characteristic imaging features.

The authors have done a commendable job. Anyone studying this small volume will know all that is needed to know about sonography of the spleen. Unfortunately, I do not think many people will read this book because it is priced at \$0.78 per page, which is not particularly cost-effective compared with much larger books on the market that have a broader scope that includes all aspects of diagnostic imaging of the spleen. Radiology departmental libraries and sonologists who have a particular interest in the spleen might wish to own this book. Should there be a second edition, I would suggest broadening the subject matter to include all imaging techniques, thus widening the book's appeal.

Arnold C. Friedman
Temple University Hospital
Philadelphia, PA 19140

The Diagnosis of Splenic Lymphoma by MR Imaging: Value of Superparamagnetic Iron Oxide

Ralph Weissleder¹
 Guillermo Elizondo^{1,2}
 David D. Stark¹
 Peter F. Hahn¹
 Javier Marfil³
 Juan F. Gonzalez³
 Sanjay Saini¹
 Luis E. Todd²
 Joseph T. Ferrucci¹

This study was designed to evaluate superparamagnetic iron oxide (AMI-25) as a contrast agent for MR to distinguish normal spleens from those diffusely infiltrated by lymphoma. As diffuse splenic involvement lacks visible tumor-tissue boundaries, signal-intensity measurements of spleens were used as a diagnostic criterion in 33 patients (lymphoma, $n = 8$; benign splenomegaly, $n = 5$; normal subjects, $n = 20$). Unenhanced MR images were insensitive (four of eight patients) and nonspecific (20 of 25 patients) in the diagnosis of lymphoma. After injection of superparamagnetic iron oxide ($40 \mu\text{mol Fe/kg}$), lymphomatous spleens showed a significantly higher signal intensity ($p < .05$) than did normal spleens or spleens enlarged by benign disease (hepatic cirrhosis, $n = 4$; spherocytosis, $n = 1$). Changes in splenic MR signal intensity unambiguously identified eight of eight lymphomatous spleens and 25 of 25 normal or enlarged spleens that did not contain lymphoma. Phagocytosis of superparamagnetic iron oxide in lymphomatous spleens is reduced because of diffuse displacement of splenic macrophages by lymphoma cells and/or by immunologic suppression of macrophage activity.

Our results suggest that superparamagnetic iron oxide (AMI-25) can improve the accuracy of MR imaging in the diagnosis of splenic lymphoma. With further development, this noninvasive technique may reduce the need for diagnostic splenectomy in lymphoma patients.

The finding of splenomegaly by physical examination or imaging studies has a sensitivity and specificity of 36% and 61%, respectively, for the diagnosis of splenic lymphoma [1]. Imaging techniques that display various splenic tissue characteristics are somewhat more reliable, with an overall accuracy rate of 75% for sonography [2], 54–64% for ^{99m}Tc sulfur colloid scanning [2, 3], and 58–65% for CT [4–6]. Unfortunately, as a consequence of these low accuracy rates, many lymphoma patients require invasive staging laparotomy with splenectomy [7]. Detection of subdiaphragmatic lymphoma is important as it may radically change the approach to treatment [8–10].

Only rare case reports have shown detection of splenic lymphoma by MR imaging [11, 12], and experimental studies suggest that unenhanced MR imaging is unreliable in distinguishing lymphoma from normal splenic tissue [13, 14]. Detection of focal splenic tumors is significantly improved when superparamagnetic iron oxide (AMI-25)-enhanced MR is used [13]. Superparamagnetic iron oxide has a specific biodistribution to reticuloendothelial cells and is excluded by cancer cells [13]. Diffusely infiltrative disease lacks macroscopic tumor-tissue boundaries, requiring a fundamentally different approach to imaging diagnosis. By using superparamagnetic iron oxide as a reticuloendothelial contrast agent, the phagocytic activity of the spleen has been used as an indicator of diffuse splenic lymphoma in an animal model [14]. This pilot study [15] was designed to evaluate this approach in humans.

Received July 20, 1988; accepted after revision September 8, 1988.

D. D. Stark is supported by American Cancer Society grants JFRA-163 and PDT-326, and is a member of the Scientific Advisory Board of Advanced Magnetics, Inc. S. Saini is supported by the Research Fund of the Radiological Society of North America.

¹ Department of Radiology, Massachusetts General Hospital and Harvard Medical School, 32 Fruit St., Boston, MA 02114. Address reprint requests to R. Weissleder.

² Nuclear Magnetic Resonance Unit, University Hospital, Av. Madero, Monterrey, Nuevo Leon, Mexico.

³ Department of Internal Medicine, University Hospital, Av. Madero, Monterrey, Nuevo Leon, Mexico.

AJR 152:175–180, January 1989
 0361-803X/89/1521-0175
 © American Roentgen Ray Society

Subjects and Methods

Patients

From July 1987 to February 1988, 33 patients at the Massachusetts General Hospital, Boston, MA, or at the University Hospital of Monterrey, Nuevo Leon, Mexico, were studied by using superparamagnetic iron oxide as a contrast agent for MR imaging. The clinical protocol was approved by the human study committees of both institutions.

Eight patients with lymphoma (Hodgkin disease, $n = 4$; non-Hodgkin lymphoma, $n = 4$) were selected for this study on the basis of the following criteria: (1) initial presentation of the disease without any prior therapy, (2) advanced stages of lymphoma with a high likelihood of splenic involvement, and (3) absence of focal tumor in the spleen. The diagnosis of lymphoma was confirmed by bone-marrow biopsy, blood smears, and/or lymph node histology in all patients [16]. The stage of disease was established by conventional methods: CT, sonography, and lymphangiography [17, 18]. Exploratory laparotomy with splenectomy was performed after the MR examination in patients with Hodgkin disease [17]. In these patients, lymphomatous involvement of the spleen was diffuse in all cases; none of the pathologic specimens showed nodules larger than 3 mm in diameter. Tissue iron was not quantified, because lymphoma patients are known to have increased spleen iron concentrations resulting from hemolysis. Furthermore, tissue concentrations of superparamagnetic iron oxide are quantified more accurately by MR than by histology [18]. In the four patients with non-Hodgkin lymphoma, laparotomy was not performed [7, 19]; the diagnosis of splenic lymphoma was suggested by demonstration of massive splenomegaly (extending into the left or right lower quadrant) in two patients and evidence of stage IV disease in two others [18]. In all four patients, splenic size decreased after the start of chemotherapy.

The normal control group had 20 consecutive patients with adenocarcinoma metastatic to the liver who had no evidence of splenic disease. Fourteen of these patients were included in a previous report [20]. This diagnosis was established by conventional imaging studies (sonography, scintigraphy, or CT) and was confirmed by biopsy of the liver.

The abnormal control group consisted of five consecutive patients with benign splenomegaly. Four of these had biopsy-proved hepatic cirrhosis with congestive splenomegaly, and one had congenital spherocytosis with splenic hyperplasia. In the patient with spherocytosis, splenectomy was performed after the MR study, confirming the absence of lymphoma.

Iron Oxide

Superparamagnetic iron oxide (ferrite), prepared by a modification of the method of Whitehead et al. [21], was obtained from Advanced Magnetics, Inc., Cambridge, MA, as AMI-25. Magnetic, biological, and toxicologic properties of AMI-25 have been described [18, 22]. The volume median diameter of particles was 80 nm (range, 50–100 nm), as measured by laser light scattering (Brookhaven BI-90 particle sizer, Brookhaven, NY). AMI-25 was provided at a concentration of 200 $\mu\text{mol Fe/ml}$ (0.2 M) and was injected at a rate of 3 ml/min. Doses of 20 and 40 $\mu\text{mol Fe/kg}$ were administered.

In all patients, spin-echo MR images were acquired before and 1 hr after each IV administration of superparamagnetic iron oxide. Thirty-one of the 33 patients received 20 $\mu\text{mol Fe/kg}$. Twelve of these 31 patients received a second dose of 20 $\mu\text{mol Fe/kg}$. Two of the 33 patients received a single dose of 40 $\mu\text{mol Fe/kg}$, followed by MR imaging.

MR Imaging

MR imaging was performed with a 0.3-T (13.3-MHz) Fonar (Beta 3000, Melville, NY) permanent magnet system ($n = 28$) and with a 0.6-T (25.1-MHz) Technicare (Solon, OH) superconducting magnet ($n = 5$). Transverse multislice images were obtained with both systems. A slice thickness of 14–15 mm and a 128×256 matrix were used. By using a body coil with a field of view of 46 cm, pixel dimensions were 3.6×1.8 mm. T1-weighted, 500/28/6 (TR/TE/excitations), and T2-weighted, 1500/42/2 and 1500/84/2, spin-echo images were acquired. The scanning time was 6.4 min for each pulse sequence. Each pulse sequence yielded seven (0.3 T) or 11 (0.6 T) simultaneously acquired slices.

Quantitative image analysis was performed by measuring the signal intensity of spleen, liver, fat, and paraspinous muscle [23]. The signal intensity of spleen was normalized to the standard deviation of background noise and expressed as signal-to-noise ratio (SNR). Spleen SNR values were considered normal within the range of the mean and two standard deviations, as established by data from the 20 normal control patients without splenic disease. The statistical significance of SNR differences among patients with splenic lymphoma, normal spleens, and benign splenomegaly was calculated by using the nonparametric Mann-Whitney U test. Spleen size was assessed by using standard cross-sectional image criteria [24].

Results

On unenhanced MR images, spleen SNRs showed a wide physiologic variation, and splenic lymphoma could not be distinguished from normal (Fig. 1; Table 1). When a normal range was defined as the mean SNR ± 2 SD, or a histogram distribution of the individually observed SNR values (Fig. 1) was used, splenic lymphoma could not be distinguished from normal spleen (Table 1). Spleen size was increased in four of the eight lymphomatous spleens (extension into left lower quadrant, $n = 3$; extension into right lower quadrant, $n = 1$), but five of 25 patients without malignancy also had splenomegaly (extension into left lower quadrant, $n = 4$; extension into right lower quadrant, $n = 1$).

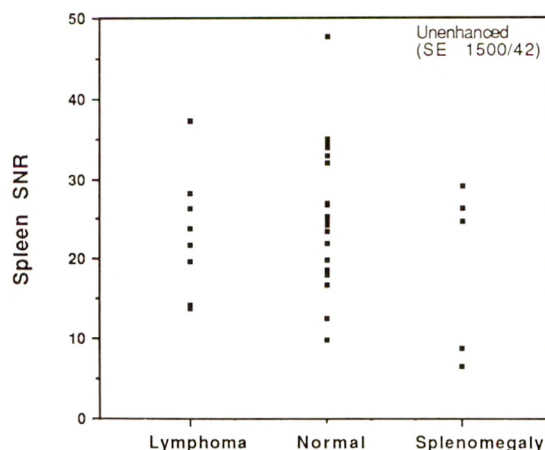


Fig. 1.—Graph shows MR image signal-to-noise ratios (SNRs) of splenic tissue obtained from noncontrast spin-echo (SE) sequences (SE1500/42) in patients with lymphoma, normal spleens, and benign splenomegaly. Because of large standard deviation of SNRs, normal spleens cannot be distinguished from lymphoma.

TABLE 1: MR Signal-to-Noise Ratios of Splenic Tissue in Patients with Normal Spleens, Lymphoma, and Benign Splenomegaly

MR Pulse Sequence: Dose of AMI-25 (μ mol Fe/kg)	Normal Subjects ($n = 20$)				Splenic Lym- phoma ($n = 8$)	Benign Splen- omegaly ($n = 5$)
	Spleen	Liver	Muscle	Fat		
Spin-echo 500/28:						
None	22.9 \pm 8.4	24.9 \pm 8.6	8.0 \pm 7.2	53.7 \pm 20.4	29.9 \pm 13.1	15.5 \pm 3.3
20	19.3 \pm 10.7	7.8 \pm 4.1 ^a	23.2 \pm 12.1	69.1 \pm 45.1	41.5 \pm 25.5	15.5 \pm 8.7
40	11.9 \pm 4.9	4.7 \pm 2.0 ^a	16.6 \pm 5.8	46.1 \pm 10.8	22.5 \pm 14.2	8.1 \pm 1.5 ^a
Spin-echo 1500/42:						
None	25.9 \pm 9.0	20.1 \pm 8.2	15.0 \pm 7.2	36.5 \pm 16.9	23.2 \pm 7.7	18.1 \pm 5.5
20	10.5 \pm 4.7 ^a	3.9 \pm 1.8 ^a	14.1 \pm 4.2	38.5 \pm 12.3	27.9 \pm 8.6 ^b	8.4 \pm 3.0 ^a
40	5.6 \pm 3.5 ^a	3.3 \pm 1.0 ^a	13.8 \pm 4.4	32.4 \pm 9.7	17.3 \pm 4.2 ^b	2.2 \pm 1.1 ^a
Spin-echo 1500/84:						
None	13.7 \pm 3.7	8.8 \pm 3.7	8.2 \pm 7.1	14.9 \pm 6.9	14.1 \pm 5.9	8.0 \pm 2.9
20	3.8 \pm 2.0 ^a	3.2 \pm 1.6 ^a	5.7 \pm 4.9	23.4 \pm 13.5	10.7 \pm 6.0	4.6 \pm 3.8
40	3.1 \pm 1.8 ^a	1.9 \pm 0.4 ^a	3.4 \pm 1.5	13.3 \pm 3.8	9.2 \pm 2.6 ^b	2.0 \pm 0.4 ^a

Note—Values are means \pm SD.^a Significant difference ($p < .05$) compared with signal-to-noise ratio of unenhanced MR images.^b Significant difference ($p < .05$) compared with signal-to-noise ratio of normal control spleens.

Normal spleens showed a consistent decrease of signal intensity after administration of 20 and 40 μ mol Fe/kg of superparamagnetic iron oxide (Figs. 2 and 3; Table 1). The signal intensity of spleen on spin-echo 500/28, 1500/42, and 1500/84 images was significantly ($p < .05$) lower after administration of 40 μ mol Fe/kg of AMI-25 than on unenhanced images. The T2-weighted spin-echo 1500/42 and 1500/84 pulse sequences were more sensitive to superparamagnetic iron oxide (SNR decrease of 78% and 77%, respectively) than was the spin-echo 500/28 sequence (48% decrease) (Fig. 3; Table 1).

Lymphomatous spleens showed a higher SNR than normal spleens did on MR images obtained after administration of superparamagnetic iron oxide (Figs. 4 and 5; Table 1). This difference was statistically significant for the spin-echo 1500/42 ($p < .05$ at a dose of 20 μ mol Fe/kg of superparamagnetic iron oxide; $p < .05$ at a dose of 40 μ mol Fe/kg) and spin-echo 1500/84 ($p < .05$ at a dose of 40 μ mol Fe/kg) pulse sequences. When individual spleen SNRs obtained from spin-echo 1500/42 images were plotted, only one measurement overlapped at 20 μ mol Fe/kg and none overlapped at 40 μ mol

Fe/kg of superparamagnetic iron oxide (Fig. 3). There was no significant difference between spleen SNRs of Hodgkin and non-Hodgkin lymphoma patients.

Enlarged but nonlymphomatous spleens showed SNRs similar to those of normal spleens before and after administration of superparamagnetic iron oxide (Figs. 4 and 6; Table 1). Spleen signal intensity on all these pulse sequences was significantly ($p < .05$) lower after administration of 40 μ mol Fe/kg than was the signal intensity on unenhanced images. The dose of 40 μ mol Fe/kg was superior to 20 μ mol Fe/kg, maximizing the separation of lymphomatous spleens from spleens enlarged by benign disease (Fig. 3).

One of the lymphoma patients vomited 5 min after administration of AMI-25 (20 μ mol Fe/kg). None of the other patients showed adverse reactions.

Discussion

Lymphoma is the most common splenic cancer and the eighth most common of all cancers in the United States. The

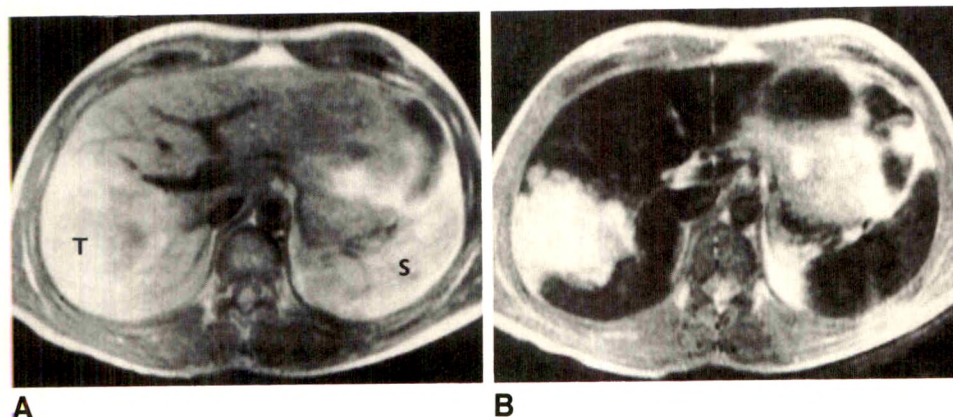


Fig. 2.—Spin-echo images, 1500/42, of normal spleen before (A) and after (B) administration of superparamagnetic iron oxide (40 μ mol Fe/kg).

A, Before administration, spleen (S) is slightly hyperintense (signal-to-noise ratio [SNR] = 23.4) relative to liver and is isointense relative to liver tumor (T).

B, After administration, profound signal loss of normal spleen (SNR = 3.2) and liver occurs. Signal intensity of hepatic tumor is unchanged and tumor is sharply delineated.

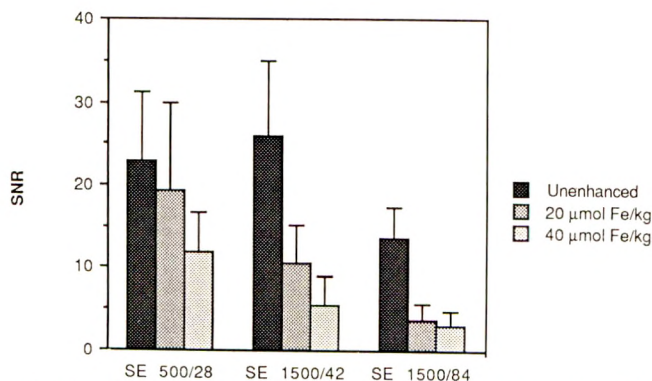
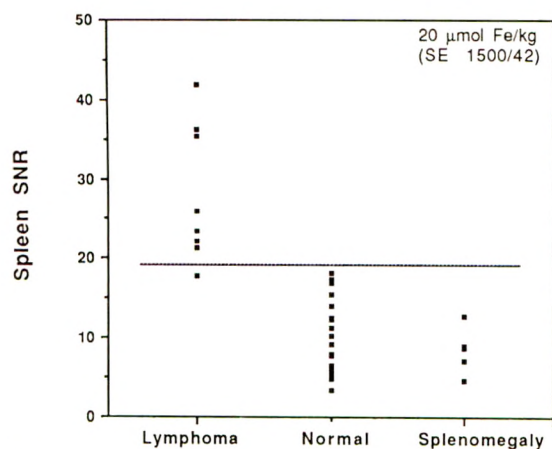
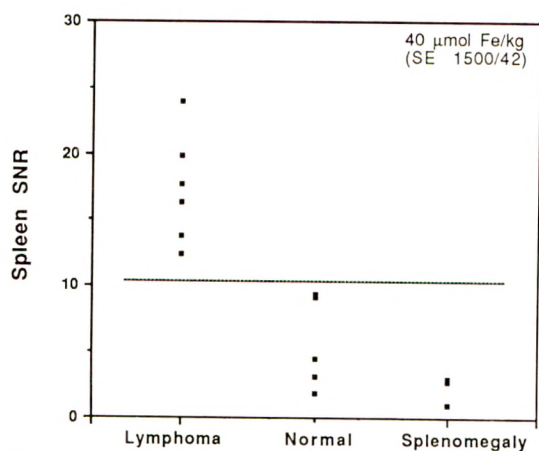


Fig. 3.—Histogram shows signal-to-noise ratios (SNRs) of normal spleens as a function of different doses of superparamagnetic iron oxide (unenhanced and 20 and 40 $\mu\text{mol Fe/kg}$ of AMI-25) and different spin-echo (SE) pulse sequences (SE 500/28, SE 1500/42, and SE 1500/84).



A



B

Fig. 4.—Graphs show splenic signal-to-noise ratios (SNRs) from spin-echo (SE) sequences (SE 1500/42) after administration of 20 $\mu\text{mol Fe/kg}$ AMI-25 (A) and 40 $\mu\text{mol Fe/kg}$ AMI-25 (B).

A, SNR values of normal spleens and spleens enlarged by benign disease have decreased because of phagocytosis of superparamagnetic iron oxide particles. SNR values of lymphomatous spleens are essentially unchanged from Fig. 1. With one exception, lymphomatous spleens can now be separated (above horizontal line) from spleens without lymphoma. B, Difference in SNR values of lymphomatous and nonlymphomatous spleens becomes marked and, in this series, separation of benign from malignant was complete (horizontal line).

annual incidence is 13/100,000, and 21,000 patients per year are subject to staging procedures [25]. Approximately one-fourth of all lymphoma patients have splenic involvement. Conventional imaging techniques are unreliable in diagnosing splenic lymphoma [1–6], and therefore noninvasive staging is of limited value. The insensitivity of CT and unenhanced MR is attributable to poor image contrast between lymphoma and normal splenic tissue. Specifically, normal spleen and tumor have similar X-ray attenuation and MR tissue characteristics, such as T1 and T2 relaxation times and proton density [11, 13].

Superparamagnetic iron oxide particles are specifically phagocytosed by organs such as spleen, liver, and bone marrow that contain reticuloendothelial cells [26]. Intracellular superparamagnetic iron oxide predominantly decreases the transverse relaxation time (T2), resulting in a loss of signal intensity on MR images. Malignant tumor cells, which are not capable of phagocytosis, displace normal reticuloendothelial cells from the parenchyma of spleen and liver. Therefore, MR signal intensity of tumor remains unchanged, whereas that of tissues containing reticuloendothelial cell decreases. Focal disease of the liver [16] and spleen [13, 27] can be imaged as a sharp transition in signal intensity, demarcating the lesion boundaries. Unfortunately, in 45% of patients with Hodgkin disease and in 70% of patients with non-Hodgkin lymphoma, splenic infiltration is microscopically diffuse or consists of miliary nodules less than 1 cm in diameter [12].

Detection of diffuse disease requires a fundamentally different quantitative approach, one that is based on measurements of the signal intensity on MR images [28]. Our results show that lymphomatous spleens appear significantly more hyperintense than do normal spleens after administration of superparamagnetic iron oxide (AMI-25). On a microscopic scale, individual lymphoma cells diffusely infiltrate normal splenic tissue, diluting the number of reticuloendothelial cells per unit weight of spleen and thus diminishing the concentration of superparamagnetic iron oxide particles [14]. In addition, reticuloendothelial cell function may be reduced in diffuse splenic disease, decreasing splenic uptake of superparamagnetic iron oxide, independent of dilution [29, 30]. As a result of either or both mechanisms, the amount of superparamagnetic iron oxide phagocytosed per unit weight of splenic tissue would be reduced, and this is manifested as increased signal intensity (less enhancement by superparamagnetic iron oxide) relative to normal spleen.

The differential diagnosis of splenomegaly is of considerable clinical importance. Approximately 30% of enlarged spleens of unknown origin are caused by lymphoma. Conversely, 30% of enlarged spleens in lymphoma patients are benign in origin [4, 19]. Whereas malignant splenomegaly is due to tumor cells displacing the red pulp, benign splenomegaly is caused most often by reactive hyperplasia and/or congestion in which the histologic structure of the red pulp is normal. Therefore, because phagocytosis is not impaired in reactive splenomegaly, splenic signal intensity decreases (in response to superparamagnetic iron oxide) as much as it does in normal spleens.

The results of this pilot study suggest that superparamagnetic iron oxide (AMI-25) can improve the accuracy of MR

Fig. 5.—Spin-echo images, 1500/42, of Hodgkin lymphoma before (A) and after (B) administration of 40 μ mol Fe/kg AMI-25.

A, Spleen size and signal intensity (signal-to-noise ratio [SNR] = 26.3) are normal.

B, Signal intensity of liver decreases, whereas that of spleen remains unchanged (SNR = 24.0). Compared with Fig. 2B (normal spleen), signal intensity of lymphomatous spleens is higher, similar to that of hepatic tumor.

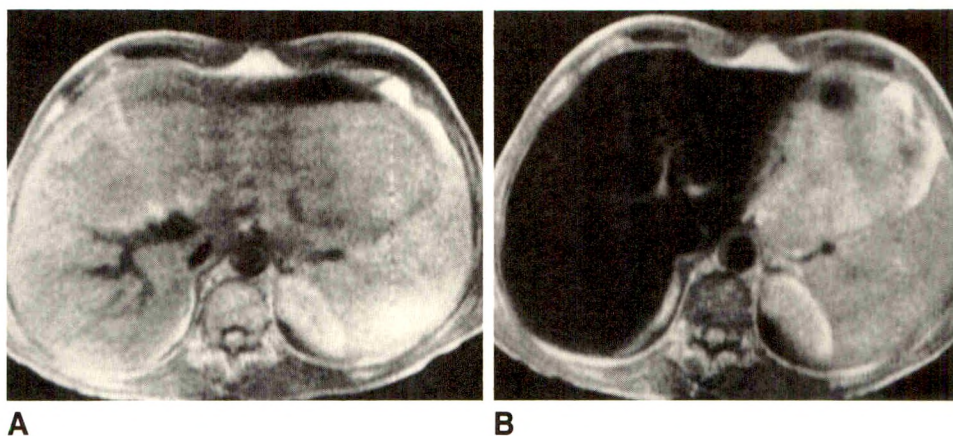
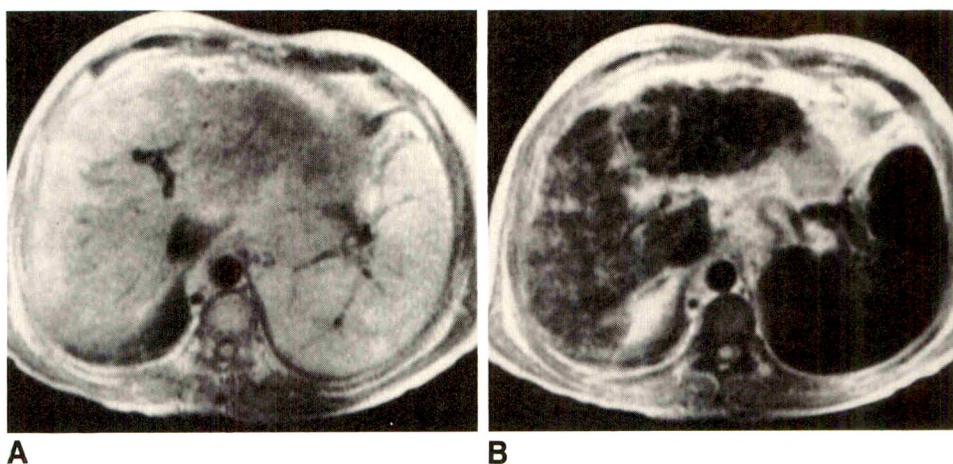


Fig. 6.—Spin-echo images, 1500/42, of benign splenomegaly due to congestion caused by hepatic cirrhosis.

A, Before administration of 40 μ mol Fe/kg AMI-25, spleen size is increased, and signal intensity is slightly higher than that of liver (signal-to-noise ratio [SNR] = 26.4).

B, After administration of 40 μ mol Fe/kg AMI-25, signal intensity of liver and spleen are decreased (SNR = 3.0), indicating phagocytosis and benign splenomegaly.



imaging in the diagnosis of splenic lymphoma, which confirms results of previous animal experiments [13, 14]. Larger prospective clinical trials should now be conducted to confirm this experience, identify limits of the method, and establish the true diagnostic sensitivity and specificity in a representative population of patients.

REFERENCES

- Glatstein E, Guernsey JM, Rosenberg SA, et al. The value of laparotomy and splenectomy in the staging of Hodgkin's disease. *Cancer* 1969;4: 709-718
- Taylor SKJW, Gazet JC, Peckham MJ, et al. Accuracy of grey-scale ultrasonography of liver and spleen in Hodgkin's disease and the other lymphomas compared with isotope scans. *Clin Radiol* 1977;28:233-238
- Silverman S, DeNardo GL, Glatstein E, et al. Evaluation of the liver and spleen in Hodgkin's disease. II. The value of splenic scintigraphy. *Am J Med* 1972;52:362-366
- Castellino RA. Imaging techniques for staging abdominal Hodgkin's disease. *Cancer Treat Rep* 1982;66:697-700
- Marglin SI, Castellino RA. Selection of imaging studies for the initial staging of patients with Hodgkin's disease. *Semin Ultrasound CT MR* 1985;6: 380-393
- Marglin SI, Castellino RA. Selection of imaging studies for the newly presenting patients with non-Hodgkin's lymphoma. *Semin Ultrasound CT MR* 1986;7:2-8
- Miller TP, Johns SE. Hodgkin's disease and non-Hodgkin's lymphomas. In: Stein JH, ed. *Internal medicine*. Boston: Little, Brown, 1987:1094-1104
- Johnson RE, Thomas LB, Schneiderman M, Glenn DW, Haferman MD, Fall FL. Preliminary experience with total nodal irradiation in Hodgkin's disease. *Radiology* 1970;96:603-608
- Kaplan HS, Rosenberg SA. Extended field radical radiotherapy in advanced Hodgkin's disease: short term results of two randomized clinical trials. *Cancer Res* 1966;26:1268-1276
- DeVita VT, Serpick AA, Carbone PP. Combination chemotherapy in the treatment of advanced Hodgkin's disease. *Ann Intern Med* 1970;73: 881-895
- Hahn PF, Weissleder R, Stark DD, et al. MR imaging of focal splenic tumors. *AJR* 1988;150:823-827
- Weissleder R, Hahn PF, Stark DD. MRI of the spleen. In: Margulis AR, Burhenne HJ, eds. *Alimentary tract radiology*, 4th ed. St Louis: Mosby, 1988:1435-1448
- Weissleder R, Hahn PF, Stark DD, et al. MR imaging of splenic metastases: ferrite-enhanced detection in rats. *AJR* 1987;149:723-726
- Weissleder R, Stark DD, Rummeny R, Compton CC, Ferruci JT. Splenic lymphoma: ferrite-enhanced MR imaging in rats. *Radiology* 1988;166: 423-430
- Freedman LS. Evaluating and comparing imaging techniques: a review and classification of study designs. *Br J Radiol* 1987;60:1071-1081
- Lukes RJ, Butler JJ. The pathology and nomenclature of Hodgkin's disease. *Cancer Res* 1966;26:1082-1084
- Rosenberg SA. Report of the committee on the staging of Hodgkin's disease. *Cancer Res* 1966;26:1310
- Weissleder R, Stark DD, Engelstad BL, et al. Superparamagnetic iron oxide: pharmacokinetics and toxicity. *AJR* 1989;152:167-173
- Quinn JJ. The lymphoproliferative disorders. In: Altman AJ, Schwartz AD, eds. *Malignant diseases of infancy, childhood, and adolescence*. Philadelphia: Saunders, 1983:239-297
- Stark DD, Weissleder R, Elizondo G, et al. Superparamagnetic iron oxide:

- clinical application as a contrast agent for magnetic resonance imaging. *Radiology* **1988**;168:297-301
21. Whitehead RA, Chagnon MS, Groman EV, Josephson L, inventors. Magnetic particles for use in preparations. U.S. patent 4,554,088. Washington, DC: U.S. Patent Office, **1985**
22. Josephson L, Lewis J, Jacobs P, Hahn PF, Stark DD. The effects of iron oxides on proton relaxivity. *Magn Reson Med* (in press)
23. Hendrick RE, Nelson TR, Hendee WR. Optimizing tissue contrast in magnetic resonance imaging. *Magn Reson Imaging* **1984**;2:193-204
24. Strijk SP, Wagener DJT, Bogman MJJT, Pauw BE, Wobbes T. The spleen in Hodgkin disease: diagnostic value of CT. *Radiology* **1985**;154:753-757
25. Horn JW, Asire AJ, Young JL, Pollack ES. *Cancer incidence and mortality in the United States*. NIH publication no. 85-1837. Bethesda, MD: National Cancer Institute, **1985**
26. Saini S, Stark DD, Hahn PF, et al. Ferrite particles: a superparamagnetic MR contrast agent for enhanced detection of liver cancer. *Radiology* **1987**;162:217-222
27. Weissleder R, Hahn PF, Stark DD, et al. Superparamagnetic iron oxide: enhanced detection of focal splenic tumors by MR imaging. *Radiology* **1988**;169:399-403
28. Weissleder R, Stark DD, Compton CC, Wittenberg J, Ferrucci JT. Ferrite-enhanced MR imaging hepatic lymphoma: an experimental study in rats. *AJR* **1987**;149:1161-1165
29. Saba TM. Physiology and physiopathology of the reticuloendothelial system. *Arch Intern Med* **1970**;126:1036-1052
30. Dornfest BS, Lipp C. Further studies of splenic RES function in rat leukemia using ^{99m}-technetium-sulphur colloid as a test clearance agent. *J Reticuloendothel Soc* **1975**;17:274-281

Technical Note

The Blunt Needle: A New Percutaneous Access Device

E. William Akins,¹ Irvin F. Hawkins, Jr., Christopher Mladinich, Richard Tupler, Roy J. Siragusa, and Richard Pry

All previously reported methods of gaining percutaneous access for interventional radiologic procedures have used needles with sharp tips. Surgeons have used blunt-tipped devices to avoid inadvertent penetration of arteries or adjacent vital structures [1, 2]. This report documents our development and clinical testing of a new blunt access needle that applies this surgical technique to interventional radiology.

Methods

The standard 18-gauge splenic needle (Cook, Bloomington, IN) has a sharp stylet within the blunt cannula. Our blunt needle was made by filing down the sharp inner stylet (Fig. 1). The commercially available versions (Cook, Bloomington, IN; National Standard, Gainesville, FL) feature an extremely smooth blunt tip and a locking hub. The 18-gauge needle was chosen because we thought that this size would truly behave as a blunt instrument, whereas a fine blunt needle theoretically could enter arteries because its tiny tip may not be "discriminating." The 18-gauge needle also permits insertion of large guidewires or aspiration, and it has enough strength that the position of the tip can be changed after insertion to provide a better angle of entry into the target.

Studies were performed in 12 mongrel dogs as follows. Blunt and sharp needle punctures were performed with direct inspection of resultant bleeding in five dogs (open model); percutaneous renal and hepatic puncture was performed in three dogs; and percutaneous, directed puncture of the renal artery opacified with barium was done in four dogs.

The blunt needle was used for 52 interventional procedures in 46 patients (18 nephrolithotomies, eight nephrostomies, 12 biliary drainages, 12 abscess drainages, and two coaxial biopsies). Informed consent was obtained. After a skin nick was made, the blunt needle

was advanced to the target in a routine manner by using fluoroscopic, sonographic, or CT guidance as needed. When the blunt needle was advanced within 2 mm of the target, sharp needles were used coaxially for all biliary drainages and nephrolithotomies.

Results

In the open model, 20 sharp needle punctures of the kidney resulted in seven instances (35%) of brisk arterial bleeding as well as slow capsular bleeding when the needle was removed. The blunt needle caused a similar amount of capsular bleeding but no brisk arterial bleeding after 50 direct renal punctures. The blunt needle displaced loops of bowel without laceration or entry into the intestines.

When a percutaneous technique was used in three dogs, the blunt needle was directed through the deep fascia down to the kidney and, in most passes, through the renal parenchyma. When a glancing needle pass was not perpendicular to the kidney, the blunt needle bounced off the renal capsule. Parenchymal entry in this circumstance required a jabbing action at the capsule. After 20 transrenal passages, aspiration through the blunt needle, as it was slowly withdrawn, revealed no arterial bleeding and only one instance of venous bleeding (5%). Using identical access routes, we verified fluoroscopically and arteriographically that the sharp needle entered arteries in 3 (38%) of 8; venous entry occurred in two other cases (25%).

In four dogs, we could not force the blunt needle to enter a barium-filled renal artery despite at least 100 direct forceful attempts. The blunt needle deformed the renal pedicle without

Received April 25, 1988; accepted after revision July 1, 1988.

¹ All authors: Department of Radiology, University of Florida, College of Medicine, Gainesville, FL 32610. Address reprint requests to E. W. Akins, Dept. of Radiology, Box J-374, JHMC, University of Florida, College of Medicine, Gainesville, FL 32610.

AJR 152:181-182, January 1989 0361-803X/89/1521-0181 © American Roentgen Ray Society

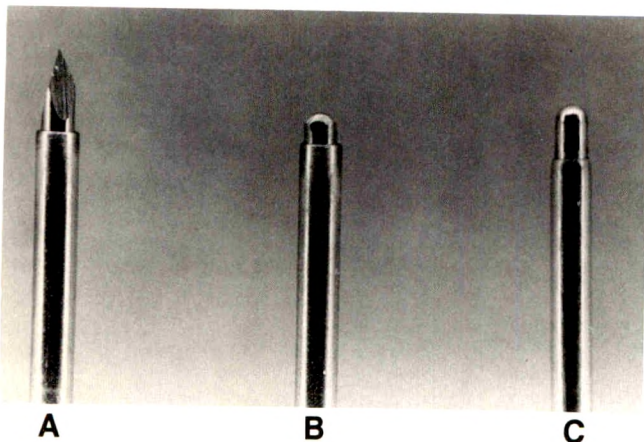


Fig. 1.—Photograph of the conventional 18-gauge splenic Cook needle with a sharp stylet (A) compared with the prototype 18-gauge blunt needle (B). The commercially available blunt needle will be made extremely smooth (C) by grinding down the tip.

arterial damage; the artery moved out of the needle path. The sharp needle entered the renal artery on the first or second attempt and caused massive extravasation in all instances.

We used the blunt needle to perform 52 procedures on 46 patients. The overall success rate was 98%. Six patients had minor complications. With moderate pressure, the blunt needle was capable of traversing organ parenchyma. Some resistance was often noted at fascial planes, but this was overcome by using a controlled jabbing motion of the needle at the entry site. The blunt needle failed to enter one kidney with dense capsular fibrosis, but it served as a coaxial trocar, allowing direction of the 22-gauge needle guide into the appropriate calix.

None of the 18 patients in whom the blunt needle was used for access in 18 endourologic procedures required transfusion for bleeding. In one case, nephroscopy revealed a thrombus but no active bleeding. In one other case, we achieved excellent initial access using the blunt needle, but the nephrolithotomy was aborted because of a pelvic tear caused by the tract dilator. In 16 other percutaneous nephroscopic procedures performed with the blunt needle, bleeding was minimal even when the tract was dilated to 36 French for rigid nephroscopy and stone removal. Eight simple nephrostomies were easily performed with the blunt needle. Either the blunt needle can be advanced into calices directly, or final access can be gained with a coaxial 22-gauge needle.

The blunt needle was used successfully for 12 percutaneous biliary drainage procedures in 11 patients. In these cases, the biliary system was first opacified with contrast material. The blunt needle was used to gain access down to the duct. Because the blunt tip impressed the duct and did not enter, we placed a 22-gauge needle guide through the wall, taking care to make a single wall puncture. A guidewire was then advanced into the duct to allow catheter placement. Patients tolerated this procedure as well as other patients had tolerated similar procedures with sharp needles.

The blunt needle was used for percutaneous abscess drainage when vascular structures or bowel was present in the pathway to be used for needle placement. Viscous pus was

aspirated through the 18-gauge cannula in more instances than would be possible through 22-gauge needles. Using the blunt needle as a coaxial trocar for insertion of a 22-gauge biopsy needle, we successfully performed two aspiration biopsies.

Discussion

Initial access for drainage procedures in radiology previously has been accomplished with a variety of entry needles, all with sharp tips that cut a tract through tissue and do not discriminate between vascular and nonvascular tissues. Less bleeding occurs when 22-gauge needles are used [3] because the smaller needle tract allows spontaneous hemostasis after inadvertent arterial puncture. However, if transarterial placement of the skinny needle occurs during the pass when the target is entered, arterial hemorrhage may occur if a large catheter is advanced through this tract. Percutaneous biliary drainage has been complicated by fatal hemorrhage [4], and hemorrhage requiring transfusion therapy also has occurred in 10–43% of percutaneous nephrolithotomies [5, 6].

Modern surgeons avoid sharp dissection, preferring to perform blunt or manual dissection of tissue planes because it is safer and generally adequate for exposure or definitive drainage. Transcerebral ventriculostomy [1] has been done with blunt drainage tubes. Periorbital anesthesia [2] has been done with blunt-tipped needles, and significant procedural hemorrhage is rare. The Cuatrecasas needle (Becton-Dickinson, Rutherford, NJ), which has a blunt stylet, has been used for Pantopaque myelography.

Our results support our hypothesis [7] that the blunt needle is able to puncture abdominal viscera and fluid collections safely and without arterial damage because of the resilience of the arterial wall. Although these results are encouraging, further studies will be required to prove whether percutaneous nephrolithotomy performed with blunt needles causes less bleeding than a procedure done with sharp needles.

Use of the blunt needle, based on the surgical premise of blunt dissection, can be applied to a wide variety of interventional radiologic procedures and is particularly applicable when inadvertent arterial or intestinal puncture is possible.

REFERENCES

1. Canter RC, Michelsen JJ, White JC, New PFJ. *Ventriculocisternostomy: long term experience*. Springfield, IL: Charles C Thomas, 1970
2. Frayer WC, Jacoby J. Local anesthesia. In: Duane TD, Jaeger EA, eds. *Clinical ophthalmology*, vol. 5. New York: Harper and Row, 1987:1–10
3. Ferrucci JT Jr, Wittenberg J, Sarno RA, Dreyfuss JR. Fine needle transhepatic cholangiography: a new approach to obstructive jaundice. *AJR* 1976;127:403–407
4. Hamlin JA, Friedman M, Stien MG, Bray JF. Percutaneous biliary drainage: complications of 118 consecutive catheterizations. *Radiology* 1986;158:199–202
5. Hunter PT, Newman RC, Finlayson B, Hawkins IF Jr. Retrograde nephrostomy in 100 patients. *World J Urol* 1985;3:2–6
6. Snyder JA, Rosenblum JL, Smith AD. Endourologic removal of staghorn calculi in the elderly: analysis of 42 cases. *Endourology* 1987;1:123–128
7. Hawkins IF, Akins EW, Mladinich C, Siragusa RJ. Transvisceral access using a blunt needle. *Semin Intervent Radiol* (in press)

Case Report

Percutaneous Treatment of Superior Vena Cava Syndrome

Paul Capek¹ and Constantin Cope

Because the superior vena cava (SVC) is a soft, compliant structure, it is much more susceptible to occlusion from compression by local processes than is the aorta. If the occlusion occurs relatively suddenly, venous pressure in the upper body increases, causing a characteristic clinical syndrome [1]. Severe occlusion may be fatal because of concomitant obstruction of the airway or an intracerebral catastrophe. Occlusion that develops slowly may not cause any clinical signs or symptoms until late because adequate collaterals have developed to allow venous drainage. The syndrome is estimated to occur in 3–4% of all patients with lung cancer. With the advent of chronic central venous catheterization, benign iatrogenic causes are becoming more common, as is shown by the following case report.

Case Report

A 44-year-old, insulin-dependent, diabetic woman presented with acute swelling of the upper extremities. The difficulties encountered with IV access due to frequent admissions for control of diabetes necessitated the insertion of a Hickman catheter. The catheter was placed via a left subclavian vein venotomy and remained in place for approximately 10 months. The patient's complaints began 4 weeks after removal of the catheter. On admission, she complained of tense swelling involving the neck, face, upper chest, and arms. The swelling did not impede ventilation but did result in a sensation of "fullness" in her throat. She did not show any neurologic dysfunction. An additional but unrelated problem was chronic dysfunctional uterine bleeding. CT of the chest showed no mediastinal tumor.

Bilateral upper-extremity venograms revealed occlusion of the superior vena cava. Contrast injection from a femoral vein catheter showed a well-defined clot in the distal SVC (Fig. 1A). In view of her

uterine bleeding, local thrombolysis was performed through the catheter that was buried in the clot. An initial bolus of 250,000 units of urokinase was delivered into the thrombus, followed by another injection of 250,000 units over a period of 10 min. Infusion was continued at 1000 units/min overnight. Plasma fibrinogen levels remained within normal limits. The next day a repeat cavogram showed patency with residual thrombus. Additionally, a stricture below the level of thrombosis was revealed for the first time (Fig. 1B). A pressure gradient of 40 mm Hg was measured across the stricture. After dilatation of the stricture with a 10-mm angioplasty balloon, the pressure gradient was reduced to 30 mm Hg. The patient was given heparin. Over the next 48 hr, her facial and arm swelling decreased dramatically and her appearance returned to normal. Because a significant pressure gradient remained, repeat angioplasty was performed 24 hr later with a single 15-mm balloon. After angioplasty, the pressure gradient was reduced to 13 mm Hg. Two weeks later, angioplasty performed with two 8-mm, high-pressure balloons positioned side by side reduced the pressure gradient further to 10 mm Hg. Residual narrowing was still present in the SVC; however, all thrombus had dissolved (Fig. 1C). Oral anticoagulants were continued, and the patient was asymptomatic 4 months after the procedure.

Discussion

Thrombolytic therapy for acute, catheter-related thrombosis of the SVC has been reported anecdotally [2–4]. In general, the thrombolytic agent used has been streptokinase administered systemically via a peripheral vein. The infusion times usually were less than 72 hr, frequently resulting in dramatic relief of symptoms. In view of our patient's dysfunctional uterine bleeding, we elected to use urokinase delivered directly into the thrombus at a rate that might minimize the

Received May 12, 1988; accepted after revision July 18, 1988.

¹ Both authors: Angiography/Interventional Radiology Section, Hospital of the University of Pennsylvania, 3400 Spruce St., Philadelphia, PA 19104. Address reprint requests to C. Cope.



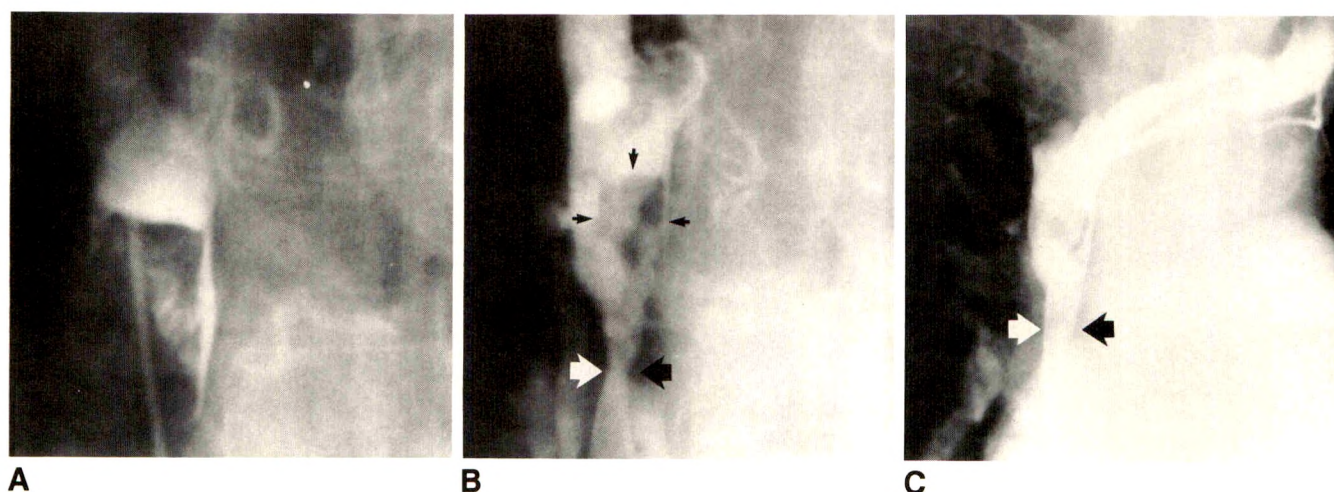


Fig. 1.—44-year-old woman with superior vena cava syndrome.

A, Initial contrast injection in superior vena cava via a catheter positioned from below shows a well-defined thrombus completely occluding outflow. B, After 24 hr of urokinase infusion into thrombus, it has shrunk (small arrows), but a stricture is revealed below clot (large arrows). C, Cavogram after angioplasty shows an improved stricture lumen (arrows) with free flow into right atrium.

systemic effect of the urokinase. Our patient experienced no significant increase in her uterine bleeding during the infusion. After the thrombolysis, an unexpected stricture of the SVC was uncovered but was safely dilated. The stricture presumably arose as a result of the previous central line tip, eroding and disrupting the SVC intima and resulting in fibrosis and narrowing of the lumen.

Transluminal balloon angioplasty has been used successfully to dilate SVC strictures without associated thrombosis [5–7]. These authors reported that dramatic relief of symptoms frequently occurred after angioplasty. The safety of venous percutaneous transluminal angioplasty has not, however, been adequately addressed. As opposed to arteries, veins are quite thin walled and pliable. Angioplasty is thought to work by endothelial disruption and intimal splitting, which could result in complete disruption of the venous wall if the dilatation is excessive [5]. In our patient, the danger was apparently offset by the scarring resulting from the reaction to the process that initially caused the stricture. This scarring apparently was quite intense because dilatation was achieved only with high-pressure balloons and considerable force on the inflating syringes.

The long-term prognosis for patients with SVC syndrome treated in this manner is unknown. The process causing the stricture may progress with further narrowing or reocclusion

of the SVC. In that case, the procedure potentially can be repeated. The relatively noninvasive nature of the lysis/angioplasty may allow the procedure to be performed repeatedly. A possible future approach may involve the use of an endovascular stent to maintain patency. This approach may preclude the thoracotomy currently necessary for a venous bypass procedure.

REFERENCES

1. Lochridge SK, Knibbe WP, Doty DB. Obstruction of the superior vena cava. *Surgery* 1979;85:14–24.
2. Ahmed N, Payne RF. Thrombosis after central venous cannulation. *Med J Aust* 1976;1:217–220.
3. Montgomery JH, D'Souza VJ, Dyer RB, Formanek AG, Prabhu SH. Non-surgical treatment of the superior vena cava syndrome. *Am J Cardiol* 1985;56:829–830.
4. Smith NL, Ravo B, Soroff HS, Khan SA. Successful fibrinolytic therapy for superior vena cava thrombosis secondary to long-term total parenteral nutrition. *J Parenter Enter Nutr* 1985;9:55–57.
5. Rocchini AP, Cho KJ, Byrum C, et al. Transluminal angioplasty of superior vena cava obstruction in a 15-month-old child. *Chest* 1982;82:506–508.
6. Sherry CS, Diamond NG, Meyers TP, et al. Successful treatment of superior vena cava syndrome by venous angioplasty. *AJR* 1986;147:834–835.
7. Ali MK, Ewer MS, Balakrishnan PV, et al. Balloon angioplasty for superior vena cava obstruction. *Ann Intern Med* 1987;107:856–857.

Computer Page

The Use of a Microcomputer to Make Rapid and Inexpensive Lecture Slides

Felix S. Chew¹

Lecture slides are a virtual necessity for radiologists who give conferences. Rapid and inexpensive methods of making excellent slides of radiographs are well known [1]; this report describes several different methods of making text and graphics slides with the aid of a microcomputer (Fig. 1).

Composing Copy

Any type of word-processing software can be used to compose the copy for slides. One can both rearrange and edit the text and preview the finished slide (Fig. 2A). Dedicated programs for composing slides also are available, and most graphic drawing programs can accept and edit text. An example of a word-processing program that allows the integration of text and graphics is Microsoft Word (Microsoft, Redmond, WA; available for both IBM-compatible and Apple Macintosh [Apple, Cupertino, CA] computers). Two examples of programs dedicated to composing visual aids for presentations (including 35-mm slides) are Pixie (Zenographics, Irvine, CA; IBM compatible) and Cricket Presents (Cricket Software, Malvern, PA; Apple Macintosh). Many other programs also are available. Some graphic drawing programs allow unusual effects, such as text along curved paths. Cricket Draw (Macintosh), for example, enables one to wrap a line of text around the circumference of a circle (or along any arbitrary curve). Most computers can display the text on the monitor in a variety of typefaces in different sizes and styles. For IBM-compatible computers, this capability requires the appropriate hardware (graphics board) and software; if

the computer has no graphics capability, the monitor may be limited to one typeface in a single size and style. All Macintosh computers and programs can display text in many different typefaces, sizes, and styles. Typefaces designed for the printed page may be less attractive when projected onto a large screen. The best readability is obtained with tall letters of simple design, close proportional spacing, and moderately heavy line weight [2]. Finished slides should be legible when held to the light and viewed without magnification and, in general, should have no more than six lines per slide and six words per line.

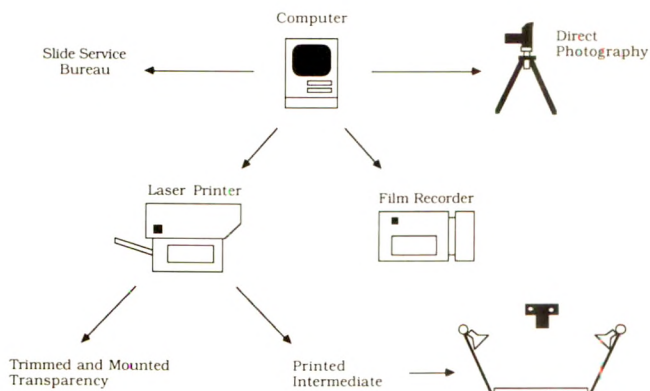
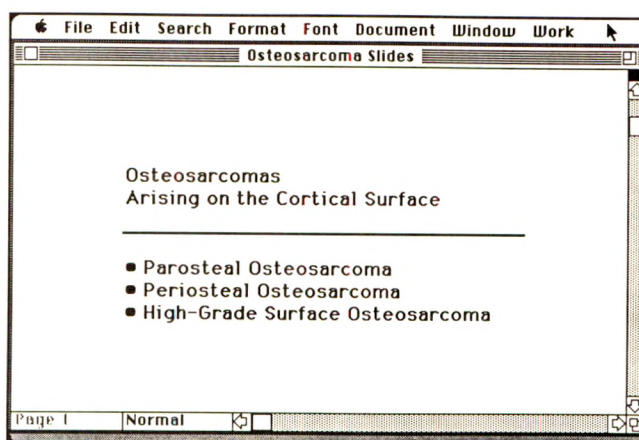


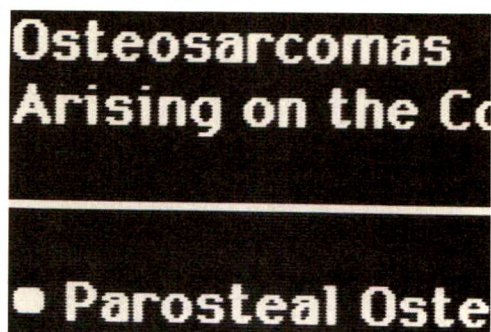
Fig. 1.—Alternative methods of making slides by using a microcomputer.

Received August 4, 1988; accepted after revision September 8, 1988.

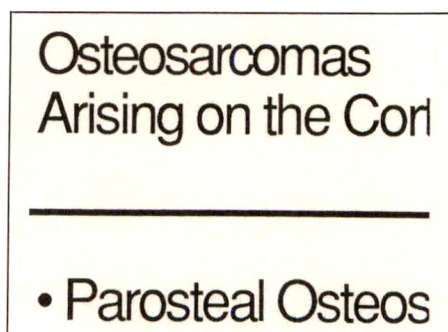
¹ Department of Radiology, State University of New York, Health Science Center at Syracuse, 750 E. Adams St., Syracuse, NY 13210. Address reprint requests to F. S. Chew.



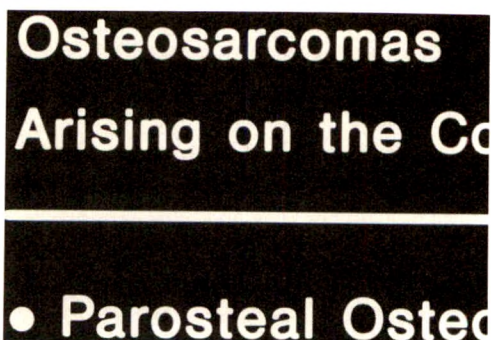
A



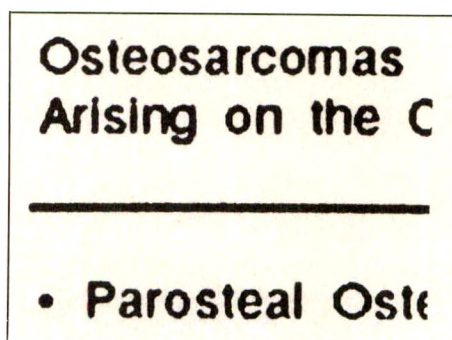
B



C



D



E

Fig. 2.—Examples of slides made by microcomputer.

A, Text slide composed by using Microsoft Word 3.01 on an Apple Macintosh SE microcomputer that was set up for making slides. Typeface is Geneva 18-point. (Figure has been reduced for reproduction.)

B, Print from slide photographed directly from monitor by using a single-lens reflex camera with 55-mm macro-focus lens, Ektagraphic HC film, 3 sec at f-3.5. Raster lines are present.

C, Print from slide made from laser-printed intermediate.

D, Print from slide made by Imagemaker (Presentation Technologies, Sunnyvale, CA), a dedicated film recorder. Film is exposed by light projected through a template with shapes of letters.

E, Photograph of transparency that was printed on a laser-xerographic printer and that has been mounted as a slide. Copy was composed in Helvetica 18-point typeface, but was reduced to 25% of original dimensions during printing. Letters are coarsely resolved with jagged edges. (Figure has been reduced for reproduction.)

TABLE 1: Technical Factors for Direct Photography of Computer Monitors

Film	Exposure Settings ^a	Processing (Time)	Final Result
Ektagraphic HC ^b	3 sec, f-3.5	Radiographic processor (90 sec)	High-contrast black-and-white negative
Rapid process copy film ^b	120 sec, f-3.5	Radiographic processor (90 sec)	Black-and-white direct positive
Polagraph HC ^c	1/8 sec, f-3.5	Processing pack (2 min) ^d	High-contrast black-and-white direct positive
Polabue BN ^c	4 sec, f-3.5	Processing pack (4 min) ^d	White letters, blue background
Ektachrome 100 ^b	1/8 sec, f-3.5 orange filter	C-41 process (send out)	White letters, blue background
Ektachrome 100 ^b	1/8 sec, f-3.5	E-6 process (send out)	Color positive

^a Exposure factors will vary considerably with screen brightness and developer conditions.

^b Eastman Kodak, Rochester, NY.

^c Polaroid, Cambridge, MA.

^d Processing pack supplied with each roll of film; requires "Polaroid 35 mm Autoprocessor" for use.

Direct Photography

A 35-mm single-lens reflex camera mounted on a tripod is best for direct photography of a computer monitor [3]. The camera should be positioned to fill the viewfinder with the text. A lens with a long focal length (at least 50 mm) will reduce the line bow (geometric distortion) at the edges of the image from the convex curvature of the monitor screen. The camera film plane must be parallel to the monitor screen, and all ambient light should be extinguished. For monitors that write black letters on a white background, exposure factors based on light-meter readings of the entire screen are substantially correct (Table 1). For monitors that write glowing letters on a dark background, exposure factors should be based on light-meter readings obtained from the brightest point on the screen. Exposure times of 1/30 sec or less may be shorter than the refresh rate of the monitor, and they should be avoided. It is prudent to bracket the film exposures until the correct settings with a particular arrangement of computer, camera, film, and processing are established. This method produces finished slides with visible raster lines and coarsely resolved letters (Fig. 2B). The smaller the letters on the monitor, the coarser their resolution.

Direct photography of red-green-blue (RGB) color monitors is generally unsatisfactory because of unsharp images and "washed out" colors [3]. The colors on RGB monitors are created by tiny, separate dots of red, green, and blue light produced by electron beams striking spatially separate red, green, and blue phosphors. Our vision blends these individual dots of light together, but the camera does not, and it records them separately [4].

Monochrome monitors with glowing letters on a dark background and RGB color monitors are both commonly used with IBM-compatible computers. Most Macintosh computers have monochrome monitors with black letters on a white background.

Printed Intermediate

The text can be printed and photographed, which eliminates raster lines but adds an intermediate step and requires the

use of a printer and a copy stand. Text printed by a laser-xerographic printer is best (Fig. 2C). Initial exposure settings should be obtained from light-meter readings of a Kodak 18% gray card (Eastman Kodak, Rochester, NY), not from the printed material itself.

Dedicated Film Recorders

Dedicated computer film recorders convert output from a microcomputer directly to film; the 35-mm slide format is universally available. A variety of software is available for the microcomputers (IBM compatible or Apple Macintosh) that drive film recorders, and film recorders make excellent text and graphics slides.

A video film recorder is a type of dedicated computer film recorder that consists of a (1) high-resolution, flat-field, cathode-ray tube monitor, (2) controlling circuitry, and (3) a camera platform. Raster line suppression is accomplished by interlacing or vibrating the raster lines during the photographic exposure. The monitor's flat field reduces geometric distortion. For color images, each phosphor color is exposed separately. The optical system is reregistered between exposures so that the dots appear exactly on top of each other. Alternatively, successive exposures of a monochrome monitor can be made through a series of three colored filters. Image components of different color are exposed through one, two, or all three filters for variable lengths of time. Film recorders that use cathode-ray tube technology generally provide images with resolution better than that of a standard microcomputer monitor.

Another type of film recorder uses a computer-controlled light source that exposes the film directly. Letters are exposed one at a time by projecting the light through a template with the shapes of the letters, an operation similar to that of a daisy wheel printer. A movable lens controls the location of the letter on the film. Lines and dots can also be plotted on the film. Exposure through a series of filters obtains different colors. The process is relatively slow, taking several minutes per slide, but the images are very sharp (Fig. 2D). A more sophisticated approach has a light beam passing over each

point on the film; the microcomputer controls whether the film is exposed.

Photographic Film

Black-and-white films that can be processed in standard 90-sec radiographic processors are ideal for making rapid and inexpensive slides. For creating slides with white copy on an opaque, black background, Kodak Ektagraphic HC is suitable; either a monitor with black letters on a white background or a printed intermediate can be photographed. This high-contrast, line-copy negative film can be developed in a standard, 90-sec radiographic processor. For slides with black copy on a gray background, Kodak Rapid Process Copy (RPC) film can be used. This direct-reversal film intended for copying radiographs works well for text and graphics slides; it is also developed in a radiographic processor. Polaroid Polagraph (Polaroid, Cambridge, MA) is a high-contrast line-copy film that yields black copy on a white background. This film is developed with an "instant" processing pack that is supplied with the film. For slides with white letters on a blue background, Polaroid Polablue BN film is suitable; a black-on-white monitor screen or a printed intermediate can be photographed. When time permits, color slide film such as Kodak Ektachrome 100 can be used [5]. For black letters on a colored background, the film is exposed through a filter of the color background desired and is developed with E-6 process (color slide processing). For white letters on a colored background, the film is exposed through a filter of color complementary to that desired for the background and is developed with C-41 process (color-negative processing). For colored letters on a background of different color, double exposure is required [5].

Projection of Printed Transparencies

Laser-xerographic printers can accept the transparency film that plain paper copiers use to make transparencies for overhead projectors. An example is Scotch 501 transparency film (3M, St. Paul, MN). If the text is composed within a 14.0 × 9.5 cm area and reduced to 25% of its original dimensions during printing, the size of the resulting image is 3.5 × 2.4 cm, exactly the size of a single frame of 35-mm camera film. This image can be trimmed from the transparency sheet with scissors and placed in a slide mount. The slides have coarsely resolved black letters on a clear background (Fig. 2E), and they can be obtained quickly and cheaply [6]. The transparency material is available in a variety of tints.

Discussion

Once the copy has been composed on the computer, slides can be made in a matter of minutes by using Ektagraphic HC or one of the Polaroid films; either the monitor or a printed intermediate can be photographed. The use of Ektachrome can be more time-consuming because of the necessity for commercial processing. Direct projection of a printed transparency is expedient in the preparation of a small number of slides, but trimming the images to the correct size for 35-mm slide mounts can be tedious and slow. Dedicated film recorders can be slow, particularly if Ektachrome is used.

The best quality slides are those made from printed intermediates or by dedicated film recorders; these slides are of professional quality. Slides made by photographing the monitor are also quite serviceable, but the printed transparencies are of marginal quality by comparison (Fig. 2).

The cost of each method depends on the film, the equipment, and the amount of time available. Ektagraphic and RPC are the least expensive methods if cost-free development in radiographic processors is available. Assuming no waste, Ektachrome is three to four times as expensive, and the Polaroid films are six to eight times as expensive. Cameras, copy stands, and laser-xerographic printers are common items in many radiology departments and probably would not be purchased for the express purpose of making text and graphics slides. The usefulness of purchasing a dedicated film recorder (\$2500–\$6000 for a "low-end" device) will depend on the local demand for text and graphics slides. All of these methods require a moderate effort, and a busy radiologist may not have time for them. An alternative is a slide service bureau. These commercial services receive microcomputer-composed copy for slides by modem or floppy disk, create slides with a dedicated film recorder, and return finished slides by courier. The marginal cost per slide can be 10 to 20 times as much as other methods, but relatively little effort would be required and no special equipment is needed.

Although each method has particular advantages over the others under certain circumstances, photography of a printed intermediate appears to be the best method overall.

REFERENCES

1. Curry TS III, Dowdey JE, Murray RC Jr. *Christensen's introduction to the physics of diagnostic radiology*, 3rd ed. Philadelphia: Lea & Febiger, 1984:295–299.
2. Ernst SB. *The ABCs of typography*. New York: Art Direction, 1977.
3. Hunter TB, Brewer M. Production of text and graphics slides on a personal computer. *AJR* 1985;144:1309–1312.
4. Wilson S. *Using computers to create art*. Englewood Cliffs, NJ: Prentice-Hall, 1986.
5. O'Neill JP Jr. 101 ways to make copy and title slides . . . some of them good! *J Biol Photogr Assoc* 1978;46:141–152.
6. Sweet H. Instant slides. *MacUser* 1988;May:219–222.

Perspective

Industry Support of Radiologic Journals and Newsmagazines

Douglas W. MacEwan¹

Radiologists welcome and respect the support of industry. Although optimal patient care is always the radiologists' primary objective, some radiologists are concerned also about the way in which industry's advertising resources are being allocated. Radiologic newsmagazines, such as *Diagnostic Imaging*, are mailed to radiologists and other health-care professionals at no cost. The goal of these publications is to influence readers who purchase medical equipment and supplies to choose the products that they advertise. These publications are supported by industry and are a strong, new presence. Their appeal lies in their ability to abstract highlights from scientific meetings and to communicate them quickly. These magazines are not peer reviewed, and they are published for profit by private entrepreneurs. Because of their large circulation, four commercial publications—*Diagnostic Imaging* (over 30,000 circulation), *Applied Radiology*, *Radiology Today*, and *Medical Electronics and Equipment News*—had 57% of the total advertising market in 1987. In contrast, the three largest peer-reviewed journals—*Radiology*, the *AJR*, and the *Journal of Nuclear Medicine*—had only 42% of the advertising market (May 13, 1988, letter mailed to *Diagnostic Imaging* advertisers and Research Department, Miller Freeman Publications, unpublished data). Between 1980 and 1987, the number of advertising pages in the *AJR* decreased by 25%, from 514 to 385 [1]. The need for a balance in the distribution of advertising pages between the scientific journals and the newsmagazines is becoming an important issue.

J. L. Doppman [2] points out that "the radiologists themselves are conferring on these publications," by allowing

incomplete abstracting of their reports, "a role that is scientifically inappropriate . . . and ultimately detrimental to the principles of our speciality." Doppman asks, "What are the risks of accepting the *Reader's Digest* approach to keeping up in this field?" and concludes, "Radiology newsmagazines fill a need but should not lead our profession." It was discouraging to learn that the following portions of Dr. Doppman's opinion were communicated in a letter to advertisers by the editors of *Diagnostic Imaging*, without the corresponding concerns. "For information on federal regulations affecting our speciality, new product announcements, the latest on the financial and corporate health of companies whose products we are considering purchasing, and beautifully crafted reviews with all the polish that professional editing and expensive graphics can provide, *Diagnostic Imaging* is outstanding." "Faculty members in our most distinguished medical schools freely lend their names to the editorial board and the list of contributors. A solicitation to write a 'state of the art' review for *Diagnostic Imaging* is acquiring the prestige of a lead article in *Radiology* or *AJR*."

O. W. Houser, on behalf of the Board of Directors of the Radiological Society of North America, recently chaired an Ad Hoc Strategic Planning Committee for Publications to plan for the future. Information was obtained by the staff of *RadioGraphics* from a questionnaire answered by radiologists in all types of practice. Some of these data are presented in Table 1. Although the survey was limited and was not expected to be used beyond the committee, the findings are reassuring. Radiologists claim that they are reading the journals carefully

Received June 13, 1988; accepted after revision August 26, 1988.

¹ Department of Radiology, Faculty of Medicine, University of Manitoba, Winnipeg, Manitoba R3A 1R9, Canada, and Dept. of Radiology, Health Sciences Centre, Room ON104, 820 Sherbrook St., Winnipeg, Manitoba R3A 1R9, Canada. Address reprint requests to D. W. MacEwan at the Health Sciences Centre.

AJR 152:189-190, January 1989 0361-803X/89/1521-0189 © American Roentgen Ray Society

TABLE 1: Radiologists' Use of Radiologic Journals

Question	AJR	Radiology	Radio- Graphics	Radiological Clinics of North America	Diagnostic Imaging
How do you read specific radiologic journals?					
From cover to cover	19	26	23	9	4
Read only selected articles	69	70	69	52	38
Just skim it	1	3	9	13	37
Rarely look at it	11	0	0	25	22
What do you do with old copies of radiologic journals?					
Throw them away	5	4	8	5	49
Save selected articles for reference	30	31	32	5	46
Save complete issues for reference	65	65	60	90	4
How useful do you find these journals in your practice?					
Very useful	66	69	62	40	14
Somewhat useful	34	29	34	47	40
Of little use	0	2	4	8	38
Of no use	0	0	0	4	8

Note.—All data are expressed as a percentage of 91 responses from 200 radiologists polled. All of these publications, except *Radiological Clinics of North America*, are received by most of the radiologists surveyed.

and keeping selected articles or the entire journal for future use. A magazine that is sponsored by a commercial enterprise is much less important.

The Canadian Association of Radiologists is evaluating the future of its journal. A questionnaire prepared with the help of a consulting firm [3] and mailed to 2200 radiologists yielded 450 responses. An analysis of the initial 216 responses yielded the following information: 79% of the respondents read selected articles, 65% rate the quality as being good, 16% suggest a need for more advertising to assist in the expansion of the journal, and 89% consider it a forum in which Canadians publish. The general thrust of a debate at the annual meeting of the Association in June 1988 favored expansion of the journal with more support from both members and industry.

Two problems become obvious from this information. The data presented in Table 1 strongly suggest that industrial firms that have switched from advertising in radiologic journals to advertising in newsmagazines may not be well served. A

continuation of this trend may diminish and distort the essential information available to radiologists on which they base decisions concerning the equipment and supplies necessary for care of patients.

The editors of the peer-reviewed radiologic journals should communicate with each other and make recommendations to their respective radiologic societies and to industry regarding efforts to prevent further loss of advertising revenues to entrepreneurial magazines. At least, these editors should discuss ways to bring the problem to the attention of radiologists, who, as authors, editors, and readers, support the throwaways and thus are contributing to the problem.

REFERENCES

1. Berk RN, Capp MP. A report to AJR readers. *AJR* 1988;151:1-4
2. Doppman JL. Who speaks for radiology? Or the threat of the throwaways. *Radiology* 1988;167:579
3. The Canadian Association of Radiologists and its activities—a membership evaluation. Montreal: Chapter Three Marketing Research Services, 1988

Perspective

Marketing Radiology and Radiologic Services

Joseph A. Marasco, Jr.¹ and Otha W. Linton²

Marketing may be defined as "an aggregate of functions involved in moving goods from producer to consumer" [1]. Marketing also refers to the organizational science that deals with the relationship between suppliers of a product or service and their customers and consumers. Marketing also is an art. Much of the discussion herein is drawn from a session on radiologic marketing held in August 1987 at the Radiology Summit Meeting in Colorado Springs, Colorado.

Background

Most radiologists and other physicians once considered business concepts such as marketing to be antithetical to the values of proper medical practice. They now perceive a need to accept such concepts. Marketing in medicine is not new. Successful physicians have marketed their practices throughout the history of medicine. Usually such marketing has been unstructured and perhaps even inadvertent on the part of the physician. Marketing "strategies" have been intuitive, and have been accepted as "the art of medicine." The physician who shows care and concern for his patient markets his practice whether he realizes it or not. The concept of being "the doctor's doctor" follows the same vein.

Competition has made the idea of marketing central to medical practice today. In more peaceful and less turbulent times, when physicians were in relatively short supply, medicine was a seller's market. The physician could consciously or unconsciously ignore the dictates of the art of medicine.

Physicians were in demand. If a physician lost a patient, there was always another one to replace him. Today, physicians are in oversupply, and this oversupply will increase in the decade ahead. Thirty years ago, there were 1.4 physicians/1000 people in the United States. The Graduate Medical Education National Advisory Committee (GMENAC) estimates that the United States needs 1.7 physicians/1000 people. The nation now has approximately 1.9 physicians/1000 people. GMENAC projects that the ratio will be approximately 2.2 physicians/1000 by the year 2000 [2]. The physician glut makes competition for patients a reality.

An excessive and increasing number of physicians competing for a relatively static or dwindling population of patients forces physicians to be less casual and more structured about marketing their services.

Competition for patients becomes less and less friendly. The promotional aspects of marketing help to intensify the competitiveness and the breakdown of collegiality. Medical advertising that may be completely proper and ethical frequently is perceived as unprofessional or cheap by some physicians.

Competition also has intensified turf battles. All manner of physicians now pursue traditional radiologic activities as ways to augment and/or replace lost revenues. Today's radiologist not only competes with other radiologists but also with family practitioners, internists, neurologists, obstetricians, and gynecologists. The problem is compounded by competition from corporations and hospitals and by price pressures from managed care and alternative delivery systems.

Received April 4, 1988; accepted after revision August 30, 1988.

¹ Department of Diagnostic Radiology, St. Francis Medical Center, Pittsburgh, PA 15201, and Dept. of Radiology, Forbes Health System, 225 Penn Ave., Pittsburgh, PA 15221. Address reprint requests to J. A. Marasco, Jr., at Forbes Health System.

² American College of Radiology, 1891 Preston White Dr., Reston, VA 22091.

The Marketing Plan

The scientific approach to marketing includes four basic steps—market research, decisions about product mix, promotion, and evaluation. These steps parallel the logical processes followed in any science—that is, analysis, decision, implementation, and monitoring. The casual viewer fixes on the most obvious element—promotion—which involves doing things or creating activities and materials. Overlooked are the research needed to define the intentions and milieu of the practice, the deliberate assessment of the strengths and weaknesses of the practice, the decisions to change elements of the practice in response to research findings, and, finally, the impact of the marketing effort on its objective—namely, the enhancement of the practice. Equally overlooked and difficult to measure is the marketing impact of the attitudes and actions of the people involved in the practice—the radiologists, technologists, clerks, receptionists, and even the parking attendants.

Market Research

Market research represents a deliberate commitment by a group to organize its efforts to create a favorable change.

Market research includes demographic, psychographic, and competitive research. Demographic research focuses on facts and figures. Psychographic research looks into the attitudes, preferences, and feelings of referring physicians and patients. Competitive research attempts to gain insight into what the competition is doing.

Most people have a general awareness of changes in their communities. However, the identification and quantification of such changes require a structured effort to gather demographic and medical data and to plot population growth, new road patterns, changes in major employers, and thus third-party payment plans, alternative payment systems, and activities of medical competitors and referring physicians. In one obvious example, if several of the largest groups of referring physicians relocate or expand into a new medical arts building, the radiology group should at least consider expanding there, too, before someone else does.

Marketing research requires a body of skills that may not come naturally to many radiologists and that may not be found among their employees. In most communities, marketing firms, advertising agencies, public relations counsel, and practice consultants now offer planning services to medical groups. The first dilemma for a radiology group interested in a marketing effort is to select appropriate help for its task. The field is open and changing. There is no American Board of Medical Marketing to reassure innocent customers. Some assistance in selecting a market research team can be found in such publications as *Marketing for the Radiologist—An Introduction*, published by the American College of Radiology [3].

External Marketing

External marketing involves those activities directed toward making customers and consumers aware of the services that

are being offered. In marketing terms, this involves decisions about product mix and promotion.

Most radiologists are comfortable with the decisions about product mix—that is, about which types of examinations and procedures should be offered and at what sites. If a hospital recruits the first neurosurgeon to the community, the need to enhance radiologic strength in this area is obvious. Less obvious are decisions about whether a current member of the group should seek special training or whether a new member with neuroradiologic competence should be recruited. If a new radiologist is to be recruited, questions about service volumes, equipment costs, coverage patterns, and ultimately promotion in the community must be addressed in an organized way.

A product-mix decision facing many radiologic groups in 1988 is the question of whether to offer direct-access screening mammography. A decision to do so goes against a long tradition of referral practice in diagnostic radiology. It raises questions about relationships with patients and other physicians, financial commitments, ongoing promotional efforts, legal liabilities, and the objectives of the practice. All of these should be defined and discussed only after the appropriate data have been collected; decisions about these matters should not be made intuitively.

On the basis of the market research findings and the decisions about product mix that follow, a practice can then consider embarking on an overt marketing program. In most cases, the radiologic group will turn to outside sources for help in preparing pamphlets; developing advertisements for newspapers, magazines, radio, or television; using public relations initiatives; and creating logos or other identifying symbols.

In making such efforts, it is important to keep in mind that the radiologists's service or product differs both from consumer items and from most other medical services. Thus, a practice must consider both its customers and its consumers.

A product or service is directed toward a consumer, defined as the person who uses the product or service. The customer is the person who determines the need and initiates the purchase. In the referral practice of both diagnostic and radiation oncology, the consumer is the patient and the customer is the referring physician. Physicians' decisions generate the demand. For screening mammography, the consumer and the customer are the same person—namely, the patient.

A radiologic group needs to develop a corporate or institutional identity in its community. This is true whether it is the only group in town or whether it has competition from other radiologists and from others offering imaging services. The group with the natural monopoly must indicate that the quality, availability, and costs of its services are so good as to negate any viable opportunity for a competitor to enter the market. The group in a competitive situation must attract itself to physicians and to patients as the chosen or preferred alternative.

Physicians are customers as members of a medical staff, as members of closed panel practice groups, and as individuals who occasionally are consumers as well. Other parts of the marketing target, if not precisely customers, are hospital management, third-party payers, government payment and

regulatory agencies, voluntary health organizations, and the community at large. Marketing to these groups involves definition of their real or latent relationships to the radiology group's service. The medical staff wants accuracy and service. The hospital wants reliability. The third-party payer wants low costs. So does the governmental paying agency. The government as regulator wants safety. The community at large wants honesty, responsibility, access, reliability, reasonableness, and a cheerful manner. A conscious effort to reflect these qualities in a radiologic group is essential to any marketing effort.

Radiologists in an academic setting gain respect by publishing their work in scholarly journals. All radiologists can enhance their prestige by participating in hospital conferences, by continuing their medical education, by serving on hospital committees, and by attending medical society affairs. However, such activities are time-consuming and detract from the radiologist's time in the practice.

The marketing of diagnostic radiology and radiation oncology to third-party payers and to government payment and regulatory agencies is achieved by a practice group through participation in efforts of medical or specialty societies. The task of persuading a Blue Shield plan or Medicare to change a coverage pattern or to increase a benefit usually relates to the entire radiologic or medical community and may depend on representation by that community through its established organizations. Hence, the well-marketed group is active in those societies.

Once committed to a marketing posture and effort, a radiology group will be involved in an ongoing set of activities. The task of evaluating the results of marketing efforts is just as important as the initial planning and market surveys. The ultimate evaluative criterion is the prosperity of the practice. If it is thriving, someone is doing something right. But it is essential to know who is doing what and how those efforts contribute toward the marketing objective.

A single marketing effort or pamphlet, for example, seldom has a positive effect. However, one poorly conceived (or executed) marketing effort can have a negative effect. It is important to measure overt marketing efforts. Usually, the same kinds of experts who plan and produce advertising and

ment, a surly technologist, or an unresponsive radiologist, especially if the patient is already nervous and apprehensive.

Internal marketing, or personal selling, clearly is the most important factor in promoting a practice. Leadership by the radiologist is vital in establishing a strong internal marketing effort. All of the employees in the office or department must feel that they are members of the team and understand the mission. This involves more than words by the radiologist; it involves example. Good relationships between members of the team are vital to providing a harmonious and effective atmosphere. The radiologist who is polite and considerate with the staff improves the chances that patients and referring physicians will receive the same treatment.

Factors that have an impact on internal marketing include the following:

1. The appointment. A pleasant and understanding approach on the telephone to the patient or the referring physician's secretary sets the tone for the remainder of the patient's treatment. The referring physician's secretary may be very influential in directing patients for referral.

2. Parking. The availability and convenience of parking to the hospital department or radiology office is more important today than ever before. If convenient parking is not available, every effort should be made to provide it.

3. Reception. Although making the appointment by telephone is the first step, the receptionist has the first face-to-face interaction with the patient. The reception area should be comfortable. But even when physical amenities are not optimal, courteous and caring receptionists may help to offset this disadvantage. The concept of guest relations is important. The receptionist must act as a sort of "ambassador" of the radiologist.

4. The technologist. The technologist sets the tone for the interaction between the radiologist and the patient. When the radiologist does not see the patient, the technologist is the representative of the radiologist.

5. The nurse. The radiology nurse usually interacts with most of the ill patients and thus plays a key role in representing the radiologist as a caring and concerned physician.

6. The radiologist. Because the practice of radiology is efficient, the radiologist may be diverted from proper interner-

office personnel and the patients is an extremely important part of internal marketing. The situation is eased when the radiologist accepts assignments and/or participates in third-party reimbursements. Delicate and sensitive handling of balance billing will enhance the image of the radiologists in both the consumer who is the patient and the customer who is the referring physician. The role of the radiologic business manager in this aspect of internal marketing is extremely important.

Marketing and Turf

Marketing and promotion can easily lead to turf battles between radiologists and others. Although economics motivates much of the competition for radiologists from other physicians, issues related to quality and availability also may play a role in turf battles. The need for increased availability of radiologists as well as the diffusion of radiologists into different areas separate from a central department (e.g., private offices, operating rooms, separate emergency room areas) suggests the possibility of lower productivity and, hence, lower per capita income. There also may be an impact on the amount of available discretionary time.

Turf battles between the radiologist and the hospital may occur as more and more outpatient radiology develops. Who gets the technical fee on outpatients? A solution to the problem could be more joint ventures between radiologists, private practitioners, and hospitals.

Marketing Education

The education of radiologists about marketing should begin during residency training. The first stage is creating awareness of the need for marketing efforts and the need for radiologists to understand, appreciate, and support this aspect of their practices. The next stage is to acquire enough information to be able to choose consultants or employees to undertake marketing activities.

This information is not easily obtained, yet some radiology practices have found their own way through the maze. Currently, the American College of Radiology is structuring an expanded marketing program directed at two levels. The first is to promote radiologic services by radiologists at the national level to third-party payers, government funding agencies, and regulators. The second is to build a program to assist radio-

logic groups with advice and materials for marketing their own practices. In this second role, the American College of Radiology program will provide counsel to groups attempting to develop their own programs, as well as workshops and other methods whereby information can be shared among radiologists. The marketing education process must be a continuing one.

Conclusion

Regardless of how sophisticated a marketing program is, the ability to meet its objective—namely, the enhancement of a radiologic practice—depends on the personal commitment of the radiologists who manage it and the willing involvement of all those who are part of the radiologic team. Radiologists must care. That care must show for all to see.

Perhaps radiology needs a slogan:

Radiology	<u>C</u> ompetent
	<u>A</u> vailable
	<u>R</u> esponsive
	<u>E</u> conomical
	<u>S</u> afe

ACKNOWLEDGMENTS

The authors thank Michael A. Lopiano, chairman of the Commission on Marketing Communications of the American College of Radiology, for his review of this manuscript. We also thank those who participated in the work group on Marketing Radiology & Radiology Services at the 1987 Summit Meeting of radiological organizations sponsored by the American College of Radiology. Their insights played a significant role in the shaping of this paper.

REFERENCES

1. *Webster's ninth new collegiate dictionary*. Springfield, MA: Merriam-Webster, 1984:728
2. *The current and future supply of physicians and physician specialists* (HRA 80-60). Washington, DC: U.S. Department of Health and Human Services, Health Resources Administration, 1980:18
3. *Marketing for the radiologist—an introduction*. Reston, VA: American College of Radiology Commission on Marketing Communications, 1987
4. Enzmann DR, Webb P. Practice management: gaining a marketing perspective on the habits of referring physicians. *Diagn Imaging*. 1985; February:47-52

From the Editorial Office

An Author's Guide to the Guidelines for Authors

Elizabeth Whalen¹

The editorial staff of the *AJR* worked long and hard to prepare the guidelines that are printed at the front of every issue of the *AJR*. We wanted to provide a helpful, thorough summary of the minimal requirements for submitted manuscripts. We also wanted to be selective enough that the guidelines could be printed on the front and back of one journal page. We thought that keeping the guidelines to this manageable length would encourage authors to read and use them. Each member of the editorial staff wrote down a "wish" list of all the characteristics that would make a submitted manuscript a "perfect" manuscript to edit and publish. The lists were pared down to the most important requirements—those features of format and content that cause the most problems if not correct when the article is accepted. Then the wording of these requirements was carefully chosen for clarity and brevity. The resulting guidelines are printed on pages A3–A5 of each issue of the journal (we added a third page, A5, for specific guidelines for special kinds of papers). When authors use the checklist, their papers tend to be accepted more quickly and edited more easily—and therefore published sooner and with fewer revisions. We encourage all authors to use the guidelines whenever they prepare an article for the *AJR*.

Because the guidelines had to be concise and fit on only one page, long descriptions and explanations were not possible. Authors can, and often do, telephone the editorial office for clarification of the guidelines, but we thought it would be helpful also to publish more complete information. Therefore, the purposes of this article are to expand the descriptions of some of the requirements listed, to provide answers to the questions most often asked by authors who submit articles to the journal, and to explain the reasons for the requirements listed in the guidelines.

Introduction to the Guidelines

The introductory paragraphs of the guidelines contain important information, although they are often overlooked by hurried authors. They give the distinct functions and addresses of the editorial office and of Williams & Wilkins, our publisher. Each of these two offices handles different aspects of the *AJR*'s publication, and authors and readers will get faster service if they start with the right office. For example, an author who submits a manuscript to the Williams & Wilkins office in Baltimore will have to wait several more days for a decision letter than the author who submits a manuscript directly to the editorial office in La Jolla, because manuscripts are not sent out for review from Baltimore. Similarly, researchers who wish to reprint text or figures from the *AJR* should contact Williams & Wilkins; if they send the request to the La Jolla office, it will be delayed because we will have to forward it to Baltimore.

The introduction provides other helpful information. Whenever an author submits a manuscript to any journal, that author must first know the kind of articles that journal publishes—*AJR* publishes "original contributions to the advancement of medical diagnosis and treatment." The same section also explains the relationship between *AJR* and *AJNR*, which allows *AJR* readers direct access to the best current neuro-radiologic research. The manuscript review and publication process is briefly described in the fourth paragraph, so that authors will understand that their articles will be (1) peer-reviewed before acceptance and (2) edited after acceptance.

The final paragraph of the introduction indicates that the *AJR* agrees with the principles outlined in "Uniform Requirements for Manuscripts Submitted to Biomedical Journals" (*Ann Intern Med* 1988;108:258–265). This document explains

¹ Publications Supervisor, American Journal of Roentgenology, 2223 Avenida de la Playa, Ste. 200, La Jolla, CA 92037. Address reprint requests to E. Whalen.

in great detail some important topics, such as previous and duplicate publication, manuscript preparation, and qualifications for authorship. We consider the "Uniform Requirements" to be a supplementary source of information for our authors. These requirements and our guidelines are so similar that any differences can be resolved easily before publication, either in revision by the author or in the editing process after acceptance.

General Guidelines for Major Papers

The section on general guidelines clearly describes the expected content of each section in a major paper. However, many letters go back to authors requesting compliance with these guidelines.

The abstract should be approximately 200 words—a 100-word abstract is too short and disappears on the page, and a 300-word abstract overwhelms the rest of the text on the first page of the article. The inclusion of actual data in the abstract helps the reader immediately see the type of research involved (e.g., whether it is a large study with statistically significant conclusions or a preliminary small series of patients that supports the need for further research). Brief descriptions of the purposes, methods, results, and conclusions of the article fulfill an important purpose of the abstract: providing readers the information needed to decide quickly if they wish to read the entire article.

In first drafts of manuscripts, material is often misplaced in the Methods, Results, and Discussion sections. The guidelines clearly indicate what type of information belongs in each section. By making the content of these sections consistent, we provide readers with easy access to the specific information desired.

Author's Checklist

The Author's Checklist is the largest part of the guidelines, and it contains detailed information for the author and the typist. If an author reads and follows this checklist carefully and gives a copy to the person who is preparing the manuscript on a typewriter or word processor, the submitted article will require fewer revisions and will be accepted more quickly.

The first several items on the checklist concern general requirements for submission. All typewritten parts of the manuscript must be double-spaced; this is a requirement that must be met before editing and typesetting can take place. Articles that are typed 1½-spaced or single-spaced present many problems for the editor and almost inevitably result in messy manuscripts that invite typographic errors during the publication process.

We must have two copies of the manuscript and two copies of *original* figures so that we can send them to two reviewers simultaneously; simultaneous review is necessary for a quick decision, and reviewers cannot judge the quality of a figure (e.g., radiograph or MR image) from a photocopy. We ask for ragged right margins (not justified) on the manuscript because justified margins cause irregular spaces between words. When we edit manuscripts with justified margins, we must make appropriate notations wherever words are very far apart

or close together; if we miss some of the space variations, the typesetter may incorporate these extra spaces or closed-up words into the final copy.

The guidelines also indicate that authors must address the issues of informed consent and NIH guidelines for experimental studies; both are important legal and ethical considerations in medical research. Finally, we request minimal use of acronyms, consistent use of metric measurements, and names and locations of manufacturers because all these features help readers to understand the methods and results quickly.

Title Page

The information on the title page is essential to expeditious handling of the manuscript. Any confusion about presentation at meetings, grant support, or—most importantly—locations of authors (including telephone number for the corresponding author) causes delays and takes time away from the process of publishing a quality journal.

Three items in the guidelines are requested to help us ensure a blind review of the manuscript in which the reviewers are not biased by knowledge of the authors' names. In the general list, we specify that authors' names should not appear on pages of the manuscript; here we request two copies of a "blind" title page, which contains the title of the article but not the authors' names or affiliations; and in the Figures section, we request that authors' names *not* be placed on the backs of the figures. Whenever any of these steps are not done by authors, they must be done by our administrative staff before review. We think that these are small requests for each author but represent an enormous task for our staff to do for all 1300 manuscripts submitted each year.

Abstract

In the section on the abstract, we repeat the length requirement and expand briefly on the preferred content. Our goal is that each *AJR* abstract gives the reader a summary of the content and conclusions of the article. The use of a second paragraph in the abstract to explain the conclusions is a relatively recent innovation designed to provide the reader with a helpful quick reference. We ask that no abbreviations or acronyms be used because we expect that some readers of the abstract will not be experts in the area of study and we think that they should be able to understand the abstract without having to search through the article for the meaning of an acronym.

References

The items in the section on references clearly apply to the typing of the manuscript. The first and most important is the numbering of references. References must be numbered consecutively in the order in which they appear in the text. This convention is again for the reader's convenience, and we think consistency in this regard is important. However, it slows down the editorial process considerably if, for example, we have to renumber 21 references because reference 5 is not mentioned until after reference 24. In addition, the renumber-

ing of references at the editing stage always carries the risk of error, and we believe that an incorrect reference citation is a serious error.

Our reference format does vary slightly from that of *Radiology* and some other medical journals. (There are only two differences between our references and those in *Radiology*: first, we omit what we consider the unnecessary period at the end of each reference, and second, our in-text reference numbers are placed in brackets rather than parentheses because we think that this is less confusing to the reader.) Our format was selected many years ago, and we continue to use it because it enables the reader or researcher to find any needed reference information easily. Especially because word processors make it easy to change formats without retyping, we consider it reasonable to ask authors to have the reference list typed in *AJR* format for submission to the *AJR*. We hope that the examples given in the guidelines will make that task easy.

Tables

The first item in the section on tables could win a prize for nonconformance by authors. Somehow, subjectively, single-spaced tables must look nicer to authors—but they are exceedingly difficult for editors and printers to deal with. Therefore, an author who submits a single-spaced table can be sure that we will request another copy that is double-spaced.

If a table is not mentioned in the text, or if Table 3 is mentioned before Table 2, we have problems similar to the ones described for numbering references. As revisions are made, the author should make sure that the references to tables in the text still reflect the correct number and content of the tables.

The request that horizontal and vertical lines be omitted is the result of our printing specifications, which are consistent and specific. It is the copy editor's job to place the rules correctly in the table, and any extraneous rules interfere with that job. The author's responsibilities are to ensure that all abbreviations are explained in a table footnote (more abbreviations are necessary in tables than in text, and sometimes the abbreviations confound the most creative copy editor); that tables do not simply repeat information given in text (if that is the case, either the table should be deleted or the text rewritten to refer to the table without giving away all its data); that arithmetic is correct; and that all the data in the table agree with data in the text and figures. Whalen's three laws of editing tables are (1) given at least 10 percentages in a table, one or more percentages will be incorrect, inconsistent with the text, or both; (2) given seven or more columns with totals, at least one total will be wrong; and (3) given a percentage or a total in a table that does not make sense, it will be impossible to determine from text or figures whether the data are wrong or the addition is faulty.

Figures and Legends

The figures are the heart and soul of the *AJR*. We spend many hours sizing them, checking proofs and revised proofs

for quality and correctness, and agonizing over the occasional miscropped or misoriented figure. We request a lot from authors in regard to figures because we know that the better the submitted figure is, the better the published figure (and article) will be.

The request for unmounted figures is one of the most controversial, solely because *Radiology* asks for mounted figures. The reason for this difference is simple and unchangeable: The two journals use different printers. The printer who produces *Radiology* prefers to shoot mounted figures; the *Radiology* staff also likes them because they are "easier to handle" and get less dirty. The printer who does the *AJR* prefers to shoot unmounted figures; we also like them because they are "easier to handle" and easier for reviewers and editors to spread out on a table in order to compare images and plan page layout. We regret the inconvenience that this difference causes for some of the authors who submit manuscripts to both journals; it is just one of those unfortunate facts of life.

Other items regarding the illustrations are based on our experiences concerning which type of original figures result in the publication of clear reproductions and an attractive page layout. We ask authors to place arrows and letters on the figures that are large enough and have enough contrast to show up when the figure is reduced in size for publication. We will ask authors to replace arrows and letters that do not meet these standards. There are two reasons for these requests: (1) authors know, better than copy editors, the exact, correct placement of letters and arrows; and (2) replacement of arrows or letters always carries the risk of damaging the photograph (which can be a much bigger problem for the copy editor than for the author).

Lack of written permission for a figure not owned by the authors (whether published previously or not) can result in deleting the figure or delaying publication until the permission is received. Such written permission from the author (and the publisher, if the figure has been published) is a legal necessity for our journal, and it applies equally to the case in which a friend is allowing an author to "use" an unpublished figure. We must have a letter from the friend indicating knowledge of and permission for use of the figure—otherwise we cannot publish the figure. Permissions to use figures can be obtained easily by the author during preparation of a manuscript, but it is a time-consuming and sometimes publication-delaying problem if an article is accepted before written permissions have been obtained.

Along with tables and references, figure legends are the items that are most often sent to us single-spaced. The legends must be double-spaced for editing and printing. Also, to avoid the problems outlined for out-of-order references, all figures must be called out in order in the text. Authors who overlook this step risk having a figure number appear in the wrong place in the text.

Copyright Agreement

The copyright agreement, although printed in very small type, contains significant contractual commitments. Every

author must sign it (we have come close to deleting an author's name in the final production stage because we had to wait so long for a signature on the copyright form), and every author who signs it should read it carefully. It not only transfers copyright for the article from the authors to the *AJR*, but it also guarantees that the manuscript is not "unlawful," that any conflict of interest or commercial interest has been revealed, that each coauthor deserves that designation in terms of contribution to the study and preparation of the article, that each coauthor takes "public responsibility" for the content, and that none of the material has been published before.

This legal document protects the *AJR* and our readers from fraudulent research and dishonest researchers. We intend our journal to be a source of solid scientific research that will advance the course of medicine. We can do this only if we know that authors who submit manuscripts to us have that same goal.

Guidelines for Special Articles

Before any author begins to write an article, the type of article to be written must be determined. Some topics do not fit easily into our "major paper" mold. There are single cases that make interesting case reports or letters to the editor; there are new techniques that can be described briefly in a technical note; and there is information that can be conveyed best by a pictorial essay, a computer-page article, or an opinion. If an author prepares one of these special types of

articles, it will serve that author well to follow the boxed guidelines on page A5 and also to use the checklist. Otherwise, drastic revisions will almost certainly be required.

Conclusion

Many authors use the checklist published in each issue of the *AJR*. Some do not, and often their articles are problematic for the reviewers, the scientific editor, and the copy editors. Every day, much time is spent in the editorial office chasing down figure permissions and author signatures for copyright forms, and more editorial time is spent replacing black-on-black (or white-on-white) or too-small arrows, correcting inconsistent data or incorrect arithmetic, and renumbering references. We would rather dedicate this time to increasing the clarity and correctness of manuscripts or examining page proofs and revised pages for errors. We request a great deal from authors because we have high expectations for the *AJR*: We know that as the quality of the submitted manuscripts improves, the quality of the journal improves.

In this article, I have tried to explain the requirements outlined in the "*AJR* Guidelines for Authors" and the reasons for those requirements. We encourage authors to telephone the editorial office with specific questions about submission of manuscripts or about any part of the publication process, and we continue to appreciate the sincere efforts of those authors who not only do good research but also cooperate with us in the attempt to give that research the high-quality publication it deserves.

Letters

Whose Turf Is Imaging? Professional Responsibility for Imaging Procedures in Hospital Practice

We read the article by Dr. Evens [1] summarizing the findings in a recent survey of the American Association of Academic Chief Residents in Radiology with great interest. We were particularly interested in the observations on cardiac radiology. However, we were dismayed to read the following: "The survey shows that cardiology/medicine departments are now responsible for cardiac angiography and cardiac sonography. If this is the case, it doesn't make sense to require radiology departments to allocate precious time and resources to these areas." From this statement, we deduce that Dr. Evens believes that diagnostic radiology departments should cease participation in cardiac radiology. Such an inference is most disturbing.

First, we disagree that performing a procedure is a prerequisite for effective and fruitful participation by the radiologist. A knowledgeable and experienced cardiac radiologist is an asset to any cardiac catheterization laboratory even if the radiologist does not actually perform the angiography. An analogy may be drawn to the value of the radiologist's interpretation of ERCP, operative cholangiograms, or retrograde pyelograms. Second, cardiac radiology is at a turning point in time, when the newer imaging techniques of cine CT and MR have the potential of returning many opportunities lost to it. For a long time to come, the newer imaging techniques will be compared with and judged against the established gold standards of cardiac angiography, sonography, and scintigraphy. This new era in cardiac imaging cannot happen without the availability of dedicated cardiac radiologists who not only are involved in imaging the pathologic changes in anatomy, but are equally capable of culling the physiologic data from such images.

Additionally, understanding cardiac anatomy and physiology is a prerequisite for expert interpretation of chest radiographs, CT scans, and MRI images; pulmonary angiograms; thoracic aortograms; and cardiac scintigrams—all of which are still in the turf of diagnostic radiologists. In our program, the time spent by radiology residents in cardiac radiology rarely exceeds 5% of their training, but we consider it time well allocated.

We also wish to emphasize one other point. A well-trained radiologist's perception of an image should be superior to a nonradiologist's perception. Thus, the radiologist's interpretation of all imaging studies should contribute to improved care for patients, whether such procedures are under the total control of the radiologist or not. This should be the basic tenet of radiology training programs. Departure from this philosophy is dangerous to our specialty. We seriously doubt that Dr. Evens would suggest that radiology residents not

bother learning to interpret ERCP or other contrast studies of the biliary tree and pancreatic ductal system performed by nonradiologists or sonograms of women with ectopic pregnancies on the premise that this would be an inefficient use of time and resources. Dr. Evens mentions that renal lithotripsy is no longer in the domain of radiologists. Although that is certainly true, radiologists are intimately involved in prelithotripsy evaluation and in management of complications after lithotripsy, thus making the knowledge of lithotripsy essential.

Thus, we strongly believe that cardiac radiologists contribute substantially to the evaluation and management of cardiac diseases and should have ample opportunities to continue to do so. Toward this end, we plan continued support of an evolving cardiopulmonary radiology fellowship in our department [2]. We sincerely hope that Dr. Evens and the rest of the academic radiology community will not be influenced by the results of the A³CR² survey to exclude significant diagnostic imaging areas from the practice of radiology in the future.

Benigno Soto

Chief, Cardiopulmonary Section

Hrudaya Nath

P. Colleen Sanders

Division of Cardiac Radiology

Robert J. Stanley

Chairman, Department of Radiology

University of Alabama at Birmingham

Birmingham, AL 35233

REFERENCES

1. Evens RG. Commentary. Whose turf is imaging? Professional responsibility for imaging procedures in hospital practice. *AJR* 1988;151:261-262
2. Nath PH, Stanley RJ. Subspecialty training in cardiopulmonary radiology. *J Thorac Imag* 1987;2:81-82

The Need for Continued Training of Residents in Cardiac Imaging

In the August 1988 issue of *AJR*, Dr. Evens [1] commented on turf battles in imaging studies. He alluded to the results of a recent A³CR² survey [2] that indicated, among other things, that both cardiac angiography and echocardiography have been almost totally taken over by cardiologists. Evens seems to think that because these two turf battles have been lost, it therefore no longer makes sense to train radiologists in these subjects or to include the subjects on the American Board of Radiology examinations.

In my opinion, this would be an extremely shortsighted approach. Like it or not, the heart remains an important part of the cardiovascular system, and cardiovascular disease is a leading cause of mortality and morbidity in the United States. If for no other reasons than these, radiologists should be thoroughly familiar with cardiac function and imaging. Cardiac angiography currently is accepted as the gold standard in diagnosing most major forms of heart disease. Echocardiography might logically be considered the silver standard, as it has supplanted angiography in diagnosing certain other cardiac abnormalities (e.g., hypertrophic cardiomyopathy and pericardial effusion). Without knowledge of these two techniques, a physician simply does not have the necessary background to undertake more advanced or complex types of cardiac imaging.

This brings me to the second, and perhaps even more important, reason for understanding these techniques: the same issue of turf. As Evens pointed out in his commentary, nuclear cardiac imaging is already the subject of controversy between radiologists and cardiologists in many hospitals, and although cardiac MR still appears to be largely within the domain of radiology, this area may well become the next battleground with our cardiology colleagues. Anyone who doubts this should read the proceedings of the 1986 symposium of the American College of Cardiology on the training in adult cardiology [3]. In that publication, the task force dealing with training of cardiology fellows in cardiac nuclear medicine and MR clearly states its belief that these studies should fall under the aegis of cardiologists. If radiologists are to maintain what turf we have left in cardiac imaging, we had better make sure that all of us and our future trainees are thoroughly grounded in the fundamentals of cardiac imaging—and this means training in cardiac angiography and echocardiography. Trying to interpret cardiac nuclear medicine or MR studies without a working knowledge of angiography and echocardiography would be like trying to interpret chest CT scans without knowing how to read a chest film. It obviously would not work.

Three decades ago when coronary angiography was developed, instead of plunging in aggressively to develop large-scale, comprehensive training programs, many radiologists put their heads in the sand and hoped the challenge from cardiology would go away. The result was that this radiologic technique is now controlled by nonradiologists. Let us not make the same mistake again.

David C. Levin

Thomas Jefferson University Hospital
Philadelphia, PA 19107

REFERENCES

1. Evens RG. Commentary. Whose turf is imaging? Professional responsibility for imaging procedures in hospital practice. *AJR* 1988;151:261-262
2. Getz TA, Evens RG. Residencies in diagnostic radiology and perception of residents: 1987 A³CR² survey. *Invest Radiol* 1988;23:308-311
3. Pohost GM, Adolph RJ, Beller GA, Fleming JW, Ritchie JL. Training in nuclear cardiology and nuclear magnetic resonance. *J Am Coll Cardiol* 1986;7:1209-1212

Reply

I respond, with appreciation, to the letters by Drs. Soto et al. and Dr. Levin on my commentary in the *AJR* [1] and the original article with data [2] in which I recommend a major change in emphasis in the training for residents in diagnostic radiology.

Drs. Soto et al. and Dr. Levin represent major academic programs at universities where radiologists retain important responsibilities for cardiac angiography and, perhaps, cardiac sonography. This is also the situation at my institution, where full-time cardiac radiologists have important supervisory and interpretative responsibilities for coronary angiography but not for cardiac sonography (cardiology has essentially full responsibility for cardiac sonography).

Neither of these letters disagrees with the data: Cardiac angiography and sonography are essentially the responsibility of the departments of cardiology and medicine. The A³CR² data [2] are clear. Radiology has a presence in only 18% of cardiac catheterization laboratories and 11% of cardiac sonography laboratories. It has primary responsibility in only 4% and 3% of the respective laboratories. Soto et al. and Levin speak to the philosophic concerns about appropriate cardiology training for radiologists and about the ongoing turf battles for a variety of cardiac imaging procedures. They suggest that if radiologists lose the battles for cardiac sonography and coronary angiography, this will be an important consideration in further turf conflicts, with ultimate harm to patient care as well as radiology.

It is my opinion that the battles for coronary angiography and cardiac sonography have already been lost, but this does not mean the loss of radiology's responsibility for many aspects of cardiac imaging and diagnosis. I hope that radiologists will continue to be a presence in the major academic centers and that they will continue to provide the level of care that is the ultimate for setting standards. However, in the 2500 or more locations in the United States providing coronary angiography, approximately 100 or fewer have any involvement of radiologists. The situation is similar in cardiac sonography.

This does not mean that radiology should give up interests in diagnostic cardiac procedures. The justification for radiology's responsibility for these procedures has never been stronger. Radiologists should be the best trained to use CT, MR, nuclear imaging, and positron-emission tomography (PET). The question is how to prepare future radiologists in these technologies.

I contend that we are wasting valuable training time by requiring 1, 2, or 3 months of training in the catheterization laboratory or in the department of cardiac sonography. This time would be best spent with radiologists who are actively pursuing the newer technologies of cardiac imaging. Of course, radiologists must understand cardiac anatomy and physiology. These do not have to be taught in the catheterization or sonographic laboratories. They can be taught in pediatric radiology, chest radiology, interventional radiology, or nuclear radiology and wherever CT, MR, and PET are performed.

Colleagues and friends can disagree about very important issues. I thank Drs. Soto et al. and Dr. Levin for interest in my commentary and agree with many of their comments. The important issue is how should radiologists be best trained for future cardiac imaging. Rather than spending important training time in laboratories outside of radiology, we should organize an approach that uses the newer technologies.

Ronald G. Evens

Washington University Medical School
Mallinckrodt Institute of Radiology
St. Louis, MO 63110

REFERENCES

1. Evens RG. Commentary. Whose turf is imaging? Professional responsibility for imaging procedures in hospital practice. *AJR* 1988;151:261-262
2. Getz TA, Evens RG. Residencies in diagnostic radiology and perception of residents: 1987 A³CR² survey. *Invest Radiol* 1988;23:308-311

Update on Informed Consent

Courts traditionally have used one of two rules to determine the amount of information a patient must be given as part of the process of informed consent. In states that use the "reasonable physician" standard, the patient must be informed of those risks and complications of the proposed procedure that reasonable physicians in that jurisdiction tell their patients under the same or similar circumstances. In states that use the "reasonable patient" standard, the burden of disclosure is higher: The physician must inform the patient of the

risks, complications, and alternative procedures about which a reasonable person would want to know in deciding whether to accept or reject the procedure.

In 1987, I published an article [1] listing the states that use the physician standard and those that use the patient standard. In that article I stated that Alabama had not yet ruled on the question. In fact, the Supreme Court of Alabama, in the case of *Thane v Smith* [2], held that Alabama had adopted the physician standard in 1985. In addition, the New Jersey Supreme Court moved from the reasonable physician rule to the reasonable patient rule this year [3]. New Jersey radiologists must now decide what a reasonable patient would want to know about the risks and benefits of a proposed procedure. They can expect the issue of informed consent to play a larger role in suits alleging negligent care.

Finally, Georgia has passed an informed consent statute that will go into effect January 1, 1989. The Georgia courts' interpretations of previous statutes resulted in Georgia being the only state in which courts had expressly denied the need for informed consent. The new statute adopts the reasonable patient standard for all surgical procedures performed under general, spinal, or major regional anesthesia; diagnostic amniocentesis; and diagnostic procedures involving the IV injection of contrast medium. On its face, the statute appears to require informed consent for IV urograms but not for arteriograms. It is a strange statute, and radiologists in Georgia should study it with their attorneys. Georgia radiologists can expect a flurry of litigation alleging inadequate consent. The Georgia courts will use the resulting cases to interpret the language of the statute.

Stewart R. Reuter

*The University of Texas Health Science Center at San Antonio
San Antonio, TX 78284-7800*

REFERENCES

1. Reuter SR. An overview of informed consent for radiologists. *AJR* 1987;148:219-227
2. *Thane v Smith*, 479 So2d 1150 (Ala. 1985)
3. *Largey v Rothman*, 540 A2d 504 (N.J. 1988)

Variations of Normal Glenoid Labrum

In the November 1987 *AJR*, McNiesh and Callaghan [1] reported on variations of the glenoid labrum as depicted by CT arthrography of the shoulder. They obtained the CT scans with the patient's arm in neutral or external rotation. In our experience and that of others [2, 3], neutral rotation of the arm is the most suitable position because the anterior and posterior components of the joint capsule are similarly relaxed. It is true that external rotation of the arm enhances the visualization of the posterior labrum. However, this is achieved at the expense of adequate visualization of the anterior capsulolabral complex. This can result in limited recognition of anterior lesions [4], which are ordinarily more common than the lesions of the posterior capsulolabral complex. As has been suggested by others [3] and by us [5], additional slices can be obtained before the end of the study if a suspected posterior lesion is observed on the initial examination, or these additional three to four slices can be obtained routinely on those patients who are suspected of having a posterior lesion.

McNiesh and Callaghan show six examples of anatomic variations from a total of 72 examinations. The examples are of morphologic variations that have been considered normal on arthroscopy. Three cases had a notched or cleaved anterior labrum. The clinical pictures of the patients are not discussed.

The normal anatomy, including normal variations and degenerative changes of the glenoid labrum, has been extensively studied by DePalma [6] and others [7]. More recently, Kohn [8] has published an anatomic evaluation of 106 shoulders. These studies have indi-

cated that various morphologic changes of the labrum, such as enlargement, fissuring, partial detachment, or attenuation, are increasingly evident with increasing age. Anatomic variations of the anterior capsulolabral complex are mainly due to developmental variations of the glenohumeral ligaments and recesses associated with these ligaments. The scapular attachment of the capsule and its ligaments can vary from near the glenoid margin to more medially at the scapular neck. The inferior glenohumeral ligament when well developed is always contiguous with the inferior glenoid labrum and on axial CT sections also may give the appearance of a notch deformity. A similar configuration may be seen when the mid glenohumeral ligament has a labral attachment. Moreover, a labral attachment can, on axial sections, be manifested as an elongated or redundant labrum. In both instances, thorough review of the adjacent sections can identify a glenohumeral ligament, which usually extends laterally and superiorly to become confluent with the capsule near its humeral attachment. Recognition of these variations is important because a cleaved, notched, or irregular labrum may also represent a deformity induced by trauma or abnormal motion of the humeral head. These morphologic changes are particularly important in athletes who may have a mild degree of joint laxity that is difficult to detect clinically. We agree with Kohn that these lesions per se may have no clinical relevance, but we believe that they may be significant diagnostic signs, especially when considered with other elements such as location, extent, and association with capsular changes.

A universally small glenoid labrum, or "deficient glenoid labrum," as referred to by McNiesh and Callaghan, also has been included in the category of variations of normal labrum. We have observed this pattern in advanced degenerative processes and in several patients who have congenital laxity and multidirectional instability of the shoulder. An attenuated anteroinferior labrum also may reflect an anterior instability.

Finally, in Figure 7A in the article by McNiesh and Callaghan, the triangular density that becomes confluent with the subscapularis tendon on subsequent images is presumed to represent the obliquely coursing free margin of this tendon. This is not likely because on Figure 7A this density is attached medially to the capsule with only a thin band. Also, the orientation of this triangular density and a cleavage between it and the structure outlined with white arrows in Figure 7B, which is probably the free margin of the subscapularis tendon, are inconsistent with this being a portion of the same tendon. This density is more likely to be a portion of the superior glenohumeral ligament, which may in fact be associated with an avulsed labrum. This is a strong possibility because no anterior labrum is visualized on any of these images.

Mahvash Rafii

*Hossein Firooznia
NYU Medical Center
New York, NY 10016*

REFERENCES

1. McNiesh LM, Callaghan JJ. Pictorial Essay. CT arthrography of the shoulder: variations of the glenoid labrum. *AJR* 1987;149:963-966
2. Schumann P, Kilcoyne RF, Matsen FA, Rogers JV, Mack LA. Double-contrast computed tomography of the glenoid labrum. *AJR* 1983;141:581-584
3. Deutch AL, Resnick D, Mink J, et al. Computed and conventional arthrography of the glenohumeral joint: normal anatomy and clinical experience. *Radiology* 1984;153:603-609
4. Callaghan JJ, McNiesh LM, DeHaven JP, Savory CG, Polly DW Jr. A prospective comparison study of double contrast computed tomography (CT) arthrography and arthroscopy of the shoulder. *Am J Sports Med* 1988;16(1):13-20
5. Rafii M, Firooznia H, Bonamo J, Minkoff J, Golimbu C. Athlete shoulder injuries: CT arthrographic findings. *Radiology* 1987;162:559-564

6. DePalma AF. *Surgery of the shoulder*, 3rd ed. Philadelphia: Lippincott, 1983:51-63, 211-241
7. Moseley HF, Overgaard B. The anterior capsular mechanism in recurrent anterior dislocation of shoulder: morphological and clinical studies with special reference to the glenoid labrum and the gleno-humeral ligaments. *J Bone Joint Surg [Br]* 1962;44-B:913-927
8. Kohn D. The clinical relevance of glenoid labrum lesions. *Arthroscopy* 1987;3(4):223-230

Reply

Our appreciation is extended to Drs. Rafii and Firooznia for their interest in and comments on our article. For the diagnostic radiologist practicing double-contrast CT arthrography of the shoulder, their comments on positioning the patient, their review of the orthopedic literature addressing morphologic changes of the labrum, and their experience with this technique should be duly recognized.

Their letter gives us the opportunity to confess that our pictorial essay was originally submitted to *AJR* as a "pitfalls" article detailing our radiologic interpretive errors verified by shoulder arthroscopy. In fact, Figures 3-8 were thought to show tears of the anterior labrum. Arthroscopy proved that the anterior labra in these figures were normal or redundant.

Gradually, through arthroscopic confirmation, we realized that the lack of a classically shaped glenoid (round or triangular) does not necessarily mean that it is torn. That was the message of the pictorial essay. The earlier literature [1] would have made us believe otherwise. We sincerely hope that Drs. Rafii and Firooznia no longer adhere to the belief that "the triangular contour of the anterior glenoid labrum is constant" [1].

As familiarity with the morphologic variants and normal anatomy is gained, sensitivity, specificity, and accuracy of CT arthrography in the assessment of labral pathologic changes will also improve.

Lawrence M. McNiesh

Uniformed Services University of the Health Sciences
Bethesda, MD 20814-4799

John J. Callaghan
Duke University Medical Center
Durham, NC 27710

REFERENCE

1. Rafii M, Firooznia H, Golimbu C, Minkoff J, Bonamo J. CT arthrography of capsular structures of the shoulder. *AJR* 1986;146:361-367

Sonography of the Postoperative Shoulder

We read with great interest the article by Mack et al. [1] on sonography of the postoperative shoulder in the May 1988 issue of the *AJR*. Their demonstration of postoperative lesions of the rotator cuff is remarkable for its high quality.

In their discussion of the anatomy of the shoulder, they refer to the subdeltoid bursa as a reflective interface between the deltoid and supraspinatus muscles. In our experience, the sonographic appearance of the subdeltoid bursa is a narrow, hypoechoic, curvilinear band bounded on both sides by two hyperechoic layers. The reason that the subdeltoid bursa, or any bursa, would have that appearance is easily understood. A bursa is a sac of flattened, fibrous connective tissue that contains a minute amount of viscous fluid. Thus, the central hypoechoic region corresponds to this fluid film separating the two walls. Because the fibrous walls of the bursa are imperceptibly thin, the outer hyperreflective layers can be attributed to a "muscle-fluid" interface.

This can be proved by positioning a 22-gauge needle with its tip in the hypoechoic region of the bursa (Fig. 1). Iodinated contrast

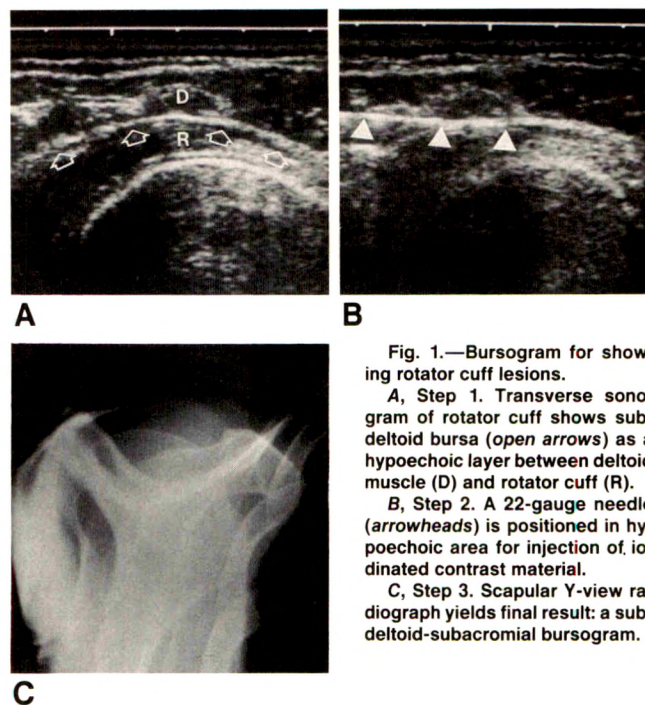


Fig. 1.—Bursogram for showing rotator cuff lesions.

A, Step 1. Transverse sonogram of rotator cuff shows subdeltoid bursa (open arrows) as a hypoechoic layer between deltoid muscle (D) and rotator cuff (R).

B, Step 2. A 22-gauge needle (arrowheads) is positioned in hypoechoic area for injection of iodinated contrast material.

C, Step 3. Scapular Y-view radiograph yields final result: a subdeltoid-subacromial bursogram.

material can then be injected, and a radiograph can be obtained. We did this in three patients, and in each case we obtained a subdeltoid bursogram.

M. van Holsbeeck

J. Introcaso
University of Michigan Hospitals
Ann Arbor, MI 48109-0326

REFERENCE

1. Mack LA, Nyberg DA, Matsen FR III, Kilcoyne RF, Harvey D. Sonography of the postoperative shoulder. *AJR* 1988;150:1089-1093

Reply

The comments of Drs. van Holsbeeck and Introcaso are greatly appreciated. They make an excellent point of anatomy regarding the appearance of the subdeltoid bursa in the normal shoulder. However, in athletes and in patients with impingement syndrome, at surgery the bursa often is noted to be up to 3 mm thick. We think that this accounts for the highly reflective nature of the bursa as illustrated in our article.

Laurence A. Mack

Frederick A. Matsen III
University of Washington
Seattle, WA 98195

Target Metastases from Bronchial Carcinoid: A Rare Form of Osteoblastic Metastases

We present a case of widespread bone metastases from bronchial carcinoid that had an unusual radiologic pattern. A 26-year-old woman had had low back pain for 1 year. Physical examination was normal except for tenderness in the back. A chest radiograph showed right

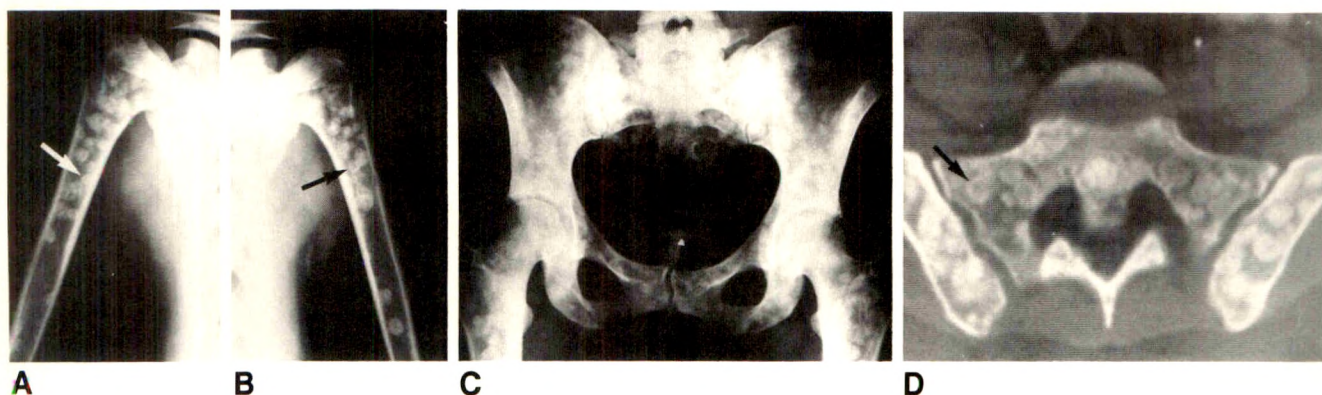


Fig. 1.—Target osteoblastic metastases from bronchial carcinoid.

A–C, Skeletal radiographs show well-defined, dense sclerotic lesions with a target appearance (arrows) in both humeri (A, B), distal end of right clavicle (A), and pelvis and femora (C).

D, CT scan shows target appearance (arrow) of sclerotic lesions involving pelvic bones.

middle lobe atelectasis. Skeletal radiographs showed multiple osteoblastic lesions in the vertebral bodies, pelvis, femora, humeri, ribs, clavicles, sternum, and skull (Figs. 1A–1C). CT examination showed the lesions had a “target” appearance (Fig. 1D). A ^{99m}Tc -methylidiphosphonate bone scan showed abnormal uptake of the radionuclide. Bronchoscopy revealed an intrabronchial tumor that subsequently was found to be a carcinoid. Results of percutaneous biopsy of the pelvis were consistent with metastatic deposits from carcinoid tumor.

Bone metastases from bronchial carcinoids are rare, but when they occur, most are osteoblastic [1, 2]. Such lesions usually progress slowly but may remain unchanged for many years. Two unusual patterns of osteoblastic metastases from bronchial carcinoid tumors have been described [2]: a radiating spiculated form that resembles osteosarcoma and a diffuse form that shows bony sclerosis with associated expansion.

Widespread target osteoblastic lesions are another unusual pattern of carcinoid metastases not described before. Despite their slow growth, the appearance of metastases may correspond to osteolysis of osteoblastic lesions as has been described in prostatic cancer [3]. Osteolysis develops centrally, leaving a rim of sclerotic bone. The distinction between osteoblastic metastases and other sclerotic bone lesions may be difficult [4]. Several causes must be considered in the differential diagnosis, including osteomesopyknosis, osteopoikilosis, pycnodysostosis, mastocytosis, osteosclerotic myeloma, and multicentric osteosarcoma.

T. Franquet
J. Barberena
C. Jiménez

Hospital “Virgen del Camino”
Pamplona 31007, Spain
F. J. Lecumberri
Clínica Universitaria de Navarra
Pamplona 31007, Spain

REFERENCES

1. Toomey F, Felson B. Osteoblastic bone metastases in gastrointestinal and bronchial carcinoids. *AJR* 1960;83:709–715
2. Peavy PW, Rogers JV Jr, Clements JL Jr, Burns JB. Unusual osteoblastic metastases from carcinoid tumors. *Radiology* 1973;107:327–330
3. Pollen JJ, Reznick RH, Talner LB. Lysis of osteoblastic lesions in prostatic cancer: a sign of progression. *AJR* 1984;142:1175–1179
4. Jacobson HG. Dense bone—too much bone: radiological considerations and differential diagnosis. Part II. *Skeletal Radiol* 1985;13:97–113

Knee Time in Femoral Arteriography

In our hospitals, arteriography of the pelvis and lower limbs is most frequently performed by using Seldinger percutaneous techniques. A 5-French pigtail catheter is inserted into the distal aorta via the femoral approach. Before the actual radiographs are made, a few milliliters of contrast medium are injected to ensure the intraluminal position of the catheter just above the bifurcation. At most, a rough estimate of blood flow in the aorta can be made. This is used to adjust the timing of the radiographs of the lower abdominal aorta and the vessels of the pelvis and the legs.

Most angiographic configurations fitted with run-off facilities are operated by a computer-card system, which enables variable preprogrammed shifts of the table and variable sequences of film throughput. To achieve a more accurate timing of the radiographs, we determine the time it takes contrast material to pass from the lower abdominal aorta to the popliteal artery. Eight to ten milliliters of contrast medium are injected for each leg, and the popliteal artery is observed under fluoroscopy. The time necessary for the contrast material to pass from the distal aorta to the popliteal artery is measured with a stopwatch. When this time was used as a guide, accurate timing of the radiographs was achieved. Fewer runs were necessary compared with those required by conventional techniques or digital subtraction angiography.

We evaluated two groups of patients who had femoral arteriography before and after the introduction of this method. In one group, estimation of the rate of blood flow and timing of the radiographs were made by evaluating the flow of contrast material in the lower abdominal aorta. A mean of 160 ml of contrast material (Telebrix 38) per study was used. Additional runs were often necessary. In the other group, estimation of the rate of blood flow was made by measuring the time necessary for the contrast material to pass from the lower abdominal aorta to the popliteal artery. Despite the additional amount of contrast material needed for the test injections (16–20 ml), the total amount needed per investigation decreased. A mean of 125 ml of contrast material per investigation was required.

Robbert J. Versteijlen
Academic Hospital Maastricht
6201 BX Maastricht, Holland
Leo E. H. Lampmann
St. Elisabeth Hospital
5000 LC Tilburg, Holland

Successful Transcatheter Arterial Embolization for the Replaced Right Hepatic Artery: A New Technique Using a Balloon Catheter and Norepinephrine Infusion

The anatomic variability of the hepatic arteries makes it difficult to perform transcatheter arterial embolization in patients who have liver tumors. We encountered a case of hepatocellular carcinoma in a patient in whom the right hepatic artery and the inferior pancreaticoduodenal artery had a long common trunk arising from the superior mesenteric artery. This anatomic variation made impossible the insertion of a catheter into the right hepatic artery.

Two embolization techniques are commonly used in patients with ordinary hepatic artery architecture when superselective catheterization into the proper hepatic artery is impossible. One is hepatic embolization from the common hepatic artery by using a balloon occlusion technique [1]. In the other technique, the hepatic blood flow is redistributed by occluding the gastroduodenal artery with a coil [2]. In this case, these two methods were attempted but failed. Therefore, we devised an alternative method and used temporary vasoconstriction rather than a coil to direct the balloon catheter into the right hepatic artery.

A 55-year-old man was admitted because of a hepatic mass. Superior mesenteric arteriography disclosed a 3-cm long common trunk of the inferior pancreaticoduodenal artery and the right hepatic artery. Tumor staining was obtained later by superselective arteriography (Fig. 1) via the common trunk. An attempt was made to insert a catheter into the right hepatic artery to perform embolization, but, because of the narrow angle between the right hepatic artery and the common trunk, the catheter entered the inferior pancreaticoduodenal artery instead of the right hepatic artery. To guide the catheter into the right hepatic artery, we used the following technique. A balloon catheter was inserted into the common trunk. After the balloon was inflated, both the right hepatic artery and the inferior pancreaticoduodenal artery were visualized by dye. If the blood flow of the inferior pancreaticoduodenal artery could be diminished, the balloon catheter could be advanced easily into the right hepatic artery. To accomplish that, we inserted the balloon catheter into the inferior pancreaticoduodenal artery (Fig. 2, upper left). The balloon was reinflated, and norepinephrine (80 μ g) in saline solution was injected into the inferior pancreaticoduodenal artery. After this artery constricted (Fig. 2, upper right), the balloon was deflated, and the catheter was drawn back to the common trunk (Fig. 2, lower left). Because of the decreased blood flow through the inferior pancreaticoduodenal artery, the inflated balloon catheter was then advanced easily into the right hepatic artery (Fig. 2, lower right). Superselective right hepatic arterial embolization was then performed by injecting a sus-

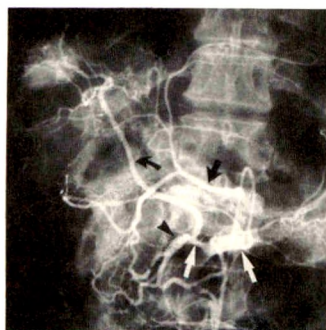


Fig. 1.—Superselective arteriogram from common trunk of inferior pancreaticoduodenal artery and right hepatic artery shows common trunk (white arrows) arises from superior mesenteric artery and branches into right hepatic artery (curved black arrow) and inferior pancreaticoduodenal artery (arrowhead). Common hepatic artery (straight black arrow) also is opacified by contrast material passing through pancreaticoduodenal arcades.

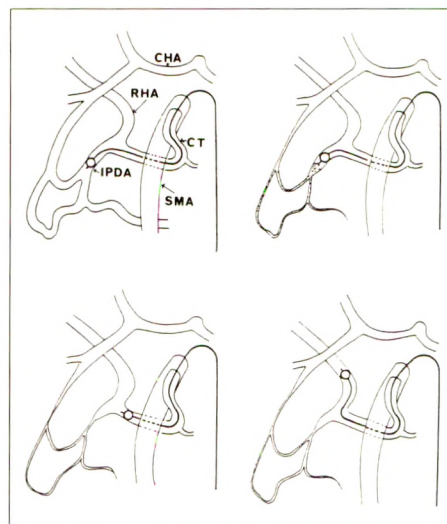


Fig. 2.—Diagrams show procedure of catheterization for transcatheter arterial embolization. CHA = common hepatic artery; RHA = right hepatic artery; CT = common trunk; IPDA = inferior pancreaticoduodenal artery; SMA = superior mesenteric artery.

Top left, Balloon catheter is inserted into inferior pancreaticoduodenal artery.

Top right, Balloon is inflated, and norepinephrine solution is injected.

Bottom left, Balloon is deflated, and catheter is retracted to common trunk.

Bottom right, Balloon is reinflated, and blood flow carries it into right hepatic artery.

pension of iodized oil (Lipiodol, 5 ml) and doxorubicin hydrochloride (Adriamycin, 10 mg), followed by absorbable gelatin sponge particles (Gelfoam) mixed with Adriamycin (10 mg).

Pharmacoangiographic techniques have been used to obtain better images of arteries or veins [3]. However, as far as we know, there is no previous report of the use of a vasoconstrictor to direct a catheter into a peripheral artery for embolization. Moreover, embolization in patients with a common trunk of the inferior pancreaticoduodenal artery and the right hepatic artery after redistribution of the inferior pancreaticoduodenal artery has not yet been reported in the English or Japanese literature. This procedure facilitates superselective catheterization when insertion of the catheter into the desired arterial branch is difficult.

Masatoshi Okazaki
Takuro Nakamura
Hideyuki Higashihara
Fumitaka Koganemaru
Yoshimi Nozaki
Fukuoka University Hospital
Fukuoka, 814-01 Japan

REFERENCES

1. Nakamura H, Tanaka M, Oi H. Hepatic embolization from the common hepatic artery using balloon occlusion technique. *AJR* 1985;145:115-116
2. Granmayeh M, Wallace S, Schwarten D. Transcatheter occlusion of the gastroduodenal artery. *Radiology* 1979;131:59-64
3. Boijesen E, Redman H. Effect of epinephrine on celiac and superior mesenteric angiography. *Invest Radiol* 1967;2:184-199

Note.—The preceding study was supported in part by the Grant-in-Aid for Cancer Research from the Ministry of Health and Welfare of Japan, a grant from the Foundation for Promotion of Clinical Research in Medicine, and a grant from the Foundation for Research in Clinical Medical Science.

Versatility of the Proximal Cope Loop Catheter

The commonly used Cope loop catheter is available in two types: proximal and distal [1]. The former has a crossed-limb loop anchor in the midpoint of the catheter; the latter has a loop at its end. We have found that the proximal loop catheter can be easily modified and introduced via the transhepatic route and the T-tube sinus tract into the bile duct system. We have placed 32 proximal loop catheters in 22 patients with various biliary conditions, including cholangiocarcinoma, biliary strictures, dislodged T-tubes, retained biliary stones, and sclerosing cholangitis. The proximal and distal Cope loop catheters and the modified proximal loop catheters that we have used are shown in Figure 1.

The distal loop catheter is commonly used for long-term biliary drainage via the percutaneous transhepatic route. When reflux of duodenal fluid into the drainage catheter is due to the presence of higher intraduodenal pressures, the proximal loop catheter is used; its distal limb is placed in the proximal jejunum or within the bile duct.

For percutaneous drainage of a high biliary obstruction, the proximal loop catheter should be modified by creating an appropriate number of side holes proximal to the loop and shortening the distal limb according to the desired level of the catheter positioning. The catheter loop is formed in the common hepatic duct distal to the obstruction. Proximal loop catheters also have been placed via the T-tube tract to drain intrahepatic biliary obstruction, to provide access to the bile duct after interventional biliary procedures, and to replace a dislodged T-tube (Fig. 2).

The advantage of the proximal loop catheter over the distal loop catheter is its longer distal limb, which not only allows the catheter to be placed in various locations but also prevents reflux of duodenal contents into the drainage catheter. The other advantage is the proximal location of the smaller loop anchor (1.5 cm in diameter), which can be formed within the bile duct. To date, we have not encountered any unusual catheter-related complications.

Francesco Doenz

Andrew Wu

Kyung Cho

University of Michigan, Medical School

Ann Arbor, MI 48109-0030

Fig. 1.—A–D, Proximal (10.2 French) (A), modified proximal (B and C), and distal (D) Cope loop catheters.

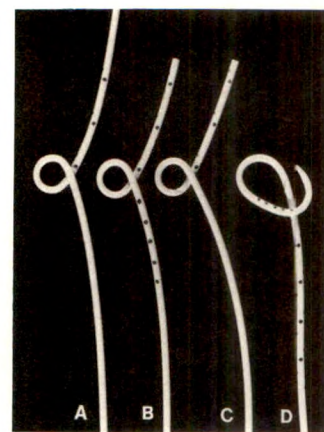
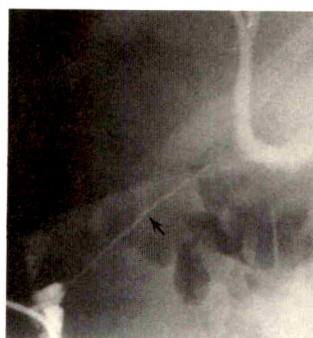


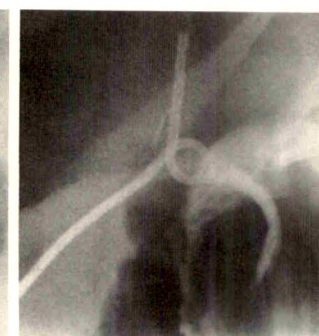
Fig. 2.—Cholangiograms show replacement of a dislodged T-tube.

A, T-tube sinus tract was opacified by injection of contrast material (arrow).

B, A modified proximal loop catheter was placed via the tract into the common hepatic duct. No sinus tract dilatation was required before catheter placement.



2A



2B

REFERENCE

1. Cope C. Use of crossed-limb anchor for percutaneous biliary bypass. *AJR* 1982;138:974–976

Letters are published at the discretion of the Editor and are subject to editing.

Letters to the Editor must not be more than two double-spaced, typewritten pages. One or two figures may be included. Abbreviations should not be used. See Author Guidelines, page A5.

Material being submitted or published elsewhere should not be duplicated in letters, and authors of letters must disclose financial associations or other possible conflicts of interest.

Letters concerning a paper published in the *AJR* will be sent to the authors of the paper for a reply to be published in the same issue. Opinions expressed in the Letters to the Editor do not necessarily reflect the opinions of the Editor.

Review of Current Literature

Since its first appearance in the summer of 1987, the Review of Current Literature section has been well received by our readership. Our experts continue to sift through a large number of journals to present the finest and most relevant articles currently published. We continue to focus on new developments in clinical medicine because few practicing radiologists have the luxury of keeping current with the literature outside their specialty. The editors would like to acknowledge the expertise and commitment of the following abstractors: Naomi Alazraki, John R. Amberg, William G. Bradley, N. Reed Dunnick, David S. Feigin, Curtis E. Green, Saskia v.W. Hilton, Michael J. Kelley, David C. Kushner, Elliott C. Lasser, George R. Leopold, Robert G. Levitt, Stephen I. Marglin, Donald Resnick, Charles A. Rohrmann, David M. Rosenbaum, Val M. Runge, David J. Sartoris, and Lee Talner.

Initials and addresses of corresponding authors are provided in parentheses for each article so that the reader can obtain reprints directly. Abstracts are printed verbatim from each journal.

The New England Journal of Medicine

Endoscopic demonstration of loss of duodenal folds in the diagnosis of celiac disease. Brocchi E, Corazza GR, Caletti G, Treggiari EA, Barbara L, Gasbarrini G, (GRC, I Patologia Medica, Nuove Patologie, Policlinico Universitario S. Orsola, Via Massarenti 9, 40138 Bologna, Italy). *N Engl J Med* 319:741-744, Sept. 1987

Among 873 patients undergoing upper gastrointestinal endoscopy for various reasons over a two-year period, four had a loss of Kerckring's folds in the descending duodenum. Endoscopic duodenal biopsy in all four patients revealed subtotal villous atrophy due to celiac disease. We undertook a prospective study to evaluate the extent to which this finding predicted celiac disease in 65 consecutive patients referred for intestinal biopsy.

Duodenal folds were absent or markedly decreased in 15 of 17 patients with subtotal villous atrophy and in 8 of 48 patients with partial villous atrophy or normal duodenal mucosa, giving a sensitivity of 88 percent and a specificity of 83 percent for this endoscopic finding with respect to celiac disease.

We recommend that all patients undergoing upper gastrointestinal endoscopy be examined for the loss or reduction of duodenal folds and, should this be found, that the examination include duodenal biopsy. The value of this procedure as an aid in the diagnosis of celiac disease should be particularly great in patients with minimal, transient, or unrelated symptoms.

Common inheritance of susceptibility to colonic adenomatous polyps and associated colorectal cancers. Cannon-Albright LA, Skolnick MH, Bishop T, Lee RG, Burt RW (LACA, Genetic Epidemiology, 410 Chipeta Way, Research Park, Salt Lake City, UT 84108). *N Engl J Med* 319:533-537, 1988

We studied 670 persons in 34 kindreds by flexible proctosigmoidoscopic examination (60 cm) to determine how frequently colorectal adenomas and cancers result from an inherited susceptibility. Kindreds were selected through either a single person with an adenomatous polyp or a cluster of relatives with colonic cancer. The kindreds all had common colorectal cancers, not the rare inherited conditions familial polyposis coli and nonpolyposis inherited colorectal cancer. Likelihood analysis strongly supported the dominant inheritance of a susceptibility to colorectal adenomas and cancers, with a gene frequency of 19 percent. According to the most likely genetic model, adenomatous polyps and colorectal cancers occur only in genetically susceptible persons; however, the 95 percent confidence interval for this proportion was 53 to 100 percent.

These results suggest that an inherited susceptibility to colonic adenomatous polyps and colorectal cancer is common and that it is responsible for the majority of colonic neoplasms observed clinically. The results also reinforce suggestions that first-degree relatives of patients with colorectal cancer should be screened for colonic tumors. This evidence of an inherited susceptibility to a cancer with well-recognized environmental risk factors supports the hypothesis that genetic and environmental factors interact in the formation and transformation of polyps.

Reduction in the rate of early restenosis after coronary angioplasty by a diet supplemented with n-3 fatty acids. Dehmer GJ, Popma JJ, van den Berg EK, et al. (GJD, Cardiac Catheterization Laboratory (111A2), Veterans Administration Medical Center, 4500 S. Lancaster Rd., Dallas, TX 75216). *N Engl J Med* 319:733-740, Sept. 1988

To determine the safety and benefit of n-3 fatty acid therapy in the prevention of early restenosis after coronary angioplasty, we conducted a randomized, unblinded study comparing a conventional antiplatelet regimen (325 mg of aspirin and 225 mg of dipyridamole per day; control group) with a similar regimen supplemented with 3.2 g of eicosapentaenoic acid per day (treatment group). Treatment began seven days before angioplasty and continued for six months afterward. All angiographic analyses were blinded and performed by a method that was validated by comparison with quantitative coronary angiography.

In 82 male patients, 103 coronary lesions were dilated. Both groups had similar base-line clinical and angiographic characteristics. The incidence of early vessel restenosis, as determined on a second angiogram three to four months after angioplasty, was 36 percent in the control group and 16 percent in the treatment group ($P = 0.026$).

The incidence of restenosis per patient was also significantly lower in the treatment group (46 vs. 19 percent). Both multiple logistic regression and Mantel-Haenszel statistical analyses demonstrated a significant independent benefit of treatment with n-3 fatty acids. No important bleeding complications developed in the treated patients.

These results, in a male population at relatively high risk for restenosis, suggest that a dietary supplement of n-3 fatty acids, administered for one week before and for six months after coronary angioplasty, is safe and reduces the occurrence of early restenosis after that procedure. Whether this beneficial effect also applies to other populations is unknown.

Cancer

Computerized tomographic prediction of extraluminal spread and prognostic implications of lesion width in esophageal carcinoma.

Lefor AT, Merino MM, Steinberg SM, et al. (H. I. Pass, Thoracic Oncology section, Surgery Branch, National Cancer Institute, National Institutes of Health, Bldg. 10, Rm. 2B07, Bethesda, MD 20892). *Cancer* 62:1287-1292, 1988

The use of preoperative computed tomographic (CT) scans of the chest in carcinoma of the esophagus to associate preoperative staging with postoperative survival is controversial. Thirty-two patients who underwent esophagectomy and reconstruction were examined with respect to a variety of variables available on preoperative evaluation, including lesion width on CT scan, lesion length on CT scan, and barium esophagogram. Each variable was evaluated for its ability to predict the presence of extraesophageal spread of tumor, as determined pathologically by logistic regression analysis. Lesions greater than 3.0 cm in width by CT scan were associated with a significantly higher incidence of extraesophageal spread. Tumor location, gender, histologic grade, presence of *in situ* lesions, vascular invasion, eosinophilia, nodal metastases, and preoperative chemotherapy had no predictive value for survival. Duration of survival was affected by the presence of esophageal spread of disease and lesion width. These results indicate that preoperative CT scanning can predict extraesophageal spread of tumor, and this is associated with overall survival.

Reprinted by permission from the American Cancer Society.

Fine-needle aspiration biopsy of cold thyroid nodules. Nathan AR, Raines KB, Lee YTM, Sakas EL, Ribbing JM (YTML, Dept. of Surgery, Tripler Army Medical Center, Honolulu, HI 96859-5000). *Cancer* 62:1337-1342, 1988

This study analyzes the results of fine-needle aspiration biopsy (FNAB) of hypofunctioning thyroid nodules performed by one physician. There were 68 patients (age range, 20 to 73 years) with 83 aspirations; 30 were interpreted as positive for neoplasm (adenoma or carcinoma), 43 were negative, and ten (12%) were technically unsatisfactory. Thyroidectomy was performed on 25 patients who had positive aspirates. Subsequent morphologic study showed that 13 patients had carcinomas, ten had adenomas, and two had adenomatoid nodules (false-positive rate of FNAB for neoplasms was 8%). One of three thyroidectomy patients with negative preoperative aspirates had a carcinoma and two had adenomas (estimated minimal false-negative rate of FNAB was 9%). Nineteen patients who underwent thyroidectomies had dynamic radioisotopic thyroid angiography. There was no correlation between the pattern of vascularity and the type of neoplasm. Ultrasound (US) study was performed on 17 patients. Both adenoma and carcinoma can be solid or partially cystic. Although approximately 33% of the nodules initially diagnosed by FNAB as follicular or papillary neoplasms had different interpretations on subsequent examination of thyroidectomy specimens, 93% of the patients selected to be operated on had either adenoma or carcinoma. Thus, in this series, FNAB of cold thyroid nodules gave more useful diagnostic information than nodule size, dynamic radioisotopic scan, or US studies.

Reprinted by permission from the American Cancer Society.

Positron emission tomography in patients with glioma: a predictor of prognosis. Alavi JB, Alavi A, Chawluk J, et al. (JBA, Hospital of the University of Pennsylvania, 3400 Spruce St., Philadelphia, PA 19104). *Cancer* 62:1074-1078, 1988

Positron emission tomography (PET) studies have been performed using 18-F-fluorodeoxyglucose in 29 adult subjects with primary brain tumors. Seventy-two percent of the patients were treated previously. The glucose metabolic state in the lesions was increased in 16 patients, and was normal or decreased in 13 patients. The hypermetabolic tumors tended to behave in a more malignant fashion. Patients with hypermetabolic tumors had a median survival of 7 months after PET scan, compared to 33 months for those with hypometabolic lesions. Among the high-grade glioma patients, the PET results separated them into a good prognosis group (hypometabolic, with 78% 1-year survival) and a poor prognosis group (hypermetabolic, with a 29% 1-year survival after PET). These results suggest that glucose metabolic studies may provide an independent measure of the aggressiveness of a brain tumor, and may supplement pathologic grading.

Reprinted by permission from the American Cancer Society.

Chest

Lobar collapse: usual and unusual forms. Mintzer RA, Sakowicz BA, Blonder JA (RAM, Dept. of Radiology, Northwestern University Medical School, Chicago, IL 60611). *Chest* 94:615-620, Sept. 1988

A systematic approach is essential to the assessment of the patient with possible lobar collapse. Evaluation of hilar size and position, mediastinal shift, fissural reorientation, diaphragm position, rib approximation, and bronchial reorientation should be performed. Conventional radiography remains the mainstay of diagnosis; CT provides anatomic-pathologic correlation.

Circulation

Randomized, double-blinded multicenter study: comparison of intracoronary single-chain urokinase-type plasminogen activator, pro-urokinase (GE-0943), and intracoronary urokinase in patients with acute myocardial infarction. Kambara H, Kawai C, Kajiwaru N, et al. (CK, Third Division, Dept. of Internal Medicine, Kyoto University Hospital, 54 Kawara-cho, Shogoin, Sakyo-ku, Kyoto 606, Japan). *Circulation* 78:899-905, 1988

Coronary recanalization rates and changes in the coagulation and fibrinolysis system were evaluated in a randomized fashion in patients with acute myocardial infarction after intracoronary administration of single-chain urokinase-type plasminogen activator (pro-urokinase: GE-0943) or urokinase. Three groups of patients were studied: group H ($n = 50$), 6,000 units pro-urokinase i.c.; group L ($n = 44$), 3,000 units pro-urokinase i.c.; and group U ($n = 54$), 960,000 IU urokinase i.c. Coronary recanalization rates determined angiographically after 45 minutes of intracoronary infusion averaged 90% in group H, 59% in group L, and 61% in group U. The differences were statistically significant between group H and the latter two groups. Pro-urokinase affected plasma proteins of the fibrinolytic system to a lesser degree than urokinase. Bleeding complications were present in one patient in group L, in none in group H, and in five in group U. Thus, intracoronary administration of 6,000 units pro-urokinase is more effective in coronary thrombolysis and causes less systemic fibrinogenolysis than intracoronary administration of urokinase.

Gastroenterology

Evolution and regression of pancreatic calcification in chronic pancreatitis: a prospective long-term study of 107 patients. Am-

mann RW, Muench R, Otto R, Buehler H, Freiburghaus AU, Siegenthaler W (RWA, Gastroenterology Service, University Hospital, Zurich, Switzerland). *Gastroenterology* 95:1018-1028, 1988

Pancreatic calcifications are virtually pathognomonic of chronic pancreatitis and develop in up to 90% of patients with alcoholic chronic pancreatitis in series with long-term results. We investigated the natural course of pancreatic calcification in a prospective longitudinal study over the past 23 yr. All patients were studied at regular intervals with particular regard to etiology, clinical findings, surgery, pancreatic function, and pancreatic calcification visible by x-ray (e.g., film series in three projections centered on the pancreas). We evaluated the findings of 107 patients with x-ray documentation of pancreatic calcification in at least three film series over a period of 4 yr or longer. Eighty-four patients had alcoholic chronic pancreatitis (group A) and 23 patients had nonalcoholic chronic pancreatitis (group B). Four hundred seventy-two film series of group A and one hundred forty-two film series of group B were reviewed independently by two expert teams. Both series were graded according to a score system in terms of intensity and distribution of pancreatic calcification (correlation of grading $r = 0.91$). The duration of calcification averaged 10 yr in group A and 12.6 yr in group B. Similar dynamic changes of pancreatic calcification were noted in groups A and B. Chronologically, three phases of evolution could be distinguished. After an initial increase (phase 1), >50% of cases reached a plateau of stationary calcification (phase 2). Approximately one-third of cases showed a marked decrease of calcification in late phases of chronic pancreatitis (phase 3). Dissolution of pancreatic stones was related primarily to duration of chronic pancreatitis (duration of calcification and marked pancreatic dysfunction), and occurred frequently (but not exclusively) in patients after ductal drainage procedures. These results indicate that spontaneous dissolution of pancreatic stones is a rather common biologic phenomenon. The factors responsible for dissolution of stones remain to be elucidated.

Reprinted with permission by the American Gastroenterological Association.

Digestive Diseases and Sciences

Infectious diarrhea in patients with AIDS. Antony MA, Brandt LJ, Klein RS, Bernstein LH (LJB, Division of Gastroenterology, Montefiore Medical Center, 111 E. 210 St., Bronx, NY 10467). *Dig Dis Sci* 33(9):1141-1146, Sept. 1988

A multitude of opportunistic infections has been documented in virtually every organ system of patients with the acquired immunodeficiency syndrome (AIDS). Prominent among these are infections of the gastrointestinal tract. However, studies of large numbers of patients documenting the frequency of such involvement are lacking. We reviewed the records of 100 patients with AIDS and assessed the frequency and organisms causing infectious diarrhea. We found diarrhea to be more common in homosexuals (80%) than heterosexuals with a risk factor of parenteral drug use (58%). In one third of all cases, no infectious etiology was found. *Myobacterium avium intracellulare* (MAI) was the most commonly identified cause of infectious diarrhea in our series, followed by cytomegalovirus, cryptosporidium, *Salmonella* spp., and herpes virus. In addition, bacteremia was documented in 43% of patients with infectious diarrhea and was most commonly due to MAI. Finally, we demonstrated that multiple concurrent infections are not uncommon (22%) in AIDS patients and that the diarrhea syndrome may not respond unless all pathogens are eradicated.

Gastrointestinal Endoscopy

Endoscopic management of malignant biliary obstruction: stents of 10 French gauge are preferable to stents of 8 French gauge. Speer AG, Cotton PB, MacRae KD (AGS, Dept. of Gastroenterology, The Royal Melbourne Hospital, Parkville, Victoria 3040, Australia). *Gastrointest Endosc* 34:412-417, 1988

To assess whether the use of large stents is justified, we have retrospectively reviewed the results of 8 French gauge (FG) stents

with pigtailed and 10 FG straight stents in the palliation of biliary obstruction due to malignancy. The incidence of cholangitis following stent insertion was significantly lower with 10 FG stents, 3 (5%), compared with 8 FG stents, 13 (34%), $p < 0.001$, χ^2 . Stent survival until blockage was significantly longer for 10 FG (median 32 weeks) compared with 8 FG (median 12 weeks), $p < 0.001$, log-rank. The superior performance of the 10 FG stents was due to their larger diameter which gives them a flow capacity much greater than the physiological bile flow. We recommend that stents of at least 10 FG diameter are used for the endoscopic palliation of biliary obstruction due to malignancy.

Video endoscopy by nurse practitioners: a model for colorectal cancer screening. Schroy PC, Wiggins T, Winawer SJ, Diaz B, Lightdale CJ (SJW, Gastroenterology Service, Memorial Sloan-Kettering Cancer Center, 1275 York Ave., New York, NY 10021). *Gastrointest Endosc* 34:390-394, 1988

The use of paramedical personnel to perform sigmoidoscopy as a screening test for colorectal cancer has been advocated as a means of increasing the availability of this test to the population at risk. A model system has been developed utilizing flexible videosigmoidoscopy performed by nurse practitioners with videotape review by physician endoscopists. Of the 100 patients studied, 36 were found to have polyps. Near excellent concordance ($\kappa = 0.72$) was observed between the nurse practitioner's findings and those of the physician. Using the physician's review as the standard, overall sensitivity and specificity of the nurse practitioner's examinations were 75% and 94%, respectively. In conclusion, videosigmoidoscopy performed by nurse practitioners and reviewed by physician endoscopists is a feasible approach to colorectal cancer screening since it is safe, provides videotape documentation to ensure quality control, and expands available resources for the performance of this examination.

The Journal of Bone and Joint Surgery

Triplane fracture of the distal tibial epiphysis: long-term follow-up. Ertl JP, Barrack RL, Alexander AH, VanBuecken K (Editorial Assistant, Clinical Investigation Dept., Naval Hospital, Oakland, CA 94627-5000). *J Bone Joint Surg [Am]* 70-A(7):967-976, Aug. 1988

The cases of twenty-three patients in whom a triplane fracture had been treated at the Naval Hospital, Oakland, California, between 1974 and 1985, were reviewed. The anatomical configuration of the fracture was confirmed in fifteen patients. Eleven of the fifteen patients had a three-fragment fracture. Plain radiographs alone did not accurately demonstrate the configuration of the fracture.

Twenty patients were asymptomatic when they were evaluated eighteen to thirty-six months after the injury, but only eight of fifteen patients were asymptomatic when they were evaluated thirty-eight months to thirteen years after the fracture. Residual displacement of two millimeters or more after reduction was associated with a less than optimum result unless the epiphyseal fracture was outside the primary weight-bearing area of the ankle.

Bipolar hemiarthroplasty for fracture of the femoral neck: clinical review with special emphasis on prosthetic motion. Bochner RM, Pellicci PM, Lyden JP (RMB, Dept. of Orthopaedic Surgery, Long Island Jewish Medical Center, 270-05 76th Ave., New Hyde Park, NY 11042). *J Bone Joint Surg [Am]* 70-A(7):1001-1010, Aug. 1988

The results of a consecutive series of 120 bipolar replacements of the femoral head that had been done for the treatment of a fracture of the femoral neck were reviewed. Ninety patients were followed for a minimum of two years. At the latest follow-up, eighty-two (91 per cent) of the patients were free of major pain, and eighty-three (92 per cent) were considered to have satisfactory motion and muscle power. Postoperative function often was limited by underlying medical problems. Seventy-five patients (83 per cent) either returned to the level of function that they had had before the fracture or used only a cane

which they had not needed previously. There was no important deterioration of the results with time.

For twenty-six of the prostheses, roentgenograms were made with the patient bearing weight in order to determine the relative motion at the two sites of articulation of the bipolar prosthesis. The roentgenograms demonstrated the presence and maintenance of motion at both bearing surfaces.

The Journal of Urology

Long-term followup in 1,003 extracorporeal shock wave lithotripsy patients. Graff J, Diederichs W, Schulze H (JG, Dept. of Urology, University of Bochum, Herne, Federal Republic of Germany). *J Urol* 140:479-483, Sept. 1988

We evaluated 1,003 patients treated with extracorporeal shock wave lithotripsy after a mean followup of 19.1 months (range 12 to 26 months). Followup excretory urograms were normal in 97 per cent of the patients. Two-thirds of the patients reported further discharge of residual fragments, mainly during the first 3 months. Rehospitalization was necessary in 57 patients. Over-all, the rate free of stones after followup was 72.2 per cent and it was not different for primary and recurrent stone patients. Rates free of stones were influenced mainly by the primary stone location and the number of stones in a renal unit. Patients with lower caliceal stones had a rate without calculi of only 57.8 per cent. Almost identical results were obtained for stones other than in the lower calix, when fragments were found in the lower calix at the time the patient was discharged from the hospital. The pre-treatment stone volume, as determined by measuring the stone area in square millimeters, did not influence the final rates free of stones for calculi up to 400 mm.², that is 2.4 cm. of a sphere. Only calculi larger than 400 mm.² showed an inverse relationship to the final rate free of stones. Multiple stones yielded a success rate of 64 per cent, with 90 per cent of the patients having regrowth of residual fragments. Serious complications during followup were not encountered.

Pediatrics

Abnormal pulmonary outcomes in premature infants: prediction from oxygen requirement in the neonatal period. Shennan AT, Dunn MS, Ohlsson A, Lennox K, Hoskins EM (ATS, Regional Perinatal Unit, Women's College Hospital, 76 Grenville St., Toronto, Ontario M5S 1B2, Canada). *Pediatrics* 82:527-532, Oct. 1988

The follow-up records of 605 infants with birth weights of less than 1,500 g, with data available for 2 years after birth, were examined for evidence of abnormal pulmonary signs or symptoms. A total of 119 infants were identified and the neonatal oxygen requirements of these infants were compared with those of 486 infants who had normal pulmonary function. A requirement for oxygen at 28 days of life had a positive predictive value for abnormal pulmonary findings at the time of follow-up of only 38%, whereas 31% of those with normal pulmonary findings at the time of follow-up were still receiving oxygen at this age. The need for oxygen at 28 days was a good predictor of abnormal findings in infants of ≥ 30 weeks' gestational age at birth but became increasingly less useful as gestational age decreased. It was found that, irrespective of gestational age at birth, the requirement for additional oxygen at 36 weeks' corrected postnatal gestational age was a better predictor of abnormal outcome, increasing the positive predictive value to 63%. The prediction of a normal outcome remained 90% for infants not receiving oxygen at this corrected gestational age.

Reprinted by permission of PEDIATRICS © 1988.

The Journal of Pediatrics

Role of conventional physiotherapy in cystic fibrosis. Reisman JJ, Rivington-Law B, Corey M, et al. (H. Levison, Hospital for Sick

Children, 555 University Ave., Toronto, Ontario M5G 1X8, Canada). *J Pediatr* 113:632-636, 1988

Because of the time and the emotional cost involved in performing daily conventional chest physiotherapy in patients with cystic fibrosis, a 3-year prospective study was undertaken to compare the long-term effects of postural drainage accompanied by percussion and the forced expiratory technique with the effects of the forced expiratory technique alone. Patients who performed the forced expiratory technique alone had mean annual rates of decline that were significantly different from zero for forced expiratory volume in 1 second ($p < 0.001$), forced expiratory flow between 25% and 75% of vital capacity ($p < 0.001$), and Shwachman clinical score ($p < 0.004$). In the group performing conventional physiotherapy with percussion and postural drainage, only the mean annual rate of decline for forced expiratory flow between 25% and 75% of vital capacity was significantly different from zero ($p < 0.03$), and it was significantly different from the mean rate of decline associated with the forced expiratory technique alone ($p < 0.04$). We conclude that conventional chest physiotherapy should remain a standard component of therapy in cystic fibrosis.

The Journal of Nuclear Medicine

Thallium-201 SPECT in coronary artery disease patients with left bundle branch block. DePuey EG, Guertler-Krawczynska E, Robbins WL (EGD, Division of Nuclear Medicine, Emory University Hospital, 1364 Clifton Rd., N.E., Atlanta, GA 30322). *J Nucl Med* 29(9):1479-1485, Sept. 1988

Fourteen patients with left bundle branch block (LBBB) underwent immediate postexercise and 3-hr delayed ²⁰¹Tl single photon emission computed tomography (SPECT) with quantitative analysis using bullseye polar maps. Test performance in detecting individual coronary artery stenosis $\geq 50\%$ demonstrated 100% sensitivity. Specificity was 100% for circumflex stenosis, 78% for right coronary stenosis, but only 10% for left anterior descending coronary stenosis. This very low specificity was due to the fact that $\frac{3}{4}$ (75%) patients with left anterior descending stenosis and also $\frac{9}{10}$ (90%) patients with normal left anterior descending coronary arteries had immediate septal perfusion defects with redistribution in all cases at 3 hr. Septal abnormalities were most marked in patients who achieved high peak heart rates (>170 bpm). Thus, with LBBB, ²⁰¹Tl SPECT is indeterminate for left anterior descending coronary disease.

Gastrointestinal Radiology

Squamous cell carcinoma of the esophagus in patients with acquired immunodeficiency syndrome. Frager DH, Wolf EL, Competiello LS, Frager JD, Klein RS, Beneventano TC (DHF, Dept. of Radiology, Montefiore Medical Center, 111 E. 210th St., Bronx, NY 10467). *Gastrointest Radiol* 13:358-360, 1988

Two patients with Acquired Immunodeficiency Syndrome (AIDS) and infectious esophagitis developed squamous cell carcinoma of the esophagus. The clinical, radiographic, and endoscopic presentations in both cases were atypical. One patient developed a focal flat lesion that imitated segmental esophagitis, and the other patient developed a superficially spreading carcinoma that mimicked diffuse esophagitis. In the setting of AIDS, a changing radiographic or endoscopic mucosal pattern requires biopsy to exclude the possibility of a superimposed squamous cell carcinoma.

Ultrasound evaluation of cholelithiasis in the morbidly obese. Slidker MS, Cronan JJ, Scola FH, et al. (JJC, Dept. of Radiology, Rhode Island Hospital, 593 Eddy St., Providence, RI 02902). *Gastrointest Radiol* 13:345-346, 1988

The ability to detect gallstones in the morbidly obese population has been questioned in recent literature. Utilizing state-of-the-art, real-time ultrasound equipment, 44 morbidly obese patients were

examined prior to gastric exclusion surgery and concomitant cholecystectomy. The 91% sensitivity and 100% specificity of gallstone detection in this series matches the results for the general population. This study provided the unique opportunity to evaluate a large number (34) of negative ultrasound examinations, with subsequent surgical confirmation yielding a negative predictive value of 97%. This confirms the continued role of ultrasound in the evaluation of cholelithiasis.

Patterns of calcifications and cholangiographic findings in hepatobiliary tuberculosis. Maglinte DDT, Alvarez SZ, Ng AC, Lapeña JL (DDTM, Dept. of Radiology, Methodist Hospital of Indiana, 1701 N. Senate Blvd., Indianapolis, IN 46202). *Gastrointest Radiol* 13:331-335, 1988

The radiologic findings on conventional examinations (plain films and cholangiograms) in a large group of patients with proven hepatobiliary tuberculosis are reviewed. The plain film findings of large "chalky" and confluent hepatic calcifications or nodal-type calcifications along the course of the common bile duct are suggestive of hepatobiliary tuberculosis. Small, discrete, scattered calcifications may be mimicked by histoplasmosis but can be differentiated from hepatobiliary tuberculosis. Obstructing defects seen on cholangiography are indicative of tuberculosis when adjacent calcifications are present. The patterns of liver calcifications could provide a clue to the diagnosis of hepatobiliary tuberculosis and its differentiation from liver calcifications of various other etiologies.

Journal of Ultrasound in Medicine

Prenatal diagnosis of pentalogy of Cantrell. Ghidini A, Sirtori M, Romero R, Hobbins JC (AG, Yale University School of Medicine, Dept. of Obstetrics and Gynecology, 333 Cedar St., P.O. Box 3333, New Haven, CT 06510). *J Ultrasound Med* 7:567-572, Oct. 1988

Ten cases of prenatal diagnosis of Pentalogy of Cantrell are reported. A uniformly fatal outcome was found confirmed by a review of similar cases prenatally diagnosed by other authors. This is at variance with the data derived from the pediatric literature. Implications in obstetrical management and parental counseling are discussed.

Reprinted with permission by the American Institute of Ultrasound in Medicine.

Magnetic Resonance Imaging

A comparison of fast spin echo and gradient field echo sequences. Tkach JA, Haacke EM (JAT, Dept. of Radiology, University Hospitals of Cleveland, Cleveland, OH 44106). *Magn Reson Imaging* 6:373-389, 1988

Optimal angle, fast repeat time, gradient field echo imaging techniques such as FISP (Fast Imaging with Steady Precession) and FLASH (Fast Low Angle Shot) often fail to discriminate disease from healthy tissue for two main reasons. First, T_1 and T_2 of the affected tissue may increase such that the ratio of T_1 to T_2 remains nearly unchanged, hence there is no contrast change with FISP. Second, T_2 weighted gradient field echo images suffer severely from T_2^* signal and resolution loss leading to a reduction in C/N. Although FLASH imaging with two separate angles can, in principle, extract the longer T_1 tumors, contrast is often not good. To overcome the inhomogeneity and contrast problems, we have implemented a FAST optimal angle spin-echo sequence with a short TE (FATE). For the first echo, FATE has the same contrast properties as FLASH with a slight decrease in signal intensity. The advantage is that the intensity of the signal does not suffer from T_2^* signal decay, hence improved contrast and disease detection via T_2 weighted FATE images is possible. Contrast-to-noise in lesion detection is also considered for CE FAST (Contrast Enhanced Fast), a T_2 -weighted version of FISP, and HYBRID.

News

Automated Percutaneous Discectomy Workshop

Radiology Postgraduate Education, University of California, San Francisco, is offering a course, Automated Percutaneous Discectomy Workshop, Jan. 14–15, at the Marriott Marco Island Resort, Marco Island, FL, and Feb. 25–26, March 25–26, and April 22–23, at the Hyatt Regency Hotel, Embarcadero, San Francisco. The course is designed to give physicians the opportunity to enter into a structured hands-on learning experience that will permit them to comprehend and accurately perform the basic technique of automated percutaneous lumbar discectomy. Attendees will work closely with an instructor, enabling them to gain an appreciation for the identification of uncomplicated lumbar herniated discs and the percutaneous surgical approach. Workshop chairmen: Clyde A. Helms and Gary Onik. Faculty: G. W. Davis, Vert Mooney, J. M. Morris, Joseph Schweigel, James Thomas, P. R. DiMartino, and Joseph Maroon. Category 1 credit: 11.5 hr. Fee: \$1000. Information: Radiology Postgraduate Education, Rm. C. 324, University of California, San Francisco, San Francisco, CA 94143-0628; (415) 476-5731.

New Application Deadline for RSNA Grants

Deadlines for the Radiological Society of North America (RSNA) Scholar Program, RSNA Fellow Program, and RNSA Seed Grants Program have been consolidated for 1989. Application materials for all of the 1989 RSNA Research and Education Fund Grants programs are due Jan. 16, 1989.

Breast Imaging Update

Radiology Postgraduate Education, University of California, San Francisco, will offer Breast Imaging Update, Jan. 21–22, at the Hyatt Regency Hotel, San Francisco. The course will provide a concentrated overview of the current status of and recent developments in breast imaging, with emphasis on the application of mammographic techniques to breast cancer screening and diagnosis. Topics will include the strengths and limitations of the full spectrum of available breast imaging techniques, practical approaches to the management of breast masses and clustered calcifications, how to tailor examinations to the specific needs of both symptomatic and asymptomatic patients, and economic and medicolegal aspects of breast cancer screening. Course director: Edward A. Sickles. Guest faculty: Myron Moskowitz. Credit: physicians, 14 hr (category 1); nurses, 14 contact hr; technologists, 14 ECE points. Fee: physicians, \$295; residents, fellows, nurses, technologists, \$195 (letter required). Information: Radiology Postgraduate Education, Rm. C 324, University of California, San Francisco, San Francisco, CA 94143-0628; (415) 476-5731.

Diagnostic Radiology Seminars, Ixtapa, Mexico

The 6th annual Ixtapa postgraduate course in diagnostic radiology will be presented by the Dept. of Radiology, University of California, San Francisco, Jan. 23–27, Camino Real, Ixtapa, Mexico. It has been designed primarily for the radiologist in general practice and provides a survey of selected subdivisions of diagnostic radiology. Topics will include recent advances in diagnostic radiology; newer techniques in subspecialty areas, such as CT, pediatric radiology, MR, chest radiology, skeletal radiology, neuroradiology, sonography, and interventional radiology; and principles and advances in MR imaging and its likely role in diagnostic radiology. Course director: Robert C. Brasch. Credit: physicians, 25 hr (category 1); nurses, 25 contact hr; technologists, 25 ECE points. Fee: physicians, \$495; residents, fellows, nurses, and technologists, \$395 (letter required). Information: Radiology Postgraduate Education, Rm. C 324, University of California, San Francisco, San Francisco, CA 94143-0628; (415) 476-5731.

Abdominal Ultrasound

The Division of Diagnostic Ultrasound, Dept. of Radiology, Thomas Jefferson University Hospital, will offer a course on abdominal ultrasound, Jan. 30–Feb. 2. Course director: Wolfgang Dahnert. Category 1 credits will be awarded. Fee: \$500. Information: Judith Superior, Education Coordinator, Thomas Jefferson University Hospital, Philadelphia, PA 19107; (215) 928-8533.

Practical Approach to Modern Chest and Musculoskeletal Imaging

The Dept. of Radiology, the University of Utah, School of Medicine, is sponsoring A Practical Approach to Modern Chest and Musculoskeletal Imaging. Alternative sessions will be offered: Feb. 5–10, at Snowbird, UT, and Feb. 26–March 3, at Park City, UT. Category 1 credit: 22 hr. Fee: practicing physicians, \$395; residents and fellows, \$150. Information: Judy Gallegos, CME Coordinator, Dept. of Radiology, The University of Utah, School of Medicine, 1A71 Medical Center, Salt Lake City, UT 84132; (801) 581-8699.

Diagnostic Imaging Update: 1989

The Dept. of Radiology, University of California, San Francisco, will present the 4th annual postgraduate course in diagnostic radiology, Feb. 19–24, at Shadow Ridge, Park City, UT. The goal of this program is to update the practicing physician in the newer technology and

clinical applications of sonography, CT, MR imaging, and interventional radiology. Nonionic and MR contrast media and the radiologist's role in AIDS will also be highlighted. Course director: Michael P. Federle. Credit: physicians, 23 hr; nurses, 23 contact hr; technologists, 23 ECE points. Fee: physicians, \$495; residents, fellows, nurses, and technologists, \$395 (letter required). Information: Radiology Postgraduate Education, Rm. C 324, University of California, San Francisco, San Francisco, CA 94143-0628; (415) 476-5731.

Perspectives in Imaging

The Dept. of Radiology, Hospital of the University of Pennsylvania, is sponsoring the 5th Annual Winter Imaging Seminar: Perspectives in Imaging, Feb. 20–24, at the Camino Real Hotel, Cancun, Mexico. This seminar will put in perspective a variety of sonographic and CT imaging procedures. Areas to be covered include chest imaging, prostate imaging, obstetric sonography, diagnostic and interventional imaging of the genitourinary tract, small bowel imaging, and neck imaging. Course director: Peter H. Arger. Guest faculty: H. S. Glazer, E. G. Grant, and C. A. Mittelstaedt. Category 1 credit: 18 hr. Fee: physicians, \$475; residents, \$350; technologists, \$225. Information: Janice Ford or Nancy Fedullo, Continuing Education, Dept. of Radiology, Hospital of the University of Pennsylvania, 3400 Spruce St., Philadelphia, PA 19104; (215) 662-6904 or 662-6982.

Ultrasound in Obstetrics and Gynecology

The Division of Diagnostic Ultrasound, Dept. of Radiology, Thomas Jefferson University Hospital, will offer a course in diagnostic ultrasound, Obstetrics and Gynecology, Feb. 27–March 3. Course director: Alfred Kurtz. Category 1 credits will be awarded. Fee: \$575. Information: Judith Superior, Education Coordinator, Thomas Jefferson University Hospital, Philadelphia, PA 19107; (215) 928-8533.

MR Winter Conference

Radiology Postgraduate Education, University of California, San Francisco, is offering Magnetic Resonance Imaging: Update 1989–Winter Conference, March 5–10, at the Cliff Lodge, Snowbird, UT. The course is designed to provide comprehensive instruction in the basic principles and instrumentation used for MR imaging. It will also provide an update on the current clinical uses of MR for the assessment of all organ systems. Program cochairmen: Charles B. Higgins and William P. Dillon. Credit: physicians, 25 hr (category 1); nurses, 25 contact hr; technologists, 25 ECE points. Fee: physicians, \$495; residents, fellows, nurses, and technologists, \$395 (letter required). Information: Radiology Postgraduate Education, Rm. C 324, University of California, San Francisco, San Francisco, CA 94143-0628; (415) 476-5731.

Musculoskeletal Imaging—The State of the Art

The Dept. of Radiology, Hoag Memorial Hospital, Newport Beach, CA, will present Musculoskeletal Imaging—The State of the Art, March 10–12, at the Four Seasons Hotel, Newport Beach. The course will concentrate on current whole-body musculoskeletal applications and clinical correlations presented by national MR experts and orthopedic surgeons. Program directors: Michael Brant-Zawadzki and Joel Lipman. Category 1 credit: 16 hr. Fee: \$375. Information: Dawne Ryals, Ryals & Associates, P. O. Box 1925, Roswell, GA 30077-1925; (404) 641-9773.

Joint American-European Course in Davos

The European Association of Radiology and the Johns Hopkins Radiological Alumni Association are sponsoring the 21st International Diagnostic Course in Davos, Switzerland, April 2–8. The topic is the thorax. The course will stress both classic and newer diagnostic imaging and interventional techniques. Other lectures and seminars will feature the anatomic and physiologic bases for radiologic-pathologic correlation and the diagnostic approach to specific pulmonary and cardiac diseases. Exhibits, quizzes, special lectures, and a film-reading session by experts will be included. Category 1 credit: 40 hr. Fee: physicians, \$400; residents, \$300. Information: B. G. Brogdon, M.D., Dept. of Radiology, University of South Alabama Medical Center, 2451 Fillingim St., Mobile, AL 36617; (205) 471-7868; or M. W. Donner, M.D., Dept. of Radiology, Johns Hopkins Hospital, Baltimore, MD 21205; (301) 955-5677.

Spring Seminar

The 1989 Spring Seminar of the Southern California Chapter of the American Association of Physicists in Medicine will be held at Caesar's Palace, Las Vegas, NV, April 5–7. This year's seminar will be combined with a full-day workshop on portal imaging. As part of the seminar, a half-day session will be allotted to quantitative flow imaging by MR. Approaches for using this technique to obtain blood flow in tumors for prediction of hyperthermic temperature distributions will be discussed. The workshop on portal imaging will emphasize real-time systems. Speakers will include investigators who are at the forefront of research and applications in this area. The workshop will be partially sponsored by the National Institutes of Health. Another feature of the program will be presentation of research by the winner or winners of the Norman A. Baily Award. Information: Dr. Norman A. Baily, Dept. of Radiology, M-010, University of California, San Diego, La Jolla, CA 92093.

The Brain, the Self, and Nuclear Medicine

The Dept. of Nuclear Medicine, University of Bonn, and the Society of Nuclear Medicine are sponsoring The Brain, the Self, and Nuclear Medicine, April 7–8, in Bonn, W. Germany. Topics will include an overview and introduction, basic sciences, resting and cognitive states of the brain, dementia, and psychiatric diseases. Conference directors: Hans J. Biersack, Michael D. Devous, and Ronald S. Tikofsky. Fee: \$100. Information: Hans J. Biersack, M.D., Professor and Chairman, Dept. of Nuclear Medicine, University of Bonn, Sigmund-Freud-Strasse 25, D-5300 Bonn 1, W. Germany.

Courses in Diagnostic Ultrasound at Bowman Gray

The Center for Medical Ultrasound, Bowman Gray School of Medicine, is sponsoring several courses in diagnostic ultrasound: Physics, April 12–14; Obstetrics, April 17–21 and June 5–9; Radiology (Abdomen), April 24–28 and June 12–16; Neurovascular, May 1–5; Echocardiology, May 15–19; and Urology, May 22–23. Category 1 credit: each course, 7 hr/day. Information: Registrar, Ultrasound Center, Bowman Gray School of Medicine, Winston-Salem, NC 27103; (919) 748-4505.

Advances in Radiology

The Dept. of Radiology, University of California, Irvine, and the Great Teachers Foundation are presenting Advances in Radiology,

April 19–May 7, in Asia (Shanghai, Guilin, Hong Kong, Bangkok, Chiang Mai, Phuket, and Singapore). The course is designed to provide interaction between American and Asian physicians and discussion of the latest concepts in radiology. Program director: Eric N. C. Milne. Category 1 credit: approximately 27 hr. Fee: \$475. Information: Dawne Ryals, Ryals & Associates, P. O. Box 1925, Roswell, GA 30077-1925; (404) 641-9773.

AFIP Musculoskeletal Radiology Review Course

The Armed Forces Institute of Pathology, the American Registry of Pathology, and the American College of Radiology will offer the 1st Annual Musculoskeletal Radiology Review Course, April 22–23, at the Holiday Inn of Bethesda, Bethesda, MD. Course directors: Richard P. Moser, Jr., and John E. Madewell. Category 1 credit: 16.5 hr. Fee: \$275. Information: Mrs. Cunningham, Dept. of Radiologic Pathology, Bldg. 93, Armed Forces Institute of Pathology, Washington, DC 20306-6000; (202) 576-2534 or 576-2535. Military and other full-time federal salaried physicians should contact the Associate Director for Education, Armed Forces Institute of Pathology, Washington, DC 20306-6000; (202) 576-2934 or 576-2939.

Differential Diagnosis in Radiology

The University of Michigan will present its 6th annual course, Differential Diagnosis in Radiology: Review Course for Residents, April 22–24, in Ann Arbor. The course format will emphasize a case-solving approach to the unknown radiograph. Differential diagnostic features of common radiographic abnormalities will be stressed in lecture and workshop settings. Category 1 credit: 20 hr. Fee: \$175. Information: D. L. Spizarny, M. D., Dept. of Radiology, Box 0326, University of Michigan Hospital, Taubman Center 2910A/0326, 1500 E. Medical Center Dr., Ann Arbor, MI 48109-0326; (313) 936-4357.

Ultrasound 1989

The Dept. of Radiology, Brigham and Women's Hospital, and Harvard Medical School are offering the 14th annual postgraduate course, Ultrasound 1989, April 23–26, at the Westin Hotel, Copley Place, Boston. A special feature of the course will be a Basics of Ultrasound day on April 23. Program director: Peter M. Doubilet. Category 1 credit: 28 hr. Fee: physicians, \$525; residents, fellows, RTs, \$350; Basics day only, \$130. Information: Dept. of Continuing Education, Harvard Med-CME, P. O. Box 825, Boston, MA 02117; (617) 732-1525.

Annual Spring Diagnostic Ultrasound Conference

The Continuing Education Committee, the Los Angeles Radiological Society (LARS), will sponsor their 14th Annual Spring Diagnostic Ultrasound Conference, April 28–30, at the Century Plaza Hotel, Los Angeles. Categorical courses will include Doppler imaging of the obstetric patient, duplex carotid sonography, prostate sonography, endovaginal sonography, and other subspecialties. Three special focus sessions and six workshop sessions will be held. Conference speakers: P. N. Burns, B. B. Gosink, J. C. Hobbins, R. B. Jeffrey, Jr., and A. B. Kurtz. Category 1 credit: up to 20 hr. Fee: nonmember physicians: \$395 (3 days) or \$345 (2 days); LARS or Ultrasound Section members, \$325 (3 days) or \$275 (2 days); nonmember technologists, \$345 (3 days) or \$295 (2 days); LARS or Ultrasound Section technologist members, \$295 (3 days) or \$245 (2 days).

Information: Los Angeles Radiological Society—SDUC, P. O. Box 91215, Los Angeles, CA 90009-1215; (213) 827-9078.

International MR Symposium in Italy

The Dept. of Radiology, Case Western Reserve Medical Center, will present Magnetic Resonance Imaging: An International Symposium in Venice and Florence, Italy, April 30–May 5. The purpose of the symposium is to provide a basic overview of both the basic science and clinical implications of MR. A trip to Tuscany and the Lake Region will follow the symposium. Program chairmen: Michael T. Modick and Plinio Rossi. Faculty: R. Felix, J. Lissner, R. Passariello, P. Pavone, P. Rossi, G. Scotti, G. Bydder, R. Longmore, D. Underwood, R. J. Alfidi, M. Brant-Zawadzki, R. Herfkens, and M. T. Modic. Category 1 credit: 27 hr. Fee: \$475. Information: Dawne Ryals, Ryals & Associates, P. O. Box 1925, Roswell, GA 30077-1925; (404) 641-9773.

Annual Mid-Pacific Diagnostic Ultrasound Conference

The Continuing Education Committee of the Los Angeles Radiological Society will sponsor the 9th Annual Mid-Pacific Diagnostic Ultrasound Conference at the Royal Waikoloan Hotel on the Big Island of Hawaii, May 2–6. This seminar, which will follow the 14th Annual Spring Diagnostic Ultrasound Conference in Los Angeles, will feature nationally recognized experts in diagnostic ultrasound. A series of morning lectures will be followed by panel discussions and presentation of interesting cases. Faculty: R. A. Filly, F. C. Laing, B. B. Gosink, and Delores Pretorius. Category 1 credit: up to 19 hr. Fee: physicians, \$395; technologists, \$295. Information: Los Angeles Radiological Society—SDUC, P. O. Box 91215, Los Angeles, CA 90009-1215; (213) 827-9078.

Sonography Symposium

The Dept. of Radiology and Radiological Sciences, Vanderbilt University Medical Center, will offer its 13th annual Sonography Symposium May 26–27 at the Opryland Hotel, Nashville, TN. Topics will include transvaginal sonography, carotid duplex sonography, color Doppler sonography, financial aspects of sonography practice, and renal and biliary lithotripsy. Guest faculty: B. B. Goldberg, B. B. Gosink, and E. A. Lyons. Category 1 credit: approximately 10 hr. Fee: \$350. Information: Sher Reed, Division of Continuing Medical Education, CCC-5326 MCN, Vanderbilt University Medical Center, Nashville, TN 37232; (615) 322-4030.

Radiology in Scandinavia and the Soviet Union

The Dept. of Radiology, University of California, San Diego School of Medicine, will present Radiology in Scandinavia and the Soviet Union, June 17–July 1, in Copenhagen, Stockholm, and Leningrad (with option to Moscow). The course is designed to provide interaction with physicians in Scandinavia and the Soviet Union and discussion of the latest concepts in radiology. Program director: Folke Brahme. Category 1 credit: approximately 28 hr. Fee: \$475. Information: Dawne Ryals, Ryals & Associates, P. O. Box 1925, Roswell, GA 30077-1925; (404) 641-9773.

CAR '89

The 3rd international symposium on computer-assisted radiology, CAR '89, will be held in Berlin, June 25–28. This symposium is

intended to serve as a forum for discussion between experts from the medical sciences (e.g., radiology, radiotherapy, nuclear medicine, orthopedics, cardiology, neurology, and surgery) and professionals from the computer and physical sciences. The aim is to evaluate the state of the art (presented in tutorials) and research results (session papers) in the area of computer-assisted radiology. Topics to be covered include generation of digital images, picture archiving and communications systems, medical work stations, and application systems. Particular emphasis will be given to the clinical relevance of results. A special session on social aspects of computer-assisted radiology is being planned. Information: CAR '89, Heinz U. Lemke, Institute for Technical Computer Science, Technical University Berlin, Sekr. CG/FR 3-3, Franklinstrasse 28-29, D-1000 Berlin 10, West Germany.

Third World Medicine—Tropical Radiology and the Problem of AIDS

The Dept. of Radiology, University of California, Irvine, and the Great Teachers Foundation will present Third World Medicine—Tropical Radiology and the Problem of AIDS, July 19–Aug 5, in East Africa (Nairobi, Maasa-Mara, Lake Baringo, Lake Turkana, Mombasa, and Lamu). The course is designed to provide interaction with leading physicians in Africa and discussion of the latest concepts in radiology and the problems of AIDS in third world countries. The faculty will consist of American and African leaders in the field of tropical radiology and AIDS. Program director: Eric N. C. Milne. Category 1 credit: approximately 27 hr. Fee: \$475. Information: Dawne Ryals, Ryals & Assoc., P. O. Box 1925, Roswell, GA 30077-1925; (404) 641-9773.

Cleveland Radiological Society Officers

The officers of the Cleveland Radiological Society for the year 1988–1989 are as follows: John Haaga, president; James A. Patterson, president-elect; Peter B. O'Donovan, secretary/treasurer; Dieter Bloser, past president; and David M. Paushter, program chairman. The new address for the society is Cleveland Clinic Foundation, Dept. of Hospital Radiology, 9500 Euclid Ave., Cleveland, OH 44195.

The American Board of Radiology Examinations

Written examinations for the American Board of Radiology (ABR) are scheduled for Oct. 5–6, 1989. Oral examinations will be held at the Executive West Hotel in Louisville, KY, June 5–9, 1989. The ABR will accept applications for admission to the examinations after July 1, but not later than Sept. 30, in the year *preceding* the year in which the examination is to be taken. For application forms and further information: Office of the Secretary, The American Board of Radiology, 300 Park, Ste. 440, Birmingham, MI 48009.

Meeting and Course Review

For the reader's convenience, a summary of upcoming meetings and courses is provided. Detailed listings are given in the *AJR* issue given in parentheses.

One-Week Visiting Fellowships in MR Imaging, times arranged, Philadelphia (April)

Fellowships in Interventional Radiology, times arranged, San Diego (May)

Fellowship Program in Diagnostic Radiology, times arranged, Ann Arbor (June)

Basic and Advanced Training in MRI, times arranged, Baltimore (Dec)

Courses in Diagnostic Ultrasound: Obstetrics, Jan. 9–13; **Radiology (Abdomen)**, Jan. 16–20; **Neurovascular**, Jan. 23–27; **Transcranial Doppler**, Jan. 30–31; **Arterial/Venous Doppler**, Feb. 1–3; **Echocardiography**, Feb. 6–10; and **Urology**, Feb. 13–14; Winston-Salem, NC (Sept)

Advanced Seminars in Diagnostic Imaging, Jan. 13–15, Laguna Niguel, CA (July)

Annual Midwinter Radiological Conference, Jan. 17–29, Los Angeles (Dec)

Courses at the University of California, San Diego: Duplex Imaging, Jan. 19–21; **Workshop on Percutaneous Diskectomy**, Jan. 21–22; **Neuroradiology Update**, Jan. 23–26; **Magnetic Resonance Imaging**, Jan. 24–27; and **MRI for Technologists—Symposium and Workshops**, Jan. 24–27; San Diego (Oct)

Perspectives in Radiology, Jan. 23–27, Miami (Sept)

Mammography and the Search for Breast Cancer, Jan. 27–29, Scottsdale, AZ (Nov)

AFIP Annual Courses: Neuroradiology Review Course, Jan 28–29; **Neuropathology Course**, begins Jan. 30; Bethesda, MD (Dec)

Annual Big Sky Radiology Conference, Jan. 29–Feb. 2, Big Sky, MT (Nov)

Annual Mid-Pacific Radiological Conference, Jan. 31–Feb. 4, Kauai, HI (Dec)

The George Simon Award, deadline for receipt of papers, Feb. 1 (Dec)

Thomas Jefferson University Hospital Courses in Diagnostic Ultrasound: Prostate Ultrasound, Feb. 3 and April 14; **Doppler Ultrasound in Vascular Diagnosis**, Feb. 15–18; Philadelphia (Oct)

Physics of Diagnostic Radiology and Radiobiology, Feb. 3–6, Chicago (Sept)

Postgraduate Course in Puerto Rico, Feb. 5–10, Hyatt Cerrymar Beach Hotel, Puerto Rico (Nov)

Practical Radiology 1989, Feb. 5–10, Vancouver, B.C. (Dec)

Annual Uroradiology Course, Feb. 7–8, Bethesda, MD (Dec)

Advanced Ultrasound Seminar: OB/GYN, Feb. 9–11, Lake Buena Vista, FL (Sept)

Annual Intermountain Imaging Conference, Feb. 11–18, Steamboat Springs, CO (Nov)

Sun Valley Imaging, Feb. 18–25, Sun Valley, ID (Oct)

Palm Beach Magnetic Resonance Imaging Update, Feb. 19–22, Palm Beach, FL (Sept)

Society of Gastrointestinal Radiologists Meeting and Postgraduate Course, Feb. 19–23, Palm Desert, CA (Sept)

Imaging the Central Nervous System, Feb. 20–24, Tucson, AZ (Oct)

Advanced Seminars in Diagnostic Imaging, Feb. 23–25, Rancho Mirage, CA (Nov)

Seminars in MRI, Feb. 25–March 4, Snowbird, UT (Nov)

University of Arizona Practical Radiology Course, Feb. 27–March 3, Tucson, AZ (Dec)

Skeletal Symposium, Feb. 27–March 3, Sun Valley, ID (Dec)

Body Imaging, Mammography, and Neuroradiology, Feb. 27–March 4, Acapulco (Nov)

Breast Disease Update VI Seminar, March 1–4, Lake Buena Vista, FL (Dec)

Magnetic Resonance Imaging Conference, March 4–8, Scottsdale, AZ (Nov)

Society of Thoracic Radiology Postgraduate Course, March 5–9, Coronado (San Diego), CA (Nov)

Masters Diagnostic Radiology Conference, March 5–10, Poipu Beach, Kauai, HI (Nov)

Computed Body Tomography 1989—The Cutting Edge, March 9–12, Bal Harbour, FL (Nov)

Symposium on Shock Wave Lithotripsy, March 10–12, Indianapolis (Dec)

Skeletal Radiology at the Pointe—1989, March 11–16, Phoenix (Nov)

Mayo Clinic Advances in Radiology, March 12–16, Phoenix (Nov)
Radiation Research Society and North American Hyperthermia Group Annual Meetings, March 18–23, Seattle (Nov)

Clinical Nuclear Medicine 1989, March 28–31, Boston (Dec)

Ultrasound in Obstetrics and Gynecology, April 3–5, Ann Arbor, MI (Dec)

National Council on Radiation Protection and Measurements Annual Meeting, April 5–6, Washington, DC (Nov)

American Osteopathic College of Radiology Mid-Year Conference, April 6–9, Washington, DC (Nov)

Society of Computed Body Tomography Annual Course, April 10–14, Washington, DC (Nov)

San Diego Residents' Radiology Review Course, April 16–21, San Diego (Nov)

Fleischner Society Symposium on Chest Disease, April 28–30, New York (Dec)

Surgical Neuroangiography, May 1–5, New York (Dec)

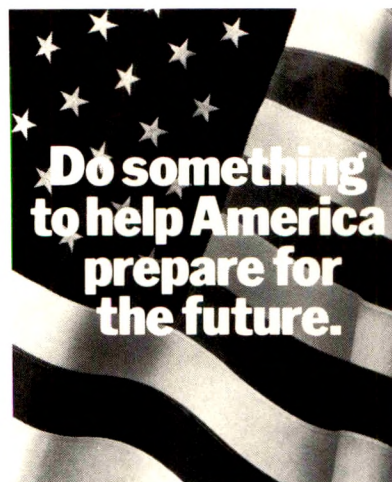
International Congress on Peer Review in Biomedical Publication, May 10–12, Chicago (Sept)

1989 International Congress of Radiology, July 1–8, Paris (May)

Society of Uroradiology Postgraduate Course, Sept. 25–28, Hilton Head, SC (Dec)

World Congress for Bronchology, Oct. 18–20, Tokyo, and Oct. 21–22, Kyoto, Japan (Nov)

AJR carries announcements of courses, symposia, and meetings of interest to its readers if received a minimum of 5 months before the event. There is no charge; receipt of items by the *AJR* Editorial Office is not acknowledged. Submit items for publication typed double-spaced. Provide title, date, location, brief description, sponsor, course directors, fees, category I credit, and address and telephone number for additional information. Faculty from the host institution will not be listed. Guest faculty names will appear **only** if initials are provided. Mail news items to *AJR* Editorial Office, 2223 Avenida de la Playa, Suite 200, La Jolla, CA 92037-3218.



Support America's colleges. Because college is more than a place where young people are preparing for their future. It's where *America* — and American business — is preparing for *its* future.

**Give to
the college of
your choice.**

**Ad
council**
A Public Service of This Publication

COUNCIL FOR AD TO EDUCATION **CEAE**

Information and Application for Membership in the American Roentgen Ray Society

General Information

The American Roentgen Ray Society, founded in 1900, has been a forum for progress in radiology since shortly after the discovery of x-rays. From its beginning and continuing to today, the ARRS has been guided by dedication to the goal of the advancement of medicine through the science of radiology and its allied sciences.

The goal of the ARRS is maintained through an annual scientific and educational meeting, and through publication of the American Journal of Roentgenology.

The annual meeting consists of instructional courses, scientific sessions, a symposium, scientific exhibits, and commercial exhibits. A special categorical course is also offered. Category I CME credits are available on an hour-for-hour basis.

The monthly American Journal of Roentgenology is a highly respected peer review journal with a worldwide subscription base. For over 75 years the AJR has been accepted as one of the best specialty journals available in the world, and this reputation grows each month.

A recently developed quarterly ARRS newsletter keeps members informed of events and general Society news.

Application Instructions

Candidates for Active Membership

1. An Active member must be a graduate of an approved medical school or hold an advanced degree in one of the physical, chemical or biological sciences and be certified by the American Board of Radiology, the American Osteopathic Board of Radiology, the Royal College of Physicians of Canada, or document training and credentials that are adequate to qualify for membership. Active members shall actively practice radiology or one of its branches in the United States or Canada. Such members are eligible to participate in all activities of the Society, including membership on committees, and have full voting privileges.
2. Application must be on an official form, signed by the applicant and at least two members of the American Roentgen Ray Society, active or emeritus, in good standing, who endorse the applicant.
3. Application fee is \$50 (payable when billed for dues).
4. Annual dues are \$125, payable on January 1 of each year following the initial year. First year dues will be invoiced following candidate election at the annual meeting. Of this amount, \$50 is for a 1-year subscription to the American Journal of Roentgenology, beginning with the July issue following election to membership.
5. Application must be received by February 1 for action during the current year's meeting.

Candidates for In-Training Membership

1. In-training members must be serving in a radiology residency program approved by the Radiology Residency Review Committee, the American Osteopathic Board of Radiology, or the Royal College of Physicians of Canada, or in an approved post-residency fellowship, or be a postgraduate student in an allied science. Training status must be verified by the program director. In-training members have special consideration in fees and subscription rates to the Society journal. Such members cannot hold Society offices or vote.
2. Application must be on an official form and signed by the applicant and by the applicant's training or residency program director.
3. In-training status is limited to a maximum of five years starting with the entrance date into the radiology residency. In the last year, each in-training member will receive an application for active membership from the Society. Those who do not apply for transfer to active membership shall be dropped from membership at the end of the fifth year, but can later apply as a new member through the process outlined for active status.
4. There is no application fee. Annual dues are \$25. Membership includes a subscription to the American Journal of Roentgenology and admission to the annual meeting without payment of the registration fee.
5. Membership applications will be acted on when received.

Corresponding Membership

A corresponding member must meet the qualifications of active membership, but reside and practice in a foreign country. Corresponding members shall pay dues and fees, but shall not have the privileges of voting nor of holding elective office.

All Applicants

1. Do not remit application fee or dues until requested.
2. Send completed forms to: American Roentgen Ray Society
1891 Preston White Drive
Reston, Virginia 22091

For ARRS
Office Use

Date Rec'd _____

I.D.# _____

AMERICAN ROENTGEN RAY SOCIETY APPLICATION FOR MEMBERSHIP

Date: _____

Category of Membership: ☐ Active
(Check One) ☐ Corresponding
☐ In-Training

Name (Please Print) _____ Degree(s) _____
First Initial Last

Mailing Address _____ Date of Birth _____
Street/Box

City/State/Country _____ Zip Code _____ Telephone () _____

A. Education: (List name of institution, years attended, and degree and type received.)

Undergraduate: _____

Graduate (Medical School, Graduate School, etc.):

Postgraduate (Internship, Residency, Fellowship, etc.):

B. Licensure:

Licensed to practice _____ in _____ since _____
(Type) (State, Province, etc.)

C. Appointments/Memberships: (In-Training applicants: skip to Section F on reverse.)

Present Appointments: Academic _____

Hospitals _____

Memberships in Scientific Societies: _____

Offices or Committee Assignments: _____

Government Service (Military or Civilian) _____ (Position) _____ (Years)

D. Credentials:

I hereby certify that I was issued a certificate of qualification in _____
(Specialty)

in _____ by the _____
(Year) (Name of Qualifying Board)

Other Credentials: _____

Signature: _____

E. References:

We, active or emeritus members in good standing of the American Roentgen Ray Society, and acquainted with the applicant, do recommend him/her for membership in the Society. (Two references are required.)

Name (Please Print) 1. _____ 2. _____

Address _____

Signatures: _____

F. IN-TRAINING APPLICANTS MUST COMPLETE THIS SECTION**Credentials:**

I certify that I am serving as a Resident/Fellow in _____
(Specialty)

at _____ . Date program began (begins): _____
(Name of Institution)

date program to end: _____ . I understand that in-training membership is limited to maximum of 5 years.

Applicant Signature: _____

Verification: (Program Director or Department Chairman *only*)

I certify that the applicant is in training at the institution named and qualifies for enrollment as a member-in-training of the American Roentgen Ray Society.

Name (Please Print) _____

Address: _____

Signature _____

Send completed form to: **American Roentgen Ray Society**
1891 Preston White Drive
Reston, Virginia 22091

American Roentgen Ray Society: Officers, Committees, and Membership Information

Officers

President: Lee F. Rogers

President-elect: Ronald G. Evens

1st Vice-president: M. Paul Capp

2nd Vice-president: John A. Kirkpatrick, Jr.

Secretary: Glen W. Hartman

Treasurer: Beverly P. Wood

Executive Council: J. Thrall, J. F. Wiot, L. F. Rogers, R. A. Gagliardi, R. G. Evens, R. N. Berk, B. P. Wood, J. E. Madewell, M. P. Capp, G. W. Hartman, B. G. Brogdon, G. R. Leopold, A. Landry, Jr., A. K. Poznanski, K. H. Vydareny, J. T. Ferrucci, Jr., W. J. Casarella, E. J. Ferris, J. A. Kirkpatrick, Jr., A. E. James, Jr., chairman

Committees

Editorial Policy: S. S. Sagel, R. J. Stanley, C. A. Rohrmann, Jr., N. O. Whitley, S. V. Hilton, J. M. Taveras, R. N. Berk, W. J. Casarella, chairman

Education and Research: C. E. Putman, C. B. Higgins, B. J. Hillman, R. A. McLeod, B. G. Brogdon, chairman

Finance and Budget: A. K. Poznanski, G. R. Leopold, J. R. Thornbury, R. C. Gedgaudas-McClees, J. Thrall, chairman

Nominating: K. L. Krabbenhoft, J. F. Wiot, G. R. Leopold, chairman

Publications: R. J. Stanley, S. S. Sagel, N. O. Whitley, C. A. Rohrmann, Jr., W. J. Casarella, chairman

Membership: E. J. Ferris, G. R. Leopold, K. H. Vydareny, A. K. Poznanski, chairman

Representatives to Other Organizations

American Board of Radiology: E. C. Klatte, L. F. Rogers, J. A. Kirkpatrick, Jr.

American College of Radiology: L. F. Rogers, G. A. Kling, R. A. Gagliardi, J. E. Madewell

American Medical Association House of Delegates: S. F. Ochsner, K. L. Krabbenhoft, alternate

American National Standards Institute: M. Haskin

National Council on Radiation Protection and Measurements: E. L. Saenger, H. L. Friedell

Meeting Arrangements

Annual Meetings: May 7-12, 1989, Hilton, New Orleans; May 13-18, 1990, Sheraton Washington, Washington, DC

Annual Meeting Committee: H. C. Carlson, G. P. Janetos, E. K. Lang, R. R. Lukin, A. Landry, Jr., chairman

Instruction Courses: R. J. Stanley, associate chairman, J. T. Ferrucci, Jr., chairman

Scientific Program: R. J. Alfidi, A. E. Robinson, J. H. Thrall, M. P. Banner, J. J. Gisvold, T. C. McLoud, R. G. Evens, chairman

Scientific Exhibits: A. A. Moss, A. V. Proto, R. J. Churchill, J. E. Madewell, chairman

ARRS Membership

An application form is printed in this issue of the Journal. For consideration at the 1989 ARRS meeting, send completed forms before February 1, 1989, to American Roentgen Ray Society, 1891 Preston White Dr., Reston, VA 22091. Active members are graduates of an approved medical or osteopathic school or hold an advanced degree in an allied science. They must practice radiology or work in an associated science in the United States or Canada and be certified by the American Board of Radiology, American Osteopathic Board of Radiology, or Royal College of Physicians of Canada or otherwise adequately document training and credentials. Corresponding members are foreign radiologists or scientists who are active in radiology or an allied science. Members-in-training are residents or fellows in radiology or postgraduate students in an allied science. Additional application forms can be obtained from the ARRS offices in Reston, VA.

Business Office

Paul Fullagar, Administrative Director, American Roentgen Ray Society, 1891 Preston White Dr., Reston, VA 22091; (703) 648-8900

Invitation to the 1989 American Roentgen Ray Society Meeting in New Orleans, LA, May 7–12, 1989

I am pleased to extend an invitation to all radiologists to attend the 89th annual meeting of the American Roentgen Ray Society in New Orleans, LA, May 7–12, 1989. In keeping with the ARRS tradition, outstanding scientific and social programs will be provided.

The excitement of a meeting set in New Orleans requires no further description. The opportunity for busy radiologists to attend a major national meeting while enjoying all that New Orleans has to offer is ideal.

The scientific program, instructional courses, and categorical course are certain to be interesting and informative (see Table 1 for schedule).

Scientific Program

Two hundred scientific papers have been selected from more than 400 abstracts. Scientific sessions will be devoted to all major body systems, angiography, interventional techniques, sonography, and mammography, as well as technologies. Special emphasis has been placed on discussion of new developments.

The innovative and extremely well-received Friday morning minisymposium is entitled "Gastrointestinal Radiology Update 1989." An outstanding faculty has been assembled for what I am sure will be a very stimulating program.

Instructional Courses

Joseph T. Ferrucci, Chairman of the Instructional Course Committee, has put together 60 instructional courses. Faculty members have been drawn from across the entire country, with emphasis on luminaries from the South. A superlative educational experience is anticipated, and advance registration is recommended.

Categorical Course

An extraordinary categorical course on genitourinary imaging (uroradiology) has been fashioned. The course covers all aspects of the field, including equipment and principles of diagnosis. This course is certain to be popular, and advance registration is advised.

TABLE 1: Summary of 1989 American Roentgen Ray Society Meeting

Sunday May 7	Monday May 8	Tuesday May 9	Wednesday May 10	Thursday May 11	Friday May 12
	8–9:30 Instructional courses	8–9:30 Instructional courses	8–9:30 Instructional courses	8–9:30 Instructional courses	8–10 Symposium: gastrointestinal imaging update
9–noon Categorical course: genitourinary imaging	10–10:30 Opening cere- monies				
	10:30–12:30 Scientific programs	10–12:30 Scientific programs	10–12:30 Scientific programs	10–12:30 Scientific programs	10:30–12:30 Symposium: gastrointestinal imaging update
1:30–3 Categorical course: genitourinary imaging	1:30–3:30 Categorical course: genitourinary imaging	1:30–3:30 Scientific programs	1:30–3:30 Scientific programs	1:30–3:30 Scientific programs	
3:30–5:30 Categorical course: genitourinary imaging	4–5:30 Instructional courses and cate- gorical course: genitourinary imaging	4–5:30 Instructional courses and cate- gorical course: genitourinary imaging	4–5:30 Instructional courses and cate- gorical course: genitourinary imaging	4–5:30 Instructional courses and cate- gorical course: genitourinary imaging	

Scientific Exhibits

The 220 scientific exhibits coordinated by John Madewell will cover the entire breadth of the field of diagnostic radiology. The technical exhibits will be integrated among the scientific exhibits to enhance the interaction of the attendees with our technical exhibitors.

Caldwell Lecture

The Honorable William Bradley, senator from New Jersey, has agreed to present the Caldwell Lecture at the 1989 meeting. The title of Senator Bradley's presentation will be "Health Care Choices for the Nineties." This promises to be one of the highlights of the meeting.

Social Events

New Orleans offers an unlimited number of diversions, and Abner M. Landry, Jr., Chairman of the Local Arrangements Committee, has engaged Crescent City Consultants to plan a variety of outstanding tours. The annual golf and tennis tournaments for attendees and their companions are scheduled for Monday. The traditional cocktail party given by the society in the exhibit area for all registrants will be Tuesday evening and will provide a convenient meeting place before an evening on the town.

This promises to be a truly outstanding event in exceptional surroundings. I hope you will be able to accept our invitation. Plan now to attend.

Ronald G. Evens
President-Elect, ARRS

Forthcoming ARRS Meeting Information

Details of the American Roentgen Ray Society Meeting in New Orleans, LA, May 7-12, 1989, will appear in the **February** and **March** 1989 issues of the *AJR*. The complete scientific program, abstracts of the instructional programs, information about social events, and hotel and travel forms will be published in the Journal.

See pages 62 and 90 of this issue for more information concerning the meeting.

Classified Advertisements

Positions Available

BOARD-CERTIFIED/ELIGIBLE GENERAL DIAGNOSTIC RADIOLOGIST to join 1 other radiologist in 41-physician, multispecialty clinic. Outpatient imaging including mammography, ultrasonography, fluoroscopy, arthrography, and general diagnosis. No night or weekend call. Small community east of Los Angeles, convenient to beaches and mountain resorts. Excellent schools. Send CV to Robert J. Thomas, M.D., The Beaver Medical Clinic, P. O. Box 3001, Redlands, CA 92373. 1-2a

ABDOMINAL IMAGING POSITION—The Johns Hopkins Hospital is pleased to offer an academic position in abdominal imaging, available immediately. Applicants as instructor, assistant professor, or associate professor will be considered. The position encompasses an integrated approach to abdominal imaging in a busy, tertiary-care institution with primary responsibilities in GI fluoroscopic procedures, CT, and MRI. A superb radiology research laboratory facility is available if desired. Please reply with CV to Bronwyn Jones, M.D., Section Head, Gastrointestinal Imaging, The Johns Hopkins Hospital, Baltimore, MD 21205; (301) 955-2351. 1a

MR, CT, ANGIOGRAPHY, INTERVENTIONAL—Seven-member, multihospital group is seeking a board-certified, fellowship-trained radiologist. Must be able to perform all facets of diagnostic imaging. Excellent opportunity. Send CV to Don F. Gowans, M.D., or Neel E. Bennett, M.D., Dept. of Radiology, Holy Cross Hospital, 1045 E. 100 S., Salt Lake City, UT 84102; (801) 350-4636. 1ap

GENERAL DIAGNOSTIC RADIOLOGIST, THOMAS JEFFERSON UNIVERSITY HOSPITAL—The Dept. of Radiology at Thomas Jefferson University Hospital in Philadelphia has an opening in July 1989 for a faculty-level, general diagnostic radiologist. An interest and/or fellowship training in abdominal radiology (GI/GU) would be helpful, but not mandatory. The individual will have the opportunity to participate in clinical activities, teaching, and research in a progressive and expanding general diagnostic division. Excellent salary and benefits are offered. Contact either Robert M. Steiner, M.D., Co-director of General Diagnostic Radiology or David C. Levin, M.D., Professor and Chairman, Dept. of Radiology, Thomas Jefferson University Hospital, 111 S. 11th St., Philadelphia, PA 19107. Thomas Jefferson University is an equal opportunity/affirmative action employer. 1-6ap

IMAGING RADIOLOGIST—THE CAROLINAS—Progressive, 12-man group seeking an exceptional individual with fellowship training or junior staff experience in body imaging. Must be board-certified and competent in a wide range of general diagnostic skills including mammography. Prosperous and reputable 650-bed community hospital planning major expansion. One hospital, 1 office practice with state-of-the-art equipment; 4 CT scanners (2 Picker, 2 GE 9800), MRI (GE Signa), and 7 ultrasound units (3 Acuson). A choice practice and excellent location in the heart of the Carolinas. Contact Box 221249, Charlotte, NC 28222. 1-3ap

TWO GENERAL RADIOLOGY MEDICAL OFFICER POSITIONS available in the Dept. of Radiology, Madigan Army Medical Center, Tacoma, WA. Serve as board-certified radiologists with responsibility for the full range of cases including the most difficult. Responsibilities include providing training and serving as a consultant to interns and residents. Contact Kathleen Derry at the Fort Lewis Civilian Personnel Office to obtain additional information and government application forms; (206) 967-2131. 1a

RADIOLOGIST—Full-time, board-certified radiologist with particular interest and experience in nuclear and ultrasound radiology desired for association in 10-man, private practice for a 660-bed, private, tertiary-care, teaching hospital with 2 regional offices. Practice is located in large midwestern city and maintains fully accredited, 4-yr, radiology residency training program. This comprehensive dept. includes 2 state-of-the-art CT scanners, a 1.5-T MRI unit, modern equipment for mammography, sonography, angiography, nuclear medicine, and a wide variety of invasive applications and procedures. Competitive salary and benefits. Full partnership, if mutually agreeable, at 3 yr. Near-future plans include manning of regional outpatient center with CT and general radiologic facilities on site. Send inquiry and CV in reply to Box N63, AJR (see address this section). 1-12ap

IMMEDIATE OPENING FOR STAFF NEURORADIOLOGIST, in the Division of Neuroradiology, to join 1 other neuroradiologist. The University of Massachusetts Medical Center is a 360-bed university hospital and medical school located in Worcester, MA, approximately 40 mi. west of Boston. The dept. consists of 19 staff, 12 residents, and 2 fellows and does approximately 105,000-110,000 exams/yr. The hospital is a major trauma center and is serviced by 2 Life Flight helicopters. The dept. is well-equipped with 2 CT scanners (a GE 9800 Quick and an 8800), a 1.5-T GE MR scanner in a stand-alone facility with a second scanner expected by Jan. 1989. There is also a 2.0-T small-bore unit for animal research. For further information, contact Edward H. Smith, M.D., Professor and Chair, Dept. of Radiology, University of Massachusetts Medical Center, 55 Lake Ave. N., Worcester, MA 01655; (508) 856-3252. UMMC is an equal opportunity/affirmative action employer. 1-3a

COASTAL CALIFORNIA—Immediate opening for board-certified radiologist to provide day-off/vacation relief. Hospital, private office, group. Sunny northern California. Ultrasound, CT, and mammography. No angiography or MRI. CA license required, malpractice insurance provided. No weekends or call. Minimum 1/2 yr coverage. Reply Box N61, AJR (see address this section). 1-3ap

INTERVENTIONAL RADIOLOGIST, ASSISTANT/ASSOCIATE PROFESSOR IN RESIDENCE—San Francisco General Hospital, Dept. of Radiology, an affiliate of the University of California, San Francisco is seeking an experienced academic radiologist to be Head of Interventional Radiology. The candidate should be experienced in a wide range of angiographic and interventional procedures, including transluminal angioplasty, embolotherapy biliary, and GI and GU interventions. The candidate will participate in all clinical, teaching, and research programs at SFGH. Radiology board certification, California medical license, and postresidency fellowship or equivalent are required. The University of California, San Francisco is an equal opportunity/affirmative action employer. Minority groups, women, and handicapped individuals are encouraged to apply. Send CV and 3 references to Michael P. Federle, M.D., Dept. of Radiology 1X55, San Francisco General Hospital, 1001 Potrero Ave., San Francisco, CA 94110. 1a

BOARD-CERTIFIED, GENERAL DIAGNOSTIC RADIOLOGIST with academic credentials to become Associate Director of Radiology and Director of Residency Training Program. Experience in clinical research required. Send CV to David Bryk, M.D., Director of Radiology, Maimonides Medical Center, 4802 Tenth Ave., Brooklyn, NY 11219. 1-2ap

INTERVENTIONAL RADIOLOGIST—Board-certified radiologist with fellowship training in vascular/interventional radiology for position starting July 1, 1989. Academic rank is at the level of assistant professor. This active clinical service performs the entire range of diagnostic and interventional procedures including embolization, angioplasty, infusion therapy, IVC filter placement, atherectomy, and laser angioplasty. A program in biliary lithotripsy is the responsibility of the section. The interventional inpatient service admits 100 patients/yr, primarily for embolization and angioplasty. The interventional clinic evaluates referred patients and patients seen in follow-up. Please send applications with CV to Donald F. Denny, Jr., M.D., Chief, Vascular and Interventional Radiology, Yale University School of Medicine, P. O. Box 3333, New Haven, CT 06510. Yale University is an equal opportunity/affirmative action employer. Applications from women and minority group members are encouraged. Application deadline is March 1, 1989. 1-2a

STAFF RADIOLOGISTS—The College of Physicians and Surgeons of Columbia University is searching for junior and senior staff radiologists for our angiography division. Salary and academic rank will be commensurate with experience and qualifications. Responsibilities include patient care, teaching, and supervising residents for junior staff level; research and demonstrated academic ability are required, in addition for senior staff level. Requirements include board eligibility or certification in diagnostic radiology for junior staff level; board certification and at least 2 yr of cardiovascular and interventional radiology experience for senior staff level. New York state medical license required; narcotics license desirable. Please send resume to Philip O. Alderson, M.D., Dept. of Radiology, 622 W. 168th St., New York, NY 10032. Columbia University is an affirmative action/equal opportunity employer. 1a

CHEST RADIOLOGY—The Dept. of Diagnostic Radiology and Nuclear Medicine at Stanford Medical School is recruiting a chest radiologist to direct and coordinate the research, teaching, and clinical activities of the chest radiology program. Stanford University is committed to increasing representation of women and members of minority groups on its faculty and particularly encourages applications from such candidates. The successful candidate should have expertise in all modern imaging modalities and have potential for excellence in research and teaching. Opportunities for research in MRI/MRS digital radiography and collaborative research with an outstanding Dept. of Electrical Engineering in medical imaging or image processing are available. This position can be at the assistant, associate, or full professor level, depending on the experience and national stature of the successful candidate. All interested candidates should send a letter of inquiry and CV to Leslie M. Zatz, M.D., Search Committee Chairman, Dept. of Diagnostic Radiology/Nuclear Medicine, Stanford University Medical Center S-072, Stanford, CA 94305. 1a

DIAGNOSTIC RADIOLOGIST—FLORIDA GULF COAST—Board-certified radiologist required for a diagnostic center located in an area offering many opportunities for enjoying outdoor activities. Experience in mammography, ultrasound, fluoroscopy, CT, and MRI required. Excellent compensation package based on revenues. Reply to Box N65, AJR (see address this section). 1ap

RADIOLOGIST—IMMEDIATE OPENING—American university-educated, board-certified/eligible M.D., with particular interest in imaging including MRI to join large, multihospital group in San Antonio, TX. Please direct inquiries and CV to P. O. Box 120310, San Antonio, TX 78212-9510. 1-4ap

PEDIATRIC RADIOLOGIST—Several faculty positions available for general pediatric imaging, pediatric neuroradiology, and nuclear medicine. Requirements include certification from ABR as well as fellowship training in pediatric radiology. Additional training in neuroradiology or nuclear medicine advisable. Academic commitment required. Contact David C. Kushner, M.D., Chairman, Dept. of Radiology, Children's Hospital National Medical Center, 111 Michigan Ave., N.W., Washington, DC 20010. 1ap

BC/BE GENERAL RADIOLOGIST WITH INTEREST IN NUCLEAR MEDICINE needed to join 6-man, hospital-based practice in Portland, OR. Position will require approximately 25% of time supervising the Nuclear Medicine Section and 75% of time doing general radiology. We are a progressive group with state-of-the-art equipment in all areas. This is a partnership position with generous salary and significant vacation time. Contact Norman Harris, M.D. or Lucien Burke, M.D., 10123 S.E. Market, Portland, OR 97216; (503) 251-6132. 1-2ap

DIAGNOSTIC RADIOLOGIST—ABDOMINAL IMAGING—The University of Missouri-Columbia Hospital and Clinics is seeking a radiologist with expertise in abdominal imaging (GI, CT, ultrasound, and MRI). Board certification required. Fellowship desirable. Tenured and nontenured tracks available at Assistant and Associate Professor levels. An equal opportunity/affirmative action employer. Address inquiries to Robert J. Churchill, M.D., Dept. of Radiology, University of Missouri-Columbia Hospital and Clinics, One Hospital Dr., Columbia, MO 65212. 1-2a

DIRECTOR, RADIATION ONCOLOGY—The University of Missouri-Columbia Hospital and Clinics is seeking a Director of Radiation Oncology. The position is a tenured track in the Dept. of Radiology. The Director will also serve as the Service Chief of the Radiation Therapy Service at the Ellis Fishel State Cancer Center. The facilities occupy 11,000 sq. ft. and include a 40 MeV Sagittaire, Dual Beam Siemens 15 MeV Accelerator, a simulator, CMS Treatment Planning Computer, and 4 Cobalt units. The candidate must provide leadership in research, teaching, clinical work, and administration. The position provides a unique opportunity for career development. Academic rank will be commensurate with previous experience. An equal opportunity/affirmative action employer. Address inquiries including CV to Robert J. Churchill, M.D., Dept. of Radiology, University of Missouri-Columbia Hospital and Clinics, One Hospital Dr., Columbia, MO 65212. 1-2a

NEURORADIOLOGIST—The University of Missouri-Columbia Hospital and Clinics is seeking a second neuroradiologist. Board certification required. Jr. or Sr. member of ASNR. Tenured and nontenured tracks available at Assistant and Associate Professor levels. An equal opportunity/affirmative action employer. Address inquiries to Robert J. Churchill, M.D., Dept. of Radiology, University of Missouri-Columbia Hospital and Clinics, One Hospital Dr., Columbia, MO 65212. 1-2a

STAFF RADIOLOGISTS—The VA Medical Center, Bay Pines, FL, affiliated with the University of S. Florida School of Medicine, is currently accepting applications for 2 staff radiologist positions. One position is required for general diagnostic radiology with MRI experience and 1 position for an interventional radiologist. Individuals should be board-certified. The Medical Center is located on the beautiful West Coast of Florida, only minutes from the Gulf of Mexico. Send CV and/or call Ann E. Esquerre, M.D., Chief, Radiology Service (114), VA Medical Center, Bay Pines, FL 33504; (813) 398-9363. An equal opportunity employer. 1a

GENERAL RADIOLOGIST—Progressive 15-member group needs additional radiologist for hospital- and office-based practice that serves part of a southwestern community with approximately 500,000 population. Position requires board certification. Training and/or experience in mammography, CT, and MRI is also needed. Contact Tulsa Radiology Associates, Inc., P.O. Box 4939, Tulsa, OK 74159. 12-2a

VASCULAR-INTERVENTIONAL RADIOLOGIST needed ASAP for well-established, progressive practice in 330-bed, major medical center in Fresno, CA. The hospital and dept. are currently undergoing major expansion. Send inquiries and current CV to L. De St. Jeor, M.D., Associate Director, Dept. of Radiology, Saint Agnes Medical Center, 1303 E. Herndon Ave., Fresno, CA 93710. 12-3ap

DIAGNOSTIC RADIOLOGIST—VA Medical Center, Muskogee, OK, is recruiting for a third board-certified or -eligible radiologist for a modern diagnostic imaging dept. Activities include routine radiography, fluoroscopy, limited angiography, digital subtraction angiography, CT, ultrasound, percutaneous biopsy, and PTC. This 230-bed facility with a large outpatient population is affiliated with the University of Oklahoma School of Medicine. Muskogee is a historic town of 43,000 located in the rolling hills of eastern Oklahoma, 45 mi. from Tulsa and 60 mi. from Fort Smith, AR. Attractions include several universities within commuting distance, all types of water sports nearby, and many wooded areas for recreation or hunting. The region is rated among the most desirable retirement areas in the nation and attracts many tourists to its beautiful azalea gardens and fascinating American Indian cultural activities. Good working hours, liberal holiday and vacation time, excellent federal benefits. Please send inquiries with CV to Eleanor P. Deed, M.D., Chief, Radiology Service (114), VA Medical Center, Honor Heights Dr., Muskogee, OK 74401. EOE. 1a

HARTFORD, CT—Actively growing practice has position available for board-certified radiologist to join an established group of 7. Practice includes hospital and private offices, performing approximately 70,000 exams per yr. Training and/or experience in CT and MRI necessary. Please send CV with correspondence to M. Lee Wallace, M.D., 40 Hart St., New Britain, CT 06052; (203) 229-2059. 1xa

CHEST RADIOLOGIST, CLEVELAND CLINIC FOUNDATION—Immediate opening for a staff, chest radiologist at the Cleveland Clinic Foundation. Internationally renowned institution with 1000-bed hospital and large, outpatient facility offering exciting opportunities for individual with clinical, teaching, and research interests. Competitive salary and very attractive benefit package. Please call and/or send CV to Moulay Meziane, M.D., Peter B. O'Donovan, M.D., Cleveland Clinic Foundation, 9500 Euclid Ave., Cleveland, OH 44195; (216) 444-0282, (216) 444-6411. 12-2ap

VASCULAR INTERVENTIONAL RADIOLOGIST—University of Virginia Medical Center, Dept. of Radiology. Tenure-track position at rank of assistant professor to professor. Salary and academic rank commensurate with experience and qualifications. Minimum requirements include M.D. with board certification in radiology and competence in angiography, interventional radiology, and special procedures. Starting date is negotiable. Please provide CV and names and addresses of 3 references. Contact Charles J. Tegtmeyer, M.D., Professor and Director, Division of Angiography, Interventional Radiology, and Special Procedures, Box 170, University of Virginia Medical Center, Charlottesville, VA 22908; (804) 924-9401. Equal opportunity/affirmative action employer. 12-1a

PACIFIC NORTHWEST—Nine-member, hospital-based group seeks a fellowship-trained radiologist, preferably CT/ultrasound. Modern 625-bed tertiary-care hospital, Sacred Heart Medical Center, and on-campus office practice. Spokane, WA, is a progressive community with outstanding recreational opportunities. Forward inquiry or CV to Hal Holte, M.D., Spokane Diagnostic Radiology, P.S., Sacred Heart Doctors' Bldg., W. 105 8th Ave., Ste. 322, Spokane, WA 99204; (509) 455-3352. 1xa

EMORY UNIVERSITY, DEPT. OF RADIOLOGY seeks a Ph.D. or M.D. with either NMR spectroscopy or imaging experience for a full-time faculty position. The candidate must be able to originate fundable research projects using NMR and collaborate with other faculty members (in or out of radiology) on NMR research. Knowledge of spin behavior is essential. Medicine, biology, or biochemistry, analog electronics, and computer science are useful skills. Two 1-m clinical imagers operating at 0.5 T and 1.5 T and a 30-cm 200-MHz instrument, all fully-programmable, will be available. The dept. is part of an 800-bed, tertiary-care complex giving ample opportunity for collaborations requiring clinical material. Seven full-time Ph.D. scientists, in the radiology dept., are currently involved in NMR. Qualified candidates please contact Thomas Dixon, M.D., Director, Frits Philips Magnetic Resonance Research Center, 419 Woodruff Memorial Bldg., Emory University, Atlanta, GA 30322. Emory University is an equal opportunity/affirmative action employer. 12-3a

ULTRASOUND STAFF RADIOLOGIST, THOMAS JEFFERSON UNIVERSITY HOSPITAL—The Dept. of Radiology at Thomas Jefferson University Hospital in Philadelphia has an immediate opening for a faculty ultrasound radiologist. This is an exciting opportunity for an individual with clinical, teaching, and research interests. Our Division of Diagnostic Ultrasound is one of the largest and best-equipped in the world. It is responsible for the full range of ultrasound exams, including general, obstetric, echocardiography, vascular, intraluminal, Doppler, interventional, and operative. Contact either Barry Goldberg, M.D., Director of Diagnostic Ultrasound, or David Levin, M.D., Professor and Chairman, Dept. of Radiology, Thomas Jefferson University Hospital, Philadelphia, PA 19107. Thomas Jefferson University Hospital is an equal opportunity/affirmative action employer. 12-6ap

BODY IMAGER—We are seeking a board-certified radiologist with postgraduate training in body imaging, CT, ultrasound, MRI, and interventional experience. 550-bed hospital in an attractive suburban setting, 25 mi. from NYC, with university-affiliated residency. Negotiable terms leading to full partnership. Please send CV to P. E. Moriarty, M.D., 151 Summit Ave., Summit, NJ 07901. 12-2ap

NUCLEAR MEDICINE—We are seeking a board-certified radiologist with postgraduate training in nuclear medicine and strong computer background. 550-bed hospital in attractive suburban setting, 25 mi. from NYC, with university-affiliated residency. Negotiable terms leading to full partnership. Please send CV to P. E. Moriarty, M.D., 151 Summit Ave., Summit, NJ 07901. 12-2ap

ULTRASOUND PHYSICIAN to join 3 hospital-based ultrasound/nuclear medicine physicians in Portland, OR. Practice includes high-risk obstetric sonography, neonatal neurosonography, color Doppler vascular sonography. Equipment includes multiple Acuson systems and multiple ATL systems. Position includes coverage for nuclear medicine. Send CV to Michael Daly, M.D., Nuclear Medicine/Ultrasound Section, Emanuel Hospital, 2801 N. Gantenbein Ave., Portland, OR 97227. 12-3a

DIAGNOSTIC RADIOLOGIST—GASTROINTESTINAL IMAGING—Yale New Haven Medical Center, Yale University School of Medicine, is seeking a radiologist with special interest in gastrointestinal imaging including barium radiography, CT, and/or ultrasound. Rank is commensurate with experience. A strong interest in patient care, research, and teaching is required. Please send inquiries along with CV to Morton Burrell, M.D., Professor of Radiology, Director of Gastrointestinal Radiology, Yale University School of Medicine, 333 Cedar St., New Haven, CT 06510. Yale University is an equal opportunity/affirmative action employer; applications from women and minority groups are encouraged. Application deadline is Feb. 1, 1989. 12-1a

ABDOMINAL RADIOLOGIST—The Abdominal Section of Emory University, Dept. of Radiology, is seeking an abdominal radiologist. The position is an exciting opportunity for an individual with teaching, clinical, and/or research interest. The individual will have access to the latest state-of-the-art equipment in fluoroscopy, ultrasound, CT, and MRI. Interested candidates should contact Michael E. Bernardino, M.D., Professor of Radiology, Director, Abdominal Division and Magnetic Resonance Imaging, Dept. of Radiology, Emory University Hospital, 1364 Clifton Rd., N.E., Atlanta, GA 30322. Emory University is an equal opportunity/affirmative action employer. 12-3a

THE DEPT. OF RADIOLOGY AT TRIPLER ARMY MEDICAL CENTER, HONOLULU, HI, is recruiting academically oriented radiologists for several divisions of the dept.: ultrasound, imaging (CT and/or MRI), interventional, chest, genitourinary, mammography, pediatric, neuro-radiology, and general diagnostic radiology. We are particularly interested in radiologists with ultrasound training or extensive experience. Our dept. offers a fully-accredited residency program with 18 residents and 15 attending full-time staff. Numerous consultants from across the country lecture on a continuing and regular basis. The hospital is a modern tertiary-care center serving the state and the entire Pacific Basin. A strong residency program, a diverse and interesting patient population, excellent equipment, and a tropical lifestyle are positive aspects of the practice. Academic credentials and/or experience are necessary. Recently graduated fellows are encouraged to apply. Board certification is mandatory. Candidates should be particularly interested in patient care, teaching, and research. Salary and benefits are competitive and generous. Tripler is an EO/EEOE employer. Please contact Dr. Mark F. Hansen, Col., MC, Chief, Dept. of Radiology, TAMC, HI 96859-5000; (808) 433-6393. Dr. Hansen will be present at the RSNA meeting. 1a

DIAGNOSTIC RADIOLOGIST—The University of S. Florida, Dept. of Radiology, is recruiting for 2 board-certified radiologists. The first position is for a general radiologist with special interest and/or experience in teaching medical students the basics of diagnostic radiology. The second position is for a diagnostic radiologist with a specialty or training in thoracic radiology. Both are combined appointments with the Tampa VA Hospital and the Dept. of Radiology, USF, at the assistant or associate professor level, commensurate with prior credentials. Competitive salary and generous fringe benefits are derived from both institutions. Both positions also involve clinical service, the teaching of radiology residents, and research. Please send letter of inquiry with CV to Michael Vermess, M.D., Professor of Radiology, Chief, Radiology Service, James A. Haley Veterans Hospital, 13000 Bruce B. Downs Blvd., Tampa, FL 33612. EOE. 1a

DIAGNOSTIC RADIOLOGIST, NUCLEAR MEDICINE POSITION—Large, private practice in desirable, rapidly growing location between Philadelphia and Princeton in Bucks County, PA, and Trenton, NJ, seeks a diagnostic radiologist with expertise in nuclear medicine, especially cardiac. Competency in general diagnostic radiology including ultrasound, CT, and mammography also required. Position available immediately or July 1989. Send letter and CV to S. Meshkov, M.D., 838 W. State St., Trenton, NJ 08618. 12-2ap

CHAIRMAN, DEPT. OF RADIOLOGY—Rose Medical Center, Denver, CO, a 300-bed, tertiary-care hospital, affiliated with the University of Colorado Health Sciences Center, is seeking a Chairman for the Dept. of Radiology. Qualifications include a strong professional base as well as administrative expertise. Please forward inquiries and CV to Chairman, Radiology Search Committee, c/o Medical Staff Office, Rose Medical Center, 4567 E. Ninth Ave., Denver, CO 80220. Rose Medical Center is an equal opportunity/affirmative action employer. 12-1a

VA MEDICAL CENTER, AUGUSTA, GA, seeks BC/BE radiologists interested in general radiology to include CT, ultrasound, and teaching. Affiliated with the Medical College of Georgia, this modern, 1100-bed, 2-unit facility is located in a progressive, southeastern city with excellent schools, moderate climate (and home of the Masters Golf Tournament), and is close to numerous major universities. An outstanding federal retirement, health, and insurance benefit package is available, plus 30 days vacation and 10 paid holidays per yr. Please send CV to Alex F. Daley, M.D., Chief, Radiology Service (114), VA Medical Center, Augusta, GA 30910; (404) 823-2236; FTS 251-2236. An equal opportunity employer. 1a

CHIEF, RADIOLOGY SERVICE, UNIVERSITY OF UTAH—AFFILIATED SALT LAKE VA HOSPITAL—Effective July 1, 1989, a position will be available for Chief of Radiology Service, Salt Lake VA Hospital. The position will be that of a full-time, university, faculty person, rank unspecified, with subspecialty interest preferably in cardiopulmonary radiology. The position will have the responsibility of coordination of VA radiology services, including supervision of VA resident rotations, medical student VA educational rotations, and supervision of VA technical and clerical personnel. The dept. is entirely new, currently under construction, planned for completion in the spring of 1989. This new dept. will include a new 2-T MRI system as well as all new radiologic equipment. Confidential inquiries and CV should be submitted to David G. Bragg, M.D., Professor and Chairman, Dept. of Radiology, University of Utah School of Medicine, Salt Lake City, UT 84132. The position will be open until Feb. 1, 1989. AA/EO employer. 12-1a

DIAGNOSTIC RADIOLOGY—Fellowship-trained radiologist desired to join 23-person expanding, established practice. Pediatric experience desirable, but not mandatory. Contact Lester Goldberg, M.D., Memorial Hospital, 3501 Johnson St., Hollywood, FL 33021; (305) 985-5886. 12-3ap

PEDIATRIC RADIOLOGIST—Yale New Haven Medical Center, Yale University School of Medicine, is seeking a pediatric radiologist for full-time faculty appointment. Academic rank is at the level of assistant or associate professor, dependent on qualifications. A strong interest in patient care, research, and teaching is required. Please send inquiries along with CV to Marc Keller, M.D., Diagnostic Radiology, Yale University School of Medicine, 333 Cedar St., New Haven, CT 06510. Yale University is an equal opportunity/affirmative action employer; applications from women and minority groups are encouraged. 11-1a

DIAGNOSTIC RADIOLOGIST—Yale University School of Medicine is seeking a radiologist with special interest in body MRI including a focus in cardiac MRI for a full-time faculty appointment. Equipment includes 2 GE 1.5-T scanners, a 2-T advanced NMR fast scanner, a 0.4-T superkinetics, a 2-T CSI, and 300- and 20-MHz spectrometers. Academic rank is at the level of assistant professor. A strong interest in patient care, research, and teaching is required. Please send inquiries along with CV to Shirley McCarthy, M.D., Ph.D., Diagnostic Radiology, Yale University School of Medicine, 333 Cedar St., New Haven, CT 06510. Yale University is an equal opportunity/affirmative action employer; applications from women and minority groups are encouraged. 11-1a

NEURORADIOLOGIST—Ten-man private group seeks BC/BE radiologist with 1- or 2-yr neuro fellowship. Strong MR skills required. Must be willing to practice general radiology in addition to neuro. Beautiful, midwestern university town. Excellent starting salary/fringes with full partnership in 2 yr. Send inquiries/CV to Joe McColley, M.D., 909 E. University St., Bloomington, IN 47401; (812) 336-9446. 11-1ap

MUSCULOSKELETAL RADIOLOGIST—The H. Lee Moffitt Cancer Center and Research Institute at the University of South Florida has an opening for a musculoskeletal radiologist with fellowship training or equivalent subspecialty experience. Interest and expertise in all imaging modalities (including MRI) and procedures related to musculoskeletal radiology are preferred. Case material is plentiful and varied including primary and secondary neoplasms, pediatric orthopedics, and a large-volume MRI load. This faculty position includes clinical service, teaching, and research; academic rank is based on qualifications. Our facility is a new, state-of-the-art complex; the compensation package is excellent. Interested candidates should contact Robert Clark, M.D., Dept. of Radiology, Moffitt Cancer Center, P. O. Box 280179, Tampa, FL 33682-0179. 11-1ap

ONCOLOGIC RADIOLOGISTS—The H. Lee Moffitt Cancer Center and Research Institute at the University of South Florida has faculty positions available for individuals with training or experience in oncologic radiology. This is an excellent opportunity to participate in all areas of oncologic imaging or to subspecialize based on expertise. The positions include clinical service, research, and teaching; academic rank is based on qualifications. Our facility is a new, state-of-the-art complex; the compensation package is excellent. Interested candidates should contact Robert A. Clark, M.D., Dept. of Radiology, Moffitt Cancer Center, P. O. Box 280179, Tampa, FL 33682-0179. 11-1ap

RADIOLOGIST—Opening for board-certified radiologist. Junior staff position. Interest or training in nuclear medicine or neuroradiology preferred. 700-bed, university-affiliated teaching hospital with fully approved residency program. Send CV to David Bryk, M.D., Director of Radiology, Maimonides Medical Center, 4802 Tenth Ave., Brooklyn, NY 11219. 11-1ap

NEURORADIOLOGIST—Immediate opening for recently trained neuroradiologist in busy, suburban practice in Southwest. Current CT, MRI, and arteriography skills required. Highly competitive salary/benefits. Send CV to Box K49, AJR (see address this section). 1xa

CENTRAL FLORIDA—Fellowship-trained, ultrasound physician to join large, tertiary-center, radiology group in central FL. Practice includes 3 hospitals and 2 outpatient depts. Send CV to Bruce R. Crossman, M.D., Dept. of Radiology, Florida Hospital, 601 E. Rollins St., Orlando, FL 32803. 11-2ap

ABDOMINAL RADIOLOGIST—The H. Lee Moffitt Cancer Center and Research Institute at the University of South Florida has a faculty position available for an abdominal radiologist with fellowship training or equivalent subspecialty experience. Interest and expertise in all imaging modalities and procedures related to abdominal radiology are preferred. The position includes clinical service, research, and teaching; academic rank is based on qualifications. Our facility is a new, state-of-the-art complex; the compensation package is excellent. Interested candidates should contact Robert Clark, M.D., Dept. of Radiology, Moffitt Cancer Center, P. O. Box 280179, Tampa, FL 33682-0179. 11-1ap

CENTRAL FLORIDA—General diagnostic radiologist to join large, tertiary-center radiology group. Specific interest in mammography to head very active women's center practice. Send CV to Bruce R. Crossman, M.D., Dept. of Radiology, Florida Hospital, 601 E. Rollins St., Orlando, FL 32803. 11-2ap

DIAGNOSTIC ONCORADIOLOGIST—The Division of Oncoradiology at the Dana-Farber Cancer Institute, a Harvard University affiliate, has an opening at the instructor/assistant professor level for a general radiologist with an interest in oncology beginning July 1989 or sooner. Patient care responsibilities with a close working relationship with the clinical staff, teaching, and research opportunities abound. There are 52 beds with a large outpatient service. All new equipment is available including a GE-9800 CT scanner. Please send CV to Maxine Jochelson, M.D., Director, Division of Oncoradiology, Dana-Farber Cancer Institute, 44 Binney St., Boston, MA 02115. 11-4a

FULL-TIME ACADEMIC NEURORADIOLOGIST—One staff position is currently available in the Division of Neuroimaging at the Children's Memorial Hospital at Chicago. The Division of Neuroimaging is a complete service with 2 CT scanners (1 is a GE-9800), 1 GE 1.5-T Signa MRI scanner (which is inhouse for children), 3 Acuson ultrasound units, myelography and cerebral angiography equipment, as well as an interventional neuroradiology program with Northwestern University. The Division has its own approved fellowship program in neuroradiology. Some training in interventional neuroradiology and/or pediatric neuroradiology is preferred, but not necessary. Send CV to Sharon E. Byrd, M.D., Director of Neuroimaging Division, Children's Memorial Hospital, 2300 Children's Plaza, Chicago, IL 60614; (312) 880-3565. 11-4ap

GU RADIOLOGIST, BRIGHAM & WOMEN'S HOSPITAL—The Dept. of Radiology at Brigham & Women's Hospital/Harvard Medical School is seeking a radiologist to direct its GU Section. The position combines clinical activities with teaching and research. Candidates must be board-certified and have experience in all aspects of GU radiology, as well as an interest/commitment to academic work. Please send CV to B. Leonard Holman, M.D., Chairman, Dept. of Radiology, Brigham & Women's Hospital, 75 Francis St., Boston, MA 02115. Harvard Medical School is an affirmative action/equal opportunity educator and employer. 11-4a

ANGIOGRAPHY/INTERVENTIONAL RADIOLOGIST—Board-certified radiologist with training in angiography/interventional radiology and competence in MRI to join 6-physician, hospital-based group practice. Must be able to perform all facets of diagnostic imaging including ultrasound, CT, nuclear medicine, and mammography. Immediate opening with excellent benefits. 380-bed hospital, 85,000 exams per yr. Send CV to William R. Balchunas, M.D., P.O. Box 9210, Pensacola, FL 32513-9210. 10-1a

ULTRASOUND STAFF RADIOLOGIST, BRIGHAM & WOMEN'S HOSPITAL—The Dept. of Radiology at the Brigham & Women's Hospital/Harvard Medical School is seeking a radiologist for a full-time, academic position in ultrasound. We perform 60-85 scans per day, including OB-GYN, abdominal, Doppler, small parts, neonatal, and interventional. Research and teaching opportunities are available. Candidate must be BC/BE with fellowship training in ultrasound. Please send CV to B. Leonard Holman, M.D., Chairman, Dept. of Radiology, Brigham & Women's Hospital, 75 Francis St., Boston, MA 02115. Harvard Medical School is an affirmative action/equal opportunity educator and employer. 11-4a

NEW ENGLAND—BC/BE diagnostic radiologist, with expertise in ultrasound, CT, and mammography, sought by 5-member office practice dept. in an established, rapidly-expanding, multispecialty, prepaid, and FFS group practice. Physician owned and directed. Send CV to Medical Director, Fallon Clinic, Inc., 630 Plantation St., Worcester, MA 01605. 11-1ap

ABDOMINAL IMAGING—A staff position is available at The Cleveland Clinic Foundation in the Section of Abdominal Imaging. The Cleveland Clinic is a 1000-bed tertiary-care facility with a large outpatient population and international referral base. The Section of Abdominal Imaging encompasses body CT, ultrasound, body MR, gastrointestinal radiology, and mammography. Sectional applicants should be fellowship-trained or possess equivalent experience. Send CV to David M. Paushter, M.D., Head, Section of Abdominal Radiology, Hospital Radiology, Cleveland Clinic Foundation, 9500 Euclid Ave., Cleveland, OH 44106. The Cleveland Clinic is an equal opportunity employer. (M-F-H-V) 11-1ap

DIAGNOSTIC RADIOLOGIST competent in interventional and MR to join growing 3-man practice in northern Arkansas. Modern hospital-based practice includes CT, ultrasound (including duplex vascular), angiography, DSA, interventional, lo-dose mammography, and computerized nuclear medicine. Mobile MR and on-site Radiation Center being added. Located in beautiful resort area of Ozark Mountains, 110 mi from Springfield, MO, 150 mi from Little Rock, and 190 mi from Memphis, and serves 100,000 area population. Excellent recreational activities in family-oriented rural environment. Competitive starting salary with full-partnership in 1 yr. Contact Marc Trager, M.D., P.O. Box 1137, Mountain Home, AR 72653; (501) 425-1760. 11-4a

BC/BE RADIOLOGIST for metropolitan-based, Nashville hospital. Close working relationship with 3 skilled radiologists. Experience required in all routine modalities (excluding MRI), as well as basic skills in angiography and specials. Excellent starting salary and vacation. Immediate need. Send CV to John Huff, M.D., 834 Brentview Dr., Nashville, TN 37220. 1ap

HARTFORD, CT—Position available for a board-certified radiologist to join an established group of 7. Practice includes hospital and 3 private offices, all fully equipped, including CT, MRI and CT experience is an essential requirement. Competitive starting salary and benefits. Please enclose CV with initial correspondence to Jeffrey Blau, M.D., 40 Hart St., New Britain, CT 06052; (203) 229-2059. 1xa

DIAGNOSTIC RADIOLOGIST, ATLANTA, GA—Position available for BC/BE radiologist experienced in neuroradiology or interventional to join a 2-man, rapidly expanding, hospital-based practice. All modalities utilized including MRI. Competitive salary with opportunity for partnership. Send CV to Vernon Markel, M.D., P.O. Box 1633, Tucker, GA 30085. 12-2ap

RADIOLOGIST—Seven-member group seeking board-certified/eligible radiologist to join progressive hospital/clinic practice in scenic western Arkansas town in Ozark foothills of approximately 100,000 population. All modalities represented in practice. Competitive salary leading to early full-partnership. Liberal fringe benefits and vacation. At least 3 mo documented MRI training necessary. Interested parties please send CV to W. T. Huskison, M.D., Radiologists, P.A., P.O. Box 3887, Ft. Smith, AR 72913, or call collect (501) 452-9416. 11-1a

VASCULAR/INTERVENTIONAL RADIOLOGIST—Position available, Dept. of Radiology, University of Pittsburgh School of Medicine, for a full-time, academically oriented, staff vascular/interventional radiologist at the assistant or associate professor level. Board certification and 1-yr. fellowship training or equivalent experience are required. Duties include clinical service, teaching, and research. Research in laser angioplasty and vascular MRI available. Cooperative research and clinical interaction are maintained with academically active departments of vascular surgery, transplant surgery, and gastroenterology. Salary and excellent benefits commensurate with rank. Please include CV with letter of inquiry to Joan Roberge, Administrator, University of Pittsburgh, Dept. of Radiology, One Children's Pl., 3946 Children's Main Tower, Pittsburgh, PA 15213. 10-1a

DIAGNOSTIC RADIOLOGIST—Eight board-certified radiologists in expanding hospital-based private practice seek BC/BE general radiologist to associate. Competence in all modalities expected with need for interventional and/or MRI training emphasized. Opportunity in midwestern city of 72,000 people offers generous compensation/vacation. Full partnership after 2 yr. Reply to Box J32, AJR (see address this section). 10-1a

BOARD-CERTIFIED OR ELIGIBLE RADIOLOGIST sought to join staff covering 4 hospitals and an outpatient clinic in S.E. Georgia. Skills must include general diagnostic, ultrasound, nuclear medicine, mammography, CT, and special procedures. Salary negotiable. Send letters of inquiry with CV and letters of reference to Director, Regional Diagnostics, P.O. Box 147, Vidalia, GA 30474; (912) 537-1150. 1xa

VASCULAR/INTERVENTIONAL RADIOLOGIST—Kansas University Medical Center, Dept. of Diagnostic Radiology. Full-time, academic, senior staff position. Salary, with excellent fringe benefits and rank negotiable. ABR certification and 1 yr of fellowship training or equivalent experience required. Address inquiries and CV to Arch W. Templeton, M.D., KUMC, 39th & Rainbow Blvd., Kansas City, KS 66103; (913) 588-6805. 10-1ap

ISRAEL, DIAGNOSTIC RADIOLOGY. Opportunities for 3-4 week or longer working vacations in a number of Israeli medical centers, on a volunteer basis. Positions varied, arrangements flexible. For information contact: Jonathan H. Fish, M.D., 1844 San Miguel Dr., #302, Walnut Creek, CA 94596; (415) 947-0560. 1xa

CROSS-SECTIONAL RADIOLOGIST, INTERVENTIONALIST—Board-certified diagnostic radiologist with fellowship training wanted to join 5-member dept. in 214-bed community hospital. Group also active in busy outpatient facilities and free-standing Magnetic Resonance Center. Primary responsibility will be ultrasound, CT, and nonangiography interventional, with back-up for primary angiographer. Competence in Doppler studies desired. Call and/or send CV attention Jon Robins, M.D., or Edward Janon, M.D., 6699 Alvarado Rd., Ste. 2100, San Diego, CA 92120; (619) 583-4214. 1xa

Fellowships and Residencies

FELLOWSHIPS IN ULTRASOUND/CT/MRI, CARDIOVASCULAR/INTERVENTIONAL, NEURORADIOLOGY/ENT, CARDIOPULMONARY, AND MRI—The Dept. of Radiology at Thomas Jefferson University Hospital offers these 5 subspecialty fellowships each yr. We have a large and extensively equipped ultrasound division that offers training in all phases of ultrasound, including cardiac, vascular, and obstetric. The dept. also has 3 modern CT scanners and a GE 1.5-T MRI unit. A second MRI unit will be installed shortly. The Cardiovascular/Interventional Division is currently being renovated and will house state-of-the-art angiography equipment with DSA. This division performs a full range of both vascular and nonvascular interventional procedures. Neuroradiology is housed in a brand new Neurosciences Imaging Center containing all imaging modalities in a single comprehensive facility. For information and applications to these 5 programs, contact Barry B. Goldberg, M.D. (US/CT/MRI), Geoffrey Gardiner, Jr., M.D. (Cardiovascular/Interventional), Carlos Gonzalez, M.D. (Neuroradiology), Robert Steiner, M.D. (Cardiopulmonary), or Matthew Rifkin, M.D. (MRI), at the Dept. of Radiology, Thomas Jefferson University Hospital, Philadelphia, PA 19107. 1c

CARDIOVASCULAR/INTERVENTIONAL RADIOLOGY FELLOWSHIP AT THOMAS JEFFERSON UNIVERSITY HOSPITAL—A 1-yr fellowship position is available starting 7/1/89. This fellowship includes experience in a wide range of diagnostic angiography and both vascular and nonvascular interventional procedures. These include balloon angioplasty, laser thermal angioplasty, thrombolytic therapy, atherectomy, intravascular stent placement, IVC filter placements, renal and biliary drainage procedures, abscess drainages, and stone retrievals. Optional training also available in coronary angiography. Facilities include state-of-the-art angiographic and digital subtraction equipment. Contact either Geoffrey A. Gardiner, Jr., M.D. or David C. Levin, M.D., Dept. of Radiology, Thomas Jefferson University Hospital, 111 S. 11th St., Philadelphia, PA 19107. Thomas Jefferson University is an equal opportunity/affirmative action employer. 1-6cp

FELLOWSHIP IN PEDIATRIC RADIOLOGY—LeBonheur Children's Medical Center/St. Jude Children's Research Hospital/University of Tennessee combined program in pediatric radiology offers a 1- or 2-yr fellowship in pediatric imaging. Experience to include general pediatric, neuro, nuclear, oncologic, neonatal, and cardiovascular radiology. Facilities include Doppler ultrasound, CT, and MRI. Opportunity to participate in MRI and other imaging research. Equal opportunity/affirmative action employer. Address inquiries to Barry D. Fletcher, M.D., Chairman, Diagnostic Imaging Dept., St. Jude Children's Research Hospital, 332 N. Lauderdale, P. O. Box 318, Memphis, TN 38101; (901) 531-2309, or Robert A. Kaufman, M.D., Director, Dept. of Radiology, LeBonheur Children's Medical Center, One Children's Plaza, Memphis, TN 38103; (901) 522-3195. 1c

UNEXPECTED FELLOWSHIP OPENING—The University of Oregon Health Sciences Center has recently funded a second position for a fellow in angiography/interventional radiology beginning July 1, 1989. 509-bed hospital. Fellow will be involved in all noncardiac diagnostic and interventional procedures. Opportunity for clinical and/or animal research. Contact Josef Rosch, M.D., Director, Vascular and Interventional Radiology, Dept. of Radiology, L-340, Oregon Health Sciences University, 3181 S.W. Sam Jackson Park Rd., Portland, OR 97201. 12-1cp

MEDICAL IMAGING FELLOWSHIP IN RADIOLOGY—The Dept. of Radiology at the Hospital of the University of Pennsylvania is currently offering a 1- or 2-yr fellowship in the Medical Imaging Section. Training will be provided in the application of computer technology to the processing of medical images. The applicant should have completed an accredited radiology training program and be board-eligible before starting the fellowship. The fellowship is part of a continuing effort by the Dept. of Radiology to bring about a symbiosis between basic science research in medical imaging and clinical radiology. Applicants should submit a CV and a list of 4 references to James F. Greenleaf, Ph.D., Acting Chief, Medical Imaging Section, Dept. of Radiology, Hospital of the University of Pennsylvania, 3400 Spruce St., Philadelphia, PA 19104-4283. The University of Pennsylvania is an affirmative action/equal opportunity employer. Minorities and women are encouraged to apply for the fellowship. 1c

FELLOWSHIP IN PEDIATRIC RADIOLOGY—Dept. of Radiology, Children's Hospital Medical Center, Cincinnati, OH, offers a 1- or 2-yr fellowship in pediatric radiology beginning July 1, 1989. Children's Hospital Medical Center is a 344-bed institution where approximately 85,000 radiologic exams are done per yr by 10 attending radiologists. Training includes all aspects of pediatric imaging including conventional radiology, neuroradiology, abdominal imaging, ultrasound, nuclear medicine, CT, MRI, and vascular/interventional techniques. Equipment includes digital fluoroscopy, Acuson and ATL ultrasound units with Doppler and color-flow Doppler capabilities, Gamma and SPECT tomographic nuclear cameras, GE 9800 Quick CT Scanner, 1.5-T GE MRI, and angiographic suite with digital vascular imaging. Requirements for the fellowship include completion of a radiology residency with training in the various subspecialties of diagnostic imaging. Contact Donald R. Kirks, M.D., Director, Dept. of Radiology, Children's Hospital Medical Center, Eland & Bethesda Aves., Cincinnati, OH 45229-2899; (513) 559-8058. 12-8cp

ONCORADIOLOGY/MAMMOGRAPHY FELLOWSHIP—The Dept. of Radiology at the Dana-Farber Cancer Institute and Brigham and Women's Hospital, which are Harvard University affiliates, offers a 1-yr fellowship position beginning July 1, 1989. All noninvasive imaging modalities involved in the diagnosis and care of cancer patients are integrated into this program. Please send CV to Maxine Jochelson, Director, Division of Oncoradiology, Dana-Farber Cancer Institute, 44 Binney St., Boston, MA 02115. 11-4c

THE NEW YORK HOSPITAL-CORNELL MEDICAL CENTER, DEPT. OF RADIOLOGY—One-yr fellowship position available beginning July 1, 1989, in GU radiology. Program will involve participation in clinical aspects of GU imaging including urography, CT, sonography, and MRI. Opportunity for research, particularly involving MRI, is offered. Applicants should be ABR certified or eligible. Interested candidates should contact and send CV to Susan Kryszewicz, M.D., Dept. of Radiology, The New York Hospital-Cornell Medical Center, 525 E. 68th St., New York, NY 10021; (212) 472-6136. 9-1c

CARDIOVASCULAR-INTERVENTIONAL RADIOLOGY FELLOWSHIP—Available July 19, 1989. One-year fellowship program at a 750-bed teaching hospital. Extensive clinical experience involving all aspects of cardiovascular imaging, interventional vascular and nonvascular procedures, and availability for clinical or animal research. Send CV and inquiries to Oscar H. Gutierrez, M.D., Dept. of Radiology, Box 648, University of Rochester Medical Center, Rochester, NY 14642. An equal opportunity employer (M/F). 9-2c

MUSCULOSKELETAL RADIOLOGY FELLOWSHIP—The Dept. of Radiology at the University of Minnesota has a 1-yr, postresidency fellowship training position in musculoskeletal radiology available at the rank of instructor (temporary, nonregular) beginning July 1, 1989. Minimum requirements include successful completion of an accredited radiology residency and board certification in radiology by beginning date of fellowship appointment. In addition to clinical practice and training, responsibilities will include graduate and undergraduate medical instruction in musculoskeletal radiology as well as assisting with related departmental research projects. Salary is negotiable and competitive and dependent on past scholarly productivity and post-M.D. experience. Applicants must be licensed, or able to obtain license, to practice medicine in the state of Minnesota before appointment date. Applications for these positions will be accepted through Feb. 28, 1989. Send letters to Harry Griffiths, M.D., Professor, Dept. of Radiology, Box 292 UMHC, University of Minnesota, 420 Delaware St. S.E., Minneapolis, MN 55455. The University of Minnesota is an equal opportunity and affirmative action educator and employer and specifically encourages applications from women and minorities. 1c

MRI FELLOWSHIP—The Dept. of Radiology at the University of Minnesota has a 1-yr, postresidency fellowship training position in MRI available at the rank of instructor (temporary, nonregular) beginning July 1, 1989. Minimum requirements include successful completion of an accredited radiology residency and board certification in radiology by beginning date of fellowship appointment. In addition to clinical practice and training, responsibilities will include graduate and undergraduate medical instruction in MRI as well as assisting with related departmental research projects. Salary is negotiable and competitive and dependent on past scholarly productivity and post-M.D. experience. Applicants must be licensed, or able to obtain license, to practice medicine in the state of Minnesota before appointment date. Applications for these positions will be accepted through Feb. 28, 1989. Send letters to Harry Griffiths, M.D., Professor, Dept. of Radiology, Box 292 UMHC, University of Minnesota, 420 Delaware St. S.E., Minneapolis, MN 55455. The University of Minnesota is an equal opportunity and affirmative action educator and employer and specifically encourages applications from women and minorities. 1c

PEDIATRIC RADIOLOGY FELLOWSHIP—The Dept. of Radiology at the University of Minnesota has a 1-yr, postresidency fellowship training position in pediatric radiology available at the rank of instructor (temporary, nonregular) beginning July 1, 1989. Minimum requirements include successful completion of an accredited radiology residency and board certification in radiology by beginning date of fellowship appointment. In addition to clinical practice and training, responsibilities will include graduate and undergraduate medical instruction in pediatric radiology as well as assisting with related departmental research projects. Salary is negotiable and competitive and dependent on past scholarly productivity and post-M.D. experience. Applicants must be licensed, or able to obtain license, to practice medicine in the state of Minnesota before appointment date. Applications for these positions will be accepted through Feb. 28, 1989. Send letters to Deborah Day, M.D., Associate Professor, Dept. of Radiology, Box 292 UMHC, University of Minnesota, 420 Delaware St. S.E., Minneapolis, MN 55455. The University of Minnesota is an equal opportunity and affirmative action educator and employer and specifically encourages applications from women and minorities. 1c

ULTRASOUND IMAGING FELLOWSHIP—The Dept. of Radiology at the University of Minnesota has a 1-yr, postresidency fellowship training position in ultrasound imaging available at the rank of instructor (temporary, nonregular) beginning July 1, 1989. Minimum requirements include successful completion of an accredited radiology residency and board certification in radiology by beginning date of fellowship appointment. Clinical responsibilities include conventional diagnostic sonography (including obstetrical and prostate studies), conventional and color flow Doppler exams (including those done in the noninvasive vascular laboratory), and sonography-guided interventional procedures. In addition to clinical practice and training, responsibilities will include graduate and undergraduate medical instruction in ultrasound imaging as well as assisting with related departmental research projects. Salary is negotiable and competitive and dependent on past scholarly productivity and post-M.D. experience. Applicants must be licensed, or able to obtain license, to practice medicine in the state of Minnesota before appointment date. Applications for these positions will be accepted through Feb. 28, 1989. Send letters to Janis Letourneau, M.D., Associate Professor, Dept. of Radiology, Box 292 UMHC, University of Minnesota, 420 Delaware St. S.E., Minneapolis, MN 55455. The University of Minnesota is an equal opportunity and affirmative action educator and employer and specifically encourages applications from women and minorities. 1c

NEURORADIOLOGY FELLOWSHIP—The Dept. of Radiology at the University of Minnesota has a 1- or 2-yr, postresidency fellowship training position in neuroradiology available at the rank of instructor (temporary, annual renewable) beginning July 1, 1989. Minimum requirements include successful completion of an accredited radiology residency and board certification in radiology by beginning date of fellowship appointment. In addition to clinical practice and training, responsibilities will include graduate and undergraduate medical instruction in neuroradiology as well as assisting with related departmental research projects. Salary is negotiable and competitive and dependent on past scholarly productivity and post-M.D. experience. Applicants must be licensed, or able to obtain license, to practice medicine in the state of Minnesota before appointment date. Applications for these positions will be accepted through Feb. 28, 1989. Send letters to Benjamin C. P. Lee, M.D., Associate Professor, Dept. of Radiology, Box 292 UMHC, University of Minnesota, 420 Delaware St. S.E., Minneapolis, MN 55455. The University of Minnesota is an equal opportunity and affirmative action educator and employer and specifically encourages applications from women and minorities. 1c

UNIVERSITY OF MASSACHUSETTS MEDICAL CENTER, Dept. of Radiology has 1-yr fellowship openings for July 1989 in vascular/interventional radiology and neuroradiology. The medical center is a 360-bed teaching hospital and medical school and a major trauma center. The dept. runs a very active clinical service and is well-equipped with 2 GE CT scanners, a 1.5-T GE MR scanner in a stand-alone facility, and 2 dedicated vascular/interventional radiology suites with Siemens and Fisher equipment. Both conventional and digital subtraction imaging capabilities are present. For further information, contact Edward H. Smith, M.D., Professor and Chair, Dept. of Radiology, University of Massachusetts Medical Center, 55 Lake Ave., N., Worcester, MA 01655; (508) 856-3252. UMMC is an equal opportunity/affirmative action employer. 1-3c

ABDOMINAL/CT IMAGING FELLOWSHIP, UNIVERSITY OF MINNESOTA—The Dept. of Radiology at the University of Minnesota has a 1-yr, postresidency fellowship training position in abdominal/CT imaging available at the rank of instructor beginning July 1, 1989. The fellowship will provide extensive clinical experience in all facets of body CT, including CT-guided biopsies and drainage procedures performed by the fellow. In addition to practical experience with the 3 Siemens CT scanners in clinical use, the fellowship will also offer participation in the many ongoing research projects at the University of Minnesota. Ample time will be provided for individual research projects, participation at meetings, and preparation of manuscripts. Minimum requirements include successful completion of an accredited radiology residency and board certification in radiology by beginning date of fellowship appointment. In addition to clinical practice and training, responsibilities will include graduate and undergraduate medical instruction in abdominal/CT imaging, as well as assisting with related departmental research projects. Salary is negotiable and competitive and dependent on past scholarly productivity and post-M.D. experience. Applicants must be licensed, or able to obtain license, to practice medicine in the state of Minnesota before appointment date. Applications for these positions will be accepted through Feb. 28, 1989. Send letters to Dr. Halvorsen, Associate Professor, Dept. of Radiology, Box 292 UMHC, University of Minnesota, 420 Delaware St. S.E., Minneapolis, MN 55455. The University of Minnesota is an equal opportunity and affirmative action educator and employer and specifically encourages applications from women and minorities. 1c

CARDIOVASCULAR/INTERVENTIONAL RADIOLOGY FELLOWSHIP—The Dept. of Radiology at the University of Minnesota has several 2-yr, postresidency fellowship training positions in cardiovascular/interventional radiology available at the rank of instructor (temporary, annual renewable) beginning July 1, 1989. Minimum requirements include successful completion of an accredited radiology residency and board certification in radiology by beginning date of fellowship appointment. Training in all interventional and angiographic techniques including coronary angiography. In addition to clinical practice and training, responsibilities will include graduate and undergraduate medical instruction in cardiovascular/interventional radiology as well as assisting with related departmental research projects. Salary is negotiable and competitive and dependent on past scholarly productivity and post-M.D. experience. Applicants must be licensed, or able to obtain license, to practice medicine in the state of Minnesota before appointment date. Applications for these positions will be accepted through Feb. 28, 1989. Send letters to Kurt Amplatz, M.D., Professor, Dept. of Radiology, Box 292 UMHC, University of Minnesota, 420 Delaware St. S.E., Minneapolis, MN 55455. The University of Minnesota is an equal opportunity and affirmative action educator and employer and specifically encourages applications from women and minorities. 1c

BREAST IMAGING 1989—The Westin Maui-Kaanapali Beach Resort, Maui, HI, Jan. 22-27, 1989. A comprehensive course that will provide a structured, up-to-date approach to the detection and diagnosis of breast cancer. A distinguished faculty will address the day-to-day problems encountered in screening and lesion analysis and provide practical solutions for those new to the field, as well as for the experienced radiologist. Sponsor: Massachusetts General Hospital. Director: Daniel B. Kopans, M.D. Contact: Harvard Medical School, Dept. of Continuing Education, Boston, MA 02115; (617) 732-1525. Fee: \$500; 20 hr of category 1 credit. 1dp

ALASKA 89—CRUISE THE INLAND PASSAGE—July 8-15, 1989, CME I accreditation, Professor Lawrence Bassett, M.D., Breast Imaging. For information, contact Medical Seminars International, 9800 D Topanga Canyon Blvd., #232, Chatsworth, CA 91311; (818) 700-9821. 1-6d

Other

VOLUNTEER SERVICES—If you are interested in doing volunteer work as a radiologist where your services are desperately needed and greatly appreciated, inquire about the program at St. Jude Hospital in St. Lucia, West Indies. For more information, contact Sister Sharee Hurtgen, c/o St. Jude Hospital, Box 331, St. Lucia, West Indies; (809) 454-6041, or Merle Piacenti, M.D.; (815) 223-4319 (5-10 p.m. CST). 1-2ep

AJR Classified Advertisements Information

Box Responses and Address for Ad Placement

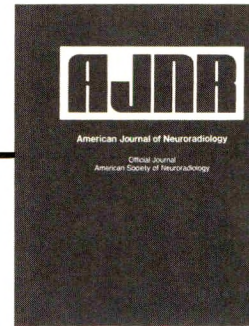
Write Box _____, AJR, 2223 Avenida de la Playa, Suite 200, La Jolla, CA 92037-3218; (619) 459-2229; FAX: (619) 459-8814.

Tutorials/Courses

SEVENTH WINTER CONGRESS, COURCHEVELLE, FRANCE—March 4-11, 1989, Category I accreditation, international faculty, MRI, CT, and ultrasound. For information, contact Medical Seminars International, 21915 Roscoe Blvd., Ste. 222, Canoga Park, CA 91304; (818) 700-9821. 11-2d

Increase your expertise in evaluating CNS lesions

AJNR American Journal of Neuroradiology



Editor: **Juan M. Taveras, MD**, Harvard Medical School; MGH

Outstanding clinical papers on every aspect of CNS imaging, including spinal diagnosis...informed coverage of head and neck radiology...clear, readable CTs, angiographs, MR imaging and ultrasound studies. These are the features you demand of a quality professional journal. You'll find them in every issue of **AJNR: American Journal of Neuroradiology**.

As you are called upon to perform and interpret more and more sophisticated diagnostic tests — from myelography to CT to newborn ultrasound studies — you need a comprehensive, reliable journal that can keep you abreast of all the latest developments. Each bimonthly issue of **AJNR** brings you timely, clinically pertinent information, as well as important clinical research presented with an eye toward immediate practical application.

Here's a brief sampling of the variety of articles you'll find in **AJNR**:

Giant Cavernous Aneurysm Associated with Trigeminal Artery: Treatment by Detachable Balloon. *Higashida RT, Halbach VV, Mehringer CM, Hieshima GB*

Intraoperative Digital Subtraction Neuroangiography: A Diagnostic and Therapeutic Tool. *Hieshima GB, Reicher MA, Higashida RT, et al.*

Characteristic Features of MR Truncation Artifacts.

Czervionke LF, Czervionke JM, Daniels DL, Haughton VM
Neuroimaging of Scuba Diving Injuries to the CNS. *Warren LP Jr, Djang WT, Moon RE, et al.*

Risk of Seizures After Myelography. *Maly P, Bach-Gansmo T, Elmqvist D*

Comparison of MR Imaging and CT in Patients with Intracranial Aneurysm Clips. *Holtas S, Olsson M, Romner B, Larsson E-M, Saveland H, Brandt L*


Comparison of MR Imaging, CT, and Angiography in the Evaluation of the Enlarged Cavernous Sinus. *Hirsch WL Jr, Hryshko FG, Sekhar LN, et al.*

Bimonthly

Personal \$115/yr **Institutions** \$135/yr

In-training \$65/yr (add \$25.00 outside the US)

ORDER FREE BY PHONE. Just call

 **1-800-638-6423** from anywhere in the US.
Maryland residents, call **1-800-638-4007**.

Williams & Wilkins

P.O. Box 23291 Baltimore, Maryland 21203



Subscribe to AJNR for 3 years and SAVE

Avoid future rate increases and ensure uninterrupted service by placing a multi-year subscription at current rates.

☐ New subscription ☐ Renewal

☐ 3 yrs ☐ 2 yrs ☐ 1 yr

☐ **Personal** \$115 ☐ **Institutions** \$135 ☐ **In-training** \$65
(add \$25.00 outside the US)

☐ Also send me the **1989 Bound Volume** at \$65.00 (\$70.00 outside the US). \$2.00 discount for orders placed before October 31, 1989, and for pre-paid orders. I understand that the bound volume is *in addition to* my regular subscription and is available only to subscribers. (To be shipped in early 1990. Sorry, bound volumes for years prior to 1989 are not available.) *All bound volume orders must be received by December 31, 1989.*

☐ Check enclosed ☐ Bill me
☐ VISA ☐ MasterCard ☐ American Express

card # _____ exp. _____

signature/P.O. # _____

printed in USA

Name _____

Address _____

City/State/Zip _____

MD residents, please add 5% sales tax. Subscription orders from outside the US must be prepaid in US dollars only.

Residents, Fellows, Interns, and Students: when applying for the in-training rate, available for 3 years, please specify name of institution and training status. Rates valid through October 31, 1989.

Please allow 8 weeks for order processing and delivery of your first issue. Surface mail delivery to countries outside the US may take up to 16 weeks. Airmail rates available upon request.

Williams & Wilkins

P.O. Box 23291
Baltimore, Maryland 21203

The Broadway Centre
2-6 Fulham Broadway
London SW6 1AA England



JNRA91 1179

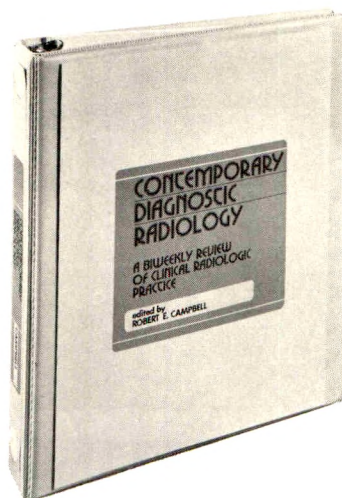
You learn from your experience with **CONTEMPORARY DIAGNOSTIC RADIOLOGY**

Editor: **Robert E. Campbell, M.D.**

A Biweekly Review of Clinical Radiologic Practice—26 issues a year!

One of your toughest jobs is keeping up with the many new developments that affect radiology. That's why you want **Contemporary Diagnostic Radiology**... an effective and convenient way to perfect your skills and maintain your professional status.

Contemporary Diagnostic Radiology is designed as a continuing education program that lets you work at your own pace. Every two weeks you'll receive an issue that covers a single topic or procedure in detail. Read the information and study the clearly reproduced radiographs—and then, if you choose, respond to a comprehensive examination in the strictest confidence. You set the pace. Each biweekly lesson brings you pertinent review of the basics in bone radiology... gastrointestinal radiology... pediatric radiology... genitourinary radiology... MR imaging... and all of the topics you want to know more about.



Contemporary Diagnostic Radiology works two ways. You may choose to subscribe to the non-scoring version, receiving every issue as an important element of your professional reading. The scoring version, however, supplements your reading and computer-coded examinations with confidential result responses, making you eligible for Continuing Medical Education credits co-sponsored by the University of Pennsylvania School of Medicine.

"As an organization for continuing medical education, the University of Pennsylvania School of Medicine designates this continuing medical education activity as meeting the criteria for 1 credit hour per bi-weekly issue in Category I for Educational Materials for the Physician's Recognition Award of the American Medical Association provided it has been completed according to instructions."

You can begin this ongoing program today. **Contemporary Diagnostic Radiology** is a year-round program, so you can join at any time. To begin your lessons, just fill out the enclosed card and return it to us. Or call **FREE** 1-800-638-6423. In Maryland call 1-800-638-4007. You'll find that **Contemporary Diagnostic Radiology** is the most efficient and inexpensive way to keep up with your dynamic field.

Williams & Wilkins

P.O. Box 23291
Baltimore, Maryland 21203



The Broadway Centre
2-6 Fulham Broadway
London SW6 1AA England

clip & mail

CONTEMPORARY DIAGNOSTIC RADIOLOGY

- ☐ **Yes!** I want to keep pace in my field! Begin my 26-issue subscription:
- ☐ Send me the scoring version (\$230)
- ☐ Send me the non-scoring version (\$180)
- ☐ Send me the resident non-scoring version (\$115) (add \$45 for optional air mail delivery outside the U.S.)
- ☐ new subscription
- ☐ renewal

name _____

address _____

city/state/zip _____

payment options

- ☐ payment enclosed
- ☐ American Express

- ☐ bill me
- ☐ MasterCard

☐ VISA

card # _____

expiration date _____

signature/P.O. # _____

Maryland residents add 5% sales tax. Subscriptions outside the U.S. must be prepaid in U.S. dollars only. Rates subject to change without notice. Please allow 8 weeks for delivery of your first issue, up to 16 weeks for surface delivery outside the U.S. Optional airmail rates add \$45 per subscription.

Residents are eligible for the special in-training rate for up to three years. When requesting this rate, please include training status and institution.



Don't forget: you can order with a **FREE** phone call at 1-800-638-6423. In Maryland, call 1-800-638-4007.

Williams & Wilkins

P.O. Box 23291
Baltimore, Maryland 21203

The Broadway Centre
2-6 Fulham Broadway
London SW6 1AA England

GET THE MOST OUT OF IMAGING PROCEDURES

NEW!

Fetal Sectional Anatomy and Ultrasonography

Lewis H. Nelson III, MD and
Walter J. Bo., PhD

Enhance your interpretive skills with the one text that helps you translate the two-dimensional images on paper to the three-dimensional image you actually see.

Combining images and drawings, this text-free atlas provides the facts you need to get the most out of ultrasonographic procedures. Anatomical sections that feature both sagittal and transverse orientation make this book easy to use during scanning, while the clearly-labeled illustrations eliminate the need for cross-referencing to tables.

Drs. Nelson and Bo have created an atlas which employs not only ultrasonography, but also magnetic resonance imaging and computer tomography as imaging modalities to present a complete reference of fetal anatomy. Serial transverse sections of a mid-pregnancy male fetus and sagittal sections of a term, anencephalic female fetus are labeled on the actual image for easy identification at a glance.

1988/224 pages/365 illustrations/6400-2/\$65.00/\$78.00 outside the US and Canada

NEW!

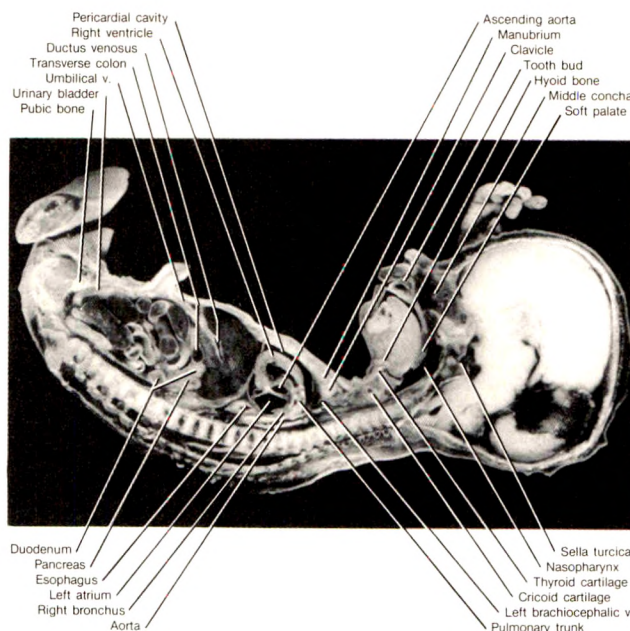
Computed Cranial and Spinal Imaging A Practical Introduction

John M. Stevens

Superb illustrations and eminent authors distinguish this new work on optimal imaging of neurological disorders.

From initial choice of imaging modality through interpretation of results, this text spells out exactly how to approach investigation and management decisions, with the strengths, limitations, and uses of CT and MRI examined clearly and in detail. Both normal and pathological appearances of the brain, spine, paranasal sinuses, and orbits are examined with extensive accompanying illustrations. You'll also find essential information on when to administer intravenous or intrathecal contrast enhancement.

1988/224 pages/illustrated/
7931-X/\$44.95 (available only in
North America)



Ordering is as easy as picking up your phone:

In the US just dial, toll-free
1-800-638-0672.

30 day FREE trial for all books! (US only)



Williams & Wilkins

428 East Preston Street
Baltimore, Maryland 21202

Broadway House
2-6 Fulham Broadway
London SW6 1AA England



STATE UNIVERSITY OF NEW YORK
HEALTH SCIENCE CENTER
AT BROOKLYN
Department of Radiology

ACADEMIC RADIOLOGY POSITIONS AVAILABLE AT ALL APPOINTMENT LEVELS

Vacancies Exist In General Radiology
and Sub-Specialty Areas

Salary level commensurate with experience and highly competitive to the greater New York area. Contact: Joshua A. Becker, M.D., Professor and Chairman, SUNY Health Science Center at Brooklyn, 450 Clarkson Avenue, Brooklyn, NY 11203. (718) 270-1503.

EO/AA Employer

DMC#C-0229

RADIOLOGISTS

Radiology Department at Marshfield Clinic (13 radiologists) is presently expanding. We are recruiting radiologists with expertise in fields of neuro-imaging, body imaging and general diagnostic radiology. Very busy clinical practice (approximately 270 physicians) and hospital practice (525 beds). Total examinations: approximately 170,000 per year and expanding. State of the art equipment in all modalities. For further information, please write or call:

Dr. William Manor
Department of Radiology

1000 North Oak Ave.
Marshfield, WI 54449
(715) 387-5261



MarshfieldClinic

*for prompt
subscription
service...*

attach label here

Please use this coupon and attach a *recent* label in the space provided when writing to us about:

- change of address
- renewal
- questions regarding your subscription

Please use the space below to indicate your *new* address.

Name of Journal _____

Name _____

Address _____

City/State/Zip _____

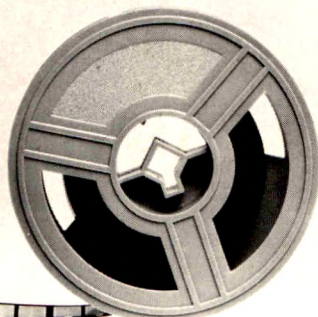
THE WILLIAMS & WILKINS COMPANY

428 East Preston Street/Baltimore, Maryland 21202

Need shelf space?

Williams & Wilkins is your source for back issues of this journal in microform.

Free Up 98%
Of Your Shelf
Space With
Microform
Conversion



MICROFILM editions are available for this journal direct from the publisher.

Many Williams & Wilkins journals as well as those journals distributed by the Publishing Services Division of Waverly Press, Inc. are also available for a single volume year or on a standing order basis.

FOR ORDERING INFORMATION:
Write to the address below or call **TOLL-FREE 1-800-638-6423**.
In Maryland call **COLLECT** 528-4105.

☐ **Please send me microform back issue ordering information for**

Journal Name _____

Name _____

Title _____

Address _____

City/State/Zip _____

Mail to:

Williams & Wilkins

Microform Sales
Attention: Yvonne Hahn
428 East Preston Street
Baltimore, Maryland 21203
or
266 Fulham Road
London SW10 9EL England

Formats available:

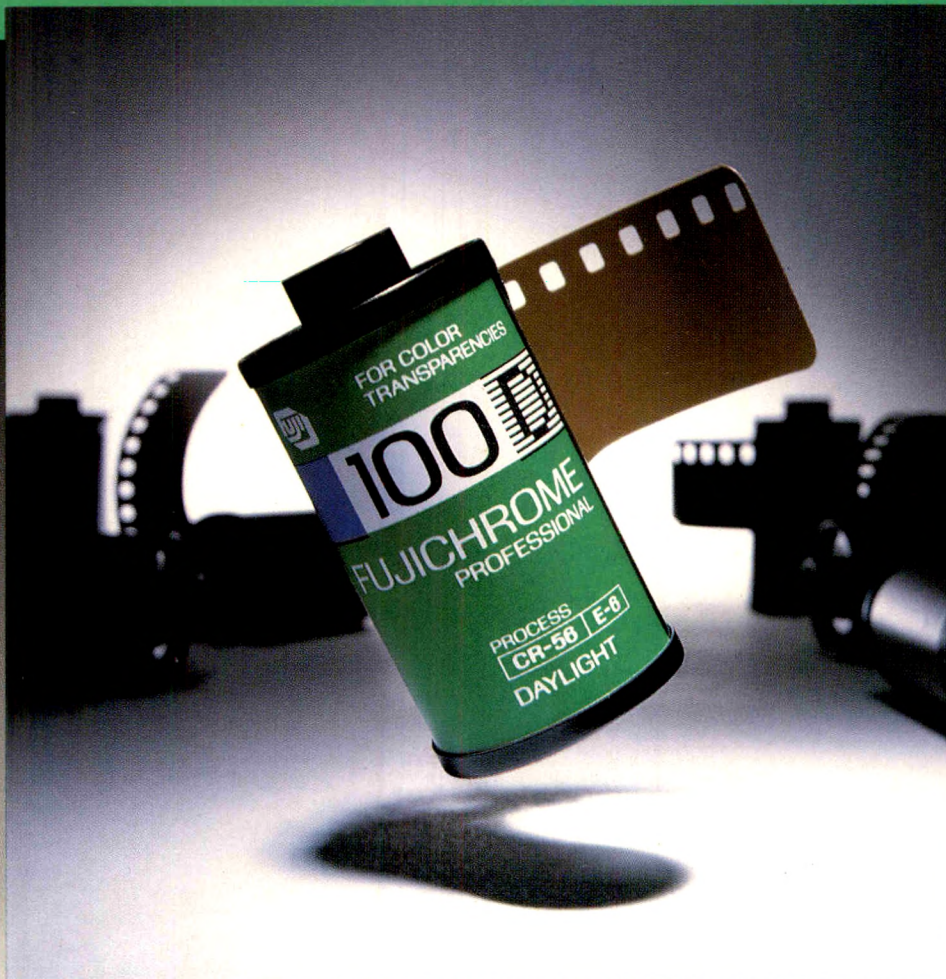
- 16-mm reel
- 35-mm reel
- 16-mm cartridge (3M or Kodak)
- positive or negative film

MICROAD 50567

INDEX TO ADVERTISERS

Berlex Imaging	A17, A18, A19, A20
Eastman Kodak	A6, A7
Elema Schonander	A23
E-Z-EM Company	Cover 2
FUJI	Cover 3
General Electric	A14, A15, A24, A25
Mallinckrodt, Inc.	A9, A10, A11, A12
Marshfield Clinic	A29
NAMIC	A2
Nuclear Associates.....	A27
Osler Institute	A26
S & S X-Ray	A17
SUNY Health Science Center at Brooklyn.....	A29
University of Southern California	A28
Winthrop Laboratories	A21, A22

We try to present an accurate index. Occasionally this may not be possible because of a last-minute change or omission.



The reason for change . . . It's better

No one likes change . . . particularly professional and serious amateur photographers. So when they began switching to Fuji color film world wide, there could only be one reason . . . the right reason. It's better!

Have you evaluated Fuji Medical radiographic films lately?

Call your Fuji representative or 800-431-1850.

CIRCLE 7 ON READER SERVICE CARD



The Reason for Change!

Durham, Chicago, Stamford, CT



PROGRESS IN RADIOLOGY

- 1 Preoperative imaging-guided needle placement and localization of clinically occult breast lesions. *Kopans DB, Swann CA*
- 11 Nonsurgical therapy of gallstones: implications for imaging. *Simeone JF, Mueller PR, Ferrucci JT*
- 19 Visual fuzzy cluster analysis of MR images. *Young SW, Ballerio C, Carrol CL*

PULMONARY RADIOLOGY

- 27 Superior mediastinal widening from spine fractures mimicking aortic rupture on chest radiographs. *Dennis LN, Rogers LE*

- 123 Case report. Torsion of normal uterine adnexa before menarche: CT appearance. *Bellah RD, Griscom NT*
- 125 Case report. Mediastinal bronchogenic cyst: prenatal sonographic diagnosis. *Young G, L'Heureux PR, Krueckeberg ST, Swanson DA*
- 128 Case report. MR imaging of double-outlet right ventricle. *Akins EW, Martin TD, Alexander JA, Knauf DG, Victorica BE*

NEURORADIOLOGY

- 131 Dyke award. Gd-DTPA-enhanced MR imaging of experimental bacterial meningitis: evaluation and comparison with CT. *Mathews VP, Kuharik MA, Ed-*

Dec 13. 11. 90

AJR

American
Journal of
Roentgenology

February 1989

This issue: ARRS Meeting Section

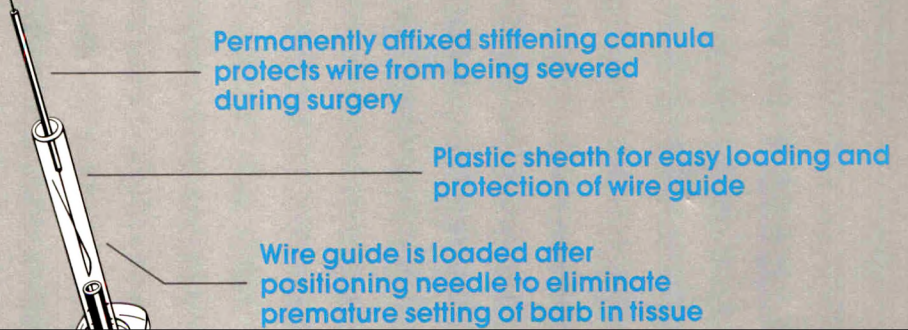
Precise localization of non-palpable lesions ...from E-Z-EM

PercuGuide™

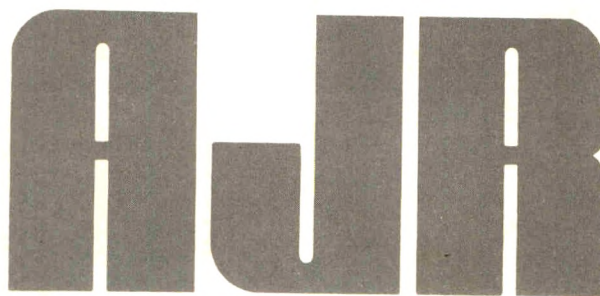
Regardless of your present method of marking non-palpable lesions, PercuGuide™ can improve upon it.

Unlike improvised markers, PercuGuide can't shift with patient movement. It won't disperse over time like a dye. And PercuGuide offers a range of refinements that no other wire guide system can match.

Afterloading of the PercuGuide wire guide eliminates any chance of the barb seating before the needle has been properly positioned. A plastic



Official Journal of the American Roentgen Ray Society



American Journal of Roentgenology
Diagnostic Imaging and Related Sciences

- Editor-In-Chief** Robert N. Berk, *La Jolla, California*
University of California, San Diego
School of Medicine and Medical Center
- Editor Emeritus** Melvin M. Figley, *Seattle, Washington*
- Associate Editor** Saskia von Waldenburg Hilton, *San Diego, California*
- Consulting Editor** Juan M. Taveras, *Boston, Massachusetts*
- Statistician** Charles C. Berry, *San Diego, California*

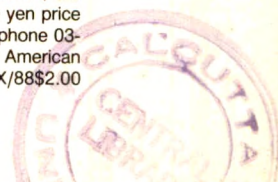
Editorial Board

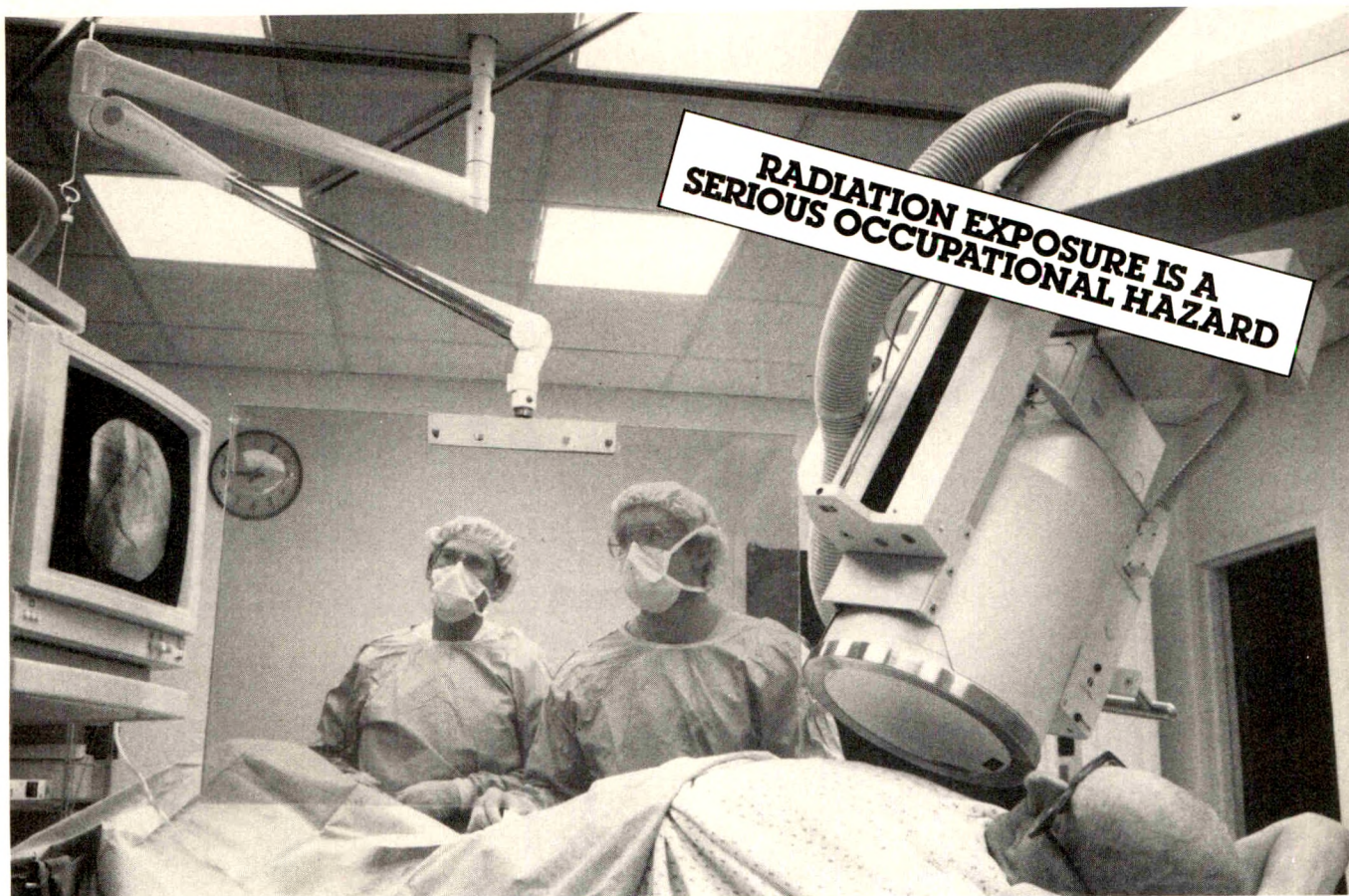
- | | | |
|-------------------------|--------------------------|--------------------|
| John R. Amberg | William R. Hendee | Peter M. Ronai |
| Itamar Aviad | John R. Hesselink | Sjef H. J. Ruijs |
| Lawrence W. Bassett | Charles B. Higgins | Carol M. Rumack |
| Gregory P. Borkowski | Melvyn T. Korobkin | Stuart S. Sagel |
| William G. Bradley, Jr. | Thomas L. Lawson | David J. Sartoris |
| Peter L. Cooperberg | Bruce L. McClennan | Stefan C. Schatzki |
| N. Reed Dunnick | Albert A. Moss | Edward A. Sickles |
| David K. Edwards | Jeffrey H. Newhouse | Barry A. Siegel |
| Ronald G. Evens | Donald L. Resnick | David D. Stark |
| David S. Feigin | Stewart R. Reuter | Edward T. Stewart |
| Paul J. Friedman | Charles A. Rohrmann, Jr. | Eric vanSonnenberg |

Editorial Staff: Margaret Levene, *managing editor*; Katie L. Spiller, Barbara Rose, Barbara L. Halliburton, and Janine Anderson, *manuscript editors*; Nancy Rydbeck, *office manager*; Sheri Smith, *administrative assistant*; Sandra L. Griffin, *administrative secretary*.

AJR, AMERICAN JOURNAL OF ROENTGENOLOGY (ISSN 0361 803X) is the official journal of the American Roentgen Ray Society and is published monthly by Williams & Wilkins, 428 E. Preston St., Baltimore, MD 21202. Annual dues include \$50 for journal subscription. Second-class postage paid at Baltimore, MD, and at additional mailing offices. Postmaster, send address changes (Form 3579) to AJR, 428 E. Preston St., Baltimore, MD 21202. Subscription rates \$100 (\$135 foreign); institutions \$110 (\$145 foreign); in training \$25 (\$50 foreign); single copy \$16 (\$19 foreign). Japanese rates include airfreight. Japanese yen price is available from our sole agent USACO Corporation, 13-12, Shimbashi 1-Chome, Minato-Ku, Tokyo 105, Japan, telephone 03-502-6471. Airmail rates furnished on request. Indexed by *Current Contents* and *Index Medicus*. Copyright © 1988 by American Roentgen Ray Society.

0361-803X/88\$2.00





Cardiac Cath and Special Procedures Personnel...

NOW YOU CAN GET GREATER RADIATION PROTECTION WITH CLEAR-Pb® Fixed-Mount Overhead X-Ray Barriers

*In 4 panoramic shield sizes...18" x 24" to 36" x 24"...
at budget-pleasing prices.*

- **Unsurpassed radiation protection;** shatter-resistant, transparent lead-plastic (0.5mm lead equivalency).
- **Bigger shielding area and panoramic visibility;** no need to reposition the barrier during procedure; protects two people, if required.
- **Easy-to-use, adjustable, spring-loaded fixed ceiling mounted suspension system;** pull down to use, push up and out of the way at the end of the procedure

Existing lead-glass overhead barriers (usually 16" x 12" or 20" x 16") are so small that when you move, you must also move the barrier to avoid exposure. Now, depending on your needs and budget, you can select from 4 CLEAR-Pb Overhead Barriers with panoramic shield sizes from 18" x 24" to 36" x 24", and get greater protection from scatter radiation.

For complete details, request Bulletin 423-44

CIRCLE 16 ON READER SERVICE CARD

NUCLEAR ASSOCIATES



A Division of VICTOREEN, INC.
100 VOICE ROAD
CARLE PLACE, NY 11514-1593 U.S.A.
(516) 741-6360
FAX (516) 741-5414

® Victoreen, Inc.

AJR Guidelines for Authors

Address new and revised manuscripts, correspondence, and classified ads to the Editor:

AJR Editorial Office
2223 Avenida de la Playa, Suite 200
La Jolla, CA 92037-3218
Telephone: (619) 459-2229; FAX: (619) 459-8814

Inquiries regarding subscriptions, display advertising, reprints, or permission to republish *AJR* material should be addressed to the publisher:

The Williams & Wilkins Co.
428 E. Preston St.
Baltimore, MD 21202 Telephone: (301) 528-4133

The *AJR* publishes original contributions to the advancement of medical diagnosis and treatment. Submitted manuscripts should not contain previously published material and should not be under consideration for publication elsewhere. Papers dealing with neuroradiology should be addressed to: American Journal of Neuroradiology, Dept. of Radiology, Massachusetts General Hospital, Boston, MA 02114. At the discretion of the *AJR* Editor, *AJNR* articles that are of interest to the general reader may be republished in the *AJR*. Neuroradiologic papers sent to the *AJR* will be forwarded to the Editorial Office of the *AJNR*.

Manuscript decisions are based on peer review. Reviewers receive manuscripts without title pages to ensure an unbiased review. Statements made in the article, including changes made by the Editor or manuscript editor, are the responsibility of the author and not of the *AJR* or its publisher. Authors will be sent the edited manuscript, galley proof, and proofs of illustrations. If the corresponding author will be unavailable to review galleys, arrangements should be made for a coauthor or colleague to read and return the proof.

The following guidelines are based on instructions set forth in the **Uniform Requirements for Manuscripts Submitted to Biomedical Journals** (*Ann Intern Med* 1988;108:258-265). Articles will be edited, however, to conform to the individual style of *AJR*.

General Guidelines for Major Papers

Abstract. Clearly state (in 200 words or less) the purpose, methods, results, and conclusions of the study. Include actual data.

Introduction. Briefly describe the purpose of the investigation, including relevant background information.

Methods. Describe the research plan, the materials (or subjects), and the methods used, in that order. Explain in detail how disease was confirmed and how subjectivity in observations was controlled.

Results. Present results in a clear, logical sequence. If tables are used, do not duplicate tabular data in text, but do describe important trends and points.

Discussion. Describe the limitations of the research plan, materials (or subjects), and methods, considering both the

purpose and the outcome of the study. When results differ from those of previous investigators, explain the discrepancy.

AUTHOR'S CHECKLIST

For priority handling, complete the following checklist, sign the copyright form on the reverse side of this page, and include both with the manuscript.

_____ Two copies of the manuscript (the original and a photocopy) and two complete sets of figures are submitted. One copy has been retained by the author.

_____ If appropriate, *AJR* Guidelines for case reports, technical notes, pictorial essays, or letters to the Editor have been followed. (See page A5.)

_____ The manuscript, including references, figure legends, and tables, is typed double-spaced on 8½ × 11 in. (21.6 × 27.9 cm) nonerasable paper. Right-hand margins are not justified.

_____ All manuscript pages are numbered consecutively beginning with the abstract. Authors' names do not appear on the manuscript pages.

_____ The manuscript is organized as follows: title page, blind title page (title only), abstract, introduction, methods, results, discussion, acknowledgments, references, tables, figure legends, and figures.

_____ Informed consent has been obtained from patients who participated in clinical investigations. If experiments were performed on animals, authors complied with NIH guidelines for use of laboratory animals.

_____ Use of unfamiliar acronyms and abbreviations is kept to a minimum. When abbreviations are used they are defined at first mention, followed by the abbreviation in parentheses.

_____ Metric measurements are used throughout, or the metric equivalent is given in parentheses.

_____ Names and locations (city and state only) of manufacturers are given for equipment and nongeneric drugs.

Title Page

_____ The following information is given: title of article; names and complete addresses (including zip code) of all authors; current addresses of authors who have moved since study; acknowledgment of grant or other assistance. The corresponding author is clearly identified, and a current address, phone number, and Fax number are given.

_____ Two copies of a blind title page are included giving only the title (without the authors' names) for use in the review process.

Abstract

_____ An abstract of approximately 200 words concisely states the purpose, methods, and results of the study in one paragraph. Actual data are included. Conclusions are stated in a second, summary paragraph.

_____ No abbreviations or reference citations are used.

References

References (not to exceed 35) are typed double-spaced starting on a separate page and are **numbered consecutively in the order in which they appear in the text**.

All references are cited in the text and are enclosed in brackets and typed on line with the text (not superscript).

Unpublished data are not cited in the reference list, but are cited parenthetically in the text, for example, (Smith DJ, personal communication), (Smith DJ, unpublished data). This includes papers submitted, but not yet accepted, for publication.

Inclusive page numbers (e.g., 333–335) are given for all references.

Journal names are abbreviated according to *Index Medicus*.

Style and punctuation of references follow the format illustrated in the following examples (all authors are listed when six or less; when seven or more authors, the first three are listed, followed by “et al.”):

Journal article

1. Long RS, Roe EW, Wu EU, et al. Membrane oxygenation: radiographic appearance. *AJR* **1986**;146:1257–1260

Book

2. Smith LW, Cohen AR. *Pathology of tumors*, 6th ed. Baltimore: Williams & Wilkins, **1977**:100–109

Chapter in a book

3. Breon AJ. Serum monitors of bone metastasis. In: Clark SA, ed. *Bone metastases*. Baltimore: Williams & Wilkins, **1983**:165–180

Paper presented at a meeting

4. Lau FS, Kirk AN. MR imaging of the spine. Presented at the annual meeting of the American Roentgen Ray Society, Washington, DC, April **1986**

Tables

Each table is typed double-spaced on a separate page without vertical or horizontal rules; each has a short, descriptive title. Tables do not exceed two pages in length and contain at least four lines of data.

Tables are numbered in the order in which they are cited in the text.

Abbreviations are defined in an explanatory note below each table.

Tables are self-explanatory and do not duplicate data given in the text or figures.

All arithmetic (percentages, totals, differences) has been double checked for accuracy, and tabular data agree with data given in the text.

Figures and Legends

Two complete sets of original figures are submitted unmounted in labeled envelopes.

Figures are clean, unscratched, 5 × 7 in. (13 × 18 cm) glossy prints with **white borders**. A separate print is submitted for each figure *part*.

All figure parts relating to one patient have the same figure number.

Each figure is labeled on the back with the figure number and an arrow indicating “top.” For black-and-white figures, labeling is done on a gummed label, which is then affixed to the back of the print. *Never* use labels on color figures, but write figure number on the back lightly in pencil. *Never* use ink on front or back of any figures.

Author’s names are *not* written on the backs of figures.

Only removable (rub-on) arrows and letters are used on the figures. Symbols are uniform in size and style and are not broken or cracked.

Images are uniform in size and magnification.

Line drawings are done in black ink on a white background. They are professional in quality, and all use the same size type. (Only glossy prints are acceptable.)

Written permission has been obtained for use of all previously published illustrations (and copies of permission letters are included), and an appropriate credit line is given in the legends.

Legends are typed double-spaced, and figure numbers correspond with the order in which the figures are cited in the text.

Transfer of Copyright Agreement, Conflict of Interest Acknowledgment, Certification of Coauthors, and Exclusive Publication Statement

Complete copyright to the article entitled: _____

is hereby transferred to the American Roentgen Ray Society (for United States government employees to the extent transferable), effective if and when the article is accepted for publication in the *American Journal of Roentgenology*. In the case of the authors who are officers or employees of the United States government, the American Roentgen Ray Society recognizes that works prepared by officers or employees of the United States government as part of their official government duties are in the public domain.

Authors reserve all proprietary rights other than copyright, such as patent rights and the right to use all or part of this article in future works of their own. The authors retain the right of replication, subject only to crediting the original source of publication and receiving written permission from the publisher.

Authors guarantee that this manuscript contains no matter that is libelous or otherwise unlawful, invades individual privacy, or infringes any proprietary rights.

Authors understand that they will receive no royalty or other compensation from the American Roentgen Ray Society or the publisher.

Authors guarantee that the editor has been or will be informed of any proprietary or commercial interest or conflicts of interest the authors may have that relate directly or indirectly to the subject of this article.

All authors certify that they have made substantive and specific intellectual contributions to the article and assume public responsibility for its content.

Finally, the authors certify that none of the material in this manuscript has been published previously or is currently under consideration for publication elsewhere.

First author/date

Second author

Third author

Fourth author

Fifth author

Sixth author

This agreement must be signed by all authors in order for the manuscript to be published.

Case Reports

A case report is a brief description of a special case that provides a message that transcends the individual patient.

Format. There is no abstract. The introduction should be a short paragraph giving the general background and the specific interest of the case. No more than one case should be described in detail (similar ones can be mentioned briefly in the discussion). Emphasis should be on the radiologic aspects; clinical information must be limited to that necessary to provide a background for the radiology. The discussion should be succinct and should focus on the specific message and relevance of radiologic methods. A review of the literature is not appropriate.

Length. Maximum of five double-spaced, typewritten pages, including the references but not the title page or figure legends.

References. Maximum of eight.

Figures. Maximum of three or four, unless the text is shortened accordingly. Legends must not repeat the text.

Tables and Acknowledgments. Not appropriate in case reports.

Technical Notes

A technical note is a brief description of a specific technique or procedure, modification of a technique, or equipment of interest to radiologists.

Format. No abstract, headings, or subheadings are required. If headings are used, they should be a combination of "Case Report," "Materials and Methods," "Results," and "Discussion." A brief one-paragraph introduction should be included to give the general background. Discussion should be limited to the specific message, including the uses of the technique or equipment. Literature reviews and lengthy case reports are not appropriate.

Length. Maximum of five double-spaced, typewritten pages, including the references but not the title page or figure legends.

References. Maximum of eight.

Figures. Maximum of two, unless the text is shortened accordingly.

Tables and Acknowledgments. Not appropriate in technical notes.

Pictorial Essays

A pictorial essay is an article that conveys its message through illustrations and their legends. Unlike other AJR articles, which are based on original research, pictorial essays serve primarily as teaching tools, like exhibits at a scientific meeting. They are not encyclopedic book chapters. No abstract is necessary.

Length. Maximum of four double-spaced, typewritten pages, including the references but not the title page or figure legends.

References. Maximum of four.

Figures. Maximum of 30 figure parts. Number should be as few as necessary to convey the message of the paper.

Tables and Acknowledgments. Not appropriate in pictorial essays.

Letters to the Editor and Replies

Letters to the Editor and Replies should offer objective and constructive criticism of published articles. Letters may also discuss matters of general interest to radiologists. Do not end a letter with a hand-written signature.

Format. All letters should be typed double-spaced on nonletterhead paper, with no greeting or salutation. Name and affiliation should appear at the end of the letter. Titles for letters should be short and pertinent. The title for a reply is simply "Reply."

Length. Maximum of two double-spaced, typewritten pages, including references.

References. Maximum of four.

Figures. Maximum of two.

Tables and Acknowledgments. Not appropriate in Letters to the Editor and Replies.

Opinions, Commentaries, and Perspectives

Opinions, commentaries, and perspectives are special articles dealing with controversial topics or issues of special concern to radiologists.

Format. Include a title page but no abstract. Headings may be used to break up the text.

Length. Maximum of five double-spaced, typewritten pages.

References. Maximum of five.

Tables and Figures. Maximum of four.

Computer Page Articles

Articles published on the computer page deal with practical computer applications to radiology.

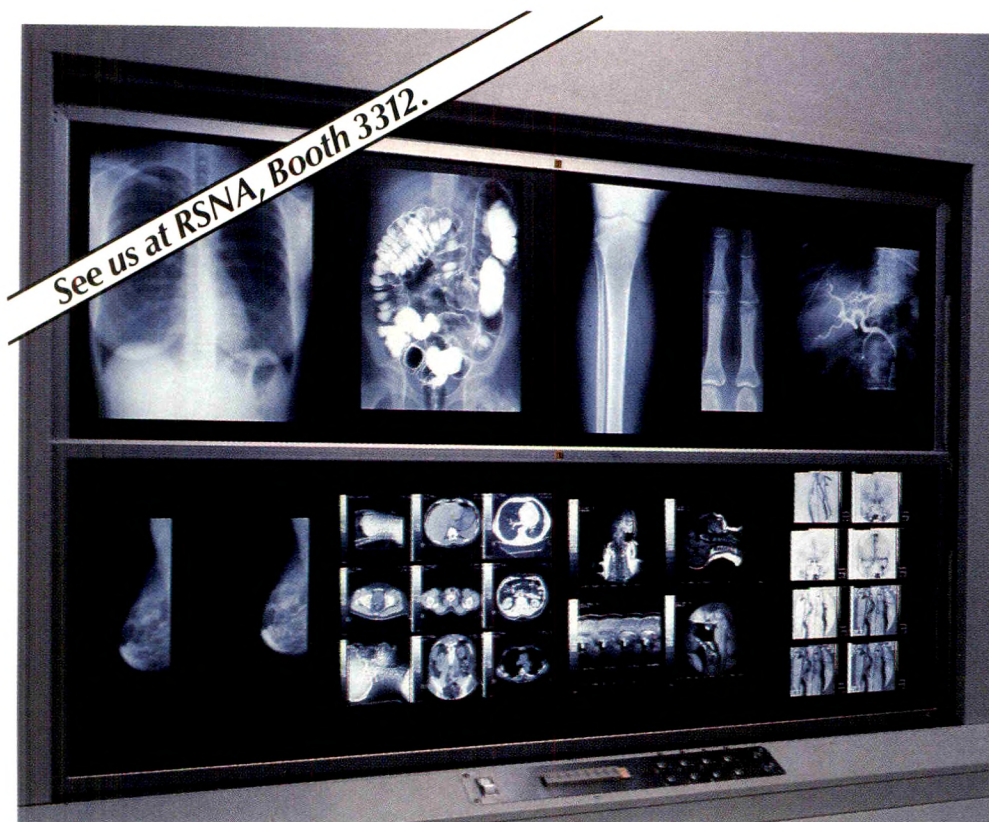
Format. Include a title page but no abstract.

Length. Maximum of eight double-spaced, typewritten pages.

References. Maximum of five.

Figures and Tables. Maximum of five. Computer printouts are not acceptable. Figures must be submitted as 5 × 7 in. glossy prints.

**THE
RIGHT FILM
FOR EVERY
SUBJECT
FROM
KODAK**



Whatever the procedure, there's always a Kodak film for the job. Always with the quality you've come to expect from Kodak.

There's a Kodak film for every diagnostic imaging modality and procedure—including extremities, mammography, photofluorography, cinefluorography, duplicating and radiation therapy. In fact, there's usually an array of films for each purpose, so there's not only one that's right for the job, but right for the particular subject as well.



They're all there when you need them, each with the consistent quality you expect from any Kodak product. All with the service and support that help make them as cost-effective as they are good. Your Kodak representative has the details.



The new vision of Kodak



AJR Business and Subscriber Information

The American Roentgen Ray Society

AJR, *American Journal of Roentgenology*, is published monthly to disseminate research on current developments in the radiologic sciences and commentary on topics related to radiology. It is published by the American Roentgen Ray Society, 1891 Preston White Dr., Reston, VA 22091; (703) 648-8992. Inquiries regarding society business, the annual ARRS meeting, and membership should be addressed to the Society at the above address.

Correspondence Concerning the AJR

Correspondence regarding display (not classified) advertising, subscriptions, address changes, reprints, and permission requests should be addressed to Williams & Wilkins, 428 E. Preston St., Baltimore, MD 21202; (301) 528-4000.

Correspondence regarding editorial matters and classified advertising should be addressed to Editorial Office, *AJR*, 2223 Avenida de la Playa, Ste. 200, La Jolla, CA 92037-3218; telephone (619) 459-2229; FAX (619) 459-8814. For information on manuscript submission, see *Guidelines for Authors*, pages A3-A5.

Subscriber Information

Subscription requests and inquiries should be sent to Williams & Wilkins, 428 E. Preston St., Baltimore, MD 21202. ARRS annual dues include \$50 for journal subscription. Subscription rates are as follows: nonmembers, \$100/year (\$135 foreign); institutions, \$110 (\$145 foreign); nonmember in-training, \$25 (\$50 foreign). Single copies of the Journal may

be purchased for \$16 (\$19 foreign). Airmail rates will be furnished on request.

Japanese rates include airfreight. Japanese yen price is available from our sole agent, USACO Corporation, 13-12, Shimbashi 1-Chome, Minato-Ku, Tokyo 105, Japan; telephone 03-502-6471.

If a subscriber receives a damaged copy of the *AJR* or fails to receive an issue, the subscriber should notify Williams & Wilkins (428 E. Preston St., Baltimore, MD 21202) within 60 days of publication (90 days for foreign subscribers) and that issue will be replaced.

Change of address information should be sent to Williams & Wilkins, 428 E. Preston St., Baltimore, MD 21202. Allow 90 days for address changes.

Copyrights, Permissions, and Reprints

The American Roentgen Ray Society holds the copyright for all material published in the *AJR*. No part of this publication may be reproduced without permission from the ARRS. Requests for such permission should be addressed to Williams & Wilkins, 428 E. Preston St., Baltimore, MD 21202.

For reprints of a particular article, please contact the author designated in the footnotes for that article.

Indexes

The *AJR* provides volume and yearly indexes (subject and author) in the June and December issues each year. *AJR* articles are also indexed in *Current Contents*, *Index Medicus*, and the cumulative index published by *Radiology*.

The image features a central, highly reflective globe showing the continents of North and South America. The globe is overlaid with a grid of orange lines. Above the globe, a larger grid of orange lines is visible, containing various abstract, high-contrast images that appear to be data or satellite imagery. The background is a deep blue gradient, and the globe casts a shadow on the surface below it.

SAFETY IN NUMBERS.



AFTER 15 MILLION



SAFETY IN NUMBERS.


Every year the numbers grow.
To date, over 500 published
studies and articles with over
75,000 patients document the
safety, tolerance, and comfort
of nonionic OMNIPAQUE.

No other nonionic contrast
medium has been studied
more!¹

And to complete the picture,
nonionic OMNIPAQUE delivers
consistently sharp images to
support your diagnoses.

Safety. Tolerance. Image quality.
Simple words. Reliable facts.

Reference: 1. Data on file, Winthrop Pharmaceuticals.

NONIONIC
OMNIPAQUE[®] 
(IOHEXOL)

THE IMAGE OF SAFETY.

PROCEDURES,* SAFETY IS A FACT.

*Approximation of over 15 million radiographic procedures worldwide is based on quantities of nonionic iohexol sold, used at recommended dosages.

See next page for important product information concerning contraindications, warnings, adverse reactions, patient selection, and prescribing and precautionary recommendations.

OMNIPAQUE® 240 300 350

INJECTION (IOHEXOL) INTRAVASCULAR

PLEASE CONSULT FULL PRODUCT INFORMATION BEFORE USING.
A SUMMARY FOLLOWS:

DESCRIPTION: OMNIPAQUE is a sterile, pyrogen- and preservative-free, nonionic, water-soluble radiographic contrast medium for intravascular administration in concentrations of 240, 300, and 350 mgI/mL. OMNIPAQUE 240 contains 518 mg of iohexol equivalent to 240 mg of organic iodine per mL; OMNIPAQUE 300 contains 647 mg of iohexol equivalent to 300 mg of organic iodine per mL; and OMNIPAQUE 350 contains 755 mg of iohexol equivalent to 350 mg of organic iodine per mL. Each milliliter of iohexol solution contains 1.21 mg tromethamine and 0.1 mg edetate calcium disodium with the pH adjusted between 6.8 and 7.7 with hydrochloric acid or sodium hydroxide. Unused portions must be discarded. Iohecol solution is sensitive to light and should be protected from exposure.

CONTRAINDICATIONS: OMNIPAQUE should not be administered to patients with a known hypersensitivity to iohecol.

WARNINGS: OMNIPAQUE should be used with extreme care in patients with severely impaired renal and/or hepatic function; severe thyrotoxicosis, hyperthyroidism, or an autonomously functioning thyroid nodule; diabetes with a serum creatinine level above 3 mg/dL. It is not recommended for use in patients with anuria.

Patients with known or suspected pheochromocytoma should receive a minimum of contrast medium if the benefit of the examination is judged to outweigh its risk; blood pressure should be monitored throughout the procedure, and measures for the treatment of hypertensive crisis should be readily available.

Contrast agents are potentially hazardous in patients with multiple myeloma or other paraproteinemia, particularly those with therapeutically resistant anuria. The combination of contrast agent and dehydration may precipitate myeloma protein in the renal tubules. No form of therapy, including dialysis, has been successful in reversing the effect. Myeloma, which occurs most commonly in persons over age 40, should be considered before instituting intravascular administration of contrast agents.

Ionic contrast media, when injected intravenously or intra-arterially, may promote sickling in individuals who are homozygous for sickle cell disease.

PRECAUTIONS: Diagnostic procedures that involve the use of radiopaque diagnostic agents should be carried out under the direction of personnel with the prerequisite training and with a thorough knowledge of the particular procedure to be performed. Appropriate facilities should be available for coping with any complication of the procedure, as well as for emergency treatment of severe reactions to the contrast agent itself. Competent personnel and emergency facilities should be available for at least 30 to 60 minutes, since severe delayed reactions have occurred (see ADVERSE REACTIONS). The possibility of serious, life-threatening, fatal, anaphylactoid, or cardiovascular reactions should always be considered (see ADVERSE REACTIONS). It is of utmost importance that a course of action be carefully planned in advance for immediate treatment of serious reactions. Preparatory dehydration is dangerous and may contribute to acute renal failure in patients with advanced vascular disease, in diabetic patients, and in susceptible nondiabetic patients (often elderly with preexisting renal disease), infants, and small children. *Patients should be well hydrated prior to and following iohecol administration.* Careful consideration of the potential risk of acute renal failure should be given before performing excretory urography in diabetic patients with diabetic nephropathy and in susceptible nondiabetic patients (often elderly with preexisting renal disease). Immediately following surgery, excretory urography should be used with caution in renal transplant recipients. The possibility of an idiosyncratic reaction in susceptible patients should always be considered (see ADVERSE REACTIONS). The susceptible population includes, but is not limited to, patients with a history of a previous reaction to contrast media, patients with a known sensitivity to iodine per se, and patients with a known clinical hypersensitivity: bronchial asthma, hay fever, and food allergies. A thorough medical history with emphasis on allergy and hypersensitivity, prior to the injection of any contrast media, may be more accurate than pretesting in predicting potential adverse reactions.

A positive history of allergies or hypersensitivity does not arbitrarily contraindicate the use of a contrast agent where a diagnostic procedure is thought essential, but caution should be exercised (see ADVERSE REACTIONS). Premedication with antihistamines or corticosteroids to avoid or minimize possible allergic reactions in such

OMNIPAQUE® injection (iohecol)

Cardiovascular System: Arrhythmias including PVCs and PACs (2%), angina/chest pain (1%), and hypotension (0.8%). Others including cardiac failure, asystole, bradycardia, tachycardia, and vasovagal reaction were reported with an individual incidence of less than 0.4%. In controlled clinical trials involving 1,213 patients, one fatality occurred. A cause-and-effect relationship between this death and iohecol has not been established.

Nervous System: Vertigo [including dizziness and lightheadedness] (0.7%), pain (3%), photomas (2%), headache (2%), and taste perversion (1%). Others including anxiety, blurred vision, fever, motor and speech dysfunction, convulsion, paresthesia, somnolence, stiff neck, hemiparesis, and nystagmus were reported, with an individual incidence of less than 0.3%.

Respiratory System: Dyspnea and laryngitis, with an individual incidence of 0.1%.

Gastrointestinal System: Nausea (2%) and vomiting (0.6%). Others including diarrhea, dyspepsia, and dry mouth were reported, with an individual incidence of less than 0.2%.

Skin and Appendages: Urticaria (0.3%) and purpura (0.1%).

Pediatric angiocardiology and urography: In controlled clinical trials involving 324 patients, adverse reactions following the use of OMNIPAQUE 300 and OMNIPAQUE 350 were generally less frequent than with adults. **Cardiovascular System:** Ventricular tachycardia (0.6%), 2:1 heart block (0.6%), hypertension (0.3%), and anemia (0.3%).

Nervous System: Pain (0.6%), fever (0.6%), and convulsion (0.3%).

Respiratory System: Congestion (0.3%) and apnea (0.3%).

Gastrointestinal System: Nausea (1%), hypoglycemia (0.3%), and vomiting (2%).

Skin and Appendages: Rash (0.3%).

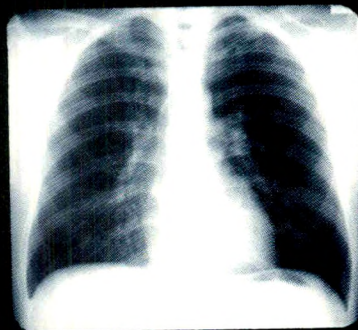
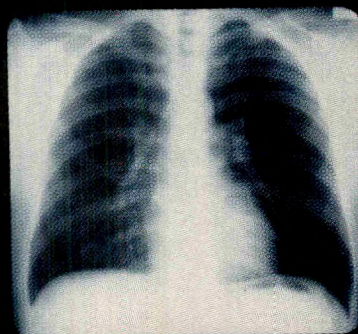
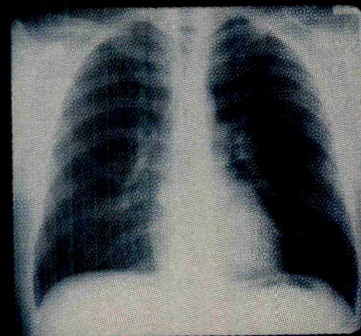
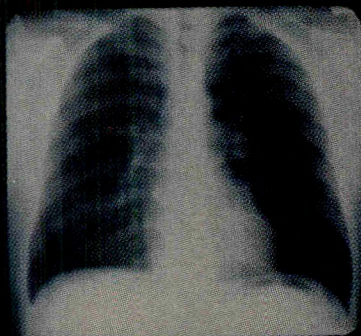
General Adverse Reactions to Contrast Media: The following reactions have been reported after administration of other intravascular iodinated contrast media, and rarely with iohecol. *Reactions due to technique:* hematomas and ecchymoses. *Hemodynamic reactions:* vein cramp and thrombophlebitis following intravenous injection. *Cardiovascular reactions:* rare cases of cardiac arrhythmias, reflex tachycardia, chest pain, cyanosis, hypertension, hypotension, peripheral vasodilatation, shock, and cardiac arrest. *Renal reactions:* occasionally, transient proteinuria, rarely, oliguria or anuria. *Allergic reactions:* asthmatic attacks, nasal and conjunctival symptoms, dermal reactions such as urticaria with or without pruritus, as well as pleomorphic rashes, sneezing, and lacrimation; rarely, anaphylactic reactions. Rare fatalities have occurred due to these or unknown causes. *Signs and symptoms related to the respiratory system:* pulmonary or laryngeal edema, bronchospasm, dyspnea; or to the nervous system: restlessness, tremors, convulsions. *Other reactions:* flushing, pain, warmth, metallic taste, nausea, vomiting, anxiety, headache, confusion, pallor, weakness, sweating, localized areas of edema (especially facial cramps), neutropenia, and dizziness. Rarely, immediate or delayed rigors can occur, sometimes accompanied by hyperpyrexia. Infrequently, "iodism" (salivary gland swellings) from organic iodinated compounds appears 2 days after exposure and subsides by the sixth day.

In general, the reactions that are known to occur upon parenteral administration of iodinated contrast agents are possible with any nonionic agent. Approximately 95% of adverse reactions accompanying the use of water-soluble intravascularly administered contrast agents are mild to moderate in degree. However, severe, life-threatening anaphylactoid reactions, mostly of cardiovascular origin, have occurred. Reported incidences of death range from 6.6 per 1 million (0.00066%) to 1 in 10,000 (0.01%). Most deaths occur during injection or 5 to 10 minutes later, the main feature being cardiac arrest, with cardiovascular disease as the main aggravating factor. Isolated reports of hypotensive collapse and shock are found in the literature. The incidence of shock is estimated to be 1 out of 20,000 (0.005%) patients.

Adverse reactions to injectable contrast media fall into two categories: chemotoxic reactions and idiosyncratic reactions.

Chemotoxic reactions result from the physicochemical properties of the contrast media, the dose, and the speed

WHICH WOULD YOU RATHER READ?



The difference is *Clear!*
S & S Illuminators provide the brightest, most even light distribution for glare-free "perfect" reading — all day long.

Our commitment to illumination excellence and innovative design has produced an extraordinarily extensive, diversified line of general and "special" purpose illuminators — with configurations to meet *Your* specifications. For example:

- Film formats include 14 x 17, 8 x 10, 14 x 36 and 14 x 51 inches. Plus 18 x 24 and 24 x 30 cm Mammography Series
- Panoramic or divided viewing sections

- High-Low intensity levels as well as high frequency, reduced glare units are available as options
- 1 - 8 banks / Single or double tier configurations
- Straight, console or full range tilt viewing
- Surface or recess mounting or mobile free-standing units
- Economy models thru deluxe models with full range of optional accessories

Tried, tested and trusted for over 40 years, S & S — the world's largest manufacturer of Motorized Viewers — has earned its reputation for setting the **standard** in illumination excellence.

Call us toll-free, or ask your local x-ray representative for our fully illustrated 100+ page catalog of Illuminators, Motorized Viewers and X-Ray Accessories.

CIRCLE 9 ON READER SERVICE CARD



S & S X-RAY PRODUCTS INC.

1101 Linwood Street
Brooklyn, NY 11208

800/347-XRAY • 718/649-8500

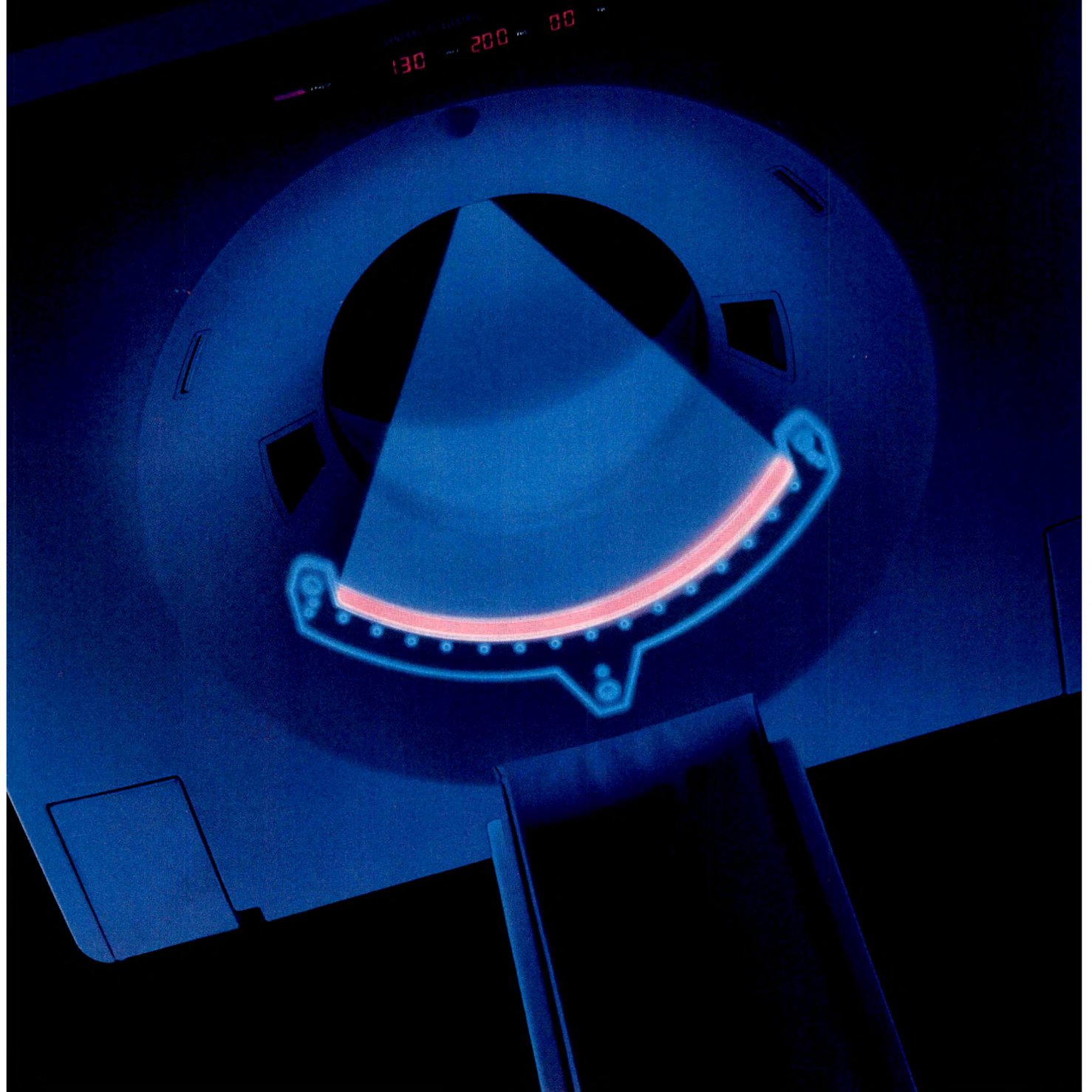
FAX 718/257-0219

The difference is Clear!

**4X Series with
High-Low Feature**
(Model 4X0001 shown)



Highlight



New light in computed tomography

GE is bringing new light to computed tomography. The CT 9800 HiLight™ Detector.

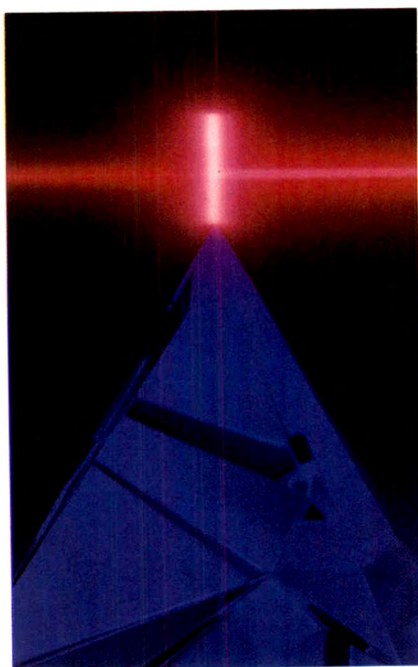
It's a revolutionary new detector from the scientists at GE that provides you with fast scan times, low dose levels, high throughput and extraordinary images.

With efficiency and sensitivity far beyond other detectors, HiLight brings even greater spatial resolution and low-contrast detectability to the CT 9800 Quick™ system.

In a standard 2-second scan, for example, spatial resolution measures 0.65 mm. In the high resolution mode—0.35 mm. Low contrast detectability is equally impressive—2.5 mm at 0.25% contrast (≤ 4 rads).

Extraordinary images

As a result, clinical images are remarkable—even by GE standards. Improved definition between grey and white matter in head studies. Superior detection of liver lesions, periaortic structures and mesenteric vasculature. Clear presentation of the smallest details of anatomy and pathology in studies of the spine, chest, inner ear and orbits.



No compromises

Perhaps the most significant aspect of imaging with the CT 9800 Quick/HiLight system is that there are no compromises. In any study you can combine fast scan times with low dose levels and still get superior images.

Which means better pediatric studies. More comprehensive dynamic scanning. More efficient throughput with fewer tube cooling delays.

Dose for dose, scan time for scan time, there is no better image quality available to you in CT today.

Still the standard

CT 9800 Quick continues to be the system by which all others are measured in computed tomography. Its standard features have always been exceptional. Routine 2-second scanning. Ability to scan, reconstruct, display and film slices in less than 16 seconds. Real-time ScoutView™ dynamic scanning. Arrange™ reformatting and a host of other features that enhance both the clinical effectiveness and efficiency of your CT department.

And now, with the HiLight Detector, we've raised our image quality standards even higher—so you can continue to provide the ultimate in CT imaging to your patients.

The CT 9800 Quick system with the HiLight Detector. An extraordinary combination from GE.

For more information, call GE Medical Systems toll free:

(800) 624-5692.



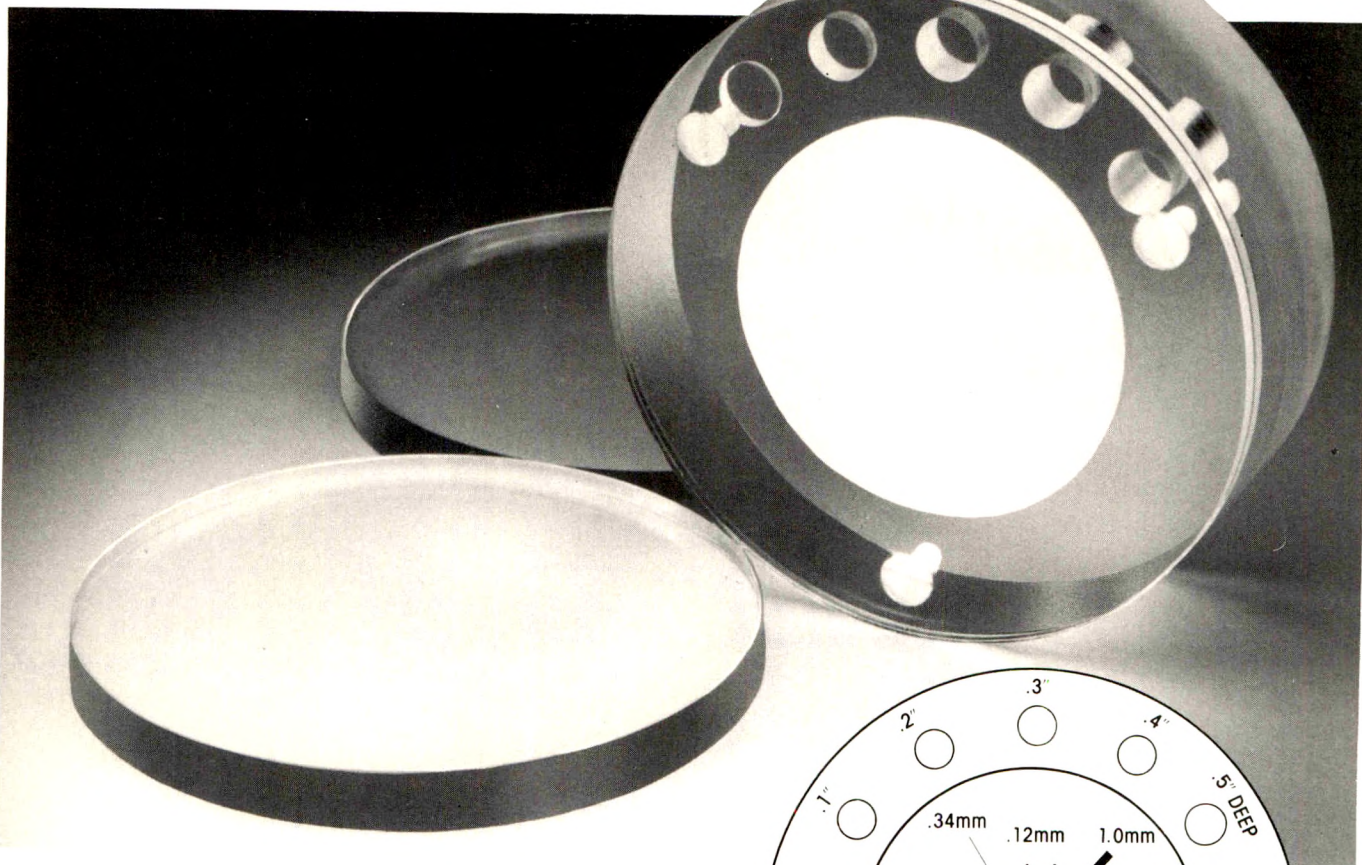
CIRCLE 3 ON READER SERVICE CARD

GE Medical Systems

*There's never been
a better time to choose GE*

Easy To Use . . . Easy to Interpret!

MAMMOGRAPHIC QA PHANTOM*

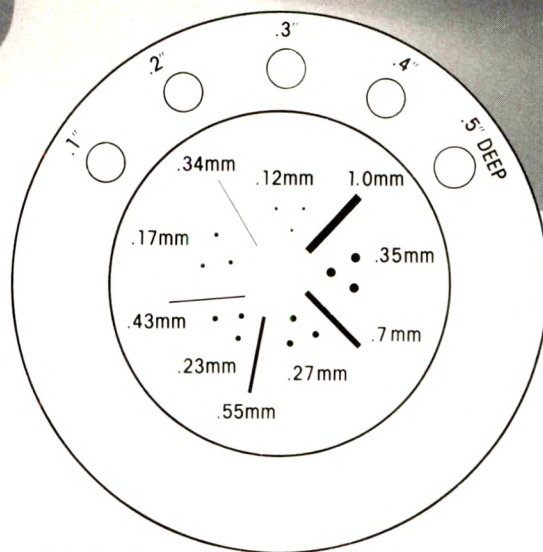


For Evaluating the Overall Imaging Performance of a Mammographic System

- Intended as an integral part of a complete mammography QA program: evaluates x-ray generator, screen-film combination and film processor.
- Contains calcium carbonate specks which better simulate actual clinical conditions ("punctate calcifications") in breast cancer.
- Uses nylon fibers to simulate "soft tissue fibrillar extensions in adipose tissue."
- Includes two additional attenuators to check phototiming linearity.
- Includes 5-step air wedge to gauge for image contrast.

76-001 Mammographic Phantom \$495.00

CIRCLE 36 ON READER SERVICE CARD



**Designed by Leonard Stanton, M.S.,
Hahnemann University, Philadelphia, PA 19102.*

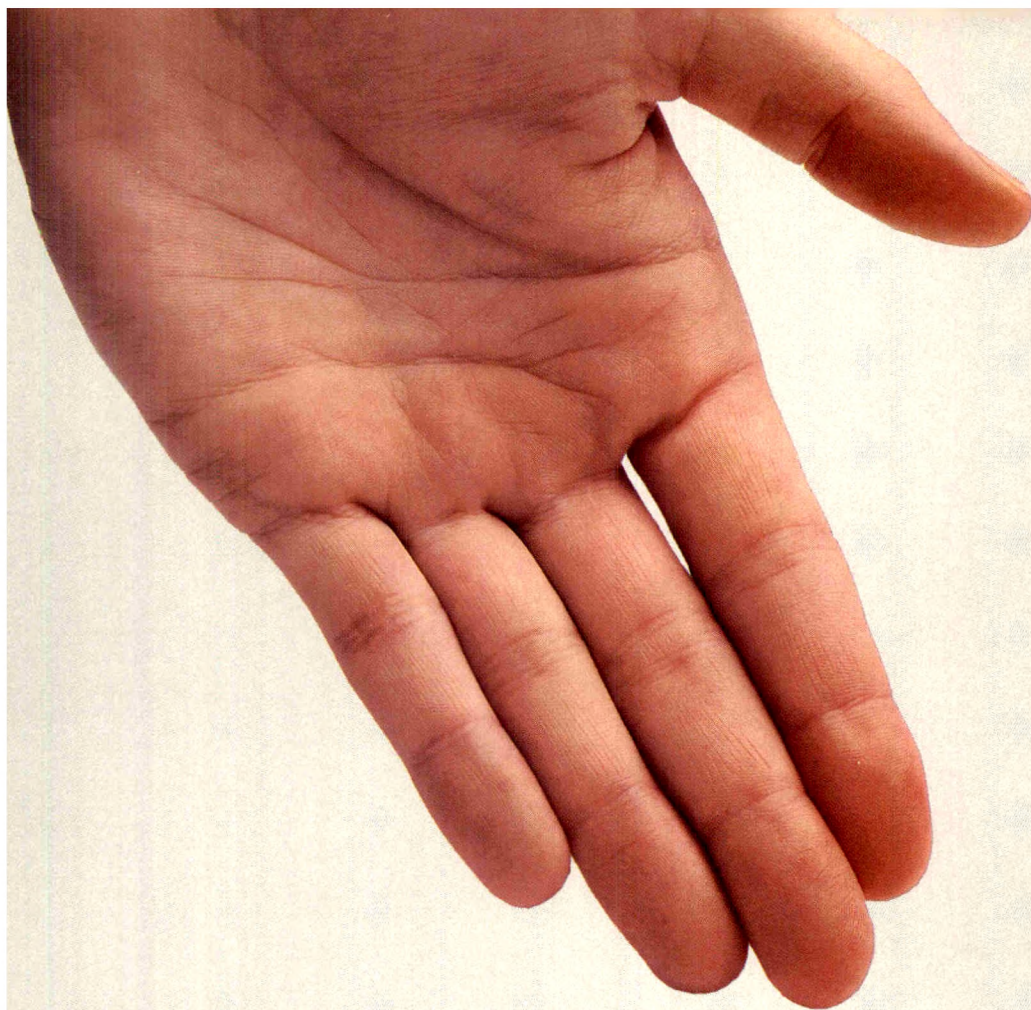
Write, or phone 516-741-6360 today!
For more details, request Bulletin 4052-44

NUCLEAR ASSOCIATES



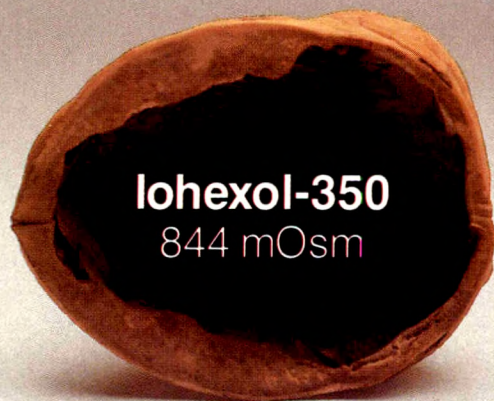
A Division of VICTOREEN, INC.
100 VOICE ROAD
CARLE PLACE, NY 11514-1593 U.S.A.
(516) 741-6350
FAX (516) 741-5414

WE CARRY A COMPLETE LINE OF MAMMOGRAPHIC QA PRODUCTS

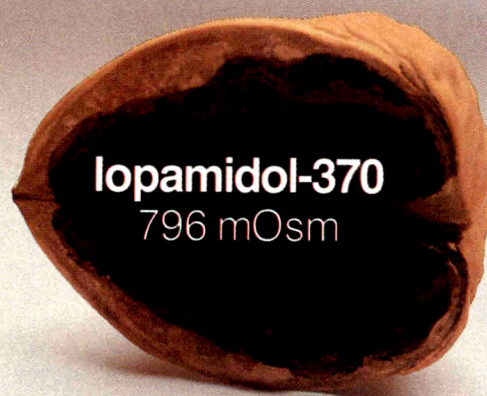


**For greater patient comfort
and the lowest osmolality,
the choice is yours...**



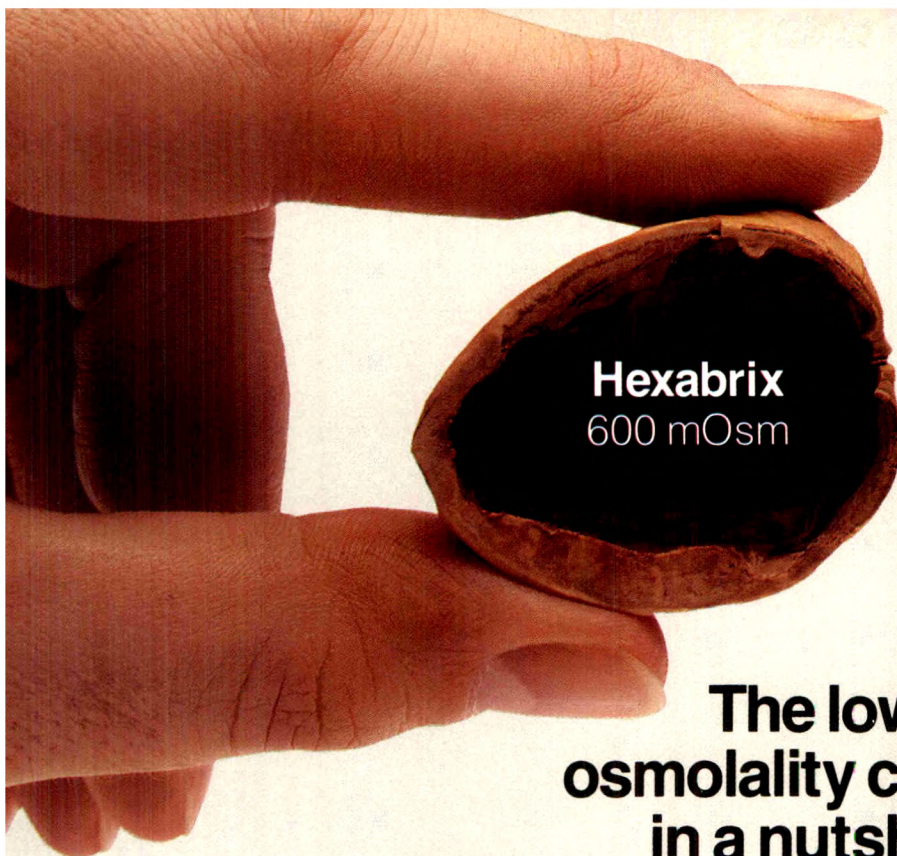


Iohexol-350
844 mOsm



Iopamidol-370
796 mOsm

F R O M M A L I



Hexabrix
600 mOsm

The low osmolality choice, in a nutshell

Compare Hexabrix with the nonionics, and you'll find that Hexabrix not only has the lowest osmolality, but also the least amount of patient discomfort in interventional procedures.

Least heat and pain

Recent comparative studies demonstrate that Hexabrix produces significantly less heat¹ and pain¹⁻³ than iopamidol and/or iohexol during arteriography procedures.¹⁻³

Less risk of clotting *in vitro*

Hexabrix has been shown to be a stronger inhibitor of clotting^{4,5} and platelet aggregation^{5,6} *in vitro* than iopamidol or iohexol.

Good angiographic technique should be followed in all procedures involving contrast media. Even when meticulous technique is used, some mixing of blood with contrast media in syringes and catheters is possible. Prolonged contact of blood and contrast media in syringes and catheters can lead to clot formation.

Lowest viscosity

Hexabrix has the lowest viscosity at 37°C (7.5 cps), compared to iohexol-350 (10.4 cps) or iopamidol-370 (9.4 cps).

HEXABRIX[†]

(ioxaglate meglumine 39.3%/
ioxaglate sodium 19.6% injection)

Please see following page for references and brief summary of prescribing information.

N C K R O D T

HEXABRIX[†] (ioxaglate meglumine 39.3%/ioxaglate sodium 19.6% injection)

HEXABRIX[®]

Each milliliter of HEXABRIX contains 393 mg of ioxaglate meglumine, 196 mg of ioxaglate sodium and 0.10 mg edetate calcium disodium as a stabilizer. The solution contains 3.48 mg (0.15 mEq) sodium in each milliliter and provides 32% (320 mg/mL) organically bound iodine.

CONTRAINDICATIONS

HEXABRIX is contraindicated for use in myelography. Refer to PRECAUTIONS concerning hypersensitivity. Hysterosalpingography should not be performed during the menstrual period, in pregnant patients, in patients with known infection in any portion of the genital tract, or in patients in whom cervical conization or curettage has been performed within 30 days. Arthrography should not be performed if infection is present in or near the joint.

WARNINGS

Serious or fatal reactions have been associated with the administration of iodine containing radiopaque media. It is of utmost importance to be completely prepared to treat any contrast medium reaction.

As with any contrast medium, serious neurologic sequelae, including permanent paralysis, can occur following cerebral arteriography, selective spinal arteriography and arteriography.

Idiosyncratic reaction in patients who have previously received a contrast medium without ill effect should always be considered. Prior to the injection of any contrast medium, the patient should be questioned to obtain a medical history with emphasis on allergy and hypersensitivity. A positive history of bronchial asthma or allergy (including food), a family history of allergy, or a previous reaction or hypersensitivity to a contrast agent may imply a greater than usual risk. Such a history may be more accurate than pre-testing in predicting the potential for reaction, although not necessarily the severity or type of reaction in the individual case. A positive history of this type does not arbitrarily contraindicate the use of a contrast agent when a diagnostic procedure is thought essential, but does call for caution. (See ADVERSE REACTIONS.)

Prophylactic therapy including corticosteroids and antihistamines should be considered for patients who present with a strong allergic history, a previous reaction to a contrast medium, or a positive pre-test since in these patients the incidence of reaction is two to three times that of the general population. Adequate doses of corticosteroids should be started early enough prior to contrast medium injection to be effective and should continue through the time of injection and for 24 hours after injection. Antihistamines should be administered within 30 minutes of the contrast medium injection. Recent reports indicate that such pre-treatment does not

insure choice for malignant tumor enhancement.

Arthrography: Strict aseptic technique is required to prevent the introduction of infection. Fluoroscopic control should be used to insure proper introduction of the needle into the synovial space and prevent extracapsular injection. Aspiration of excessive synovial fluid will reduce the pain on injection and prevent the dilution of the contrast agent. It is important that undue pressure not be exerted during the injection.

Hysterosalpingography: Caution should be exercised in patients suspected of having cervical or tubal carcinoma to avoid possible spread of the lesion by the procedure. Delayed onset of pain and fever (1-2 days) may be indicative of pelvic infection.

Carcinogenesis, Mutagenesis, Impairment of Fertility: No long-term animal studies have been performed to evaluate carcinogenic potential. However, animal studies suggest that this drug is not mutagenic and does not affect fertility in males or females.

Pregnancy Category B: Reproduction studies have been performed in rats and rabbits at doses up to two times the maximum adult human dose and have revealed no evidence of impaired fertility or harm to the fetus due to HEXABRIX. There are, however, no adequate and well-controlled studies in pregnant women. Because animal reproduction studies are not always predictive of human response, this drug should be

Technique reactions: Extravasation with burning pain, hematomas, ecchymosis and tissue necrosis, vascular constriction due to injection rate, thrombosis and thrombophlebitis.

Neurological reactions: Spasm, convulsions, aphasia, syncope, paresis, paralysis resulting from spinal cord injury and pathology associated with the syndrome of transverse myelitis, visual field losses which are usually transient but may be permanent, coma and death.

Other reactions: Headache, trembling, shaking, chills without fever, hyperthermia and lightheadedness. Temporary renal shutdown or other nephropathy.

Pediatric angiocardiology has been complicated by intramural injection with marked adverse effects on cardiac function.

During selective coronary arteriography with or without left ventriculography, patients may have clinically insignificant ECG changes. The following adverse effects have occurred in conjunction with the administration of iodinated intravascular contrast agents for this procedure: hypotension, shock, anginal pain, myocardial infarction, cardiac arrhythmias (bradycardia, ventricular tachycardia, ventricular fibrillation) and cardiac arrest. Fatalities have been reported. Complications to the procedure include dissection of coronary arteries, dislodgement of atheromatous plaques, perforation, hemorrhage and thrombosis.

Following peripheral arteriography, hemorrhage and throm-

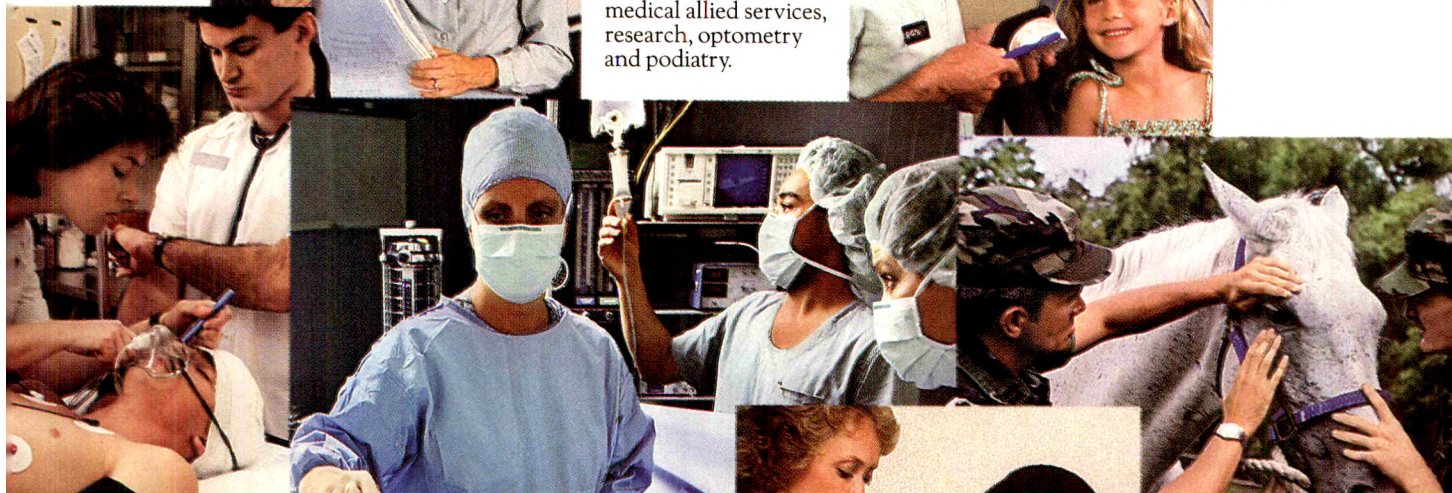
The Army Nurse Corps provides nursing services.



The Medical Service Corps provides health care services in pharmacy, supply and administration, medical allied services, research, optometry and podiatry.

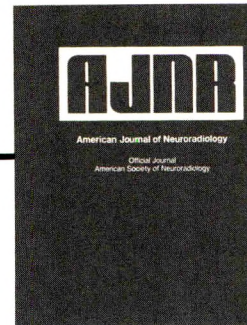


The Army Dental Corps provides dental services.



Increase your expertise in evaluating CNS lesions

AJNR American Journal of Neuroradiology



Editor: **Juan M. Taveras, MD**, Harvard Medical School; MGH

Outstanding clinical papers on every aspect of CNS imaging, including spinal diagnosis...informed coverage of head and neck radiology...clear, readable CTs, angiographs, MR imaging and ultrasound studies. These are the features you demand of a quality professional journal. You'll find them in every issue of **AJNR: American Journal of Neuroradiology**.

As you are called upon to perform and interpret more and more sophisticated diagnostic tests — from myelography to CT to newborn ultrasound studies — you need a comprehensive, reliable journal that can keep you abreast of all the latest developments. Each bimonthly issue of **AJNR** brings you timely, clinically pertinent information, as well as important clinical research presented with an eye toward immediate practical application.

Here's a brief sampling of the variety of articles you'll find in **AJNR**:

Giant Cavernous Aneurysm Associated with Trigeminal Artery: Treatment by Detachable Balloon. *Higashida RT, Halbach VV, Mehlinger CM, Hieshima GB*

Intraoperative Digital Subtraction Neuroangiography: A Diagnostic and Therapeutic Tool. *Hieshima GB, Reicher MA, Higashida RT, et al.*

Characteristic Features of MR Truncation Artifacts.

Czervionke LF, Czervionke JM, Daniels DL, Haughton VM
Neuroimaging of Scuba Diving Injuries to the CNS. *Warren LP Jr, Djang WT, Moon RE, et al.*

Risk of Seizures After Myelography. *Maly P, Bach-Gansmo T, Elmqvist D*

Comparison of MR Imaging and CT in Patients with Intracranial Aneurysm Clips. *Holtas S, Olsson M, Romner B, Larsson E-M, Saveland H, Brandt L*


Comparison of MR Imaging, CT, and Angiography in the Evaluation of the Enlarged Cavernous Sinus. *Hirsch WL Jr, Hryshko FG, Sekhar LN, et al.*

Bimonthly

Personal \$115/yr **Institutions** \$135/yr

In-training \$65/yr (add \$25.00 outside the US)

ORDER FREE BY PHONE. Just call

 **1-800-638-6423** from anywhere in the US.
Maryland residents, call **1-800-638-4007**.

Williams & Wilkins

P.O. Box 23291 Baltimore, Maryland 21203



Subscribe to AJNR for 3 years and SAVE

Avoid future rate increases and ensure uninterrupted service by placing a multi-year subscription at current rates.

☐ New subscription ☐ Renewal

☐ 3 yrs ☐ 2 yrs ☐ 1 yr

☐ **Personal** \$115 ☐ **Institutions** \$135 ☐ **In-training** \$65
(add \$25.00 outside the US)

☐ Also send me the **1989 Bound Volume** at \$65.00 (\$70.00 outside the US). \$2.00 discount for orders placed before October 31, 1989, and for pre-paid orders. I understand that the bound volume is *in addition to* my regular subscription and is available only to subscribers. (To be shipped in early 1990. Sorry, bound volumes for years prior to 1989 are not available.) *All bound volume orders must be received by December 31, 1989.*

☐ Check enclosed ☐ Bill me
☐ VISA ☐ MasterCard ☐ American Express

card #

exp.

signature/P.O. #

printed in USA

Name

Address

City/State/Zip

MD residents, please add 5% sales tax. Subscription orders from outside the US must be prepaid in US dollars only.

Residents, Fellows, Interns, and Students: when applying for the in-training rate, available for 3 years, please specify name of institution and training status. Rates valid through October 31, 1989.

Please allow 8 weeks for order processing and delivery of your first issue. Surface mail delivery to countries outside the US may take up to 16 weeks. Airmail rates available upon request.

Williams & Wilkins

P.O. Box 23291
Baltimore, Maryland 21203

The Broadway Centre
2-6 Fulham Broadway
London SW6 1AA England



JNRA91 1179

MUSCLE.



Financial Strength. The muscle of a company. The power to invest in an industry. And to improve the quality of health care worldwide.

At Picker we put our financial strength to work for you. Bringing you new products, excellent service, advanced technologies, and customer support programs that make your job easier. While building a solid, profitable company is good news to us, it's also good news to you. Because we've put those profits to work to help you improve patient care. With over 70 years of experience in diagnostic imaging,

Picker is a growing global corporation. Our commitment to the future has never been greater. Our financial resources have never been stronger. Your choice of Picker products has never been better. For more information write Picker International, 595 Miner Rd., Highland Heights, Ohio 44143.



PICKER

THE IMAGE OF EXCELLENCE

The name
that started
a revolution.

*the
leader*

GOLYTELY[®]

PEG-3350 and Electrolytes for Oral Solution

CIRCLE 35 ON READER SERVICE CARD

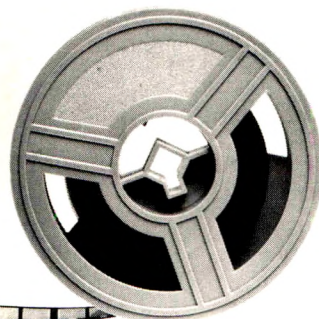
LABORATORIES, INC.
Braintree

© 1989 Braintree Laboratories, Inc.
TRE-1035

Need shelf space?

**Williams & Wilkins is your
source for back issues of
this journal in microform.**

Free Up 98%
Of Your Shelf
Space With
Microform
Conversion



MICROFILM editions are available
for this journal direct from the
publisher. Many Williams &
Wilkins journals as well as those
journals distributed by the
Publishing Services Division of
Waverly, Inc., are also available for
a single volume year or on a
standing order basis.

FOR ORDERING INFORMATION:
Write to the address below or call
TOLL FREE 1-800-638-6423.
In Maryland call **1-800-638-4007.**

☐ **Please send me microform
back issue ordering information
for** _____

Journal Name _____

Name _____

Title _____

Address _____

City/State/Zip _____

Mail to:

Williams & Wilkins

Microform Sales

Attention: Yvonne Hahn

428 East Preston Street

Baltimore, MD 21202

-or-

The Broadway Centre

2-6 Fulham Broadway

London SW6 1AA England

Formats available:

- 16-mm reel
- 35-mm reel
- 16-mm cartridge
(3M or Kodak)
- positive or negative film

MICA92 1193

Review Article

Modern Diagnostic Imaging in Joint Disease

Murray K. Dalinka,¹ Morrie E. Kricun, Michael B. Zlatkin, and Claire A. Hibbard

The introduction of new imaging techniques in recent years has greatly expanded the possibilities for the investigation of musculoskeletal disorders. In many circumstances, this has complicated the investigation of clinical problems because universal agreement on the utility of the various procedures in specific conditions has not yet been reached. In this article, we review the use of available techniques for the diagnosis and evaluation of joint disease, emphasizing the role each plays in specific circumstances.

Lower Extremity

Hip

Ischemic necrosis.—Ischemic necrosis can occur in any of the major joints, and the principles are the same regardless of location. In patients with osteonecrosis, MR is the most sensitive diagnostic imaging technique [1]. The hip, the most commonly studied area, will be used as the model for discussion.

Scintigraphy is more sensitive than plain radiography but is less sensitive and less specific than MR imaging [2–4]. Its sensitivity can be increased by using pinhole collimation and single-photon emission computerized tomography (SPECT) scanning [5] and is decreased in the presence of bilateral disease. In the early stages of ischemic necrosis, a bone scan may depict a negative or photopenic defect. In later stages, the bone scan becomes less specific, with increased uptake caused by remodeling and repair [5]. The tomographic images

obtained with SPECT may enable one to detect the more specific photopenic defect that is obscured by acetabular uptake on planar scintigraphy [5]. Occasionally, cases of osteonecrosis have been reported in which nuclear medicine scans and biopsy were positive and MR imaging was normal [3, 5].

Dihlmann [6] described an asterisk seen in the center of the femoral head on CT that represented the convergence of the normal weight-bearing trabeculae. In patients with ischemic necrosis, the sharply defined trabeculae lose their definition and extend to the articular margin. Magid et al. [7] used CT with multiplanar reconstruction to stage patients with ischemic necrosis. They found that this increased the detection rate of ischemic necrosis and changed the staging of the disease, often leading to changes in therapy. Sartoris et al. [8] used three-dimensional reconstruction to create polyethylene models that they compared with the resected femoral heads. They thought that these techniques did not add to the diagnostic information present on axial images but did increase conspicuity of the lesions. Mitchell et al. [9] reported that CT was superior to MR imaging in the diagnosis of fractures associated with ischemic necrosis. The total area of the head involved and the presence or absence of associated fractures may help determine whether conservative surgery is feasible [9].

Our patients with suspected ischemic necrosis of the hip are studied by MR with the use of a body coil and short and long TR/TE images in the coronal plane. Others have used special surface coils and added sagittal or axial imaging to better define the area of abnormality [10]. The appearance of

Received August 1, 1988; accepted October 20, 1988.

¹ All authors: Department of Radiology, Hospital of the University of Pennsylvania, 3400 Spruce St., Philadelphia, PA 19104. Address reprint requests to M. K. Dalinka.

ischemic necrosis on MR imaging is variable [9, 11]. On short TR (1000 or less)/short TE (less than 40) T1-weighted images, there is replacement of all or part of the high signal of fat in the femoral head. The overwhelming majority of lesions have a low-signal crescentic rim, usually in the anterior portion of the femoral head. The area within this rim may contain high, low, or intermediate signal [12]. Occasionally, an area of low signal extends beyond the crescentic margin into the femoral neck. On long TR/long TE T2-weighted images, 2000–2500/60–80 (TR/TE), the central zone may fade like fat, stay bright like blood, go from dark to bright like edema, or stay dark like fibrous tissue [12]. On T2-weighted images, an area of high signal is commonly seen within the low-signal margin; this is thought to represent granulation tissue [12] and its presence adds specificity to the diagnosis [12] (Fig. 1). Mitchell et al. [12] have graded ischemic necrosis on the basis of these signal characteristics. These authors have also found premature conversion to fatty marrow [13] and increased joint fluid in patients with ischemic necrosis [14].

Miscellaneous hip disorders.—Arthrography may show communicating iliopsoas bursae, which may present as inguinal masses [15, 16]. Other synovial cysts or bursae communicating with the joint can also be depicted [16], as can large anterior pseudobursae from recurrent anterior hip dislocation [17]. Arthrography has been used in the detection of nonopaque loose bodies and adhesive capsulitis in patients with unexplained chronic hip pain and osteopenia [18, 19]. When capsular constriction is seen without other intraarticular abnormalities, the pain usually resolves spontaneously, as in adhesive capsulitis of the shoulder [19].

Sonography, CT [20], and MR can all depict abnormal cysts and bursae about the hip, even those that are noncommunicating. We think that MR is preferable to CT and sonography because of its high contrast and multiplanar imaging capability. Arthrography should be limited to patients in whom aspiration is necessary or when the diagnosis is in doubt after noninvasive imaging.

Knee

Internal derangement.—Arthrography, usually with double-contrast and fluoroscopy, was the procedure of choice in the

diagnosis of internal derangements of the knee in the late 1960s and, in many institutions, until the late 1970s or early 1980s. Some authors later advocated CT with [21] or without [22–24] contrast material in the diagnosis of meniscal tears. In the past 10–15 years, the use of arthroscopy has led to a tremendous decrease in the number of imaging studies performed for internal derangement, although the two studies are often complementary [25].

With the advent of MR imaging, there have been a resurgence of interest and a marked increase in the number of imaging studies performed for internal derangements of the knee [26–35].

MR is painless, even in the acutely injured patient. The structures within and about the knee joint are depicted in exquisite detail with a diagnostic accuracy that compares favorably with arthrography [33, 34]. The use of specialized surface coils and a small field of view (16 cm or less) enables one to perform a high-resolution study within a reasonable period of time (40 min or less).

Most abnormalities about the knee can be seen on T1-weighted (short TR/TE) sagittal images (Fig. 2A). We also use T2-weighted sagittal images to obtain an arthrogram effect and to increase our confidence level. Fast-scanning techniques are also excellent in depicting meniscal abnormalities (Fig. 2B). T2-weighted images better show joint effusions and other cysts about the knee. Coronal images are helpful in the diagnosis of "bucket-handle tears," discoid menisci (Fig. 3), and degenerative tears of the free edge of the meniscus. We do not use coronal T2-weighted images routinely; however, they are particularly helpful in the evaluation of the acutely injured knee because collateral ligament tears are well depicted [34].

The fibrocartilaginous menisci often contain linear or globular areas of high signal within them. These high-signal areas may represent mucoid degeneration or meniscal tears pathologically [35, 36]. Stoller et al. [35] have graded meniscal signal. Globular areas within the menisci are considered grade 1, linear areas not reaching the surface are considered grade 2, and linear areas reaching the articular surface of the meniscus are classified as grade 3. Grade 3 menisci are considered meniscal tears (Fig. 2), whereas grades 1 and 2

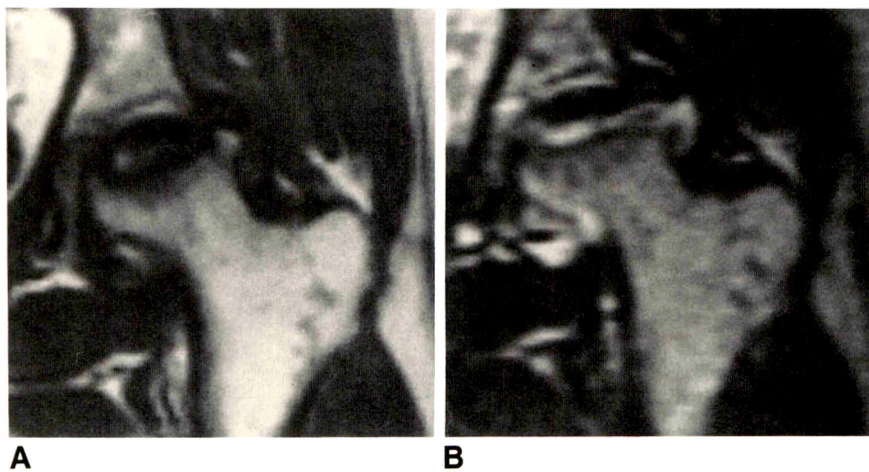


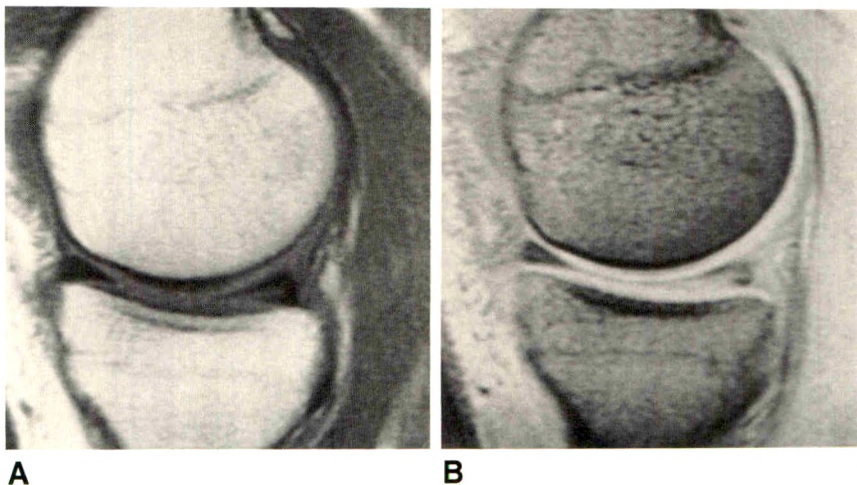
Fig. 1.—Ischemic necrosis of femoral head.

A, Short TR/TE (600/20) spin-echo image shows large area of ischemic necrosis in femoral head outlined by crescentic area of low signal.

B, Long TR/TE (2500/80) spin-echo image shows area of high signal just proximal to low-signal margin of lesion. Area of signal void is present proximal to that. Signal void area is considered fibrouslike. Area that converts to high signal on T2-weighted image represents granulation tissue.

Fig. 2.—A, Slightly, T1-weighted (1000/20) sagittal spin-echo image of knee shows oblique tear of posterior horn of medial meniscus.

B, Gradient-echo image (497/10, 90° flip angle) shows tear. Linear high signal (grade 2) in anterior horn of medial meniscus is better seen than in A. Articular cartilage turns bright on this sequence.



are considered degenerative menisci and are usually intact at surgery [37]. The finding of grade 3 meniscal signal correlates with the surgical findings of a tear in over 90% of cases [37].

The knee is placed in slight external rotation within the surface coil; this enables the anterior cruciate ligament to be seen in its entirety with sagittal imaging [38]. Usually, the anterior cruciate ligament can be seen with 5-mm-thick sections; however, in a small percentage of normal patients, it will not be seen with this technique. We use 3-mm sagittal sections with short TR/TE (600/20) images and 5-mm sections with long TR/TE (2500/20, 80) images. When this technique is used, we think that failure to visualize the anterior cruciate ligament indicates that the ligament is torn. Lee et al. [38] reported a sensitivity of 95% and a specificity of 100% in the diagnosis of anterior cruciate ligament tears. MR imaging criteria consisted of an irregular wavy contour of the anterior attachment of the ligament, high-signal intensity within the ligament, and disruption of the normal ligamentous contour.

MR imaging in patients with internal derangement may also depict marrow abnormalities thought to represent occult fractures [39]. These lesions are not rare, but their effect on patient outcome is uncertain at the present time.

Cartilaginous abnormalities can be detected with routine imaging techniques but are often better shown with fast-scanning MR imaging. Some authors advocate gadolinium-DTPA for this purpose [40, 41]. Gadolinium has not been approved for intraarticular injection, and its use turns MR into an invasive study. Mesgarzadeh et al. [42] evaluated 12 patients with osteochondritis dissecans. They thought that MR imaging could directly visualize loose and displaced fragments and help differentiate in situ loosening from unstable lesions.

Yulish et al. [43] showed a high correlation between MR imaging and surgical findings in a small number of patients with chondromalacia of the patella. CT has also been used in the evaluation of the patellofemoral joint [44–46].

Meniscal cysts and nonspecific ganglion cysts can be easily identified by MR imaging [47]. They can also be evaluated by CT [48] or sonography. MR imaging can also depict the intraarticular abnormalities usually present with meniscal

cysts (Fig. 3) and not uncommonly associated with popliteal cysts [49].

Knowledge of the pitfalls in MR imaging [50] should help in further improving the diagnostic ability of this technique. Preliminary experience with volumetric acquisition and gradient-echo scanning suggests that these refinements may increase the sensitivity of standard MR of the knee [50–52].

We think that MR imaging is the technique of choice in the diagnosis of internal derangements of the knee. Knee arthrography and/or CT arthrography should be used only if MR imaging is not available.

Miscellaneous.—MR imaging is helpful in the evaluation of marrow abnormalities, including osteonecrosis. In the evaluation of ischemic necrosis of the knee, we perform a standard knee examination and obtain a coronal short TR/TE image of the opposite knee because bilateral disease may exist, even in patients with unilateral symptoms [53]. If the initial spin-echo images are negative, chemical-shift imaging (Dixon technique) may be added as an optional sequence to increase the sensitivity of the study. MR imaging can depict the marrow abnormalities and associated meniscal and articular cartilage pathology [53].

MR imaging has been used in the evaluation of pigmented villonodular synovitis for which the findings are characteristic [54]. Hemosiderin deposition is depicted as a low-signal area that decreases in signal intensity on T2-weighting (Fig. 4). This is caused by the preferential T2 shortening of hemosiderin caused by its paramagnetic effects [55], which are particularly sensitive to fast-scanning techniques and enhanced with higher field strengths. Hemosiderin is also deposited in the synovium in patients with hemophilia and rheumatoid arthritis; hence, the findings are characteristic but not pathognomonic. In hemophilia, one can assess the synovium, articular cartilage [56], subchondral bone, periarticular abnormalities [57], and associated pseudotumors [58]. This can be done with sonography also, often in conjunction with CT [59–61].

Ankle

Ligaments and tendons.—Plain films of the ankle, including stress views, are often not helpful in patients with severe

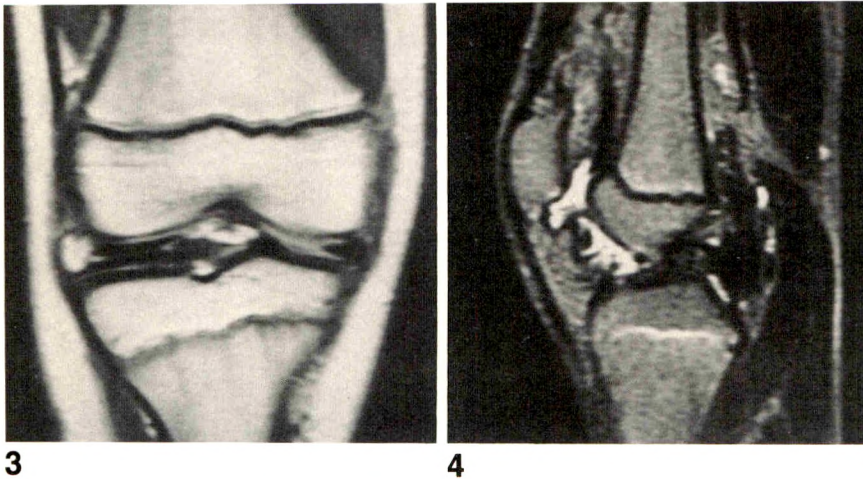


Fig. 3.—Long TR/intermediate TE (2500/40) spin-echo image shows torn, diskoid lateral meniscus with associated meniscal cyst.

Fig. 4.—Long TR/TE (2500/80) spin-echo image of knee shows fluid in knee, with signal void in and posterior to suprapatellar bursa caused by deposition of hemosiderin.

ankle sprains. Ankle arthrography has been used in the diagnosis of acute ligamentous ruptures, particularly in those for whom surgery is contemplated [62–64]. Most investigators used single-contrast arthrography with 6–10 ml of contrast agent. Double-contrast techniques with 0.5 ml of contrast material and 8–12 cm³ of air have been used, particularly when loose bodies or talar dome osteochondral fractures are suspected [65].

The location of the extravasated contrast material or filling of the peroneal tendon sheaths is dependent on the ligamentous disruptions. False-negative ankle arthrograms occur if the study is delayed beyond a few days because the leak of contrast material is often sealed by thrombin [62]. If the peroneal tendon sleeves fill without an associated tear of the anterior talofibular ligament, this suggests chronic lateral instability. Small recesses may be seen adjacent to the lateral malleolus in patients with chronic instability; however, there was no correlation between the small recesses and the location of the lesions observed surgically [66]. Posttraumatic adhesive capsulitis has also been reported on arthrography; it may be caused by intracapsular fracture or soft-tissue injury [67].

Spiegel and Staples [68] reported that arthrography was highly useful in selected patients but was not infallible. In their experience, calcaneofibular ligament tears never occurred in the absence of significant anterior capsular injury. False-negative results were encountered when two ligaments were torn because the contrast material escaped along the path of least resistance and often did not show the additional ligamentous pathology [68]. Sauser et al. [69] compared ankle arthrography with stress radiography in acute ankle injuries. They found a high false-negative rate with stress radiography. In a series of 600 patients, 30 surgically proved, ankle arthrography was more sensitive than stress films taken during anesthesia in determining the site of ligamentous ruptures [70].

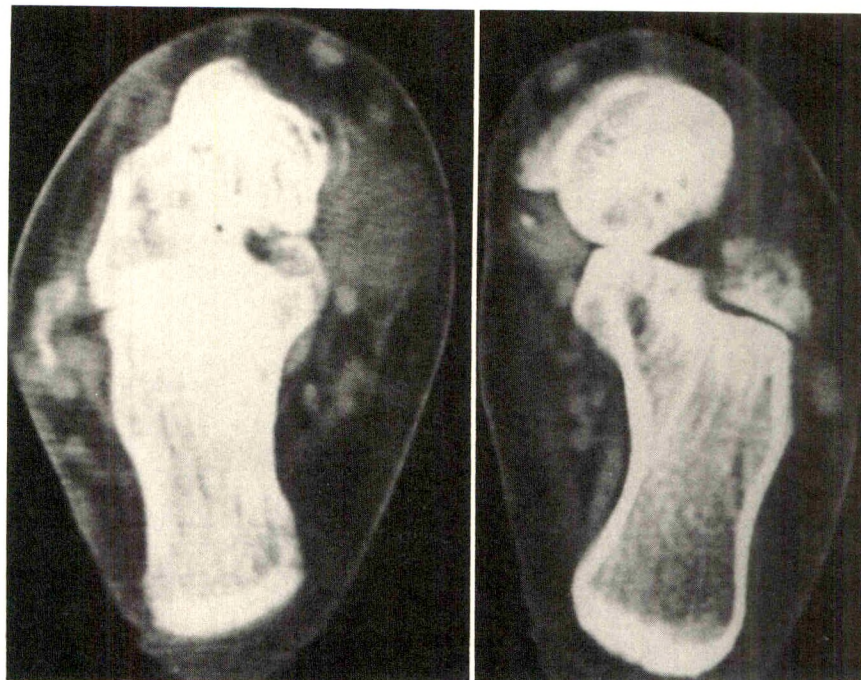
Tenography, particularly of the common peroneal tendon, has been used in patients with persistent hindfoot pain and previous calcaneal fractures [71]. Gilula et al. [72] performed tenography in eight patients with suspected tenosynovitis. They thought that the abnormal tenograms could be corre-

lated with failure of conservative therapy. Unfortunately, tenography is invasive and may be difficult to perform, particularly if the ankle is painful and swollen and the tendon itself cannot be palpated.

CT has been used in studying the tendons about the ankle with and without (Fig. 5) associated fractures [73–75]. In most cases, both feet are scanned at the same time with sections varying between 4 and 5 mm in thickness [73]. The axial plane is often used in a neutral anatomic position. The normal tendon is depicted as a rounded area of increased density surrounded by adjacent fat [73]. Rosenberg et al. [74] used CT to evaluate 25 patients with peroneal tendon abnormalities. They demonstrated subluxation, dislocation, entrapment, and tenosynovitis of the peroneal tendons and described the normal CT anatomy of these structures. Rosenberg et al. [75] also described the CT findings in posterior tibial tendon ruptures, a cause of acquired flatfoot in the adult. Plain films often show periostitis of the medial malleolus, which should suggest the possibility of this diagnosis [75]. These ruptures are often degenerative and may be partial or complete. Early tendon rupture may have a bulbous appearance with cystic or linear lucencies [76]. Later, a portion of the tendon becomes attenuated because of hemorrhage with scar formation [76]. Complete ruptures present as a gap within the tendon [76].

We think that the excellent soft-tissue contrast of MR imaging and its multiplanar capability make it the imaging technique of choice in the diagnosis of ligamentous and tendon abnormalities about the ankle [77, 78]. In evaluating the Achilles tendon by MR, Quinn et al. [79] could distinguish partial tears, complete ruptures, chronic tendonitis, and uncomplicated surgical repairs. The normal tendons lack signal and therefore appear black on all imaging sequences. In patients with partial tendon ruptures, areas of high signal appear within the structure of the tendon on both T1- and T2-weighted sequences. These areas of high signal are thought to represent hemorrhage [79]. Complete ruptures are detected as a gap or discontinuity within the tendon often associated with hemorrhage and edema [79]. Surgically repaired tendons are seen as continuous structures with inhomogeneous signal [79]. Chronic tendonitis causes tendon

Fig. 5.—Axial CT scan shows large posterior tibial tendon on right with low density in region of tendon sheath in patient with chronic posterior tibial tendonitis.



thickening [79]. Sagittal images often do not show the tendon in its entirety; axial images depict the tendon within its sheath.

Tarsal coalition.—CT is an excellent technique for the diagnosis of tarsal coalitions [80–83], particularly those between the sustentaculum tali and the talus. In this condition, the plain films and clinical findings may point to or suggest the diagnosis but may not show the medial portion of the anterior subtalar joint, a common site of coalition [84]. Bone scanning may depict increased uptake in the subtalar joint and about the superior talus or talonavicular articulation, suggesting the diagnosis [84]. Subtalar arthrography has been suggested by Kaye et al. [85], but its invasive nature has limited its usefulness.

Deutsch et al. [82] reported that coronal CT imaging could show the site of coalition and depict associated lesions. Stoskopf et al. [83] found that the diagnosis was often missed on plain films and that nuclear medicine was nonspecific and lacked morphologic detail. They studied five cases of tarsal coalition with CT scanning; four had been called normal on plain films and the fifth required five axial views before the diagnosis was established. CT was diagnostic in all cases [83]. Coronal CT scans were best for sustentacular-talar coalitions; longitudinal sections were best for showing coalitions of the calcaneonavicular articulation [83]. When CT is used, both feet can be examined simultaneously because the condition may be bilateral. The size of the coalition and associated ankle abnormalities may be shown. The ankle can be examined after surgery to assess the status and possible recurrence of fusion [86].

Cartilaginous abnormalities.—Kaye [65] used double-contrast arthrography to evaluate the integrity of the articular cartilage of the ankle joint. Tomography can be used to supplement arthrography to allow more precise evaluation of the cartilage. Heare et al. [87] used coronal CT after double-

contrast ankle arthrography to evaluate four patients with osteochondral fractures (osteochondritis dissecans) of the ankle. A detached fragment, which is a relative indication for surgery, was shown in one of their cases.

Yulish et al. [88] used MR imaging to evaluate 10 osteochondral lesions of the talus. MR can detect the status of the overlying articular cartilage, defects in the underlying bone (Fig. 6), the interface between the underlying bone and the normal structures, and the presence and location of loose bodies [88].

Three-dimensional imaging.—Woolson et al. [89] developed three-dimensional models of a cadaveric ankle from CT images. They suggested that these images could be used for enhanced diagnostic ability, planning surgery, and designing custom prostheses. Although the technology for three-dimensional imaging has been available for some time, enthusiasm for its use in the ankle and other joints is not widespread.

Upper Extremity

Shoulder

Routine radiography should be performed before more sophisticated imaging techniques. Occasionally, the presence of a subtle fracture, calcific deposits, or the classic changes of chronic rotator cuff tear may eliminate the need for further imaging studies.

Killoran et al. [90] popularized shoulder arthrography in the 1960s. It can depict complete and partial tears of the rotator cuff and has been considered the gold standard for the diagnosis of complete rotator cuff tears for many years. Both single- and double-contrast techniques have been used with excellent results. Proponents of double-contrast arthrography state that the size of the tear and the condition of the

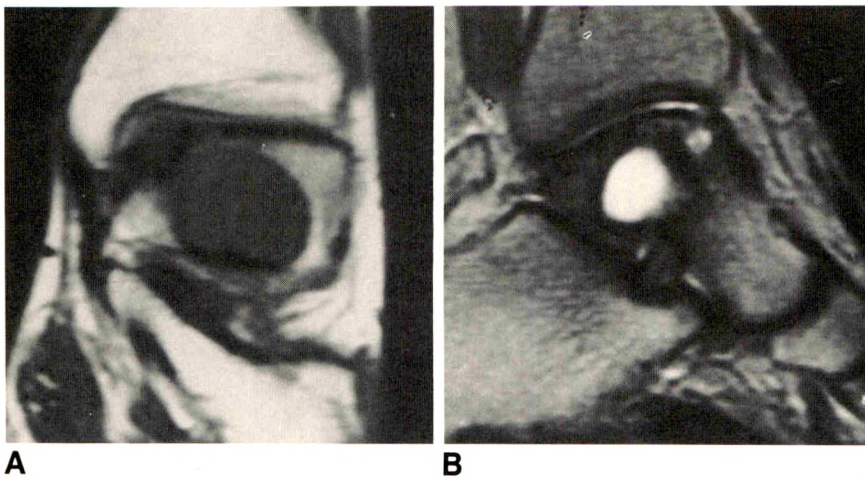


Fig. 6.—Osteochondral defect associated with large intraosseous geode of talus.

A, Short TR/TE (600/20) spin-echo MR image shows talar dome defect and large, well-defined lesion in talus.

B, Long TR/TE (2500/80) sagittal spin-echo image shows defect in superior aspect of talus and small channel connecting it to large talar lesion, which is filled with fluid.

remaining cuff can better be ascertained with this technique [91, 92]. Mink et al. [93] thought that double-contrast studies were as sensitive and accurate as single-contrast studies in the diagnosis of rotator cuff tears. The site of disruption was visualized in 93% of 581 tears. The size of the defect and condition of the torn remaining tendon edges were also well seen. Kilcoyne and Matsen [94] and Vezina et al. [95] performed thin-section upright tomography following arthrography to measure the size of rotator cuff tears. The tomographic findings correlated with the surgical results and provided more information than arthrography alone [94, 95].

Hall et al. [96] have shown that morbidity from shoulder arthrography is somewhat dependent on the amount of contrast material injected, and hence, morbidity is least with double-contrast techniques. These authors suggested that the contrast agent be aspirated when the tear is shown fluoroscopically. Use of nonionic or monovalent polymeric contrast agents is associated with a lower incidence of morbidity than are standard contrast agents [97]. We use double-contrast techniques with 0.5–2 ml of Conray 60% (iothalamate methylglucamine, Mallinckrodt, St. Louis, MO) and approximately 10 cm³ of room air. The smaller amount (0.5 ml) of contrast material is used when the study is followed by CT; in those cases, we add 0.3 ml of 1/1000 epinephrine to the contrast agent to delay resorption of contrast material [96].

Calvert et al. [98] performed arthrography after surgical repair of the rotator cuff in 20 patients. In 18 of the 20, a defect of the rotator cuff was shown; however, 17 patients had complete relief of pain, and 15 had a full range of shoulder elevation. These results suggested that complete closure is not necessary for a good, functional result.

Arthrography has been used in the diagnosis of adhesive capsulitis when small joint capacity, resistance to pressure, and extravasation have been used to make the diagnosis [90]. Resnik et al. [99] reported that pressure measurements were of value in the accurate assessment of the presence

by painless full-range-of-motion exercises that led to an increased range of motion [100].

The glenoid labrum is difficult to examine on routine double-contrast arthrography. El Khoury et al. [101] introduced arthrotomography of the glenoid labrum in a modified axial position.

In 1982, Danzig et al. [102] reported on the use of CT after double-contrast arthrography in the evaluation of labral abnormalities. The ease of performance and diagnostic accuracy of this study quickly led to its acceptance in the evaluation of the glenoid labrum and other capsular structures [103–106]. This technique can show tears in the labra (Fig. 7), abnormalities in the capsular attachments (Fig. 7), and bony pathologic changes. CT arthrotomography is useful also in studying patients who redislocate after surgery; it can depict the direction of instability and other capsular, muscle, and tendon abnormalities [107]. In comparing computed and conventional arthrotomography, Deutsch et al. [108] found CT arthrotomography preferable because it was more comprehensive, required less radiation and expertise, and was better tolerated in patients with pain. It has virtually replaced arthrotomography in most institutions. Beltran et al. [109] have used CT arthrography in the sagittal plane to evaluate abnormalities of the rotator cuff. They found it more accurate than routine arthrography.

Sonography has been used in the detection of rotator cuff tears [110–112] and abnormalities of the biceps tendon [112, 113]. Positive findings in rotator cuff tears include focal hyperechogenicity, discontinuity or gap in the rotator cuff, filling defects and cuff irregularities, and thickening of the cuff with foci of increased or decreased echogenicity [114]. In 106 patients in one series, the sensitivity and specificity of sonography in detecting a rotator cuff tear were 91%. The negative predictive value was 95%, and the positive predictive value was 84% [112]. These authors thought that sonography was superior to arthrography in the examination of the biceps tendon. The major limitation of sonography is thought to be

symptoms. They were able to detect recurrent cuff tears and differentiate them from an intact rotator cuff. Others believe that sonography is difficult to master and not as sensitive as arthrography (Miller CL, Karasick D, Kurtz AB, Fenlin J, in press at *Skeletal Radiology*).

The normal anatomy [118–120] and tears of the rotator cuff (Fig. 8) [121–125] are well depicted by MR imaging. We have used paired surface coils and off-center field-of-view and oblique imaging to obtain high resolution and highly accurate evaluations of the rotator cuff. In our experience, the coronal oblique view is the most sensitive and most accurate plane for the diagnosis of rotator cuff disease [123, 124]. We believe that MR imaging is the diagnostic technique of choice in the evaluation of pathologic changes of the rotator cuff.

MR imaging may show tendonitis, which is depicted as high signal within the normal signal-void tendon [123–125]. Irregularities in the tendon also can be shown [123–125]. In patients with complete tears of the rotator cuff, the tendon becomes discontinuous and the overlying subacromial-subdeltoid fat may be obliterated (Fig. 8) [125]. T2-weighted imaging may depict fluid in the joint and subacromial-subdeltoid bursa. Retraction and atrophy of the muscle as well as fatty replacement can be identified [123–125].

Zlatkin et al. [126] found that the capsular mechanism of the shoulder could be shown well by using MR imaging. Kieft et al. [127] compared MR imaging and CT arthrography in patients with recurrent anterior dislocation of the shoulder. They found MR imaging useful in the assessment of capsular and labral abnormalities (Fig. 9) and thought that it might eventually replace CT for these patients. Our recent experience with 12 surgically proved cases tends to support this finding. The importance of high-resolution axial images with thin slices and the use of T1- and T2-weighted sequences aid in the evaluation of these abnormalities.

MR imaging may show changes in patients with impingement syndrome. Increased signal in the supraspinatus tendon, direct tendon and bursal compression, acromioclavicular joint

hypertrophy, and spur formation about the acromion can be identified [128, 129].

Subacromial bursography has been used in conjunction with plain films in the diagnosis of impingement syndrome and subacromial bursitis [130–132]. Also, it can detect incomplete tears of the superior surface of the rotator cuff [133]. Subacromial bursography is difficult to perform and interpret and is rarely used in clinical practice.

Elbow

Fluoroscopy may be helpful in the determination of the location of loose bodies and should be performed before arthrography [134]. Intraarticular loose bodies move freely with flexion and extension, whereas those that are extracapsular are wedged within the joint and move little, if at all [134]. Arthrography of the elbow may be performed by using single- or double-contrast techniques, depending on the indications for examination; fluoroscopy, tomography, or CT may be used in conjunction with the arthrogram.

Arthrography may be performed after the reduction of a dislocated elbow. However, some authors have found it unreliable in this situation [135]. Mink et al. [136] performed positive-contrast arthrography in two patients with recurrent elbow dislocation; in one patient, polytomography followed the arthrogram. These authors demonstrated the primary lesion, defined the degree of ligamentous laxity, and identified associated loose bodies.

Pavlov et al. [137] combined double-contrast arthrography with filming in a gravity-dependent position. The positive contrast material settled to the bottom of the joint cavity, and the air rose. This technique showed cartilaginous loose bodies and the status of the articular cartilage. Eto et al. [138] reported that arthrotomography was best in showing loose bodies and abnormalities of the articular cartilage. They thought that the increased accuracy of this technique was worth the additional time, radiation exposure, and expense.

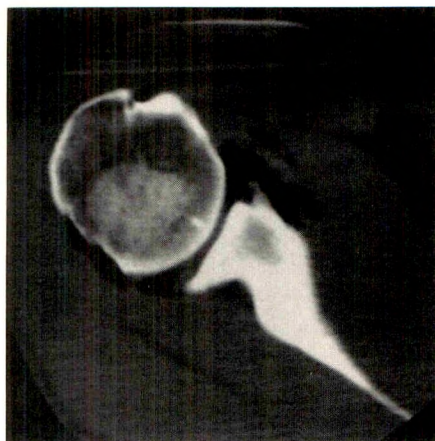
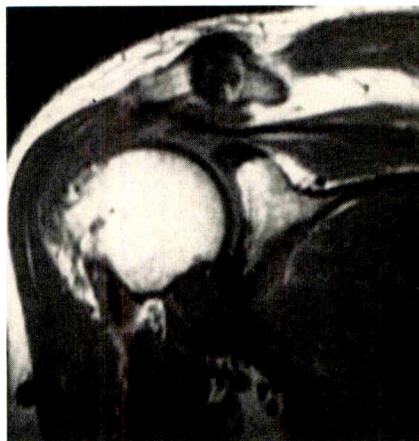
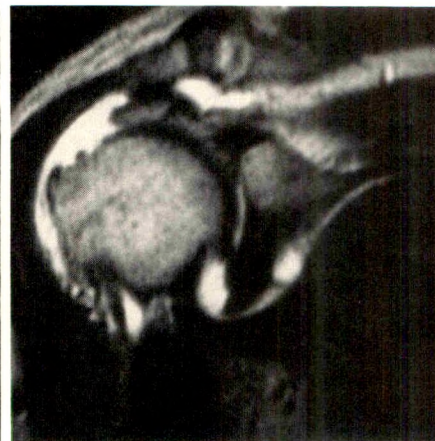


Fig. 7.—CT arthrotomogram shows absent labrum with detached capsule. Superior glenohumeral ligament is seen within large subscapularis bursa.



A



B

Fig. 8.—Rotator cuff tear.
A, Short TR/TE (800/20) spin-echo MR image shows large tear in supraspinatus tendon with loss of subdeltoid fat stripe. Acromioclavicular joint is hypertrophied and is impinging on rotator cuff.
B, Long TR/TE (2500/80) spin-echo image shows large joint effusion and fluid in subacromial-subdeltoid bursa. Joint and bursa communicate through large rotator cuff tear.

Teng et al. [139] compared conventional radiography, conventional tomography, double-contrast arthrography, and arthrotomography; they concluded that conventional tomography was sufficient for the detection or exclusion of osteocartilaginous loose bodies and that arthrotomography rarely improved the diagnostic accuracy of noncontrast methods.

CT can be performed after arthrography, with images obtained in the axial and coronal planes. One can achieve excellent visualization of the articular surfaces and evaluate loose bodies in patients with osteochondritis dissecans [140] (Fig. 10).

Recently, MR imaging has been used to define the intra- and extracapsular anatomy of the elbow in exquisite detail [141, 142]. The ligaments, articular cartilage, and neuromuscular structures are well depicted. Loose bodies, cartilaginous defects, synovial cysts, tumors, and other abnormalities about the elbow can be identified in this fashion. Despite limited experience with MR imaging of the elbow, the rapid technologic developments in MR imaging and the results in other joints suggest an optimistic result.

Wrist

We have used bone scanning as a screening procedure in patients with wrist pain and normal radiographs because a normal scan may preclude additional studies [143].

Fluoroscopy and videotaping may show dynamic abnormalities such as momentary subluxation, which are not depicted by other imaging techniques [144, 145]. Braunstein et al. [146] think that fluoroscopy should be performed in all patients with suspected ligamentous abnormalities. In their opinion, limiting the use of arthrography to patients who have negative findings on fluoroscopy would be cost-effective. The combination of the two studies [147] led to a specific anatomic diagnosis in 76% of cases.

Arthrography of the wrist must be interpreted in light of the clinical history and physical examination. Intercompartmental wrist communications increase with increasing age, and pi-

sotriquetral communications are frequently identified in normal patients [148]. Gilula and others [149, 150] thought that fluoroscopic observation with sequential spot films during injection would help localize the specific ligamentous abnormalities. On postinjection overhead films, the site of disruption may not be evident because contrast material may enter the scapholunate or naviculolunate space in a retrograde fashion, obscuring the site of abnormality.

Resnick et al. [151] thought digital arthrography was the ideal method of depicting contrast flow; they showed that filling of the midcarpal joint could also occur with pisotriquetral-hamate perforation. Manaster [152] demonstrated scaphotrapezoid tears with this technique and indicated that these, too, may lead to radiocarpal-midcarpal communications. Pittman et al. [153] added air to the positive-contrast digital subtraction examination and reported cases in which tears were seen after injection of air that were not visible on the contrast study.

Tirman et al. [154] thought that injecting the midcarpal joint would detect incomplete and small tears not visible on radiocarpal arthrography. Levinson et al. [155] used a three-injection technique in which radiocarpal arthrography was followed by midcarpal and distal radioulnar joint injections. In their series, radiocarpal arthrography alone failed to detect 17% of midcarpal communications and missed all cases of proximal detachment of the triangular fibrocartilage. We currently use the three-compartment technique in patients who have normal radiocarpal arthrograms.

Wrist arthrography can be used in the evaluation of the triangular fibrocartilage. Perforations of the triangular fibrocartilage are more common in patients with extension of the ulna beyond the distal radius (positive ulnar variance) [156]. In one series of 60 patients with persistent disability after Colles fracture, the triangular fibrocartilage was torn in 45% of cases [157].

Radiocarpal arthrography also has been used in the evaluation of arthritic disorders and can be abnormal in patients with normal radiographs. The findings include corrugation of

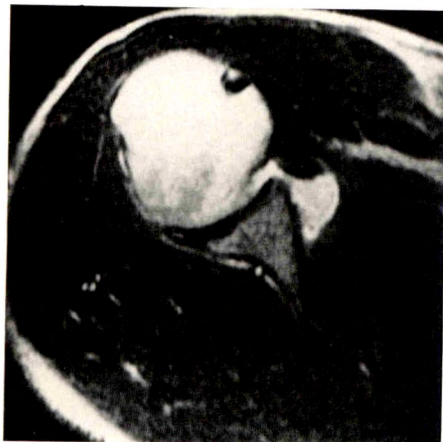


Fig. 9.—Long TR/TE (2500/80) axial spin-echo MR image shows absent anterior glenoid labrum and detached capsule with effusion. This image is comparable with that seen on CT arthrography in Fig. 7.



Fig. 10.—Anteroposterior CT arthrotomogram shows osteochondral defect in capitellum covered by articular cartilage.



Fig. 11.—Short TR/TE (600/20) spin-echo image shows interruption of triangular fibrocartilage at its radial aspect.

the synovial cavity, communications between the radiocarpal and midcarpal compartments, and radiocarpal and distal radioulnar joints. Additional, less common findings include filling of the extensor tendon sheaths and periarticular lymphatics [158, 159]. Findings are etiologically nonspecific and can be seen in inflammatory arthritis and tuberculous synovitis [160].

Arthrography may be helpful in differentiating nonunion from fibrous union of the scaphoid. In patients with nonunion, contrast material enters the fracture line and midcarpal joint; no contrast material enters the fracture line in patients with fibrous union [161]. Arthrography may also detect adhesive capsulitis in patients with persistent joint pain after trauma. Findings include decreased joint capacity, small recesses, and incomplete opacification of the joint caused by adhesions [162].

Injection of the radiocarpal joint in patients with wrist ganglia will show communications of the ganglion with the joint in two-thirds of patients [163]. These communications are usually not detected with direct injection of the ganglion (gangliography), suggesting that the connection functions like a valve.

Arthrotomography of the wrist has been performed in cadavers by Berger et al. [164, 165]. They found that lateral tomography depicted the radiocapitate and radiotriquetral ligaments [164] and anteroposterior tomography could be used to classify tears of the triangular fibrocartilage complex [165].

MR imaging of the wrist is being evaluated currently [166–168]. We have used specially designed surface coils to obtain high-resolution, thin-section images of the wrist. The triangular fibrocartilage can be evaluated with MR imaging, and disruptions are depicted best in the coronal plane (Fig. 11). Axial images may show radioulnar joint disruptions, which are usually associated with abnormalities of the triangular fibrocartilage. These can also be diagnosed by axial CT [169, 170]; supination and pronation images are sometimes added to those obtained in the neutral position [170]. Disruptions of the intercarpal ligaments also can be depicted; however, at the present time, we do not feel confident in excluding small tears of these structures on the basis of MR imaging results. Other abnormalities about the wrist that can be depicted on MR include ischemic necrosis, ganglia, tendonitis, synovitis, and tumors.

REFERENCES

- Mitchell MD, Kundel HL, Steinberg ME, Kressel HY, Alavi A, Axel L. Avascular necrosis of the hip: comparison of MR, CT, and scintigraphy. *AJR* 1986;147:67–71
- Markisz JA, Knowles JR, Altchek DW, Schneider R, Whalen JP, Cahill PT. Segmental patterns of avascular necrosis of the femoral heads: early detection with MR imaging. *Radiology* 1987;162:717–720
- Beltran J, Herman LJ, Burk JM, et al. Femoral head avascular necrosis: MR imaging with clinical-pathologic and radionuclide correlation. *Radiology* 1988;166:215–220
- Collier BD, Carrera GF, Johnson RP, et al. Detection of femoral head avascular necrosis in adults by SPECT. *J Nucl Med* 1985;26:979–987
- Kulkarni MV, Tarr RR, Kim EE, McArdle CB, Partain CL. Potential pitfalls of magnetic resonance imaging in the diagnosis of avascular necrosis. *J Nucl Med* 1987;28:1052–1054
- Dihlmann W. CT analysis of the upper end of the femur: the asterisk sign and ischaemic bone necrosis of the femoral head. *Skeletal Radiol* 1982;8:251–258
- Magid D, Fishman EK, Scott WW Jr, et al. Femoral head avascular necrosis: CT assessment with multiplanar reconstruction. *Radiology* 1985;157:751–756
- Sartoris JD, Resnick D, Gershuni D, Bielecki D, Meyers M. Computed tomography with multiplanar reformation and 3-dimensional image analysis in the preoperative evaluation of ischemic necrosis of the femoral head. *J Rheumatol* 1986;13:153–163
- Mitchell DG, Kressel HY, Arger PH, Dalinka M, Spritzer CE, Steinberg ME. Avascular necrosis of the femoral head: morphologic assessment by MR imaging, with CT correlation. *Radiology* 1986;161:739–742
- Shuman WP, Castagno AA, Baron RL, Richard ML. MR imaging of avascular necrosis of the femoral head: value of small-field-of-view sagittal surface-coil images. *AJR* 1988;150:1073–1078
- Totty WG, Murphy WA, Ganz WI, Kumar B, Daum WJ, Siegel BA. Magnetic resonance imaging of the normal and ischemic femoral head. *AJR* 1984;143:1273–1280
- Mitchell DG, Rao VM, Dalinka MK, et al. Femoral head avascular necrosis: correlation of MR imaging, radiographic staging, radionuclide imaging, and clinical findings. *Radiology* 1987;162:709–715
- Mitchell DG, Rao VM, Dalinka M, et al. Hematopoietic and fatty bone marrow distribution in the normal and ischemic hip: new observations with 1.5-T MR imaging. *Radiology* 1986;161:199–202
- Mitchell DG, Rao V, Dalinka M, et al. MRI of joint fluid in the normal and ischemic hip. *AJR* 1986;146:1215–1218
- Staple TW. Arthrographic demonstration of iliopsoas bursa extension of the hip joint. *Radiology* 1972;102:515–516
- Sartoris DJ, Danzig L, Gilula L, Greenway G, Resnick D. Synovial cysts of the hip joint and iliopsoas bursitis: a spectrum of imaging abnormalities. *Skeletal Radiol* 1985;14:85–94
- Guyer B, Levinsohn EM. Recurrent anterior dislocation of the hip: case report with arthrographic findings. *Skeletal Radiol* 1983;10:262–264
- Murphy WA, Siegel MJ, Gilula LA. Arthrography in the diagnosis of unexplained chronic hip pain with regional osteopenia. *AJR* 1977;129:283–287
- Lequesne M, Becker J, Bard M, Witvoet J, Postel M. Capsular constriction of the hip: arthrographic and clinical considerations. *Skeletal Radiol* 1981;6:1–10
- Peters JC, Coleman GB, Turner ML, et al. CT evaluation of enlarged iliopsoas bursa. *AJR* 1980;135:392–394
- Ghelman B. Meniscal tears of the knee: evaluation of high-resolution CT combined with arthrography. *Radiology* 1985;157:23–27
- Manco LG, Kavanaugh JH, Fay JJ, Bilfield BS. Meniscus tears of the knee: prospective evaluation with CT. *Radiology* 1986;159:147–151
- Manco LG, Kavanaugh JH, Lozman J, Colman ND, Bilfield BS, Fay JJ. Diagnosis of meniscal tears using high-resolution computed tomography. *J Bone Joint Surg [Am]* 1987;69-A:498–502
- Passariello R, Trecco F, de Paulis F, Masciocchi C, Bonanni G, Zobel BB. Meniscal lesions of the knee joint: CT diagnosis. *Radiology* 1985;157:29–34
- Levinsohn EM, Baker BE. Prearthrotomy diagnostic evaluation of the knee: review of 100 cases diagnosed by arthrography and arthroscopy. *AJR* 1980;134:107–111
- Burk DL Jr, Kanal E, Brunberg JA, Johnstone GF, Swensen HE, Wolf GL. 1.5-T surface-coil MRI of the knee. *AJR* 1986;147:293–300
- Burk DL Jr, Dalinka MK, Kanal E, Brunberg JA. High resolution MR imaging of the knee. In: Kressel HY, ed. *Magnetic resonance annual* 1988. New York: Raven, 1988:1–36
- Gallimore GW Jr, Harms SE. Knee injuries: high-resolution MR imaging. *Radiology* 1986;160:457–461
- Reicher MA, Rauschnig W, Gold RH, Bassett LW, Lufkin RB, Glen W Jr. High-resolution magnetic resonance imaging of the knee joint: normal anatomy. *AJR* 1985;145:895–902
- Reicher MA, Bassett LW, Gold RH. High-resolution magnetic resonance imaging of the knee joint: pathologic correlations. *AJR* 1985;145:903–909
- Reicher MA, Hartzman S, Bassett LW, Mandelbaum B, Duckwiler G, Gold RH. MR imaging of the knee. Part I. Traumatic disorders. *Radiology* 1987;162:547–551
- Reicher MA, Hartzman S, Duckwiler GR, Bassett LW, Anderson LJ, Gold RJ. Meniscal injuries: detection using MR imaging. *Radiology*

- 1986;159:753-757
33. Mink JH, Levy T, Crues JV III. Tears of the anterior cruciate ligament and menisci of the knee: MR imaging evaluation. *Radiology* 1988;167:769-774
34. Mink JH, Reicher MA, Crues JV. *Magnetic resonance imaging of the knee*. New York: Raven, 1987:1-178
35. Stoller DW, Martin C, Crues JV III, Kaplan L, Mink JH. Meniscal tears: pathologic correlation with MR imaging. *Radiology* 1987;163:731-735
36. Hajek PC, Gyls-Morin VM, Baker LL, Sartoris DJ, Haghighi P, Resnick D. The high signal intensity meniscus of the knee: magnetic resonance evaluation and in vivo correlation. *Invest Radiol* 1987;22:883-890
37. Crues JV III, Mink J, Levy TL, Lotysch M, Stoller DW. Meniscal tears of the knee: accuracy of MR imaging. *Radiology* 1987;164:445-448
38. Lee JK, Yao L, Phelps CT, Wirth CR, Czajka J, Lozman J. Anterior cruciate ligament tears: MR imaging compared with arthroscopy and clinical tests. *Radiology* 1988;166:861-864
39. Yao L, Lee JK. Occult intraosseous fracture: detection with MR imaging. *Radiology* 1988;167:749-751
40. Gyls-Morin VM, Hajek PC, Sartoris DJ, Resnick D. Articular cartilage defects: detectability in cadaver knees with MR. *AJR* 1987;148:1153-1157
41. Hajek PC, Baker LL, Sartoris DJ, Neumann CH, Resnick D. MR arthrography: anatomic-pathologic investigation. *Radiology* 1987;163:141-147
42. Mesgarzadeh M, Sapega AA, Bonakdarpour A, et al. Osteochondritis dissecans: analysis of mechanical stability with radiography, scintigraphy, and MR imaging. *Radiology* 1987;165:775-780
43. Yulish BS, Montanez J, Goodfellow DB, Bryan PJ, Mulopulos GP, Modic MT. Chondromalacia patellae: assessment with MR imaging. *Radiology* 1987;164:763-766
44. Martinez S, Korobkin M, Fondren FB, Hedlund LW, Goldner LJ. Computed tomography of the normal patellofemoral joint. *Invest Radiol* 1983;18:249-253
45. Martinez S, Korobkin M, Fondren FB, Hedlund LW, Goldner JL. Diagnosis of patellofemoral malalignment by computed tomography. *J Comput Assist Tomogr* 1983;7:1050-1053
46. Boven F, Bellemans A-M, Geurts J, De Boeck H, Potvliege R. The value of computed tomography scanning in chondromalacia patellae. *Skeletal Radiol* 1982;8:183-185
47. Burk DL Jr, Dalinka MK, Kanal EM, et al. Meniscal and ganglion cysts of the knee: MR evaluation. *AJR* 1988;150:331-336
48. Passariello R, Masciocchi C, Zobel BB, DePaulis F, Trecco F. Computed tomography of meniscal cysts of the knee joint. *Eur J Radiol* 1987;7:83-86
49. Herman LJ, Beltran J. Pitfalls in MR imaging of the knee. *Radiology* 1988;167:775-781
50. Hagggar AM, Froelich JW, Hearshen DO, Sadasivan K. Meniscal abnormalities of the knee: 3DFT fast-scan GRASS MR imaging. *AJR* 1988;150:1341-1344
51. Spritzer CE, Vogler JB, Martinez S, et al. MR imaging of the knee: preliminary results with a 3DFT GRASS pulse sequence. *AJR* 1988;150:597-603
52. Tyrrell RL, Gluckert K, Pathria M, Modic MT. Fast three-dimensional MR imaging of the knee: comparison with arthroscopy. *Radiology* 1988;166:865-872
53. Pollack MS, Dalinka MK, Kressel HY, Lotke PA, Spritzer CE. Magnetic resonance imaging in the evaluation of suspected osteonecrosis of the knee. *Skeletal Radiol* 1987;16:121-127
54. Spritzer CE, Dalinka MK, Kressel HY. Magnetic resonance imaging of pigmented villonodular synovitis: a report of two cases. *Skeletal Radiol* 1987;16:216-219
55. Gomori JM, Grossman RI, Hackney DB, Goldberg HI, Zimmerman RA, Bilaniuk LT. Variable appearances of subacute intracranial hematomas on high-field spin-echo MR. *AJR* 1988;150:171-178
56. Yulish BS, Lieberman JM, Strandjord SE, Bryan PJ, Mulopulos GP, Modic MT. Hemophilic arthropathy: assessment with MR imaging. *Radiology* 1987;164:759-762
57. Kulkarni MV, Drolshagen LF, Kaye JJ, et al. MR imaging of hemophilic arthropathy. *J Comput Assist Tomogr* 1986;10:445-449
58. Wilson DA, Prince JR. MR imaging of hemophilic pseudotumors: case report. *AJR* 1988;150:349-350
59. Wilson DJ, McLardy-Smith PD, Woodham CH, MacLarnon JC. Diagnostic ultrasound in haemophilia. *J Bone Joint Surg [Br]* 1987;69-B:103-107
60. Hermann G, Yeh H-C, Gilbert MS. Computed tomography and ultrasonography of the hemophilic pseudotumor and their use in surgical planning. *Skeletal Radiol* 1986;15:123-128
61. Shirkhoda A, Mauro MA, Staab EV, Blatt PM. Soft-tissue hemorrhage in hemophilic patients. *Radiology* 1983;147:811-814
62. Brostrom L, Liljedahl S-O, Lindvall N. Sprained ankles. II. Arthrographic diagnosis of recent ligament ruptures. *Acta Chir Scand* 1965;129:485-499
63. Lindholmer E, Foged N, Jensen J Th. Arthrography of the ankle. *Acta Radiol [Diagn] (Stockh)* 1977;19:585-598
64. Ala-Ketola L, Puranen J, Kolvisto E, Puupera M. Arthrography in the diagnosis of ligament injuries and classification of ankle injuries. *Radiology* 1977;125:63-68
65. Kaye JJ. The ankle. In: Freiburger RG, Kaye JJ, eds. *Arthrography*. New York: Appleton-Century-Crofts, 1979:237-260
66. Dory MA. Arthrography of the ankle joint in chronic instability. *Skeletal Radiol* 1986;15:291-294
67. Goldman AB, Katz MC, Freiburger RH. Posttraumatic adhesive capsulitis of the ankle: arthrographic diagnosis. *AJR* 1976;127:585-588
68. Spiegel PK, Staples OS. Arthrography of the ankle joint: problems in diagnosis of acute lateral ligament injuries. *Radiology* 1975;114:587-590
69. Sauser DD, Nelson RC, Lavine MH, Wu CW. Acute injuries of the lateral ligaments of the ankle: comparison of stress radiography and arthrography. *Radiology* 1983;148:653-657
70. van Moppes FI, van den Hoogenband CR, van Engelshoven JMA, Betts-Brown A. Arthrography, talar tilt and surgical findings after inversion trauma of the ankle. *ROFO* 1981;134:413-416
71. Resnick D, Goergen RG. Peroneal tenography in previous calcaneal fractures. *Radiology* 1975;115:211-213
72. Gilula LA, Oloff L, Caputi R, Destouet JM, Jacobs A, Solomon MA. Ankle tenography: a key to unexplained symptomatology. Part II. Diagnosis of chronic tendon disabilities. *Radiology* 1984;151:581-587
73. Rosenberg ZS, Feldman F, Singson RD, Kane R. Ankle tendons: evaluation with CT. *Radiology* 1988;166:221-226
74. Rosenberg ZS, Feldman F, Singson RD. Peroneal tendon injuries: CT analysis. *Radiology* 1986;161:743-748
75. Rosenberg ZS, Hajss MH, Noto AM, et al. Rupture of the posterior tibial tendon: CT and surgical findings. *Radiology* 1988;167:489-493
76. Rosenberg ZS, Feldman F, Singson RD, Price GJ. Peroneal tendon injury associated with calcaneal fractures: CT findings. *AJR* 1987;149:125-129
77. Beltran J, Noto AM, Mosure JC, Shamam OM, Weiss KL, Zuelzer WA. Ankle: surface coil MR imaging at 1.5 T. *Radiology* 1986;161:203-209
78. Beltran J, Noto AM, Herman LJ, Lubbers LM. Tendons: high-field-strength, surface coil MR imaging. *Radiology* 1987;162:735-740
79. Quinn SF, Murray WT, Clark RA, Cochran CF. Achilles tendon: MR imaging at 1.5 T. *Radiology* 1987;164:767-770
80. Pineda C, Resnick D, Greenway G. Diagnosis of tarsal coalition with computed tomography. *Clin Orthop* 1986;208:282-288
81. Sarno RC, Carter BL, Bankoff MS, Semine MC. Computed tomography in tarsal coalition. *J Comput Assist Tomogr* 1984;8:1155-1160
82. Deutsch AL, Resnick D, Campbell G. Computed tomography and bone scintigraphy in the evaluation of tarsal coalition. *Radiology* 1982;144:137-140
83. Stoskopf CA, Hernandez RJ, Kelikian A, Tachdjian MO, Dias LS. Evaluation of tarsal coalition by computed tomography. *J Pediatr Orthop* 1984;4:365-369
84. Goldman AB, Pavlov H, Schneider R. Radionuclide bone scanning in subtalar coalitions: differential considerations. *AJR* 1982;138:427-432
85. Kaye JJ, Ghelman B, Schneider R. Talocalcaneonavicular joint arthrography for sustentacular-talar tarsal coalitions. *Radiology* 1975;115:730-731
86. Marchisello PJ. The use of computerized axial tomography for the evaluation of talocalcaneal coalition. *J Bone Joint Surg [Am]* 1987;69-A:609-611
87. Heare MM, Gillespy T III, Bittar ES. Direct coronal computed tomography arthrography of osteochondritis dissecans of the talus. *Skeletal Radiol* 1988;17:187-189
88. Yulish BS, Mulopulos GP, Goodfellow DB, Bryna PJ, Modic MT, Dollinger BM. MR imaging of osteochondral lesions of talus. *J Comput Assist Tomogr* 1987;11:296-301

89. Woolson ST, Dev P, Fellingham LL, Vassiliadis A. Three-dimensional imaging of the ankle joint from computerized tomography. *Foot Ankle* 1985;6:2-6
90. Killoran PJ, Marcove RC, Freiburger RH. Shoulder arthrography. *AJR* 1968;103:658-668
91. Ghelman B, Goldman AB. The double contrast shoulder arthrogram: evaluation of rotator cuff tears. *Radiology* 1977;124:251-254
92. Goldman AB, Ghelman B. The double-contrast shoulder arthrogram. *Radiology* 1978;127:655-663
93. Mink JG, Harris E, Rappaport M. Rotator cuff tears: evaluation using double-contrast shoulder arthrography. *Radiology* 1985;157:621-623
94. Kilcoyne RF, Matsen FA III. Rotator cuff tear measurement by arthro-pneumotomography. *AJR* 1983;140:315-318
95. Vezina JA, Des Marchais JE, Beauregard CG. Double-contrast arthro-tomography of the shoulder: correlation of radiological and surgical findings in complete rotator cuff tears. *J Can Assoc Radiol* 1985;36:183-188
96. Hall FM, Rosenthal DI, Goldberg RP, Wyshak G. Morbidity from shoulder arthrography: etiology, incidence, and prevention. *AJR* 1981;136:59-62
97. Hall FM, Goldberg RP, Wyshak G, Kilcoyne RF. Shoulder arthrography: comparison of morbidity after use of various contrast media. *Radiology* 1985;154:339-341
98. Calvert PT, Packer NP, Stoker DJ, Bayley JIL, Kessel L. Arthrography of the shoulder after operative repair of the torn rotator cuff. *J Bone Joint Surg [Br]* 1986;68-B:147-150
99. Resnik CS, Fronek J, Frey C, Gershuni D, Resnick D. Intra-articular pressure determination during glenohumeral joint arthrography: preliminary investigation. *Invest Radiol* 1984;19:45-60
100. Gilula LA, Schoenacker PL, Murphy WA. Shoulder arthrography as a treatment modality. *AJR* 1978;131:1047-1048
101. El-Khoury GY, Albright JP, Yousef MMA, Montgomery WJ, Tuck SL. Arthro-tomography of the glenoid labrum. *Radiology* 1979;131:333-337
102. Danzig L, Resnick D, Greenway G. Evaluation of unstable shoulders by computed tomography: a preliminary study. *Am J Sports Med* 1982;10:138-141
103. McNiesh LM, Callaghan JJ. CT arthrography of the shoulder: variations of the glenoid labrum. *AJR* 1987;149:963-966
104. Rafii M, Firooznia H, Golimbu C, Minkoff J, Bonamo J. CT arthrography of capsular structures of the shoulder. *AJR* 1986;146:361-367
105. Singson RD, Feldman F, Bigliani L. CT arthrographic patterns in recurrent glenohumeral instability. *AJR* 1987;149:749-753
106. Shuman WP, Kilcoyne RF, Matsen FA, Rogers JV, Mack LA. Double-contrast computed tomography of the glenoid labrum. *AJR* 1983;141:581-584
107. Singson RD, Feldman F, Bigliani LU, Rosenberg ZS. Recurrent shoulder dislocation after surgical repair: double-contrast CT arthrography: work in progress. *Radiology* 1987;164:425-428
108. Deutsch AL, Resnick D, Mink JH, et al. Computed and conventional arthro-tomography of the glenohumeral joint: normal anatomy and clinical experience. *Radiology* 1984;153:603-609
109. Beltran J, Gray LA, Bools JC, Zuelzer W, Weis LD, Unverferth LJ. Rotator cuff lesions of the shoulder: evaluation by direct sagittal CT arthrography. *Radiology* 1986;160:161-165
110. Mack LA, Matsen FA, Kilcoyne RF, Davies PK, Sickler ME. US evaluation of the rotator cuff. *Radiology* 1985;157:205-209
111. Middleton WD, Edelstein G, Reinus WR, Melson GL, Totty WG, Murphy WG. Sonographic detection of rotator cuff tears. *AJR* 1985;144:349-353
112. Middleton WD, Reinus WR, Totty WG, Melson CL, Murphy WA. Ultrasonographic evaluation of the rotator cuff and biceps tendon. *J Bone Joint Surg [Am]* 1986;68-A:440-450
113. Middleton WD, Reinus WR, Totty WG, Melson CL, Murphy WA. US of the biceps tendon apparatus. *Radiology* 1985;157:211-215
114. Harcke AT, Grissom LE, Finkelstein MS. Evaluation of the musculoskeletal system with sonography. *AJR* 1988;150:1253-1261
115. Middleton WD, Reinus WR, Melson GL, Totty WG, Murphy WA. Pitfalls of rotator cuff sonography. *AJR* 1986;146:555-560
116. Mack LA, Nyberg DA, Matsen FR III, Kilcoyne RF, Harvey D. Sonography of the postoperative shoulder. *AJR* 1988;150:1089-1093
117. Crass JR, Craig EV, Feinberg SB. Sonography of the postoperative rotator cuff. *AJR* 1986;146:561-564
118. Seeger LL, Ruszkowski JT, Bassett LW, Kay SP, Kahmann RD, Ellman H. MR imaging of the normal shoulder: anatomic correlation. *AJR* 1987;148:83-91
119. Kieft GJ, Bloem JL, Obermann WR, Verbout AJ, Rozing PM, Doornbos J. Normal shoulder: MR imaging. *Radiology* 1986;159:741-745
120. Middleton WD, Kneeland JB, Carrera GF, et al. High-resolution MR imaging of the normal rotator cuff. *AJR* 1987;148:559-564
121. Kneeland JB, Middleton WD, Carrera GF, et al. MR imaging of the shoulder: diagnosis of rotator cuff tears. *AJR* 1987;149:333-337
122. Kneeland JB, Carrera GF, Middleton WD, et al. Rotator cuff tears: preliminary application of high-resolution MR imaging with counter rotating current loose-gap resonators. *Radiology* 1986;160:695-699
123. Zlatkin MB, Dalinka MK, Kressel HY. Magnetic resonance imaging of the shoulders. In: Kressel HY. *Magnetic resonance quarterly* 1989. New York: Raven, 1988
124. Zlatkin MB, Dalinka MK, Kressel HY. Magnetic resonance imaging of the shoulder. In: Torg JS, ed. *Current therapy in sports medicine*, vol 2. Ontario:Decker (in press)
125. Zlatkin MB, Reicher MA, Kellerhouse LE, McDade W, Vetter L, Resnick D. The painful shoulder: MR imaging of the glenohumeral joint. *J Comput Assist Tomogr* 1988;12:995-1001
126. Zlatkin MB, Bjorkengren AG, Gylys-Morin V, Resnick D, Sartoris DJ. Cross-sectional imaging of the capsular mechanism of the glenohumeral joint. *AJR* 1988;150:151-158
127. Kieft GJ, Bloem JL, Rozing PM, Obermann WR. MR imaging of recurrent anterior dislocation of the shoulder: comparison with CT arthrography. *AJR* 1988;150:1083-1087
128. Kieft GH, Bloem JL, Rozing PM, Obermann WR. Rotator cuff impingement syndrome: MR imaging. *Radiology* 1988;166:211-214
129. Seeger LL, Gold RH, Bassett LW, Ellman H. Shoulder impingement syndrome: MR findings in 53 shoulders. *AJR* 1988;150:343-347
130. Strizak AM, Danzig L, Jackson DW, Greenway G, Resnick D, Staple T. Subacromial bursography. *J Bone Joint Surg [Am]* 1982;64-A:196-201
131. Hardy DC, Vogler JB III, White RH. The shoulder impingement syndrome: prevalence of radiographic findings and correlation with response to therapy. *AJR* 1986;147:557-561
132. Cone RO III, Resnick D, Danzig L. Shoulder impingement syndrome: radiographic evaluation. *Radiology* 1984;150:29-33
133. Fukuda H, Mikasa M, Yamanaka K. Incomplete thickness rotator cuff tears diagnosed by subacromial bursography. *Clin Orthop* 1987;223:51-58
134. Hudson TM. Joint fluoroscopy before arthrography: detection and evaluation of loose bodies. *Skeletal Radiol* 1984;12:199-203
135. Josefsson PO, Andren L, Gentz CF, Johnell O. Arthrography of the dislocated elbow joint. *Acta Radiol [Diagn]* (Stockh) 1984;25:143-145
136. Mink JH, Eckardt JJ, Grant TT. Arthrography in recurrent dislocation of the elbow. *AJR* 1981;136:1242-1244
137. Pavlov H, Ghelman B, Warren RF. Double-contrast arthrography of the elbow. *Radiology* 1979;130:87-95
138. Eto RT, Anderson PW, Harley JD. Elbow arthrography with the application of tomography. *Radiology* 1975;115:283-288
139. Teng MM, Murphy WA, Gilula LA, et al. Elbow arthrography: a reassessment of the technique. *Radiology* 1984;153:611-613
140. Singson RD, Feldman F, Rosenberg ZS. Elbow joint: assessment with double-contrast CT arthrography. *Radiology* 1986;160:167-173
141. Middleton WD, Macrander S, Kneeland JB, Froncisz W, Jesmanowicz A, Hyde JS. MR imaging of the normal elbow: anatomic correlation. *AJR* 1987;149:543-547
142. Bunnell DH, Fisher DA, Lawrence LW, Gold RH, Ellman H. Elbow joint: normal anatomy on MR images. *Radiology* 1987;165:527-531
143. Dalinka MK. Evaluation of the painful wrist. In: Heuck FJW, Donner MW, eds. *Radiology today IV*. New York: Springer-Verlag, 1987:165-169
144. Protas JM, Jackson WT. Evaluating carpal instabilities with fluoroscopy. *AJR* 1980;135:137-140
145. White SJ, Louis DS, Braunstein EM, Hankin FM, Greene TL. Capitulum-lunate instability: recognition by manipulation under fluoroscopy. *AJR* 1984;143:361-364
146. Braunstein EM, Vyadreny KH, Louis DS, Hankin FM. Cost effectiveness of wrist fluoroscopy and arthrography in the evaluation of obscure wrist pain. *Orthopedics* 1986;9:1504-1506
147. Braunstein EM, Louis DS, Greene TL, Hankin FM. Fluoroscopic and arthrographic evaluation of carpal instability. *AJR* 1985;144:1259-1262
148. Trentham DE, Hamm RL, Masi AT. Wrist arthrography: review and

- comparison of normals, rheumatoid arthritis and gout patients. *Semin Arthritis Rheum* 1975;5:105-120
149. Gilula LA, Totty WG, Weeks PM. Wrist arthrography: the value of fluoroscopic spot viewing. *Radiology* 1983;146:555-556
150. Gilula LA, Hardy DC, Totty WG, Reinus WR. Fluoroscopic identification of torn intercarpal ligaments after injection of contrast material. *AJR* 1987;149:761-764
151. Resnick D, Andre M, Kerr R, Pineda C, Guerra J Jr, Atkinson D. Digital arthrography of the wrist: a radiographic-pathologic investigation. *AJR* 1984;142:1187-1190
152. Manaster BJ. Digital wrist arthrography: precision in determining the site of radiocarpal-midcarpal communication. *AJR* 1986;147:563-566
153. Pittman CC, Quinn SF, Belsole R, Green T, Rayhack J. Digital subtraction wrist arthrography: use of double contrast technique as a supplement to single contrast arthrography. *Skeletal Radiol* 1988;17:119-122
154. Tirman RM, Weber ER, Synder LL, Koonce TW. Midcarpal wrist arthrography for detection of tears of the scapholunate and lunotriquetral ligaments. *AJR* 1985;144:107-108
155. Levinsohn EM, Palmer AK, Coren AB, Zinberg E. Wrist arthrography: the value of the three compartment injection technique. *Skeletal Radiol* 1987;16:539-544
156. Levinsohn EM, Palmer AK. Arthrography of the traumatized wrist. *Radiology* 1983;146:647-651
157. Mohanti RC, Kar N. Study of triangular fibrocartilage of the wrist joint in Colles' fracture. *Injury* 1980;11:321-324
158. Ranawat CS, Harrison MO, Jordan LR. Arthrography of the wrist joint. *Clin Orthop* 1972;83:6-12
159. Resnick D. Arthrography in the evaluation of arthritic disorders of the wrist. *Radiology* 1974;113:331-340
160. Dalinka MK, Osterman AL, Lynch R, Harty M. Wrist arthrography. In: Goldsmith HS, ed. *Practice of surgery*. Philadelphia: Harper & Row, 1982:65-85
161. Roy C, Godin C, Dussault RG. Complementary role of wrist arthrography in non-union of scaphoid fractures. *J Can Assoc Radiol* 1985;36:194-196
162. Maloney MD, Sauser DD, Hanson EC, Wood VE, Thiel AE. Adhesive capsulitis of the wrist: arthrographic diagnosis. *Radiology* 1988;167:187-190
163. Andren L, Eiken O. Arthrographic studies of wrist ganglions. *J Bone Joint Surg [Am]* 1971;53-A:299-302
164. Berger RA, Blair WF, El-Khoury GY. Arthrotomography of the wrist: the palmar radiocarpal ligaments. *Clin Orthop* 1984;186:224-229
165. Berger RA, Blair WF, El-Khoury GY. Arthrotomography of the wrist: the triangular fibrocartilage complex. *Clin Orthop* 1983;172:257-264
166. Koenig H, Lucas D, Meissner R, Phys D. The wrist: a preliminary report on high-resolution MR imaging. *Radiology* 1986;160:463-467
167. Weiss KL, Beltran J, Shamam OM, Stilla RF, Levey M. High-field MR surface-coil imaging of the hand and wrist. Part I. Normal anatomy. *Radiology* 1986;160:143-146
168. Weiss KL, Beltran J, Lubbers LM. High-field MR surface-coil imaging of the hand and wrist. Part II. Pathologic correlations and clinical relevance. *Radiology* 1986;160:147-152
169. Mino DE, Palmer AK, Levinsohn EM. Radiography and computerized tomography in the diagnosis of incongruity of the distal radio-ulnar joint. *J Bone Joint Surg [Am]* 1985;67-A:247-252
170. Wechsler RJ, Wehbe MA, Rifkin MD, Edeiken J, Branch HM. Computed tomography diagnosis of distal radioulnar subluxation. *Skeletal Radiol* 1987;16:1-5

Progress in Radiology

Dual-Energy Radiographic Absorptiometry for Bone Densitometry: Current Status and Perspective

David J. Sartoris¹ and Donald Resnick^{1,2}

Bone mineral analysis plays an important role in both detecting and managing osteoporosis and other forms of metabolic bone disease. However, the concept of bone density measurement, particularly as applied to screening for osteoporosis, has recently been challenged by the internal medicine community, owing in part to the suboptimal nature of existing methods [1, 2]. The most widely used of these currently include single-photon absorptiometry (SPA), dual-photon absorptiometry (DPA), and quantitative CT [3, 4]. SPA is used to measure bone mineral content of the distal radius and os calcis, and some investigators have found that measurements made at these anatomic sites do not correlate well with measurements made in the spine and hip, which are much more important sites of fracture in osteopenic states [5]. Quantitative CT can measure only the spine without sophisticated data processing, uses an expensive piece of equipment in demand for other studies, involves high radiation doses, and is subject to measurement errors (single-energy) owing to varying fat content of the marrow [6, 7]. DPA, which measures an integral of cortical and trabecular bone in the spine or hip, has problems including less-than-ideal precision and image spatial resolution, periodic expensive source replacement, and a long examination time [8, 9].

In response to these dilemmas, an innovative approach to noninvasive bone densitometry, dual-energy radiographic absorptiometry (DRA), has recently been introduced by three independent manufacturers (Hologic, Inc., Waltham, MA; Lunar, Madison, WI; and Norland, Fort Atkinson, WI). This report

describes the background, design, performance, and preliminary results derived by DRA, with comparative reference to conventional methods. The emphasis on the system developed by Hologic reflects the authors' personal experience and is in no way intended to suggest its superiority over other equipment of this type.

Background

DRA is a new approach to measuring bone mineral content in the spine, the hip, and other anatomic sites. The technique is similar in concept to DPA but has many additional advantages. DRA uses an X-ray tube rather than a radioisotopic source and consequently has higher resolution (1.5 mm FWHM [full-width at half-maximum]) and greater speed (5 vs 20 min) than existing DPA instruments do. More importantly, DRA makes possible a major improvement in precision, a feature that is expected to significantly enhance the clinical usefulness of projectional-type measurements. Table 1 provides an overview of the principal characteristics of DRA as compared with other widely used methods for measuring bone mineral content. DRA is appropriately thought of as a new generation of bone densitometer that, although similar in operation to DPA, offers important technical and performance advantages.

One of the major advantages associated with the use of an X-ray source over a radioisotope is its intensity. An X-ray

Received April 29, 1988; accepted after revision October 14, 1988.

¹ Department of Radiology, University of California, San Diego, Medical Center, and University of California, San Diego, School of Medicine, 225 Dickinson St., H-756, San Diego, CA 92103. Address reprint requests to D. J. Sartoris.

² Department of Radiology, Veterans Administration Medical Center, 3350 La Jolla Village Dr., San Diego, CA 92161.

TABLE 1: Comparison of Bone Mineral Measurement Systems

Variable	Single-Photon Absorptiometry	Dual-Photon Absorptiometry	Single-Energy Quantitative CT	Dual-Energy Radiographic Absorptiometry
Radiation source	^{125}I	^{153}Gd	X-ray	X-ray
Dose (skin exposure in mR)	$\approx 6-18$	1-10	100-1000	<3
Examination time (min)	10 (radius)	20-30 (spine)	5-10 (spine)	5 (spine)
Source renewal (months)	6	12-18	NA	NA
Examination sites	Distal radius, os calcis	Spine, femur	Spine, femur	Spine, femur, total body
Precision (% CV):				
In vitro	1-2	1-2	0.5	0.4
In vivo	3	2-3	1.3	1
Accuracy (%)	1	1-3	5-15	9
Trabecular vs integral measurement	Integral	Integral	Trabecular	Integral
Fat error relevant?	No	No	Yes	No

Note.—NA = not applicable; CV = coefficient of variation.

source with an average tube current of 1 mA produces 500 to 1000 times more photon flux than does a 1-Ci (3.7×10^{10} Bq) gadolinium-153 source used in conventional DPA systems. In order to take advantage of the intense beam produced by an X-ray source, the issues of source stability and beam hardening must be addressed.

A dual-energy projection approach to bone densitometry with the use of an X-ray tube source was pioneered during the 1960s and 1970s in Scandinavia as the technique X-ray spectrophotometry [10-12]. Subsequently, a comparable approach to bone mass measurements in the femoral neck using a General Electric (Milwaukee, WI) prototype imaging unit was reported [13, 14]. In cadaveric femurs, positive simple linear correlation was observed between DRA measurements and dry density; ash fraction; cross-sectional cortical bone area; and, to a lesser degree, force required for fracture. However, DRA measurements did not correlate with trabecular bone volume, failure time, or Singh trabecular grade. DRA results related linearly to mineral-equivalent solution (K_2HPO_4) concentration and showed long-term reproducibility in repeated specimen studies [15].

DRA of the proximal femur subsequently was performed successfully in patients for densitometric evaluation, using the same General Electric prototype system [13]. Age-related regression plots were derived for both women and men, with correlative reference to clinical and laboratory parameters. Although promising clinical results were obtained, the system did not function ideally as a bone densitometer because it had been designed primarily for dual-energy imaging [16] and delivered a relatively high radiation dose.

Equipment for DRA

In the Federal Drug Administration-approved system developed by Hologic (model QDR-1000), a self-contained X-ray source mounted beneath the patient provides alternating pulses at 70 and 140 kVp. A "raster scan" (X-Y) pattern and tight beam collimation are used in conjunction with a calibra-

tion disk containing various X-ray-absorbing materials. The patient:calibration-material attenuation ratio is independent of all variations in the source or detectors and compensates for beam hardening. The software of this device currently is available for the lumbar spine (Fig. 1) and proximal femur, and future planned upgrades include a total-body scanning capability.

A competitive system for DRA bone densitometry using an X-ray tube photon source has recently been developed by a manufacturer of DPA equipment (DPX, Lunar Radiation Corp., Madison, WI). This prototype differs from the Hologic unit in its approach to energy separation (selective constant-potential K-edge filtration as opposed to alternate tube pulsing at different voltages), as well as the resultant effective beam energies (40/70 vs 43/110 keV). An inherently stable, low-scatter (operator exposure <0.25 mR [$<6.44 \times 10^{-8}$ C/kg] per scan at 1 m), relatively monochromatic beam thus exposes each pixel uniformly to both energies with negligible effect of tissue thickness and/or composition. An integral-line scintillation detector and photomultiplier tube are used for photon counting, and software currently allows densitometric analysis of the spine (Fig. 2) and proximal femur, with future versions planned for the tibia, proximal humerus, radius, and total body (including percent lean/fat soft-tissue characterization) [17]. The footprint of this system is about 25% smaller than that of the Hologic unit (2.23 vs 2.97 m²). Regional scans of the spine or femur require about 4-6 min with either scanner.

Norland Corp. (Fort Atkinson, WI) has recently announced the development of a work-in-progress X-ray bone densitometer (model XR26). The device features whole-body scanning capability using a K-edge filtered X-ray source. Preliminary specifications include a 5-min scan time, 1-mm image spatial resolution, and precision error of less than 1.0%.

Performance

DRA offers high-resolution images, which contribute greatly to the precision of measurements. The clear visualization of

the intervertebral spaces (Fig. 3) ensures that the exact original region of interest is remeasured on subsequent scans. The images generated with DPA may not show a clear boundary between vertebrae (especially in patients with low bone-mineral content) and can fail to show osteophytes, severe compression fractures, and ligamentous or aortic calcification that adversely affect the reliability of the data. The higher scan speed, automatic internal reference system, and high-resolution imaging capabilities of the Hologic DRA sys-

tem combine to provide a significant improvement over conventional DPA equipment in clinical testing for osteoporosis.

At the University of California Medical Center in San Diego, short- and long-term precision of the Hologic system and the Lunar DP3 DPA unit has been examined by using two phantom types: (1) three mineral-equivalent cylinders of variable diameter (simple geometry) and (2) the Hologic calcium hydroxyapatite standard modeled as four lumbar vertebrae (complex geometry). Each instrument had a significantly ($p <$

Fig. 1.—Representative patient report from Hologic system depicts calculation of bone mineral density for L1, L2, L3, and L4 and the four levels combined. gHA = grams of hydroxyapatite.

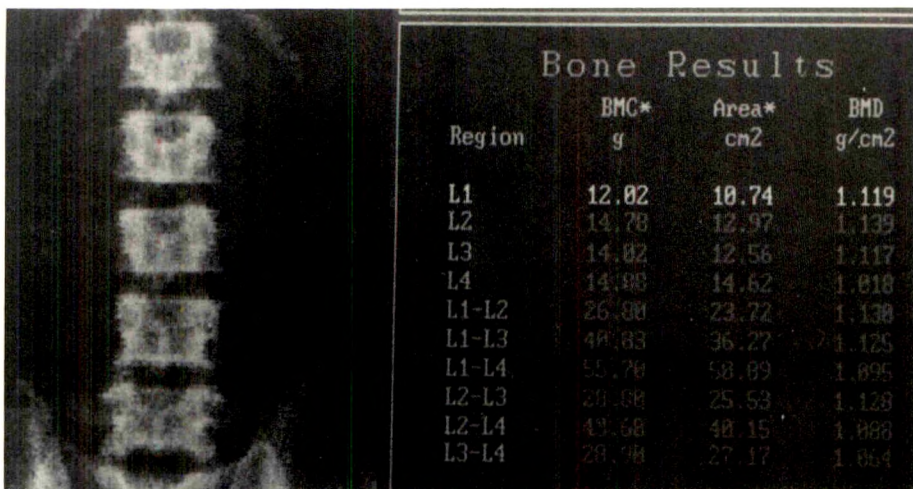
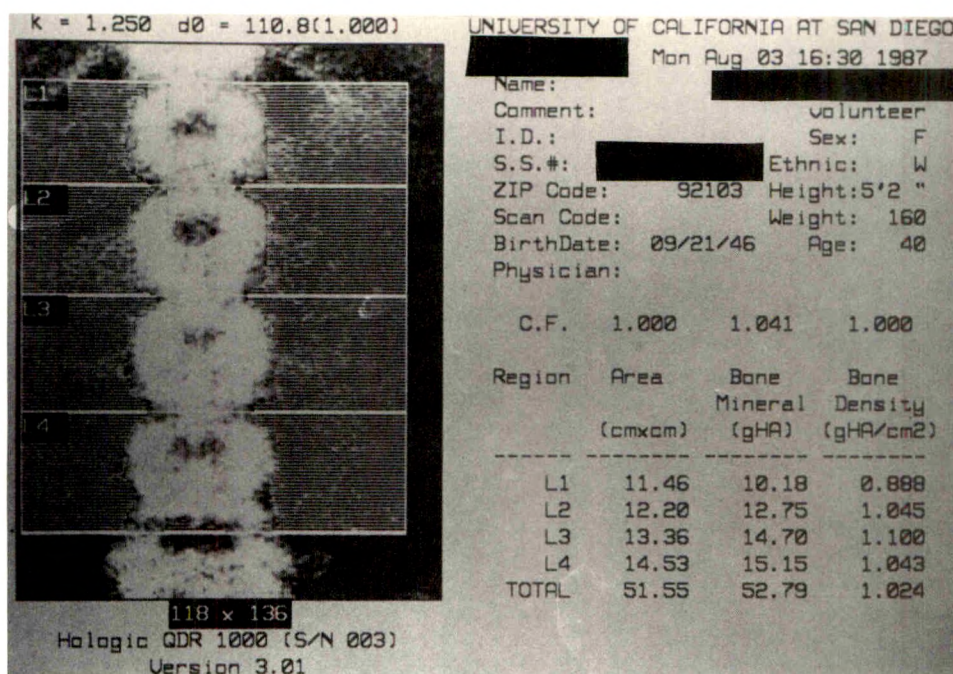


Fig. 2.—Representative scan image of lumbar spine from dual-energy radiographic absorptiometry with Lunar system.

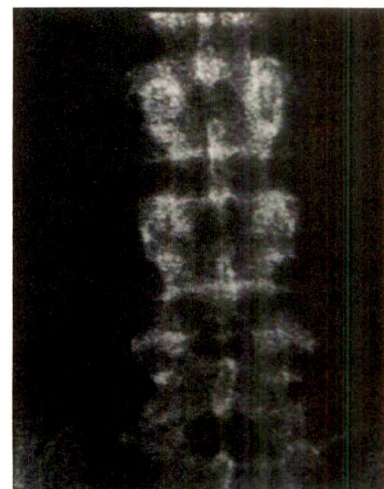


Fig. 3.—Representative scan images of lumbar spine from dual-energy radiographic absorptiometry with Hologic system.

.05) smaller coefficient of variation (CV) for data obtained with the simple-geometry vs the complex-geometry phantom. The short-term precision was slightly better than the long-term precision for DRA (mean CV = 0.88% vs 0.97%). For DPA, the short-term precision was slightly worse than the long-term precision (mean CV = 2.92% vs 2.57%). DRA was approximately three times more precise (long-term) than DPA was for both phantoms, a difference that was statistically significant ($p < .01$). The accuracy of DRA as assessed by repetitive scanning of a phantom containing known K_2HPO_4 concentrations (0–200 mg/ml) was high ($r = .99$, SEE = 0.007, slope = 1.04, constant = -0.003 , and standard error of coefficient = 0.024) [18].

In an attempt to rapidly develop a normative data base for DRA, lumbar spine examinations at the same institution are currently offered free of charge to any volunteer. Calculated best-fit regression equations for age-related bone loss are being derived for approximately 1000 women and 200 men 18–100 years old. Mean interlevel variation is also being determined. To date, these studies have indicated that DRA is capable of measuring age-related bone loss in both genders [19].

At the Mayo Clinic in Rochester, MN, the Hologic instrument has also been compared with a Lunar DP3 in phantoms and patients. DRA had better (1.4% vs 1.7%) precision, improved accuracy, and reduced beam-hardening effect with increasing patient thickness. Both instruments showed no effect of changing fat levels in the body (0–40% fat). A greater effect of composition and of distance from the tabletop was shown for DRA. Results in patients were consistently lower with DRA by 10% owing to differences in area calibration between the two techniques. Correlation between results in patients was $r = .99$, with an SEE of 0.02 for the range of bone mineral from 0.92 to 1.39 g/cm² [20].

Comparison of DRA with more conventional densitometric methods in vivo has been performed at the University of California Medical Center in San Diego [21, 22]. Dual-energy X-ray results correlated well with prior DPA scans over a DRA density range of 0.568 to 1.52 g/cm². Among patients having both examinations in the lumbar spine, linear regression gave an excellent value of $r = .95$, with an SEE of 0.036. The best-fit regression equation was $DPA = 1.067 \times DRA + 0.163$ over the L1–L4 region. The standard error of the coefficient was 0.035 [23].

In contrast, dual-energy X-ray results were not predictive of quantitative CT trabecular bone densities in a small heterogeneous group of patients. We found no correlation in the data, whether we used average results or values for L1 in isolation [24]. These results conflict with previously reported studies indicating correlations of 0.5 to 0.8 between quantitative CT and DPA [4], possibly owing to patient selection bias and the relatively small series included in the DRA investigation. In a limited study using images of highly variable quality, lateral DRA scans were used to calculate central vertebral body trabecular bone density. There was improved correlation between this approach and quantitative CT measurements. This relationship could potentially show marked

improvement with increased X-ray exposure [24]. Because there is not a consensus that quantitative CT has better diagnostic sensitivity than DRA or DPA does, the observed correlations should not be interpreted as a clinical "criterion."

In another study conducted at the University of California Medical Center in San Diego, DRA of the lumbar spine was compared with DPA of the lumbar spine and proximal femur in 52 patients (33 women and 19 men) with rheumatoid arthritis. Of the two vertebral measurements, DRA correlated less well with femoral data than DPA did in both genders. High correlation was documented between DRA and DPA of the lumbar spine. No significant relationship between bone density and age was observed, regardless of gender, site, or measurement technique. Bone densities in the spine and proximal femur were significantly reduced for both genders among the rheumatoid population as compared with controls [25].

In addition to the reported studies described previously, a large number of clinical investigations using DRA are currently in progress at the University of California in San Diego. The technology is being used to evaluate patients with chronic renal failure on dialysis or after transplantation, as well as pediatric patients, including children with inborn errors of metabolism and patients with cancer, as well as normal subjects. The effects of various chemotherapeutic regimens on bone density in adult oncology patients and osteopenia in younger women with amenorrhea from a variety of causes are also being studied. DRA also has shown early promise as a sensitive method for detecting and monitoring the course of disuse osteopenia as a model for the weightless environment.

Summary and Perspective

Because most hospitals currently possess CT equipment for body examinations, CT is currently the most widely available means for obtaining bone density information noninvasively. In addition, CT has been shown to be a better predictor of vertebral crush fracture risk than any other available densitometric method. However, single-energy quantitative CT has specific disadvantages, including a higher radiation dose than DPA or DRA has (several hundred millirad), limited accuracy because of bone marrow fat deposition [26–28], the need for sophisticated software to evaluate the proximal femur or cortical bone [29, 30], and potentially limited scanner availability. As discussed in detail elsewhere in this report, DRA offers improvements in these areas, and despite its projectional nature with inherent poorer sensitivity because of an inability to selectively measure high-turnover cancellous bone, the potential for improved lateral evaluation of the spine exists in the future, owing to the high photon flux (approximately 1000-fold greater than DPA) afforded by this technique. Such an approach may permit approximation of the high sensitivity currently afforded only by selective cancellous measurements using quantitative CT. Although the utility of DRA of the spine as compared with CT remains to be established in large series, DRA appears to be a more acceptable approach to hip measurements.

DPA has become the most widely used dedicated method for noninvasive bone densitometry in the axial skeleton because of its ability to study the proximal femur as well as the spine at an acceptable radiation dose [8, 9]. However, in addition to the less-than-ideal precision already discussed, DPA has important drawbacks, including poor image spatial resolution with concomitant inability to recognize potential causes of falsely elevated bone density values in the spine (compression fractures with callus, osteophytosis, degenerative sclerosis, ligamentous or aortic calcification); the need for expensive periodic replacement of gadolinium-153 sources (approximately \$6000 per source, recommended every 6–12 months and mandatory every 18 months); a relatively long examination time (20–30 min per site) with greater patient inconvenience and lower throughput; and the inability of users to analyze raw scan data independent of system software [3]. DRA improves on each of these limitations at a generally lower radiation exposure as compared with DPA, but also mandatorily includes low-turnover compact bone (60–80% of total) and extraneous calcification or ossification. The technique has exhibited an approximately three-fold greater precision in phantom, specimen, and patient studies [16–24]; manifests an image spatial resolution of about 1.5 mm (vs 2–10 mm for DPA); requires an X-ray tube replacement only about every 7 years; and requires an examination time of approximately 5–6 min per site. Because the cost of DRA is acceptably higher than that for DPA, DRA probably will replace DPA in the near future. It appears that the only current advantages of DPA are greater experience and a more extensive normative data base.

SPA remains competitive with DRA from the standpoint of radiation dose, examination time, and technical ease. SPA offers advantages in the areas of equipment cost and patient inconvenience. However, periodic (every 4–6 months) source replacement and suboptimal precision (particularly at sites of higher cancellous bone content) remain significant problems as compared with DRA. Because most investigators believe that direct assessment of axial high-risk fracture sites (spine and hip) is preferable to indirect prediction from appendicular measurements, DRA ultimately may become used more widely, despite its disadvantages as compared with SPA.

In conclusion, on the basis of extremely preliminary and as yet unpublished results, DRA appears to be an improved densitometric method that has significant advantages over existing techniques and that should allow for more accurate and precise evaluation of osteopenia. The lack of adequately high precision has been an important factor limiting widespread adoption of DPA testing. The introduction of DRA now appears to provide the ability to detect small changes in bone mineral with a precision of better than 1%. The high precision of DRA that has been shown so far ultimately may render it an extremely powerful tool for the detection and follow-up of abnormal bone loss in patients at risk for osteoporosis. The shorter required scanning time of this technology may result in the additional significant advantage of lower cost and/or more available third-party reimbursement due to higher patient throughput.

ACKNOWLEDGMENTS

We thank Jeffrey Borders, Alex Chang, Mark Green, Charles Ho, Alan Hochberg, Brian Howard, James A. Hunter, Amy J. Kenrick, Richard Kim, Margaret Marshall, Richard B. Mazess, Avraham Moscona, Elena Ramos, Jay A. Stein, and Carlene Wright for assistance in manuscript preparation.

REFERENCES

- Cummings SR, Black D. Should perimenopausal women be screened for osteoporosis? *Ann Intern Med* 1986;104:817–823
- Ott S. Should women get screening bone mass measurements? *Ann Intern Med* 1986;104(6):974–976
- Kimmel PL. Radiologic methods to evaluate bone mineral content. *Ann Intern Med* 1984;100:908–911
- Reinbold WD, Genant HK, Reiser UJ, Harris ST, Ettinger B. Bone mineral content in early-postmenopausal and postmenopausal osteoporotic women: comparison of measurement methods. *Radiology* 1986;160:469–478
- Riggs BL, Wahner HW, Dunn WL, et al. Differential changes in bone mineral density of the appendicular and axial skeleton with aging: relationship to spinal osteoporosis. *J Clin Invest* 1981;67:328–335
- Richardson ML, Genant HK, Cann CE, et al. Assessment of metabolic bone diseases by quantitative computed tomography. *Clin Orthop* 1985;195:224–238
- Firooznia H, Golimbu C, Rafii M, Schwartz MS. Rate of spinal trabecular bone loss in normal perimenopausal women: CT measurement. *Radiology* 1986;161:735–738
- Riggs BL, Wahner HW, Seeman E, et al. Changes in bone mineral density of the proximal femur and spine with aging. Differences between the postmenopausal and senile osteoporosis syndromes. *J Clin Invest* 1982;70:716–723
- LeBlanc AD, Evans HJ, Marsh C, Schneider V, Johnson PC, Jhingan SG. Precision of dual photon absorptiometry measurements. *J Nucl Med* 1986;27:1362–1365
- Gustafsson L, Jacobson B, Kusoffsky L. X-ray spectrophotometry for bone-mineral determinations. *Med Biol Eng Comput* 1974;12:113–118
- Jacobson B. X-ray spectrophotometry in vivo. *AJR* 1964;91:202–210
- Dalen N, Jacobson B. Bone mineral assay: choice of measuring sites. *Invest Radiol* 1974;9(3):174–185
- Sartoris DJ, Sommer FG, Marcus R, Madvig P. Bone mineral density in the femoral neck: quantitative assessment using dual-energy projection radiography. *AJR* 1985;144:605–611
- Brody WR, Butt G, Hall A, Macovski A. A method for selective tissue and bone visualization using dual energy scanned projection radiography. *Med Phys* 1981;8:353–357
- Sartoris DJ, Sommer FG, Kosek J, Gies A, Carter D. Dual-energy scanned projection radiography in the evaluation of femoral neck strength, density and mineralization. *Invest Radiol* 1985;20:476–485
- Sartoris DJ, Sommer FG, Oppenheimer DA. Preliminary report. Dual-energy scanned projection radiography of osseous metastatic disease. *Invest Radiol* 1985;20:983–988
- Mazess RB, Sorenson J, Hanson JA. Performance of an X-ray dual-photon scanner. Presented at the second international workshop on Non-Invasive Bone Measurements: Methodological Problems. Bone Mineral Measurements by Photon Absorptiometry, Leuven, Belgium, September 1987
- Hunter JA, Sartoris DJ, Stein A, et al. Quantitative dual-energy digital radiography versus dual-photon absorptiometry: in vitro precision and accuracy. Presented at the annual meeting of the Association of University Radiologists, New Orleans, LA, April 1988
- Sartoris DJ, Ramos E, Stein JA, Resnick D. Quantitative dual-energy digital projection radiography of the lumbar spine: normative database and inter-level variation. Presented at the annual meeting of the Association of University Radiologists, New Orleans, LA, April 1988
- Wahner HW, Brown ML, Dunn WL, Morin R, Stein J. Evaluation of a new instrument for bone mineral analysis based on quantitative digital radiography. Presented at the second international workshop on Non-Invasive

Bone Measurements: Methodological Problems. Bone Mineral Measurements by Photon Absorptiometry, Leuven, Belgium, September 1987

21. Ho C, Sartoris DJ, Stein JA, Andre M, Resnick D. Dual-energy projection radiographic bone densitometry: comparison to existing methods. Presented at the second international workshop on Non-Invasive Bone Measurements: Methodological Problems. Bone Mineral Measurements by Photon Absorptiometry, Leuven, Belgium, September 1987
22. Sartoris DJ, Stein JA, Ramos E, et al. Quantitative dual-energy digital radiography of the spine: comparison to dual-photon absorptiometry and quantitative computed tomography. Presented at the international workshop on Bone and Soft Tissue Densitometry, Buxton, Derbyshire, England, September 1987
23. Borders J, Sartoris DJ, Stein JA, Ramos E, Resnick D. Quantitative dual-energy digital projection radiography of the lumbar spine: comparison to dual-photon absorptiometry in patients. Presented at the annual meeting of the American Roentgen Ray Society, San Francisco, CA, May 1988
24. Borders J, Sartoris DJ, Stein JA, Ramos E, Resnick D. Quantitative dual-energy digital projection radiography of the lumbar spine: comparison to quantitative computed tomography in patients. Presented at the annual meeting of the American Roentgen Ray Society, San Francisco, CA, May 1988
25. O'Malley M, Kenrick AJ, Sartoris DJ, et al. Quantitative dual-energy digital projection radiography of the spine versus dual-photon absorptiometry of the spine and proximal femur in rheumatoid arthritis: relationship to clinical parameters. *Radiology* (in press)
26. Mazess RB. Errors in measuring trabecular bone by computed tomography due to marrow and bone composition. *Calcif Tissue Int* 1983;35:148-152
27. Mazess RB, Vetter J. The influence of marrow on measurement of trabecular bone using computed tomography. *Bone* 1985;6:349-351
28. Laval-Jeantet AM, Roger B, Bouysse S, Bergot C, Mazess RB. Influence of vertebral fat content on quantitative CT density. *Radiology* 1986;159:463-466
29. Sartoris DJ, Andre M, Resnick C, Resnick D. Trabecular bone density in the proximal femur: quantitative CT assessment. *Radiology* 1986;160:707-712
30. Lambiase R, Sartoris DJ, Fellingham L, Andre M, Resnick D. Vertebral mineral status: assessment with single- versus multi-section CT. *Radiology* 1987;164:231-236



Scientific Program (200 papers)

Instructional Courses (60 hours)

Categorical Course on
Genitourinary Radiology

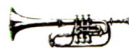
The Caldwell Lecture

Award Papers

Scientific Exhibits

Social, Golf, and Tennis Programs

Guest Programs



Come to the American Roentgen Ray Society

89th

ANNUAL MEETING



New Orleans Hilton May 7-12, 1989

Progress in Radiology

Perfluorooctylbromide: A New Contrast Agent for CT, Sonography, and MR Imaging

Robert F. Mattrey¹

Perfluorochemicals are a class of compounds composed entirely of carbon and fluorine atoms. They were made famous when Clark and Gollan [1] demonstrated their oxygen-carrying potential by submerging normal mice in the liquid for an extended period of time. These mice suffered no ill effects while they were submerged or afterward [1]. Perfluorochemicals, like oil, are immiscible with water and cannot be given intravenously unless emulsified [2]. Fluosol-DA (Alpha Therapeutics Corp., Los Angeles, CA) and PFOB-100% (Fluoromed Pharm, La Mesa, CA) are two emulsions that have been given intravenously to human subjects [3, 4].

Perfluorooctylbromide (PFOB), a fluorochemical in which one bromine atom is substituted for fluorine, is radiopaque on radiography and CT [5–10]. PFOB has been used in human subjects in its neat form (pure unemulsified liquid) for radiography of the gastrointestinal tract and for bronchography (Long DM, unpublished data). IV perfluorochemical emulsions given to animals [11–13] and humans [14] are effective sonographic contrast agents. Because these compounds, in the neat form, have no hydrogen atoms, they are effective negative oral contrast agents for MR imaging [15, 16]. These agents can also be imaged with MR when coils are tuned to the Larmor frequency of the ¹⁹F nucleus [17]. Clinical trials with IV PFOB as a CT and a sonographic contrast agent have begun in Europe. Preliminary reports are extremely encouraging [4].

Physical Properties, Pharmacokinetics, and Toxicity of PFOB

Perfluorochemicals, including PFOB, are inert and have high gas solubility, low surface tension, and very low toxicity when ingested or inhaled [18, 19]. Because of these unique properties they are used extensively in industry as cleansers, lubricants, and propellants [18]. These compounds actually behave like a liquefied gas. Some are extremely volatile, like freon, whereas others are extremely stable. They accumulate in human tissues when inhaled, ingested, or given intravenously. The length of time they remain in the body is related to their molecular weight and vapor pressure (volatility); the more volatile they are the shorter their half-life, which can range from minutes to years [20, 21]. Those with very short half-lives (hours) cannot be used intravenously because they produce pulmonary emphysema as they evaporate out of the pulmonary capillaries into the interstitium [21]. IV PFOB-100%, given to rats at a dose of 1.5 g/kg, has a half-life of 3 days, which is long enough to be safe and short enough to be practical [22]. Fluosol-DA 20%, the first perfluorochemical used in humans intravenously, consists of two perfluorochemicals, perfluorodecalin and perfluorotripropylamine (their half-lives are 6 and 63 days, respectively) [21].

PFOB, which is twice as dense as water, is emulsified in pure lecithin to produce 100% weight per volume emulsion

Received August 2, 1988; accepted after revision October 4, 1988.

R. F. Mattrey is the recipient of Research and Career Development Award NCI-K08-CA01319.

¹ Department of Radiology, Magnetic Resonance Institute, UCSD Medical Center, 410 W. Dickinson St., San Diego, CA 92103.

(1 g PFOB in 1 ml emulsion) with particle sizes 0.1- to 0.2- μ m in diameter [23]. These particles, unable to leak out of normal capillaries, are limited to the intravascular space. PFOB is removed from blood by two competitive mechanisms, phagocytosis by the reticuloendothelial system and evaporation through the lung. In rats, the PFOB half-life in blood was approximately 6 hr after the infusion of 2.5 g/kg [22]. In rats, 99.8% of the IV PFOB dose is eliminated in the expired air. The remainder is eliminated in feces during the first few days, probably from bile excretion, and none is eliminated in urine [22]. Early clinical data from the European trials suggest a shorter blood half-life in man.

IV PFOB is eliminated without breakdown of its chemical structure. No acute hemodynamic effects of the lecithin-based 100% PFOB emulsion occurred when 1 g (1 ml)/kg was given as an IV bolus to dogs (Mattrey RF, unpublished data). The 7-day LD₅₀ of PFOB in rats is 45 g/kg with an LD₅₀ to diagnostic dose ratio of 22:1 [22]. No subacute or chronic toxicity of PFOB is expected.

More than 95% of the oral PFOB dose is excreted by the gastrointestinal tract within 24 hr [5]. No LD₅₀ could be measured in rats when dosages in excess of 64 ml/kg were ingested [5, 24]. PFOB has been taken orally by approximately 60 human subjects at dosages of 2–12 ml/kg. Extensive laboratory studies before and at various time intervals up to 3 days after PFOB ingestion showed no effect [15, 16]. Although some absorption occurs after ingestion, miniscule levels are detectable in tissues that are five orders of magnitude smaller than would be found if 1 g/kg were given intravenously. An IV dose of 1 g/kg has no detectable toxic effect [22].

Computed Tomography

Although urographic contrast agents are ideal for renal CT scanning, they are suboptimal for imaging the blood pool and various organs on CT. These agents are lost to the extravascular space because they quickly diffuse into and equilibrate with the interstitial fluid. Because PFOB remains intravascular, the dose can be titrated to provide the blood enhancement desired on CT, and the degree of enhancement will be the

same throughout the arteries, veins, and cardiac chambers (Fig. 1) [9]. With the 6-hr blood half-life of PFOB, this enhancement persists long enough to allow ample time for CT imaging. Tissues enhance to a degree commensurate with their blood volume [25]. Blood-pool enhancement of tissues with PFOB on CT is comparable to labeled RBC blood-pool scanning in nuclear medicine. PFOB on CT should allow the differentiation of intrahepatic tumors from hemangiomas, because intrahepatic tumors have less blood than liver does and hemangiomas are essentially a blood pool. This hypothesis would of course require testing in the clinical setting.

EOE-13 (ethiodized oil emulsion), like PFOB, is taken up by the reticuloendothelial system of the liver and spleen [8, 26]. EOE-13 does not enhance blood vessels. It has a sensitivity of 90% for the detection of liver tumors, which is considered to be the best of all CT techniques [27]. The reason for the less than perfect sensitivity is because small lesions are confused with comparable-sized intrahepatic vessels and vice versa [28]. However, unlike EOE-13 enhancement, the simultaneous enhancement of the vascular space with PFOB renders lesions the only unopacified structures within the liver (Fig. 2), potentially providing greater than the 90% sensitivity in the detection of liver lesions achieved with EOE-13.

Within minutes to hours after PFOB is given, enhancement of abscess wall and tumors begins; enhancement peaks at 1–4 days. Accumulation of PFOB in these sites is thought to occur by either transcapillary leak through abnormal neoplastic or inflammatory vascular beds, accumulation of PFOB-filled macrophages, or both. That transcapillary leakage occurs is evidenced by tumor rim enhancement minutes after infusion [29] and the presence of PFOB particles in the perivascular space when lecithin is stained with a fat stain [17]. By 48 hr, all of PFOB in these sites is within macrophages that are then present in large numbers when compared with controls [8, 10]. It is not clear how these PFOB-filled macrophages accumulate in lesions. They may have taken up PFOB elsewhere, become activated as has been suggested [30], and accumulated in immunologically active sites; or they may have been residents of these sites or recruited to these sites to phagocytose the PFOB particles present in the interstitium.



Fig. 1.—Transverse CT scans at level of heart in pig before and after IV administration of 5 g/kg perfluorooctylbromide (PFOB).

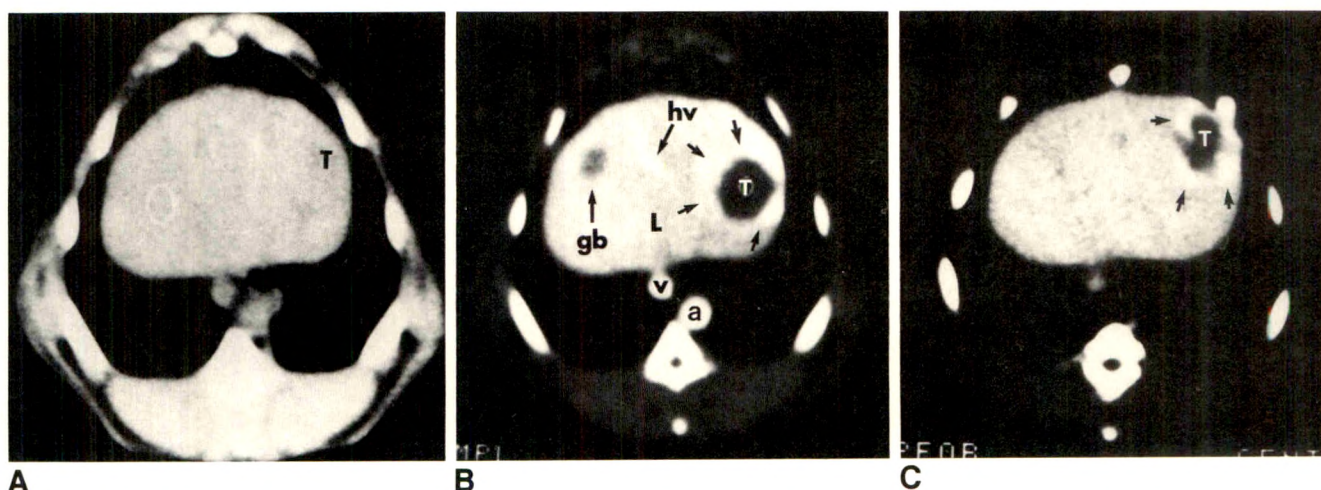


Fig. 2.—Transverse CT scans of rabbit at level of Vx2 tumor implanted in liver.

A, Before perfluorooctylbromide (PFOB). Tumor (T) is isodense relative to liver and paraspinal muscles.

B, 5 min after 5 g/kg PFOB. Liver (L) and blood vessels, including intrahepatic veins (hv), enhance significantly relative to tumor and paraspinal muscles. There is a faint hypervascular tumor rim (small arrows).

C, 48 hr later. Tumor rim has become hyperintense relative to liver (arrows).

a = aorta; v = vena cava; gb = gallbladder.

Lesion enhancement has been documented by both CT and sonography after the administration of PFOB [8, 10–13, 29]. In fact, it appears that PFOB accumulates in any region where macrophages are found, including tumors [8, 11, 12, 14, 29], abscesses [10, 31], and injured [32] or infarcted [13] tissues. This leads to enhancement of the area on CT in proportion to the degree of inflammation [32]. An application of great clinical potential may be the use of PFOB as a CT contrast agent to improve the detection of abscesses. In rabbits in which hepatic and peritoneal abscesses were induced, PFOB produced dense enhancement of abscess wall on CT 2 days after infusion of the compound [10]. Although liquefied centers of hepatic abscesses could be seen without PFOB, PFOB made it possible to determine the extent of the inflammation (Fig. 3). Although the peritoneal abscesses were not visible on CT without PFOB, they were all identified after PFOB administration [10].

Sonography

Perfluorochemicals are effective contrast agents for sonog-

sion [29]. This is also true of liver tumors (Fig. 4). Increased echogenicity in proportion to the degree of vascularity may allow sonography to be used to estimate the degree of tissue perfusion, visualize areas of infarction, and tumors.

Doppler signals and their color rendition enhance significantly as a result of PFOB [33], which lasts for hours because of the long blood half-life of PFOB. Doppler signals, including color, become detectable from submillimeter vessels as well as vessels not seen on the gray-scale image [33]. This capability should have a significant impact on deep Doppler applications, where small or deep vessels reflect weak signals.

Perfluorochemicals also enhance the liver and spleen because of their uptake by the reticuloendothelial cells for at least 2 days after their administration [11–14]. In humans, Fluosol-DA 20% produced significant liver and spleen enhancement 24 hr after a dose of 2.4 g/kg, allowing the visualization of unenhanced tumors [14].

As with CT, macrophages that accumulate in lesions become visible sonographically. In patients, the IV administration of Fluosol caused significant rim or diffuse echogenic en-

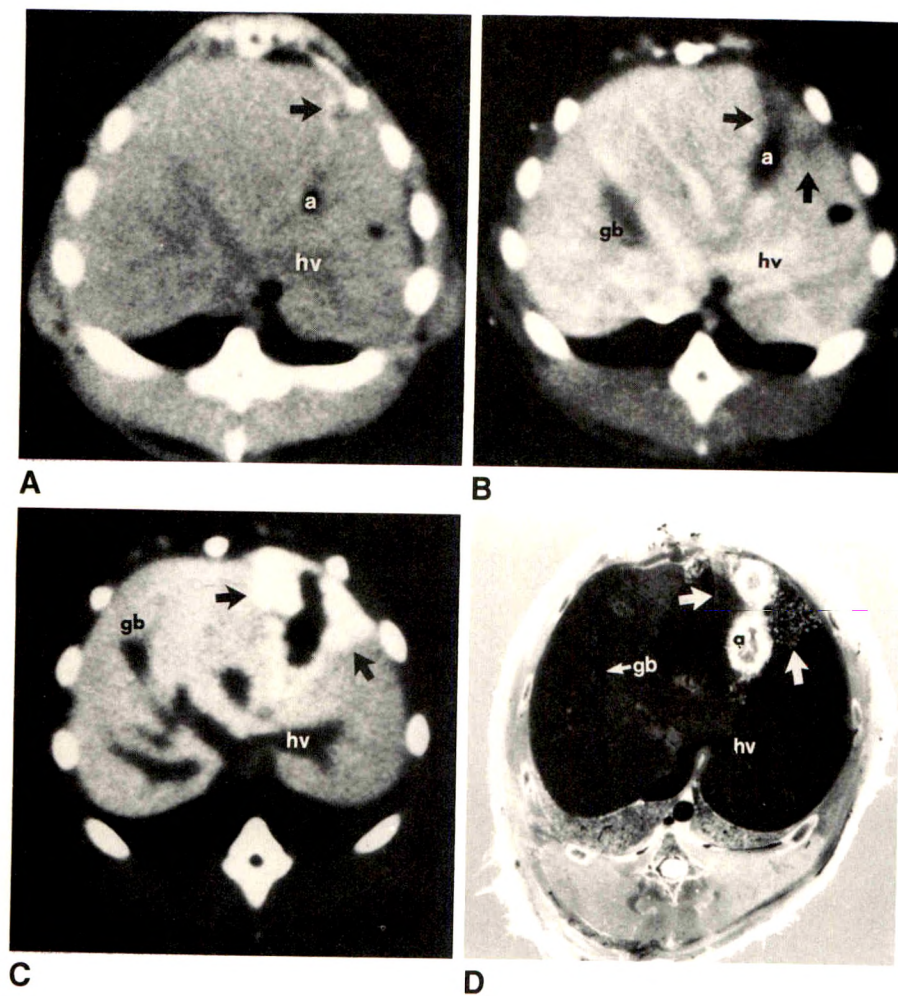


Fig. 3.—Transverse CT scans of rabbit at level of abscess in liver.

A, Before perfluorooctylbromide (PFOB). Faint calcification is seen at abscess (a) margin (arrow).

B, 5 min after 5 g/kg PFOB. Liver and blood vessels, including intrahepatic veins (hv), enhance significantly relative to abscess, phlegmon about abscess (arrows), and paraspinal muscles. Phlegmon does not enhance significantly.

C, 48 hr later. Dense enhancement of phlegmon (arrows) extends beyond abscess wall. Intrahepatic vessels are less dense than liver.

D, Anatomic section at approximate level of C shows phlegmon (arrows) extending beyond confines of abscess.

gb = gallbladder.

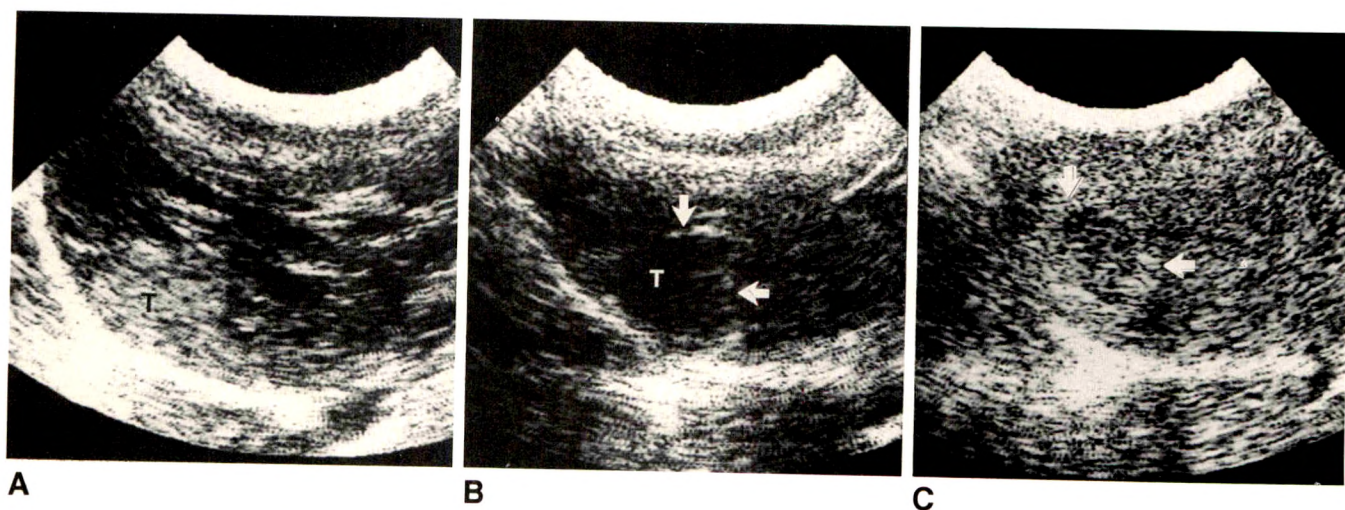


Fig. 4.—Longitudinal sonograms of liver at level of Vx2 tumor of rabbit in Fig. 2.

A, Before perfluorooctylbromide (PFOB). Tumor (T) is hyperechoic relative to surrounding liver.

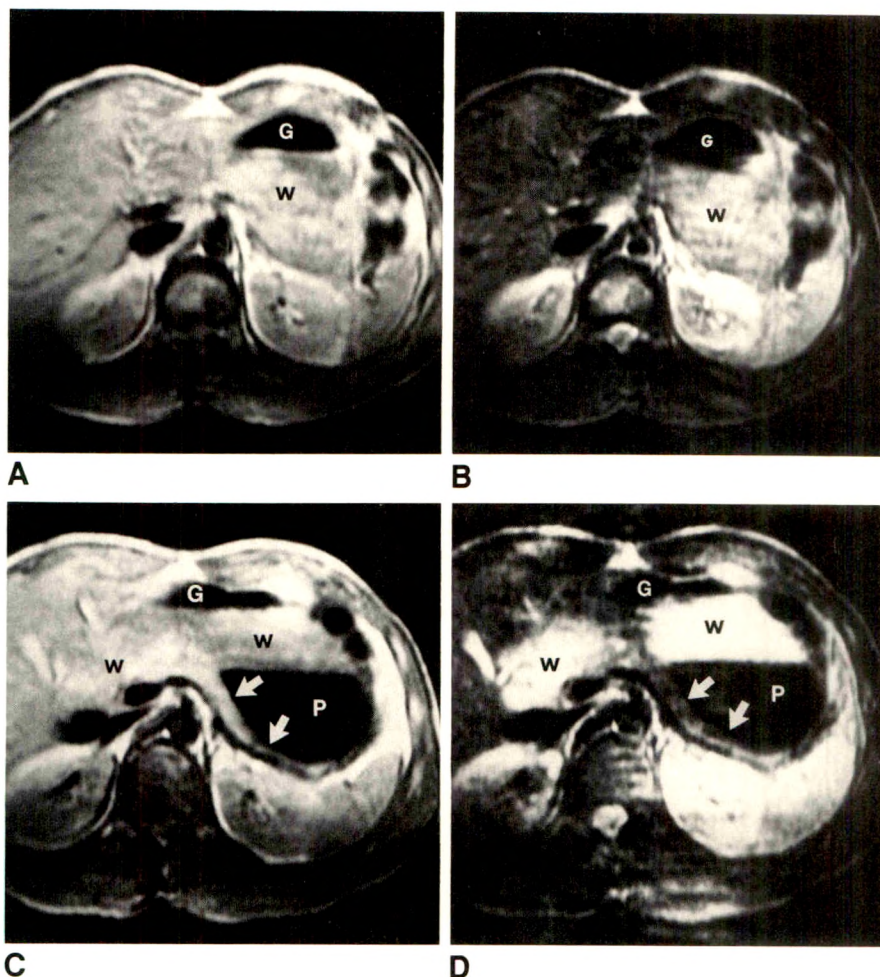
B, 30 min after 5 g/kg PFOB. Tumor is hypoechoic relative to liver. There is faint rim enhancement (arrows).

C, 48 hr later. Tumor rim is echogenic (arrows).

Fig. 5.—Transverse MR images at level of pancreas of volunteer before and after ingestion of 500 ml neat perfluorooctylbromide (PFOB).

A and B, Hydrogen-density (2000/20) (A) and T2-weighted (2000/70) (B) images before PFOB ingestion. Pancreas is not visible because of water (W) in gastric fundus.

C and D, Hydrogen-density (C) and T2-weighted (D) images obtained with same technique 5 min after PFOB ingestion. Clear visualization of pancreas (arrows) contrasts with PFOB-filled gastric fundus. Air-fluid-fluid level with water (W) floating between gas (G) and PFOB (P).



barium or Hypaque because of their low surface tension [5]; and (4) they are tasteless, odorless, and have no side effects [5, 24]. The use of PFOB was shown to be feasible in rats and humans [15]. PFOB significantly darkened bowel lumen on T1-weighted, hydrogen-density, and T2-weighted images (Fig. 5) [16].

MR Imaging of the ^{19}F Nucleus

Fluorine is the next best nucleus for MR applications after hydrogen, because it has 100% natural isotopic abundance and has an 83% sensitivity relative to hydrogen. ^{19}F in PFOB can be imaged to show the vascular pool, liver, spleen, and macrophage collections [17, 34].

^{19}F MR imaging or spectroscopy can be used to estimate tissue oxygen tension percutaneously. Neat PFOB can carry more than twice as much oxygen as whole blood can [2]. Dissolved molecular oxygen is paramagnetic, affecting T1 shortening of ^{19}F [35]. Tissue oxygen tension can be estimated by appropriate MR techniques, because oxygen in perfluorocarbons is carried passively and is in equilibrium with tissue oxygen tension [2], and the ^{19}F relaxation rate is linearly related to oxygen tension dissolved in the perfluorocarbon

[35]. Fishman et al. [36] showed signal-intensity changes in various tissues in rats when respired oxygen tension was changed from 20% to 100%. Therefore, these agents can be used to detect ischemic tissues and to monitor the efficacy of therapy. Although this technique is feasible and of great interest, its accuracy and potential utility in vivo have not yet been documented.

REFERENCES

1. Clark LC, Gollan F. Survival of mammals breathing organic liquids equilibrated with oxygen at atmospheric pressure. *Science* 1966;152:1755-1756
2. LeBlanc M, Riess JG. Artificial blood substitutes based on perfluorochemicals. In: Banks RE ed. *Preparation, properties, and industrial applications of organofluorine compounds*. Chichester, England: Ellis Horwood, 1982:83-138
3. Tremper KK, Freidman AE, Levine EM, Lapin R, Camarillo D. The preoperative treatment of severely anemic patients with a perfluorochemical oxygen-transport fluid, Fluosol-DA. *N Engl J Med* 1982;307:277-283
4. Bruneton JN, Falewee MN, Balu-Maestro C, Normand F, Mattrey RF. Perfluorooctylbromide and hepatosplenic computed tomography: preliminary clinical study. *Invest Radiol* 1988;23[suppl]:5306-5307
5. Long DM, Liu M, Szanto PS, et al. Efficacy and toxicity studies with radiopaque perfluorocarbon. *Radiology* 1972;105:323-332

6. Long DM, Lasser EC, Sharts CM, Multer FK, Nielsen M. Experiments with radiopaque perfluorocarbon emulsions for selective opacification of organs and total body angiography. *Invest Radiol* **1980**;15:242-247
7. Young SW, Enzmann DR, Long DM, Muller HH. Perfluorooctylbromide contrast enhancement of malignant neoplasms: preliminary observations. *AJR* **1981**;137:141-146
8. Mattrey RF, Long DM, Multer F, et al. Perfluorooctylbromide: a reticulo-endothelial specific and a tumor imaging agent for computed tomography. *Radiology* **1982**;145:755-758
9. Mattrey RF, Peck WW, Slutsky RA, Higgins CB. Perfluorooctylbromide as a blood pool imaging agent for computed tomography. *J Comput Assist Tomogr* **1984**;8:739-744
10. Mattrey RF, Andre M, Campbell J, et al. Specific enhancement of intra-abdominal abscesses with perfluorooctylbromide for computed tomography. *Invest Radiol* **1984**;19:438-446
11. Mattrey RF, Scheible FW, Gosink BB, Leopold GR, Long DM, Higgins CB. Perfluorooctylbromide: a liver and spleen specific and a tumor imaging ultrasound contrast material. *Radiology* **1982**;145:759-762
12. Mattrey RF, Leopold GR, vanSonnenberg E, Gosink BB, Scheible FW, Long DM. Perfluorochemicals as liver and spleen seeking ultrasound contrast agents. *J Ultrasound Med* **1983**;2:173-176
13. Mattrey RF, Andre MP. Ultrasonic enhancement of myocardial infarction with perfluorocarbon compounds. *Am J Cardiol* **1984**;54:206-210
14. Mattrey RF, Strich G, Shelton RE, et al. Perfluorochemicals as ultrasound contrast agents for tumor imaging and hepatosplenography: preliminary clinical results. *Radiology* **1987**;163:339-443
15. Mattrey RF, Hajek P, Gyls-Morin VM, et al. Perfluorochemicals as gastrointestinal contrast agents for MR imaging: preliminary studies in rats and humans. *AJR* **1987**;148:1259-1263
16. Mattrey RF, Hilpert PL, Levine D, Long DC. PFOB as a negative oral MR contrast agent identifies bowel: clinical results. Presented at the annual meeting of the Association of University Radiologists, New Orleans, May **1988**; (abstr) *Invest Radiol* **1988**;23:S3
17. Ratner AV, Muller HH, Bradley-Simpson B, et al. Detection of tumors with ^{19}F magnetic resonance imaging. *Invest Radiol* **1988**;23:361-364
18. Slinn DSL, Green SW. Fluorocarbon fluids for use in the electronics industry. In: Banks RE, ed. *Preparation, properties, and industrial applications of organofluorine compounds*. Chichester, England: Ellis Horwood, **1982**:45-82
19. Ubel FA, Sorenson SD, Roach DE. Health status of plant workers exposed to fluorochemicals: a preliminary report. *Am Ind Hyg Assoc Jour* **1980**;41:584-589
20. Riess JG. Reassessment of criteria for the selection of perfluorochemicals for second-generation blood substitutes: analysis of structure/property relationships. *Artif Organs* **1984**;8:44-56
21. Naito R, Yokohama K. Perfluorochemical blood substitutes FC-43 emulsion, Fluosol-DA 20% and 35% for preclinical studies as a candidate for erythrocyte substitution. The Green Cross Corps Technical Information Series no. 5, 7/1981:37, 84, 161-169
22. Burgan AR, Long DM, Mattrey RF, et al. Results of pharmacokinetic and toxicologic studies with PFOB emulsions. Presented at the International Symposium on Artificial Blood Substitutes, Montreal, Canada, May **1987**
23. Long DC, Fallano R, Riess JG, et al. Preparation and applications of highly concentrated PFOB emulsions. Presented at the International Symposium on Artificial Blood Substitutes, Montreal, Canada, May **1987**
24. Mai-Shian L, Long DM. Perfluorooctylbromide as a diagnostic contrast medium in gastroenterography. *Radiology* **1977**;122:71-76
25. Hillman BJ, Stanley ML, Tracey P, Swindell W, Long DM. CT determination of renal and hepatic microvascular volumes in experimental acute renal failure. *Invest Radiol* **1982**;17:41-45
26. Vermess M, Doppman JL, Sugarbaker PH, et al. Computed tomography of the liver and spleen with intravenous lipid contrast material: review of 60 examinations. *AJR* **1982**;138:1063-1071
27. Sugarbaker PH, Vermess M, Doppman JL, Miller DL, Simon R. Improved detection of focal lesions with computerized tomographic examination of the liver using ethiodized oil emulsion (EOE-13) liver contrast. *Cancer* **1984**;54:1489-1495
28. Patronas N, Miller DL, Girtan M. Experimental comparison of EOE-13 and perfluorooctylbromide for the CT detection of hepatic metastases. *Invest Radiol* **1984**;19:570-573
29. Mattrey RF, Mitten R, Peterson T, Long CD. Vascular ultrasonic enhancement of tissues with perfluorooctylbromide for renal tumor detection (abstr). *Radiology* **1987**;165[suppl]:76
30. Miller ML, Stinnett D, Clark LC Jr. Ultrastructure of tumoricidal peritoneal exudate cells stimulated in vivo by perfluorochemical emulsions. *Reticuloendothel Soc* **1980**;27:105-118
31. Shelton RE, Brown JJ, Ogino MT, Johnson KK, Mitten RM, Mattrey RF. Efficacy and toxicity of perfluorooctylbromide in the CT diagnosis of hepatic abscesses (abstr). *Invest Radiol* **1985**;20:S15
32. Sartoris DJ, Guerra J Jr, Mattrey RF, et al. Perfluorooctylbromide as a contrast agent for computed tomographic imaging of septic and aseptic arthritis. *Invest Radiol* **1986**;21:49-55
33. Hilpert PL, Mattrey RF, Mitten R, Peterson T. Intravenous ultrasonic contrast agents to enhance systemic arterial Doppler signal. Presented at the annual meeting of the Association of University Radiologists, New Orleans, May **1988**; (abstr) *Invest Radiol* **1988**;23:S9
34. Ratner AV, Hurd R, Muller HH, et al. ^{19}F magnetic resonance of the reticuloendothelial system. *Magn Reson Med* **1987**;5:548-554
35. Clark LC, Ackerman JL, Thomas Sr, Millard RW. High contrast tissue and blood oxygen imaging based on fluorocarbon ^{19}F NMR relaxation. *Magn Reson Med* **1984**;1:135-136
36. Fishman JE, Joseph PM, Floyd TF, Mukherji B, Sloviter HA. Oxygen sensitive ^{19}F NMR imaging of the vascular system in vivo. *Magn Reson Imaging* **1987**;5:279-285

Progress in Radiology

New Perspectives in Thrombus-Specific Imaging: Radiolabeled Monoclonal Antibodies

Zvi H. Oster¹ and Prantika Som

The Challenge

A new era, the "thrombolytic era," has recently been hailed [1]. This enthusiastic proclamation is based mainly on the impressive achievements of thrombolytic therapy in improving the prognosis of patients with myocardial infarction [2-7]. Direct intraarterial administration of thrombolytic agents requiring coronary artery catheterization was used initially [8-10] and is still indicated in peripheral vascular disease and arterial graft occlusions [11, 12]. However, the currently accepted route of administration of thrombolytic agents in coronary artery thrombosis is by IV infusion, making the procedure available even to hospitals without cardiac catheterization laboratories. In addition to coronary thrombosis, thrombolytic therapy has also been evaluated in a variety of other thrombotic conditions, including superior mesenteric artery occlusion [13], renal artery thromboembolism [14], and obstruction of prosthetic valves [15]. In cerebrovascular events, thrombolysis has been found to give inconclusive results and also to carry greater and more hazardous risks as compared with thrombolysis in other organs [16, 17]. Venous thrombosis and pulmonary embolism have been the subject of several clinical trials [1, 18, 19], but thrombolysis has not yet been established as a routine therapy in these conditions.

The efficacy of thrombolytic therapy in opening vascular occlusions due to thrombus or embolism is indisputable. At the same time, thrombolysis is characterized by significant

risks: high prevalence of major side effects (mainly bleeding) and reocclusion. Removal of the major cause of arterial stenosis, the atheromatous plaques, has to be done mechanically by balloon angioplasty, laser-aided techniques, or bypass surgery.

This therapeutic approach poses challenges that cannot be answered by currently available diagnostic techniques. Determining the presence of thrombus at a site of vascular stenosis or occlusion is crucial in deciding whether thrombolytic therapy is indicated or whether to institute a maintenance infusion to prevent reocclusion after therapy. Because of the lack of a noninvasive test, decisions on initiation of therapy and determination of dose are empiric, based on results from large clinical trials indicating a positive outcome. The ability to determine the indication for thrombolytic therapy or to individualize the dose is not possible because of the lack of specific tests. Monitoring the clotting/fibrinolytic systems or other laboratory biochemical parameters does not seem to answer these questions [1, 20]. Frequently, incomplete lysis and reocclusion occur after thrombolytic therapy [21-23], and, at present, these occurrences can be assessed only by angiography. However, because bleeding at "access sites" is the most frequent complication of thrombolytic therapy, prevention can best be attained by minimizing the number of interventions causing tissue and blood vessel trauma during therapy. Therefore, a noninvasive method, if available, could help in the selection of patients suitable for thrombolytic or maintenance therapy, or those patients who need emergency

Received August 22, 1988; accepted after revision October 19, 1988.

Supported in part by the United States Department of Energy, contract no. DE-AC02-76CH00016.

¹ Both authors: Department of Radiology, School of Medicine, State University of New York at Stony Brook, Stony Brook, NY 11794, and Medical Department, Brookhaven National Laboratory, Upton, NY 11973. Address reprint requests to Z. H. Oster at the State University of New York at Stony Brook.

percutaneous transluminal coronary angioplasty or coronary bypass surgery to salvage ischemic myocardium.

The need for achieving a "systemic lytic state" for effective dissolution of occluding thrombi [24], or whether only a local, "regionalized" approach is sufficient, is still debated [1]. It seems that a test to determine the presence of active, continuously forming thrombus would be of help to determine on an individual basis the minimally effective dose. Thus, the risks of bleeding and of other side effects that seem to be dose-dependent [25–27] could be minimized.

Clinical studies indicate that the efficacy of thrombolytic therapy in acute myocardial infarction decreases significantly with elapsed time after the appearance of symptoms [2–7]. The term "lytic window" has been coined (up to 4–6 hr) to indicate the time of greatest efficacy of thrombolytic therapy in salvaging ischemic myocardium. Moreover, it was found that delayed reperfusion not only is ineffective but may increase myocardial injury by the action of oxygen-derived free radicals, generated during late tissue reoxygenation. Various strategies have been proposed for restricting the damage induced by free radicals [28, 29], but early reperfusion and prevention of free-radical formation seem to be the best alternatives. It seems, therefore, that a thrombus-specific diagnostic method could provide important information for treating patients with active thrombi amenable to lytic therapy.

The following is a brief description of the currently available thrombus-specific diagnostic techniques and their limitations, and a review of newer methods and their potential perspectives.

Currently Available Thrombus-Specific Agents

Radioiodinated fibrinogen, first proposed in 1968 [30] and later improved to become a bedside procedure [31], is limited to the diagnosis of deep-vein thrombosis in extremities. Because of the low sensitivity and specificity of the ^{125}I -labeled fibrinogen method, the search for better methods continued. Over the years, radioiodinated plasminogen [32], $^{99\text{m}}\text{Tc}$ -labeled plasmin [33], radiolabeled urokinase [34, 35], $^{99\text{m}}\text{Tc}$ -labeled streptokinase [34, 36], and ^{131}I -labeled streptokinase [34, 37] were evaluated. Radioiodinated fibrinogen-derived fragment E was also evaluated for its usefulness in the diagnosis of deep-vein thrombosis [38]. None of the methods described earlier seem to fulfill the expectations to become of practical use.

Blood-cell labeling with indium-111, first described by McAfee and Thakur [39], was later applied to platelets [40–42], enabling extensive studies of thromboembolic diseases. Thus, deposition of ^{111}In -labeled platelets was shown in experimental coronary artery bypass [43], infective endocarditis [44], experimental coronary thrombi [45], and arterial wall injury caused by balloon angioplasty [46–48]. By using this technique, researchers showed that aspirin prevents platelet accumulation at sites of endothelial damage, both in experimental animals [49] and in humans [47]. Deposition of platelets on atherosclerotic lesions [50], thrombogenic catheters [51], experimental prosthetic valves [52], and aortic aneurysms [53] also was shown. Ventricular mural thrombi that show platelet accumulation seem to embolize more frequently than do "hematologically nonactive" thrombi, which are negative on ^{111}In -labeled platelet scans and can be shown

by echocardiography only [54]. Attempts also were made to visualize coronary artery thrombi [55–57]. ^{111}In -labeled platelet scintigraphy was also actively evaluated in cerebrovascular disease. Deposition of platelets on carotid artery atherosclerotic plaques and in patients with transient ischemia was demonstrated [58–61]. However, in order to image the platelets at these sites, a second injection of a blood-pool agent was considered by some as necessary for subtracting the high levels of intravascular radioactivity [62]. Deep-vein thrombosis and pulmonary embolism also have been studied with ^{111}In -labeled platelets [63–67]. However, only partially successful results limited to thrombi in extremities were obtained [68]. Anticoagulation therapy seems to cause significantly high rates of false-negative results [67, 68].

Although a decade has passed since ^{111}In -labeled platelets for thrombus imaging were first described [40], the method has not yet become a routine clinical procedure and is mainly still limited to investigational purposes. The reasons for this state are the need for careful separation of autologous platelets before radiolabeling, the lengthy and complex preimaging preparation, and the need for delayed imaging. Meaningful results can be obtained only in areas of low blood-pool background, and therefore imaging of coronary thrombi and pulmonary and cerebral emboli was not successful. The radiopharmaceutical, ^{111}In -labeled platelets, can be given in relatively small amounts, less than 1 mCi (37 MBq), resulting in low-count images. A 30,000-count image may take 10–15 min to acquire. In addition, the slow blood clearance causing high-body background activity requires delayed imaging 24–48 hr after injection so as to enable clearance of blood background and to attain target-to-nontarget ratios that are adequate for detection of discrete foci of increased platelet accumulation.

Therefore, the methods that use radioiodinated fibrinogen and ^{111}In -labeled platelets are not suitable for providing the answers needed for the decision of initiating, continuing, or reinstituting fibrinolytic therapy in high-blood-pool organs such as the heart and brain. Because researchers have shown that for maximal tissue salvage, thrombolytic therapy must be started as soon as possible and no later than 2–4 hr after the appearance of symptoms [2–7], neither method is adequate because rapid imaging is not possible.

New Thrombus-Specific Imaging Agents

A new approach to thrombus imaging is the use of radio-labeled monoclonal antibodies directed against platelets or fibrin. Although murine monoclonal antibodies have been extensively investigated for tumor imaging [69], few applications to nonmalignant processes have been described. Polyclonal antibodies against fibrinogen/fibrin had been evaluated earlier, albeit without great success [70–74].

Radiolabeled Monoclonal Antiplatelet Antibodies

The first successful attempt for thrombus-specific imaging with a monoclonal antiplatelet antibody was described by us in 1985 [75]. An antibody, 7E3, directed against the IIb/IIIa glycoprotein complex on the platelet surface was developed [76–78] and evaluated in an animal model of venous and arterial thrombosis [75]. Before injection into animals with

experimental thrombi, ^{111}In -labeled 7E3 was preincubated for 45 min with autologous blood. Imaging of thrombi in carotid arteries, femoral arteries, segmental pulmonary arteries, jugular and femoral veins, and right ventricle was possible 1.0–1.5 hr after injection (Fig. 1). Thrombi 2–10 hr old could thus be detected, but 48-hr-old thrombi were not visible in dogs. Within 20–30 min after injection, 50% of the injected radioactivity cleared from the blood. No side effects, decrease in platelet count, or increased bleeding tendency were observed in 18 dogs. In vitro studies showed that saturation of 5% or less of the platelet binding sites does not cause any detectable change in platelet function. The antibody protein dose, therefore, was kept well below this level. The 7E3 antibody is now under evaluation as a therapeutic antiplatelet agent [78].

After the successful experimental results with ^{111}In -labeled 7E3 for thrombus imaging, we evaluated a second monoclonal antibody, 50H.19. The antibody 50H.19 was converted to fragments and pretinned in kit vials, for subsequent labeling with $^{99\text{m}}\text{Tc}$ according to a method described earlier [79].

This labeled preparation, consisting mainly of 50H.19 F(ab') (85%) and F(ab')₂ (15%), has been evaluated in dogs and in vitro on human blood [80]. Labeling with $^{99\text{m}}\text{Tc}$ was performed by adding 5–30 mCi (185–1110 MBq) $^{99\text{m}}\text{Tc}$ pertechnetate in 2 ml of saline to the incubation vial containing 150 μg pretinned antibody fragments. After incubation for 30–45 min at room temperature, the solution was passed through a radio-pharmaceutical filter column (Filtech, Summa Medical Corp., Albuquerque, NM) to remove the unbound pertechnetate;

after this, the preparation was ready for injection. Recovery of $^{99\text{m}}\text{Tc}$ after filtration was $93 \pm 3\%$; thin-layer chromatography showed that $97 \pm 6\%$ was protein-bound. In vitro binding of $^{99\text{m}}\text{Tc}$ -labeled 50H.19 to citrated blood showed that $58 \pm 3\%$ of the radioactivity was in the cellular fraction in dogs and $61 \pm 2\%$ in the cellular fraction of human blood. In dogs, $56 \pm 5\%$ of the injected dose in vivo was found in the cellular fraction. In vitro studies showed that 57% of the radioactivity became bound to in vitro preformed clots and $70 \pm 3\%$ to in vivo formed clots. In humans, binding to in vitro preformed clots was $75 \pm 6\%$. Blood clearance studies in dogs showed a reduction of 50% of the initial activity within 3–6 min after IV injection, and 18–24% of the injected activity was excreted in the urine collected during the first 3 hr after injection. Immunohistochemical studies showed intense and exclusive binding of $^{99\text{m}}\text{Tc}$ -labeled 50H.19 to platelets. The antibody was evaluated in dogs with experimental thrombi induced by transcatheter placement of copper coils or aluminum balls. Thrombi were thus induced in peripheral veins (jugular, femoral), in segmental pulmonary arteries (carotid, femoral), and in the right ventricle. Spontaneous thrombi formed on catheters placed for venous blood sampling and intimal damage occurred at catheter insertion sites in arteries and veins. The $^{99\text{m}}\text{Tc}$ -labeled 50H.19 was injected 1–3 hr after thrombus induction, and imaging was started immediately and continued for 4 hr. Imaging of peripheral thrombi was possible 1 hr after antibody injection, and the optimal imaging time for thrombi in the trunk was 2 hr after injection (Fig. 2).

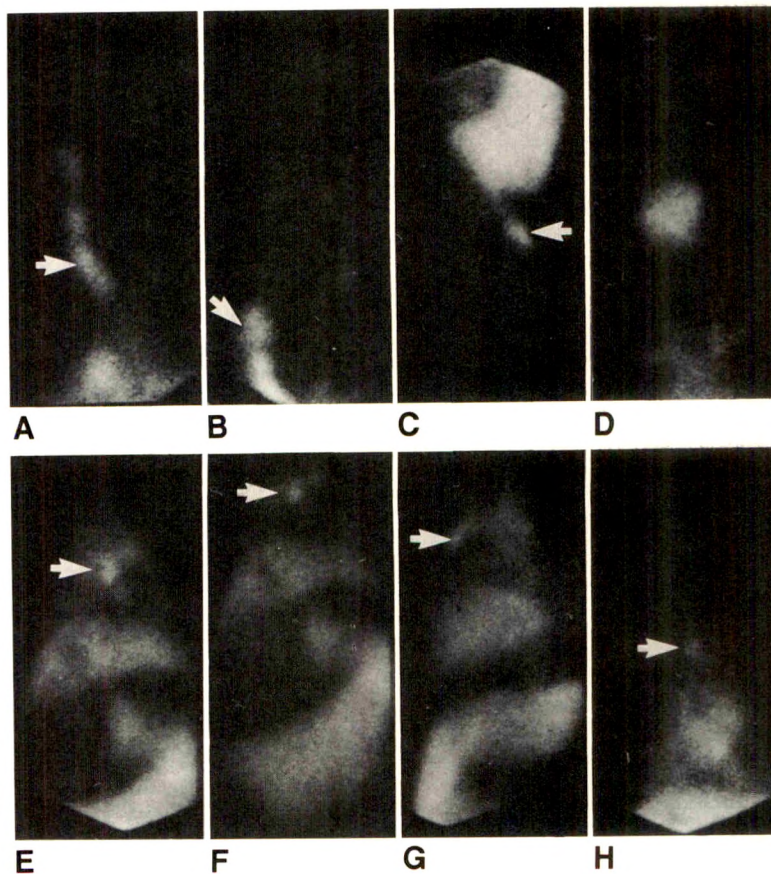


Fig. 1.—Scintigrams of experimental thrombi in dogs 75–120 min after IV injection of 3 mCi (111 MBq) ^{111}In -labeled antiplatelet antibody 7E3.

A, Right common carotid artery thrombus (arrow); persistent activity in lungs (bottom).

B, Thrombus in right jugular vein (arrow). Compare with contralateral side.

C, Spontaneous thrombus around catheter in left femoral vein (arrow); bottom of spleen shows intense uptake.

D, Thrombus in right common carotid artery and clotted hematoma.

E–G, Thrombus in segmental pulmonary artery of right lung (arrows) on anterior, posterior, and lateral views. Note blood-pool activity in spleen and liver.

H, Thrombus in superior vena cava and areas of endothelial damage in jugular vein due to catheter (arrow). Heart and dome of liver are visible also.

In all 15 dogs, there was consistent visualization of thrombi in veins, arteries, and right ventricle, as well as in areas of intimal damage. Blood-pool subtraction or image enhancement was not necessary for thrombus visualization. A ^{99m}Tc -labeled, nonspecific antibody (MOPC-21), labeled and evaluated under the same conditions as the specific antibody (50H.19), did not show accumulation in thrombi. The ex vivo thrombus to blood (percent injected dose/g) ratio of ^{99m}Tc -labeled 50H.19 was on the average 15.

We extended this work with ^{99m}Tc -labeled 50H.19 to an animal model of mesenteric vascular occlusion [81, 82]. When similar experimental techniques were used to induce vascular occlusions, the ^{99m}Tc -labeled antibody fragments were shown to accumulate in infarcted bowel and became visible on scintigrams 90–120 min after injection (Fig. 3). No accumulation of ^{99m}Tc -labeled MOPC-21, the nonspecific antibody, was detected in dogs with mesenteric occlusion. The ex vivo

scintigrams with ^{99m}Tc -labeled 50H.19 showed high accumulation in the experimentally occluded ileal or jejunal vessels. In addition, accumulation in the infarcted bowel was seen, which most probably represented small intramural thrombi (Fig. 3c).

Thrombus radioimmunoimaging in humans by means of a different antiplatelet antibody, P256, has been reported by Peters et al. [83]. Although originally only a limited number of subjects were studied (Fig. 4), results of further studies seem to be encouraging [84].

Radiolabeled Monoclonal Antifibrin Antibodies

Other investigators choosing a different approach have developed radiolabeled monoclonal antifibrin antibodies for thrombus localization [85, 86]. Two antibodies, 59D8 [85] and T2G1S [86], share the same epitope on the fibrin molecule that becomes exposed after cleavage of the fibrinogen

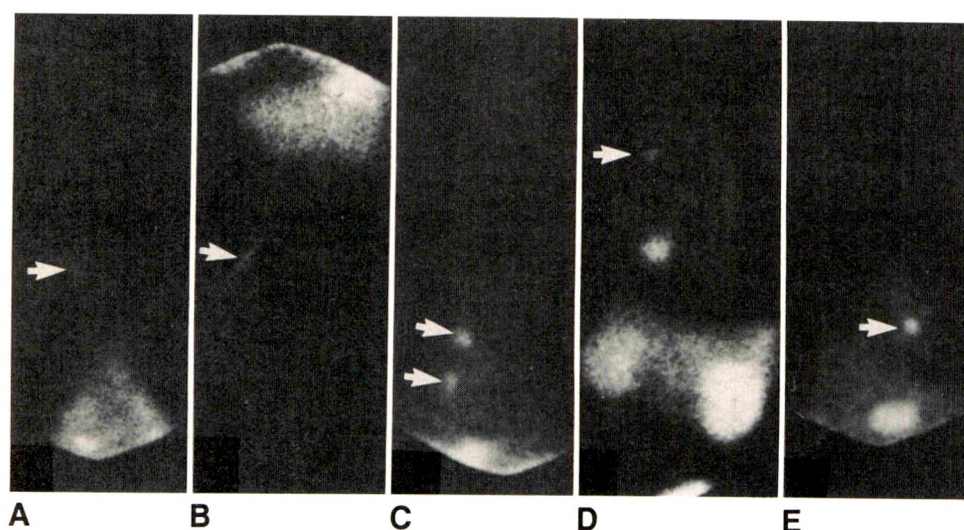


Fig. 2.—Scintigrams of thrombi in dogs 60–180 min after IV injection of 5 mCi (185 MBq) ^{99m}Tc -labeled antiplatelet antibody 50H.19.

A, Thrombus in right common carotid artery (arrow); lungs are seen at bottom.

B, Thrombus in right femoral vein (arrow). Lower pole of spleen (top) shows high uptake.

C, Two thrombi in segmental pulmonary arteries in right lung (arrows). Focal activity at lower part of image represents gallbladder.

D and E, Thrombus in segmental pulmonary artery (arrows), anterior (D) and lateral (E) views. Note kidneys and gallbladder.

(Reprinted from [80], with permission.)

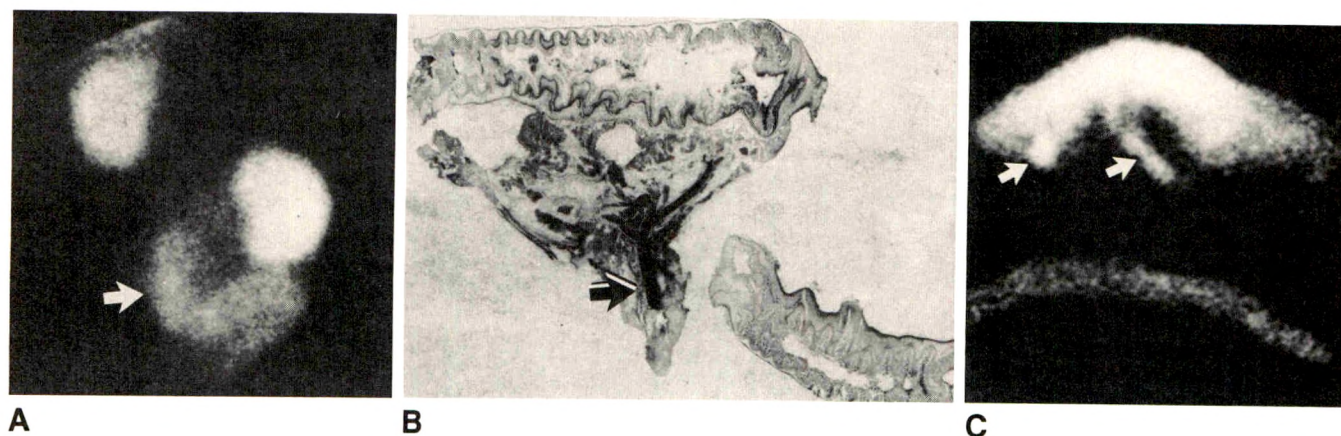


Fig. 3.—A, Scintigram of dog (anterior abdomen) 150 min after IV injection of 3.5 mCi (130 MBq) ^{99m}Tc -labeled antiplatelet antibody 50H.19. Experimentally induced infarcted bowel is clearly seen (arrow). Note activity in kidneys.

B, Macrosection of bowel segment and occluded mesentery (left) as compared with normal bowel (right bottom). Note thrombus in occluded vessel (arrow) and dilatation and edema of bowel wall.

C, Ex vivo scintigram of same dog. In addition to accumulation of ^{99m}Tc -labeled 50H.19 in infarcted bowel wall, there is uptake in thrombosed mesenteric vessels (arrows).

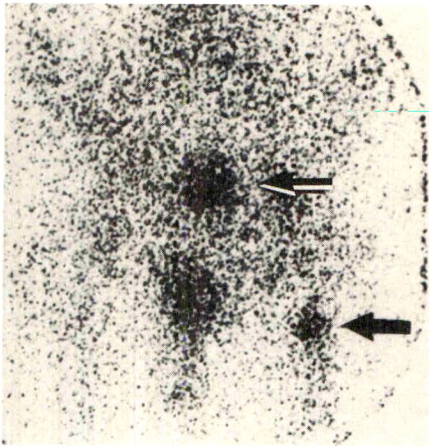


Fig. 4.—Scintigram of lower pelvis of 81-year-old man with deep-vein thrombosis 72 hr after IV injection with antiplatelet antibody fragments, ^{111}In -labeled P256 F(ab')₂. Activity in left femoral vein (lower arrow) is consistent with deep-vein thrombosis. Note urinary excretion (upper arrow). (Courtesy of J. P. Lavender and A. W. J. Stuttle, London.)

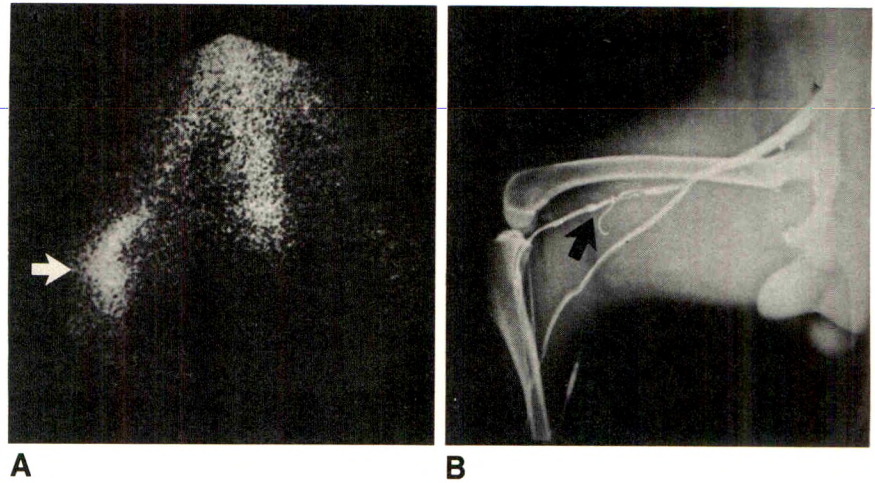


Fig. 5.—A, Scintigram of experimental venous thrombus (arrow) in dog 20 hr after IV injection of 240 μCi (8.9 MBq) ^{111}In -labeled monoclonal antifibrin fragment, T2G1S F(ab')₂. B, Venogram shows thrombus induced by Gianturco coil (arrow). (Courtesy of J. G. McAfee, B. J. Kudryk, S. F. Rosebrough, and Z. D. Grossman, Syracuse, NY.)

molecule. ^{131}I -labeled antifibrin antibody was first evaluated in a dog model of deep-vein thrombosis [87]. Imaging of fresh thrombi was possible only 24–48 hr after injection; the delay was probably caused by the prolonged blood clearance ($T_{1/2} = 46$ hr). Imaging of coil-induced “older” thrombi in the dog by using the same compound has been reported [88]. However, researchers [88, 89] have questioned whether coil-induced thrombi in the dog ever become “old.” Dogs have an extremely active fibrinolytic system, and the presence of the coil in the circulation may act as a continuous thrombogenic stimulus creating conditions that may be different from normal “aging” of thrombus. ^{111}In -labeled Fab fragments of 59D8 were also evaluated as a potential agent for imaging old thrombi in rabbits and dogs [89]. The average half-life in the circulation in dogs was 8 ± 1 hr, and, therefore, images at 3–4 hr showed only the blood-pool distribution pattern. Moreover, thrombi that embolized to the lungs could not be detected even on delayed images. Fab' fragments of $^{99\text{m}}\text{Tc}$ -labeled antifibrin antibody (T2G1S) have been used recently in experimental animals [90], and various labeled fragment preparations were evaluated [91]. Indium-111-labeled F(ab')₂ (Fig. 5) seems to have the best characteristics for thrombus imaging in the dog [91].

The first human trials of ^{111}In -labeled antifibrin antibody have been reported recently [92–94]. These studies indicate the safety and relative efficacy (high sensitivity) of the antifibrin technique in detecting deep-vein thrombosis (Fig. 6). The radiation dosimetry data of the 2-mCi (74-MBq) dose of ^{111}In -labeled 59D8 used in these studies have not been published yet.

Future Perspectives

Radiolabeled monoclonal antiplatelet antibody preparations have significant advantages over antifibrin antibodies (Table

1). Imaging is possible within a much shorter time after injection, and thrombi in organs with high blood-pool activity (e.g., lungs and heart) can be detected. Antifibrin antibodies were shown to be effective for the detection of deep-vein thrombosis in experimental animals and in humans. Thrombus detection in other organs has not yet been reported. Although theoretical considerations seem to indicate that antifibrin agents may be preferable for imaging older thrombi, the results from various reports are not conclusive because of methodologic problems related to the model of old thrombi. The half-life of antifibrin antibodies in the circulation is long, and therefore imaging can be performed several hours after injection, even when fragments are used [92], thus limiting the use of this method to nonemergency situations. The prolonged persistence in the circulation of antifibrins resulting in high body background and low target-to-nontarget ratios probably causes the difficulties in detecting thrombi in high-blood-pool organs also. The lack of circulating antigen has been disputed, because 59D8 and T2G1S may also bind to split fibrin products that are released into the circulation during fibrinogenesis. On the other hand, although antiplatelet antibodies encounter large amounts of antigenic sites on the platelets in the circulation, an adequate contrast between target (thrombus) and nontarget is achieved within a short time. The mechanisms responsible for this phenomenon have not yet been elucidated. Several possibilities may be considered. Possibly, the particulate platelet/antibody complex clears faster because it is recognized by the spleen and removed at a faster rate, as compared with nonparticulate antigen/antibody complexes. Another possibility is that the antibody may have a higher affinity for activated platelets, as compared with nonactivated platelets, and therefore fast accumulation in the clot occurs, increasing the local concentration and possibly lowering blood activity by urinary excretion.

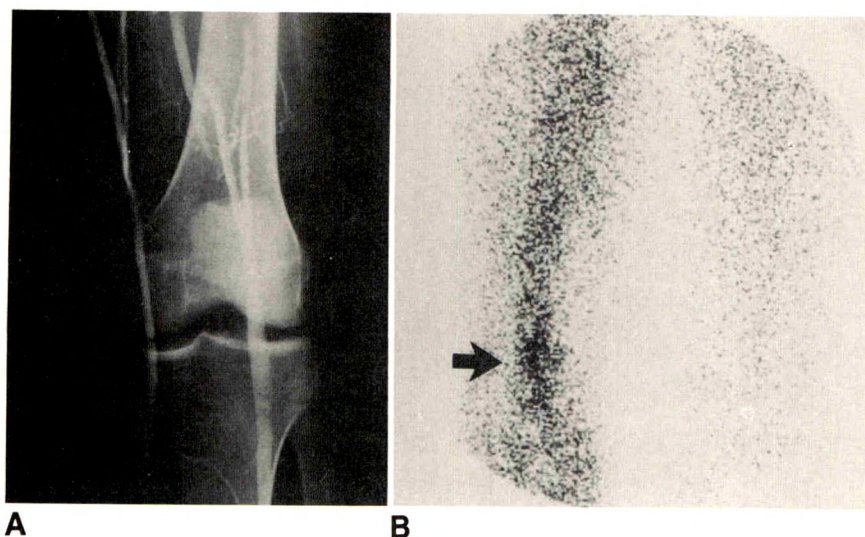


Fig. 6.—A, Contrast venogram shows thrombosis in popliteal area of patient.

B, Scintigram of same area 18 hr after injection of 2 mCi (74 MBq) ^{111}In -labeled antifibrin antibody fragments. Increased activity is noted in area corresponding to site of thrombosis (arrow).

(Courtesy of A. Alavi, Hospital of the University of Pennsylvania, Philadelphia, PA, and Centocor, Malverne, PA.)

TABLE 1: Comparison of Some Thrombus-Specific Imaging Agents

	^{111}In -labeled Platelets	^{111}In -labeled 7E3	$^{99\text{m}}\text{Tc}$ -labeled 50H.19	^{111}In -labeled 59D8	$^{99\text{m}}\text{Tc}$ -labeled T2G1S
Preparation/labeling:					
Platelet separation	Needed	Not needed	Not needed	Not needed	Not reported
Complexity	High	Moderate	Minimal	Moderate	Not reported
Time	Long (~4 hr)	Moderate (~3 hr)	Short (1 hr)	Moderate (~3 hr)	Not reported
Isotope	^{111}In	$^{111}\text{In}/^{123}\text{I}$	$^{99\text{m}}\text{Tc}$	^{111}In	$^{99\text{m}}\text{Tc}$
Imaging Time (hr):					
Extremities	4–24	3	1.5–2.0	4–25	2–4
Trunk	24–48	3	1.5–2.0	Not reported	Not reported

Note.—7E3 = whole monoclonal antiplatelet antibody [75]; 50H.19 = fragments of monoclonal antibody reacting with platelets [80]; 59D8 = fragments of monoclonal antifibrin antibody [91]; T2G1S = fragments of monoclonal antifibrin antibody [90].

Despite our deficient understanding of the mechanisms responsible for faster thrombus-binding and blood clearance that enable early thrombus imaging, it seems that antiplatelet antibodies, $^{99\text{m}}\text{Tc}$ -labeled 50H.19 in particular, may become valuable diagnostic aids for improving the selection of patients before thrombolytic therapy and for thrombus detection in general. Thrombus-specific imaging will enable the administration of thrombolytic therapy only to patients with thrombi that are amenable to lysis. Perfusion may then be reestablished when maximal tissue salvage is possible, thus avoiding unnecessary treatment and potentially serious side effects. If clinical trials in humans confirm the results obtained in experimental animals, thrombus radioimmunoscintigraphy will become a simple, effective, and noninvasive clinical diagnostic technique with wide applications in thromboembolic conditions.

ACKNOWLEDGMENTS

We thank E. Roche for her highly skillful secretarial help in manuscript preparation and Morton A. Meyers for his valuable comments.

REFERENCES

- Marder VJ, Sherry S. Thrombolytic therapy: current status. Part I. *N Engl J Med* 1988;318:1512–1520
- European Cooperative Study Group for Streptokinase Treatment in Acute Myocardial Infarction. Streptokinase in acute myocardial infarction. *N Engl J Med* 1979;301:797–802
- The TIMI Study Group. The thrombolysis in myocardial infarction (TIMI) trial: phase I findings. *N Engl J Med* 1985;312:932–936
- ISIS Collaborative Group. Results of a large randomized trial of intravenous streptokinase and oral aspirin in acute myocardial infarction (abstr). *J Am Coll Cardiol* 1988;11:232A
- Gruppo Italiano per lo Studio della streptochinasi nell' Infarto miocardico (GISSI). Effectiveness of intravenous thrombolytic treatment in acute myocardial infarction. *Lancet* 1986;1:397–402
- Koren G, Weiss AT, Hasin Y, et al. Prevention of myocardial damage in acute myocardial ischemia by early treatment with intravenous streptokinase. *N Engl J Med* 1985;313:1384–1389
- Guerci AD, Gerstenblith G, Brinker JA, et al. A randomized trial of intravenous tissue plasminogen activator for acute myocardial infarction with subsequent randomization for elective coronary angioplasty. *N Engl J Med* 1987;317:1613–1618
- Ganz W, Ninomiya K, Hashida J, et al. Intracoronary thrombolysis in acute myocardial infarction: experimental background and clinical experience. *Am Heart J* 1981;102:1145–1149
- Swan HJ. Thrombolysis in acute evolving myocardial infarction: a new potential for myocardial salvage. *N Engl J Med* 1983;308:1354–1355
- Rentrop KP, Feit F, Blanke H, et al. Effects of intracoronary streptokinase and intracoronary nitroglycerin infusion on coronary angiographic patterns and mortality in patients with acute myocardial infarction. *N Engl J Med* 1984;311:1457–1463
- Belkin M, Belkin B, Buckman CA, Strautt JJ, Lowe R. Intra-arterial fibrinolytic therapy: efficacy of streptokinase vs urokinase. *Arch Surg* 1986;121:769–773
- McNamara TO, Fischer JR. Thrombolysis of peripheral arterial and graft

- occlusions: improved results using high-dose urokinase. *AJR* **1985**; 144:769-775
13. Flickinger EG, Johnsrude IS, Ogburn NL, Weaver MD, Pories W. Local streptokinase infusion for superior mesenteric artery thromboembolism. *AJR* **1983**;140:771-772
 14. Steckel A, Johnston J, Fraley DS, Bruns FJ, Segal DP, Adler S. The use of streptokinase to treat renal arterial thromboembolism. *Am J Kidney Dis* **1984**;4:166-170
 15. Roudaut M-F, Ledain L, Roudaut R, Besse P, Boisseau MR. Thrombolytic treatment of acute thrombotic obstruction with disk valve prostheses: experience with 26 cases. *Semin Thromb Hemost* **1987**;13:201-205
 16. Del Zoppo GS, Zeumer H, Harker LA. Thrombolytic therapy in stroke: possibilities and hazards. *Stroke* **1986**;17:595-607
 17. Sloane MA. Thrombolysis and stroke: past and future. *Arch Neurol* **1987**;44:748-768
 18. Goldhaber SZ, Buring JE, Lipnick RJ, Hennekens CH. Pooled analyses of randomized trials of streptokinase and heparin in phlebographically documented acute deep venous thrombosis. *Am J Med* **1984**;76:393-397
 19. Goldhaber SZ, Vaughan DE, Markis JE, et al. Acute pulmonary embolism treated with tissue plasminogen activator. *Lancet* **1986**;2:886-889
 20. Austin GE, Lynn M, Hollman J. Laboratory test results as predictors of recurrent coronary artery stenosis following angioplasty. *Arch Pathol Lab Med* **1987**;111:1158-1162
 21. Brown BG, Gallery CA, Badger RS, et al. Incomplete lysis of thrombus in the moderate underlying atherosclerotic lesion during intracoronary infusion of streptokinase for acute myocardial infarction: quantitative angiographic observations. *Circulation* **1987**;73:653-661
 22. Braunwald E, Knatterud GL, Passamani E, Robertson TL, Solomon R. Update from the thrombolysis in myocardial infarction trial (abstr). *J Am Coll Cardiol* **1987**;10:970
 23. Gold HK, Leinbach RC, Carabedian HD, et al. Acute coronary reocclusion after thrombolysis with recombinant human tissue-type plasminogen activator: prevention by a maintenance infusion. *Circulation* **1986**;73:347-352
 24. Fletcher AP, Alkjaersig N, Sherry S. The maintenance of a sustained thrombolytic state in man. I. Induction and effects. *J Clin Invest* **1959**;38:1096-1100
 25. Topol EJ, Bell WR, Weisfeldt ML. Coronary thrombolysis with recombinant tissue-type plasminogen activator: a hematologic and pharmacologic study. *Ann Intern Med* **1985**;103:837-843
 26. Rao AK, Pratt C, Berke A, et al. Thrombolysis in myocardial infarction (TIMI) trial—phase I: hemorrhagic manifestations and changes in plasma fibrinogen and the fibrinolytic system in patients treated with recombinant tissue plasminogen activator and streptokinase. *J Am Coll Cardiol* **1988**;11:1-11
 27. Lew AS, Laramée P, Cercek B, Shah PK, Ganz W. The hypotensive effect of intravenous streptokinase in patients with acute myocardial infarction. *Circulation* **1985**;72:1321-1326
 28. Burton KP, McCord JM, Ghai G. Myocardial alterations due to free-radical generation. *Am J Physiol* **1984**;246:H776-H783
 29. Werns SW, Shea MJ, Lucchesi BR. Free radicals and myocardial injury: pharmacologic implications. *Circulation* **1986**;74:1-5
 30. Atkins P, Hawkins LA. The diagnosis of deep-vein thrombosis of the leg using ¹²⁵I-fibrinogen. *Br J Surg* **1968**;55:825-830
 31. Kakkar VV, Nicolaides AN, Renney JT, Friend JR, Clarke MB. ¹²⁵I-labelled fibrinogen test adapted for routine screening for deep-vein thrombosis. *Lancet*; **1970**;1:540-542
 32. Harwig SL, Harwig JF, Sherman LA, Coleman RE, Welch MJ. Radioiodinated plasminogen: an imaging agent for pre-existing thrombi. *J Nucl Med* **1977**;18:42-45
 33. Persson BRR, Darte L. Labeling plasmin with technetium-99m for scintigraphic localization of thrombi. *Int J Rad Appl Instrum [A]* **1977**;28:97-104
 34. Som P, Rhodes BA, Bell WR. Radiolabeled streptokinase and urokinase and their comparative biodistribution. *Thromb Res* **1975**;6:247-253
 35. Krohn KA, Knight LC. Radiopharmaceuticals for thrombus detection: selection, preparation and critical evaluation. *Semin Nucl Med* **1977**;7:219-228
 36. Persson BRR, Kempf V. Labeling and testing of ^{99m}Tc-streptokinase for the diagnosis of deep vein thrombosis. *J Nucl Med* **1975**;16:474-477
 37. Siegel ME, Malmud LS, Rhodes BA, Bell WR, Wagner HN Jr. Scanning of thromboemboli with ¹³¹I-streptokinase. *Radiology* **1972**;103:695-696
 38. Knight LC, Maurer AH, Robbins PS. Fragment E, labeled with I-123 in the detection of venous thrombosis. *Radiology* **1985**;156:509-514
 39. McAfee JG, Thakur ML. Survey of radioactive agents for in vitro labeling of phagocytic leukocytes. I. Soluble agents. *J Nucl Med* **1976**;17:480-487
 40. Thakur ML, Welch MJ, Joist JH, Coleman RE. Indium-111 labeled platelets: studies on preparation and evaluation of in vitro and in vivo function. *Thromb Res* **1976**;9:345-357
 41. Heaton WA, Davis HH, Welch MJ, et al. Indium-111: a new radionuclide label for studying human platelet kinetics. *Br J Haematol* **1979**;42:613-622
 42. Hawkes RJ, Hawker LM, Wilkinson AR. Use of indium-111/oxine to label human platelets. *Lancet* **1978**;2:483
 43. Dewanjee MK, Fuster V, Kaye MP, Josa M. Imaging platelet deposition with ¹¹¹In-labeled platelets in coronary artery bypass grafts in dogs. *Mayo Clin Proc* **1978**;53:327-331
 44. Riba AL, Thakur ML, Gottschalk A, Andriole VT, Zaret BL. Imaging experimental infective endocarditis with indium-111-labeled blood cellular components. *Circulation* **1979**;59:336-343
 45. Riba AL, Thakur ML, Gottschalk A, Zaret BL. Imaging experimental coronary artery thrombosis with indium-111 platelets. *Circulation* **1979**;60:767-775
 46. Kadir S, Hill-Zabel RL, Tsan MR. Evaluation of arterial injury due to balloon angioplasty by ¹¹¹In-labeled platelets. *J Nucl Med* **1983**;22:234-238
 47. Cunningham DA, Kumar B, Siegel BA, Gilula LA, Totty WG, Welch MJ. Aspirin inhibition of platelet deposition at angioplasty sites: demonstration by platelet scintigraphy. *Radiology* **1984**;151:487-490
 48. Pope CF, Ezekowitz MD, Smith EO, et al. Detection of platelet deposition at the site of peripheral balloon angioplasty using indium-111 platelet scintigraphy. *Am J Cardiol* **1985**;55:495-497
 49. Park JH, Beltman MA, Adelman B, et al. In vivo imaging and evaluation of platelet accumulation vs. time at arterial injury site. *Invest Radiol* **1985**;20:287-292
 50. Davis HH, Heaton WA, Siegel BA, et al. Scintigraphic detection of atherosclerotic lesions and venous thrombi in man by indium-111-labeled autologous platelets. *Lancet* **1978**;1:1186-1187
 51. Lipton MH, Doherty PW, Goodwin DA. Evaluation of catheter thrombogenicity in vivo with indium-labeled platelets. *Radiology* **1980**;135:191-194
 52. Dewanjee MK, Trastek VF, Tago M, Torianni M, Kaye MP. Noninvasive radioisotopic technique for detection of platelet deposition on bovine pericardial mitral-valve prosthesis and in vitro quantification of visceral microembolism in dogs. *Trans Am Soc Artif Intern Organs* **1983**;29:188-193
 53. Ritchie JL, Stratton JR, Thiele B, et al. Indium-111 platelet imaging for detection of platelet deposition in abdominal aneurysms and prosthetic arterial grafts. *Am J Cardiol* **1981**;47:882-889
 54. Stratton JR, Ritchie JL. The effects of antithrombotic drugs in patients with left ventricular thrombi: assessment with indium-111 platelet imaging and two-dimensional echocardiography. *Circulation* **1984**;69:561-568
 55. Fox KA, Bergmann SR, Mathias CJ, et al. Scintigraphic detection of coronary artery thrombi in patients with acute myocardial infarction. *J Am Coll Cardiol* **1984**;4:975-986
 56. Dewanjee MK. Cardiac and vascular imaging with labeled platelets and leukocytes. *Semin Nucl Med* **1984**;14:154-187
 57. Bergmann SR, Lerch RA, Mathias CJ, Sobel BE, Welch MJ. Noninvasive detection of coronary thrombi with In-111 platelets: concise communication. *J Nucl Med* **1983**;24:130-135
 58. Davis HH, Siegel BA, Sherman LA, et al. Scintigraphic detection of carotid atherosclerosis with indium-111-labeled autologous platelets. *Circulation* **1980**;61:982-988
 59. Powers WJ, Siegel BA, Davis HH, Mathias CJ, Clark HB, Welch MJ. Indium-111 platelet scintigraphy in cerebrovascular disease. *Neurology* **1982**;32:938-943
 60. Kessler C, Reuther R, Berentelg J, Kimmig B. The clinical use of platelet scintigraphy with ¹¹¹In-oxine. *J Neurol* **1983**;229:255-261
 61. Goldman M, Leung JO, Aukland A, Hawker RJ, Drolc Z, McCollum CN. Indium-111 platelet imaging, Doppler spectral analysis and angiography compared in patients with transient cerebral ischaemia. *Stroke* **1983**;14:752-756
 62. Isaka Y, Kimura Y, Yoneda S, et al. Platelet accumulation in carotid atherosclerotic lesions: semiquantitative analysis with indium-111 platelets and technetium-99m human serum albumin. *J Nucl Med* **1984**;25:556-563
 63. McIlmoyle G, Davis HH, Welch MJ, Primeau JL, Sherman LA, Siegel BA. Scintigraphic diagnosis of experimental pulmonary embolism with In-111-

- labeled platelets. *J Nucl Med* **1977**;18:910-914
64. Knight LC, Primeau JL, Siegel BA, Welch MJ. Comparison of In-111-labeled platelets and iodinated fibrinogen for the detection of deep vein thrombosis. *J Nucl Med* **1978**;19:891-894
 65. Davis HH, Siegel BA, Sherman LA, Heaton WA, Welch MJ. Scintigraphy with In-111 labeled autologous platelets in venous thromboembolism. *Radiology* **1980**;136:203-207
 66. Sostman HD, Neumann RD, Loke J, et al. Detection of pulmonary embolism in man with ¹¹¹In-labeled autologous platelets. *AJR* **1982**;138:945-947
 67. Ezekowitz MD, Pope CF, Sostman HD, et al. Indium-111 platelet scintigraphy for the diagnosis of acute venous thrombosis. *Circulation* **1986**;73:668-674
 68. Seabold JE, Conrad GR, Kimball DA, Ponto JA, Bricker JA. Pitfalls in establishing the diagnosis of deep venous thrombophlebitis by indium-111 platelet scintigraphy. *J Nucl Med* **1988**;29:1169-1180
 69. Dick HM. Monoclonal antibodies in clinical medicine. *Br Med J* **1985**;291:762-764
 70. Spar IL, Goodland RL, Schwartz SI. Detection of preformed venous thrombi in dogs by means of ¹³¹I-labeled antibodies to dog fibrinogen. *Circ Res* **1965**;17:322-329
 71. Reich T, Reynolds BM, Healey M, Wang MCH, Jacobson JH. Detection of venous thrombosis in the human by means of radioiodinated antifibrin-fibrinogen antibody. *Surgery* **1966**;60:1211-1215
 72. Kramer RS, Ashburn WL, Vasko JS, Morrow AG. Detection of intracardiac thrombi using radio-iodinated antifibrinogen (RIAF) and precordial scanning. *Ann Surg* **1967**;166:173-182
 73. Spar IL, Perry JM, Benz LL, et al. Detection of left atrial thrombi: scintillation scanning after administration of ¹³¹I-rabbit antibodies to human fibrinogen. *Am Heart J* **1969**;78:731-739
 74. Bosnjakovic VB, Jankovic BD, Horvat J, Cvoric J. Radiolabeled antihuman fibrin antibody: a new thrombus-detecting agent. *Lancet* **1977**;1:452-454
 75. Oster ZH, Srivastava SC, Som P, et al. Thrombus radioimmunoscintigraphy: an approach using monoclonal antiplatelet antibody. *Proc Natl Acad Sci USA* **1985**;82:3465-3468
 76. Collier BS, Peerschke EI, Scudder LE, Sullivan CA. A murine monoclonal antibody that completely blocks the binding of fibrinogen to platelets produces a thrombosthenic-like state in normal platelets and binds to glycoprotein IIb and/or IIIa. *J Clin Invest* **1983**;72:325-338
 77. Collier BS. A new murine monoclonal antibody reports an activation-dependent change in the conformation and/or microenvironment of the platelet glycoprotein IIb/IIIa complex. *J Clin Invest* **1985**;76:101-108
 78. Collier BS, Folts JD, Scudder LE, Smith SR. Antithrombotic effect of a monoclonal antibody to the platelet glycoprotein IIb/IIIa receptor in an experimental animal model. *Blood* **1986**;68:783-786
 79. Rhodes BA, Torvestad DA, Breslow K, et al. ^{99m}Tc-labeling and acceptance testing of radiolabeled antibodies and antibody fragments. In: Rhodes BA, Burchiel SW, eds. *Tumor imaging*. New York: Masson, **1982**:111-123
 80. Som P, Oster ZH, Zamora PO, et al. Radioimmunoimaging of experimental thrombi in dogs using technetium-99m-labeled monoclonal antibody fragments reactive with human platelets. *J Nucl Med* **1986**;27:1315-1320
 81. Oster ZH, Som P, Zamora PO, et al. The diagnosis of mesenteric thrombosis with Tc-99m 59H.19: a monoclonal antiplatelet antibody (abstr). *J Nucl Med* **1988**;29:886
 82. Oster ZH, Som P, Zamora PO. Mesenteric vascular occlusion: a new diagnostic method using a radiolabeled monoclonal antibody reactive with platelets. *Radiology* (in press)
 83. Peters AM, Lavender JP, Needham SG, et al. Imaging thrombus with radiolabeled monoclonal antibody to platelets. *Br Med J* **1986**;293:1525-1527
 84. Lavender JP. In-vivo studies with an antiplatelet monoclonal antibody, P256 (abstr). In: *Proceedings of new approaches to radiolabelling blood cells and imaging thrombus and inflammation*. London, February **1988**; Nuclear Medicine Communications (in press)
 85. Hui KY, Haber E, Matsueda GR. Monoclonal antibodies to a synthetic fibrin-like peptide bind to human fibrin, but not fibrinogen. *Science* **1983**;222:1129-1132
 86. Kudryk BJ, Rohoza A, Ahadi M, Chin J, Wiebe E. Specificity of a monoclonal antibody for the NH₂ terminal region of fibrin. *Mol Immunol* **1984**;21:89-94
 87. Rosebrough SF, Kudryk BJ, Grossman ZD, et al. Radioimmunoimaging of venous thrombi using iodine-131 monoclonal antibody. *Radiology* **1985**;156:515-517
 88. Rosebrough SF, Grossman ZD, McAfee JG, et al. Aged venous thrombi: radioimmunoimaging with fibrin-specific monoclonal antibody. *Radiology* **1987**;162:575-577
 89. Knight LC, Maurer AH, Ammar IA, Shealy DJ, Mattis JA. Evaluation of indium-111-labeled anti-fibrin antibody for imaging vascular thrombi. *J Nucl Med* **1988**;29:494-502
 90. Knight LC, Maurer AH, Ammar IA, Epps LA, Dean RT, Berger HJ. Imaging venous thrombi in dogs with Tc-99m antifibrin antibody (abstr). *J Nucl Med* **1988**;29:745
 91. Rosebrough SF, Grossman ZD, McAfee JG, et al. Thrombus imaging with indium-111 and iodine-131-labeled fibrin-specific monoclonal antibody and its F(ab')₂ and F(ab) fragments. *J Nucl Med* **1988**;29:1212-1222
 92. Alavi A, Gupta N, Berger H, et al. Detection of venous thrombosis with In-111 labeled antifibrin (59D8) antibody imaging (abstr). *J Nucl Med* **1988**;29:825
 93. Peltier P, Plamchon B, Tefaucal P, et al. Imaging venous thrombi using antifibrin monoclonal antibody (abstr). *J Nucl Med* **1988**;29:806
 94. Bourgeois P, Feremans W, Van Gysel JP. In-111 labeled antifibrin antibodies (AFab) in the diagnosis of vein thrombosis (VT): first results (abstr). *J Nucl Med* **1988**;29:807

The Diagnosis of Pulmonary Nodules: Comparison Between Standard and Inverse Digitized Images and Conventional Chest Radiographs

Martin E. Sheline¹
Inna Brikman
David M. Epstein
Jonathan L. Mezrich
Harold L. Kundel
Ronald L. Arenson

We compared plain chest radiographs, standard (bones white) digitized images, and inverse-intensity (bones black) images to determine their ability to identify pathologically confirmed malignant pulmonary nodules. The images were digitized by using a photo-optical laser scanner and were displayed on a 1024 × 1024 × 8 bit system capable of operator-controlled magnification (2× or 4×) and nonlinear (logarithmic/exponential) contrast transformation in both standard and inverse-intensity modes. Receiver-operator curve analysis was used to study the detection performance of six observers who viewed 40 images obtained in 15 normal subjects and 25 abnormal subjects. There was no statistically significant difference in the area under the ROC curve between the standard digital images and the plain chest radiographs. However, ROC areas were significantly greater ($p \leq .05$) for inverse-intensity digital images when compared with either standard-intensity digital images or plain chest radiographs.

These results suggest that inverse-intensity images may have some advantages in the detection of pulmonary nodules.

The purpose of this project was to compare plain chest radiographs, standard (bones white) digitized images, and inverse-intensity (bones black) digitized images to determine their usefulness in detecting pulmonary nodules. Several studies have been done recently comparing digitized images and digitizing systems with conventional plain radiographs [1–6]. The systems studied have used multiple features, including edge enhancement, inverse intensity, magnification, contrast transformation, and scrolling. Some studies have shown that conventional radiographs are superior in detecting pneumothoraces and mild interstitial disease, probably reflecting the higher resolution of plain films [3, 4]. When nodules are located in the mediastinum or behind the heart, digitized images may be better than plain radiographs [3, 5] because the local contrast can be adjusted by the use of either window and level controls or by a suitable intensity transformation.

Until recently, the inverse-intensity digital display mode had not been tested and compared with conventional radiographs and standard digitized images. However, MacMahon et al. [7] found that, for a variety of radiographic findings including pneumothorax, interstitial disease, bone lesions, and pulmonary nodules, diagnostic accuracy was greater with conventional films than with video display, and standard digitized images were more accurate than inverse-intensity images. We specifically concentrated on a comparison of these three image-display techniques to assess any inherent advantages in the detection of pulmonary nodules. We designed the study, both by selection of cases and by selection of readers, to isolate any possible differences between the three imaging methods.

Materials and Methods

Of the 40 posteroanterior chest radiographs that were selected, 15 were normal and 25 showed single or multiple pulmonary nodules. The 25 positive films were obtained in patients with pathologically proved pulmonary malignancy; each of these patients had had a chest

Received July 25, 1988; accepted after revision October 3, 1988.

This work was supported in part by grant #HL33332 from the National Institute of Heart, Lung, and Blood Diseases, United States Public Health Service.

¹ All authors: Department of Radiology, Hospital of the University of Pennsylvania, 3400 Spruce St., Philadelphia, PA 19104. Address reprint requests to D. M. Epstein.

AJR 152:261–263, February 1989
0361–803X/89/1522–0261
© American Roentgen Ray Society

radiograph on which the pulmonary tumor had been missed when the films were interpreted routinely. The films chosen were the earliest radiographs on which the presence and location of a nodule could, in retrospect, be confirmed unanimously by a panel of three radiologists. This sample was biased toward difficult cases under the assumption that if image processing is to be useful, it must help with diagnosis of the cases that are ordinarily missed. The normal cases were chosen from a series of healthy people who had had follow-up for several years to establish the absence of a tumor. The age range of the normal subjects (27–94 years) was similar to that of the patients with malignancy. The radiologists who selected the films did not participate in interpreting the studies.

Digitized images were made of all 40 films by using a photo-optical laser scanner with 200- μ m resolution (Film Digital Radiograph System [DRS-1], Du Pont, Wilmington, DE). Images were displayed on a Ramtek RM9460 display station (Ramtek, Santa Clara, CA). The digitizer and the display station have been described in detail elsewhere [1–3, 8]. We displayed digitized images of 1024 \times 1024 pixels with an 8-bit gray scale (256 shades of gray). Inverse images were obtained by subtracting each pixel's gray scale from 255. Normal and inverse-intensity images were treated as separate categories, and the reviewers were not allowed to use the operator-controlled inverse capabilities of the system. The reviewers were allowed to use the two- or four-power magnification software and to perform nonlinear (logarithmic/exponential) contrast transformation of the images. Six radiology residents-in-training independently reviewed the 40 cases in each of three modes: radiographs, normal-intensity digitized images, and inverse-intensity digitized images. They were allowed to examine the images at their own pace. In order to prevent any bias or learning, groups of eight studies from each of the three categories (plain film, standard digitized, and inverse digitized) were reviewed in separate, randomized blocks. The six radiology residents saw the films in different randomized sequences.

So that the residents would have some familiarity with interpreting digital images, several cases not used in the study were reviewed before starting the study. Plain radiographs, standard digital images, and inverse images were displayed side-by-side. For this study, the radiologists recorded their confidence level as either low, medium, or high for detecting the presence or absence of at least one pulmonary nodule for each of the four quadrants of the image (the readers were asked to make incidental note of granulomas, calcified lymph nodes, and nipple shadows but not to include them as nodules). The scoring was done on the basis of quadrants. There were a total of 40 quadrants containing at least one nodule and 120 quadrants without nodules. The ROC curves were compared for each of the three image-display categories to determine which method was superior in detecting lung nodules.

The ROC area (A) and the standard error (SE) were calculated for each viewing mode by using the jackknife method of Dorfman and Berbaum [9]. This method pools the response data from a group of observers. Two viewing techniques were then compared by using the approach of Hanley and McNeil [10]. The critical ratio, z , was calculated as

$$z = \frac{A_1 - A_2}{(SE_1^2 + SE_2^2 - 2rSE_1SE_2)^{1/2}} \quad (1)$$

where A_1 and A_2 are the ROC areas for two viewing techniques, SE_1 and SE_2 are the standard errors, and r is the correlation between the two techniques. This correlation is derived from the average ROC area and from the correlation coefficient for paired observer responses. Kendall's tau was used as the correlation coefficient. The average value for the six observers was used, and the value of r was taken from the table published by Hanley and McNeil [10].

Results

The pooled results from the RSCORE-J jackknife program for each of the three viewing modes are given in Table 1. A composite ROC curve for each of the three techniques is shown in Figure 1. The difference between pairs of viewing modes is given in Table 2. The difference between inverse video images and plain radiographs for pooled data was significant, with $p = .008$. The difference between inverse and normal video images had a p of .055, which is just at the borderline of significance when $p = .050$ is used as a criterion. The difference between normal video images and plain radiographs was not found to be significant ($p = .18$).

TABLE 1: Area Under the Receiver Operating Characteristic Curves and Population Standard Error for Three Display Techniques

Technique	Area Under ROC Curve	Standard Error
Film	0.72	0.05
Normal digital video	0.75	0.06
Inverse digital video	0.86	0.06

Note.—Area and standard error were estimated by the jackknife procedure RSCORE-J [9]. ROC = receiver operating characteristic.

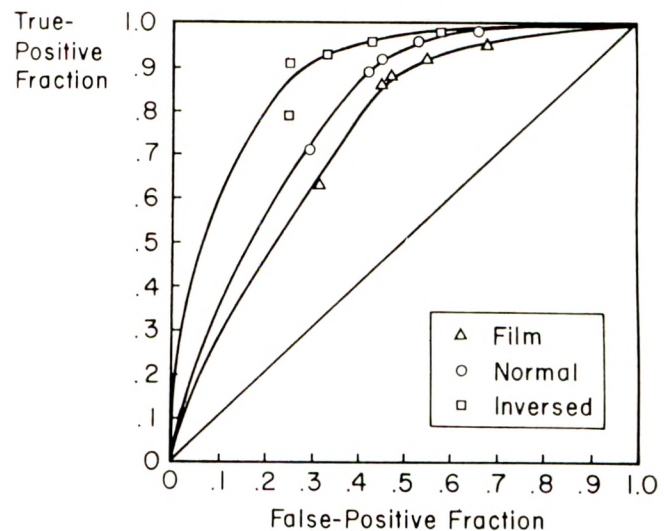


Fig. 1.—Receiver operating characteristic curves of pooled data for inverse images, normal images, and plain radiographs.

TABLE 2: A Comparison of Performance Between Different Display Techniques by Calculating the Difference in the Areas of Their Receiver Operating Characteristic Curves

Comparison	ΔA	r	z	p
Film vs normal	0.05	.42	0.93	.18
Normal vs inverse	0.09	.47	1.60	.055
Film vs inverse	0.14	.40	2.39	.008

Note.—Numbers in ΔA column show the difference in the areas of ROC curves, r is the average correlation coefficient, z is the critical ratio calculated by using equation 1 (see Materials and Methods), and p is the corrected ratio derived from the normal distribution. ROC = receiver operating characteristic.

Discussion

It appears that for the detection of nodules, there may be an advantage in displaying images in inverse intensity. In our study, every attempt was made to eliminate bias toward normal-intensity images (digitized and plain films). We used radiology residents, because we thought that more experienced radiologists, with much more experience with plain films, might be biased in favor of normal images. No attempt was made to simulate a "real practice"; reviewers were allowed to read films at their own pace.

By using pathologically confirmed lung tumors that were missed during regular interpretation, we were able to include cases in which the plain film findings were questionable. In some of these cases, the findings may have been more visible on inverse-display images. The inverse- and normal-intensity images were obtained from the same digitizer data and were displayed on the same display station. Both the magnification and the nonlinear contrast transformation were available for either technique. Therefore, any difference in observer performance when viewing normal-display and inverse-display images presumably represents a real difference between the two techniques. The difference between inverse and normal video images was more than twice that between normal video and plain radiographs, indicating that the digitization of images was a less significant factor than the mode in which they were displayed—that is, as inverse- or normal-intensity images. Although the difference between the inverse display and the normal display was just at the borderline of statistical significance ($p = .055$), we believe that inverse images may have an intrinsic advantage over normal images, especially in light of the many biases toward normal-intensity images (such as more familiarity with normal images).

The fact that observer performance was better with both types of digitized images than with plain radiographs may reflect the ability to manipulate contrast on the digital system. Other authors [3–5] have reported that digitized images are useful in identifying pulmonary nodules. A recent study by MacMahon et al. [7] evaluated hard-copy, standard, and inverse-intensity digitalized images but did not permit observer manipulation of the video controls, window width, or brightness. This may account for the fact that their degree of accuracy in detecting pulmonary nodules was lower with inverse-intensity images than with standard digitized images

and hard copy. Our study suggests that, although digitized images clearly do not contain any more information than plain radiographs, the format and image manipulation possible with digitized systems may present pulmonary nodules in a more recognizable fashion, especially those obtained from under- or overexposed areas of radiographs.

ACKNOWLEDGMENTS

We are indebted to the radiology residents at the University of Pennsylvania for their time and effort in reviewing the images used in this study: Phil Bergey, Stuart Bobman, Theresa Chan, Elliott Lerner, and Robert Lipman. We thank Du Pont and Digital Equipment for generous gifts of equipment and Karen L. Weiss and John Kahler for help in preparing the manuscript.

REFERENCES

1. Kundel HL, Mezrich JL, Brikman I, et al. Digital chest imaging: comparison of two film digitizers with a classification task. *Radiology* **1987**;165:747–752
2. Kundel H. Visual perceptions and image display terminals. *Radiol Clin North Am* **1986**;24:69–77
3. Goodman LR, Foley WD, Wilson CR, Rimm AA, Lawson TL. Digital and conventional chest images: observer performance with film digital radiography system. *Radiology* **1986**;158:27–33
4. MacMahon H, Vyborny CJ, Metz CE, Doi K, Sabeti V, Solomon SL. Digital radiography of subtle pulmonary abnormalities: an ROC study of the effect of pixel size on observer performance. *Radiology* **1986**;158:21–26
5. Chakraborty DP, Breatnach ES, Yester MV, Soto B, Barnes GT, Fraser RG. Digital and conventional chest imaging: a modified ROC study of observer performance using simulated nodules. *Radiology* **1986**;158:35–39
6. Armstrong JD II, Sorenson JA, Nelson JA, et al. Clinical evaluation of unsharp masking and slit scanning techniques in chest radiography. *Radiology* **1983**;147:351–356
7. MacMahon H, Metz CE, Doi K, Kim T, Giger ML, Chan H-P. Digital chest radiography: effect on diagnostic accuracy of hard copy, conventional video, and reversed gray scale video display formats. *Radiology* **1988**;168:669–673
8. van der Voorde F, Arenson RL, Kundel HL, et al. Development of a physician-friendly digital image display console. *PACS IV, SPIE* **1986**;626:541–548
9. Dorfman DD, Berbaum KS. RSCORE-J: Pooled rating method data: a computer program for analyzing pooled ROC curves. *Behav Res Methods Instruments Comput* **1986**;18:452–462
10. Hanley JA, McNeil BJ. A method of comparing the areas under receiver operating characteristic curves derived from the same cases. *Radiology* **1983**;148:839–843

Book Review

Principles of Radiopharmacology. Edited by Harald Deckart and Peter H. Cox. Boston: Nijhoff, 262 pp., 1987. \$67

The preface states that this volume represents the written version of 22 lectures presented at training courses in radiopharmacy and radiopharmacology under the sponsorship of the European Societies of Nuclear Medicine. The preface is refreshingly honest, pointing out that (1) developments in the field have been complex, (2) the volume is thus wide-ranging, (3) the styles of presentation are not uniform, (4) partial overlapping occurs between chapters, and (5) the book "is designed for specialists working in nuclear medicine centres."

Chapter 1 devotes 17 pages to the "Fundamentals of Radioactivity." (Why do this if the book is intended for specialists?) The following chapters cover radionuclide production with small accelerators, radionuclide generator systems, and a review of several radiopharmaceuticals (particularly iodine and technetium, with briefer mention of indium, thallium, and several others). Chapter 5 contains the reference list for the two previous chapters and is said to "provide a historical overview." Chapter 6 reviews some recent developments, such as generator systems, ^{99m}Tc complexes, liposomes, and "metabolically active materials" (including metaiodobenzyl guanidine, selenomethylnorcholesterol, iodoamphetamine, and monoclonal antibodies). The following five chapters deal with structure-activity relationships of ^{99m}Tc -radiopharmaceuticals, indium complexes, protein-based radiopharmaceuticals, ^{125}I -labeled proteins for radioimmunoassays, radiopharmacokinetics, and principles of radiopharmacology. After a chapter on stable-isotope pharmaceuticals, the final eight deal with development and evaluation of new radiopharmaceuticals, good pharmacy practice, quality control, adverse reactions to radiopharmaceuticals, interaction of pharmaceuticals and radiopharmaceuticals (two

parts), toxicity and safety of radiopharmaceuticals, and calculations of absorbed dose.

Chapters 7 and 8, much of 13, and parts of several others are devoted to ^{99m}Tc compounds. Because these play a central role in many clinical studies in nuclear medicine, it is perhaps not an over-emphasis. As the preface hints, there is redundancy, and the writing styles in various chapters vary from smooth to exceedingly bumpy. This has to be balanced against the fact that an enormous amount of information is presented in 262 pages. The book has a number of idiosyncrasies. For example, the index has eight entries for radiosynovectomy but only five for radioiodide therapy of hyperthyroidism (and that is listed under "treatment"). The term "specific activity" does not appear in the index but can be found on page 18 with the statement "mass activity concentration S (formerly specific activity)." However, mass activity concentration is not in the index either. The back cover has an incomprehensible statement about "stable isotope-labelled radiopharmaceuticals for diagnostics." This is balanced by chapter 14, which states that both stable-isotope pharmaceuticals and radionuclides involved in pharmaceuticals should be referred to as "nuclear pharmaceuticals."

The volume will be of interest to radiopharmacists and is suited as a reference item in a departmental collection.

Richard P. Spencer
University of Connecticut Health Center
Farmington, CT 06032

Case Report

Pulmonary Edema Due to Ingestion of Organophosphate Insecticide

Cheng Li,¹ Wallace T. Miller,² and Jennifer Jiang³

Organophosphate insecticides, of which there are dozens, are the most widely used agricultural insecticides in the United States and throughout the world [1]. The best known organophosphates are parathion and malathion. It has been estimated that 325,000 agricultural workers in the United States will be exposed each year to these two organophosphates alone [1]. Worldwide, organophosphates are the pesticides most commonly involved in human poisoning, and in some countries they rival hypnotics as the most common suicidal poison [2]. The major radiographic finding in acute organophosphate poisoning is pulmonary edema [3]. We report 10 cases of pulmonary edema caused by accidental or deliberate ingestion of DDVP (O,O-dimethyl O-(2,2-dichlorovinyl)phosphate or dichlorvos), a commonly used organophosphate pesticide.

Case Report

An 18-year-old woman drank 50 ml of 80% DDVP in a suicide attempt after a family quarrel. Ten minutes later, she developed severe abdominal pain, headache, blurred vision, and nausea. Gastric lavage was carried out promptly at a local clinic and 5.0 mg of atropine sulfate was given intramuscularly. The patient was then transferred to the emergency room of Chao-Yong Hospital, where she was comatose, unresponsive to stimuli, and cyanotic; her other symptoms were excessive salivation and bronchial secretions. Vital signs were temperature 37.8°C, pulse 112/min, respiration 48/min, and blood pressure 90/70. The patient's pupils were constricted and unresponsive to light, and there were diffuse rales throughout the lung fields. A portable chest radiograph (Fig. 1) showed diffuse alveolar edema and cardiomegaly. The patient was given an additional 10 mg of atropine and 1 g of protopam and was treated with nasal oxygen and IV fluids and antibiotics. She gradually regained consciousness, and a chest radiograph made 4 days after admission was normal.

Discussion

We collected 13 cases of DDVP ingestion over 10 years at Chao-Yong Hospital in Beijing, China. Ten of these 13 cases were associated with acute pulmonary edema. The 13 patients included 10 women and three men with an age range from 11 to 38 years. Twelve of the 13 patients ingested 25–50 ml of DDVP in suicide attempts. The remaining patient accidentally ingested one mouthful, which he subsequently spat out. All patients presented with coma or semicoma and excessive lacrimation and salivation 30 min to 9 hr after ingestion. Several were incontinent of urine and feces, and several were cyanotic and/or hypotensive. In 11 patients, the cause of the coma was recognized as organophosphate poisoning. These 11 patients were treated with pralidoxime chloride (PAM, protopam, 2-PAM) and atropine, and all patients survived, recovering completely in 2–5 days. In the other two patients, organophosphate poisoning was not diagnosed in the emergency room, and both subsequently died. One of these patients had pulmonary edema at autopsy, and the second did not. Nine of the 11 remaining patients had pulmonary edema on the initial supine portable chest radiograph.

Although many cases of organophosphate poisoning have been reported, these 13 cases are the first cases described that are caused by DDVP. This is a widely used pesticide, and probably other poisoning has occurred but has not been reported.

All organophosphate derivatives are rapidly absorbed through the gastrointestinal tract, the respiratory tract, the skin, and/or the mucous membranes [4]. Very rapid absorption can occur through the conjunctiva. Having several drops of organophosphate splashed in the eye has been fatal in

Received July 6, 1988; accepted after revision August 25, 1988.

¹ Department of Radiology, Hospital of the University of Pennsylvania, 3400 Spruce St., Philadelphia, PA 19104, and Department of Radiology, Chao-Yong Hospital, Beijing, China.

² Department of Radiology, Hospital of the University of Pennsylvania, 3400 Spruce St., Philadelphia, PA 19104. Address reprint requests to W. T. Miller.

³ Department of Medicine, Chao-Yong Hospital, Beijing, China.

several instances [2]. The 13 cases in this report are all caused by ingestion of the pesticide, but acute poisoning has been reported by all other routes mentioned. Accidental poisoning is a well-recognized hazard among farmers and crop dusters [2, 5].

The organophosphate insecticides are all cholinesterase inhibitors of varying potency. The most toxic of these compounds are the "nerve gases" used in chemical warfare. Of the insecticides, parathion is considered among the "most dangerous group," malathion among the "least dangerous," and DDVP "dangerous" [5].

The pharmacologic and toxicologic actions of the organophosphates primarily result from inhibition of acetylcholinesterase of the nervous system. Muscarinelike action results from accumulation of acetylcholine at the ends of postganglionic cholinergic nerves, which supply the smooth and cardiac muscles and exocrine glands. Nicotinellike effects result from accumulation of the neurotransmitter in the autonomic ganglia and at nerve endings in voluntary muscles [6]. These physiologic actions of acetylcholine result in clinical symptoms, which initially are usually headache, nausea, vomiting, sweating, blurred vision, weakness, pallor, diarrhea, and abdominal pain. Psychiatric symptoms, such as depression,

anxiety, decrease in mental alertness, or agitation, may be a manifestation of more chronic poisoning. In more severe acute cases, patients may also have increased salivation and lacrimation, muscle fasciculation, convulsions, cyanosis, dyspnea, shock, and cardiac arrhythmias. Organophosphate poisoning may also result in coma or death [6]. Death is attributed to hypoxia due to interference with the respiratory system by severe pulmonary edema and excessive respiratory tract secretion, coupled with paralysis of the respiratory muscles and failure of the respiratory center [6].

Pulmonary edema is a frequent clinical occurrence in organophosphate poisoning (Figs. 1–3) and has been observed also in lungs at autopsy [3, 7]. It has been attributed to the muscarinic action of the insecticide [6]. Accumulated acetylcholine also has complicated effects on the cardiovascular system. Initially, tachycardia and hypertension may be seen, but the predominant influence on the heart appears to be bradycardia and weakened cardiac contraction. This may be a contributing factor to the pulmonary edema [3]. Hypoxia may also play a role in the production of pulmonary edema by increasing capillary permeability.

Early recognition of poisoning is important because treatment with atropine and pralidoxime may save lives [5]. The two patients in this study who were not recognized in the emergency room as poisoned by organophosphates both died. There are many causes of pulmonary edema in the emergency-room patient. The diagnosis of organophosphate poisoning should be considered in the appropriate clinical situation.

REFERENCES

1. Sittig M, ed. *Handbook of toxic and hazardous chemicals and carcinogens*. 2nd ed. Paul Ridge, NJ: Noyes, 1985
2. Kopel FB, Starobin S, Gribetz I, Gribetz D. Acute parathion poisoning: diagnosis and treatment. *J Pediatr* 1962;61:898–902
3. Bledsoe FH, Seymour EQ. Acute pulmonary edema associated with parathion poisoning. *Radiology* 1972;103:53–56
4. Eitzman DV, Wolfson SL. Acute parathion poisoning in children. *Am J Dis Child* 1967;114:397–400
5. Milby TH. Prevention and management of organophosphate poisoning. *JAMA* 1971;216:2131–2133
6. Namba T, Nolte CT, Jackrel J, Grob D. Poisoning due to organophosphate insecticides: acute and chronic manifestations. *Am J Med* 1971;50:475–492
7. Kass JB, Khamapirad T, Wagner ML. Pulmonary edema following skin absorption of organophosphate insecticide. *Pediatr Radiol* 1978;7:113–115

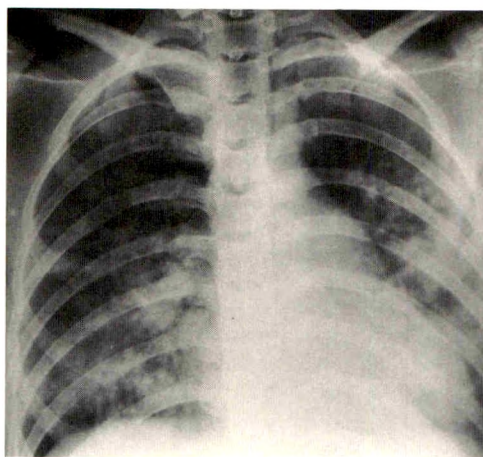
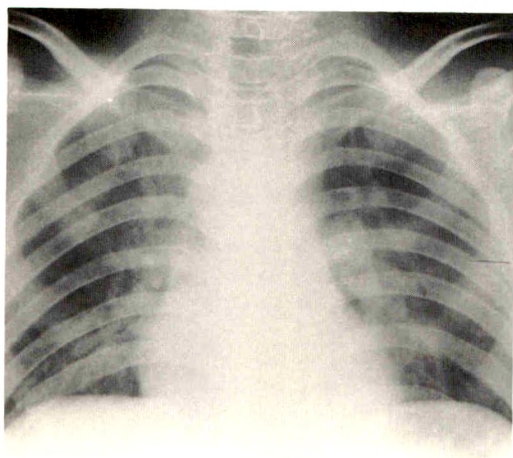
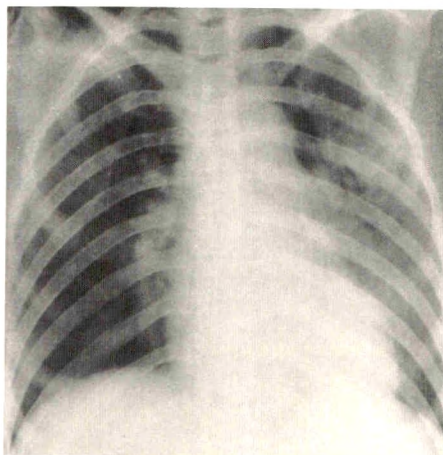


Fig. 1.—18-year-old woman drank 50 .nl of 80% DDVP in an attempted suicide. A chest radiograph made 30 min later shows bilateral pulmonary edema and cardiomegaly, which cleared in 4 days.



2



3

Fig. 2.—11-year-old boy accidentally ingested one mouthful of diluted DDVP, which he rapidly spat out. Chest radiograph made 4 hr later shows bilateral interstitial edema, which cleared 48 hr later.

Fig. 3.—25-year-old woman ingested 25–30 ml of 80% DDVP. A chest radiograph made 1 hr later shows patchy pulmonary edema, primarily in the left lung. The heart is also slightly enlarged. These changes cleared in 3 days.

CT Evaluation of Suspected Hepatic Metastases: Comparison of Techniques for IV Contrast Enhancement

David M. Paushter^{1,2}
 Robert K. Zeman¹
 Mark L. Scheibler^{1,3}
 Peter L. Choyke¹
 Mark H. Jaffe¹
 Letitia R. Clark¹

Although IV injection of contrast material is widely used for detection and follow-up of hepatic metastases on CT, the optimal method of contrast enhancement has not yet been defined. A prospective study was performed in 50 consecutive patients with suspected hepatic metastases. Lesion size and detectability were compared on unenhanced CT scans, scans obtained during a bolus injection of contrast material (early bolus phase), and scans obtained during a rapid infusion after the loading bolus. A total of 60 hepatic lesions were evaluated in 26 patients, 19 with histologic confirmation of metastases and seven with strong supportive evidence. The bolus phase allowed detection of 15% more lesions than did examination during the rapid-infusion phase. Lesion size varied, depending on the timing and method of contrast administration; the largest measurements were obtained during bolus injection of contrast material. In addition, bolus administration of contrast material subjectively resulted in the best lesion detection.

Because the three techniques of IV contrast enhancement may produce different size measurements, sequential examinations must be tailored appropriately. Scanning during the bolus phase is technically possible with current CT equipment and is recommended as the primary CT screening examination for hepatic metastases.

Although CT is used routinely for the detection and follow-up of hepatic metastases, the specific role of IV contrast enhancement has engendered considerable debate [1-14]. Historically, this debate has focused on the accuracy of enhanced vs nonenhanced images [2-4]. It is now recognized that IV contrast enhancement is essential, and the controversy has shifted to the optimal method for delivering the contrast material and the timing of the scans. A recent survey of the members of the Society of Body Computed Tomography revealed wide variability in the methods used to administer contrast material and inconsistencies in the terminology that has been used to describe these techniques in the literature [1].

The purpose of this study was twofold: (1) to compare lesion size and conspicuity with the use of noncontrast, bolus, and bolus-plus-drip-infusion techniques, and (2) to compare the sensitivity of the three techniques for the detection of lesions.

Subjects and Methods

Fifty patients with known or suspected hepatic masses were examined prospectively during a 5-month period. Three sequential techniques were used for each patient: (1) complete liver CT without IV contrast material, (2) dynamic incremental limited liver CT during a machine-injected IV bolus of contrast material, and (3) complete liver CT during a rapid drip of IV contrast material given after a loading bolus. Informed consent for the study was obtained from all the patients.

All examinations were performed on a General Electric CT/T-9800 scanner (General Electric Medical Systems, Milwaukee, WI) with 1-cm-thick contiguous sections. Radiographic technical factors were 120 kVp, 200 mA, and a 2-sec scanning time. The field of view was held constant for each patient's study, and all images were photographed with a window of 350 H and a level of 45 H.

Received April 27, 1988; accepted after revision September 27, 1988.

¹ Department of Radiology, Georgetown University Hospital, 3800 Reservoir Rd., N.W., Washington, DC 20007-2197.

² Present address: Department of Radiology, Cleveland Clinic Foundation, 9500 Euclid Ave., Cleveland, OH 44106. Address reprint requests to D. M. Paushter.

³ Present address: University of North Carolina, Magnetic Resonance Imaging Center, Research Bldg. D, Campus Box 7515, Mason Farm and Daniels Rd., Chapel Hill, NC 27599-7515.

AJR 152:267-271, February 1989

0361-803X/89/1522-0267

© American Roentgen Ray Society

Noncontrast scans were obtained nondynamically from the liver dome to the inferior margin of the right lobe of the liver. After this, a dynamic sequence during a bolus of contrast material was initiated. Contrast material was administered through a 20-gauge angiographic catheter inserted in a dorsal hand or forearm vein by using a MedRad MK-IV dedicated CT injector (MedRad Inc., Pittsburgh, PA). Dynamic imaging was begun 15 sec after initiation of a 50-ml bolus of 60% urographic contrast material (diatrizoate meglumine and diatrizoate sodium) with an injection rate of 2 ml/sec. Therefore, scanning was started after 30 ml of contrast material had been mechanically injected. Seven to nine contiguous 10-mm dynamic sections were obtained in 70 sec to include the central bulk of the liver. There was an obligatory interscan delay of 6 sec/scan in addition to the 2-sec scan time.

After the bolus of contrast material was injected, a 100-ml "wide-open" drip of 60% urographic contrast material was started immediately. Scanning was begun after scanner reprogramming, which required 1 1/4 min. The entire liver was reexamined with 10-mm contiguous sections during the drip infusion. Scans were obtained at a preprogrammed rate with a 2-sec scan time and 10-sec interscan delay.

All studies were reviewed blindly by two authors to determine lesion size, number, and detectability. The noncontrast, bolus, and bolus-plus-drip-infusion studies were compared at carefully matched levels through the central bulk of the liver. In examinations showing multiple metastatic lesions, the maximum diameters of up to three separate and discrete masses, which were well visualized with at least two of the three contrast techniques, were measured to determine which method yielded the largest diameter. The lesions to be measured were agreed on during simultaneous readings by the two reviewers, although size measurements were obtained separately and the two reviewers' results were averaged. Masses smaller than 1 cm were excluded to prevent partial-volume averaging and respiratory misregistration. Only measurement differences greater than 20% were considered significant when the various phases of contrast enhancement were compared for the same reason.

Detectability represents a subjective determination of the ease of visualization of an abnormality [5]. This depends on multiple factors, including lesion size, relative attenuation/vascularity when compared with the remainder of the liver, location, and margin contour. This

variable was compared for each of the three contrast techniques in an attempt to account for a number of factors that affect the radiologic interpretation of the CT examinations.

Twenty-six (52%) of the 50 examinations were considered positive for hepatic metastatic disease. Overall, 60 metastatic lesions were evaluated. Primary neoplasms within this group included colon (eight patients); breast (six); pancreas adenocarcinoma (three); lung (three); stomach (two); and pancreas islet cell, carcinoid, renal cell, and melanoma (one each).

Although 19 of 26 patients had tissue confirmation of their metastatic disease, seven patients did not undergo liver biopsy. These patients did, however, have a known primary tumor, and their follow-up examinations showed interval enlargement or increase in number of presumed hepatic metastases. This was taken as adequate evidence to support the diagnosis of hepatic metastases.

Results

The assessment of lesion size was compared among the three scanning techniques. When present, a hypervascular rim was included in the measurement of lesion size. Rim enhancement was identified in eight (31%) of 26 patients. The bolus study showed rim enhancement on 21 (35%) of 60 measured metastases; the bolus-plus-drip phase showed rim enhancement on 15 (25%) of 60. All rim-enhancing lesions imaged during the bolus examination had a visually denser rim than those imaged during the bolus-plus-drip part of the study (Fig. 1).

Lesion size varied from 1 to 10 cm (mean, 3.5). The bolus phase yielded the largest measurement in 16 (27%) of 60 measured metastases. The loading bolus-plus-drip-infusion technique yielded the largest size in only one (2%) of the 60 masses, and the noncontrast study yielded the largest size in five (8%). In the other metastases measured, more than one technique resulted in the same largest measurements.

The three techniques of contrast administration were compared to determine the number of metastatic deposits that

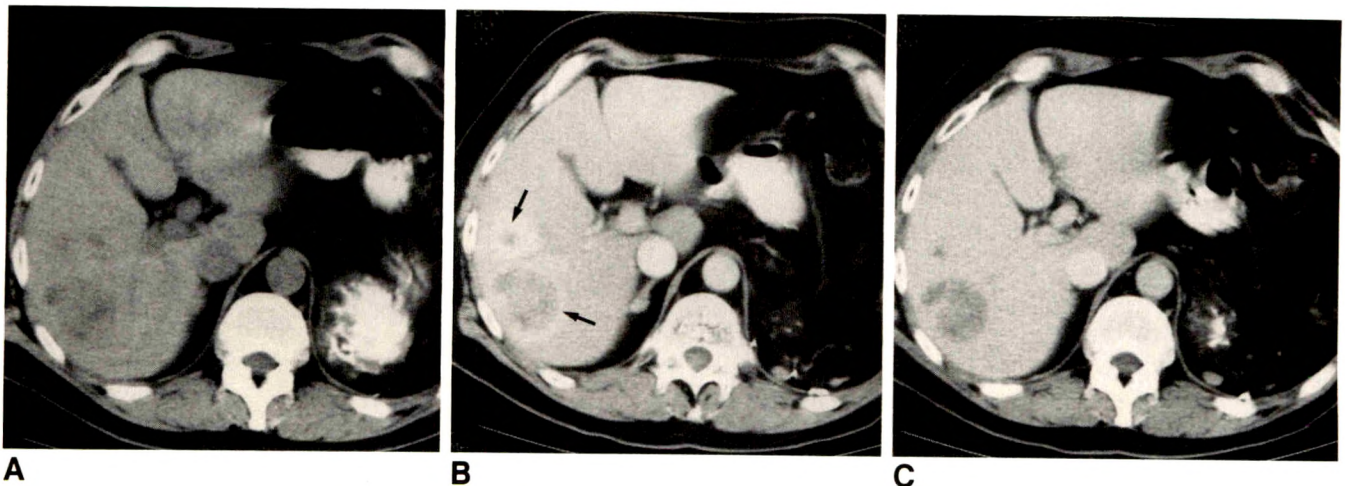


Fig. 1.—CT scans of patient with liver metastases from renal cell carcinoma.

A, Noncontrast scan shows two areas of decreased attenuation in right lobe of liver.

B, Scan obtained during bolus phase shows marked rim enhancement (arrows) with significant increase in size measurements.

C, Scan obtained during bolus-plus-drip phase shows overall size measurements and detectability have diminished compared with bolus phase.

could not be identified by using a single method. The bolus technique detected 60 lesions. Noncontrast scans visualized 54 lesions, and the loading bolus-plus-drip-infusion study revealed only 51 lesions. Thus, 15% of the lesions seen on the bolus phase were not evident on the loading bolus-plus-drip-infusion examination (Figs. 2 and 3). The noncontrast and loading bolus-plus-drip-infusion techniques each resulted in one false-negative examination. Of the three patients with classically hypervascular tumors (pancreas islet cell carcinoma, renal cell carcinoma, and carcinoid), noncontrast images of the liver detected no lesions that were not apparent on the dynamic bolus study.

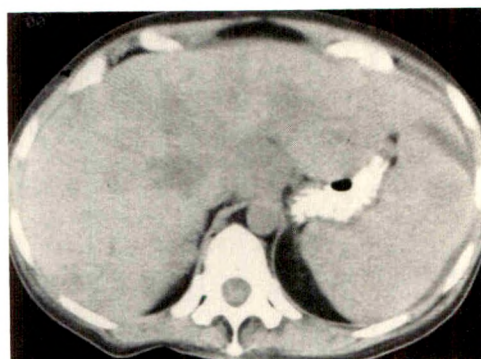
When subjectively asked to select a single contrast technique that provided the best lesion detectability, the bolus was clearly preferred in 39 (65%) of 60 measured metastases. By comparison, a noncontrast study was the preferred technique in only four (7%) and the combined bolus-plus-drip phase in five (8%) of the evaluated 60 lesions. In the remainder of the metastases, two or more techniques were thought to provide best detectability. This subjective superiority of the bolus method was considered multifactorial in that lesion detection was aided by the presence of a hypervascular rim and better delineation of lesion contour, particularly with infiltrating metastases. Rim enhancement was denser during the bolus part of the study than during the infusion examination in all patients with this type of enhancement.

Discussion

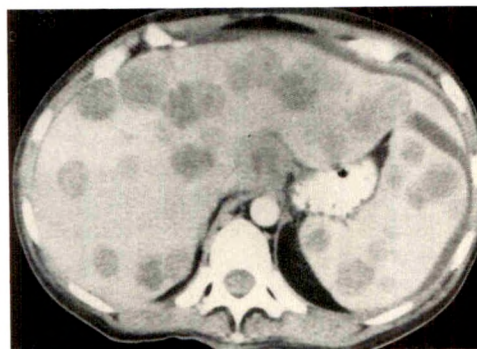
Dynamic CT during a bolus injection of contrast material has been shown to be superior to imaging the liver during a

drip infusion [5-9]. Although most studies have come to this conclusion, none have studied the same patients by looking at the conspicuity of the same lesions with both techniques for administration of contrast material. Administration of a loading bolus before infusion is a variation of the bolus technique, which evolved to "stretch" the contrast injection and obtain high levels of circulating contrast material while allowing the CT scanner to keep pace with the delivery of the contrast material. In this study, enhanced incremental dynamic CT performed during a 50-ml bolus of contrast material detected 15% more hepatic metastases than did scans obtained during a 100-ml drip infusion after a 50-ml loading bolus. The latter technique and specific distribution of contrast volume were chosen for evaluation because it is a popular enhancement strategy in use by 41% of the institutions represented in the Society of Body Computed Tomography [1]. The relatively low dosage of contrast material used for the dynamic part of the study does put the bolus method at a disadvantage, but this low dose was used to keep the patient's total load of contrast material under 42 g of iodine. Despite the "low dose" of the contrast bolus used, the initial bolus-phase dynamic study still proved superior in detecting lesions, as compared with the loading bolus-plus-drip-infusion method.

Burgener and Hamlin [12, 13] have defined three phases of contrast enhancement. The bolus phase represents a difference greater than 30 H between the aorta and inferior vena cava, lasting less than 1 min after bolus administration of contrast material. Contrast material immediately begins to redistribute from the intravascular to extravascular space. The nonequilibrium phase is defined as a difference between 10 and 30 H between aorta and inferior vena cava, indicative



A



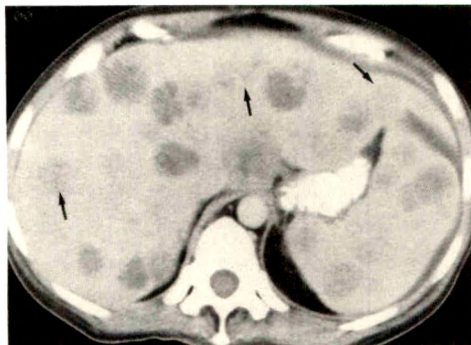
B

Fig. 2.—CT scans of patient with liver metastases from melanoma.

A, Nonenhanced scan shows poorly defined areas of decreased attenuation within liver.

B, During bolus, several metastatic deposits in left lobe of liver are seen that were not seen on noncontrast study. Improved visualization of lesion margin is noted throughout right and caudate lobes.

C, Scan obtained during bolus-plus-drip phase of study again identifies several metastatic deposits in left lobe of liver not visualized on noncontrast study. Numerous lesions (arrows) are not seen as distinctly as they were on comparable level of bolus study.



C

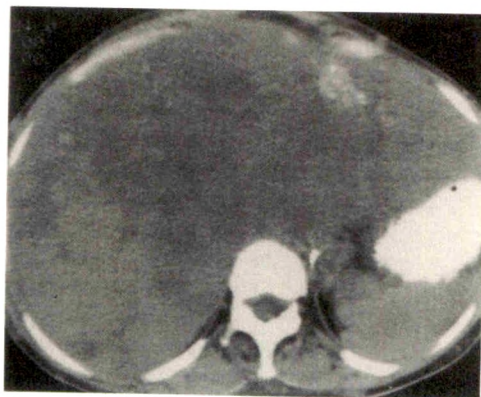
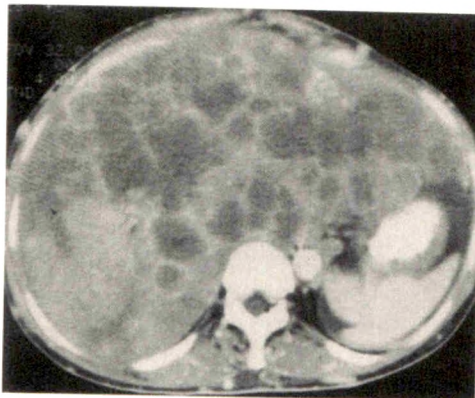
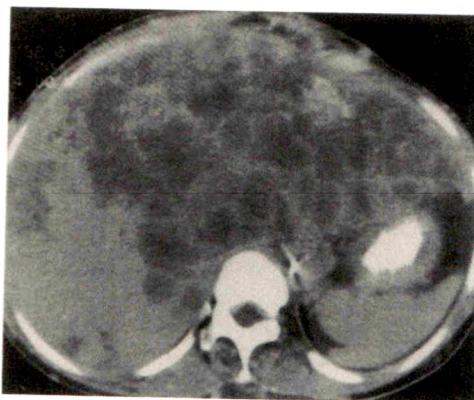
**A****B****C**

Fig. 3.—CT scans of patient with liver metastases from mucinous adenocarcinoma of the colon.

A. Noncontrast examination optimally visualizes calcification in hepatic metastases.

B. During bolus phase, metastases appear more discrete when compared with noncontrast and bolus-plus-drip (C) phases. In addition, thrombosis of inferior vena cava with multiple subcutaneous collaterals is best imaged during bolus administration of contrast material.

C. During bolus-plus-drip phase, metastases are less discrete than during bolus portion of study.

of relatively high levels of intravascular contrast material compared with its concentration in the interstitial space. The nonequilibrium phase ceases rapidly after the end of the bolus administration but may be extended for the duration of a subsequent drip infusion of contrast material. Although not the original intent of the authors, this concept has been erroneously extrapolated to imply that scanning during a drip infusion given after a loading bolus is adequate for lesion detection. Our work does not support that contention. In fact, the bolus-plus-drip-infusion phase resulted in more missed lesions and smaller size measurements than did the other two techniques evaluated in our series. The equilibrium phase represents an arteriovenous difference of less than 10 H when intravascular and interstitial concentrations of contrast material equilibrate and decline at an equal rate. This occurs approximately 2 min after bolus administration of contrast material or immediately after cessation of a drip infusion.

Traditionally, dynamic CT has referred to imaging with a CT scanner preprogrammed to complete a series of exposures as fast as possible and with minimal interscan delay. Bolus injection of contrast material is implied, but the timing of that injection relative to the initiation and termination of imaging often is not clear. In general, the majority of respondents to the Society of Body Computed Tomography survey [1] thought that if a 40-g load of iodine was injected over 3 min and the scans were completed within that interval, the examination qualified as "dynamic" regardless of whether the CT scanner was preprogrammed for a dynamic sequence or whether serial scans were obtained with deferred reconstruc-

tion. The intent of imaging the liver within 3 min is to complete scanning before the onset of the equilibrium phase when contrast material disperses more equally in the hepatic parenchyma and tumor interstitial space, causing isodensity of hepatic metastases [9, 12, 13].

Although Burgener and Hamlin [13] found no significant difference between visualization of hepatic masses between the bolus and nonequilibrium phases, in their series scanning was started *after* completion of the IV injection of a bolus of contrast material. Because of this delay and slower scanning techniques, the bolus and nonequilibrium phases were "lumped together" and jointly considered better for lesion detection than was the equilibrium phase. In our study, an "early" bolus scanning technique was used while contrast material was being administered. Our data specifically distinguish the bolus from the nonequilibrium phase and support the concept that imaging during the bolus phase is superior. This may have implications for future investigations for the role of fast cine CT scanners in hepatic imaging. Our technique required an obligatory 1¼-min delay between imaging the bolus and drip-infusion portions of the study, although the drip infusion was started immediately after completion of the bolus sequence. Possibly, circulating levels of contrast material during the drip infusion were lower than could be obtained without this obligatory tube cooling and reprogramming delay.

The superior lesion conspicuity seen during the bolus phase most likely is multifactorial. Hepatic tumors receive their blood supply primarily from the hepatic artery, whereas most of the

liver circulation is from the portal venous system [15]. Maximal rim enhancement of liver metastases should occur with high arterial levels of circulating contrast material. In our study, arterial rim enhancement occurred in 35% of lesions analyzed. Similar results have been reported by Freeny and Marks [11]. In the present series, rim enhancement was visually densest during the bolus phase. In addition, recirculation of contrast material through the portal venous system further increases overall hepatic attenuation, making the relatively hypovascular interior of metastases more apparent as negative defects.

Three patients had liver metastases from typically hypervascular primary tumors. Noncontrast scans detected no lesions that were missed on the dynamic examinations in this series. Bressler et al. [16] reported that highly vascular metastases may not be visible during bolus contrast enhancement. They used a technique in which scanning was started during the nonequilibrium phase, 60 sec after the onset of an IV bolus of contrast material. In their series, an early bolus phase was not included. Our technique differed substantially in that scanning was begun 15 sec after a bolus injection of contrast material was started. Because of the small number of patients with potentially hypervascular metastases in our study, we cannot definitely conclude that the early bolus phase is superior to the nonequilibrium phase for detection of hypervascular metastases. More work is needed to look at this subgroup of lesions. In our series, all examinations were reviewed with a window of 350 H to maintain uniformity in comparing contrast enhancement techniques. Frequently, noncontrast studies are reviewed with a lower window (150–200 H). Therefore, our data on nonenhanced CT may have been put at a disadvantage as compared with images photographed with a narrower window.

The impact of lesion detectability on patient care and prognosis has been stressed in the literature previously [7]. The variability in lesion size that results from different strategies for administration of contrast material has not received the same attention. In our study, the greatest lesion diameter was consistently seen during the bolus phase, as compared with the nonequilibrium phase obtained during the loading bolus-plus-drip-infusion study or a noncontrast examination. Therefore, serial CT studies must be appropriately tailored and different methods of contrast administration be considered when interpreting these examinations.

We recommend imaging during the bolus phase as the primary CT scanning method for evaluating hepatic metastases. In our institution, a single 100-ml bolus is injected mechanically at a rate of 1 ml/sec. Imaging is started 15 sec after the bolus is begun, and imaging is completed within 15 sec after the end of the injection. Our currently recommended dose of contrast material has increased with a concomitant decrease in injection rate, so as to allow imaging of the entire

liver. At the time that this investigation was conducted, tube-cooling delays limited us to seven to nine sections during the bolus injection. With recent software advances and a graphite tube on the GE 9800 "Quick" scanner, 14 sections (2-sec scan, 5-sec interscan delay) at 400 mAs with table incrementation may easily be obtained during the power-injected bolus of contrast material. With this technique, the hepatic veins usually are well opacified by the second dynamic scan. Also, a 150-ml bolus of contrast material could be used and the start of scanning could be delayed until 30 sec after beginning the bolus to assure optimal opacification of the hepatic veins. When hypervascular metastases are suspected, unenhanced scans are added to our screening protocol; further data are being collected regarding the need for these additional images.

REFERENCES

1. Zeman RK, Clements LA, Silverman PM, et al. CT of the liver: a survey of prevailing methods for administration of contrast material. *AJR* 1988;150:107–109
2. Moss AA, Schrumph J, Schnyder P, Korobkin M, Shimshak RR. Computed tomography of focal hepatic lesions: a blind clinical evaluation of the effect of contrast enhancement. *Radiology* 1979;131:427–430
3. Alfidi RJ, Haaga JR, Havrilla TR, Pepe RG, Cook SA. Computed tomography of the liver. *AJR* 1976;127:69–74
4. Stanley RJ, Sagel SS, Levitt RG. Computed tomography of the body: early trends in application and accuracy of the method. *AJR* 1976;127:53–67
5. Berland LL, Lawson TL, Foley WD, Melrose BL, Chintapalli KN, Taylor AJ. Comparison of pre- and post-contrast CT in hepatic masses. *AJR* 1982;138:853–858
6. Foley WD, Berland LL, Smith DF, Thorsen MK. Contrast enhancement technique for dynamic hepatic computed tomographic scanning. *Radiology* 1983;147:797–803
7. Alpern MB, Lawson TL, Foley WD, et al. Focal hepatic masses and fatty infiltration detected by enhanced dynamic CT. *Radiology* 1986;158:45–49
8. Araki T, Itai Y, Furui S, Tasaka A. Dynamic CT densitometry of hepatic tumors. *AJR* 1980;135:1037–1043
9. Young SW, Turner RJ, Castellino RA. A strategy for the contrast enhancement of malignant tumors using dynamic computed tomography and intravascular pharmacokinetics. *Radiology* 1980;137:137–147
10. Marchal GJ, Baert AL, Wilms GE. CT of noncystic liver lesions: bolus enhancement. *AJR* 1980;135:57–65
11. Freeny PC, Marks WM. Patterns of contrast enhancement of benign and malignant hepatic neoplasms during dynamic and delayed CT. *Radiology* 1986;160:613–618
12. Burgener FA, Hamlin DJ. Contrast enhancement of hepatic tumors in CT: comparison between bolus and infusion techniques. *AJR* 1983;140:291–295
13. Burgener FA, Hamlin DJ. Contrast enhancement in abdominal CT: bolus versus infusion. *AJR* 1981;137:351–358
14. Freney PC, Marks WM, Ryan JA, Bolen JW. Colorectal carcinoma evaluation with CT: preoperative staging and detection of post-operative recurrence. *Radiology* 1986;158:347–353
15. Ackerman NB, Lien WM, Kondi ES, Silverman NA. The blood supply of experimental liver metastasis. I. The distribution of hepatic artery and portal vein blood to "small" and "large" tumors. *Surgery* 1969;66:1067–1072
16. Bressler EL, Alpern MB, Glazer GM, Francis IR, Ensminger WD. Hypervascular hepatic metastases: CT evaluation. *Radiology* 1987;162:49–51

Dynamic Hepatic CT Scanning

W. Dennis Foley¹

Contrast-enhanced hepatic CT scan techniques used to evaluate suspected metastatic disease vary widely, largely because of a lack of consensus on contrast load, scanning sequence, and factors affecting lesion detectability.

In contrast-enhanced studies, the rate and amount of contrast material delivered to normal hepatic parenchyma and to focal tumors should depend on local blood supply and the degree of cellularity, fibrosis, and necrosis in each region. Normal hepatic parenchyma is best enhanced by rapid and sustained delivery of a large contrast bolus (45–50 g iodine administered over 2–2½ min), not by an infusion technique (42 g iodine delivered over 5–10 min). Most hepatic metastases are hypovascular in relation to hepatic parenchyma and have areas of fibrosis and necrosis into which contrast media diffuse at relatively slow rates. Better liver-to-lesion contrast is achieved with bolus than infusion techniques because parenchyma is more enhanced and less contrast medium diffuses into the interstitial spaces of tumors.

In order to understand the pharmacokinetics of contrast material delivery and diffusion following sustained bolus injection (42–50 g iodine over 2–2½ min), three distinct phases can be considered [1, 2]. During the bolus phase, there is marked vascular and parenchymal enhancement, which peaks at the end of injection. This is followed by a short “nonequilibrium phase” in which vascular enhancement declines relatively rapidly before equilibrating with parenchymal enhancement. The rapid drop in vascular enhancement results from continuing intravascular to extravascular contrast redistribution in liver parenchyma. The third, or equilibrium, phase is one of gradually declining vascular and parenchymal

enhancement reflecting renal filtration. Contrast material diffuses into the interstitial spaces of tumors during all three phases. With bolus contrast delivery, tumor enhancement occurs during the relatively short time of contrast delivery and nonequilibrium or redistribution. With bolus contrast, there is less time for tumor enhancement to occur during the relatively short contrast delivery and nonequilibrium or redistribution phases than with the sustained nonequilibrium phase induced by an infusion. As Paushter et al. point out, in the preceding article [3], persistent “nonequilibrium” achieved by infusion techniques does not guarantee lesion detectability equivalent to that achieved with bolus contrast delivery.

In order to obtain complete hepatic CT coverage via bolus contrast delivery, an incremental dynamic scan technique with short scan times, short interscan delays, and technical factors to optimize image quality is necessary. The combination of bolus contrast delivery and incremental dynamic scan should ensure greater lesion detectability than an infusion technique. This working hypothesis, which has been assumed correct for several years, has been tested by Paushter et al. [3]. Their comparison of noncontrast, bolus dynamic, and bolus-plus-drip-infusion nondynamic techniques confirms the superiority of the bolus dynamic approach in terms of the number of lesions detected, delineation of lesion margins, determination of lesion size, and overall conspicuity. Significantly, Paushter et al. found that noncontrast scanning resulted in slightly more detected lesions than the loading bolus-plus-drip-infusion technique and that some lesions were smaller on the loading bolus-plus-drip-infusion technique than on the non-contrast study. Thus, the loading bolus-plus-drip-infusion

This article is a commentary on the preceding article by Paushter et al.

¹ Department of Radiology, Medical College of Wisconsin, 8700 W. Wisconsin Ave., Milwaukee, WI 53226. Address reprint requests to W. D. Foley.

technique was even less efficacious than a noncontrast scan. Obviously, contrast-enhancement techniques should be used to improve, not diminish, lesion detectability.

The incremental dynamic hepatic CT scan with bolus contrast delivery should be used in a broad range of patients with suspected hepatic metastasis, which is most common in patients with primary malignancies involving the colon, lung, breast, pancreas, or endometrium and in those with melanoma or sarcomas. Tumors that may be hypervascular in relation to normal hepatic parenchyma (e.g., primary hepatoma and metastases from pancreatic islet cell tumor, carcinoid, and renal carcinoma) may be isodense during an incremental dynamic hepatic CT scan obtained during bolus contrast administration [4].

Paushter et al. describe their dynamic CT scan as being acquired during the "early bolus phase" and state that hypervascular lesions are less likely to be isodense with their approach than with dynamic techniques in which the onset of scanning is delayed for 45 sec rather than 15 sec after the beginning of bolus injection. However, a 45-sec scan delay has two purposes. First, hepatic parenchymal enhancement is greater at 45 sec than 15 sec and reaches a relative plateau at that time. Second, hepatic veins are positively enhanced at 45 sec and not at 15 sec, allowing detected lesions in the cephalad portion of the liver to be localized to specific lobes and segments. In the timing sequence used by Paushter et al. [3], most of the hepatic scans are obtained after the end of injection, during the phase of intravascular to extravascular contrast redistribution before contrast equilibrium is obtained. In essence, they used a smaller bolus and earlier dynamic scan than Bressler et al. [4] or Alpern et al. [5], but they still obtained scans both during contrast material delivery and in the early nonequilibrium phase. The consensus, as Paushter et al. state, is that patients with suspected hypervascular tumors should have both a noncontrast and a dynamic postcontrast study. The dynamic postcontrast study still may detect hypervascular metastases or other multifocal sites of hepatoma not apparent on the precontrast examination.

A number of practical issues affect the choice of hepatic CT scan technique in individual practices. The CT scanner should be capable of rapid repetitive scanning at contiguous levels with scan techniques that can detect low-contrast lesions equal in diameter to the slice thickness used. The scan repetition rate should be between 7 and 10 contiguous scans per minute so that the liver can be evaluated over 1½–2½ min, depending on hepatic size. Relatively rapid incremental dynamic scanning requires the cooperation of the patient for controlled breathing between individual scans or between sequences of scans obtained during one breath-hold. This prevents slice misregistration due to unequal respiration, which can result in lesions being missed because of overlapping slices and missing segments in scans that are contiguous in space but not contiguous anatomically.

If the radiologist has access to suitable CT equipment and a cooperative patient, the second issue affecting the use of dynamic scanning with bolus contrast delivery is the amount of contrast material used. In our practice, we administer 50 g of iodine load to patients with normal cardiorenal function. One hundred eighty milliliters of 60% contrast material is

injected over 140 sec (5 ml/sec for 10 sec and 1 ml/sec for 130 sec). For routine hepatic CT scanning, Paushter et al. advocate 100–150 ml of contrast material injected at 1 ml/sec. Many years of angiographic experience has shown clearly that 3 ml/kg/hr is a tolerable load of contrast material when given to patients with normal renal function. In our practice, the formula is adjusted to 3 ml/kg in 2 min. Rate of delivery has no deleterious effect on renal function, as we have demonstrated with serial postprocedure determinations of serum creatinine at 24, 48, and 72 hr and 7 days after the procedure [2]. In addition, patients with normal cardiac function can tolerate an acute intravascular volume expansion of 1 l. One hundred eighty milliliters of 60% ionic contrast material is equivalent to approximately 750 ml of normal saline. In our practice, only a few patients with cardiac decompensation have required evaluation for suspected hepatic metastases. Evaluation of these patients should be tailored to each individual by using noncontrast CT and other alternative imaging techniques including sonography and isotope scans.

A volume flow rate injector that can be operated by a technologist from the CT scan console is an integral component of an incremental dynamic bolus contrast-enhanced hepatic CT study. Contrast given by hand injection is not as accurate in its timing, not as reproducible, and not as convenient. With volume flow rate injectors, contrast material is delivered through standard angiographic catheters (19 or 20 gauge) either 1¼ in. (3.2 cm) or 2 in. (5.1 cm) in length preferably into antecubital veins, at rates that vary between 5 ml/sec (initial 10 sec) and 1 ml/sec (subsequent 130 sec). A volume flow rate injector ensures consistent contrast delivery, an important feature in patients having sequential CT scans to assess tumor response to chemotherapy or radiation therapy.

Given the convenient feature of a volume flow rate injector operated by the CT technologist, the radiologist can supervise to ensure that the examination is tailored to the particular patient's circumstances. For example, a patient with suspected recurrent carcinoma of the rectum would best be evaluated with an abdomen/pelvis CT technique in which the initial component of the study is a dynamic hepatic sequence. A patient undergoing staging CT for carcinoma of the lung could be evaluated with an abdomen/thorax CT study in which the initial scan sequence is a dynamic hepatic CT, programmed in a caudal to cephalic sequence from the tip of the right hepatic lobe to the dome of the right hemidiaphragm. The radiologist or a designated assistant, such as a second technologist or nurse, must palpate the injection site to ensure that the contrast material delivered through the plastic venous cannula does not extravasate. If extravasation occurs, the injection should be stopped immediately.

The optimal method for delivering IV contrast through antecubital veins is to position the patient's arm at a right angle to the chest by placing the palm of the hand against the face of the CT gantry. This ensures that injected contrast material is not constricted at the thoracic outlet.

If the four factors discussed above (CT scanner performance, a proper understanding of contrast material tolerance and toxicity, availability of a volume flow rate injector, and

Intrahepatic Cholangiographic Abnormalities in Liver Transplants: Correlation with Biopsy Evidence of Rejection and Other Disorders

Jeanne Bauman¹
William L. Campbell¹
A. Jake Demetris²
Albert B. Zajko¹

We investigated the cholangiographic appearance of intrahepatic bile ducts in 56 liver transplants and correlated the findings with biopsy evidence of acute rejection and other histologic diagnoses. Mild to moderate narrowing, stretching, separation, and poor filling of the bile ducts were common. Narrowing was present in 69 (92%) of 75 studies and was at least moderate in degree in 14 (19%). Duct separation was seen on 39 (58%) of 67 cholangiograms and was usually mild but was more pronounced in 10 (15%). In 22 (25%) of 89 studies, 10 or fewer branch ducts were filled. Cholangiographic abnormalities were more marked in patients with biopsy diagnoses of moderate-severe and partially treated acute rejection than with findings of mild rejection or nonspecific histology. Portal tract cellular infiltration and edema, liver swelling and, possibly, loss of small bile ducts correlated with the radiologic changes. However, the severity of the radiographic changes varied in all histologic categories.

Acute rejection contributes to intrahepatic duct narrowing, separation, and poor filling on cholangiography in liver transplants, but the cause of the changes is probably multifactorial. Cholangiography is limited as a test for rejection and other hepatic parenchymal abnormalities in individual patients, but it may provide evidence supporting the need for liver biopsy in the evaluation of hepatic dysfunction after transplantation.

A variety of hepatic parenchymal disorders may develop in liver allografts. The most important is rejection, which occurs in more than 37% of liver transplants [1] and is the most common cause of hepatic dysfunction after transplantation [2]. Rejection and other parenchymal disorders are diagnosed most definitively by liver biopsy. However, cholangiography often is performed first in such patients because the clinical presentations of a number of complications after transplantation are nonspecific. Intrahepatic cholangiographic abnormalities may be observed in liver transplants [3]. The ability to recognize signs of rejection or other parenchymal disorders on cholangiography would be useful in determining allograft status and in further directing the diagnostic evaluation.

The purpose of this study was threefold: (1) to determine the type and prevalence of intrahepatic cholangiographic abnormalities in a population of both viable and failing liver allografts in which concurrent liver biopsy was performed, (2) to discover what pathologic processes are associated with intrahepatic cholangiographic abnormalities, and (3) to determine whether cholangiography has clinical value in detecting allograft rejection and other parenchymal disorders.

Materials and Methods

The study group consisted of 54 liver-transplant patients (56 liver allografts) who underwent cholangiography and liver biopsy between October 1984 and February 1987. The most common indication for postoperative cholangiography was abnormal liver function tests. Other indications included unexplained fever, suspected bile leak, and possible T-tube obstruction or malposition. Liver biopsies were performed because of unexplained postoperative hepatic dysfunction. All patients had cholangiogram-biopsy intervals of no more than

Received August 15, 1988; accepted after revision October 12, 1988.

¹ Department of Radiology, University of Pittsburgh School of Medicine, Presbyterian-University Hospital, Pittsburgh, PA 15213. Address reprint requests to W. L. Campbell.

² Department of Pathology, University of Pittsburgh School of Medicine, Pittsburgh, PA 15213.

AJR 152:275-279, February 1989
0361-803X/89/1522-0275

© American Roentgen Ray Society

3 days. None of the patients had cholangiographic findings that could be associated with decreased intrahepatic duct opacification, such as incomplete donor common duct filling, dislodged T-tube, or large leaks of contrast material.

Eight-nine cholangiograms with pathologic correlation were available for review. Included were 83 postoperative T-tube cholangiograms, three surgical cholangiograms, two percutaneous transhepatic cholangiograms, and one endoscopic retrograde cholangiogram. Most cholangiograms were obtained early in the postoperative course; 78 (88%) of 89 were obtained within 5 weeks of transplantation. Twenty-four (27%) were obtained in the first postoperative week; 26 (29%) were obtained in the second postoperative week, when acute rejection is most likely to occur. Thirteen of the 89 cholangiograms in nine patients were of allografts that eventually failed and required retransplantation. The mean interval between cholangiography and retransplantation was 41 days (range, 3–190).

Eighty-six biopsies (92 diagnoses) were reviewed. The number of biopsy diagnosis-cholangiogram pairs with a maximum cholangiogram-biopsy interval of 3 days was 95; 60 had a maximum interval of 1 day.

T-tube cholangiography was performed by resident and staff radiologists by hand injection of 30% meglumine diatrizoate. The volume of contrast material injected was variable and depended on the volume of the biliary system and on the rate of flow into the duodenum. Rapid injection was avoided to prevent overdistension of ducts. Optimal biliary tree opacification was considered to consist of filling of the common duct as well as primary, secondary, and some tertiary intrahepatic ducts. In some patients in whom initial intrahepatic duct filling was not optimal, injection with the patient in a slight Trendelenburg position was used. Percutaneous transhepatic and endoscopic retrograde cholangiography were performed in standard fashion with an attempt to opacify the common duct and intrahepatic ducts.

Three intrahepatic duct parameters were evaluated: (1) narrowing, (2) separation, and (3) degree of filling. Evaluation was based on the radiograph from each cholangiogram that showed maximum intrahepatic duct filling. Severity of narrowing and separation of intrahepatic ducts were graded subjectively on a scale of 0–10, with 0 representing normal. The degree of filling was quantified by counting the number of end branches visualized at their most peripheral points of opacification. The grading was performed by two radiologists without knowledge of the histopathologic diagnoses.

One pathologist experienced in the interpretation of liver-transplant histopathology reviewed the biopsy material without knowledge of the radiographic findings. Biopsies were analyzed for changes indicative of acute rejection as well as other histopathologic diagnoses. Acute rejection changes were classified as mild, moderate, severe, or partially treated.

Cholangiographic changes were correlated with histopathologic diagnoses. The statistical significance of cholangiographic differences among pathologic diagnoses was tested by Wilcoxon rank sum analysis. Because the rapidity with which the pathologic processes might wax or wane was not precisely known, analyses were performed both for a subgroup of cases with 1-day cholangiogram-biopsy intervals as well as for the whole study group with a maximum of 3-day intervals.

Results

Cholangiography

On some cholangiograms, intrahepatic filling was too limited (fewer than six ducts filled) to permit meaningful assessment of duct narrowing or separation. Accordingly, the numbers of cholangiograms evaluated for narrowing and separation were each less than the number assessed for duct filling.

Seventy-five cholangiograms were evaluated for intrahepatic duct narrowing. The mean grade of duct narrowing was 3.5 (range, 0–10). Some degree of narrowing of ducts was seen in 69 (92%) of 75 studies. Moderate to marked narrowing (grade > 5) was present in 14 (19%) of 75.

Sixty-seven cholangiograms were evaluated for intrahepatic duct separation. The mean grade of separation was 1.1 (range, 0–5). No cholangiogram received a grade greater than 5 (moderate separation). At least some separation of branches was noted in 39 (58%) of 67 cholangiograms. More than mild separation (grade > 2) was present in 10 (15%) of 67.

The mean number of intrahepatic ducts filled in 89 cholangiograms was 23.4 (range, 1–86). Forty-three (48%) of 89 cholangiograms showed 20 or fewer ducts filled, and 22 (25%) of 89 showed 10 or fewer ducts opacified.

Narrowing typically appeared as a generalized smooth attenuation of all intrahepatic ducts. Ducts often had a stretched or straightened appearance (Fig. 1). Separation and poor filling were also generalized processes without predisposition for any one portion of the liver (Fig. 2). Focal strictures were not encountered in the study group.

Pathology

Of 86 biopsies, 45 (52%) showed changes of acute rejection. Of these, twenty-seven (31%) were graded as mild rejection, 12 (14%) were graded as moderate or severe rejection, and six (7%) revealed changes of partially treated acute rejection. Sixteen (19%) biopsies showed nonspecific or essentially normal findings. Other histopathologic diagnoses were viral infection (seven), moderate or greater cholestasis (six), preservation injury (six), ischemia/infarction (six), acute cholangitis (five), and chronic rejection (one). Six biopsies had two diagnoses.

Histologic findings considered to be diagnostic of acute rejection consisted of a predominantly mononuclear, portal-tract infiltrate consisting of lymphocytes and monocytes with fewer neutrophils and eosinophils (Fig. 3). The infiltrate was associated with inflammation and damage of the bile ducts with subendothelial accumulation of lymphoid cells. The portal infiltrate in some instances extended beyond the limiting plate into the periphery of the lobule and was associated with periportal hepatocyte necrosis [4, 5].

The grading of acute rejection was based on the degree of portal inflammation combined with the presence or absence of arteritis and/or centrilobular hepatocellular necrosis. Partially treated rejection was diagnosed when a previous diagnosis of rejection was followed by a biopsy showing diminished inflammatory cellularity but continued endothelial and biliary epithelial changes.

Histologic findings in chronic rejection consisted of mild to moderate, mononuclear portal-tract infiltration; damage to and loss of small ductules; and arteriolar thickening [4].

Cholangiographic-Pathologic Correlation

Cholangiographic changes were similar and most marked in the groups with moderate-severe and partially treated acute

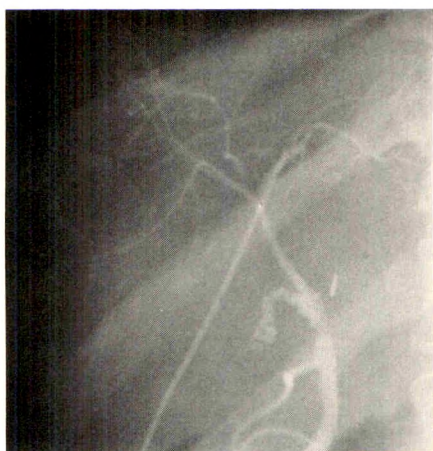
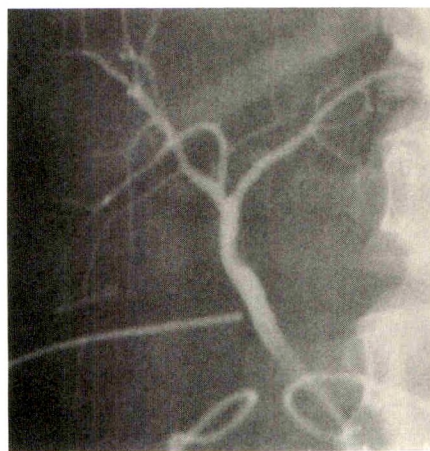
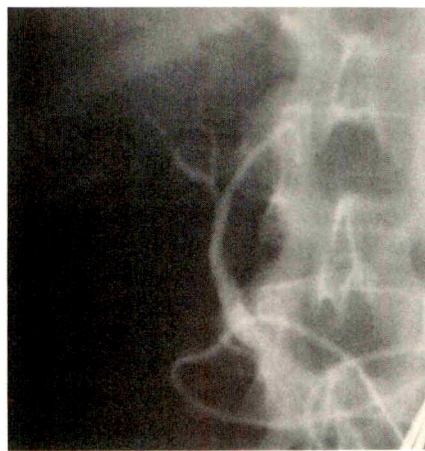


Fig. 1.—T-tube cholangiogram 9 days after transplantation shows diffuse smooth narrowing of intrahepatic ducts and slight duct separation. Branch filling is normal. Liver biopsy the same day revealed moderate acute rejection.



A



B

Fig. 2.—T-tube cholangiograms show development of poor intrahepatic branch filling in acute rejection.

A, 11 days after transplantation. Intrahepatic duct filling is normal. Liver biopsy 1 day later showed mild acute rejection.

B, 7 weeks after transplantation. Intrahepatic branch filling is markedly decreased. Liver biopsy 1 day later revealed severe acute rejection. Retransplantation was performed 1 month later.

rejection. Correlation between cholangiography and liver biopsy diagnosis was slightly better when the cholangiogram-biopsy interval was 1 day rather than up to 3 days. One-day cholangiogram-biopsy interval data were used for computation of statistical significance, sensitivity, and specificity.

Duct narrowing.—The mean grade of duct narrowing was 4.8 (range, 1–6) for moderate-severe rejection and 4.4 (range, 1–6) for the combined group of moderate-severe and partially treated rejection. The mean grade was 2.3 (range, 0–6) for the nonspecific (normal) group ($p = .05$). Mild rejection showed a 3.4 (range, 1–7) mean grade of narrowing. Differences between the rejection and nonspecific groups were slightly less when the interval between cholangiography and biopsy was up to 3 days.

A duct-narrowing grade of 4 or more was 71% sensitive for moderate-severe and partially treated rejection. Specificity

was 52% for moderate-severe and partially treated rejection and 73% for any histopathologic abnormality.

Duct separation.—Mean grade for separation of ducts was 1.6 (range, 0–2) for moderate-severe rejection, 0.9 (range, 0–3) for mild rejection, and 0.7 (range, 0–3) for nonspecific (normal) changes. The mean grade for the combined group of moderate-severe and partially treated rejection was 2.0 (range, 0–5) ($p = .05$). Values were nearly identical when the interval between cholangiogram and biopsy was up to 3 days.

A duct separation grade of 2 or more was 80% sensitive for moderate-severe and partially treated rejection. Specificity was 74%.

Duct filling.—The mean number of intrahepatic ducts opacified was 15.9 (range, 2–33) in moderate-severe rejection vs 26.9 (range, 3–60) in mild rejection and 27.6 (range, 8–86) in the nonspecific (normal) group. In the combined group of moderate-severe and partially treated rejection, the mean number of ducts filled was 13.4 (range, 1–33) ($p = .05$). Findings were similar if the radiologic changes were correlated with biopsies performed up to 3 days after cholangiography, but differences were not statistically significant.

The finding of 10 or fewer filled intrahepatic ducts gave a sensitivity of 45%, and 20 or fewer filled ducts yielded a sensitivity of 82% for moderate-severe/partially treated rejection. Specificity for moderate-severe/partially treated rejection was 79% for 10 or fewer ducts filled and 62% for 20 or fewer ducts filled. Specificity for any histopathologic abnormality was 83% and 58% for 10 or fewer and 20 or fewer ducts filled, respectively.

Other considerations.—In the nonspecific (normal) group, two (13%) of 16 cholangiograms could not be evaluated for narrowing or separation because too few ducts were filled. In mild rejection, six (19%) of 31 could not be evaluated for narrowing and eight (26%) of 31 could not be evaluated for separation. In moderate to severe rejection, three (25%) of

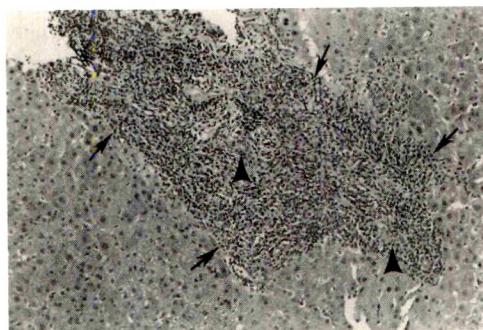


Fig. 3.—Photomicrograph of liver biopsy in moderate acute cellular rejection shows exclusively portal tract inflammation (arrows) with resultant portal expansion. Bile ducts (arrowheads) are embedded within infiltrate and show reactive changes and intraepithelial inflammatory cells. (H and E, original magnification $\times 150$)

12 cholangiograms had poor filling, preventing evaluation of either variable.

To determine if changes in radiologic parameters might be diagnostically significant, we compared postoperative cholangiograms with previous operative cholangiograms. In acute rejection, duct narrowing and separation were increased on postoperative cholangiograms compared with operative cholangiograms. Cholangiograms in moderate-severe rejection exhibited an average of 8.8 fewer ducts filled than were seen on operative cholangiography. The mean number of ducts filled on postoperative cholangiography with normal biopsy was 1.5 ducts more than on operative cholangiography. However, comparison with operative cholangiography did not improve the correlation of cholangiographic findings with biopsy. Correlation was hampered by the unavailability of operative cholangiograms in more than one-half of the study group.

Cholangiography was also correlated with other liver biopsy diagnoses (Table 1). Although the numbers of cases of each diagnosis were relatively small, all pathologic groups tended to show more narrowing than the nonspecific group did, with preservation injury and cholestasis showing changes of a degree comparable with that in moderate-severe/partially treated acute rejection. Cholestasis and viral infection exhibited the greatest, albeit still mild, duct separation changes. Moderate to severe cholestasis, ischemia, and viral infection showed decreased duct filling compared with nonspecific histology, but the degree was not as great as was found in moderate-severe/partially treated acute rejection. Cholangiographic differences between the various nonrejection biopsy diagnoses and the nonspecific group were not statistically significant.

Discussion

The primary role of cholangiography after liver transplantation is to evaluate for extrahepatic bile duct obstruction or leak as a cause of hepatic dysfunction [3, 6]. Detection of such abnormalities is essential because early surgical or interventional radiologic treatment may be required.

Intrahepatic duct changes in liver allografts have received relatively little attention. Focal abnormalities are uncommon and include strictures and leakage of contrast material, changes strongly suggestive of hepatic artery occlusion [7]. Intrahepatic duct sludge, stones, and communicating hepatic

abscesses are relatively rare, often occurring in the setting of stasis and/or cholangitis. The most common intrahepatic duct changes after transplantation are generalized narrowing and stretching and, less frequently, separation and poor filling of branches. The prevalence, cause, and clinical significance of these changes have been incompletely understood.

Intrahepatic duct narrowing was the most frequent radiologic abnormality seen in our patients, being present to at least a slight degree in 92% of studies; moderate to marked changes were seen in 19% of cases. Duct separation was the next most frequent abnormality, being appreciated on 58% of cholangiograms and to at least a mild or moderate degree in 15%. Decreased duct filling of 10 or fewer branches opacified was encountered in 25% of studies in this series.

The early postoperative appearance and radiologic characteristics of these intrahepatic duct changes suggest that they are the result of a relatively acute, generalized hepatic parenchymal abnormality. However, the exact cause of the changes cannot be inferred from the radiologic appearance. Previous experience with cholangiography in acute or subacute hepatic parenchymal processes (e.g., acute hepatitis) in either nontransplant or transplant patients is extremely limited [8, 9]. Intrahepatic duct attenuation and stretching reminiscent of that seen in our patients has been reported in nontransplant patients with fatty livers [8].

Graft rejection is the most common complication after transplantation, and an association with intrahepatic duct abnormalities has been noted in some cases [3]. One study found the cholangiographic changes of poor filling, stretching, and attenuation in five of 11 patients with complete liver failure from rejection. Similar changes were also seen in infarction and infection, suggesting a nonspecific response to various pathologic processes [9]. The clinical value of this early study was limited by the relatively small number of patients, inclusion only of livers that failed completely, and relatively long cholangiogram-biopsy intervals of up to 20 days.

The most pronounced cholangiographic changes in our patients were seen in moderate-severe and partially treated acute rejection. Differences from normal subjects were statistically, although weakly, significant. Cholangiography in mild rejection showed more duct narrowing than normal allografts did, but not to a degree that was statistically significant. Although the numbers of patients were small, other pathologic processes exhibited some of the findings encountered in acute rejection (Table 1). For example, all nonrejection path-

TABLE 1: Intrahepatic Cholangiography in Liver Transplants: Nonrejection Biopsy Diagnoses

Diagnosis	Maximum 1-Day/3-Day Cholangiogram-Biopsy Interval			
	Cholangiogram-Biopsy Pairs (No.)	Duct Narrowing (Mean Grade)	Duct Separation (Mean Grade)	Ducts Opacified (Mean No.)
Cholestasis	4/7	5.0/5.1	2.3/2.2	19.0/24.3
Viral infection	4/7	2.8/3.6	1.6/2.2	20.3/25.6
Preservation injury	4/6	4.0/4.2	0.7/0.8	28.0/27.5
Ischemia	3/6	3.0/3.8	1.0/1.8	20.7/18.8
Cholangitis	2/4	3.0/3.3	1.5/1.3	31.0/22.2
Chronic rejection	1/1	3.0/3.0	0/0	29.0/29.0

ologic diagnoses showed a trend toward more duct narrowing than normals did, some (preservation injury and cholestasis) as much as occurred in moderate-severe rejection. Others (e.g., ischemia and viral infection) tended to show less ductal filling than normals did. However, moderate-severe/partially treated rejection was notable for exhibiting the most marked abnormalities in all three of the measured cholangiographic parameters. Correlation was better, albeit only slightly so, when biopsy was performed within 1 day rather than up to 3 days after cholangiography.

The cholangiographic findings in acute rejection can be explained by the pathology. During rejection episodes, the liver allograft frequently is swollen [10], a finding that explains the tendency toward separation of intrahepatic ducts. Increased intrahepatic pressure [1] and portal expansion caused by inflammation and edema may compress the lumina of ductules (Fig. 3). Also, reactive epithelial biliary changes with cell enlargement and/or frank luminal disruption often result in a loss of visible lumina in small bile ducts, and these changes offer a reasonable explanation for some examples of poor filling and luminal narrowing on cholangiography. The similarity between radiographic abnormalities in partially treated rejection and those in moderate-severe rejection perhaps reflects a more severe underlying process in these patients, with persistent clinical abnormality requiring repeated cholangiography and biopsy.

Although acute rejection of at least moderate severity was the pathologic process most associated with diffuse intrahepatic ductal abnormalities, variation in cholangiographic appearance was present in all histopathologic categories. Several factors probably contribute to the less-than-perfect correlation between cholangiography and liver biopsy histology. In early acute rejection, the pathologic changes may be very focal, making the diagnosis susceptible to sampling error [4]. In some biopsies, more than one pathologic process may be at work (e.g., rejection and viral infection). Radiologic-pathologic correlation may be difficult to the degree that histopathologic changes in the various entities are not completely specific. Also, the interpretation of the cholangiographic changes of narrowing, stretching, and separation is somewhat subjective. Variations in cholangiographic technique may influence the degree of branch filling, a variable that presumably affected our abnormal and normal groups equally in this study. However, some care and experience may be required to interpret these radiologic signs in the individual patient. Finally, evidence based on CT and correlative pathology suggests that liver allografts may develop portal-tract cellular infiltration and/or lymphatic engorgement

[11, 12]. These changes have been reported to be associated with rejection [11]. We have observed similar CT findings in nonrejecting allografts, suggesting that the changes may be nonspecific in some patients. We speculate that this periportal infiltration/engorgement may contribute to some of the cholangiographic abnormalities observed in liver allografts.

In conclusion, mild to moderate intrahepatic duct narrowing, separation, and poor filling are commonly seen on cholangiograms in liver transplants. These changes correlate most closely with biopsy evidence of acute rejection, but other parenchymal disorders and perhaps nonspecific factors probably also contribute to their occurrence. Cholangiography is limited as a test for rejection in individual patients, but may provide evidence supporting the need for liver biopsy, especially when no extrahepatic biliary complication is seen.

ACKNOWLEDGMENT

We thank Maggie Zdrodowski for help in manuscript preparation.

REFERENCES

1. Demetris AJ, Lasky S, Van Thiel DH, Starzl TE, Dekker A. Pathology of hepatic transplantation: a review of 62 adult allograft recipients immunosuppressed with a cyclosporine/steroid regimen. *Am J Pathol* 1985; 118:151-161
2. Esquivel CO, Jaffe R, Gordon RD, Iwatsuki S, Shaw BW Jr, Starzl TE. Liver rejection and its differentiation from other causes of graft dysfunction. *Semin Liver Dis* 1985;5:369-374
3. Zajko AB, Campbell WL, Bron KM, et al. Cholangiography and interventional biliary radiology in adult liver transplantation. *AJR* 1985;144: 127-133
4. Demetris AJ, Jaffe R, Starzl TE. A review of adult and pediatric post-transplant liver pathology. *Pathol Annu* 1987;22:347-386
5. Fennell RH, Roddy HJ. Liver transplantation: the pathologist's perspective. *Pathol Annu* 1979;14(part 2):155-182
6. Campbell WL, Zajko AB. Chapter 62A. Radiology of liver transplantation. In: Taveras JM, Ferrucci JT, eds. *Radiology: diagnosis/imaging/intervention*, vol. 4. Philadelphia: Lippincott, 1988:1-7
7. Wood RP, Shaw BW Jr, Starzl TE. Extrahepatic complications of liver transplantation. *Semin Liver Dis* 1985;5:377-384
8. Rohrmann CA Jr, Ansel HJ, Ayoola EA, Silvis SE, Vennes JA. Endoscopic retrograde intrahepatic cholangiogram: radiographic findings in intrahepatic disease. *AJR* 1977;128:45-52
9. Dominguez R, Cuervas-Mons V, Van Thiel DH, Lecky JW, Starzl TE. Radiographic features of liver allograft rejection. *Gastrointest Radiol* 1986;11:326-329
10. Starzl TE, Iwatsuki S, Van Thiel DH, et al. Evolution of liver transplantation. *Hepatology* 1982;2:614-636
11. Wechsler RJ, Munoz SJ, Needleman L, et al. The periportal collar: a CT sign of liver transplant rejection. *Radiology* 1987;165:57-60
12. Marineck B, Barbier PA, Becker CD, Mettler D, Ruchti C. CT appearance of impaired lymphatic drainage in liver transplants. *AJR* 1986;147: 519-523

Book Review

The Alimentary Tract. The Hollow Organs and Salivary Glands. (Vol. 4 of *A Textbook of Radiological Diagnosis*, ed. 5.) Edited by K. C. Simpkins. London: H. K. Lewis, 754 pp., 1988. £85

This text, volume 4 of the seven volumes of *A Textbook of Radiological Diagnosis*, is written by fellows of the Royal College of Radiologists who are experts in gastrointestinal disease. Although the book has many authors, redundancy is minimal, and the text is a pleasing mix of history, technique, pathogenesis, and radiology. Traditional contrast-enhanced examinations of the hollow viscera are emphasized. Cross-sectional techniques and interventional radiology are considered in a subsequent volume.

The initial chapters of the text are organized anatomically. Individual chapters consider general pathologic processes occurring within specific organs or organ systems. Chapters on technique emphasize details of performance of contrast-enhanced examinations and endoscopy. The final five chapters consider special clinical problems, such as the acute abdomen, gastrointestinal bleeding, abdominal abscesses and fluid collections, tropical diseases, and pediatric gastroenterology.

The contributions are high quality and generally quite informative. These characteristics are highlighted by the chapter on colonic neoplasia by Dr. Bartram, which is exceptionally well organized and

illustrated, and appropriately and specifically referenced. A chapter by Drs. Beckly and Stevenson discussing relative merits of colonoscopy and barium enema provides a useful discussion of selection of patients and strategies for evaluation by means of these complementary techniques. This chapter is also enhanced by four pages of color illustrations of pathologic material viewed by colonoscopy and microscopy.

Although the size (754 pages) and the cost (£85) might dissuade some from purchasing this text, its resource value cannot be overemphasized. It contains summary material that is not available elsewhere. Its value for initial reading and as a reference text will make it an important component of the library of the radiologist, surgeon, gastroenterologist, or other physician who has an interest in gastrointestinal disease.

Charles A. Rohrmann
University of Washington Hospital
Seattle, WA 98195

CT Findings of Clonorchiasis

Byung Ihn Choi¹
 Hyung Jin Kim¹
 Man Chung Han¹
 Young Soo Do¹
 Moon Hee Han¹
 Suck Hong Lee²

Clonorchiasis is a snail-transmitted trematodiasis caused by Chinese liver fluke, *Clonorchis sinensis*. Forty-two patients with the disease were examined with CT. Seventeen patients had clonorchiasis alone, and 25 patients had clonorchiasis with hepatobiliary malignancies (20 cholangiocarcinomas, four hepatocellular carcinomas, one carcinoma of the ampulla of Vater). In three of the 17 patients with clonorchiasis alone, the CT scans were normal. In 14 patients (82%), CT showed diffuse, minimal, or mild dilatation of the intrahepatic bile ducts. None of the patients had marked dilatation. The extrahepatic biliary tree was normal in all 17 patients. All 25 patients with clonorchiasis and hepatobiliary malignancies had diffuse dilatation of the intrahepatic bile ducts on CT, including 18 patients with minimal or mild dilatation and seven patients with marked dilatation. All seven patients with marked dilatation had extrahepatic biliary malignancies. *Clonorchis sinensis* per se or thickening of the bile duct wall could not be recognized on CT scans. Additional abnormalities evident on CT included pyogenic liver abscesses in two patients and gallstones in five patients.

The diagnosis of clonorchiasis can be suspected when CT shows diffuse, uniform, and minimal or mild dilatation of the intrahepatic bile ducts, particularly in the periphery of the liver, without evidence of extrahepatic biliary dilatation.

Clonorchis sinensis is an important human parasite that is widely distributed in southern Korea, China, Taiwan, Japan, and countries in Southeast Asia [1-3]. The number of *Clonorchis* carriers worldwide is estimated to be 38 million [4]. Most human infections involve the intrahepatic bile ducts and occasionally the gallbladder and extrahepatic bile duct. In heavy infections, flukes may be found in the pancreas and duodenum [1, 3]. Although cholangiographic findings of clonorchiasis have been reported [5], to our knowledge, the CT appearance of clonorchiasis has not been described previously.

We present our experience with 42 patients with proved clonorchiasis, all of whom had CT scans.

Subjects and Methods

During a 4-year-period, 370 patients, including 203 patients from Seoul National University Hospital and 167 patients from Pusan National University Hospital, were diagnosed as having clonorchiasis on the basis of the stool and/or intradermal test for *Clonorchis sinensis*. The formalin-ether sedimentation techniques for the stool test and veronal-buffered saline (VBS) extract (VBS antigen, 1:10,000 dilution) of adult worms of *Clonorchis sinensis* for the intradermal test were used in every patient. Of the 370 patients, 42 underwent CT scans of the abdomen for evaluation of associated tumors or for reasons other than clonorchiasis. The hospital records and CT examinations of 42 patients with clonorchiasis were reviewed retrospectively. Twenty-eight patients were from Seoul National University Hospital, and 14 were from Pusan National University Hospital. The diagnosis of clonorchiasis was made on the basis of the stool examination in 19 patients and the intradermal test in seven patients; the diagnosis was made during the surgical resection of the associated tumors in the other 16 patients.

Received July 12, 1988; accepted after revision August 23, 1988.

This work was supported by the Special Research Grant (1988) from Seoul National University Hospital, Seoul, Korea.

¹ Department of Radiology, College of Medicine, Seoul National University, 28 Yeongun-Dong, Chongro-Ku, Seoul 110-744, Korea. Address reprint requests to B. I. Choi.

² Department of Radiology, College of Medicine, Pusan National University, 1-10, Ami-Dong, Suhu-Ku, Pusan 602-073, Korea.

AJR 152:281-284, February 1989

0361-803X/89/1522-0281

© American Roentgen Ray Society

Thirty-seven patients were men, and five patients were women. The average age of the patients was 52 years (range, 34–73 years). Clinical and laboratory data were reviewed in all patients. Initial signs and symptoms included abdominal pain or discomfort (25 patients), palpable mass (five patients), jaundice (five patients), and fever (two patients). Thirty-two patients had elevated serum alkaline phosphatase, and 17 patients had elevated serum bilirubin. Twenty-three patients had elevated eosinophil counts.

All CT examinations were performed with a CT/T 8800 or CT 9800 scanner (General Electric, Milwaukee, WI). Contiguous 10-mm axial sections were obtained, and a bolus injection of 120 ml of 60% meglumine iothalamate (Telebrix 30; Guerbet Laboratories, Aulnay-Sous-Bois Cedex, France) was administered and then followed by serial CT slices.

The patients were divided into two groups: Group 1 included patients with clonorchiasis alone, and group 2 included patients with clonorchiasis and hepatobiliary malignancy. The CT scans of these patients were analyzed for the degree and pattern of dilatation of the biliary tree, thickening of the bile duct wall, and the presence of associated abnormalities.

Results

In the 17 patients with clonorchiasis alone, CT scans showed diffuse dilatation of the intrahepatic bile ducts in 14 patients (82%) (Table 1). In three patients, the scans were normal. The degree of dilatation was minimal in four patients (Fig. 1A) and mild in 10 patients (Fig. 1B). None of the patients showed marked dilatation. The pattern of intrahepatic biliary dilatation was diffuse and uniform. The extrahepatic bile duct and gallbladder were normal in all patients. In no patient could *Clonorchis sinensis* per se be identified, and none had thickening of bile duct wall. Associated abnormalities on CT scans in the hepatobiliary system were pyogenic liver abscess in two patients (Fig. 2A), gallstones in two patients, and pancreatic pseudocyst in one patient.

Twenty-five patients with clonorchiasis had associated hepatobiliary malignancies including 20 cholangiocarcinomas (Fig. 2B), four hepatocellular carcinomas (Fig. 2C), and one carcinoma of the ampulla of Vater. In 20 patients with cholangiocarcinomas, 10 had peripheral cholangiocarcinomas, seven had hilar cholangiocarcinomas (including four intrahepatic main ductal cholangiocarcinomas), and three had common bile duct carcinomas. CT scans in all 25 patients showed diffuse dilatation of the intrahepatic bile ducts. The degrees of dilatation were minimal in seven, mild in 11, and marked in four (Fig. 1C). The pattern of intrahepatic biliary dilatation was diffuse and uniform. None of the 18 patients with minimal or mild biliary dilatation had extrahepatic malignancies. Of the seven patients with severe intrahepatic biliary dilatation, three had hilar cholangiocarcinomas, three had common bile duct carcinomas, and one had carcinoma of the ampulla of Vater. Of the seven, four had dilatation of the extrahepatic biliary tree (three had cholangiocarcinomas of the common bile ducts

TABLE 1: CT Findings in 42 Cases of Clonorchiasis

CT Finding	Clonorchiasis Alone (n = 17)	Clonorchiasis with Hepatobiliary Cancer (n = 25)	Total (n = 42)
Normal	3	0	3
Biliary duct dilatation			
Intrahepatic			
Minimal	4	7	11
Mild	10	11	21
Marked	0	7	7
Extrahepatic	0	4	4

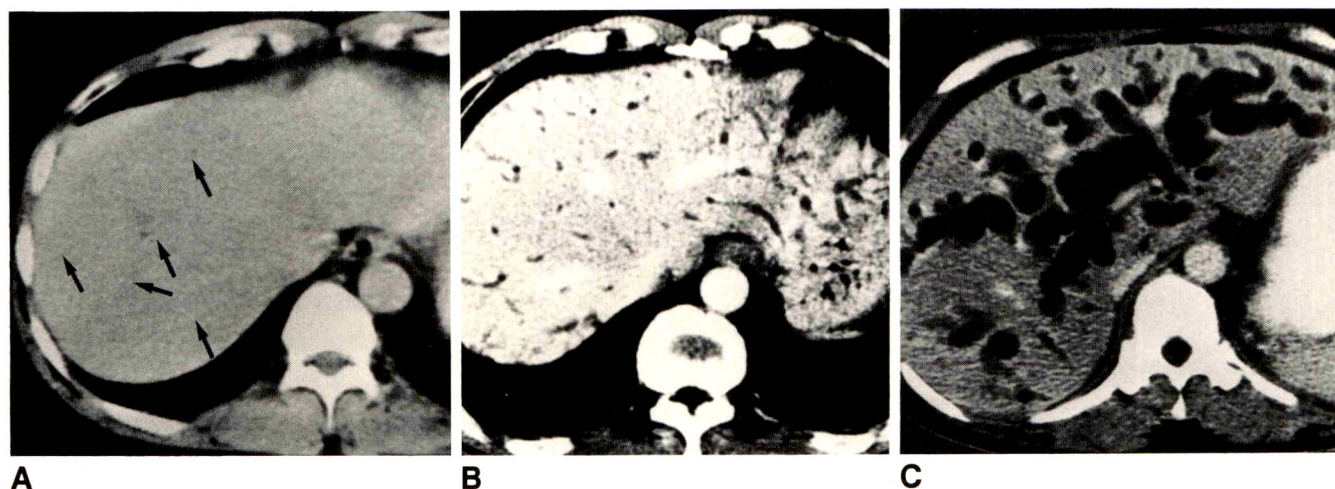


Fig. 1.—Intrahepatic biliary dilatation in three patients with clonorchiasis.

A, Minimal degree of dilatation. CT scan shows subtle dilatation of intrahepatic ducts (arrows). Patient had no associated tumor.

B, Mild degree of dilatation. CT scan shows diffuse, uniform dilatation of intrahepatic bile ducts, particularly in periphery of liver. Extrahepatic biliary tree was normal. Patient had no associated tumor.

C, Marked degree of dilatation. CT scan shows diffuse dilatation of bile ducts. Peripheral ducts are tortuous. Extrahepatic biliary tree was also dilated. Patient had carcinoma of ampulla of Vater in addition to clonorchiasis.

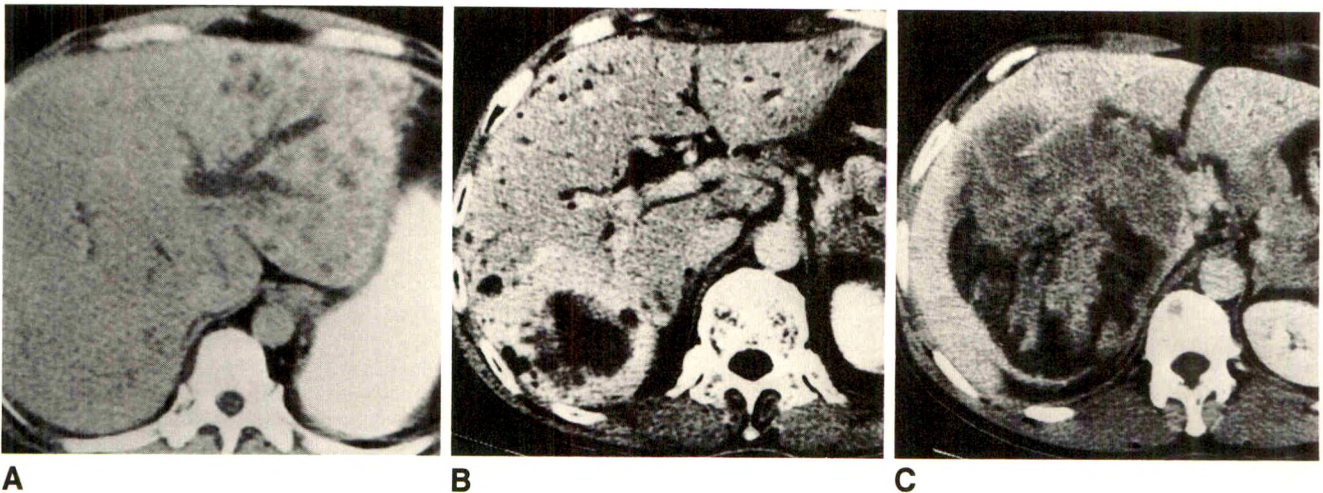


Fig. 2.—Associated hepatobiliary abnormalities in patients with clonorchiasis.

A, Pyogenic liver abscess. CT shows mild, diffuse dilatation of intrahepatic bile ducts and multiple small, round, low-density areas in left lobe of liver due to liver abscesses.

B, Cholangiocarcinoma, peripheral type. CT scan shows irregular, low-density mass with peripheral contrast enhancement in posterior segment of right lobe of liver. Intrahepatic bile ducts show mild, diffuse dilatation.

C, Hepatocellular carcinoma. CT scan shows huge, low-density mass with irregular, central necrotic area in the liver. Minimal dilatation of intrahepatic bile ducts is also seen.

and one had ampullary carcinoma). The gallbladder was distended in four patients. Neither *Clonorchis sinensis* per se nor thickening of the bile duct wall could be identified on CT scans in any of the patients. Three patients had gallstones.

Discussion

The life cycle of *Clonorchis sinensis* has been well documented [1–3]. The definitive hosts of *Clonorchis sinensis* are humans, dogs, hogs, wild cats, martens, badgers, minks, weasels, and rats. The eggs, shed by the adult worm, are deposited in the biliary tree of these animals, enter the intestine, and are passed with the feces. On reaching water, the eggs are ingested by snails. Although several species of snails serve as the first intermediate hosts, *Parafossarulus* and *Bithynia* are probably the most important. Within the snail, the eggs undergo metamorphosis for 4–5 weeks, after which the cercariae erupt. These have the capacity to penetrate the scales of freshwater fish. Numerous species of freshwater fish, mostly belonging to *Cyprinidae*, serve as the second intermediate hosts. After a development period of several weeks, cercariae become encysted in muscle. Humans and

80%, depending on the region of the country [6]. Men are more commonly infected than women [3]. The higher percentage of clonorchiasis in men is probably related to dietary habits. In rural endemic areas, there is a tradition of eating raw freshwater fish, soaked simply in vinegar or red-pepper mash, as an appetizer when drinking rice wine at social gatherings. Because women infrequently participated in such rituals, they are less frequently exposed to the infection.

The clinical symptoms depend on the degree of infection. Most patients with mild infections have no symptoms. Early symptoms include general malaise, abdominal discomfort, and diarrhea. Abdominal pain, enlarged liver, and jaundice subsequently develop. In 10–40% of patients, peripheral eosinophilia may accompany a fluctuating jaundice that usually is obstructive in nature. In the late stage of severe cases, portal hypertension, splenomegaly, ascites, and edema occur [7].

Clonorchiasis should be suspected in a patient who develops manifestations of hepatic or biliary disease and who has a history of ingesting raw freshwater fish in an endemic area. However, the diagnosis is based on the discovery of worms or eggs in the stool or bile drainage [1]. Formalin-ether

In our series, the CT features of clonorchiasis were typical. Diffuse, minimal, or mild dilatation of intrahepatic bile ducts, particularly in the periphery of the liver and without evidence of extrahepatic biliary dilatation, occurred in 32 of the 42 cases. In fact, none of the patients who had clonorchiasis without hepatobiliary malignancy had marked dilatation of the intrahepatic bile duct. Seven patients with severe intrahepatic biliary dilatation had a malignant tumor that was obstructing the biliary tree. Four patients had a malignant tumor of the common bile duct or ampulla of Vater that caused extrahepatic biliary dilatation.

Uniform dilatation of the biliary tree from the main bile ducts in the porta hepatis to the ducts in the periphery of the liver

stones, and ductal dilatation usually is irregular and sometimes shows segmental distribution [17]. In sclerosing cholangitis, both primary and secondary, the bile ducts may have a beaded appearance on CT. The ducts appear to be discontinuous, rather than progressively dilating centrally, and they may have a short serpiginous course and show irregular luminal caliber [18]. Congenital cystic dilatation of the intrahepatic bile ducts shows multiple low-density, branching, tubular structures, which are characteristic of dilated ducts communicating with focal cystic spaces [19]. In metastatic tumor, the clinical presentation and the history serve to differentiate these patients from those with clonorchiasis. Additionally, the tumor mass is usually visible focally compressing

Periportal Low-Attenuation Areas on CT: Value as Evidence of Liver Transplant Rejection

Sheldon B. Kaplan¹
 Jules H. Sumkin¹
 William L. Campbell¹
 Albert B. Zajko¹
 A. Jake Demetris²

CT scans of liver transplants may show periportal areas that are lower in attenuation than adjacent portal veins and liver. These areas appear as low-density rims that surround or parallel the portal vein and its intrahepatic branches as well as the immediate subhepatic portal area. In order to determine the value of periportal low attenuation as an indicator of rejection, we reviewed the CT scans of 37 liver transplant patients with biopsy evidence of either acute rejection (12 patients) or nonspecific change without rejection (25 patients). Low-attenuation areas around peripheral portal branches were identified in six of 12 patients with rejection and in four of 25 patients with nonspecific change (sensitivity, 50%; specificity, 84%; accuracy, 73%). The correlation between peripheral periportal low attenuation and rejection was statistically significant ($p < .05$). Periportal low attenuation in a central location was seen in eight of 12 patients with acute rejection and in 14 of 25 patients with nonspecific change (sensitivity, 67%; specificity, 44%; accuracy, 51%). The correlation was not statistically significant. Low-attenuation areas were evident on scans obtained either with or without IV contrast enhancement.

Periportal low-attenuation areas are commonly seen on CT scans of liver transplants. Peripheral areas correlate with acute rejection, but other factors probably contribute to their occurrence. Central areas do not correlate with acute rejection. Low sensitivity and relatively low accuracy limit the usefulness of peripheral periportal low attenuation as a sign of acute liver allograft rejection.

The CT finding of a rim of low attenuation surrounding the intrahepatic portal veins in liver transplants has been recently described [1, 2]. Wechsler et al. [2] termed the finding the *periportal collar sign* and considered it to be evidence of acute allograft rejection. Another reported cause of this appearance is dilatation of periportal lymphatics severed at transplantation [1].

We have frequently observed rims of low attenuation around central as well as peripheral hepatic portal branches in the livers of transplant patients, many of whom were not undergoing graft rejection. Therefore, to determine the validity of this finding as a sign of acute allograft rejection, we studied the CT scans of 37 liver transplant patients (12 with and 25 without biopsy evidence of graft rejection).

Materials and Methods

Thirty-seven liver transplant patients 22–60 years old (mean, 42) who underwent abdominal CT scanning between December 1984 and September 1986 were included in the study. Criteria for inclusion in the study consisted of liver biopsy performed within 7 days of the CT scan and a histologic diagnosis of either moderate to severe acute rejection (12 patients) or nonspecific change (i.e., essentially normal) (25 patients) as determined by the pathologist of record for each case. If more than one CT scan was obtained within the prescribed period of time for any individual patient, only the first scan was included in the study.

Indications for CT were ascertained from the radiology reports and/or medical records. Indications included: exclude abscess or evaluate known fluid collection (22), rule out hemorrhage (five), evaluate pancreatitis (four), determine liver volume (two), and evaluate for hepatic dysfunction (four).

Received July 29, 1988; accepted after revision September 27, 1988.

¹ Department of Radiology, University of Pittsburgh School of Medicine, Presbyterian-University Hospital, DeSoto at O'Hara Sts., Pittsburgh, PA 15213. Address reprint requests to J. H. Sumkin.

² Department of Pathology, University of Pittsburgh School of Medicine, Pittsburgh, PA 15213.

AJR 152:285–287, February 1989

0361–803X/89/1522–0285

© American Roentgen Ray Society

The diagnosis of acute graft rejection was based on histologic criteria reported previously [3]. The absence of rejection was established if there were no histologic features specific for acute rejection or any other graft syndrome [3].

CT scans were interpreted by two radiologists who were blinded to the biopsy results. Periportal low attenuation was defined as areas surrounding the portal vein and its branches that were clearly less radiodense than the adjacent portal veins or liver. A distinction between central and peripheral periportal low attenuation was made by dividing the liver and the immediately subjacent extrahepatic portal area into three concentric zones of approximately equal radial thickness, centered around the main portal vein. Low-attenuation areas in the inner or central zone nearest the main portal vein were classified as "central." Those occurring in the middle and outer zones of the liver were classified as "peripheral." In general, the central zone included the area around the main portal vein and its first-order branches. CT scans were classified as either positive or negative for peripheral and/or central periportal low attenuation.

All CT scans were obtained on GE 8800 or 9800 scanners. Fourteen scans were obtained with and 23 without IV contrast material. These numbers include only the contrast-enhanced scans for two patients who had scans both before and after an IV contrast agent during the same examination. Six of the patients who received IV contrast material exhibited rejection; eight did not. Six of the patients who did not receive IV contrast material exhibited rejection; 17 did not.

A Fischer's exact two-tailed analysis was performed to evaluate for a correlation between the finding of a hypodense rim and acute rejection. Because such testing is valid only when applied to data in which samples are independent of each other, only one CT scan was included for any individual patient.

Results

Ten (27%) of 37 CT scans showed peripheral low-attenuation rims. Of 12 CT scans in patients with biopsy evidence of acute rejection, six showed peripheral periportal low-attenuation areas and six did not (Fig. 1). CT scans in four of the 25 patients without rejection showed such areas, and the other 21 scans did not (Fig. 2). Thus, the sensitivity of the

sign as an indication of graft rejection was 50%, the specificity was 84%, and the accuracy was 73%. A statistically significant correlation was found between the presence of the sign and biopsy evidence of acute rejection ($p < .05$).

Twenty-two (60%) of 37 scans showed central low-attenuation rims. Central periportal rims were seen on eight of 12 CT scans in the acute rejection category and on 14 of 25 in the group with nonspecific histologic findings. Sensitivity and specificity were 67% and 44%, respectively, as an indicator of rejection; accuracy was 51%.

All 10 scans that showed peripheral periportal rims of low attenuation also exhibited central low-attenuation rims. However, of 22 patients with central periportal low attenuation, peripheral low attenuation was absent in 12.

Of 14 scans obtained with IV contrast material, peripheral periportal low attenuation was observed in three (21%) and central low attenuation in seven (50%). Of 23 noncontrast scans, peripheral low-attenuation rims were seen in seven (30%) and central low-attenuation areas in 15 (65%).

Discussion

Acute rejection is the most common and important cause of hepatic dysfunction after transplantation; it occurs in at least 37% of liver allografts [4]. Liver biopsy is the definitive means of diagnosing and grading the severity of this complication. The imaging evaluation of hepatic dysfunction after transplantation, which often includes patients with graft rejection, usually is performed with duplex sonography and cholangiography. However, CT may be performed in patients suspected of having an abdominal complication such as abscess or hemorrhage. As allograft rejection may also be present in such patients, reliable CT evidence of rejection would be useful.

Our data confirm a previously reported association between CT evidence of periportal low-attenuation areas and acute allograft rejection [2]. The correlation between the two was statistically significant, albeit weakly. Overall accuracy of the

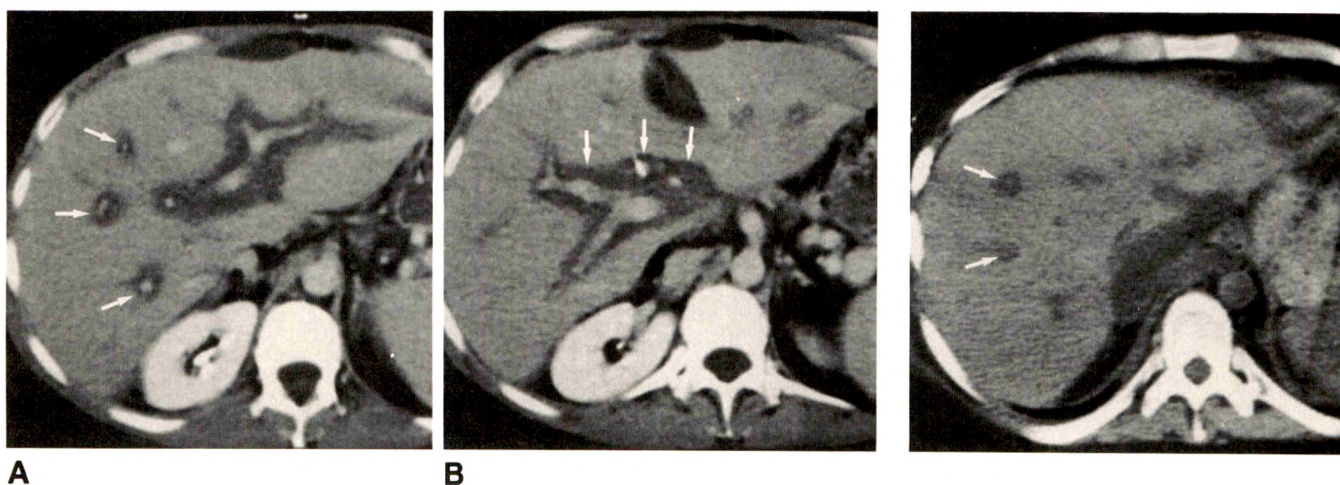


Fig. 1.—CT scans with IV contrast material show periportal low attenuation in patient with biopsy-proved acute hepatic allograft rejection.

A, Peripheral periportal low-attenuation areas (arrows).

B, Central periportal low-attenuation rim (arrows).

Fig. 2.—CT scan without IV contrast material in transplant patient without graft rejection shows peripheral periportal low-attenuation areas (arrows).

sign was 73%. Although the sign was reasonably specific (84%) in our series, its sensitivity was low (50%). The low sensitivity is inconsistent with the findings of the prior study [2]. Centrally located periportal rims of low attenuation were not significantly associated with rejection. Thus, in our experience, periportal low attenuation is of relatively limited clinical value in the detection of allograft rejection.

Periportal low-attenuation areas in both peripheral and central locations were evident on scans obtained with or without IV contrast material. In only two of 37 patients were CT scans obtained before and after administration of IV contrast material as part of the same examination. Low-attenuation areas were not evident on either scan for either patient. We cannot, therefore, directly compare the effect of IV contrast material on the finding in the same patient. In some cases, IV contrast enhancement significantly increased the density of the portal vein making the periportal low attenuation more striking, but the finding was easily seen without IV contrast material in both peripheral and central locations.

Factors other than acute rejection may contribute to periportal low attenuation on CT scans of liver transplants [1, 2]. Lymphatic dilatation and lymphedema, caused by severed lymphatic channels at transplantation, have been described based on clinical observation and animal studies [1]. We have frequently observed periportal rims shortly after transplantation in patients with subhepatic fluid collections in which the more peripheral changes appear to be extensions of more prominent subhepatic and central periportal processes. Indeed, in our study, peripheral rims were never observed in the absence of central periportal low-attenuation areas, although the converse frequently was true. Presumed periportal lymphedema or lymphatic dilatation has been observed in nontransplant patients with conditions such as tumor or post-traumatic hematoma, which might predispose to obstruction of hepatic lymph channels. Similar findings have been described in patients with chronic congestive heart failure [5]. We have also seen a similar CT appearance created by diffuse bile leakage in bile duct necrosis caused by hepatic artery thrombosis after transplantation [6]. Infectious causes also

have been reported [2]. Thus, two or more factors, sometimes operating concurrently, may contribute to the production of periportal low attenuation. The combination of underlying lymphatic obstruction with superimposed acute rejection may be a frequent occurrence.

In summary, CT periportal rims of low attenuation are commonly seen in liver transplants and probably have multiple causes. Although an association with acute rejection has been confirmed when the finding is seen peripherally, the relatively low accuracy and sensitivity of the finding limits its use as evidence of rejection. Other possible causes of this sign include lymphedema and dilated lymphatics, chronic congestive heart failure, tracking of subhepatic and central periportal fluid, and bile leakage in hepatic artery thrombosis after transplantation.

ACKNOWLEDGMENTS

We thank Lori Dobrzynski for assistance in data collection and Pam Sorensen and Maggie Zdrodowski for manuscript preparation.

REFERENCES

1. Marincek B, Barbier PA, Becker CD, Mettler D, Ruchti C. CT appearance of impaired lymphatic drainage in liver transplants. *AJR* 1986;147:519-523
2. Wechsler RJ, Santiago JM, Needleman L, et al. The periportal collar: a CT sign of liver transplant rejection. *Radiology* 1987;165:57-60
3. Demetris AJ, Jaffe R, Starzl TE. A review of adult and pediatric posttransplant liver pathology. In: Rosen PP, Fechner RE, eds. *Pathology annual*, part II. 1987;22:347-386
4. Demetris AJ, Lasky S, Van Thiel DH, Starzl TE, Decker A. Pathology of hepatic transplantation: a review of 62 adult allograft recipients immunosuppressed with a cyclosporine/steroid regimen. *Am J Pathol* 1985;118:151-161
5. Koslin DB, Stanley RJ, Berland LL, Shin MS, Dalton SC. Hepatic perivascular lymphedema: CT appearance. *AJR* 1988;150:111-113
6. Campbell WL, Zajko AB. Radiology of liver transplantation. In: Taveras JM, Ferrucci JT, eds. *Radiology: diagnosis, imaging, intervention*. Philadelphia: Lippincott, 1988;ch. 62:1-7

Videotape Review

RSNA Today, Vol. 2, No. 3. Oak Brook, IL: The Radiological Society of North America, 1988. \$75; by subscription, 4 issues annually at \$225 for RSNA members and \$275 for nonmembers (VHS videotape)

This videotape runs for approximately 1 hr and covers three subjects: Nonpeptic Inflammatory Disease of the Esophagus, by Harvey M. Goldstein; Lumbar Disk Disease: Anatomic Considerations and Imaging Controversies, panel discussion by Stephen A. Kieffer, Victor M. Haughton, and Michael T. Modic; and Imaging in Radiation Oncology, by James A. Purdy and George T. Y. Chen.

This new educational service offered by the Radiological Society of North America (RSNA) provides the subscriber with four cassettes per year, covering new developments and current problems in radiology for the practicing radiologist. The format may include lectures, panel discussions, or interviews.

This particular tape starts out with a short demonstration of the double-contrast technique of examining the esophagus and a discussion of nonpeptic inflammatory disease of the esophagus. Examples of opportunistic infection, medication- or radiation-induced esophagitis, and Crohn disease of the esophagus are illustrated. Although these conditions are less frequently encountered than peptic esophagitis, they are becoming more important, particularly in those practices dealing with immunocompromised patients.

The next segment consists of three presentations on lumbar disk disease and a panel discussion. A brief introduction about the etiology of low back pain is followed by a pathologic-radiologic correlation of the normal and degenerative lumbar disks, demonstrating the normal aging changes of the disk and the mechanism of herniation of the nucleus pulposus through the annular tear. The algorithmic approach for evaluating low back pain is explained, including the role of plain films, myelography, CT, and MR. This is followed by a panel discussion by the three neuroradiologists on the relative value of these techniques, particularly MR and CT. Although the speakers explore some controversies, no consensus is established except that this diagnostic process is still in flux and requires further study.

The final segment is a brief discussion of imaging in radiation oncology by two physicists involved in planning radiation therapy. CT and MR imaging are used to provide information on both anatomic structure and density. By using interactive raster-scan graphic devices and specialized hardware for the computation of radiation doses, diagnostic information can be synthesized, the anatomy can be delineated, radiation therapy can be simulated, the dose distribution can be calculated, and treatment can be verified. An example of the integration of MR and CT of the brain is then shown, with a graphic simulator showing three-dimensional images in real time.

The quality of the images displayed on this tape is exceptionally good. The discussions are quite superficial because of the time constraints and are designed to encourage further study by the viewer, a pursuit facilitated by an accompanying bibliography.

The choice of three totally different subjects makes the educational experience less than ideal. Emphasis on three aspects of one anatomic system or technique would be preferable in such a short period of time. As it is, the brevity of the second and third segments reminds me of the previews of coming attractions seen in the cinema rather than a feature film. The highly professional television-style production will probably appeal to the busy practitioner who wants to be kept current with the new developments in radiology, but it will not substitute for continuing medical education in the form of conferences, courses, or independent study of journals and books.

Herbert F. Gramm
New England Deaconess Hospital
Harvard Medical School
Boston, MA 02215

The Sonographic Diagnosis of Acute Gangrenous Cholecystitis: Importance of the Murphy Sign

Joseph F. Simeone¹
 James A. Brink¹
 Peter R. Mueller¹
 Carolyn Compton²
 Peter F. Hahn¹
 Sanjay Saini¹
 Stuart G. Silverman¹
 Glen Tung¹
 Joseph T. Ferrucci¹

The sonographic Murphy sign is defined as the presence of maximal tenderness elicited by direct pressure of the transducer over a sonographically localized gallbladder. The reported prevalence of this sign is more than 95% in patients with acute cholecystitis. In this series of 18 patients with pathologically proved gangrenous cholecystitis, the sonographic Murphy sign was positive in only six (33%). Clinical examination showed a positive Murphy sign in eight patients (44%), diffuse abdominal pain in nine patients (50%), and no pain in one patient (6%). Other sonographic findings included pericholecystic fluid (10), thickening of the gallbladder wall (10), and a dilated gallbladder (five).

Our experience suggests that the absence of the Murphy sign increases the possibility of gangrenous cholecystitis in patients with abdominal pain and sonographic findings of cholecystitis.

The sonographic Murphy sign is defined as the presence of maximal tenderness elicited by direct pressure of the transducer over a sonographically localized gallbladder. Gangrenous cholecystitis is a rare form of acute cholecystitis with a clinical presentation occasionally indistinguishable from that of acute nongangrenous cholecystitis. Gangrenous cholecystitis has a mortality rate of up to 22% and a complication rate of 16–25% as compared with acute nongangrenous cholecystitis, which has a mortality rate of 0.5–6% and a complication rate of 6–15% [1]. Early diagnosis and surgery are necessary in gangrenous cholecystitis to avoid this high morbidity and mortality. In contrast, acute nongangrenous cholecystitis may be treated conservatively with antibiotics initially, followed by elective surgery [2]. Consequently, the sonographic recognition of gangrenous cholecystitis has significant ramifications.

Previous radiologic reports have stressed the predictive value of the sonographic Murphy sign in diagnosing acute nongangrenous cholecystitis, but they have not commented on its value in gangrenous cholecystitis. Our purpose was to determine the importance of the sonographic Murphy sign in establishing the diagnosis of gangrenous cholecystitis.

Materials and Methods

Between 1983 and 1987, a total of 1482 cholecystectomies were performed at our institution. We retrospectively reviewed the sonograms, final pathologic reports, and hospital records of 18 cholecystectomy patients who had a proved diagnosis of gangrenous gallbladder in this period. Gangrenous cholecystitis was defined pathologically as transmural hemorrhagic or liquefactive necrosis in most of the gallbladder wall. Clinical records were studied to determine if patients had diabetes, diffuse abdominal pain, diffuse tenderness, focal pain and tenderness, or the Murphy sign on physical examination (presence of focal pain in the right upper quadrant on palpation during deep inspiration). The patients' general condition and the presence of leukocytosis and fever at the time of presentation were determined. The surgical reports were studied to determine the presence of cholelithiasis, perforation of the gallbladder, omental phlegmon, inflamed porta hepatitis, inflamed mesentery, and gallbladder

Received July 28, 1988; accepted after revision September 23, 1988.

¹ Department of Radiology, Massachusetts General Hospital, Boston, MA 02114. Address reprint requests to J. F. Simeone.

² Department of Pathology, Massachusetts General Hospital, Boston, MA 02114.

AJR 152:289–290, February 1989

0361–803X/89/1522–0289

© American Roentgen Ray Society

empyema. The pathologic reports were studied to determine the presence of perforation of the gallbladder, fibrosis, adhesions, necrosis, and gangrenous cholecystitis.

Real-time sonography was performed by a radiologist in every case. The sonographic reports were reviewed for the presence or absence of the sonographic Murphy sign. The sonograms were studied to determine the presence of cholelithiasis, pericholecystic fluid, gallbladder-wall thickening, size and shape of the gallbladder (replacement of the normal pear shape by a more spherical shape), contraction of the gallbladder, and gallbladder emphysema.

During the study, evaluation of the sonographic Murphy sign was made as part of the sonographic examination in all patients.

Results

Of the 18 patients, four presented with fever and leukocytosis, and two presented with leukocytosis and no fever. Three patients had diabetes. On physical examination, eight patients had a positive Murphy sign, and 10 patients had a negative Murphy sign. Of these 10, nine (50% of the total) had generalized abdominal pain. No abdominal pain was reported in one patient.

The sonographic Murphy sign was observed and reported in only six (33%) of the 18 patients. Other sonographic findings were variable. Cholelithiasis was present in 17 (94%) of the 18 patients. The next most common findings were pericholecystic fluid and thickening of the gallbladder wall, each noted in 10 patients (56%). The gallbladder was dilated in five patients (28%) and contracted in one patient (6%). Gallbladder emphysema was noted in one patient (6%). In one patient, the sonogram revealed only gallstones with no Murphy sign.

The surgical findings were perforation in five (28%), inflamed porta hepatitis in five (28%), inflamed mesentery in four (22%), omental phlegmon in three (17%), and gallbladder empyema in one (6%). The pathologic findings were gangrene in 18 (100%), perforation in five (28%), and fibrosis and adhesions in three (17%).

Discussion

The prevalence of gangrenous cholecystitis in patients presenting with right upper quadrant pain in our hospital was 1.2% during the 5-year period of this report. However, the importance of making this diagnosis clinically is emphasized by the high mortality (22%) and complication rates (16–25%) of gangrenous cholecystitis when compared with acute nongangrenous cholecystitis [1]. Therefore, early and accurate diagnosis of this condition is important.

The sonographic Murphy sign is defined as the presence of maximal tenderness elicited by direct pressure of the transducer over a sonographically localized gallbladder. The sign is negative if no tenderness is present or if tenderness is

the same over the gallbladder as it is in adjacent regions [1]. The sonographic Murphy sign has been shown to be present in 98.8% of 497 suspected cases of acute cholecystitis [1]. The presence of cholelithiasis in conjunction with a positive sonographic Murphy sign has a 92% positive predictive value in the diagnosis of acute nongangrenous cholecystitis [3].

Only 33% of our patients with gangrenous cholecystitis had a positive sonographic Murphy sign. This is significantly lower than the higher 95% prevalence reported in patients with acute nongangrenous cholecystitis [3]. The physical examination revealed a Murphy sign in about 44% of patients, diffuse abdominal pain in 50% of patients, and no pain in 6% of patients.

The mechanism by which pain is elicited from the gallbladder is complex. In acute nongangrenous cholecystitis, gallbladder distension and mural inflammation stimulate visceral afferent nerves in the muscular and serosal layers of the gallbladder via the autonomic nervous system [4, 5]. Thus, compression of the distended inflamed gallbladder by a sonographic transducer causes maximal pain. Once these nerves die, as they do in gangrenous cholecystitis, transmural necrosis produces inflammation of the adjacent parietal peritoneum, stimulating intercostal branches of the spinal nerves and producing generalized right upper quadrant pain in the T5–T11 dermatomes. The right phrenic nerve branches in the right hemidiaphragm may also be stimulated, producing additional referred right shoulder pain [5].

We have observed that a positive sonographic Murphy sign is less prevalent in patients with gangrenous cholecystitis than in patients with acute nongangrenous cholecystitis. When an inflamed gallbladder is apparent on sonography, absence of the Murphy sign may indicate the presence of gangrene.

ACKNOWLEDGMENTS

We gratefully acknowledge the assistance of ultrasound technologists Jean Lamere, Jane Kelley, Joan Coakley, Janice Gullickson, and Barbara Hoyler. We thank Andrea Kacos for preparing the manuscript.

REFERENCES

1. Ralls PW, Halls J, Lapin SA, Quinn MF, Morris UL, Boswell W. Prospective evaluation of the sonographic Murphy sign in suspected acute cholecystitis. *JCU* 1982;10:113–115
2. Glenn F. Surgical management of acute cholecystitis in patients 65 years of age and older. *Ann Surg* 1981;193(2):56–59
3. Ralls PW, Colletti PM, Lapin SA, et al. Real-time sonography in suspected acute cholecystitis. *Radiology* 1985;155:767–771
4. Warwick R, Williams PL, eds. *Graves anatomy*, 35th ed. (British). Philadelphia: Saunders, 1973:1311–1312
5. Sabiston DC, ed. *Textbook of surgery*, 11th ed. Philadelphia: Saunders, 1977:879

Technical Note

The Use of Color Doppler Sonography to Distinguish Dilated Intrahepatic Ducts from Vascular Structures

Philip W. Ralls,¹ Donald S. Mayekawa, Kevin P. Lee, Meade B. Johnson, and James Halls

Diagnostic sonography has depended on morphologic signs to distinguish dilated intrahepatic ducts from vascular structures. Unfortunately, the double-channel (parallel-tract or shotgun) sign [1, 2] has limited usefulness, especially in differentiating small ducts from vessels, [1, 3, 4]. We assessed the capabilities of color Doppler sonography in patients with dilated intrahepatic ducts.

Subjects and Methods

Twenty-six patients with known intrahepatic dilatation were selected for color Doppler imaging (QAD I, Quantum Medical Systems, Issaquah, WA). Most patients were scanned with 5-MHz, linear-array transducers. A few patients were scanned with a 3-MHz, linear-array transducer that became available near the end of the study. Patients were selected for scanning if intrahepatic biliary dilatation had been detected by some other imaging technique, either CT (23 patients) or direct cholangiography (three patients). The size of the dilated intrahepatic ducts ranged from 2 to 10 mm. In 25 of the 26 patients, intrahepatic ductal dilatation could be detected by conventional gray-scale sonography. Although an attempt was made to scan consecutive patients, it is unlikely that all patients with dilated intrahepatic ducts were scanned. No patients were excluded from color Doppler scanning for any reason. Color Doppler imaging usually was easiest to perform in the left lobe of the liver. This was related to access difficulties with the linear-array transducer and the limited depth at which color could be detected (approximately 9 cm with the 5-MHz transducer). The most superficial portions of the right lobe usually could be imaged by using the intercostal technique. The only criterion for diagnosis of intrahepatic ductal dilatation was the presence of one

or more small tubular structures that did not show color-coded flow on Doppler imaging (Fig. 1).

Ten patients without biliary dilatation on CT were scanned as normal control subjects.

Examiners performing color Doppler sonography had preliminary knowledge of the presence or absence of intrahepatic biliary dilatation in the subjects studied.

Results

Dilated intrahepatic ducts were successfully differentiated from small vessels with color Doppler in all 26 patients. One patient with a gallbladder carcinoma had intrahepatic ductal dilatation that was missed on a previous sonogram. This was the only patient in whom dilated intrahepatic ducts were not identified on gray-scale images alone. It is uncertain if other patients might have been misdiagnosed with gray-scale sonography had the examiners not known that intrahepatic ductal dilatation was present. Subjectively, it was easier to differentiate ducts from vessels with color Doppler sonography in all 26 patients.

No dilated intrahepatic bile ducts were detected in the 10 control patients who did not have biliary dilatation.

Discussion

Doppler sonography has been used to help discriminate bile ducts from vessels in the porta hepatis [5]. We and others [6] have found sample-volume Doppler technically difficult and

Received June 21, 1988; accepted after revision August 9, 1988.

¹All authors: Department of Radiology, University of Southern California School of Medicine, Los Angeles County/USC Medical Center, Los Angeles, CA 90033. Address reprint requests to P. W. Ralls, Box 631, 1200 N. State St., Los Angeles, CA 90033.

AJR 152:291-292, February 1989 0361-803X/89/1522-0291 © American Roentgen Ray Society

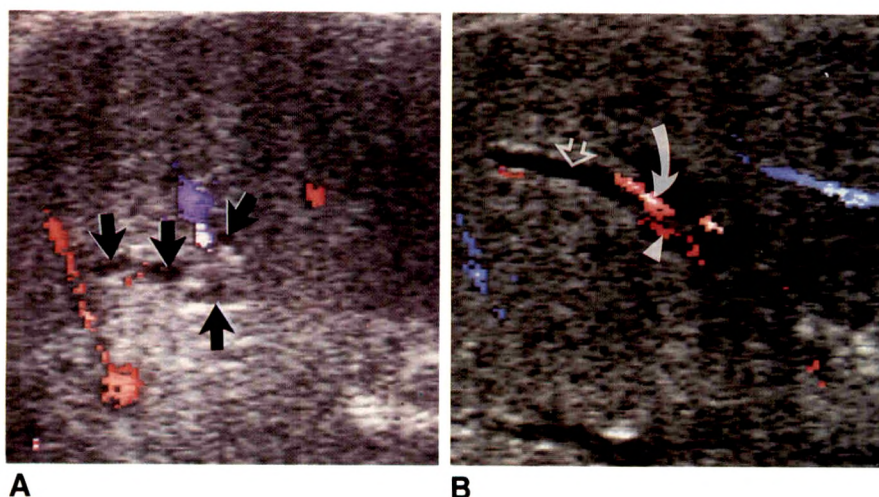


Fig. 1.—A and B, Transverse color Doppler sonograms of liver. Flow is detected in small arterial and venous structures. No flow is detected within small, dilated intrahepatic ducts. Note ease with which vessels can be differentiated from dilated ducts, even when they are adjacent to one another. Note dilated duct (open arrow in B) adjacent to vessels with color-coded flow. In B, portal vein is shown by arrowhead; curved arrow indicates hepatic artery.

tedious in evaluating suspected intrahepatic tubular abnormalities. Color Doppler passively displays flow information, facilitating differentiation of ducts from vessels. Although our study has limitations, it suggests that color Doppler imaging may be useful in this problem area. Despite the inherent limitations of the color Doppler system we used (linear-array transducer with a large footprint and concomitant access problems; limited depth sensitivity with a 5-MHz transducer), we obtained definite information in all patients. We had anticipated difficulty in detecting signal in the left-sided intrahepatic vessels because they generally course parallel to the skin surface. The resulting Doppler angle (90°) might be expected to result in no signal. Color flow usually was noted even in vessels that seemed to be parallel to the transducer. When little or no flow was detected, a slight rocking motion of the transducer revealed color flow in vessels.

Our data, because of the design limitations of this study, do not provide a reliable assessment of the accuracy of color Doppler sonography in diagnosing suspected intrahepatic biliary dilatation. Nevertheless, color Doppler sonography appears to be sensitive in detecting dilated intrahepatic ducts.

Color Doppler also allows an easier and more confident diagnosis of intrahepatic ductal dilatation than does gray-scale or duplex Doppler sonography. Thus, color Doppler sonography appears to be a promising technique, capable of improving ease of diagnosis and, perhaps, accuracy in the assessment of intrahepatic biliary dilatation.

REFERENCES

1. Conrad MR, Landay MJ, Janes JO. Sonographic "parallel channel" sign of biliary tree enlargement in mild to moderate obstructive jaundice. *AJR* 1978;130:279-286
2. Willi UV, Teele RL. Hepatic arteries and the parallel-channel sign. *JCU* 1979;7:125-127
3. Mueller PR. Jaundice. In: Simeone J, ed. *Clinics in diagnostic ultrasound*, vol. 14. *Coordinated diagnostic imaging*. New York: Churchill Livingstone, 1984:25-56
4. Bressler EL, Rubin JM, McCracken S. Sonographic parallel channel sign: a reappraisal. *Radiology* 1987;164:343-346
5. Berland LL, Lawson TL, Foley WD. Porta hepatis: sonographic discrimination of bile ducts from arteries with pulsed Doppler with new anatomic criteria. *AJR* 1982;138:833-840
6. Wing VW, Laing FC, Jeffrey RB, et al. Sonographic differentiation of enlarged hepatic arteries from dilated intrahepatic bile ducts. *AJR* 1985;145:57-61

Color Doppler Ultrasound of the Normal Testis

William D. Middleton¹
David A. Thorne
G. Leland Melson

Color Doppler ultrasound with point spectral analysis was performed on 30 testes of 15 asymptomatic volunteers. Intratesticular arteries and testicular capsular arteries were imaged in all 30 cases. Waveforms from these vessels were similar and consistently showed a low-impedance pattern with high levels of diastolic flow. This reflects the low vascular resistance of the testis. Supratesticular arteries were also identified in all 30 cases. In addition to the low-impedance-type waveforms from the testicular artery, waveforms obtained in the supratesticular region also originated from the deferential and/or cremasteric arteries. This resulted in some waveforms with high-impedance patterns, reflecting the high vascular resistance of the epididymis and peritesticular tissues.

We believe that color Doppler ultrasound is capable of reliably showing the normal testicular arterial anatomy by imaging intraarterial blood flow. Knowledge of the normal color Doppler appearance and waveform characteristics of the testicular artery should aid in diagnosing scrotal conditions that alter blood flow.

High-resolution color Doppler ultrasound has recently made it possible to noninvasively image and evaluate small vessels in superficial organs. Applications in the thyroid gland and neonatal brain already have been described [1–3]. We think that color Doppler ultrasound will also be useful in evaluating vascular disorders in the scrotum. This study was performed to determine the normal color Doppler ultrasound appearance of the testis and to establish the velocity waveform parameters that can be expected in normal patients.

Subjects and Methods

Bilateral testicular scans were obtained in 15 young asymptomatic volunteers. A commercially available color Doppler ultrasound unit (QAD1 Angiodynography, Quantum Medical Systems, Issaquah, WA) was used. With this unit, blood flow is identified and its direction (either toward or away from the transducer) is determined by detection and analysis of phase shifts in the returning echoes. Red and blue colors are assigned to flowing blood depending on the direction of flow. Color shading depends on the Doppler frequency shift of the returning echoes, and higher-frequency shifts are assigned a whiter shade of red or blue. Stationary tissue is identified as motionless because it does not produce a phase shift in the returning echoes. It is then assigned gray-scale values as in conventional gray-scale sonography. The resulting real-time image displays conventional gray-scale information while simultaneously showing the temporal and spatial characteristics of blood flow in color.

As with conventional duplex Doppler, range-gated pulsed Doppler interrogation can be performed with color Doppler ultrasound. The sample volume for this particular unit is fixed at 0.6 by 1.5 mm. This small size ensures that any given waveform originates from a single vessel. The gate is positioned over the vessel of interest identified on the real-time image. The Doppler frequency shift originating from the blood flow in that vessel is displayed below the image. This frequency information can be converted to velocity information by determining the direction of blood flow with an angle indicator (Fig. 1).

The volunteers studied were 28–35 years old (mean, 30). None had a history of testicular torsion, infection, or significant trauma. All were examined while they were supine. Real-time

Received July 18, 1988; accepted after revision September 23, 1988.

Presented at the annual meeting of the American Roentgen Ray Society, San Francisco, CA, May 1988.

¹ All authors: Mallinckrodt Institute of Radiology, Washington University School of Medicine, 510 S. Kingshighway Blvd., St. Louis, MO 63110. Address reprint requests to W. D. Middleton.

AJR 152:293–297, February 1989

0361–803X/89/1522–0293

© American Roentgen Ray Society

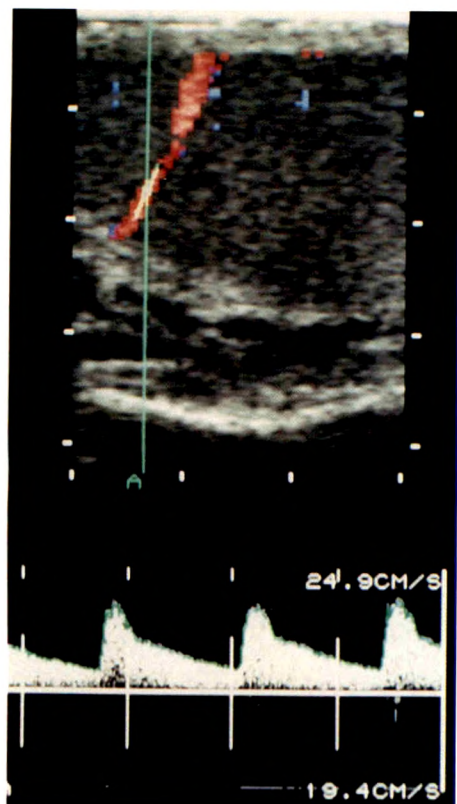


Fig. 1.—Color Doppler ultrasound image and velocity waveform from intratesticular artery. Vessel is identified on real-time image, and range-gated cursor is placed over region of interest. Doppler frequency shift obtained from vessel is converted to velocity by correcting for angle of blood flow, as with conventional duplex Doppler.

scans were obtained in standard longitudinal and transverse planes. In each volunteer, a prospective search was made for suprastesticular, capsular, and intratesticular arteries (Fig. 2). When these vessels were identified, the scanning plane was adjusted to elongate and optimally visualize the vessels. Point spectral analysis was performed on the largest vessel identified in each category. Sampling was performed until consistent, reproducible waveforms were obtained. The examinations were recorded digitally on videotape and subsequently reviewed on a frame-by-frame basis by using a cine loop function.

The frequencies of visualization of the suprastesticular, capsular, and intratesticular arteries were determined by an analysis of the real-time images. Analysis of the velocity waveforms from these three groups of vessels included determination of peak systolic velocity, end-diastolic velocity, resistive index (systolic velocity minus diastolic velocity divided by systolic velocity), and pulsatility index (maximum velocity minus minimum velocity divided by mean velocity). All examinations were performed with a linear-array transducer operating at 7.5 MHz for both imaging and Doppler interrogation. Low flow settings were used to ensure optimum visualization of the small testicular arteries and to optimize detection of lower-velocity diastolic flow. At this setting, velocities as low as 0.3 cm/sec can be detected. This improved sensitivity to low flow velocities is accompanied by a narrower range of frequencies that can be sampled without high-

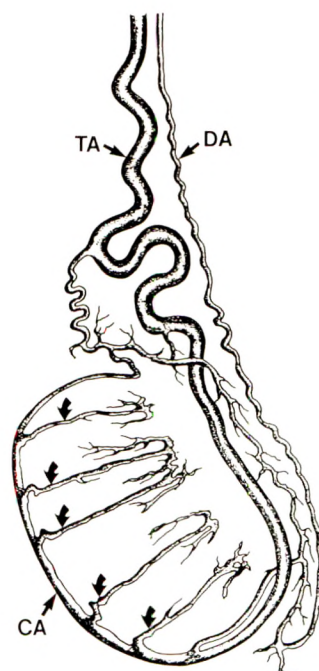


Fig. 2.—Testicular (TA) and deferential (DA) arteries. Cremasteric artery has been omitted for simplicity. Capsular arteries (CA) are seen around periphery of testes. Centripetal arteries (curved arrows) are directed toward mediastinum. Recurrent rami are branches of centripetal arteries, which are directed away from mediastinum. Note anastomosis between DA and TA.

frequency aliasing. However, aliasing was never encountered at the low flow velocities seen in the scrotum. Threshold levels were adjusted to maximize visualization of testicular vessels while avoiding artifactual color assignment due to system noise.

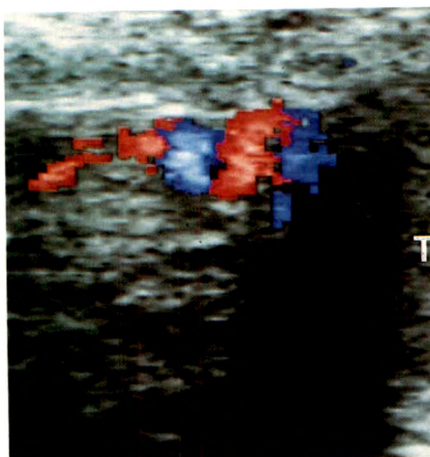
Results

Suprastesticular arteries were visualized bilaterally in all volunteers. Typically, they were tortuous with areas of flow toward and away from the transducer seen in different segments of the same vessel (Fig. 3). Peak systolic velocities ranged from 7.5 to 27.7 cm/sec (mean, 14.0 cm/sec), and end-diastolic velocities ranged from 0 to 4.7 cm/sec (mean, 1.9 cm/sec). Resistive indexes ranged from 0.63 to 1.00 (mean, 0.84), and pulsatility indexes ranged from 1.3 to 5.9 (mean, 3.0).

Capsular arteries were also visualized bilaterally in all volunteers. They were seen along the outer margin of the testis in either longitudinal or transverse planes (Fig. 4). Peak systolic velocities ranged from 5.0 to 23.4 cm/sec (mean, 11.9 cm/sec), and end-diastolic velocities ranged from 1.8 to 9.2 cm/sec (mean, 4.0 cm/sec). The resistive indexes ranged from 0.46 to 0.78 (mean, 0.66), and the pulsatility indexes ranged from 0.82 to 2.3 (mean, 1.3).

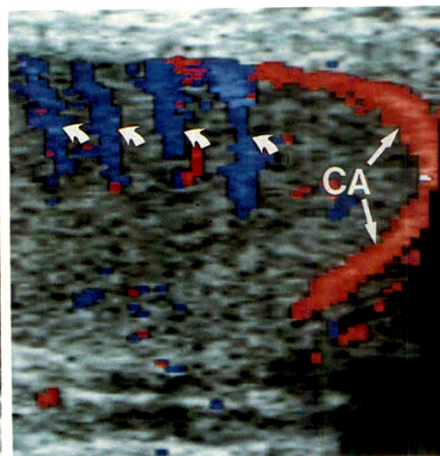
Intratesticular arteries were also visualized bilaterally in all cases. They were relatively straight and were best seen in certain "vascular" planes. These planes generally were oblique to the standard longitudinal and transverse planes. In many cases, both centripetal arteries and their recurrent rami were identified (Fig. 5). Peak systolic velocities ranged from 4.0 to 19.1 cm/sec (mean, 9.7 cm/sec), and diastolic velocities ranged from 1.6 to 6.9 cm/sec (mean, 3.6 cm/sec). Resistive indexes ranged from 0.48 to 0.75 (mean, 0.62), and pulsatility indexes ranged from 0.7 to 2.3 (mean, 1.3).

Fig. 3.—Doppler image shows longitudinal view of suprastesticular artery. Its tortuosity results in different color assignment to portions of vessel; flow is directed toward and away from transducer. Upper pole of testis (T) is on right of image.



3

Fig. 4.—Doppler image shows longitudinal view of testis with capsular artery (CA) at inferior pole with multiple centripetal arteries (curved arrows) arising from it.

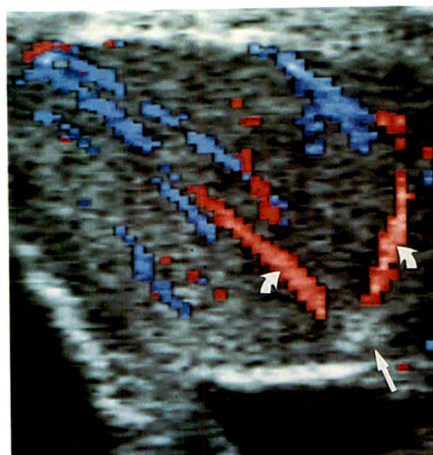


4

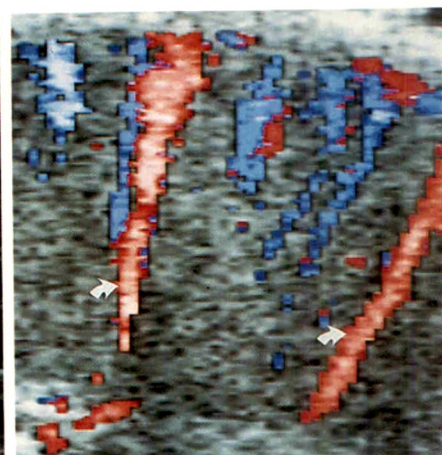
Fig. 5.—Doppler images of intratesticular arteries.

A, Transverse view shows centripetal arteries (curved arrows) in red, with flow directed toward mediastinum (straight arrow), and recurrent rami in blue, with flow directed away from mediastinum.

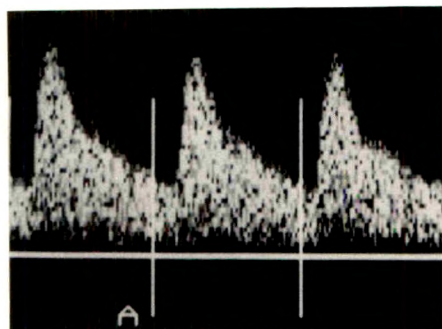
B, Longitudinal view shows centripetal arteries in red (arrows) and recurrent rami in blue.



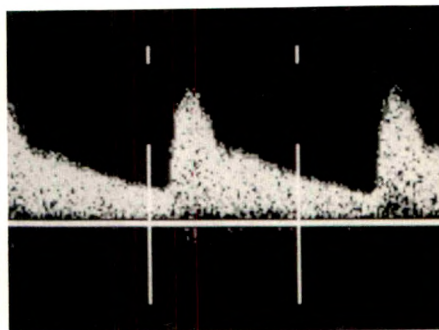
A



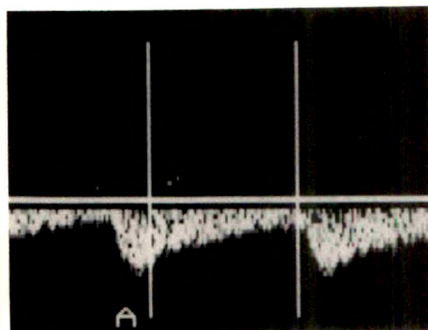
B



A



B



C

Fig. 6.—Pulsed Doppler waveforms from capsular artery (A), centripetal artery (B), and recurrent ramus (C) show low-impedance pattern with high levels of diastolic flow. Recurrent rami waveform is below baseline because of its opposite flow direction with respect to centripetal artery.

Review and comparison of the waveforms from the three groups of vessels resulted in the subjective impression that the capsular and intratesticular waveforms were similar and relatively constant in their appearance, whereas the suprastesticular waveforms were more variable in appearance (Figs. 6 and 7). The distribution of resistive indexes and pulsatility indexes from the three groups of vessels confirms this subjective impression (Figs. 8 and 9). Also apparent from these

graphs is a certain amount of overlap between the suprastesticular waveforms and the waveforms of the capsular and intratesticular arteries.

In this study, no attempt was made to systematically identify testicular veins. However, in two instances, a vein was clearly seen immediately adjacent to an intratesticular artery. In both cases, venous waveforms were obtained from pulsed Doppler interrogation of these vessels (Fig. 10).

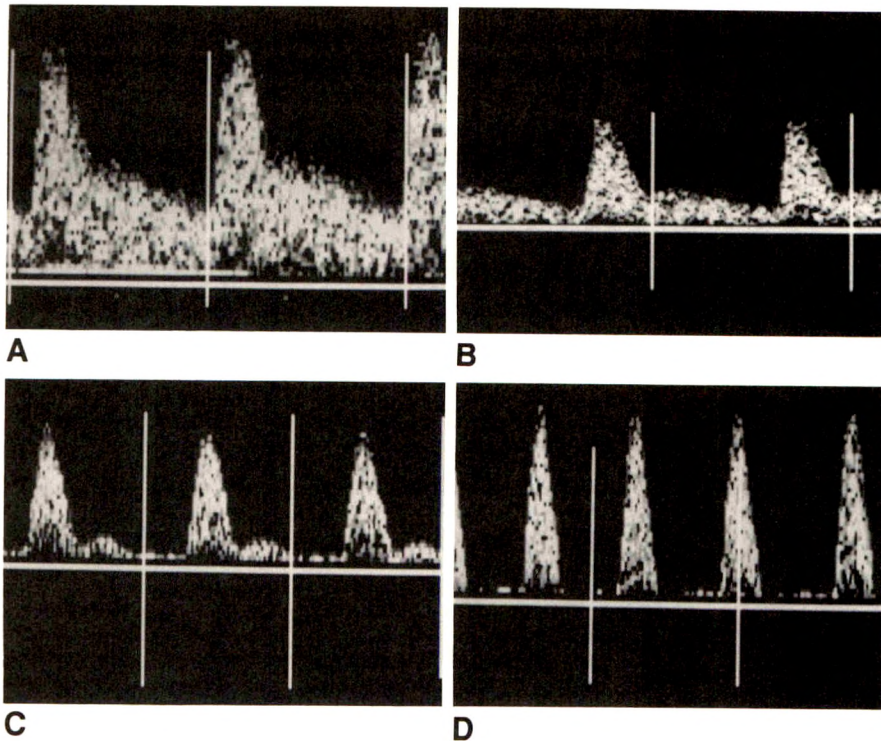


Fig. 7.—Velocity waveforms from suprastesticular arteries of different volunteers show variability of waveforms with progressively decreasing diastolic flow from A to D.

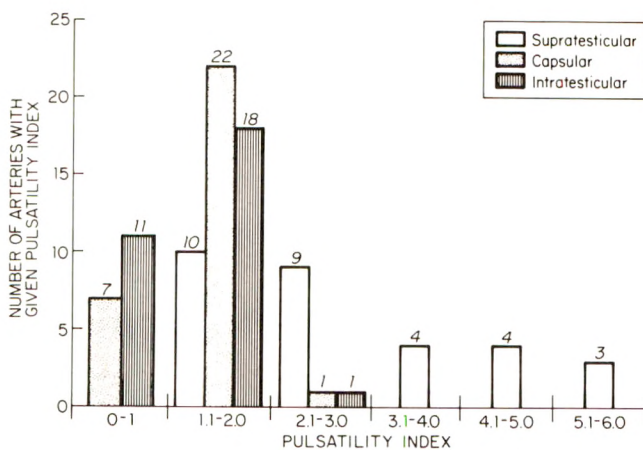


Fig. 8.—Distribution of pulsatility indexes from suprastesticular, capsular, and intratesticular arteries.

Discussion

Blood flow to the testis is supplied by several arteries [4]. The testicular arteries arise from the anterior aspect of the aorta just below the level of the renal arteries. They enter the spermatic cord at the internal inguinal ring with the other cord structures. At the posterosuperior aspect of the testis, the testicular artery divides into branches that pierce the tunica albuginea and run along the periphery of the testis in a layer known as the tunica vasculosa. These capsular arteries in the tunica vasculosa supply centripetal branches that enter the testicular parenchyma and run toward the mediastinum. At the mediastinum, the centripetal arteries arborize into recur-

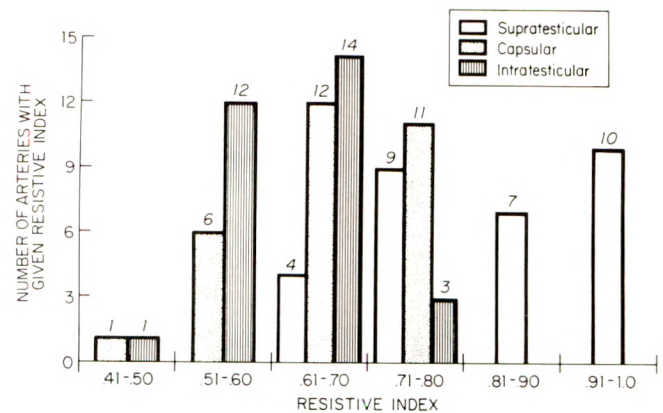
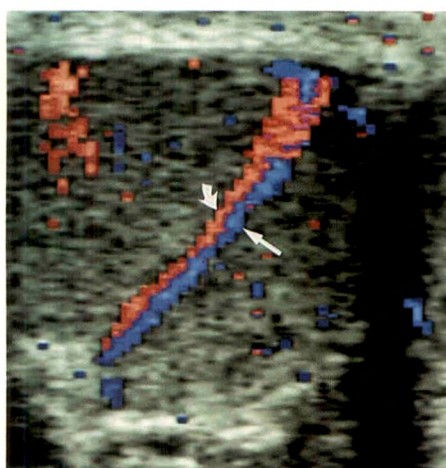


Fig. 9.—Distribution of resistive indexes from suprastesticular, capsular, and intratesticular arteries.

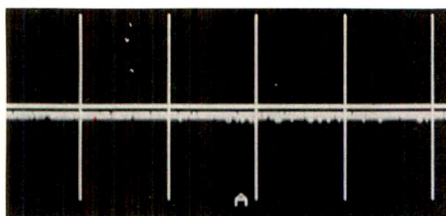
rent rami that run in the opposite direction, away from the mediastinum (Fig. 1) [4].

Color Doppler ultrasound accurately reflects this arterial anatomy. In all 30 testes imaged, identification of capsular and intratesticular arteries was relatively easy. The morphology of these vessels as portrayed with color Doppler ultrasound corresponded well with the described anatomic morphology. However, some exaggeration in size of tiny vessels such as those examined in this study does occur because of limitations in lateral resolution. Velocity waveforms from the capsular and intratesticular arteries showed high levels of antegrade diastolic flow throughout the cardiac cycle. This reflects the low vascular resistance of the testis.

Color Doppler ultrasound was also capable of reliably iden-



A



B

Fig. 10.—Intratesticular vein.

A, Transverse view shows centripetal artery (curved arrow) in red and small adjacent vein (straight arrow) in blue.

B, Velocity waveform from vein confirms venous flow pattern.

tifying suprastesticular arteries in this group of normal volunteers. However, the velocity waveforms obtained from these vessels were quite variable. In some cases there was a high-impedance-type waveform with sharp, narrow systolic peaks and no diastolic flow. In other cases, the waveforms were similar to those obtained from the capsular and intratesticular vessels.

This variability most likely resulted from sampling different vessels. In addition to the testicular artery, the spermatic cord also contains the deferential and cremasteric arteries. These arteries primarily supply the epididymis and the peritesticular scrotal tissues; however, they also contribute a variable amount of blood to the testis via anastomoses with the testicular artery. We think that the high-resistance waveforms obtained in the suprastesticular region originated from the deferential and cremasteric arteries and reflect the high vascular resistance of these extratesticular scrotal tissues. The lower-resistance waveforms obtained in the suprastesticular region presumably originated from the testicular artery and therefore are similar to the capsular and intratesticular vessels.

Knowledge of the expected waveform characteristics of the scrotal arteries is important if color Doppler ultrasound is

to have a role in evaluating testicular disease. For instance, demonstration of blood flow in the suprastesticular region does not necessarily imply perfusion of the testis unless the waveform pattern is of a low-impedance type. High-impedance waveforms may originate from arteries other than the testicular artery. On the other hand, if there is an increase in diastolic flow in arteries that normally supply extratesticular tissues, then some form of peritesticular hyperemia, such as an inflammatory process, exists.

We think that subjective analysis of the morphology of the Doppler waveforms is adequate to characterize and differentiate testicular and peritesticular arteries. However, several indexes also can be used to provide objective characterization of these arteries. The pulsatility index is more sensitive in identifying abnormal waveforms because it takes into account the mean velocity. Unfortunately, not all instruments provide for this calculation. Therefore, we have also calculated resistive indexes because these can be calculated easily [5]. Either index can be used to complement the subjective analysis.

The results of this study apply only to equipment similar to that used in this study. Detection of small scrotal vessels and low levels of diastolic flow is dependent on the overall sensitivity of the unit and on the transmitted Doppler frequency. We have not attempted to reproduce these results with other equipment or with other transducers in our own unit.

In summary, we think that color Doppler ultrasound is capable of consistently and accurately visualizing the testicular arteries in normal individuals. In the suprastesticular region, variable waveforms are to be expected. Capsular and intratesticular waveforms consistently show a low-impedance pattern. Knowledge of these normal color Doppler ultrasound characteristics should be valuable in the evaluation of abnormalities that affect scrotal blood flow, such as torsion, orchitis, and epididymitis.

ACKNOWLEDGMENTS

We thank Mary A. Middleton for manuscript review and Lynn Losse for manuscript preparation.

REFERENCES

1. Ralls PW, Mayekawa DS, Lee KP, et al. Color-flow Doppler sonography in Graves disease: the "thyroid inferno." *AJR* 1988;150:781-784
2. Taylor GA, Short BL, Glass P, Ichord R. Cerebral hemodynamics in infants undergoing extracorporeal membrane oxygenation: further observations. *Radiology* 1988;168:163-167
3. Mitchell DG, Merton D, Needleman L, et al. Neonatal brain: color Doppler imaging. Part 1. Technique and vascular anatomy. *Radiology* 1988;167:303-306
4. Setchell BP. Testicular blood supply, lymphatic drainage and secretion of fluid. In: Johnson AD, Gowes WR, Vandemark NL, eds. *The testis*. New York: Academic Press, 1970:101-239
5. Nelson TR, Pretorius DH. The Doppler signal: where does it come from and what does it mean? *AJR* 1988;151:439-447

American Roentgen Ray Society

89th Annual Meeting

May 7–12, New Orleans, LA

1989 Caldwell Lecturer



The Honorable William Bradley

United States Senator from New Jersey

“Health Care Choices for the 90s”

Wilms Tumor (Nephroblastoma) in the Adult Patient: Clinical and Radiologic Manifestations

Farhad Kioumehri¹
Sachiko T. Cochran²
Lester Layfield³
Issa Yaghmai¹
Caroline Ngo¹
Stanley R. Smith⁴

Wilms tumor (nephroblastoma), a primary renal neoplasm containing primitive blastema and embryonic glomerulotubular structures, is seen rarely in adults. To identify clinical and radiologic criteria for preoperative diagnosis of adult Wilms tumor, we studied 29 cases reported in the literature from 1975 to 1987 (all patients were 15 years old or older) and four newly diagnosed cases. The mean age of patients was 30 years; 80% were less than 35 years old. Each patient presented with a large, rapidly growing, abdominal mass (average duration of symptoms, <2 months), had no constitutional symptoms (e.g., weight loss, fever), and otherwise were healthy (80%). Twenty-six patients had IV or retrograde pyelograms. Twenty-three showed a nonspecific mass effect. In seven (78%) of nine patients, abdominal CT scans showed a large, inhomogeneous mass with large areas of low density and increased enhancement of the compressed remaining normal renal parenchyma, which resembled a pseudocapsule. In five (63%) of eight patients, sonograms showed a complex mass with large cystic components. In 18 (82%) of 22 patients, arteriograms showed a hypovascular mass with fine wavy or zigzag (creeping-vine) neovascularity.

We conclude that a rapidly growing renal mass in a young patient (<35 years old) that is shown to be complex and cystic by CT or sonography and that is hypovascular with fine, wavy neovascularity on arteriography is suggestive of adult Wilms tumor (75–80%). An awareness of this constellation of findings may be helpful in diagnosing this unusual tumor before surgery.

Wilms tumor (nephroblastoma) in adults is rare and represents 0.5% of all renal neoplasms [1]. Nephroblastoma is only one of 53 synonyms for this tumor. The number of cases reported in the literature is difficult to determine owing to controversy over the pathologic diagnosis. There is also uncertainty about whether all the reported cases actually represent adult Wilms tumors or whether they are sarcomatoid renal carcinomas instead [2].

Kilton et al. [3] compiled the following criteria for the diagnosis of adult Wilms tumor: (1) presence of a primary renal neoplasm, (2) presence of a primitive blastematos spindle or round-cell component, (3) formation of abortive or embryonal tubular or glomeruloid structures, (4) absence of tumor diagnostic of renal cell carcinoma, and (5) age over 15 years.

Previous papers have reported that adult Wilms tumor cannot be recognized specifically before surgery. To identify clinical and radiologic findings that might suggest the diagnosis of adult Wilms tumor before surgery, we reviewed the cases reported in the literature and our four new cases.

Materials and Methods

We reviewed all 29 cases of adult Wilms tumor reported in the literature from 1975 to 1987 [1–14]. Also, a computer search of the pathologic records at multiple medical centers (Olive View, UCLA, Harbor/UCLA, LA County/USC Medical Center, and Burns Clinic Medical Center) identified four new cases of adult Wilms tumor. These 33 cases were reviewed by a

Received August 30, 1988; accepted after revision October 3, 1988.

¹ Department of Radiology, Olive View Medical Center, 14445 Olive View Dr., Sylmar, CA 91342. Address reprint requests to F. Kioumehri.

² Department of Radiology, UCLA School of Medicine, 10833 Le Conte Ave., Los Angeles, CA 90024.

³ Department of Pathology, UCLA School of Medicine, Los Angeles, CA 90024.

⁴ Department of Radiology, Burns Clinic Medical Center P.C., 560 W. Mitchell Ave., Petoskey, MI 49770.

AJR 152:299–302, February 1989
0361–803X/89/1522–0299
© American Roentgen Ray Society

pathologist to confirm that they were indeed adult Wilms tumor. Of these cases, 26 (79%) had IV or retrograde pyelograms, nine (27%) had abdominal CT scans, eight (24%) had sonograms, and 23 (70%) had angiograms.

The clinical data that were collected included the patient's age and sex, side of tumor, type and duration of symptoms, record of weight loss, and presence of hematuria and metastasis. Radiologic data included appearance of tumor on IV or retrograde pyelography, abdominal CT, sonography, or angiography.

Four new cases were analyzed. Two of these are illustrated in Figures 1 and 2. The third patient was a 15-year-old girl who pre-

sented to the UCLA Medical Center with a large, nontender, rapidly growing, left-sided abdominal mass. There was no weight loss or hematuria. An abdominal CT scan showed a large, inhomogeneous mass with cystic and solid components, arising from the left kidney. A renal arteriogram showed a hypovascular mass with a few small, irregular vessels extending into the mass. No filling defect was seen on the inferior venacavogram. The fourth patient was a 68-year-old man in whom a right lower-pole renal mass was identified incidentally on IV pyelography. Sonography showed a complex, solid mass. The mass was hypovascular on renal arteriography. Normal renal arteries were stretched around the mass, which had a fine neovascularity.

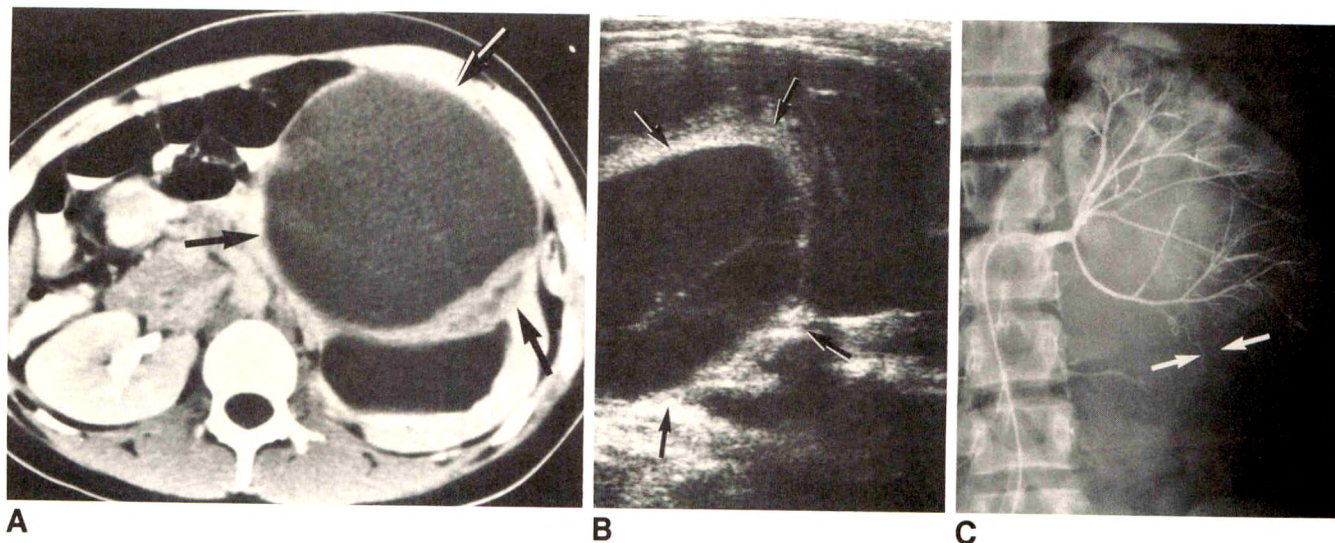


Fig. 1.—18-year-old woman with a rapidly growing abdominal mass. There was no weight loss or hematuria.

A, Enhanced abdominal CT scan shows a large, inhomogeneous, exophytic mass arising from left kidney and extending to anterior abdominal wall; there is a huge cystic component anteriorly and a dilated calyx posteriorly. Cystic component is denser than fluid in calyx. Solid component shows less enhancement than that seen in normal parenchyma (pseudocapsule) (arrows).

B, Sonogram shows a large, complex, mostly cystic mass with septation involving lower pole of kidney (arrows) and a dilated upper-pole calyx.

C, Selective left renal arteriogram shows a hypovascular mass arising from lower pole of kidney and some neovascularity extending into tumor (arrows). No clot was seen on an inferior venacavogram (not shown).

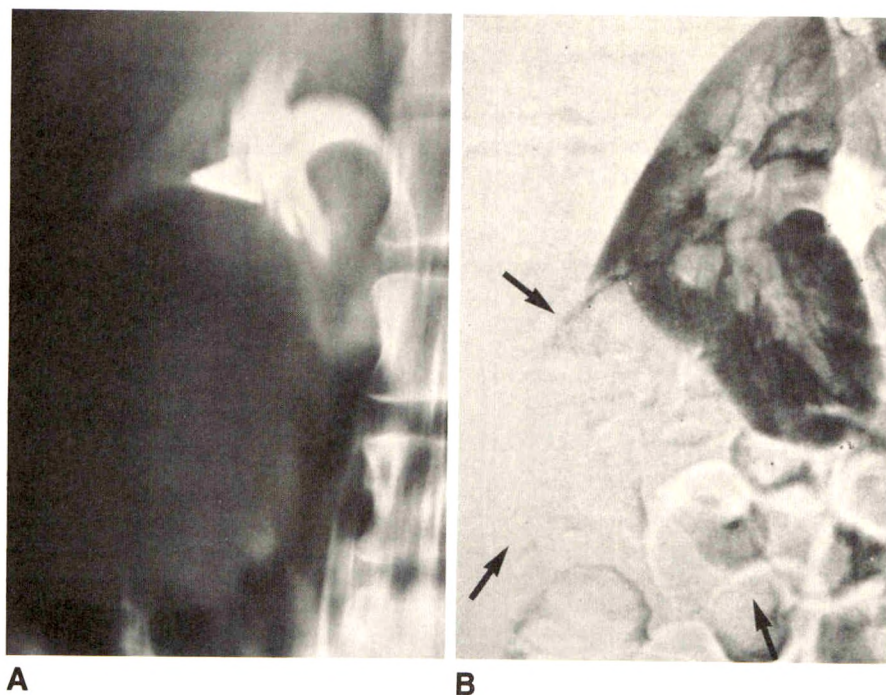


Fig. 2.—18-year-old woman with an enlarging right lower quadrant mass.

A, IV pyelogram shows a large, radiolucent mass in right lower pole. Cyst puncture revealed clear, light amber fluid. Wall of cyst was smooth on contrast examination. However, malignant cells were found on cytologic examination.

B, Arteriogram shows an avascular mass with no tumor vessels (arrows).

No tumor thrombus was seen on inferior venacavography. The metastatic workup was negative.

Results

Clinical Findings

Twenty-six (79%) of the 33 patients reviewed were 35 years old or younger (average age, 30; range, 15–84). There were 17 women and 16 men. In 18 patients, the tumor was in the right kidney; in 15 patients, it was in the left kidney. In 10 (59%) of the 17 women, the tumor was on the left side; in 11 (69%) of the 16 men, the tumor was on the right side.

Symptoms included abdominal pain of short duration related to a rapidly growing abdominal mass. Pain in the abdomen, flank, or back was noted in 22 (88%) of 25 cases and was not present in three cases (12%). (Data were not available in eight [24%] of 33 cases.) A palpable abdominal mass or abdominal fullness was present in 19 (79%) of 24 cases and was absent in five cases (21%). (No data were available in nine [27%] of 33 cases.) Duration of symptoms ranged from 1 day to 8 months. In 17 (71%) of 24 patients, the symptoms lasted 3 months or less. Six patients presented with weight loss. Hematuria was present in 15 (58%) of 26 patients and was absent in 11 patients (42%). (In seven of 33 [21%] cases, no data were available.)

Nine (28%) of 32 patients had metastases at the time of presentation. In one patient, no data were available. The most common locations were the lung and the liver.

Radiologic Findings

Twenty-six (79%) of 33 patients had an IV or retrograde pyelogram. In 23 (88%) of the 26 a mass was shown in the kidney. In two patients, these masses contained calcifications. Three patients had no kidney function on the side of the tumor. Two of these three patients had a clot in the inferior vena cava.

Nine (27%) of 33 patients had abdominal CT scans. In seven (78%) of the nine an inhomogeneous mass was seen with large areas of low density and less contrast enhancement than that seen in normal parenchyma; in these patients, the compressed normal renal parenchyma appeared as a pseudocapsule. In the other two patients, the masses were homogeneous on CT. Three patients showed no thrombus in the inferior vena cava, two showed thrombus, and in four no data were available. Para-aortic lymph nodes (one case), perinephric fat involvement (one case), and liver metastases (one case) also were shown by CT.

Eight (24%) of 33 patients had sonograms. Five (63%) of eight patients had a complex, largely cystic mass, with some solid components. The remaining three patients had a solid echogenic mass. Two sonograms showed venous thrombus.

Twenty-two (67%) of 33 patients had renal arteriograms. In 18 (82%) of these 22 patients masses were hypovascular; in two, masses were vascular; and in two, masses were hypervascular. The hypovascular masses contained fine zig-zag, wavy neovascularity that extended into the tumor.

Inferior venacavography were performed in nine (27%) of 33 patients. Six (67%) of the nine were negative, one was positive, and two were false positive.

Follow-up data were available in 18 patients in whom there was radiologic, surgical, or pathologic information about the renal vein and inferior vena cava. Metastases developed in five of six patients in whom the renal vein and/or inferior vena cava was positive for tumor thrombus (follow-up, 3 months to 2 years). Six of 12 patients in whom the renal vein and/or inferior vena cava was negative for tumor thrombus were free of disease during follow-up (10 months to 7½ years).

Pathologic Findings

Most of the tumors were large, solitary, unilateral masses that were well circumscribed grossly but not encapsulated. Areas of hemorrhage were described grossly in eight of 33 cases, and necrosis was found in 13 cases. Although radiologic imaging showed inferior vena caval involvement in eight cases, invasion was documented pathologically in three. In the 26 cases in which slides or adequate pathologic descriptions were available, no cases appeared to have true anaplasia as defined by the National Wilms' Tumor Study criteria. Also, no rhabdoid or clear cell variants were reported. Most cases appeared to be mixed blastemal and epithelial (13 cases) or blastemal predominant neoplasms (nine cases).

Discussion

Wilms tumor is a childhood neoplasm; in 85% of cases, it occurs before the patient is 6 years old. Only 1% of these tumors occur in patients older than 15 years. Two hundred cases have been reported in adults, but it is unclear whether all of these cases were adult Wilms tumors; some of them may have been sarcomatoid renal carcinomas or some other renal neoplasm [1, 2, 4]. The diagnostic criteria for Wilms tumor include the presence of abortive or embryonic glomerulotubular structures within an immature spindle-cell stroma. These structures are not found in renal cell carcinoma. Some renal cell carcinomas can have glandular elements and an abundance of sarcomatous or undifferentiated cells. These cases can be misinterpreted as Wilms tumors [2]. The absence of fetal renal tissue points against the diagnosis of Wilms tumor [5]. The most common location of nephrogenic blastema is the subcapsular portion of the renal cortex [15], which explains this neoplasm's common appearance as an exophytic mass. Microscopically, no difference exists between adult and childhood Wilms tumor. Both have epithelial, stromal, and blastemal elements [15].

Clinically, adult Wilms tumor usually presents in young patients as a large, rapidly growing abdominal mass, but the disease can be seen at any age; the oldest patient reported was 84 years old [7]. In our study as well as that of Byrd et al. [16], the mean age of patients was 30 years. This is in contrast to the study by Bailey et al. [7] in which patients presented between the fourth and sixth decades. Renal cell carcinoma occurs in an older population than does adult Wilms tumor. Women are affected more often than men [8, 15–17]. Renal cell carcinoma, however, is seen predominantly in men.

Usually the tumor is very large and is palpable, in contrast to renal cell carcinoma in which the tumors are generally

smaller and often are less palpable at the time of presentation.

IV pyelography showed a nonspecific mass effect or, on rare occasions, a nonfunctioning kidney. A horseshoe kidney was reported in one patient with adult Wilms [7]. One patient had a large, calcified mass [9]. Calcifications are rare in adult Wilms tumor but may be seen because of hemorrhage or necrosis within the lesion.

Although the number of cases studied by high-resolution CT is limited, the findings in adult Wilms tumor are characteristic. Abdominal CT shows a large, well-defined, exophytic, inhomogeneous mass that is cortical in origin. Large areas of low density are present without contrast enhancement. After IV contrast administration, the solid component shows variable enhancement, and the remaining normal parenchyma shows greater enhancement; the normal parenchyma appears as a pseudocapsule around the tumors (75%). Nonenhancing areas representing foci of necrosis and hemorrhage are common. These findings are similar to those in childhood Wilms tumor [8, 15]. Renal cell carcinoma generally presents as a smaller, infiltrative tumor when compared with Wilms tumor [17].

Sonographic studies of adult Wilms tumor typically show a large, complex mass with large cystic components. This is in contrast to renal cell carcinoma, which usually is a solid mass [1, 17, 18]. The sonographic pattern is identical to childhood Wilms; however, in the adult, the mass tends to be much larger [1].

Angiograms in the reviewed cases of adult Wilms tumor showed a hypovascular mass with neovascularity extending to the tumor with a "spaghetti pattern" or "creeping-vine" appearance. In the study by Hartman et al. [17], a comparison was made between Wilms tumor and renal cell carcinoma in patients in the second decade of life. Seven (87%) of eight cases of Wilms tumor showed hypo- to moderate vascularity without arteriovenous shunting, but eight of 10 cases of renal cell carcinoma showed a moderate to hypervascular mass with arteriovenous shunting. In a study of Wilms tumor in children [15], angiographic findings were described as "poor vascularity with some neoformation of vessels, having a fine wavy or zig-zag pattern." This is similar to our angiographic findings in adult Wilms tumor.

Although invasion of the renal vein and inferior vena cava are not used as part of the staging classification, patients with involvement of the vein had a much poorer outcome than those without involvement and also had high stages of tumors. In this study, 83% of patients with tumor involvement in the renal vein or inferior vena cava developed metastases, whereas 50% of patients with no venous involvement were free of disease at follow-up. The rate of venous involvement seems to be similar to renal cell carcinoma so that this observation is not a useful differential point.

By evaluating the clinical and radiologic presentation of 33 patients with adult Wilms tumor, we conclude that 75–80% of patients have characteristic clinical and/or radiologic findings that may be useful in suggesting the diagnosis before surgery. The presence of a large, rapidly growing abdominal

mass in an otherwise healthy young patient that shows as a complex mass on sonography and as an inhomogeneous mass with variable enhancement and pseudocapsule on CT is highly suggestive of Wilms tumor. Hypovascularity of the mass on arteriography with a few zigzag lines of neovascularity extending to the mass is also characteristic. This is in contrast to renal carcinoma, which usually is solid and smaller than Wilms tumor, is hypervascular and has arteriovenous shunting on arteriography, occurs at an older age, and involves more constitutional symptoms. Multilocular cystic nephroma should also be considered in the differential diagnosis. This benign renal tumor, which is seen more frequently in children, also can occur in adults (predominantly women). The tumor is well encapsulated and contains numerous noncommunicating cysts. Occasionally, calcifications are present and the tumor is hypovascular on arteriography.

ACKNOWLEDGMENTS

We thank Paul Dickman for providing the UCLA/Harbor case, Howard Mindell for bringing a new case to our attention, and Sharon Simpson and Cynthia Shirley for editing and typing the manuscript.

REFERENCES

1. Kumar R, Amparo EG, David R, Fagan CJ, Moretti LB. Adult Wilms' tumor: clinical and radiographic features. *Urol Radiol* 1984;6:164–169
2. Babaian RJ, Skinner G, Waisman J. Wilms' tumor in the adult patient: diagnosis, management and review of the world medical literature. *Cancer* 1980;45:1713–1719
3. Kilton L, Matthews MJ, Cohen MH. Adult Wilms tumor: report of prolonged survival and review of literature. *J Urol* 1980;124:1–5
4. Roth DR, Wright J, Cawood CD, Pranke DW. Nephroblastoma in adults. *J Urol* 1984;132:108–110
5. Vorstman B, Rothwell D. Wilms tumor in adult patient. *Urology* 1982;20:628–630
6. Denes FT, Nahas WC, Alfer V. Adult Wilms' tumor. *Urology* 1982;19:187–189
7. Bailey LE, Durkee CT, Werner AL, Finley RK Jr. Wilms tumors in adults. *Am Surg* 1987;53:149–155
8. Fishman EK, Hartman DS, Goldman SM, Siegelman SS. The CT appearance of Wilms tumor. *J Comput Assist Tomogr* 1983;7:659–665
9. Merten DF, Yang SS, Bernstein J. Wilms tumor in adolescence. *Cancer* 1976;37:1532–1538
10. Bard RH, Greenwald ES, Kalnicki S, Sablay LB. Adult Wilms tumor treated with radiotherapy and chemotherapy: a case report. *J Urol* 1979;121:679–680
11. Greco A, Perry MC. Wilms' tumor in an adult. *South Med J* 1981;74:622–624
12. Chung TS, Reyes CV, Stefani SS. Wilms tumor in adults. *Urology* 1984;24:275–277
13. Hagiwara M, Tachibana M, Jitsukawa S, et al. Multimodal treatment of advanced adult Wilms tumor. *J Urol* 1982;127:535–538
14. Morrison IS. The ultrasonic and angiographic appearances of Wilms tumors in adults. *Australas Radiol* 1985;29:345–348
15. Bennington JL, Beckwith JB. *Tumors of the kidney, renal pelvis and ureter*. Washington, DC: Armed Forces Institute of Pathology, 1975:31–81
16. Byrd RL, Evans AE, D'Angio GJ. Adult Wilms tumor: effect of combined therapy on survival. *J Urol* 1982;127:648–651
17. Hartman DS, Davis CJ Jr, Madewell JE, Friedman AC. Primary malignant renal tumors in the second decade of life: Wilms tumor versus renal cell carcinoma. *J Urol* 1982;127:888–891
18. Chan HSL, Daneman A, Gribbin M, Martin DJ. Renal cell carcinoma in the first two decades of life. *Pediatr Radiol* 1983;13:324–328

Percutaneous, Large-Bore, Suprapubic Cystostomy: Technique and Results

Nicholas Papanicolaou¹
Richard C. Pfister¹
Barry N. Nocks²

A technique to insert large-bore suprapubic cystostomy catheters (18-French or larger) percutaneously, under radiologic imaging guidance, is described in 15 men who required long-term drainage of the bladder. This single-stage procedure is carried out under local anesthesia with optional IV sedation. It consists of rapid enlargement of the percutaneous track by means of a balloon dilatation catheter followed by insertion of a self-retaining Foley cystostomy catheter through a peel-away sheath. No complications associated with the placement of the catheters occurred, and long-term patient compliance has been satisfactory.

Our results suggest that percutaneous, large-bore suprapubic cystostomy may be a preferred alternative to surgical cystostomy.

Percutaneous suprapubic cystostomy has long been used for the treatment of acute urinary retention, regardless of cause, when standard urethral catheterization of the bladder is either impossible or contraindicated [1-4]. The placement of a small-diameter trocar suprapubic catheter is quick and safe and requires only local anesthesia. Although effective in urgent situations, this cystostomy system is not suitable for long-term drainage of the bladder, primarily because of the small lumen of the catheter and the sutures required for securing it.

Surgical placement of large cystostomy catheters (20- to 30-French) usually requires hospitalization, spinal or general anesthesia, and an open procedure [5]; their use in high-risk anesthesia patients cannot be advocated. Because of these shortcomings, we inserted large-bore cystostomy catheters percutaneously in 15 patients in whom long-term bladder drainage was necessary. The technique, complications, and long-term compliance were reviewed to establish the safety and effectiveness of the procedure.

Materials and Methods

Between February 1987 and July 1988, we inserted percutaneously large-diameter suprapubic cystostomy catheters (18 French or larger) in 15 men (31-95 years old (median age, 69). Eight patients had a combination of neurogenic bladder (CNS disorders, cerebrovascular disease, or spinal cord injury) and mechanical obstruction of the bladder outlet (enlarged prostate). Three patients had radiation cystitis with refractory bladder spasms. In two, severe urethral trauma had been caused by motor vehicle accidents. One had multiple urethral strictures and severe coronary artery disease, and one developed pyocystitis of his defunctionalized bladder. Urodynamic assessment of neuromuscular function of the bladder and sphincter and voiding cystography were performed in all patients except the two patients with urethral trauma and the patient with pyocystitis. Intermittent catheterization of the bladder or placement of an indwelling catheter was deemed inapplicable in these rehabilitation patients, as were sphincterotomy and continuous penile condom drainage. With the exception of the two trauma cases, the remaining 13 patients were poor surgical and anesthesia risks. In three patients, percutaneous insertion of a suprapubic catheter without imaging guidance was unsuccessful.

Received August 30, 1988; accepted after revision October 6, 1988.

Presented at the annual meeting of the American Roentgen Ray Society, San Francisco, CA, May 1988.

¹Department of Radiology, Division of Uroradiology, Massachusetts General Hospital, and Department of Radiology, Harvard Medical School, Boston, MA 02114. Address reprint requests to N. Papanicolaou, Dept. of Radiology, Massachusetts General Hospital, Boston, MA 02114.

²Urological Service, Massachusetts General Hospital, and Department of Surgery, Harvard Medical School, Boston, MA 02114.

AJR 152:303-306, February 1989
0361-803X/89/1522-0303

© American Roentgen Ray Society



The procedure was performed with the patient under local anesthesia (Fig. 1). In addition, IV sedation and analgesia (morphine sulfate, meperidine hydrochloride, midazolam, diazepam, or fentanyl) were used in 10 patients. Under fluoroscopy, the urinary bladder was opacified and distended via a suprapubic 20-gauge needle or a transurethral catheter (Fig. 1). In most cases, 300–400 ml of dilute contrast material (allowing visualization of the guidewire in the bladder) displaced bowel loops away from the needle path and provided direct visualization of the bladder for subsequent insertion of the cystostomy catheter. A paramedian oblique approach above the symphysis pubis and a 19-gauge needle-sheath system were used to enter the anterior bladder wall (Fig. 2A). On aspiration of urine, the needle was exchanged for a 0.97-mm (0.038-in.) torque guidewire, which was coiled into the bladder. The skin opening at the site of the puncture was widened, and a balloon dilatation catheter (8–10 mm [24–30 French] in diameter and 10 cm long) was inserted over the wire. The percutaneous track was then rapidly dilated for 3–4 min (Fig. 2B). In seven cases, further dilatation of focal areas of persisting narrowing was performed by using rigid fascial dilators before the track could easily accommodate the peel-away sheath. The peel-away sheath-dilator system (38-PFISTER-B-021583, Cook, Inc., Bloomington, IN) was then inserted over the guidewire into the bladder (Fig. 2C). The size of the sheath selected was 2 French sizes larger than the cystostomy catheter to be placed. The dilator was then removed, and a 5-ml Foley catheter balloon, with an end hole or removed tip, was inserted over the guidewire into the vesical lumen (Fig. 2D). The catheter balloon was inflated once satisfactory position of the tube was confirmed. The peel-away sheath was then removed, the retention balloon was pulled snug against the anterior bladder wall, and the catheter was put to drainage (Fig. 1). A sterile dressing

was applied around the catheter entry site. We did not suture the catheter to the skin, because the retention balloon effectively secured good position and comfortable wear. Within 4–6 weeks after cystostomy, the percutaneous track was mature enough to allow easy replacement of the catheter by the urologist in the office.

Results

All attempts at catheter placement with the use of radiologic imaging under local anesthesia were successful. No immediate complications have occurred after large-bore suprapubic cystostomy. The catheters have been tolerated well, and their care and function have been satisfactory for periods up to 1.5 years (minimum, 3 weeks; mean, 9 months). Both trauma patients and the patient with pyocystitis had their suprapubic drainage discontinued 2–3 months after recovery of the urethral injuries and sterilization of the bladder, respectively. After removal of the catheter, the percutaneous tracks closed promptly within 2–3 days. One patient with malignant melanoma and neurogenic bladder died of metastases 3 weeks after placement of the catheter. Two of the 11 long-term cystostomies were complicated transiently by urinary tract infections, which were controlled with oral trimethoprim-sulfamethoxazole. All 11 remaining patients have been maintained on suprapubic cystostomy drainage, oral antimicrobial prophylaxis, and catheter changes every 3 months.

Discussion

Long-term drainage of the urinary bladder has been accomplished by various methods, including an indwelling catheter, intermittent catheterization, transurethral sphincterotomy with continuous condom drainage, and suprapubic cystostomy [2, 6–8]. The choice of management depends on the type of neurogenic bladder, the presence of obstruction of the bladder outlet, age and medical condition of the patient, and expected compliance and care after discharge from the hospital. Among the catheter methods, the suprapubic one is best tolerated by patients who are physically unable or psychologically unwilling to catheterize themselves. In men, intermittent catheterization is an uncomfortable procedure, especially in the presence of urethral strictures or prostatic enlargement; it is ideally suited to patients who do not have mechanical obstruction. Also, in certain long-term chronic care facilities intermittent catheterization often is not a viable option.

The percutaneous trocar method of suprapubic cystostomy via 8- or 12-French Silastic catheters has been useful for the short-term treatment of urinary retention of any cause and for temporary urinary diversion at any age. For long-term management, however, a larger-bore catheter to facilitate irrigation and drainage is desirable. For this purpose, Ingram [9] described a stylet-trocar cystostomy system accommodating 12- and 16-French catheters, which he successfully used in 86 gynecologic patients.

The surgical placement of a large cystostomy tube is a simple procedure technically; however, it carries with it the

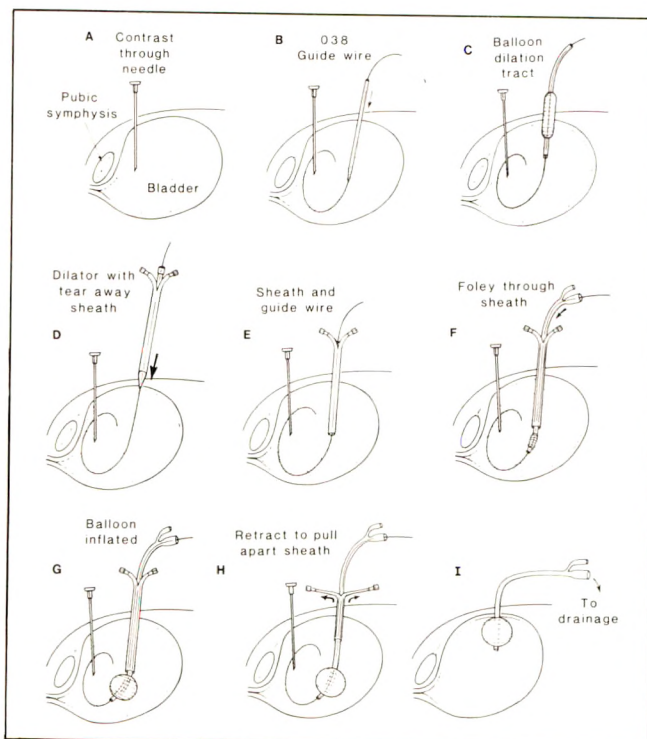


Fig. 1.—Successive steps (A–I) in percutaneous placement of large Foley catheter for suprapubic cystostomy.

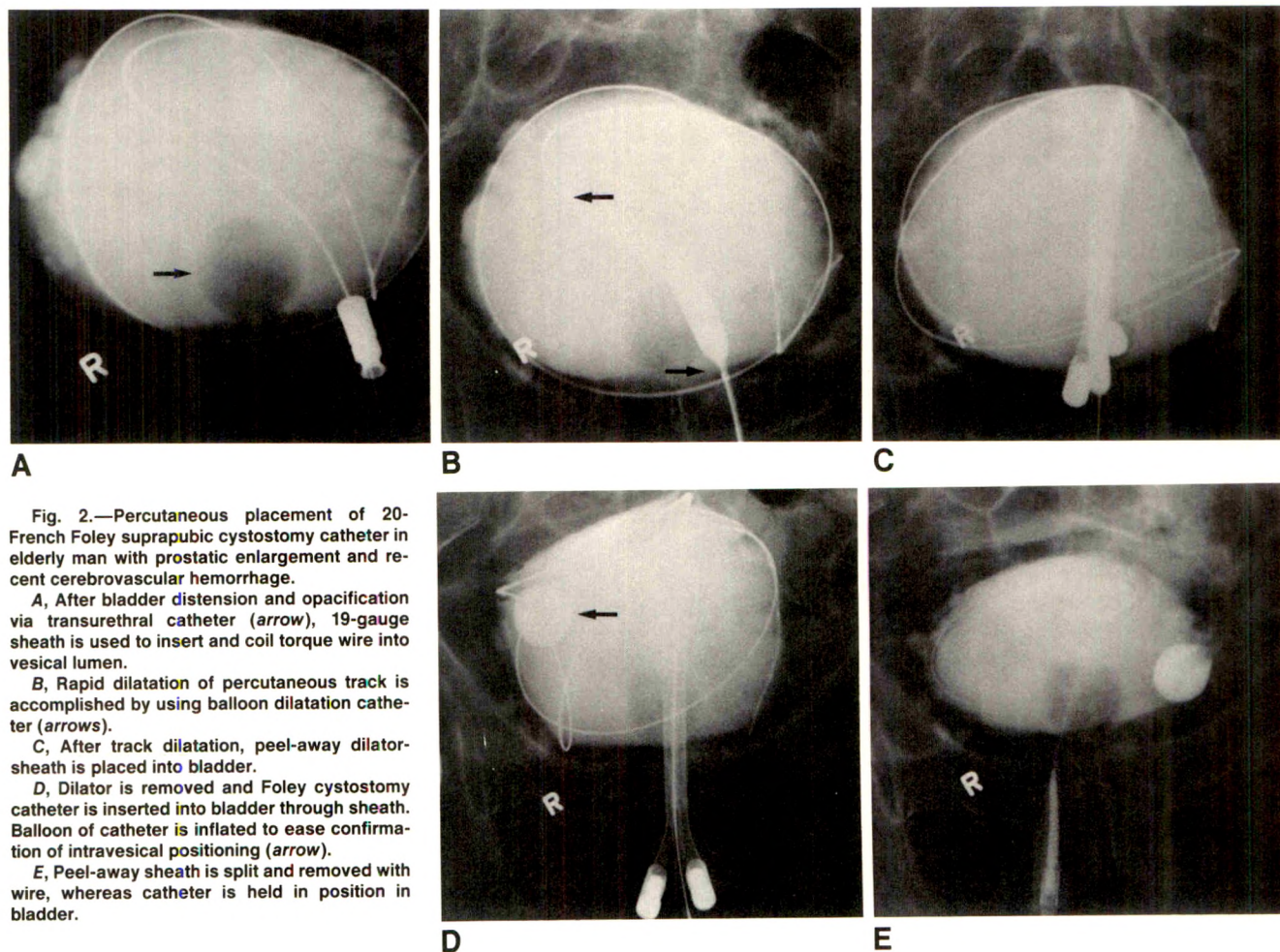


Fig. 2.—Percutaneous placement of 20-French Foley suprapubic cystostomy catheter in elderly man with prostatic enlargement and recent cerebrovascular hemorrhage.

A, After bladder distension and opacification via transurethral catheter (arrow), 19-gauge sheath is used to insert and coil torque wire into vesical lumen.

B, Rapid dilatation of percutaneous track is accomplished by using balloon dilatation catheter (arrows).

C, After track dilatation, peel-away dilator-sheath is placed into bladder.

D, Dilator is removed and Foley cystostomy catheter is inserted into bladder through sheath. Balloon of catheter is inflated to ease confirmation of intravesical positioning (arrow).

E, Peel-away sheath is split and removed with wire, whereas catheter is held in position in bladder.

risks and expense of anesthesia, open surgery, and hospitalization. Therefore, percutaneous placement of a similar-size tube is advantageous and was performed as an outpatient procedure in two of our cases.

The procedure was safely performed with imaging guidance in all patients, including three patients in whom blind placement of a suprapubic cystostomy catheter by others had failed. The technique is applicable to both men and women. Men are more likely to undergo the procedure because of anatomic considerations, such as longer urethra and presence of the prostate, which are often associated with bladder outlet obstruction. Fluoroscopy is of great aid in selecting the site of entrance into the bladder (junction of mid and lower third) and final placement of the catheter; the area of the trigone should be spared trauma and irritation to avoid bladder spasms. Skin infection is circumvented by securing the catheter with simple intravesical balloon inflation and omitting sutures.

Catheters that were 18 French or larger provided satisfactory drainage. Although a peel-away sheath 2 French sizes larger than the cystostomy catheter is usually appropriate, sheath and catheter should be matched with each other before placement. Imprecise size labeling and manufacturing

variations in the size of the deflated balloon on the Foley catheter shaft may result in a mismatch; a 4-French difference may then be required for successful placement.

Potential complications after suprapubic cystostomy placement include perivesical hemorrhage, hematuria, transgression of bowel loops, perforation of the bladder, catheter fragmentation resulting in an intravesical foreign body, and catheter malfunction [1, 10, 11]. Hematuria is always present, but usually is transient and insignificant. By distending the bladder during placement of the cystostomy catheter, adjacent bowel loops are displaced superiorly or laterally and are less likely to be injured. The concomitant use of sonography should further ensure that bowel loops have indeed been displaced, thus making the procedure safer. Bladder distension also makes through-and-through perforation of the bladder unlikely, because the opposing vesical walls are widely separated.

Both infection and stone formation have been associated with long-standing bladder catheters, including those used for suprapubic cystostomy [6–8, 12–14]. In addition, patients who have indwelling urethral catheters or who are on intermittent catheterization may develop urethral strictures. The suprapubic type is less likely to cause infection than is the

indwelling urethral catheter and it also compares favorably with intermittent catheterization [7, 13].

In summary, our experience indicates that percutaneous placement of a large-bore suprapubic cystostomy catheter under the guidance of radiologic imaging is a single-stage, safe, and well-tolerated procedure for patients requiring long-term drainage of the urinary bladder.

REFERENCES

- Hodgkinson CP, Hodari AA. Trocar suprapubic cystostomy for postoperative bladder drainage in the female. *Am J Obstet Gynecol* **1966**;96:773-781
- Cook JB, Smith PH. Percutaneous suprapubic cystostomy after spinal cord injury. *Br J Urol* **1976**;48:119-121
- Morehouse DD. Emergency management of urethral trauma. *Urol Clin North Am* **1982**;9:251-254
- Retik AB, Perlmutter AD. Temporary urinary diversion in infants and young children. In: Walsh PC, Gittes RF, Perlmutter AD, Stamey TA, eds. *Campbell's urology*, 5th ed. Philadelphia: Saunders, **1986**:2116-2136
- Lieber MM, Utz DC. Open bladder surgery. In: Walsh PC, Gittes RF, Perlmutter AD, Stamey TA, eds. *Campbell's urology*, 5th ed. Philadelphia: Saunders, **1986**:2640-2641
- Perkash I. Problems with decatheterization in long-term spinal cord injury patients. *J Urol* **1980**;124:249-253
- Noll F, Russe O, Kling E, Botel U, Schreiter F. Intermittent catheterisation versus percutaneous suprapubic cystostomy in the early management of traumatic spinal cord lesions. *Paraplegia* **1988**;26:4-9
- Anderson RU. Urinary tract infections in spinal cord injury patients. In: Walsh PC, Gittes RF, Perlmutter AD, Stamey TA, eds. *Campbell's urology*, 5th ed. Philadelphia: Saunders, **1986**:888-899
- Ingram JM. Suprapubic cystostomy by trocar catheter: a preliminary report. *Am J Obstet Gynecol* **1972**;113:1108-1112
- Noller KL, Pratt JH, Symmonds RE. Bowel perforation with suprapubic cystostomy: report of two cases. *Obstet Gynecol* **1970**;48[suppl]:67-69.
- Frymire LJ. Comparison of suprapubic versus Foley drains. *Obstet Gynecol* **1971**;38:239-244
- Donovan WH, Stolov WC, Clowers DE, Clowers MR. Bacteriuria during intermittent catheterization following spinal cord injury. *Arch Phys Med Rehabil* **1978**;59:351-357
- Schaeffer AJ. Catheter-associated bacteriuria. *Urol Clin North Am* **1986**;13:735-747
- Donovan WH, Kiriak MD, Clowers DE. Intermittent bladder emptying via urethral catheterization of suprapubic cystocath: a comparison study. *Arch Phys Med Rehabil* **1977**;58:291-296

Case Report

Renal Lymphangiomyoma—A Rare Cause of a Multiloculated Renal Mass

Jill E. Jacobs,¹ Steven K. Sussman, and Marc F. Glickstein

We report a case of renal lymphangiomyoma that presented as a multiloculated renal mass on both CT and sonography. Lymphangiomyomas are rare lesions that arise from the proliferation of smooth muscle in the walls of lymphatics [1–4]. Lymphangiomyomas usually occur in lymphangiomyomatosis syndrome when there is associated characteristic pulmonary involvement. However, they can occur without associated thoracic disease, and in such cases, they usually involve retroperitoneal lymph nodes [2]. We are unaware of any previous reports of lymphangiomyoma presenting as a renal mass.

Case Report

During routine physical examination, a 79-year-old man was found to have right-sided abdominal fullness, heme-positive stools, and anemia. A barium enema showed a cecal mass, but a soft-tissue mass also was found in the right renal fossa. An abdominal sonogram revealed that most of the renal parenchyma on the right was replaced by a multiloculated cystic mass (Fig. 1A). The left kidney appeared normal. Contrast-enhanced CT showed a small residuum of functioning renal parenchyma and a large, predominately cystic multiloculated mass with thin septa (Fig. 1B). A diagnosis of multilocular cystic nephroma was suggested. A right nephrectomy and right hemicolectomy were performed. A carcinoma of the colon was found. The kidney measured 19 × 11 × 9 cm and weighed 1400 g. A small portion of preserved renal parenchyma was noted along the inferior aspect of the hilum, but the remainder of the parenchyma was composed of multiple fluid-filled cystlike spaces (Fig. 1C). Tubular epithelium lined the septa between the cysts. In addition, prominent smooth muscle within the septa indicated a significant muscle com-

ponent to the lesion. The final histologic diagnosis was renal lymphangiomyoma.

Discussion

Lymphangiomyomas are rare lesions that arise from the proliferation of smooth muscle in the walls of lymphatics [1–4]. More than half of the reported cases of lymphangiomyomas occur in lymphangiomyomatosis syndrome when the syndrome is associated with characteristic smooth-muscle proliferation along pulmonary lymphatic channels, producing honeycombing, chylous effusions, and spontaneous pneumothoraces [4]. Lymphangiomyomas can occur without pulmonary involvement, with most reported cases involving retroperitoneal lymph node chains, usually in a multifocal distribution [2]. Lymphangiomyomas, whether occurring with or without the associated pulmonary syndrome, have been reported exclusively in women [1–4]. Because patients with tuberous sclerosis have pulmonary and lymph node involvement identical to that reported in lymphangiomyomatosis, it is thought that lymphangiomyomatosis may be a "forme-fruste" of tuberous sclerosis [5, 6]. Although certain renal masses (i.e., renal angioliipomas) have been associated with both tuberous sclerosis and lymphangiomyomatosis syndrome [6], renal lymphangiomyomas have not been described. Remancik et al. [7] described a renal mass in a patient with lymphangiomyomatosis that had soft-tissue density on CT, without evidence of fat. Based on the associated angiographic findings of multiple small aneurysms, the diag-

Received June 20, 1988; accepted July 8, 1988.

¹ All authors: Department of Radiology, Hartford Hospital, 80 Seymour St., Hartford, CT 06106. Address reprint requests to J. E. Jacobs.

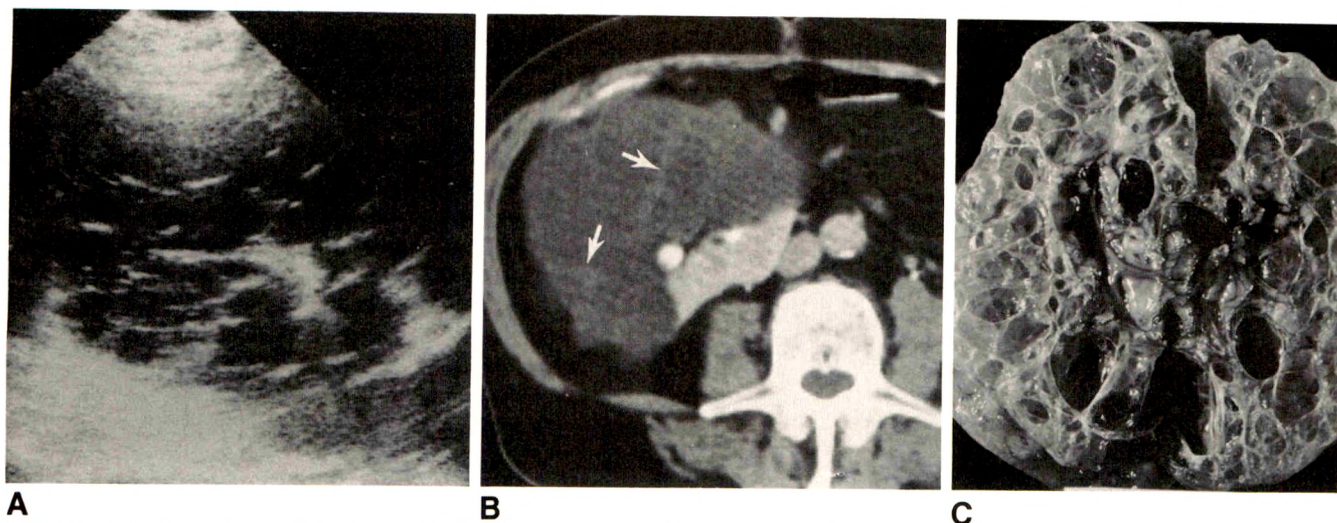


Fig. 1.—**A**, Sagittal renal sonogram shows multiple clustered cystic masses with echogenic septa replacing normal renal parenchyma.
B, Contrast-enhanced CT shows a fluid-density renal mass with only a few functioning renal parenchyma. Multiple septa (arrows) are present but not as clearly visible as with sonography.
C, The kidney is largely replaced by multiple fluid-filled cystlike spaces. Septa between cysts were lined with tubular epithelium and contained prominent smooth muscle.

nosis of a renal hamartoma (presumably angiomyoma) was suggested.

Our case is unique in a number of ways. To our knowledge, neither lymphangioma nor lymphangiomyomatosis syndrome has been reported in a man. In addition, aside from a single report of lymphangiomyoma occurring in the adrenal gland [4], no other reports discuss lymphangiomyomas in a solitary organ outside of the lymphatic system.

A myriad of causes can result in the radiologic appearance of a multiloculated renal mass. This diverse group of entities has been reviewed recently by Hartman et al. [8]. The main diagnostic considerations in a middle-aged adult include multilocular cystic nephroma, renal cell carcinoma, localized renal cystic disease, and echinococcal cyst. In middle-aged patients, multilocular cystic nephroma usually occurs in women. Herniation of the multilocular mass into the renal pelvis is a finding that may suggest this type of nephroma [8]. Approximately 5% of cases of renal cell carcinoma may have a multilocular appearance, but features such as intravascular extension, metastases, and associated solid areas in the tumor mass help to suggest this diagnosis [8]. The mass in localized renal cystic disease usually has an ill-defined, poorly demarcated appearance because there is no capsule. Other simple cysts are often seen in the adjacent parenchyma [8].

Hydatid disease often has associated hepatic lesions, daughter cysts, and hydatid sand, which may layer dependently in the cystic mass [8].

REFERENCES

1. Cornog JL, Enterline HT. Lymphangiomyoma, a benign lesion of chyliferous lymphatics synonymous with lymphangiopericytoma. *Cancer* 1966;19:1909-1930
2. Wolff M. Lymphangiomyoma: clinicopathologic study and ultrastructural confirmation of its histogenesis. *Cancer* 1973;31:988-1007
3. Joliat G, Stalder H, Kapanci Y. Lymphangiomyomatosis: a clinico-anatomical entity. *Cancer* 1973;31:455-461
4. Carrington CB, Cugell DW, Gaensler EA, et al. Lymphangiomyomatosis: physiologic-pathologic-radiologic correlations. *Am Rev Respir Dis* 1977;116:977-995
5. Jao J, Gilbert S, Messer R. Lymphangiomyoma and tuberous sclerosis. *Cancer* 1972;25:1188-1192
6. Monteforte WJ, Kohnen PW. Angiomyolipomas in a case of lymphangiomyomatosis syndrome: relationships to tuberous sclerosis. *Cancer* 1974;34:317-321
7. Rumancik WM, Bosniak MA, Rosen RJ, Hulnick D. Atypical renal and pararenal hamartomas associated with lymphangiomyomatosis. *AJR* 1984;142:971-972
8. Hartman DS, Davis CJ, Sanders RC, Johns TT, Smirniotopoulos J, Goldman SM. The multiloculated renal mass: considerations and differential features. *RadioGraphics* 1987;7:29-52

Anticoagulant Effects of Contrast Materials: In Vitro Study of Iohexol, Ioxaglate, and Diatrizoate

Pasteur Rasuli¹
William A. McLeish²
D. Ian Hammond¹

It has been reported that clot formation may occur when blood is mixed directly with nonionic contrast medium in a syringe during angiography. To investigate this possibility, we performed three in vitro experiments to determine the anticoagulant properties of a low-osmolar, nonionic contrast medium (iohexol); a low-osmolar, ionic medium (ioxaglate); and a high-osmolar, ionic medium (diatrizoate). In the first experiment, human arterial blood was incubated at room temperature in an angiographic syringe with each of the three media for 60 min, after which the mixture was filtered for clots. In the second experiment, the clotting times of venous blood in heparinized saline or serial dilutions of the three agents were determined. In the third experiment, the partial thromboplastin time of platelet-poor plasma in heparinized saline or serial dilutions of the three agents was measured. No clots were observed in any of the arterial blood samples. Iohexol prolonged the normal 15-min clotting time of venous blood to 160 min, compared with a clotting time of at least 330 min for ioxaglate and diatrizoate. Iohexol prolonged the normal 36-sec partial thromboplastin time of platelet-poor plasma to 40 sec, compared with 50 sec for diatrizoate and 54 sec for ioxaglate.

Our data show that iohexol, like ioxaglate and diatrizoate, inhibits clot formation when mixed with blood in a syringe. It prolongs the clotting time to approximately the same degree as 600 U/l of heparinized saline, but to a lesser degree than the other two media. All three media have a minimal effect on the partial thromboplastin time. Our results do not show any risk of clot formation in the usual clinical setting in which there is inadvertent mixing of blood with iohexol, ioxaglate, or diatrizoate in an angiographic syringe.

Clot formation has been reported in blood mixed with a nonionic contrast medium in a plastic syringe [1] and has been attributed to the reduced anticoagulant effect of the nonionic media compared with that of the conventional contrast media. Because a small amount of blood might be mixed inadvertently with contrast material in the angiographic syringe housed in a power injector, we decided to test the relative anticoagulant properties of a low-osmolar, nonionic medium (iohexol: Omnipaque 350, Winthrop Pharmaceuticals, Aurora, Ont.); a low-osmolar, ionic medium (ioxaglate: Hexabrix 350, Mallinckrodt Inc., Pointe Claire, Quebec); and a conventional high-osmolar, ionic contrast medium containing diatrizoate (Hypaque-M, 60%, Winthrop Pharmaceuticals, Aurora, Ont.).

One experiment was designed to recreate the clinical situation in which clotting might be a hazard owing to the inadvertent mixing of arterial blood with contrast medium in an angiographic syringe. We also designed two bench studies that used standard dilution-curve techniques to measure the anticoagulant properties of the three contrast media in whole blood and in platelet-poor plasma and to compare them with heparin, a known potent anticoagulant.

Materials and Methods

In the first experiment, 30 adult patients undergoing peripheral or abdominal arteriography were included in the study. No patient received anticoagulants or antiplatelet medication

Received July 20, 1988; accepted after revision September 22, 1988.

¹ Department of Radiology, Ottawa General Hospital, University of Ottawa, 501 Smyth Rd., Ottawa, Ontario K1H 8L6, Canada. Address reprint requests to P. Rasuli.

² Department of Laboratory Medicine, Ottawa General Hospital, University of Ottawa, Ottawa, Ontario K1H 8L6, Canada.

AJR 152:309-311, February 1989
0361-803X/89/1522-0309
© American Roentgen Ray Society

before angiography. After insertion of the catheter but before the injection of contrast material, 1 ml of arterial blood was drawn from the catheter into an angiographic syringe (Clear Vu, Liebel-Flarsheim, Cincinnati, OH) containing 49 ml of iohexol, ioxaglate, or diatrizoate. The syringe was left undisturbed at room temperature for 60 min. The syringe contents were then passed through a paper cloth (Chix, Johnson & Johnson, New Brunswick, NJ) to identify blood clots 0.1 mm or larger in diameter. Fine clumps of material were placed on a microscope slide, coverslipped, and examined microscopically.

In the second experiment, venous blood was obtained from a healthy volunteer, and the clotting times of the blood alone and the blood mixed with serial dilutions of heparin in saline or each of the three contrast materials in saline were determined. Dilutions of heparin in saline were prepared to yield concentrations of 6000, 1800, 600, 180, 60, 18, and 6 U/l. Serial dilutions of each of the three contrast media in saline were prepared to yield concentrations of 100%, 30%, 10%, 3%, and 1% vol/vol. One milliliter of venous blood was added to 1 ml of each of the dilutions of heparin or contrast media in both glass and plastic tubes; the two liquids were mixed and incubated at 20°C. All tubes were observed for clotting at intervals of up to 5 hr.

In the third experiment, we measured the partial thromboplastin time of platelet-poor plasma mixed with either serial dilutions of heparinized saline or one of the three contrast materials in saline. Platelet-poor plasma was prepared by centrifuging pooled blood from five normal volunteers at 2800 rpm for 10 min in a tabletop centrifuge. Serial dilutions of heparinized saline were prepared to yield concentrations of 8000, 6000, 4000, and 2000 U/l. Normal saline was used as a solution of 0 U/l. Serial dilutions of each of the three contrast media in saline were prepared to yield concentrations of 80%, 60%, 40%, and 20% by volume. A fibrometer (Becton-Dickinson, Cockeysville, MD) was used to determine partial thromboplastin times: 0.1 ml of thromboplastin reagent were incubated with 0.09 ml of platelet-poor plasma at 37°C for 1 min. Then 0.01 ml of either contrast medium or heparinized saline were added, and the mixture was incubated for 5 min. At the end of this period, 0.1 ml of calcium chloride was added and the clotting times were observed. This was done for each of the dilutions of the three contrast media and for each of the dilutions of the heparinized saline. All measurements were made in duplicate.

Results

No clots were observed in the arterial blood incubated with contrast material in syringes. In 20 of the 30 syringes containing the nonionic media, RBC aggregation occurred. In half of the 20 syringes in which aggregation occurred, the aggregates were visible in the syringe and were readily dispersed by shaking the syringe [2]. In the other half, the aggregates were visible only after filtration of the syringe contents as small clumps adhering to the filter, which were readily dispersed by pouring saline solution over them. Microscopic examination confirmed that these were clumps of RBCs and not clots.

Undiluted iohexol prolonged the clotting time of venous blood in a plastic tube to 160 min (Fig. 1) and in a glass tube to 80 min. The normal clotting time for this blood was 15 min in plastic and 10 min in glass. At 5.5 hr, we ended the experiment; no clotting had occurred in the blood mixed with undiluted ioxaglate or diatrizoate, or with heparinized saline at a concentration of 1800 U/l or greater.

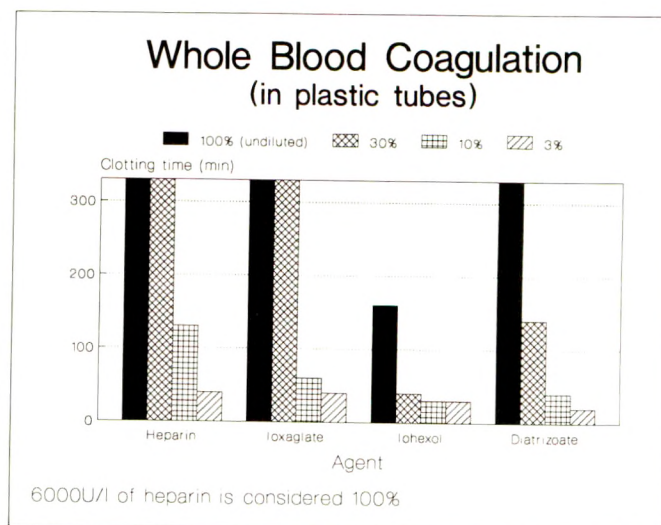


Fig. 1.—Graph shows comparison of anticoagulant effects of heparin, ioxaglate, iohexol, and diatrizoate on whole blood as measured in plastic tubes in vitro.

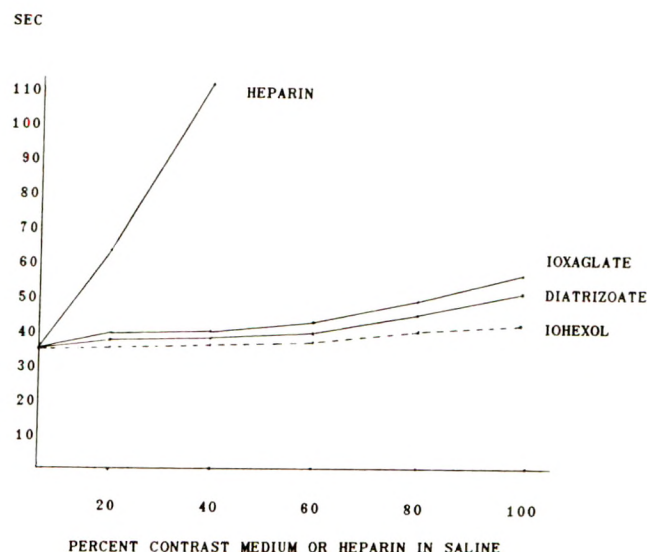


Fig. 2.—Graph shows effect of various contrast media and heparin on partial thromboplastin time. A concentration of 10,000 U/l of heparin in saline was used as 100% solution.

The effects of the contrast media and heparin on the partial thromboplastin times are shown in Figure 2. The control partial thromboplastin time of 36 sec was prolonged to 40 sec in undiluted iohexol, 50 sec in undiluted diatrizoate, and 54 sec in undiluted ioxaglate.

Discussion

Our principal focus was the investigation of clot formation in arterial blood mixed with nonionic contrast medium in the angiographic syringe. Unlike the angiographic catheter, the angiographic syringe housed in a power injector cannot be

flushed readily, and it is the only site where blood might remain in direct contact with contrast medium for more than a few minutes. Conventional high-osmolar, ionic contrast media are known to be capable of modulating various physiologic pathways at the cellular and humoral levels [3], and their anticoagulant effect is thought to be due to a combination of their ionic strength, their osmolality, and their toxicity [4]. The new low-osmolar, nonionic media with their reduced inherent chemotoxicity have been shown to be only mildly anticoagulant both in vivo and in vitro [4, 5].

Robertson [1] reported the isolation of one small clot and a fibrin thread from one of two plastic syringes containing 2 ml of arterial blood that had been standing for 30 min in 5 ml of nonionic contrast medium. He also reported clot formation in venous blood after 70 min of incubation with nonspecified contrast media mixed with heparin. Because nonionic media are in widespread use, it is important to determine the risk of clot formation with these compounds. We expanded on the design of Robertson in several ways. We used more samples so as to reduce the influence of spurious coagulation should clots have formed in any of the catheters from which arterial blood was initially drawn. We also tried to recreate the angiographic setting by (1) using 1 ml of blood and 49 ml of contrast media since in clinical practice the amount of blood that might be aspirated inadvertently into an angiographic syringe would rarely exceed 1 ml and (2) using dedicated angiographic syringes instead of small hand-held syringes.

Chix paper cloth, which will trap clots 0.1 mm or larger in diameter, was used in our study as a filter to screen the samples because precalibrated laboratory filter papers were found to require at least 20 min to filter 50 ml of sample contents, during which time artifactual clotting might have occurred. We also chose to measure the anticoagulant properties of the three contrast media by using laboratory dilution-curve techniques similar to those used by Stormorken et al. [5] and to compare these with heparin, a known potent anticoagulant.

Our results do not show any risk of clot formation in the usual clinical setting in which there is inadvertent mixing of blood with iohexol, ioxaglate, or diatrizoate in an angiographic syringe, although aggregation or clumping of RBCs does occur in iohexol. Aggregation is a physiologic phenomenon that occurs rapidly whenever blood flow is brought to rest [6]. RBC aggregates usually are of microscopic size but sometimes are large enough to be seen with the naked eye. A blood clot, on the other hand, consists of RBCs and WBCs trapped in a fibrin mesh. Erythrocyte aggregation sometimes can be seen in heparinized blood, in which fibrin does not form. Unlike clot formation, RBC aggregation is readily reversible. The hyperosmolality, ionicity, and inherent chemotoxicity of the conventional contrast media probably all contribute to their inhibition of aggregation [7-9], and it is perhaps not surprising that iohexol, which is more nearly physiologic in all of these respects, does permit RBC aggregation.

The results of our in vitro studies are similar to those of Dawson et al. [4] and Stormorken et al. [5] and confirm that all three contrast media have an inhibitory effect on blood coagulation. Undiluted Omnipaque 350 prolonged the clotting time of whole blood in plastic tubes to 160 min, which was similar to the anticoagulant effect of heparinized saline at a concentration of 600 U/l. Both ioxaglate and diatrizoate were more strongly anticoagulant than iohexol was, and at full strength both of these media inhibited clot formation for 5.5 hr, at which point we chose to stop the study because an angiogram would never last 5.5 hr. Qualitatively similar but less anticoagulant effect in whole blood was found when clotting times were measured in glass tubes because glass is a more potent activator of the extrinsic pathway of coagulation than plastic is. These results bear out the observations of Dawson et al. [4] that iohexol does not prolong the clotting time of whole blood to the same degree as do the conventional contrast media or ioxaglate.

In platelet-poor plasma, none of the media were strongly anticoagulant. The rank of effect was the same as for the clotting times: ioxaglate was more anticoagulant than diatrizoate, and diatrizoate was more anticoagulant than iohexol. This is similar to the effect observed by Stormorken et al. [5].

ACKNOWLEDGMENTS

We thank Monique Sutherland for technical assistance in performing the coagulation studies and Margaret Crosbie for secretarial assistance.

REFERENCES

1. Robertson HJF. Blood clot formation in angiographic syringes containing nonionic contrast media. *Radiology* 1987;162:621-622
2. Rasuli P. Blood clot formation in angiographic syringes containing nonionic contrast media (letter). *Radiology* 1987;165:582
3. Fareed J, Moncada R, Messmore HL Jr, Walenga JM, Hoppensteadt D, Wehrmacher WH. Molecular markers of contrast media-induced adverse reactions. *Semin Thromb Hemost* 1984;10:306-328
4. Dawson P, Hewitt P, Mackie IJ, Machin SJ, Amin S, Bradshaw A. Contrast, coagulation and fibrinolysis. *Invest Radiol* 1986;21:248-252
5. Stormorken H, Skälpe IO, Testart MC. Effect of various contrast media on coagulation, fibrinolysis, and platelet function: an in vitro and in vivo study. *Invest Radiol* 1986;21:348-354
6. Raininko R, Ylinen SL. Effect of ionic and nonionic contrast media on aggregation of red blood cells in vitro: a preliminary report. *Acta Radiol [Diagn]* (Stockh) 1987;28:87-92
7. Aspelin P, Stohr-Liessen M, Almen T. Effect of iohexol on human erythrocytes. I. Changes of red cell morphology in vitro. *Acta Radiol [suppl]* (Stockh) 1980;362:117-122
8. Aspelin P, Birk A, Almen T, Kiesewetter H. Effect of iohexol on human erythrocytes. II. Red cell aggregation in vitro. *Acta Radiol [suppl]* (Stockh) 1980;362:123-125
9. Issitt PD, Issitt CH. *Applied blood group serology*, 2nd ed. Oxnard, CA: Spectra Biologicals, 1975:3-20

Book Review

Imaging Anatomy of the Knee Region. Anatomy-CT-NMR: Frontal Slices, Sagittal Slices, Horizontal Slices. By Henri Sick and Jean-Louis Burguet. Munich: J. F. Bergmann Verlag, 88 pp., 1988. \$115

This new atlas provides a comprehensive imaging-anatomic correlative insight into structural relationships relevant to the interpretation of CT and MR studies of the knee. Its French authors are to be complimented for developing an extremely valuable practical tool that is a timely publication because of the increasing application of MR to the investigation of knee dysfunction. In general, the book can serve either as a tool for learning the cross-sectional anatomy of this articulation or as a reference review book for individuals who have previous knowledge of the subject.

This atlas specifically includes anatomic slices of the region of the knee studied in the three fundamental spatial planes (coronal, sagittal, and axial), the corresponding views obtained by CT of the same anatomic specimens, equivalent axial CT views of the knee, and MR images of the knee studied at the same levels in the same spatial planes. The anatomic material comes from 20 adults who were less than 50 years old and free of any articular pathologic condition. For any plane of section, all the anatomic slices presented come from the same specimen. The *in vivo* CT slices were obtained from young healthy volunteers, and all corresponding MR images come from the same patient.

CT views presented in this work were obtained with a total-body scanner (CE 10,000, Compagnie Generale de Radiologie). Sections were performed with the knee extended. The incrementations were 5 mm for coronal and sagittal planes and 10 mm for the axial plane. CT settings were 120 kV, 80 mA, 6.8 sec, 130- and 260- (coronal and sagittal) and 130-mm (axial) fields of view, 1-mm slice thickness, and 512×512 matrix.

Coronal and sagittal gross anatomic slices were 5 mm thick; axial slices were 10 mm thick. Each slice was photographed near a centrimetric scale, allowing determination of the real size of specific structures.

The MR images also were acquired with total-body equipment (Magniscan, Compagnie Generale de Radiologie) with a superconducting magnet operated at 0.5 T. The extended knees were positioned in the center of the main magnetic field, placed into a cervical emitting-receiving coil, and immobilized with plastic-foam cushions. The field of view thus achieved was 200 mm in diameter. A spin-echo

sequence was performed by using a TR of 450 msec and a TE of 26 msec. The data-acquisition matrix was 256×256 . The slice thickness was 5 mm, with a 5-mm increment for sagittal and coronal views and a 10-mm increment for axial views.

Positive aspects of the book include its large page size (10×13 in. [25.4×33 cm]), which allows all images at a given anatomic level to be viewed simultaneously; its detailed structural labeling; its inclusion of numerous anatomic levels in each of the three major planes of interest (axial, coronal, and sagittal); and its comprehensive index of specific structures. A short, up-to-date reference list and a concise table of contents are also provided. Negative features of the atlas include the use of relatively low-field-strength MR images with somewhat dark reproduction in certain instances, slight degradation of some CT scans by streak artifacts, failure to include anatomic sections in color, and limitation of its content to a single articulation. The rather brief text (preface, introduction, and materials and methods) also suffers from less-than-optimal translation from French into English. As compared with available general atlases of cross-sectional imaging, the work is far more comprehensive in its depiction of the knee but, by definition, more limited in scope.

The book would be of particular value to residents, fellows, and practicing radiologists who are in the process of learning to interpret MR examinations of the knee. Clinicians in orthopedic surgery and rheumatology would also find the atlas useful for evaluating cross-sectional imaging studies performed on their patients. The work would also be beneficial as a learning aid for medical students enrolled in gross anatomy courses. The book would be an appropriate and reasonably priced acquisition for MR reading rooms, radiology departmental libraries, and general biomedical libraries and would enhance the instructional materials of institutions offering visiting fellowships in MR.

David J. Sartoris
University of California, San Diego, Medical Center
San Diego, CA 92103

Pictorial Essay

The Subclavian Triangle: CT Analysis

Richard J. Wechsler,¹ Vijay M. Rao,¹ and Lois M. Newman²

The subclavian triangle of the neck is a clinically important anatomic compartment. Diseases of the vessels and lymph nodes located in this region cause a variety of clinical syndromes and are a harbinger of many systemic diseases. Therefore, a complete understanding of the CT anatomy and pathology of the area is important. The purpose of this essay is to increase this understanding.

Materials and Methods

The clinical material is drawn from nearly 3000 CT studies of the subclavian triangle performed over the past 6 years at our institution. All patients were scanned with a Technicare 2020 or 1440 high-performance scanner or a General Electric 9800 scanner. Contiguous axial scans were obtained in either 10- or 5-mm sections. IV contrast material was administered unless contraindicated.

Anatomy

The subclavian triangle, a subdivision of the posterior triangle of the neck, serves in part as the root of the neck and is contiguous with the thoracic inlet and axilla (Fig. 1) [1]. The upper boundary is formed by the inferior belly of the omohyoid muscle. While the clavicular attachment of the trapezius muscle marks the lateral extension, the lateral border of the anterior scalene muscle, lying deep to the sternocleidomas-

toid muscle, forms the medial border. The base is formed by the clavicle, the subclavius muscle, the first digitation of the serratus anterior muscle, and the first rib. The muscular floor is formed by the middle and posterior scalene muscles.

At the level of the seventh cervical and first thoracic vertebrae, brachial plexus roots are formed between the anterior and middle scalene muscles. The internal jugular vein is atop the scalene muscles and the carotid artery is atop the longus colli muscle. The transverse cervical vessels cross the triangle (Fig. 2).

In the lower part of the subclavian triangle, as the scalene muscles insert into the first rib, the subclavian vein is separated from the subclavian artery by the anterior scalene muscle. The subclavius muscle inserts on the clavicle. The pectoralis muscles are anterior, and the serratus anterior and levator scapulae muscles are posterior (Fig. 3).

Pathology

Brachial Plexopathy

The most important application of CT in evaluating brachial plexopathies is in the evaluation of cancer patients with brachial plexus signs. The presence of a local mass with or without paravertebral extension on CT is highly suggestive if not indicative of recurrent or metastatic tumor (Fig. 4) [2]. Osseous invasion of tumor sometimes can be detected on

Received August 9, 1988; accepted after revision October 25, 1988.

¹ Department of Radiology, Suite 3607, Thomas Jefferson University Hospital, 111 S. 11th St., Philadelphia, PA 19107. Address reprint requests to R. J. Wechsler.

² Department of Anatomy, Jefferson Medical College, Philadelphia, PA 19107.

AJR 152:313-317, February 1989 0361-803X/89/1522-0313 © American Roentgen Ray Society

Key to Abbreviations Used in Figures

Aa	axillary artery
Ab	abscess
AS	anterior scalene muscle
Av	axillary vein
BP	brachial plexus
C	common carotid artery
Cl	clavicle
ES	Ewing sarcoma
J	internal jugular vein
LC	longus colli muscle
LS	levator scapulae muscle
M	mass
MS	medial and posterior scalene muscles
MT	metastases
NF	neurofibroma
O	inferior belly of omohyoid muscle
PM	pectoralis muscles
R	rib
SA	serratus anterior muscle
S Art.	subclavian artery
SCM	sternocleidomastoid muscle
Sv	supracapsular vessel (artery)
T	trapezius muscle
TCv	transverse cervical vessel (artery)

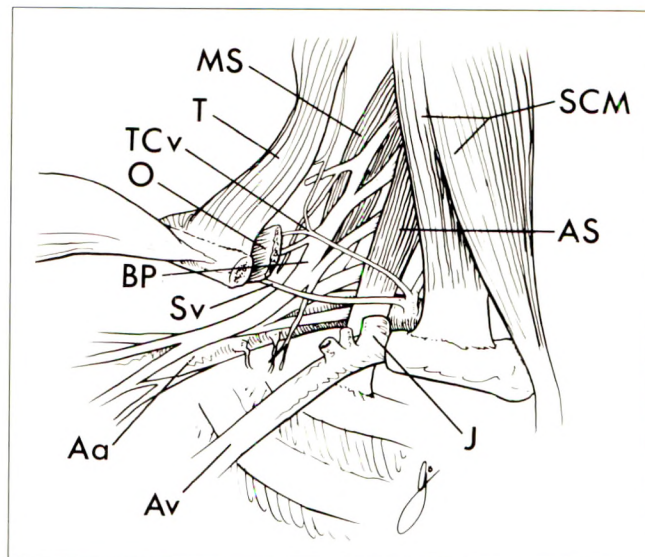


Fig. 1.—Subclavian triangle. Anterior boundary is formed by sternocleidomastoid muscle. Roof and lateral wall are bounded by inferior belly of omohyoid muscle. Scalene muscles form medial wall. Trapezius muscle is posterior boundary. Brachial plexus traverses triangle. See abbreviation key in left column.

supraclavicular fossa between the anterior and middle scalene muscles is almost diagnostic of these tumors (Fig. 6). CT also can confirm the diagnosis of subcostal fat, vascular processes, and superior sulcus tumors affecting the brachial plexus. CT delineates the depth of invasion in relation to the subclavian vessels, trachea, esophagus, and chest wall, as well as the relationship of the tumor to the brachial plexus (Fig. 7).

Lymphadenopathy

Diseases originating in the scalp, nuchal, pectoral, deltoid, and brachial areas as well as in the mediastinal, diaphragmatic, breast, parotid, and sternocleidomastoid regions may

CT when radiographs and bone scans are normal. Although a diffuse loss of tissue planes on CT can be due to tumor infiltration, it is more suggestive of radiation changes (Fig. 5).

CT also is valuable in the evaluation of a thoracic apical mass originating or growing into the supraclavicular fossa. The technique is an excellent means of diagnosing primary brachial plexus tumors. An apical mass extending from the

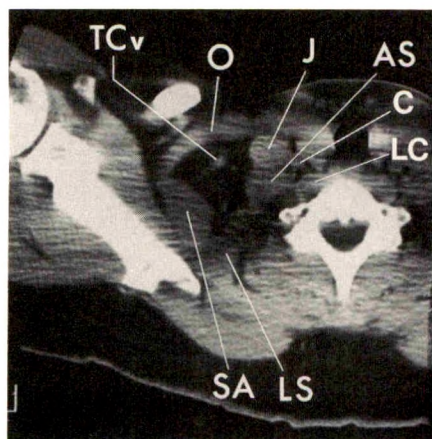


Fig. 2.—Upper part of subclavian triangle. Omohyoid muscle forms anterior and lateral boundary of subclavian triangle with serratus anterior and levator scapulae serving as posterior boundary. Internal jugular vein lies in front of anterior scalene muscles and carotid artery in front of longus colli muscle. Note transverse cervical vessels crossing subclavian triangle. See abbreviation key, in left column.

Fig. 3.—Lower part of subclavian triangle. Anterior scalene muscle separates anterior subclavian vein from subclavian artery and brachial plexus. Pectoralis muscles are anterior while serratus anterior muscle is posterior. Subclavius muscle (arrow) inserts on clavicle.

See abbreviation key, page 314.

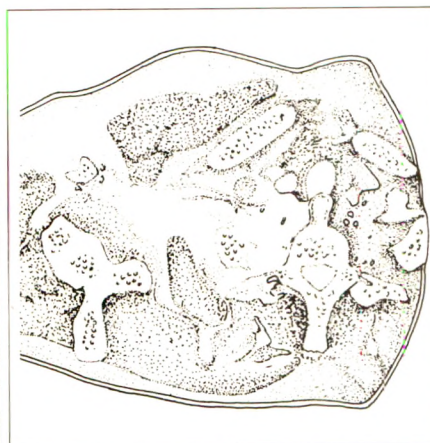
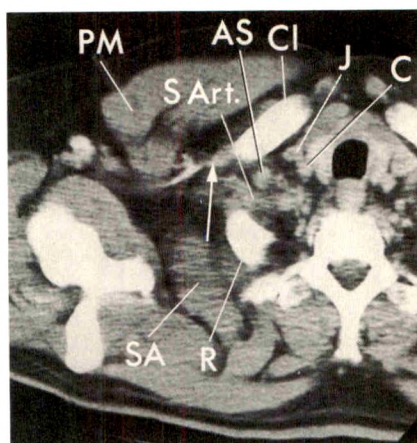
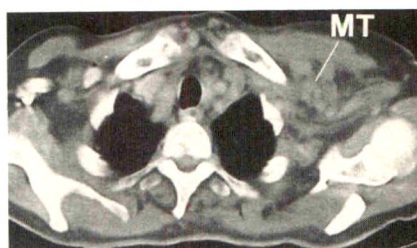
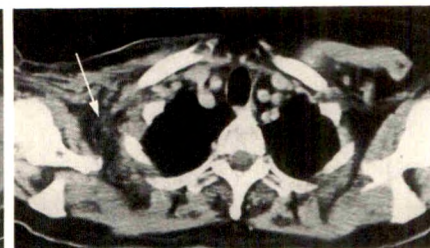


Fig. 4.—71-year-old woman with metastases (MT) in left subclavian triangle from vaginal carcinoma. Subclavian vessels are deviated posteriorly.



4



5

Fig. 5.—56-year-old woman with breast cancer. CT scan 6 months after radiation therapy shows right subclavian triangle stranding (arrow).

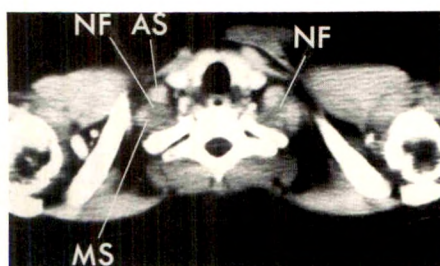


Fig. 6.—26-year-old woman with neurofibromatosis. CT scan shows bilateral enlargement of brachial plexus with splaying of anterior and middle scalene muscles by neurofibromas.

See abbreviation key, page 000.

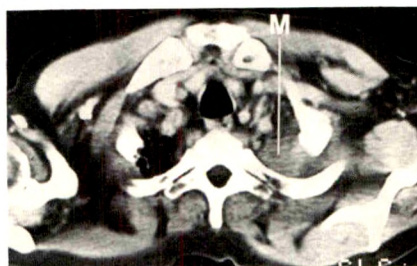
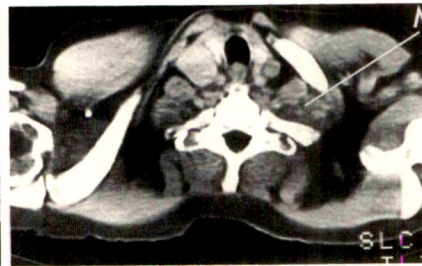


Fig. 7.—52-year-old woman with sarcoidosis and superior sulcus tumor. Axial CT scans reveal extension of mass (M) into supraclavicular fossa and involvement of brachial plexus.



present with adenopathy in the subclavian triangle. CT findings of lymph node disease include increase in the size and number of the nodes as well as obliteration to juxtanodal planes. Usually normal nodes in this region are not seen on CT [3].

Metastases from tumors in any part of the body, especially

the lung, breast, stomach, or esophagus, occur in the subclavian triangle (Fig. 8). Metastatic squamous cell carcinoma presents as a mass with a hypodense center due to necrosis (Fig. 9). On the other hand, adenopathy due to lymphomatous involvement generally presents as a homogeneous enhancing mass (Fig. 10).

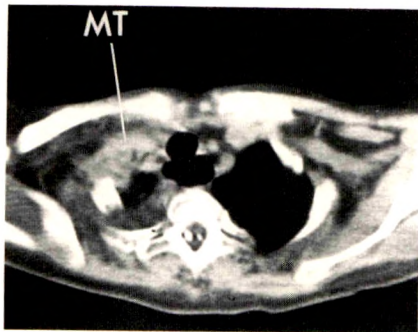


Fig. 8.—61-year-old man with Horner syndrome. CT scan shows metastasis (MT) from esophageal cancer in right subclavian triangle.

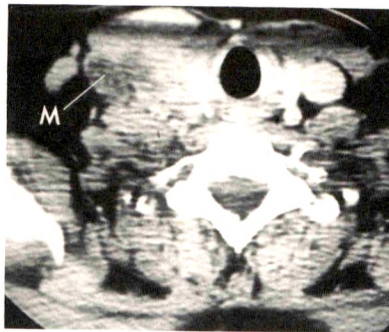


Fig. 9.—62-year-old man with squamous cell carcinoma. CT scan shows mass (M) with central lucency, characteristic of metastases to lymph nodes with central necrosis.

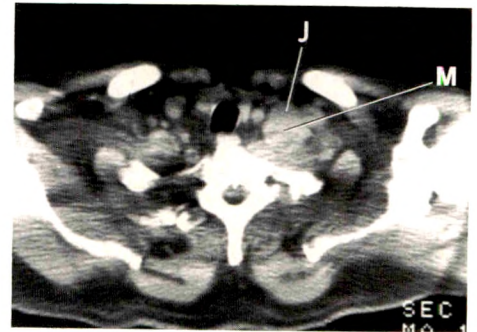
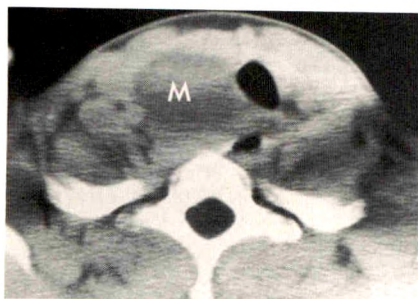
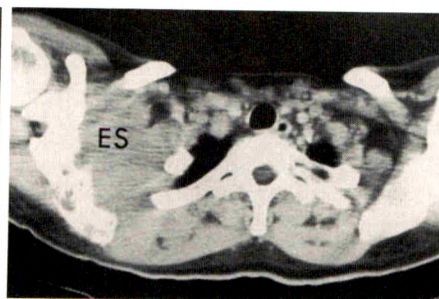


Fig. 10.—64-year-old man with lymphoma. CT scan shows homogeneous enhancing mass (M) due to lymphoma involving left brachial plexus. Jugular vein (J) is compressed by mass. Note normal contralateral scalene muscles.



11



12

Fig. 11.—19-year-old woman with cystic hygroma. CT scan reveals low-density mass (M) laterally displacing internal jugular vein and internal carotid artery.

Fig. 12.—32-year-old woman with Ewing sarcoma (ES) of scapula. Note local extension into subclavian triangle.

Adenopathy also may be caused by local or regional inflammatory processes. These nodes usually are homogeneous and well defined on CT. Tuberculous adenitis, although uncommon, is found in patients who have emigrated from an endemic region. When there is active pulmonary tuberculosis, the nodes may have a homogeneous or low-density center with ringlike areas of enhancement around it [4]. Generally, however, CT has not been useful in separating malignant from inflammatory lymphadenopathy.

Primary Tumors

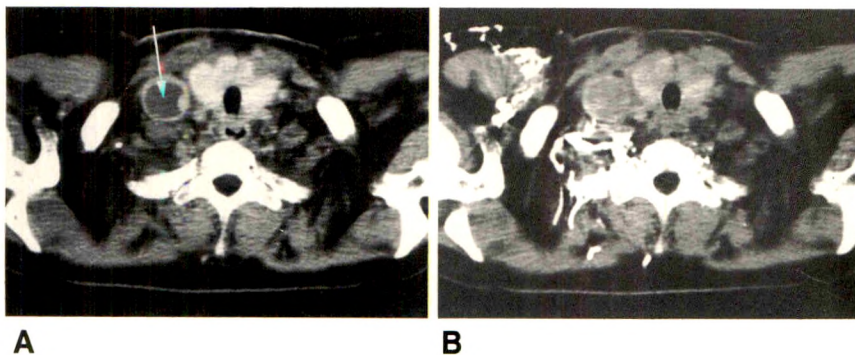
Primary tumors in the subclavian triangle are rare. Cystic hygromas usually occur in the first 2 years of life but may not be apparent until later in childhood. CT reveals a water-density mass that is homogeneous, round, smooth, and sharply outlined (Fig. 11). Other mesenchymal tumors such as lipomas,

liposarcomas, fibrohistiocytoomas, and rhabdomyosarcomas also involve this region. Local extension of tumors from lung, scapula, and neck also occurs (Fig. 12).

Vascular Lesions

Aneurysms of the subclavian artery may be visible on CT as saccular outpouchings of the artery on contrast-enhanced scans. Arterial rupture may cause obliteration of the vessel margins and perivascular fascial planes.

Obstruction of the superior vena cava can result from neoplasm, granulomatous disease, complication of catheter insertion, and trauma. In the presence of venous obstruction, blood from the arm is diverted into collateral venous pathways. Opacification of the venous plexus of the subclavian triangle, the transverse cervical vein, or muscular branches



A

B

Fig. 13.—34-year-old man.

A, CT scan shows jugular vein thrombosis (arrow).

B, Opacification of venous plexus of subclavian triangle, a reliable clue to underlying superior vena cava obstruction.

(Courtesy of Kenneth Neigut, Germantown Hospital and Medical Center, Philadelphia, PA.)

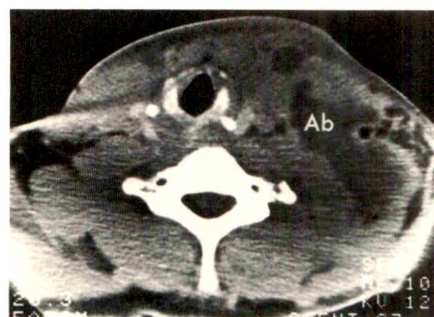


Fig. 14.—27-year-old man with neck abscess (Ab). Note loss of soft-tissue planes and extension into scalene and levator scapulae muscles.

of the axillary vein is a reliable clue to underlying obstruction of the superior vena cava (Fig. 13) [5].

Infection

Acute abscesses occur in the subclavian fossa. Subclavian triangle infections can originate in the neck (Fig. 14), although they extend from the axilla more frequently [1]. An abscess is seen on CT as a mass with varying density that may have rim enhancement. Frequently, skin thickening and fatty infiltration are seen. Differential diagnosis includes nodal mass, tumor, seroma, and hematoma.

REFERENCES

1. Wechsler RJ. *Cross sectional analysis of the chest and abdominal wall*. St. Louis: Mosby, 1989
2. Gebarski KS, Glazer GM, Gebarski SS. Brachial plexus: anatomic, radiologic, and pathologic correlation using computed tomography. *J Comput Assist Tomogr* 1982;6:1058-1063
3. Goldberg RP, Austin RM. Computed tomography of axillary and supraclavicular adenopathy. *Clin Radiol* 1985;36:593-596
4. Reede DL, Bergeron RT. Cervical tuberculous adenitis: CT manifestations. *Radiology* 1985;154:701-704
5. Engle IA, Auh YH, Rubenstein WA, Sniderman K, Whalen JP, Kazam E. CT diagnosis of mediastinal and thoracic inlet obstruction. *AJR* 1983;141:521-526

Book Review

Atlas of Fetal Skeletal Radiology. By Asher Ornoy, Zvi Borochowitz, Ralph Lachman, and David L. Rimoin. Chicago: Year Book Medical, 136 pp., 1988. \$75

This publication aims to facilitate the prenatal diagnosis of specific skeletal dysplasias. It does so by providing the obstetric sonographer with a successive progression of normal skeletal growth and with examples of various skeletal disorders that occur during fetal life.

The book is divided into three chapters. Chapter 1 is a 16-page textual review of normal embryonic and fetal chondroosseous development that is illustrated with multiple histologic sections, many derived from original work by the authors on fetuses 11–27 weeks old. The normal ossification of major bones is traced from its inception to its completion after puberty. Chapter 2 contains frontal and lateral radiographs of fetuses 10–27 weeks old. The radiographs are scaled to actual size or half size, with supplemental magnification of the smallest fetuses. Each progressive week-by-week developmental stage is accompanied by a well-organized table describing the interim changes occurring in each major bone. Chapter 3 consists of single examples of 19 skeletal disorders illustrated by frontal radiographs of fetuses that are between 18 and 34 weeks. The tabular legends are organized in a manner similar to those adjoining the images of normal fetuses. The tables include the mode of genetic transmission for each entity, which would be helpful in counseling patients about future pregnancies. However, the tables do not include prognosis, which would be helpful in counseling patients about termination of pregnancy. Also not included in the tables is a differential diagnosis

pointing out the salient differences among superficially similar entities, which might be of considerable assistance to the initiate.

The atlas is supplemented by an appendix containing the International Nomenclature of Constitutional Diseases of Bone (European Society of Pediatric Radiology, May 1983) and by a useful and complete index. References are given generously in each section of the book.

The book is organized logically and is well written; the tabular information is concise. Pertinent facts from the text in chapter 1 are carried over to the figure legends to facilitate integration of text and illustrations, but the histologic sections could be clarified by a more liberal use of arrows and labels. The quality of the radiographs, although satisfactory overall, is spotty, ranging from excellent to very poor, especially in some of the lateral projections.

This book does not claim to be an exhaustive treatise of skeletal malformations; rather it is a specialized volume that would not be useful to the resident or general radiologist. However, it does provide a succinct, albeit limited, reference for the radiologist who is interested in refining the clinical diagnosis of fetal skeletal disorders.

Marta Hernanz-Schulman
Vanderbilt University Medical Center
Nashville, TN 37232

Flexion Teardrop Fracture of the Cervical Spine: Radiographic Characteristics

Kwang S. Kim¹
 Harry H. Chen
 Eric J. Russell
 Lee F. Rogers

Teardrop fracture of the cervical spine is a confusing and loosely used term, often referring to any fracture with a triangular fragment in the involved body. The flexion teardrop fracture is a specific entity that should not be confused with other types of injury with a teardrop fragment. In a radiographic analysis of 45 patients with flexion teardrop fracture, the most characteristic feature was posterior displacement of the upper column of the divided cervical spine, observed in 78% of the cases. Other radiographic characteristics included backward displacement of the posterior fragment of the involved body, widening of the interlaminar and interspinous spaces, widening of the facet joint with backward displacement of the inferior facet, and kyphotic deformity of the cervical spine at the level of injury. The injury was frequently associated with sagittal-body and laminar fractures and occurred predominantly at the C5 level.

The flexion teardrop fracture (FTDF) is a common injury of the cervical spine that often has a devastating outcome [1-3]. Its name is derived from the characteristic triangle-shaped fragment that fractures from the anteroinferior corner of the vertebral body, and that resembles a drop of water dripping from the vertebral body. The posterior fragment of the divided body is displaced backward into the spinal canal. The lesion is also characterized by complete disruption of both the anterior and posterior ligamentous structures, resulting in marked instability at the site of injury [4].

The characteristic neurologic injury accompanying the FTDF is the anterior cord syndrome. This syndrome consists of quadriplegia with loss of pain, temperature, and touch sensations, and preservation of the posterior column senses of position, motion, and vibration [1, 4].

Neurologic consequences are usually severe with the FTDF; however, in some cases there are incomplete deficits or even intact neurologic status [2, 5]. Radiographic diagnosis of this unstable injury is, therefore, therapeutically important. Unfortunately, diagnostic confusion exists between the FTDF and other fractures with a teardrop fragment. While the radiographic features of FTDF have been described by many authors since the initial description by Schneider and Kahn in 1956 [4], there has been no comprehensive radiographic description of this entity in the literature. We present a complete radiographic analysis of 45 patients with FTDF and discuss the characteristic and differential features of FTDF as compared with other fractures with a teardrop fragment.

Subjects and Materials

We reviewed the records of 45 patients with flexion teardrop fractures who were admitted to the Midwest Spinal Cord Injury Unit of the Northwestern Memorial Hospital between May 1982 and June 1987. The cases were selected on the basis of availability of lateral radiographs, polytomograms, and medical records. Most of the cases were referred from outlying community hospitals, and the initial lateral radiograph was available for review in 20 cases. Serial lateral radiographs and anteroposterior and lateral views of polytomograms,

This article appears in the November/December 1988 issue of *AJNR* and the February 1989 issue of *AJR*.

Received December 2, 1987; accepted after revision March 8, 1988.

¹ All authors: Department of Diagnostic Radiology, Northwestern Memorial Hospital and Northwestern University Medical School, Olson Pavilion, 710 N. Fairbanks Court, Chicago, IL 60611. Address reprint requests to K. S. Kim.

AJR 152:319-326, February 1989
 0361-803X/89/1522-0319
 © American Roentgen Ray Society

obtained after traction tongs were applied, were available in all cases. The purpose of polytomography as a requirement for selection of the cases was to analyze all components of the injury that might not have been revealed on the plain cervical films. The diagnosis of FTDF was based on the characteristic appearance of the involved body and on evidence of disruption of the anterior and posterior ligamentous structures as described by Schneider and Kahn [4] and others [1, 5, 6]. In five cases, CT was available for review. Sagittal images were reformatted from the 3-mm axial slices.

FTDF was the result of diving accidents in 18 cases (40%), motor vehicle accidents in 13 cases (29%), falls in 12 cases (27%), and other types of injury in two cases (4%). The neurologic status after injury was complete quadriplegia in 25 cases (56%), incomplete quadriplegia in 14 cases (31%), and intact in six cases (13%).

Results

The Vertebral Body

In the lateral view, the involved vertebral body was divided into two fragments: the smaller anterior triangular fragment and the larger posterior fragment. The anterior aspect of the anterior fragment was generally aligned with that of the ver-

tebral body below, although in some cases it was displaced and rotated anteriorly beyond the anterior vertebral body line. In all cases, the posterior inferior aspect of the posterior fragment was displaced backward in relation to the superior aspect of the vertebral body below (Figs. 1–6). The displacement varied from 1 mm to the total body width, and was reduced by varying degrees after application of traction tongs (Figs. 3B, 5A, 5B). However, the posterior displacement was evident on at least one of the serial lateral radiographs or on the polytomogram during application of traction tongs. The superior aspect of the posterior fragment, on the other hand, was in normal alignment with the inferior aspect of the vertebral body above in all but four cases (91%). In these four cases, the backward displacement of the superior aspect was much less than that of the inferior aspect. The fractured vertebral body showed an anterior wedging deformity in 39 (87%) of 45 cases.

Signs of Ligamentous Disruption

In addition to fragmentation of the vertebral body with backward displacement of the posterior fragment, another

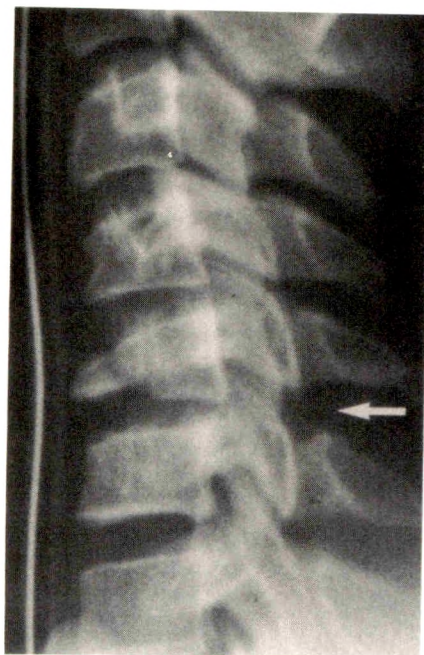


Fig. 1.—14-year-old with incomplete quadriplegia at C6 as a result of diving accident. Lateral radiograph, obtained after traction tongs are applied, shows flexion teardrop fracture at C5 with a mild degree of kyphotic angulation. Posterior fragment is slightly displaced backward in inferior aspect; disk space between posterior fragment and vertebral body below is narrowed; interlaminar and interspinous spaces are widened at C5–C6 (arrow); C5–C6 facet joint is widened; and fractured C5 body shows anterior wedging deformity. There is also compression deformity in anteroinferior aspect of C4 body.

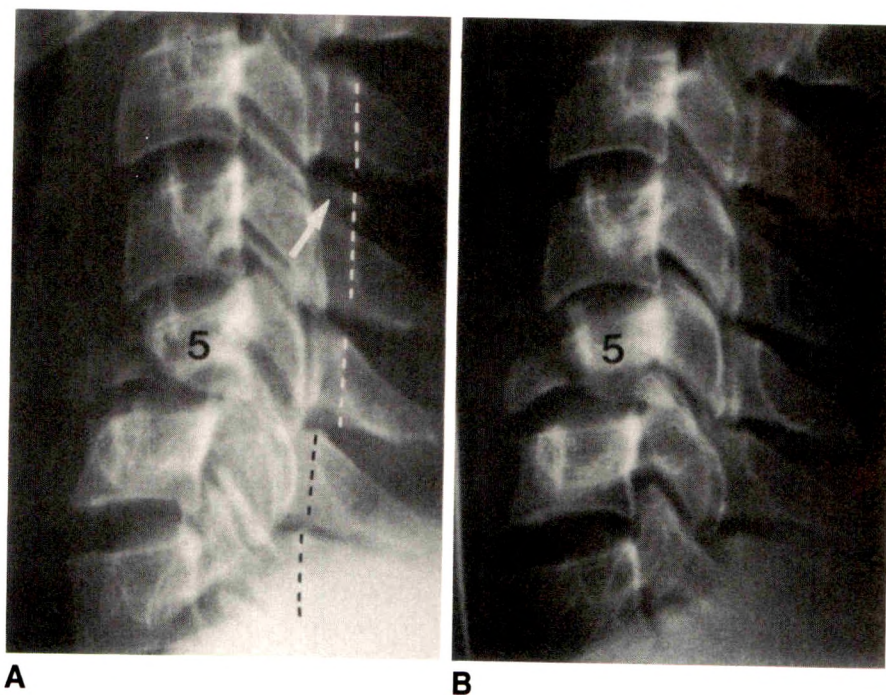


Fig. 2.—28-year-old man with incomplete quadriplegia at C6 as a result of falling accident.

A, Lateral radiograph, obtained before traction tongs are applied, shows flexion teardrop fracture at C5 with backward displacement of posterior fragment in inferior aspect. Interlaminar and interspinous spaces are not widened; spinolaminar line of upper column (white dashed line) is displaced backward in relation to that of lower column (black dashed line); there is a moderate degree of kyphotic deformity at level of injury; and disk space between posterior fragment and vertebral body below is narrowed while the disk space between anterior fragment and vertebral body below is normal. There are sagittal fractures in C5 and C6 bodies, and multiple laminar fractures at C4, C5, and C6 (not shown except for C4 laminar fracture, which is indicated by arrow). There is also prevertebral soft-tissue swelling.

B, Lateral radiograph, obtained after traction tongs have been applied, shows that kyphotic angulation and posterior displacement of spinolaminar line of upper column are improved. However, backward displacement of posterior fragment of fractured body and a slight degree of posterior displacement of spinolaminar line of upper column are still appreciated.

Fig. 3.—29-year-old man with complete quadriplegia at C5 as a result of motor vehicle accident.

A, Lateral radiograph, obtained before traction tongs are applied, shows flexion teardrop fracture at C5 with a marked degree of backward displacement of posterior fragment of fractured body. Inferior facet of C5 (arrow) is displaced backward in relation to superior facet of C6. Interlaminar and interspinous spaces are widened at C5–C6; spinolaminar line of upper column is displaced posteriorly in relation to that of lower column; and disk space between posterior fragment and vertebral body below is lost while disk space between anterior fragment and vertebral body below is normal. The anterior fragment is aligned with lower column, and there is widening of prevertebral soft-tissue space.

B, Lateral polytomogram, obtained after traction tongs have been applied, shows that backward displacement of posterior fragment of fractured body and posterior offset of spinolaminar line of upper column are improved but still persist.

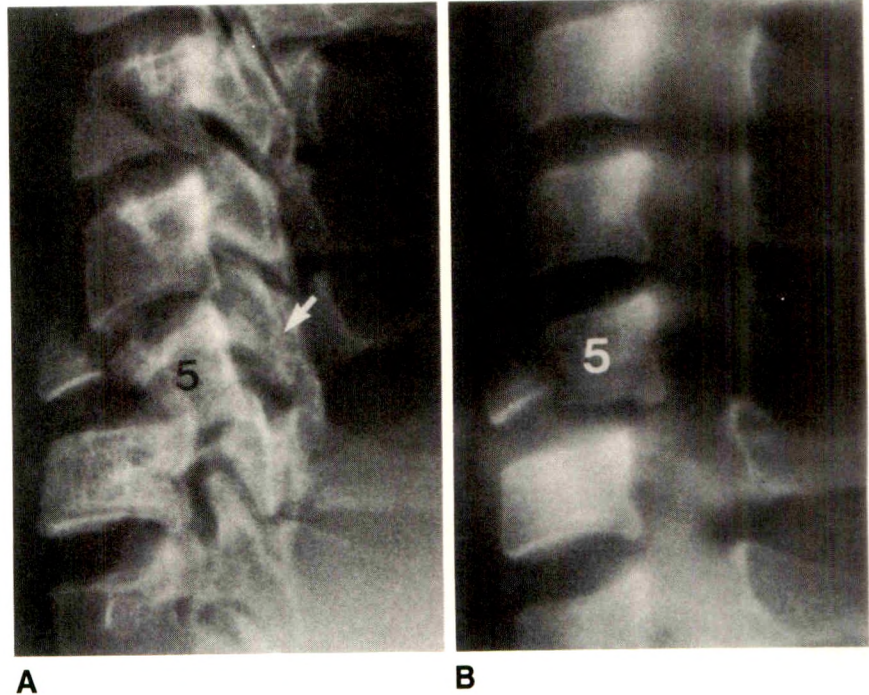
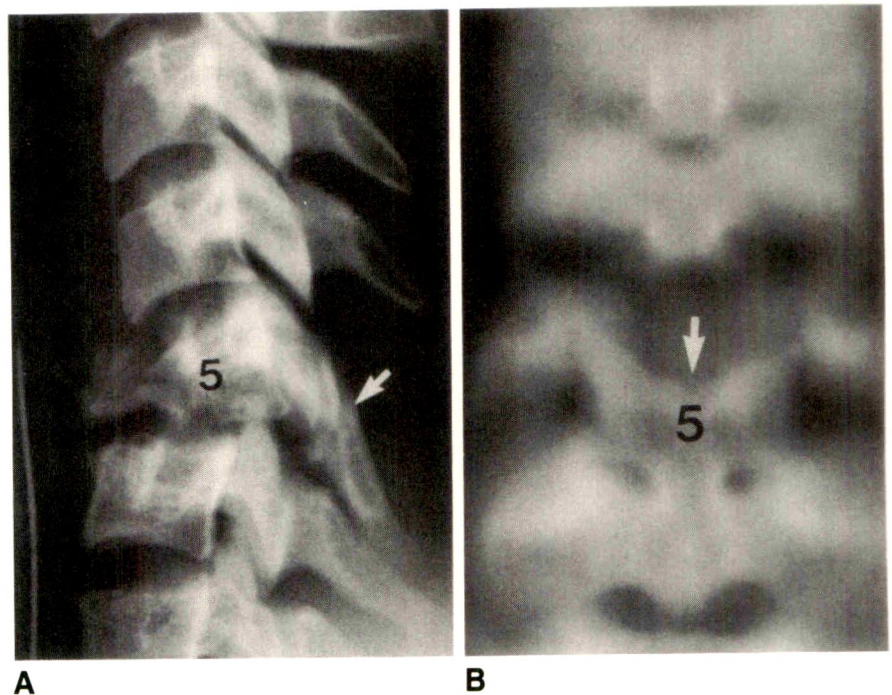


Fig. 4.—19-year-old man with complete quadriplegia at C5 as a result of motor vehicle accident.

Lateral radiograph (A) and anteroposterior polytomogram (B), obtained after traction tongs have been applied, show flexion teardrop fracture at C5 with kyphotic angulation and backward displacement of posterior fragment. C5 laminae are fractured and displaced downward (arrow) with paradoxical narrowing of C5–C6 interlaminar and interspinous spaces. Interlaminar and interspinous spaces are widened at C4–C5.



essential characteristic of FTDF was evidence of complete disruption of the anterior and posterior ligamentous structures.

The disk space. While the disk space between the anterior fragment and the vertebral body below was usually maintained, the disk space between the posterior fragment and the vertebral body below was narrowed in all 20 cases (100%) for which the initial radiographs were available (Figs. 2A, 3A, 6). The disk space remained narrowed, changed to normal,

or widened after application of traction tongs, depending on the weight applied (Figs. 2B, 3B, 5A, 5B).

The facet joint. The facet joint between the level of injury and the one below was widened in all cases (100%). There was a varying degree of posterior displacement of the inferior facet in relation to the superior facet below in 29 (64%) of 45 cases (Figs. 2, 3A, 4A, 5A, 6). On polytomograms, widening of the facet joint space was observed in two or more adjacent levels on one or both sides in 39 (87%) of 45 cases.

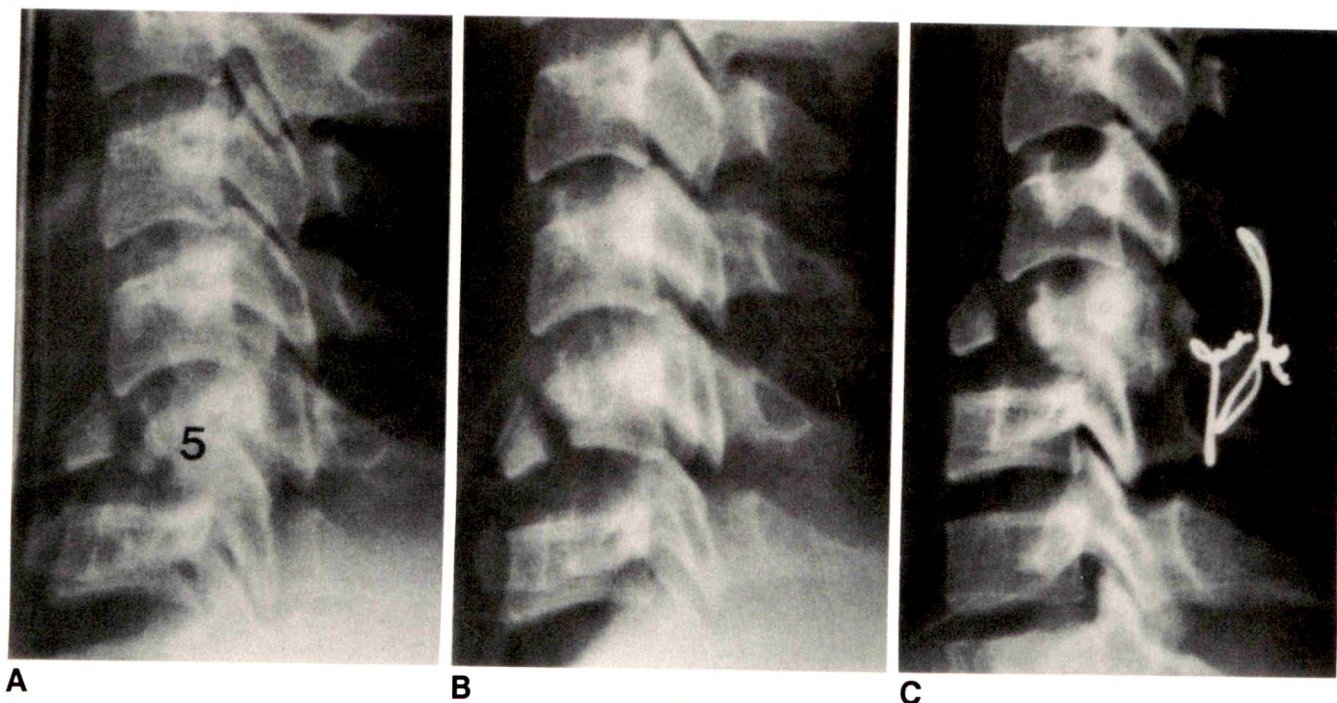


Fig. 5.—20-year-old man with complete quadriplegia at C6 as a result of motor vehicle accident.

A, Lateral radiograph, obtained after traction tongs have been applied, shows flexion teardrop fracture at C5 with kyphotic angulation and backward displacement of posterior fragment. There is a substantial degree of posterior displacement of inferior facet of C5 in relation to superior facet of C6. The C4–C5 interlaminar and interspinous spaces are widened due to C5 bilaminar fracture and disruption of C4–C5 ligamentous structures. The spinolaminar line of upper column above C5 level is slightly displaced backward in relation to that of lower column.

B, With further increase in traction weight, alignment is improved with reduction of both the kyphotic angulation and the backward displacement of posterior fragment. The spinolaminar line is now almost anatomical. Distraction force causes widening of disk space, facet joint, and interlaminar and interspinous spaces at C5–C6. C4–C5 interlaminar and interspinous spaces remain widened.

C, After a posterior fusion, posterior displacement of upper column is evident. C5 lamina is displaced downward with narrowing of interlaminar and interspinous spaces at C5–C6. Interlaminar and interspinous spaces above are widened. The disk space between posterior fragment and vertebral body below is narrowed.

The interlaminar and interspinous spaces. Of the 20 cases in which the initial lateral radiographs were available, eight (40%) showed widening of the interlaminar and interspinous spaces between the level of injury and the one below (Figs. 3A, 6). In five (25%) of the cases, the spaces were narrowed due to downward displacement of the fractured laminae; the spaces above were widened in these five cases. In the remaining seven cases (35%), the interlaminar and interspinous spaces were not widened (Fig. 2A). Of the 25 cases in which the initial lateral radiographs were not available, six (24%) showed widening of the interlaminar and interspinous spaces between the levels of inquiry and the one below on one of the serial lateral radiographs obtained after cervical traction (Fig. 1). In seven (28%) of the cases, the spaces were narrowed due to downward displacement of the fractured laminae; the spaces above were widened in these seven cases (Figs. 4, 5). In 12 (48%) of the cases, the interlaminar and interspinous spaces were not widened.

Kyphotic deformity of the cervical spine at the level of injury. A varying degree of kyphotic deformity of the cervical spine was present at the level of injury in 18 (90%) of 20 cases on the initial lateral radiographs (Figs. 2A, 3A, 6) and 13 (52%) of 25 cases on one of the serial lateral radiographs obtained after traction tongs were applied (Figs. 1, 4A, 5A).

Posterior displacement of the upper column. The cervical spine was divided into the upper and lower columns at the level of injury, following complete disruption of the anterior and posterior ligamentous structures. By observing the alignment of the spinolaminar line, posterior displacement of the upper column in relation to the lower one was seen at the level of injury in 16 (80%) of 20 cases before application of traction tongs (Figs. 2A, 3A). In the remaining 25 cases, evaluation was made with the serial lateral radiographs and polytomograms after traction tongs were applied. Posterior displacement of the upper column was still evident in 19 (76%) of these 25 cases (Figs. 4A, 5A). In some cases with a marked degree of kyphotic angulation at the level of injury, the upper column was inclined forward in such a way that it appeared deceptively displaced forward. However, the upper column immediately above the level of injury was invariably displaced backward (Fig. 6). When the kyphotic angulation was reduced after traction tongs were applied, backward displacement of the entire upper column often became evident.

Distraction. In 12 (27%) of 45 cases there was widening of the disk, facet, and interlaminar and interspinous spaces on one of the serial lateral radiographs obtained after traction tongs were applied (Fig. 5B).



Fig. 6.—26-year-old woman with complete quadriplegia at C5 as a result of motor vehicle accident. Lateral radiograph, obtained before traction tongs are applied, shows flexion teardrop fracture at C5 with a marked degree of kyphotic angulation at level of injury. Upper column is inclined forward in such a way that it appears deceptively displaced forward. However, both the posterior fragment of the fractured body and the inferior facet of C5 are markedly displaced backward. Interlaminar and interspinous spaces are widened at C4–C5 and at C5–C6. The small anterior fragment is aligned with lower column.

Sagittal Body and Laminar Fractures

These fractures were evaluated with polytomography. A sagittal fracture was noted in 39 (87%) of 45 cases. Of these 39 cases, the sagittal fracture was present at the level of injury in all but one. In 13 (33%) of these 39 cases, the sagittal fractures were present at two or more adjacent levels. A laminar fracture, unilateral or bilaminar, was present in 38 (84%) of 45 cases. Of these 38 cases, the laminar fracture was noted at the level of injury in all but one. The laminar fracture was present at two or more adjacent levels in 12 (32%) of 38 cases. The laminar fracture was usually associated with the sagittal fractures in the body. The associated laminar fracture was present in 52 (96%) of 54 vertebrae with sagittal fractures.

Level of Injury

In two (4%) of 45 cases, the FTDFs were noted at two levels, the C4 and the C5 in one case, and the C5 and the C6 in the other. Of the remaining 43 cases, the lesion was at the C5 level in 31 cases (72%), the C6 level in eight cases (19%), and the C4 level in four cases (9%).

Associated Prevertebral Soft-Tissue Swelling

This was evident in 27 (60%) of 45 cases (Figs. 2A, 3A), questionable in 10 (22%) of the cases, and not present in eight (18%) of the cases.

Associated Spine Fracture Distant from the Level of Injury

In three (7%) of 45 cases, there were fractures of the spine distant from the FTDF: Jefferson fracture of C1 in two cases, and a burst fracture of L1 in one case.

CT Features

Axial CT scans with sagittal reformation were obtained in five cases. CT appeared superior to polytomography in detecting the sagittal-body and posterior-element fractures. These fractures were more clearly defined on the axial CT scans, although none were missed on the polytomograms. However, the reformatted sagittal images from the 3-mm axial slices were inferior to the lateral polytomograms and even to the lateral plain cervical films.

Relationship Between the Radiographic Features and Neurologic Status

In five (83%) of six cases with normal neurologic status, there were no sagittal-body or laminar fractures. A sagittal-body fracture was present in all but one of the remaining 39 cases with complete or incomplete neurologic deficits. The posterior displacement of the posterior fragment of the body and the upper column was mild in the cases with normal neurologic status compared with those with complete or incomplete neurologic deficits. There was no differentiating radiographic feature between the group with complete quadriplegia and the one with incomplete neurologic deficits.

Discussion

Teardrop fracture of the cervical spine is a confusing term [2, 7] that is often loosely used to describe any fracture with a triangular fragment of the body without indicating the mechanism of injury. The FTDF is a specific entity that should not be confused with other types of fractures with a teardrop fragment [1, 4–6].

The FTDF results from a combination of forceful flexion and axial compression of the cervical spine (Fig. 7A) that occurs when the neck is flexed and the head strikes a solid object, as in diving into shallow water, hitting the dashboard in a motor vehicle accident, or falling [1, 3, 5–7].

The anteroinferior margin of the involved vertebral body is fractured by a shear stress with compressive loading and the major portion of the body is displaced backward into the spinal canal. The intervertebral disk between the major fragment and the vertebral body below is disrupted. The reciprocal distractive force that occurs in the posterior column of the spine results in disruption of the posterior ligamentous structures [1]. Thus, the cervical spine is divided into an upper and a lower column at the level of injury. The line of disruption separates the anterior and posterior fragment of the body, the disk space between the posterior fragment and the body below, the facet joint, and the interspinous space (Figs. 7B–7D).

Radiographic evaluation of the FTDF is best made with initial lateral radiographs obtained before applying a traction device. However, these radiographs are often of limited quality because of the difficulty in positioning the seriously injured patient. In 25 (56%) of 45 cases, initial lateral radiographs were not available when the patient was referred to our institution. Our study demonstrated that the radiographic characteristics of FTDF could still be appreciated on serial lateral films and on polytomograms in most cases, despite the altered deformity of the cervical spine after traction tongs were applied.

In lateral radiographs, the characteristic feature is the displaced posterior fragment of the involved body, although the injury derives its name from the appearance of the anterior fragment. While the anterior fragment is aligned with the lower column, the posterior fragment is displaced backward as a unit with the upper column relative to the vertebral body below (Figs. 1–7). This feature, when observed at the C5 or adjacent level, strongly implies the diagnosis of FTDF. If such a displacement is found, the next step is the search for signs of disruption of the anterior and posterior ligamentous structures. The disk space narrowing between the posterior fragment and the vertebral body below indicates disruption of the disk. The offset of the anterior and the posterior vertebral body lines at the level of injury is suggestive of disruption of the anterior and posterior longitudinal ligaments. The widening of the facet joint, interlaminar space, and interspinous space represents disruption of the facet joint capsule, ligamentum

flavum, and the interspinous ligament, respectively (Figs. 7B–7D).

The facet joint capsules are thin and lax, contributing little to the strength of the spine [8]. The widening of this joint space is frequently observed in other types of injury, including simple compression and burst fractures. Facet joint space widening alone is not indicative of complete disruption of the posterior ligamentous structures. However, the presence of a substantial degree of posterior displacement of the inferior facet may be indicative of complete disruption (Figs. 3A, 4A, 5A, 5C, 6).

Widening of the interlaminar and interspinous spaces has been stressed by previous authors in establishing the diagnosis of FTDF [1, 6]. However, the interlaminar and interspinous spaces between the level of injury and the one below were widened in only eight (40%) of 20 cases without traction tongs (Figs. 3A, 6) and in six (24%) of 25 cases with traction tongs (Fig. 1). The spaces were paradoxically narrowed due to downward displacement of the fractured laminae in five (25%) of 20 cases without traction tongs and in seven (28%) of 25 cases with traction tongs (Figs. 4, 5A). The spaces above were widened in these 12 cases. The widening of the interlaminar and interspinous spaces is indicative of disruption of the posterior ligamentous structures but not necessarily specific to FTDF: a distractive hyperflexion injury, which includes a flexion sprain injury, with unilateral or bilateral facet locking [3], may produce widening of the interlaminar and interspinous spaces.

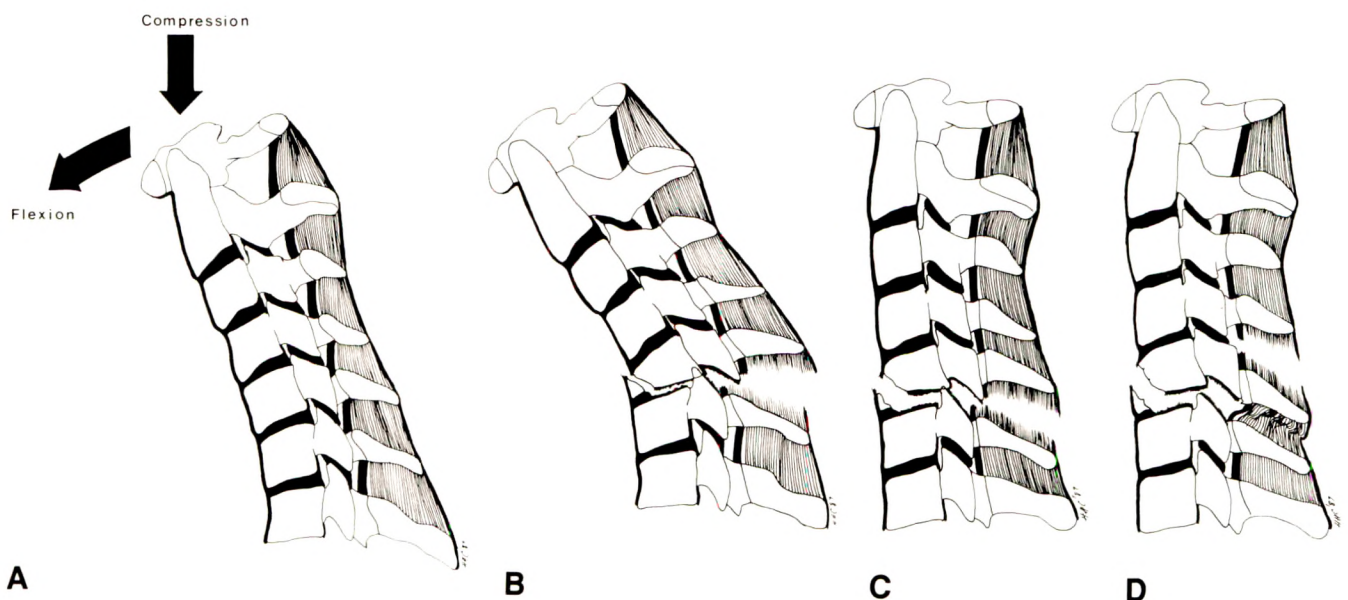


Fig. 7.—A and B, Diagrams show mechanism of flexion teardrop fracture (A) and resultant deformity (B).

C, Drawing shows altered deformity after traction tongs have been applied. Alignment is improved with reduction of both the kyphotic angulation and the posterior displacement of upper column. However, some degree of posterior displacement of posterior fragment of fractured body and posterior offset of spinolaminar line of upper column often persists. Distraction force may cause widening of disk space, facet joint, and interlaminar and interspinous spaces between the level of injury and the one below.

D, Variation of C. In some cases of bilaminar fracture at the level of injury, the interlaminar and interspinous spaces between the level of injury and the one below are paradoxically narrowed due to downward displacement of fractured laminae. Interlaminar and interspinous spaces above are widened with torn ligamentum flavum and interspinous ligament.

However, we believe that posterior displacement of the upper column at the level of injury is a specific feature of FTDF, observed in 35 (78%) of the 45 cases. This was demonstrated by a posterior step-off of the spinolaminar line at the level of injury (Figs. 2, 3, 4A), or at one level above in some patients with a bilaminar fracture (Figs. 5A, 5C). Posterior step-off of the anterior and posterior vertebral body lines provided additional evidence of posterior displacement of the upper column.

In 12 (27%) of the 45 cases, a distraction force following application of the traction tongs produced widening of the disk space, facet joint, and interlaminar and interspinous spaces at the level of injury (Fig. 5B). This allowed us to more easily define the line that divided the cervical spine into the unstable upper and lower columns.

A sagittal fracture in the involved body was present in 39 (87%) of the 45 cases. A laminar fracture was usually associated with the sagittal-body fracture. This high incidence of sagittal-body and laminar fractures associated with FTDF reflects the severity of the axial load compression [9].

The level of injury was predominantly at the C5 level,

reported at these levels, to the best of our knowledge, in the literature. This observation may be of some diagnostic value.

CT appeared to be of limited value in evaluating FTDF. CT was superior to polytomography in detecting the sagittal-body fracture, laminar fracture, and spinal stenosis [10]. However, the radiographic characteristics of FTDF were observed in the lateral view of the cervical spine. The comparable sagittal image was reformatted from the 3-mm axial slices and this was inferior to the lateral view of the polytomograms and even to the lateral plain cervical films.

An attempt was made to correlate the radiographic features and neurologic status of the patients. In five (83%) of the six cases with intact neurologic status, no sagittal-body or laminar fracture was present. This was compared with the presence of these fractures in 38 (97%) of 39 cases with complete or incomplete neurologic deficits. The posterior displacement of the posterior fragment of the body and the upper column was mild in the group with normal neurologic status as compared with the group with quadriplegia. Although the number of cases is too small to draw a meaningful implication, the absence of the sagittal-body and laminar fractures and a mild degree of posterior displacement of the posterior body

spine. There was no statistically significant differentiating feature between the group with complete neurologic deficits and the one with incomplete deficits.

Diagnostic confusion may occur between the FTDF and the other types of injury with a teardrop fragment in the involved body. A burst fracture produces fractures of the involved body with a smaller anterior and a larger posterior fragment that is retropulsed into the spinal canal. The posterior fragment is displaced posteriorly in the superior aspect as well as in the inferior aspect (Fig. 8). This is in contradistinction to the FTDF, in which the posterior displacement of the posterior fragment takes place in the inferior aspect and not in the superior aspect. In the burst fracture, the posterior ligamentous structures are essentially intact [1, 6, 11] and there is no widening of the interlaminar or interspinous space nor disruption of the spinolaminar line, although the facet joint space may be widened.

An extension injury may produce an avulsion fragment from the anteroinferior corner of the body, simulating a teardrop fragment of the FTDF. The involved body may be displaced posteriorly on the body below; however, the similarity should end here. The posterior ligamentous structures are intact and there is no kyphotic deformity of the cervical spine in the extension injury.

A distractive flexion injury may produce fractures of the body similar to those of the FTDF when the axial compression load is sufficiently forceful [2]. The sagittal-body and the laminar fractures may be present. The distractive force produces disruption of the posterior ligamentous structures with widening of the interspinous space, and kyphotic deformity of the cervical spine may also be present. These features are in common with those of FTDF; however, the cervical spine above the level of injury is displaced forward and often associated with unilateral or bilateral facet locking (Fig. 9). In contrast, the upper column is displaced backward in FTDF.

In conclusion, the radiographic characteristics of FTDF are as follows:

1. In the lateral radiographs, the involved vertebral body is divided into a smaller anterior fragment and a larger posterior fragment, which are displaced backward in the inferior aspect. The disk space between the posterior fragment and the vertebral body below is narrowed.

2. The upper column of the divided cervical spine is displaced backward in relation to the lower one at the level of injury. This feature, together with the appearance of the vertebral body, is diagnostic of FTDF.

3. If posterior displacement of the upper column is not present, widening of the interlaminar and interspinous spaces is supportive of the diagnosis of FTDF, provided there is no forward subluxation or dislocation of the cervical spine above the level of injury.

4. Widening of the facet joint space alone is not indicative of complete disruption of the posterior ligamentous structures. However, a substantial degree of posterior displacement of the inferior facet in relation to the superior facet below at the level of injury is suggestive of FTDF.

5. Sagittal-body and laminar fractures are frequently associated with FTDF at levels that are the same as or adjacent to the level of injury. The bilaterally fractured laminae at the level of injury were displaced inferiorly, in some cases, with paradoxical narrowing of the interlaminar and interspinous spaces between the level of injury and the one below. The interlaminar and interspinous spaces between the level of injury and the one above were widened in these cases.

6. FTDF occurred predominantly at the C5 level and less frequently at the C4 and the C6 levels, but it was never encountered at the C3 or the C7 level.

REFERENCES

1. Harris JH, Edeiken-Monroe B. *The radiology of acute cervical spine trauma*, 2nd ed. Baltimore: Williams & Wilkins, 1987
2. Lee C, Kim KS, Rogers LF. Triangular cervical body fragments: diagnostic significance. *AJR* 1982;138:1123-1132
3. Allen BL, Ferguson RL, Lehmann TR, O'Brian RP. A mechanistic classification of closed, indirect fractures and dislocations of the lower cervical spine. *Spine* 1982;7(1):1-27
4. Schneider RC, Kahn EA. Chronic neurological trauma to the spine and spinal cord. Part I. The significance of the acute flexion or "teardrop" fracture dislocation of the cervical spine. *J Bone Joint Surg (Am)* 1956;38:985-997
5. Gehweiler JA, Osborne RL, Becker RF. *The radiology of vertebral trauma*. Philadelphia: Saunders, 1980
6. Scher AT. "Teardrop" fractures of the cervical spine: radiologic features. *S Afr Med J* 1982;61:355-356
7. White AA, Panjabi MM. *Clinical biomechanics of the spine*. Philadelphia: Lippincott, 1978
8. Halliday DR, Sullivan CR, Hollinshead WH, Bahn RC. Torn cervical ligaments: necropsy examination of normal cervical region. *J Trauma* 1964;4:219-232
9. Lee C, Kim KS, Rogers LF. Sagittal fractures of the cervical vertebral body. *AJR* 1982;139:55-60
10. Acheson MB, Livingston RR, Richardson ML, Stimac GK. High resolution CT scanning in evaluation of cervical spine fractures: comparison with plain film examination. *AJR* 1987;148:1179-1185
11. Holdworth F. Fractures, dislocations and fracture dislocation of the spine. *J Bone Joint Surg (Am)* 1970;52(A):1534-1551

MR Imaging of the Pars Interarticularis

David W. Johnson¹
Gregory N. Farnum²
Richard E. Latchaw
S. Michael Erba³

MR imaging of the lumbar spine has become a useful method for the noninvasive evaluation of low back pain. However, bone abnormalities are more difficult to detect than soft-tissue lesions, such as herniated disk. We reviewed 14 MR images of the lumbar spine in adults with spondylolisthesis. These were correlated with CT scans and plain films in all cases. From the CT scans and plain films we found that seven patients had spondylolysis and that seven had other causes for their spondylolisthesis. It was our opinion that the MR images suggested an abnormality of the pars interarticularis in all seven of the cases confirmed to have spondylolysis and in six of the seven patients that did not have spondylolysis. We also studied four cadaver lumbar spines, obtained as blocks of tissue, and scanned in the coronal, sagittal, and axial planes with MR and in the sagittal and axial planes with CT. The tissue blocks were then sectioned in the sagittal plane. Spondylolysis is suggested on sagittal MR images when there is an interruption of the marrow signal in the pars as uninterrupted from the superior to

in the sagittal plane for anatomic evaluation and correlation with the imaging studies. All were scanned on the GE 1.5-T magnet in the sagittal, axial, and coronal planes using both a single-echo sequence, 600–800/25/2 (TR/TE/excitations), 256 × 256 matrix, and 16-cm field of view, and a multi-spin-echo sequence, 2500–3000/20–25/2–4, 128 × 256 or 256 × 256 matrix, and 16-cm field of view. The factors for the multiecho sequence were varied slightly in an effort to optimize scanning time and signal-to-noise ratio. All were scanned with a 5-mm slice thickness and 1-mm gap. Either the head or knee coil was used depending on the size of the block of tissue. One specimen was scanned on a GE 8800 CT scanner using contiguous 1.5-mm slices, and the other three specimens were scanned on the GE 9800 scanner using contiguous 3-mm slices. Bone algorithms were used for all images.

Clinical Study

We received 14 MR images of the lumbar spine in adults with spondylolisthesis. Patients included nine men and five women whose ages ranged from 18 to 63 years old. The MR images were correlated

with CT scans and plain films in all cases. All patients were imaged on a GE 1.5-T system with a 5.5 × 11-in. planar coil. Our standard lumbar spine protocol includes imaging in the sagittal and axial planes with a multi-spin-echo sequence (3000/20–25/2), 128 × 256 matrix, 5-mm slice thickness, and 1-mm gap. The field of view was 20–24 cm in the sagittal plane and 16–20 cm in the axial plane, depending on the girth of the patient. No special imaging technique was employed to improve visualization of the posterior elements. We applied the hypothesis that if pars defects on CT scans and plain films are appreciated by a break in the bone continuity, then on sagittal MR images a pars defect will be appreciated by a break in the continuity of the marrow signal. In other words, there must be an uninterrupted marrow signal from the superior to the inferior facet to indicate a normal pars interarticularis.

Results

A summary of the cadaveric and clinical findings is illustrated schematically in Figure 1.

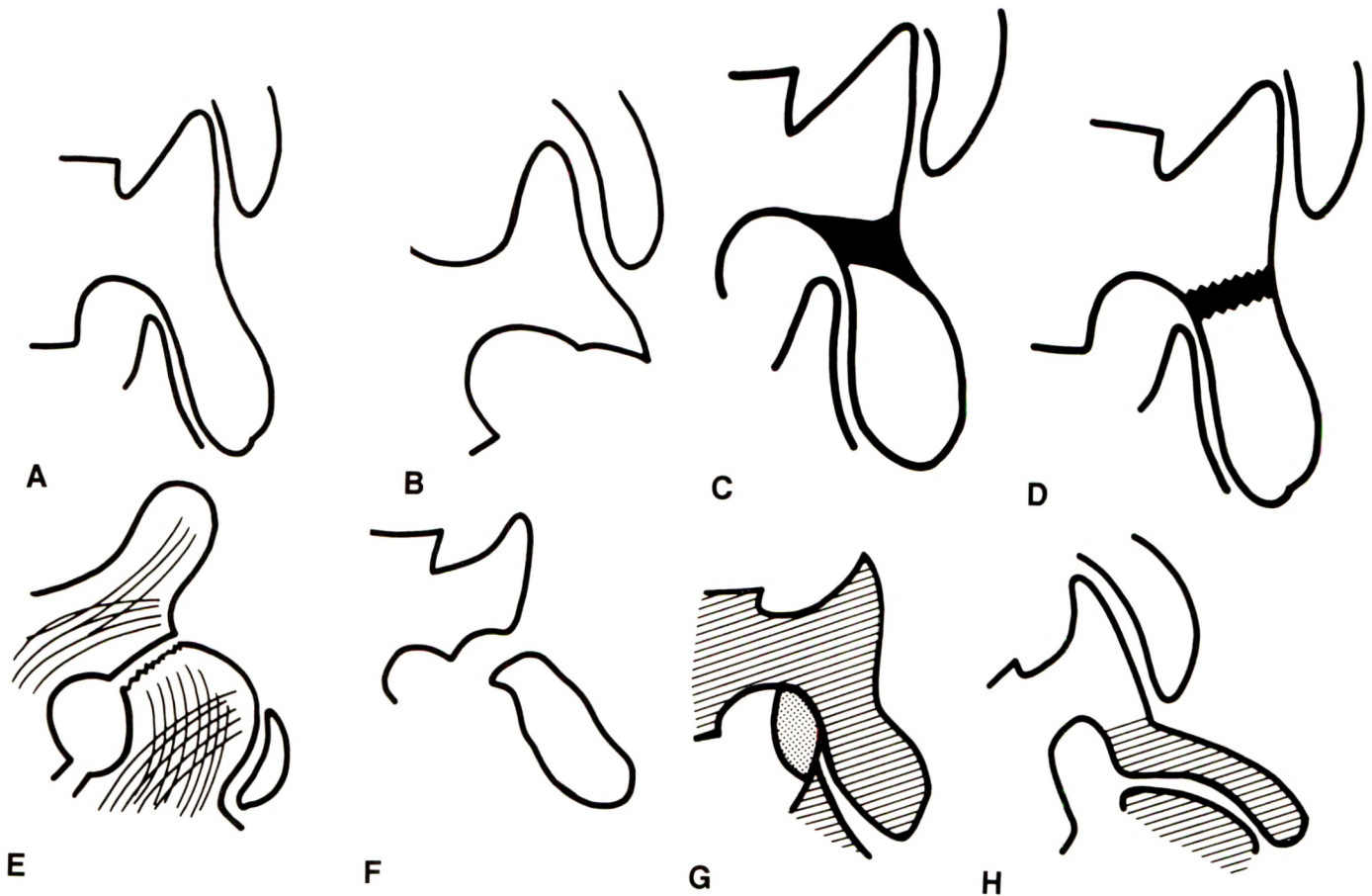


Fig. 1.—Schematic drawings summarize sagittal MR findings of clinical and cadaver studies.

- A, Normal pars, no sclerosis, marrow signal intact from superior to inferior facet.
- B, Partial facetectomy.
- C, Normal but sclerotic pars, marrow signal interrupted.
- D, Spondylolysis with sclerotic margins, no gap.
- E, Partial volume imaging of S1 superior facet and L5 pedicle simulating a break in the pars.
- F, Spondylolysis with gap.
- G, Metastatic disease with diffusely abnormal marrow signal (*diagonal lines*) and adjacent soft tissue mass (*dotted area*).
- H, Thin, sclerotic pars, degenerated facet with abnormal marrow signal (*diagonal lines*).

Cadaver Study

All the cadaver specimens had varying degrees of degenerative disk and facet changes at L4–L5 and L5–S1. None had spondylolysis, spondylolisthesis, blastic or lytic metastatic disease, or evidence of prior surgery or trauma. Of the 16 pars surveyed in four cadavers at L4 and L5, two had interruption of the marrow signal by MR. Direct sagittal CT revealed bone sclerosis. Figure 2 illustrates the CT and MR findings and the corresponding anatomic sections.

Clinical Study

From the CT scans and plain films we found that seven patients had bilateral spondylolysis and that seven had other causes for their spondylolisthesis. Four had degenerative spondylolisthesis; one had laminectomy, partial facetectomy, and posterior fusion; and one had metastatic breast carcinoma. One patient had an elongated, thin, sclerotic pars with degenerative changes in the posterior facets. MR suggested an abnormality of the pars interarticularis in all of the seven cases with confirmed spondylolysis and in six of the seven cases that did not have spondylolysis. Figures 3 and 4 illustrate the findings of spondylolysis (compare with Figs. 1D and 1F). By applying the criteria of an intact marrow signal from the superior to the inferior facet, we found four situations in which the pars can simulate spondylolysis on sagittal MR

images: (1) sclerosis of the neck of the pars, Figure 4 (compare with Fig. 1C); (2) partial volume imaging of the spur arising from the superior facet slightly lateral to the pars, Figure 5 (compare with Fig. 1E); (3) partial facetectomy, Figure 6 (compare with Fig. 1B); and (4) blastic metastatic replacement of the marrow of the pars, Figure 7 (compare with Fig. 1G).

Discussion

Slippage of the spine or "luxation of the lumbosacral joint" was described earlier [6] but Kilian [7] introduced the term spondylolisthesis to describe a forward slip of L5 on S1. The Greek word *olisthesis* means to slip or slide. Because the lordotic curve causes a downward tilt of the anterior aspect of the upper sacral endplate and usually of the lower lumbar endplate, the term spondylolisthesis has become synonymous with forward displacement of the upper vertebral body down the slope of the superior endplate of the lower vertebral body. The term retrolisthesis refers to posterior displacement of the upper vertebral body upon the lower. Though lateral plain films, sagittal CT scans, or MR images suggest a symmetric forward slip, most of the time the slip is asymmetric, causing a rotatory component [8].

Newman [9] classified spondylolisthesis into five types, as follows: type I, dysplastic—the result of an associated congenital abnormality of the arch of S1 and L5; type II, isthmic—





Fig. 3.—63-year-old woman with low back pain and history of L2–L5 laminectomy.

Fig. 6.—62-year-old man with history of laminectomy and fusion presented with acute exacerbation of bilateral lower-extremity weakness.

A and B, Adjacent sagittal MR images (3000/25/2) separated by 6 mm fail to identify entire pars/inferior facet structure (arrows) at L5. Left side is depicted. Plain films revealed fusion of L4-S1 and partial inferior facetectomies bilaterally at L5.

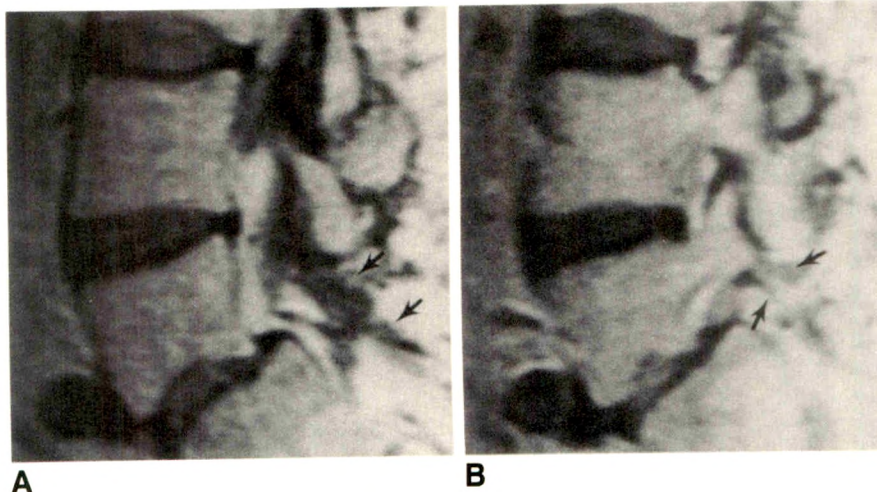
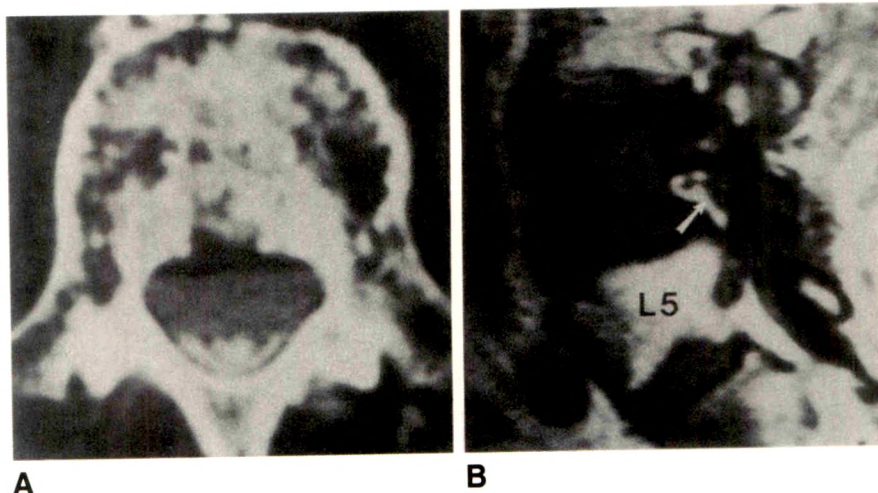


Fig. 7.—63-year-old man with history of metastatic breast cancer with new onset of radicular type right leg pain.

A, Axial CT scan of L4 shows blastic changes in the body and posterior elements but no spondylolysis.

B, Sagittal MR image (3000/25/2) shows abnormally low marrow signal in the body, pars, and inferior facet of L4 and the superior facet and pars of L5 with soft tissue narrowing the L4-L5 neural foramen (arrow), all compatible with metastasis.



the result of a defect in the pars interarticularis that may be (a) a fatigue fracture, (b) an elongated but intact pars, or (c) an acute fracture; type III, degenerative—the result of a long-standing intersegmental instability and degeneration of the disk and facets; type IV, traumatic—the result of fractures in areas of the posterior elements other than the pars interarticularis; and type V, pathologic—the result of generalized or localized bone disease.

Symptoms

Symptoms of spondylolisthesis run the whole gamut from no symptoms to mild or severe, and intermittent to constant backache with or without radicular complaints. There may also be no complaint of backache despite symptoms and signs of nerve root compression or cauda equina syndrome. Stenosis of the neural foramina at the level of the slip and in some cases secondary degenerative spurs further narrowing the foramina are important factors in nerve root compression in this syndrome [10].

Imaging

CT has added much to the plain-film and myelographic evaluation of spondylolisthesis, particularly because of the superior resolution of small bone abnormalities of the neural arch and the added soft-tissue detail that facilitates the evaluation of spinal canal and neural foraminal stenosis. The "incomplete ring" sign describes the axial CT findings of spondylolysis [11]. However, the presence of a grade I spondylolisthesis may be missed if only the axial images are evaluated. Often, sagittal and coronal reformatting of high-resolution axial images add a new perspective to foraminal stenosis and the interrelationships of anomalies, slips, fractures, or bone spurs in three-dimensional space [12, 13]. The use of a midline sagittally reformatted image can demonstrate the presence of the pseudobulging disk at the level of the slip [14].

MR has proved to be a significant addition to the imaging of the lumbar spine. It has for the first time revealed noninvasively the internal architecture of the disk itself [1-3] and

its degree of hydration relative to other disks in the sagittal image. The detection of disk herniation is comparable to, and in some cases surpasses, CT and myelography [2, 4, 5]. This is not the case, however, regarding bone structures. Because of the lack of signal from solid structures—namely the cortical bone and trabeculae—bone abnormalities manifest themselves by signal changes in the marrow and by their effects on surrounding soft tissues. MR has demonstrated great sensitivity to bone marrow abnormalities. Moore et al. [15] reported an increase in T1 relaxation times in the bone marrow of children with acute lymphocytic leukemia. With aging, fat replaces hematopoietic marrow causing a decrease in T1 and T2 relaxation times [16]. Aseptic necrosis of the bone marrow is manifested as a prolonged T1 relaxation time [17]. MR has a high sensitivity and specificity for vertebral osteomyelitis, demonstrating prolonged T1 and T2 relaxation times in the vertebral body [18]. Neoplasms demonstrate prolonged T1 and T2 relaxation times in the vertebral body, often appearing multiple, of varying size and location [19]. If these tumors cause an osteoblastic response, there is a shortened T2 relaxation time. Gross features of fractures/dislocations of the vertebral body can also be easily appreciated, particularly with respect to encroachment upon the spinal canal and compression of the cord [20].

In our study, we found that the optimal images for evaluating the pars interarticularis were the short TR/short TE or long TR/short TE sequence. These factors optimize signal-to-noise ratio and allow the greatest contrast between marrow and the signal void of cortical bone. There is no best plane for evaluating the entire pars interarticularis because it is obliquely oriented to the sagittal, coronal, and axial planes. The sagittal plane is more useful than the other two for several reasons. The obliquity of the pars in the sagittal plane is minimal and a 5-mm slice thickness properly positioned will also include the pedicle, superior, and inferior facets. Abnormal marrow signal in the pars can be easily compared with adjacent marrow containing structures in the same image. In those individuals without scoliosis the pars interarticularis of all the lumbar segments can be evaluated on one or occasionally two adjacent sagittal images. Furthermore, spondylolisthesis and foraminal stenosis are best appreciated in the sagittal plane. These are secondary findings, of course, and may not coexist with a pars abnormality; but these findings are more obvious, indicating a closer study of the images to ascertain the cause.

Our high false-positive rate was most likely due to the rather inclusive wording of the hypothesis. An interruption in the continuity of the marrow signal cannot be synonymous with a break in the pars because any process that replaces marrow (i.e., lytic or blastic metastasis or bony sclerosis) should alter the marrow signal. The false positives encountered in our series had other features that were unique to themselves. The patient with metastasis (Fig. 7) had lesions in other marrow-containing structures and soft-tissue metastasis in the neural foramen. The patient with partial inferior facetectomy (Fig. 6) on two adjacent images had no clearly defined inferior facet. The false break in the pars encountered in those with degenerative facet disease was due to partial volume averaging of the superior facet spur and the adjacent

pedicle (Figs. 2 and 5). However, one should be able to identify correctly the superior facet arising from the lower vertebral segment, and on the more medial adjacent image the intact pars should be seen. Sclerosis of the pars is the false-positive appearance that most resembles spondylolisthesis when there is minimal spondylolisthesis. Higher grades of spondylolisthesis due to spondylolysis (\geq grade II) should leave a gap in the pars defect (Fig. 4). Our true positives all demonstrated marrow abnormalities limited only to the pars itself, corresponding closely with the extent of abnormality seen on plain films and/or CT.

In conclusion, much information can be gleaned from the routine sagittal MR. Pars abnormalities can be detected without the use of additional sequences. The exact nature of the pars abnormality may remain obscure, but by using our criteria, one can acquire information from the routine sagittal MR that may raise the level of suspicion sufficiently to recommend CT and/or plain-film corroboration.

REFERENCES

1. Pech P, Haughton VM. Lumbar intervertebral disk: correlative MR and anatomic study. *Radiology* 1985;156:699-701
2. Modic MT, Pavlicek W, Weinstein MA, et al. Magnetic resonance imaging of intervertebral disk disease. *Radiology* 1984;152:103-111
3. Aguila LA, Piraino DW, Modic MT, Dudley AW, Duchesneau PM, Weinstein MA. The intranuclear cleft of the intervertebral disk: magnetic resonance imaging. *Radiology* 1985;155:155-158
4. Maravilla KR, Lesh P, Weinreb JC, Selby DK, Mooney V. Magnetic resonance imaging of the lumbar spine with CT correlation. *AJNR* 1985;6:237-245
5. Edelman RR, Shoukimas GM, Stark DD, et al. High resolution surface-coil imaging of lumbar disk disease. *AJR* 1985;144:1123-1129
6. Stone KH. The etiology of spondylolisthesis. *J Bone Joint Surg* 1963;45B:39-59
7. Kilian HF. *Schilderungen neuer Beckenformen und ihres Verhaltens im Leben*. Mannheim:Verlag von Basserman & Mathy, 1854
8. Farfan HF. The pathological anatomy of degenerative spondylolisthesis. *Spine* 1980;5:412-418
9. Newman PH. The etiology of spondylolisthesis. *J Bone Joint Surg* 1963;45B:39-59
10. Edelson JG, Nathan H. Nerve root compression in spondylolysis and spondylolisthesis. *J Bone Joint Surg* 1986;68B:596-599
11. Langston JW, Gavatt ML. "Incomplete ring" sign: a simple method for CT detection of spondylolysis. *J Comput Assist Tomogr* 1985;9:728-729
12. Rothman SLG, Glenn WV. CT multiplanar reconstruction in 253 cases of lumbar spondylolysis. *AJNR* 1984;5:81-90
13. Rothman SLG, Glenn WV, Kerber CW. Multiplanar CT in the evaluation of degenerative spondylolisthesis. A review of 150 cases. *Comput Radiol* 1985;9:223-232
14. Teplick JG, Laffey PA, Berman A, Haskin ME. Diagnosis and evaluation of spondylolisthesis and/or spondylolysis on axial CT. *AJNR* 1985;7:479-491
15. Moore SG, Gooding CA, Brasch RC, et al. Bone marrow in children with acute lymphocytic leukemia: MR relaxation times. *Radiology* 1986;160:237-240
16. Doms GC, Fisher MR, Hricak H, Richardson M, Crooks LE, Genant HK. Bone marrow imaging: magnetic resonance studies related to age and sex. *Radiology* 1985;155:429-432
17. Modic MT, Weinstein MA, Pavlicek W, et al. Nuclear magnetic resonance imaging of the spine. *Radiology* 1983;148:757-762
18. Modic MT, Feiglin DH, Piraino DW, et al. Vertebral osteomyelitis: assessment using MR. *Radiology* 1985;157:157-166
19. Modic MT, Masaryk T, Paushter D. Magnetic resonance imaging of the spine. *Radiol Clin North Am* 1986;24:229-245
20. McArdle CB, Crofford MJ, Mirfakhraee M, Amparo EG, Calhoun JS. Surface coil MR of spinal trauma: preliminary experience. *AJNR* 1986;7:885-893

Incidental Detection of Hematopoietic Hyperplasia on Routine Knee MR Imaging

Andrew L. Deutsch¹
 Jerrold H. Mink¹
 Fred P. Rosenfelt²
 Alan D. Waxman³

An unusual appearance of the marrow of the distal femur, characterized by confluent foci of diminished signal intensity replacing the normally expected bright signal of fatty marrow on all pulse sequences, was encountered in 10 asymptomatic patients undergoing routine knee MR imaging. This prompted initial concern about the possibility that this appearance was due to lymphoma or occult myeloproliferative malignancy. All patients were mild to moderately obese, and all but one were women. Peripheral blood analysis was obtained in nine patients and was normal in five. The other four were cigarette smokers with a peripheral leukocytosis. Bone-marrow biopsy of the distal femur in two patients and of the iliac crest in three, performed to exclude malignancy, showed hypercellular but otherwise normal-appearing hematopoietic (red) marrow. The patients have been followed for 4–15 months without evidence of malignancy.

We conclude that extensive foci of hematopoietic marrow may be encountered incidentally in patients undergoing MR examination. Careful follow-up to date suggests that this most likely represents a benign process and that patients in whom this appearance is encountered can be managed conservatively.

MR has the capacity to differentiate hematopoietic and fatty marrow with great precision, as well as to detect abnormalities of marrow with high sensitivity [1–11]. In the course of routine knee MR imaging for internal derangement, we encountered patients with MR evidence of hyperplastic hematopoietic (red) marrow replacing the normally fatty (yellow) marrow in the long bones around the knee. These findings caused concern that they might be due to a lymphoma or a myeloproliferative malignancy. As a result, the first four patients had a bone-marrow biopsy to exclude this possibility.

We describe the typical MR findings of hematopoietic hyperplasia in 10 patients, review the clinical findings in these patients, and describe the histologic features of the bone marrow.

Materials and Methods

We reviewed the MR examinations and medical records of 10 patients whose MR imaging studies showed foci of hematopoietic marrow in the long bones about the knee. The MR images had been obtained for suspected abnormalities of the knee joint. The appropriate cases were found by recall of all scans obtained between January 1987 and April 1988 (approximately 1400 studies) that had the coded diagnosis of "marrow." The patients were 32–72 years old. Nine of the 10 patients were women.

All MR examinations were performed on a 1.5-T Signa system (General Electric, Milwaukee, WI). The technique has been described in detail [12]. The examinations were performed with the patient supine and the knee externally rotated 10°–20°. An initial coronal T1-weighted imaging sequence, 800/20 (TR/TE), was performed with two excitations, a 5-mm image section, and no interslice gap. A 16-cm field of view and 128 × 256 matrix were used. A sagittal sequence was selected from the coronal. A spin-echo, multiecho sequence, 2000/20,80, was obtained again with a 16-cm field of view and 5-mm slice thickness.

Four patients underwent comprehensive hematologic/oncologic evaluation (physical examination, peripheral blood analysis, and marrow biopsy). Complete blood counts with cell

Received August 12, 1988; accepted after revision October 10, 1988.

¹ Department of Diagnostic Radiology, Section of Musculoskeletal Radiology, Cedars-Sinai Medical Center, 8700 Beverly Blvd., Los Angeles, CA 90048. Address reprint requests to A. L. Deutsch.

² Department of Medicine, Cedars-Sinai Medical Center, Los Angeles, CA 90048, and Department of Medicine, University of California, Los Angeles, Medical Center, Los Angeles, CA 90024.

³ Department of Nuclear Medicine, Cedars-Sinai Medical Center, Los Angeles, CA 90048, and Department of Radiology, University of Southern California Medical Center, Los Angeles, CA 90033.

AJR 152:333–336, February 1989
 0361–803X/89/1522–0333
 © American Roentgen Ray Society

differentials were available in nine patients. Open biopsy of the distal femur was accomplished in two patients, and percutaneous trephine biopsy of the iliac crest was performed in the three other patients. (One patient underwent both open biopsy of the distal femur and closed biopsy of the iliac crest.) Conventional knee radiographs were available in eight patients. Survey MR of the pelvis and opposite extremity was done in one patient. The patients have been followed clinically since MR imaging for 4–15 months; one patient with chronic leukocytosis has been followed clinically for 12 years.

Results

All MR examinations showed extensive regions of diminished signal intensity replacing the normally expected bright

signal of fatty marrow on all pulsing sequences. These changes were best seen on the T1-weighted sequences (Fig. 1). The abnormal foci were confluent and broad-based and extensively involved the distal metaphysis of the femur in all patients with striking epiphyseal sparing. The proximal tibial metaphysis was involved with similar findings in two patients, and the proximal fibular metaphysis was involved in one patient. The abnormal areas did not significantly increase in signal intensity on T2-weighted images (Fig. 2).

Conventional radiographs, available in eight patients, were normal. A limited MR survey in one patient showed abnormal foci within the distal femur in the opposite extremity (Fig. 3). The pelvis and contralateral proximal femur were normal.

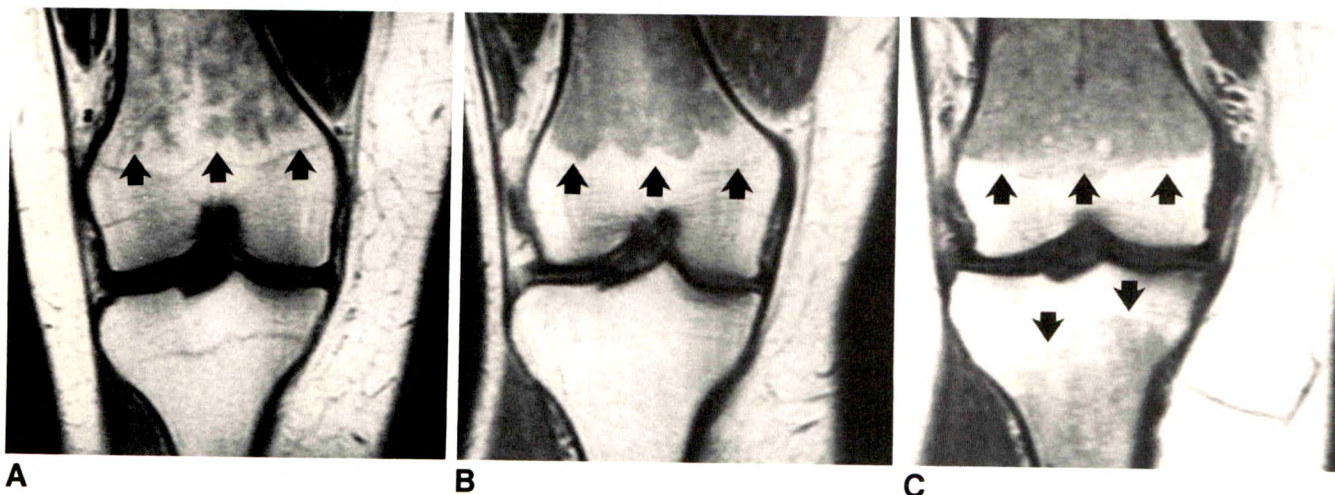


Fig. 1.—Hematopoietic hyperplasia. Spectrum of changes.

A, Coronal image, 800/20, in 30-year-old obese woman shows multiple partially confluent linear-to-ovoid areas of decreased signal within distal femoral metaphysis (arrows). Epiphysis is spared and proximal tibia is uninvolved.

B, Coronal spin-echo image, 800/20, in 47-year-old obese woman. Peripheral foci of red marrow are more confluent (arrows). Note that epiphysis is spared and there is no involvement of tibia.

C, Coronal spin-echo image, 800/20, in 41-year-old woman. There is marked confluent broad-based diminution of normally expected high signal within distal femoral metaphysis (arrows). Proximal tibia shows less extensive involvement. Note epiphyseal sparing.

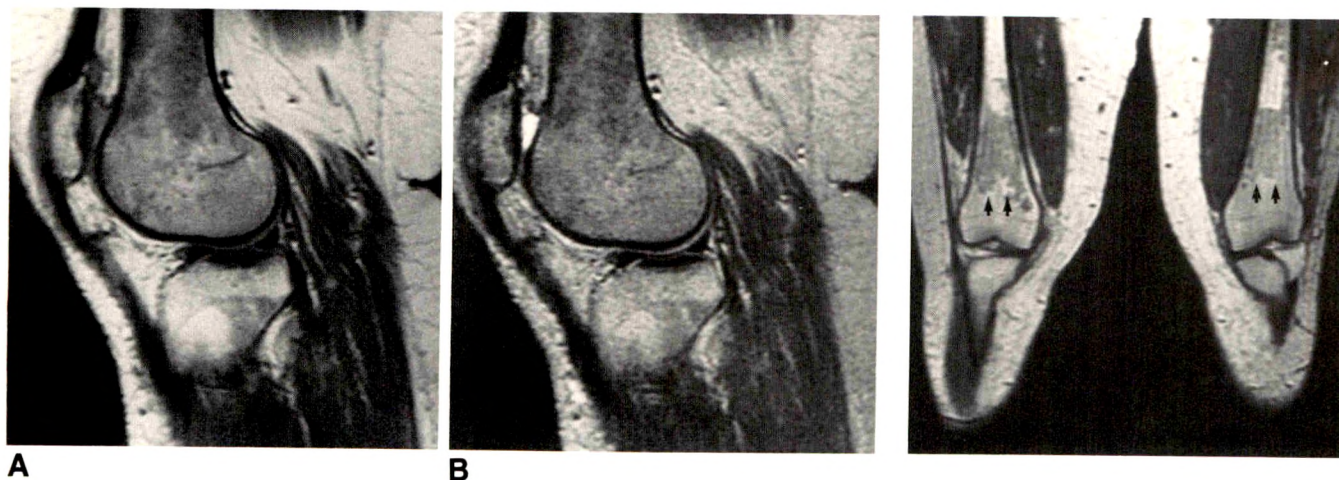


Fig. 2.—Hematopoietic hyperplasia.

A, Sagittal spin-echo sequence, 2000/20, shows confluent foci of decreased signal within distal femoral metaphysis.

B, Sagittal spin-echo image, 2000/80, shows no increase in signal intensity within hyperplastic marrow.

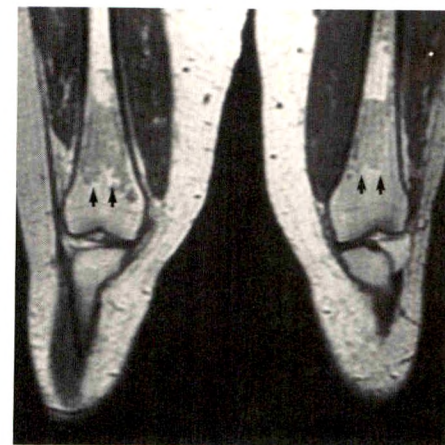


Fig. 3.—Limited MR survey. Coronal image, 800/20, of both distal femurs obtained as part of MR survey in 36-year-old moderately obese woman. Note focal, nearly symmetric, and increasingly confluent areas of decreased signal within distal femurs bilaterally (arrows).

Physical examination revealed all patients to be mildly to moderately obese with weights of 130–210 lb. (59–95.5 kg). Medical history and a review of systems resulted in no common clinical findings except for a history of cigarette smoking in six patients. Menstrual histories were unremarkable.

Analysis of the peripheral blood was normal in five patients and abnormal in four. The abnormal results included mild to moderate leukocytosis with WBCs of 12,000–16,000/ μ l. No differential shift was present. All patients with leukocytosis were cigarette smokers. Hemoglobin, hematocrit, and RBC indexes were normal in all patients. No reticulocytosis was noted. One patient had a documented 12-year history of mild leukocytosis of unknown cause.

Posterior iliac crest biopsy, performed in three patients, showed mild to moderate hypercellularity without evidence of malignancy. The hematopoietic to fat ratio ranged from 60:40 to 70:30. The granulocytic series showed complete and normal maturation. Erythroid series showed normoblastic maturation. The myeloid:erythroid ratio was approximately 3:1 in all patients. Lymphocytes were normal. Iron stores were normal to slightly increased. Open biopsy of the distal femur, performed in two patients, revealed hypercellular but otherwise normal-appearing hematopoietic marrow uncharacteristic for this location (Fig. 4). The marrow cellularity was 30% in one patient and 50% in the other patient who underwent open biopsy.

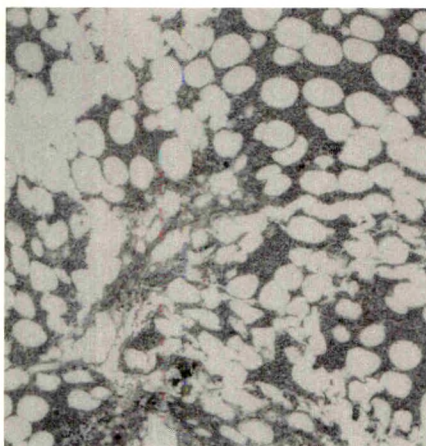
Discussion

In the fetus, bone marrow is entirely hematopoietic (red). After birth, conversion to fatty marrow begins in the distal extremities, followed by the epiphyses and midshaft of the long bones (Fig. 5). By young adulthood, hematopoietic marrow is confined to the axial skeleton, proximal humeri, femoral neck, and intertrochanteric regions [2, 6]. Hematopoietic marrow is composed of both cellular elements and varying degrees of fat, with the fat intimately mixed with the cellular

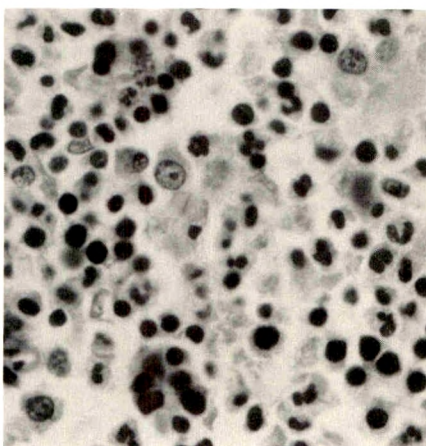
elements [6]. The percentage of fat within the red marrow progressively increases with age. The mixture of fat and water constituents results in each contributing significantly to signal intensity. On spin-echo imaging, hematopoietic marrow has lower to intermediate signal intensity on both T1- and T2-weighted images as compared with fatty marrow [1, 5]. It has additionally been suggested that nonuniform magnetic susceptibility caused by intracellular iron in hematopoietic marrow may contribute to T2 shortening, and thus to the decreased signal intensity of hematopoietic marrow compared with fatty marrow on spin-echo imaging [6]. Yellow marrow is characterized by high signal intensity on T1-weighted images, which decreases slightly on T2-weighted scans. The high signal relates to the nearly exclusive contribution from aliphatic protons and reflects the low cellularity of fatty marrow [1, 6]. The contrast between red and yellow marrow is maximized on T1-weighted scans [3, 5]. Phase-contrast images provide more contrast between fatty and hematopoietic marrow than do standard T1-weighted spin-echo images [8].

Hematopoietic requirements in the adult normally are satisfied by the red marrow existing in the axial skeleton and proximal femora and humeri. Under conditions of stress, yellow marrow can undergo reconversion to hematopoietic marrow [2]. The yellow marrow elements do not themselves actually convert, but rather the conditions permit for hyperplasia of the existing hematopoietic elements. This phenomenon is most commonly observed in chronic anemias (particularly hemolytic types) and infiltrative marrow disorders, both benign and malignant, such as Gaucher disease, myelofibrosis, myeloma, and metastatic disease. Fatty marrow "reconversion" begins proximally and extends distally, the reverse of physiologic marrow conversion [2, 13].

The marrow changes depicted by MR in this series appeared to follow the reverse pattern of reconversion. In no case were changes present in the tibia and fibula in the absence of extensive femoral involvement. Peripheral marrow extension in otherwise normal individuals has not, to our



A



B

Fig. 4.—Femoral biopsy.
A, Low-power photomicrograph of distal femoral biopsy specimen reveals marked increase in marrow cellularity (30%) for this anatomic site. (H and E, $\times 40$)
B, High-power photomicrograph shows normal maturation of all cell lines. (H and E, $\times 500$)

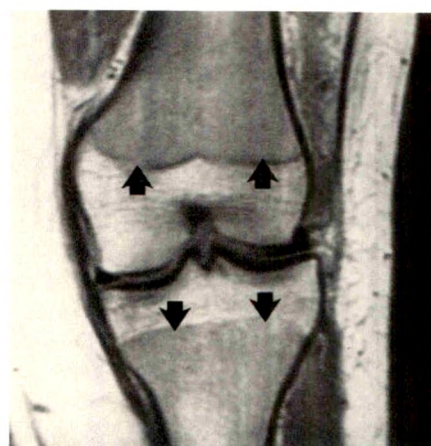


Fig. 5.—Normal child. Coronal spin-echo image, 800/20, of left knee of 11-year-old girl. Note uniform decreased signal of metaphyseal regions of tibia and femur reflecting normal distribution of hematopoietic marrow in this age group (arrows). Epiphysis shows normal fatty marrow.

knowledge, been reported previously as a finding in marrow scintigraphy [14]. Prior scintigraphic marrow imaging has been performed primarily with ^{99m}Tc -sulfur colloid or ^{111}In -chloride as the imaging agents. The basis for marrow imaging with radiocolloids relates to their phagocytosis by the reticuloendothelial system [14]. As such, radiocolloid methods afford only an indirect depiction of marrow hematopoietic function. Indium-111 may be a more direct indicator of marrow hematopoietic function because it binds to transferrin and partially acts as an iron analog before incorporation into protoporphyrin nine. The apparent discordance between the MR findings reported in our series and the previous scintigraphic experience may reflect differences in sensitivity between the two methods. This, however, must remain speculative at this time because we have not had an opportunity to critically evaluate this question.

No unifying basis could be identified to account for the changes in the peripheral marrow in our patients. All patients were mild to moderately obese, and all but one were women. Menstrual histories were unremarkable (one patient was postmenopausal), and there were no known hormonal abnormalities. A moderate leukocytosis was observed in four of the patients, and these four patients were all cigarette smokers. The association of leukocytosis and cigarette smoking has been recognized previously and is believed to represent a direct effect of smoking, probably related to chronic bronchitis [15]. No gender differences have been observed with regard to this latter phenomenon. The leukocytosis observed in the group of smokers does not explain the presence of the finding in the one smoking patient without leukocytosis and the four nonsmokers.

The differential diagnosis of hematopoietic hyperplasia incorporates a spectrum of marrow disorders including malignancies, chronic anemias, and nonneoplastic infiltrative disorders. The concern with regard to possible lymphoma or occult myeloproliferative malignancy led to biopsy in the first four patients in whom these MR findings were incidentally encountered. Acute leukemias, given their severe systemic findings, are clinically unlikely to be detected incidentally on routine knee MR. Chronic granulomatous leukemia, which may be asymptomatic in up to 20% of patients at the time of diagnosis, could possibly be encountered initially on MR performed for internal derangement. The MR appearance of leukemic infiltration of the marrow has been well described and could pose a significant problem in differential diagnosis based solely on the MR appearance, particularly when marked hypercellularity is present [4, 7, 11]. The epiphyseal sparing observed in all of our patients may be of some value in the differential diagnosis because this finding suggests a less significant insult and lesser degree of recruitment of yellow marrow. In addition, no areas of increased signal intensity were identified on T2-weighted images in patients with hematopoietic hyperplasia. This contrasts with what is sometimes observed with malignant marrow processes. Analysis of the peripheral blood should allow the diagnosis of chronic leukemia to be established. Chronic anemias, particularly sickle cell, are associated with marked expansion of hematopoietic marrow [16]. Although the MR appearance could be strikingly similar to hematopoietic hyperplasia, the history and analysis of the peripheral blood will allow the diagnosis to be established. Both primary hemosiderosis or hemosiderosis caused by multiple blood transfusions show more marked

diminution in signal intensity than is observed with hematopoietic hyperplasia and should not be confused on the basis of MR examination. Gaucher disease could present a nearly identical MR appearance, but one should be able to differentiate it clinically [10]. In addition, the Erlenmeyer flask deformity seen in some patients with Gaucher disease is distinctive of this entity. Infiltration of marrow caused by lymphoma, myeloma, and primary malignancy usually has a more nodular and masslike appearance than has been encountered with incidental depiction of hematopoietic hyperplasia.

With the increased use of MR for evaluation of articular disease, incidental depiction of marrow abnormalities probably will be encountered increasingly. We have frequently observed smaller isolated foci of red marrow that are characteristically situated both posteriorly and peripherally within the distal femur in younger adults of both genders well into their third decade. These foci, however, are far less extensive than those reported here and have been assumed to be within normal limits, although they have not been studied critically. On the basis of our experience to date, when the marrow pattern described in this article is detected incidentally in patients, particularly in mildly to moderately obese women, the findings can be considered to most likely reflect a benign process. A complete examination and analysis of the peripheral blood are recommended in all of these patients. If these parameters are normal, the patients can be followed conservatively, and the findings need not necessitate biopsy.

REFERENCES

- Porter EA, Shields AF, Olson DO. Magnetic resonance imaging of bone marrow disorders. *Radiol Clin North Am* 1986;24(2):269-289
- Kricum ME. Red-yellow marrow conversion: its effect on the location of some solitary bone lesions. *Skeletal Radiol* 1985;14:10-19
- Dooms GC, Fisher MR, Hricak H, Richardson M, Crooks LE, Genant HK. Bone marrow imaging: magnetic resonance studies related to age and sex. *Radiology* 1985;155:429-432
- Daffner RH, Lupetin AR, Dash N, Deeb ZL, Sefczek RJ, Schapiro RL. MRI in the detection of malignant infiltration of bone marrow. *AJR* 1986;146:353-358
- Kaplan PA, Asleson RJ, Klassen LW, Duggan MJ. Bone marrow patterns in aplastic anemia: observations with 1.5-T MR imaging. *Radiology* 1987;164:441-444
- Mitchell DG, Rao VW, Dalinka W, et al. Hematopoietic and fatty bone marrow distribution in the normal and ischemic hip: new observations with 1.5-T MR imaging. *Radiology* 1986;161:199-202
- Moore SG, Gooding CA, Brasch RC. Bone marrow in children with acute lymphocytic leukemia: MR relaxation times. *Radiology* 1986;160:237-240
- Wisner GL, Rosen BR, Buxton R, Stark DD, Brady TS. Chemical shift imaging of bone marrow: preliminary experience. *AJR* 1985;145:1031-1037
- Hajck PC, Baker LL, Goodbar JE, et al. Focal fat deposition in axial bone marrow: MR characteristics. *Radiology* 1987;167:245-249
- Lanir A, Hadar H, Cohen I, et al. Gaucher disease: assessment with MR imaging. *Radiology* 1986;161:239-244
- McKinstry SC, Steiner RE, Young AT, Jones L, Swirsky D, Aber V. Bone marrow in leukemia and aplastic anemia: MR imaging before, during, and after treatment. *Radiology* 1987;162:701-707
- Mink JH, Reicher MA, Cruess JV III. *Magnetic resonance imaging of the knee*. New York: Raven, 1987
- Piney A. The anatomy of the bone marrow. *Br Med J* 1922;2:792-799
- Price DC. Bone marrow scintigraphy. In: Matin P, ed. *Clinical nuclear medicine*. Garden City, NY: Medical Examination Publishing, 1986:92-116
- Friedman GD, Stegelaub AB, Seltzer CC, Feldman R, Cohen MF. Smoking habits and the leukocyte count. *Arch Environ Health* 1973;26:137-139
- Rao VM, Fishman M, Mitchell DG, et al. Painful sickle cell crisis: bone marrow patterns observed with MR imaging. *Radiology* 1986;161:211-215

Pictorial Essay

Imaging of Pigmented Villonodular Synovitis with Emphasis on MR Imaging

James S. Jelinek,^{1,2} Mark J. Kransdorf,^{1,2} Joseph A. Utz,^{1,2} B. Hudson Berrey, Jr.,^{2,3} Jeffrey D. Thomson,³ Richard D. Heekin,³ and Mark S. Radowich^{1,2}

Pigmented villonodular synovitis (PVNS) is a term given to a family of benign proliferative lesions of the synovium of the joint, bursa, and tendon sheath. It is seen in both localized and diffuse forms. The localized form typically involves the small bones of the hands and usually is termed nodular synovitis, giant cell tumor of tendon sheath, fibrous histiocytoma of synovium, or pigmented nodular synovitis. The diffuse form, the subject of this essay, usually occurs in the large joints and is termed PVNS. Pathologically, PVNS is characterized by multinucleated giant cells with a characteristic pigmentation due to both intra- and extracellular hemosiderin [1, 2]. The imaging studies of seven patients with PVNS were reviewed, and the findings seen on radiography, arthrography, sonography, bone scintigraphy, angiography, CT, and MR are illustrated. Several lesions that mimicked PVNS on MR are also shown, and their distinguishing features are discussed.

Materials and Methods

One hundred eight-two patients with musculoskeletal diseases were evaluated by MR at our institution. Sixty-four of these patients had soft-tissue tumors, of which seven were pathologically proved cases of PVNS. The diagnosis of PVNS was suggested preoperatively in all but one case. Four cases that mimicked PVNS on MR studies are discussed also. All patients with PVNS were evaluated by the orthopedic surgery service and had surgical biopsy. All patients

had plain radiographs and MR examinations. In addition, five patients had CT. Angiography was performed in two patients, and five patients had three-phase bone scintigraphy. Arthrograms were available in two patients, and one patient was examined with real-time sonography.

MR studies were performed on a 1.5-T superconducting MR imager (Technicare Inc., Solon, OH) or a 0.6-T superconducting MR imager (Picker International, Highland Heights, OH). Images were obtained by using both T1-weighted (200–700/20–40 [TR/TE]) and T2-weighted (1400–2200/40–100) spin-echo sequences. The MR studies were compared with results of the other imaging techniques.

Results

There were seven pathologically proved cases of PVNS. The diagnosis of four abnormalities that mimicked PVNS on MR included hip and knee synovial chondromatosis, hemangioma of the elbow, and rheumatoid arthritis of the knee. The cases of PVNS were located at the knee (three cases), the hip (three cases), and the ankle (one case).

Plain radiographs showed normal bones on both sides of the joint in two cases. In four of the five remaining cases, either a soft-tissue mass or joint effusion in addition to erosive bone changes was discernible on the radiographs (Fig. 1A). The remaining patient had well-defined, sclerotic bone erosions without a joint effusion or soft-tissue mass. Four of the lytic bony changes were on both sides of the joint, and in one

Received August 8, 1988; accepted after revision October 4, 1988.

¹ Department of Radiology, Walter Reed Army Medical Center, Washington, DC 20307. Address reprint requests to J. S. Jelinek.

² Department of Radiology, Uniformed Services University of Health Sciences, Bethesda, MD 20012.

³ Department of Orthopedic Surgery, Walter Reed Army Medical Center, Washington, DC 20307.

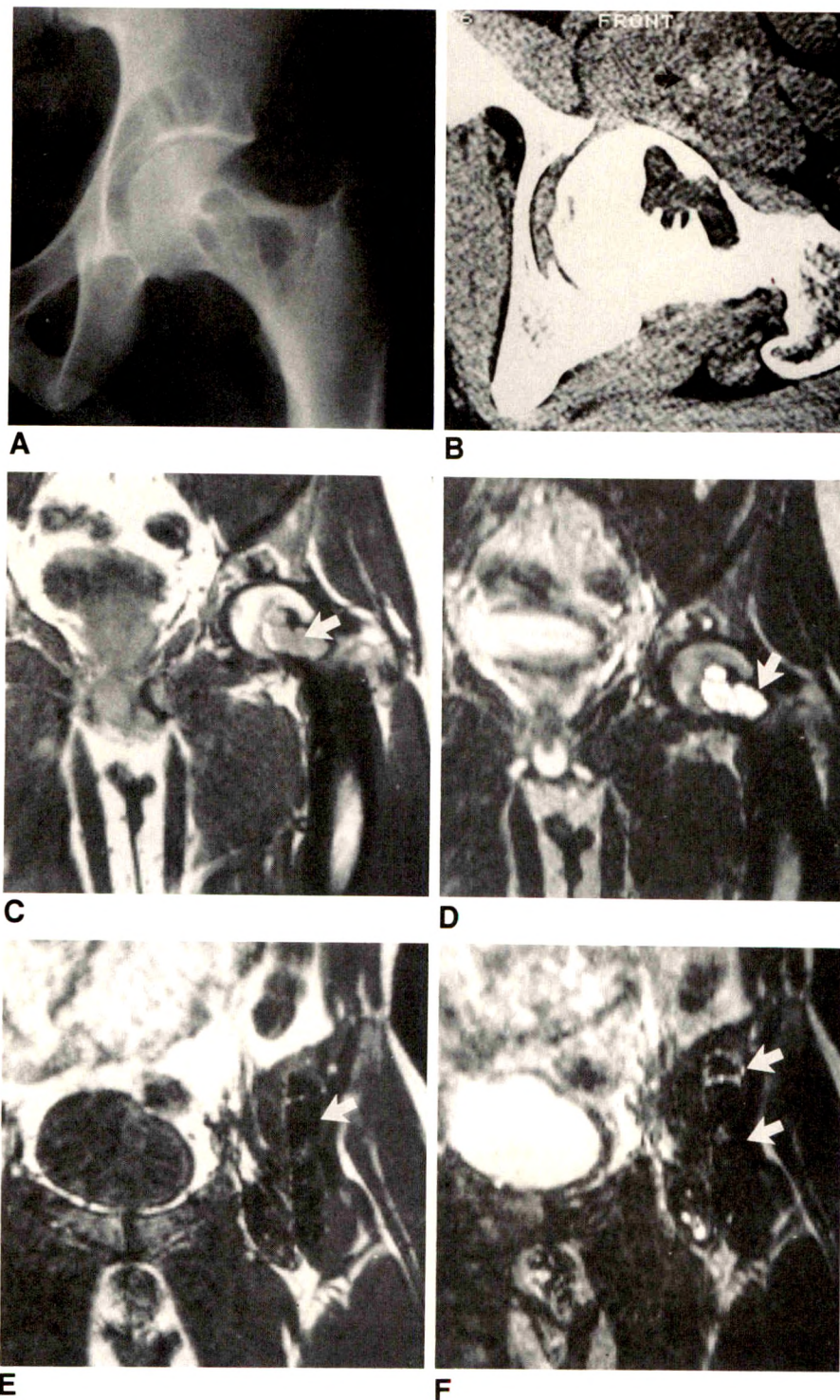


Fig. 1.—Pigmented villonodular synovitis of the hip.

A, Radiograph of left hip shows geographic lytic lesions with well-defined sclerotic margins on both sides of joint, consistent with synovial process.

B, Corresponding axial image from noncontrast CT scan at level of femoral neck shows geographic lesion, which is primarily intraosseous with small defect in anterior cortex as only communication with joint space. Soft-tissue mass with focal region of increased density anteriorly (arrow) may represent calcification or deposition of hemosiderin.

C and D, Coronal T1-weighted (700/33) (C) and T2-weighted (1000/100) (D) MR images show bony changes that correspond to those on plain films. Signal from region of bony defects shows typical mixed signal. Bony septa or ridges crossing lesion on plain film are seen here as fine linear streaks of signal void (arrows).

E and F, T1-weighted (700/33) (E) and T2-weighted (1000/100) (F) MR images show area of markedly decreased signal intensity on both pulse sequences within soft tissues in distribution similar to area of increased flow on bone scan. Decreased signal is caused by deposition of hemosiderin within hypervascular tumor mass (arrows).

case bone changes were apparent on only one side of the joint.

Three-phase bone scintigraphy was performed in five patients. All patients had increased flow and blood pool in the regions of the soft-tissue masses. Those patients with lytic defects seen on either plain-film radiography or CT had increased bone uptake of radionuclide on delayed images in the region of those defects. The large extraarticular soft-

tissue components showed subtle areas of increased activity on delayed images in one case.

Real-time sonography, performed in one patient with PVNS of the knee, showed a complex mass within an enlarged bursa. The interior of the bursa contained fluid with echogenic synovial masses and septations (Fig. 2A).

The two angiograms showed vascular masses with numerous irregular vessels, "tumor" blush, and slight arteriovenous

Fig. 2.—Pigmented villonodular synovitis (PVNS) of the knee.

A, Sonogram shows soft-tissue mass with both cystic and solid components (arrows).

B, Arteriogram shows soft-tissue mass posterior and medial to proximal tibia. Mass has neovascularity with irregularity and puddling of contrast material as well as a "tumor blush." Mass is indistinguishable from malignant soft-tissue tumor.

C and D, T1-weighted (480/22) (C) and T2-weighted (2000/80) (D) MR images reveal areas of markedly decreased signal on both spin-echo sequences suggesting calcification, flowing blood, or hemosiderin deposition (arrows). This is mixed with areas of prolonged T1 and T2 relaxation times consistent with synovial fluid. Lack of calcification or large vessels as noted on plain-film radiographs and angiogram indicate hemosiderin as cause of decreased signal on the MR images. This suggests PVNS as likely cause of soft-tissue mass.

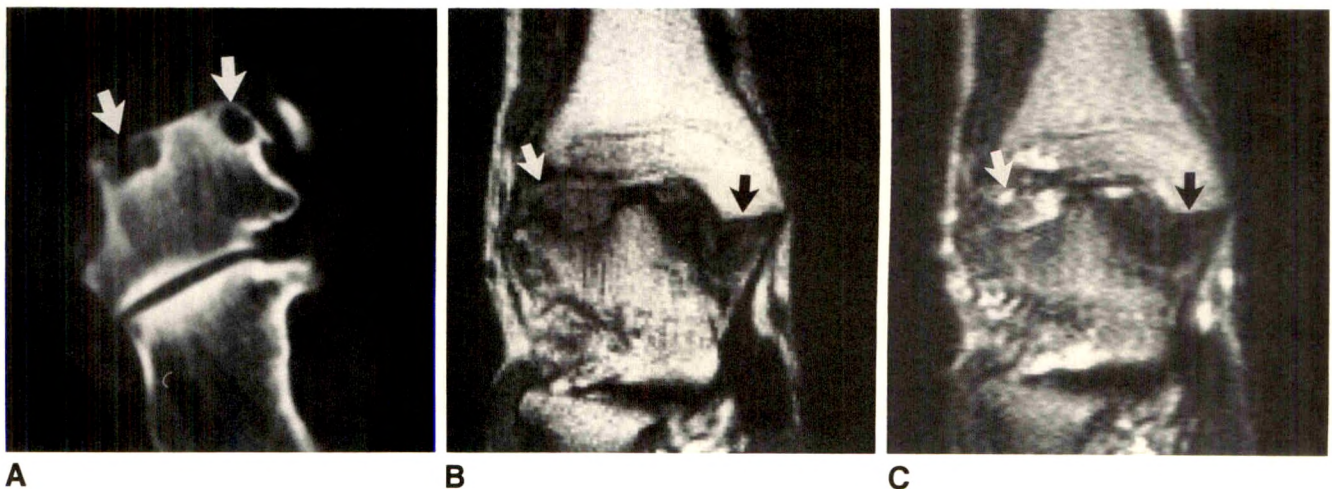
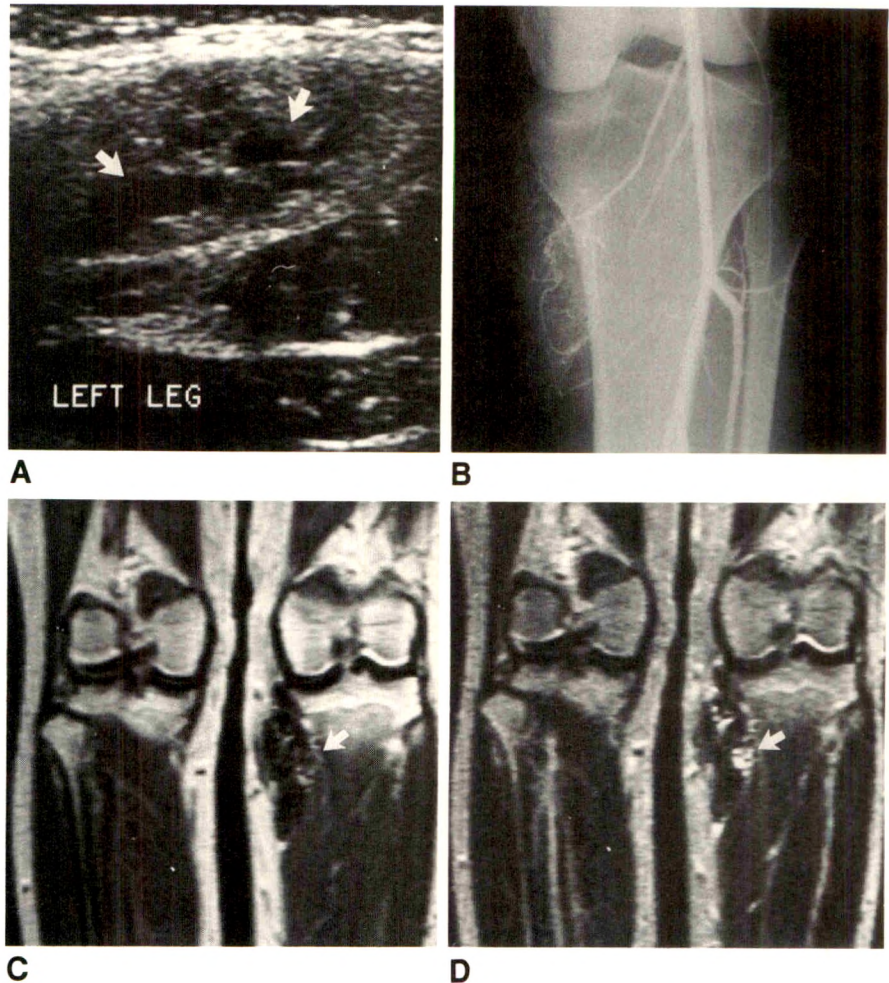


Fig. 3.—Pigmented villonodular synovitis (PVNS) of the ankle.

A, CT scan of right foot shows geographic lesions (arrows) in talus. Similar lesions were also present in distal tibia (not shown). Lesions have a sclerotic margin and may be mistaken for subchondral bone cysts.

B and C, Coronal MR images, T1-weighted (400/22) (B) and T2-weighted (2000/100) (C), show diffuse involvement of talus, far exceeding that expected on plain films and CT scan. Intermediate signal intensity noted in lateral aspect of tumor (white arrows) is consistent with any synovial process; however, areas of decreased signal in medial aspect of talus (black arrows) are thought to be caused by hemosiderin within synovium, most consistent with PVNS.

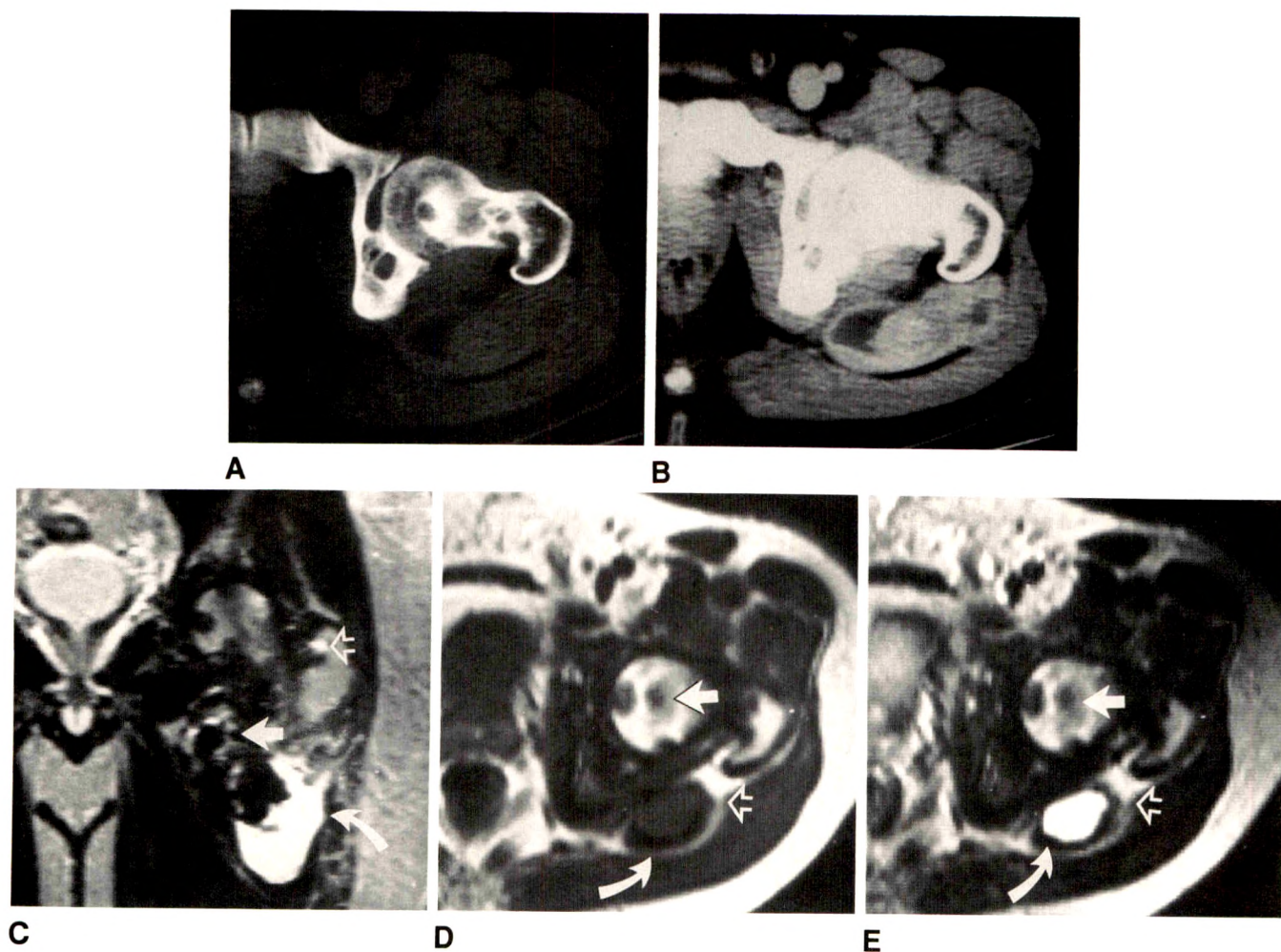
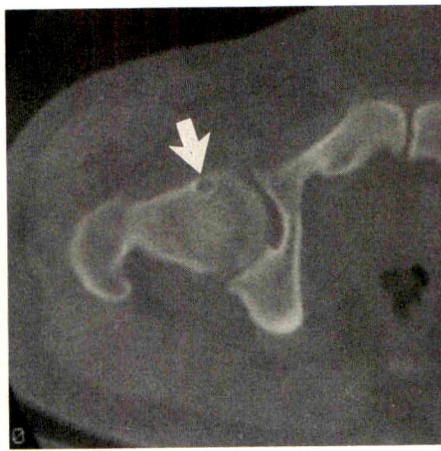


Fig. 4.—Pigmented villonodular synovitis (PVNS) of the hip.
A, Axial CT scan at level of femoral head and neck at bone window setting shows geographic lesions with sclerotic margins in both femur and acetabulum.
B, CT scan, Soft-tissue window setting accentuates soft-tissue mass posterior to hip joint with rim enhancement, enhancing nodules, and surrounding fluid.



Fig. 5.—Pigmented villonodular synovitis of the knee. Double-contrast arthrogram shows diffusely enlarged joint with nodular masses within synovium. Aspiration of rust brown-tinged fluid is characteristic. Incidental note is made of fibrous cortical defect in distal femur.



A



B

Fig. 6.—Synovial chondromatosis simulating pigmented villonodular synovitis (PVNS).

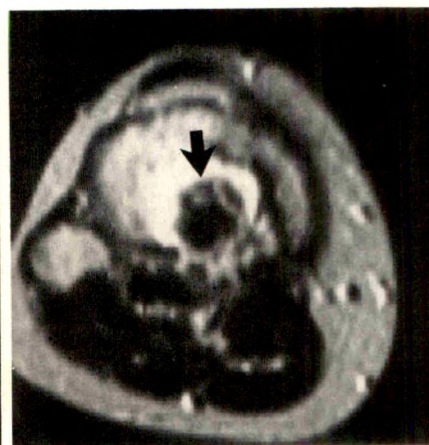
A, CT scan shows well-defined erosion (arrow) of anterior aspect of femoral head. No definite synovial mass is identified.

B, T1-weighted MR image (600/200) shows synovial mass as cause of erosion. Signal intensity within mass is similar to that of skeletal muscle (arrow), suggesting lack of hemosiderin deposition, which would be atypical for classical PVNS. Biopsy-proved synovial chondromatosis. This is a nonspecific MR examination; however, homogeneous appearance was not seen in any of our patients with PVNS.

Fig. 7.—A and B, Rheumatoid arthritis simulating pigmented villonodular synovitis (PVNS). Sagittal T1-weighted (450/21) (A) and axial T2-weighted (2000/100) (B) MR images of patient with biopsy-proved rheumatoid arthritis show large bone erosion (arrows) with homogeneous signal intensity similar to adjacent skeletal muscle on sagittal T1-weighted image. Axial T2-weighted image reveals hypointense mass surrounded by area of hyperintense signal consistent with synovial fluid. Axial T2-weighted image is indistinguishable from T2-weighted images of patients with PVNS. However, homogeneous T1-weighted image is less typical and has not been observed by us in other patients with PVNS.



A



B

joint was present with multiple lobulated filling defects. Double-contrast arthrography enhanced the appearance of synovial nodules (Fig. 5).

The MR appearance of PVNS seen in these seven patients was that of a heterogeneous synovial process that in five cases extended away from the joint space (Figs. 1E, 1F, 2C,

2D, 3B, 3C, 4D, and 4E). The lesions contained significant areas of intermediate signal intensity and hypointensity when compared with skeletal muscle on all spin-echo sequences. The lytic bone lesions were seen as well on MR as on CT (Figs. 1C, 1D, 1F, 3B, 3C, and 4E). Joint effusions were present in four cases and were manifest as areas of low



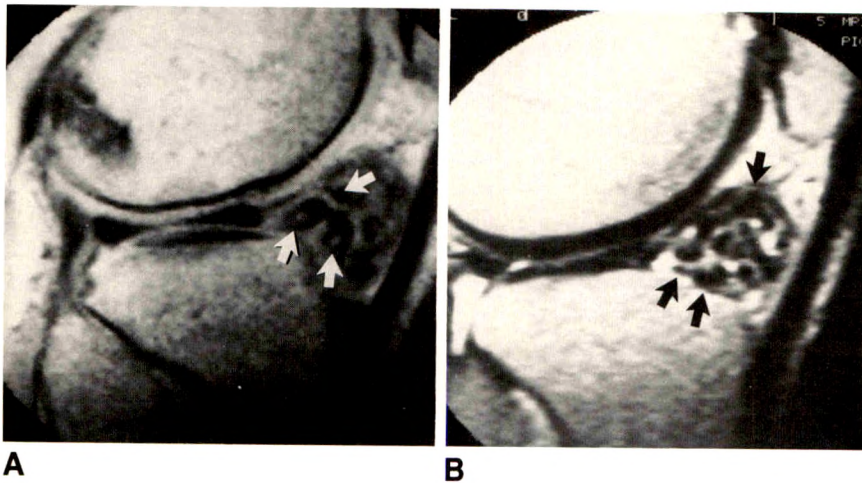


Fig. 8.—A and B, Osteochondromatosis simulating pigmented villonodular synovitis (PVNS). T1-weighted (700/12) (A) and T2-weighted (2100/100) (B) MR images of left knee show synovial mass with decreased signal intensity (arrows) similar to that seen in PVNS. Plain-film radiography showed round, calcified bodies within knee joint typical of osteochondromatosis.



Fig. 9.—Hemangioma mimicking pigmented villonodular synovitis (PVNS). Sagittal T1-weighted MR image (500/33) of soft-tissue mass adjacent to olecranon. Note that signal intensity on T1-weighted image is similar to that of skeletal muscle (solid arrow). Within mass, small, well-defined areas of decreased signal (open arrow) on both T1-weighted image and T2-weighted image (not shown) might be interpreted as area of hemosiderin deposition suggesting PVNS. Plain-film radiograph showed phleboliths corresponding to these areas, which strongly suggested pathologically proved hemangioma.

signal on T1-weighted images, with marked hyperintensity on T2-weighted images (Figs. 4C–4E).

Discussion

PVNS is a highly vascular synovial mass with a tendency to erode bone and to bleed [1, 2]. The vascularity of the mass is best appreciated on nuclear medicine flow studies and angiography. Unfortunately, the vascularity of the lesion mimics malignant soft-tissue diseases. The vascular nature of the mass is not apparent on MR. Areas of decreased signal intensity corresponding to vessels are not apparent within or around the soft-tissue masses on any MR examination. This may be due to either the size of the vessels or the lack of contrast between the flowing blood and the other larger areas of decreased signal thought to be a result of deposition of hemosiderin.

The masslike nature of PVNS frequently is manifested as bone erosion on both sides of the joint. This was seen in five of our seven patients. The CT appearance of these erosions often is that of an intraosseous mass. The tendency of the lesion to bleed results in deposition of hemosiderin, which results in decreased signal on both T1- and T2-weighted

images. This was seen in all of our seven cases of PVNS and three of four cases previously reported in the literature [3, 4]. This appearance was not seen in two of four cases that mimicked PVNS on MR and were later shown not to be PVNS (Figs. 6 and 7). The two cases with hypointensity on all spin-echo sequences had significant calcified or ossified bodies in the joint spaces that were seen clearly on plain-film radiography and suggested that these were not cases of PVNS (Figs. 8 and 9).

REFERENCES

1. Dowart RH, Genant HK, Johnston WH, Morris JM. Pigmented villonodular synovitis of synovial joints: clinical, pathologic, and radiologic features. *AJR* 1984;143:877–885
2. Madewell JE, Sweet DE. Tumors and tumor like lesions in or about joints. In: Resnick D, Niwayama G, eds. *Diagnosis of bone and joint disorders*, 1st ed. Philadelphia: Saunders, 1981:2733–2735
3. Spitzer CE, Dalinka MK, Kressel HY. Magnetic resonance imaging of pigmented villonodular synovitis: report of two cases. *Skeletal Radiol* 1987;16:316–319
4. Kottal RA, Vogler JB, Matamoras A, Alexander AH, Cookson JL. Pigmented villonodular synovitis: a report of magnetic resonance imaging in two cases. *Radiology* 1987;163:551–553

Case Report

Cerebellar Atrophy Caused by High-Dose Cytosine Arabinoside: CT and MR Findings

Lucy Miller,¹ Michael P. Link,² Saba Bologna,² and Bruce R. Parker¹

High-dose cytosine arabinoside has been used recently in the treatment of refractory leukemias in both adults and children. Cerebellar dysfunction is well recognized as an adverse effect of this high-dose systemic therapy; it is not seen at conventional doses or with intrathecal administration. Although such effects are often mild or transient, severe toxicity with permanent sequelae or death has been reported [1-6].

The results of cross-sectional imaging in such cases have not been reported previously. Recently, we have seen two cases of cerebellar atrophy recognizable on CT and MR in children with clinical evidence of cytosine arabinoside toxicity.

Case Report

A 2-year-old boy with acute promyelocytic leukemia received a cumulative IV dose of 48 g/m² of cytosine arabinoside during two induction courses of chemotherapy, which also included daunorubicin and 50 mg of intrathecal cytosine arabinoside. Two weeks after completion of the second induction course, he developed CNS symptoms consisting of eye-rolling spells, which were thought to represent seizures, and truncal ataxia rendering him unable to stand or walk. CT of the brain at this time was within normal limits. Electroencephalogram showed diffuse slowing without focality, and CSF examination revealed no evidence of infection or CNS involvement with leukemia. Remission was achieved and was maintained with a regimen including etoposide, 5-azacytidine, and daunorubicin, but no more cytosine arabinoside was administered. Although cerebellar symptoms gradually decreased, there was residual ataxia. Repeat head CT performed 8 months later showed interval development of marked symmetric atrophic change limited to the cerebellum. The fourth ventricle was enlarged, and CT showed diffuse thinning of folia and widening of the cerebellar sulci (Fig. 1A). MR revealed similar findings of diffuse cerebellar atrophy (Fig. 1B). Parenchymal signal intensity was normal. No supratentorial abnormalities were identified on either CT or MR.

Discussion

In the case described, evidence of cerebellar atrophy was found on cross-sectional imaging in a child who had developed

ataxia after treatment with high-dose cytosine arabinoside. Identical imaging findings were seen in a 6-year-old girl examined with CT and MR 6 months after the onset of irreversible ataxia and speech disturbance (Fig. 2). She had received the same chemotherapeutic regimen; her symptoms began after a cumulative dose of 36 g/m² of cytosine arabinoside. Three neurologically asymptomatic patients on this regimen had normal CT and MR scans 5-18 months after chemotherapy.

Cerebellar toxicity related to systemic administration of high-dose cytosine arabinoside is a well-recognized and scientifically proved entity. It is characterized by acute onset of global cerebellar dysfunction that occurs soon after administration of the agent and that gradually resolves, to various degrees, after treatment with the drug is stopped [1-10]. The toxic effect is reported to be cumulative [11] and dose-related, occurring primarily in patients who have received a total dose of 36 g/m² or more [1-6]. Pathologic examination in fatal cases has shown necrosis of Purkinje cells, particularly in the depths of cortical sulci, with relative sparing at the crests of the folia and in the most posterior/inferior portion of the cerebellum [1, 2, 7]. Our cases had clinical courses compatible with drug toxicity without evidence of tumor, infection, or metabolic disturbance to account for cerebellar symptoms.

In previously reported cases in which CT was performed, CT abnormalities were not described [1, 3, 8, 9], and gross pathologic findings were normal [7, 10]. In these studies, CT or autopsy examination was performed within a few weeks of the onset of symptoms. We report two cases in which evidence of cerebellar degeneration was shown by cross-sectional imaging, including CT and MR, on examinations performed several months after the onset of symptoms. In one case, a CT scan performed acutely was normal. Aside from the loss of tissue mass, no parenchymal abnormality was shown by CT either in the acute phase or on delayed examination. Delayed studies with MR revealed normal parenchymal signal. Neither patient was imaged with MR in the acute phase.

Received June 8, 1988; accepted after revision August 16, 1988.

¹ Department of Diagnostic Radiology and Nuclear Medicine, Division of Diagnostic Radiology, The Children's Hospital at Stanford and Stanford University Medical Center, Stanford, CA 94305. Address reprint requests to B. R. Parker, Stanford University Medical Center, Room S-058, Stanford, CA 94305.

² Division of Hematology-Oncology, The Children's Hospital at Stanford, 520 Sand Hill Rd., Palo Alto, CA 94304.

AJR 152:343-344, February 1989 0361-803X/89/1522-0343 © American Roentgen Ray Society

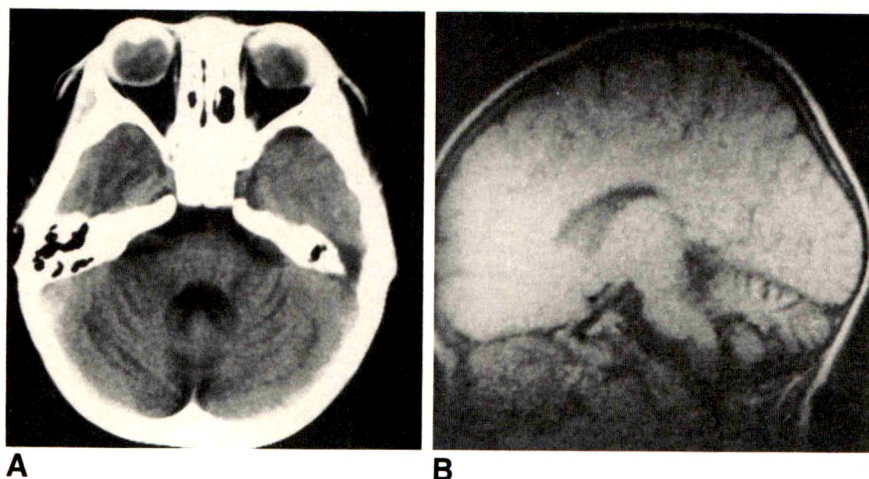


Fig. 1.—A and B, CT scan (A) of posterior fossa and sagittal MR image (B) obtained 8 months after treatment with high-dose cytosine arabinoside show prominent cerebellar sulci indicative of cerebellar atrophy. Signal intensity on MR image is normal.

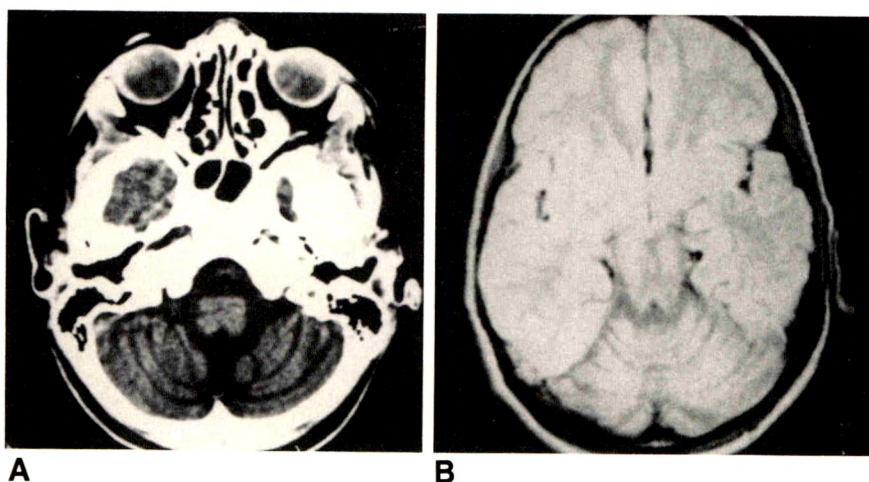


Fig. 2.—A and B, CT scan (A) and axial MR image (B) obtained 6 months after treatment with high-dose cytosine arabinoside show changes of cerebellar atrophy. Signal intensity on MR image is normal.

Some reports suggest that the toxic effects of high-dose cytosine arabinoside are cumulative [11], which raises the possibility of subclinical brain damage. If this is the case, abnormal findings on cross-sectional imaging may predict which asymptomatic patients undergoing therapy are at risk for developing cerebellar toxic reactions on subsequent courses. No abnormalities were revealed by CT or MR in our small group of asymptomatic patients, but prospective evaluation of a large number of patients is needed to determine whether acute changes in parenchymal signal reflect cellular damage.

We conclude that morphologic changes of the cerebellum related to the known toxicity of high-dose cytosine arabinoside can be seen on noncontrast CT scans performed several months after the onset of symptoms. MR is also capable of showing these changes, but it appears to offer no additional diagnostic information in this setting. Whether MR performed in the acute phase may be clinically useful in evaluating early or subclinical cellular damage remains to be determined.

REFERENCES

1. Lazarus HM, Herzig RH, Herzig GP, Phillips GL, Roessman U, Fishman DJ. Central nervous system toxicity of high-dose systemic cytosine arabinoside. *Cancer* 1981;48:2577-2582
2. Winkelman MD, Hines JD. Cerebellar degeneration caused by high-dose cytosine arabinoside: a clinicopathological study. *Ann Neurol* 1983;14(5):520-528
3. Barnett MJ, Richards MA, Ganesan TS, et al. Central nervous system toxicity of high-dose cytosine. *Semin Oncol* 1985;12(2)[suppl 3]:227-232
4. Herzig RH, Lazarus HM, Wolff SN, Phillips GL, Herzig GP. High-dose cytosine arabinoside therapy with and without anthracycline antibiotics for remission reinduction of acute nonlymphoblastic leukemia. *J Clin Oncol* 1985;3(7):992-997
5. Herzig RH, Lazarus HM, Herzig GP, Coccia PF, Wolff SN. Central nervous system toxicity with high-dose cytosine arabinoside. *Semin Oncol* 1985;12(2)[suppl 3]:233-236
6. Hwang T, Yung WKA, Estey EH, Fields WS. Central nervous system toxicity with high-dose ara-c. *Neurology* 1985;35:1475-1479
7. Salinsky MC, Levine RL, Aubuchon JP, Schutta HS. Acute cerebellar dysfunction with high-dose ara-c therapy. *Cancer* 1983;51:426-429
8. Lopez JA. Acute cerebellar toxicity after high-dose cytarabine associated with CNS accumulation of its metabolite, uracil arabinoside. *Cancer Treat Rep* 1984;68(10):1309-1310
9. Early AP, Preisler HD, Slocum H, Rustum YM. A pilot study of high-dose 1-B-D-arabinofuranosylcytosine for acute leukemia and refractory lymphoma: clinical response and pharmacology. *Cancer Res* 1982;42:1587-1594
10. Dworkin LA, Goldman RD, Zivin LS, Fuchs PC. Cerebellar toxicity following high-dose cytosine arabinoside. *J Clin Oncol* 1985;3(5):613-616
11. Bengier A, Browman GP, Walker IR. Clinical evidence of a cumulative effect of high-dose cytarabine on the cerebellum in patients with acute leukemia: a leukemia intergroup report. *Cancer Treat Rep* 1985;69(2):240-241

Case Report

Aortico-Left Ventricular Tunnel: Diagnosis by Cine Angiocardiography

De-Wen Guo¹

Aortico-left ventricular tunnel is an extremely rare congenital anomaly. Its early recognition is important because the lesion can be corrected surgically [1]. The case presented here was the first confirmed case encountered at Shanghai Chest Hospital; the patient was treated successfully by surgery.

Case Report

A 5-year-old girl was admitted to the hospital with a chief complaint of dyspnea and palpitations. Plain radiograph of the chest revealed a moderate degree of cardiomegaly with a cardiothoracic ratio of 0.59. The ascending aorta was slightly dilated, the pulmonary segment was flat, and the apex was displaced downward and leftward, denoting left ventricular enlargement. Pulmonary vascularity appeared normal. Two-dimensional echocardiography in the long-axial view of the left ventricle revealed a tubelike, echo-free area at the anterior wall of the root of the aorta. The preliminary diagnosis was rupture of an aortic aneurysm or coronary arteriovenous fistula. A ventricular septal defect combined with aortic insufficiency also was considered.

The left heart was catheterized, and angiography was performed. Pressure in the aorta was 128/60 mm Hg, and left ventricular pressure was 120/8 mm Hg. The blood oxygen saturation levels in both were 95%. Aortography was performed with a pigtail catheter; the cine technique was used in the long-axial-oblique (left anterior oblique 60° + cranial 30°) projection. When the root of the aorta was filled with contrast material, a fistulous channel was visualized in the diastolic phase from the right aortic sinus to the left ventricle (Fig. 1A). The ascending aorta was dilated (Fig. 1B). A second injection was made in the left ventricle, and the entire course of the abnormal channel was visualized again (Fig. 1C). Angiocardiographic diagnosis of aortico-left ventricular tunnel was strongly suggested. For further con-

firmation of the diagnosis, aortic catheterization was performed. A straight-tipped catheter was manipulated into the opening in the aortic sinus and into the left ventricle. A diagnosis of aortico-left ventricular tunnel was established.

At surgery, an oval opening approximately 8 mm in diameter was found about 5 cm above the level of the coronary ostium. A probe could be pushed through the abnormal channel into the outflow tract of the left ventricle. The aortic opening of the tunnel was closed by four interrupted mattress sutures and reinforced by a second layer of 5-0 stitches.

Discussion

In 1961, Edwards [2] described a case in which communication existed between aorta and left ventricle. In 1963, Levy et al. [3] reported three other such cases in detail. They introduced the term aortico-left ventricular tunnel and suggested the congenital origin of this entity. An extensive review of the literature by Humes et al. [4] indicated that from 1961 to 1986, 48 cases were reported. Hovaguimian et al. [5] added two more cases in 1988. This rare anomaly was seen more frequently in males (75%) than in females [1].

The gross pathology in our case was similar to that in most of the cases described in the literature. The tunnel arises from the right aortic sinus, passes behind the infundibulum of the right ventricle, and threads through the upper part of the interventricular septum to enter the outflow tract of the left ventricle. Hovaguimian et al. [5] proposed that aortico-left ventricular tunnel could be classified into four types on the basis of local anatomic findings: (1) a simple tunnel with a

Received May 24, 1988; accepted after revision August 18, 1988.

¹ Department of Radiology, Shanghai Chest Hospital, 241, Huai Hai Xi Lu, Shanghai, People's Republic of China. Address reprint requests to D-W. Guo.

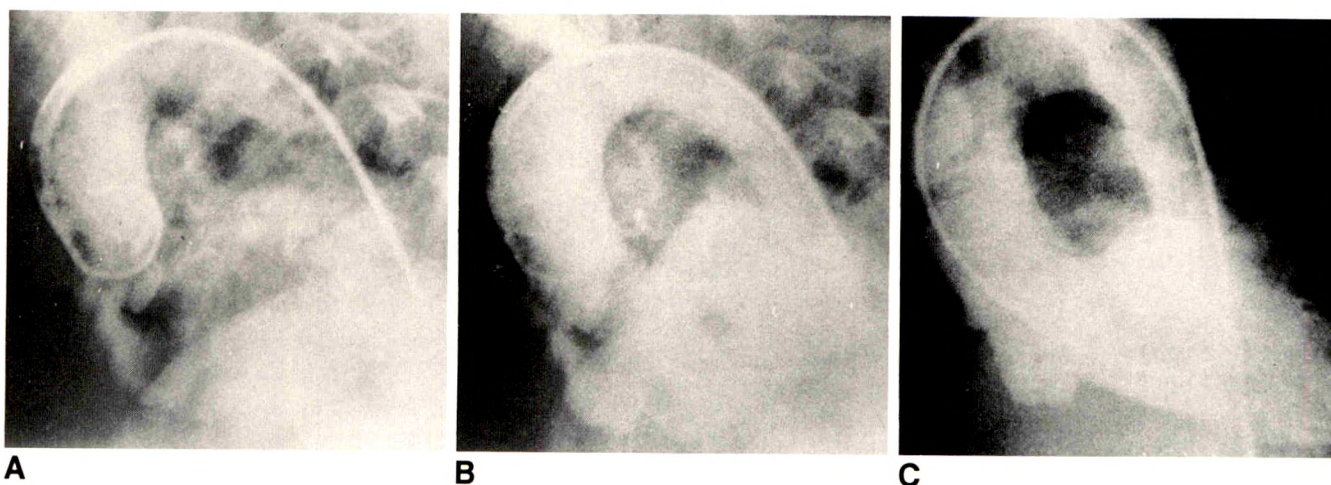


Fig. 1.—A, Early frame of cine film obtained during aortography shows a fistulous channel in diastolic phase from slightly dilated right aortic sinus to left ventricle. An aneurysmal dilatation was seen around the middle of the somewhat tortuous channel. No regurgitation was seen through aortic valve. B, A later frame shows dilatation at ventricular end of tunnel. Left ventricle was filled in a retrograde fashion. C, Cine film obtained during left ventriculography shows tunnel from ventricular side during systole. Aorta was filled through both aortic valvular opening and tunnel.

slitlike opening, (2) a large extracardiac aortic wall aneurysm with an oval opening, (3) an intracardiac aneurysm of septal portion of the tunnel, and (4) a combination of extra- and intracardiac aneurysms. (Our case may be classified as type 3.)

The use of two-dimensional and pulsed Doppler echocardiography has been described, and the value of such noninvasive techniques has been emphasized [4–6].

However, we think that precise pathologic anatomy and hemodynamic changes can be shown best by cine aortography and cine-left ventriculography. Angiography shows the morphology of the tunnel, the location and size of its aortic orifice, and its relationship to the aortic sinus (especially to the right sinus and its corresponding aortic leaflet. Exaggerated pulsation at the root of the aorta and left ventricle also can be seen. We think that all these changes can be shown best with routine projections supplemented by axial-angulated views.

Cine angiocardiographic study is mandatory in postoperative follow-up for detecting the development of (or accentuation of) aortic insufficiency, which occurs frequently in cases of aortico-ventricular tunnel [6, 7]. Tuna and Edwards [8] pointed out that deficient support of the aortic root in relation to the right aortic sinus is present and appears to underlie the development of aortic insufficiency.

Aortico-ventricular tunnel may be complicated by bicuspid aortic valve, aortic stenosis, pulmonic stenosis, absent right coronary artery, aortic sinus aneurysm, and aneurysm of the ventricular septum [1]. We found no sign of aortic insufficiency in our case during follow-up study 1 year after surgery.

In the differential diagnosis of this condition, rupture of an aneurysm of the sinus of Valsalva, coronary arteriovenous fistula, ventricular septal defect combined with aortic insufficiency, and isolated congenital aortic insufficiency should all

be considered [1, 5]. Rupture of an aneurysm of the sinus of Valsalva deserves special attention in that aortography may reveal aneurysm formation from the right aortic sinus with a regurgitant jet from the ruptured opening, and the morphology of the jet may sometimes mimic a fistulous channel. However, it is the outflow or sinus portion of the right ventricle that is directly filled, not the left ventricle. Rupture of an aneurysm of the sinus of Valsalva into the left ventricle was not seen in our series of 90 proved cases of ruptured sinus or sinus aneurysm [9]. Anatomically, this was considered to be impossible by Levy et al. [3].

REFERENCES

1. Levy MJ, Schachner A, Blieden LC. Aortico-left ventricular tunnel: collective review. *J Thorac Cardiovasc Surg* 1982;84:102–109
2. Edwards JE. *Atlas of acquired disease of the heart and great vessels*, vol. 3. Philadelphia: Saunders, 1961:1142
3. Levy MJ, Lillehei CW, Anderson RC, Amplatz K, Edwards JE. Aortico-left ventricular tunnel. *Circulation* 1963;27:841–853
4. Humes RA, Hagler DJ, Julsrud PR, Levy JM, Feldt RH, Schaff HV. Aortico-left ventricular tunnel: diagnosis based on two-dimensional echocardiography, color flow Doppler imaging, and magnetic resonance imaging. *Mayo Clin Proc* 1986;61:901–907
5. Hovaguimian H, Cobanoglu A, Starr A. Aortico-left ventricular tunnel: a clinical review and new surgical classification. *Ann Thorac Surg* 1988;45:106–112
6. Turley K, Silverman NH, Teitel D, Mavroudis C, Snider R, Rudolph A. Repair of aortico-left ventricular tunnel in the neonate: surgical, anatomic and echocardiographic considerations. *Circulation* 1982;65:1015–1020
7. Serino W, Andrade JL, Ross D, de Leval M, Somerville J. Aortico-left ventricular communication after closure: late postoperative problems. *Br Heart J* 1983;49:501–506
8. Tuna IC, Edwards JE. Aortico-left ventricular tunnel and aortic insufficiency. *Ann Thorac Surg* 1988;45:5–6
9. Guo D-W, Cheng TO, Lin ML, Gu ZQ. Aneurysm of the sinus of Valsalva: a roentgenologic study of 105 Chinese patients. *Am Heart J* 1987;114:1169–1177

Efficacy of MR vs CT in Epilepsy

E. R. Heinz¹
 T. R. Heinz²
 R. Radtke³
 R. Darwin¹
 B. P. Drayer⁴
 E. Fram¹
 William T. Djang¹

We studied 59 seizure patients with CT, MR, and EEG to determine the efficacy of each in the detection of an epileptogenic focus. EEG was most sensitive (67%), MR was next (53%), and CT was least sensitive (42%). MR detected an abnormality in five patients (8%) in whom CT was negative. EEG was positive in each of these patients. CT failed to demonstrate any focal lesion not detected by MR. MR and CT detected focal abnormalities in seven patients (12%) who had negative EEGs. Five of the seven patients had brain tumors. Eighteen of the 26 patients who underwent surgery had positive CT and MR; 14 of these patients had tumors. The remaining eight patients who had surgery all had temporal lobectomies for intractable seizures; none had tumors. In the complex partial seizure subgroup of 34 patients, MR was positive in 44%, CT was positive in 29%, and EEG was positive in 80%.

We consider MR to be the imaging procedure of choice for the detection of an epileptogenic focus in seizure patients. When indicated, CT may be performed as a second procedure to try to distinguish neoplasm from thrombosed vascular malformations and other lesions.

MR imaging is an important new imaging technique. As it is expensive, and because it competes with a good existing imaging method—CT—it is important to determine the efficacy of MR vs CT as it applies to the detection of epileptogenic foci in seizure patients. Further, if MR is significantly superior to CT, and CT fails to detect any disease not detected on MR, then it may be possible to use MR only in the evaluation of future seizure patients. For this reason, all patients with seizures who had MR and CT examinations between January 1985 and June 1986 were analyzed. After the sensitivities of MR and CT were determined, the sensitivity of each of these methods was compared with that of EEG.

Materials and Methods

Seventy-two patients with seizures had neuroimaging studies between January 1985 and June 1986. Of these, 59 patients had CT, MR, and EEG studies. Many of the patients in this series were referred to our epilepsy center for chronic, medically intractable seizures. Twenty-six of these patients ultimately had surgery. We reviewed CT, MR, and EEG data to determine the efficacy of each in the detection of epileptogenic foci.

All of the CT examinations were performed on a GE 8800 or 9800 scanner. All patients had contrast enhancement. Slice thickness was 10 mm. MR imaging was performed on a 1.5-T GE system with spin-echo pulse sequences, 500/25 and 2000/40,80 (TR/TE). Section thickness was 5 mm. MR was considered "positive" when an increased signal intensity was noted on the T2-weighted images when compared with the signal from the opposite hemisphere or when a mass was detected. Although structural lesions with very intense signal (long T2 relaxation time) were thought more likely to be intrinsic neoplasms, and foci with a less intense signal were thought more likely to be mesial sclerosis or gliosis, for purposes of sensitivity and tabulation in this study, each has simply been called "positive."

EEG was performed routinely; electrophysiologic studies were supplemented by 3- to 7-day hospitalizations with continuous TV and simultaneous EEG recording so that seizures

This article appears in the November/December 1988 issue of *AJNR* and the February 1989 issue of *AJR*.

Received September 21, 1987; accepted after revision March 8, 1988.

¹ Department of Radiology, Box 3808, Duke University Medical Center, Durham, NC 27710. Address reprint requests to E. R. Heinz.

² Department of Surgery, Mary Hitchcock Clinic, Hanover, NH 03755.

³ Department of Medicine, Duke University Medical Center, Durham, NC 27710.

⁴ Department of Radiology, Barrow Neurological Institute and St. Joseph's Hospital, Phoenix, AZ 85013.

AJR 152:347-352, February 1989
 0361-803X/89/1522-0347
 © American Roentgen Ray Society

could be detected and recorded during sleep as well as during waking hours. An EEG was considered positive when epileptiform activity was noted, whether or not slow waves were present. In addition, depth electrodes were placed in 11 (18.6%) of the 59 patients; eight of the 11 electrodes were placed in patients who had negative imaging studies. The contribution of depth electrode data in the remaining three was excluded from this study because depth electrode place-

ment is very invasive and should not be used in comparing non-invasive studies. These data have been included in another publication [1].

Results

The results are summarized in part in Tables 1–3. Overall MR displayed an abnormal signal in 31 (53%) of the 59 patients. In no instance did MR fail to detect a lesion seen on CT. When patients with positive EEGs were added to those with negative EEGs and positive MR, 44 (79%) of the 59 patients had positive findings. MR was positive in five patients (16%) in whom CT was negative. Three of the patients with negative CT and positive MR scans had subtle, poorly defined hyperintense foci in the temporal lobe on T2-weighted images. Two of the three had aspiration partial lobectomies with relief of seizures. An aspiration lobectomy was used early in the series; this technique did not permit classical neuropathologic examination in these two patients, but no tumor was found. The third had bitemporal EEG foci and is being treated medically. One patient had atrophy, and one patient was thought to have vascular disease.

TABLE 1: CT and MR Findings in Seizure Patients

	MR+ (n = 31)		MR–, CT– (n = 28)
	CT+	CT–	
Operated:			
Neoplasms	14	0	0
Other	4	2	8
Subtotal	18	2	8 ^a
No operation	8	8	20 ^b
Total	26	10	28

^a Three of these patients had mesial sclerosis.

^b Drug therapy.

TABLE 2: Seizure Patients with Negative CT and Positive MR Findings

Case No.	Age	Gender	Clinical Findings	MR Findings	Radiologic Diagnosis	Pathology
1	17	F	CPS, 14 years	↑ intensity on T2-weighted images of medial temporal lobe (L)	Probable gliosis	No pathologic tissue identified ^a
2	32	F	CPS	↑ intensity focus on T2-weighted images of medial temporal lobe (L)	Focal atrophy, ?gliosis	No pathologic tissue identified ^a
3	19	F	CPS	↑ intensity focus (subtle) on T2-weighted images of medial temporal lobe (L)	?Gliosis	Not operated
4	60	M	CPS vs dementia	↑ intensity on T2-weighted images of temporal lobe (L)	Atrophy	Not operated
5	73	F	Seizure	Single 1-cm high-intensity focus on T2-weighted images of left frontotemporal area (subcortical)	Vascular disease	Not operated

Note.—L = left; CPS = complex partial seizure(s).

^a In these two early cases, aspiration partial lobectomy was used; lobectomy or partial lobectomy has been used subsequently.

TABLE 3: Seizure Patients with Negative EEG, Positive CT, and Positive MR Findings

Case No.	Age	Gender	Clinical Findings	CT/MR Localization	Pathology
6	33	F	CPS, 5 years	↑ intensity focus in temporal parietal area	Oligoastrocytoma
7	17	M	Focal seizures, 6 months	High convexity in right frontoparietal area	Pleomorphic astrocytoma
8	17	F	Intractable temporal-lobe seizures	Left temporal lobe	Astrocytoma
9	59	M	Focal seizures, 6 months	↑ intensity in left frontoparietal area involving cortex	Oligodendroglioma
10	60	M	Elemental partial seizures, right leg weakness	↑ intensity on T2-weighted images in left centrum semiovale	Glioma
11	43	M	Motor vehicle accident, age 16	Left focal temporal atrophy	Focal atrophy; not operated
12	12	M	Elementary partial seizures	↑ intensity on T2-weighted images in left parietal area	Hemiplegic migraine; not operated

Note.—CPS = complex partial seizure(s).

Both MR and the CT were positive in seven patients who had negative EEG findings; five of these seven patients had tumors, one had hemiplegic migraine, and one had focal atrophy after cerebral trauma.

In the complex partial seizure subgroup of 34 patients, MR was positive in 15 (44%), CT was positive in 10 (29%), and EEG was positive in 27 (80%).

Twenty-six (44%) of the 59 patients had lobectomies or partial lobectomies. Of these 26, 14 (54%) had neoplasms.

Eighteen of the 26 patients who underwent surgery had positive CT and MR scans; 14 of these patients had tumors. The remaining eight patients who had surgery had no CT or MR abnormalities and had temporal lobectomies for intractable seizures; none had tumors. Two had subpial aspiration lobectomies in which no diagnosis could be made, three had mesial sclerosis, and in three no diseased tissue was found. Twenty-eight patients, including eight with positive MR scans, did not undergo surgery. These patients are being managed with drug therapy. In 19 of the 26 patients who underwent surgery, seizure control was a major goal. Fourteen (74%) of these 19 are now seizure-free, and four (21%) are greatly improved, with a greater than 75% reduction in the incidence of seizures. One patient was improved but had less than a 75% reduction of seizures. The mean follow-up period was 20.5 months (range, 12–30 months).

Discussion

Several reports have addressed the use of MR in surveying seizure patients for a seizure focus that might lead to epilepsy surgery. Laster et al. [2] reported 100 patients with CPS;

Latack et al. [3] reported 50 patients with CPS, 14 of whom underwent positron emission tomography as well. Twenty-three of the patients had positive MR. We thought it would be useful to provide statistics on consecutive patients with seizures between January 1985 and June 1986 as an overall indicator of the efficacy of MR vs CT, and to compare both imaging techniques with the existing neurologic standard, EEG. Our series is exceptional because of the large number of tumors found, because of the relatively large number of patients who have had lobectomies for treatment of their seizures, and, finally, because of the high percentage of surgical cures of the epilepsy.

The results of our study are summarized in part in Tables 1–3. Of the five patients with positive MR and negative CT results, three had subtle but definite increased signal in the temporal lobe on T2-weighted images. Two of these went on to have a partial lobectomy by aspiration at craniotomy (Figs. 1 and 2); these patients were thought to have had mesial sclerosis or gliosis, but because of the nature of the surgical resection, histology was not available. Since then, en bloc removal of the mesial temporal structures during temporal lobectomy has been used at our institution. This allows excellent histologic analysis of the hippocampus and amygdala, and one hopes will provide pathologic correlation with the mesial temporal abnormalities on T2-weighted images. The third patient had similar subtle focal increased signal on T2-weighted images of the temporal lobe, but because of bilateral EEG findings this patient did not have surgery. MR appears to have the capacity to detect abnormal foci on T2-weighted images within the temporal lobe that are not visible on enhanced CT scans of the brain. Each of the two patients with

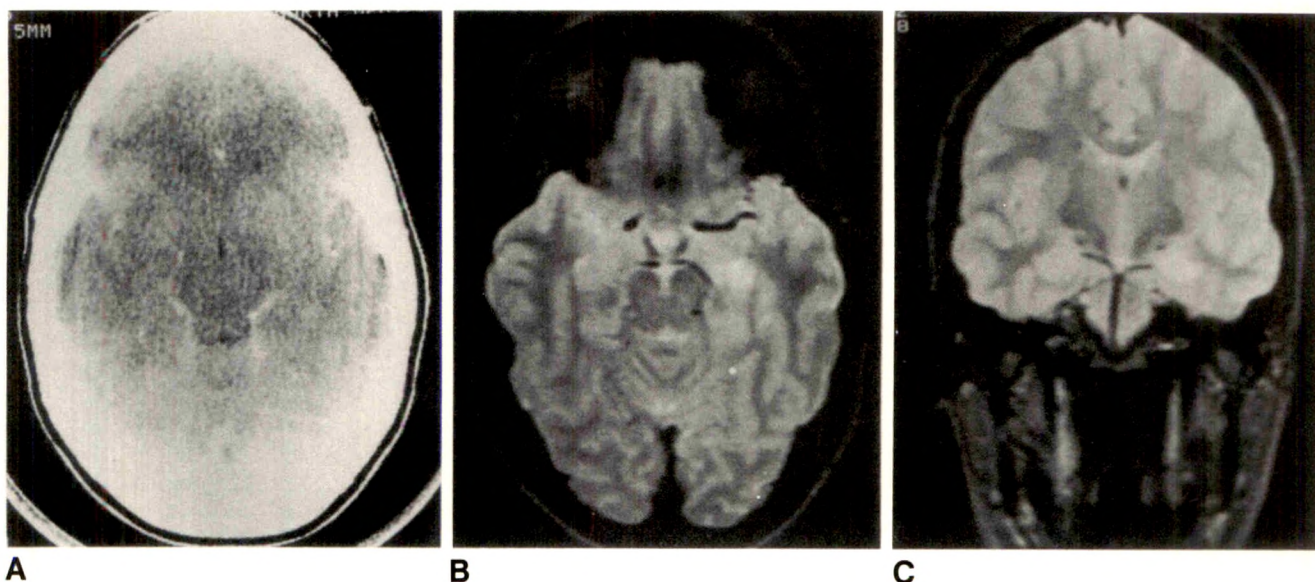


Fig. 1.—Case 1: 17-year-old woman with complex partial seizures for 14 years. Scalp EEG: left spike focus. Depth electrodes: left temporal focus. CT negative; MR positive.

A, Contrast-enhanced CT scan is normal.

B, Axial MR image, 2500/80. Hyperintense focus in medial third of left temporal lobe.

C, Coronal MR image, 2500/80. Hyperintense focus on fully T2-weighted sequence is in pes hippocampi.

Partial temporal lobectomy was performed by aspiration. (This technique subsequently was changed to partial lobectomy with en bloc removal of specimen.) No tumor was found.

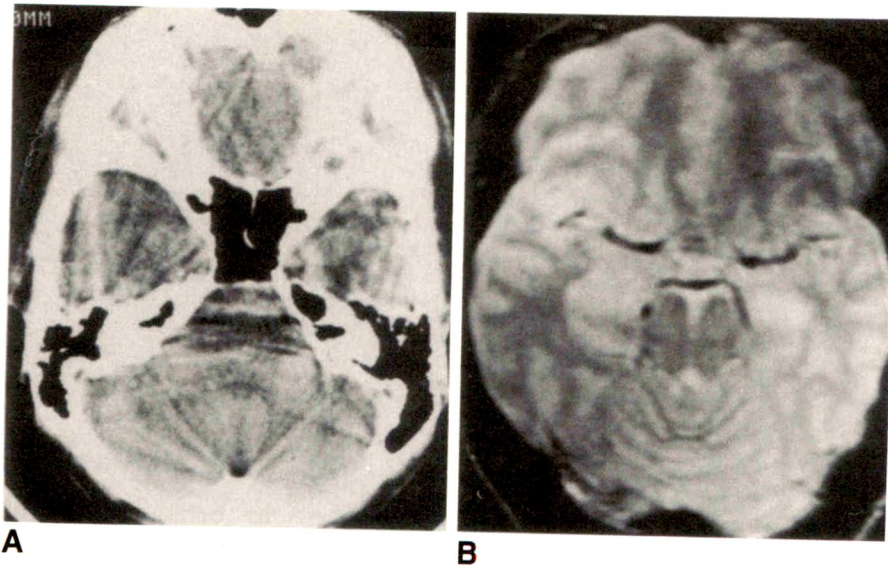


Fig. 2.—Case 2: 32-year-old woman with complex partial seizures for 31 years. Scalp EEG: focus in left temporal lobe.

A, Contrast-enhanced CT scan shows no enhancing structural lesion. However, note that left temporal fossa is slightly smaller than right.

B, Axial T2-weighted MR image, 2500/80. Hyperintense focus in medial third of left temporal lobe. Also, volume of left temporal lobe may not be as great as right.

Left temporal lobectomy was performed by aspiration. No tumor was found.

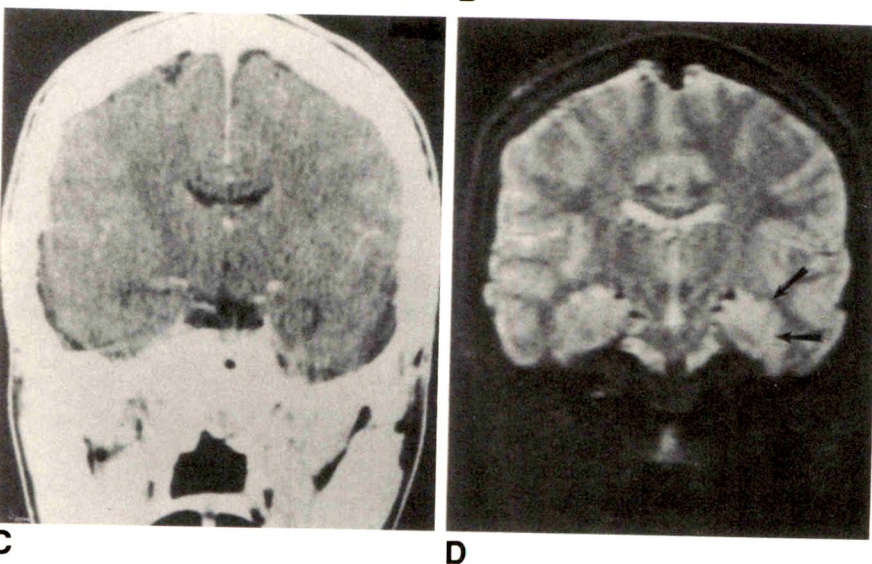
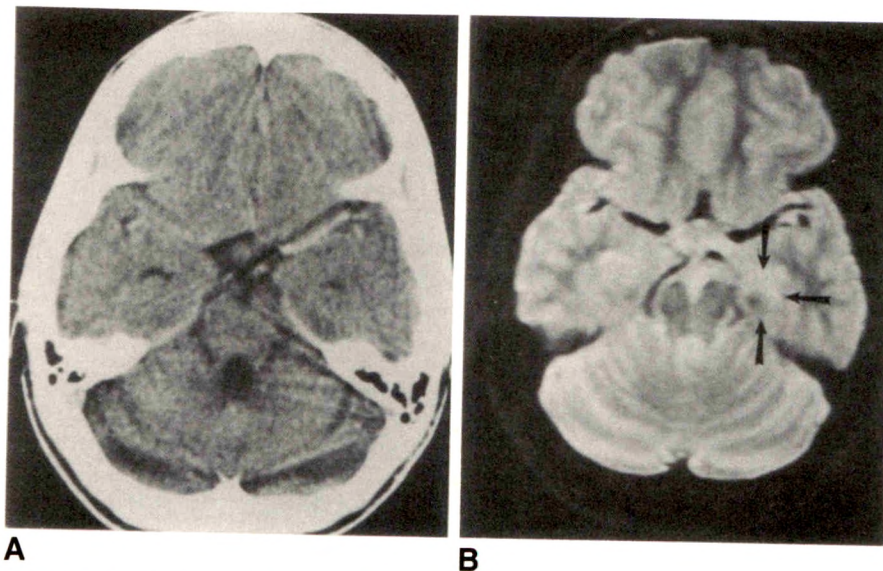


Fig. 3.—Case 3: 19-year-old woman with intractable partial complex seizures.

A, Axial contrast-enhanced CT scan shows no abnormality in left temporal lobe.

B, Axial MR image, 2500/80, shows hyperintense focus in left temporal lobe (arrows). Medications altered with control of seizures. No operation.

C, Coronal contrast-enhanced CT scan shows no definite structural lesion.

D, Coronal MR image, 2500/80. Definite hyperintense focus in medial portion of left temporal lobe (arrows).

This patient was thought to have an abnormality, but, based on Figs. 1 and 2, the lesion was thought to be mesial sclerosis or gliosis, and not a brain tumor. Because the abnormality was located in her dominant hemisphere and her seizures could be controlled with an altered drug regimen, she has been followed medically.

positive MR and negative CT results are seizure-free after partial aspiration lobectomies. Therefore, the capacity of MR to display a signal abnormality in the brain at the site of an epileptogenic focus is superior to that of CT. However, at least three of our patients had lobectomies after positive EEG and negative MR and CT scans, and were shown to have prominent mesial sclerosis on histology. It appears that although mesial sclerosis may be associated with positive MR findings, it also may be present in patients with negative MR images of the temporal lobe.

The determination of increased T2 signal from the temporal lobe is not always straightforward. Frequently a "shading" artifact is seen in which one temporal lobe has a higher-intensity T2 signal than the opposite side. Another artifact is

created by carotid artery pulsations, which are projected over the temporal lobes when the phase-encoding direction is at right angles to the sagittal plane of the head. When one patient with questionable findings was placed in the scanner and the phase-encoding direction was altered by 90° to parallel the sagittal axis of the head, the "lesion" disappeared. We now routinely image seizure patients with the phase-encoding gradient in the sagittal plane.

Although other series have demonstrated intrinsic neoplasms on MR that were not detected on CT, none of our tumors were in this category. However, in at least three patients said to have positive MR and CT scans, the CT changes were minimal. In two of the three only a 2- to 3-mm calcification in the temporal lobe was detected. In contrast,

Fig. 4.—Case 13: 18-year-old man with complex partial seizures for 10 years. Scalp EEG: left spike focus.

A, CT scan shows small calcification in medial third of left temporal lobe.

B, MR image obtained with low-field-strength magnet at another institution. High-intensity focus in medial 50% of left temporal lobe on T2-weighted image.

Left temporal lobectomy revealed astrocytoma.

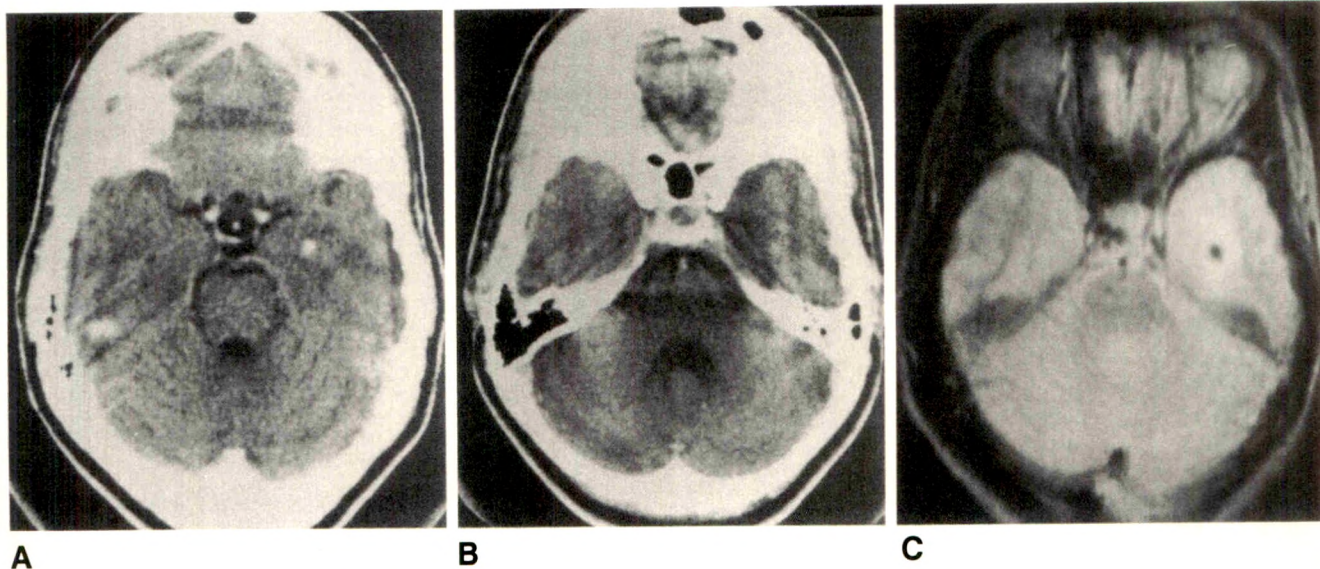
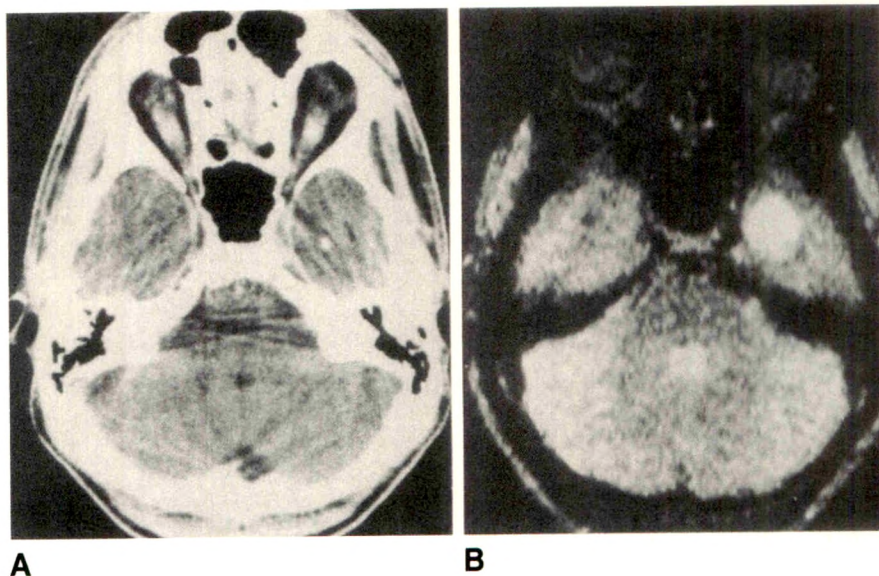


Fig. 5.—Case 14: 28-year-old woman with complex partial seizures for 5 years.

A, Contrast-enhanced CT scan shows a 3- to 4-mm density in medial third of left temporal lobe. Nonenhanced scan showed this to be calcium.

B, Slightly inferior section shows no convincing tissue abnormality.

C, MR image, 2500/40, shows high-intensity focus surrounding focal area of signal void, which corresponds to calcification in A. Lobectomy confirmed an astrocytoma.

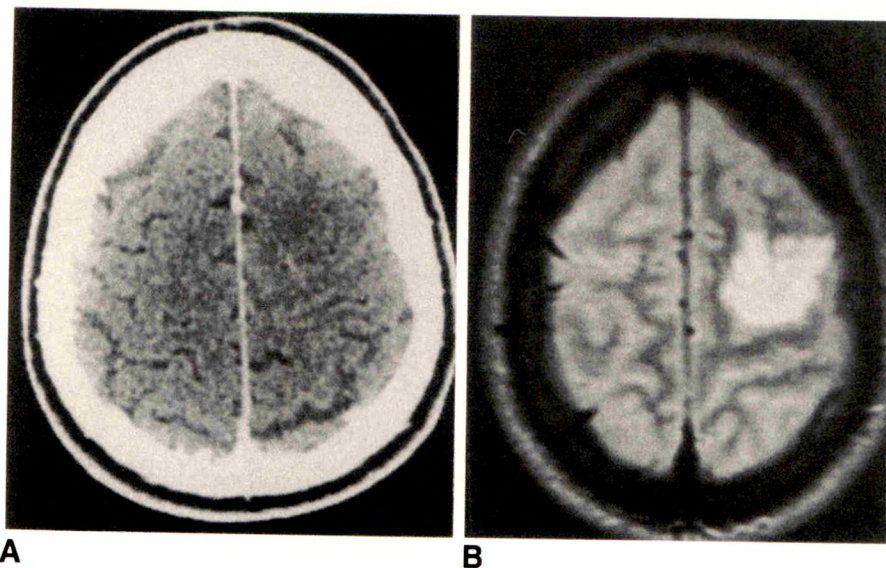


Fig. 6.—Case 9: 59-year-old man with elemental partial seizures for 3 weeks. No scalp EEG focus detected.

A, Contrast-enhanced CT scan. High-convexity sulci are less conspicuous on left. Slight hypodensity. No other mass effect.

B, T2-weighted MR image, 2500/80. Large hyperintense focus in frontoparietal area of left high convexity.

Surgery yielded oligodendroglioma.

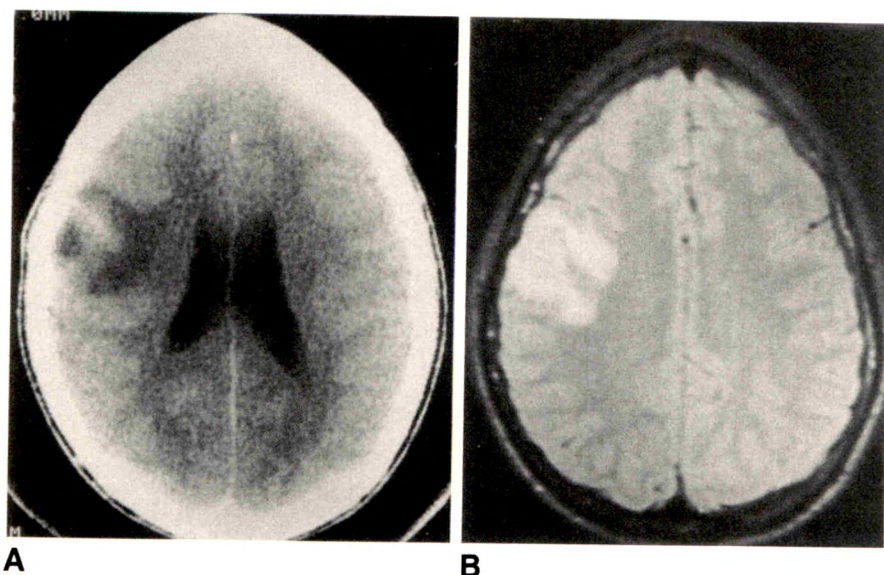


Fig. 7.—Case 7: 17-year-old man with new onset of complex partial seizures. Scalp EEG: negative.

A, Contrast-enhanced CT scan shows focal mass, probably intrinsic neoplasm.

B, T2-weighted MR image, 2500/80. Focal mass is surrounded by hyperintense cortex with adjacent vasogenic edema of high intensity.

Surgery revealed astrocytoma. This is an example of a patient with a neoplasm in whom the EEG was normal.

MR showed an obvious large area of increased intensity on T2-weighted images (Figs. 3–5).

MR was able to document a potential seizure focus in 31 (53%) of the 59 patients in our study (Figs. 6 and 7). In no instance did MR fail to detect a lesion seen on CT. When EEG was performed, and then supplemented by MR, 44 (79%) were shown to have an abnormality as the probable cause of the seizures.

The complex partial seizure subgroup comprised 34 patients. MR was positive in 15 (44%) and CT was positive in 10 (29%). Not unexpectedly, the EEG was positive in 27 (80%). These statistics are comparable to those in the series of Latack et al. [3], in which MR scans were abnormal in 42%. Forty to fifty percent of patients with complex partial seizures are considered to be appropriate candidates for lobectomy [4] because their seizures cannot be controlled medically and lobectomy may provide a cure or significant relief. MR is a major advance in the presurgical evaluation of these surgical candidates. In our series 94% of carefully selected patients were significantly improved or seizure-free after lobectomy.

In summary, EEG remains the most sensitive test for the localization of an epileptogenic focus. MR is the most efficacious imaging test in the evaluation of seizure patients for defining a potential surgical focus as a cause for the epilepsy. CT did not detect any lesion not seen by MR. Therefore, on the basis of our series and the two series that compare the sensitivities of MR and CT [2, 3], there appears to be no specific need to perform CT when MR is normal. However, as MR has a high sensitivity but poor specificity, CT may be done as a second procedure to try to distinguish neoplasm from thrombosed vascular malformations and other lesions.

REFERENCES

1. Radtke RA, McNamara JO, Lewis DV, Heinz ER. Usefulness of MRI in pre-surgical evaluation of intractable complex partial seizures. *Epilepsia* 1986;27:612
2. Laster DW, Penry JK, Moody DM, et al. Chronic seizure disorders: contribution of MR imaging when CT is normal. *AJNR* 1985;6:177–180
3. Latack JT, Abou-Khalil BW, Siegel GJ, Sackellares JC, Gabrielsen TO, Aisen AM. Patients with partial seizures: evaluation by MR, CT, and PET imaging. *Radiology* 1986;159:159–163
4. Rodin EA. *Prognosis in epilepsy*. Springfield, IL: Thomas, 1968:179–262

Absence of the Septum Pellucidum: A Useful Sign in the Diagnosis of Congenital Brain Malformations

A. James Barkovich^{1,2}
David Norman²

In a review of more than 2000 MR images of the brain we identified 35 patients with absence of the septum pellucidum. These patients were divided into seven basic groups as follows: septo-optic dysplasia; schizencephaly; holoprosencephaly; agenesis of the corpus callosum; chronic, severe hydrocephalus; basilar encephaloceles; and porencephaly/hydranencephaly. Absence of the septum pellucidum was never seen as an isolated finding. By using data gathered from the review of the MR scans of patients in this study, we devised a diagnostic algorithm to aid in the classification of these patients.

Absence of the septum pellucidum can provide a valuable clue to the diagnosis of malformations of the brain.

Absence of the septum pellucidum is reported to be an unusual anomaly that occurs in an estimated 2 to 3 individuals per 100,000 people in the general population [1]. When observed, this anomaly should serve as a clue to the presence of associated anomalies, including holoprosencephaly, septo-optic dysplasia, abnormalities of the corpus callosum, and Chiari II malformation [1].

The purpose of this study was to identify the underlying brain anomalies in 35 consecutive patients in whom absence of the septum pellucidum was demonstrated by MR imaging, to characterize these malformations, and to develop an algorithmic approach to their diagnosis.

Subjects and Methods

Absence of the septum pellucidum was identified in 35 patients selected from 2007 MR images of the brain obtained over a 2½-year period at the University of California at San Francisco and at the San Francisco Magnetic Resonance Center. Patients' ages ranged from 2 days to 23 years (mean, 2.3 years). Developmental abnormalities occurred as follows: septo-optic dysplasia (seven patients), schizencephaly (six patients), Chiari II malformation (seven patients), aqueductal stenosis (five patients), holoprosencephaly (four patients), encephaloceles (three patients—two with associated callosal agenesis), agenesis of the corpus callosum with interhemispheric cyst (two patients), porencephaly (two patients), and hydranencephaly (two patients). Three of the patients with septo-optic dysplasia also had schizencephaly. No cases of absence of the septum pellucidum were identified without associated anomalies. All patients were imaged on a 1.5-T GE imager. Imaging parameters included 5-mm thick axial spin-echo (SE) sections with 2500/35,70 (TR/TEs) and sagittal SE images with 600/20 (TR/TE). In some patients, coronal SE 600/20 images were also obtained. The coronal views were especially useful for assessing the interhemispheric fissure in suspected holoprosencephaly and for evaluating the optic chiasm in suspected septo-optic dysplasia.

The images were evaluated retrospectively for the presence or absence, size, location, and appearance of the following structures: corpus callosum, fornices, falx cerebri, interhemispheric fissure, lateral ventricles, optic nerves, optic chiasm, cerebral cortex, cerebral white matter, and clefts within the cerebral hemispheres. The results were then compiled and contrasted and an algorithm was devised to facilitate diagnosis (Fig. 1).

This article appears in the November/December 1988 issue of *AJNR* and the February 1989 issue of *AJR*.

Received October 23, 1987; accepted after revision February 29, 1988.

The views expressed in this article are those of the authors and do not reflect the official policy or position of the Department of the Army, Department of Defense, or the U.S. Government.

¹ Department of Radiology, Letterman Army Medical Center, Presidio of San Francisco, CA 94129-6700. Address reprint requests to Medical Editing HSHH-CI-ME.

² Department of Radiology, Neuroradiology Section, University of California School of Medicine, San Francisco, CA 94143.

AJR 152:353-360, February 1989
0361-803X/89/1522-0353
© American Roentgen Ray Society

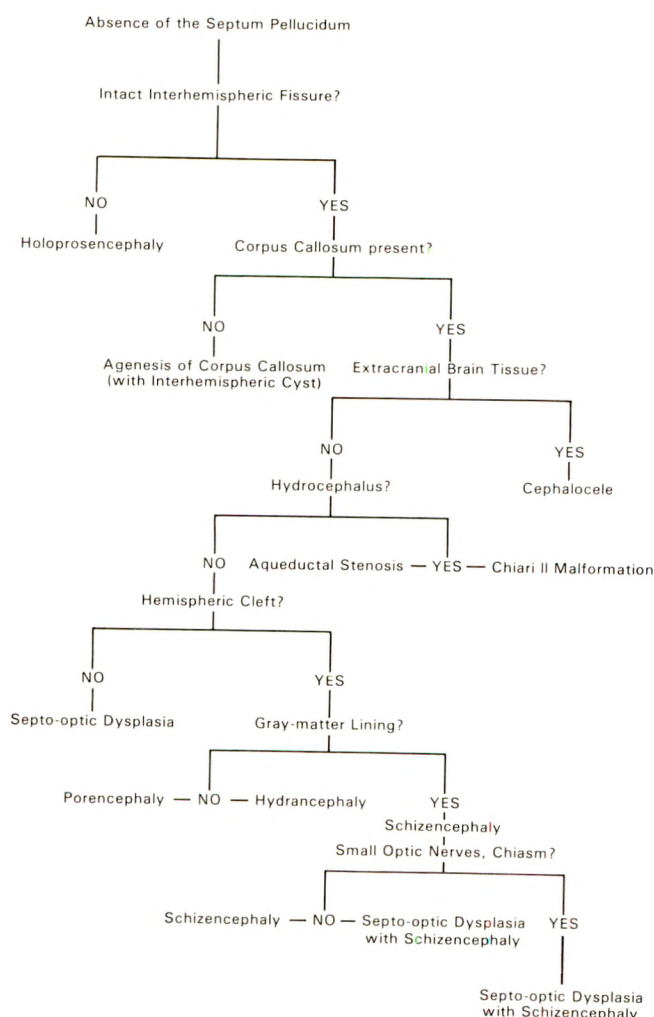


Fig. 1.—Algorithm to facilitate diagnosis of underlying brain anomaly in patients with absence of septum pellucidum.

Results

Septo-optic Dysplasia (Seven Patients)

The septum was completely absent in these seven patients. In all of these subjects, the fornix was present but low in location. The fornix was attached to the postero-inferior aspect of the splenium of the corpus callosum (Fig. 2). The corpus callosum was present in all seven patients, but exhibited a focal narrowing in three of the patients with associated schizencephaly. The location of the callosal narrowing correlated with that of the cleft. (One patient with a frontal cleft had a focal narrowing of the genu, two with parietal clefts had narrowing of the callosal body.) This correlation of a callosal narrowing with the location of a hemispheric cleft has been previously described [2]. The falx and interhemispheric fissure were intact and complete. The optic nerves and/or optic chiasm were subjectively small in four of the seven patients. The frontal horns had a square appearance on coronal images in all seven patients; inferior pointing of the frontal horns was identified in three. In the three patients with schizencephaly,

the lateral ventricles were of normal size. Of the four patients without schizencephaly, two had enlarged lateral ventricles with diminished white matter in the centrum semiovale and the cortical sulci were shallow. In a third patient the ventricular enlargement was unilateral.

Schizencephaly (Six Patients)

The anterior-most 1 cm of the septum was present in one patient; complete absence was noted in the other five. The fornix was present, but low with posterior displacement of the attachment to the splenium in all six patients. The corpus callosum, falx, and interhemispheric fissure were intact and complete except for focal thinning of the corpus callosum, as described above. The optic nerves and chiasm were small in two of the patients, both of whom also had septo-optic dysplasia. In the three patients in whom the frontal horns were not involved by the cleft, the frontal horns had a square appearance. The frontal horns were distorted in the three patients in whom they were involved by clefts (Fig. 3). The cerebral cortex was thickened with an irregular gray matter-white matter junction and shallow sulci along and adjacent to the cleft.

Aqueductal Stenosis (Five Patients)

There was marked hydrocephalus in all five patients. The septum was partially absent in two of the five patients (Fig. 4), nearly completely absent in one, and completely absent in two subjects. In the patients with partial absence of the septum, the middle of the septum was absent but the most anterior, posterior, superior, and inferior portions were present. The septum was progressively thinner close to the absent center (Fig. 4). The fornix was inferiorly displaced in all five cases. The corpus callosum, falx, interhemispheric fissure, optic nerves, and optic tracts showed no developmental abnormality. The corpus callosum was stretched, the frontal horns ballooned, the cortex flattened, and the white matter thinned by the marked hydrocephalus. No other abnormalities were noted.

Chiari II Malformation (Seven Patients)

All seven patients had ventriculoperitoneal shunts for severe hydrocephalus. The septum was completely absent in four patients and absent except for a few remnants in three of the seven. The appearance of the septal remnants at the periphery and of the inferiorly displaced fornices was identical to that of the remnants of septum in the patients with aqueductal stenosis. In all seven patients, the rostrum and splenium of the corpus callosum were absent, and the falx was completely formed in all seven subjects, but was fenestrated in three. The interhemispheric fissure was complete in all seven patients, but in three of the children it was off-center as a result of gyral interdigitations (Fig. 5). The frontal horns of the lateral ventricles were enlarged as a result of hydrocephalus. The trigones and occipital horns were enlarged by

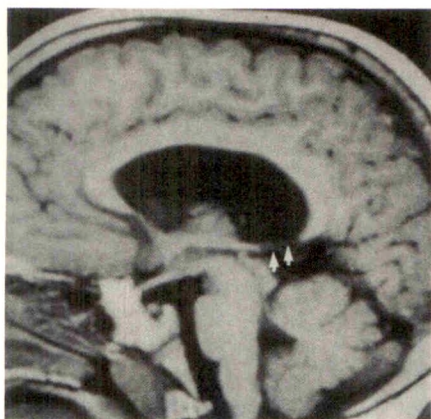


Fig. 2.—Midline sagittal SE 600/20 MR image of patient with septo-optic dysplasia. Fornix (arrows) is low in position, meeting splenium of corpus callosum posteriorly and inferiorly. Axial images of this patient showed absence of septum pellucidum.

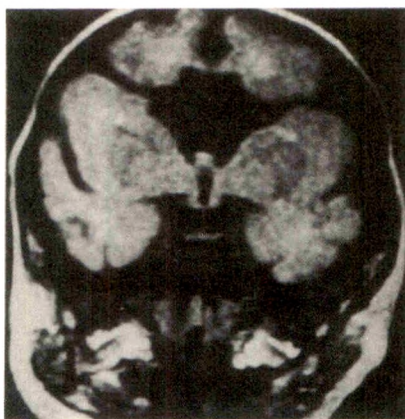


Fig. 3.—Coronal SE 600/20 MR image of patient with bilateral schizencephaly. Septum pellucidum is completely absent. Shape of frontal horns is distorted by clefts.

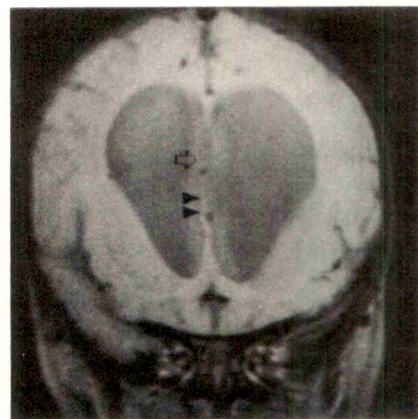
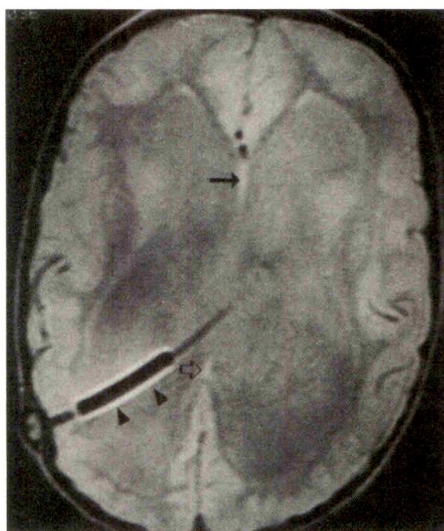
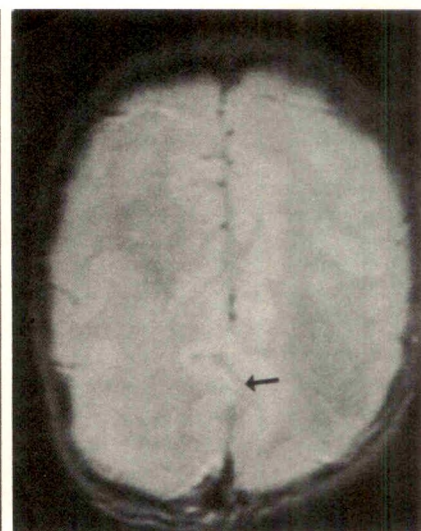


Fig. 4.—Coronal SE 2500/35 MR image of patient with severe hydrocephalus resulting from aqueductal stenosis. Septum is thin inferiorly (arrowheads) and absent centrally (arrow). A wide range of thinning and partial absence of septum was seen in patients with aqueductal stenosis and Chiari II malformation. Pressure necrosis of septum, resulting from longstanding hydrocephalus, may be the cause of these septal anomalies.



A



B

Fig. 5.—Chiari II malformation.

A, Axial SE 2500/35 MR image at level of bodies of lateral ventricles. A ventriculostomy tube is in place in right lateral ventricle (arrowheads). Only the most anterior 2 cm (closed arrow) and most posterior 1 cm (open arrow) of septum are present at this level.

B, Axial SE 2500/35 MR image above lateral ventricles. Gyri of cerebral hemispheres interdigitate through an area of falx fenestration (arrow). This is a helpful sign in diagnosing Chiari II malformation.

a combination of chronic hydrocephalus and colpocephaly. The mantle of the cerebral white matter was slightly thinned. The cerebral cortex, optic nerves, and optic chiasm were normal in all seven patients.

Holoprosencephaly (Four Patients)

The septum was completely absent in all four patients who had holoprosencephaly. Three patients had semilobar holoprosencephaly and one had lobar holoprosencephaly. The frontal lobes were entirely fused in two of the infants with semilobar holoprosencephaly. The frontal lobes were fused in

the posterior frontal region in the third patient with semilobar holoprosencephaly and in the patient with the lobar variety. None of the four patients had a detectable corpus callosum or fornix. The frontal horns were unformed in the three patients with the semilobar form; they were present, but hypoplastic, in the child with the lobar form. The cerebral cortex and white matter were normal in appearance in the child with lobar holoprosencephaly and in two of the three patients with the semilobar variety. In the third infant with the semilobar form, the cortex was thickened with multiple heterotopias and diminished thickness of the white matter. The optic nerves and chiasm appeared normal in all four patients.

Cephaloceles (Three Patients)

The septum was completely absent in all three patients. In the two patients with frontonasal encephaloceles, there was agenesis of the corpus callosum in one and atrophy of the corpus callosum in the other. In the third patient, with a sphenoidal encephalocele, there was agenesis of the corpus callosum. The fornix was absent in the two patients with callosal agenesis; in the patient with callosal atrophy, the fornix was low with a posteriorly displaced attachment to the splenium. The frontal horns were squared and the ventricles otherwise normal in the patient with an intact corpus callosum; the frontal horns were crescent shaped and the trigones dilated (colpocephaly) in the two patients with agenesis of the corpus callosum. The optic chiasm and intracranial optic nerves were stretched and displaced by the cephaloceles. The interhemispheric fissure and falx cerebri were normal in all three patients. The cerebral cortex and white matter were normal except for stretching near the site of the cephaloceles.

Agenesis of the Corpus Callosum (Two Patients)

In each of two patients who had agenesis of the corpus callosum there was a large associated interhemispheric cyst. The septum and the fornix were completely absent in both patients. The frontal horns were crescentic in shape, and there was colpocephaly in both patients. The interhemispheric fissure was widened by the cyst. The optic nerves and optic chiasm, cerebral cortex, and cerebral white matter were normal.

Porencephaly (Two Patients)

Two patients had CSF-intensity clefts, which were not lined by gray matter, in the cerebral hemispheres. Both patients had complete absence of the septum. The corpus callosum was complete but uniformly thin, and the amount of cerebral white matter was generally reduced in both patients. In one patient, the fornix was absent on the side of the lesion; in the other, the fornix was not well-evaluated. The ipsilateral frontal horns communicated with and were distorted by the clefts. The cerebral cortex, falx, interhemispheric fissure, and optic systems were normal.

Hydranencephaly (Two Patients)

Two patients had complete absence of the hemispheres, except for small foci of remaining tissue in the inferomedial frontal and medial temporal lobes. The septum was completely absent, as were the corpus callosum, fornix, ventricles, interhemispheric fissure, optic systems (except for the optic nerves), and the vast majority of the cerebral cortex and white matter. The falx cerebri was intact in both patients.

Discussion

Proper classification of the dysmorphic brain is most important because of the very different prognoses associated

with the different anomalies of the brain. For example, patients with holoprosencephaly are nearly always severely developmentally retarded and rarely live for more than a few years, while those with callosal agenesis can have normal intelligence and lead normal lives. Results of this study indicate that absence of the septum pellucidum can serve as a useful indicator of additional brain malfunction. In our series, associated anomalies included septooptic dysplasia, schizencephaly, holoprosencephaly, agenesis of the corpus callosum, porencephaly/hydranencephaly, basilar encephaloceles, and chronic severe hydrocephalus (Chiari II malformation and aqueductal stenosis). Absence of the septum pellucidum may be reason to develop an algorithmic approach to distinguish among these anomalies (Fig. 1).

The septum telencephali is a term coined by Andy and Stephen [3, 4] to denote the midline structure located in the rostral telencephalon. It is bounded dorsally by the body of the corpus callosum; rostrally by the subcallosal gyrus, hippocampal continuation, and genu of the corpus callosum; rostroventrally by the nucleus accumbens and subcallosal gyrus; and caudoventrally by the anterior commissure, preoptic area, and anterior hypothalamus. It is bounded laterally by the lateral ventricles. Phylogenetically and functionally, the septum has been divided into two components. A thin, membranous, superior portion that contains glial cells and fiber bundles has been called the septum gangiosum [5], but will be referred to in this article as the septum pellucidum as defined by Andy and Stephen. This structure is seen only in higher primates. The caudally located subdivision of the septum telencephali contains well-developed nuclei that correspond with those seen in lower forms of life. This structure is called the septum verum (septum gliosum of Kuhlenbeck) [5]. The septum verum is not clearly differentiated from the subcallosal gyrus or paraterminal gyrus below, nor from the septum pellucidum above. Within the septum verum are the septal nuclei, the nucleus of the diagonal band of Broca, the bed nucleus of the anterior commissure, and the bed nucleus of the stria terminalis [4]. The septum verum contains multiple fiber systems and essentially acts as a central relay station. It is linked with the hippocampus by fornix fibers, with the preoptic and hypothalamic nuclei by the median forebrain bundle, with the amygdaloid nuclei by the stria terminalis, and with the habenula and colliculi by way of the stria medullaris. The diagonal band of Broca runs medially within the ventral septum and relates the limbic system with the olfactory apparatus. In view of the septum verum's function as a regulatory station linking the diencephalon with the limbic system, it is not surprising that its absence may be associated with a rather severe clinical manifestation [1].

The embryological development of the septum pellucidum has not been clearly elucidated. Rakic and Yakovlev [6] have hypothesized that the leaves of the septum form as a result of cavitation of the medial inferior commissural plate during formation of the corpus callosum (Fig. 6A). The commissural plate is a deep midline structure deriving from the primitive lamina terminalis at the rostral end of the neural tube. The anterior commissure, hippocampal commissure, and corpus callosum develop from this structure. Rakic and Yakovlev suggest that after the corpus callosum forms in a certain

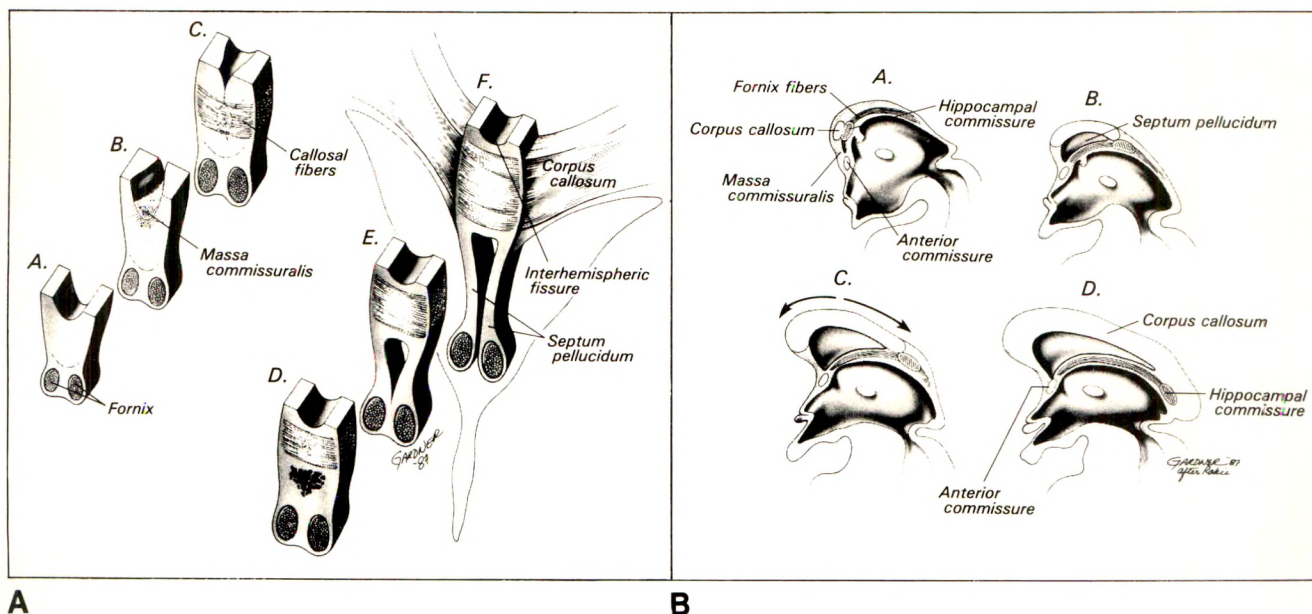


Fig. 6.—Schematic drawings illustrate major theories about formation of septum pellucidum.

A, Rakic and Yakovlev [6] have suggested that the leaves of the septum form as a result of cavitation of the medial, inferior aspect of commissural plate after corpus callosum has formed from the plate in a certain region. The thin remaining walls of commissural plate in this region become the leaves of the septum while the cavitory center becomes the cavum septi pellucidi.

B, Abbie [7] and Kuhlenbeck [5] contend that the septum forms early in the caudal commissural plate and then undergoes progressive stretching between the anterior commissure, hippocampal commissure, and corpus callosum.

area, the remaining walls of the commissural plate in this region become the leaves of the septum pellucidum, while the cavitory center becomes the cavum septi pellucidi. The leaves then fuse, in most people, starting posteriorly and progressing rostrally sometime after birth. Others [1, 5, 7] contend that the septum forms early (sixth or seventh week of gestation) in the caudal commissural plate and then undergoes progressive stretching between the anterior commissure, hippocampal commissure, and corpus callosum; the stretching is a result of progressive growth of the corpus callosum and fornix (Fig. 6B). The results of this study are not sufficient to substantiate either theory, although the fact that in one patient with schizencephaly the most anterior 1 cm of the septum was the only part formed suggests formation in an anterior to posterior direction, as suggested by Abbie [7] and Kuhlenbeck [5].

In all patients with absence of the septum pellucidum, the frontal horns, if not distorted by a cleft, had a square appearance. This sign has been described in association with septo-optic dysplasia. It appears that in fact the squaring is a consequence of absence of the septum, and is not specific for a single disease. The fornix consistently occupies an abnormally low position in patients with absence of the septum. The caudal displacement of its attachment to the splenium also appears to be a nonspecific consequence of absence of the septum.

The low position of the fornix in these patients presumably results simply from absence of the tethering effect of the septum. When the septum is present, it holds the fornix well above the velum interpositum. When the septum is absent, the bodies of the fornices settle inferiorly onto the velum interpositum. The only other condition in which this low for-

niceal position is seen is hydrocephalus of the lateral ventricles, in which the septum is stretched and the fornix inferiorly displaced.

The holoprosencephalies are probably the most devastating brain anomalies associated with absence of the septum pellucidum. The basic underlying defect is a lack of induction of the forebrain within the primitive lamina terminalis, which varies in degree [8–10]. The defect in the primitive lamina terminalis results in a lack of formation of the corpus callosum and septum pellucidum. The distinguishing radiographic feature of the holoprosencephalies is a lack of complete separation of the cerebral hemispheres; the hemispheres will be fused in at least one area, usually in the frontal lobes [11]. This fusion was seen only in the patients with holoprosencephaly and in no others. The initial step in the evaluation of patients with absence of the septum pellucidum, therefore, should be examination of the interhemispheric fissure for evidence of fusion of the hemispheres.

Since the corpus callosum and septum pellucidum both derive from the commissural plate and the corpus callosum forms first, absence of the septum in patients with absence of the corpus callosum is consistent with the known embryological development. Absence of the septum may not be readily recognized on cross-sectional imaging exams, because the third ventricle assumes an abnormally high position in the large monoventricle. The high third ventricle is interposed between the lateral ventricles, and the bodies of the lateral ventricles are compressed from the medial aspect by the longitudinal callosal bundles of Probst [12–15] (Fig. 7). A similar appearance may be seen in "agenesis of the corpus callosum with interhemispheric cyst" [16]. In these patients, a large CSF-containing structure continuous with the ventric-

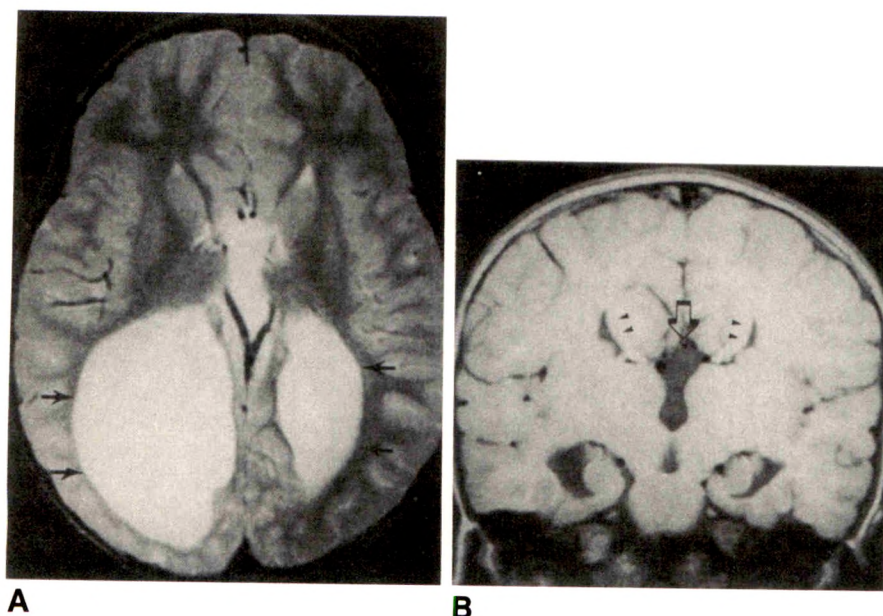


Fig. 7.—Agenesis of corpus callosum.

A, Axial SE 2500/70 MR image. Absence of septum pellucidum is not readily apparent because abnormally high-positioned third ventricle is interposed between lateral ventricles. Note enlarged atria and occipital horns of lateral ventricles (colpocephaly), characteristic of agenesis of the corpus callosum (arrows).

B, Coronal SE 600/20 MR image reveals abnormally high position of third ventricle (open arrow) and longitudinal bundles of Probst (arrowheads) impressing the medial aspects of lateral ventricles.

ular system extends upward into the interhemispheric fissure, and the separation between the lateral and third ventricles is lost, giving the appearance of a monoventricle (Fig. 8). Agenesis of the corpus callosum is easily detected on the mid-sagittal image. The major differentiation is from holoprosencephaly, a diagnosis that has already been eliminated from consideration by identification of a complete interhemispheric fissure, in this case widened by the "cyst."

Two of the three patients with encephaloceles also had agenesis of the corpus callosum, a well-known association in basilar encephaloceles [17]. Basilar encephaloceles may be a result of an abnormality of the primitive lamina terminalis; hence, anomalies of the corpus callosum and septum pellucidum are not surprising. The diagnosis of encephalocele is usually made on clinical grounds. Imaging is done to look for the presence of associated malformations and to determine the location of the vascular structures in the involved region [18]. Since the vast majority of encephaloceles are in the midline, the diagnosis can be made radiographically on the midline sagittal image at the same time the corpus callosum is evaluated. The encephalocele appears as soft tissue extending beyond the calvaria through a calvarial defect. On MR, the low-intensity signal of the calvaria is interrupted at the site of the defect (Fig. 9).

Patients who have Chiari II malformation and patients who have aqueductal stenosis are grouped together in our algorithm, because both groups of patients demonstrate the same spectrum of septal absence. (The patients with the least severe hydrocephalus had a normal septum, and they were not included in this study.) Increasingly large areas of septal fenestration developed as the hydrocephalus became more profound in degree (Fig. 4). In patients with the most severe hydrocephalus, the septum was completely absent. Therefore, the absence of the septum in these patients is presumably the result of septal necrosis from longstanding, severe hydrocephalus. In the present study, all the patients with

aqueductal stenosis and Chiari II malformation had severe hydrocephalus and complete or near-complete absence of the septum. The next step in the algorithmic approach, therefore, should be assessment of ventricular size. If there is severe hydrocephalus, sagittal images should be assessed for evidence of tectal beaking; a low, vertical fourth ventricle; a cervicomedullary kink; or herniation of the cerebellum below the foramen magnum. These findings are diagnostic of Chiari II malformation [19–24]. In the absence of these findings, the sylvian aqueduct should be assessed for evidence of narrowing. Diminished flow through the aqueduct can be substantiated on an axial nongated MR image with a long repetition time. Absence of a CSF flow void within the aqueduct supports a diagnosis of aqueductal stenosis [25], although a flow void is absent in a significant number (approximately 10%) of patients without aqueductal disease. A more precise method for evaluating flow through the aqueduct is to do a flow-sensitive, axial, gradient-recalled echo sequence through the level of the aqueduct. A single slice should be obtained by using a flip angle of 50°, TR of 150, and TE of 12.5. Lack of a high signal intensity in the aqueduct supports the diagnosis of a stenotic aqueduct.

In the absence of aqueductal stenosis or Chiari II malformation, the images should be examined for clefts communicating with the lateral ventricles. If no cleft is seen, the patient should be examined for evidence of optic nerve hypoplasia and hypothalamic-pituitary dysfunction. These findings are diagnostic of DeMorsier syndrome (septo-optic dysplasia) [26–28]. Examination of the optic nerves is best done clinically, since, in our experience, the optic nerves and chiasm are normal in appearance on MR in about half the patients with DeMorsier syndrome.

When a cleft is present, differentiation should be made between an early developmental or a late destructive lesion. Both the encephaloclastic porencephalies and the developmental schizencephalies are known to be associated with

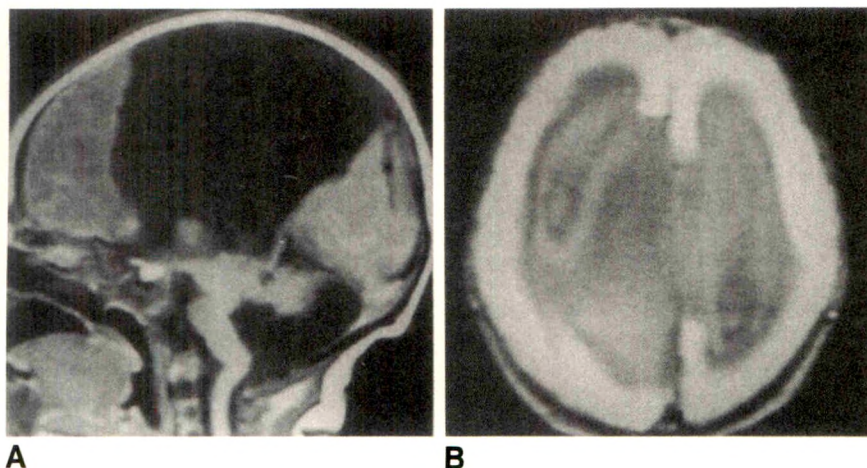


Fig. 8.—Agenesis of corpus callosum with interhemispheric cyst.

A, Sagittal SE 600/20 MR image. Inferior cerebellar vermis is absent, medulla is kinked, and there is a large fourth ventricle-cisterna magna cyst. These findings are diagnostic of Dandy-Walker malformation. Corpus callosum is absent and CSF extends upward from third ventricle between the cerebral hemispheres to inner table of skull.

B, Axial SE 2500/35 MR image. The appearance is that of a large monoventricle as seen in nearly all patients with absence of septum pellucidum.

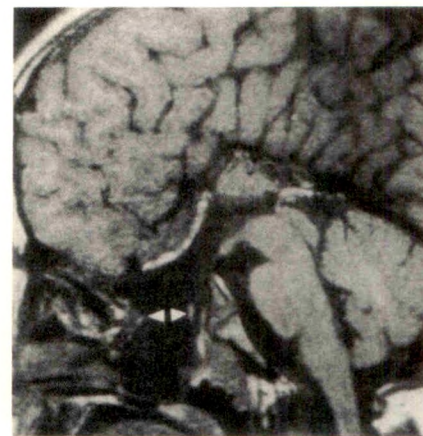


Fig. 9.—Sagittal SE 600/20 MR image of patient with sphenoidal encephalocele. The defect in skull base is seen as a CSF-intensity structure extending through skull base (arrowheads). Note associated agenesis of corpus callosum.

absence of the septum pellucidum [1, 29–32]. These entities can be distinguished by the appearance of the cleft. In schizencephaly, the cleft results from a disturbed migration of neuroblasts from the germinal matrix in the subependymal region of the ventricle; this cleft is lined by gray matter [30]. In porencephaly, the cleft results from destruction of tissue after neuroblast migration has begun [32]; gray matter lining of the cleft is absent. Hydranencephaly is classified as a porencephaly; however, this destructive lesion is much more extensive. In hydranencephaly, the entire hemisphere is destroyed, except for areas in the inferomedial frontal and posteromedial temporal regions and the deep central gray matter.

If a gray-matter-lined cleft is present, the optic nerves and chiasm must be examined because of the association between schizencephaly and septo-optic dysplasia. As discussed earlier, the clinical examination is the most important factor in this assessment.

In summary, absence of the septum pellucidum is an uncommon finding in imaging studies of the brain. In this series, it was never an isolated finding. Moreover, when this anomaly is identified, it provides a valuable clue to underlying brain malformation. A diagnostic algorithm is provided to facilitate the diagnostic process.

REFERENCES

1. Bruyn GW. Agenesis septi pellucidi, cavum septi pellucidi, cavum Vergae, and cavum veli interpositi. In: Vinken PJ, Bruyn GW, eds. *Handbook of clinical neurology*, vol. 30. *Congenital malformations of the brain and skull. Part I*. Amsterdam: North Holland, 1977:299–336.
2. Barkovich AJ, Norman D. Anomalies of the corpus callosum: correlation with further anomalies of the brain. *AJNR* 1988;9:493–501.
3. Andy OJ, Stephen H. Phylogeny of the primate septum telencephali. In: Hassler J, Stephen H, eds. *Evolution of the forebrain*. Stuttgart: Thieme, 1966:389–399.
4. Andy OJ, Stephen H. The septum in the human brain. *J Comp Neurol* 1968;133:383–410.
5. Kuhlbeck H. Some comments on the development of the human corpus callosum and septum pellucidum. *Acta Anat Nippon* 1969;44:245–256.
6. Rakic P, Yakovlev PI. Development of the corpus callosum and cavum septi in man. *J Comp Neurol* 1968;132:45–72.
7. Abbie AA. The origin of the corpus callosum and the fate of the structures related to it. *J Comp Neurol* 1939;70:9–44.
8. Yakovlev PI. Pathoarchitectonic studies of cerebral malformations. III. Arrhinencephalies (holotelencephalies). *J Neuropathol Exp Neurol* 1959;18:22–55.
9. DeMyer W. Holoprosencephaly (cyclopia-arhinencephaly). In: Vinken PJ, Bruyn GW, eds. *Handbook of clinical neurology*, vol. 30. *Congenital malformations of the brain and skull. Part I*. Amsterdam: North Holland, 1977:431–478.
10. Fitz CR. Holoprosencephaly and related entities. *Neuroradiology* 1983;25:225–238.
11. Yokota A, Oota T, Matsukado Y. Dorsal cyst malformations. Part I. Clinical study and critical review on the definition of holoprosencephaly. *Childs Brain* 1984;11:320–341.
12. Loeser JD, Alvord EC Jr. Agenesis of the corpus callosum. *Brain* 1968;91:553–570.
13. Probst FP. Congenital defects of the corpus callosum—morphology and encephalographic appearances. *Acta Radiol [Diagn] (Suppl) (Stockh)* 1973;331:1–152.
14. Kendall BE. Dysgenesis of the corpus callosum. *Neuroradiology* 1983;25:239–256.
15. Davidson HD, Abraham R, Steiner RE. Agenesis of the corpus callosum: magnetic resonance imaging. *Radiology* 1985;155:371–373.
16. Swett HA, Nixon GW. Agenesis of the corpus callosum with interhemispheric cyst. *Radiology* 1975;114:641–645.
17. Yokota A, Matsukado Y, Fuwa I, Moroki K, Nagahiro S. Anterior basal encephalocele of the neonatal and infantile period. *Neurosurgery* 1986;19:468–478.
18. Diebler C, Dulac O. Cephaloceles: clinical and neuroradiological appearance. Associated cerebral malformations. *Neuroradiology* 1983;25:199–216.
19. Naidich TP, Pudlowski RM, Naidich JB. Computed tomographic signs of Chiari II malformation. II: Midbrain and cerebellum. *Neuroradiology*

- 1980;134:391-398
20. Naidich TP, Pudlowski RM, Naidich JB. Computed tomographic signs of the Chiari II malformation. III: Ventricles and cisterns. *Neuroradiology* 1980;134:657-663
 21. Naidich TP, McLone DG, Fulling KH. The Chiari II malformation: Part IV. The hindbrain deformity. *Neuroradiology* 1983;25:179-197
 22. Peach B. Arnold-Chiari malformation. Anatomic features of 20 cases. *Arch Neurol* 1965;12:613-621
 23. Peach B. Cystic prolongation of the fourth ventricle. An anomaly associated with the Arnold-Chiari malformation. *Arch Neurol* 1964;11:609-612
 24. Variend S, Emery JL. Cervical dislocation of the cerebellum in children with meningocele. *Teratology* 1976;13:281-290
 25. Sherman JL, Citrin CM, Bowen BJ, Gangarosa RE. MR demonstration of altered cerebrospinal fluid flow by obstructive lesions. *AJNR* 1986;7:571-579
 26. DeMorsier G. Agenesie du septum pellucidum avec malformation du tractus optique. La dysplasie septo-optique. *Schweiz Arch Neurol Psychiatr* 1956;77:267-293
 27. Hoyt WF, Kaplan SL, Grumbach MM, Glaser TS. Septo-optic dysplasia and pituitary dwarfism. *Lancet* 1970;1:893-894
 28. Manelfe C, Rochiccioli P. CT of septo-optic dysplasia. *AJR* 1979;133:1157-1160
 29. Miller GM, Stears JC, Guggenheim MA, Wilkening GN. Schizencephaly: a clinical and CT study. *Neurology* 1984;34:997-1001
 30. Barkovich AJ, Chuang SH, Norman D. MR of neuronal migration anomalies. *AJNR* 1987;8:1009-1017, *AJR* 1988;150:179-187
 31. Barkovich AJ, Norman D. MR imaging of schizencephaly. *AJNR* 1988;9:297-302, *AJR* 1988;150:1391-1396
 32. Raybaud C. Destructive lesions of the brain. *Neuroradiology* 1983;25:265-291

Intracranial Oligodendrogliomas: Imaging Findings in 35 Untreated Cases

Ya-Yen Lee¹
Pamela Van Tassel

The radiographic findings in 35 cases of untreated intracranial oligodendrogliomas were reviewed. The mean age of the patients was 34.6 years, and seizure disorder and headache were the most frequent presenting symptoms. Slightly less than two-thirds of the tumors were histologically pure and almost half were low-grade. Most lesions were cerebral and peripheral in location, and the majority were in the frontal lobes. On CT the tumors were usually hypo- or isodense. Contrast enhancement of tumor occurred in nearly half the cases, and was usually mild and poorly defined. Tumor calcification often occurred, and hemorrhage or cystic formation was not infrequent. Occasionally, calvarial erosion was associated with the tumors because of their peripheral location and slow-growing nature. The lesions were usually sharply demarcated and without edema. MR most frequently revealed hypointense lesions on T1-weighted images and abnormal hyperintensity on T2-weighted scans. In regard to grading or purity of oligodendrogliomas, no significant correlations were found except for a suggestion that higher-grade and mixed tumors tend to enhance more often on CT.

The radiographic features of oligodendroglioma are quite characteristic but not pathognomic. A high preoperative suspicion might lead to more appropriate tumor management. MR, although less sensitive in detecting tumor calcification, is superior to CT in defining the tumor extent, which is beneficial for surgical and postsurgical radiotherapy planning.

Oligodendrogliomas are relatively uncommon primary brain neoplasms and account for 4–7% of all primary intracranial gliomas [1, 2]. They occur more frequently in young adults and tend to involve the frontal lobes of the cerebrum. Oligodendrogliomas often contain other glial elements, and approximately 50% of the tumors generally classified as oligodendrogliomas consist of mixed-cell forms [1]. The presence of a mixed-cell population and the absence of characteristic cytoplasmic clearing in frozen biopsy material make the intraoperative diagnosis of oligodendroglioma challenging [3]. Furthermore, the higher cellularity and nuclear/cytoplasmic ratio as well as the nonprognostic increased mitotic activity of oligodendrogliomas may lead to misdiagnosis of more malignant anaplastic astrocytoma, which might alter or defer a proper surgical resection. A high index of suspicion on preoperative imaging studies may contribute to a proper frozen section diagnosis. With the advances in neuroimaging in recent years, the diagnostic capability of brain tumor imaging has vastly improved. We review the CT and MR features of intracranial oligodendrogliomas and attempt to correlate these with the histologic tumor purity and grading.

Materials and Methods

The pretreatment imaging studies of 35 patients with surgically proved oligodendrogliomas were reviewed retrospectively. All patients had pre- and postcontrast CT, which was performed on a variety of scanners. Most of the studies were obtained on high-resolution scanners. More recently, 11 patients also had preoperative MR, which was performed on

This article appears in the January/February 1989 issue of *AJNR* and the February 1989 issue of *AJR*.

Received February 17, 1988; accepted after revision May 25, 1988.

¹ Both authors: Division of Diagnostic Imaging, Department of Diagnostic Radiology, M. D. Anderson Hospital and Tumor Institute at Houston, The University of Texas System Cancer Center, 1515 Holcombe Blvd., Houston, TX 77030. Address reprint requests to Y.-Y. Lee.

AJR 152:361–369, February 1989
0361–803X/89/1522–0361
© American Roentgen Ray Society

(No.)	T2-MR (No.)	Ca ⁺⁺ (No.)	Hemorrhage (No.)	Cystic Formation (No.)	Calvarial Erosion (No.)	Edema (No.)
6	Hyperintense (7)	(6)	(3)	(1)	(3)	Present (2) Absent (10) Unknown (3)
2	Hyperintense (2)	(3)	(2)	(2)	(1)	Present (4) Absent (4)
1	-	(0)	(0)	(1)	(0)	Present (1) Unknown (1)
1	Hyperintense (2)	(4)	(2)	(3)	(1)	Present (4) Absent (2) Unknown (2)
1	-	(1)	(0)	(1)	(1)	Present (1)

either a 1.5-T GE Signa unit or a 0.35-T Dasonics MT/S scanner with images obtained with spin-echo T1-weighted, proton-density, and T2-weighted pulse sequences. Slice thickness ranged from 5 to 10 mm, and the majority of studies were done using a 5-mm slice thickness.

All of the pathologic specimens were collected from subtotal or total resections. Tumor composed of at least a 75% oligodendroglial element was categorized as a pure oligodendrogloma, with a mixed tumor containing less than 75% oligodendrogloma. Mixed gliomas with predominant nonoligodendroglial elements were excluded from this study. Histologic grading of oligodendrogloma was modified after Smith's classification [4]. In low-grade oligodendrogloma, the neoplastic cells are fairly uniform, with round or polygonal shapes, and there is a characteristic retraction artifact of the cytoplasm, which forms a clear halo that surrounds the nuclei. The nuclear/cytoplasmic (N/C) ratio is less than one-third. There is no vascular endothelial proliferation or necrosis. In intermediate-grade (or anaplastic) oligodendrogloma, there is an increased N/C ratio and mild nuclear pleomorphism. Increased cell density may produce a "back-to-back" appearance. Vascular endothelial proliferation may be present but necrosis is not seen. In high-grade oligodendrogloma (glioblastoma multiforme with oligodendroglial features), the tumor is very cellular and highly pleomorphic, with a high N/C ratio. Necrosis is present along with abundant vascular endothelial proliferation.

Medical records were reviewed for patient's gender, presenting symptoms, interval between initial symptoms and diagnosis, and age at time of diagnosis.

The radiographic parameters studied for the tumors were size, configuration, location, CT density and contrast enhancement of tumor matrix, tumor intensities of T1- and T2-weighted MR images,

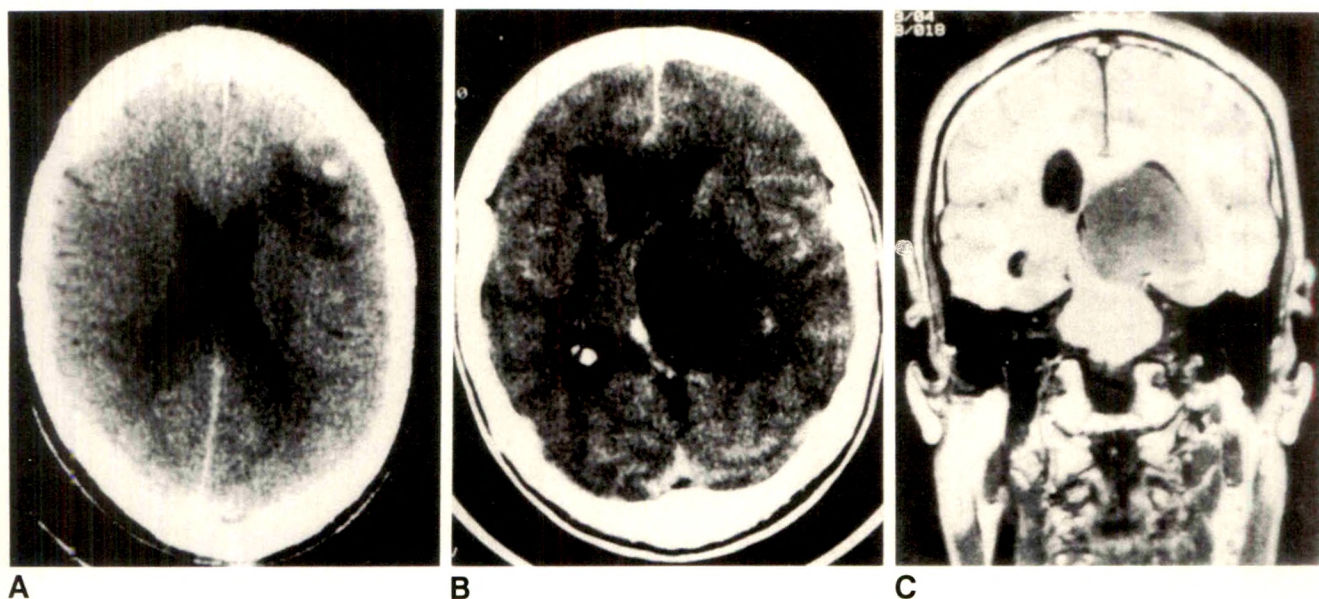


Fig. 1.—A, Peripheral, pure low-grade oligodendroglioma. Hypodense nonenhancing characteristics of tumor matrix with a fleck of calcification. B and C, Central pure low-grade oligodendroglioma. MR image (600/25) clearly demonstrates the absence of intraventricular extension of this subependymal thalamic tumor.

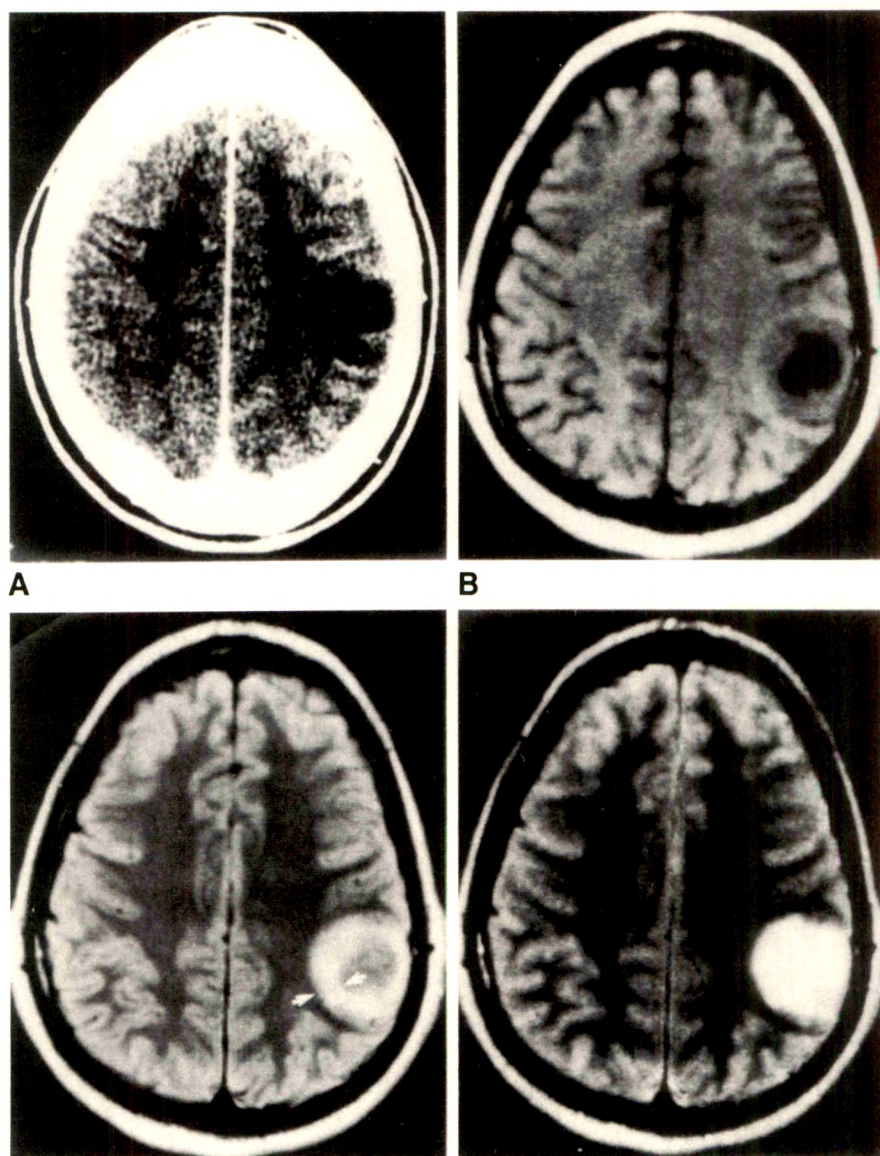


Fig. 2—Mixed intermediate-grade oligodendroglioma.

A, Postcontrast CT shows hypodense nonenhancing tumor peripherally in left parietal lobe with poorly defined borders.

B–D, MR images (500/30, 2000/30, and 2000/90, respectively). Tumor margins are sharply delineated, with demonstration of a central cystic component; the best demarcation of tumor (arrows in C) from surrounding normal tissue and cyst is on the proton-density image (C, 2000/30).

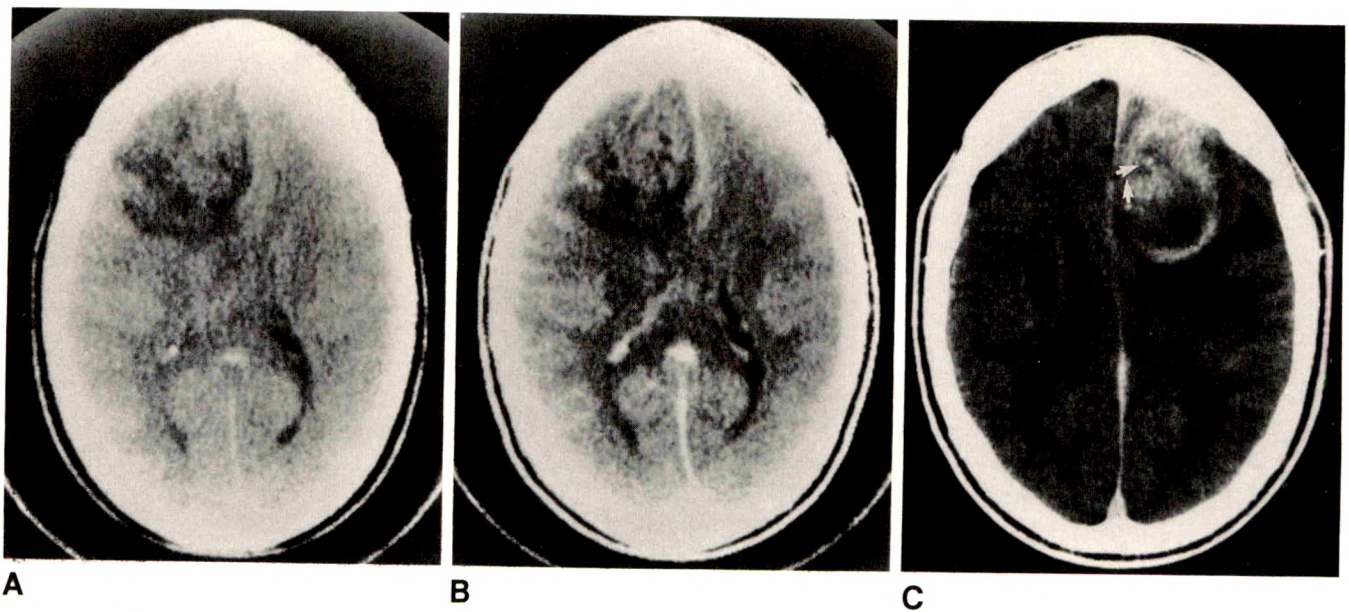


Fig. 3.—A and B, Pre- (A) and post- (B) contrast CT of a pure intermediate-grade oligodendroglioma. Contrast enhancement of the tumor is mild and poorly defined.
C, Postcontrast CT of a mixed intermediate tumor with uncommon strong enhancement of the solid portion of the tumor. Note minute matrix calcifications (arrows) and cystic formation.

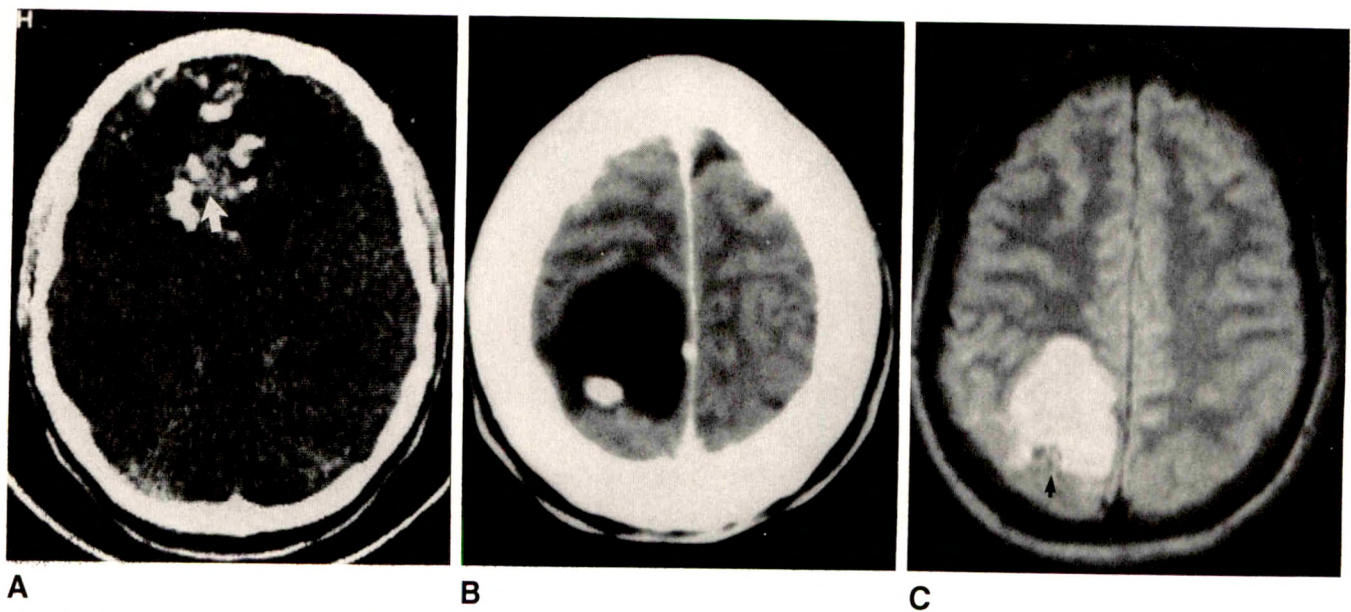


Fig. 4.—A, Extensive scattered calcifications in a mixed intermediate-grade oligodendroglioma. Poorly defined tumor enhancement (arrow) is noted.
B and C, Noncontrast CT (B) and MR, 2000/56, (C) of a pure low-grade tumor. Note poorly defined low signal at tumor calcification (arrow in C), which is clearly demonstrated on CT.

$\times 7 \times 6$ cm. On CT the tumor margins were sharp in 17 cases (49%) and poorly margined in 18 (51%). Indistinct tumor margins on CT became sharply margined on MR in eight of nine cases (Fig. 2).

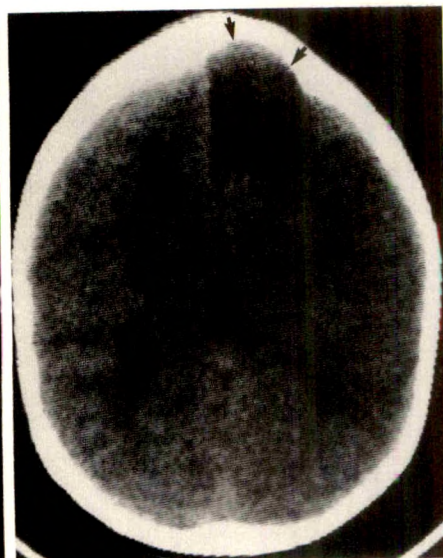
On the noncontrast CT scans the tumor matrix was hypodense to brain parenchyma in 20 cases (57%) and isodense

in eight (23%). Two were extremely hyperdense due to extensive tumor hemorrhage, and five were mixed. CT contrast enhancement of tumor was noted in 16 patients (46%) and was faint and poorly defined in all but two (Fig. 3). Sixteen cases had no definite tumor enhancement, and two could not be evaluated due to extensive tumor hemorrhage. Of the 15

Fig. 5.—Postcontrast CT of a hemorrhagic pure intermediate-grade oligodendroglioma. The large acute hematoma obscures the underlying tumor.



5



6

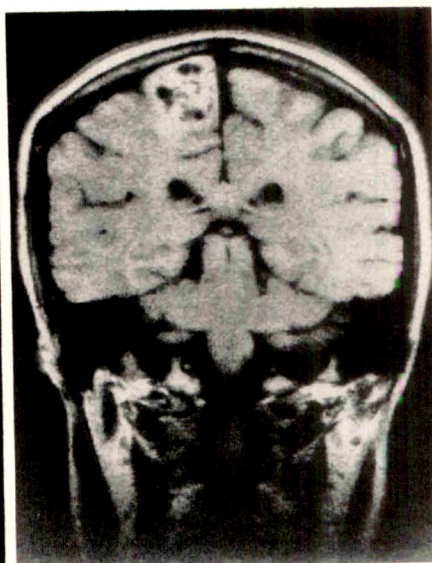
Fig. 6.—Pure low-grade oligodendroglioma. Note erosion of overlying calvarium (arrows) from this peripheral tumor, which was oval, hypodense, and nonenhancing.



A



B



C

Fig. 7.—A and B, T1-weighted, 450/25, (A) and T2-weighted, 2500/100, (B) MR images of the patient shown in Fig. 6. Typical but nonspecific hypointensity on T1-weighted image and hyperintensity on T2-weighted image. Also clearly shown is the extension of tumor into the diploë of overlying frontal bone.

C, Uncommon hyperintense tumor with areas of signal void created by matrix calcification on T1-weighted MR image (500/40) of a mixed intermediate-grade oligodendroglioma.

pure low-grade oligodendrogliomas, three enhanced on CT, as did four of eight pure intermediate-grade tumors. Among the 12 mixed oligodendrogliomas, all enhanced except for one low-grade and two intermediate-grade tumors. There was a tendency for mixed- or higher-grade tumors to have contrast enhancement.

Tumor calcifications were identified on CT in 14 patients (40%), appearing as clumps in six and as flecks in eight (Fig. 4). Known calcifications were undetectable on MR in two

cases. Calcifications were seen in 40% of pure low-grade tumors, 38% of pure intermediate-grade tumors, 44% of mixed intermediate-grade tumors, and in the only mixed high-grade tumor. Tumoral hemorrhage was noted on CT in seven patients (20%). Two were so extensive that a nonhemorrhagic part of tumor could not be identified (Fig. 5). Hemorrhage was seen in three pure low-grade, two pure intermediate-grade, and two mixed intermediate-grade tumors. A cystic component was seen in seven oligodendrogliomas (20%). There was

no consistent correlation of tumoral calcification, hemorrhage, or cystic formation with tumor purity or grading.

Owing to tumor hypodensity and absence of contrast enhancement, assessment of possible associated edema could not be made on CT in 12 patients. In the remaining 23 patients, edema was absent in 14 and present in nine. In 11 MR studies, edema was present in three and absent in four of seven cases of hypodense, nonenhancing tumors with uncertainty of associated edema on CT. Therefore, in a total of 30 patients the presence of edema could be correlated with histopathologic findings. Among 20 pure oligodendrogliomas (12 low-grade, and eight intermediate-grade), six were associated with edema (30%). Six of 10 mixed tumors (one low-grade, eight intermediate-grade, and one high-grade) were positive for edema (60%). Edema was present in three of 13 low-grade tumors (23%) and nine of 17 more malignant (intermediate- or high-grade) tumors (53%).

Associated calvarial erosion, caused by the peripheral location and slow-growing character of tumor, was present in six cases (17%) (Fig. 6). This was seen in three pure tumors that were low-grade, one pure intermediate-grade, one mixed intermediate-grade, and one mixed high-grade lesion.

Of the 11 cases that had MR imaging (Fig. 7), seven were pure low-grade oligodendrogliomas. Six of these were hypointense on T1-weighted images and one had mixed areas of hypo- and hyperintensity. Two pure intermediate-grade tumors also were hypointense. There were two mixed tumors with one demonstrating hypointensity and the other mixed intensity on T1-weighted scans. Hyperintensity of tumor was observed on T2-weighted images in all 11 cases. No significant differences in T1 or T2 intensity were noted regarding the purity or grading of the tumors. Late-echo images to a TE

of 100 were obtained in four patients and did not provide additional information.

Discussion

Oligodendroglioma is a relatively slow-growing primary brain tumor, and the diagnosis is usually preceded by a long history of symptoms, frequently a seizure disorder or headaches [2, 5, 6]. However, with easy access to modern non-invasive neuroimaging techniques, such as CT or MR, the interval between initial presentation and diagnosis of tumor has been greatly reduced. As shown in our series, slightly over half the cases (51%) were diagnosed within 6 months from the onset of symptoms.

Histologically, the oligodendroglioma is often in a mixed form [1]. In our series about one-third were mixed tumors that also contained minor components of astrocytoma or anaplastic astrocytoma. It should be mentioned that the high-grade oligodendrogliomas, either pure or mixed, are often categorized as glioblastoma multiforme because of the presence of necrosis, and therefore the reported incidence of higher-grade oligodendrogliomas may not be accurate.

As also described in the literature, almost all the lesions in this series, either pure or mixed, are located peripherally in the cerebrum, with a definite propensity for the frontal lobe [2, 5]. Intraventricular and posterior fossa lesions are very rare [7, 8], and neither one was found in our series. Oligodendrogliomas are often round or oval in shape and frequently are sharply margined. A significant number of cases with poorly defined tumor margins on CT demonstrated sharp margination on MR. Furthermore, MR provided better delineation of tumor in the anatomic sites where inherent computer

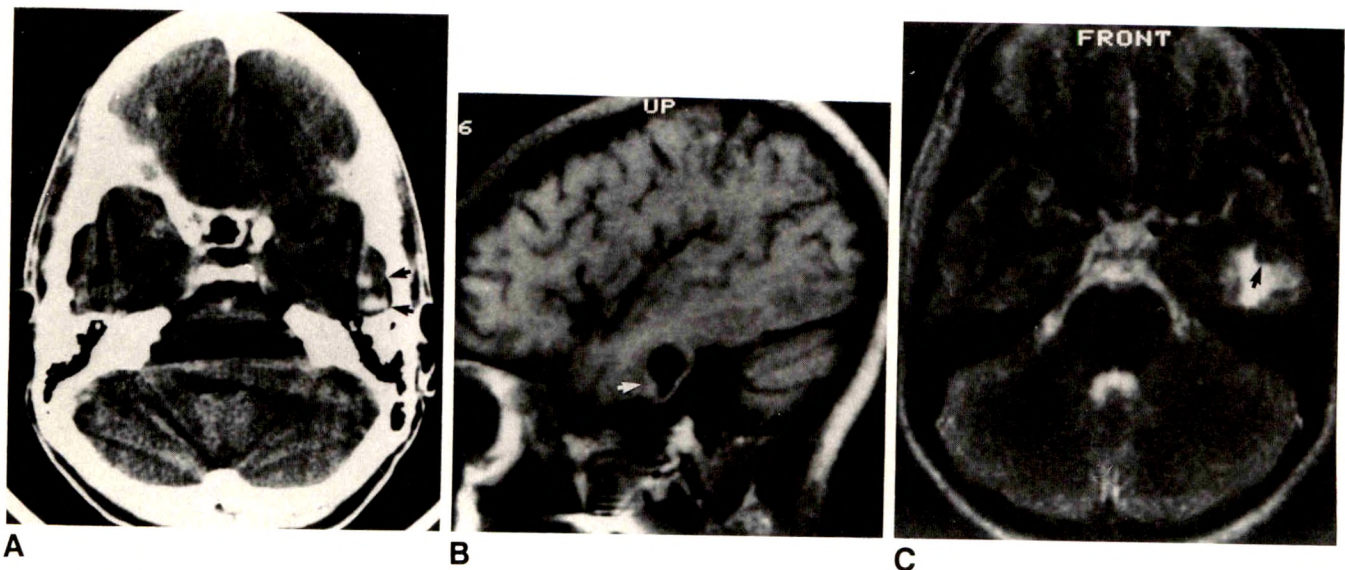


Fig. 8.—A–C, Contrast CT (A), T1-weighted, 500/30 (B), and T2-weighted, 2500/90, (C) MR images of a pure low-grade oligodendroglioma. Tumor calcifications (arrows in A) are far better appreciated on CT. However, the tumor margins and cystic component, obscured by computer artifacts on CT, are clearly shown on MR. Solid tumor nodule (arrows in B and C), proved at surgery, is sharply demonstrated.

Fig. 9.—Left pure low-grade oligodendroglioma.

A, Precontrast CT shows no definite abnormality.

B, Postcontrast CT after infusion of 300 ml of 30% iodinated contrast. A small poorly defined enhancing mass is identified in the medial aspect of left frontal lobe.

C, Repeat study after infusion of 200 ml of 76% iodinated contrast. The lesion becomes better defined and larger.

D, MRI image (2000/20) best demonstrates the tumor borders.

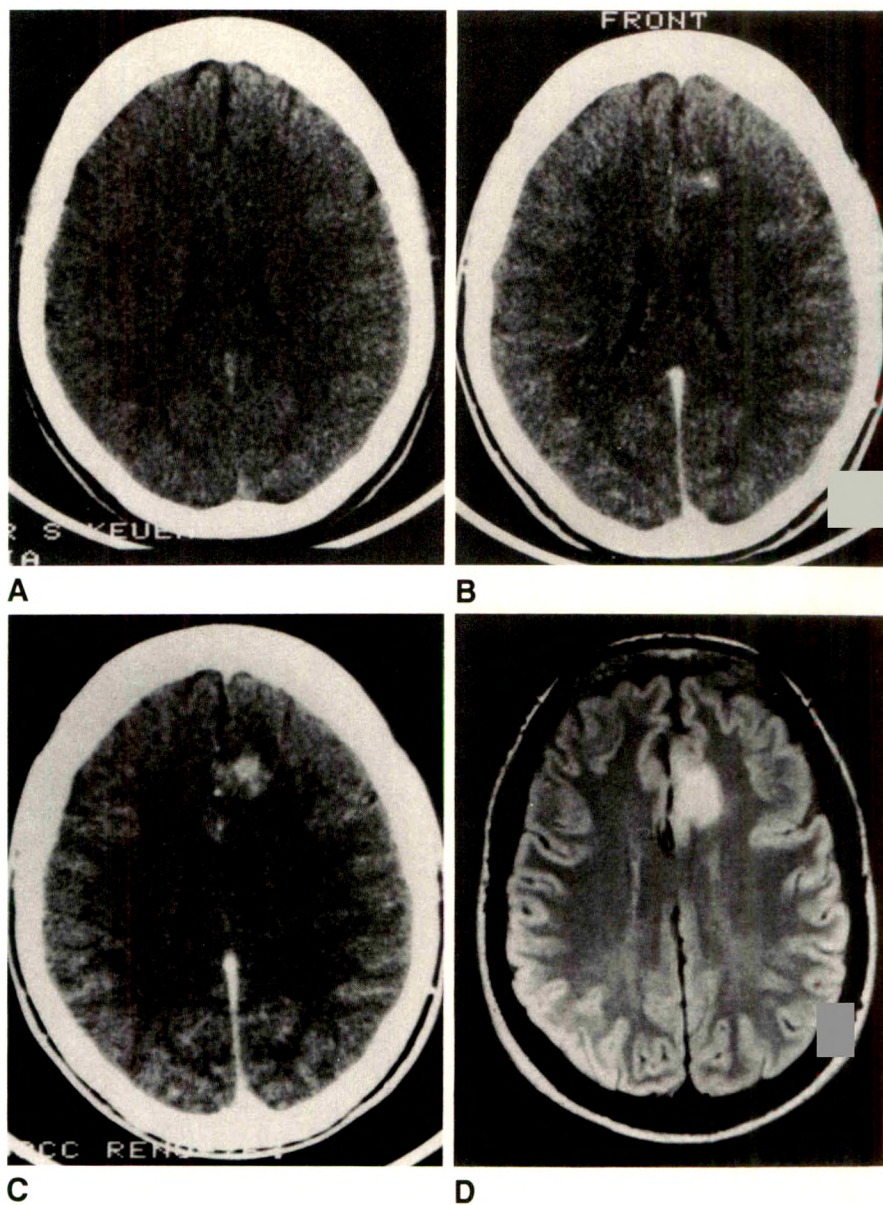
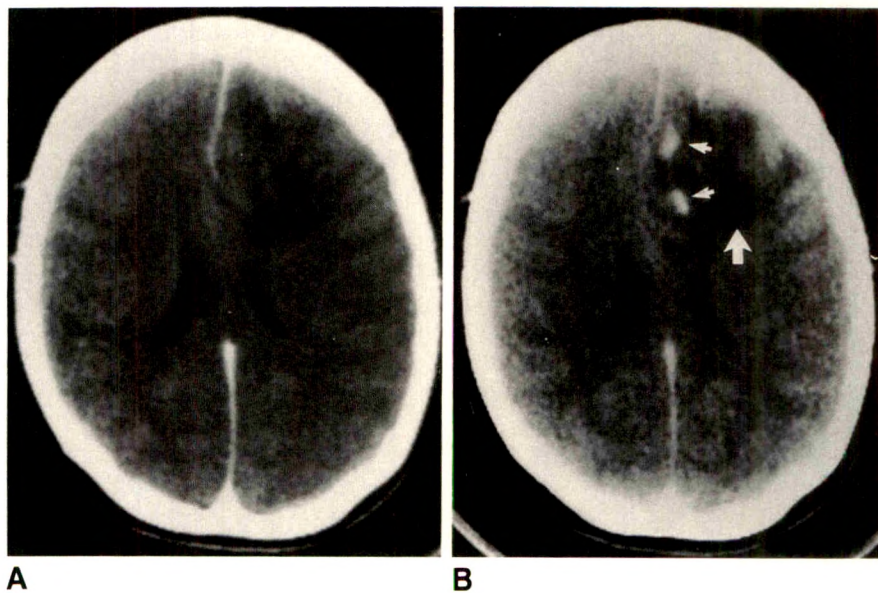


Fig. 10.—27-year-old woman with sudden-onset grand mal seizures.

A, Initial contrast CT. A poorly margined hypodense nonenhancing mass is identified in left frontal lobe with minimal mass effect. Patient refused surgery and radiotherapy after becoming symptom-free with anticonvulsant medication.

B, Contrast CT 5 years later, after patient developed severe frontal lobe dysfunction. The tumor did not progress in size and the matrix remained hypodense and nonenhancing; however, tumor calcifications (small arrows) and cystic formation (large arrow) have occurred. Pure intermediate-grade oligodendroglioma.



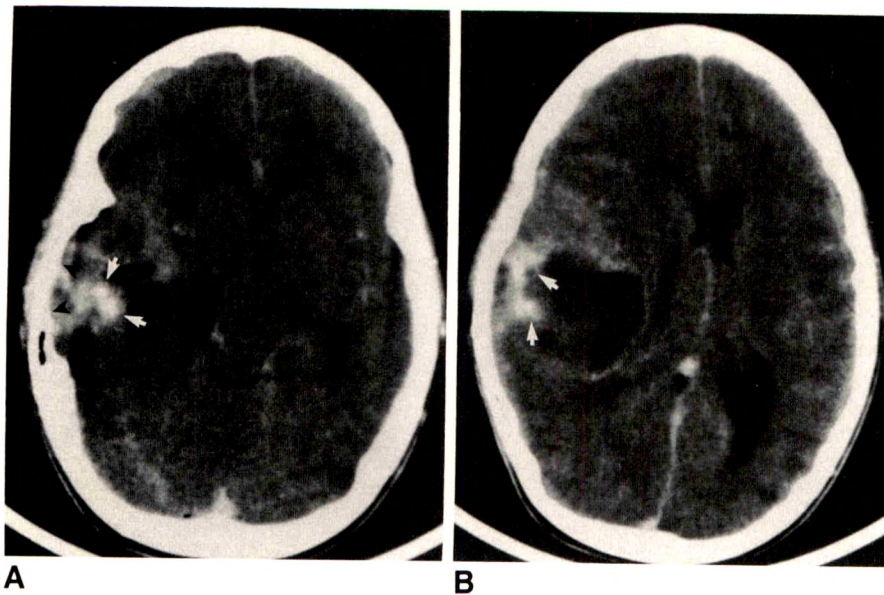


Fig. 11.—Mixed high-grade oligodendroglioma.

A and B, Postcontrast CT shows multilobulated temporal mass with large cystic or necrotic component, compatible with a glioblastoma multiforme. However, the presence of tumor calcifications (arrows) and calvarial erosion (arrowheads in A), with minimal surrounding edema, favors a lower-grade malignancy and suggests oligodendroglioma.

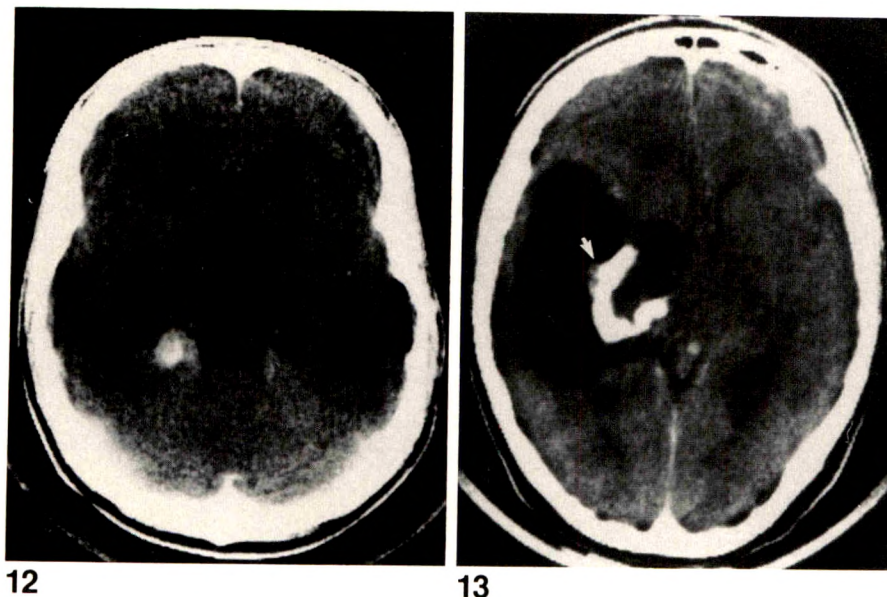


Fig. 12.—Postcontrast CT shows typical ganglioglioma presenting as a calcified and enhancing mass in the right posterior medial temporal lobe.

Fig. 13.—Postcontrast CT shows large cystic mass with dense calcification and minimal enhancement (arrow). Surgery revealed an astrocytoma with xanthochromic cystic fluid from old hemorrhage.

artifacts and limited imaging planes precluded detailed evaluation (Fig. 8). This improvement of tumor delineation should facilitate not only presurgical planning of tumor resection, but also postsurgical radiotherapy if needed [9]. On CT the tumor matrix is often either hypo- or isodense, and occasionally hyperdense due to tumoral hemorrhage. Nearly half the tumors enhanced on CT after IV administration of contrast medium. The tumor enhancement tended to be poorly defined and heterogeneous. Pathologic correlation revealed that higher-grade and mixed tumors more often demonstrated enhancement on CT. CT tumor enhancement is often better with the double contrast technique (Fig. 9).

Tumor calcification is often better defined on CT than MR; however, based on our observations in this series of cases, it seems to have no direct correlation with the purity or the grade of the tumors. The same observation is made with respect to tumor hemorrhage. A cystic component has been

said to have a significant correlation with the malignancy of oligodendroglioma [10]. This observation was not made in our series. Instead, there is a suggestion that time may play a role in the development of this finding as well as the tumor calcification (Fig. 10). As expected, edema is less often observed in the pure or low-grade oligodendrogliomas. Occasionally noted is calvarial erosion in association with slow-growing, peripherally located oligodendrogliomas. This observation also appeared to be independent of the tumor purity or grade.

With the application of high-resolution CT and MR, the differential diagnosis of oligodendroglioma is relatively limited to that of a few primary brain tumors. The high-grade oligodendroglioma may be difficult to differentiate from the more frequent glioblastoma multiforme. However, the presence of tumor calcification, a peripheral location, and the sometimes associated calvarial erosion might indicate a lower malignancy

of the tumor and suggest the proper diagnosis (Fig. 11). Ganglioglioma, an even more indolent tumor, will frequently present as calcified mass and cause diagnostic difficulty [11]; however, its propensity to involve the temporal lobe and deep cerebral tissue may provide a differentiating clue (Fig. 12). Occasionally, astrocytoma with dystrophic calcification from old hemorrhage may also look like an oligodendroglioma (Fig. 13). The most difficult lesion to differentiate is astrocytoma or low-grade anaplastic astrocytoma presenting as a hypodense, nonenhancing mass on CT. However, these astrocytic tumors tend to be deeper in location and to extend along the fiber tracts, and usually lack calcifications.

The diagnosis of oligodendroglioma on frozen section can be challenging. The high cellularity and high nuclear/cytoplasmic ratio of some oligodendrogliomas, with the absence of classic cytoplasmic halos in frozen material, might cause a misdiagnosis of anaplastic astrocytoma. Since the usual prognosis of oligodendroglioma is somewhat better than that of anaplastic astrocytoma, a high index of suspicion of the former on the presurgical CT and MR may prompt a correct histologic diagnosis, leading to more appropriate management of the tumor.

REFERENCES

1. Rubinstein LJ. Tumors of the central nervous system. In: *Atlas of tumor pathology*, series 2, fascicle 6. Armed Forces Institute of Pathology, Bethesda, MD: 1972:85-104
2. Mork SJ, Lindegaard KF, Halvorsen TB, et al. Oligodendroglioma: incidence and biological behavior in a defined population. *J Neurosurg* 1985;63:881-889
3. Bruner JM. Oligodendroglioma: diagnosis and prognosis. *Semin Diagn Pathol* 1987;4:251-261
4. Smith MT, Ludwig CL, Godfrey AD, Armburstamacher VW. Grading of oligodendrogliomas. *Cancer* 1983;52:2107-2114
5. Ludwig CL, Smith MT, Godfrey AD, et al. A clinicopathological study of 323 patients with oligodendrogliomas. *Ann Neurol* 1986;19:15-21
6. Chin HW, Hazel JJ, Kim TH, Webster JH. Oligodendrogliomas. A review of two hundred cases. *Cancer* 1980;45:1458-1466
7. Dolinskas CA, Simeone FA. CT characteristics of intraventricular oligodendrogliomas. *AJNR* 1987;8:1077-1082
8. Packers RJ, Sutton LN, Borke LB, et al. Oligodendroglioma of the posterior fossa in childhood. *Cancer* 1985;56:195-199
9. Shuman WP, Griffin BR, Haynor DR, et al. The utility of MR in planning the radiation therapy of oligodendroglioma. *AJNR* 1987;8:93-98
10. Vonofakos D, Marcu H, Hacker H. Oligodendrogliomas: CT patterns with emphasis on features indicating malignancy. *J Comput Assist Tomogr* 1979;3:783-788
11. Dorne HL, O'Gorman AM, Melanson D. Computed tomography of intracranial gangliogliomas. *AJNR* 1986;7:281-285

FORTHCOMING ARTICLES

PROGRESS IN RADIOLOGY

Percutaneous transthoracic needle aspiration: a review. *Perlmutter LM, Johnston WW, Dunnick NR*

SPECIAL ARTICLES

On teaching radiology to medical students: challenges for the nineties. *Squire LF*

Commentary. On teaching radiology to medical students. *Ott DJ, Bohrer SP*

PULMONARY RADIOLOGY

Cine-gradient-refocused MR imaging of central pulmonary emboli. *Posteraro RH, Sostman HD, Spritzer CE, Herfkens RJ*

Cardiac masses: assessment by MR imaging. *Lund JT, Ehman RL, Julsrud PR, Sinak LJ, Tajik AJ*

1988 ARRS Executive Council Award. Detection of pneumothorax: comparison of digital and conventional chest imaging. *Fajardo LL, Hillman BJ, Pond GD, Carmody RF, Johnson JE, Ferrell WR*

MAMMOGRAPHY

Case report. Pectoralis muscle simulating a breast mass. *Meyer JE, Stomper PC, Lee RR*

Evaluation of a dual-screen, dual-emulsion mammography system. *Jackson VP, Harrill CD, White SJ, Gillespie KR, Mail JT, Katz BP*

GASTROINTESTINAL RADIOLOGY

Imaging of pancreatic neoplasms: comparison of MR and CT. *Steiner E, Stark DD, Hahn PF, et al.*

Pictorial essay. MR imaging of liver neoplasms. *Rummeny E, Saini S, Wittenberg J, et al.*

Hepatic lymphoma in cyclosporine-treated transplant recipients: sonographic and CT findings. *Honda H, Franken EA Jr, Barloon TJ, Smith JL*

MR differentiation of hepatocellular carcinoma from cavernous hemangioma: complementary roles of FLASH and T2 values. *Ohtomo K, Itai Y, Yoshida H, Kokubo T, Yoshikawa K, Iio M*

Increased prevalence of cholelithiasis in patients with abdominal aortic aneurysm: sonographic evaluation. *Schuster JJ, Raptopoulos V, Baker SP*

Large colonic neoplasms missed by endoscopy. *Glick SN, Teplick SK, Balfe DM, et al.*

Case report. Giant fibrovascular polyp of the esophagus: CT and MR findings. *Whitman GJ, Borkowski GP*

Case report. Direct percutaneous drainage of an obstructed afferent loop. *Maile CW, Hanna PD*

Technical note. An internalized double-J catheter for percutaneous transgastric cystogastrostomy. *Sacks BA, Greenberg JJ, Porter DH, et al.*

Technical note. A new technique for removing occluded double mushroom-tipped biliary endoprostheses. *Yeung EY-C, O'Donnell C, Carvalho P, Adam A*

Technical note. Scrape biopsy of malignant biliary stricture through percutaneous transhepatic biliary drainage tracts. *Yip CKY, Leung JWC, Chan MKM, Metreweli C*

GENITOURINARY RADIOLOGY

Changes in the epididymides after vasectomy: sonographic findings. *Jarvis LJ, Dubbins PA*

Duplex Doppler sonography of renal transplants: lack of sensitivity and specificity in establishing pathologic diagnoses. *Genkins SM, Sanfilippo FP, Carroll BA*

SKELETAL RADIOLOGY

Digital skeletal radiography: spatial resolution requirements for detection of subperiosteal resorption. *Murphey MD*

Immature bone infarcts: findings on plain radiographs and MR scans. *Munk PL, Helms CA, Holt RG*

MR of osteochondritis dissecans and avascular necrosis of the mandibular condyle. *Schellhas KP, Wilkes CH, Fritts HM, Omlie MR, Lagrotteria LB*

Pre- and postoperative MR imaging of the craniocervical junction in rheumatoid arthritis. *Larsson E-M, Holtås S, Zygmunt S*

PEDIATRIC RADIOLOGY

Ectopic ureterocele without ureteral and caliceal dilatation (ureterocele disproportion): findings on urography and sonography. *Share JC, Lebowitz RL*

Case report. Diagnosis of pulmonary hemosiderosis by MR imaging. *Rubin GD, Edwards DK III, Reicher MA, Doemeny JM, Carson SH*

Efficacy of chest radiography in pediatric intensive care. *Sivit CJ, Taylor GA, Hauser GJ, et al.*

Sonography of the painful hip in children: 500 consecutive cases. *Miralles M, Gonzalez G, Pulpeiro JR, et al.*

MR imaging of periventricular leukomalacia in childhood. *Flodmark O, Lupton B, Li D, et al.*

Percutaneous drainage of traumatic pancreatic pseudocyst in children. *Jaffe RB, Arata JA Jr, Matlak ME*

NEURORADIOLOGY

Herniation of the suprasellar visual system and third ventricle into empty sella: morphologic and clinical considerations. *Kaufman B, Tomsak RL, Kaufman BA, et al.*

MR and CT of masses of the anterosuperior third ventricle. *Wagenspack GA, Guinto FC Jr*

Subdural and epidural empyemas: MR imaging. *Weingarten K, Zimmerman RD, Becker RD, Heier LA, Haimes AB, Deck MDF*

³¹P spectroscopy in thrombolytic treatment of experimental cerebral infarct. *Lee BCP, Brock JM, Fan T, et al.*

VASCULAR RADIOLOGY

Pseudoaneurysm and arteriovenous fistula after femoral artery catheterization: association with low femoral punctures. *Altin RS, Flicker S, Naidech HJ*

Color Doppler sonography of hemodialysis vascular access: comparison with angiography. *Middleton WD, Picus DD, Marx MV, Melson GL*

Insertion of subclavian hemodialysis catheters in difficult cases: value of fluoroscopy and angiographic techniques. *Selby JB, Tegtmeyer CJ, Amodeo C, Bittner L, Atuk NO*

PERSPECTIVE

On journals: the competition for minds and money. *Brogdon BG*

FROM THE EDITORIAL OFFICE

Why we edit. *Whalen E*

Color Doppler Ultrasound Imaging of Lower-Extremity Venous Disease

W. Dennis Foley¹
 William D. Middleton²
 Thomas L. Lawson¹
 Scott Erickson¹
 Francisco A. Quiroz¹
 Stephanus Macrander^{1,3}

A color Doppler ultrasound imaging device was used to evaluate 475 patients with suspected lower-extremity venous thrombosis. Occlusive and nonocclusive femoral and popliteal thrombi were detected in 200 studies (42%). In phase 1 of the study (240 examinations), peripheral augmentation with the use of periodic calf compression was required to show color flow throughout the femoropopliteal venous segment. In phase 2 (235 examinations), with a software upgrade to enhance detectability of slow flow, spontaneous flow could be appreciated in the normal, partly thrombosed, and recanalized femoral popliteal veins without augmentation. Augmentation was often necessary to view tibioperoneal veins. Of the total study group, conventional venography was performed for correlation in 47 patients. In the other patients, clinicians relied on the color Doppler test for the definitive diagnosis of the presence or absence of femoral popliteal venous thrombosis and treated these patients on the basis of the color Doppler test result. In the femoral veins, color Doppler studies and venography agreed in all 12 positive and 35 negative cases. In the popliteal veins, there was agreement in five isolated popliteal thromboses and in 10 femoral popliteal thromboses; there were two false-negative color Doppler studies of isolated popliteal thromboses. In four patients, Doppler studies detected nonocclusive thrombus not evident on venography.

Color Doppler imaging is easy to perform and does not require augmentation to view color flow in the femoropopliteal venous segment. Eccentric thrombus and partially canalized thrombus can be shown. Initial experience suggests color Doppler imaging may be useful in the detection of tibioperoneal venous thrombosis.

Color Doppler ultrasound is a new technical development that provides a combination gray-scale or tissue image and a dynamic-color-flow vascular image [1, 2]. Recent studies have documented the high sensitivity and specificity of real-time B-mode sonography with compression technique in the evaluation of suspected femoral popliteal venous thrombosis [3, 4]. Color Doppler imaging combines the advantages of a compression sonographic technique with the additional advantage that the flow lumen is defined in color in a manner analogous to that achieved with iodinated contrast agents.

This report details our experience in the use of color Doppler extremity venography, with particular emphasis on the diagnosis of recanalized thrombus and early evaluation of the technique in tibioperoneal venous imaging.

Materials and Methods

In the first 22 months of operation, 475 venous color Doppler studies were performed at the Medical College of Wisconsin for suspected deep-vein thrombosis. Patients were referred from either medical inpatient services or outpatient clinics.

The color Doppler studies were performed by using a sequential linear-array system with 7.5- and 5.0-MHz transducers (QAD I Quantum Medical Systems, Issaquah, WA). All studies were performed with a fluid-filled, plastic, wedge-shaped standoff attached directly to the transducer. This created an angle between the sound beam and the longitudinal axis of vessels running parallel to the skin surface. Returning echoes were analyzed for amplitude,

Received June 30, 1988; accepted after revision September 23, 1988.

¹ Department of Radiology, Medical College of Wisconsin, 8700 W. Wisconsin Ave., Milwaukee, WI 53226. Address reprint requests to W. D. Foley.

² Department of Radiology, Mallinckrodt Institute of Radiology, Washington University School of Medicine, 510 S. Kingshighway Blvd., St. Louis, MO 63110.

³ Radiology Associates of Appleton, S.C., 424 E. Wisconsin Ave., Ste. 103, Appleton, WI 54912.

AJR 152:371-376, February 1989
 0361-803X/89/1522-0371
 © American Roentgen Ray Society

phase, and frequency shift. Amplitude data provided a gray scale or tissue image; phase and frequency shifts were produced by moving targets (RBCs). Color assignment (either red or blue) depended on flow direction with respect to the transducer and was selected by the operator. Color saturation or hue reflected the extent of frequency shift, which was dependent on flow velocity and the angle of the sound beam in relation to the longitudinal axis of the flow lumen. High-frequency shifts resulted in greater color saturation toward the whiter shades of red and blue. The amplitude of the Doppler signal was dependent on power output, reflectivity of the moving RBCs, and receiver gain. The amplitude of the color flow signal on the video-display terminal was controlled by a display threshold setting. With the 7.5-MHz probe (3 cm in length), the image repetition rate was 18 frames/sec at a depth of 4 cm and 12 frames/sec at a depth of 6 cm. With the 5.0-MHz transducer (4 cm in length), the image repetition rate was 12 frames/sec at a depth of 6 cm, nine frames/sec at a depth of 9 cm, and seven frames/sec at a depth of 11.5 cm.

Transverse and longitudinal images of the common femoral vein and superficial femoral vein were obtained with the patient supine and the leg slightly externally rotated. The proximal medial saphenous and profunda femoral vein were also imaged routinely. The popliteal vein was studied with the patient decubitus and the knee flexed to approximately 30°. All venous segments were examined for the characteristics of venous flow and the effects of compression.

We recorded on videotape selected segments in the longitudinal and transverse planes of the common femoral vein; saphenofemoral junction; superficial femoral and profunda femoral vein junction; proximal, middle, and distal superficial femoral vein; and popliteal vein. These selected recordings were then available for subsequent replay and analysis. Point spectral analysis was not performed; this was unnecessary because all relevant Doppler information was encoded as a color-flow signal throughout the full length of the venous segment being imaged at any one time.

In the last 10 months of the study, upgraded software, in conjunction with a slow pulse repetition frequency for the color-flow component of the sonographic image, enabled operators to portray color-flow signals in the tibioperoneal veins from the ankle to the knee. When imaging the tibioperoneal venae comitantes, the transverse plane was preferred to the longitudinal plane. In the transverse plane, color-flow venous signal from both venae comitantes of a selected tibioperoneal vessel could be imaged simultaneously. These veins were examined with the patient supine and the knee slightly flexed, internally rotated for the anterior tibial venae comitantes and externally rotated for the posterior tibial and peroneal venae comitantes. In the longitudinal plane, with a sagittal, parasagittal, or coronal projection, it often was not possible to include both venae comitantes within the ultrasonic beam profile. When using the longitudinal imaging plane, the anterior tibial venae comitantes were imaged in a sagittal or parasagittal projection and the peroneal and posterior tibial venae comitantes in a coronal projection. In this phase of the study, 235 patients were evaluated.

Of the total 475 patients studied, correlative venograms were obtained at the request of the referring medical service in 47 patients, 31 before the installation of the slow-flow sensitivity software upgrade and 16 subsequent to installation. In other patients, clinicians using the published literature relating to compression B-mode sonography [3, 4] relied on the color Doppler test for the definitive diagnosis of the presence or absence of femoral popliteal venous thrombosis. Patients with demonstrated femoropopliteal venous thrombosis were treated with anticoagulation or caval filters as appropriate. Patients without evidence of femoropopliteal thrombosis on color Doppler imaging were not treated.

Of the 47 patients who had color Doppler and venographic examinations, the studies were performed independently by different radi-

ologists who were unaware of the results of the other diagnostic technique. The examinations were interpreted prospectively, and the prospective results were used in comparative analysis. Of the 31 studies performed before the software upgrade, comparison was made only in the femoropopliteal venous system. Of the 16 studies performed after the software upgrade, comparison included the tibioperoneal veins in addition to the proximal deep veins. Patients who had both color Doppler and venographic examinations were 35–80 years old; 60% were men and 40% were women. There was a similar age and gender distribution in the 428 other patients, who had color Doppler examinations but did not have venography.

Results

Normal Examinations

In lower-extremity venous imaging, in which vessels run parallel to the skin surface without tortuosity, all venous segments were encoded in blue and corresponding arteries in red. Normal phasic venous flow caused by respiration could be appreciated on the real-time color image in a normal femoral popliteal venous system (Fig. 1). Venous flow in the lower extremity was decreased during inspiration and increased during expiration. Flow reversal caused by the Valsalva maneuver or by heart pressures elevated on the right or localized to the upper surface of normal valve cusps was documented easily. Arterial flow reversal in early diastole, which is a normal phenomenon in lower-extremity arteries with triphasic flow characteristics, was also seen easily.

In the first 12 months of operation, with the use of an initial production-type QAD I system, color-flow venous signal in the mid and distal superficial femoral vein in most patients was appreciated only with augmentation created by distal calf compression. In the final 10 months of operation, with upgraded software, color-flow venous signal throughout the full length of the femoral popliteal venous segments could be appreciated in all normal patients without augmentation. In normal patients, the color-flow signal occupied the full cross-sectional area of the venous lumen during maximum venous flow. Normal veins were uniformly compressible, with apposition of the anterior and posterior venous walls. Compression was shown best in the transverse plane, because the compressing transducer often displaced the underlying vein medially or laterally in the longitudinal plane.

Spontaneous or augmented color-flow signals from the venae comitantes of the anterior and posterior tibial and the peroneal arteries were detectable, with the slow-flow-sensitivity software upgrade, in the proximal and distal calf (Fig. 2). In only a minority of patients were spontaneous, phasic flow signals elicited from deep veins of the calf. Most patients required augmentation, which in the latter part of the study was provided by a mechanical sleeve compressor at ankle level (Venodyne model EPS 400, Division of Advanced Instruments, Needham Heights, MA). This mechanical compressor cycled once every 5 sec.

Venous Thrombosis

Venous thrombosis was diagnosed in 42% of all femoral and popliteal veins. Intraluminal thrombus was recognized as

Fig. 1.—Longitudinal view of proximal superficial femoral vein shows normal phasic venous flow. Femoral artery (red) is anterior to femoral vein (blue). Minimal flow signal is appreciated in profunda artery, which, owing to the use of the mechanical plastic sleeve offset, is almost parallel to the face of the transducer.

A, Flow is minimal or absent in superficial femoral vein during inspiration.

B, Normal venous flow is seen during expiration.

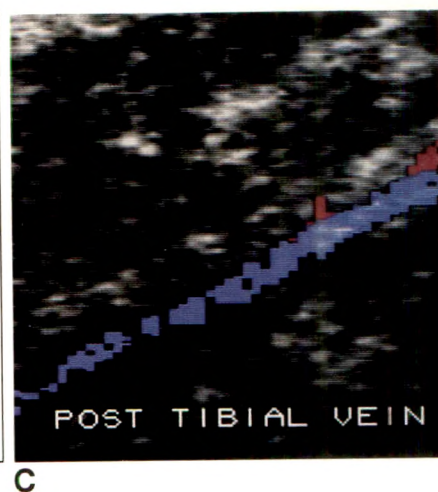
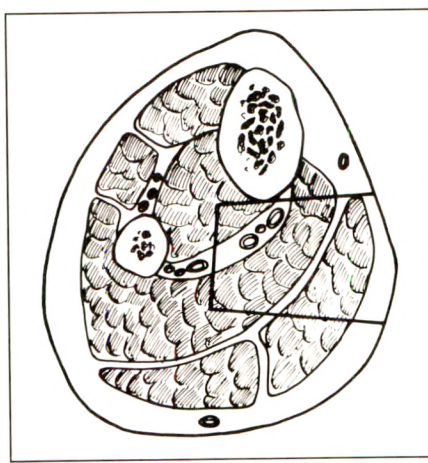
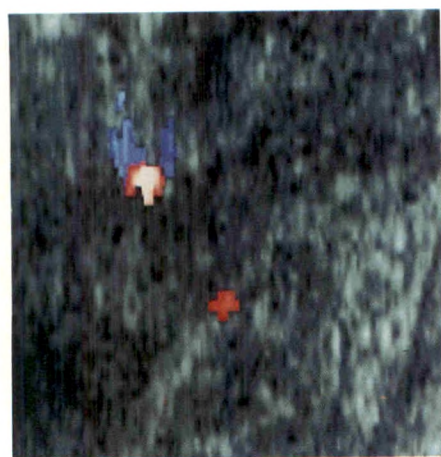
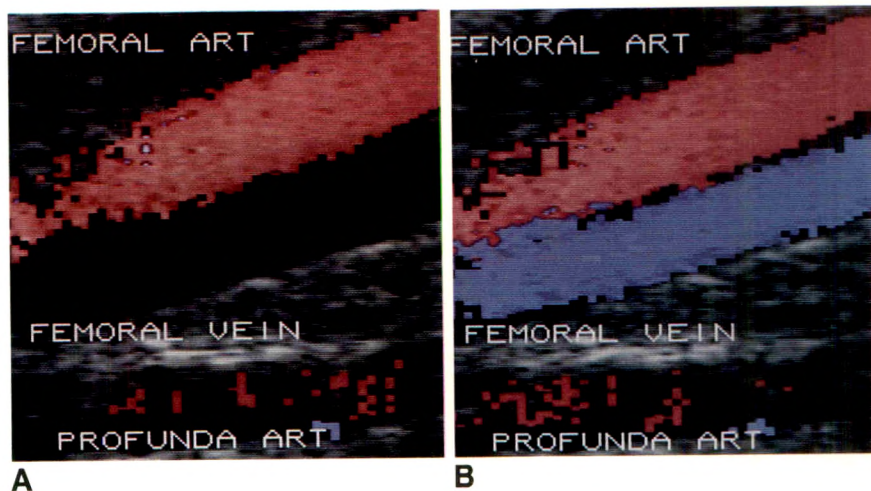


Fig. 2.—A, Transverse view of patent posterior tibial venae comitantes in proximal calf. Two normal venae comitantes are seen adjacent to posterior tibial artery.

B, Accompanying anatomic cross-sectional line drawing illustrates location and depth of field of color Doppler image obtained with 7.5-MHz probe. Top of image is anterior; bottom is posterior.

C, Segmental longitudinal view of posterior tibial vein in proximal calf. Although normal venous flow patterns are appreciated in patent tibioperoneal veins, spatial resolution of ultrasound images does not appear sufficient to exclude minor degrees of recanalized thrombus.

Fig. 3.—Segmental longitudinal view of mid thigh shows partly occluding thrombus with eccentric flow channels (arrows) in mid superficial femoral vein.

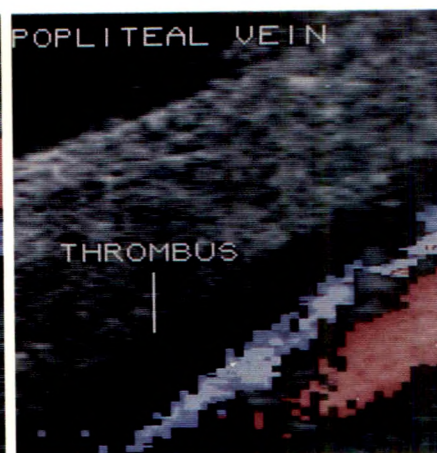
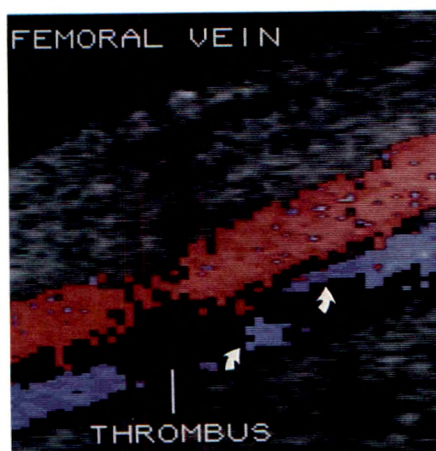


Fig. 4.—Eccentric mural thrombus in popliteal vein. Thrombus is predominantly on posterior wall of popliteal vein. Color Doppler study does not distinguish between acute, partially occluding thrombus and old recanalized thrombus.

an intraluminal echogenic filling defect, which in most acute deep vein thromboses expanded the venous lumen. Thrombi were recognized in both the transverse and longitudinal planes when evaluating the femoropopliteal venous system. Hypoechoic clot could be distinguished from intraluminal echoes due to rouleaux formation by the presence or absence of the color-flow signal. Extension of superficial femoral vein or saphenous vein thrombus to the common femoral vein could be documented easily. In contradistinction to an acute hypoechoic thrombus, chronic thrombus was relatively echogenic and did not expand the venous lumen. Patients with recanalized thrombus had torturous eccentric flow channels filled with color-flow signal (Fig. 3). With the slow-flow-sensitivity software upgrade, more flow signal from the eccentric channels could be appreciated than when the normal-sensitivity mode was used. Nonocclusive mural thrombus had a single eccentric flow lumen (Fig. 4). Periarterial and intramuscular collateral veins could be recognized owing to spontaneous color flow within their lumen. Collateral veins could be seen entering the femoral vein above a segmentally occluding thrombus.

Color Doppler Imaging and Venography

Of the 47 patients who had color Doppler and conventional venography, 10 had femoral popliteal venous thrombosis, two had isolated femoral vein thrombosis, and seven had isolated

the color Doppler study showed recanalized thrombus, although the conventional contrast venogram failed to fill the femoral venous segment (Fig. 5). In these patients, the contrast material injected into a superficial foot vein flowed preferentially via superficial saphenous collaterals to the proximal saphenofemoral junction. The color Doppler studies were performed with augmentation produced by distal calf compression. The conventional venograms were obtained in the standard manner with the patient in a semiupright position and the use of ankle tourniquets.

In the separate subset of 16 patients in whom imaging of the tibioperoneal veins could be compared, there was agreement between both techniques in the 12 negative and four positive cases (Fig. 6). Isolated calf vein thrombosis occurred in none of the positive cases.

Discussion

Contrast venography is the accepted gold standard in the diagnosis of lower-extremity deep vein thrombosis. However, the technique is invasive, is painful for the patient, and carries the possibility of chemically induced phlebitis and resultant phlebothrombosis in 1–2% of examinations [5, 6]. For these reasons, clinicians have evaluated various indirect noninvasive tests, including continuous-wave Doppler sonography, impedance plethysmography, and ^{125}I -fibrinogen scanning as

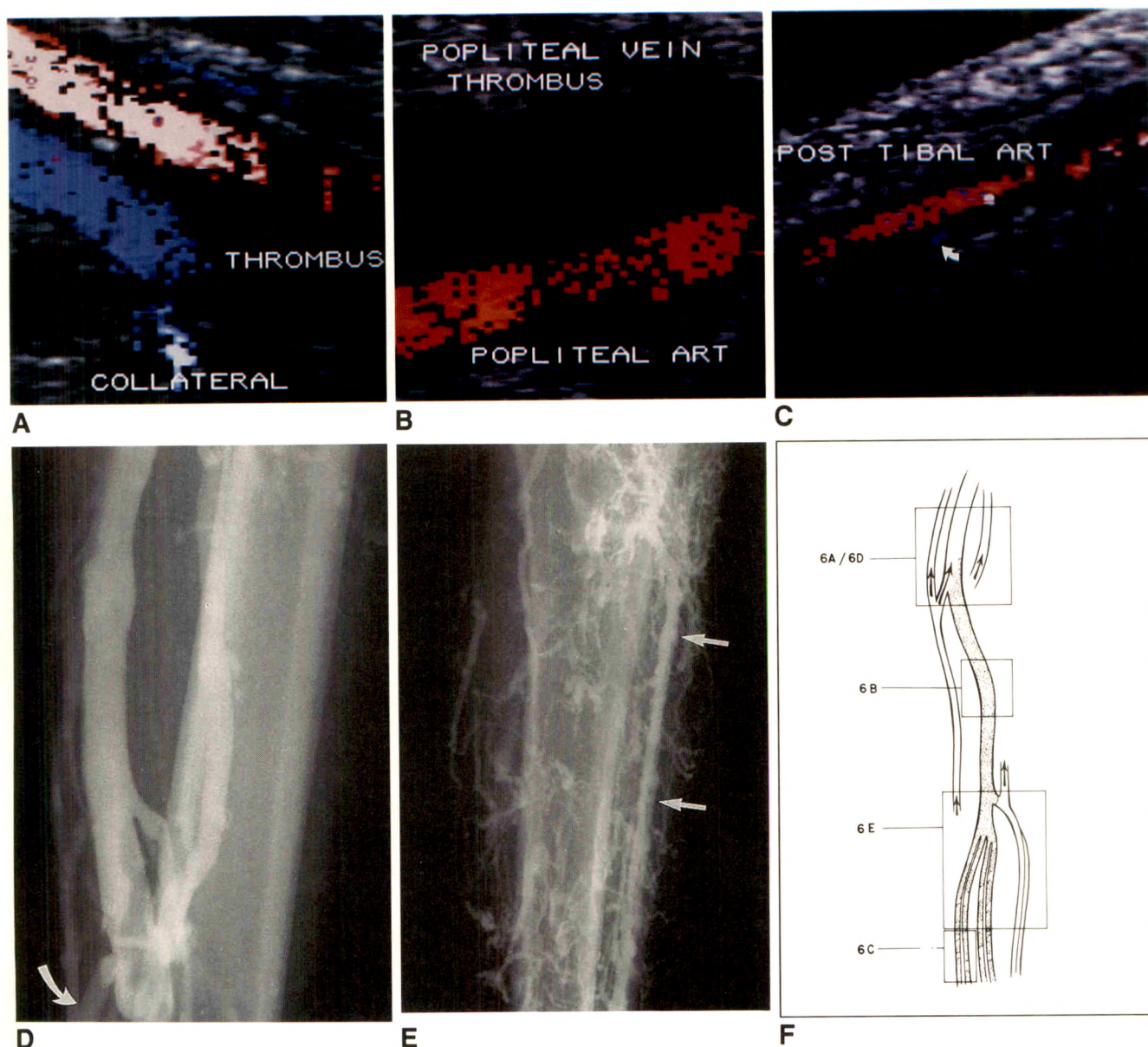


Fig. 6.—Popliteal, posterior tibial, and peroneal venous thrombosis.

A, Longitudinal color Doppler image at level of adductor region in left distal thigh shows patent superficial femoral vein filled by venous collateral. There is echo-free thrombus in distal femoral vein.

B, Longitudinal color Doppler study shows expanding echo-free thrombus in the popliteal vein.

C, Segmental longitudinal view of posterior tibial artery in distal calf. Minimal venous color flow signal is seen adjacent to posterior tibial artery (arrow). Venous flow signal in posterior tibial vein was not appreciated in mid or proximal calf.

D, Contrast venogram shows upper extent of popliteal vein thrombus in distal thigh. Note collateral inflow (arrow) corresponding to venous collaterals seen on color Doppler study (A).

E, Contrast venogram shows almost completely occlusive thrombi in posterior tibial and peroneal veins and patent anterior tibial vein (arrows). Patent anterior tibial vein was also seen on color Doppler study. Popliteal vein was completely occluded.

F, Schematic diagram shows locations of color Doppler images in distal thigh (A), knee (B), and distal calf (C) and venogram at distal thigh (D) and proximal calf (E).

therapy on the basis of these noninvasive test results [7, 8]. However, other investigators, whose results with plethysmography are less impressive (sensitivity, 60–70%), advise the use of a contrast venogram in patients with a negative plethysmogram who are known to be at high risk for deep vein thrombosis [11, 12]. In addition, patients with a positive

plethysmogram who have a clinical condition that could result in a false-positive examination, such as cardiac failure or pelvic mass, should have a contrast venogram [11, 12].

¹²⁵I-fibrinogen scanning is of major value in detecting calf vein thrombi and is a useful complement to plethysmography, which has a low sensitivity in detecting calf vein thrombi.

However, the 72-hr delay in obtaining the test result and the low sensitivity to thrombus more than 7 days old make the test an unsuitable screening examination for most hospital inpatients.

Initial results with compression B-mode sonography are very encouraging [3, 4]. This technique uses direct visualization of the femoral popliteal venous lumen with compression to confirm venous patency. As such, it is a direct noninvasive study, as compared with plethysmography and continuous-wave Doppler sonography, which are indirect noninvasive studies. Plethysmography evaluates venous capacitance and emptying rate; continuous-wave Doppler sonography evaluates isolated spectral wave forms from the popliteal, medial saphenous, and common femoral veins and the venous flow response to augmentation and the Valsalva maneuver.

Color Doppler imaging combines the advantages of compression sonography with the ability to visualize spontaneous venous flow in color without the injection of contrast material. With the advent of the slow-flow-sensitivity software upgrade, spontaneous color-flow signal outlining the full cross-sectional area of the femoral popliteal vein during maximum flow can be appreciated in normal patients. Augmentation to enhance the Doppler signal is unnecessary; thus, the examination is simplified considerably. In these patients, compression to document the absence of intraluminal thrombosis appears unnecessary. The permanent record of this anatomic and physiologic test is maintained on videotape and can be replayed for analysis. The major advantage of color Doppler venous imaging would appear to be demonstration of recanalized venous segments that cannot be shown by compression B-mode sonography. With recanalized thrombi, the venous lumen contains an admixture of echogenic clot (noncompressible) and anechoic spaces, which could represent either additional soft clot or recanalized lumen. The recanalized luminal segments can be shown without augmentation by using the slow-flow-sensitivity software upgrade. These recanalized segments may not be seen on conventional venography when the major portion of the peripherally injected contrast material is diverted into superficial collateral veins.

False-negative results occurred in two of 17 patients with popliteal vein thrombosis evaluated by color Doppler imaging and contrast venography. Complete reliance cannot be placed on a negative test in the presence of clinical findings suggestive of venous thrombosis.

Early experience in imaging the tibioperoneal veins suggests that the color Doppler technique has the potential to produce a total lower-extremity venous imaging study noninvasively. Both continuous-wave Doppler sonography and plethysmography have reported sensitivities of 20% or less in the evaluation of calf vein thrombosis [7, 8, 12]. ¹²⁵I-fibrinogen scanning, although it has a reported sensitivity of 60% in the diagnosis of calf vein thrombosis [8], may not provide a definite answer for 72 hr after injection; is probably insensitive to clot more than 7 days old; and may give false-positive results for femoropopliteal venous thrombosis in the acute postoperative period, particularly in patients who have had hip or leg surgery. Spontaneous phasic flow in the venae

comitantes of the tibioperoneal veins can be shown by the slow-flow-sensitivity mode of the color-flow instrument. However, preliminary results suggest that augmentation, preferably by a mechanical sleeve compressor at ankle level, will be necessary for most patients. Further evaluation of the accuracy and reproducibility of color Doppler imaging and MR imaging with the fast-scan technique (partial-flip-angle gradient-recalled echo) [13] in the detection of both above-knee and below-knee venous thrombosis would be of interest. As a practical matter, color Doppler imaging has a significant advantage over MR imaging in that it is a portable technique that can be performed in the intensive care unit.

The clinical value of a total-extremity (thigh and calf), noninvasive but direct imaging test of the deep venous system is difficult to assess at this time. Some authorities suggest that pulmonary embolism, as a consequence of undiagnosed and untreated deep venous thrombosis confined to the calf, is extremely rare. These authorities suggest that serial noninvasive studies (plethysmography and continuous-wave Doppler sonography) are effective means of detecting progression of previously undiagnosed calf vein thrombosis to femoral popliteal thrombosis before there is a significant risk of pulmonary embolism [8]. Whether provision of an accurate and repeatable noninvasive test for the diagnosis of both femoral popliteal and calf deep vein thrombosis would alter this mode of practice is uncertain.

REFERENCES

1. Middleton WD, Foley WD, Lawson TL. Flow reversal in the normal carotid bifurcation: color-Doppler flow imaging analysis. *Radiology* 1988;167:207-210
2. Mitchell DG, Needleman L, Bessi M, et al. Femoral artery pseudoaneurysm: diagnosis with conventional duplex and color-Doppler US. *Radiology* 1987;165:687-690
3. Cronan JJ, Dorfman GS, Scola FH, Schepps V, Alexander J. Deep venous thrombosis: US assessment using vein compression. *Radiology* 1987;162:191-194
4. Vogel P, Laing FC, Jeffrey RB, Wing VW. Deep venous thrombosis of the lower extremity: US evaluation. *Radiology* 1987;163:747-751
5. Bettman MA, Paulin S. Leg phlebography: the incidence, nature, and modification of undesirable side effects. *Radiology* 1977;122:101-104
6. Bettman MA, Salzman EW, Rosenthal D, et al. Reduction of venous thrombosis complicating phlebography. *AJR* 1980;134:1169-1172
7. Hull R, Hirsh J, Sackett DL, et al. Combined use of leg scanning and impedance plethysmography in suspected venous thrombosis: an alternative to venography. *N Engl J Med* 1977;296:1497-1500
8. Hull R, Hirsh J, Sackett DL. Replacement of venography in suspected venous thrombosis by impedance plethysmography and ¹²⁵I-fibrinogen leg scanning: a less invasive approach. *Ann Intern Med* 1981;94:12-15
9. Moser KM, Brach BB, Dolan GF. Clinically suspected deep venous thrombosis of the lower extremities: a comparison of venography, impedance plethysmography, and radiolabeled fibrinogen. *JAMA* 1977;237:2195-2198
10. Sumner DS, Lambeth A. Reliability of Doppler US in the diagnosis of acute venous thrombosis both above and below the knee. *AJR* 1979;138:205-210
11. Ramchandani P, Soulen R, Fedullo L, Gaines V. Deep vein thrombosis: significant limitations of noninvasive tests. *Radiology* 1985;156:47-49
12. Holden RW, Klatte EC, Park HM, et al. Efficacy of noninvasive modalities for the diagnosis of thrombophlebitis. *Radiology* 1981;141:63-66
13. Spritzer CE, Sussman SK, Bunder RA, Saeed M, Herfkens RJ. Deep venous thrombosis evaluation with limited flip-angle, gradient refocused MR imaging: preliminary experience. *Radiology* 1988;166(2):371-375

Budd-Chiari Syndrome: The Results of Duplex and Color Doppler Imaging

Edward G. Grant¹
 Rita Perrella¹
 Franklin N. Tessler¹
 Juan Lois¹
 Ronald Busutt²

This study was designed to evaluate duplex and color-flow Doppler imaging as potential noninvasive methods of diagnosing patients with Budd-Chiari syndrome and following them after surgery. Five patients with confirmed hepatic venoocclusive disease were imaged. All five underwent duplex Doppler examinations; three were also evaluated with color-flow Doppler. The hepatic vasculature was examined in all five patients; decompressive mesoatrial shunts were present and were evaluated in four of the five patients. Color-flow Doppler precisely defined intrahepatic, portal, and inferior vena caval circulatory dynamics. Correlation with angiography was excellent. In the two patients in whom hepatic vasculature was evaluated with duplex Doppler alone, the results were less impressive. Intrahepatic flow abnormalities were identified, but the sites of occlusion were not determined convincingly. Signals transmitted from the heart and the inability to visualize the hepatic veins made duplex Doppler evaluation problematic. Duplex Doppler was able to define patency and the direction of flow in the portal vein and inferior vena cava.

Our results suggest that color-flow Doppler is an excellent technique for the initial evaluation of patients suspected of having Budd-Chiari syndrome. In the evaluation of decompressive mesoatrial shunts, color-flow Doppler produced dramatic images. However, both duplex and color-flow Doppler were highly accurate in determining the patency of decompressive shunts. Either duplex or color-flow Doppler may be used as the primary imaging procedure to determine shunt patency.

Thrombosis of the hepatic veins was originally described by Budd in the mid-nineteenth century [1]. More than 50 years later, Chiari [2] recognized the classic triad of hepatomegaly, ascites, and abdominal pain as the clinical manifestation of hepatic venoocclusive disease. The actual site of the occlusion varies in what has come to be known as Budd-Chiari syndrome; the occlusion may be located at any level from the hepatic venules to the inferior vena cava. Although Budd-Chiari syndrome may be associated with polycythemia rubra vera, various neoplasms, pregnancy, use of oral contraceptives, leukemia, and trauma, the exact cause is never determined in approximately two-thirds of the cases [3, 4]. In a few patients, particularly those of Asian origin, a congenital web may obstruct the inferior vena cava or hepatic veins [5].

The necessity for an initial, often extensive radiologic evaluation is not surprising given the broad spectrum of anatomic abnormalities associated with Budd-Chiari syndrome [6]. After the diagnosis is established, most patients with Budd-Chiari syndrome require a decompressive shunt. Shunts in Budd-Chiari syndrome are constructed to divert blood away from a congested liver via the portal vein [7, 8]. The frequency of complications in these often complex decompressive shunts is relatively high [8] and adds further to the overall number of radiographic procedures performed.

Since the 1950s, angiography has been the mainstay of diagnosis in patients with Budd-Chiari syndrome, both before and after surgery [9-11]. Angiography, in fact, remains the definitive technique. Unfortunately, angiography is invasive and

Received August 5, 1988; accepted after revision September 7, 1988.

¹ Department of Radiological Sciences, UCLA School of Medicine, 10833 LeConte Ave., Los Angeles, CA 90024. Address reprint requests to E. G. Grant.

² Department of Surgery, UCLA School of Medicine, 10833 LeConte Ave., Los Angeles, CA 90024.

AJR 152:377-381, February 1989

0361-803X/89/1522-0377

© American Roentgen Ray Society

frequently the hepatic veins cannot be opacified beyond their ostia [12]. Numerous less-invasive techniques, including nuclear medicine [13], sonography [14–17], CT [15, 17], and most recently MR imaging, [18] have had various degrees of success in characterizing the underlying vascular lesions in Budd-Chiari syndrome and evaluating the patency of decompressive shunts [18, 19].

These radiographic techniques may all contribute important information about patients with Budd-Chiari syndrome. However, a portable, noninvasive examination would be desirable both before and after surgery. Doppler imaging is, therefore, an appealing technique in patients with Budd-Chiari syndrome. Duplex Doppler has been used with considerable success in the evaluation of the hepatic vasculature and various portosystemic shunts [20–23]. Color-flow Doppler, only recently available for use in the abdomen, would also seem to have considerable potential. We undertook this study to assess the possible roles of duplex and color-flow Doppler in the diagnosis of Budd-Chiari syndrome and in the evaluation of decompressive shunts in the same patients.

Subjects

During the past year, five patients with Budd-Chiari syndrome were referred to our institution. All patients were female, ranging in age from 8 to 64 years (average age, 32 years). In two of the five patients, the exact cause of hepatic venoocclusive disease was never established. In one, polycythemia rubra vera was present; in another, an autoimmune process with elements of lupus was diagnosed. In the fifth patient, a congenital web occluded the hepatic veins. Four of the five patients required decompressive (mesoatrial or cavoatrial) shunts because significant pressure gradients existed between the inferior vena cava and the right atrium. The child with the congenital web was treated successfully with percutaneous angioplasty. Among the patients with shunts, sonograms were all performed after the initial surgery. The child who had angioplasty was scanned both before and after the procedure. Clinical follow-up showed that one patient died in the immediate postoperative period; two are well with patent decompressive shunts. The fourth patient who had surgery is being treated conservatively and is relatively well compensated in spite of

a thrombosed mesoatrial shunt. The patient with the congenital web is doing well 10 months after angioplasty.

All five patients underwent abdominal sonography (Ultramark 4, Ultramark 8, and Ultramark 9, Advanced Technology Laboratories, Bothell, WA); 2.25-, 3.0-, or 5.0-MHz transducers were used. Duplex Doppler examinations were performed with a mechanical sector scanner, whereas color Doppler imaging used phased-array technology. Both duplex and color-flow Doppler examinations included spectral analysis. Duplex Doppler was used a total of nine times to assess the hepatic vasculature and/or the status of decompressive shunts. At least one duplex Doppler examination was performed in all five of our patients. In three patients, color-flow Doppler imaging was used, and in all three cases, both the hepatic vasculature and the mesoatrial shunts were evaluated. In all cases, sonographic examinations were performed without knowledge of previous imaging/angiographic findings. Sonographic scans were later compared with other techniques including angiography (eight examinations in four patients), CT (two examinations in two patients), and MR imaging (four examinations in three patients). Descriptions of the pertinent imaging procedures are given in the legends to Figures 1–5.

The overall appearance of the architecture of the liver was evident in all patients on the real-time sonograms. The real-time sonographic findings in Budd-Chiari syndrome, however, have been described elsewhere [14–17] and will not be discussed here.

Results

Hepatic Vasculature

In all cases, color-flow imaging correctly determined the status of the hepatic veins and the direction of flow, if present. Areas of occlusion were clearly evident. Likewise, patency and direction of flow in both the portal vein and the inferior vena cava were readily apparent. Vascular junctions/anastomoses were clearly shown, as were intrahepatic collaterals. Two patients were evaluated with duplex Doppler only. Reversed flow was detected in the hepatic veins of one (the child with the congenital web), but the site of obstruction was not definitely determined. In the other patient, an emergency bedside scan was performed with emphasis on the status of her recently placed mesoatrial shunt. Hepatic veins, however,

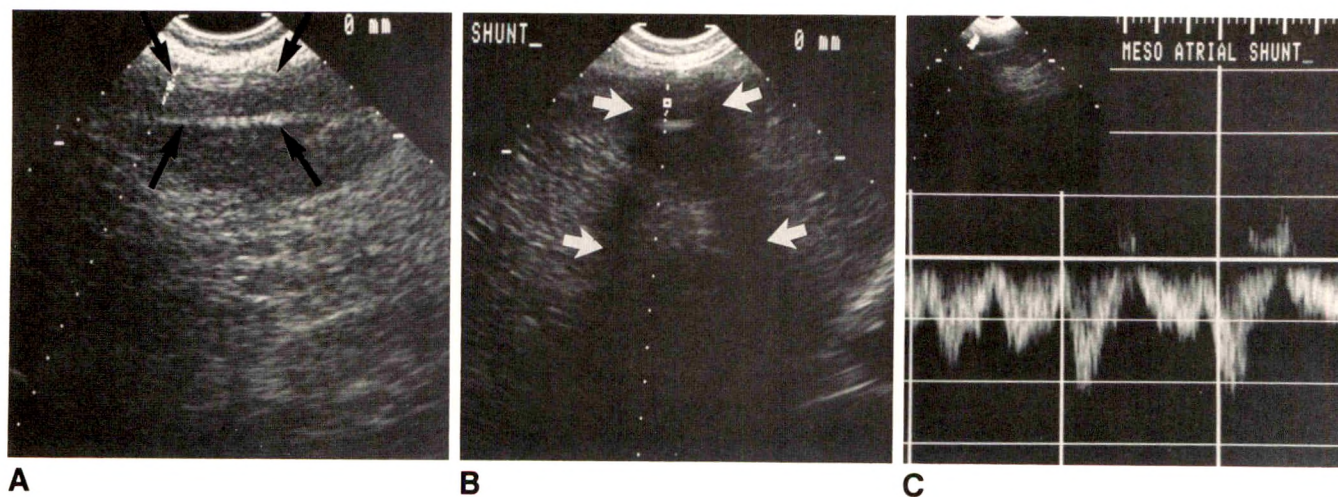


Fig. 1.—A, Longitudinal sonogram of right subcostal area shows superficial location of mesoatrial shunt (arrows).
B, Transverse sonogram of right subcostal area shows "lateral shading" (arrows); ultrasound beam is deflected by edge of graft.
C, Doppler signal from mesoatrial shunt confirms patency and verifies that flow is in a cephalad direction; flow pattern is strongly influenced by right atrium.

Fig. 2.—Color Doppler imaging in patient with patent mesoatrial shunt.

A, Flow in shunt is dramatically shown by presence of color. Color changes from red to blue as flow vector changes from approaching to receding in relationship to Doppler beam.

B, Portal vein (arrow) is patent, but flow is reversed and appropriately directed toward mesoatrial shunt. Blue color indicates flow away from transducer. As with all Doppler technology, color flow is extremely angle-sensitive.

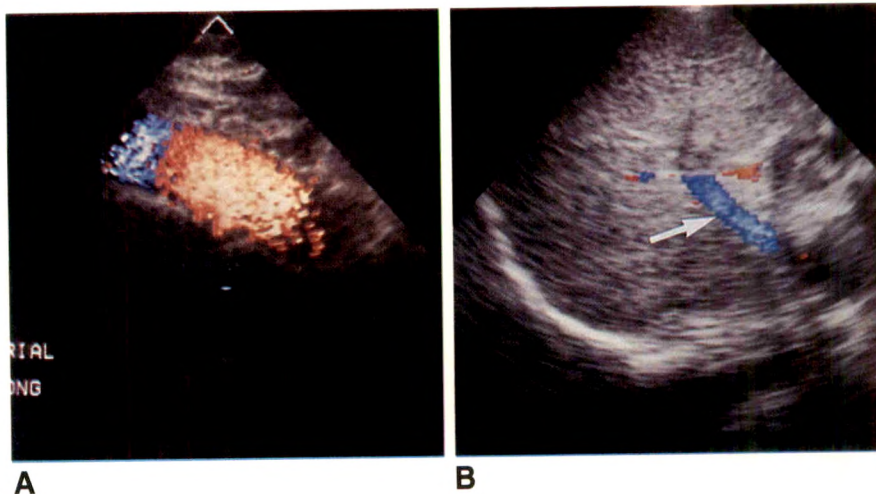


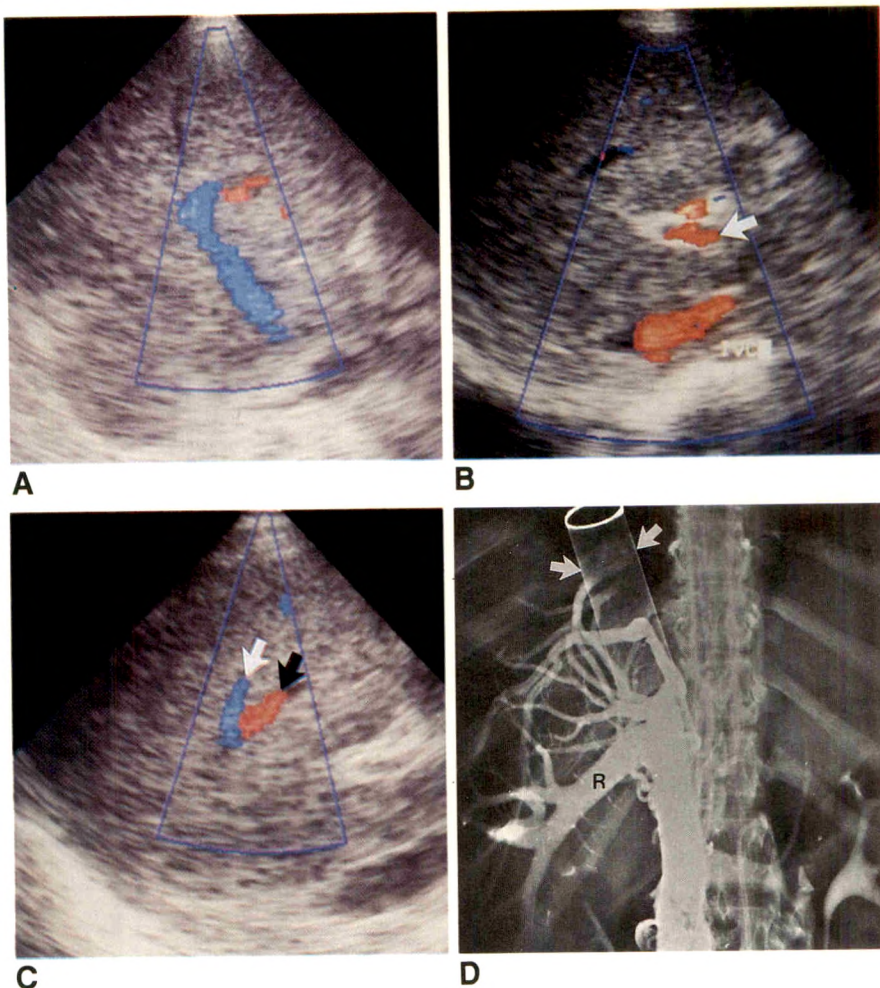
Fig. 3.—Complete thrombosis of mesoatrial shunt was shown by color-Doppler examination and confirmed by MR imaging (not shown).

A, Transverse color Doppler image through right upper quadrant reveals large, patent right hepatic vein. Blue color indicates that flow is directed normally (away from transducer, toward inferior vena cava). Right hepatic vein was easily followed into inferior vena cava by real-time scanning.

B, Longitudinal color Doppler image shows reversed flow in inferior vena cava but shows normally directed flow in portal vein (arrow). Nature of sector format makes evaluation of directional flow dynamics somewhat more complicated than it might appear initially. Flow in inferior vena cava is directed caudally but is angled toward transducer/Doppler beam at the point in question. Portal flow, however, is directed cephalad but is also angled toward transducer/Doppler beam. This section shows both vessels nicely in one plane. Realistically, however, confirmation of directionality must be made for each individual vessel and may require scanning from multiple vantage points to ensure that the assigned color truly reflects the direction of flow.

C, Longitudinal section from periphery of right lobe of liver shows hepatic vein flow dynamics typical of patients who do not have adequate decompression by mesoatrial shunt. Flow in one hepatic vein branch is directed normally (white arrow), whereas its counterpart is reversed (black arrow) and carries blood toward collaterals on surface of liver. Other intrahepatic flow abnormalities identified included a large left-to-right intrahepatic collateral and small superficial hepatic veins in left lobe of liver that were reversed in direction.

D, Inferior venocavogram confirms occlusion of inferior vena cava and presence of a large patent right hepatic vein (R). Injection of portal system (not shown) confirmed thrombosis of mesoatrial shunt (arrows).



could not be identified with either real-time or Doppler sonography.

Decompressive Shunts

Color-flow Doppler, with either 5.0- or 3.0-MHz transducer, showed the patency of the shunts dramatically. The anastoma-

mosis with the native vessel was visualized clearly in both patients who had patent grafts. Likewise, duplex scanning with a 5.0-MHz transducer clearly showed appropriately directed flow in all cases. Spectral analysis (from both color-flow and duplex Doppler) showed a triphasic pattern in all of the shunts; this undoubtedly was a reflection of right atrial

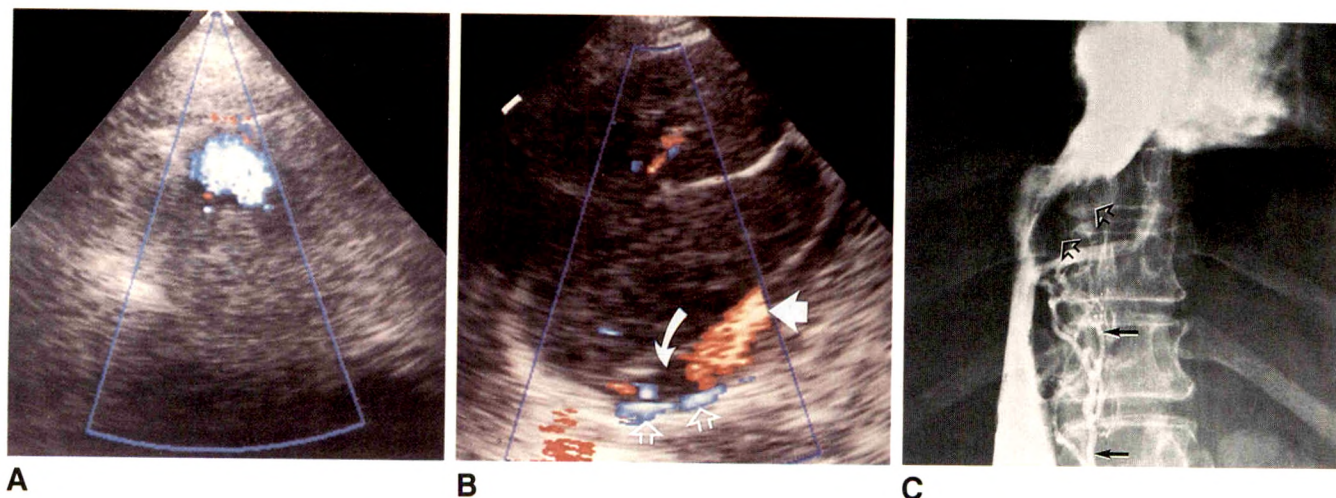


Fig. 4.—A, Transverse color Doppler image in right subcostal area shows a patent mesoatrial shunt.
 B, Longitudinal color Doppler image of inferior vena cava reveals reversed flow (straight arrow) inferior to a large defect (curved arrow) in color column at area of confluence of hepatic veins. Minimal flow (open arrows) was observed to pass by this partial obstruction.
 C, Venacavogram obtained before surgery confirms presence of filling defect in inferior vena cava (open arrows); closed arrows indicate collaterals.

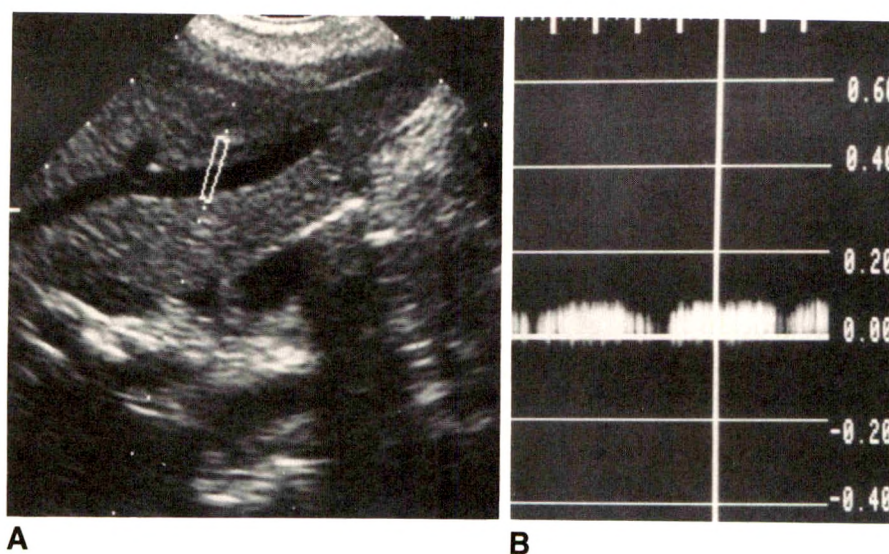


Fig. 5.—Longitudinal duplex scan through inferior portion of right lobe of liver in patient with hepatic vein web. Scan was performed before angioplasty.

A, Branch of right hepatic vein becomes larger as it approaches surface of liver.

B, Spectral analysis confirms reversed flow in right hepatic vein branch. Intrahepatic vascular dynamics are similar to those shown in Fig. 3, in which the patient had a thrombosed mesoatrial shunt.

contractility. In both of two duplex scans performed early in the study with 3.0-MHz transducers, the mesoatrial shunts were not seen.

Discussion

The nature of Budd-Chiari syndrome and the frequent need for postoperative shunt evaluation make accurate radiologic assessment an essential part of the diagnosis and treatment of this disease. Although biopsy and venography are essential, an accurate, noninvasive technique would be welcome. Almost every available imaging technique has been used to establish the diagnosis of Budd-Chiari syndrome. Conventional sonography and CT may be suggestive of hepatic venoocclusive disease, but each has inherent drawbacks and neither is pathognomonic [24]. Although scintigraphy may

produce a classical appearance of increased uptake or enlargement of the caudate lobe, the recent series of Powell-Jackson et al. [25] identified this sign in only 17% of their patients. MR imaging has been advocated recently as the most advantageous method of evaluating the hepatic vasculature and imaging postoperative shunt complications [24].

Little attention has been given to the possibility of using Doppler either before or after surgery in Budd-Chiari syndrome. This apparent lack of attention may be due in part to the rarity of the disease. More likely, however, the lack of success in diagnosing Budd-Chiari syndrome with duplex Doppler rests on the difficulty of definitively identifying the hepatic veins in a swollen liver. The hepatic veins in the normal liver are seen easily, and the presence of the characteristic triphasic Doppler signal confirms their patency [26]. Many causes of hepatomegaly, however, result in sufficient compression of the hepatic veins to render them nonvisible

to real-time sonography, although they are patent. At the opposite end of the spectrum, the hepatic veins in patients with cirrhosis are almost never visible with real-time sonography and therefore are equally difficult to localize with duplex Doppler. Cardiac pulsations are also prominently transmitted into the left lobe of the liver and further complicate the duplex-Doppler diagnosis of middle and left hepatic vein occlusion.

The ability of duplex Doppler to adequately evaluate the hepatic vasculature in Budd-Chiari syndrome seems limited. Color Doppler imaging, however, offers considerably more diagnostic information. Color-flow imaging gives a real-time overview of all vascular events within the plane of section. The hepatic veins need not be seen by real-time sonography. In this regard, the middle and left hepatic veins are situated almost parallel to the Doppler beam when scanning is done in the transverse plane at the level of the xyphoid. This angle allows optimum reception of their Doppler signals. Conversely, the right hepatic vein is imaged best from a lateral intercostal approach, again optimizing the Doppler angle. Color Doppler imaging compared very favorably with angiography in the evaluation of the hepatic vasculature. Our preliminary experience suggests that color Doppler imaging has the potential to become the initial screening technique in patients suspected of having Budd-Chiari syndrome.

The duplex Doppler evaluation of the hepatic vasculature in Budd-Chiari syndrome is admittedly problematic. The lack of emphasis on duplex Doppler in the postoperative patient, however, is curious. To the best of our knowledge, only Chezmar and Bernardino [19] have actually described its use. In their series of nine patients with Budd-Chiari syndrome, two underwent duplex Doppler evaluation to establish patency of their mesoatrial shunts. In the three studies performed, shunt patency was implied if portal vein flow was reversed. The study concluded that although "Doppler sonography would be the ideal primary screening modality because of its low cost, availability and portability . . . the shunt itself is usually difficult to evaluate directly because the graft impedes sound transmission" [19].

Color-flow Doppler yielded dramatic images of mesoatrial shunts in our patients. Duplex Doppler, however, was also 100% successful in determining shunt patency, the main clinical question to be answered. An explanation for our success in imaging mesoatrial shunts may come from two early scans in which the shunt was not seen. Both of these scans were performed with a 3.0-MHz transducer. The optimum focal zone of such transducers is relatively deep (6–10 cm), and mesoatrial grafts lie directly beneath the anterior abdominal wall at the subcostal level. The synthetic material in the graft also causes considerable attenuation of the sound beam. Generalized attenuation coupled with the marked "lateral shading" [27] that originates from the sides of the graft when sectioned in the transverse plane (Fig. 1) certainly add to the difficulty of imaging mesoatrial shunts. Knowledge of the graft's location, however, should enable the operator to obtain an adequate assessment of patency by using a transducer with an optimum focal zone in the near field.

In our series, both duplex (with a 5.0-MHz transducer) and color-flow Doppler were 100% successful in evaluating the patency of decompressive shunts. Because of the advantages of sonography, duplex or color-flow Doppler sonography should be the primary screening technique to establish patency of mesoatrial shunts in patients after surgery.

ACKNOWLEDGMENT

The authors thank Ellen Knight for her assistance in preparing the manuscript.

REFERENCES

- Budd G. *On diseases of the liver*. London: John Churchill, 1845:146
- Chiari H. Veber die selbständige Phlebitis Obliterans der Hauptstämme der Vanae Hepaticae als Todesursache. *Beitr Pathol Anat* 1899;26:1–17
- Millikan WJ, Henderson JM, Sewell CW, et al. Approach to the spectrum of Budd-Chiari syndrome: which patients require portal decompression? *Am J Surg* 1985;149:167–176
- Clain D, Freston J, Kreel L, Sherlock S. Clinical diagnosis of the Budd-Chiari syndrome. *Am J Med* 1967;43:544–554
- Hirooka M. Embryonic abnormality as the pathogenesis of membranous obliteration of the inferior vena cava in the hepatic portion. *Acta Hepat Jpn* 1969;10:566–577
- Parker RG. Occlusion of the hepatic veins in man. *Medicine* 1959;38:369–397
- Longer B, Stone RM, Colapinto RF, Meinkop M, Phillips MJ, Fisher MM. Clinical spectrum of the Budd-Chiari syndrome and its surgical management. *Am J Surg* 1975;129:137–145
- Cameron JL, Kadir S, Pierce WS. Mesoatrial shunt: a prosthesis modification. *Surgery* 1984;96:114–116
- Brink AJ, Botha D. Budd-Chiari syndrome: diagnosis by hepatic venography. *Br J Radiol* 1955;28:330–331
- Levander M, Ponten J. Budd-Chiari's syndrome diagnosed by means of phlebography in case of retroperitoneal sarcoma. *Acta Med Scand* 1959;163:251–255
- Redmond PL, Karir S, Kaufman SL, White RI, Cameron JL. Mesoatrial shunts for Budd-Chiari syndrome and inferior vena cava thrombosis: angiographic and hemodynamic evaluations. *Radiology* 1987;163:131–134
- Deutsch V, Rosenthal T, Adar R, Mozes M. Budd-Chiari syndrome: study of angiographic findings and remarks on etiology. *Radiology* 1972;116:430–439
- Tavil AS, Wood EJ, Kreel L, Jones EA, Gregory M, Sherlock S. The Budd-Chiari syndrome: correlation between hepatic scintigraphy and the clinical, radiological and pathological findings in nineteen cases of hepatic venous outflow obstruction. *Gastroenterology* 1975;68:509–518
- Menu Y, Alison D, Lorphelin JM, Valla D, Belghiti J, Nahum H. Budd-Chiari syndrome: US evaluation. *Radiology* 1985;157:761–764
- Harter LP, Gross BH, St. Hilaire J, Filly RA, Goldberg HI. CT and sonographic appearance of hepatic vein obstruction. *AJR* 1982;139:176–178
- Makuuchi M, Hasegawa H, Yamazaki S, Moriyama N, Takayasu K, Okazaki M. Primary Budd-Chiari syndrome: ultrasonic demonstration. *Radiology* 1984;152:775–779
- Becker CD, Scheidegger J, Marincek B. Hepatic vein occlusion: morphologic features on computed tomography and ultrasonography. *Gastrointest Radiol* 1986;11:305–311
- Stark DD, Hahn PF, Trey C, Clouse ME, Ferrucci JT. MRI of the Budd-Chiari syndrome. *AJR* 1986;146:1141–1148
- Chezmar JL, Bernardino ME. Mesoatrial shunt for the treatment of Budd-Chiari syndrome: radiologic evaluation in eight patients. *AJR* 1987;149:707–710
- Patriquin H, Lafortune M, Burns PN, Dauzat M. Duplex Doppler examination in portal hypertension: technique and anatomy. *AJR* 1987;149:71–76
- Alpern MB, Rubin JM, Williams DM, Capek P. Porta hepatis: duplex Doppler US with angiographic correlation. *Radiology* 1987;162:53–56
- Nelson RC, Lovett KE, Chezmar JL, et al. Comparison of pulsed Doppler sonography and angiography in patients with portal hypertension. *AJR* 1987;149:77–81
- Dalen K, Day DL, Ascher NL, et al. Imaging of vascular complications after hepatic transplantation. *AJR* 1988;150:1285–1290
- Murphy FB, Steinberg HV, Shires GT, Martin LG, Bernardino ME. The Budd-Chiari syndrome: a review. *AJR* 1986;147:9–15
- Powell-Jackson PR, Karani J, Ede RJ, Hylton M. Ultrasound scanning and ^{99m}Tc sulphur colloid scintigraphy in diagnosis of Budd-Chiari syndrome. *Gut* 1986;27:1502–1506
- Taylor KJW, Burns PN, Woodcock JP, et al. Blood flow in deep abdominal and pelvic vessels: ultrasonic pulsed-Doppler analysis. *Radiology* 1985;154:487
- Sommer FG, Filly RA, Minton MJ. Acoustic shadowing due to refractive and reflective effects. *AJR* 1979;132:973–977

Embolotherapy of a High-Flow False Aneurysm by Using an Occlusion Balloon, Thrombin, Steel Coils, and a Detachable Balloon

Gary K. Lammert,^{1,2} Dimitri Merine,¹ Robert I. White, Jr.,³ Elliot K. Fishman,¹ and James K. Porterfield⁴

Percutaneous techniques for the embolization of pseudoaneurysms have been well described. We encountered a mycotic renal artery pseudoaneurysm in a patient who was considered to be a poor surgical candidate. Successful embolization was accomplished by using an occlusion balloon, stainless steel coils, thrombin, and a detachable balloon.

Case Report

A 65-year-old man was treated for *Staphylococcus aureus* endocarditis 8 months before admission. Three months after completing a course of IV antibiotics he complained of pain in his chest and right flank. On physical examination, the right flank was tender on palpation. Laboratory data, including blood cultures and echocardiography, were unremarkable. Cardiac catheterization showed severe coronary artery disease for which the patient underwent emergent bypass surgery. A CT scan of the abdomen was subsequently performed and showed nonfunction of an atrophic right kidney and a large mass immediately adjacent to the origin of the right renal artery (Fig. 1A). An aortogram confirmed the presence of a mycotic renal artery pseudoaneurysm (Fig. 1B). No therapy was performed owing to the patient's tenuous cardiac status and postoperative complications, including sternal wound dehiscence. A repeat CT examination per-

formed 5 months later (not shown) showed that the pseudoaneurysm had enlarged slightly. Because rupture of the pseudoaneurysm was considered inevitable, the patient was admitted for definitive treatment. Because his cardiac function remained compromised, he was considered a poor surgical candidate and transcatheter embolotherapy was undertaken.

A 6.5-French Cobra catheter (Cook, Bloomington, IN) was used to engage the orifice of the pseudoaneurysm. Injection of contrast material showed rapid, turbulent flow in and out of the pseudoaneurysm via a short narrow neck. A 7-French, end-hole, wedge-pressure catheter (Critikon, Tampa, FL) with a 10-mm balloon was placed into the pseudoaneurysm. With the balloon inflated and drawn firmly against the internal orifice of the neck of the pseudoaneurysm, four 15-mm Gianturco coils (Cook, Bloomington, IN) were introduced into the body of the pseudoaneurysm; then 3500 U of thrombin (Thrombostat, Parke Davis, Morris Plains, NJ) (500 U/ml) were injected over 5 min (Fig. 1C). Repeat aortography showed incomplete thrombosis. Six more Gianturco coils were then introduced, followed by administration of an additional 3500 U of thrombin via the wedge-pressure catheter. Repeat aortography showed near-complete thrombosis. Finally, the residual neck of the pseudoaneurysm was sealed with a detachable 2-mm silicone balloon (Beckton-Dickinson, Lincoln Park, NJ) inflated with 0.6 ml of a 50-50 sterile water/iodipamide meglumine mixture. A final aortogram showed occlusion of the aneurysm (Fig. 1D). Nonheparinized saline flush was used throughout the case.

Received May 13, 1988; accepted after revision August 4, 1988.

¹ Russell H. Morgan Department of Radiology & Radiologic Sciences, The Johns Hopkins Medical Institutions, Baltimore, MD 21205-2191.

² Present address: Department of Radiology, The Cleveland Clinic Foundation, 9500 Cleveland Ave., Cleveland, OH 44195. Address reprint requests to G. K. Lammert.

³ Department of Diagnostic Imaging, Yale New Haven Hospital, 20 York St., New Haven CT 06510.

⁴ Department of Cardiology, The Johns Hopkins Medical Institutions, Baltimore, MD 21205-2191.

AJR 152:382-384, February 1989

0361-803X/89/1522-0382

© American Roentgen Ray Society

Fig. 1.—Right renal artery pseudoaneurysm before, during, and after successful thrombosis.

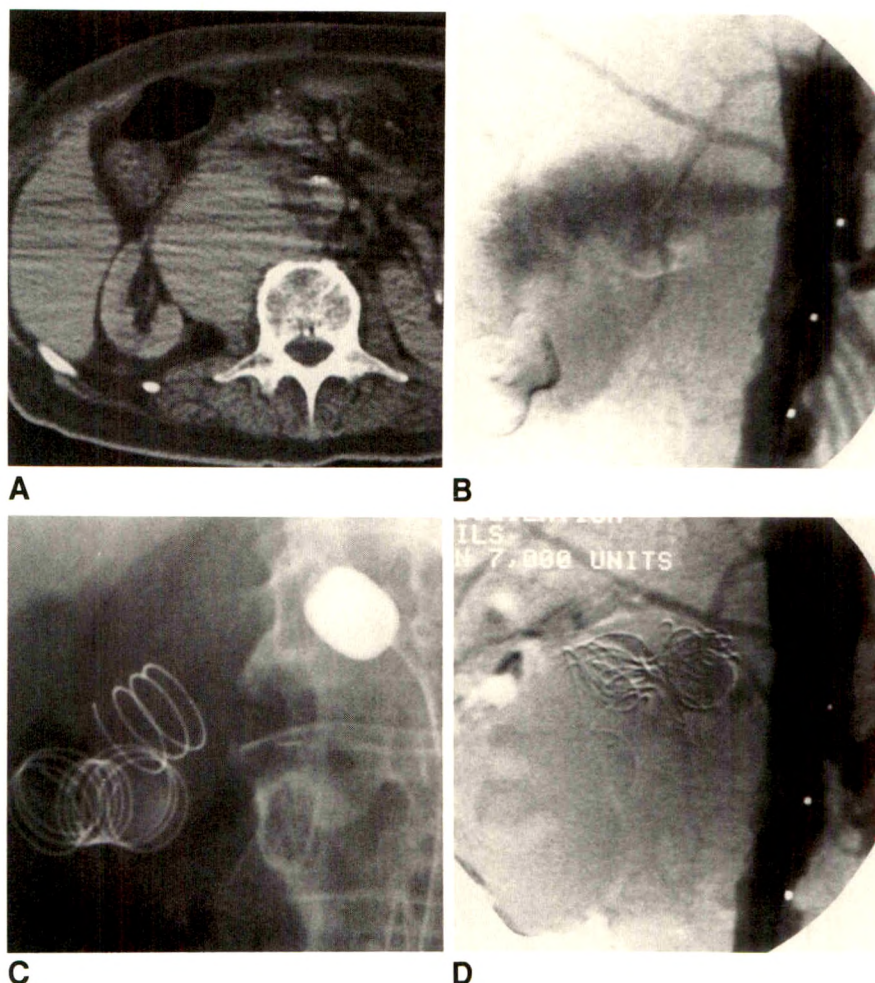
A, Nonenhanced CT scan obtained before embolization shows large pseudoaneurysm adjacent to right kidney measuring approximately 10 cm in diameter.

B, Intraarterial digital subtraction aortogram shows filling of right renal artery pseudoaneurysm via a narrow neck.

C, A 7-French end-hole wedge-pressure catheter in place for introduction of coils and thrombin. A total of 10 specially made 15 mm × 5 cm stainless steel coils were introduced along with 7000 units of thrombin.

D, Postembolization aortogram shows thrombosis of pseudoaneurysm.

A nonenhanced CT scan (not shown) performed 3 months after embolization showed reduction of thrombosed aneurysm to approximately 5 cm in diameter.



The patient had mild nausea and low-grade fever for 48 hr after the procedure; this was thought to be due to a postembolic syndrome. Subsequently the patient did well. A CT scan performed 3 months after embolization showed a marked decrease in the size of the thrombosed pseudoaneurysm.

Discussion

Despite adequate antibiotic therapy, mycotic aneurysms remain a life-threatening complication of bacterial endocarditis. A series of mycotic aneurysms reported by Kaufman et al. [1] showed an overall mortality of 67%. Mycotic aneurysms develop in about 25% of patients with bacterial endocarditis, with the aorta and coronary and pulmonary arteries being the most common sites of involvement [2]. Development of mycotic aneurysms of the renal arteries is uncommon. As of 1985, only 20 cases had been reported in the literature [3, 4]. Recognition and treatment of mycotic aneurysms are important for two reasons: (1) An aneurysmal sac may serve as a persistent source of infection even when blood cultures are sterile. (2) Expansion and fatal rupture may result if they are left untreated.

Traditionally, management of chronic mycotic aneurysms and posttraumatic pseudoaneurysms required surgical resection. Recently, percutaneous catheter techniques have been shown to be effective alternatives to surgery. These techniques have been especially helpful in patients considered to be poor surgical risks.

Recent case reports [5, 6] have described percutaneous treatment of pseudoaneurysms by occlusion of the vessel proximal and distal to the site of origin. This was not possible in our patient because of the location of the pseudoaneurysm. In one of these reports [5], an attempt to pack a pseudoaneurysm with coils failed. In that patient, coils alone were used to fill the pseudoaneurysm. The authors conclude that treatment must cause thrombosis at the site of vessel disruption in order to prevent leakage via new tissue planes and thus recurrence of pseudoaneurysm. Use of a detachable balloon to seal the neck of the pseudoaneurysm was probably helpful in preventing reformation of the aneurysm in our patient.

Cope and Zeit [7] have used direct percutaneous injection of thrombin into pseudoaneurysms that are not amenable to transcatheter methods. These authors point out that the success of thrombin injection depends on its concentration

and the degree of stasis within the aneurysm. Use of an occlusion balloon in this high-flow aneurysm permitted increased stasis, so thrombin could exert maximal clotting effect. The occlusion balloon also provided a margin of safety by preventing thrombus from embolizing to the systemic circulation. The thrombin concentration was kept as high as possible while still allowing an adequate injection volume to provide good mixing within the large aneurysm.

The introduction of a foreign body (stainless steel coils) into a potentially infected space should be considered an additional risk of this procedure. However, surgery was not considered a viable alternative, and the coils were thought to be vital in providing a matrix for the thrombin-induced clot in this large pseudoaneurysm.

In summary, percutaneous catheter techniques provide an alternative to surgery in the treatment of pseudoaneurysms. In this case, an occlusion balloon, thrombin, stainless steel coils, and a detachable balloon were effective in thrombosing

a large pseudoaneurysm in a patient who was thought to be unable to withstand the stress of major surgery.

REFERENCES

1. Kaufman SL, White RI, Harrington DP, Barth KH, Siegelman SS. Protean manifestations of mycotic aneurysms. *AJR* **1978**;131:1019-1025
2. Weinstein L. Life-threatening complications of infective endocarditis and their management. *Arch Intern Med* **1986**;146:953-957
3. Pezzuli FA, Purnell FM, Rotterdam HZ. Renal artery mycotic aneurysm. *NY State J Med* **1984**;5:260-261
4. Stavas IM, Reinke DB, Miller RP. Mycotic aneurysm of the renal artery: CT appearance. *Br J Radiol* **1985**;59:401-402
5. Glanz S, Gordon D, Scafani S. Percutaneous coil embolization in the management of peripheral mycotic aneurysms. *Cardiovasc Intervent Radiol* **1987**;10:198-201
6. Fedullo LM, Meranze SG, McLean GK, Burke DR. Embolization of a subclavian artery aneurysm with steel coils and thrombin. *Cardiovasc Intervent Radiol* **1987**;10:134-137
7. Cope C, Zeit R. Coagulation of aneurysms by direct percutaneous thrombin injection. *AJR* **1986**;147:383-387

Case Report

Fat-Shift Artifact Simulating Aortic Dissection on MR Images

Chaim S. Lotan,¹ Gregory B. Cranney, Mark Doyle, and Gerald M. Pohost

MR imaging has been shown to be an important technique for the diagnosis and follow-up of patients with suspected or proved aortic disease [1-3]. High-field MR systems yield a greater signal-to-noise ratio and are now in widespread use. However, the chemical shift between water and fat is greater with these systems than with lower-field systems and may cause problems in image interpretation. In the present case, a dissection of the thoracic aorta was suspected on the basis of an MR feature that later was proved to be an artifact caused by the water-fat chemical-shift effect.

Case Report

A 66-year-old man was referred for evaluation of the thoracic aorta before undergoing surgery for an abdominal aneurysm. Five years earlier, he had presented to another institution, where he underwent thoracic aortography. The aortogram was interpreted as depicting a small aortic dissection for which medical treatment was instituted. The patient subsequently improved and was discharged while taking beta blockers and receiving antihypertensive therapy.

MR imaging was performed by using a 1.5-T Philips Gyroscan system. Gated spin-echo images of the thoracic and abdominal aorta were acquired in the axial, coronal, and sagittal planes. The possibility of an intimal flap on the concave side of the aortic arch and descending aorta was suggested by an apparent 5-mm separation of the intima from the surrounding tissue (Figs. 1A and 1B). Gradient-echo imaging did not identify a differential flow pattern in the region of the suspected false lumen.

Coronary angiography, performed to evaluate risk before surgery, showed only subcritical coronary disease. Aortography, performed after MR imaging, disclosed a normal thoracic aorta. On his fourth day in the hospital, the patient died suddenly. An autopsy revealed pulmonary emboli and a tortuous aorta with diffuse atherosclerotic

involvement. Aortic dissection could not be found on either macroscopic or microscopic examination.

Discussion

Recent studies have suggested that MR imaging can correctly diagnose, stage, and follow various aortic diseases [1-3]. With a spin-echo pulse sequence, there is high contrast between the intimal flap and the low signal present in rapidly flowing blood. When cine MR (gradient-echo) imaging also is performed, the combination usually can identify the proximal and distal extent of the dissection, the precise involvement of the arch vessels, and the communication between the true and false lumens [4, 5]. Thus MR imaging offers a complete assessment of patients with suspected aortic dissection and currently appears to be more sensitive than any other noninvasive imaging technique [6].

A growing number of imaging centers are currently using high-field magnets (1-2 T) to improve the signal-to-noise ratio and to permit concurrent in vivo spectroscopy studies. For imaging purposes, a disadvantage of such systems is the increase in the chemical shift between water and fat (fat shift). However, even with low-field systems, under certain imaging conditions (e.g., noise-reduction strategies), the fat shift can also be significant.

In proton MR spectroscopy, fat and water molecules are spectrally separated by 3.5 ppm. The corresponding frequency (Hz) separation is directly proportional to the strength of the static magnetic field, which for a field of 1.5 T is 224 Hz. In MR imaging, spatial information is also encoded by spectral shifts induced by magnetic gradients. In the present study, the frequency separation per pixel was 80 Hz. There-

Received May 13, 1988; accepted after revision July 20, 1988.

C. S. Lotan and G. B. Cranney are research fellows in the Division of Cardiovascular Disease, Dept. of Medicine, University of Alabama at Birmingham, Birmingham, AL 35294. C. S. Lotan is the recipient of a Fulbright Scholarship.

This work was supported in part by the University of Alabama at Birmingham Center for Research and Development; the Callaway Foundation; the IDH SCOR (2P50 HL 17667); and Philips Medical Systems, N. America.

¹ All authors: Division of Cardiovascular Disease, Department of Medicine, University of Alabama at Birmingham, Birmingham, AL 35294. Address reprint requests to G. M. Pohost.

AJR 152:385-386, February 1989 0361-803X/89/1522-0385 © American Roentgen Ray Society

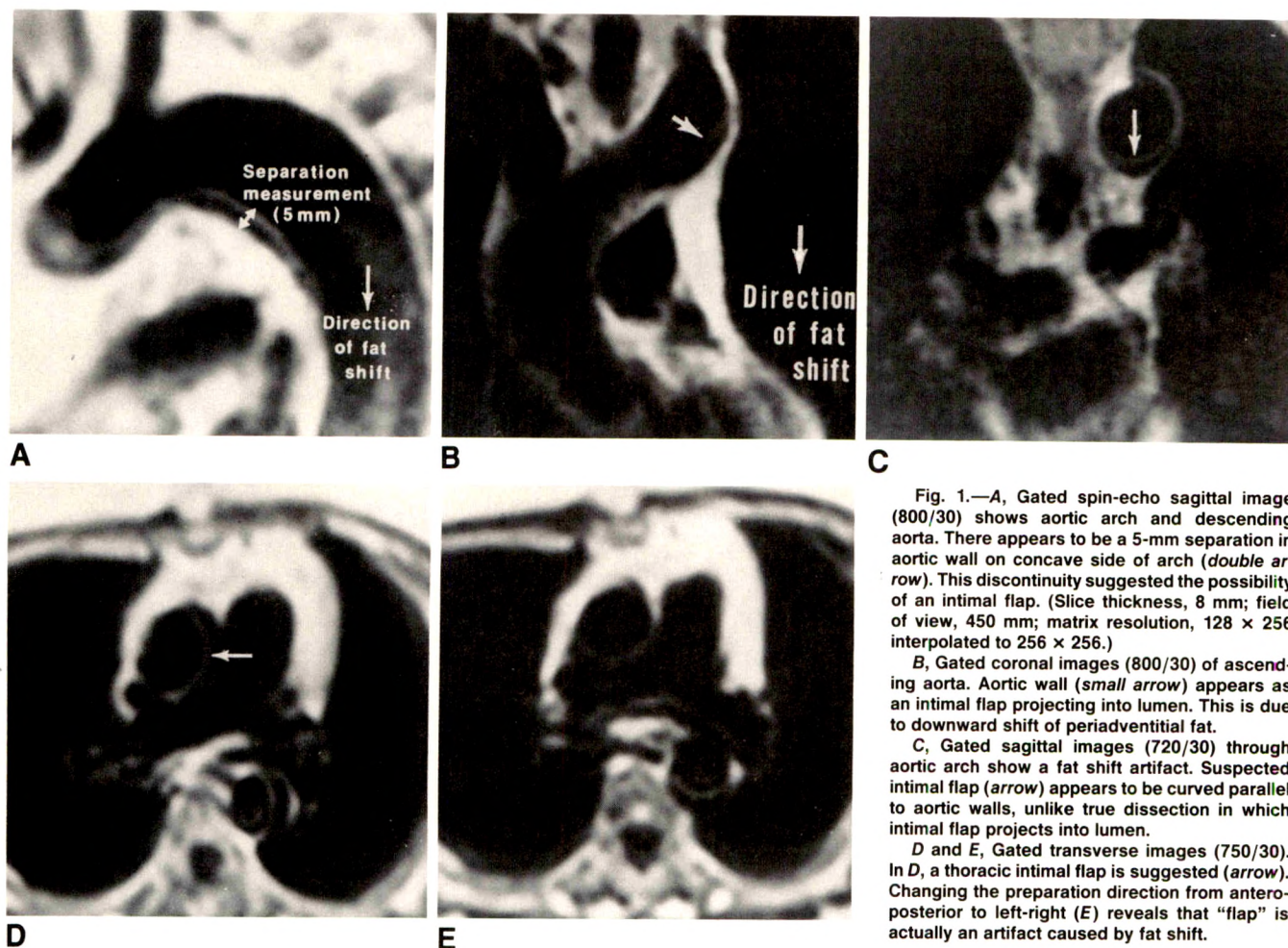


Fig. 1.—A, Gated spin-echo sagittal image (800/30) shows aortic arch and descending aorta. There appears to be a 5-mm separation in aortic wall on concave side of arch (double arrow). This discontinuity suggested the possibility of an intimal flap. (Slice thickness, 8 mm; field of view, 450 mm; matrix resolution, 128 × 256 interpolated to 256 × 256.)

B, Gated coronal images (800/30) of ascending aorta. Aortic wall (small arrow) appears as an intimal flap projecting into lumen. This is due to downward shift of periaortic fat.

C, Gated sagittal images (720/30) through aortic arch show a fat shift artifact. Suspected intimal flap (arrow) appears to be curved parallel to aortic walls, unlike true dissection in which intimal flap projects into lumen.

D and E, Gated transverse images (750/30). In D, a thoracic intimal flap is suggested (arrow). Changing the preparation direction from anteroposterior to left-right (E) reveals that "flap" is actually an artifact caused by fat shift.

fore, the fat shift corresponded to 2.78 pixels (224 Hz/80 Hz/pixel), or 5.0 mm (pixel size = 1.8 mm).

Large blood vessels frequently are surrounded by fat, which varies in both extent and distribution. In spin-echo images, the shifted fat may cause the appearance of a double lumen or may imitate an intimal flap. The location of this "double lumen" will depend on the precise distribution of fat.

In this particular case, the fact that the patient had a history of thoracic aortic dissection heightened the suspicion that there was an intimal flap. On reviewing this and other cases, we suggest several approaches that may assist the operator in differentiating fat shift from true dissection: (1) In fat shift artifacts, the intimal flap usually is found to be curved parallel to the aortic walls, unlike the true dissection in which the intimal flap can be observed to project into the lumen on cross-sectional images (Fig. 1C). (2) The fat shift is always in the direction of the measurement. Thus in questionable cases, changing the direction of the measurement will change the direction of the fat shift (Figs. 1D and 1E). (3) The magnitude and direction of the fat shift should be readily available by using the software. Usually, however, the same information can be obtained by observing other tissue interfaces in the image. (4) The fat shift can be reduced by increasing the strength of the gradients. However, this can lead to a de-

crease in the signal-to-noise ratio and thus cause degradation of image quality.

Under certain conditions (e.g., moderate high-field gradients or weak low-field gradients), significant fat shift can occur. This can cause artifacts that can imitate an intimal flap. Awareness of the fat-shift phenomenon should prevent such misinterpretation.

REFERENCES

1. Barentz JO, Ruijs JHJ, Heystarten JMJ, Buskens F. Magnetic resonance imaging of the dissected thoracic aorta. *Br J Radiol* 1987;60:499-502
2. Kersting-Sommerhoff BA, Sechtem UP, Schiller NB, Lipton MJ, Higgins CB. MR imaging of the thoracic aorta in Marfan's syndrome. *J Comput Assist Tomog* 1987;11:633-639
3. Geisinger MA, Risius B, O'Donnell JA, et al. Thoracic aortic dissections: magnetic resonance imaging. *Radiology* 1985;155:407-412
4. Dinsmore RE, Wedeen VJ, Miller SW, et al. MRI of dissection of the aorta: recognition of the intimal tear and differential flow velocities. *AJR* 1986;146:1286-1288
5. Cranney GB, Lotan CS, Helmcke F, Nanda NC, Pohost GM. Diagnosis of thoracic aortic dissection using nuclear magnetic resonance imaging—comparison with other imaging modalities (abstr). Proceedings of the meeting of the Cardiac Society of Australia and New Zealand 1988:14
6. Goldman AP, Kotler MN, Scanlon MH, et al. The complementary role of magnetic resonance imaging, Doppler echocardiography, and computed tomography in the diagnosis of dissecting thoracic aneurysms. *Am Heart J* 1986;111:970-981

Chemotherapy and Embolization via the Inferior Epigastric Artery for the Treatment of Primary and Metastatic Cancer

Francis O'Keeffe¹
James G. Lorigan
Chusilp Charnsangavej
C. H. Carrasco
William R. Richli
Sidney Wallace

We evaluated the results of arterial chemotherapy and embolization via the inferior epigastric artery and its branches in 10 patients with a variety of primary and metastatic neoplasms supplied by that vessel. A total of 15 infusions and five occlusions were performed. There were no complications related to arteriography, indwelling catheters, or arterial occlusion. The effects on tumor bulk ranged from complete necrosis in one patient to partial necrosis in three patients. Surgical resection was facilitated in four of six patients. Local recurrence of tumor occurred in two of these patients. Three of four patients with intractable pain had effective relief.

Our experience suggests that transarterial therapy of tumors supplied by the inferior epigastric artery or its branches is a safe procedure and may be useful in tumor management.

Transcatheter arterial embolization and chemoinfusion are frequently used in the management of neoplasms [1-4]. The inferior epigastric artery and its branches may provide the main blood supply to tumors in the pelvis and anterior portion of the abdomen. We describe our experience with chemoinfusion and occlusion of these vessels in 10 patients with a variety of primary and metastatic neoplasms supplied by the inferior epigastric artery.

Materials and Methods

Our study group included six men and four women (age range, 20-63 years). Pathologic diagnoses included metastatic melanoma in three; metastatic carcinoma of the penis in two; and endometrial sarcoma, osteosarcoma, giant cell tumor, metastatic renal cell carcinoma, and metastatic hemangiopericytoma in one each. The tumors were located in the external iliac and inguinal nodes in four patients, anterior abdominal wall in two, iliosacral region in two, and ischial tuberosity and inferior pubic ramus in one each.

The aim of therapy was to reduce tumor bulk and facilitate surgical resection in six patients and to alleviate pain in four. Pain relief was assessed subjectively by the patient and objectively by the level of analgesia required. Effect of therapy on tumor bulk was determined by CT examination in 10 patients, by arteriography in nine patients, and by subsequent surgical findings in five patients.

Catheterization of the inferior epigastric and anomalous obturator vessels was performed by using a catheter with a double or modified double curve. In most patients (nine of 10), we used a 5-French polyethylene catheter and a contralateral approach. In one patient, an ipsilateral approach was used, and in one patient, a 6.5-French Cobra C-1 visceral catheter (Cook, Bloomington, IN) was used. Depending on arterial flow, contrast medium was injected at a rate of 1-2 ml/sec, for a total of 4-10 ml.

CT arteriography was performed in three patients with the catheter positioned in either the inferior epigastric artery (one patient) or in the anomalous obturator vessel originating from the inferior epigastric artery (two patients) to confirm tumor blood supply before therapy (Fig. 1). CT scans were obtained with 10-mm collimation, usually with a scan time of 2 sec and a 1.5-sec interscan delay, and were begun at the onset of injection of contrast material. Thirty percent iodinated contrast material (diatrizoate meglumine) was injected at 1-2 ml/sec by

Received July 13, 1988; accepted after revision September 23, 1988.

¹ All authors: Division of Diagnostic Imaging, Department of Diagnostic Radiology, The University of Texas M. D. Anderson Cancer Center, 1515 Holcombe Blvd., Houston, TX 77030. Address reprint requests to F. O'Keeffe.

AJR 152:387-390, February 1989
0361-803X/89/1522-0387

© American Roentgen Ray Society

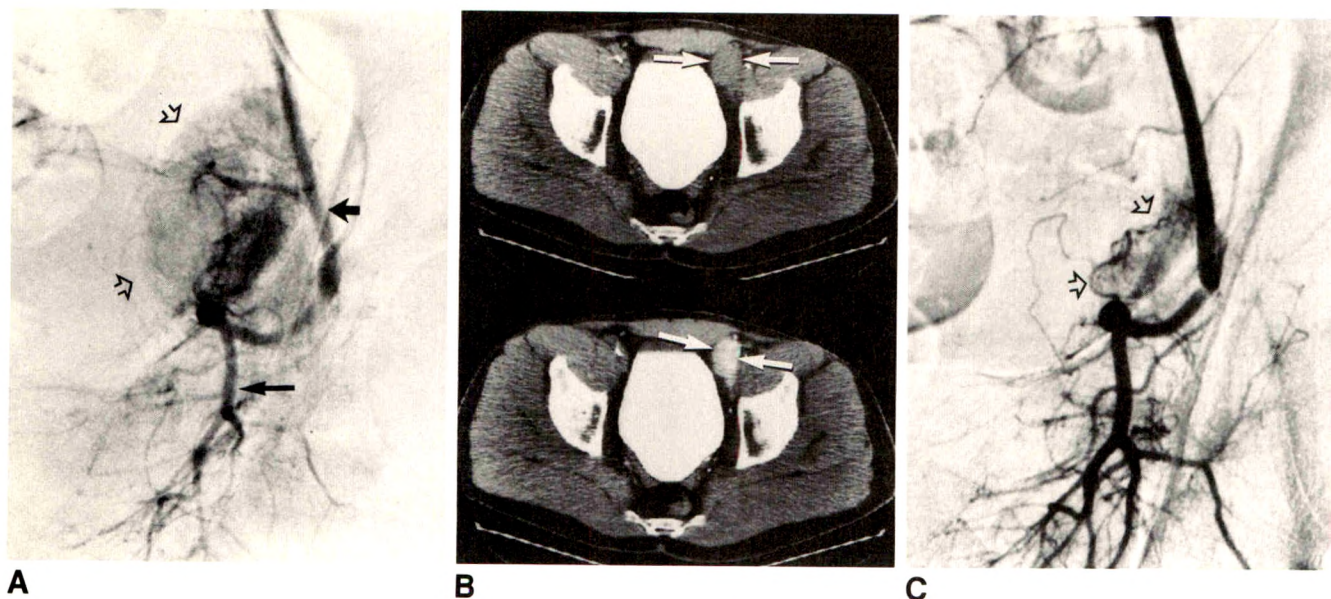


Fig. 1.—Case 3: Metastatic melanoma to left external iliac node.

A, Selective inferior epigastric arteriogram shows hypervascular mass (open arrows) receiving blood supply from inferior epigastric artery (short solid arrow) and anomalous obturator (long solid arrow) arising from inferior epigastric artery.

B, CT scans before (top) and after (bottom) injection of contrast medium into inferior epigastric-obturator arterial trunk show enhancement of nodal mass (arrows), confirming tumor blood supply.

C, Selective inferior epigastric arteriogram 1 month after first chemoinfusion of inferior epigastric-obturator trunk shows reduction in tumor size (arrows). Complete tumor necrosis was found at surgery.

means of a mechanical injector (Mark IV, Medrad, Pittsburgh, PA) and was continued throughout the scan period. The number of scans obtained and the amount of contrast material injected were determined by precontrast scanning through the region of interest.

Embolic materials used for vessel occlusion included 2- to 3-mm cubes of gelatin sponge (Gelfoam, Upjohn, Kalamazoo, MI), 150- to 590- μ m particles of polyvinyl alcohol foam (Ivalon, Unipoint, High Point, NC), and in one patient a stainless steel coil with a 3-mm helix. Chemotherapeutic agents are listed in Table 1. In two patients, only embolization was performed.

Results of the 10 patients treated by intraarterial therapy are outlined in Table 1. All tumors received blood supply from either the inferior epigastric artery or an anomalous obturator artery arising from the inferior epigastric. A total of 15 infusions and five occlusions were performed. Nine chemotherapy infusions and three embolizations of inferior epigastric arteries were performed in six patients. Six infusions and two occlusions of anomalous obturator arteries arising from the inferior epigastric were performed in four patients. Three embolizations were performed to redistribute tumor arterial flow to a single artery and thus facilitate the effect of infusion. The other two embolizations were performed to reduce tumor bulk and thus alleviate pain.

Results

Of four patients with painful lesions, two had good relief of pain, one had moderate relief, and one had no relief. Pain eased within a few hours to 2 days after therapy, and persisted for 6–32 weeks. Pain relief was associated with evidence of bone healing in one patient (Fig. 2). In six patients, therapy was aimed at reducing tumor bulk to facilitate surgical

resection. This was eventually attempted in five patients, although in one of these only partial resection was possible because of vascular involvement. One patient had complete tumor necrosis and at 2 years after resection had no measurable disease. Three patients had incomplete tumor necrosis. Two patients had no evidence of response to therapy. Tumors were hypervascular in nine patients, and reduced tumor vascularity was seen on posttreatment angiograms in eight. In two of the five patients who had undergone resection, local recurrence of tumor after resection occurred over intervals of 1–6 months.

There were no complications related to arteriography, indwelling catheters, or arterial occlusion. Two patients had abdominal pain that was thought to be related to infusion of cisplatin. In the first patient, severe pain developed in the left inferior rectus muscle area 1 day after infusion and lasted 48 hr. Previous infusion of the same vessel (anomalous obturator artery) had been uneventful. CT examination showed no abnormality in this region. In the second patient, moderate lower abdominal pain developed when the cisplatin infusion was started. CT examination subsequently revealed an area of low attenuation in the left rectus muscle. At surgery, necrotic tumor involvement of the rectus muscles was found.

Chemodermatitis, a local cutaneous reaction to the chemotherapy, developed in one after infusion of cisplatin via an anomalous obturator vessel. This reaction consisted of a painful tender erythematous area approximately 10 cm in diameter in the suprapubic region (presumably in the inferior epigastric territory), which subsided within 10 days.

TABLE 1: Summary of Patients Treated by Inferior Epigastric Arterial Chemotherapy or Embolization

Case No.	Diagnosis	Previous Therapy	Arterial Chemotherapy	Embolization Site & Method	Anatomy	Follow-Up
1	Carcinoma, penis; inguinal metastases	Cisplatin and 5-fluorouracil; no response	Cisplatin and bleomycin, medial femoral circumflex $\times 2$	R inferior epigastric with Gelfoam	Classical	Partial necrosis; local recurrence 1 month after resection
2	Endometrial sarcoma; bladder/abdominal wall recurrence	Radiotherapy; systemic chemotherapy 1 year earlier	Cisplatin, bilateral inferior epigastric $\times 2$; bilateral internal iliac $\times 1$	Gluteal vessels with steel coils	Anomalous obturator	Almost complete necrosis; resected; local recurrence at 6 months
3	Metastatic melanoma: L inguinal, iliac	Inguinal dissection, systemic chemotherapy; no response	Cisplatin, L obturator $\times 2$	None	Anomalous obturator	Complete necrosis; resection at 1 month; no recurrence at 2 years
4	Metastatic melanoma: R inguinal, iliac	Inguinal dissection, systemic chemotherapy; no response	Cisplatin, R external iliac $\times 3$; R obturator $\times 1$	R inferior epigastric with Gelfoam distal to tumor supply	Classical	Partial necrosis; resection at 1 month; disseminated at 7 months
5	Osteosarcoma, iliosacral; severe pain	None	Cisplatin, R obturator $\times 2$	None	Anomalous obturator	Moderate pain relief for 8 months
6	Metastatic melanoma, bladder/suprapubic	Surgical resection; arterial chemotherapy 2 years earlier	Cisplatin, $\times 2$	None	Classical	Partial necrosis; resected at 4 months; disseminated at 2 years
7	Carcinoma, penis; inguinal metastases	Perinectomy; inguinal dissection; recurrence	Cisplatin and bleomycin, L inferior epigastric $\times 1$; both internal pudendal $\times 1$	None	Classical	No change on CT; died after 2 months
8	Giant cell tumor, iliosacral/L5; lung metastases; severe pain	Laminectomy, L5; chemotherapy; no response	None	L inferior epigastric, L fourth lumbar, L deep femoral circumflex with 175 mg Ivalon/Gelfoam	Classical	Progression; no pain relief
9	Metastatic renal cell carcinoma, L inferior pubic ramus; pain	L nephrectomy; R adrenalectomy	None	L obturator, L external pudendal with 100 mg Ivalon/Gelfoam	Anomalous obturator	Relief of pain for 6 weeks, until death
10	Metastatic hemangiopericytoma, R ischium; severe pain	Irradiation with no response after 6 weeks	Cisplatin, R obturator $\times 2$; R internal iliac $\times 2$	Redistribution, R obturator with 3-mm coil	Anomalous obturator	Relief of pain for 6 months, until death

Note.—Anomalous obturator indicates origin from inferior epigastric artery. Redistribution directs tumor blood flow to a single artery by occluding other arterial supply. R = right; L = left.

Discussion

The inferior epigastric vessels or anomalous obturator arteries arising from them may supply tumors in a variety of locations. When planning transcatheter arterial therapy for tumors in the external iliac, anterior abdominal wall, inguinal, or ischial regions, blood supply from these vessels should be sought. The inferior epigastric artery usually arises from the external iliac artery just above the inguinal ligament but may originate up to 6 cm above it. It infrequently arises from either the common femoral or the obturator artery. Occasionally, it is formed by two branches, one derived from the external iliac artery, the other from the internal iliac artery. It divides below the umbilicus into two or three branches that anastomose

with the superior epigastric branch of the internal mammary and lower intercostal arteries. The obturator artery has an anomalous origin from the inferior epigastric artery in 13–28% of cases (Fig. 2). The origin of the obturator artery may differ on either side. The course and vascular supply territory of these vessels have been well described [5–7]. CT arteriography via these vessels can provide precise information on tumor blood supply and thus direct arterial therapy. This may be especially helpful with hypovascular tumors.

In this series, the effects on tumor bulk ranged from partial to complete necrosis, and surgical resection was facilitated in four of six patients. Response depends on many variables, including tumor blood flow, intratumor disposition and concentration over time of the drug infusion, and the intrinsic

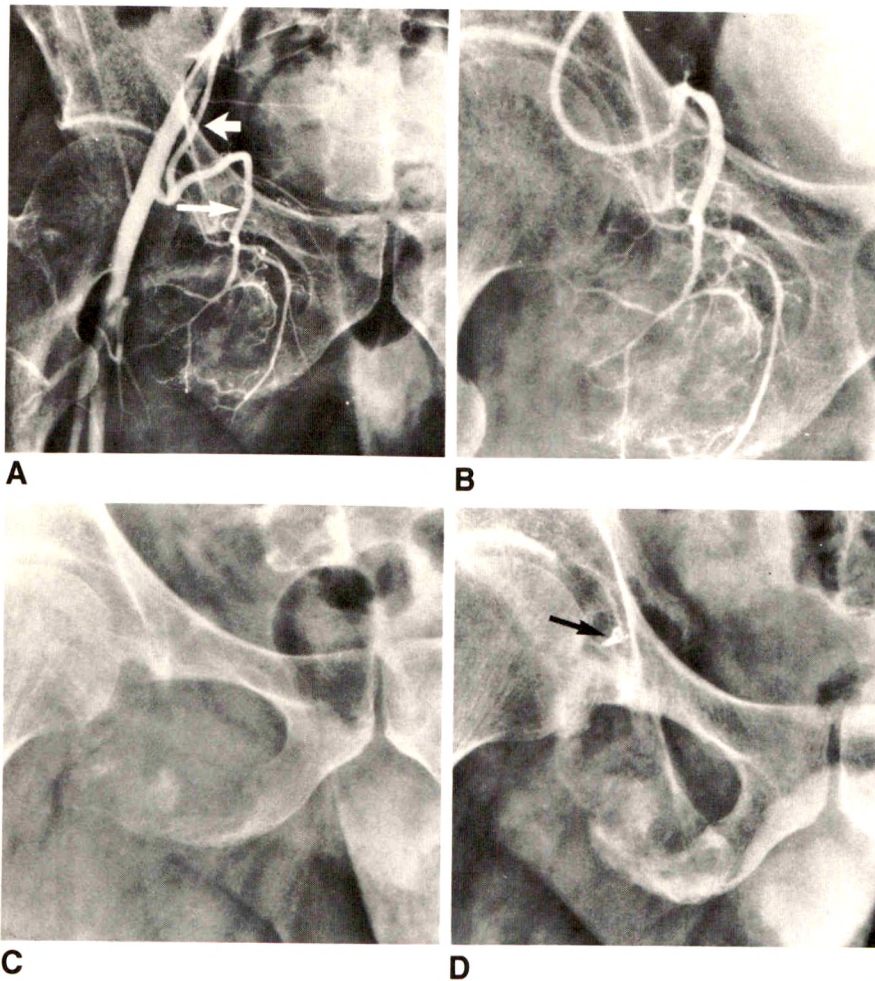


Fig. 2.—Case 10: Metastatic hemangiopericytoma to right ischium.

A, External iliac arteriogram shows blood supply to tumor is from obturator artery (long arrow) arising from inferior epigastric artery (short arrow). Tumor also received blood supply from anterior trunk of internal iliac artery (not shown).

B, Selective catheterization of obturator artery was performed for chemoinfusion of this vessel, and subsequently it was occluded to redistribute tumor arterial supply to a single vessel for further arterial chemotherapy.

C and D, Conventional radiographs before chemoinfusion (C) and 4 months after chemoinfusion (D) show reparative bone formation. Opacity over right hip joint (arrow) is a stainless steel coil in obturator artery that was placed to redistribute flow from obturator to anterior internal iliac trunk. This was then infused.

sensitivity of the tumor to the agent [4]. Reduction in tumor bulk is more likely if blood supply is from a single blood vessel where the catheter can be placed selectively [8]. This was shown clearly in our third case, in which blood supply was almost exclusively from one vessel.

Relief of pain by transarterial chemotherapy or occlusion of tumor arterial supply presumably is due to decreased tumor vascularity and subsequent reduction of tumor growth. In patients with tumor involvement of bone, diminished pressure on the nerve fibers of the periosteum probably contributes to pain relief. Failure to control pain, as occurred in one of our patients, seems more likely when multiple collaterals feed the tumor [9].

Apart from transcatheter therapy in the management of tumors, knowledge of the inferior epigastric vascular territory may help in the diagnosis of tumor origin and is also important to avoid inadvertent trauma when performing percutaneous lower abdominal procedures, or when embolization of this vessel is required as a result of trauma [10, 11].

Our experience suggests that the inferior epigastric artery and its branches may be infused and embolized without significant complications. The planning of such treatment requires a knowledge of variant anatomy.

REFERENCES

1. Chuang V, Wallace S, Carrasco CH, Charnsangavej C. Embolization as a therapeutic modality. *Cancer Bull* 1984;36:15-20
2. Jitendra V, Huben R, Wajzman Z, Pontes JE. Therapeutic embolization of pelvic metastases of renal cell carcinoma. *J Urol* 1984;131:647-649
3. Chuang V, Wallace S. Arterial infusion and occlusion in cancer patients. *Semin Roentgenol* 1981;1:13-25
4. Kavanagh J. Regional chemotherapeutic approaches to the management of pelvic malignancies. *Cancer Bull* 1984;36:52-55
5. Goss CM. *Gray's anatomy*, 27th ed. Philadelphia: Lea & Febiger, 1959:694-696
6. Braithwaite J. Variations in origin of the parietal branches of the internal iliac artery. *J Anat* 1952;86:423-430
7. Pick J, Anson A, Ashley F. The origin of the obturator artery. *Am J Anat* 1942;70:317-342
8. Charnsangavej C, Chuang V, Wallace S, Soo C, Bowers T. Angiographic appearance of recurrent malignant melanoma before and after intra-arterial chemotherapy. *Radiology* 1982;142:347-349
9. Kudo S, Chuang V, Wallace S, Bechtel W, Mir S. Middle sacral arteriography: diagnostic and therapeutic implications. *Radiology* 1984;151:65-67
10. Schlakman BN, Meranza G, McLean GK, Burke DR. Inferior epigastric artery laceration following cystostomy tube placement: angiographic diagnosis and control. *J Intervent Radiol* 1986;1:77-78
11. Wittich GR, Helmer M, Mortinger H, et al. Radiological anatomy of the inferior epigastric artery. Presented at the annual meeting of the Association of University Radiologists, New Orleans, April 1988

Technical Note

A Technique for Pulmonary Artery Catheterization in Patients with Right Ventricular Enlargement

Arthur C. Waltman¹ and T. Gregory Walker^{1,2}

A variety of techniques for performing pulmonary arteriography from a femoral approach have been described [1-8]. Many of these use either a Grollman pulmonary catheter or a standard pigtail catheter. The configuration of the catheter can be modified by applying various curves directly to the catheter [4-6] or by using different guidewire combinations [2, 7, 8]. In patients with normal-sized cardiac chambers, these techniques are usually satisfactory. However, in patients who have marked enlargement of the right ventricular chamber, catheterization may be difficult. We describe a simple guidewire modification for reliable catheterization of the pulmonary artery in such patients.

Materials and Methods

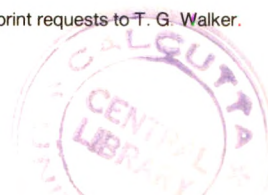
Our standard technique for pulmonary arteriography is a modification of that described by Grollman and Renner [8]. We use a transfemoral route of access and a standard 7.1-French pigtail catheter. After a percutaneous femoral vein catheterization, the catheter is advanced into the right atrium. A tip-deflecting guidewire is used to direct the pigtail catheter across the tricuspid valve into the right ventricle. When the catheter enters the right ventricle, the deflector tension is released, but the wire is left within the catheter. The

catheter is rotated counterclockwise and simultaneously advanced upward into the right ventricular outflow tract. Once in the outflow tract, the catheter is usually easily advanced into the main pulmonary artery. Use of the deflector wire to stiffen the pigtail catheter often facilitates this step. This maneuver may not be successful, however, in patients with marked enlargement of the right ventricular cavity. In such cases, after the pigtail catheter has been advanced into the right ventricle, the tip-deflecting guidewire is replaced with the stiff end of a 0.038-in. (0.99-mm) fixed-core guidewire that has been manually shaped into a tight S configuration. Each curve of the S has a radius of curvature of approximately 5 mm (Fig. 1A). This curved guidewire is carefully passed through the catheter to a point just proximal to the coiled pigtail portion. Passing the guidewire through the catheter may be slightly difficult and often requires greater force than is normally used. The acuteness of the two curves in the wire will diminish as it is advanced through the catheter. However, the guidewire retains sufficient curvature to cause the catheter to assume the same configuration. This S configuration directs the catheter tip upward into the right ventricular outflow tract, where it can be advanced over the fixed guidewire into the main pulmonary artery (Fig. 1B-D). In order to avoid the possibility of vascular perforation, the stiff end of the guidewire must never be allowed to straighten out the pigtail coil or protrude beyond the catheter tip. Once the pigtail catheter has been advanced into the main pulmonary artery, it can be positioned selectively in either the right or left pulmonary artery, by using a tip-deflecting guidewire when necessary.

Received June 20, 1988; accepted after revision July 27, 1988.

¹ Both authors: Department of Radiology, Massachusetts General Hospital and Harvard Medical School, Boston, MA 02114.

² Present address: Department of Radiology, Boston University Medical Center, 88 E. Newton St., Boston, MA 02118. Address reprint requests to T. G. Walker.



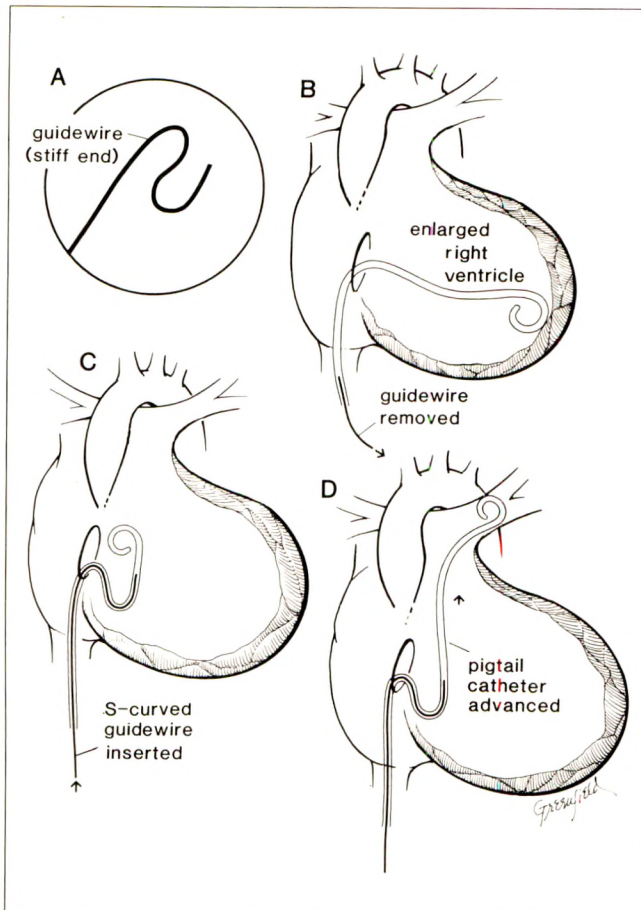


Fig. 1.—Schematic diagram of technique for pulmonary artery catheterization in patients with enlarged right ventricles.

A, Stiff end of 0.038-in. (0.99-mm) guidewire modified into tight S configuration. Each limb has a radius of curvature of approximately 5 mm.

B, With right ventricular enlargement, pigtail catheter tip preferentially seeks cardiac apex or interventricular septum.

C, Introduction of modified guidewire causes catheter to assume same configuration, thus directing pigtail tip cephalad toward pulmonary outflow tract.

D, Pigtail catheter advanced over fixed guidewire into the main pulmonary artery.

Discussion

For pulmonary arteriography we use a standard pigtail catheter rather than the Grollman catheter, because the Grollman catheter tends to seek the upper-lobe and middle-lobe pulmonary arteries [5]. In patients with marked dilatation of the right ventricular chamber, however, directing a pigtail catheter cephalad into the right ventricular outflow tract is often difficult. Often the catheter will preferentially advance into the right ventricular apex instead. Continued unsuccessful attempts to maneuver the catheter tip into the outflow tract may produce cardiac arrhythmia, because the catheter may irritate the interventricular septum.

In such patients, introduction of a guidewire modified as described will cause the pigtail catheter to assume this same configuration. Such a configuration directs the catheter tip cephalad and into the pulmonary outflow tract. It is not necessary to exchange the pigtail catheter for a specially shaped catheter. Furthermore, the modification is easy to do and uses readily available materials.

REFERENCES

1. Grollman JH Jr, Gyepes MT, Helmer E. Transfemoral selective bilateral pulmonary arteriography with a pulmonary-artery-seeking catheter. *Radiology* 1970;96:202-204
2. Courey WR, deVillasante JM, Waltman AC. A quick, simple method of percutaneous transfemoral pulmonary arteriography. *Radiology* 1974;113:475-477
3. Glenn JH, Ranniger K. A new variation of the technique of transfemoral arteriography. *Radiology* 1975;117:473
4. Beachley MC, Tisnado J, Konerding K, Vines FS. Alternate technique for pulmonary arteriography. *AJR* 1980;134:195-196
5. Ledor K, Ben-Avi HA, Ben-Avi DD, Abramowitz JG. A lower lobe-seeking pulmonary artery catheter. *Radiology* 1987;165:286-287
6. Tempkin DL, Ladika JE. New catheter design and placement technique for pulmonary arteriography. *Radiology* 1987;163:275-276
7. Kozak BE, Röscher J. Curved guide wire for percutaneous pulmonary angiography. *Radiology* 1988;167:864-865
8. Grollman JH, Renner JW. Transfemoral pulmonary angiography: update on technique. *AJR* 1981;136:624-626

Perspective

Radiologic Physics Instruction for Diagnostic Radiologists: Results of an Opinion Survey

Committee on Training of Radiologists, American Association of Physicists in Medicine¹

A survey of radiologists who recently were certified by the American Board of Radiology was conducted in the winter of 1984–1985 by the Committee on Training of Radiologists of the American Association of Physicists in Medicine (AAPM). The subject of the survey was the radiologists' overall impressions of the quality of the physics instruction they received during their residencies (not solely board preparation). The survey population was selected from a list, provided by the American College of Radiology (ACR), of 3000 radiologists who had been certified within the 5 years preceding the survey. From that group, approximately 1000 names were selected (every third entry) for the mailing, which yielded a total of 354 responses. No attempt was made to ensure that the demographic distribution of requests matched the demographic distribution of radiologists. In fact, the resultant distribution was determined solely by response (second mailings were not performed).

The survey consisted of 33 questions, with space for comments. The first eight questions were intended to identify the demographics of the survey population, including factors such as the size of the residency program attended, specialty at the time of the survey, and size of practice. The remaining 25 questions dealt with the format of the physics training received, continuing education pursuits since that time, and the radiologists' perceptions of their level of understanding and the importance of various topics.

Results

For completeness, the full text of the survey is reprinted in the appendix, with responses listed as total number and percent in each category. The results are summarized here.

Objective Responses

Demographics.—Sixty-three percent of the respondents were general diagnostic radiologists. Forty-nine percent were based in community hospitals; 19% were in university teaching hospitals. The study group was representative of a wide range of practice sizes as measured by local population, number of hospital beds, number of radiologists in practice, or number of examinations performed per year. For example, 21% of the respondents practiced in communities with populations of less than 50,000, whereas 18% practiced in communities with populations of more than 1 million. Physics training during residency was most often (65%) conducted by a physicist who was knowledgeable about both diagnostic imaging and radiation therapy. A physicist did not participate in the training of 4% of the respondents.

General Opinion of Physics.—At the time of residency, 39% thought that radiologic physics was a "potentially useful but necessary evil forced on me by certification requirements." For the same question, 31% chose the option "important part

Received July 20, 1988; accepted after revision September 7, 1988.

¹ The following committee members were particularly involved in this project: Robert L. Dixon, F. Marc Edwards, E. Russell Ritenour, and Richard L. Morin. Address reprint requests to Executive Officer, American Association of Physicists in Medicine, 335 E. 45th St., New York, NY 10017.

of residency, but not very interesting." In retrospect, it is clear that the two choices are not mutually exclusive, so an unambiguous answer to the opinion question was not obtained. For example, physics could be useful, important, a necessary evil, and uninteresting all at the same time. In any case, it is probably fair to pool both of these responses as an opinion of "uninteresting" or "drudgery" and to include the 3% who thought that it was a "useless evil forced upon me by certification requirements." Thus, a total of 72% of the respondents had a negative opinion of physics as it appeared in their programs; 28% considered it an "important and interesting part of residency." However, 72% have attempted to continue their physics training since the end of their residencies by attending courses and seminars at national meetings and through self-study. Forty-eight percent attempt to follow physics and technologic articles in the literature.

Relevance and Competence.—Respondents were asked to rank the relative importance of various topics in radiologic physics and their current level of understanding of those topics. The rankings were to be carried out on a scale of 1–5, where 1 indicated the lowest level. The relative-importance scores tended to fall slightly above 3 with a standard deviation of 1. Only two topics, "patient dose as a function of examination technique" and "effect of technique factors on image quality" had a mean score greater than 4. Level-of-understanding scores tended to fall slightly below 3, with a standard deviation of 1.

Usefulness.—Another series of questions dealt with the respondents' ability to use their physics knowledge to perform tasks and their perception of the importance of these tasks. In this series, the scores tended toward a level of ability of slightly less than 3, with an importance score of 3.5 for most tasks. Again, the only tasks for which the mean level of importance scores were greater than 4 were "suggest technique factors to technologists when image quality is unsatisfactory" and "explain the risk of radiation vs benefit to fellow physicians and to the general public." A final objective question asked if they thought their knowledge or lack of knowledge about radiologic physics had had an effect on the quality of patient care. Roughly one-third answered yes, one-third answered no, and one-third did not answer.

Subjective Responses

The final question solicited written suggestions for improvement of content and instructional methods for radiologic physics education. Fifty-three percent of the respondents (186) chose to include comments and suggestions; these are summarized in the following paragraph. The full text of their comments is available from the AAPM Committee on Training of Radiologists.

A number of common themes were shared among the responses; seven of these are summarized in Table 1. By far the most common suggestion was that physics instruction emphasize the practical/clinical applications of theory and deemphasize more esoteric topics such as mathematical derivations and circuit diagrams. Suggestions that are not

TABLE 1: Summary of Subjective Responses (186 Total Responses)

Suggestion	No. of Times Mentioned
Courses should include less theory and more practical clinical applications.	64
More laboratory work and demonstrations should be used.	14
Physics curriculum should be standardized.	13
Patient dose and risk estimation should be more extensively discussed.	9
More information about computers should be given.	8
A textbook should be used and followed.	8
The physicist should be more aware of clinical problems.	8

included in Table 1 but that were mentioned at least three times included the following: (1) There should be more coverage of methods for evaluation and specification of radiologic equipment. (2) Radiologists should work as technologists for at least 1 month. (3) The overall quality of the physicists as teachers should be improved. (4) Audiovisual material for self-instruction should be developed. (5) Physics training should be spread throughout the residency and should not be concentrated in the year before the board examinations.

Conclusions

Seventy-two percent of the respondents expressed a negative opinion of the physics instruction that they received during their residencies, but these same respondents nonetheless have continued to study physics. This suggests that radiologists actually do consider physics to be a worthwhile endeavor, even though this was not their perception during their residencies.

The respondents indicated a need for emphasis on subjects that are directly relevant to everyday practice. Although they acknowledged the need for an understanding of basic physics principles, they clearly perceived that theory had been over-emphasized. The suggestion was to emphasize physics in action rather than physics as a discipline, along with more practical, hands-on experience and the use of images to illustrate points.

The survey data discussed here are several years old and therefore do not reflect some of the more recent topics of technologic interest in radiology. In addition, many materials are now available (for example, ACR Physics Film Teaching Files, ACR/AAPM Syllabus, RSNA Physics Symposia) that would aid in resident training in physics. However, the concerns expressed by the respondents were rather basic—for example, a need for a more standardized curriculum—and are therefore still relevant. These data should serve as a useful baseline for future studies as the AAPM, the ACR, and other interested organizations work toward the improvement of radiologic physics instruction.

Appendix

Radiologic Physics for Diagnostic Radiologists:
Questionnaire

General Background Data

1. Which of the following best describes your own daily practice of radiology? (Choose one.)
 - 63% (221) a. Diagnostic radiology including nuclear medicine
 - 18% (64) b. Diagnostic radiology except nuclear medicine
 - 1% (5) c. Nuclear medicine
 - 8% (27) d. Specials/interventional
 - 7% (26) e. CT/ultrasound
 - 3% (11) f. Other
2. What is the population of community in which you practice?
 - 3% (12) a. <10,000
 - 19% (66) b. 10,000–50,000
 - 17% (61) c. 51,000–100,000
 - 17% (59) d. 101,000–250,000
 - 11% (40) e. 251,000–500,000
 - 13% (45) f. 501,000–1,000,000
 - 18% (62) g. >1,000,000
3. Which one of the following best describes the practice site where you spend most of your professional time? (Choose one.)
 - 49% (172) a. Community hospital
 - 19% (66) b. Office and hospital practice
 - 19% (67) c. University teaching hospital
 - 2% (7) d. Private office or independent clinic
 - 8% (28) e. Federal hospital
 - 3% (11) f. State/county/city hospital
4. What is the size of the hospital in which you practice?
 - 1% (3) a. Not applicable (private office or clinic)
 - 2% (7) b. <50 beds
 - 16% (55) c. 51–150 beds
 - 27% (96) d. 151–300 beds
 - 20% (70) e. 301–450 beds
 - 18% (63) f. 451–600 beds
 - 16% (57) g. >600 beds
5. What is the size of your radiology practice, in number of examinations/year performed by your group?
 - 2% (6) a. <10,000 examinations/year
 - 22% (78) b. 11,000–40,000 examinations/year
 - 20% (69) c. 41,000–70,000 examinations/year
 - 18% (62) d. 71,000–100,000 examinations/year
 - 11% (37) e. 101,000–130,000 examinations/year
 - 4% (15) f. 131,000–160,000 examinations/year
 - 15% (52) g. >160,000 examinations/year
 - 9% (31) h. No answer/do not know
6. How many radiologists are in your practice?
 - 19.4% (68) a. 1–3
 - 27.9% (98) b. 4–6
 - 14.8% (52) c. 7–9
 - 8.3% (29) d. 10–12
 - 6.3% (22) e. 13–15
 - 4.3% (15) f. 16–18
 - 2.8% (10) g. 19–21
 - 2.8% (10) h. 22–24
 - 2.0% (7) i. 25–34

Appendix—continued

- 2.6% (9) j. 35–44
- 0.9% (3) k. >45
- 8.0% (28) l. no answer

Educational Background Data

7. What was the size of the residency program you attended, as measured by the average number of all radiology residents in training (PG1 to PG5)?
 - 3% (12) a. <5 residents
 - 15% (51) b. 5–10 residents
 - 19% (66) c. 11–15 residents
 - 24% (85) d. 16–20 residents
 - 19% (65) e. 21–25 residents
 - 20% (70) f. >25 residents
8. Did you have a fellowship year? If so, in what subspecialty?
 - 50% (176) a. No fellowship year
 - 8% (27) b. Neuroradiology
 - 20% (69) c. CT
 - 20% (69) d. Ultrasound
 - 10% (34) e. Nuclear medicine
 - 13% (45) f. Other (specify) _____
9. How many years have elapsed since the completion of your residency?
 - 3.7 ± 1.8 yrs
10. What type of physics education or training did you have? (Circle more than one answer, if appropriate.)
 - 0% (1) a. None
 - 40% (142) b. Individual reading/self-taught
 - 22% (77) c. Review course taken to prepare for the ABR examination
 - 16% (56) d. Formal lectures or seminars taught by physician
 - 94% (329) e. Formal lectures or seminars taught by physicist
11. If some of your physics education or training was provided by a physicist, how would you describe his or her background?
 - 4% (13) a. Not applicable because physicist did not participate in residency training program
 - 8% (28) b. Physicist whose primary background was in radiation therapy and who had little apparent knowledge of diagnostic imaging
 - 65% (227) c. Physicist with background and knowledge in both radiation therapy and diagnostic imaging
 - 24% (83) d. Physicist whose primary background and knowledge were in diagnostic imaging and who had little apparent knowledge in radiation therapy
12. At the time of residency, what was your opinion of physics?
 - 3% (9) a. Useless evil forced on me by certification requirements
 - 39% (136) b. Potentially useful but necessary evil forced on me by certificate requirements
 - 31% (109) c. Important part of residency, but not very interesting
 - 28% (98) d. Important and interesting part of residency
13. Since completion of your residency, how have you continued your education in physics or radiologic equipment/technology? (Circle more than one if necessary.)

Appendix—continued

28% (97)	a. Have not attempted to continue my physics education
9% (33)	b. Attended physics refresher course(s) at professional society meetings (e.g., RSNA, ARRS, SNM)
18% (64)	c. Attended medical refresher courses at professional society meetings that specifically covered physics as part of the course
7% (26)	d. Attended hospital or local institutional seminars or talks given by in-house or consulting physicist
45% (157)	e. Talked with medical imaging industry representatives (e.g., sales representatives, product specialists) and read their educational/promotional brochures
40% (140)	f. Self-study/independent reading in the literature
	14. If you have participated in physics continuing education courses, what topic(s) were covered?
62% (218)	a. Not applicable since none attended
1% (3)	b. Attended but do not recall topic(s)
16% (57)	c. CT
13% (46)	d. Ultrasound
6% (21)	e. Radiation protection
13% (46)	f. Nuclear medicine imaging
8% (27)	g. Radiobiology/risks of radiation
27% (96)	h. MR imaging
13% (47)	i. Digital subtraction imaging/picture archiving and communication
1% (2)	j. Other(s) (specify) _____
	15. Do you currently attempt to follow articles on physics and technology in the literature? If yes, please indicate which journals.
52% (182)	a. Do not follow these articles
46% (161)	b. <i>Radiology</i>
38% (132)	c. <i>American Journal of Roentgenology</i>
2% (8)	d. <i>British Journal of Radiology</i>
9% (32)	e. <i>Applied Radiology</i>
1% (3)	f. <i>Medical Physics</i>
1% (3)	g. <i>Physics in Medicine and Biology</i>
5% (18)	h. Others (specify) _____

Use of Physics Training

In the following questions, you are asked to assess two different aspects of various topics in radiologic physics. "Level of Understanding" refers to your current degree of knowledge concerning a particular topic. "Level of Understanding" should reflect the quantity and quality of your training during residency as well as subsequent loss or gain of knowledge. "Relative Importance" should reflect your judgment of how important knowledge of a given topic is to the practice of radiology, regardless of your current level of understanding. For instance, you may have received and retained considerable training concerning a topic that, in your experience, has little importance in radiology. The numeric system used is: 1 = lowest level, 5 = highest level.

	Level of Understanding	Relative Importance
16. Types and performance characteristics of X-ray generators	2.75 ± 0.97	3.09 ± 1.05
17. X-ray tube design rating and performance	2.72 ± 0.99	3.20 ± 1.08

Appendix—continued

	Level of Understanding	Relative Importance
18. Types and performance characteristics of intensifying screens	3.15 ± 1.05	3.62 ± 0.95
19. Film development and rapid processing	2.96 ± 0.96	3.45 ± 1.04
20. Film characteristics	3.10 ± 0.98	3.80 ± 1.04
21. Selection of the film/screen combination most appropriate for a particular procedure	2.90 ± 1.05	3.97 ± 0.97
22. Conventional (focused) tomography	3.42 ± 1.02	3.20 ± 1.05
23. Principles and performance characteristics of image intensifiers and video (TV system)	2.75 ± 1.01	3.35 ± 1.00
24. Patient dose as a function of examination techniques	3.39 ± 1.05	4.17 ± 1.02
25. Effect of technique factors on image quality	3.44 ± 1.05	4.20 ± 0.99
26. Principles and performance characteristics of digital fluoroscopic imaging systems	2.42 ± 1.05	3.34 ± 1.12
27. Radiation safety shielding calculations for radiology room design	2.30 ± 1.13	3.29 ± 1.17
28. Image quality descriptors such as modulation transfer function, radiographic contrast, and quantum mottle	2.86 ± 1.02	3.01 ± 1.05
29. Basic principles of digital computers	2.39 ± 1.26	3.17 ± 1.26
30. Principles and performance characteristics of special procedures equipment	2.71 ± 1.06	3.35 ± 1.03
31. Ultrasonic transducers	3.31 ± 1.00	3.59 ± 0.91
32. Ultrasonic imaging equipment and display	3.09 ± 1.00	3.61 ± 0.86
33. TM mode ultrasound equipment and display	2.31 ± 1.11	2.58 ± 1.12
34. Doppler ultrasound equipment and display	2.37 ± 1.05	2.88 ± 1.04
35. CT equipment and data-acquisition geometries	3.12 ± 1.10	3.60 ± 0.89
36. CT reconstruction techniques	2.70 ± 1.19	3.35 ± 1.09
37. CT image display techniques	2.92 ± 1.20	3.40 ± 1.11
38. Relationship of CT equipment and technique factors to CT image quality and artifacts	3.10 ± 1.14	3.69 ± 1.01
39. Radionuclide and radiopharmaceutical production and safety	2.92 ± 1.10	3.54 ± 1.10
40. Gamma cameras and collimators (principles and equipment performance)	3.08 ± 1.83	3.34 ± 0.98
41. Emission tomographic imaging (principles and equipment performance)	1.91 ± 1.13	2.22 ± 1.18
42. Nuclear cardiologic imaging (principles and equipment)	2.77 ± 1.15	3.31 ± 1.05
43. Computer applications in nuclear medicine	2.47 ± 1.23	3.31 ± 1.22

Appendix—continued

How adequately prepared do you feel you are to do the following: (1 = not adequate; 5 = very adequate). Please rate the relative importance of each item:

	Level of Adequacy	Level of Importance
44. Compare technical performance characteristics of equipment	2.58 ± 1.02	3.70 ± 0.98
45. Develop "generic" purchase specifications	2.12 ± 1.04	3.33 ± 1.09
46. Suggest technique factors to technologists when image quality is unsatisfactory	3.00 ± 1.19	4.13 ± 1.00
47. Help design an effective quality assurance program for your own specialty	2.78 ± 1.08	3.77 ± 1.01
48. Understand and assess the impact of digital image acquisition, storage, and retrieval	2.60 ± 1.19	3.38 ± 1.01
49. Understand and assess the impact of MR imaging	2.29 ± 1.20	3.38 ± 1.24
50. Explain the risk of radiation vs benefit to fellow physicians and to the general public	3.56 ± 1.07	4.25 ± 0.81
51. Evaluate the appropriateness and effectiveness of a radiation safety program for your department	2.96 ± 1.12	3.74 ± 0.98

Appendix—continued

	Level of Adequacy	Level of Importance
52. Deal with state and federal radiation regulatory agencies	2.49 ± 1.13	3.55 ± 1.20
53. Do you think that your knowledge or lack of knowledge about radiologic physics has had an effect on patient care? If so, please comment briefly.		
a. Yes 35% (127)		
b. No 27% (96)		
c. No answer 36% (128)		
54. What suggestions do you have to improve the content and instructional methods used for radiologic physics education?		

Note.—Total number of respondents = 354. Numbers in parentheses indicate actual number of respondents for each question. ABR = American Board of Radiology; RSNA = Radiological Society of North America; ARRS = American Roentgen Ray Society; SNM = Society of Nuclear Medicine.

ACKNOWLEDGMENT

We thank the American College of Radiology for providing the mailing list and labels used in this study.

The reader's attention is directed to the commentary on this article, which appears on the following pages.

Physics Instruction in Radiology

William R. Hendee¹

Of all the procedural specialties in medicine, radiology is the one most closely attuned to the basic sciences, especially physics. In the early years, physicians worked in close association with physicists to identify the useful clinical applications of X-rays, to develop devices such as X-ray tubes and fluorescent screens, and to establish standards for acceptable exposures and images. Later, innovations in X-ray imaging such as the rotating anode and image intensifier were combined with new imaging methods such as nuclear medicine and sonography to expand the horizons of diagnostic imaging. These developments reflected the continued extension of developments in physics into the clinical arena of radiology. Almost from the beginning, training and certification in radiology have included physics as a reflection of the importance of this basic science to diagnostic imaging.

The advent of CT in the early 1970s accentuated the importance of physics training in radiology. This technology introduced the digital computer as an integral component of imaging systems and stimulated development of several new imaging techniques in radiology, including cardiovascular nuclear medicine, single-photon and positron-emission tomography, real-time sonography, digital angiography and radiography, and MR imaging. Its insertion of reconstruction mathematics between the accumulation of imaging data and the formation of diagnostic images complicated the techniques of ensuring that the image reflected conditions in the patient and not in the imaging process. An improved understanding of the physics of image formation and display became necessary, together with at least a passing acquaintance with the language of physics to facilitate communication between ra-

diologists and the increased number of physicists and engineers working in radiology departments.

Today radiology is a highly technical discipline, and work on picture archiving and communications systems (PACS), new imaging methods, and the need for quantitative verification of the clinical usefulness of radiologic procedures promise to make it even more complex in the future. At the same time, competition is sure to increase between radiology and other medical specialties for privileges to perform radiologic examinations. One way for radiology to buttress itself against these turf invasions is to ensure not only that radiologists can interpret images more accurately, but also that they can optimize patient data acquired for the production of images. The latter approach requires that radiologists have a reasonable understanding of the physics underlying image production processes.

Recognition of the continuing need for an improved understanding of the physics of imaging probably explains the efforts of 72% of polled radiologists to continue their physics training after completion of their residency, as reported in the preceding article [1]. This recognition is reassuring, because it is the best insurance imaginable against the aggressive behavior of other specialists toward the province of radiologists. A solid understanding of the sciences underlying radiology, when combined with experience in performing imaging techniques and interpreting diagnostic images, is the optimum way to ensure that radiology continues to be practiced in the best interest of the patient.

A disturbing feature of the article, however, is the conclusion that 72% of the polled radiologists also found physics an

This article is a commentary on the preceding article.

¹ Northwestern University School of Medicine, 303 E. Chicago Ave., Chicago, IL 60611, and Medical College of Wisconsin, Milwaukee County Medical Complex, 8700 W. Wisconsin Ave., Milwaukee, WI 53226. Address reprint request to W. R. Hendee, American Medical Association, 535 N. Dearborn St., Chicago, IL 60610.

uninteresting subject, drudgery, or a useless evil as it was presented during their residency. This statistic brings to the surface an inescapable dichotomy between recognition of the importance of physics and the opinion of its value as it is taught in typical residency programs. It is a dichotomy that should not be ignored by directors of residency programs, and it should be considered especially by those responsible for physics instruction of residents.

Unlike other instructional programs in radiology, physics is too often inserted almost as an afterthought into the residency curriculum and taught by individuals with little understanding of the clinical implications of the subject. Frequently its presence is explained solely on the basis that questions about physics are asked on the certification examination. Under these circumstances, the reluctance of residents to learn physics is matched by the lack of enthusiasm of physicists to teach it. In addition, some physicists, like some radiologists, are simply not very good teachers. The difference is that

several radiologists teach in residency programs, whereas usually only one, or at best two or three, physicists teach in the same programs.

The preceding article [1] raises important issues for directors of residency programs and, especially, for physicists teaching residents. Surely we can all emphasize the importance of physics in radiology, and those of us responsible for teaching it can do a far better job of explaining physics and making it relevant to the clinical arena. Physics is essential to everything we do in radiology; how to make it understandable and interesting to residents is a challenge that must be met in the best interest of radiologists and the future of radiology.

REFERENCE

1. Committee on Training of Radiologists, American Association of Physicists in Medicine. Perspective. Radiologic physics instruction for diagnostic radiologists: results of an opinion survey. *AJR* 1989; 152:393-397

Invitation to the 1989 American Roentgen Ray Society Meeting in New Orleans, LA, May 7-12, 1989

I am pleased to extend an invitation to all radiologists to attend the 89th annual meeting of the American Roentgen Ray Society in New Orleans, LA, May 7-12, 1989. In keeping with the ARRS tradition, outstanding scientific and social programs will be provided.

The excitement of a meeting set in New Orleans requires no further description. The opportunity for busy radiologists to attend a major national meeting while enjoying all that New Orleans has to offer is ideal.

The scientific program, instructional courses, and categorical course are certain to be interesting and informative (see Table 1 for schedule).

Scientific Program

Two hundred scientific papers have been selected from more than 400 abstracts. Scientific sessions will be devoted to all major body systems, angiography, interventional techniques, sonography, and mammography, as well as technologies. Special emphasis has been placed on discussion of new developments.

The innovative and extremely well-received Friday morning minisymposium is entitled "Gastrointestinal Radiology Update 1989." An outstanding faculty has been assembled for what I am sure will be a very stimulating program.

Instructional Courses

Joseph T. Ferrucci, Chairman of the Instructional Course Committee, has put together 60 instructional courses. Faculty members have been drawn from across the entire country, with emphasis on luminaries from the South. A superlative educational experience is anticipated, and advance registration is recommended.

Categorical Course

An extraordinary categorical course on genitourinary imaging (uroradiology) has been fashioned. The course covers all aspects of the field, including equipment and principles of diagnosis. This course is certain to be popular, and advance registration is advised.

TABLE 1: Summary of 1989 American Roentgen Ray Society Meeting

Sunday May 7	Monday May 8	Tuesday May 9	Wednesday May 10	Thursday May 11	Friday May 12
	8-9:30 Instructional courses	8-9:30 Instructional courses	8-9:30 Instructional courses	8-9:30 Instructional courses	8-10 Symposium: gastrointestinal imaging update
9-noon Categorical course: genitourinary imaging	10-10:30 Opening cere- monies				
	10:30-12:30 Scientific programs	10-12:30 Scientific programs	10-12:30 Scientific programs	10-12:30 Scientific programs	10:30-12:30 Symposium: gastrointestinal imaging update
1:30-3 Categorical course: genitourinary imaging	1:30-3:30 Categorical course: genitourinary imaging	1:30-3:30 Scientific programs	1:30-3:30 Scientific programs	1:30-3:30 Scientific programs	
3:30-5:30 Categorical course: genitourinary imaging	4-5:30 Instructional courses and cate- gorical course: genitourinary imaging	4-5:30 Instructional courses and cate- gorical course: genitourinary imaging	4-5:30 Instructional courses and cate- gorical course: genitourinary imaging	4-5:30 Instructional courses and cate- gorical course: genitourinary imaging	

Scientific Exhibits

The 220 scientific exhibits coordinated by John Madewell will cover the entire breadth of the field of diagnostic radiology. The technical exhibits will be integrated among the scientific exhibits to enhance the interaction of the attendees with our technical exhibitors.

Caldwell Lecture

The Honorable William Bradley, senator from New Jersey, has agreed to present the Caldwell Lecture at the 1989 meeting. The title of Senator Bradley's presentation will be "Health Care Choices for the Nineties." This promises to be one of the highlights of the meeting.

Social Events

New Orleans offers an unlimited number of diversions, and Abner M. Landry, Jr., Chairman of the Local Arrangements Committee, has engaged Crescent City Consultants to plan a variety of outstanding tours. The annual golf and tennis tournaments for attendees and their companions are scheduled for Monday. The traditional cocktail party given by the society in the exhibit area for all registrants will be Tuesday evening and will provide a convenient meeting place before an evening on the town.

This promises to be a truly outstanding event in exceptional surroundings. I hope you will be able to accept our invitation. Plan now to attend.

Ronald G. Evens
President-Elect, ARRS

1989 American Roentgen Ray Society Section on Instruction: Courses and Symposium

Joseph T. Ferrucci, Director

Sixty instructional courses will be presented during the 89th annual meeting of the American Roentgen Ray Society (ARRS) beginning Monday, May 8, and continuing through Thursday, May 11. Each of the instructional courses will be 90 min long. In addition, there will be a week-long categorical course on genitourinary radiology and a half-day symposium on gastrointestinal imaging.

The categorical course in genitourinary imaging will have 14.5 hr of instruction and will begin on Sunday, May 7, and conclude on Thursday, May 11. The symposium on gastrointestinal imaging will be on Friday, May 12, from 8 a.m. to 12:15 p.m. All courses carry Category 1 credit on an hour-to-hour basis.

Registration Information

To register for courses, complete the meeting registration form in this section and mail promptly. Tickets will also be available at the Instruction Course Registration Desk, New Orleans Hilton, for courses that have not been sold out. All courses will take place in the headquarters' hotel.

After reviewing the course abstracts, select three for each day. List the course number and name of the first instructor on the registration form. Please note that the -01 residents'-masters' tutorials are intended primarily for residents and that attendance will be limited.

All who register for the categorical course in genitourinary imaging (including ARRS members) must pay a fee of \$75 and must take the entire series of classes. The categorical course totals 14.5 hr of instruction and includes a syllabus.

Course Schedule

Sunday, May 7, through Thursday, May 11

The categorical course in genitourinary imaging will have 14.5 hr of instruction over 5 days. Table 1 lists topics and instructors.

Monday, May 8, through Friday, May 12

A total of 60 courses will be offered (Table 2) plus a symposium on gastrointestinal radiology. Course abstracts and a list of faculty follow.

Monday, May 8

101. What's new in pediatric radiology: chest and gastrointestinal. Kirkpatrick JA, Singleton E. This presentation is mainly the result of the newer and more sophisticated methods of imaging that were not available a few years ago. The instructors of this course have had the experience of being trained in the older methods of chest and gastrointestinal imaging and have been compelled to learn and keep up with each succeeding imaging technique, including sonography, CT, and, now, MR. Although the diseases are the same, the imaging approach has changed. Accompanying this has been the obvious improvement in diagnosis, especially those conditions requiring surgical correction. Conventional chest radiographs and conventional contrast studies of the gastrointestinal tract remain basic, "first look," important examinations. Lesions involving the chest often require additional studies, especially CT, which add another dimension in anatomic location, differentiate between cystic and solid masses, and provide information on mediastinal masses and pleural lesions. The use of CT in neoplasms of the chest is extremely important. MR imaging may, under certain conditions, be helpful but should not be a part of the routine workup of chest abnormalities. Maternal sonographic studies have enabled prenatal diagnosis of gastrointestinal lesions, including congenital obstructive lesions and diaphragmatic hernias. The use of sonography in the evaluation of pyloric stenosis and air reduction of intussusception are now substitutes for barium studies in many institutions. CT also has been extremely useful in many abnormalities of the gastrointestinal tract. A discussion of the importance of these newer methods of imaging for pediatric chest and gastrointestinal lesions and a prediction of future advances in this field will be presented.

102. Vascular sonography. Gooding GAW. Duplex Doppler technology, including the introduction of color, enables the examiner to find a vessel rapidly, detect flow, and assess the velocity profile and the morphology of the vessel. This discussion will focus on practical applications of these techniques. (1) In the diagnosis of deep venous thrombosis of the lower extremities, a Doppler signal per se does not necessarily exclude the possibility of thrombosis. Ancillary abnormalities that occur with deep venous thrombosis include diminished or absent augmentation of the venous signal, an enlarged vein that fails to expand during the Valsalva maneuver, and lack of venous compressibility. These procedures are best performed on the iliac, common femoral, superficial and deep femoral, popliteal, and superficial saphenous veins. Venous sonography also can be used to evaluate obstruction of the superior vena cava. In the abdomen, it can be used in the evaluation of portal hypertension and renal vein thrombosis. (2) The primary use of duplex Doppler studies in arterial evaluation has been in the assessment of the carotid system. This evaluation de-

TABLE 1: Categorical Course on Uroradiology

Day/Time	Topic (Presenter)
Sunday, May 7	Contrast Media/Infection/Renal Masses (Moderators: Pollack [a.m.] and Mellins [p.m.])
10:00–10:10 a.m.	Welcome and Introduction
10:10–10:50 a.m.	Contrast media. Comparison of ionic and nonionic agents: pharmacology, physiology, and guidelines for practical usage (Katzberg)
10:50–11:30 a.m.	Toxicity and reactions to contrast media (Pfister)
11:30–Noon	Evaluation of the azotemic patient (Talner)
Break	
1:30–2:15 p.m.	Acute renal infections (McClennan)
2:15–3:00 p.m.	Chronic renal infections (Kenny)
Break	
3:30–4:15 p.m.	Cystic diseases of the kidney (Hartman)
4:15–5:00 p.m.	Neoplasms of the kidney (Stanley)
Monday, May 8	Prostate/Bladder/Scrotum (Moderator: Davidson)
1:30–2:15 p.m.	Imaging of the urinary bladder (Hattery)
2:15–2:45 p.m.	Epidemiology and natural history of carcinoma of the prostate (Amis)
2:45–3:15 p.m.	Ultrasonography of the prostate (Rifkin)
Break	
3:45–4:15 p.m.	CT and MRI of the prostate (Hricak)
4:15–5:00 p.m.	Imaging of the scrotum (Rosenfield)
Tuesday, May 9	Stone Disease (Moderator: Newhouse)
3:30–4:05 p.m.	Radiological aspects of urolithiasis (Bush)
4:05–4:40 p.m.	Extracorporeal stone therapy (ESWL) (LeRoy)
4:40–5:15 p.m.	Interventional Procedures in Urolithiasis (Banner)
Wednesday, May 10	Impotence and Erectile Insufficiency (Moderator: Lang)
3:30–4:00 p.m.	Pathology and physiology of impotence (Goldstein)
4:00–4:45 p.m.	Radiology of impotence (Bookstein)
4:45–5:15 p.m.	Radiology of penile prostheses (Cohan)
Thursday, May 11	Retroperitoneum (Moderator: Hartman)
3:30–4:05 p.m.	Adrenal imaging (Dunnick)
4:05–4:40 p.m.	Perinephric disease (Levine)
4:40–5:15 p.m.	Retroperitoneal disease (Lee)

depends on characterization of visible plaque (homogeneous, inhomogeneous, ulcerated, hemorrhagic) and on Doppler characteristics (e.g., waveform, velocities). This is an extremely accurate technique that is best used as a screening device to select those patients who then may be candidates for angiography. Duplex Doppler studies also can be used in the evaluation of abdominal arteries. The most common application in this area is assessment of renal transplants.

103. Fetal measurements for estimating age and fetal growth. Hadlock FP. Fetal sonography has become almost routine practice in clinical obstetrics. The most important components of such an examination are an anatomic survey and a biometric evaluation of fetal age and/or growth. In this session, I will focus on assessment of fetal age by both quantitative and qualitative methods; emphasis

will be on the use of the multiple-parameter approach, including what role the newer measurements (e.g., foot length) may play. I will also describe methods for analyzing the appropriateness of fetal growth and for predicting term birth weight from early third-trimester examinations.

104. Some thoughts on the functional aspects of a radiology department. Janower ML. The goal of every hospital radiology department is to provide optimal radiologic services at reasonable costs. In order to achieve this objective, every effort must be made to organize the department properly to ensure maximal use of increasingly limited resources. This talk will explore many of the basic principles pertaining to the organizational aspects of the department. Topics to be covered will include scheduling and performance of the examination, interpretation of films, operation of the file room, and production of the radiologic report. Determination of the appropriate number of personnel, the status of radiology information systems, and the potential usefulness of picture archiving and retrieval will also be discussed.

105. MR of the head and neck. Bryan N, Zinreich SJ. Excellent soft-tissue discrimination and the multiplanar capability of MR result in numerous applications in imaging of the head and neck. However, because of differences in the types of soft tissue, the complex intermix of air and bone compartments, and unique aspects of motion, MR techniques specifically designed for this anatomic region should be considered. With appropriate MR pulse sequences, anatomic detail such as the pharyngeal fascia and pathologic abnormalities such as tongue base neoplasia can be evaluated as never before. This course is intended to review MR techniques optimized for the head and neck, to demonstrate anatomically unique capabilities of MR, and to show pathologic conditions best evaluated by MR. Specific anatomic regions to be considered include the nose and paranasal sinuses, pharynx, oral cavity, larynx, and other soft-tissue structures of the neck.

106. Gallbladder imaging: 1989. Leopold GR, Amberg JR. Biliary lithotripsy is stimulating renewed interest in gallbladder imaging. Although in recent years sonography has assumed a dominant role in the detection of stones, oral cholecystography seems to be making a comeback. In terms of absolute detection of calculi, it is clear that sonography has the advantage. If the consideration is accurate portrayal of stone number and size, then oral cholecystography seems better. Other considerations are the prospect of serial studies and the relative costs of the two procedures. To further confuse matters, commercially available lithotripsy units have different ways (X-ray, sonography) of localizing stones. This course will attempt to explore the interrelationships between all available methods, placing in perspective the role of each in diagnosing a broad spectrum of gallbladder disease.

107. Imaging in thoracoabdominal trauma: a review and update. Mirvis SE, Foley WD. Thoracoabdominal trauma is the major cause of death among young adults in the United States. Prompt recognition of potentially life-threatening injuries is crucial to optimize patient management. This instructional course will review the major diagnostic features of injuries commonly encountered in blunt thoracoabdominal trauma. The section on blunt thoracic trauma will review the various radiographic appearances of pneumothoraces, pneumomediastinum, pneumopericardium, hemomediastinum, pulmonary contusion and laceration, chest wall injuries, diaphragmatic rupture, and esophageal and tracheal disruption. The potential applications of CT to the diagnosis of both initial injury and delayed complications of

TABLE 2: American Roentgen Ray Society Instructional Courses: May 8–May 11, 1989

Topic	Monday	Tuesday	Wednesday	Thursday
Morning (all sessions begin at 8 a.m.)				
Residents'-masters' tutorial: up close & personal	101. What's new in pediatric radiology: chest and gastrointestinal. <i>Kirkpatrick, Singleton</i>	201. The analytic approach to the film (an imaging discipline). <i>Edeiken, Jacobson</i>	301. Old masters. <i>Reeder</i>	401. Interventional uro radiology. <i>Lang</i>
Vascular	102. Vascular sonography. <i>Gooding</i>	202. Angiography of the extremities. <i>Crummy, McDermott</i>	302. Deep venous thrombosis: sonographic diagnosis and treatment by inferior vena caval filter. <i>Cronan, Dorfman</i>	402. Duplex and color-flow Doppler imaging of the abdomen, pelvis, and extremities. <i>Merritt</i>
Pediatrics and obstetrics	103. Fetal measurements for estimating age and fetal growth. <i>Hadlock</i>	203. Obstetric sonography and the detection of fetal anomalies. <i>Callen, Manco-Johnson</i>	303. Tumors and tumorous lesions of the kidney in infant and child. <i>Rabinowitz</i>	403. Pediatric body MR imaging: fact or fantasy. <i>Bisset, Kirks</i>
Nuclear medicine/radiologic practice	104. Some thoughts on the functional aspects of a radiology department. <i>Janower</i>	204. Nuclear cardiology in clinical practice. <i>Thrall</i>	304. Legal aspects of radiologic practice. <i>Reuter</i>	404. SPECT imaging in clinical nuclear medicine. <i>Handmaker, Bunker</i>
Neuroimaging I	105. MR of the head and neck. <i>Bryan, Zinreich</i>	205. Supratentorial tumors. <i>Davis</i>	305. Intraoperative neurosonography. <i>Quencer</i>	405. Craniocerebral trauma. <i>Kieffer, Cacayorin</i>
Gastrointestinal	106. Gallbladder imaging: 1989. <i>Leopold, Amberg</i>	206. CT and sonography of acute gastrointestinal lesions. <i>Jeffrey, Megibow</i>	306. CT-sonography-guided biopsies: practical approaches, pitfalls, and new techniques. <i>Charboneau, Reading</i>	406. Pattern approach to gastrointestinal radiology. <i>Eisenberg</i>
Thorax and Abdomen	107. Imaging in thoracoabdominal trauma: a review and update. <i>Mirvis, Foley</i>	207. Diagnostic imaging techniques in the clinical management of metastatic disease. <i>Steckel, Kagan</i>	307. Radiographic manifestations of chronic obstructive pulmonary disease. <i>Stark</i>	407. Complications of IV drug abuse: hits, blows, and stuff for the nose. <i>McCarroll, Roszler</i>
Skeletal	108. Imaging the knee: current status. <i>Totty, Wilson</i>	208. The radiology of vertebral trauma. <i>Daffner</i>	308. Imaging the acutely injured cervical spine. <i>Swischuk, Harris</i>	408. Needle biopsy of the musculoskeletal system. <i>Rosenthal</i>
Sonography	109. Sonographic imaging equipment. <i>Goldstein</i>	209. Sonography image interpretation: is it real or is it an artifact? <i>Cooperberg</i>	309. Endoluminal sonography: transvaginal and transrectal. <i>Bree, Madrazo</i>	409. Sonography of the rotator cuff and of the infant's hip. <i>Crass, Harcke</i>
Chest	110. CT of the mediastinum with MR correlation. <i>Sagel, Glazer</i>	210. Practical approach to intensive-care chest radiology. <i>Spirn, Goodman</i>	310. MR imaging of the thorax. <i>McLoud, Drucker</i>	410. Lung tumor staging. <i>Zerhouni, Pugatch</i>
Afternoon (all sessions begin at 4 p.m.)				
Neuroimaging II	111. Use of gadolinium in imaging brain lesions. <i>Hasso</i>	211. CT of disk diseases and spinal stenosis. <i>Helms</i>	311. Imaging of intracranial neoplasms. <i>Hesselink, Press</i>	411. The radiologic evaluation of paranasal sinus disease and facial trauma: conventional films, CT, and MR. <i>Weber</i>
Magnetic resonance	112. MR of the retroperitoneum, kidneys, adrenals, and pelvis. <i>Fritzsche, Weinreb</i>	212. Abdominal MR. <i>Nelson, Chezmar, Bernardino</i>	312. Technical advances in clinical MR: contrast agents, fast scanning, surface coils. <i>Saini, Edelman, Kneeland</i>	412. Practical aspects of MR image interpretation. <i>Bradley, Stark</i>
New technology	113. Shock-wave lithotripsy. <i>Ferrucci</i>	213. PET scanning. <i>Hubner, Besozzi, Buonocore</i>	313. Percutaneous laser angioplasty. <i>McCowan, Casteñeda-Zúñiga, Ferris</i>	413. Computer-assisted three-dimensional imaging: state of the art. <i>Fishman, Ney</i>
Breast	114. Analyzing the mammogram. <i>Kopans</i>	214. Screening mammography: rationale, implementation, economics, and malpractice consideration. <i>Sickles</i>	314. Film mammography: current practices and results. <i>Gisvold</i>	414. Screen-film mammography: equipment, technique, and interpretation. <i>Feig</i>
Interventional	115. Sedation and pain control for radiologists. <i>Lieberman, Neff</i>	215. Interventional radiology in the biliary tract: from drainage to lithotripsy. <i>Casarella, Kaufman, Torres</i>	315. Radiologic aspects of liver transplantation. <i>Campbell, Zajko</i>	415. Angioplasty: 1989. <i>Waltman, Levin</i>

thoracic trauma, such as empyema and adult respiratory distress syndrome, will be discussed. The series on abdominal trauma will focus on the role of CT in the initial and serial evaluation of blunt injury to the liver, spleen, pancreas, kidneys, mesentery, and bowel. The role of angiography in hepatic, renal, and pelvic injury and in treatment of delayed bleeding as well as the role of urography and cystography will be discussed.

108. Imaging the knee: current status. Totty WG, Wilson AJ. Changing technology provides new methods for looking at old problems. The recent development of MR imaging is changing the way in which abnormalities of the knee are evaluated. MR has provided us with a noninvasive method to directly image many structures that were invisible to older methods, were seen indirectly, or required invasive techniques. This course will review the major methods for imaging the knee, including conventional radiology and tomography, arthrography, CT, scintigraphy, and MR. Each imaging method will be explored to discover its strengths and weaknesses. The place of each technique in a cost-effective and complete workup of disease will be evaluated. Injuries to both the bony and the soft-tissue elements of the knee will be discussed, along with arthritis, tumors, and osteochondroses. The contribution of each technique to the evaluation of each disorder will be illustrated. An evaluation scheme based on the patient's clinical picture and the information provided by each imaging technique will be developed.

109. Sonographic imaging equipment. Goldstein A. The purpose of this course is to keep radiologists current in all of the latest technical advances in sonography. It is designed to be useful to both experienced and inexperienced users. The latest types of sonographic imaging equipment will be presented, along with typical clinical images, and discussed in terms of operational principles and clinical usefulness. Detailed criteria will be presented to aid in the cost-effective purchase of sonographic imaging equipment. These criteria will be available as a handout to the attendees. Those techniques for assessment of image quality that have been found effective in evaluation of equipment by clinical personnel will be presented and will be illustrated by clinical scans.

110. CT of the mediastinum with MR correlation. Sagel SS, Glazer HS. CT has evolved as the method of choice for performing tomography in patients with known or suspected mediastinal abnormalities. This course will emphasize the vital role of CT in the detection, characterization, and determination of disease extent. Proper technique, including the use of IV contrast media and dynamic scanning, and the criteria used to diagnose pathologic alteration will be discussed and illustrated. The clinical indications for applying CT will be reviewed, with emphasis on delineation and diagnosis of mediastinal lymphadenopathy, benign and malignant masses, thoracic aortic abnormalities and anomalies, and thymic lesions. Common problems in differential diagnosis and potential sources of interpretative error will be addressed. The current role of MR imaging in the evaluation of mediastinal masses and vascular abnormalities will be described, and the advantages and limitations of both CT and MR will be stressed.

111. The use of gadolinium in imaging brain lesions. Hasso AN. The U.S. Food and Drug Administration recently approved the use of Magnevist (gadopentetate dimeglumine) brand of gadolinium-DTPA. Magnevist is a chelated paramagnetic agent that enhances MR images by causing a decrease in the T1 and T2 relaxation times. The

magnetic moment produced by Magnevist results in a relatively large local magnetic field, which enhances the relaxation rates of water protons in the vicinity of the paramagnetic agent. The ideal dose of contrast medium depends on body weight and is given according to a sliding scale, not to exceed 20 ml. The injection of contrast medium is followed by a 5-ml normal saline flush. The MR imaging should be completed within 1 hr of injection of the agent. Magnevist does not pass through an intact blood-brain barrier but will pass through the capillary and endothelial cells whenever damage caused by injury, tumor, infection, or infarction exists. This presentation will outline the use of gadolinium in imaging lesions of the CNS. Brain neoplasms, including intra- and extraaxial and metastatic tumors will be shown. The use of gadolinium in cases of meningitis, encephalitis, granulomatous infections, and abscess formation will also be presented. Other occasional uses of gadolinium in demyelinating diseases, subacute infarctions, and traumatic or radiation injuries will be discussed.

112. MR of the retroperitoneum, kidneys, adrenals, and pelvis. Fritzsche PJ, Weinreb J. Continuing improvements in image quality and sequence flexibility have increased confidence in using MR for evaluating the retroperitoneum, kidneys, adrenals, and pelvis. The availability of fast imaging with gradient echos has provided additional information in the evaluation of both vascular flow and hemorrhage. In evaluation of the retroperitoneum, kidneys, and adrenals, MR is used as a problem-solving technique when other imaging techniques are equivocal or when use of iodinated contrast medium is contraindicated. MR can detect renal masses greater than 3 cm in diameter, but it is better suited to characterization of masses and staging of malignancy. The advantages of MR in staging of renal and adrenal neoplasms include demonstration of tumor origin and local extension, evaluation of vascular patency, and determination of metastatic lymphadenopathy. In evaluation of the female and male pelvis, MR appears to be more useful for staging than for diagnosis of pelvic neoplasms. In endometrial malignancy, MR can assess extension into the myometrium and parametrium, assess uterine leiomyomas, and differentiate between uterine and adnexal masses. In cervical carcinoma, MR is used for tumor localization and assessment of local spread. Recurrent tumors and fibrosis in patients who have undergone pelvic surgery or radiation often can be distinguished. MR is more useful than CT for staging of prostate tumors as it can be used to evaluate periprostic extension of tumor, extension into the bladder base, and seminal vesicles.

113. Shock-wave lithotripsy. Ferrucci JT. This course will discuss technical and clinical issues relating to shock-wave lithotripsy, especially biliary tract applications. Shock waves are high-pressure waves that can pass through tissues without causing damage and that undergo focusing at a remote site to produce a localized high-pressure zone for the therapeutic fragmentation effects. Clinical lithotripters produce shock waves by three different principles: spark gap, electromagnetic, and piezoelectric. Significant differences in pressures achieved, the size of the focal zone, and the amount of pain and tissue damage produced exist among these approaches. Different manufacturers' design solutions for second-generation lithotripter technology will be discussed, including the type of focusing device, image localization, and provision for ancillary radiographic procedures. All commercial lithotripter systems will be capable of treating both gallbladder and urinary calculi. The second portion of the course will be devoted to clinical biliary lithotripsy and related techniques for chemical litholytic adjuvant therapy of cholesterol gallstones. Fragmentation rates of different manufacturers will be compared, the rationale and results of drug adjuvant therapy will be detailed, and considerations for pretreatment imaging of gallstones will be discussed.

114. Analyzing the mammogram. Kopans DB. Because there is a clear benefit to finding small, clinically occult breast cancers, high-quality mammography is necessary to permit their earlier detection. The ultimate decision in mammographic interpretation is whether to perform a biopsy. The marked variation of normal and benign morphology and the overlap with malignant morphology present a broad array of interpretative enigmas for the radiologist. Many of these can be solved by an organized approach to breast imaging, with attention to the morphologic reflection of the cellular processes involved. A practical approach to mammographic analysis will be presented, including a simple, accurate, structured imaging report. The discussion will outline techniques for problem solving and will address the keys to guide follow-up studies, aspiration, and biopsy.

115. Sedation and pain control for radiologists. Lieberman RP, Neff C. Expert use of sedative and local anesthetic drugs greatly facilitates many radiologic procedures, especially angiography, interventional procedures, pediatric CT, and MR. This session will address many issues related to sedation and pain control: the importance of the preprocedure visit, choices of benzodiazepine and narcotic drugs, oral premedication, use of IV drugs, sedative regimens for children, and treatment of benzodiazepine and narcotic drug overdoses, including the use of specific antagonists. Throughout our discussion, we will stress safety and appropriate monitoring. We will also cover short- and long-acting local anesthetic drugs, including toxicity, allergy, and alternatives to the "caine" anesthetics; techniques of local anesthesia; celiac plexus block; ankle block for venography; and pericatheter injection for pain relief after biliary drainage.

Tuesday, May 9

201. The analytic approach to the film (an imaging discipline). Edeiken J, Jacobson HG. Diagnostic radiology is an imaging discipline that reflects with considerable accuracy gross pathologic changes that are transmitted through the image techniques used by the radiologist. In the "approach to the film," a series of diagnostic parameters are considered in an organized fashion. Such an orderly evaluation generally permits an intelligent perusal of the findings in a given case and often results in a correct diagnosis, even in difficult cases. This approach implies adoption of the concept that the film speaks a basic language and that the radiologist functions as an interpreter of that language. If the language is understood, the interpretation should be accurate. This instructional course is planned to evaluate a number of cases of skeletal abnormalities representative of different subcategories (e.g., trauma, infection, neoplasm). In this connection, it will also be stressed that because different types of benign disease may simulate malignant disorders, it is extremely important for the radiologist to recognize the subtle signs that distinguish the pseudomalignant pattern of a benign disorder from a true malignancy. It is hoped that residents in the group will volunteer to demonstrate the process of applying analytic techniques by using the various parameters selected.

202. Angiography of the extremities. Crummy AB, McDermott JC. Angiography of the extremities is the most common contrast-enhanced vascular examination performed by radiologists. The particular requirements of percutaneous transluminal angioplasty, especially distal to the knee; of vascular bypasses to the tibial arteries; and of venograms to assess problems related to Hickman and other venous infusion catheters have appreciably changed the performance of these studies. We will present our techniques for arteriography

and venography of the extremities and the use of these techniques in the diagnosis of various conditions. Technical considerations will include (1) selection of entry site; (2) catheters and special guidewires; (3) filming sequences; (4) method of recording (conventional films or digital subtraction angiography); and (5) augmentation of flow by exercise, ischemia, or drugs. The use of roadmapping techniques as an aid for the puncture of vessels with poor or absent pulsations, for selective catheterization, and for the placement of balloons for transluminal angioplasty will be discussed. A regimen including hydration and use of dopamine to reduce the risk of renal failure in diabetics or other patients with elevated creatinine levels will be outlined. The increasing interest in the surgical correction of venous insufficiency due to incompetent venous valves has led to wider use of retrograde venography of the lower extremities. The technique and interpretation of retrograde venography will be covered.

203. Obstetric sonography and the detection of fetal anomalies.

Callen P, Manco-Johnson ML. Guidelines for antepartum obstetric sonography have been approved by the American College of Radiology and the American Institute of Ultrasound in Medicine since 1985, and one of these guidelines deals with the evaluation of fetal anatomy. Six anatomic locations should be examined: the cerebral ventricles, spine, stomach, urinary bladder, umbilical cord insertion site on the fetus, and the renal region. It is apparent, therefore, that the antenatal diagnosis of fetal intracranial abnormalities, renal abnormalities, and spinal abnormalities is an expected and essential part of the obstetric sonographic examination. Visualization of the fetal kidneys should be possible by the 18th week of gestation, and their size can be compared with graphs that give normal values for various gestational ages. Fetal hydronephrosis is common, and the level of obstruction can often be determined by careful sonographic examination. Cystic diseases of the kidney are the next most common; they can be divided into four groups: (1) infantile polycystic kidney disease, (2) multicystic dysplastic kidney, (3) adult polycystic kidney disease, and (4) cystic dysplasia. These lesions can be differentiated sonographically. The fetal cerebral ventricles can be visualized as early as 12–14 weeks menstrual age, and ventricular enlargement can be diagnosed confidently as early as 18–20 weeks. An accurate diagnosis can often be made in such conditions as hydrocephalus, agenesis of the corpus callosum, Dandy-Walker cyst, alobar holoprosencephaly, schizencephaly, intracranial hemorrhage, intracranial teratomas, and anencephaly. The evaluation of the fetal spine is extremely important. Detection of meningomyelocele can be quite difficult because of the potentially small size of the lesion. Careful transverse scanning through each vertebral body and posterior elements is necessary, with adequate visualization of the skin, soft tissues, and ossification centers of the posterior arches. If time allows, a basic approach to skeletal dysplasias and the four-chamber cardiac view will also be discussed.

204. Nuclear cardiology in clinical practice. Thrall JH. Nuclear cardiology embraces multiple imaging procedures aimed at diagnosing cardiac disease and monitoring heart function. In current practice, three major procedures encompass the majority of clinical applications: the ^{99m}Tc -pyrophosphate infarct-avid scan, the thallium-201 myocardial perfusion scan, and the radionuclide ventriculogram or radioangiocardigram. In this session, the rationale, basic technique, clinical application, and accuracy of the respective procedures will be presented. Applications in the evaluation of patients with coronary heart disease will be emphasized. A strategy for selection of patients for each of the respective procedures will be presented within the framework of an analysis of the efficacy of the procedures. In addition to the clinically well-established techniques, a number of newer methods of imaging the heart, including positron-emission tomogra-

phy (PET) will be briefly presented, with emphasis on rationale, information available, and potential for clinical use in the near future.

205. Supratentorial Tumors. Davis DO.

Extra-axial: meningioma and malignant meningioma.

Intra-axial: astrocytoma (low grade [grade 1], anaplastic [grade 2], and glioblastoma multiforme [grades 3-4]); lymphoma; metastases; and other.

Detection: nonspecific high signal on long TR-TE images, with/without masses.

Analysis: location, relationship to outer cortical surface and bone, grading of astrocytomas with gadolinium, inflammatory vs lymphoma, and stroke vs tumor.

Postoperative change: radiation/postchemotherapeutic changes and other diagnostic considerations.

206. CT and sonography of acute gastrointestinal lesions. Jeffrey RB, Megibow AJ. This course will focus on the unique contribution of noninvasive imaging with CT and sonography in the diagnosis of a variety of acute gastrointestinal disorders. Topics to be covered include acute appendicitis, small bowel and colonic ischemia, obstruction, blunt trauma to the bowel, diverticulitis, and colitis. Strengths and weaknesses of CT and sonography will be discussed as well as use of imaging to guide appropriate interventional procedures.

207. Diagnostic imaging techniques in the clinical management of metastatic disease. Steckel RJ, Kagan AR. Diagnostic imaging techniques are critical for evaluating the possibility of metastatic disease, either as screening procedures in patients who have newly diagnosed malignancies or as diagnostic procedures when other findings suggest the presence of metastasis. The initial treatment and the prognosis will often depend on one or more imaging examinations to evaluate the possibility of metastases. After diagnosis, imaging of metastatic lesions can be used to determine progression or response to treatment. Therefore, the appropriate integration of diagnostic imaging techniques and clinical management is a therapeutic necessity. CT and MR provide new opportunities in this regard when combined with sonography and standard radiographic and nuclear medicine techniques. The appropriate workups for metastatic disease will be discussed for several common malignancies and for various metastatic sites. Case problems illustrating the use of imaging techniques in reaching decisions about clinical management will also be presented and will be discussed with course participants.

208. The radiology of vertebral trauma. Daffner RH. Trauma to the vertebral skeletal column is one of the most common injuries encountered in the daily practice of radiology. The prompt assessment of bone and soft-tissue abnormalities in the patient who has a spinal injury is of paramount importance in stabilizing any existing neurologic abnormalities and in preventing additional ones. Furthermore, the inherent stability of the injured vertebral column must be assessed to determine the need for surgical intervention and restoration of normal function. This course will be in four parts. Part 1, technique, will discuss plain-film, CT, and MR imaging as they apply to the evaluation of the patient who has a spinal injury. Part 2, "fingerprints" of vertebral injuries, revolves around a mechanistic classification of injuries broken into four categories: flexion, extension, shearing, and rotation. The distinct radiographic findings or fingerprints of each type of injury will be discussed. Part 3, the ABCs of vertebral trauma, will discuss the overall radiologic approach to these injuries in regard to abnormalities

of alignment, bony integrity, cartilage or joint space, and soft tissue. Finally, Part 4, the radiologic assessment of vertebral stability, will define stable and unstable injuries and will discuss the five main parameters that are used to determine the presence of an unstable lesion.

209. Sonographic interpretation: is it real or is it an artifact?

Cooperberg PL. Most general sonologists do not need to understand all of the physics involved in the production of sonographic images. However, many types of artifacts that are not related to anatomic structures within the body can appear on sonographic images. It is important to understand the underlying physical principles to appreciate the causes of these artifacts and to be able to differentiate spurious echoes from real pathologic changes. Among the types of artifacts to be described, displayed, and explained are reverberation artifacts, ring-down artifacts, off-axis artifacts, and the various kinds of acoustic shadowing. Although a review of these types of pitfalls in sonographic diagnosis may suggest that diagnoses never can be made, these difficulties arise only rarely, and most of the time clinically useful diagnoses are possible.

210. A practical approach to intensive-care chest radiology. Spirn PW, Goodman LR. Whether working in tertiary-care facilities or community hospitals, today's radiologists are called on to provide an ever-increasing proportion of their services to critically ill patients. The lion's share of this is chest radiology in intensive care units. This presentation will suggest practical strategies for dealing with the technical, logistic, and diagnostic problems encountered in providing effective intensive-care radiology. Topics to be discussed include optimizing the image, organizing film handling and review, evaluating support and monitoring devices, differentiating among cardiopulmonary abnormalities, augmenting the chest film with other imaging studies, and future trends in intensive-care radiology.

211. CT of disk disease and spinal stenosis. Helms CA. CT examination of the lumbar spine for diagnosis of disk disease, spinal stenosis, or both has replaced myelography as the procedure of choice in most institutions. This is appropriate only if high-quality imaging is used and sound diagnostic principles are followed. This instructional course will review the appropriate scanning protocols and the diagnostic capabilities and limitations that can be expected with CT scanning of the lumbar space. Pitfalls in diagnosis of disk disease will be addressed. Spinal stenosis will be discussed in categories of central canal, lateral recess, and neuroforaminal involvement. MR imaging and myelographic enhanced CT will be mentioned as alternatives to plain CT scanning, and the diagnostic accuracy of the techniques will be discussed. Use of CT in evaluating patients for surgery, treatment with chymopapain, and percutaneous nucleotomy will be discussed also.

212. Abdominal MR. Nelson RC, Chezmar JL, Barnardino ME. This course will describe state-of-the-art MR techniques for imaging the upper abdomen at both low and high magnetic field strengths. Four organs will be discussed in detail: liver, pancreas, adrenals, and kidneys. Techniques to be discussed include (1) strategies for suppressing motion artifacts, for minimizing scan times, and for optimizing detection of focal lesions; (2) use of routine spin-echo and inversion-recovery sequences and applications of gradient-echo and chemical-shift imaging; and (3) the role of paramagnetic contrast agents. Specific clinical issues to be presented include tissue characterization of focal hepatic and adrenal masses, staging of renal tumors, and morphologic and parenchymal changes in diffuse disease

processes, such as cirrhosis and hemochromatosis. The strengths and weaknesses of MR and other techniques will be emphasized to determine the best methods for imaging the abdomen in 1989.

213. PET scanning. Hubner KF, Besozzi MC, Buonocore E. PET is the only technique that makes it possible to measure regional metabolic and biochemical processes in the living heart, the brain, and other tissues, including neoplasms. Until recently, PET remained in the realm of scientific adventure, but now it is on the threshold of becoming a routine diagnostic tool in modern medicine. Ischemic heart disease, the chemistry and metabolic activity of a multitude of neurologic disorders, and cancer can now be examined by PET in a clinical rather than a research setting. The short-lived cyclotron products needed for PET have necessitated considerable investment in space, hardware, laboratory facilities, and sophisticated personnel. The development of smaller cyclotrons and automated methods of synthesis have reduced cost and promise to bring PET closer to clinical reality. This course will cover the basic physical and chemical principles and techniques of PET and will deal with newer commercial approaches to solve basic problems. The logistics and practical details involved in establishing a clinical PET center will be presented. The course should meet the needs of radiologists, cardiologists, neurologists, and nuclear medicine physicians. Specific clinical applications of PET will be discussed and should be of interest not only to clinicians but also to researchers interested in PET applications in biomedical research.

214. Screening mammography: rationale, implementation, economics, and malpractice considerations. Sickles EA. Mammographic screening for breast cancer is being done with increasing frequency. Growing numbers of radiologists are interpreting more and more such examinations. This course will supply practical suggestions on how to improve the efficiency of screening operations and also will provide sufficient background information for educating referring physicians and patients on the life-saving potential of breast cancer screening. I will begin by discussing the most important evidence supporting the practice of screening mammography and by answering the most common criticisms levied against it. Next, I will cover the key aspects of screening practice, including equipment selection, siting considerations, imaging and operational procedures, interpretation, and reporting. The aim will be to emphasize techniques that produce high-quality examinations in the most cost-efficient manner. I will conclude by discussing the increasing role that industry and insurance companies will play in supporting screening mammography, legislative efforts to broaden health care coverage for screening, and concerns about increased malpractice exposure resulting from reading evergrowing numbers of examinations and from accepting women into screening programs without referrals.

215. Interventional radiology in the biliary tract: from drainage to lithotripsy. Casarella WJ, Kaufman SL, Torres WE. Interventional radiology of the biliary tract will be discussed in three separate segments. The first will focus on technical considerations, complications, and expected results of biliary drainage procedures. Derivatives of biliary drainage, such as transluminal dilatation of bile duct strictures, biopsies, and dissolution and extraction of stones, will be included in the second part. Pitfalls in the application of the technique will be emphasized. The radiologist's involvement in removal of biliary stones will be summarized. The technique and results of stone extraction percutaneously as well as through T-tube tracts will be discussed. The principles and practice of extracorporeal biliary lithotripsy and the organizational problems in managing a biliary lithotripsy center are the subjects of the third part of the course.

Wednesday, May 10

301. Old masters. Reeder M. This instructional course for residents and other interested participants is specifically designed to review important diagnostic signs, patterns, and differential diagnosis in chest and skeletal radiology. Emphasis will be placed on accurate analysis of radiographs to ferret out all of the intrinsic clues and data on the film and arrive at a specific radiographic pattern, then reviewing the differential diagnosis or "gamut" for that pattern, and, finally, triangulating to the most likely diagnosis by virtue of known clinical and laboratory information about the patient. Important signs of alveolar vs interstitial diseases, lobar collapse, the silhouette sign, and other clues referable to pulmonary disease will be stressed. In the skeletal system, analysis of the various destructive patterns within bone, the significance of various periosteal reactions, patterns of sclerosis, and matrix production will be emphasized, and appropriate gamuts will be reviewed for each pattern. It is hoped the resident will learn how senior radiologists use an understanding of these signs and patterns to arrive at the most likely diagnosis in routine as well as atypical cases, especially because pulmonary and skeletal radiology still account for more than 50% of all radiographic examinations, even in this era of advanced technology.

302. Deep venous thrombosis: sonographic diagnosis and treatment by inferior vena caval filter. Cronan JJ, Dorfman GS. Deep venous thrombosis (DVT) affects nearly 20 million patients per year in the United States. Up to 600,000 cases of pulmonary embolism also occur. Sonography of the lower extremities is an accepted technique to evaluate for DVT. It has been rigorously evaluated in many controlled series and has been shown to function effectively in the clinical setting. Sonography involving both compression and Doppler techniques will be evaluated. Sonographic parameters for diagnosing acute DVT will be discussed, as well as potential problems with chronic changes that may mimic acute DVT. A historical view of techniques used for the diagnosis of DVT will be included for completeness. The treatment of DVT is not without consequence. Anticoagulation is associated with morbidity in 15–30% of cases. Inadequate treatment is responsible for pulmonary emboli. Nonpharmacologic control of DVT by means of the percutaneous filter will be emphasized. Indications for caval interruption will be discussed. The technique of placement, the consequences of placement, and the anticipated success rate will be discussed. We will emphasize the venous insertion site and our assessment that insertion is relatively innocuous. We will review the newest filter devices that will soon be marketed. The presentation will use videotapes and slides of duplex sonographic examinations of veins, as well as videotapes of caval filter placement, to demonstrate actual how-to-do-it techniques.

303. Tumors and tumorous lesions of the kidney in infant and child. Rabinowitz JG. This course will analyze all of the mass lesions involving the kidney and surrounding structures that occur in the newborn and infant. Detailed discussion will be given to the pathology, pathogenesis, embryology, and differential diagnosis of these lesions. The radiographic evaluation will proceed along two parallel planes: the "old" and the "new." The old approach will show the features seen with conventional radiography, and the new approach will show the features seen by the newer imaging techniques. Particular stress will be given to the differential diagnosis of certain lesions (e.g., congenital hydronephrosis and multicystic dysplastic kidney, Wilms tumor, neuroblastoma). The major features of other important conditions, such as polycystic kidneys, neonatal adrenal hemorrhage, duplication, mesoblastic nephroma, nephroblastomatosis as related to Wilms tumor, and many other lesions will also be discussed in detail.

304. Legal aspects of radiologic practice. Reuter SR. The number of law suits against radiologists has increased progressively in recent years, and we are now number three behind surgeons and obstetricians in frequency of being sued. Suits can generally be divided into failure to diagnose, procedure-related injuries, slips and falls, and administrative misadventures. These causes of suits will be discussed in a risk-management approach, along with such current legal issues as consent for IV injections of contrast agents and the use of ionic and nonionic contrast medium. Courts are increasingly finding a duty on the part of the radiologist to ensure that abnormal radiologic findings are transmitted effectively to the referring physicians, and these cases will be discussed. Finally, some of the legal aspects relating to "turf" issues of radiologists, including the liability of non-radiologists who practice radiology, and some of the legal issues relating to expert witnesses in suits against radiologists will be discussed.

305. Intraoperative neurosonography. Quencer RM. Real-time sonography during neurosurgical procedures involving the brain and spine has a significant impact on operative management and the patient's outcome in a wide range of diseases. This presentation will include (1) a discussion of the techniques involved in intraoperative neurosonography; (2) a description of the normal sonographic anatomy of the spine, spinal cord, and brain; and (3) a demonstration of the practical importance of sonography in neoplastic, developmental, degenerative, inflammatory, and traumatic abnormalities of the CNS. Emphasis will also be placed on correlating the preoperative MR and CT studies with the surgical findings and showing how, in a step-by-step manner, sonography helps to direct and focus the surgical procedure. Directing tissue biopsies of the brain and cord, assuring proper placement of shunt catheters in hydrocephalic ventricles and in syringohydromyelic cavities, assessing the effect of procedures designed to decompress bone and disk material from cord tissue and nerve roots in both trauma and nontraumatic diseases (disk herniation, spondylosis), and directing the surgery in various spinal dysraphic states are among the many uses of intraoperative sonography that will be presented.

306. CT- and US-guided biopsies: practical approaches, pitfalls, and new techniques. Charboneau JW, Reading CC. The technique of percutaneous CT- or US-guided needle biopsy has emerged as one of the significant advances in radiology in the past decade. It is now a widely accepted, safe, and accurate technique for evaluating suspected malignant masses. Today, improved accuracy is possible because of several factors, including (1) use of larger bore (16–19 gauge) needles to improve histologic diagnosis, (2) use of coaxial technique (e.g., 21 gauge through 18 gauge) to decrease the need for multiple passes, and (3) use of phased-array sonographic transducers to improve needle visualization for biopsy of small masses. The emphasis of this course will be on common and unique approaches and pitfalls in the biopsy of the following regions: liver, pancreas, spleen, adrenal, kidney, paraaortic lymph nodes, presacral mass, thyroid, parathyroid, and cervical lymph nodes.

307. Radiographic manifestations of chronic obstructive pulmonary disease. Stark P. This course will demonstrate the radiographic manifestations of asthma and its complications, bronchopulmonary allergic aspergillosis, small airways disease, chronic bronchitis, emphysema, bronchiectases, and cystic fibrosis. Plain chest radiographs, CT scans, and bronchograms will be shown. The pertinent epidemiologic, etiologic, pathologic, and clinical data will be presented. This should be a detailed review of common (and some less common) conditions encountered in daily practice and should help the radiologist in the diagnostic workup of patients who have airways disease.

308. Imaging the acutely injured cervical spine. Swischuk LE, Harris JH. The subject of this instructional course will be the radiologic evaluation of the patient suspected of having an acute cervical spine injury. Topics to be covered include acute cervical spine injuries in the infant and child, with particular emphasis on acute injuries; the radiographic appearance of those characteristics of normal growth and development of the cervical spine that may simulate—or be mistaken for—acute injuries; the advantages and limitations of plain-film radiography and tomography, multiplanar CT, three-dimensional CT, and MR in the evaluation of acute cervical spine trauma; the appropriate sequence of imaging procedures as dictated by the patient's condition; the radiographic features of anterior subluxation and hyperextension dislocation (both often poorly understood, but relatively common and clinically significant cervical spine injuries) and the role of MR in each. Each presenter will provide time in his segment for questions from the audience.

309. Endoluminal sonography: transvaginal and transrectal. Bree RL, Madrazo B. Transvaginal pelvic sonography has become an accepted and important technique in evaluating the female pelvis for many obstetric and gynecologic conditions. This high-resolution technique allows much earlier and more accurate diagnosis of pregnancy and can accurately assess complications of early pregnancy, including abortions and extrauterine gestations. A detailed study of the fetus in the first trimester allows for earlier detection of anomalies. In the gynecologic patient, accurate assessment of the uterus, fallopian tubes, and ovaries can supplement, and possibly replace, the trans-abdominal sonogram. Specific applications of this technique include evaluation of cystic and solid adnexal masses, free fluid, pelvic inflammation, adenomyosis, leiomyomata, endometrial pathologic processes, and intrauterine devices. Transvaginal pelvic scanning is ideal for care of patients undergoing fertility stimulation, particularly in the in vitro fertilization clinic for evaluation of follicles and aspiration of ova. Interventional procedures using the transvaginal probe have been performed in selected patients. Advantages of transvaginal scanning include high degree of acceptance by patients because of the comfort of the probe, the fact that the patient does not have to have a full bladder, and improved definition of pathologic entities because of the higher resolution. Transrectal sonography has become an accepted technique in the evaluation of the prostate. The prostate can be evaluated in those patients who have palpable nodules or strong clinical or biochemical suggestion of prostatic carcinoma. Details of prostatic anatomy and its relationship to prostatic carcinoma will be discussed. Controversy over the value of prostate sonography for screening of prostate cancer is ongoing. Prostate biopsy via a guided transrectal approach will be discussed, and the results will be compared with those of other prostate biopsy techniques. Transrectal sonography has been used to stage both prostate cancer and cancers of the rectum. Results of these procedures and their clinical application will conclude the course.

310. MR imaging of the thorax. McLoud TC, Drucker EA. This course will review MR imaging of the thorax, including preferred pulse sequences, respiratory and cardiac gating, and gradient-echo techniques. Imaging of mediastinal masses will be discussed, with emphasis on CT correlation. The course will also deal with the role of MR imaging in the staging of bronchogenic carcinoma, with particular reference to the imaging of mediastinal nodal metastases and chest wall and mediastinal invasion. The relative value of MR vs CT in the imaging of the pulmonary hila will also be discussed. The latter part of the refresher course will deal with MR imaging of vascular lesions, including aortic aneurysms, aortic dissection, and pulmonary emboli. Emphasis will be placed on techniques used to optimize vascular imaging.

311. Imaging of intracranial neoplasms. Hesselink JR, Press GA. The course will cover all aspects of imaging of intracranial tumors. Selection of the proper imaging technique will be discussed. The CT and MR appearances of extra- and intraaxial tumors will be reviewed, as well as the variations of these lesions. Differential diagnosis according to both the characteristics of individual tumors and the compartmental localization within the intracranial cavity will be emphasized. The patterns of tumoral hemorrhage will also be covered. Paramagnetic enhancement with Gd-DTPA will be discussed in detail to give the registrants an understanding of the mechanisms of enhancement, methods of administration and imaging, indications for its use, and the normal enhancing structures within the CNS. Enhancement patterns of individual tumors will be used in differential diagnosis.

312. Technical advances in clinical MRI: contrast agents, fast scanning, and surface coils. Saini S, Edelman R, Kneeland JB. This instructional course will focus on clinical applications of recent developments in contrast-enhanced MR (Saini), fast scanning techniques (Edelman), and surface coils (Kneeland). The principles of pharmaceutical manipulation of MR contrast and practical considerations for their clinical application will be explored. Gd-DTPA is now approved for clinical use, and its role in imaging diseases of the brain, spinal cord, and abdomen will be discussed. Clinical results with investigational magnetopharmaceuticals, including ferrites and hepatobiliary contrast agents, will also be presented. Clinical applications with fast scanning techniques that are useful for reducing motion artifacts and maximizing patient throughput will be discussed, with particular reference to rapid MR myelography, fast three-dimensional imaging of the knee, dynamic imaging of the temporomandibular joint, breath-hold imaging of the upper abdomen, imaging of hemorrhage, flow imaging, MR cineangiography, and dynamic contrast studies. Results of investigations with ultrafast (subsecond) imaging techniques will also be presented. The basic principles of surface-coil operation and practical considerations with regard to the use of these coils will be presented. Clinically relevant applications of surface coils, partial-volume coils, full-volume coils, intracavity coils, and coil arrays will be shown.

313. Percutaneous laser angioplasty. McCowan TC, Castañeda-Zúñiga WR, Ferris EJ. The therapeutic use of laser energy transmitted through fiber-optic bundles placed percutaneously in the vascular system has recently received considerable attention from radiology, other medical specialties, and the public. Although still experimental in many ways, laser systems are now in use clinically, and all interventional radiologists should be familiar with the current status of lasers to treat atherosclerotic vascular disease. This course will review these important issues and topics: (1) laser-tissue interaction (thermal, mechanical, photoablative), with emphasis on the effects of different lasers (argon ion, neodymium:yttrium aluminum garnet, excimer, etc.), wavelengths, and pulse sequences on plaque dissolution and tissue injury; (2) the various laser systems now available or projected to be available for clinical use, including the laser and fiber-tip configuration, and the relative advantages and disadvantages of each; (3) practical clinical tips on performing laser angiography; (4) critiques of reported human trials; and (5) future directions in laser angiography.

314. Film mammography: current practices and results. Gisvold JJ. Breast imaging is now a busy area in most radiology departments. Mammography is the primary examination. Sonography is an adjunctive study important for complete evaluation of certain types of lesions. Current techniques for mammography and sonography will

be reviewed. Preoperative wire localization is a vital part of the biopsy procedure for nonpalpable lesions. Early results with fine-needle aspiration biopsy of nonpalpable lesions by using stereotaxic X-ray guidance will be discussed. Evaluation of indeterminate mammographic findings by using methodology that has long proved useful will be reviewed. Knowing the results of the work we do is important. Many systems have been developed with this purpose in mind. Results from the Mayo Clinic's breast imaging and surgical experience will be presented.

315. Radiologic aspects of liver transplantation. Campbell WL, Zajko A. Liver transplantation is playing an increasing role in the management of end-stage hepatic disease. Diagnostic imaging and interventional radiology are used extensively in the care of liver transplant patients. This course will review the role of the radiologist in liver transplantation, beginning with the initial evaluation of the patient to determine suitability for operation. After a brief review of the surgical procedure and its variations, the normal postsurgical imaging anatomy will be described. The balance of the presentation will deal with various posttransplant complications, some virtually unique to liver transplantation, with which the radiologist may be significantly involved. These include problems stemming from biliary and vascular anastomoses, other abdominal complications, allograft rejection, and extraabdominal problems. Finally, the important role of interventional radiology in the management of the complications of liver transplantation will be described and illustrated.

Thursday, May 11

401. Interventional uroradiology. Lang EK. The indications for percutaneous nephrostomy, decompression, management of sepsis, and entry to the collecting system are discussed. Expanded use of this technique for seating of ureteric stents; dilatation of ureteric strictures; reentry procedures from the distal ureter into the bladder; bypass drainage of a dehiscent system; and manipulation and extraction of calculi, foreign bodies, and projectiles are likewise covered. A number of antegrade, retrograde, and combined techniques; usage of different reinforcement guidewires, exchange sheaths, and peel sheaths; and bimanual manipulation for advancement and seating of stents under adverse conditions are discussed theoretically and illustrated by appropriate examples. Risks of different techniques and precautionary steps to avoid complications are presented. Last, results for different interventions are analyzed on the basis of available statistics so members of the audience can develop the algorithmic pathway best suited to their circumstances.

402. Duplex and color-flow Doppler imaging of the abdomen, pelvis, and extremities. Merritt CRB. Changes in tissue function are often associated with changes in blood flow, and methods that allow visualization of organ perfusion are of potential clinical importance. Pulsed Doppler and Doppler color-flow imaging now provide insights into such vascular changes throughout the body, allowing characterization of the presence and direction of flow. Primary vascular disease, including aneurysm, pseudoaneurysm, and dissection, may be evaluated. In the abdomen, Doppler imaging aids in the assessment of portal, hepatic, splenic, and mesenteric vein flow; evaluation of shunt patency; identification of tumor vascularity; measurement of renal blood flow; and diagnosis of transplant rejection. Recently, important roles for Doppler imaging in detection and evaluation of placental, umbilical, and fetal blood flow have been reported. In the extremities, Doppler imaging is assuming an increasing important role in the diagnosis of arterial and venous disease.

403. Pediatric body MR imaging: fact or fantasy? Bisset GS, Kirks DR. The applications and advantages of MR imaging in pediatric neuroradiology are well known. In recent years, however, MR has emerged as a diagnostic technique in body imaging. This course will explore the current clinical applications for and potentials of body MR imaging in infants and children. Selecting appropriate techniques and tailoring the examination are especially important in infants and children to achieve optimal diagnostic information. This instructional course will provide an overview of body MR imaging and its challenges in this group of patients. Preparation, sedation, monitoring, pulse sequences, and clinical indications for body MR will be emphasized. New and unique techniques, use of surface coils, and pediatric potentials will be discussed. MR imaging applications in the chest, cardiovascular system, abdomen, pelvis, soft tissues, and extremities of children will be illustrated.

404. SPECT imaging in clinical nuclear medicine. Handmaker H, Bunker SR. The shift toward tomography with the newer morphologic imaging techniques of CT, sonography, and MR is challenging nuclear medicine to optimize the inherently limited spatial resolution of its uniquely physiologic imaging procedures. It is therefore logical that single-photon emission CT (SPECT), with its considerable improvements in contrast resolution, is displacing conventional planar scintigraphic routines so rapidly. This evolution toward tomography has been facilitated by major technologic advances in the processing of computerized images. It also is not surprising that SPECT is accepted so readily by the medical community; the tomographic image format provides convenient correlation with CT, sonography, and MR. Our experience over the past 4 years indicates that SPECT provides improved sensitivity and specificity to existing procedures. SPECT is the preferred technique for all exercise- and dipyridamole-stress thallium-201 myocardial perfusion examinations, limited ^{99m}Tc -methylenediphosphonate skeletal evaluations, and ^{99m}Tc -sulfur colloid studies of the liver and spleen. Additional studies can be performed with SPECT as a function of available camera time and the potential for improved diagnostic yield from tomography. Currently, approximately 50% of our department's procedures and revenues are generated by SPECT studies. It is our belief that with the development of newer and more specific radiopharmaceuticals and the continued availability of SPECT techniques, this figure eventually may exceed 75%.

405. Craniocerebral trauma. Kieffer SA, Cacayorin ED. Even before the advent of CT, it was evident that the management of the patient with head trauma was little affected by the demonstration of a skull fracture on plain radiographs. With CT, not only was the diagnostic evaluation of the injured patient notably improved, but also the entire management of the injury and its sequelae were facilitated. The role of MR in the diagnosis and management of craniocerebral trauma is still emerging. In the acutely injured patient, CT remains the neuro-radiologic examination of choice. However, it is already clear that MR is more sensitive than CT for the demonstration of injuries involving the white matter, the inferior surfaces of the brain, and the brainstem and in the assessment of subacute and chronic intra- and extraaxial hemorrhage. Close correlation between clinical status and radiologic findings is essential for optimal patient management in craniocerebral trauma. This presentation will examine the imaging characteristics of both the early (hematoma, contusion) and late (hydrocephalus, gliosis, atrophy) effects of trauma on the intracranial contents. The results of injury to the intra- and extracerebral blood vessels (infarction, hemorrhage, fistulization) will also be considered.

406. Pattern approach to gastrointestinal radiology. Eisenberg RL. The practicing radiologist performing gastrointestinal examinations is

often unaware of the underlying disease and is presented with a specific set of findings for which a differential diagnosis and rational diagnostic approach must be suggested. This course will discuss a variety of radiologic patterns of specific portions of the gastrointestinal tract, including ulceration, narrowing, thickened folds, filling defects, and obstruction. For each pattern a differential diagnosis will be presented. This will be followed by radiographic illustrations of the disease entities and a discussion of differential points that should aid in arriving at the proper diagnosis.

407. Complications of IV drug abuse: hits, blows, and stuff for the nose. McCarroll K, Roszler M. IV drug abuse and cocaine abuse are increasing problems in all areas of the country. These patients have protean complications involving almost all organ systems, many of which are potentially fatal. The radiologic manifestations of these complications are unique. This presentation will first demonstrate the local complications of IV drug usage by using two dangerous injection routes as examples, the "groin hit" and "pocket (neck) shot." The complications encountered as a result of systemic bacterial seeding, which may involve the musculoskeletal, pulmonary, cardiovascular, neurologic, renal, and gastrointestinal systems will then be shown. Inhalation of crack cocaine may result in neurologic, cardiovascular, or obstetric complications. The preparation and mode of administration of the abused substances and the radiographic appearance of the complications will be presented.

408. Needle biopsy of the musculoskeletal system. Rosenthal DI. Needle biopsy of the musculoskeletal system cannot be considered a single procedure. Three distinctly different techniques are required for biopsies of soft tissue (or completely destroyed bone), densely mineralized tissue, or soft tissue located behind a bony cortex (such as the marrow cavity). Different types of equipment are required for each. In addition, adequate biopsy of primary tumors of the musculoskeletal system, and many infections, requires rather large specimens. Metastatic lesions frequently can be diagnosed on the basis of cytologic aspirates. Radiologic guidance can be provided by either fluoroscopy or CT. The choice depends on the anatomic difficulty of the site, which in turn determines potential complications. In this talk, we will consider each type of biopsy and illustrate our preferred equipment and technique. Potential complications will be addressed.

409. Sonography of the rotator cuff and of the infant's hip. Crass JR, Harcke HT. This refresher course will review the recently developed roles of sonography in the evaluation of the rotator cuff and of the infant's hip. Sonography of the rotator cuff is used primarily for the diagnosis of tears of the cuff; sonography also may play a role in diagnosis of the subacromial impingement syndrome. The anatomy of the rotator cuff will be reviewed as it relates to scanning technique. Easily learned methods of positioning the patient and methods of scanning that result in consistently diagnostic images will be demonstrated. The spectrum of sonographic findings in both the normal and the abnormal tendon will be illustrated. An approach to the abnormal but apparently intact tendon will also be presented, including a discussion of the abnormally echogenic tendon. Sonography of infants' hips is used both to detect congenital dislocation and/or dysplasia and to monitor the hip during treatment. It is a highly accurate method because structures not visualized on plain films are clearly identified. The dynamic method of evaluation will be reviewed, with emphasis on the three routine views and stress maneuvers. Normal sonograms will be compared with cases of subluxation and dislocation to emphasize the spectrum of abnormality in congenital dislocation of the hip. Integration of sonography with other imaging techniques will be discussed.

410. Lung tumor staging. Zerhouni E, Pugatch R. This course will review current concepts in lung cancer staging from initial workup to surgical management. The differential diagnosis of focal lung disease by CT and MR will be addressed with specific emphasis on workup of peripheral pulmonary nodules using densitometric as well as morphologic characteristics. Optimal strategies for effective preoperative diagnosis will be outlined. The management of lung cancer will be addressed using the new staging schemes adopted at the 4th World Conference on Lung Cancer, 1984. The advantages and limitations of imaging will be discussed with particular emphasis of critical determinants such as invasion of major structures, lymph node assessment, and adrenal imaging. The course will provide the attendee with a working knowledge of current management pathways in lung cancer with emphasis on the specific roles of imaging.

411. The radiologic evaluation of paranasal sinus disease and facial trauma: conventional films, CT, and MR. Weber AL. This course deals with the radiologic evaluation of the paranasal sinuses and of facial trauma. Before a discussion of the various disease entities, the normal radiographic anatomy will be presented. This will be followed by a description of normal variations, including developmental anomalies. Next, the different pathologic entities, including inflammatory disease, polyposis, mucocoeles, and benign and malignant tumors, will be illustrated. All radiologic techniques (including plain sinus films, CT, and MR) will be discussed, in conjunction with the case presentations. Special emphasis will be placed on the indications and value of the various radiographic studies. The radiographic findings will be covered in detail, along with the pertinent clinical signs and symptoms. The plain-film and CT findings of facial fractures also will be discussed briefly.

412. Practical aspects of MR image interpretation. Bradley WG, Stark DD. This is a practical course aimed at those who already read CT scans and now will also be interpreting MR images. The focus is on the unique information in MR that distinguishes it from CT. The following questions are addressed: What determines the proton density, T1, and T2 of a particular tissue; how and why do these parameters change in certain disease states? How does the protein content affect signal intensity? What are the magnetic properties of tissue and contrast agents? Why do some substances (e.g., methemoglobin, and Gd-DTPA) increase signal intensity, whereas others (e.g., deoxyhemoglobin, hemosiderin, iron oxides) decrease signal intensity? What is magnetic susceptibility? diamagnetism? paramagnetism? superparamagnetism? Why do flowing blood and CSF sometimes appear dark and sometimes bright? Exactly how do time-of-flight effects, turbulence, and odd-echo dephasing decrease signal intensity, whereas flow-related enhancement, even-echo rephasing, and diastolic pseudogating increase signal intensity? How are intraluminal pathologic changes distinguished from high-intensity flow effects? What determines MR image contrast in the traditional spin-echo and inversion-recovery images and in the new fast methods with reduced flip angles? Principles of pulse-sequence optimization will be discussed by using clinical examples of brain and body pathologic changes. Tricks, pitfalls, and efficient diagnostic strategies will be examined in detail.

413. Computer-assisted three-dimensional imaging: state of the art. Fishman EK, Ney DR. Advances in computer technology and computer graphics have provided the opportunity for a new generation of three-dimensional imaging systems. In this session, we will

review the basic concepts and techniques involved in three-dimensional imaging. This will include a discussion of the reconstruction algorithms (volumetric-rendering technique vs thresholding technique) commonly used and of the principles involved in image processing and display. The clinical applications of three-dimensional imaging will then be addressed, with a review of several of the common applications. Specific emphasis will be placed on the advantages of three-dimensional imaging over routine transaxial CT scans only. The technique of the CT examination, CT scan parameters, and image formatting will be reviewed and specific recommendations made. The clinical applications reviewed will include orthopedic (trauma, congenital disorders, dysplasias, and degenerative diseases), plastic surgery (soft tissues, craniofacial tissues), oncologic (tumor imaging, planning radiation therapy), and general surgery (tumor imaging, presurgical planning). The advantages in each of the specific areas will be addressed and reviewed with clinical examples. Finally, some recent and future applications of three-dimensional imaging, including custom design of prosthetic implants, computer-simulated surgery, and analysis of joint motion will be presented.

414. Screen-film mammography: equipment, technique, and interpretation. Feig SA. Unless screen-film images have high contrast and resolution and include as much breast tissue as possible, even the best mammographer will not be able to see very early cancers. Thus, the first part of the course will provide clinically relevant information on mammographic technique for the practicing radiologist. Topics will include generator types, focal-spot size and composition, phototiming, compression devices, grids, and magnification; aspects of film processing, such as development time, temperature, chemistry, and quality control; and breast positioning for routine and supplementary views. Examples of lesions that were missed or misinterpreted because of technical factors will be shown. Methods to recognize and correct improper technique on screen-film mammography will be discussed. The second part of the course will emphasize recognition of subtle signs of early breast cancer and its distinction from normal and benign lesions. The use of special projections, magnification mammography, and sonography to determine the need or lack of need for biopsy will be discussed. Guidelines for interpretation of mammograms will be considered.

415. Angioplasty: 1989. Waltman AC, Levin DC. Peripheral and renal angioplasty can be considered relatively mature procedures, having now been in widespread clinical use for about 8 years. This course will review the indications, techniques, clinical and angiographic results, long-term success rates, and complications of these procedures. Newer technical innovations, such as lasers, laser thermal probes, intravascular stents, and atherectomy catheters, will be reviewed. A brief discussion will also be included of certain political and economic issues, such as "turf battles" with other medical specialties, credentialing criteria, and the advisability of setting up an interventional radiology admitting service.

Friday, May 12

Symposium on gastrointestinal radiology. See Table 3 for topics and instructors. Register on registration form for this complimentary program.

TABLE 3: Gastrointestinal Radiology 1989. Focus: New Problems, New Solutions

Session/Time	Topic (Presenter)
The Immune System and Its Deficiencies	
8:00 a.m.	Immune diseases and the small intestine (<i>Olmsted</i>)
8:20 a.m.	AIDS and the GI radiologist (<i>Federle</i>)
8:50 a.m.	Iatrogenic immune suppression (<i>Jones</i>)
The Bile Ducts: Linking Diagnosis and Therapy	
9:25 a.m.	Diagnostic radiology of the bile ducts—1989 (<i>Balfe</i>)
9:45 a.m.	Innovative intervention in biliary disease (<i>Teplick</i>)
10:15 a.m.	Biliary lithotripsy (<i>Ferrucci</i>)
New Horizons in Oncology: Focus on Cancer of the Rectum	
10:50 a.m.	Imaging and immunity: monoclonal antibodies (<i>Wahl</i>)
11:10 a.m.	Cross-sectional imaging: staging and recurrence (<i>Thompson</i>)
11:35 a.m.	Endosonography in the rectosigmoid (<i>Hill</i>)

Note.—There is no fee for this symposium. However, to facilitate planning, please register on the meeting registration form.

ACR Luncheon Presentations on Socioeconomics of Radiology

A series of luncheon presentations on the socioeconomic aspects of radiology will be arranged by the American College of Radiology (ACR). A box lunch will be provided. The presentations do not conflict with other elements of the program. Advance registration is required. Cost per session is \$12.

Date, Topic, Speaker

Monday, May 8: Governmental Issues, Otha W. Linton, associate executive director, ACR
 Tuesday, May 9: Standards Setting, Jerome H. Shapiro, M.D.
 Wednesday, May 10: Status and Update on RVS, James M. Moorefield, M.D.
 Thursday, May 11: Mammography Screening Program, Gerald D. Dodd, M.D.

Faculty List

Amberg, John R., University of California, San Diego
 Amis, E. Stephen, Jr., Columbia University
 Balfe, Dennis M., Mallinckrodt Institute of Radiology
 Banner, Marc P., University of Pennsylvania
 Bernardino, Michael E., Emory University Hospital
 Besozzi, Myrwood C., University of Tennessee
 Bisset, George S., Children's Hospital Medical Center
 Bookstein, Joseph J., University of California, San Diego
 Bradley, William G., Jr., Huntington Medical Research Institute
 Bree, Robert L., University of Michigan
 Bryan, Nicholas, Johns Hopkins Hospital
 Buonocore, Edward, University of Tennessee
 Bunker, Stephen R., Children's Hospital of San Francisco
 Bush, William H., University of Washington
 Cacayorin, Edwin D., Upstate Medical Center
 Callen, Peter, University of California, San Francisco
 Campbell, William L., Presbyterian University Hospital
 Casarella, William J., Emory University Hospital
 Castaneda-Zuniga, R. Wilfrido, University of Minnesota Hospitals
 Charboneau, William J., Mayo Clinic
 Chezmar, Judith L., Emory University Hospital
 Cooperberg, Peter L., University of British Columbia
 Cohan, Richard H., Duke University
 Crass, Jeffrey R., Cleveland Metropolitan General Hospital
 Cronan, John J., Rhode Island Hospital
 Crummy, Andrew B., University of Wisconsin
 Daffner, Richard H., Allegheny General Hospital
 Davis, David O., George Washington University
 Davidson, Alan J., Uniformed Services University of Health Sciences
 Dorfman, Gary S., Rhode Island Hospital
 Drucker, Elizabeth A., Pomona Valley Community Hospital
 Dunnick, N. Reed, Duke University
 Edeiken, Jack, M. D. Anderson Hospital
 Edelman, Robert R., Beth Israel Hospital
 Eisenberg, Ronald L., Louisiana State University Medical Center
 Federle, Michael, University of California, San Francisco
 Feig, Stephen A., Jefferson Medical College
 Ferris, Ernest J., University of Arkansas for Medical Sciences
 Ferrucci, Joseph T., Massachusetts General Hospital
 Fishman, Elliott K., Johns Hopkins Hospital
 Foley, W. Dennis, Milwaukee County Hospital
 Fritzsche, Peggy J., Loma Linda University Medical Center
 Gisvold, John J., Mayo Clinic
 Glazer, Harvey S., Mallinckrodt Institute of Radiology
 Goldstein, Alan, Detroit Receiving Hospital
 Goldstein, Irwin, Boston University Medical School
 Gooding, Gretchen A., V. A. Medical Center, San Francisco
 Goodman, Lawrence, Milwaukee County Hospital
 Hadlock, Frank P., Baylock College of Medicine
 Handmaker, Hirsch, Children's Hospital, San Francisco
 Harcke, H. Theodore, Alfred I. Dupont Institute
 Harris, John J., University of Texas Medical School
 Hartman, David S., Uniformed Services University of the Health Sciences
 Hartman, Glen W., Mayo Clinic Foundation
 Hasso, Anton N., Loma Linda University Medical Center
 Hattery, Robert R., Mayo Clinic Foundation
 Helms, Clyde A., University of California, San Francisco

- Hesselink, John, University of California, San Diego
Hill, Michael C., George Washington University Medical Center
Hricak, Hedvig, University of California, San Francisco
Hubner, Karl F., University of Tennessee
Jacobson, Harold G., Montefiore Medical Center
Janower, Murray L., Saint Vincent Hospital
Jeffrey, R. Brooke, San Francisco General Hospital
Jones, Bronwyn, Johns Hopkins Hospital
Kagan, A. Robert, University of California, Los Angeles
Katzberg, Richard W., University of Rochester
Kaufman, Stephen J., Emory University Hospital
Kenney, Philip J., University of Alabama
Kieffer, Stephen A., Upstate Medical Center
Kirkpatrick, John A., Children's Hospital Medical Center, Boston
Kirks, Donald R., Children's Hospital Medical Center, Cincinnati
Kneeland, Bruce, Milwaukee County General Hospital
Kopans, Daniel B., Massachusetts General Hospital
Lang, Erich K., Louisiana State University Medical Center
Lee, Joseph K. T., Washington University
Leopold, George R., University of California, San Diego
Leroy, Andrew J., Mayo Clinic Foundation
Levin, David C., Thomas Jefferson University Hospital
Levine, Errol, University of Kansas, Kansas City
Lieberman, Robert P., University of Nebraska Medical Center
Madrazo, Beatrice, Henry Ford Hospital
Manco-Johnson, Michael, University of Colorado
McCarroll, Kathleen, Detroit Receiving Hospital
McCowan, Timothy, University of Arkansas for Medical Sciences
McClennan, Bruce L., Washington University
McDermott, John C., University of Wisconsin
McLoud, Theresa C., Massachusetts General Hospital
Megibow, Alec J., New York University Medical Center
Mellins, Harry Z., Brigham and Women's Hospital
Merritt, Christopher B., Ochsner Clinic
Mirvis, Stuart E., University of Maryland
Neff, Courtney C., Salem Hospital
Nelson, Rendon C., Emory University Hospital
Newhouse, Jeffrey H., Columbia University
Ney, Derek, Johns Hopkins Hospital
Olmstead, William W., George Washington University Medical Center
Pfister, Richard C., Massachusetts General Hospital
Press, Gary, University of California, San Diego
Pollack, Howard M., University of Pennsylvania
Pugatch, Robert, Brigham and Women's Hospital
Quencer, Robert M., Miami School of Medicine
Rabinowitz, Jack G., Mount Sinai Medical Center
Reading, Carl C., Mayo Clinic
Reeder, Maurice M., Fronk Clinic
Reuter, Stewart R., University of Texas Health Sciences Center
Rifkin, Matthew D., Thomas Jefferson University
Rosenfield, Arthur T., Yale University
Rosenthal, Daniel I., Massachusetts General Hospital
Roszler, Myer, Detroit Receiving Hospital
Sagel, Stuart S., Mallinckrodt Institute of Radiology
Saini, Sanjay, Massachusetts General Hospital
Sickles, Edward, University of California, San Francisco
Singleton, Edward, Texas Children's Hospital
Spirn, Paul, Thomas Jefferson University Medical Center
Stanley, Robert J., University of Alabama
Stark, David D., Massachusetts General Hospital
Stark, Paul, Loma Linda University Medical Center
Steckel, Richard J., University of California, Los Angeles
Swischuk, Leonard J., University of Texas Medical School
Teplick, Steven, Hahnemann University School of Medicine
Talner, Lee B., University of California, San Diego
Thompson, William M., University of Minnesota
Thrall, James H., Massachusetts General Hospital
Torres, William E., Emory University School of Medicine
Totty, William G., Mallinckrodt Institute of Radiology
Wahl, Richard L., The University of Michigan Medical Center
Waltman, Arthur C., Massachusetts General Hospital
Weber, Alfred C., Massachusetts Eye and Ear Infirmary
Weinreb, Jeffrey, New York University Medical Center
Wilson, Anthony J., Mallinckrodt Institute of Radiology
Zajko, Albert B., University of Pittsburgh
Zerhouni, Elias, Johns Hopkins Hospital
Zinreich, S. James, Johns Hopkins Hospital

American Roentgen Ray Society 1989 Scientific Program

The scientific program is divided into parallel sessions so that registrants may choose topics related to their interests. A total of 189 papers will be presented Monday–Thursday, May 8–11. In addition, on Wednesday afternoon, May 10, a special session will be devoted to award-winning papers and the Caldwell Lecture, to be given by the Honorable William Bradley, Senator from New Jersey. On Friday, May 12, there will be a special 4-hr symposium, Gastrointestinal Radiology 1989: New Problems, New Solutions.

Monday, May 8, 10:30 a.m.–12:30 p.m.

I. Interventional Radiology: I

10:30 1. Atherectomy with the Simpson atherectomy device in the management of arterial stenosis. Maynar M, Castañeda F, Letourneau JG, Cabrera V, Hunter DW, Amplatz K, Castañeda-Zúñiga WR

10:42 2. Infrapopliteal artery angioplasty: follow-up and factors influencing clinical response. Bakal CW, Sprayregen S, Raden M, Cynamon J, Ascer E, Gupta S, Veith FJ

10:54 3. The use of corticosteroids to prevent early restenosis following percutaneous transluminal angioplasty. Tsai FY, Myers TV, Parker J, Shah D

11:06 4. PTA in the treatment of Budd-Chiari syndrome. Martin LG, Alspaugh JP, Kaufman SL

11:18 5. Logistical considerations of biliary ESWL. Nelson RC, Rowland GA, Steinberg HV, Torres WE

11:30 6. Ultrasonography in cholecystolithiasis: the requirements for biliary lithotripsy. Mathieson JR, So CB, Malone DE, Becker CD, Burhenne HJ

11:42 7. In vitro assays of gallstone solubility: comparison of a new catheter agitator, hand injection, and solvents alone. vanSonnenberg E, Cox J, Hofmann AF, Casola G, Varney RR, D'Agostino H, Ainge G

11:54 8. Gallstone dissolution: selection of patients, procedural considerations and follow-up. vanSonnenberg E, Casola G, Varney RR, Cox J, Zakko S, Jinich H, Hoyt DB, Zornow M, Hofmann AF

12:06 9. Interventional urological applications of the glidewire. Banner MP, Amendola MA, Pollack HM

II. Magnetic Resonance: I

10:30 10. MR imaging of the soft tissues of the hand. Richard O, Souissi M, Rigot J, Cyna Gorse F, Chabrias J, Moreau JF

10:42 11. Skeletal stigmata of major concomitant soft-tissue injury. Feldman F, Singson RD, Staron RB

10:54 12. MR of temporomandibular joint disorders: experience in 635 patients. Palacios E, Valvassori G, Shannon M, Dobben G

11:06 13. MRI of stressed anterior cruciate ligaments. Rijke AM, Goitz HT, Gay SB

11:18 14. MRI diagnosis of injury to the lateral ligaments of the ankle. Rijke AM, Goitz HT, Gay SB

11:30 15. Interactive linear combinations of magnetic resonance images of joints. Drace J, Resendes M

11:42 16. Distal radioulnar joint subluxation: comparative studies with MRI and CT. Staron RB, Feldman F, Singson RD

11:54 17. Spectrum of appearance of marrow in the pediatric spine: stir imaging. Moore SG

12:06 18. MR imaging of pediatric hematologic disorders. Murayama S, Mulvihill DM, Robinson AE

III. Chest

10:30 19. Bronchiectasis & bronchiolitis obliterans in heart-lung transplant recipients: radiologic and pathologic correlation. Skeens JL, Fuhrman CR, Yousem SA

10:42 20. Endotracheal surfactant and prematurity—new insights. Macones AJ, Mulhern CB, Wolfson BJ, Fisher MS, Friss HE

10:54 21. Conventional analog vs computed chest radiography: ROC study of observer performance. Brown K, Morioka C, Aberle DR, Batra P, Huang HK, Milos MJ, Balter S

11:06 22. Accuracy of identification of support devices on portable radiographs: a comparison of digital vs conventional filming. Thompson MJ, Kubicka RA, Smith C, Smith SM

11:18 23. Computed radiography: a study of observer performance with a high-resolution dedicated chest unit. Batra P, Aberle DR, Brown K, Milos M, Wong A, Komori M, Huang HK

11:30 24. Radiologic diagnosis of esophageal malposition of endotracheal tubes. Smith GM, Reed JC, Choplin RH

11:42 25. Demonstration of calcium in carcinoma of the lung. Mahoney MC, Shipley RT, Corcoran HL

11:54 26. Double lung transplantation. Weisbrod GL, Herman

SJ, Rappaport DC, Patterson GA, Cooper JD, Chamberlain D, Toronto Lung Transplant Group

12:06 27. The anterior wall stripe of the left lower lobe bronchus on lateral chest radiographs: CT correlative study. Lang EV,

Friedman PJ

Tuesday, May 9, 10:00 a.m.–12:30 p.m.

IV. Magnetic Resonance: II

10:00 28. Superparamagnetic iron oxide: clinical use for imaging tissue perfusion in vascular liver tumors. Hahn PF, Stark DD, Weissleder R, Saini S, Elizondo G, Wittenberg J, Ferrucci JT

10:12 29. Ferrite-enhanced MRI of focal hepatic lesions: controlled comparison with contrast-enhanced CT and noncontrast MR. Fretz CJ, Stark DD, Metz CE, Shen JH, Wittenberg J, Simeone J, Hahn PF, Weissleder R, Elizondo G, Saini S, Ferrucci JT

10:24 30. MR imaging of the liver using long TR motion artifact suppression imaging (MAST). Phillips JJ, Clifford PD, Chiu LC

10:36 31. Utility of phase-contrast pulse-sequence in the detection of liver metastases. Rummeny E, Saini S, Stark DD, Weissleder R, Hahn PF, Mueller P, Wittenberg J, Ferrucci JT

10:48 32. Comparative MR imaging at 0.5 and 1.5 Tesla in the evaluation of focal hepatic lesions. Steinberg HV, Alarcon JJ, Nelson RC, Chezmar JL, Bernardino ME

11:00 33. Preoperative MRI evaluation of liver transplant candidates. Fulmer JM, Hurst DC, Harms SE, Goldstein RM, Klintmalm G

11:12 34. High-field (1.5 T) MR imaging of pancreatic transplant acute rejection. Sironi S, Secchi A, Pozza G, Del Maschio A

11:24 35. Correlation between Gaucher infiltration of liver/spleen and bone with MRI. Gendal ES, Hermann G, Mendelson DS, Janus CL

11:36 36. Use of contrast agents in MRI of liver tumors: study of four different substances in an animal model. Hamm B, Taupitz M

11:48 37. Ultrafast MR imaging of the pancreas at 2.0 T: initial clinical evaluation. Saini S, Stark DD, Pykett IL, Rzedzian RR, Ferrucci JT

12:00 38. MRI of acoustic neuromas poststereotactic radiosurgery. Robinson JD, To SYC, Lufkin RB, Rand RW, Hanafey WN

12:12 39. MRI of postamputation neuromas. Singson RD, Feldman F, Staron RB

V. Computed Tomography: I

10:00 40. Computed tomographic lateral ventricular asymmetry: brain structural correlates. Stein M, Grosman H, Perrin RG, St. Louis EL, Gray R

10:12 41. Determination of ischemia utilizing SPECT IMP and HMPAO imaging: comparison with CT. Mountz JM, Dougherty MH, Speed NM, Schwartz JA, Gross MD

10:24 42. The accuracy of CT in the diagnosis of chronic lung disease. Bergin CJ, Bell D, Coblenz C, Chiles C, Castellino RA

10:36 43. Neonatal tracheobronchomegaly: cine CT evaluation. Sato Y, Kao S, Wagener J, Smith W, Parker S

10:48 44. High-resolution computed tomography (HRCT) in tracheobronchomegaly (Mounier-Kuhn syndrome). Buschman DL, Corsello PR, Iseman M, Goble M

11:00 45. Occult pneumothorax: CT diagnosis and its clinical implication. Gilpin JW, Wolfman NT, Ditesheim JA, Meredith JW

11:12 46. Ultrafast computed tomography in the diagnosis of aortic aneurysms and dissections. Rooholamini SA, Stanford W

11:24 47. Ultrafast CT of upper airway obstruction in symptomatic postoperative patients with esophageal atresia and tracheoesophageal fistula. Kao SCS, Smith WL, Sato Y, Franken EA Jr, Kimura K, Soper RT

11:36 48. High-resolution CT scanning in allergic bronchopulmonary aspergillosis (ABPA). Buschman DL

11:48 49. The role of radiology in metastatic carcinoma of unknown primary: a retrospective analysis. Khoury G, Monteferrante M, Choy O, Pinto M

12:00 50. Malignant melanoma: computed tomography of subcutaneous metastases. Patten RM, Shuman WP, Teefy S

12:12 51. CT-determined organ volumes after bone marrow transplantation for mucopolysaccharidosis. Day DL, Whitley CB, Krivit W, Drake DG

VI. Ultrasound: I

10:00 52. Reproducibility of Doppler ultrasound estimates of internal carotid artery stenosis. Polak JF, Cutler S

10:12 53. Color Doppler ultrasound of pseudoaneurysms. Middleton WD, Melson GL

10:24 54. Endovaginal sonography in the evaluation of benign pelvic masses. Leibman AJ, Kruse BD

10:36 55. Ectopic pregnancy: criteria and accuracy of endovaginal sonographic diagnosis. Thorsen MK, Lawson TL, Miller D, Aiman JE, McAsey ME, Erickson S, Quiroz F, Perret RS

10:48 56. Endoscopic ultrasonography in the preoperative staging of gastric neoplasm—comparison with dynamic CT and MRI. Botet JF, Lightdale C, Brennan M, Heelan RT, Turnbull A

11:00 57. Renal transplant resistive index (RI) elevation in the absence of rejection. Pozniak M, Kelcz F

11:12 58. Intraoperative ultrasound during resection of primary hepatic tumors in pediatric patients. Grewe GM, Brewer WH, Krummel TM, Thomas BL, Benator RM

11:24 59. Sonographic features of ovarian teratomas in pediatric patients. Sisler C, Siegel MJ

11:36 60. Duplex sonography of parathyroid adenomas. Riedy K, White EM, Simeone JF, Jarosky MJ, Eisenstein MM

11:48 61. Infected hip prosthesis: sonographic findings. Graif M, Kessler A, Salai M, Mouallem M, Horoszewski H, Itzhak Y

12:00 62. Ultrasound versus CT as guidance modality and for follow-up of percutaneously drained abscesses. Clayton J, Wells W, Lang EK

12:12 63. Sonographic diagnosis of gallbladder perforation. Levy HM, Jaffe RM, Newhouse JH, Seldin DW

Tuesday, May 9, 1:30-3:30 p.m.

VII. Bone: I

1:30 64. CT measurement of the calcaneal varus angle in the normal and fractured hindfoot. Vu MV, Richardson ML, Vincent LM, Sangeorzan BJ, Patten RM

1:42 65. Occult fractures of the carpals and metacarpals: demonstration by computed tomography. Hindman BW, Kulik WJ, Lee G, Avolio RE

1:54 66. In vivo MRI imaging confirmation of pathology of hyperextension dislocation (HD). Yeakley JW, Fenstermacher MJ, Harris JH Jr.

2:06 67. The radiographic appearance of low velocity bullets. Gray DGK, Guyot DR, Kling GA

2:18 68. Cervical spine annulus vacuum: a degenerative phenomenon. Bohrer SP, Chen YM

2:30 69. Acute injuries to the lateral ligaments of the ankle, comparison of quantitative stress radiography and arthrography. Rijke AM, Jones B, Vierhout PA

2:42 70. Three-dimensional computerized simulation of bone fracture angulation and displacement as dependent on the incident angle of X-ray beam. McEnery KW, Lambiase RL

2:54 71. Calcific tendonitis of the long head of the biceps brachii occurring distal to the glenohumeral joint. Goldman AB

3:06 72. Development and clinical application of digital book cassette tomography within an emergency radiology department. Milos MJ, Widoff BE, Nichols T, Lagmay RD

3:18 73. Aseptic necrosis of the femoral head: progression of MRI appearance following core decompression and grafting. Chan T, Dalinka M, Steinberg M, Kressel H, Zlatkin M

VIII. Computed Tomography: II

1:30 74. CT diagnosis of pneumatosis intestinalis. White EM, Ghahremani GG, Zeman RK

1:42 75. Detection of postsurgical complications in patients with ulcerative colitis and ileo-anal pouches. Thoeni RF, Fell S

1:54 76. CT evaluation of enterovaginal and vesicovaginal fistula. Kuhlman JE, Fishman EK, Scatarige JC

2:06 77. Kurkenberg tumors: CT features and growth characteristics. Kuhlman JE, Hruban RH, Fishman EK

2:18 78. Computed tomography of the postpartum pelvis. Garagiola DM, Gibson L, Tarver RD, Rogers RE, Wass JL

2:30 79. Evaluation of an abbreviated abdominal-pelvic computed tomography blunt trauma protocol. Milos MJ, Widoff BE, Kadell-Wootton BM, Weiner M, Hiatt JR

2:42 80. Normal variations of pelvic fat distribution: implications on CT staging of pelvic tumors. Li KCP, Mastin ST, Ros PR

2:54 81. Quantitative comparison of three-dimensional rendering CT data classification techniques. Ney DR, Fishman EK, Gerber JD, Beck TJ

3:06 82. Evaluation of oncologic patient with bone pain: value of CT with two- and three-dimensional reconstruction. Fishman EK, Order SE, Kuhlman JE

3:18 83. Inpatient precision in QCT bone mineral measurements. Morin RL, Brown ML, Wahner HW, Karsell PR, Berquist TH

IX. Breast

1:30 84. Sonographic appearance and ultrasound-guided fine-needle aspiration of breast carcinomas less than 1 cm³ in volume. Fornage BD, Sneige N, Paulus DF, Martin JE

1:42 85. Aspiration biopsy of nonpalpable breast lesions with stereotactic guidance. Merritt CRB, Bergeron RB, Sullivan MA, Bluth EI, McBurney D, Mitchell WT, McKinnon WM, Kirsch P

1:54 86. Breast cancer: mammographic and sonographic findings in the augmented breast. Leibman AJ, Kruse BD

2:06 87. Focal breast fibrosis: mimic of breast carcinoma. Mendelson EB, Bohm-Velez M, Freimanis M, Bhagwanani DH, Rishi US, Lamas C

2:18 88. Radiographic evaluation of the augmented breast. Douglas KP, Bluth EI, Sauter ER, McKinnon WMP, Bergeron RA, Merritt CRB, Sullivan MA

2:30 89. Radiographic features of recurrent breast carcinoma after segmental resection and radiation therapy. Baratz A, Harris K, Costa Greco M, Britton C, Poller W, Ilkhanipour Z

2:42 90. Pathological correlation of non-neoplastic conditions which simulate malignancy on mammography. Crosby DL, Koukoulis G, Harten JN, Adler YT

2:54 91. Evaluation of a mammographic stereotactic device for localization, fine needle aspiration cytology, and core biopsy of suspicious lesions. Fajardo LL

3:06 92. Effect of 3-minute film processing on dose and image quality in mammography. Skubic SE, Yagan R

3:18 93. Short-term mammographic follow-up of low-suspicion lesions: compliance rate and diagnostic yield. Pennes DR, Rebner M, Helvie MA

Wednesday, May 10, 10:00 a.m.–12:30 p.m.

X. Bone: II

10:00 94. Combined 99m-technetium methylene diphosphonate bone/111-indium leukocyte imaging in sickle cell bone infarction. Gilarsky BP, Fajman WA, Eckman JR, Taylor AT

10:12 95. Radiographic evaluation of new bone formation in Ilizarov distraction techniques. Young JWR, Kostrubiak IS, Resnik CS, Paley D

10:24 96. Early bone marrow changes following radiation: magnetic resonance evaluation. Stevens SK, Moore SG, Gaudette M, Kaplan ID

10:36 97. Magnetic resonance imaging of sacroiliitis. Murphy MD, Wetzel LH, Bramble JM, Levine E, Simpson K, Lindsley HB

10:48 98. The effects of jogging on the MR examination of the knee in normal volunteers. Kursunoglu S, Schwaighofer B, Ho C, Resnick D, Sartoris DJ

11:00 99. Abnormalities of triangular fibrocartilage: arthrographic, magnetic resonance, and surgical correlation. Moore S, Parker B, Brody G

11:12 100. MR imaging of the triangular cartilage and ligaments of the wrist: correlation with three compartment digital arthrography and anatomic sections. Gundry C, Kursunoglu S, Schwaighofer B, Kang HS, Zlatkin MB, Sartoris DJ, Resnick DL

11:24 101. Giant cell tumor (GCT): CT vs MRI in preoperative planning. Salomon CG, Gitelis S, Petasnick JP, Turner DA, Charters J, Quast M, Templeton A

11:36 102. Combined therapy for extremity soft tissue sarcomas: the role of MR. Ekstrom JE, Shuman WP, Conrad EU, Richardson ML

11:48 103. Differentiating skeletal neoplasm from non-neoplastic process: value of MR and Gd-DTPA. Harkens KL, Yuh WTC, Kathol MH, Moore TE, McGuire CW, Hawes DP, El-Khoury GY

XI. Interventional Radiology: II

10:00 104. The use of the Simpson atherectomy catheter in the management of complete arterial obstructions. Maynar M, Reyes R, Pulido JM, Castañeda F, Letourneau JG, Cabrera V, Hunter DW, Amplatz K, Castañeda-Zúñiga WR

10:12 105. Percutaneous atherectomy as an alternative treatment for postangioplasty obstructing intimal flaps. Maynar M, Letourneau JG, Castañeda F, Cabrera V, Hunter DW, Amplatz K, Castañeda-Zúñiga WR

10:24 106. Mesenteric ischemia in aortic dissection: a new mechanism. Williams DM, Andrews JC, Messina LM

10:36 107. Correlation of MR, CT, and angiography in diagnosis of surgically proved brain arteriovenous malformation. Ryals TJ, Yuh WTC, Sickels WJ, Sato Y, Cornell SH

10:48 108. Cystic arterial adventitial disease: the progression of disease and long-term follow-up. Moradian GP, Castañeda-Zúñiga WR, Hunter DW, Velasquez G, Amplatz K

11:00 109. The Simon nitinol inferior vena cava filter. Simon M, Kim D, Porter D, Kleshinski S

11:12 110. Comparison of duplex ultrasound versus inferior vena cavogram in follow-up of patients post-inferior vena caval filter placement. Epstein DH, Moradian GP, Schlam BW, Castañeda F, Coleman CC, Hunter DW, Castañeda-Zúñiga WR, Amplatz K

11:24 111. Superselective chemotherapy delivered via target catheters. Lang EK

11:36 112. Fluoroscopically guided percutaneous gastrotomy and gastroenterostomy: results and complications. Hicks ME, Picus D, Marx MV, Lang EV, Weyman PJ

11:48 113. Percutaneous drainage of psoas abscesses and fluid collections: technical aspects, results and pitfalls. D'Agostino H, vanSonnenberg E, Casola G, Varney RR, Ainge GD, Dillard J, Jhala S

XII. Gastrointestinal

10:00 114. The use of gallbladder ultrasonography and oral cholecystography in the evaluation of potential candidates for biliary lithotripsy. Torres WE, Maurer DE, Steinberg HV

10:12 115. Percutaneous cholecystostomy: does transhepatic puncture preclude a transperitoneal catheter route? Bernstein JE, Nemcek AA, Vogelzang RL

10:24 116. The histologic basis of biliary stricture dilatation. Haskin PH, Brandon JC, Conti P, Najjar D, Teplick SK, Howell L, Haskin ME

10:36 117. Biliary stricture dilatation: results in chronic inflammatory processes. Vogelzang RL, Nemcek AA Jr

10:48 118. Gallstone recurrence after cholecystolithotomy. Chow K, Gibney RG, So CB, Rowley VA, Burhenne HJ

11:00 119. Dissolution of cholesterol and cholesterol/calcium gallstones with MTBE and monooctanoin. Oldershaw JH, Epstein NF, Potter JE, Clouse ME

11:12 120. Analysis of various radiographic features in attempting to differentiate cholesterol and pigment gallstones. Steinberg HV, Maurer DE, Torres WE

11:24 121. Intussusception in children: should the indications for radiologic reduction be broadened? Barr LL, Stansberry SD, Swischuk LE

11:36 122. The modified barium swallow (cookie swallow) for evaluation of patients with dysphagia. Richman LS, Lorman JS

11:48 123. Contribution of enteroclysis in small bowel obstructions. Schmutz G, Nguyen D, Jeung MY

Thursday, May 11, 10:00 a.m.–12:30 p.m.**XIII. Magnetic Resonance: III**

10:00 124. Magnetic resonance imaging of carotid artery flow and quantitation of blood flow velocity by phase-sensitive technique. Buonocore E, Besozzi MC

10:12 125. High-field (1.5T) MR imaging of stage 1 endometrial carcinoma. Sironi S, Belloni C, Taccagni L, Del Maschio A

10:24 126. Superparamagnetic iron oxide: pharmacokinetics

11:12 142. CT evaluation of the extrahepatic biliary system: duct visualization and wall characteristics. Schulte SJ, Baron RL, Teefey SA, Rohrmann CA, Freeny PC, Shuman WP

11:24 143. Prognostic CT criteria for liver metastases comparison of CT findings with survival data. Halvorsen R, Llerena J, Wesen C, Letourneau JG, Graves K

11:36 144. The role of abdominal CT in pancreatic transplants with bladder drainage. Kayes M, Sutherland DER, Dunn D, Halvorsen R, Letourneau JG

Thursday, May 11, 1:30 p.m.–3:30 p.m.

XVI. Genitourinary

1:30 160. Role of US-guided biopsy in diagnosis of prostate cancer. Llerena J, Castañeda F, Drake DG, Ercole C, Hulbert JC, Fraley E, Hunter DW, Castañeda-Zúñiga WR, Letourneau JG

1:42 161. A nonsurgical approach for BPH: prostatic urethroplasty with balloon catheter: long-term results. Castañeda F, Hulbert JC, Maynar M, Ercole C, Reddy PK, Letourneau JG, Castañeda-Zúñiga WR, Hunter DW, Amplatz K

1:54 162. Mechanism of prostatic urethroplasty with balloon catheter. Castañeda F, Maynar M, Hulbert JC, Repa I, Letourneau JG, Reddy PK, Hunter DW, Castañeda-Zúñiga WR, Amplatz K

2:06 163. Applications of color-flow and spectral Doppler ultrasound in the evaluation of vasculogenic impotence. Quam J, King B, Brakke D, James EM, Lewis R, Parulkar BG, Barrett D

2:18 164. The role of imaging in the diagnostic evaluation of impotence. Kryszewicz S, Mellinger BC

2:30 165. Functional versus cicatricial obstruction of the fallopian tubes: assessment by selective salpingography. Lang EK, Roniger W, Dunaway H

2:42 166. MR imaging of pelvic masses in pregnancy. Kier R, Scoutt L, McCarthy S, Wain S, Viscarillo R, Schwartz P

2:54 167. Intraperitoneal contrast enhanced CT: increased detection of intraperitoneal metastases. Panushka C, Halvorsen R Jr, Letourneau JG, Adcock L

3:06 168. Renal cell carcinoma: evaluation of inferior vena cava invasion using MRI with fast scanning ("grass") technique. Amendola MA, Pollack HM, Kressel HY, Gefter WB, Banner MP, Schnall MD, Glickstein MF, Wein AJ

3:18 169. CT identification of lower GU tract injuries. Kane NM, Francis IR, Ellis JH

XVII. Bone: III

1:30 170. 2-D and 3-D CT assessment of congenital hip dysplasia in the older child and young adult. Magid D, Fishman EK, Sponseller PD, Brooker AF Jr

1:42 171. Animated 2-D/3-D imaging of slipped capital femoral epiphysis. Magid D, Fishman EK, Sponseller PD, Griffin PP, Thompson JD

1:54 172. Three-dimensional reconstruction from 2DFT and 3DFT magnetic resonance images: applications in the musculoskeletal system. Lang P, Stoller D, Lindquist T, Heuck A, Steiger P, Felix R, Genant HK

2:06 173. Animated 2-D/3-D assessment of ankle fractures. Magid D, Michelson JD, Fishman EK

2:18 174. Comparison of external vs internal rotation of the humerus for CT arthrography of the shoulder. Jonsson K, Pennes DR, Buckwalter K, Braunstein EM, Blasier RB, Wojtyś EM

2:30 175. Contrast and nuclear arthrography in loosening of the uncemented hip prosthesis. Swan JS, Braunstein EM, Capello WN, Wellman HN

2:42 176. Radiographic assessment of acetabular allograft following cemented, porous coated, and bipolar total hip arthroplasty. Nikpoor N, Aliabadi P, Weissman B

2:54 177. percutaneous catheter drainage of infected joints. Agee MW, Renner JB

3:06 178. Carpal instability in rheumatoid arthritis. White HA, Braunstein EM, Krohn K

3:18 179. Dual-energy radiography for vertebral bone densitometry following renal transplantation: comparison to clinical parameters and quantitative computed tomography. Kim R, Howard B, Sartoris DJ, Ramos E, Steiner R, Stein JA, Resnick D

XVIII. Ultrasound: II

1:30 180. Application of color-flow Doppler ultrasound and evaluation of erectile dysfunction. Schwartz AN, Wang K, Mack L, Berger R, Lowe M, Cyr D, Feldman M, Graney DO

1:42 181. Color Doppler imaging of the acute scrotum. Lerner RM, Mevorach RA, Rabinowitz R

1:54 182. Does color-coded duplex sonography improve the diagnosis of scrotal diseases? Fobbe F, Hamm B, Heidt P, Koennecke H-C, Dietzel M, Wolf K-J

2:06 183. Duplex Doppler sonography in the diagnosis of veno-occlusive disease. Abu-Yousef MM, Brown BP, Gingrich RD, LaBrecque DR

2:18 184. Color-flow imaging and the assessment of upper extremity deep venous thrombosis. Knudson GJ, Wiedmeyer DA, Erickson S, Foley WD, Lawson TL, Quiroz FA, Macrander S

2:30 185. Duplex-pulsed Doppler ultrasound in the evaluation of portal hypertension: pitfalls and limitations. Parvey HR, Eisenberg RL, Giyanani V, Krebs CA

2:42 186. Duplex and color flow Doppler imaging of Budd-Chiari syndrome. Grant EG, Perrella R, Tessler F, Lois J, Busuttill R

2:54 187. Color-flow Doppler evaluation of focal hepatic lesions. Marn CS, Rubin JM, Francis IR, Ensminger WD, Hutton TL, Walker-Andrews S

3:06 188. Renal transplant artery stenosis: diagnosis with duplex sonography. Tessler FN, Grant EG, Perrella RR, Boechat MI, Hall TR, Dietrich RB

3:18 189. Duplex Doppler ultrasound in suspected transplant renal artery stenosis. Snider JF, Hunter DW, Moradian GP, Castañeda-Zúñiga WR, Letourneau JG

1989 ARRS Meeting: Local Activities and Tennis and Golf Tournaments

The 89th annual meeting of the American Roentgen Ray Society (ARRS) in New Orleans, LA, will feature activities for members, nonmembers, spouses, and friends. Abner M. Landry, Jr., heads the Local Arrangements Committee and has planned the local programs. The tennis tournament will be arranged and supervised by David R. Hunter; the golf tournament will be arranged and supervised by Dr. Landry. To register for these events, please complete the registration form in this issue.

Golf Tournament

The annual golf tournament will be held at the English Turn Country Club on Monday, May 8. The golf course at the club was designed by Jack Nicklaus and is the new home of the USF&G New Orleans Open. Buses will leave the New Orleans Hilton Riverside and Towers at 11 a.m. and will return by 6 p.m. There will be a buffet lunch at 11:30 a.m. and a shotgun start at 12:30 p.m. Participants must bring their own golf clubs and shoes. The pro shop and clubhouse will be open, and there will be a bar. The fee for the golf tournament is \$75 and includes transportation, luncheon, greens fees, and prizes.

Men's and Women's Tennis Tournaments

The annual Men's and Women's Tennis Tournaments will be held at the New Orleans Hilton Riverside and Towers on Monday, May 8, from 1:30 to 4:30 p.m. Please register early so arrangements can be made to accommodate all who wish to play. Appropriate dress is required. The fee of \$50 includes luncheon, court fees, and balls.

Local Program

Reservations for the social program are limited. To avoid disappointment, send in the reservation form immediately. Reservations will be filled in the order in which they are received. Because guarantees are required for all events,

reservations must be received by April 20, 1989. Tickets for all events will be included in the registration packet. Prices for these events include transportation; meals where indicated; escorts and guides; and all entrance fees, taxes, and gratuities. Prices do not include alcoholic beverages with meals. On Sunday, May 7, from 2 to 5 p.m., and on Monday, May 8, from 8 to 11 a.m., remaining tickets for events will be sold at the meeting registration desk. These tickets may be sold at a slightly higher cost. Refunds are available if the ARRS office in Reston, VA, receives a written cancellation request by April 20, 1989. No cancellations will be accepted by telephone. Refunds will be issued at the meeting on Sunday and Monday only if the returned tickets can be resold. ARRS reserves the right to cancel an event if registration is insufficient. In that case, refunds will be issued.

Sunday, May 7

Overview of New Orleans, 1-4 p.m. Take a whirlwind tour of New Orleans by chartered motor coach. The tour goes through the fabled Vieux Carré and Jackson Square areas and then on to Esplanade Avenue, a lovely vista of 19th century architecture. Next you will proceed to Bayou St. John, where you will tour Pitot House, an authentically restored West Indies-style plantation house dating to the 18th century, and then on to beautiful Lake Pontchartrain, whose width is spanned by the Causeway, the world's longest bridge. Down the road a piece you will enter the University section, home to Tulane and Loyola universities, where you will see quaint streetcars, horse-drawn candy wagons, and an amazing variety of architectural styles. Last but not least, you will pass through the luxurious splendor of the Garden District and return to the hotel via the central business district. Fee: \$20.

Evening on the Mississippi, 7:30-10 p.m. Take a nostalgic trip down "Ole Man River" and witness the history and excitement of one of the oldest cities in the South. Stroll a short distance from the hotel to the Mississippi Riverboat *Creole Queen*. A jazz band will welcome you as you board and entertain you during the excursion. You will be treated to New Orleans style hors d'oeuvres and open bars. A banjo player will stroll the decks and play for your enjoyment. Fee: \$52.

Monday, May 8

Plantations of Old Louisiana, 9 a.m.-4 p.m. Chartered motor coaches will meet you at the hotel for a trip into

Louisiana's plantation past. Your first stop is Houmas House, languid setting of the Bette Davis thriller "Hush, Hush, Sweet Charlotte," and once the centerpiece of a 20,000-acre sugar plantation. You will also visit Nottoway, the South's largest plantation home. Amidst the gracious grandeur of this American castle of the South, you will partake of a Creole-fare luncheon. Motor coaches will return you to the hotel at the end of the tour. Fee: \$37.

Dinner at Gallier Hall, 8–10:30 p.m. Chartered motor coaches will transport you to Gallier Hall, one of the finest examples of Greek Revival architecture in the United States, and the seat of city government for more than 100 years. Cocktails and hors d'oeuvres will be served in the Mayor's Parlor; dinner in the Grand Ballroom will follow. A jazz band will entertain during dinner. Fee: \$65.

Tuesday, May 9

Elegant Homes of New Orleans, 9:30 a.m.–3:30 p.m. Depart by chartered motor coach to the Vieux Carré, where you will visit the Hermann-Grimm House, built in 1831 by a German immigrant. Here you will be entertained by skilled docents who cook original-period recipes and use the same techniques as those of cooks in the 1800s. Refreshments will be served. Next you will proceed to the Garden District, a residential haven of a very different flavor, where you will visit a historic private home where the life-style today is as elegant as it was 100 years ago. Culminating this tour will be lunch at Commander's Palace, one of New Orleans's most pleasurable dining experiences. You will be returned to your hotel via scenic St. Charles Ave. Fee: \$50.

Wednesday, May 10

Creole Connection, 9–11:30 a.m. Join Joe Cahn, owner of the New Orleans School of Cooking, at the Prince Conti Hotel to learn the secrets of authentic Creole cooking. In just

3 hr, you will learn how to recreate the magic of New Orleans in your own kitchen. You will receive complimentary recipes of all dishes prepared for your tasting pleasure. After the program you may return to the hotel via motor coach or explore the French Quarter on your own. Fee: \$25.

Audubon Zoo Tour and River Cruise, 12:30–5 p.m. After a short walk from the hotel, you will board the authentic sternwheeler *Cotton Blossom* for a 7-mile cruise to Audubon Zoo, one of the best zoos in the nation and home to more than 1200 animals. In the Louisiana Cypress Swamp Exhibit, you will see living examples of Louisiana wildlife, such as alligators, turtles, and nutria. While at the zoo you will enjoy box lunches under the oaks, surrounded by many furry and feathered friends. You will be returned to the hotel via chartered motor coach. Fee: \$31.

Evening Overlooking the Mississippi, 7–10 p.m. Walk across the street from the Hilton to the Plimsoll Club, one of New Orleans's most spectacular private facilities. Located atop the World Trade Center, this setting provides a breathtaking panoramic view of the city. You can look down bustling Canal St. or turn toward a kaleidoscopic harbor scene that might include naval vessels, cruise ships, and freighters flying flags from round the world. The Galvez Room will be a marvelous setting for sipping a cocktail and tasting elegant New Orleans hors d'oeuvres while enjoying the sounds of a talented pianist. Dinner will be served in the elegant crystal and damask-appointed Versailles Room. Fee: \$75.

Thursday, May 11

Cajun Swamp Tour, 11 a.m.–2:30 p.m. Chartered motor coaches will transport you to a typical Louisiana swamp where you will take a boat ride and catch glimpses of the indigenous wildlife, such as nutria, alligators, and egrets. Along the way your guide will recount the history of the Cajuns and their relationship with the Creoles, Americans, and Indians. Lunch will be served at a local seafood restaurant. Fee: \$50.

Meeting and Local Activities Registration Form: ARRS 89th Annual Meeting May 7-12, 1989, New Orleans, LA

If you plan to attend, please complete this form. Official badges and program booklets will be available at the ARRS Registration Desk, New Orleans Hilton Riverside and Towers. **There will be no confirmations before the meeting.** Preregistration by mail will be accepted until April 7. On-site registration will be available.

Make all checks payable to: American Roentgen Ray Society

Mail to: American Roentgen Ray Society
1891 Preston White Drive
Reston, VA 22091

Please type or print:

Registrant

Last Name First Name or Initials

Street

City State ZIP Code

Accompanying Guest

Name (Accompanying person's name to be printed on badge)

Street

City State ZIP Code

Check those desired:

Registra-
tion fee:

- ☐ Member ARRS None
- ☐ Nonmember \$250
- ☐ Physician in training
(please fill where indicated below) \$25
- ☐ Course faculty, presenter of
scientific paper, scientific
exhibitor (circle one) None
- ☐ ACR luncheon course,
Monday, May 8 \$12
- ☐ ACR luncheon course,
Tuesday, May 9 \$12
- ☐ ACR luncheon course,
Wednesday, May 10 \$12
- ☐ ACR luncheon course,
Thursday, May 11 \$12
- ☐ Categorical course on genitourinary
imaging \$75
- ☐ Social program (see next
page) _____
- Total enclosed** _____

Section on Instruction

Please register early for Instructional Courses. Attendance is limited. List first, second, and third choices for each day by course number. Ticket orders are filled according to postmark. ARRS members, nonmembers, and those in radiology training may take all courses without charge except the categorical course. **For the categorical course, all must pay \$75. All who wish to attend courses must complete this section. Residents and nonmembers must pay the meeting registration fee also.**

Course tickets will be available at the ARRS Registration Desk at the New Orleans Hilton Riverside and Towers on and after Saturday, May 6, at 1 p.m.

Complete section at right for courses other than the categorical course. Be sure to fill out second and third choices for each day.

Course Choices	Morning			Afternoon		
	1st	2nd	3rd	1st	2nd	3rd
Monday						
Tuesday						
Wednesday						
Thursday						

Friday _____ Check if you wish to attend the gastrointestinal symposium (only course offered this day).

For Physicians in Training:

_____ is in training in my department.

Training Program Director _____

Institution _____ Date _____

(OVER)

Local Activities

No refunds after April 20

Sunday, May 7, 1–4 p.m., Overview of New Orleans	_____ tickets @ \$20	\$ _____
Sunday, May 7, 7:30–10 p.m., Evening on the Mississippi	_____ tickets @ \$52	\$ _____
Monday, May 8, 9 a.m.–4 p.m., Plantations of Old Louisiana	_____ tickets @ \$37	\$ _____
Monday, May 8, 8–10:30 p.m., Dinner at Gallier Hall	_____ tickets @ \$65	\$ _____
Tuesday, May 9, 9:30 a.m.–3:30 p.m., Elegant Homes of New Orleans	_____ tickets @ \$50	\$ _____
Wednesday, May 10, 9–11:30 a.m., Creole Connection	_____ tickets @ \$25	\$ _____
Wednesday, May 10, 12:30–5 p.m., Audubon Zoo/River Cruise	_____ tickets @ \$31	\$ _____
Wednesday, May 10, 7–10 p.m., Evening Overlooking the Mississippi	_____ tickets @ \$75	\$ _____
Thursday, May 11, 11 a.m.–2:30 p.m., Cajun Swamp Tour	_____ tickets @ \$50	\$ _____

Preregistration is required.

Annual ARRS Golf Tournament, Monday, May 8

The tournament will be at the English Turn Country Club, New Orleans, LA. Transportation, luncheon, greens fee, cart, and prizes are included in the \$75 fee. Preregistration is important.

Name: _____ Telephone: _____
Address: _____
Hotel: _____ Handicap (if any) _____
My foursome includes (list handicaps): _____
_____ tickets @ \$75 \$ _____

Men's and Women's Tennis Tournaments, Monday, May 8

The tournaments will be at the New Orleans Hilton Riverside and Towers, New Orleans, LA. Tennis attire is required. Fee of \$50 includes luncheon, court fees, and balls.

Name: _____ Telephone: _____
Address: _____
_____ tickets @ \$50 \$ _____

Hotel Registration Form: ARRS 89th Annual Meeting May 7-12, 1989, New Orleans Hilton Riverside and Towers New Orleans, LA

Mail to:**ARRS Housing Bureau**

New Orleans Hilton Riverside and Towers

Attention: Reservations Office

Poydras at the Mississippi

New Orleans, LA 70140

(PLEASE MAKE CHECKS PAYABLE TO THE NEW ORLEANS HILTON RIVERSIDE AND TOWERS—NOT TO THE ARRS)

Individual guest name _____

Address _____

City & State _____ ZIP _____

Arrival date/time _____ Departure date/time _____

Individual requesting reservation _____

Address _____

City & State _____ ZIP _____

Please forward with your reservation a deposit of one night's room rate to be applied to the last night of your scheduled stay, or provide credit card information to guarantee your reservation. The hotel accepts American Express, Diners Club, Carte Blanche, Visa, Master Card, and Hilton credit cards. The deposit will hold your room until 6 a.m. of the morning following your scheduled arrival date. In the event of an early departure, the deposit is nonrefundable unless the hotel is notified prior to or at the time of check-in. Cancellation notice of 14 days is required for a deposit refund.

Check accommodations desired

Room Category	Rate
Singles	
Main	_____ \$108
Riverside	_____ \$118
Towers	_____ \$132
Doubles	
Main	_____ \$124
Riverside	_____ \$134
Towers	_____ \$148
1-bedroom suite	_____ \$290/390
2-bedroom suite	_____ \$375/475

Deposit amount (1 night's rate) \$ _____

☐ Check enclosed
☐ Credit card: _____
 Type of card _____ Exp. date _____

Card number _____

Signature _____

Important Information:

1. Reservations must be received by the New Orleans Hilton Riverside and Towers/ARRS Housing Bureau no later than April 7 to be assured of written confirmed accommodation. Reservations after that time are subject to availability. We urge you to make your reservations promptly.
2. Written confirmation of your reservation will be sent to you by the hotel.
3. To change or cancel reservations, please call either Hilton Reservations Service at 1-800-HILTONS or the hotel directly at (504) 561-0500.
4. If you plan to share a room, please send in only one housing form. Be sure to list all names of occupants of rooms. Assignment is delayed until complete information is received.
5. Check-in is after 3 p.m., or earlier if the room is available. Check-out time is 1 p.m.
6. Parking is available at the hotel.

Transportation Discounts

United Airlines is offering special airfares to the 1989 ARRS meeting for travel to and from New Orleans between May 3 and 16 inclusive. To obtain a 5% discount from any United available/applicable fare (MaxSavers and first class included) or a 40% discount off standard coach fares (all restrictions waived), telephone (toll-free) 1-800-521-4041 between the hours of 8:00 a.m. and 11:00 p.m. EST and immediately reference special ARRS account number 9099D. For travel to and from Canada, United will offer published Canadian meeting fares in selected markets. This discount can be as much as 35% off normal coach fares. No discounts are permitted from Mexico, the Bahamas, or the Orient. In addition, ARRS attendees who fly on United (as outlined above) will be eligible for a special drawing. The prize is one complimentary round-trip ticket good for travel in the continental United States before November 1, 1989 (holiday periods excluded).

Delta Airlines is also offering special airfares for travel to and from New Orleans between May 4 and 15 inclusive. To obtain a 5% discount from any Delta available/applicable fare or a 40% discount off standard coach fares (all restrictions waived), telephone (toll-free) 1-800-241-6760 between 8:00 a.m. and 8:00 p.m. EST and reference account number M-0045. Travel from Canada will apply at a 35% discount. No discounts are available for international travel. All fares are subject to change without notice. To obtain the best discount available, make your reservations as early as possible.

Budget Rent A Car is offering special rental rates for attendees of the 1989 ARRS meeting. These rates range from \$32 per day for an economy-sized car to \$38 per day for a full-sized four-door, based on a 3-day minimum rental. Rates are good for 1 week before and 1 week after the meeting. Make reservations by calling (toll-free) 1-800-772-3773; identify yourself as an attendee of the American Roentgen Ray Society annual meeting.

1989 ARRS Meeting Summary, May 9-12, 1989 New Orleans, LA

A comprehensive description of the meeting, including the scientific program, Categorical Course in Genitourinary Imaging, and instructional courses, appears in this issue of the *AJR*. A special loose insert on the meeting also accompanies this issue. Meeting and registration forms will be found in the February and March issues. These may be photocopied.

Accreditation

All courses and scientific sessions carry AMA Category I credit on an hour-for-hour basis.

Meeting Format

Scientific Program. Sessions will be grouped in parallel sessions, Monday–Thursday. A total of 189 scientific papers will be presented. In addition, on Wednesday, May 10, the afternoon session will feature award papers and the Caldwell Lecture, which will be delivered by Senator Bill Bradley (D-NJ). On Friday, there will be a special symposium on gastrointestinal imaging.

Categorical Course in Genitourinary Imaging. This 15.5-hr course will be Sunday–Thursday.

Luncheon Sessions. Registrants may enroll in special luncheon sessions, Monday–Thursday. A box lunch will be provided.

Exhibits

Scientific and Technical Exhibits and Case of the Day Presentations will be presented in the Grand Salon of the New Orleans Hilton Riverside and Towers, Monday–Thursday, May 8–11. The Case of the Day will be presented by Marilyn Siegel of Washington University and Mallinckrodt Institute, St. Louis, MO.

Local Activities

General Reception. Tuesday evening, May 9, for all registrants.

Golf Tournament. Monday, May 8, English Turn Country Club. Transportation leaves the hotel at 11 a.m.; shotgun start is at 12:30 p.m.

Men's and Women's Tennis Tournaments. Monday, May 8, at the New Orleans Hilton Riverside and Towers, New Orleans, LA.

Local Tours. Sunday, May 7, 1–4 p.m., Overview of New Orleans; 7:30–10 p.m., Evening on the Mississippi; Monday, May 8, 9 a.m.–4 p.m., Plantations of Old Louisiana; 8–10:30 p.m., Dinner at Gallier Hall; Tuesday, May 9, 9:30 a.m.–3:30 p.m., Elegant Homes of New Orleans; Wednesday, May 10, 9–11:30 a.m., Creole Connection; 12:30–5 p.m., Audubon Zoo/River Cruise; 7–10 p.m., Evening Overlooking the Mississippi; Thursday, May 11, 11 a.m.–2:30 p.m., Cajun Swamp Tour. No refunds after April 20.

Meeting Registration

Preregistration will be accepted until April 7. There will be on-site registration. Official badges and program books will be available at the registration desk, New Orleans Hilton Riverside and Towers. No confirmations will be mailed.

Course Registration

Register early—enrollment is limited. List first, second, and third choices for each period. Also, indicate whether you wish to take the categorical course. Deadline for mail registrations is April 7. All ticket orders will be filled by postmark. Course tickets will not be mailed. Tickets will be available on and after Sunday, May 6 (after 1 p.m.), at the ARRS registration desk in the New Orleans Hilton Riverside and Towers. There will be on-site registration for courses not already filled.

Hotel Registration

Reservations are handled by the ARRS Housing Bureau, New Orleans Hilton Riverside and Towers, Attn: Reservations Office, Poydras at the Mississippi River, New Orleans, LA 70140. These must be received by April 7. Make check payable to New Orleans Hilton Riverside and Towers.

Fees

Meeting:

ARRS members and resident members	No fee
Nonmembers	\$250
Nonmember physicians in training (with verification)	25
Categorical course (all who attend)	75
Luncheon sessions/each	12
Golf tournament	75
Tennis tournaments	50
Local tours	20–75

Cancellations and Fee Refunds

Fees will be refunded only if cancellation is received by April 20, 1989. Send to American Roentgen Ray Society, 1891 Preston White Drive, Reston, VA 22091.

Transportation Discounts

United and Delta airlines are offering discounts, up to 40%, on airfares. For United, call (800) 521-4041 and mention ARRS account number 9099D. For Delta, call (800) 241-6760 and reference account number M-0045.

Budget Rent A Car is offering special rates on car rentals. Call (800) 772-3773 and mention that you are attending the American Roentgen Ray Society annual meeting.

American Roentgen Ray Society: Officers, Committees, and Membership Information

Officers

President: Lee F. Rogers

President-elect: Ronald G. Evens

1st Vice-president: M. Paul Capp

2nd Vice-president: John A. Kirkpatrick, Jr.

Secretary: Glen W. Hartman

Treasurer: Beverly P. Wood

Executive Council: J. Thrall, J. F. Wiot, L. F. Rogers, R. A. Gagliardi, R. G. Evens, R. N. Berk, B. P. Wood, J. E. Madewell, M. P. Capp, G. W. Hartman, B. G. Brogdon, G. R. Leopold, A. Landry, Jr., A. K. Poznanski, K. H. Vydareny, J. T. Ferrucci, Jr., W. J. Casarella, E. J. Ferris, J. A. Kirkpatrick, Jr., A. E. James, Jr., chairman

Committees

Editorial Policy: S. S. Sagel, R. J. Stanley, C. A. Rohrmann, Jr., N. O. Whitley, S. V. Hilton, J. M. Taveras, R. N. Berk, W. J. Casarella, chairman

Education and Research: C. E. Putman, C. B. Higgins, B. J. Hillman, R. A. McLeod, B. G. Brogdon, chairman

Finance and Budget: A. K. Poznanski, G. R. Leopold, J. R. Thornbury, R. C. Gedgaudas-McClees, J. Thrall, chairman

Nominating: K. L. Krabbenhoft, J. F. Wiot, G. R. Leopold, chairman

Publications: R. J. Stanley, S. S. Sagel, N. O. Whitley, C. A. Rohrmann, Jr., W. J. Casarella, chairman

Membership: E. J. Ferris, G. R. Leopold, K. H. Vydareny, A. K. Poznanski, chairman

Representatives to Other Organizations

American Board of Radiology: E. C. Klatte, L. F. Rogers, J. A. Kirkpatrick, Jr.

American College of Radiology: L. F. Rogers, G. A. Kling, R. A. Gagliardi, J. E. Madewell

American Medical Association House of Delegates: S. F. Ochsner, K. L. Krabbenhoft, alternate

American National Standards Institute: M. Haskin

National Council on Radiation Protection and Measurements: E. L. Saenger, H. L. Friedell

Meeting Arrangements

Annual Meetings: May 7-12, 1989, Hilton, New Orleans; May 13-18, 1990, Sheraton Washington, Washington, DC

Annual Meeting Committee: H. C. Carlson, G. P. Janetos, E. K. Lang, R. R. Lukin, A. Landry, Jr., chairman

Instruction Courses: R. J. Stanley, associate chairman, J. T. Ferrucci, Jr., chairman

Scientific Program: R. J. Alfidi, A. E. Robinson, J. H. Thrall, M. P. Banner, J. J. Gisvold, T. C. McLoud, R. G. Evens, chairman

Scientific Exhibits: A. A. Moss, A. V. Proto, R. J. Churchill, J. E. Madewell, chairman

ARRS Membership

An application form is printed in the January issue of the *Journal*. For consideration at the 1989 ARRS meeting, send completed forms before February 1, 1989, to American Roentgen Ray Society, 1891 Preston White Dr., Reston, VA 22091. Active members are graduates of an approved medical or osteopathic school or hold an advanced degree in an allied science. They must practice radiology or work in an associated science in the United States or Canada and be certified by the American Board of Radiology, American Osteopathic Board of Radiology, or Royal College of Physicians of Canada or otherwise adequately document training and credentials. Corresponding members are foreign radiologists or scientists who are active in radiology or an allied science. Members-in-training are residents or fellows in radiology or postgraduate students in an allied science. Additional application forms can be obtained from the ARRS offices in Reston, VA.

Business Office

Paul Fullagar, Administrative Director, American Roentgen Ray Society, 1891 Preston White Dr., Reston, VA 22091; (703) 648-8900

Letters

CT and Sonographic Features of Pseudomyxoma Peritonei

The availability of abdominal sonography and CT have made possible the noninvasive diagnosis of pseudomyxoma peritonei.

A 38-year-old woman had massive abdominal distension, anorexia, and a marked weight loss of 2 months duration. Examination revealed a cachectic woman with ascites and multiple, soft, cervical polyps evident on speculum vaginal examination. Hemoglobin was 13.1 g/dl, and the erythrocyte sedimentation rate was 96 mm in the first hour.

Sonography showed echogenic ascites with interspersed hypoechoic areas. The intestines were displaced posteriorly. The ovaries were not identified. CT confirmed the presence of ascites (8 H). Scallopings of the hepatic margin and formation of septa not seen on sonography were visualized on CT (Fig. 1A). Several irregular structures (20 H) were seen within the fluid. Some had well-defined rims and central hypoattenuation (Fig. 1B).

At laparotomy, the peritoneal cavity contained 12 l of gelatinous material. Both ovaries contained multiloculated cysts measuring up to 12 cm in diameter, some of which were seen exuding mucinous material. Histologically, the ovaries showed a mucinous cystadenocarcinoma with spread to the cervix and omentum.

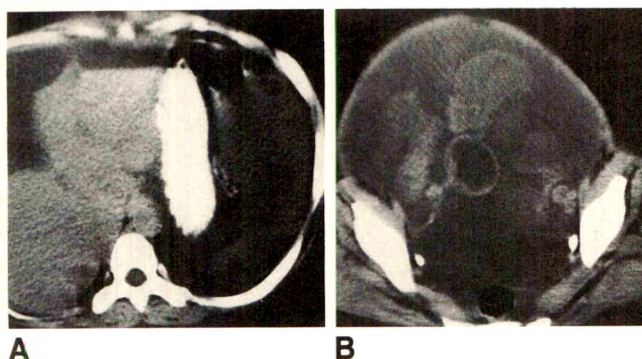


Fig. 1.—Pseudomyxoma peritonei.

A, CT scan at level of liver shows septated ascites and scalloping of surface of liver.

B, CT scan through pelvis shows ascites containing several structures, one of which has a well-defined rim. The latter was a large mucin-containing cyst arising from right ovary.

Sonographic features of pseudomyxoma peritonei include intra-abdominal masses, ascites with multiple septations, and echogenic masses. CT findings include low-density masses, calcification, scalloping of liver margins, septations, intrahepatic low-attenuation lesions, and posterior displacement of intestines [1–3].

In our case, CT showed hepatic scalloping, ascites, and posterior displacement of the intestines. Irregular structures within the ascites on CT were identified as the ovaries at laparotomy.

P. S. Lawate

S. P. Singh

M. P. Jasper

R. William

M. V. Bharathi

D. D. K. Rolston

Christian Medical College Hospital
Vellore 632 004, India

REFERENCES

1. Seshul MB, Coulam CM. Pseudomyxoma peritonei: computed tomography and sonography. *AJR* 1981;136:803–806
2. Foster DR. Ultrasound findings in pseudomyxoma peritonei. *Australas Radiol* 1985;29:39–41
3. Yeh H-C, Shafir MK, Slater G, Meyer RJ, Cohen BA, Geller SA. Ultrasonography and computed tomography in pseudomyxoma peritonei. *Radiology* 1984;153:507–510

Bilateral Blurring of Vision After Administration of Contrast Medium During IV Digital Subtraction Angiography

We recently saw an unusual adverse reaction after intravascular administration of Urografin 76% (sodium and meglumine diatrizoate) during IV digital subtraction angiography in two patients. Both were young adult men with a recent onset of moderate hypertension and no history of allergy to iodinated contrast medium. A 5-French high-flow pigtail catheter was placed in the middle of the right atrium, and the position was checked by injecting 4 ml of Urografin 76%. No untoward reaction was noted after this test injection. Subsequently, after the injection of a bolus of contrast medium (30 ml at 20 ml/sec), the patients complained of bilateral blurring of vision, which subsided within a few minutes. No significant change in blood pressure occurred during the episodes of blurring. No neurologic deficit was observed, and the patients had no other complaints.

Adverse reactions to iodinated contrast media occur in 5–8% of all intravascular injections and are more common after IV injections [1, 2]. These are probably not related to the age, sex, or weight of the patient, except for a slight variance in the younger and lower weight groups [3]. Patients who have underlying cardiac disease have a higher risk of these reactions developing, but no direct relationship with hypertension has been described [4]. Even though many types of adverse reactions have been reported [1–4], we found no previous mention of bilateral blurring of vision after IV administration of contrast medium.

Various mechanisms responsible for these adverse reactions have been described [1]. Both our patients had underlying hypertension, and we have otherwise not seen this type of adverse reaction in a large population of patients undergoing IV digital subtraction angiography, suggesting that the underlying hypertension was in some way related to the blurring of vision.

Sanjiv Sharma

Mira Rajani

All India Institute of Medical Sciences
New Delhi, 110029, India

REFERENCES

1. McClennan BL. Low osmolality contrast media: premises and promises. *Radiology* 1987;162:1–8
2. Shehadi WH. Adverse reactions to intravascularly administered contrast media: a comprehensive study based on a prospective survey. *AJR* 1975;124:145–152
3. Shehadi WH, Toniolo G. Adverse reactions to contrast media. *Radiology* 1980;137:299–302
4. Ansell G, Tweedie MCK, West CR, Evans P, Couch L. The current status of reactions to intravenous contrast media. *Invest Radiol* 1980;15: S32–S39

Stress Fracture of the Os Peroneum

A 25-year-old obese woman had a snapping sensation along the lateral aspect of the right foot that occurred while she was walking. Plain radiographs made the next day were interpreted as negative. Pain continued for 5 weeks despite conservative treatment. When she came to the hospital 6 weeks after the injury, she had pain during ambulation only. Her mother stated that the patient had "walked on the outside of her feet all of her life." Physical examination revealed only tenderness at the cubocalcaneal joint. Magnification oblique views of the foot were made to evaluate a possible fracture of the os peroneum suggested on the conventional films (Fig. 1). A normal os peroneum was seen on the left side. Radionuclide (^{99m}Tc -MDP) bone scan showed increased uptake at the os peroneum, confirming the diagnosis of fracture. The patient was treated by immobilization in a cast. Follow-up telephone calls at 6 and 10 months after the injury revealed improvement in the symptoms: only mild pain on prolonged activity.

Fractures of sesamoid bones are rare. The os peroneum, embedded in the peroneus longus tendon as the tendon enters the cuboid sulcus, is identified on only 14–26% of radiographs of the feet. It may be bipartite (19%), tripartite (4%), or multipartite (1%) [1]. Reports of fracture of the os peroneum have been few and certainly less frequent than reports of rupture of the peroneal tendon. One mechanism for fracture is dorsiflexion at the ankle, similar to that causing rupture of the tendon [2, 3]. An alternative cause involves repeated muscular traction, resulting in microfractures and, ultimately, clinical stress fractures. Meurman [4] reported one case of stress fracture of the os peroneum among a series of 827 stress fractures in soldiers, and Burman and Lapidus [1] described two women who had suspected fracture of the os peroneum and clinical manifestations of peroneal tenosynovitis.

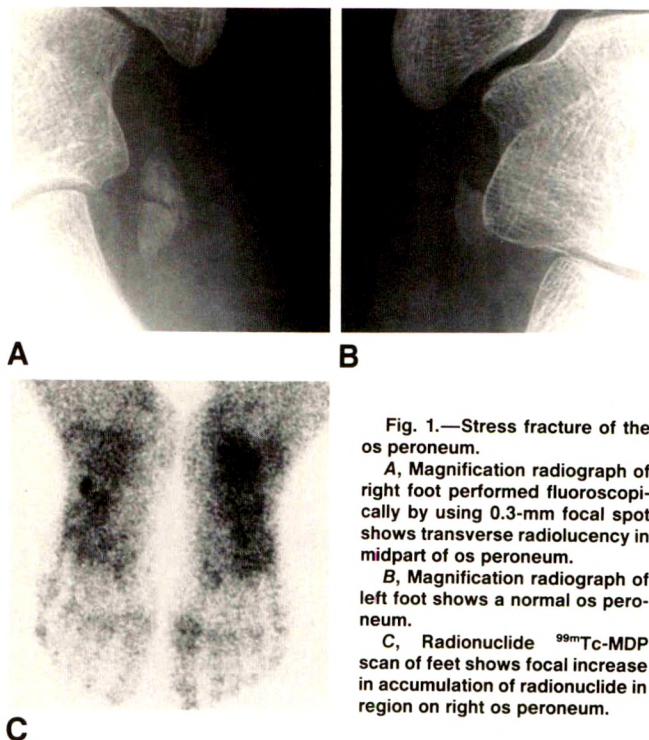


Fig. 1.—Stress fracture of the os peroneum.

A, Magnification radiograph of right foot performed fluoroscopically by using 0.3-mm focal spot shows transverse radiolucency in midpart of os peroneum.

B, Magnification radiograph of left foot shows a normal os peroneum.

C, Radionuclide ^{99m}Tc -MDP scan of feet shows focal increase in accumulation of radionuclide in region on right os peroneum.

This case is the third report of radiographic evidence of stress fracture of the os peroneum and the first case to be confirmed by scintigraphy. Violent dorsiflexion did not precede the onset of symptoms. This case also points out the value of magnification views and scintigraphy in making the diagnosis. Because the os peroneum may be multipartite, diagnosis based on the findings on plain films may be difficult. Thus, these supporting studies are useful in instances in which radiographic diagnosis is not certain.

Martin R. Crain

Georges Y. El-Khoury

The University of Iowa Hospitals and Clinic
Iowa City, IA 52242

REFERENCES

1. Burman MS, Lapidus PW. The functional disturbances caused by the inconstant bones and sesamoids of the foot. *Arch Surg* 1931;22:936–975
2. Mains DB, Sullivan RC. Fracture of the os peroneum. *J Bone Joint Surg [Am]* 1973;55-A(7):1529–1530
3. Tehranzadeh J, Stoll DA, Gabriele OM. Case 271. *Skeletal Radiol* 1984;12:44–47
4. Meurman KOA. Less common stress fractures in the foot. *Br J Radiol* 1981;54:1–7

Isolation of the Right Subclavian Artery

I read the recent case report by Mathieson et al. [1] with great interest. The authors state that isolation of the right subclavian artery has not been reported before. It is ironic that our paper, "Isolation of a Subclavian Artery" [2], in which we described three cases of isolation of the right subclavian artery, was published in the *AJR*. To the best of our knowledge, this condition was first reported by Barger et al. in 1954 [3]. Mathieson et al. found that blood pressure in both arms was equal despite the presence of closure of the right ductus and consequent subclavian steal. Such was the case in our patients

as well. Hence, in patients with tetralogy of Fallot, it is necessary to exclude isolation of the subclavian artery before attempting a Blalock-Taussig shunt.

Hrudaya Nath
The University of Alabama at Birmingham
Birmingham, AL 35233

REFERENCES

1. Mathieson JR, Silver SF, Culham JAG. Case report. Isolation of the right subclavian artery. *AJR* 1988;151:781-782
2. Nath PH, Castaneda-Zuniga W, Zollkofer C, et al. Isolation of a subclavian artery. *AJR* 1981;137:683-688
3. Barger JD, Creasman RW, Edwards JE. Bilateral ductus arteriosus associated with interruption of the aortic arch. *Am J Clin Pathol* 1954;24:441-444

Reply

Dr. Nath has brought to our attention the previous report [1] in which he and his colleagues included three cases of isolated right subclavian artery. Their case 6 was a patient with complex congenital heart disease, visceral heterotaxy, and bilateral patent ductus. Cases 7 and 8 had bilateral ductus. Case 8 was the most similar to ours because of closure of the right-sided ductus.

Dr. Nath also refers to an earlier case (Barger et al. [2]) of right-sided isolation of the subclavian artery associated with arch interruption. Our case [3] apparently is the only one of isolated right subclavian artery without other arch anomalies or associated left-sided ductus. We agree with Dr. Nath's concern for potential problems with shunt surgery in the presence of an isolated subclavian artery.

J. A. Gordon Culham
British Columbia's Children's Hospital
Vancouver, B.C. V6H 3V4

REFERENCES

1. Nath PH, Castaneda-Zuniga W, Zollkofer C, et al. Isolation of a subclavian artery. *AJR* 1981;137:683-688
2. Barger JD, Creasman RW, Edwards JE. Bilateral ductus arteriosus associated with interruption of the aortic arch. *Am J Clin Pathol* 1954;24:441-444
3. Mathieson JR, Silver SF, Culham JAG. Case report. Isolation of the right subclavian artery. *AJR* 1988;151:781-782

Drug Testing at the Oral Boards?

With the memories of the Seoul Olympics still painfully fresh, it seems most appropriate to examine the use of performance-enhancing drugs among radiologists. Beta-blockers have been shown to be useful in the management of acute situation stress [1, 2], and few experiences in the life of a radiologist are more acutely stressful than the oral boards. On the basis of an informal survey of residents, it appears that these drugs are already being used. These agents have been banned by the International Olympic Committee, and drug testing is enforced for sports such as shooting, fencing, and diving in which the somatic manifestations of stress can dramatically impair an athlete's performance [3].

A fundamental difference between amateur athletic competition and the boards is that an athlete chooses to compete, but residents must take the boards. Nevertheless, it is just as unfair to allow use of performance-enhancing drugs at the boards as it is to allow their use at a sporting event. Short of instituting drug testing, it seems

naive to think that the American Board of Radiology could by decree eliminate use of beta-blockers at the boards.

We believe that the perceived need for such drugs could be minimized by better preparing residents to deal with the stress of the examinations. Many radiology programs spend much more conference time generating stress than teaching residents how to deal with it, and stress will remain an integral and often important part of oral examinations. Beta-blockers should be banned from the oral boards, but radiology training programs must prepare residents to handle the stress of these examinations if such a ban is to be respected.

Alex Mamourian
Robert Sefczek
Penn State University Hospital
Hershey, PA 17033

REFERENCES

1. Lehrer PM, Rosen RC, Kostic JB, Greenfield D. Treating stage fright in musicians: the use of beta blockers. *NJM* 1987;84(1):27-33
2. James IM. Beta blockers and acute situational stress. *Clin Neuropharmacol* 1986;9(suppl 4):423-425
3. U.S. Olympic Committee Drug Newsletter, May 31, 1985

A New Radiologic Sign of Ruptured Pulmonary Hydatid Cyst

Hydatid cysts represent the larval form of the canine intestinal tapeworm *Echinococcus granulosus* and are encountered worldwide. Structurally, they consist of a tough outer pericyst that protects a delicate inner endocyst from which brood capsules and daughter cysts develop. They may be difficult to distinguish from other cystic and cavitory lesions. We describe the unique CT appearance of a ruptured hydatid cyst of the lung.

A 23-year-old woman had had a dull ache in the right lower chest for 4 months. Two months before admission, she had an episode of wheezing, coughing, and flushing, with subsequent bouts of coughing and breathlessness. The chest radiograph revealed a cavity with multiple internal rings in the right lower lobe associated with a pleural effusion (Fig. 1A). A CT scan showed the cyst to better advantage (Fig. 1B). At thoracotomy, a ruptured hydatid cyst was identified and removed.

Most hydatid cysts are asymptomatic. Clinical manifestations, when they occur, are frequently those of a space-occupying lesion [1]. Occasionally, however, rupture of the cyst may be the first sign. When the cyst ruptures or is punctured, serious anaphylactic complications may occur.

A variety of signs on chest radiographs that denote different appearances produced by air within the cyst have been described [1]. The crescent sign is produced by air between the pericyst and the fluid-filled endocyst. The double-arch sign denotes air outlining both the pericyst and the endocyst. The water-lily sign is produced by the endocysts floating on top of the fluid. The daughter-cyst sign is seen within the cyst when air outlines the daughter cyst at the bottom. Not all of these signs are pathognomonic of a hydatid cyst. The crescent sign may be seen with an intracavitary fungus ball or blood clot, pulmonary gangrene, cavitating malignancy, and so forth [1, 2]. The daughter-cyst sign also may be mimicked by an intracavitary fungus ball or blood clot [3]. Even the time-honored water-lily sign may not be pathognomonic [2].

The chest radiograph and CT scan of our patient showed the partially crumpled membranes of the mother and daughter cysts as multiple rings. This ring-within-a-ring appearance has not been documented previously as a finding in hydatid cyst. Unlike the other



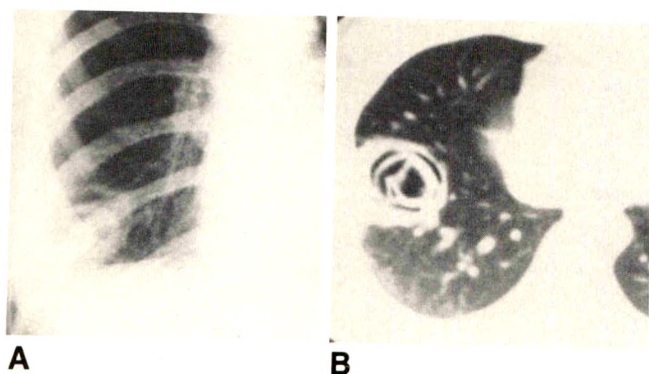


Fig. 1.—Ruptured pulmonary hydatid cyst.

A, Chest radiograph shows cystic lesion in right lower lobe with a small pleural effusion.

B, CT scan shows multiple rings due to crumpled membranes of mother and daughter cysts.

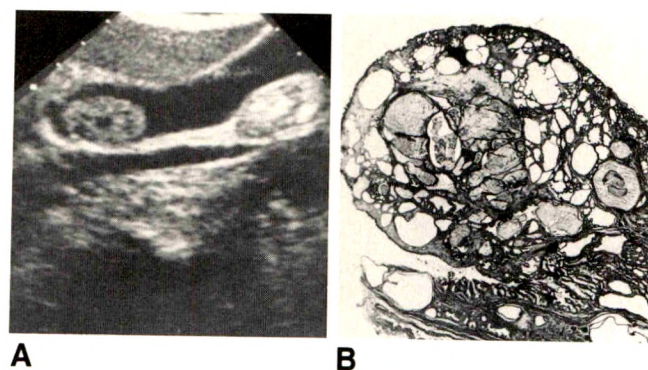


Fig. 1.—Heterotopic gastric mucosa in the gallbladder.

A, Sonogram shows circumscribed mass in gallbladder.

B, Low-power photomicrograph shows structure of heterotopia. Note enlarged glandular cavities.

signs, the genesis of this sign depends solely on intracavitary endocysts. As such, it is pathognomonic of this disease.

Shashi Aggarwal

Alka Kumar

Sima Mukhopadhyay

Manorama Berry

All India Institute of Medical Sciences, Ansari Nagar,
New Delhi 110029, India

REFERENCES

1. Balikian JP, Mudarris FF. Hydatid disease of the lungs: a roentgenologic study of 50 cases. *AJR* 1974;122:692-707
2. Felson B. *Chest roentgenology*. Philadelphia: Saunders, 1973:314-349
3. Saksook FA, Fahl MH, Rizk GK. Computed tomography of pulmonary hydatid disease. *J Comput Assist Tomogr* 1986;10:226-232

Heterotopic Gastric Mucosa in the Gallbladder

We present a case of gastric heterotopia in the gallbladder that appeared to be a tumor on sonography. To our knowledge, this sonographic finding has not been described before.

A 77-year-old woman had sonography because of nonspecific abdominal pain. The sonogram showed a 2-cm mass in the neck of the gallbladder (Fig. 1A). Pathologic examination of the gallbladder after cholecystectomy showed that the lesion was composed of gastric fundal mucosa covered with mucus-secreting columnar epithelium (Fig. 1B). The mass contained normal fundic glands with chief cells and parietal cells and a mild, chronic inflammatory infiltrate. Elsewhere the gallbladder was normal.

Heterotopia is the presence of well-differentiated normal tissue in an abnormal location. In the gallbladder, heterotopic islands of gastric mucosa, intestinal mucosa, pancreatic tissue, and liver tissue have been reported [1]. Heterotopic gastric mucosa has also been noted in the duodenum, where it is visible as a polypoid mass or prominent areae gastricae in the base of the duodenal bulb [2]. Gastric fundal mucosa with specialized chief and parietal cells probably could not be formed by metaplasia of gallbladder epithelium. The abnormality is more likely congenital, formed from displaced anlagen or by a developmental error of multipotential cells [3]. In almost all cases, the heterotopic tissue is located in the neck of the gallbladder or in the adjacent cystic duct [4]. The heterotopia forms either a nodule in the wall of the gallbladder [3] or a mucosal lesion resembling a polyp. Chronic cholecystitis is often present, possibly because of peptic

secretions produced by the heterotopic glands [4]. The major complication is peptic ulceration of the gallbladder with perforation and hemorrhage [4].

P. Pradines

M. Brauner

I. Legrand

M. Sibony

B. Garin

Hôpital Jean Verdier

93143 Bondy Cedex, France

REFERENCES

1. Kalman PG, Stone RM, Phillips MJ. Heterotopic gastric tissue of the bile duct. *Surgery* 1981;81:384-386
2. Agha FP, Ghahremani GG, Tsang TK, Victor TA. Heterotopic gastric mucosa in the duodenum: radiographic findings. *AJR* 1988;150:291-294
3. Whittaker LD Jr, Lynn HB, Dockerty MB, Stickler GB. Heterotopic gastric mucosa in the wall of the cystic duct: report of a case. *Surgery* 1967;62:382-385
4. Larsen EH, Diederich PJB, Sorensen FB. Peptic ulcer in the gallbladder: a case report. *Acta Chir Scand* 1985;151:575-576

The Three Lines: Origin of Sonographic Landmarks of the Fetal Head

We were pleased to read that Hertzberg et al. [1] found that the lines to either side of the midline echo of the fetal brain arise from small cerebral blood vessels rather than from the lateral ventricular walls. Clearly, they were unaware of our autopsy studies [2, 3] showing the same findings. We showed that these lines are separate from the lateral ventricular walls, and we proposed that they arose from cortical blood vessels. In fact, if the brain is removed from the skull and scanned at an oblique angle, different cortical vessels radiating from the superolateral angle of the lateral ventricle are detected when the vessels are at right angles to the ultrasound beam. To our regret, our findings have not been accepted for many years. We hope that their rediscovery by Hertzberg et al. will ensure that these parallel lines in the fetus and neonate are no longer misnamed as arising from the lateral ventricular wall.

Lachlan Ch. de Crespigny

Hugh P. Robinson

St. Andrew's Hospital

East Melbourne, 3002 Australia

REFERENCES

1. Hertzberg BS, Bowie JD, Burger PC, Marshburn PB, Djang WT. The three lines: origin of sonographic landmarks in the fetal head. *AJR* 1987; 149:1009-1012
2. de Crespigny LCh, Robinson HP. The anatomical basis for the ultrasound diagnosis of cerebroventricular haemorrhage and its sequelae. *Ultrasound Med Biol* 1982;8:593-603
3. de Crespigny LCh. Intraventricular haemorrhage. In: Bennett MJ, ed. *Ultrasound in perinatal care*. New York: Wiley & Sons, 1984:157-181

Reply

We thank Drs. de Crespigny and Robinson for their letter about our recent article [1]. We agree that their autopsy studies did indeed show that in the neonate, small cerebral blood vessels account for lines corresponding to those seen in the fetus during antenatal sonography [2]. We were pleased to learn that using a different approach, in a different population of patients, Drs. de Crespigny and Robinson arrived at the same conclusion proposed in our article: The lines seen on axial scans above the level of the thalamus do not originate from the lateral walls of the lateral ventricles but rather correspond to small blood vessels.

We regret that despite running the usual literature searches before publishing our study, we were unaware of the work of de Crespigny and Robinson and, as a result, did not credit them. We suspect that this occurred because the title of their article emphasizes cerebroventricular hemorrhage rather than normal intracranial anatomy, the material deals with newborns rather than with intrauterine hydrocephalus, and, as they themselves state, their findings did not receive wide acceptance. It is unfortunate that for so many years after their article was published, these lines were assumed to originate from the lateral ventricles and were erroneously used as markers to evaluate for hydrocephalus. We hope that with the additional work recently published by our group, the concept that these lines do not originate from the ventricular walls will finally receive the wide clinical acceptance it deserves.

Barbara S. Hertzberg
James D. Bowie
Peter C. Burger
Paul B. Marshburn
William T. Djang
Duke University Medical Center
Durham, NC 27710

REFERENCES

1. Hertzberg BS, Bowie JD, Burger PC, Marshburn PB, Djang WT. The three lines: origin of sonographic landmarks in the fetal head. *AJR* 1987; 149:1009-1012
2. de Crespigny LCh, Robinson HP. The anatomical basis for the ultrasound diagnosis of cerebroventricular haemorrhage and its sequelae. *Ultrasound Med Biol* 1982;8:593-603

Pelvic Abscess Complicated by a Subarachnoid Fistula

Acquired subarachnoid fistulas of the spinal cord are rare and often have catastrophic consequences. A case is described in which a confusing clinical presentation led to an unusual method of diagnosis.

A 63-year-old man with recurrent squamous cell carcinoma of the sacrum arising from a pilonidal cyst was admitted for a right hemipelvectomy. A musculocutaneous flap from the right thigh was mobilized to fill in the hemipelvic defect. The right ureter was accidentally

damaged, necessitating primary repair. Three Jackson-Pratt surgical drains were placed within the surgical wound.

Two of the drains were promptly removed. The third continued to drain 300 ml of yellow, serous fluid daily, suggesting a urine leak. The patient subsequently became febrile, and cultures of the drainage fluid became positive for several microorganisms. The patient denied having headache, meningismus, or back or leg pain.

CT of the pelvis (Fig. 1) showed the hemipelvectomy deformity. The drain was seen with its tip terminating directly posterior to a defect in the posterior sacral canal. Although the margins of the thecal sac were not clearly visualized at this level, it seemed probable that its dorsal aspect abutted the drain. A poorly defined region of mixed attenuation anterior to the drain suggested an abscess.

Under fluoroscopic guidance, approximately 100 ml of 30% meglumine diatrizoate were injected through the drain. An 8 × 10 cm abscess cavity was identified anterior and inferior to the drain. Further injection of contrast medium resulted in abrupt filling of the subarachnoid space with visualization of the cauda equina.

A high lumbar spinal drain was placed, and the remaining Jackson-Pratt drain was removed. After a week of treatment with broad-spectrum antibiotics, the fever resolved. A myelogram showed no fistula.

Most acquired subarachnoid fistulas of the spinal cord result from penetrating or severe blunt trauma. The thoracic spine is the most common site where fistulas are usually to the pleural space [1, 2]. Iatrogenic causes from spinal and thoracic surgery are unusual [2].

This case is unusual because of the absence of meningismus, headache, or neurologic deficit. The clinical presentation was further confused by the intraoperative damage of the right ureter. Consequently, the method of diagnosis was also unusual. To my knowledge, sinographic demonstration of a spinal subarachnoid fistula has not been reported before.

John C. Chaloupka
Emory University Hospital
Atlanta, GA 30322

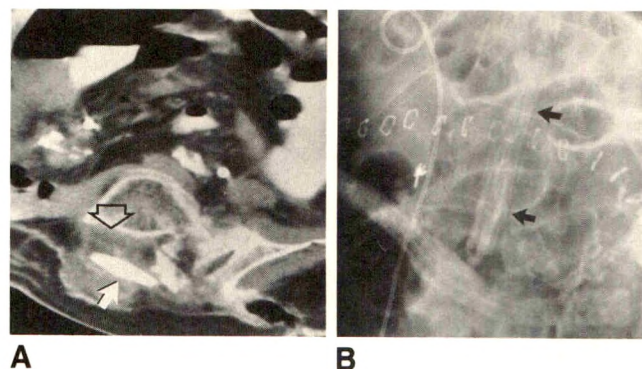


Fig. 1.—Pelvic abscess complicated by a subarachnoid fistula.

A, CT scan of pelvis shows hemipelvectomy defect and drain (closed arrow) abutting posterior thecal sac. A poorly defined region of mixed attenuation is seen both to right of thecal sac and anterior to drain (open arrow).

B, Sinogram obtained after injection of contrast material into drain shows a communication between abscess and subarachnoid space. Cauda equina is visualized (arrows). A right ureteral stent is in place.

REFERENCES

1. Lovaas ME, Castillo RG, Deutschman CS. Traumatic subarachnoid-pleural fistula. *Neurosurgery* 1985;17:650-652
2. Qureshi MM, Roble DC, Gindin RA, Scudamore HH. Subarachnoid-pleural fistula: case report and review of the literature. *J Thorac Cardiovasc Surg* 1986;91:238-241

Angiographic Demonstration of Esophagojejunal Venous Shunt in a Patient with Esophagojejunostomy and Esophageal Varices

To our knowledge, the occurrence of esophageal varices in patients with esophagojejunostomy has not been reported. We describe a patient who had bleeding esophageal varices 7 years after a total gastrectomy. Angiography revealed an esophagojejunal shunt.

A 72-year-old man presented with massive hematemesis. Seven years earlier, he had had a total gastrectomy with splenectomy and esophagojejunostomy for gastric adenocarcinoma. Two years earlier, a diagnosis of chronic active hepatitis had been made. Endoscopy showed large bleeding esophageal varices that abruptly ended at the esophagojejunostomy anastomosis. Superior mesenteric arteriography showed hepatopetal portal blood flow and a large ascending jejunal vein with hepatofugal flow (Fig. 1). Endoscopic sclerotherapy stopped the bleeding. Contrast material injected into a large varix 1 cm above the anastomosis flowed in a cephalic direction. Retrograde flow into jejunal veins was noted after high-pressure injection of contrast medium. Follow-up endoscopy 1 year later showed no recurrence of the varices.

Unusual locations of varices are characteristic in patients with portal hypertension who have had gastrointestinal surgery [1]. In our case, the occurrence of esophageal varices was surprising because these are unusual after gastrectomy and splenectomy. Angiography and direct venography showed that the varices were the result of a communication between jejunal and esophageal veins. This may have been the result of collateral flow directly across the esophagojejunal anastomosis or through periesophageal veins. Communications across anastomoses are not surprising considering the frequent recurrence of esophageal varices after devascularization and transection procedures [2].

Jean-François Bretagne
Olivier Loréal
Isabelle Le Jean-Colin
Jean-Luc Raoul
Joseph Gastard
CHU Pontchaillou
35033 Rennes, France

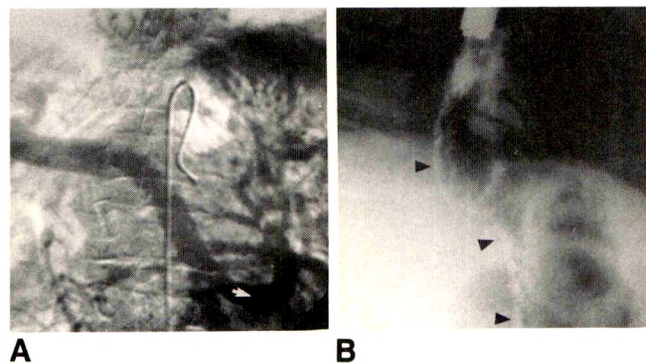


Fig. 1.—Esophagojejunal venous shunt in a 72-year-old man with esophagojejunostomy and esophageal varices.

A, Superior mesenteric arteriogram shows hepatopetal portal blood flow and a large jejunal vein with hepatofugal flow (arrow).

B, Venogram of intravariceal injection of contrast material during endoscopic sclerotherapy shows retrograde flow into jejunal veins (arrowheads).

REFERENCES

1. Fee HJ, Taylor JB, O'Connell TX. Bleeding intestinal varices associated with portal hypertension and previous abdominal surgery. *Am Surg* 1977;43:760-762
2. Koyanagi N, Iso Y, Higashi H, Kitano S, Sugimachi K. Recurrence of varices after esophageal transection: intra-operative and post-operative assessment by endoscopy. *Br J Surg* 1988;75:9-11

Periaortic Leukemic Infiltration

Leukemic infiltrates begin as small perivascular aggregates that progressively diffuse through the stroma of the affected organ [1]. Overall, intrathoracic radiographic manifestations of uncomplicated leukemia are uncommon; the most common are hilar and mediastinal lymphadenopathy (7% and 10%, respectively) [2].

A 52-year-old woman had a 2-month history of fatigability, night sweats, and petechia. Laboratory studies at admission revealed a hematocrit of 18%; a WBC count of 18,100, with 90% blast forms (Auer body positive); and a platelet count of 35,000. A chest radiograph showed bilateral displacement of the paraspinal lines (Fig. 1). Chest CT showed a concentric soft-tissue mass with bilateral paraspinal and pleural extensions surrounding a normal-sized descending aorta. MR was performed also to rule out a chronic dissection. No intimal flap was seen.

Because the finding of periaortic infiltration was incidental, the patient's condition was stable, and thrombocytopenia was present, invasive procedures were not performed. Follow-up CT 3 weeks after the start of chemotherapy showed a decrease in the size of the soft-tissue mass around the aorta and spine and in the size of the pleural extensions. A follow-up chest film obtained 5 weeks after the first one showed a marked decrease in the widening of the paraspinal lines.

We believe that our patient's lack of symptoms related to the periaortic infiltration, the concentric nature of the soft-tissue mass, and the decrease in size after chemotherapy argue strongly that this finding was due to leukemic infiltration of the periaortic soft tissues.

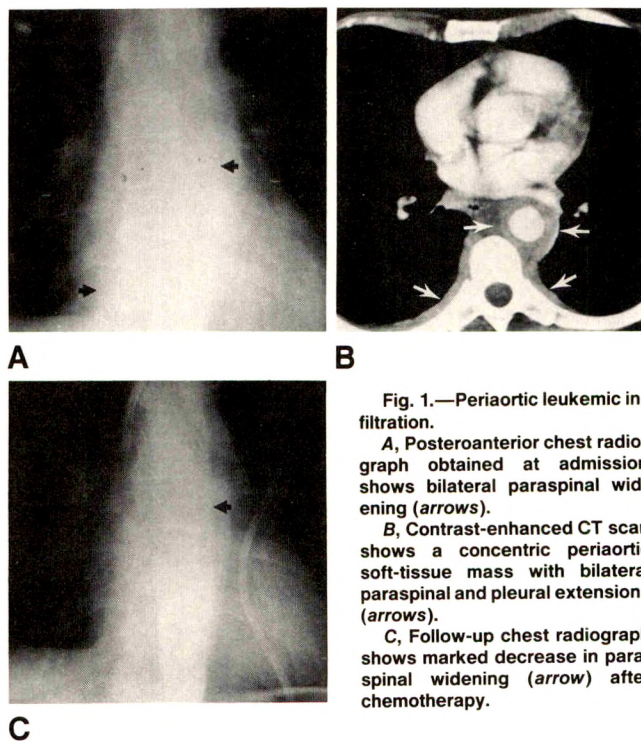


Fig. 1.—Periaortic leukemic infiltration.

A, Posteroanterior chest radiograph obtained at admission shows bilateral paraspinal widening (arrows).

B, Contrast-enhanced CT scan shows a concentric periaortic soft-tissue mass with bilateral paraspinal and pleural extensions (arrows).

C, Follow-up chest radiograph shows marked decrease in paraspinal widening (arrow) after chemotherapy.

No similar cases have been reported. A single pathologically proved case of ruptured abdominal aortic aneurysm due to myelogenous leukemic infiltration has been reported, establishing that infiltration of the aortic wall does occur [3]. We hope that knowledge of this entity will help prevent unnecessary intervention in a high-risk patient.

Suzanne T. Mastin
Barbara G. Steinbach
Pablo R. Ros
University of Florida
Gainesville, FL 32610

REFERENCES

1. Robbins SL, Cotran FS, Kumar V. Diseases of white cells, lymph nodes and spleen. In: *Pathologic basis of disease*, 3rd ed. Philadelphia: Saunders, 1984:653-705
2. Klatte EC, Yardley J, Smith EB, et al. The pulmonary manifestations and complications of leukemia. *AJR* 1963;89:598-609
3. Shifrin EG, Drenger B, Matzner Y, Kaplan L. Ruptured inflammatory abdominal aortic aneurysm due to acute myelomonoblastic leukemia. *J Cardiovasc Surg (Torino)* 1987;28(1):32-34

Letters are published at the discretion of the Editor and are subject to editing.

Letters to the Editor must not be more than two *double-spaced*, typewritten pages. One or two figures may be included. Abbreviations should not be used. See Author Guidelines, page A5.

Material being submitted or published elsewhere should not be duplicated in letters, and authors of letters must disclose financial associations or other possible conflicts of interest.

Letters concerning a paper published in the *AJR* will be sent to the authors of the paper for a reply to be published in the same issue. Opinions expressed in the Letters to the Editor do not necessarily reflect the opinions of the Editor.

Review of Current Literature

Initials and addresses of corresponding authors are provided in parentheses for each article so that the reader can obtain reprints directly. Abstracts are printed verbatim from each journal.

The New England Journal of Medicine

Echocardiographic findings in autosomal dominant polycystic kidney disease. Hossack KF, Leddy CL, Johnson AM, Schrier RW, Gabow PA (KFH, Division of Cardiology, Denver General Hospital, 777 Bannock St., No. A009, Denver, CO 80204). *N Engl J Med* 319(14):907-912, 1988

Echocardiography, including Doppler analysis, was performed to assess the prevalence of cardiac abnormalities in 163 patients with autosomal dominant polycystic kidney disease, 130 unaffected family members, and 100 control subjects. In these three groups, the prevalence of mitral-valve prolapse was 26, 14, and 2 percent, respectively ($P < 0.0005$). A higher prevalence of mitral incompetence (31, 14, and 9 percent, respectively; $P < 0.005$), aortic incompetence (8, 3, and 1 percent, respectively; $P < 0.05$), tricuspid incompetence (15, 7, and 4 percent, respectively; $P < 0.02$), and tricuspid-valve prolapse (6, 2, and 0 percent, respectively; $P < 0.02$) was also found in the patients with polycystic kidney disease.

These findings reflect the systemic nature of polycystic kidney disease and support in the hypothesis that the disorder involves a defect in the extracellular matrix and the cardiac abnormalities are an expression of that defect.

Cancer

Metastatic pattern in recurrent breast cancer: special reference to intrathoracic recurrences. Kamby C, Vejborg I, Kristensen B, Olsen LO, Mouridsen HT (CK, Dept. of Oncology ONA, The Finsen Institute, Rigshospitalet, 49, Strandboulevarden, DK-2100 Copenhagen, Denmark). *Cancer* 62:2226-2233, 1988

The anatomical and temporal patterns of recurrence were studied in 401 patients with first recurrence of breast cancer. All patients underwent the same scheduled investigation program: history, physical examination, blood tests, bone scanning, bilateral iliac crest biopsy, radiologic bone survey, chest x-rays, and ultrasound scanning of the liver. The current article focuses on the diagnosis of intrathoracic (ITH) recurrence. Most patients recurred in a single site and 50% of the recurrences were diagnosed within the first 2 years from initial diagnosis. Chest x-ray revealed ITH recurrence in 27% (109 patients), and in 8% the lung, pleura, and/or mediastinum were the only signs of recurrence. Generally, the status of primary demographic, clinical, and pathoanatomical characteristics were not predictive as to the development of ITH recurrence, although patients with pleural recurrences often had centrally located primary tumors,

locally advanced disease, and often received adjuvant radiotherapy. Clinical symptoms and signs of ITH recurrence were present in only one third of the patients, and the diagnostic specificity and sensitivity of serum lactate dehydrogenase were only 33% and 85%, respectively. Since ITH recurrences often are silent, and since recurrence in this site may have both prognostic and therapeutical implications, routine chest x-ray is indicated in all patients with first recurrence of breast cancer.

Reprinted by permission from the American Cancer Society.

Thromboembolic events in patients with malignant superior vena cava syndrome and the role of anticoagulation. Adelstein DJ, Hines JD, Carter SG, Sacco D (DJA, Cleveland Metropolitan General Hospital, 3395 Scranton Rd., Cleveland, OH 44109). *Cancer* 62:2258-2262, 1988

In patients with superior vena caval obstruction resulting from malignancy, the importance of vena caval thrombosis and the role of anticoagulation are incompletely understood. The authors discuss this aspect of the management of 25 patients with malignant superior vena cava syndrome. Ten patients were retrospectively reviewed after having been clinically diagnosed without venography, and treated without anticoagulation. Five thromboembolic complications occurred, two of which proved fatal. Fifteen patients were prospectively evaluated by angiography and then treated with anticoagulants. Angiographic evidence of intraluminal subclavian vein or superior vena caval thrombosis was found in five of these patients, and no thromboembolic complications occurred. Of the 20 patients ultimately anticoagulated, two fatal intracranial hemorrhages developed. The authors suggest the need for randomized prospective trials if the role of venography and anticoagulation in this syndrome is to be determined.

Reprinted by permission from the American Cancer Society.

Mediastinal osteosarcoma with extension to lungs in a patient treated for Hodgkin's disease. Catanese J, Dutcher JP, Dorfman HD, Andres DF, Wiernick PH (JPD, Albert Einstein College of Medicine, 1825 Eastchester Rd., Bronx, NY 10461). *Cancer* 62:2252-2257, 1988

This article reports a patient with Hodgkin's disease in remission after combined modality therapy who developed metastatic pulmonary osteosarcoma, subsequently found to originate in soft tissue of the mediastinum, within a field irradiated 11 years previously. This patient developed a series of radiotherapy-induced complications in addition to osteosarcoma. Only 16 cases of extraskeletal osteosarcoma after radiation treatment have been reported, none originating in the mediastinum. To the authors' knowledge, this is the first reported case of extraskeletal osteosarcoma occurring in a patient previously treated for Hodgkin's disease and with the sarcoma originating within the irradiated field.

Reprinted by permission from the American Cancer Society.

Chest

"Density mask": an objective method to quantitate emphysema using computed tomography. Müller NL, Staples CA, Miller RR, Abboud RT (NLM, Dept. of Radiology, University of British Columbia and Vancouver General Hospital, Vancouver, B.C., Canada). *Chest* 94:782-787, 1988

We used a computed tomography (CT) scanner program ("density mask") that highlights voxels within a given density range to quantitate emphysema by defining areas of abnormally low attenuation. We compared different density masks, mean lung attenuation, visual assessment of emphysema and the pathologic grade of emphysema in 28 patients undergoing lung resection for tumor. In each patient, a single representative CT image was compared with corresponding pathologic specimens of tissue. There was good correlation between the extent of emphysema as assessed by the density mask and the pathologic grade of emphysema. The optimal attenuation level to define areas of emphysema may vary in different scanners, but, once determined for a particular scanner, the density mask accurately assesses the extent of emphysema and eliminates interobserver and intraobserver variability. It has the added advantage of determining the exact percentage of lung parenchyma showing changes consistent with emphysema.

Circulation

Magnetic resonance imaging with gadolinium-DTPA for detecting cardiac transplant rejection in rats. Konstam MA, Aronovitz MJ, Runge VM, et al. (MAK, Box 108, Tufts University-New England Medical Center, 750 Washington St., Boston, MA 02111). *Circulation* 78[suppl III]:III-87-94, 1988

To date, no noninvasive tool has gained widespread acceptance as an adequate substitute for endomyocardial biopsy for the diagnosis and grading of cardiac transplant rejection. We examined the potential role of magnetic resonance imaging with gadolinium (Gd)-diethylenetriamine penta-acetic acid (DTPA) image enhancement for the diagnosis of cardiac graft rejection. We studied 15 rats with heterotopic cardiac transplants, nine of which received no immunosuppression, and six of which received cyclosporine, azathioprine, and methylprednisolone. The animals underwent magnetic resonance imaging, which was immediately followed by sacrifice (2-12 days after transplant). Myocardial image enhancement was assessed on T1-weighted images performed before and after administration of Gd-DTPA, 0.5 mmol/kg. Histological specimens were graded I, II, or III to indicate increasing severity of rejection. In the absence of rejection, Gd-DTPA induced mild homogeneous myocardial enhancement. Ten of 11 cases with Grade II or III rejection manifested one or more areas of intense myocardial enhancement. The extent and distribution of intense myocardial enhancement corresponded to the severity and distribution of histological rejection. Quantitative myocardial enhancement, expressed as the ratio of maximal signal intensity after Gd-DTPA to signal intensity before Gd-DTPA administration, separated Grade I animals (1.61 ± 0.27 ; mean \pm SD) from Grades II (2.89 ± 0.58) and III (3.10 ± 0.77 ; $p < 0.01$) animals. In conclusion, cardiac transplant rejection is characterized by intense T1-weighted image enhancement after administration of Gd-DTPA. Magnetic resonance imaging with Gd-DTPA thus has potential application in the clinical diagnosis of cardiac transplant rejection.

Intrathoracic spatial location of specified coronary segments on the normal human heart: applications in quantitative arteriography, assessment of regional risk and contraction, and anatomic display. Dodge JT Jr, Brown BG, Bolson EL, Dodge HT (BGB, Cardiology Division, RG-22, University of Washington School of Medicine, Seattle, WA 98195). *Circulation* 78:1167-1180, 1988

The clinically important coronary segmental anatomy has been described in a format useful for quantitative analysis and standardized display. We have determined the intrathoracic location and course of each of the 23 coronary artery segments and branches commonly

used for clinical description of disease. Measurements were averaged from perpendicular angiographic view-pairs in 37 patients with normal-sized hearts. Each segment or branch is described by several points along its course; each point is specified in polar coordinates as the radial distance from the principal coronary ostium and by angles about the patient, corresponding to those describing rotation in c-arm radiographic systems. This computer-assisted measurement method is accurate to within ± 0.2 cm (SD) and $\pm 2^\circ$ in phantom studies. Coronary segment location among a group of normal-sized hearts can be specified to within ± 1.0 cm (SD). For example, the left anterior descending coronary artery segment at the apex of the heart is 12.2 ± 1.0 cm from the left coronary ostium, $32 \pm 4^\circ$ to the left of the anteroposterior axis, and at $46 \pm 7^\circ$ of caudal angulation. There are several clinically important applications of this new knowledge. First, this anatomic format provides the basis for estimating regional myocardial contraction and the relative size of the myocardial region at risk from a given arterial occlusion. Second, precise knowledge of "normal" segment location greatly simplifies the computation of dimensional correction factors for quantitative arteriography. Third, viewing angles most appropriate for videodensitometric assessment of lesion lumen area may be computed from these data. The theoretical basis and numerical values needed for most of the above estimates are provided. Finally, a computer program has been written to generate a three-dimensional tree-branch vascular model from these anatomic locations. This easily used interactive program aids in teaching coronary angiographic anatomy and, of importance, permits selection of viewing angles that "best" visualize the traditionally difficult parts of the coronary tree.

Gastroenterology

Sphincter of Oddi dysfunction: a clinical controversy. Steinberg WM (WMS, Dept. of Medicine, George Washington University, Washington, DC). *Gastroenterology* 95:1409-1415, 1988

This report analyzes the literature on sphincter of Oddi dysfunction as it applies to biliary-type pain. The sensitivities and specificities of the tests used to diagnose this condition (e.g., size of bile duct, drainage time of bile duct, provocative tests with morphine, sphincter of Oddi manometry) are poorly defined. Recent studies suggest that noninvasive tests such as quantitative nuclear scintigraphy and fatty meal sonography may aid in diagnosing functional common bile duct obstruction. Continuous manometry of the biliary tree with microtransducer technologies may allow a greater understanding of the causes of pain in this group of patients. Only 1 case report of pharmacologic management for this disorder exists in the literature. Endoscopic sphincterotomy may be helpful in relieving the pain that occurs in this condition but is associated with increased risks. There is no consensus in the literature as to the best test that will predict response to sphincterotomy. Controlled trials of medical therapies are needed.

Reprinted with permission by the American Gastroenterological Association.

Duplex ultrasound measurement of postprandial intestinal blood flow: effect of meal composition. Moneta GL, Taylor DC, Helton WS, Mulholland MW, Strandness DE Jr (GLM, Dept. of Surgery, University of Washington, Seattle, WA). *Gastroenterology* 95:1294-1301, 1988

Duplex ultrasound was used to evaluate the effects of 350-cal, 300-ml protein, fat, carbohydrate, and mixed (Ensure-Plus) liquid meals on celiac, superior mesenteric, and femoral artery blood flow in 7 healthy volunteers. Ingestion of separate water and mannitol solutions served as controls for volume and osmolarity. Duplex parameters of peak systolic velocity, end-diastolic velocity, mean velocity, and volume flow were determined before, and serially for 90 min after, ingestion of each test meal. Maximal changes were compared with baseline values. There were no significant changes in any of the blood flow parameters derived from the celiac or femoral arteries after any test meal ingested. In contrast, maximal changes in all superior mesenteric artery parameters were increased significantly over baseline ($p < 0.05$) after each of the test meals except

water, with end-diastolic velocity showing proportionally the greatest increase. The study demonstrates that duplex ultrasound can provide a noninvasive means of studying the reactivity of the splanchnic arterial circulation to different stimuli and documents differing blood flow responses to variation of nutrients.

Reprinted with permission by the American Gastroenterological Association.

Complications of surgical and percutaneous nonendoscopic gastrostomy: review of 233 patients. Ho C-S, Yee ACN, McPherson R (C-SH, Dept. of Radiology, Toronto General Hospital, Toronto, Ontario, Canada). *Gastroenterology* 95:1206-1210, 1988

A retrospective study was undertaken to compare the complications of surgical feeding gastrostomy in 100 consecutive patients with those of percutaneous nonendoscopic gastrostomy in 133 consecutive patients. The age and sex distribution and indications for gastrostomy were similar in both groups. Thirty-day mortality in the surgical group was 12% and in the percutaneous group 7.5%. Complications requiring surgical treatment occurred in 8% and 1.5% of the surgical and percutaneous patients, respectively. Significant nonsurgical complications, such as bleeding, aspiration, and myocardial infarction, occurred in 11% of patients undergoing surgical gastroscopy and 3.0% of those with percutaneous gastrostomy. Minor complications, such as mild wound infection and pericatheter leakage, occurred in 14% of surgical patients and in 0.7% of percutaneous patients. Overall, there were significantly fewer complications with percutaneous gastrostomy than with surgical gastrostomy ($p < 0.01$). We conclude that percutaneous, nonendoscopic gastrostomy is safer than surgical gastrostomy and hence the preferred method for long-term enteral feeding.

Reprinted with permission by the American Gastroenterological Association.

Sensitivity and specificity of microscopic examination of gallbladder bile for gallstone recognition and identification. Ramond M-J, Dumont M, Belghiti J, Erlinger S (M-JR, Service d'Hépatologie, INSERM U-24, Clichy, France). *Gastroenterology* 95:1339-1343, 1988

During cholecystectomy, gallbladder bile and gallstones were obtained from 77 patients and gallbladder bile was obtained from 39 patients free of stones (11 patients had biliary stenosis). According to their chemical composition, gallstones were classified as cholesterol ($n = 46$) or pigment ($n = 31$) stones. In patients with gallstones (a) cholesterol crystals better helped to identify cholesterol gallstones (sensitivity, 87%; specificity, 97%; positive predictive value, 97%) than did an abnormal cholesterol saturation index of bile (sensitivity, 93%; specificity, 48%; positive predictive value, 73%); (b) the presence of cholesterol crystals was significantly related to the cholesterol content of gallstones and the bile cholesterol saturation index; and (c) bilirubinate crystals, when present alone (without cholesterol crystals), were good predictors of pigment gallstones (sensitivity, 71%; specificity, 93%; positive predictive value, 88%). In the absence of stones, bilirubinate crystals were present in 9 of 28 patients without biliary stenosis (4 with alcoholic cirrhosis and 2 with alcoholic pancreatitis) and 8 of 11 patients with biliary stenosis. In the absence of stones, cholesterol crystals were present in 2 of 28 patients without biliary stenosis and in 4 of 11 patients with biliary stenosis, suggesting that bile stasis can induce cholesterol crystal formation.

Reprinted with permission by the American Gastroenterological Association.

Paraneoplastic visceral neuropathy as a cause of severe gastrointestinal motor dysfunction. Chinn JS, Schuffler MD (JSC, Dept. of Medicine, University of Washington School of Medicine, Seattle, WA). *Gastroenterology* 95:1279-1286, 1988

The purpose of this study was to define the cause of severe gastrointestinal motor dysfunction in 7 patients with lung cancer. Six patients had small cell carcinoma and 1 patient had pulmonary carcinoid. Their ages ranged from 58 to 74 yr. All had intestinal pseudoobstruction and obstipation/constipation; 6 of 7 patients had gastroparesis; 4 of 4 patients had esophageal peristaltic abnormalities; and 2 patients had neurogenic bladders, autonomic insufficiency,

and peripheral neuropathy. Five of 7 patients had dilated small bowel with 4 of them showing slow transit of barium; 2 of 7 patients had dilated colons; and 3 of 7 patients had slow colonic transit. Five patients died 4-9 mo after onset of gastrointestinal symptoms, and 2 survived. Postmortem or surgical samples of the esophagus, stomach, small bowel, and colon showed neuron and axon degeneration and dropout, lymphoplasmacytic infiltration, and glial cell proliferation within the myenteric plexus of 6 patients. The antrum from the seventh patient had inflammatory cells within the myenteric plexus but without neuron dropout. Neuron numbers were significantly less than normal in each area of the gastrointestinal tract. Thus, we conclude that lung cancer may be complicated by severe gastrointestinal motor dysfunction resulting from visceral neuropathy of the myenteric plexus, a paraneoplastic effect of the cancer.

Reprinted with permission by the American Gastroenterological Association.

Digestive Diseases and Sciences

Short-term effects of bile diversion on postgastrectomy gastric histology. Bechi P, Amorosi A, Mazzanti R, Buccarelli A, Pantalone D, Cortesini C (PB, Clinica Chirurgica III viale Morgagni 85, 50134 Firenze, Italy). *Dig Dis Sci* 33(10):1288-1296, Oct. 1988

Twelve partially gastrectomized subjects who have consecutively undergone total biliary diversion for severe bilious vomiting were studied before and after operation in order to assess the effects of surgery on gastric histology and enterogastric reflux. Before and six months after operation, the following protocol was performed: (1) blood examinations including serum basal gastrin; (2) endoscopy with multiple gastric biopsies; and (3) quantitation of bile acids in the gastric aspirate. Of the preoperative symptoms, bilious vomiting and heartburn completely disappeared postoperatively in all the subjects. Fasting bile reflux was significantly reduced (bile reflux was annulled in six and considerably lowered in the remaining six subjects), and erythema of the gastric mucosa completely disappeared in all the subjects after diversion. Among histological findings, while a significant regression of foveolar hyperplasia was found both in the perianastomotic area and in the body of gastric remnant, none of the other aspects identifiable in postgastrectomy gastric mucosa (chronic gastritis changes included) were affected by diversion. These results show that biliary diversion is effective in correcting reflux, bilious vomiting, erythema, and foveolar hyperplasia of the gastric mucosa and confirm the suggested relationship between bile reflux and gastric foveolar hyperplasia.

Frequency of upper gastrointestinal lesions in patients with liver cirrhosis. Sacchetti C, Capello M, Rebecchi P, et al. (M Ponz de Leon, Istituto di Patologia Medica, Policlinico, via del Pozzo 71, 41100, Modena, Italy). *Dig Dis Sci* 33(10):1218-1222, Oct. 1988

The frequency of gastroduodenal lesions has been investigated in 142 patients with liver cirrhosis of various degrees of severity and in 63 patients with mild liver disease (controls) in whom liver biopsy excluded nodular regeneration. Cirrhotic patients were subdivided in three groups according to the Pugh modification of the Child-Turcotte criteria. Although the frequency of peptic ulcer was not different, gastroduodenal erosions were observed more frequently in cirrhotics than in controls (29.6% vs 11.1%, $P < 0.01$). The occurrence of erosions was related to the severity of the disease: in Child A and B patients their frequency was 21 and 26% respectively, but rose to 48.4 (15 of 31 vs 7 of 63 in controls, $P < 0.001$) in the Child C group. Both mild and severe gastroduodenitis occurred more frequently, although not significantly, in patients with liver cirrhosis. All together one or more endoscopic lesions were observed in almost 60% of cirrhotics but only in 25.4% of controls ($P < 0.001$). In conclusion, our data do not show an increased prevalence of peptic ulcer in cirrhotic patients; in contrast, liver cirrhosis is significantly associated with the endoscopic finding of gastroduodenal erosions, especially in the more advanced stages of the disease. These findings would suggest a cautious use, in cirrhotic patients, of drugs which may

damage the gastroduodenal mucosa; moreover, long-term administration of antacids or of other drugs with a protective effect on gastroduodenal mucosa might be taken into consideration for Child C patients.

The Journal of Bone and Joint Surgery

Heterotopic ossification as a complication of acetabular fracture: prophylaxis with low-dose irradiation. Bosse MJ, Poka A, Reinert CM, Ellwanger F, Slawson R, McDevitt ER (MJB, Dept. of Orthopedic Surgery, United States Naval Hospital, Portsmouth, VA 23708). *J Bone Joint Surg [Am]* 70-A(8):1231-1237, Sept. 1988

In a retrospective review of thirty-seven patients who had operative treatment for thirty-eight complex acetabular fractures, postoperative low-dose irradiation was administered to seventeen patients (eighteen fractures) to suppress heterotopic ossification. All of the patients had been operated on through either an extended iliofemoral incision or a modified extended iliofemoral incision.

The prophylactic radiation was administered using a low-dose protocol; most of the patients received 1,000 rads in 200-rad increments, starting on the third postoperative day. The incidence of heterotopic ossification in the eighteen irradiated limbs was much lower than in the twenty patients who comprised the control group (50 per cent compared with 90 per cent). Only two of the irradiated limbs had Class-3 heterotopic ossification as described by Brooker et al., and no patient had Class-4 (ankylosis of the hip). Of the twenty control-group patients, ten had severe heterotopic ossification: Class 3 in seven and Class 4 in three.

The difference in the incidence of severe (Class-3 or 4) heterotopic ossification between the two groups of patients was significant ($p < 0.01$).

Clinical Orthopaedics and Related Research

Vascular complications in orthopedic surgery. Chervu A, Quinones-Baldrich WJ (WJQ-B, Section of Vascular Surgery, Dept. of Surgery, UCLA School of Medicine, 72-160 CHS, 10833 LeConte Ave., Los Angeles, CA 90024). *Clin Orthop* 235:275-288, Oct. 1988

Vascular complications may be seen secondary to trauma or in the perioperative period following elective surgery. Prompt recognition and correction of these problems are of utmost importance to assure functional viability of the affected extremity. Evaluation may be complicated by the presence of preexisting atherosclerotic occlusive disease in the elderly patient. Relevant points in the history and physical examination include mechanism of injury, preexisting disease, evaluation of motor and sensory function, and presence and character of pulses. Noninvasive vascular studies should be obtained in all patients. Absolute indications for angiography include absent pulses, signs and symptoms of ischemia, a bruit, and a posterior knee dislocation; decreased pulses, a significant hematoma, and proximity of the fracture fragment are relative indications. Controversial issues in the management of combined orthopedic and vascular injuries include the use of internal versus external fixation, the use of prosthetic versus autogenous material, and the need for venous reconstruction. Popliteal artery trauma is still associated with a high limb loss rate, and careful evaluation of knee injuries is necessary. Vascular compromise may also complicate joint replacement surgery. These complications are preventable, and management is greatly simplified by a detailed preoperative evaluation.

The Journal of Urology

Transrectal ultrasonography in the diagnosis and staging of carcinoma of the prostate. Andriole GL, Kavoussi LR, Torrence RJ, Lepor H, Catalona WJ (GLA, Division of Urologic Surgery, Washington University School of Medicine, 4960 Audubon Ave., St. Louis, MO 63110). *J Urol* 140:758-760, Oct. 1988

Transrectal prostatic ultrasonography is a potentially valuable means to evaluate the prostate of men with suspected carcinoma. We studied 118 patients with this modality before histological evaluation of the prostate (20 underwent radical prostatectomy, 75 core needle biopsy and aspiration cytology, and 23 transurethral resection of the prostate). Transrectal ultrasonography was more efficient than digital rectal examination in the staging of carcinoma of the prostate before radical prostatectomy. The value of transrectal ultrasonography in the diagnosis of prostatic cancer in men with an abnormal-feeling prostate on digital rectal examination is less certain, since 10 of 75 patients (13 per cent) in this group had a falsely positive scan. The predictive value of a scan positive for malignancy was 37 per cent. Further refinements in the technique of transrectal prostatic ultrasonography are needed to realize fully the diagnostic potential of this imaging modality.

British Journal of Urology

The effect of unilateral experimental testicular torsion on spermatogenesis and fertility. Ryan PC, Whelan CA, Gaffney EF, Fitzpatrick JM (PCR, Dept. of Urology, Meath Hospital, Heytesbury St., Dublin 8, Ireland). *Br J Urol* 62:359-366, 1988

Significant subfertility exists in patients following unilateral testicular torsion, implying bilateral testicular disease. Immunological activation has been detected after experimental torsion and the present study sought to demonstrate immunologically mediated effects on contralateral spermatogenesis following experimental torsion, as well as quantifying ipsilateral damage. Early and late effects of torsion on bilateral spermatogenesis were studied at 1 and 6 months in 10 groups each containing 20 rats. Gross and histological examination, direct immunofluorescence tests, vas deferens counts and copulation studies were performed. Severe ipsilateral damage was noted, even after brief torsion periods. No contralateral testicular effects, immunological or otherwise, were observed. Ipsilateral damage after torsion may have been underestimated. There is no damage to contralateral testicular exocrine function following unilateral experimental torsion.

Pediatrics

Natural history of fetal ventriculomegaly. Hudgins RJ, Edwards MSB, Goldstein R, et al. (MSBE, % The Editorial Office, 1360 Ninth Ave, Ste. 210, San Francisco, CA 94122). *Pediatrics* 82:692-697, 1988

The natural history of in utero ventriculomegaly was defined by a retrospective review of the outcome of 47 fetuses evaluated during a 5-year period by the Fetal Treatment Program at the University of California. In 20 fetuses, a diagnosis of ventriculomegaly associated with other severe abnormalities was made early in pregnancy. Termination of pregnancy was elected in 19 of 20 cases, and no fetus survived. In five fetuses, the diagnosis was made late in pregnancy and was associated with severe abnormalities. Fetuses were handled in a routine obstetric fashion and none survived. Of the other 22 fetuses 19 had stable and two had progressive ventriculomegaly; in one case, ventriculomegaly resolved in utero. Nineteen of these fetuses have survived, 13 with normal intellectual development and six with moderately to severely delayed development. Associated abnormalities were detected with ultrasonography in 74% of fetuses; there was a 20% false-negative rate of detection. Ventriculomegaly was isolated and progressive in two fetuses. In both cases, fetuses were delivered at term, and postnatally a shunting procedure was performed. Both children are neurologically normal. From our results and a review of the literature, which supports our findings, we were unable to define a group of fetuses with in utero ventriculomegaly that would benefit from in utero shunting.

The Journal of Pediatrics

Oligohydramnios, renal insufficiency, and ileal perforation in preterm infants after intrauterine exposure to indomethacin. Vanhaesebrouck P, Thiery M, Leroy JG, et al. (PV, Neonatal Intensive Care Unit, Dept. of Pediatrics, University of Ghent, De Pintelaan 185, B-9000 Ghent, Belgium). *J Pediatr* 113:738-743, Oct. 1988

Three preterm infants exposed antenatally to indomethacin developed a characteristic syndrome consisting of edema and hydrops with a bleeding disorder at birth, oliguric renal failure during the first 3 postnatal days, and acute pneumoperitoneum resulting from localized ileal perforation(s) at the end of the first week of life. Despite the value of indomethacin for arresting preterm labor, the physician must take into account the potential hazards of drug toxicity.

The Journal of Nuclear Medicine

Combined bone scintigraphy and indium-111 leukocyte scans in neuropathic foot disease. Schauwecker DS, Park HM, Burt RW, Mock BH, Wellman HN (DSS, Division of Nuclear Medicine, Wishard Memorial Hospital, 1001 W. 10th St., Indianapolis, IN 46202). *J Nucl Med* 29(10):1651-1655, Oct. 1988

It is difficult to diagnose osteomyelitis in the presence of neurotrophic osteoarthropathy. We performed combined [^{99m}Tc]MDP bone scans and indium-111 (^{111}In) leukocyte studies on 35 patients who had radiographic evidence of neuropathic foot disease and clinically suspected osteomyelitis. The [^{111}In]leukocyte study determined if there was an infection and the bone scan provided the anatomic landmarks so that the infection could be localized to the bone or the adjacent soft tissue. Seventeen patients had osteomyelitis and all showed increased [^{111}In]leukocyte activity localized to the bone, giving a sensitivity of 100%. Among the 18 patients without osteomyelitis, eight had no accumulation of [^{111}In]leukocytes, seven had the [^{111}In]leukocyte activity correctly localized to the soft tissues, two

had [^{111}In]leukocyte activity mistakenly attributed to the bone, and one had [^{111}In]leukocyte accumulation in a proven neuroma which was mistakenly attributed to bone. These three false-positive results for osteomyelitis reduced the specificity to 83%. Considering only the 27 patients with a positive [^{111}In]leukocyte study, the combined bone scan and [^{111}In]leukocyte study correctly localized the infection to the soft tissues or bone in 89%. Uninfected neurotrophic osteoarthropathy does not accumulate [^{111}In]leukocytes. We found the combined bone scan and [^{111}In]leukocyte study useful for the detection and localization of infection to soft tissue or bone in patients with neuropathic foot disease.

Journal of Ultrasound in Medicine

The ultrasound appearance of radiation-induced hepatic injury: correlation with computed tomography and magnetic resonance imaging. Garra BS, Shawker TH, Chang R, Kaplan K, White RD (BSG, Dept. of Radiology, Georgetown University Hospital, 3800 Reservoir Road N.W., Washington, DC 20007). *J Ultrasound Med* 7:605-609, Nov. 1988

The ultrasound findings in three cases of radiation induced hepatic injury are described and compared with computed tomography and magnetic resonance imaging findings. Fatty infiltration of the liver was present in two of the cases in which concurrent chemotherapy was being administered. On ultrasound B-scans, the regions of radiation injury were hypoechoic relative to the remainder of the liver. This finding was more obvious in the patients with fatty livers. CT scans on the patients with fatty infiltrated livers showed higher attenuation in the irradiated region than in unexposed liver. In the patient where no fatty infiltration was present, the radiated section of liver had lower attenuation consistent with previous reports. Magnetic resonance imaging showed decreased signal in the exposed areas on T1 weighted images.

Reprinted with permission by the American Institute of Ultrasound in Medicine.

American Roentgen Ray Society Residents' Award Papers, 1989

The ARRS announces competition for the 1989 President's Award and two Executive Council Awards for the best papers concerning the clinical application of the radiologic sciences.

Awards

The winner of the President's Award will receive a certificate and a \$1000 prize. The winners of the two Executive Council Awards will each be given a certificate and a prize of \$500. The winners will be announced on March 15, 1989. Winning papers will be presented at the ARRS annual meeting at the New Orleans Hilton, New Orleans, LA, May 7-12, 1989. Winning papers will be submitted for early publication in the *American Journal of Roentgenology*. All other papers will be returned to the authors.

Regulations

Eligibility is limited to residents or fellows in radiology who have not yet completed 4 years of approved training in a radiologic discipline. A letter from the resident's department chairman attesting to this status must accompany the manuscript. The resident must be the sole or senior author and be responsible for all or most of the project.

Submitted manuscripts must not exceed 5000 words and have no more than 10 illustrations. Four copies of the manuscript and illustrations are required. Submitted manuscripts should not contain previously presented or published material and should not be under consideration for publication elsewhere.

Deadline for submissions is February 10, 1989. Send papers to

B. G. Brogdon, M.D.
Chairman, Committee on Education & Research
American Roentgen Ray Society
Department of Radiology
University of South Alabama Medical Center
2451 Fillingim Street
Mobile, AL 36617

News

Snowmass 1989: MR & CT of the Head and Spine

The Florida Radiological Society and the Joint Committee on Education, AANS and CNS, are cosponsoring Snowmass 1989: MR & CT of the Head and Spine, Feb. 11-18, at the Hotel Wildwood, Snowmass, CO. This comprehensive, educational symposium is designed to expand current imaging applications in clinical medicine. The format will include formal lectures, case studies, and clinical teaching sessions structured to illustrate appropriate use of MR and CT studies of the head and spine. Faculty: W. G. Bradley, M. N. Brant-Zawadzki, R. E. Decker, Romeo Ethler, E. A. Eikman, Glenn Forbes, K. D. Grant, R. R. Lukin, J. D. Miller, L. H. Miller, L. R. Muroff, C. L. Partain, R. M. Quencer, J. F. Sackett, R. B. Schilling, and M. A. Solomon. Category 1 credit: up to 20 hr. Fee: physicians and scientists, \$395; residents, fellows, and military personnel, \$275; nurses and technologists, \$225. Information: Florida Radiological Society, Program Committee, P. O. Box 17241, Tampa, FL 33682; (813) 873-2090 or (800) 338-5901.

Orthopedic Radiology

The Dept. of Radiology, Brigham and Women's Hospital, and the Dept. of Continuing Education, Harvard Medical School, will offer the postgraduate course, Orthopedic Radiology, March 6-8, at the Hyatt Regency Hotel, Cambridge, MA. Program director: Barbara N. Weissman. Category 1 credit: 22 hr. Fee: physicians, \$425; residents, fellows, and RTs, \$300. Information: Dept. of Continuing Education, Harvard Med-CME, P. O. Box 825, Boston, MA 02117; (617) 732-1525.

Neonatal Brain

The Dept. of Radiology, Division of Diagnostic Ultrasound, Thomas Jefferson University Hospital, is offering a course on ultrasound evaluation of the neonatal brain, March 9-10. The course will cover the basics and more advanced areas such as color Doppler imaging of the neonatal cerebrovascular circulation. This is an all-didactic program. It includes lectures, case analyses, and video demonstrations but does not include hands-on experience scanning infants. Program coordinators: Don Mitchell and Matthew Pasto. Category 1 credits will be awarded. Fee: \$275. Information: Judith Superior, Education Coordinator, Division of Ultrasound, Thomas Jefferson University Hospital, 7th Floor Main Bldg., 10th and Sansom Sts., Philadelphia, PA 19107; (215) 928-8533.

PET: Imaging of Brain Chemistry

The Johns Hopkins Medical Institutions are sponsoring PET: Imaging of Brain Chemistry, March 16-18, at the Johns Hopkins Medical Institutions, Thomas B. Turner Bldg., Baltimore, MD. This symposium will cover the basic principles and applications of positron-emission tomography in biomedical research and clinical practice. Course director: Henry N. Wagner, Jr. Category 1 credit: 14 hr. Fee: physicians, \$390; residents, \$290. Information: Joan Liston, Assistant Coordinator, The Johns Hopkins Medical Institutions, Office of Continuing Education, Turner Bldg., 720 Rutland Ave., Baltimore, MD 21205; (301) 955-2959; or Julia W. Buchanan, Course Codirector, (301) 955-8582.

Snowmass 1989: Practical Magnetic Resonance Imaging

The Florida Radiological Society is sponsoring Snowmass 1989: Practical Magnetic Resonance Imaging, March 18-25, at the Silver-tree Hotel, Snowmass, CO. The symposium is designed for those who order, perform, and interpret MR studies. The format combines formal lectures and question-and-answer sessions. Faculty: W. G. Bradley, J. V. Crues III, R. B. Dietrich, Donald Longmore, R. B. Lufkin, L. R. Muroff, R. M. Quencer, J. S. Ross, M. A. Solomon, D. D. Stark, and J. C. Weinreb. Category 1 credit: up to 20 hr. Fee: physicians and scientists, \$425; residents, fellows, and military personnel, \$300; nurses and technologists, \$250. Information: Florida Radiological Society, Program Committee, P. O. Box 17241, Tampa, FL 33682; (813) 873-2090 or (800) 338-5901.

St. Moritz 1989: Advances in Diagnostic Imaging

St. Moritz 1989: Advances in Diagnostic Imaging will be held March 25-April 2 at the Palace Hotel, St. Moritz, Switzerland. This 9th annual symposium is designed for those who order, perform, and interpret MR and interventional radiologic studies. Indications for these studies and strengths and limitations of the procedures will be stressed. Faculty: Robert Eberhard, E. A. Eikman, Donald Longmore, Rene Marti, L. R. Muroff, Thomas Norlindh, Peter Soklic, Gered Stuckmann, Peter Vock, Gustav von Schulthess, and Christoph Zollkofer. Category 1 credit: up to 20 hr. Fee: physicians and scientists, \$395; residents, fellows, and military personnel, \$275; nurses and technologists, \$225. Information: Florida Radiological Society, Program Committee, P. O. Box 17241, Tampa, FL 33682; (813) 873-2090 or (800) 338-5901.

University of Wisconsin CT Conference

The Dept. of Radiology and Continuing Medical Education, University of Wisconsin, School of Allied Health Professions, will present the University of Wisconsin CT Conference, March 31–April 1, at the University of Wisconsin Hospital, Madison, WI. Participants at the conference will review and discuss the latest developments in CT. Category 1 credit: pending. Information: Sarah Z. Aslakson, University of Wisconsin, School of Allied Health Professions, Continuing Education Program, 2715 Marshall Ct., Madison, WI 53705; (608) 263-2856.

Obstetrics and Gynecology

The Dept. of Radiology, Division of Diagnostic Ultrasound, Thomas Jefferson University Hospital, is sponsoring courses on ultrasound in obstetrics and gynecology April 3–7, May 22–26, and June 5–9. The courses cover the full range of ultrasound applications in evaluation of the fetus and the female pelvis. Approximately two-thirds of the program is devoted to obstetrics and the remainder to gynecology. The program includes a thorough review of current techniques of

Judith Superior, Education Coordinator, Division of Diagnostic Ultrasound, Thomas Jefferson University Hospital, 7th Floor Main Bldg., 10th and Sansom Sts., Philadelphia, PA 19107; (215) 928-8533.

Radiology Review Course

The University of Florida, College of Medicine, will offer Radiology Review Course, April 16–21, at the Hyatt Orlando, Disney World/Epcot Center, FL. Category 1 credit: up to 38 hr. Fee: physicians and scientists, \$425; residents, fellows, and military personnel, \$325. Information: Florida Radiological Society, Program Committee, P. O. Box 17241, Tampa, FL 33682; (813) 873-2090 or (800) 338-5901.

Tissue Characterization in MR-Imaging

Tissue Characterization in MR-Imaging will be held April 18–21 at the Penta Hotel, Wiesbaden, Federal Republic of Germany. Topics to be covered include relaxation parameters, pattern recognition, signal mechanisms and influences, and clinical results. Different pos-

Magnetic Resonance Imaging 1989: National Symposium

The Florida Radiological Society is sponsoring Magnetic Resonance Imaging 1989: National Symposium, April 30–May 5, at the Hyatt Orlando, Disney World/Epcot Center, FL. Persons who attend this 6th annual symposium may register for the entire program or for separate mini-symposia: MRI of the Head and Spine, April 30–May 3; Orthopedic Magnetic Resonance Imaging, May 3–4; or MRI of the Body and Heart, May 3–5. Category 1 credit: entire program, 42 hr; head and spine, 26 hr; orthopedics, 15 hr; and body and heart, 24 hr. Fee: entire program: physicians and scientists, \$575; residents, fellows, military personnel, nurses, and technologists, \$300; each mini-symposium: physicians and scientists, \$395; residents, fellows, military personnel, nurses, and technologists, \$225. Information: Florida Radiological Society, Program Committee, P. O. Box 17241, Tampa, FL 33682; (813) 873-2090; or (800) 338-5901.

The Leading Edge in Diagnostic Ultrasound

The Dept. of Radiology, Division of Diagnostic Ultrasound, Thomas Jefferson University Hospital, is sponsoring The Leading Edge in Diagnostic Ultrasound, May 10–13, at Resorts International Hotel and Casino, Atlantic City, NJ. This annual conference is devoted to state-of-the-art practice and recent advances in medical diagnostic ultrasound. It provides updates in all the major specialties, including abdomen, pelvis, obstetrics, and neonatal brain, and information on newer applications, such as color-flow Doppler imaging and endoscopy. The format will include formal lectures, Meet the Professor and film-review sessions, and categorical courses and workshops. Self-evaluation examinations will be offered each morning to help participants determine their levels of expertise in the various applications of diagnostic ultrasound. The preconference tutorial for 1989 will be on ultrasound of the prostate, with special emphasis on endorectal scanning. Program director: Barry B. Goldberg. Information: Judith Superior, Education Coordinator, Division of Diagnostic Ultrasound, Thomas Jefferson University Hospital, 7th Floor Main Bldg., 10th and Sansom Sts., Philadelphia, PA 19107; (215) 928-8533.

Imaging, Intervention, Ireland—1989

The Dept of Radiology, Charlotte Memorial Hospital and Medical Center, Charlotte, NC, is sponsoring Imaging, Intervention, Ireland—1989, Sept. 2–10, in Dublin, Cong, and New Market, Ireland. The course is designed to provide interaction with leading physicians in Ireland and discussion of the newest concepts in imaging and intervention. Program directors: Patrick Carey and Michael Kelley. Category 1 credit: approximately 27 hr. Fee: \$475. Information: Dawne Ryals, Ryals & Associates, P. O. Box 1925, Roswell, GA 30077-1925; (404) 641-9773.

Update in Chest Radiology

The Dept. of Radiology, University of California, Irvine, and the Great Teachers Foundation will present Update in Chest Radiology, Sept. 10–23, in England and Scotland (London, Bath, Bowness on Windermere, Gleneagles, Edinburgh, and Chester). The course is designed to provide interaction with leading physicians in England and Scotland and discussion of the latest concepts in chest radiology. Program director: Eric N. C. Milne. The faculty will include American and United Kingdom leaders in the field of chest radiology. Category

1 credit: approximately 27 hr. Fee: \$475. Information: Dawne Ryals, Ryals & Associates, P. O. Box 1925, Roswell, GA 30077-1925; (404) 641-9773.

The American Board of Radiology Examinations

Written examinations for the American Board of Radiology (ABR) are scheduled for Oct. 12–13, 1989, and Sept. 27–28, 1990. Oral examinations will be held at the Executive West Hotel in Louisville, KY, June 5–9, 1989, and June 4–8, 1990. The ABR will accept applications for admission to the examinations after July 1, but not later than Sept. 30, in the year preceding the year in which the examination is to be taken. For application forms and further information: Office of the Secretary, The American Board of Radiology, 300 Park, Ste. 440, Birmingham, MI 48009.

Meeting and Course Review

For the reader's convenience, a summary of upcoming meetings and courses is provided. Detailed listings are given in the AJR issue given in parentheses.

- One-Week Visiting Fellowships in MR Imaging**, times arranged, Philadelphia (April)
- Fellowships in Interventional Radiology**, times arranged, San Diego (May)
- Fellowship Program in Diagnostic Radiology**, times arranged, Ann Arbor (June)
- Basic and Advanced Training in MRI**, times arranged, Baltimore (Dec)
- Annual Big Sky Radiology Conference**, Jan. 29–Feb. 2, Big Sky, MT (Nov)
- Abdominal Ultrasound**, Jan. 30–Feb. 2, Philadelphia (Jan)
- Annual Mid-Pacific Radiological Conference**, Jan. 31–Feb. 4, Kauai, HI (Dec)
- The George Simon Award**, deadline for receipt of papers, Feb. 1 (Dec)
- Courses in Diagnostic Ultrasound: Arterial/Venous Doppler**, Feb. 1–3; **Echocardiography**, Feb. 6–10; and **Urology**, Feb. 13–14; Winston-Salem, NC (Sept)
- Thomas Jefferson University Hospital Courses in Diagnostic Ultrasound: Prostate Ultrasound**, Feb. 3; **Doppler Ultrasound in Vascular Diagnosis**, Feb. 15–18; Philadelphia (Oct)
- Physics of Diagnostic Radiology and Radiobiology**, Feb. 3–6, Chicago (Sept)
- Postgraduate Course in Puerto Rico**, Feb. 5–10, Hyatt Cerromar Beach Hotel, Puerto Rico (Nov)
- Practical Radiology 1989**, Feb. 5–10, Vancouver, B.C. (Dec)
- Practical Approach to Modern Chest and Musculoskeletal Imaging**, Feb. 5–10, Snowbird, UT, and Feb. 26–March 3, Park City, UT (Jan)
- Annual Uroradiology Course**, Feb. 7–8, Bethesda, MD (Dec)
- Advanced Ultrasound Seminar: OB/GYN**, Feb. 9–11, Lake Buena Vista, FL (Sept)
- Annual Intermountain Imaging Conference**, Feb. 11–18, Steamboat Springs, CO (Nov)
- Sun Valley Imaging**, Feb. 18–25, Sun Valley, ID (Oct)
- Palm Beach Magnetic Resonance Imaging Update**, Feb. 19–22, Palm Beach, FL (Sept)
- Society of Gastrointestinal Radiologists Meeting and Postgraduate Course**, Feb. 19–23, Palm Desert, CA (Sept)
- Diagnostic Imaging Update: 1989**, Feb. 19–24, Park City, UT (Jan)

- Imaging the Central Nervous System**, Feb. 20–24, Tucson, AZ (Oct)
- Perspectives in Imaging**, Feb. 20–24, Cancun, Mexico (Jan)
- Advanced Seminars in Diagnostic Imaging**, Feb. 23–25, Rancho Mirage, CA (Nov)
- Automated Percutaneous Discectomy Workshop**, Feb. 25–26, March 25–26, and April 22–23, San Francisco (Jan)
- Seminars in MRI**, Feb. 25–March 4, Snowbird, UT (Nov)
- University of Arizona Practical Radiology Course**, Feb. 27–March 3, Tucson, AZ (Dec)
- Skeletal Symposium**, Feb. 27–March 3, Sun Valley, ID (Dec)
- Ultrasound in Obstetrics and Gynecology**, Feb. 27–March 3, Philadelphia (Jan)
- Body Imaging, Mammography, and Neuroradiology**, Feb. 27–March 4, Acapulco (Nov)
- Breast Disease Update VI Seminar**, March 1–4, Lake Buena Vista, FL (Dec)
- Magnetic Resonance Imaging Conference**, March 4–8, Scottsdale, AZ (Nov)
- Society of Thoracic Radiology Postgraduate Course**, March 5–9, Coronado (San Diego), CA (Nov)
- Masters Diagnostic Radiology Conference**, March 5–10, Poipu Beach, Kauai, HI (Nov)
- MR Winter Conference**, March 5–10, Snowbird, UT (Jan)
- Computed Body Tomography 1989—The Cutting Edge**, March 9–12, Bal Harbour, FL (Nov)
- Symposium on Shock Wave Lithotripsy**, March 10–12, Indianapolis (Dec)
- Musculoskeletal Imaging—The State of the Art**, March 10–12, Newport Beach, CA (Jan)
- Skeletal Radiology at the Pointe—1989**, March 11–16, Phoenix (Nov)
- Mayo Clinic Advances in Radiology**, March 12–16, Phoenix (Nov)
- Radiation Research Society and North American Hyperthermia Group Annual Meetings**, March 18–23, Seattle (Nov)
- Clinical Nuclear Medicine 1989**, March 28–31, Boston (Dec)
- Joint American-European Course in Davos**, April 2–8, Davos, Switzerland (Jan)
- Ultrasound in Obstetrics and Gynecology**, April 3–5, Ann Arbor (Dec)
- National Council on Radiation Protection and Measurements Annual Meeting**, April 5–6, Washington, DC (Nov)
- Spring Seminar**, April 5–7, Las Vegas (Jan)
- American Osteopathic College of Radiology Mid-Year Conference**, April 6–9, Washington, DC (Nov)
- The Brain, the Self, and Nuclear Medicine**, April 7–8, Bonn, W. Germany (Jan)
- Society of Computed Body Tomography Annual Course**, April 10–14, Washington, DC (Nov)
- Courses in Diagnostic Ultrasound at Bowman Gray: Physics**, April 12–14; **Obstetrics**, April 17–21 and June 5–9; **Radiology (Abdomen)**, April 24–28 and June 12–16; **Neurovascular**, May 1–5; **Echocardiology**, May 15–19; and **Urology**, May 22–23; Winston-Salem, NC (Jan)
- San Diego Residents' Radiology Review Course**, April 16–21, San Diego (Nov)
- Advances in Radiology**, April 19–May 7, Asia (Shanghai, Guilin, Hong Kong, Bangkok, Chiang Mai, Phuket, and Singapore) (Jan)
- AFIP Musculoskeletal Radiology Review Course**, April 22–23, Bethesda, MD (Jan)
- Differential Diagnosis in Radiology**, April 22–24, Ann Arbor (Jan)
- Ultrasound 1989**, April 23–26, Boston (Jan)
- Fleischner Society Symposium on Chest Disease**, April 28–30, New York (Dec)
- Annual Spring Diagnostic Ultrasound Conference**, April 28–30, Los Angeles (Jan)
- International MR Symposium in Italy**, April 30–May 5, Venice and Florence, (Jan)
- Surgical Neuroangiography**, May 1–5, New York (Dec)
- Annual Mid-Pacific Diagnostic Ultrasound Conference**, May 2–6, Big Island of Hawaii (Jan)
- International Congress on Peer Review in Biomedical Publication**, May 10–12, Chicago, IL (Sept)
- Sonography Symposium**, May 26–27, Nashville, TN (Jan)
- Radiology in Scandinavia and the Soviet Union**, June 17–July 1, Copenhagen, Stockholm, and Leningrad (Jan)
- CAR '89**, June 25–28, Berlin (Jan)
- 1989 International Congress of Radiology**, July 1–8, Paris (May)
- Third World Medicine—Tropical Radiology and the Problem of AIDS**, July 19–Aug 5, East Africa (Nairobi, Maasa-Mara, Lake Baringo, Lake Turkana, Mombasa, and Lamu) (Jan)
- Society of Uroradiology Postgraduate Course**, Sept. 25–28, Hilton Head, SC (Dec)
- World Congress for Bronchology**, Oct 18–20, Tokyo, and Oct. 21–22, 1989, Kyoto, Japan (Nov)

AJR carries announcements of courses, symposia, and meetings of interest to its readers if received a minimum of 5 months before the event. There is no charge; receipt of items by the *AJR* Editorial Office is not acknowledged. Submit items for publication typed double-spaced. Provide title, date, location, brief description, sponsor, course directors, fees, category I credit, and address and telephone number for additional information. Faculty from the host institution will not be listed. Guest faculty names will appear **only** if initials are provided. Mail news items to *AJR* Editorial Office, 2223 Avenida de la Playa, Suite 200, La Jolla, CA 92037-3218.

Classified Advertisements

Positions Available

CHAIRMAN, DEPT. OF RADIOLOGY—Rose Medical Center, Denver, CO, a 300-bed, tertiary-care hospital, affiliated with the University of Colorado Health Sciences Center, is seeking a Chairman for the Dept. of Radiology. Qualifications include a strong professional base as well as administrative expertise. Please forward inquiries and CV to Chairman, Radiology Search Committee, c/o Medical Staff Office, Rose Medical Center, 4567 E. Ninth Ave., Denver, CO 80220. Rose Medical Center is an equal opportunity/affirmative action employer. 2-3a

ISRAEL, DIAGNOSTIC RADIOLOGY. Opportunities for 3-4 week or longer working vacations in a number of Israeli medical centers, on a volunteer basis. Positions varied, arrangements flexible. For information contact: Jonathan H. Fish, M.D., 1844 San Miguel Dr., #302, Walnut Creek, CA 94596; (415) 947-0560. 2xa

DIAGNOSTIC RADIOLOGIST—Seeking a board-certified/board-eligible, general radiologist, with family practice experience, to join senior radiologist in established private office and hospital radiology practice. Live in a lovely and historic southwestern Virginia town located 15 mi from a busy airport and larger city. Starting salary guaranteed \$100K, with only 12 mo to full salary and full partnership. Two mo vacation first year, negotiable thereafter. Reply with CV to Box H21, AJR (see address this section). 2ap

BC/BE RADIOLOGIST for metropolitan-based, Nashville hospital. Close working relationship with 3 skilled radiologists. Experience required in all routine modalities (excluding MRI), as well as basic skills in angiography and specials. Excellent starting salary and vacation. Immediate need. Send CV to John Huff, M.D., 834 Brentview Dr., Nashville, TN 37220. 2ap

DIAGNOSTIC RADIOLOGIST position available with multispecialty ambulatory clinic. Semitropical Texas Gulf Coast location. Experience in ultrasound, mammography, fluoroscopy, and nuclear medicine. Competitive compensation packet with opportunity to become shareholder. Fee-for-service practice environment. Contact Amanda Fuhro, Valley Diagnostic Medical & Surgical clinic, P.A., 2200 Haine Dr., Harlingen, TX; (512) 421-5199. 2-3ap

BC GENERAL DIAGNOSTIC RADIOLOGIST, willing to travel in beautiful central Idaho. Affiliation with a major group with primary coverage of 2 rural hospitals. Skills needed include fluoroscopy/special procedures, ultrasonography, and mammography. For further information, please contact Karen Kellie, Administrator, P. O. Box 906, McCall, ID 83638; (208) 634-2221, or Avery Pratt, M.D., St. Alphonsus Regional Medical Center, Boise, ID 83706; (208) 378-2031. 2a

DIAGNOSTIC RADIOLOGIST—Eight board-certified radiologists in expanding hospital-based private practice seek BC/BE general radiologist to associate. Competence in all modalities expected with need for interventional and/or MRI training emphasized. Opportunity in midwestern city of 72,000 people offers generous compensation/vacation. Full partnership after 2 yr. Reply to Box J32, AJR (see address this section). 2-5a

PACIFIC NORTHWEST—Opportunity for BC/BE general diagnostic radiologists to join group of 5 board-certified radiologists. Experience in all modalities desired. Practice includes 2 hospitals and private office in Southern Oregon. Contact:

DIAGNOSTIC RADIOLOGIST, PACIFIC NORTHWEST: MRI, CT, AND ULTRASOUND—Progressive group of 4 radiologists seeks board-certified radiologist with subspecialty interest and expertise in MRI, CT, and ultrasound. Busy dynamic practice in regional medical center hospital, privately owned MRI center (presently mobile unit — planning for fixed site, fall 1989), plus private outpatient office. Located in beautiful recreation area in the inland Northwest. World-class lakes for boating and sailing. Excellent skiing, hunting, and fishing. Family-oriented environment 30 min from Spokane. Competitive starting salary with full partnership in 1 yr. Send CV to Richard Hehn, M.D., Radiology Associates of North Idaho, 1104 Ironwood Dr., Coeur d'Alene, ID; (208) 667-0686. 2-4ap

TWO RADIOLOGISTS NEEDED to join expanding 4-person group in Duluth, MN. Competence required in general radiology, ultrasound, CT, nuclear medicine, interventional radiology, and mammography. MRI helpful. Competitive salary leading to full partnership. Generous fringes. Send inquiry with CV to F. Ekberg, M.D., St. Luke's Hospital, 915 E. First St., Duluth, MN 55805. 2ap

DIAGNOSTIC RADIOLOGIST—Radiologists seek board-certified radiologist with experience in CT, nuclear medicine, general radiology, and ultrasound including Doppler, for a hospital-based, private practice in 225-bed general hospital in Forest Hills, NY. Immediate opening leading to partnership. Contact M. Tartell, M.D.; (718) 544-5858. 2-4ap

BOARD-CERTIFIED/ELIGIBLE RADIOLOGIST to join a hospital and multioffice group practice in N. central Connecticut. Applicant should be competent in all imaging modalities including CT and MRI. Training in interventional radiology is desirable but not essential. Salary first yr leading to full partnership. J. Danigelis, M.D., 151 Berle Rd., S. Windsor, CT 06074. 2ap

DIAGNOSTIC RADIOLOGIST—Ten-man, private practice group seeks BC/BE diagnostic radiologist. Candidate must have at least 1-yr fellowship in CT/ultrasound, MRI, angio/interventional, or nuclear medicine. Practice covers 2 hospitals and an outpatient office with a total of 120,000 exams/yr. Beautiful midwestern university town. Excellent salary/fringes with early partnership arrangement. Send CV or call Joe McColley, M.D., 909 E. University St., Bloomington, IN 47401; (812) 336-9446. 2-4ap

DIAGNOSTIC RADIOLOGIST—The UCLA Dept. of Radiological Sciences is seeking a board-certified radiologist for its Primary Care/Family Practice Section. Position requires strong interests in teaching, patient care, and knowledge of abdominal CT for evaluation of trauma. Send application, including CV and names and addresses of 3 references, or inquiries to Hooshang Kangaroo, M.D., Chairman, Dept. of Radiological Sciences, UCLA Medical Center, Los Angeles, CA 90024-1721, an EO/AA employer that encourages applications from members of minority groups and women. 2-7a

SKELETAL RADIOLOGIST—The UCLA Dept. of Radiological Sciences has a full- or half-time faculty position available in skeletal radiology. Candidate must be board-certified, have a clinical background in skeletal radiology, and have a strong interest in teaching. Send application, including CV and names and addresses of 3 references, or inquiries to Hooshang Kangaroo, M.D.,

IMMEDIATE OPENING—BC/BE radiologist, full- or part-time, to join 2 radiologists in outpatient imaging center. General diagnostics includes MRI. Flexible hrs, weekdays only, no weekends or call. Generous salary and vacation leading to early partnership. Send CV to L. Carr, M.D., 342 22nd Ave. N., Nashville, TN 37203. 2-3ap

ANGIOGRAPHER/INTERVENTIONAL RADIOLOGIST—The Dept. of Radiology at the University of Washington is seeking a board-certified radiologist for the Section of Angiography and Interventional Radiology. Dept. has recently undergone major expansion. Facilities at University Hospital, Harborview Medical Center, the VA Medical Center, and Children's Hospital and Medical Center include a PET scanner, several CT and MRI units, a full complement of angiographic capabilities, and the newly developed Imaging Research Center. Salary is commensurate with rank based on established level of the University of Washington School of Medicine. Submit CV to Albert A. Moss, M.D., Professor and Chairman, Dept. of Radiology, SB-05, University of Washington, Seattle, WA 98195. The University of Washington is an affirmative action employer and encourages applications from women and minorities. 2a

WE ARE SEEKING AN EXPERIENCED BOARD-ELIGIBLE/CERTIFIED NUCLEAR MEDICINE PHYSICIAN to join our clinical and research radiology faculty at the University of Washington to assume major responsibility for directing patient-care services at Harborview Medical Center, an affiliate institution. There are complete state-of-the-art clinical facilities plus an imaging research center which includes nuclear, angiographic, MRI, and PET imaging suites. Major research in nuclear medicine includes radiolabeled antibodies; osteoporosis; positron studies of cancer, heart, and lung; and extensive work in radiochemistry and computer sciences. There are 6 full-time students in nuclear medicine plus research fellows and active medical-student teaching. Will consider assistant or associate professor level. Salaries are highly competitive. The University of Washington is an equal opportunity employer. Please contact Charles H. Chesnut, III, M.D., Professor, Radiology and Medicine, Director, Osteoporosis Research Center, Division of Nuclear Medicine, University of Washington, Seattle, WA 98195. 2a

ABDOMINAL IMAGER—The University of Washington's Dept. of Radiology has an opening for an academically oriented radiologist in the area of abdominal imaging, including gastrointestinal and genitourinary radiology, with expertise in CT and ultrasound. This position will also involve interventional radiology of the abdomen including biopsies and abscess drainage. Responsibilities include instructing medical students and residents, and conducting research. Applicants must possess board certification in radiology plus 1-yr related fellowship or clinical experience in radiology postresidency. Send letter and resume to Albert A. Moss, M.D., Dept. of Radiology, SB-05, University of Washington, Seattle, WA 98195. The University of Washington is an equal opportunity employer. 2a

RADIOLOGIST—Board-certified/eligible radiologist wanted to join 3 board-certified radiologists in busy, university-affiliated, community hospital near Boston. Area offers many educational and recreational opportunities. We seek a general radiologist with demonstrated ability in mammography, angio/interventional, ultrasound, and CT.

BODY IMAGING FACULTY POSITIONS—The Georgetown University Medical Center is seeking board-certified academic radiologists with experience in body imaging (CT, ultrasound, MRI, GI). Appointments will be at the assistant or associate professor level. Clinical responsibilities can be tailored to reflect the candidates' interests. Equipment includes Diasonics, Acuson, and ATL ultrasound units, GE 9800 CT scanners, Siemens 1.5-T MR, and a Varian 4.7-T spectral imager for animal research. Over 10,000 body imaging studies are performed annually including a wide range of invasive procedures, Doppler, endovaginal and transrectal sonography, neurosonography, and biliary lithotripsy. An active research affiliation exists with the NIH. Submit CV in confidence to Robert K. Zeman, M.D. or Paul M. Silverman, M.D., Dept. of Diagnostic Radiology, Georgetown University Hospital, 3800 Reservoir Rd., N.W., Washington, DC 20007. An equal opportunity/affirmative action employer. 2ap

WILMINGTON, NORTH CAROLINA—Group of 8 radiologists seeking fellowship-trained neuroradiologist and general diagnostic imaging radiologist with staff-level experience. This 400-bed, university-affiliated, regional-referral hospital has all diagnostic imaging capabilities including GE Signa 1.5-T MRI, 2 GE 9800 CT scanners, Toshiba SPECT system, and complete angio/interventional suites. Busy private outpatient office. Progressive growing community in Cape Fear area of coastal North Carolina. Address CV to John Remington, M.D., 2212 Delaney Ave., Wilmington, NC 28403. 2-4ap

DIAGNOSTIC RADIOLOGIST—Noblewood Imaging, Inc. at Riverview Hospital is seeking a BC/BE radiologist for general diagnostic radiology. Salary commensurate with experience, with full partnership after 2 yr of service. Riverview is a 124-acute-bed, 31-extended-care facility, 20 min NW of Indianapolis, IN. Radiologic services currently provided include CT, ultrasound, MRI, vascular and interventional radiology, myelography, mammography, arthrography, plus general radiology. We have recently started construction of a new breast diagnostic center with 3 mammography suites and 1 ultrasound suite. This facility will be completed in Jan. 1989. Fringe benefits include 6-wk vacation annually, full insurance coverage, and retirement plan. Interested applicants should forward their CV and references to Frank E. Mercho, M.D., Chief, Dept. of Radiology, Riverview Hospital, 395 Westfield Rd., Noblesville, IN 46060; (317) 776-7160. 2ap

TEMPLE UNIVERSITY SCHOOL OF MEDICINE is seeking a Chairman for the Dept. of Diagnostic Imaging. The dept. consists of Divisions of: (1) Diagnostic Radiology, (2) Nuclear Medicine, and (3) Pediatric Radiology at St. Christopher's Hospital for Children. Candidates should have demonstrated leadership in clinical practice, teaching, and research and must have strong administrative skills. Inquiries and nominations should be addressed to A. Richard Kendall, M.D., Professor and Chairman, Dept. of Urology, Temple University School of Medicine, 3401 N. Broad St., Philadelphia, PA 19140. Applications will be accepted up to Feb. 15, 1989. Temple University is an equal opportunity/affirmative action employer. 2a

RADIOLOGISTS, IMMEDIATE OPENINGS—Five-member group with 1 hospital and 2 centers (1 MRI) seeks 2 radiologists. Applicants should be proficient in all areas of radiology. Also applicants with an MRI/neuroradiology fellowship or nuclear medicine fellowship preferred. Competitive salary with excellent benefits leading to full partnership. Please reply to W. M. Colaiaica, M.D., Dept. of Radiology, Roger Williams General Hospital, 825 Chalkstone Ave., Providence, RI 02908. 2a

DIAGNOSTIC RADIOLOGIST, CLEVELAND, OH—Position available for BC/BE radiologist to join hospital group at Saint Luke's Hospital. Prefer individual with previous practice experience or fellowship training, with interest in MRI and/or interventional radiology. Submit CV to R. L. Boltuch, M.D., Director, Dept. of Radiology, Saint Luke's Hospital, Cleveland, OH 44104. 2-4ap

DELAWARE PRACTICE—Combine the advantages of an active, hospital-based radiology practice with the appeals of a beautiful, historic Delaware town. Our client, a modern, progressive, 200+ bed, community hospital dominates 160,000+ coverage area. Present 5 physicians (30 techs) require expansion to handle rapidly escalating number of exams. FY89 exams/procedures: 80,000 (FY88: 66,000). Equipment includes Philips CT, Diasonics MR, current interventional units, 2 gamma cameras (1 SPECT), 4 ultrasound units (2 CFM Dopplers). Hospital and satellites total 14 rooms. Call is from home and is shared equally. Enjoy collegial support and desirable lifestyle. Tree-lined streets, excellent schools, abundant, reasonably priced housing, cultural diversions of Baltimore, DC, Philadelphia (under 2 hr), and clean Delaware beaches (under 1 hr). We seek 2 BC (or recently eligible) radiologists. General training (as opposed to subspecialty fellowship preparation) appropriate for this vacancy. For full details send CV to Carla Fox, MedQuest, Inc., P. O. Box MQ, Devault, PA 19432; (215) 640-3774. 2a

FRANCIS SCOTT KEY MEDICAL CENTER, a member of the Johns Hopkins health system, seeks a radiologist interested in an exciting career in a stimulating environment. FSKMC is a 572-bed teaching hospital on a 130-acre campus currently undergoing extensive redevelopment. We are seeking a radiologist interested in an active teaching position associated with Johns Hopkins residents and fellows using all current radiological modalities. Baltimore's famous Inner Harbor offers the cultural diversity of a thriving metropolitan area, the close proximity of suburban living, and a wealth of outdoor/recreational opportunities. Please send CV to Stanford M. Goldman, M.D., Dept. of Radiology, Francis Scott Key Medical Center, 4940 Eastern Ave., Baltimore, MD 21224; (301) 550-0212. EOE/M/H/O/V. 2ap

SECTION CHIEF, NEURORADIOLOGY, with experience in ENT and noninvasive imaging needed for research, patient care, and teaching in 489-bed, adult, tertiary-care facility. Assistant to associate professor depending on qualifications. Equal opportunity/affirmative action employer affiliated with Harvard Medical School. Submit CV to Melvin E. Clouse, M.D., Dept. of Radiology, New England Deaconess Hospital, 185 Pilgrim Rd., Boston, MA 02215. 2ap

BOARD-CERTIFIED/ELIGIBLE GENERAL DIAGNOSTIC RADIOLOGIST to join 1 other radiologist in 41-physician, multispecialty clinic. Outpatient imaging including mammography, ultrasonography, fluoroscopy, arthrography, and general diagnosis. No night or weekend call. Small community east of Los Angeles, convenient to beaches and mountain resorts. Excellent schools. Send CV to Robert J. Thomas, M.D., The Beaver Medical Clinic, P. O. Box 3001, Redlands, CA 92373. 1-2a

COASTAL CALIFORNIA—Immediate opening for board-certified radiologist to provide day-off/vacation relief. Hospital, private office, group. Sunny northern California. Ultrasound, CT, and mammography. No angiography or MRI. CA license required, malpractice insurance provided. No weekends or call. Minimum 1/2 yr coverage. Reply Box N61, AJR (see address this section). 1-3ap

GENERAL DIAGNOSTIC RADIOLOGIST, THOMAS JEFFERSON UNIVERSITY HOSPITAL—The Dept. of Radiology at Thomas Jefferson University Hospital in Philadelphia has an opening in July 1989 for a faculty-level, general diagnostic radiologist. An interest and/or fellowship training in abdominal radiology (GI/GU) would be helpful, but not mandatory. The individual will have the opportunity to participate in clinical activities, teaching, and research in a progressive and expanding general diagnostic division. Excellent salary and benefits are offered. Contact either Robert M. Steiner, M.D., Co-director of General Diagnostic Radiology or David C. Levin, M.D., Professor and Chairman, Dept. of Radiology, Thomas Jefferson University Hospital, 111 S. 11th St., Philadelphia, PA 19107. Thomas Jefferson University is an equal opportunity/affirmative action employer. 1-6ap

INTERVENTIONAL RADIOLOGIST—Board-certified radiologist with fellowship training in vascular/interventional radiology for position starting July 1, 1989. Academic rank is at the level of assistant professor. This active clinical service performs the entire range of diagnostic and interventional procedures including embolization, angioplasty, infusion therapy, IVC filter placement, atherectomy, and laser angioplasty. A program in biliary lithotripsy is the responsibility of the section. The interventional inpatient service admits 100 patients/yr, primarily for embolization and angioplasty. The interventional clinic evaluates referred patients and patients seen in follow-up. Please send applications with CV to Donald F. Denny, Jr., M.D., Chief, Vascular and Interventional Radiology, Yale University School of Medicine, P. O. Box 3333, New Haven, CT 06510. Yale University is an equal opportunity/affirmative action employer. Applications from women and minority group members are encouraged. Application deadline is March 1, 1989. 1-2a

RADIOLOGIST—IMMEDIATE OPENING—American university-educated, board-certified/eligible M.D., with particular interest in imaging including MRI to join large, multihospital group in San Antonio, TX. Please direct inquiries and CV to P. O. Box 120310, San Antonio, TX 78212-9510. 1-4ap

BOARD-CERTIFIED, GENERAL DIAGNOSTIC RADIOLOGIST with academic credentials to become Associate Director of Radiology and Director of Residency Training Program. Experience in clinical research required. Send CV to David Bryk, M.D., Director of Radiology, Maimonides Medical Center, 4802 Tenth Ave., Brooklyn, NY 11219. 1-2ap

TWO GENERAL RADIOLOGY MEDICAL OFFICER POSITIONS available in the Dept. of Radiology, Madigan Army Medical Center, Tacoma, WA. Serve as board-certified radiologists with responsibility for the full range of cases including the most difficult. Responsibilities include providing training and serving as a consultant to interns and residents. Contact Kathleen Derry at the Fort Lewis Civilian Personnel Office to obtain additional information and government application forms; (206) 967-2131. 2a

STAFF RADIOLOGISTS—The VA Medical Center, Bay Pines, FL, affiliated with the University of S. Florida School of Medicine, is currently accepting applications for 2 staff radiologist positions. One position is required for general diagnostic radiology with MRI experience and 1 position for an interventional radiologist. Individuals should be board-certified. The Medical Center is located on the beautiful West Coast of Florida, only minutes from the Gulf of Mexico. Send CV and/or call Ann E. Esquerra, M.D., Chief, Radiology Service (114), VA Medical Center, Bay Pines, FL 33504; (813) 398-9363. An equal opportunity employer. 2a

DIAGNOSTIC RADIOLOGIST—ABDOMINAL IMAGING

—The University of Missouri-Columbia Hospital and Clinics is seeking a radiologist with expertise in abdominal imaging (GI, CT, ultrasound, and MRI). Board certification required. Fellowship desirable. Tenured and nontenured tracks available at Assistant and Associate Professor levels. An equal opportunity/affirmative action employer. Address inquiries to Robert J. Churchill, M.D., Dept. of Radiology, University of Missouri-Columbia Hospital and Clinics, One Hospital Dr., Columbia, MO 65212. 1-2a

DIRECTOR, RADIATION ONCOLOGY—The University of Missouri-Columbia Hospital and Clinics is seeking a Director of Radiation Oncology. The position is a tenured track in the Dept. of Radiology. The Director will also serve as the Service Chief of the Radiation Therapy Service at the Ellis Fischel State Cancer Center. The facilities occupy 11,000 sq. ft. and include a 40 MeV Sagittaire, Dual Beam Siemens 15 MeV Accelerator, a simulator, CMS Treatment Planning Computer, and 1 Cobalt unit. The candidate must possess

IMAGING RADIOLOGIST—THE CAROLINAS

Progressive, 12-man group seeking an exceptional individual with fellowship training or junior staff experience in body imaging. Must be board-certified and competent in a wide range of general diagnostic skills including mammography. Prosperous and reputable 650-bed community hospital planning major expansion. One hospital, 1 office practice with state-of-the-art equipment; 4 CT scanners (2 Picker, 2 GE 9800), MRI (GE Signa), and 7 ultrasound units (3 Acuson). A choice practice and excellent location in the heart of the Carolinas. Contact Box 221249, Charlotte, NC 28222. 1-3ap

CHEST RADIOLOGIST, CLEVELAND CLINIC FOUNDATION

—Immediate opening for a staff, chest radiologist at the Cleveland Clinic Foundation. Internationally renowned institution with 1000-bed hospital and large, outpatient facility offering exciting opportunities for individual with clinical, teaching, and research interests. Competitive salary and very attractive benefit package.

IMMEDIATE OPENING FOR STAFF NEURORADIOLOGIST

in the Division of Neuroradiology, to join 1 other neuroradiologist. The University of Massachusetts Medical Center is a 360-bed university hospital and medical school located in Worcester, MA, approximately 40 mi. west of Boston. The dept. consists of 19 staff, 12 residents, and 2 fellows and does approximately 105,000-110,000 exams/yr. The hospital is a major trauma center and is serviced by 2 Life Flight helicopters. The dept. is well-equipped with 2 CT scanners (a GE 9800 Quick and an 8800), a 1.5-T GE MR scanner in a stand-alone facility with a second scanner expected by Jan. 1989. There is also a 2.0-T small-bore unit for animal research. For further information, contact Edward H. Smith, M.D., Professor and Chair, Dept. of Radiology, University of Massachusetts Medical Center, 55 Lake Ave. N., Worcester, MA 01655; (508) 856-3252. UMMC is an equal opportunity/affirmative action employer. 1-3a

THE DEPT. OF RADIOLOGY AT TRIPLER ARMY MEDICAL CENTER, HONOLULU, HI

EMORY UNIVERSITY, DEPT. OF RADIOLOGY seeks a Ph.D. or M.D. with either NMR spectroscopy or imaging experience for a full-time faculty position. The candidate must be able to originate fundable research projects using NMR and collaborate with other faculty members (in or out of radiology) on NMR research. Knowledge of spin behavior is essential. Medicine, biology, or biochemistry, analog electronics, and computer science are useful skills. Two 1-m clinical imagers operating at 0.5 T and 1.5 T and a 30-cm 200-MHz instrument, all fully-programmable, will be available. The dept. is part of an 800-bed, tertiary-care complex giving ample opportunity for collaborations requiring clinical material. Seven full-time Ph.D. scientists, in the radiology dept., are currently involved in NMR. Qualified candidates please contact Thomas Dixon, M.D., Director, Frits Philips Magnetic Resonance Research Center, 419 Woodruff Memorial Bldg., Emory University, Atlanta, GA 30322. Emory University is an equal opportunity/affirmative action employer. 12-3a

DIAGNOSTIC RADIOLOGIST, NUCLEAR MEDICINE POSITION—Large, private practice in desirable, rapidly growing location between Philadelphia and Princeton in Bucks County, PA, and Trenton, NJ, seeks a diagnostic radiologist with expertise in nuclear medicine, especially cardiac. Competency in general diagnostic radiology including ultrasound, CT, and mammography also required. Position available immediately or July 1989. Send letter and CV to S. Meshkov, M.D., 838 W. State St., Trenton, NJ 08618. 12-2ap

VA MEDICAL CENTER, AUGUSTA, GA, seeks BC/BE radiologists interested in general radiology to include CT, ultrasound, and teaching. Affiliated with the Medical College of Georgia, this modern, 1100-bed, 2-unit facility is located in a progressive, southeastern city with excellent schools, moderate climate (and home of the Masters Golf Tournament), and is close to numerous major universities. An outstanding federal retirement, health, and insurance benefit package is available, plus 30 days vacation and 10 paid holidays per yr. Please send CV to Alex F. Daley, M.D., Chief, Radiology Service (114), VA Medical Center, Augusta, GA 30910; (404) 823-2236; FTS 251-2236. An equal opportunity employer. 2a

DIAGNOSTIC ONCORADIOLOGIST—The Division of Oncoradiology at the Dana-Farber Cancer Institute, a Harvard University affiliate, has an opening at the instructor/assistant professor level for a general radiologist with an interest in oncology beginning July 1989 or sooner. Patient care responsibilities with a close working relationship with the clinical staff, teaching, and research opportunities abound. There are 52 beds with a large outpatient service. All new equipment is available including a GE-9800 CT scanner. Please send CV to Maxine Jochelson, M.D., Director, Division of Oncoradiology, Dana-Farber Cancer Institute, 44 Binney St., Boston, MA 02115. 11-4a

FULL-TIME ACADEMIC NEURORADIOLOGIST—One staff position is currently available in the Division of Neuroimaging at the Children's Memorial Hospital at Chicago. The Division of Neuroimaging is a complete service with 2 CT scanners (1 is a GE-9800), 1 GE 1.5-T Signa MRI scanner (which is inhouse for children), 3 Acuson ultrasound units, myelography and cerebral angiography equipment, as well as an interventional neuroradiology program with Northwestern University. The Division has its own approved fellowship program in neuroradiology. Some training in interventional neuroradiology and/or pediatric neuroradiology is preferred, but not necessary. Send CV to Sharon E. Byrd, M.D., Director of Neuroimaging Division, Children's Memorial Hospital, 2300 Children's Plaza, Chicago, IL 60614; (312) 880-3565. 11-4ap

GU RADIOLOGIST, BRIGHAM & WOMEN'S HOSPITAL—The Dept. of Radiology at Brigham & Women's Hospital/Harvard Medical School is seeking a radiologist to direct its GU Section. The position combines clinical activities with teaching and research. Candidates must be board-certified and have experience in all aspects of GU radiology, as well as an interest/commitment to academic work. Please send CV to B. Leonard Holman, M.D., Chairman, Dept. of Radiology, Brigham & Women's Hospital, 75 Francis St., Boston, MA 02115. Harvard Medical School is an affirmative action/equal opportunity educator and employer. 11-4a

ULTRASOUND STAFF RADIOLOGIST, BRIGHAM & WOMEN'S HOSPITAL—The Dept. of Radiology at the Brigham & Women's Hospital/Harvard Medical School is seeking a radiologist for a full-time, academic position in ultrasound. We perform 60-85 scans per day, including OB-GYN, abdominal, Doppler, small parts, neonatal, and interventional. Research and teaching opportunities are available. Candidate must be BC/BE with fellowship training in ultrasound. Please send CV to B. Leonard Holman, M.D., Chairman, Dept. of Radiology, Brigham & Women's Hospital, 75 Francis St., Boston, MA 02115. Harvard Medical School is an affirmative action/equal opportunity educator and employer. 11-4a

DIAGNOSTIC RADIOLOGIST competent in interventional and MR to join growing 3-man practice in northern Arkansas. Modern hospital-based practice includes CT, ultrasound (including duplex vascular), angiography, DSA, interventional, lo-dose mammography, and computerized nuclear medicine. Mobile MR and on-site Radiation Center being added. Located in beautiful resort area of Ozark Mountains, 110 mi from Springfield, MO, 150 mi from Little Rock, and 190 mi from Memphis, and serves 100,000 area population. Excellent recreational activities in family-oriented rural environment. Competitive starting salary with full-partnership in 1 yr. Contact Marc Trager, M.D., P. O. Box 1137, Mountain Home, AR 72653; (501) 425-1760. 11-4a

HARTFORD, CT—Position available for a board-certified radiologist to join an established group of 7. Practice includes hospital and 3 private offices, all fully equipped, including CT, MRI and CT experience is an essential requirement. Competitive starting salary and benefits. Please enclose CV with initial correspondence to Jeffrey Blau, M.D., 40 Hart St., New Britain, CT 06052; (203) 229-2059. 2xa

DIAGNOSTIC RADIOLOGIST—Eight board-certified radiologists in expanding hospital-based private practice seek BC/BE general radiologist to associate. Competence in all modalities expected with need for interventional and/or MRI training emphasized. Opportunity in midwestern city of 72,000 people offers generous compensation/vacation. Full partnership after 2 yr. Reply to Box J32, *AJR* (see address this section). 2-5a

BOARD-CERTIFIED OR ELIGIBLE RADIOLOGIST sought to join staff covering 4 hospitals and an outpatient clinic in S.E. Georgia. Skills must include general diagnostic, ultrasound, nuclear medicine, mammography, CT, and special procedures. Salary negotiable. Send letters of inquiry with CV and letters of reference to Director, Regional Diagnostics, P. O. Box 147, Vidalia, GA 30474; (912) 537-1150. 2xa

CENTRAL FLORIDA—General diagnostic radiologist to join large, tertiary-center radiology group. Specific interest in mammography to head very active women's center practice. Send CV to Bruce R. Crossman, M.D., Dept. of Radiology, Florida Hospital, 601 E. Rollins St., Orlando, FL 32803. 11-2ap

ULTRASOUND PHYSICIAN to join 3 hospital-based ultrasound/nuclear medicine physicians in Portland, OR. Practice includes high-risk obstetric sonography, neonatal neurosonography, color Doppler vascular sonography. Equipment includes multiple Acuson systems and multiple ATL systems. Position includes coverage for nuclear medicine. Send CV to Michael Daly, M.D., Nuclear Medicine/Ultrasound Section, Emanuel Hospital, 2801 N. Gantenbein Ave., Portland, OR 97227. 12-3a

CROSS-SECTIONAL RADIOLOGIST, INTERVENTIONALIST—Board-certified diagnostic radiologist with fellowship training wanted to join 5-member dept. in 214-bed community hospital. Group also active in busy outpatient facilities and free-standing Magnetic Resonance Center. Primary responsibility will be ultrasound, CT, and nonangiography interventional, with back-up for primary angiographer. Competence in Doppler studies desired. Call and/or send CV attention Jon Robins, M.D., or Edward Janon, M.D., 6699 Alvarado Rd., Ste. 2100, San Diego, CA 92120; (619) 583-4214. 2xa

Fellowships and Residencies

DUKE UNIVERSITY, DEPT. OF RADIOLOGY offers 1- or 2-yr fellowship positions in chest radiology, neuroradiology, vascular/interventional radiology, musculoskeletal radiology, CT, ultrasound, MRI, abdominal imaging, pediatric radiology, and nuclear medicine beginning July 1990. The dept. runs an active, clinical service with top-quality equipment including 4 GE 9800-Quick CT scanners, 3 GE 1.5-T MRI units, and 4 fully-equipped vascular/interventional laboratories. In addition to their clinical responsibilities, fellows are provided academic time to pursue investigational interests. Applications should be completed by April 1, 1989 so that interviews can be scheduled for late spring/early summer. For further information and applications, please contact Mrs. Debbie Sykes at the Dept. of Radiology, Box 3808, Duke University Medical Center, Durham, NC 27710; (919) 681-2711. 2-4c

DIAGNOSTIC RADIOLOGY RESIDENCY POSITIONS—The University of Miami/Jackson Memorial Medical Center, Dept. of Radiology, is offering 1 third- and 1 fourth-yr diagnostic radiology residency position beginning July 1989. Our program was recently approved for an increase in total number of positions. UM/JMMC is a 1300-bed, tertiary referral center serving Miami, FL, the Southeast, and Latin America. The Dept. of Radiology currently performs approximately 250,000 exams/yr with 33 faculty, 22 residents, and 8 fellows (5 in neuroradiology and 3 in interventional/CT/ultrasound). If interested, please contact by phone or letter with CV, Sandra A. Oldham, M.D., Dept. of Radiology (R-109), University of Miami School of Medicine, P. O. Box 016960, Miami, FL 33101; (305) 549-6894. AA/EOE. 2-6c

ABDOMINAL IMAGING FELLOWSHIP—Unexpected opening at PG4 or 5 level available July 1989 for 1 yr. Subspecialty training in all modalities including ultrasound, CT, MRI, and lithotripsy. Diagnostic radiology residency prerequisite. Contact Arnold C. Friedman, M.D., Director, Abdominal Imaging Section, Dept. of Diagnostic Imaging, Temple University Hospital, Broad & Ontario Sts., Philadelphia, PA 19140; (215) 221-4216. EOE. 2c

NEURORADIOLOGY FELLOWSHIP—Two-yr beginning July 1, 1989. Exposure to all aspects of clinical/academic neuroradiology. Participation in research/teaching. Send cover letter/CV to John R. Jinkins, M.D., Chief, Division of Neuro-radiology, The University of Texas Health Science Center, 7703 Floyd Curl Dr., San Antonio, TX 78284-7800. 2-3cp

FELLOWSHIP IN MRI NEURO AND BODY—The Christ Hospital and James N. Gamble MR Institute offers a 1-yr fellowship in neuro and body MR and CT. Approximately 4000 MR exams/yr and 7000-8000 CT exams/yr. Two GE 9800 Quick and 1 GE 1.5-T MR unit. Academic endeavors including papers and chapter publication encouraged. The Christ Hospital is an 870-bed multispecialty and specialty hospital. Please send CV and 2 letters of reference to Stephen J. Pomeranz, M.D., Division of Radiology and Magnetic Resonance, The Christ Hospital, 2139 Auburn Ave., Cincinnati, OH 45219 or telephone Mrs. Maricarol Glaze at (513) 369-2949. 2-4cp

THE DEPT. OF RADIOLOGY AT THE TORONTO GENERAL HOSPITAL invites applications for the following 1-yr fellowships beginning July 1, 1989: **FELLOWSHIP IN THORACIC IMAGING**—This program offers extensive, in-depth exposure to all aspects of thoracic imaging, including plain film radiography, chest tomography (approximately 250 studies/yr), ICU radiology (56-bed ICU), thoracic CT (650 studies/yr), nuclear lung scanning (700 studies/yr), and transthoracic needle biopsy (500/yr). There is close liaison with the Divisions of Pulmonary Pathology, Cytopathology, Pulmonary Medicine (6 full-time chest physicians), and Thoracic Surgery (5 full-time non-cardiac thoracic surgeons). **FELLOWSHIP IN MUSCULOSKELETAL RADIOLOGY**—This position offers extensive clinical experience in arthrography, CT, MRI, and trauma radiology. There are opportunities for participation in research and teaching. The Toronto General Hospital is a 1000-bed, tertiary- to quaternary-care institution and is a primary teaching affiliate of the Faculty of Medicine at the University of Toronto. The fellowships are open to individuals who have completed an accredited residency in radiology. Application, including CV and references, should be sent to C.S. Ho, M.B., Acting Radiologist-in-Chief, Dept. of Radiology, Toronto General Hospital, 200 Elizabeth St., Toronto, Ontario, M5G 2C4. 2-3cp

WINTHROP FELLOWSHIP IN ABDOMINAL IMAGING—The Cleveland Clinic Foundation is offering 2 fellowship positions, each encompassing 1 yr of advanced training in body CT, ultrasound, and body MR, beginning July 1, 1990. One of these positions is supported by Winthrop Corporation in order to advance expertise and research in the field of abdominal imaging. The Cleveland Clinic Foundation is a 1000-bed, tertiary-care hospital with an international referral source and large outpatient population. The fellowship positions allow subspecialty training on state-of-the-art equipment, including ultrasound- and CT-guided interventional procedures. Please submit CV and 2 letters of reference to David M. Paushter, M.D., Hospital Radiology, Cleveland Clinic Foundation, 9500 Euclid Ave., Cleveland, OH 44106. 2-3cp

UNIVERSITY OF MASSACHUSETTS MEDICAL CENTER, Dept. of Radiology has 1-yr fellowship openings for July 1989 in vascular/interventional radiology and neuroradiology. The medical center is a 360-bed teaching hospital and medical school and a major trauma center. The dept. runs a very active clinical service and is well-equipped with 2 GE CT scanners, a 1.5-T GE MR scanner in a stand-alone facility, and 2 dedicated vascular/interventional radiology suites with Siemens and Fisher equipment. Both conventional and digital subtraction imaging capabilities are present. For further information, contact Edward H. Smith, M.D., Professor and Chair, Dept. of Radiology, University of Massachusetts Medical Center, 55 Lake Ave., N., Worcester, MA 01655; (508) 856-3252. UMMC is an equal opportunity/affirmative action employer. 1-3c

CARDIOVASCULAR/INTERVENTIONAL RADIOLOGY FELLOWSHIP AT THOMAS JEFFERSON UNIVERSITY HOSPITAL—A 1-yr fellowship position is available starting 7/1/89. This fellowship includes experience in a wide range of diagnostic angiography and both vascular and nonvascular interventional procedures. These include balloon angioplasty, laser thermal angioplasty, thrombolytic therapy, atherectomy, intravascular stent placement, IVC filter placements, renal and biliary drainage procedures, abscess drainages, and stone retrievals. Optional training also available in coronary angiography. Facilities include state-of-the-art angiographic and digital subtraction equipment. Contact either Geoffrey A. Gardiner, Jr., M.D. or David C. Levin, M.D., Dept. of Radiology, Thomas Jefferson University Hospital, 111 S. 11th St., Philadelphia, PA 19107. Thomas Jefferson University is an equal opportunity/affirmative action employer. 1-6cp

FELLOWSHIP IN PEDIATRIC RADIOLOGY—Dept. of Radiology, Children's Hospital Medical Center, Cincinnati, OH, offers a 1- or 2-yr fellowship in pediatric radiology beginning July 1, 1989. Children's Hospital Medical Center is a 344-bed institution where approximately 85,000 radiologic exams are done per yr by 10 attending radiologists. Training includes all aspects of pediatric imaging including conventional radiology, neuro-radiology, abdominal imaging, ultrasound, nuclear medicine, CT, MRI, and vascular/interventional techniques. Equipment includes digital fluoroscopy, Acuson and ATL ultrasound units with Doppler and color-flow Doppler capabilities, Gamma and SPECT tomographic nuclear cameras, GE 9800 Quick CT Scanner, 1.5-T GE MRI, and angiographic suite with digital vascular imaging. Requirements for the fellowship include completion of a radiology residency with training in the various subspecialties of diagnostic imaging. Contact Donald R. Kirks, M.D., Director, Dept. of Radiology, Children's Hospital Medical Center, Elland & Bethesda Aves., Cincinnati, OH 45229-2899; (513) 559-8058. 12-8cp

ONCORADIOLOGY/MAMMOGRAPHY FELLOWSHIP—The Dept. of Radiology at the Dana-Farber Cancer Institute and Brigham and Women's Hospital, which are Harvard University affiliates, offers a 1-yr fellowship position beginning July 1, 1989. All noninvasive imaging modalities involved in the diagnosis and care of cancer patients are integrated into this program. Please send CV to Maxine Jochelson, Director, Division of Oncoradiology, Dana-Farber Cancer Institute, 44 Binney St., Boston, MA 02115. 11-4c

CARDIOVASCULAR-INTERVENTIONAL RADIOLOGY FELLOWSHIP—Available July 19, 1989. One-year fellowship program at a 750-bed teaching hospital. Extensive clinical experience involving all aspects of cardiovascular imaging, interventional vascular and nonvascular procedures, and availability for clinical or animal research. Send CV and inquiries to Oscar H. Gutierrez, M.D., Dept. of Radiology, Box 648, University of Rochester Medical Center, Rochester, NY 14642. An equal opportunity employer (M/F). 9-2c

Tutorials/Courses

MARCH 31-APRIL 1, 1989—Urologic Ultrasound Imaging: A Practical Approach to Prostate, Kidney, Bladder, and Scrotal Scanning with Matthew Rifkin and Peter Scardino, Hilton Head, SC. Fee: \$250. Contact Ruth Harker, Teknar, Inc., 267 Wolfner Dr., Fenton, MO 63026; (800) 233-3605. 2-3d

ALASKA 89—CRUISE THE INLAND PASSAGE—July 8-15, 1989, CME I accreditation, Professor Lawrence Bassett, M.D., Breast Imaging. For information, contact Medical Seminars International, 9800 D Topanga Canyon Blvd., #232, Chatsworth, CA 91311; (818) 700-9821. 1-6d

AUGUST 1988-JUNE 1989—The Dept. of Radiology, cosponsored by the University of California San Diego School of Medicine, is offering 1- to 8-wk visiting fellowships in imaging for physicians interested in updating their knowledge of diagnostic ultrasound, including carotid and abdominal duplex scanning or a combination of ultrasound and abdominal CT (abdominal CT is not offered as an independent rotation). Faculty: Drs. George Leopold, Barbara Gosink, Dolores Pretorius, Robert Mattrey, Giovanna Casola, and Eric vanSonnenberg. Accreditation: AMA Category I, 40-hr/each wk attended. For information, contact Elizabeth Novak, UCSD Medical Center, Ultrasound Div., 225 Dickinson St., San Diego, CA 92103; (619) 543-6657. 2d

SEVENTH WINTER CONGRESS, COURCHEVELLE, FRANCE—March 4-11, 1989, Category I accreditation, international faculty, MRI, CT, and ultrasound. For information, contact Medical Seminars International, 21915 Roscoe Blvd., Ste. 222, Canoga Park, CA 91304; (818) 700-9821. 11-2d

Other

VOLUNTEER SERVICES—If you are interested in doing volunteer work as a radiologist where your services are desperately needed and greatly appreciated, inquire about the program at St. Jude Hospital in St. Lucia, West Indies. For more information, contact Sister Sharee Hurtgen, c/o St. Jude Hospital, Box 331, St. Lucia, West Indies; (809) 454-6041, or Merle Piacenti, M.D.; (815) 223-4319 (5-10 p.m. CST). 1-2ep

AJR Classified Advertisements Information

Box Responses and Address for Ad Placement

Write Box _____, AJR, 2223 Avenida de la Playa, Suite 200, La Jolla, CA 92037-3218; (619) 459-2229; FAX: (619) 459-8814.



CHALLENGE 89

DECISIONS IN IMAGING

London, England

June 24-30, 1989

This didactic course will afford participants approximately 25 Category I CME credits and be presented through lectures and case discussions. Topics in **Magnetic Resonance Imaging**, **Computed Tomography** and **Ultrasonography** will be offered in a correlative manner discussing the proper uses of each modality and the results that can be obtained. The program is sponsored by **University Imaging Associates**, and will be presented by noted **University of Southern California** faculty members and a renowned faculty from Great Britain. The course immediately precedes the **INTERNATIONAL CONGRESS OF RADIOLOGY IN PARIS** and will allow participants to enjoy the **WIMBLEDON TENNIS TOURNAMENT**, and continue on, if desired, to the International Congress. Course sessions will extend from June 25th-29th. One day's sessions will be held at Addenbrookes Hospital in Cambridge, England and another day will be at the National Heart and Chest Hospital in London.

INVITED FACULTY

William D. Boswell, Jr., M.D.

University of So. California
Los Angeles, California

Graham Bydder, M.D.

Hammersmith Hospital
London, England

Patrick Colletti, M.D.

University of So. California
Los Angeles, California

David Cosgrove, M.D.

Royal Marsden Hospital
London, England

James M. Halls, M.D.

University of So. California
Los Angeles, California

Christine Heron, M.D.

St. George's Hospital
London, England

Andrew Hine, M.D.

Central Middlesex Hospital
London, England

Janet Husband, M.D.

Royal Marsden Hospital
London, England

Donald Longmore, M.D.

National Heart & Chest Hospital
London, England

Dr. Rod Mohiaddin

National Heart & Chest Hospital
London, England

Philip W. Ralls, M.D.

University of So. California
Los Angeles, California

Simon Rees, M.D.

National Heart & Chest Hospital
London, England

Brian Worthington, M.D.

University of Nottingham
Nottingham, England

Richard Underwood, M.D.

National Heart & Chest Hospital
London, England

Ian R. Young, M.D.

Hirst Research Center
Wembley, England

Chi-Shing Zee, M.D.

University of So. California
Los Angeles, California

Meeting Coordinator: Ronald J. Friedman, M.D., University of Southern California

Registration Information: Payable in U.S. Dollars and drawn on a U.S. Bank to **University Imaging Associates**, \$450 to March 31, 1989. Thereafter \$495.

Fellows, Residents, Interns, Technicians, Nurses with letter — Less \$100.

For Registration or Further Meeting Information:

University Imaging Associates

Los Angeles County — USC Medical Center

Box 66, 1200 North State Street

Los Angeles, California 90033

Telephone: (213) 226-7245

RADIOLOGISTS

Radiology Department at Marshfield Clinic (13 radiologists) is presently expanding. We are recruiting radiologists with expertise in fields of neuroimaging, body imaging and general diagnostic radiology. Very busy clinical practice (approximately 270 physicians) and hospital practice (525 beds). Total examinations: approximately 170,000 per year and expanding. State of the art equipment in all modalities. For further information, please write or call:

Dr. William Manor
Department of Radiology

1000 North Oak Ave.
Marshfield, WI 54449
(715) 387-5261



Marshfield Clinic

INDEX TO ADVERTISERS

American Society of Head & Neck Radiology	A34
Berlex Imaging	A21
Braintree Laboratories	A32
Corometrics Medical Systems ...	A33, A34, A35, A36
Eastman Kodak	A6, A7
E-Z-EM Company	Cover 2
FUJI	Cover 3
General Electric	A18, A19
Mallinckrodt, Inc.	A25
Nuclear Associates.....	A20
Philips Medical Systems	A9, A10
Picker International	A31
S & S X-Ray	A17
University of Southern California	A37
U.S. Army	A29
Winthrop Laboratories	A13, A14, A15, A16

We try to present an accurate index. Occasionally this may not be possible because of a last-minute change or omission.

**Spend 3½ days
in Toronto.
Earn 20 CME credits.**

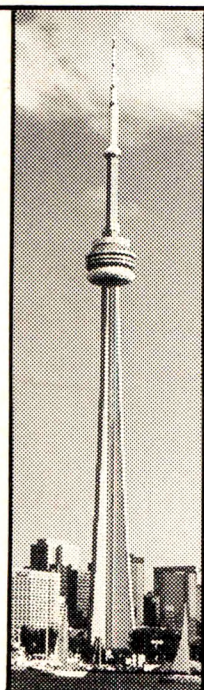
**Attend the 20th Annual
Conference and Postgraduate
Course in Head and Neck
Radiology – May 17-21, 1989**

We invite you to attend this 3½ day course on subspecialty areas within the field of Head and Neck Radiology. Seminars will cover a variety of topics, including presentations of free papers, proven cases, and resident award paper.

Social activities begin with an opening cocktail

reception and continue through Saturday's dinner at a medieval castle overlooking the city.

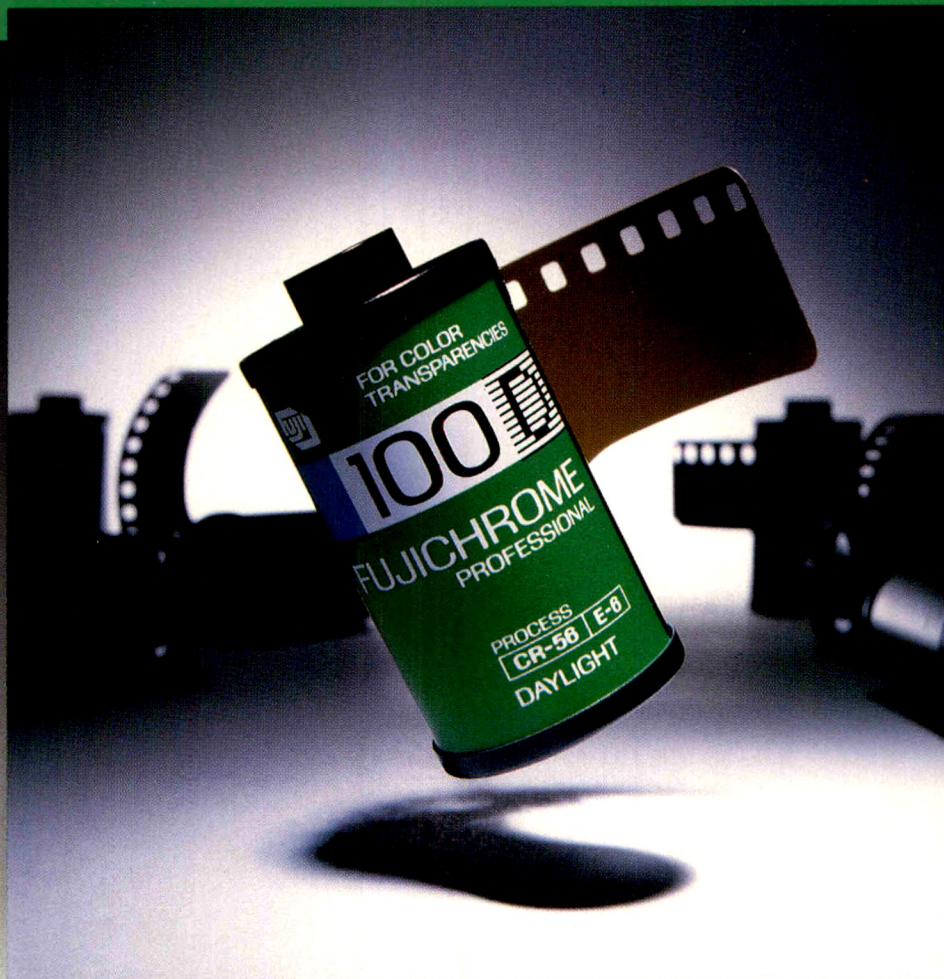
**For registration information, call (312) 574-6906
Registration Deadline: April 4, 1989**



Toronto's CN Tower



AMERICAN SOCIETY OF
HEAD AND NECK RADIOLOGY
1415 W. 22nd Street, Tower B Oak Brook, Illinois 60521



The reason for change . . . It's better

No one likes change . . . particularly professional and serious amateur photographers. So when they began switching to Fuji color film world wide, there could only be one reason . . . the right reason. It's better!

Have you evaluated Fuji Medical radiographic films lately?

Call your Fuji representative or 800-431-1850.

CIRCLE 7 ON READER SERVICE CARD



The Reason for Change!

Burbank - Chicago - Stamford, CT.



REVIEW ARTICLE

- 229 Modern diagnostic imaging in joint disease. *Dalinka MK, Kricun ME, Zlatkin MB, Hibbard CA*

PROGRESS IN RADIOLOGY

- 241 Dual-energy radiographic absorptiometry for bone densitometry: current status and perspective. *Sartoris DJ, Resnick D*
 247 Perfluorooctylbromide: a new contrast agent for CT, sonography, and MR imaging. *Mattrey RF*
 253 New perspectives in thrombus-specific imaging: radiolabeled monoclonal antibodies. *Oster ZH, Som P*

CARDIOPULMONARY RADIOLOGY

- 261 The diagnosis of pulmonary nodules: comparison between standard and inverse digitized images and conventional chest radiographs. *Sheline ME, Brikman I, Epstein DM, Mezrich JL, Kundel HL, Arenson RL*
 265 Case report. Pulmonary edema due to ingestion of organophosphate insecticide. *Li C, Miller WT, Jiang J*

GASTROINTESTINAL RADIOLOGY

- 267 CT evaluation of suspected hepatic metastases: comparison of techniques for IV contrast enhancement. *Paushter DM, Zeman RK, Scheibler ML, Choyke PL, Jaffe MH, Clark LR*
 272 Commentary. Dynamic hepatic CT scanning. *Foley WD*
 275 Intrahepatic cholangiographic abnormalities in liver transplants: correlation with biopsy evidence of rejection and other disorders. *Bauman J, Campbell WL, Demetris AJ, Zajko AB*
 281 CT findings of clonorchiasis. *Choi BI, Kim HJ, Han MC, Do YS, Han MH, Lee SH*
 285 Periportal low-attenuation areas on CT: value as evidence of liver transplant rejection. *Kaplan SB, Sumkin JH, Campbell WL, Zajko AB, Demetris AJ*
 289 The sonographic diagnosis of acute gangrenous cholecystitis: importance of the Murphy sign. *Simeone JF, Brink JA, Mueller PR, et al.*
 291 Technical note. The use of color Doppler sonography to distinguish dilated intrahepatic ducts from vascular structures. *Ralls PW, Mayekawa DS, Lee KP, Johnson MB, Halls J*

GENITOURINARY RADIOLOGY

- 293 Color Doppler ultrasound of the normal testis. *Middleton WD, Thorne DA, Melson GL*
 299 Wilms tumor (nephroblastoma) in the adult patient: clinical and radiologic manifestations. *Kiourmehr F, Cochran ST, Layfield L, Yaghmai I, Ngo C, Smith SR*
 303 Percutaneous, large-bore, suprapubic cystostomy: technique and results. *Papanicolaou N, Pfister RC, Nocks BN*
 307 Case report. Renal lymphangiomyoma—a rare cause of a multiloculated renal mass. *Jacobs JE, Sussman SK, Glickstein MF*

CONTRAST MATERIAL

- 309 Anticoagulant effects of contrast materials: in vitro study of iohexol, ioxaglate, and diatrizoate. *Rasuli P, McLeish WA, Hammond DI*

MUSCULOSKELETAL RADIOLOGY

- 313 Pictorial essay. The subclavian triangle: CT analysis. *Wechsler RJ, Rao VM, Newman LM*
 319 Flexion teardrop fracture of the cervical spine: radiographic characteristics. *Kim KS, Chen HH, Russell EJ, Rogers LF*
 327 MR imaging of the pars interarticularis. *Johnson DW, Farnum GN, Latchaw RE, Erba SM*

- 333 Incidental detection of hematopoietic hyperplasia on routine knee MR imaging. *Deutsch AL, Mink JH, Rosenfelt FP, Waxman AD*
 337 Pictorial essay. Imaging of pigmented villonodular synovitis with emphasis on MR imaging. *Jelinek JS, Kransdorf MJ, Utz JA, et al.*

PEDIATRIC RADIOLOGY

- 343 Case report. Cerebellar atrophy caused by high-dose cytosine arabinoside: CT and MR findings. *Miller L, Link MP, Bologna S, Parker BR*
 345 Case report. Aortico-left ventricular tunnel: diagnosis by cine angiocardiography. *Guo D-W*

NEURORADIOLOGY

- 347 Efficacy of MR vs CT in epilepsy. *Heinz ER, Heinz TR, Radtke R, et al.*
 353 Absence of the septum pellucidum: a useful sign in the diagnosis of congenital brain malformations. *Barkovich AJ, Norman D*
 361 Intracranial oligodendrogliomas: imaging findings in 35 untreated cases. *Lee Y-Y, Van Tassel P*

VASCULAR AND INTERVENTIONAL RADIOLOGY

- 371 Color Doppler ultrasound imaging of lower-extremity venous disease. *Foley WD, Middleton WD, Lawson TL, Erickson S, Quiroz FA, Macrander S*
 377 Budd-Chiari syndrome: the results of duplex and color Doppler imaging. *Grant EG, Perrella R, Tessler FN, Lois J, Busuttill R*
 382 Case report. Embolotherapy of a high-flow false aneurysm by using an occlusion balloon, thrombin, steel coils, and a detachable balloon. *Lammert GK, Merine D, White RI Jr, Fishman EK, Porterfield JK*
 385 Case report. Fat-shift artifact simulating aortic dissection on MR images. *Lotan CS, Cranney GB, Doyle M, Pohost GM*
 387 Chemotherapy and embolization via the inferior epigastric artery for the treatment of primary and metastatic cancer. *O'Keeffe F, Lorigan JG, Charnsangavej C, Carrasco CH, Richli WR, Wallace S*
 391 Technical note. A technique for pulmonary artery catheterization in patients with right ventricular enlargement. *Waltman AC, Walker TG*

RADIOLOGIC PHYSICS

- 393 Perspective. Radiologic physics instruction for diagnostic radiologists: results of an opinion survey. *Committee on Training of Radiologists, American Association of Physicists in Medicine*
 398 Commentary. Physics instruction in radiology. *Hendee WR*

1989 ARRS MEETING SECTION

- 400 Meeting invitation
 402 Section on instruction
 415 Scientific program
 421 Local activities
 423 Registration forms
 426 Airline discounts
 427 Meeting summary

OTHER CONTENT

- 370 Forthcoming articles
 428 American Roentgen Ray Society information
 429 Letters
 436 Review of current literature
 440 ARRS 1989 residents' award papers information
 441 News
 Book and videotape reviews 264, 280, 288, 312, 318
 Classified advertisements
 A3 Guidelines for authors
 A8 AJR business and subscriber information

Acc 13.11.90

AJR

American
Journal of
Roentgenology

March 1989

PercuCut™ Cut-Biopsy Needles from E-Z-EM provide reliable results in virtually all soft-tissue biopsies. Patented, specially designed "keyhole" cutting-edges on the cannula tip precisely core tissue samples. Ultra-thin-wall tubing maximizes sample size while minimizing needle gauge and patient trauma.

Three PercuCut needle designs allow the physician complete flexibility in obtaining a biopsy sample.

Cut-Biopsy Needle—a keyhole cutting-edge cannula with stylet. Includes a unique syringe which creates and maintains negative pressure during the biopsy procedure.

Coaxial Sheath Cut-Biopsy Needle—a three-part sheath/cannula/stylet design for multiple samples through a single puncture. Our unique aspirating syringe system is also included.

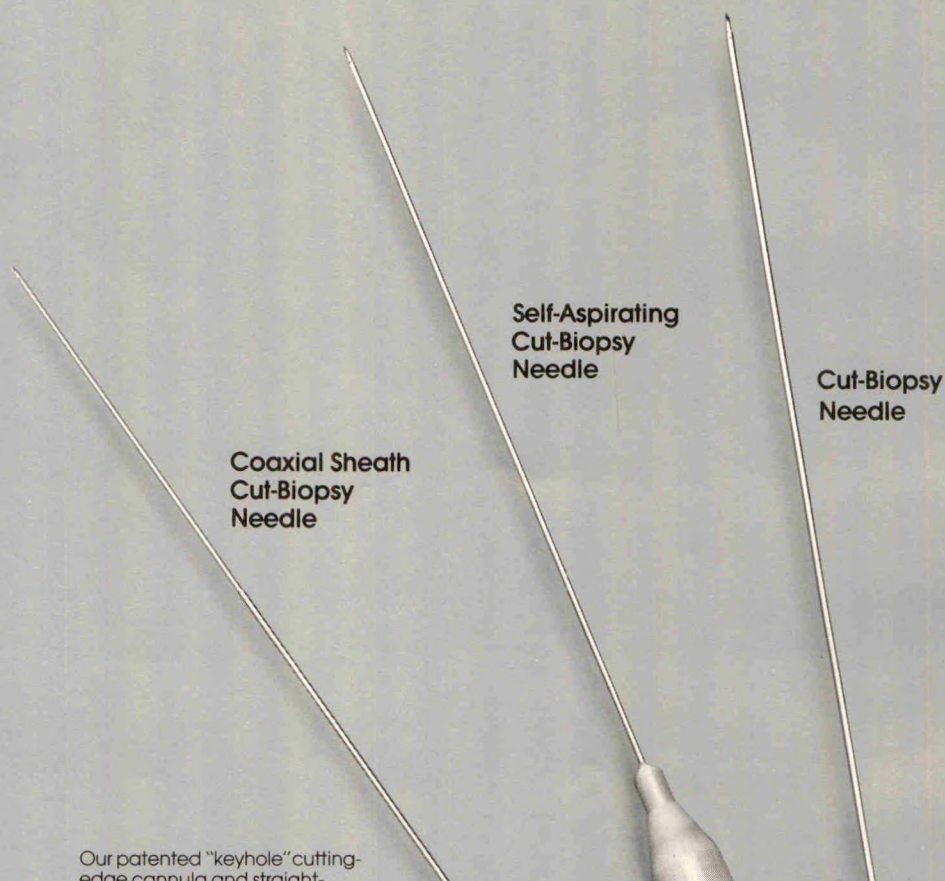
Self-Aspirating Cut-Biopsy Needle—a biopsy needle that combines our keyhole-cutting technology with a specially designed self-aspirating diaphragm hub which permits one-hand operation without a syringe.

PercuCut Needles have proven their ability to provide excellent, reliable histological and cytological samples in virtually all soft-tissue biopsies. All use a straight-tracking trocar pointed stylet for precise placement, and are available in gauges and lengths to suit any application.

For additional information on all

Reliable histological
and cytological
fine needle
aspiration biopsies
...from E-Z-EM

PercuCut™



Official Journal of the American Roentgen Ray Society



American Journal of Roentgenology
Diagnostic Imaging and Related Sciences

- Editor-In-Chief** Robert N. Berk, *La Jolla, California*
University of California, San Diego
School of Medicine and Medical Center
- Editor Emeritus** Melvin M. Figley, *Seattle, Washington*
- Associate Editor** Saskia von Waldenburg Hilton, *San Diego, California*
- Consulting Editor** Juan M. Taveras, *Boston, Massachusetts*
- Statistician** Charles C. Berry, *San Diego, California*

Editorial Board

- | | | |
|-------------------------|--------------------------|--------------------|
| John R. Amberg | William R. Hendee | Peter M. Ronai |
| Itamar Aviad | John R. Hesselink | Sjef H. J. Ruijs |
| Lawrence W. Bassett | Charles B. Higgins | Carol M. Rumack |
| Gregory P. Borkowski | Melvyn T. Korobkin | Stuart S. Sagel |
| William G. Bradley, Jr. | Thomas L. Lawson | David J. Sartoris |
| Peter L. Cooperberg | Bruce L. McClennan | Stefan C. Schatzki |
| N. Reed Dunnick | Albert A. Moss | Edward A. Sickles |
| David K. Edwards | Jeffrey H. Newhouse | Barry A. Siegel |
| Ronald G. Evens | Donald L. Resnick | David D. Stark |
| David S. Feigin | Stewart R. Reuter | Edward T. Stewart |
| Paul J. Friedman | Charles A. Rohrmann, Jr. | Eric vanSonnenberg |

Editorial Staff: Margaret Levene, *managing editor*; Katie L. Spiller, Barbara Rose, Barbara L. Halliburton, and Janine Anderson, *manuscript editors*; Nancy Rydbeck, *office manager*; Sheri Smith, *administrative assistant*; Sandra L. Griffin, *administrative secretary*.

AJR, AMERICAN JOURNAL OF ROENTGENOLOGY (ISSN 0361 803X) is the official journal of the American Roentgen Ray Society and is published monthly by Williams & Wilkins, 428 E. Preston St., Baltimore, MD 21202. Annual dues include \$50 for journal subscription. Second-class postage paid at Baltimore, MD, and at additional mailing offices. Postmaster, send address changes (Form 3579) to AJR, 428 E. Preston St., Baltimore, MD 21202. Subscription rates \$100 (\$145 foreign); institutions \$110 (\$155 foreign); in training \$25 (\$70 foreign); single copy \$16 (\$19 foreign). Japanese rates include airfreight. Japanese yen price is available from our sole agent USACO Corporation, 13-12, Shimbashi 1-Chome, Minato-Ku, Tokyo 105, Japan, telephone 03-502-6471. Airmail rates furnished on request. Indexed by *Current Contents* and *Index Medicus*. Copyright © 1989 by American Roentgen Ray Society. 0361-803X/89\$2.00

NOW THERE'S AN EASY WAY TO MONITOR RADON LEVELS



Digital Radon Monitor Systems

- Evaluated and accepted by the U.S. Environmental Protection Agency.
- Continuously monitors radon gas — anywhere.
- Digital display of current and long-term average concentrations.
- Easy to install — easy to operate — no lab analysis required.
- Measures radon concentration from 0.1 to 999 pCi/l.
- Data Logger model stores concentration values for up to 90 data points.
- Data Logger model prints data in tabular and graphic form.

NUCLEAR ASSOCIATES

For more details, request Bulletin 4142-44

CIRCLE 16 ON READER SERVICE CARD



A Division of VICTOREEN, INC.
100 VOICE ROAD
CARLE PLACE, NY 11514-1593 U.S.A.
(516) 744-6900

AJR Guidelines for Authors

Address new and revised manuscripts, correspondence, and classified ads to the Editor:

AJR Editorial Office
2223 Avenida de la Playa, Suite 200
La Jolla, CA 92037-3218

Telephone: (619) 459-2229; FAX: (619) 459-8814

Inquiries regarding subscriptions, display advertising, reprints, or permission to republish *AJR* material should be addressed to the publisher:

The Williams & Wilkins Co.
428 E. Preston St.

Baltimore, MD 21202 Telephone: (301) 528-4133

The *AJR* publishes original contributions to the advancement of medical diagnosis and treatment. Submitted manuscripts should not contain previously published material and should not be under consideration for publication elsewhere. Papers dealing with neuroradiology should be addressed to: American Journal of Neuroradiology, Dept. of Radiology, Massachusetts General Hospital, Boston, MA 02114. At the discretion of the *AJR* Editor, *AJNR* articles that are of interest to the general reader may be republished in the *AJR*. Neuro-radiologic papers sent to the *AJR* will be forwarded to the Editorial Office of the *AJNR*.

Manuscript decisions are based on peer review. Reviewers receive manuscripts without title pages to ensure an unbiased review. Statements made in the article, including changes made by the Editor or manuscript editor, are the responsibility of the author and not of the *AJR* or its publisher. Authors will be sent the edited manuscript, galley proof, and proofs of illustrations. If the corresponding author will be unavailable to review galleys, arrangements should be made for a coauthor or colleague to read and return the proof.

The following guidelines are based on instructions set forth in the **Uniform Requirements for Manuscripts Submitted to Biomedical Journals** (*Ann Intern Med* 1988;108:258-265). Articles will be edited, however, to conform to the individual style of *AJR*.

General Guidelines for Major Papers

Abstract. Clearly state (in 200 words or less) the purpose, methods, results, and conclusions of the study. Include actual data.

Introduction. Briefly describe the purpose of the investigation, including relevant background information.

Methods. Describe the research plan, the materials (or subjects), and the methods used, in that order. Explain in detail how disease was confirmed and how subjectivity in observations was controlled.

Results. Present results in a clear, logical sequence. If tables are used, do not duplicate tabular data in text, but do describe important trends and points.

Discussion. Describe the limitations of the research plan, materials (or subjects), and methods, considering both the

purpose and the outcome of the study. When results differ from those of previous investigators, explain the discrepancy.

AUTHOR'S CHECKLIST

For priority handling, complete the following checklist, sign the copyright form on the reverse side of this page, and include both with the manuscript.

_____ Two copies of the manuscript (the original and a photocopy) and two complete sets of figures are submitted. One copy has been retained by the author.

_____ If appropriate, *AJR* Guidelines for case reports, technical notes, pictorial essays, or letters to the Editor have been followed. (See page A5.)

_____ The manuscript, including references, figure legends, and tables, is typed double-spaced on 8½ × 11 in. (21.6 × 27.9 cm) *nonerasable* paper. Right-hand margins are not justified.

_____ All manuscript pages are numbered consecutively beginning with the abstract. Authors' names do not appear on the manuscript pages.

_____ The manuscript is organized as follows: title page, blind title page (title only), abstract, introduction, methods, results, discussion, acknowledgments, references, tables, figure legends, and figures.

_____ Informed consent has been obtained from patients who participated in clinical investigations. If experiments were performed on animals, authors complied with NIH guidelines for use of laboratory animals.

_____ Use of unfamiliar acronyms and abbreviations is kept to a minimum. When abbreviations are used they are defined at first mention, followed by the abbreviation in parentheses.

_____ Metric measurements are used throughout, or the metric equivalent is given in parentheses.

_____ Names and locations (city and state only) of manufacturers are given for equipment and nongeneric drugs.

Title Page

_____ The following information is given: title of article; names and complete addresses (including zip code) of all authors; current addresses of authors who have moved since study; acknowledgment of grant or other assistance. The corresponding author is clearly identified, and a current address, phone number, and Fax number are given.

_____ Two copies of a blind title page are included giving only the title (without the authors' names) for use in the review process.

Abstract

_____ An abstract of approximately 200 words concisely states the purpose, methods, and results of the study in one paragraph. Actual data are included. Conclusions are stated in a second, summary paragraph.

_____ No abbreviations or reference citations are used.

References

References (not to exceed 35) are typed double-spaced starting on a separate page and are **numbered consecutively in the order in which they appear in the text**.

All references are cited in the text and are enclosed in brackets and typed on line with the text (not superscript).

Unpublished data are not cited in the reference list, but are cited parenthetically in the text, for example, (Smith DJ, personal communication), (Smith DJ, unpublished data). This includes papers submitted, but not yet accepted, for publication.

Inclusive page numbers (e.g., 333–335) are given for all references.

Journal names are abbreviated according to *Index Medicus*.

Style and punctuation of references follow the format illustrated in the following examples (all authors are listed when six or less; when seven or more authors, the first three are listed, followed by "et al."):

Journal article

1. Long RS, Roe EW, Wu EU, et al. Membrane oxygenation: radiographic appearance. *AJR* **1986**;146:1257–1260

Book

2. Smith LW, Cohen AR. *Pathology of tumors*, 6th ed. Baltimore: Williams & Wilkins, **1977**:100–109

Chapter in a book

3. Breon AJ. Serum monitors of bone metastasis. In: Clark SA, ed. *Bone metastases*. Baltimore: Williams & Wilkins, **1983**:165–180

Paper presented at a meeting

4. Lau FS, Kirk AN. MR imaging of the spine. Presented at the annual meeting of the American Roentgen Ray Society, Washington, DC, April **1986**

Tables

Each table is typed double-spaced on a separate page without vertical or horizontal rules; each has a short, descriptive title. Tables do not exceed two pages in length and contain at least four lines of data.

Tables are numbered in the order in which they are cited in the text.

Abbreviations are defined in an explanatory note below each table.

Tables are self-explanatory and do not duplicate data given in the text or figures.

All arithmetic (percentages, totals, differences) has been double checked for accuracy, and tabular data agree with data given in the text.

Figures and Legends

Two complete sets of original figures are submitted unmounted in labeled envelopes.

Figures are clean, unscratched, 5 × 7 in. (13 × 18 cm) glossy prints with **white borders**. A separate print is submitted for each figure *part*.

All figure parts relating to one patient have the same figure number.

Each figure is labeled on the back with the figure number and an arrow indicating "top." For black-and-white figures, labeling is done on a gummed label, which is then affixed to the back of the print. *Never* use labels on color figures, but write figure number on the back lightly in pencil. *Never* use ink on front or back of any figures.

Author's names are *not* written on the backs of figures.

Only removable (rub-on) arrows and letters are used on the figures. Symbols are uniform in size and style and are not broken or cracked.

Images are uniform in size and magnification.

Line drawings are done in black ink on a white background. They are professional in quality, and all use the same size type. (Only glossy prints are acceptable.)

Written permission has been obtained for use of all previously published illustrations (and copies of permission letters are included), and an appropriate credit line is given in the legends.

Legends are typed double-spaced, and figure numbers correspond with the order in which the figures are cited in the text.

Transfer of Copyright Agreement, Conflict of Interest Acknowledgment, Certification of Coauthors, and Exclusive Publication Statement

Complete copyright to the article entitled: _____

is hereby transferred to the American Roentgen Ray Society (for United States government employees to the extent transferable), effective if and when the article is accepted for publication in the *American Journal of Roentgenology*. In the case of the authors who are officers or employees of the United States government, the American Roentgen Ray Society recognizes that works prepared by officers or employees of the United States government as part of their official government duties are in the public domain.

Authors reserve all proprietary rights other than copyright, such as patent rights and the right to use all or part of this article in future works of their own. The authors retain the right of replication, subject only to crediting the original source of publication and receiving written permission from the publisher.

Authors guarantee that this manuscript contains no matter that is libelous or otherwise unlawful, invades individual privacy, or infringes any proprietary rights.

Authors understand that they will receive no royalty or other compensation from the American Roentgen Ray Society or the publisher.

Authors guarantee that the editor has been or will be informed of any proprietary or commercial interest or conflicts of interest the authors may have that relate directly or indirectly to the subject of this article.

All authors certify that they have made substantive and specific intellectual contributions to the article and assume public responsibility for its content.

Finally, the authors certify that none of the material in this manuscript has been published previously or is currently under consideration for publication elsewhere.

First author/date

Second author

Third author

Fourth author

Fifth author

Sixth author

This agreement must be signed by all authors in order for the manuscript to be published.

Case Reports

A case report is a brief description of a special case that provides a message that transcends the individual patient.

Format. There is no abstract. The introduction should be a short paragraph giving the general background and the specific interest of the case. No more than one case should be described in detail (similar ones can be mentioned briefly in the discussion). Emphasis should be on the radiologic aspects; clinical information must be limited to that necessary to provide a background for the radiology. The discussion should be succinct and should focus on the specific message and relevance of radiologic methods. A review of the literature is not appropriate.

Length. Maximum of five double-spaced, typewritten pages, including the references but not the title page or figure legends.

References. Maximum of eight.

Figures. Maximum of three or four, unless the text is shortened accordingly. Legends must not repeat the text.

Tables and Acknowledgments. Not appropriate in case reports.

Technical Notes

A technical note is a brief description of a specific technique or procedure, modification of a technique, or equipment of interest to radiologists.

Format. No abstract, headings, or subheadings are required. If headings are used, they should be a combination of "Case Report," "Materials and Methods," "Results," and "Discussion." A brief one-paragraph introduction should be included to give the general background. Discussion should be limited to the specific message, including the uses of the technique or equipment. Literature reviews and lengthy case reports are not appropriate.

Length. Maximum of five double-spaced, typewritten pages, including the references but not the title page or figure legends.

References. Maximum of eight.

Figures. Maximum of two, unless the text is shortened accordingly.

Tables and Acknowledgments. Not appropriate in technical notes.

Pictorial Essays

A pictorial essay is an article that conveys its message through illustrations and their legends. Unlike other AJR articles, which are based on original research, pictorial essays serve primarily as teaching tools, like exhibits at a scientific meeting. They are not encyclopedic book chapters. No abstract is necessary.

Length. Maximum of four double-spaced, typewritten pages, including the references but not the title page or figure legends.

References. Maximum of four.

Figures. Maximum of 30 figure parts. Number should be as few as necessary to convey the message of the paper.

Tables and Acknowledgments. Not appropriate in pictorial essays.

Letters to the Editor and Replies

Letters to the Editor and Replies should offer objective and constructive criticism of published articles. Letters may also discuss matters of general interest to radiologists. Do not end a letter with a hand-written signature.

Format. All letters should be typed double-spaced on nonletterhead paper, with no greeting or salutation. Name and affiliation should appear at the end of the letter. Titles for letters should be short and pertinent. The title for a reply is simply "Reply."

Length. Maximum of two double-spaced, typewritten pages, including references.

References. Maximum of four.

Figures. Maximum of two.

Tables and Acknowledgments. Not appropriate in Letters to the Editor and Replies.

Opinions, Commentaries, and Perspectives

Opinions, commentaries, and perspectives are special articles dealing with controversial topics or issues of special concern to radiologists.

Format. Include a title page but no abstract. Headings may be used to break up the text.

Length. Maximum of five double-spaced, typewritten pages.

References. Maximum of five.

Tables and Figures. Maximum of four.

Computer Page Articles

Articles published on the computer page deal with practical computer applications to radiology.

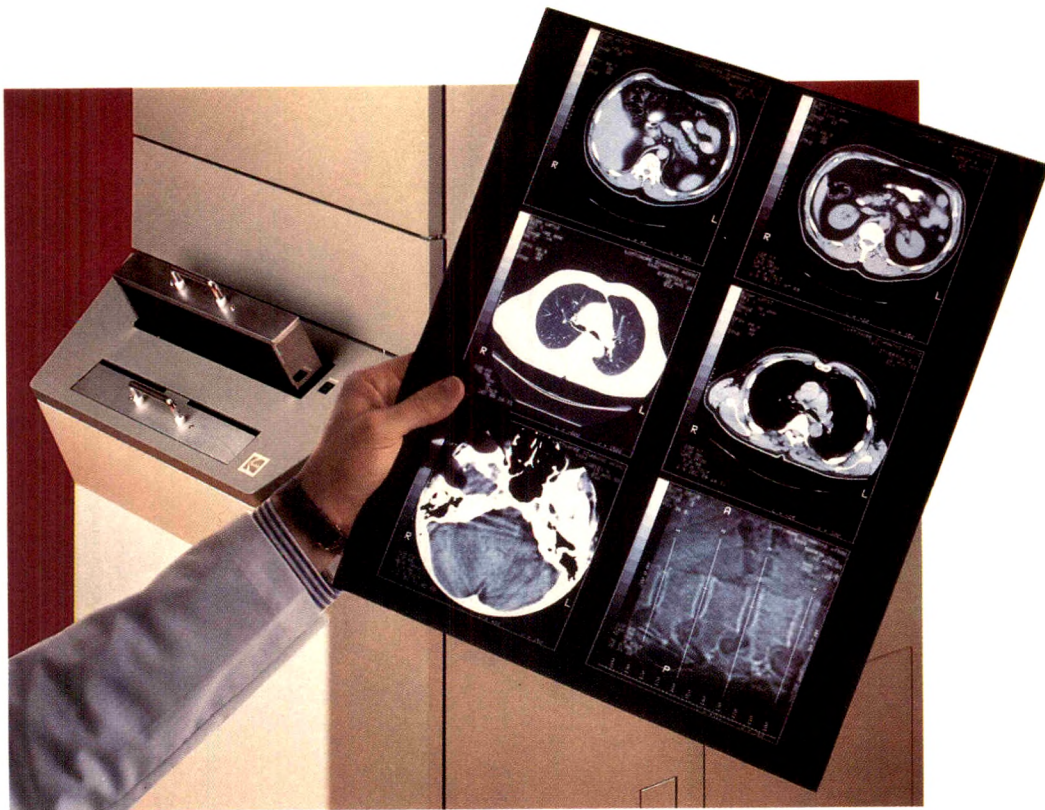
Format. Include a title page but no abstract.

Length. Maximum of eight double-spaced, typewritten pages.

References. Maximum of five.

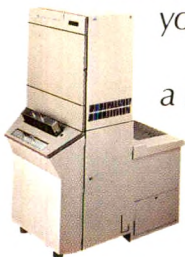
Figures and Tables. Maximum of five. Computer printouts are not acceptable. Figures must be submitted as 5 × 7 in. glossy prints.

**STEP UP
TO LASER
IMAGING
WITH
KODAK**



***Introducing the Kodak Ektascan laser printer, model 100.
The quality of digital imaging for today's and tomorrow's
imaging systems.***

Now you can have consistent, artifact-free, high-resolution digital images from current and future imaging systems. The new Kodak Ektascan laser printer, model 100, is available with custom interfaces for CT, MRI and DSA. Flexible tone scaling gives you the look you like on Kodak Ektascan laser imaging film. And a compact 28 x 30-inch footprint makes it ideal for mobile applications. Part of a complete Kodak imaging system, the Ektascan laser printer, docked to a Kodak processor, gives you maximum productivity.



Ask your Kodak representative for details, or specify a Kodak Ektascan laser printer when you order an imaging system.

The digital imaging advantage.

The new vision of Kodak



AJR Business and Subscriber Information

The American Roentgen Ray Society

AJR, *American Journal of Roentgenology*, is published monthly to disseminate research on current developments in the radiologic sciences and commentary on topics related to radiology. It is published by the American Roentgen Ray Society, 1891 Preston White Dr., Reston, VA 22091; (703) 648-8992. Inquiries regarding society business, the annual ARRS meeting, and membership should be addressed to the Society at the above address.

Correspondence Concerning the *AJR*

Correspondence regarding display (not classified) advertising, subscriptions, address changes, reprints, and permission requests should be addressed to Williams & Wilkins, 428 E. Preston St., Baltimore, MD 21202; (301) 528-4000.

Correspondence regarding editorial matters and classified advertising should be addressed to Editorial Office, *AJR*, 2223 Avenida de la Playa, Ste. 200, La Jolla, CA 92037-3218; telephone (619) 459-2229; FAX (619) 459-8814. For information on manuscript submission, see Guidelines for Authors, pages A3-A5.

Subscriber Information

Subscription requests and inquiries should be sent to Williams & Wilkins, 428 E. Preston St., Baltimore, MD 21202. ARRS annual dues include \$50 for journal subscription. Subscription rates are as follows: nonmembers, \$100/year (\$145 foreign); institutions, \$110 (\$155 foreign); nonmember in-training, \$25 (\$70 foreign). Single copies of the Journal may

be purchased for \$16 (\$19 foreign). Airmail rates will be furnished on request.

Japanese rates include airfreight. Japanese yen price is available from our sole agent, USACO Corporation, 13-12, Shimbashi 1-Chome, Minato-Ku, Tokyo 105, Japan; telephone 03-502-6471.

If a subscriber receives a damaged copy of the *AJR* or fails to receive an issue, the subscriber should notify Williams & Wilkins (428 E. Preston St., Baltimore, MD 21202) within 60 days of publication (90 days for foreign subscribers) and that issue will be replaced.

Change of address information should be sent to Williams & Wilkins, 428 E. Preston St., Baltimore, MD 21202. Allow 90 days for address changes.

Copyrights, Permissions, and Reprints

The American Roentgen Ray Society holds the copyright for all material published in the *AJR*. No part of this publication may be reproduced without permission from the ARRS. Requests for such permission should be addressed to Williams & Wilkins, 428 E. Preston St., Baltimore, MD 21202.

For reprints of a particular article, please contact the author designated in the footnotes for that article.

Indexes

The *AJR* provides volume and yearly indexes (subject and author) in the June and December issues each year. *AJR* articles are also indexed in *Current Contents*, *Index Medicus*, and the cumulative index published by *Radiology*.

P L A T I N U M



PHILIPS



CLINICALLY SUPERIOR BY DESIGN

To perceive the Philips Platinum as merely another new ultrasound system with superficial modifications would be a serious oversight.

It is, instead, the outcome of a major undertaking to combine unsurpassed clinical utility, unexcelled image quality and exceptional user comfort into a single, reliable and upgradeable system.

Platinum has been designed to provide you with the highest performance available in every modality: Linear Array, Sector Array, Doppler and color Doppler imaging.

Wide Aperture Linear Arrays, with Variable Focal Windowing™, incorporate 128 active transmit/receive channels and exacting pitch for unsurpassed image resolution.

Sector Arrays fea-

ture maximized aperture size and equal-pitch circular elements for lower phase error than today's high-performance annular arrays.

Equally important, Platinum offers you a multitude of innovative and unique design features such as the convenient mouse

to access drop-down menus, the floating console,

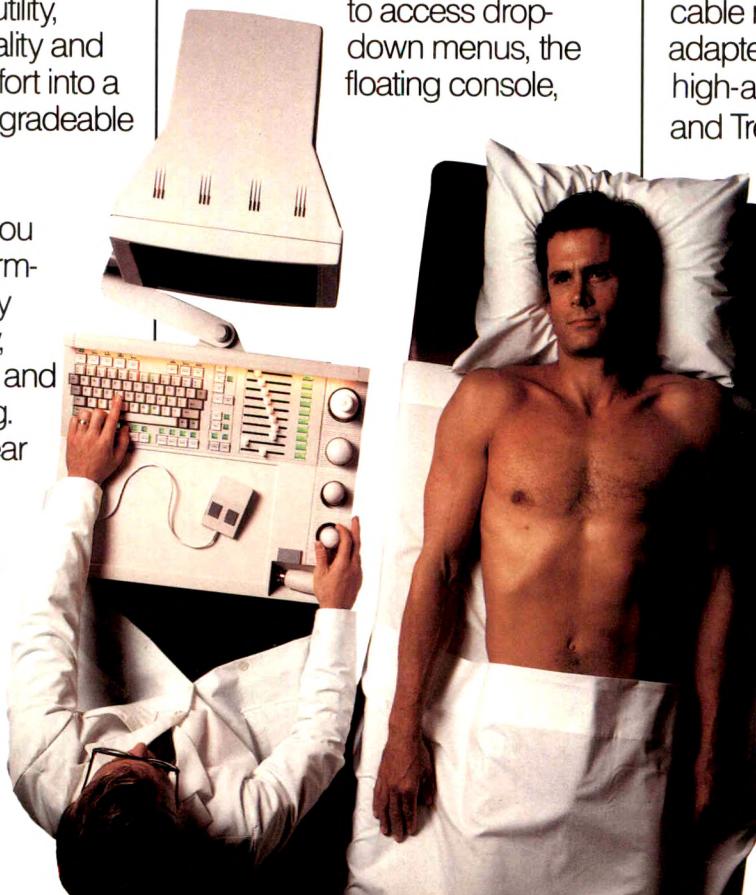


For safety and transducer protection, cables retract automatically.

cable management, operator-adapted software, lightweight high-accessibility transducers and Trend Analysis, which not

only make the system a pleasure to use, but enhance the diagnostic process.

Interactive Data Packages™ (IDP's) simplify calculations, store pertinent data for quick recall during evaluation, and graph expected normals for a variety of exams. Platinum's electronics allow Doppler and color Doppler imaging to be added easily later on.



Philips Platinum Clinically Superior By Design

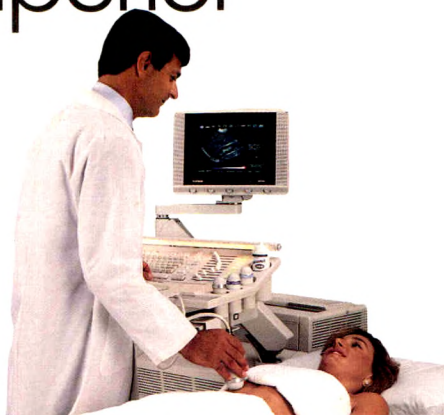
Philips Platinum is the first ultrasound system that actually adapts to the attributes of the individual operator, while at the same time accommodates all types of examinations in comfort.

The floating console allows the examiner to approach the patient from a choice of angles and still maintain complete control over all functions.

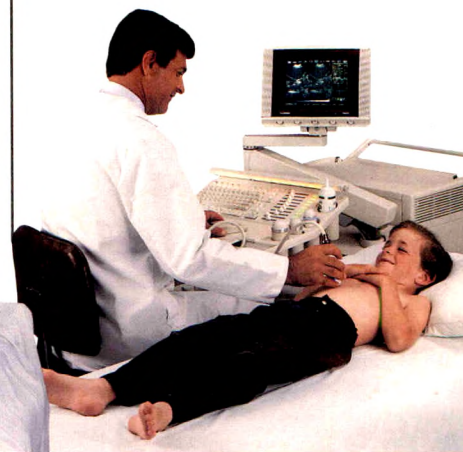
Additionally, Platinum has been built with foresight and upgradeability to maintain its clinical value during the years ahead.

To see the new and advanced ultrasound system that is clinically superior by design, call (714) 556-7608, TELEX: 683-6070. Or contact Philips Ultrasound International, 2722 South Fairview Street, Santa Ana, California 92704, U.S.A.

From Any Point of View



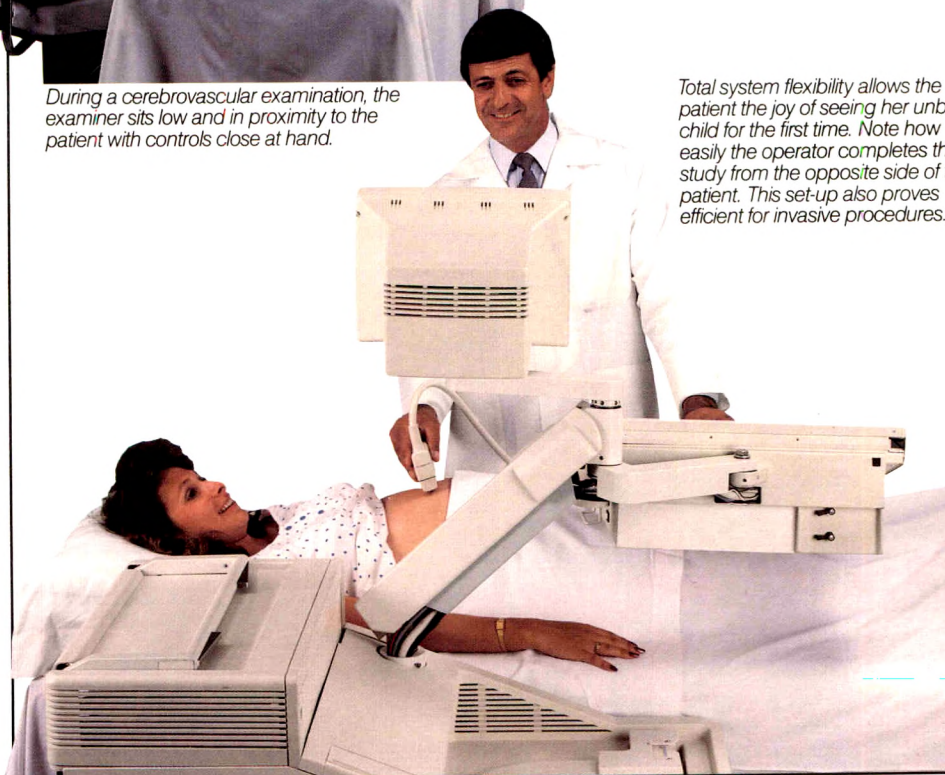
With all controls conveniently at hand, the examiner can concentrate completely on the ultrasonic data and the welfare of the patient.



While scanning the abdomen of a pediatric patient, Platinum allows the examiner to sit high for detailed surveillance.



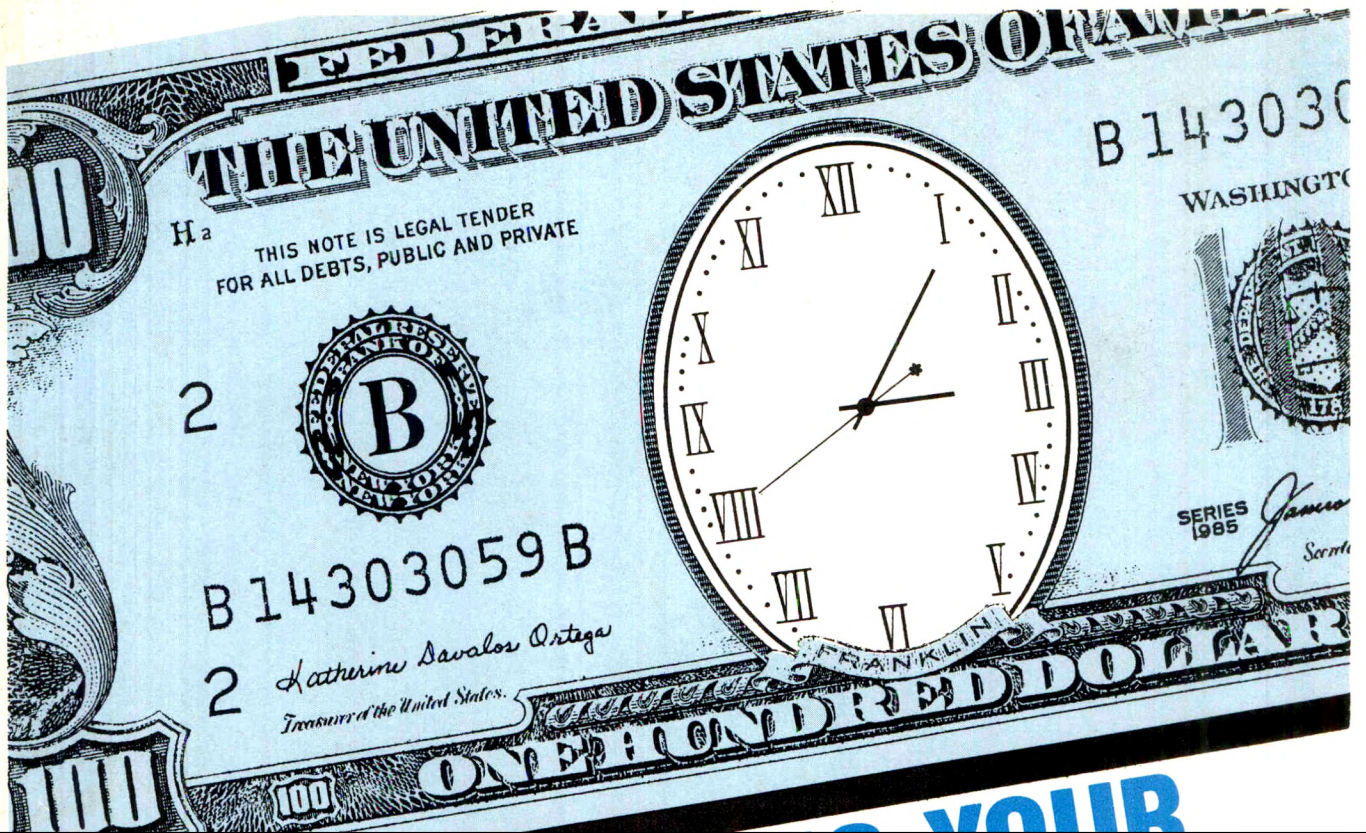
During a cerebrovascular examination, the examiner sits low and in proximity to the patient with controls close at hand.



Total system flexibility allows the patient the joy of seeing her unborn child for the first time. Note how easily the operator completes the study from the opposite side of the patient. This set-up also proves efficient for invasive procedures.



PHILIPS





GE Medical Systems



Presenting CT Pace

Productivity without compromise

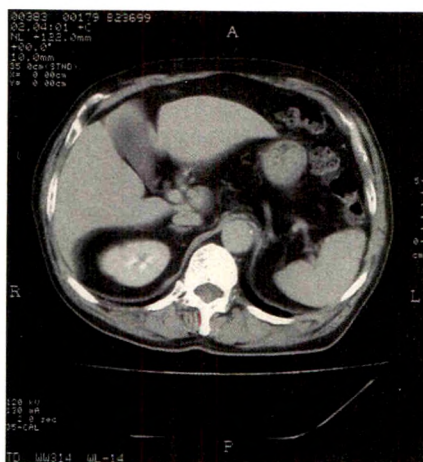
The CT Pace™ system from GE meets the productivity demands of today's fast-paced radiology departments.

CT Pace is the first CT system capable of *simultaneous* scanning, reconstruction, image display and analysis.

Accelerated productivity

With the revolutionary Parallax™ computer architecture, reconstruction proceeds uninterrupted as you perform up to eight scans per minute—twelve in a dynamic mode.

Innovative parallel processing delivers unprecedented system response—as soon as you give a command, CT Pace is ready to perform. The result—freedom to work at your own pace.



2 sec, 10 mm abdominal scan demonstrates the gallbladder and cystic duct, the spleen and associated vasculature and the superior pole of the right kidney.

Exceptional images

With its Paraview™ data acquisition system, CT Pace produces the clear, detailed images you expect from GE. The system uses 825 detectors and a 512² reconstruction matrix for excellent images, routinely acquired in two to three seconds.

Secure investment

In today's competitive environment true economy goes beyond an affordable price. State-of-the-art engineering makes CT Pace extremely reliable. Compact size, light weight and low power requirements keep site preparation costs and installation time to a minimum. And CT Pace is backed by our highly trained service and support team.

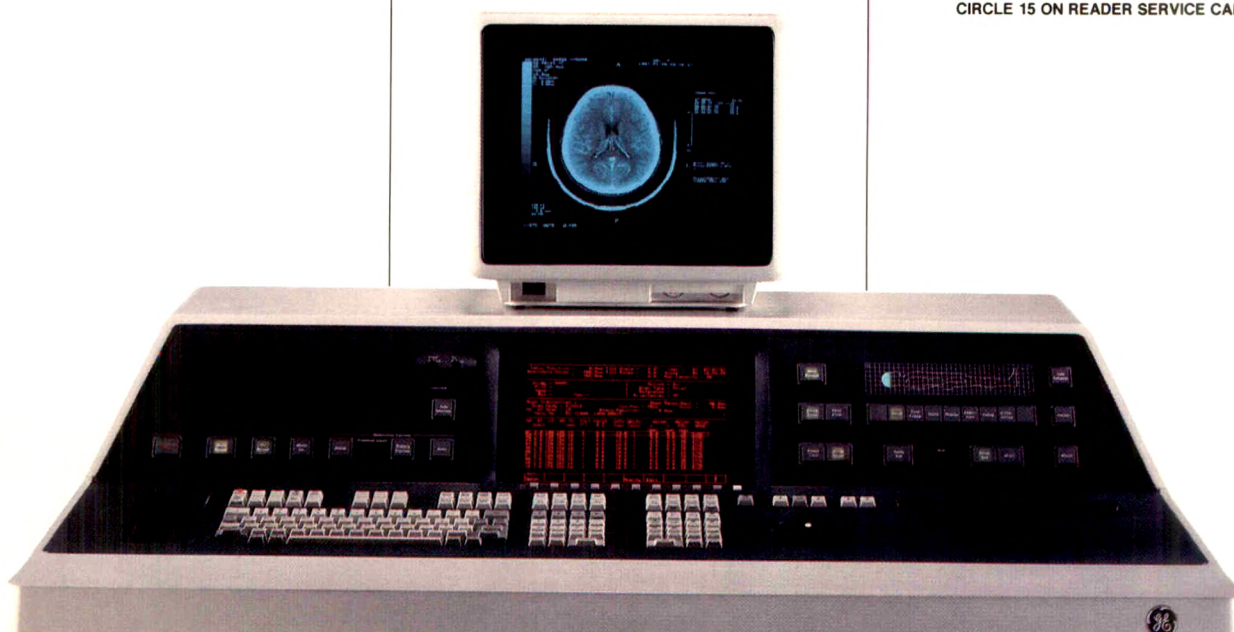


Hydraulic table lowers smoothly to just 38 cm from the floor.

Find out more about the new pacesetter in computed tomography. Call GE Medical Systems.

(800) 624-5692.

CIRCLE 15 ON READER SERVICE CARD



You learn from your experience with

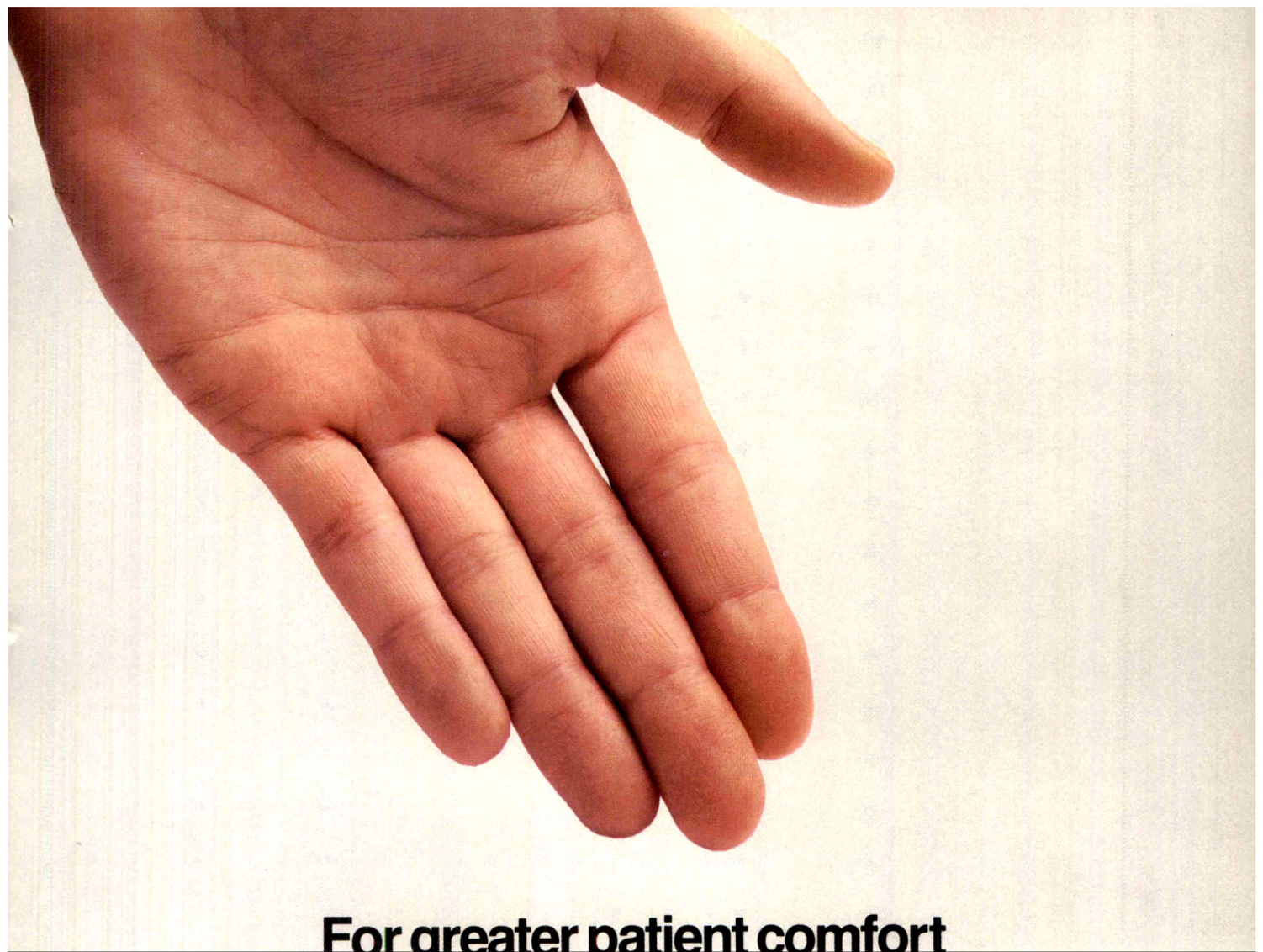
CONTEMPORARY DIAGNOSTIC RADIOLOGY

Editor: Robert E. Campbell, M.D.

A Biweekly Review of Clinical Radiologic Practice—26 issues a year!

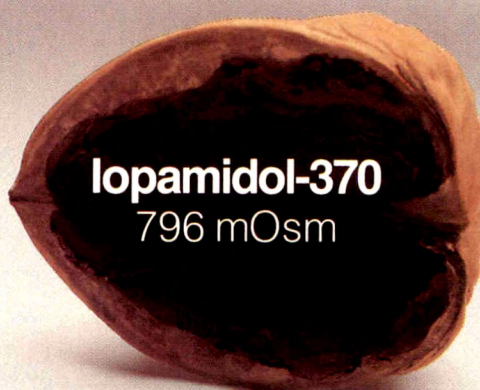
One of your toughest jobs is keeping up with the

Contemporary Diagnostic Radiology works two

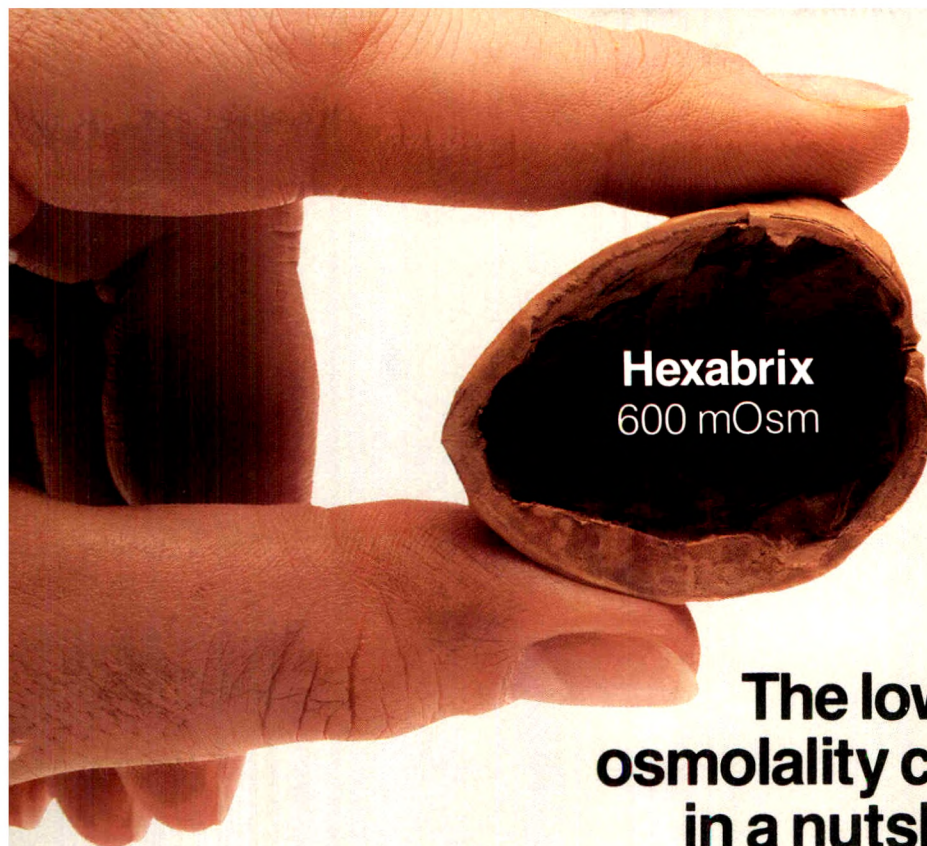


For greater patient comfort





F R O M M A L L



Hexabrix
600 mOsm

The low osmolality choice, in a nutshell

Compare Hexabrix with the nonionics, and you'll find that Hexabrix not only has the lowest osmolality, but also the least amount of patient discomfort in interventional procedures.

Least heat and pain

Recent comparative studies demonstrate that Hexabrix produces significantly less heat¹ and pain¹⁻³ than iopamidol and/or iohexol during arteriography procedures.¹⁻³

Less risk of clotting *in vitro*

Hexabrix has been shown to be a stronger inhibitor of clotting^{4,5} and platelet aggregation^{5,6} *in vitro* than iopamidol or iohexol.

Good angiographic technique should be followed in all procedures involving contrast media. Even when meticulous technique is used, some mixing of blood with contrast media in syringes and catheters is possible. Prolonged contact of blood and contrast media in syringes and catheters can lead to clot formation.

Lowest viscosity

Hexabrix has the lowest viscosity at 37°C (7.5 cps), compared to iohexol-350 (10.4 cps) or iopamidol-370 (9.4 cps).

HEXABRIX[†]

(ioxaglate meglumine 39.3%/
ioxaglate sodium 19.6% injection)

Please see following page for references and brief summary of prescribing information.

I N C K R O D T

HEXABRIX[†] (ioxaglate meglumine 39.3%/ioxaglate sodium 19.6% injection)

HEXABRIX[®] Each milliliter of HEXABRIX contains 393 mg of ioxaglate meglumine, 196 mg of ioxaglate sodium and 0.10 mg edetate calcium disodium as a stabilizer. The solution contains 3.48 mEq (0.15 mEq) sodium in each milliliter and provides 32% (320 mg/mL) organically bound iodine.

CONTRAINDICATIONS

HEXABRIX is contraindicated for use in myelography. Refer to PRECAUTIONS concerning hypersensitivity. Hysterosalpingography should not be performed during the menstrual period, in pregnant patients, in patients with known infection in any portion of the genital tract, or in patients with known cervical ceratoma or curettage has been performed within 30 days. Arthrography should not be performed if infection is present in or near the joint.

WARNINGS

Serious or fatal reactions have been associated with the administration of iodine containing radiopaque media. It is of utmost importance to be completely prepared to treat any contrast medium reaction.

As with any contrast medium, serious neurologic sequelae, including permanent paralysis, can occur following cerebral arteriography, selective spinal arteriography and arteriography of vessels supplying the spinal cord. The injection of a contrast medium should never be made following the administration of vasopressors, since they strongly potentiate neurologic effects.

In patients with subarachnoid hemorrhage, a rare association between contrast administration and clinical deterioration, including convulsions and death, has been reported. Therefore, administration of intravascular iodinated contrast media in these patients should be undertaken with caution.

A definite risk exists in the use of intravascular contrast agents in patients who are known to have multiple myeloma. In such instances anuria has developed, resulting in progressive uremia, renal failure and eventually death. Although neither the contrast agent nor dehydration has separately proved to be the cause of anuria in myeloma, it has been speculated that the combination of both may be a causative factor. The risk in myelomatous patients is not a contraindication to the procedure; however, partial dehydration in the preparation of these patients for the examination is not recommended since this may predispose to precipitation of myeloma protein in the renal tubules. No form of therapy, including dialysis, has been successful in reversing the effect. Myeloma, which occurs most commonly in persons over 40, should be considered before instituting intravascular administration of contrast agents.

Administration of radiopaque materials to patients known or suspected to have pheochromocytoma should be performed with extreme caution. It is the opinion of the physician, the possible benefits of such procedures outweigh the considered risks, the procedures may be performed, however, the amount of radiopaque medium injected should be kept to an absolute minimum. The blood pressure should be assessed throughout the procedure, and measures for treatment of a hypertensive crisis should be available.

Since intravascular administration of contrast media may promote sickling in individuals who are homozygous for sickle cell disease, fluid restriction is not advised.

In patients with advanced renal disease, iodinated contrast media should be used with caution and only when the need for the examination dictates, since excretion of the medium may be impaired. Patients with combined renal and hepatic disease, those with severe hypertension or congestive heart failure and recent renal transplant recipients present an additional risk.

Renal failure has been reported in patients with liver dysfunction who were given an oral cholecystographic agent followed by an intravascular iodinated radiopaque agent and also in patients with occult renal disease, notably diabetes and hypertension. In these classes of patients there should be no fluid restriction and every attempt made to maintain normal hydration prior to contrast medium injection; since dehydration is the single most important factor influencing further renal impairment.

Caution should be exercised in performing contrast medium studies in patients with endotoxemia and/or those with elevated body temperatures.

Reports of thyroid storm occurring following the intravascular use of iodinated radiopaque agents in patients with hyperthyroidism or with an autonomously functioning thyroid nodule, suggest that this additional risk is evaluated before use of this drug. Iodine-containing contrast agents may alter the results of thyroid function tests which depend on iodine estimation, e.g., PBI, and may also affect results of radioactive iodine uptake studies. Such tests, if indicated, should be performed prior to the administration of this preparation.

PRECAUTIONS

Diagnostic procedures which involve the use of iodinated intravascular contrast agents should be carried out under the direction of personnel skilled and experienced in the particular procedure to be performed. All procedures utilizing contrast media carry a definite risk of producing adverse reactions. While most reactions are minor, life-threatening and fatal reactions may occur without warning, and this risk must be weighed against the benefit of the procedure. A fully equipped emergency cart, or equivalent supplies and equipment, and personnel competent in recognizing and treating adverse reactions of all types should always be available. If a serious reaction should occur, immediately discontinue administration. Since severe delayed reactions have been known to occur, emergency facilities and competent personnel should be available for at least 30 to 60 minutes after administration. (See ADVERSE REACTIONS.)

Preparatory dehydration is dangerous and may contribute to acute renal failure in infants, young children, the elderly, patients with pre-existing renal insufficiency, patients with multiple myeloma, patients with advanced vascular disease and diabetic patients.

Acute renal failure has been reported in diabetic patients with diabetic nephropathy and in susceptible non-diabetic patients (often elderly with pre-existing renal disease) following the administration of iodinated contrast agents. Therefore, careful consideration of the potential risks should be given before performing this radiographic procedure in these patients.

Severe reactions to contrast media often resemble allergic responses. This has prompted the use of several provocative pretest methods, none of which can be relied on to predict severe reactions. No conclusive relationship between severe reactions and antigen-antibody reactions or other manifestations of allergy has been established. The possibility of an

idiosyncratic reaction in patients who have previously received contrast medium without ill effect should always be considered. Prior to the injection of any contrast medium, the patient should be questioned to obtain a medical history with emphasis on allergy and hypersensitivity. A positive history of bronchial asthma or allergy (including food), a family history of allergy, or a previous reaction or hypersensitivity to a contrast agent may imply a greater than usual risk. Such a history may be more accurate than pre-testing in predicting the potential for reaction, although not necessarily the severity or type of reaction in the individual case. A positive history of this type does not arbitrarily contraindicate the use of a contrast agent when a diagnostic procedure is thought essential, but does call for caution. (See ADVERSE REACTIONS.)

Prophylactic therapy including corticosteroids and antihistamines should be considered for patients who present with a strong allergic history, a previous reaction to contrast medium, or a positive pre-test since in these patients the incidence of reaction is two to three times that of the general population. Adequate doses of corticosteroids should be started early enough prior to contrast medium injection to be effective and should continue through the time of injection and for 24 hours after injection. Antihistamines should be administered within 30 minutes of the contrast medium injection. Recent reports indicate that such pre-treatment does not prevent serious life-threatening reactions, but may reduce both their incidence and severity. A separate syringe should be used for these injections.

General anesthesia may be indicated in the performance of some procedures; in selected patients, however, a higher incidence of adverse reactions has been reported in these patients, and may be attributable to the inability of the patient to identify untoward symptoms or to the hypotensive effect of anesthesia which can prolong the circulation time and increase the duration of contact of the contrast agent.

Angiography should be avoided whenever possible in patients with homocystinuria because of the risk of inducing thrombosis and embolism.

PRECAUTIONS FOR SPECIFIC PROCEDURES

Pediatric Arthrography. It is advisable to monitor for ECG and vital signs changes throughout the procedure.

When large individual doses are administered, sufficient time should be allowed for any observed changes to return to or near baseline prior to making the next injection.

Caution should be used when making right heart injections in patients with pulmonary hypertension or incipient heart failure; since this may lead to increased right side pressures with subsequent bradycardia and systemic hypotension. Patients with pulmonary disease present additional risks.

Caution is advised in cyanotic infants since apnea, bradycardia, other arrhythmias and a tendency to acidosis are more likely to occur.

Since infants are more likely to respond with convulsions than are adults, the amount of total dosage of contrast medium is particularly important. Repeated injections are hazardous in infants weighing less than 7 kg, particularly when these infants have pre-existing compromised right heart function or obliterated pulmonary vascular beds.

Selective Coronary Arteriography with or without left ventriculography. During the administration of large doses of HEXABRIX, continuous monitoring of vital signs is desirable. Caution is advised in the administration of large volumes to patients with incipient heart failure because of the possibility of aggravating the pre-existing condition. Hypotension should be corrected promptly since it may result in serious arrhythmias.

Special care regarding dosage should be observed in patients with right ventricular failure, pulmonary hypertension, or stenotic pulmonary vascular beds because of hemodynamic changes which may occur after injection into the right heart outflow tract.

Peripheral Arteriography. Moderate decreases in blood pressure occur frequently with intra-arterial (brachial) injections. This change is usually transient and requires no treatment, however, the blood pressure should be monitored for approximately ten minutes following injection.

Extreme caution during injection of the contrast agent is necessary to avoid extravasation and fluoroscopy is recommended. This is especially important in patients with severe arterial disease.

Cerebral Arteriography. Cerebral angiography should be performed with special caution in patients with advanced arteriosclerosis, severe hypertension, cardiac decompensation, recently recent cerebral thrombosis or embolism, and migraine.

Intra-Arterial Digital Subtraction Angiography. The risks associated with IA-DSA are those usually attendant with catheter procedures. Following the procedure, gentle pressure hemostasis is required, followed by observation and immobilization of the limb for several hours to prevent hemorrhage from the site of arterial puncture.

Patient motion, including respiration and swallowing, can result in misregistration leading to image degradation and non-diagnostic studies.

Intravenous Digital Subtraction Angiography. The risks associated with IV-DSA include those usually attendant with catheter procedures and include intramural injections, vessel dissection and tissue extravasation. The potential risk is reduced when small test injections of contrast medium are made under fluoroscopic observation to insure that the catheter tip is properly positioned and, in the case of peripheral placement, that the vein is of adequate size.

Patient motion, including respiration and swallowing, can result in misregistration leading to image degradation and non-diagnostic studies.

Peripheral Venography. Special care is required when venography is performed in patients with suspected thrombosis, phlebitis, severe ischemic disease, local infection or a totally obstructed venous system.

Extreme caution during injection of contrast media is necessary to avoid extravasation and fluoroscopy is recommended. This is especially important in patients with severe arterial or venous disease.

Excretory Urography. Infants and small children should not have any fluid restrictions prior to excretory urography. (See WARNINGS and PRECAUTIONS concerning preparatory dehydration.)

Contrast Enhancement in Body Computed Tomography. Patient cooperation is essential since patient motion, including respiration, can markedly affect image quality. The use of an intravascular contrast medium can obscure tumors in patients undergoing CT evaluation of the liver, resulting in a false negative diagnosis. Dynamic CT scanning is the procedure of choice for malignant tumor enhancement.

Arthrography. Strict aseptic technique is required to prevent the introduction of infection. Fluoroscopic control should be used to insure proper introduction of the needle into the synovial space and prevent extravascular injection. Aspiration of excessive synovial fluid will reduce the pain on injection and prevent the dilution of the contrast agent. It is important that undue pressure not be exerted during the injection.

Hysterosalpingography. Caution should be exercised in patients suspected of having cervical or tubal carcinoma as avoid possible spread of the lesion by the procedure. Delayed onset of pain and fever (1-2 days) may be indicative of pelvic infection.

Carcinogenesis, Mutagenesis, Impairment of Fertility. No long-term animal studies have been performed to evaluate carcinogenic potential. However, animal studies suggest that this drug is not mutagenic and does not affect fertility in males or females.

Pregnancy Category B. Reproduction studies have been performed in rats and rabbits at doses up to two times the maximum adult human dose and have revealed no evidence of impaired fertility or harm to the fetus due to HEXABRIX. There are, however, no adequate and well controlled studies in pregnant women. Because animal reproduction studies are not always predictive of human response, this drug should be used during pregnancy only if clearly needed.

Nursing Mothers. Ioxaglate salts are excreted unchanged in human milk. Because of the potential for adverse effects in nursing infants, bottle feedings should be substituted for breast feedings for 24 hours following the administration of this drug.

Pediatric Use. Safety and effectiveness in children has been established in pediatric angiography and intravenous excretory urography. Data have not been submitted to support the safety and effectiveness of HEXABRIX in any other indication. (Precautions for specific procedures receive comment under that procedure.)

ADVERSE REACTIONS

Adverse reactions to injectable contrast media fall into two categories: Chemotoxic reactions and idiosyncratic reactions.

Chemotoxic reactions result from the physicochemical properties of the contrast media, the dose and the speed of injection. All hemodynamic disturbances and injuries to organs or vessels perfused by the contrast medium are included in this category.

Idiosyncratic reactions include all other reactions. They occur more frequently in patients 20 to 40 years old. Idiosyncratic reactions may or may not be dependent on the dose injected, the speed of injection, the mode of injection and the radiographic procedure. Idiosyncratic reactions are subdivided into minor, intermediate and severe. The minor reactions are self-limited and of short duration; the severe reactions are life-threatening and treatment is urgent and mandatory.

NOTE: Not all of the following adverse reactions have been reported with HEXABRIX. Because HEXABRIX is an iodinated intravascular contrast agent, all of the side effects and toxicity associated with agents of this class are theoretically possible, and this should be borne in mind when HEXABRIX is administered.

Severe, life-threatening anaphylactoid reactions, mostly of cardiovascular origin, have occurred following the administration of HEXABRIX as well as other iodine-containing contrast agents. Most deaths occur during injection or 5 to 10 minutes later; the main feature being cardiac arrest with cardiovascular disease as the main aggravating factor. Isolated reports of hypotensive collapse and shock are found in the literature. Based upon clinical literature, reported deaths from the administration of conventional iodinated contrast agents range from 6.6 per 1 million (0.00066 percent) to 1 in 10,000 patients (0.01 percent).

Regardless of the contrast agent employed, the overall estimated incidence of serious adverse reactions is higher with coronary arteriography than with other procedures. Cardiac decompensation, serious arrhythmias, or myocardial ischemia or infarction may occur during coronary arteriography and left ventriculography.

The most frequent adverse reactions are nausea, vomiting, facial flush and a feeling of body warmth. These are usually of brief duration. In double-blind clinical trials, HEXABRIX produced less discomfort upon injection (pain and heat) when compared to various other contrast agents. Other reactions include the following:

Hypersensitivity reactions. Dermal manifestations of urticaria with or without pruritus, erythema and maculopapular rash. Dry mouth. Swelling. Conjunctival symptoms. Facial, peripheral and angioneurotic edema. Symptoms related to the respiratory system include sneezing, nasal stuffiness, coughing, choking, dyspnea, chest tightness and wheezing, which may be initial manifestations of more severe and infrequent reactions including asthmatic attack, laryngospasm and bronchospasm with or without edema, pulmonary edema, apnea and cyanosis. Rarely, these allergic-type reactions can progress into anaphylaxis with loss of consciousness, coma, severe cardiovascular disturbances, and death.

Cardiovascular reactions. Generalized vasodilation, flushing and venospasm. Occasionally thrombosis or rarely, thrombophlebitis. Extremely rare cases of disseminated intravascular coagulation resulting in death have been reported. Severe cardiovascular responses include rare cases of hypotensive shock, coronary insufficiency, cardiac arrhythmia, fibrillation and arrest. These severe reactions are usually reversible with prompt and appropriate management, however, fatalities have occurred.

Technique reactions: Extravasation with burning pain, hematomas, ecchymosis and tissue necrosis, vascular constriction due to injection rate, thrombosis and thrombophlebitis.

Neurological reactions: Spasm, convulsions, aphasia, syncope, paresis, paralysis resulting from spinal cord injury and pathology associated with the syndrome of transverse myelitis, visual field losses which are usually transient but may be permanent, coma and death.

Other reactions: Headache, trembling, shaking, chills with or without fever, hyperthermia and lightheadedness. Temporary renal shutdown or other nephropathy.

Pediatric angiography has been complicated by intravascular injection with marked adverse effects on cardiac function.

During selective coronary arteriography with or without left ventriculography, patients may have clinically insignificant ECG changes. The following adverse effects have occurred in conjunction with the administration of iodinated intravascular contrast agents for this procedure: hypotension, shock, anginal pain, myocardial infarction, cardiac arrhythmias (bradycardia, ventricular tachycardia, ventricular fibrillation) and cardiac arrest. Fatalities have been reported. Complications to the procedure include dissection of coronary arteries, dislodgement of atheromatous plaques, perforation, hemorrhage and thrombosis.

Following peripheral arteriography, hemorrhage and thrombosis have occurred at the puncture site of the percutaneous injection. Brachial plexus injury has been reported following axillary artery injection.

The major causes of cerebral arteriographic adverse reactions appear to be repeated injections of the contrast material, administration of doses higher than those recommended, the presence of occlusive atherosclerotic vascular disease and the method and technique of injection. Adverse reactions are normally mild and transient. A feeling of warmth in the face and neck is frequently experienced. Infrequently, a more severe burning discomfort is observed. Transient visual hallucinations have been reported. Serious neurological reactions that have been associated with cerebral angiography and not listed under Adverse Reactions include stroke, amnesia and respiratory difficulties. Visual field defects with anopia and reversible neurological deficit lasting from 24 hours to 48 hours have been reported. Confusion, disorientation with hallucinations, and absence of vision sometimes lasting for one week have also been reported. Cardiovascular reactions that may occur with some frequency are bradycardia and either an increase or decrease in systemic blood pressure. The blood pressure change is transient and usually requires no treatment. Arthrography may induce joint pain or discomfort which is usually mild and transient but occasionally may be severe and persist for 24 to 48 hours following the procedure. Effusion requiring aspiration may occur in patients with rheumatoid arthritis. Fever and pain, cramping and tenderness of the abdomen have been reported following hysterosalpingography.

OVERDOSAGE

Overdosages may occur. The adverse effects of overdosage are life-threatening and affect mainly the pulmonary and cardiovascular systems. The symptoms may include cyanosis, bradycardia, acidosis, pulmonary hemorrhage, convulsions, coma and cardiac arrest. Treatment of an overdose is directed toward the support of all vital functions and prompt institution of symptomatic therapy.

Ioxaglate salts are dialyzable.

The intravenous LD₅₀ values of HEXABRIX (in grams of iodine/kilogram body weight) were 11.2 g/kg in mice, >8 g/kg in rats, >6.4 g/kg in rabbits and >10.2 g/kg in dogs.

DOSAGE AND ADMINISTRATION

Details on dosage are provided in the package insert. CONSULT FULL PACKAGE INSERT BEFORE USE.
Rev. Jan 1987

References:

1. Stris MG, Laerum F: Iohexol and ioxaglate in peripheral angiography. *Acta Radiologica* 1987; 28:767-770.
2. Smith DC, Yahnku PY, Maloney MD, et al: Three new low-osmolality contrast agents: A comparative study of patient discomfort. *Am J Neuroradiol* 1988; 9:137-139.
3. Murphy WA, Campbell DR, Fraser DB: Pain in peripheral arteriography: An assessment of conventional versus ionic and non-ionic low-osmolality contrast agents. *J Can Assoc Radiol* 1988; 39:103-106.
4. Engelhart JA, Smith D, Bull BS, et al: Aspirated blood and low-osmolality contrast agents: An embolic hazard? Presented at the 73rd Meeting of the Radiological Society of North America, Chicago, IL, Dec 1, 1987.
5. Mosier LD, Joist JH, Chance D, et al: In vitro effects of ionic and nonionic contrast media on coagulation, platelet function, and fibrinolysis. Presented at the 73rd Meeting of the Radiological Society of North America, Chicago, IL, Nov 30, 1987.
6. Stormorken H, Skape IO, Testart MC: Effect of various contrast media on coagulation, fibrinolysis, and platelet function: An in vitro and in vivo study. *Invest Radiol* 1986; 21:348-354.



Changing the look of medicine.

Diagnostic Products Division

Mallinckrodt, Inc.

Post Office Box 5840

St. Louis, MO 63134

CIRCLE 22 ON READER SERVICE CARD

For orders,

medical and/or

professional assistance

call

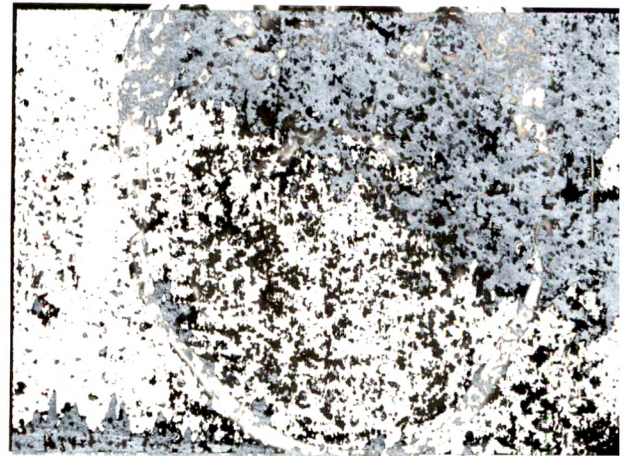
(800) 325-3688 TOLL FREE

CONFIRMED LESION

CONFIRMED LESION /Acoustic neuroma

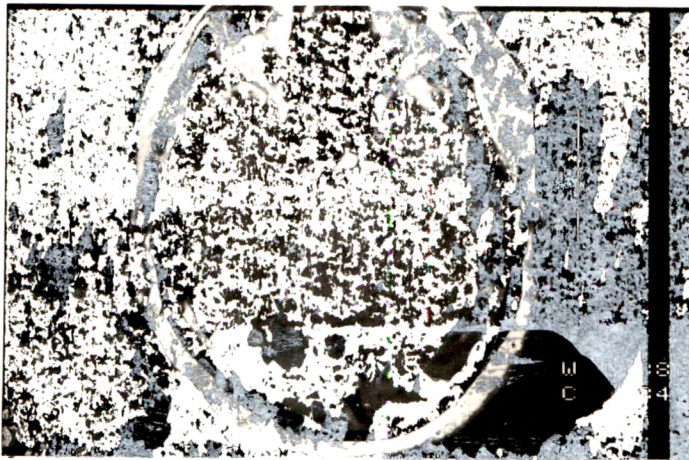


T1-weighted MRI scan pre-MAGNEVIST® injection.
(TR 400, TE 20)



T1-weighted MRI scan post-MAGNEVIST® injection
confirmed intracranial acoustic neuroma.
(TR 400, TE 20)

DEMONSTRATED SECOND TUMOR/Meningioma



T1-weighted MRI scan pre-MAGNEVIST® injection.
(TR 400, TE 20)



T1-weighted MRI scan post-MAGNEVIST® injection
demonstrated second tumor in patient with
acoustic neuroma. (TR 400, TE 20)

Delineates and defines intracranial lesions.

In clinical trials, which included double-blind as well as open-label controlled studies, post-MAGNEVIST® injection T1 scans showed quantitative increase in contrast, differentiating surrounding tissue from mass lesion.¹

Contrast enhancement to facilitate diagnosis.

In the majority of patients, diagnostic ability was facilitated or improved by enhanced contrast with MAGNEVIST® injection.

CONTRAST ENHANCEMENT TO FACILITATE DIAGNOSIS¹

Type of Study	No. of Patients	%
Double-blind	37/57	65
Open-label	70/113	62

© 1989, Berlex Laboratories, Inc. All rights reserved.

Increased number of lesions detected

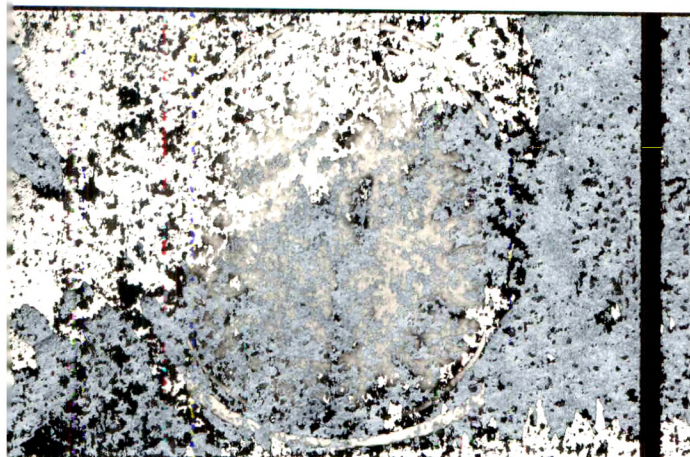
NUMBER OF LESIONS DETECTED¹

Result of Study	Type of Study	MAGNEVIST® injection	
		No. of Patients	%
Increased no of lesions postinjection	Double-blind	10/43*	23
Lesions seen postinjection but not preinjection	Open-label	16/113*	14
	Open-label	66/232	28
	Total	92/388	24

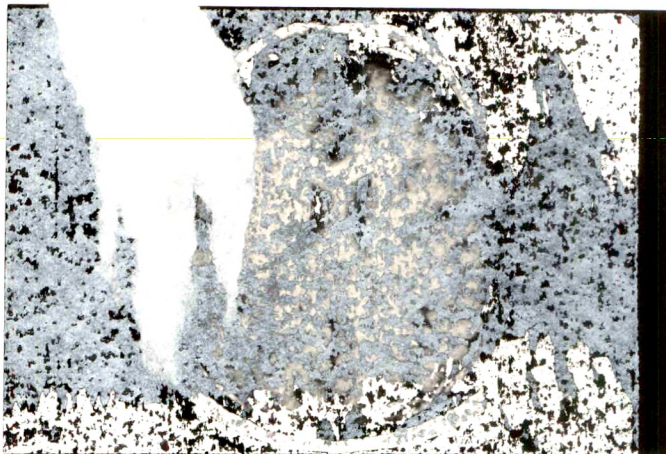
* The question was answered only for patients with contrast enhancement.

T1-WEIGHTED MRI - PRE-POST MAGNEVIST®

DETECTED LESIONS/Metastases

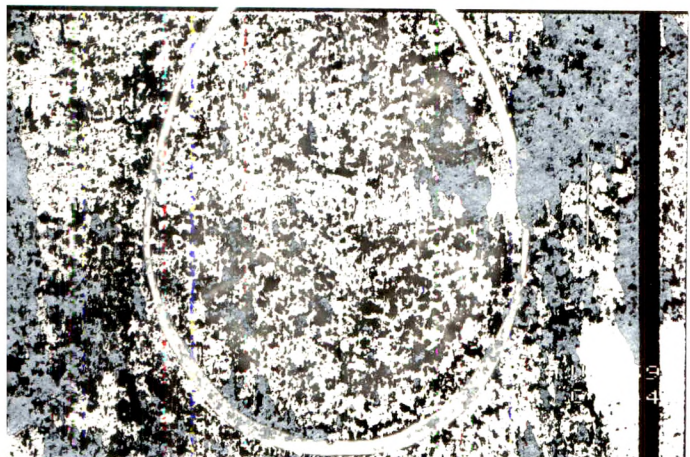


T1-weighted MRI scan pre-MAGNEVIST® injection.
(TR 600, TE 20)

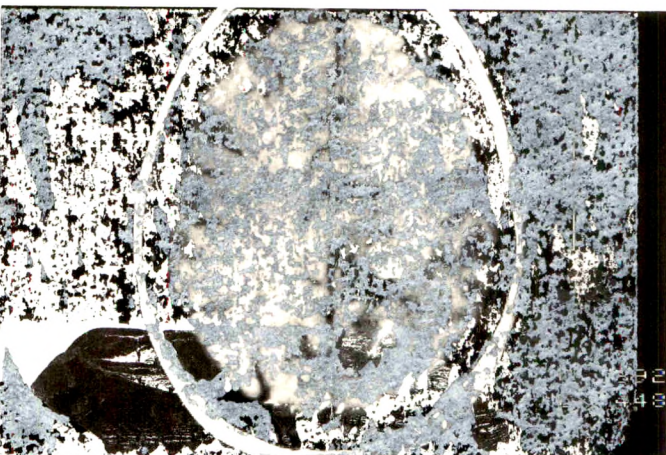


T1-weighted MRI scan post-MAGNEVIST® injection demonstrated lesions not detected preinjection.
(TR 600, TE 20)

CLEAR DELINEATION OF LESION/Glioma



T1-weighted MRI scan pre-MAGNEVIST® injection.
(TR 650, TE 20)



T1-weighted MRI scan post-MAGNEVIST® injection showed improved delineation of lesion.
(TR 650, TE 20)

Safety profile. In clinical trials, MAGNEVIST® injection was well tolerated.¹

INCIDENCE OF ADVERSE REACTIONS AMONG 410 PATIENTS

Type of Reaction	% of Patients With Adverse Reactions Related to MAGNEVIST® Injection	Total Reactions
Headache*	4.9%	9.8%
Nausea	3.4%	4.1%
Vomiting	1.5%	1.7%
Other†	<1.0%	<2.0%

*The majority of headaches were transient in nature.
†In clinical trials, two cases of hypotension were reported.

- In clinical trials, 15% to 30% of patients experienced an asymptomatic transient rise in serum iron.
- The safety of MAGNEVIST® injection in patients with hemolytic disorders has not been studied.

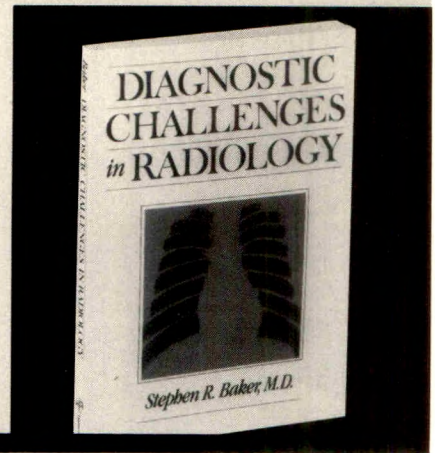
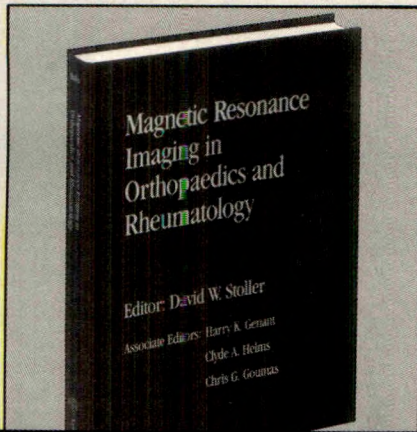
Magnevist®
(gadopentetate dimeglumine) INJECTION

Please see Warnings, Precautions and Adverse Reactions sections in full prescribing information for MAGNEVIST® injection on last page of this advertisement.

¹ Data on file, Berlex Laboratories, Inc.



Hone your professional skills
with these
totally current,
lavishly
illustrated
new books



Magnetic Resonance Imaging in Orthopaedics and Rheumatology

by David W. Stoller, M.D.
Harry K. Genant, M.D.
Clyde A. Helms, M.D.
Chris G. Goumas, M.D.

5 Contributors

MRI has the inherent ability to image soft as well as hard tissues,

ORDER
YOUR
COPIES
TODAY!

Diagnostic Challenges in Radiology

by Stephen R. Baker, M.D.

Even today, with the availability of ultrasonography, MRI, and computed tomography, most radiologic examinations still could be classified as low technology—encompassing long established but relatively simple studies such as plain films, barium studies, and intravenous urography. Long underemphasized, these basic imaging techniques now invite renewed interest in the light of cost containment and patient accountability.

Reliable, intellectually stimulating studies

Why physicians depend on Senographe mammography.

Image quality. It's the reason that more physicians use Senographe® systems than any other kind of mammography equipment.

Designed around the world's most advanced mammography x-ray tube technology, Senographe systems from GE deliver:

- **Unsurpassed image quality for complete diagnostic confidence in these difficult studies.**
- **Superb contrast and detail with the shortest exposure times of any system on the market.**
- **Consistent, accurate compression and excellent reproducibility.**

20 years of refinements

Senographe systems were the first dedicated mammography units. Today we have the largest installed base in the world. This

clinical experience has produced technological refinements that are simply not available on other systems. The Senographe 600T, for example, offers:

- **True 0.1 mm and 0.3 mm focal spots, with the highest mA in the industry—minimizing exposure time and the effects of patient motion.**
- **1.5x and 1.85x magnification for detailed examination of suspicious areas.**
- **AUTOCOMP™ II, an exclusive photo-timing system that reduces examination times and virtually eliminates retakes.**
- **Leading-edge accessories such as Stereotix™, our computerized stereotactic device for fine needle biopsy and localization.**

System-wide quality

All Senographe systems are built to the most exacting specifica-

tions. Our low-cost screening unit, for example, has the same superior image quality as the 600T—the quality you need for early detection of minute lesions.

Senographe systems are exceptionally easy to install—just plug them in—and operate. And they're backed by the in-depth training, service and support that you've come to expect from GE.

For additional information on the fine points of Senographe mammography, contact your GE Representative or call toll free:

(800) 624-5692



CIRCLE 3 ON READER SERVICE CARD



GE Medical Systems

*There's never been
a better time to choose GE*

A conceptual image featuring a globe in the center, showing the Americas. The globe is overlaid with a grid of orange lines. Above the globe, a larger grid of orange lines is visible, with abstract, swirling patterns in shades of blue and white. The background transitions from a dark blue at the top to a lighter blue at the bottom. The text "SAFETY IN NUMBERS." is written in a bold, white, sans-serif font at the bottom.

SAFETY IN NUMBERS.



SAFETY IN NUMBERS.


Every year the numbers grow.
To date, over 500 published
studies and articles with over
75,000 patients document the
safety, tolerance, and comfort
of nonionic OMNIPAQUE.

No other nonionic contrast
medium has been studied
more!¹

And to complete the picture,
nonionic OMNIPAQUE delivers
consistently sharp images to
support your diagnoses.

Safety. Tolerance. Image quality.
Simple words. Reliable facts.

Reference: 1. Data on file. Winthrop Pharmaceuticals.

NONIONIC
OMNIPAQUE[®] 
(IOHEXOL)

THE IMAGE OF SAFETY.

PROCEDURES,* SAFETY IS A FACT.

*Approximation of over 15 million radiographic procedures worldwide is based on quantities of nonionic iohexol sold, used at recommended dosages.

See next page for important product information concerning contraindications, warnings, adverse reactions, patient selection, and prescribing and precautionary recommendations.

Progress in Radiology

Percutaneous Transthoracic Needle Aspiration: A Review

Louis M. Perlmutter,^{1,2} William W. Johnston,³ and N. Reed Dunnick¹

Since the first report in 1883 [1], percutaneous transthoracic needle aspiration (TTNA) has become an efficacious and relatively safe procedure for the diagnosis of a variety of benign and malignant neoplasms, as well as inflammatory processes. Two major factors, advances in imaging technology and improvements in cytopathology, have contributed to this development. High-resolution fluoroscopy with image intensification and television monitoring provides excellent visualization of lesions that were not seen with older technology [2]. With improved visualization, lesions can be approached with a greater margin of safety and accuracy. When CT is used, even smaller lesions may be detected. These lesions can be biopsied under CT guidance, or CT can be used to aid in localization of lesions biopsied under fluoroscopic control.

With improved cytopathologic techniques, diagnoses can be made on smaller amounts of material than are required for histologic examination. This allows the use of small aspirating needles, which are safer than the large-bore cutting needles previously required for histologic preparation of biopsy material.

The procedure of a TTNA involves several steps, beginning with identifying the lesion and ending with patient follow-up. The expected benefit of the information gained from the aspiration must be weighed against the potential complications. The aspiration should be performed in the most safe and efficient manner, with fluoroscopy and chest radiographs obtained after the procedure to detect pneumothorax.

In this review, we will discuss the indications and contraindications for TTNA; the preparation of the patient; and the technical aspects, complications, treatment of complications, and diagnostic efficacy.

Indications

TTNA may be used to diagnose a variety of chest lesions. These include almost any abnormality seen by an imaging technique, including plain chest radiography, CT, and sonography. Not only can lesions of the lung parenchyma be evaluated, but also mediastinal, hilar, pleural, and chest wall diseases can be diagnosed by TTNA. Although most lesions diagnosed by TTNA are neoplastic (either benign or malignant), inflammatory disease can also be elucidated. This includes inflammatory masses as well as parenchymal infiltrates. The specimen from a suspected inflammatory lesion can be either cultured or inspected microscopically with the use of special stains.

Contraindications

In most patients, the diagnostic benefit of the procedure far outweighs the risks of a complication. This is especially true when the alternative approach is thoracotomy. The major contraindication to TTNA is a bleeding diathesis. The aerated lung does not provide sufficient soft tissue to tamponade a bleeding vessel. Patients may experience mild hemoptysis

Received June 10, 1988; accepted after revision October 31, 1988.

¹ Department of Radiology, Box 3808, Duke University Medical Center, Durham, NC 27710. Address reprint requests to N. R. Dunnick.

² Present address: Wake Radiology Diagnostic Imaging, Inc., P. O. Box 19366, Raleigh, NC 27619.

³ Department of Pathology, Box 3712, Duke University Medical Center, Durham, NC 27710.

needle via an extension tubing. Several short excursions are made through the lesion while strong suction is applied by the syringe. If the lesion is visible on lateral fluoroscopy, the depth of the excursions can be controlled by observing the lateral fluoroscopic monitor. Two to three aspirations are made. The patient is then instructed to hold his breath in expiration, and the needle is removed.

The specimen is injected into a container filled with a balanced salt solution and given to the cytotechnologist for an immediate consultation. The cellular material should be within the barrel of the needle and not within the syringe. The contents of the needle are expelled onto a slide or into a small amount of the balanced salt solution. Excellent smears are easily prepared by gently laying one slide over the slide holding the drops of expelled material, permitting the weight of the upper slide to spread the material, pulling the slides apart horizontally, and quickly dropping them into 95% ethyl alcohol.

In our institution, the following procedure is followed: From the aspirate, two direct smears are prepared for immediate wet fixation in 95% ethyl alcohol and staining with the Papanicolaou method. The remaining aspirate is then ejected into a balanced salt solution and brought to the cytopathology laboratory for further procedures. Aliquots of this cellular suspension are processed for membrane filters, direct smears, cytocentrifuge specimens, and cell blocks. For an immediate consultation, the unfixed cellular suspension is stained with a 0.4% aqueous solution of toluidine blue. By this procedure, an immediate assessment of the cellular content of the aspirate can be given and the aspiration repeated if necessary. All of the cellular preparations are screened by cytotechnologists and are then referred to a cytopathologist for final diagnostic interpretation.

If the quick stain results are negative (i.e., acellular, hypocellular, or otherwise equivocal), we repeat the aspiration process and wait for the results of the final stain. Although some researchers have determined that as many as six separate aspirations may be needed for a diagnosis, in general, only two aspirations are required for a diagnosis [9]. The final stain is generally available the next day. Johnsrude et al. [10] found this approach to decrease the rate of pneumothorax by about 50%. However, Miller et al. [11] determined that immediate cytologic assessment did not significantly change complication rates nor did it increase diagnostic accuracy. The role of repeat biopsy is therefore unclear. A negative quick stain does not necessarily mean that the final diagnosis is negative. The incidence of these discordant results is not known.

Hilar and mediastinal lesions can be biopsied fluoroscopically by using the same technique if they can be clearly visualized. The preferred approach, however, for most of these lesions is biopsy under CT control. This allows confirmation of the needle tip within the lesion. Also, the relationship of a mass with other structures can be determined, and large vessels can be avoided [12-14].

Although CT has been used to biopsy lesions that cannot be seen with fluoroscopy, it is awkward and time-consuming. Furthermore, few busy departments can afford time on the CT scanner for these biopsy procedures. The primary role of CT is to aid fluoroscopic localization by defining precisely the location of a lesion and its relationship to adjacent structures. In certain situations, however, the only way to approach a lesion is under CT control. VanSonnenberg et al. [15] recently reviewed a large series of lesions that were not visualized fluoroscopically and had to be aspirated under CT control. They performed aspirations on pulmonary or pleural lesions that were small, near a major vessel, either not seen or poorly visualized on a conventional radiograph, or simply inaccessible.

With increasing economic awareness, hospital administrators will place more pressure on physicians to perform TTNA as an outpatient procedure. The safety, efficacy, and cost-effectiveness of TTNA on 348 outpatients was discussed by Stevens and Jackman [16]. A diagnostic thoracotomy was avoided in 31%, resulting in great eco-

nomic benefits. Although 41% of their patients experienced a pneumothorax, only 10% required chest tubes, which were usually managed on an outpatient basis.

Complications

Although death from pulmonary hemorrhage and air embolism has been reported, it is extremely rare. In an extensive review of the literature, Sinner [17] found reports of only four deaths due to hemorrhage. These cases were performed by using large-bore needles. In a survey involving more than 5000 patients, Herman and Hessel [18] found major hemorrhage only in patients undergoing trephine biopsy with large-bore needles. Major hemorrhage occurred in only about 5% of patients in this group. Woolf [19], who used an 18-gauge needle, found an 8.4% occurrence rate of moderate hemoptysis.

By comparison, smaller needles are safer. When Stanley et al. [20] studied the use of 22- and 23-gauge Chiba needles in 458 lung biopsies, they found only five episodes of hemoptysis, all of which were self-limited and resolved spontaneously. In a smaller series, Chin and Yee [21] encountered no episodes of hemoptysis when the Chiba needle was used.

Air embolism is rare. Sinner [17] reported two suspected cases in a series of almost 2700 cases. Westcott [22] reported one case radiologically documented at autopsy, whereas Tolly et al. [23] recently reported a case documented by CT.

Other complications, including implantation of malignant cells into the needle tract [24], spread of tumor cells, infection of the pleural space (empyema), and bleeding in the chest wall are extremely rare [17].

The most common complication continues to be pneumothorax. The development of pneumothorax after TTNA has been attributed to a number of factors including the size of the needle used, the number of times the visceral pleura is punctured, and the presence of obstructive lung disease [25]. This last factor was recently studied by Fish et al. [4], who found that the risk of pneumothorax increased significantly in patients whose pulmonary function tests indicated obstructive lung disease.

The occurrence rates of pneumothorax after TTNA reported in the literature range from 5% to 57%, with 2% to 17% requiring a chest tube [18, 26-30]. Our own pneumothorax rate is almost 25%, with just under one-half requiring chest tube insertion [31]. Even the exclusive use of the Chiba needle has not decreased the occurrence rates of pneumothorax [20, 21, 31]. Also, experimental work is under way to prevent pneumothorax after TTNA by injection of compressed collagen plugs across the pleural space and lung after the procedure. The results have been promising in animals, and currently, human studies are being done [32].

Patients undergoing TTNA tend to be older, have a higher frequency of smoking and chronic lung disease, and have a more limited respiratory reserve than the general population. Also, in this group of patients, a pneumothorax is least well tolerated. Therefore, detecting pneumothorax in a timely and efficient manner is essential.

outpatients with a true-positive rate of 86% for the diagnosis of malignancy. Poe and Kallay [42] reported similarly good results in their series of outpatient TTNA's.

Conclusions

TTNA has evolved as a useful procedure with a high diagnostic efficacy and a low complication rate. Technical developments have contributed to its efficacy while refinements in cytopathologic techniques have made it safer. Because smaller amounts of tissue are required for a reliable diagnosis, smaller needles may be used. The ability of the radiologist to treat pneumothorax expeditiously not only enhances safety, but also promotes acceptance of the procedure.

18. Herman PG, Hessel SJ. The diagnostic accuracy and complications of closed lung biopsies. *Radiology* **1977**;125:11-14
19. Woolf CR. Applications of aspiration lung biopsy with a review of the literature. *Dis Chest* **1954**;25:286-301
20. Stanley JH, Fish GD, Andriole JG, et al. Lung lesions: Cytologic diagnosis by fine-needle biopsy. *Radiology* **1987**;162:389-391
21. Chin WS, Yee IST. Percutaneous aspiration biopsy of malignant lung lesions using the Chiba needle. An initial experience. *Clin Radiol* **1978**;29:617-619
22. Westcott JL. Air embolism complicating percutaneous needle of the lung. *Chest* **1973**;63:108-110
23. Tolly TL, Feldmeier JE, Czernecki D. Air embolism complicating percutaneous lung biopsy. *AJR* **1988**;150:555-556
24. Müller NL, Bergin CJ, Miller RR, Ostrow DN. Seeding of malignant cells into the needle tract after lung and pleural biopsy. *J Can Assoc Radiol* **1986**;37:192-194
25. Greene RE. Transthoracic needle aspiration biopsy. In: Athanasoulis CA,

Perspective

On Teaching Radiology to Medical Students: Challenges for the Nineties

Lucy Frank Squire¹

About 30 years ago, medical students began to realize how much they needed good instruction in radiology in order to function well as clinicians after graduation. In the intervening three decades, their needs in this regard have also been recognized by many academic radiology chairs, and, to some extent at least, effective teaching programs have been organized for them. However, most of this teaching is offered in elective periods in the third and/or fourth years of medical school. In only a few schools have such programs been incorporated into the curriculum as required instruction. Hence, in many schools, some students graduate each year with little or no formal instruction in radiology, and they must be considered incompletely trained physicians.

Many schools report at least a token effort toward instruction in radiologic anatomy [1-3] in the first year, either in the form of whole-class lectures by members of the radiology staff or displayed radiographs in the anatomy laboratories. In only a few schools, however, is cross-sectional anatomy studied in tandem with CT so that students learn anatomic relationships and morphology existing in the living patient, despite the fact that academic anatomists at their meetings have repeatedly expressed interest in such collaborative teaching (Talbert G, personal communication).

The crux of the problem behind this still deficient pattern of instruction in so vital a discipline as radiology is, of course, the perceived burden of teaching. Emerging in the first half of the century and exploding in its importance to medicine in the third quarter, radiology has a newcomer's position in the formal curriculum in the preparation of young doctors for practice. The staffs of the classic clinical departments of

medicine and surgery have long shouldered their proper burdens in the academic curriculum, and their responsibilities as teachers are taken for granted by deans and curriculum committees throughout the country.

Radiology, once widely considered a technical method adjunctive to diagnosis (as were the various laboratory procedures), has become the keystone to modern diagnosis [4]. The complexity of its constantly changing relationship to the current practice of medicine and surgery demands the participation of radiologists everywhere at conferences. Consultation between surgeons, internists, and radiologists on a daily basis (and as a guide to the more efficient and cost-effective management of patient care) has become almost automatic and is accepted by everyone. This consultation has evolved from necessity because the imaging field has so rapidly outdistanced the imaging knowledge of clinicians. Unless this can be rectified by a more appropriate program of instruction for medical students (the clinicians of the future), radiologists will continue to spend an enormous amount of time in daily consultation and conference, some of which could surely be avoided if they were working with more informed colleagues.

If academic radiology department chairs and their staffs continue to think of teaching as a burden, they will be unlikely to put much energy into the pursuit of an appropriate place in the required curriculum of our medical schools [5, 6]. Therefore, the purpose of this article is to help to acquaint them with some methods we have been using for the past 20 years with a variety of self-instructional, small-group, independent study systems that have proved extraordinarily effective without the expenditure of large blocks of faculty time.

Received August 29, 1988; accepted September 23, 1988.

¹ 1 W. 72nd St., New York, NY 10023. Address reprint requests to L. F. Squire.

TABLE 1: Time Spent by Students With and Without Instructor

Situation: Activity	No. of Hours
Instructor present:	
Lectures	16
Rotating exhibits (second and third hours)	14
Procedures	15
Other	5
Total	50
Instructor not present:	
Audiovisual seminars	23
Film packets	18
Rotating exhibits (first hour)	7
Other solo activities	12
Total	60

provide well-chosen new material that is interesting and provocative without the use of rare cases not relevant to the basic block of data that the student will need to command at graduation. It is a temptation for all of us to use what we call "great cases" (generally so-called because they relieve the monotony of daily routine for the instructor). Such cases probably will confuse students and depress their desire to learn. Students are best served by our use of imaging material that is basic and illustrates in a classic way disease conditions that someone in the student group will have seen during their third-year clinical experience. If imaging cases are arranged for them with this in mind, the correlation of clinical data with imaging becomes logical to students and functions as a mnemonic aid to learning. It also affords a superb review of medicine, because radiology intersects virtually all medical problems today.

The Use of Cluster Learning

Our programming of imaging material depends largely on what we term *cluster learning*, in that a cluster of similar cases is presented for viewing together, the students being asked to find the similarities or contrasts between the cases. For example, students would be shown four or five films of patients with lobar pneumonia with consolidation of various parts of the lung, and they would be asked to identify the involved lobe or segment in each and to predict the history and physical findings. Conversely, students might be shown examples of air-space disease to contrast with examples of interstitial disease, all viewed simultaneously, a short clinical description being given for each "patient." The group is asked to make certain decisions and is then supplied with answers and discussion, either on audiotape or in printed material that they read aloud. In this way, students can learn a great deal about radiology and its relation to clinical medicine by themselves and without an instructor. Cluster learning provides students with a large volume of material viewed, building their confidence in their ability to make basic decisions.

This technique also can be used to stress the importance of their supplying the radiologist with clinical data when they are requesting imaging studies. One way in which we do this is to give the student group material showing bilateral dissem-

ination of interstitial pulmonary disease, four or five films that are so similar that they cannot be differentiated radiologically. We withhold the clinical data while the student group attempts to arrive at a diagnosis from the films alone. The answer booklet then supplies the clinical data and the ultimate resolution of the diagnosis. From this exercise, the students learn that the interpretation of radiographs often cannot be definite without clinical correlation, and this exercise teaches them better than any pronouncement by a lecturer how vital the clinical data are to the interpretation of the films.

The Organization of the Fourth-Year Course

Each month our students are given a schedule on the first day that identifies for each hour in the month precisely what activity is assigned. One-half of the time students work without any instructor. All work is done in small groups (two to six students working together from the prepared material). Thirty students per month is our usual quota, and we divide them into six groups of five. Each group soon develops a harmonious relationship among its members, and they are reluctant to be rearranged, although on occasion we do reassign them for some activities so that they can interact with different members of the larger group. In general, we find that a positive gain results if students work with a group that they are accustomed to and know. String quartets get better the longer they play together.

A variety of small-group formats have been invented to afford change in activity, hour-for-hour through the day. This enhances stimulation and lessens fatigue. During the month, each of the six groups works its way through 23 hr of slide/tape seminars [7] and 18 hr of programmed material consisting of packets of films with question-and-answer booklets for guidance and instruction. For example, two of the six groups (A + B) will work through an audiovisual (slide/tape) program in two small sound-proofed rooms from 8 to 9 a.m. Then for the next hour the two groups move to the large classroom, where each group studies and discusses programmed sets of film copies at two banks of light boxes on opposite walls of the room, working independently and not disturbing each other's group discussion.

At 9 a.m., another two groups of students (C + D) occupy the two small theaters and perform the required tasks built into the same slide/tape seminar the first two groups have just completed. At the end of the second hour, the four groups change places, the A and B groups performing the next slide/tape seminar while the C and D groups work through programmed film sets in the classroom. The alternating activities of the four groups complete the morning in the teaching suite without the participation of an instructor but regulated by a full-time secretary. We believe that it is important to change the format by which the groups learn every hour; sustained activity of one kind for 2 or 3 hr is not as effective.

Meanwhile, on the same morning, the students in the E + F groups have been assigned (in pairs) to the various procedure areas in the two hospitals of the medical center. In general, morning procedure rotations are to gastrointestinal imaging, angiography, CT, sonography, emergency radiology, and the film-reading desks, where, of course, the students

books are kept on open shelves for use during work, and, although they may not be removed from the teaching suite, these are used constantly by the students at work there.

At registration the first day, each student receives a packet that contains the schedules with assignments to programmed independent study for each day as well as to the procedure rotations in the hospital. The packet also contains handouts consisting of notes prepared by each lecturer related to the subject material covered in that lecture, so that students need not try to take notes in a partially darkened room. Students seldom find it necessary to take notes during the independent study small-group sessions.

Algorithm Workups

During the final week of the month, we schedule several round-table sessions for the entire group of 30 students and an instructor to derive algorithms for optimal patient workups in a variety of disease conditions. These sessions are carried out in relation to groups of problem cases assigned to all students in advance, and they prepare workup plans before class. Any student may be called on to discuss the workup of any "patient," and, after the student presentation of each, the discussion becomes general and the instructor answers questions as needed but refrains from lecturing. As much as possible, the instructor develops the algorithm from student suggestions. We find that by the final week our students are quite ready for this type of learning format. Naturally the group can develop much better workup algorithms than those any single student can produce. The instructor guides them without lecturing, and students say this learning format is extremely valuable to them.

Evaluation of the Student's Accomplishment

At the end of the month, students take an examination lasting 2 hr. Fifty questions constitute a practical examination in which true-false statements are related to 50 slides (none of which the students have seen before). For these, the student needs to be able to recognize the presence or absence of a particular imaging finding or to relate it to the statement of a clinical situation. This exercise is followed by a written examination composed of an additional 50 multiple-choice questions on theory taken from reading material, handouts, and lectures. The two examinations are scored by the teaching secretary and the course director in a period of about 1½ hr. Examinations come from a carefully validated pool of 300 questions that are continuously supplemented with new questions [9, 10]. The examination is changed each month, although some questions may be reused. Evaluations for the dean's office are written by the course director from such criteria as the examination scores, procedure rotation write-ups, and in-class subjective notes supplied by staff after rotating exhibits.

Conclusions

In one type of radiology elective still widely offered in this country, a single student essentially sits at the elbow of the

radiologist watching him get his work done. Such a student would be fortunate indeed to be able to have explained to him the clinical correlation of imaging findings in 20 patients during a single day's observation. In contrast, our students get through a total of 2500 proved film cases, not counting those contained in the assigned reading material. Moreover, these students have spent one-half of their time actively participating in a small-group approach to materials programmed for them, but complete the material at their own pace and without the interference of an instructor.

We believe that this system results in much more indelible learning and that it is flexible enough to fit different personalities and learning preferences among the students. Most of the students soon appreciate the advantages of group endeavor, in which a rich pool of background reading and clinical experience can be drawn on during the discussion, because each student contributes data no other student possesses. Only a few students are aware at the beginning of the month how much they stand to learn about consultation techniques from this type of group endeavor with their peers. We believe that more small-group learning should be the educational pattern of the future, replacing to a major extent the classic techniques of learning from lectures and books and passive observation.

At the moment we use no small-group computer-assisted instruction in radiology [11, 12], but with the new video techniques available we see an important place for such instruction in the future. Whereas computer-assisted learning in the past has largely involved one student to one machine, we confidently expect that computer-assisted small-group participation will be an exciting new mode of learning radiology as we enter the 21st century. The development of these techniques will certainly depend on the evolution of a reward system for teaching and the time spent in the preparation of such learning materials.

REFERENCES

1. Bassett LW, Squire LF. Anatomy instruction by radiologists. *Invest Radiol* 1985;20(9):1008-1010
2. Bennett R. The value of radiology in teaching anatomy to medical students. *Australas Radiol* 1968;12:64-68
3. Forrester D. Teaching anatomy through radiology. *Radiology* 1971;100:561-565
4. Morgan RH. The emergence of radiology as a major influence in American Medicine. *AJR* 1971;111:449-462
5. Lalli AF. Radiology: a medical school requirement. *Radiology* 1973;108:217-218
6. Squire LF, Novelline RA. Radiology should be a required part of the medical school curriculum. *Radiology* 1985;156:243-244
7. Squire LF, Blotnick V, Becker JA. Self-instruction in radiology for medical students. *Radiology* 1972;105:681-684
8. Squire LF, Twersky N, Pais JM, et al. More effective devices for teaching undergraduate radiology. *Radiology* 1975;117:63-65
9. Johnson TH. Medical school radiology teaching and examination methods. *Radiology* 1969;93:443-446
10. Novelline RA, Squire LF, Whitley JE. Written and practical testing of medical students in radiology. *Radiology* 1982;143:795-797
11. Renfrew D, Elkhowsy G, Jacoby C. Computer-assisted instruction in radiology. *Radiology* 1982;143:574
12. Jacoby CG, Smith WL, Albanese MA. An evaluation of computer-assisted instruction in radiology. *AJR* 1984;143:675-677

The reader's attention is directed to the commentary on this article, which appears on the following pages.

rangement obviously involves using well-conceived self-instructional materials, such as those designed by Dr. Squire. Dedicated space to permit small-group learning and adequate secretarial support are the first prerequisites needed if medical-student education in radiology is to reach the high caliber achieved by Dr. Squire. Programmed materials are available commercially or can be created to suit the needs of the medical student. The traditional methods of teaching students that we mentioned earlier should be discouraged or relegated to a secondary role.

Finally, faculty commitment to medical-student education, especially in the form of the director, is a must. Medical-student training in radiology is Dr. Squire's full-time commitment during the teaching months at her institution. Fortunately, her chairman realizes the importance of allocating

faculty time to student education and has been completely supportive of her efforts. Often in academic radiology, the director of medical-student education is a junior faculty member who may be too overwhelmed with patient-care responsibilities, resident teaching, and research obligations to devote more than a minimal effort to organizing and running a medical-student rotation. Even more discouraging is the usual lack of incentive to consider medical-student education as a possible academic subspecialty in radiology. Department chairpersons should encourage faculty interested in training medical students and allow them enough time for this activity. Only if all of these requirements are met satisfactorily can the concept of small-group learning in radiology be implemented for a large number of students.



Scientific Program (200 papers)

Instructional Courses (60 hours)

Categorical Course on
Genitourinary Radiology

The Caldwell Lecture

Award Papers

Scientific Exhibits

Social, Golf, and Tennis Programs

Guest Programs



Come to the
American Roentgen Ray Society
89th
ANNUAL MEETING



New Orleans Hilton
May 7-12, 1989

Cine-Gradient-Refocused MR Imaging of Central Pulmonary Emboli

Robert H. Posteraro¹
H. Dirk Sostman¹
Charles E. Spritzer¹
Robert J. Herfkens^{1,2}

We studied the use of MR imaging with a limited-flip-angle, gradient-refocused pulse sequence to show central pulmonary emboli in 11 patients and to distinguish acute from chronic emboli. The central pulmonary vasculature was imaged by using a cine-limited-flip-angle (cine-MR) pulse sequence with 63/13 (TR/TE) and a 30° flip angle (θ), as well as standard spin-echo sequences. Patients were selected on the basis of suspicion of central pulmonary embolism and correlative studies done within 24 hr of the MR examination. Correlations with other studies were based on the original MR report and blinded review of the MR images by two observers in consensus. Emboli were shown in all cases by cine-MR, and they corresponded to the locations of angiographic abnormalities and mismatched perfusion defects on scintigraphy. In three patients considered to have acute pulmonary embolus on the basis of angiography, the cine-MR studies were consistent with acute pulmonary embolus in two patients and chronic pulmonary embolus in one patient (however, in that patient pathologic examination showed chronic embolism). In one case in which angiography led to the diagnosis of acute and chronic pulmonary embolism, the cine-MR study showed acute embolism. In three patients thought to have chronic pulmonary embolus on the basis of angiography, the cine-MR study was interpreted as representing acute embolus in one patient and chronic embolus in two patients.

In this highly selected, small group of patients, cine-MR imaging was accurate in showing central pulmonary embolism.

Spin-echo MR imaging at low and medium field strengths has been used as a noninvasive method for showing pulmonary emboli [1-5]. Shortcomings of this technique include spurious results due to flow artifacts [4-6], spatial resolution inferior to angiography, degradation of image quality by physiologic motion, poor differentiation between thrombus and airless lung [5], and confounding signal from endobronchial mucous plugs [7]. Spin-echo MR imaging also is unable to distinguish between chronic and acute pulmonary emboli [8]; such a distinction is desirable because it could affect therapeutic decisions.

We compared cine-MR with spin-echo MR imaging for showing central pulmonary emboli in 11 patients and evaluated the ability of each technique to distinguish between acute and chronic emboli.

Subjects and Methods

Eleven patients (six men and five women) were studied from July 1986 to July 1988. Acute pulmonary embolism was diagnosed clinically in seven patients, and chronic pulmonary embolism was diagnosed in four patients. Patients were selected for MR imaging on the basis of either a ventilation/perfusion (V/Q) scan with at least one larger-than-segmental perfusion defect or a pulmonary arteriogram. We included only those MR scans that had been obtained within 24 hr of the pulmonary arteriogram, the V/Q scan, or surgery. Five patients underwent radionuclide V/Q imaging, pulmonary arteriography, and MR imaging; four had V/Q scintigraphy and MR imaging; two had pulmonary arteriography and MR imaging. Two patients subsequently underwent pulmonary embolectomy.

Received August 30, 1988; accepted after revision November 11, 1988.

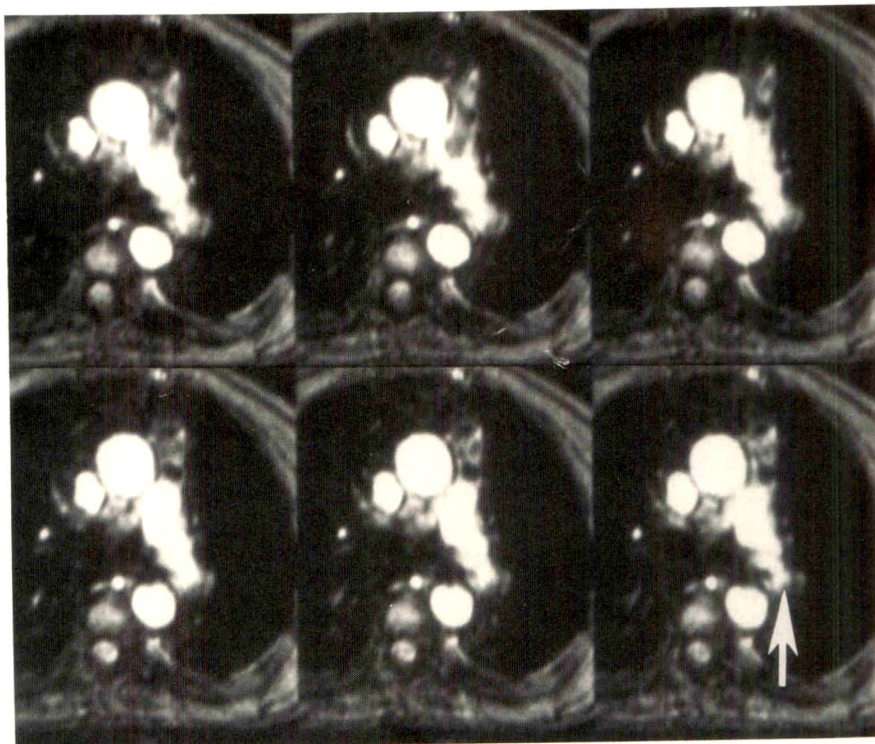
This work was supported by Public Health Service grants NCI-RO1-CA43916, NHLBI-RO1-36806, and NHLBI-RO1-39601.

¹ Department of Radiology, Box 3808, Duke University Medical Center, Durham, NC 27710. Address reprint requests to H. D. Sostman.

² Present address: Cedars-Sinai Medical Center, Los Angeles, CA 90048.

AJR 152:465-468, March 1989
0361-803X/89/1523-0465
© American Roentgen Ray Society

Fig. 3.—Six frames from a cine-MR study show narrowing and eccentric thickening of left pulmonary artery (arrow, lower right frame) consistent with chronic embolism. These findings were confirmed with pulmonary arteriography.



consensus of opinion was used in that analysis. The reference standard for presence and location of pulmonary emboli was arteriography, if this was performed, or a mismatched defect on V/Q imaging if no arteriogram was done. The reference standard for acute vs chronic embolus was pathology (if embolectomy was done) or arteriography (if embolectomy was not done).

Results

The results are shown in Table 1. Nine patients had V/Q images and seven had pulmonary arteriograms. In all patients who had V/Q scintigraphy, the images were interpreted as showing a high probability for pulmonary embolism. Five of these patients also had pulmonary arteriograms; all were positive for acute and/or chronic pulmonary emboli. Both patients who did not undergo scintigraphy had pulmonary arteriograms, which were consistent with chronic pulmonary embolism.

All of the cine-MR studies were interpreted as showing acute or chronic emboli in locations that corresponded to arteriographic or scintigraphic abnormalities. However, no emboli were identified distal to lobar branches by cine-MR. Five of the nine spin-echo MR examinations were interpreted as positive for embolism, and four were considered equivocal.

Discussion

TABLE 1: Imaging Results in 11 Patients with Pulmonary Emboli

V/Q Scintigraphy	Pulmonary Arteriogram	Cine-MR	Spin-Echo MR
HP	Acute ^a	Chronic	Embolus
HP	Acute	Acute	Equivocal
HP	Acute	Acute	Equivocal
HP	Not done	Acute	Embolus
HP	Not done	Acute	Embolus
HP	Not done	Acute	Not done
HP	Not done	Acute	Embolus
HP	Acute + chronic	Acute	Equivocal
Not done	Chronic	Acute	Embolus
HP	Chronic	Chronic	Not done
Not done	Chronic	Chronic	Equivocal

Note.—V/Q = ventilation/perfusion; HP = high probability of pulmonary embolus; Acute = acute pulmonary embolus; Chronic = chronic pulmonary embolus; Embolus = pulmonary embolus (no differentiation of acute from chronic was possible on spin-echo MR).

^a This patient underwent pulmonary embolectomy, and histologic examination showed chronic, not acute, pulmonary embolism.

establish or exclude the diagnosis of pulmonary embolism. Currently, this can only be accomplished with pulmonary arteriography, an unpleasant and not entirely safe procedure. In addition, noninvasive imaging studies currently are not able to distinguish acute from chronic embolism.

Several studies of spin-echo MR imaging of pulmonary embolism have been reported [1, 5]. Problems encountered in

Cardiac Masses: Assessment by MR Imaging

Jeffrey T. Lund¹
 Richard L. Ehman¹
 Paul R. Julsrud¹
 Lawrence J. Sinak²
 Abdul J. Tajik²

The purpose of this study was to assess the role of MR imaging for evaluating suspected cardiac tumors or paracardiac masses involving the heart. Sixty-one patients with clinical or radiologic evidence of cardiac masses were imaged with ECG-gated MR at 1.5 T (22 patients) or 0.15 T (39 patients). Fifty-one patients had echocardiography previously. Among the tissue diagnoses were myxoma (six); fibroma, rhabdomyoma, plasma cell granuloma, lipomatous hypertrophy of the atrial septum, mesothelioma, and thymoma (two each); and leiomyosarcoma, lymphoma, metastatic carcinoid, melanoma, malignant fibrous histiocytoma, hemangiopericytoma, and lung spindle cell sarcoma (one each). MR imaging demonstrated masses in 50 patients (82%); they were centered in the heart in 32, pericardial in nine, and juxtacardiac in nine. MR imaging provided diagnostic information that affected clinical management or surgical planning in 53 patients (87%), including 11 (18%) in whom cardiac mass was excluded by MR.

The ability to provide a global view of cardiac anatomy and other unique capabilities of MR imaging give the procedure an important role in the diagnosis and preoperative assessment of cardiac masses.

At present, echocardiography is the most important noninvasive technique for imaging the heart [1-7]. Generally, it is the initial imaging procedure used. Nevertheless, certain of the inherent advantages of MR imaging suggest that the technique has an important role in cardiac imaging [2, 8, 9]. These include the ability to provide high contrast between flowing blood and soft tissue and to allow imaging of the heart in any plane [2, 7-9].

The objective of this study was to assess the role of MR imaging for evaluation of patients with cardiac tumors and to determine how MR imaging can contribute to their management.

Materials and Methods

Between September 1983 and May 1987, 61 patients with suspected cardiac masses seen at the Mayo Clinic were examined with MR imaging. The 32 male and 29 female patients were 3 months to 82 years old (mean, 51 years). In some cases, patients had MR because a cardiac tumor was suspected on the basis of the history and physical examination, but in the great majority, MR was performed to confirm and evaluate masses initially recognized by CT or two-dimensional echocardiography. Two-dimensional echocardiography was performed in 51 patients; CT was performed in 25. In three patients, two with myxomas and one with metastatic melanoma, the lesion was detected during coronary angiography and ventriculography. Forty-three patients had chest radiographs, of which 14 showed a cardiac mass or mass adjacent to the heart. In many patients, two or more imaging procedures had been performed before referral for MR imaging.

Cardiac MR imaging was performed in the 61 patients with the spin-echo technique and cardiac gating. Twenty-two patients were imaged on a 1.5-T Signa machine (General Electric, Milwaukee, WI) with a TE of 20-25 msec, a TR that was ECG-gated to every beat, a section thickness of 0.5-1.0 cm, 256 views, two signal averages, a field of view of 32-48 cm, and the spatial presaturation technique [10]. Thirty-nine patients were imaged on a 0.15-T Picker

Received August 15, 1988; accepted after revision October 12, 1988.

Presented at the annual meeting of the American Roentgen Ray Society, San Francisco, May 1988.

¹ Department of Diagnostic Radiology, Mayo Clinic and Foundation, Rochester, MN 55905. Address reprint requests to R. L. Ehman.

² Division of Cardiology and Internal Medicine, Mayo Clinic and Foundation, Rochester, MN 55905.

AJR 152:469-473, March 1989

0361-803X/89/1523-469

© American Roentgen Ray Society

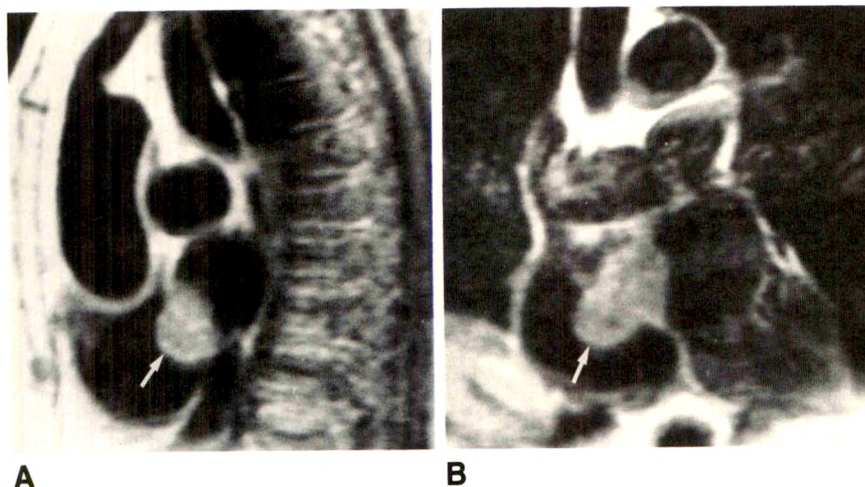


Fig. 4.—A and B, Typical atrial myxoma (TE = 25 msec). Sagittal (A) and coronal (B) views show bilobed atrial myxoma (arrows) centered in interatrial septum and extending into both atria.



Fig. 5.—Benign cardiac mass. MR image (TE = 24 msec) of primary cardiac fibroma involving left ventricular free wall (arrow).

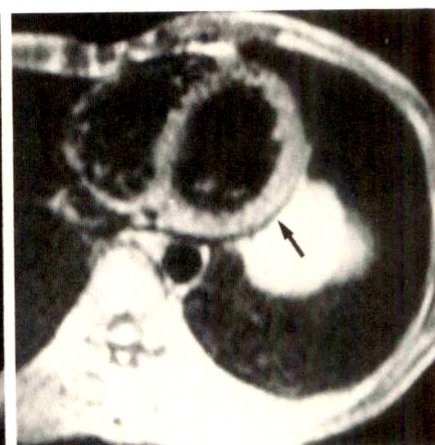
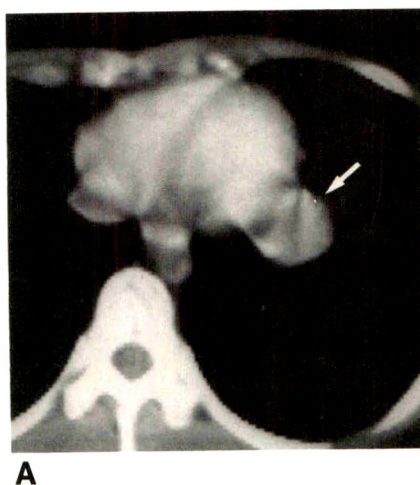


Fig. 6.—MR demonstration of no pericardial involvement by this lung mass altered the surgical approach.

A, CT image shows 4-cm mass adjacent to left ventricle (arrow). There is a suggestion of pericardial involvement by mass, but artifact makes accurate assessment difficult.

B, Axial MR image (TE = 25 msec) at level similar to CT scan clearly shows normal, thin, low-intensity pericardial line (arrow).

niques correctly evaluated pericardial involvement by scar tissue caused by radiation therapy, but only MR showed no pericardial involvement in four other patients. The pericardium in one patient with partial absence of the pericardium due to prior surgical resection of adherent plasma cell granuloma was correctly evaluated by MR but was not imaged by either echocardiography or CT.

Information provided by MR imaging contributed to a decision against surgery in 26 patients. Eleven of these patients had negative examinations and eight had a benign process, such as occurred in the two patients with lipomatous hypertrophy of the atrial septum. The role of MR imaging was easiest to document in the seven patients who were shown to have unresectable tumors. MR clearly showed unresectability due to the extent of myocardial involvement in a patient with pericardial mesothelioma metastatic to the liver (Fig. 2).

MR provided guidance for planning surgery in 25 patients. In two patients, a thoracotomy rather than a median sternotomy was performed on the basis of information obtained from the MR examination. One of these patients was found

to have a left lung mass on a chest film. Echocardiography suggested that the mass was cystic. CT examination suggested pericardial involvement (Fig. 6A). On MR, the mass had internal inhomogeneity, which is characteristic of soft tissue but not of fat or fluid. There was no transpericardial involvement (Fig. 6B). On the basis of these findings, a thoracotomy rather than a median sternotomy was performed. Surgery revealed a primary lung spindle cell sarcoma with no pericardial involvement.

Discussion

In ECG-gated MR imaging, the TR interval cannot be chosen freely but is determined by the RR interval of the patient's ECG. The typical TR and TE values on spin-echo ECG-gated MR imaging fall into the category of partial-saturation spin-echo sequences. Such sequences tend not to differentiate between various nonfatty soft tissues. Nevertheless, the combination of intensity characteristics, morphologic information, and clinical data allowed a correct diagnosis to be made in several cases. Qualitative tissue characterization was possi-

low spin density of the fibrous component of the pericardium [8, 23].

The low spin-echo intensity of the pericardium is explained partly by the presence of a phase discontinuity artifact [13, 24–26]. The shearing action between the visceral and parietal pericardium results in a large local velocity gradient causing a reduction in signal intensity from the volume elements spanning the pericardium. Focal absence of the low-intensity pericardial line implies that no shearing motion is present across the pericardium at that point. Such lack of shearing motion can be caused by transpericardial tumor invasion or inflammatory adhesions. This sign assisted reliable MR imaging diagnosis of pericardial involvement in some cases of hepatocellular carcinoma (Fig. 7), mediastinal fibrosarcoma (Fig. 8), and recurrent osteogenic sarcoma of the sternum (Fig. 9), which were confirmed at surgery.

It appears that, while echocardiography will continue to be the primary imaging technique for detecting cardiac masses, MR imaging can play a significant complementary role. The most compelling indication for MR imaging is preoperative assessment of patients with known cardiac masses. In our series, it helped to determine whether to operate and aided surgical planning.

REFERENCES

1. Fyke FE, Seward JB, Edwards WD, et al. Primary cardiac tumors: experience with 30 consecutive patients since the introduction of two dimensional echocardiography. *J Am Coll Cardiol* 1985;5:1465–1473
2. Council on Scientific Affairs. Report of the Magnetic Resonance Imaging Panel. Magnetic resonance imaging of the cardiovascular system. *JAMA* 1988;259:253–259
3. Go RT, O'Donnell JK, Underwood DA, et al. Comparison of gated cardiac MRI and 2D echocardiography of intracardiac neoplasms. *AJR* 1988;151:1005–1008
4. Higgins CB. Overview of MR of the heart—1986. *AJR* 1986;146:907–918
5. Boxer RA, LaCorte MA, Singh S, et al. Diagnosis of cardiac tumors in infants by magnetic resonance imaging. *Am J Cardiol* 1985;56:831–832
6. Feinlee JP, Ehman RL. Spatial presaturation: a method for suppressing flow artifacts and improving depiction of vascular anatomy in MR imaging. *Radiology* 1987;164:559–564
7. Levine RA, Weyman AE, Dinsmore RE, et al. Noninvasive tissue characterization: diagnosis of lipomatous hypertrophy of the atrial septum by nuclear magnetic resonance imaging. *J Am Coll Cardiol* 1986;7:688–692
8. Amparo EG, Higgins CB, Farmer D, Gamsu G, McNamara M. Gated MRI of cardiac and paracardiac masses: initial experience. *AJR* 1984;143:1151–1156
9. Zeitler E, Kaiser W, Schuierer G, et al. Magnetic resonance imaging of aneurysms and thrombi. *Cardiovasc Intervent Radiol* 1986;8:321–328
10. Choyke PL, Kressel HY, Reichek N, et al. Nongated cardiac magnetic resonance imaging: preliminary experience at 0.12 T. *AJR* 1984;143:1143–1150
11. Herfkens RJ, Higgins CB, Hricak H, et al. Nuclear magnetic resonance imaging of the cardiovascular system: normal and pathologic findings. *Radiology* 1983;147:749–759
12. Conces DJ, Vix VA, Klatte EC. Gated MR imaging of left atrial myxomas. *Radiology* 1985;156:445–447
13. Stark DD, Higgins CB, Lanzer P, et al. Magnetic resonance imaging of the pericardium: normal and pathologic findings. *Radiology* 1984;150:469–474
14. Sechtem U, Tscholakoff D, Higgins CB. MRI of the abnormal pericardium. *AJR* 1986;147:245–252
15. Conti VR, Saydjari R, Amparo EG. Paraganglioma of the heart, the value of magnetic resonance imaging in the preoperative evaluation. *Chest* 1986;90:604–606
16. Winkler M, Higgins CB. Suspected intracardiac masses: evaluation with MR imaging. *Radiology* 1987;165:117–122
17. Come PC, Riley MF, Markis JE, Malagold M. Limitations of echocardiographic techniques in evaluation of left atrial masses. *Am J Cardiol* 1981;48:947–953
18. Seward JB, Khandheria BK, Oh JK, et al. Transesophageal echocardiography: technique, anatomic correlations, implementation, and clinical application of the heart: a review of the experience in 172 subjects. *Radiology* 1985;155:671–679

**1988 ARRS
Executive Council
Award**

**Detection of Pneumothorax:
Comparison of Digital and Conventional
Chest Imaging**

Laurie L. Fajardo¹
Bruce J. Hillman¹
Gerald D. Pond¹
Raymond F. Carmody¹
James E. Johnson¹
William R. Ferrell²

To investigate radiologists' performance at interpreting digital radiographic images, we compared the detectability of pneumothoraces on computed radiographic chest images with 0.2-mm pixel size (2.5 lp/mm) with their detectability on matched conventional screen-film images (5 lp/mm). Eight radiologists reviewed 50 computed and 50 screen-film chest radiographs from 25 patients with pneumothoraces and 25 patients with other (or no) abnormalities. Four of the readers who best detected pneumothoraces on screen-film examinations performed worse when interpreting computed radiographic studies; the other four readers detected pneumothoraces similarly with both techniques. No relationship was found between the size of a pneumothorax and its likelihood of detection by either technique.

These results raise concerns about implementing computed radiography for comprehensive chest imaging.

Despite the emergence of numerous computerized imaging techniques, most images are still obtained in an analog fashion and displayed on film [1]. However, computed radiography systems based on photostimulable plates provide excellent imaging for excretory urography and for some facets of musculoskeletal and chest radiography [2-8]. As a result, investigators are now focusing further on how well radiologists interpret digital images, particularly in comparison with their ability to detect specific abnormalities on conventional screen-film radiographs [2-7, 9].

To evaluate further the clinical suitability of digital chest imaging, we investigated whether radiologists could adequately detect pneumothoraces on images generated by a state-of-the-art commercial computed radiography system (TCR, model 210; Toshiba, Tustin, CA) with 0.2-mm image pixel size. Our rationale for conducting this experiment was that pneumothorax is an important clinical condition that is radiographically manifest as a fine, linear density. As such, its visualization is representative of subtle, high-frequency pulmonary structures, the identification of which is limited by resolution constraints imposed

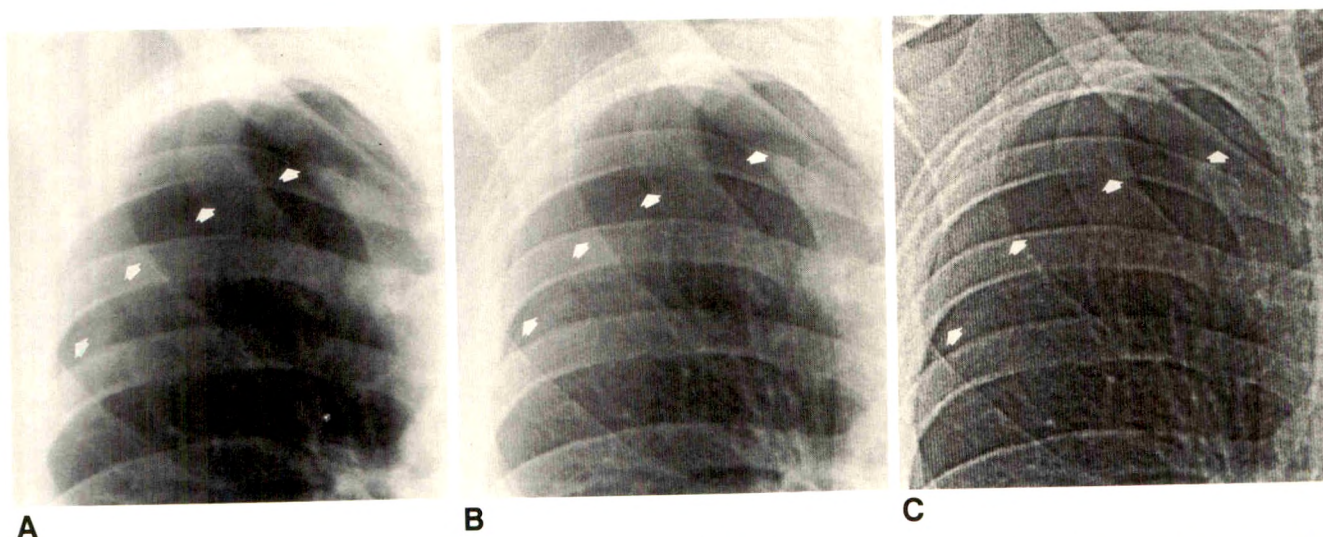


Fig. 1.—Conventional screen-film (A), computed (B), and frequency-modified computed (C) radiographs show a right apical pneumothorax (arrows).

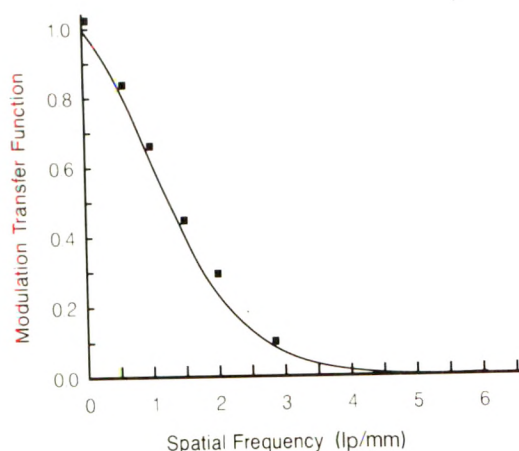


Fig. 2.—Graph shows modulation transfer function for computed radiography system when a 36 × 36 cm imaging plate is used.

with screen-film radiography, if computed radiography were truly equivalent to screen-film imaging for the detection of pneumothoraces (see Appendix). The four models of the trinomial distribution we tested were (1) 10% of readers perform better with each technique, 80% about the same; (2) 20% of readers perform better with each technique, 60% about the same; (3) 33% of readers perform better with each technique, 34% about the same; (4) 40% of readers perform better with each technique, 20% about the same.

We also tested the relationship between detectability and the size of pneumothorax for each technique. Two individuals traced the lung and pneumothorax outlines from each screen-film radiograph with a sensitized stylus on a sensitized tablet of an image analyzer (model MOT-3, Carl Zeiss, New York, NY). Electronic signals generated by the tracing process are relayed to a computer that calculates the two-dimensional areas of the pneumothorax and involved lung. These areas were expressed as the percentage of pneumothorax, that is, the ratio of pneumothorax area to total lung area [(pneumothorax area/lung area) × 100]. When the percentage of pneumothorax was greater than 10%, we required agreement of the calculations within 5% or recalculated the areas; for images with percentage of pneumothorax less than 10%, measurements were recalculated if they did not agree within 2%. When a sufficient level of agreement was

obtained, we averaged the concurring results. Pearson coefficient correlation analysis was used to evaluate the relationship between the size of pneumothorax and the probability of detection by computed radiography and screen film.

Results

Sensitivity for the eight individual readers in detecting pneumothoraces ranged from 0.76 to 0.92 for screen film, and 0.64 to 0.84 for computed radiography; specificity ranged from 0.84 to 1.00 for screen film, and 0.88 to 1.00 for computed radiography (Table 2). Four of the eight readers correctly identified pneumothoraces on screen-film much more often than on computed images. These radiologists (readers 2, 6, 7, and 8) were, on average, 27.5% more sensitive in interpreting screen-film chest images. None of the other four radiologists had higher sensitivity in reviewing computed than screen-film images; the difference in sensitivity between the two technologies was no greater than 5% for any of these four readers. Only readers 5 and 6 had a greater

TABLE 2: Sensitivity, Specificity, and ROC Curve Areas for Screen Film and Computed Radiography in Detecting Pneumothoraces

Reader	Sensitivity		Specificity		ROC Curve Analysis		
	SF	CR	SF	CR	SF Area	CR Area	% Diff
1	0.76	0.72	1.00	1.00	0.910	0.913	+0.3
2	0.88	0.68	0.88	0.88	0.962	0.857	-10.9
3	0.76	0.76	0.92	0.92	0.890	0.898	+0.9
4	0.84	0.80	0.96	1.00	0.929	0.915	-1.5
5	0.88	0.84	1.00	0.88	0.950	0.930	-2.1
6	0.92	0.68	0.84	0.92	0.962	0.902	-6.2
7	0.80	0.64	1.00	1.00	0.968	0.824	-14.9
8	0.92	0.76	0.96	0.96	0.931	0.884	-5.0

Note.—ROC = receiver operating characteristic, SF = screen film, CR = computed radiography, % Diff = percent difference between SF and CR = [(CR - SF)/SF].

differences in radiologists' performances in detecting high-frequency, low-contrast abnormalities such as pneumothoraces and interstitial thickening [3-5]. These studies, which dealt with small numbers of these types of abnormalities, have provided conflicting results, variously indicating spatial resolution requirements of 0.4-mm [3], 0.2-mm [5], and 0.1-mm [4] pixel sizes. The biphasic nature of our results suggests that influences other than spatial resolution may be important in explaining why radiologists detect pneumothoraces less well on computed than on screen-film images. The radiologists who were among the most proficient in interpreting the screen-film images performed much more poorly with computed radiography images; the other four radiologists' performances with screen-film and computed radiography differed little. Granted, it is possible to hypothesize that the former group in some manner made better use than the latter group of the greater spatial resolution that screen-film radiology offers. However, an alternative explanation suggested by the dichotomy of performances is that subtle diagnostic clues are portrayed better on the screen film than on the computed images, clues that are better exploited by the more proficient radiologists. Apparent differences between the two technologies that might contribute to explaining our result include computed radiography's lesser spatial resolution, greater image noise, and smaller image size, and radiologists' relative unfamiliarity with computed radiography. Indeed, several of these factors may have been important in influencing our results. The effects of each of these, and perhaps other influences, bear further investigation.

As with any imaging study that uses selected cases and a small group of radiologist readers, questions will arise about the generalizability of our results. Our cases were not randomly selected, nor can we be sure that the 25 pneumothoraces that composed the case material are representative of all pneumothoraces encountered in clinical practice. Nonetheless, these considerations are not germane to the purpose of the study. Insofar as the selected cases portray pneumothoraces that, if discovered, would affect clinical care, the sample is useful in determining whether computed radiography permits detection comparable with screen-film radiography of an important selection of pneumothoraces. The radiologist readers were chosen primarily on the basis of their willingness to participate in the study. Although they were not randomly selected, because their number is a sizable fraction (47%) of our 17-member group, the readers are representative of our department. To the extent that radiologists in our department are like those in other groups, similar performances can be expected in interpreting computed and screen-film chest images.

In summary, our study indicates that some radiologists will detect pneumothoraces less well on digital chest images than on screen-film examinations. We chose to investigate the detectability of pneumothoraces because we think pneumothorax is representative of other high-frequency, low-contrast abnormalities, the adequate depiction of which is important to chest diagnosis. Because an imaging system capable of supplanting conventional chest radiography should fulfill the need to visualize adequately all clinically important structures, there should be concern over fully implementing computed

radiography for clinical chest diagnosis. Further psychophysical research is needed to determine what improvements are needed in physical factors of the computed radiography system and/or radiologists' interactions with computed images.

Appendix

As described in the analysis section, we tested the hypothesis that the two methods did not differ in detectability of pneumothorax using the one-tailed paired *t* test. This test indicated that computed radiography was less effective ($p < .003$). However, this test assumes an approximately normal distribution of differences in detectability and is weighted in proportion to the size of differences in detectability among readers. Thus, in principle, the null hypothesis—that radiologists detect pneumothoraces equally well with computed and screen-film radiography—could be inappropriately rejected using the *t* test because of several large differences in performance.

Indeed, our interpretation of the data suggests that a categorical approach, which does not weight differences among readers performances according to magnitude, better reflects the results of the experiment, where some readers did as well with either method and some interpreted computed radiographs less accurately. Using this categorical approach, we determined whether our result could have occurred by chance by calculating the total probability of the possible outcomes that are as favorable to computed radiography as what we observed and the outcomes less favorable to computed radiography than what we observed. Our null hypothesis was that computed and screen-film technologies are equivalent for detecting pneumothoraces.

With the outcome we observed, this is easy to do. Even assuming a difference of 1% or less as the criterion for doing about the same with both methods, no reader did better with computed radiography. Hence, we need to sum the probability of all the outcomes in which no reader detects pneumothoraces better with computed radiography and the probability of all the outcomes in which no fewer readers than we observed do better with screen-film images. Outcomes for which any readers do better with computed radiography, even if "balanced" by more readers detecting pneumothoraces better with screen-film images, are ones that are more favorable to computed radiography, because they would demonstrate the possibility that computed radiography could be used more effectively than screen-film images.

Our null hypothesis (i.e., that the two technologies are equivalent) was that a reader taken at random had probability p_w of doing worse with computed radiography, probability p_s of doing about as well with both technologies, and probability p_b of doing better with computed radiography, where $p_b = p_w$. Such a distribution is represented by the multinomial with three possible outcomes, the trinomial. In this experiment, none of eight readers performed better with computed radiography and *M* of eight performed equally well with both methods (the value of *M* depending on the level of difference in performance accepted as equivalent). The probability of getting results at least as unfavorable for computed radiography as those we obtained is the sum of the probability of all the outcomes in which no reader does better with computed radiography and the probability of all the outcomes in which no fewer than *M* do better with screen film. It is given by the following equation:

$$\sum_{m=0}^M \left[\frac{8!}{m!(8-m)!} \right] (p_w)^{8-m} (p_s)^m.$$

Thus, our trinomial test is ad hoc, developed specifically for the results of this study. It does not represent a general test for the performance of any two radiographic systems.

Case Report

Pectoralis Muscle Simulating a Breast Mass

Jack E. Meyer,¹ Paul C. Stomper, and Roland R. Lee

Dedicated mammographic units feature rigid compression systems that optimize the visualization of breast detail. The adjacent ribs, some muscle, and a minute layer of normal tissue cannot be included in the standard views when this technique is used. Occasionally, either a breast mass close to the chest wall is not visualized or only the anterior aspect

of such a mass is imaged on the film. This geographic limitation increases the potential for false-negative mammograms [1].

Similarly, a normal structure not seen in its entirety may simulate a malignant mass. In well-positioned and compressed breasts imaged in the oblique projection, the pecto-

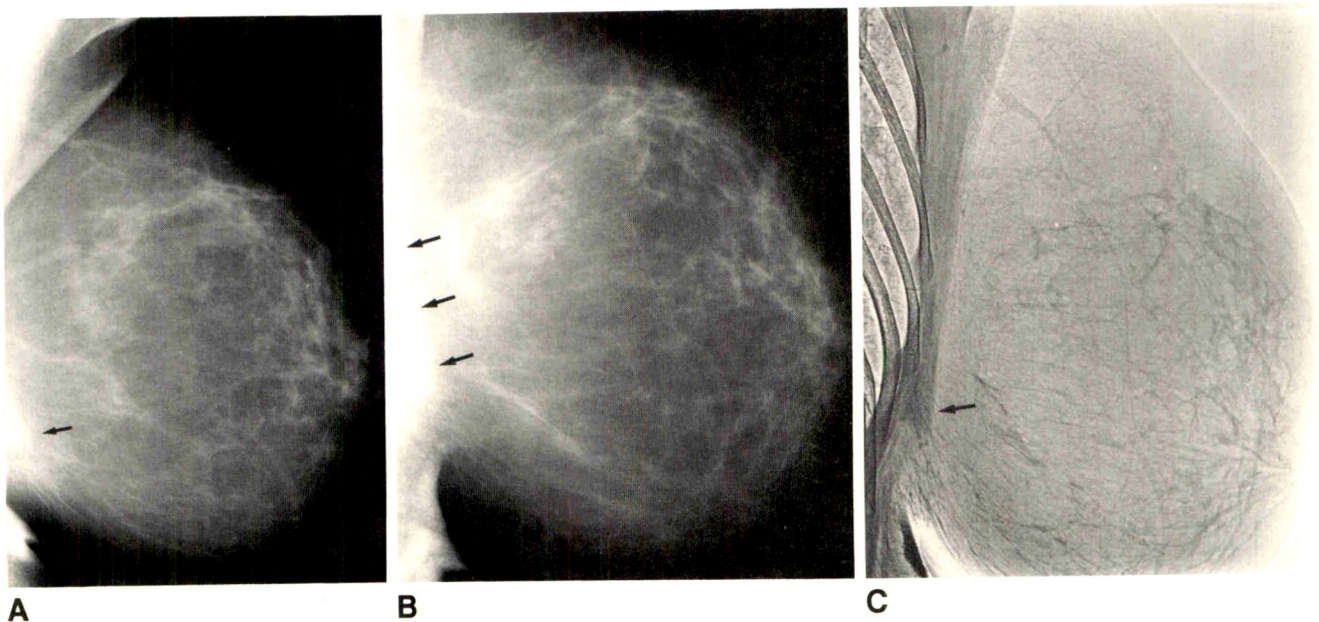


Fig. 1.—A, Right oblique mammogram shows an irregular, 1.5-cm, triangular density deep in inferior portion of right breast (arrow). B, Medial-lateral slightly angulated projection shows density is part of normal pectoralis muscle (arrows). Several skin calcifications are present. C, Right medial-lateral xeromammogram performed 1 year earlier more clearly shows inferior portion of pectoralis muscle (arrow).

Received July 11, 1988; accepted after revision October 10, 1988.

¹ All authors: Department of Radiology, Brigham and Women's Hospital, Harvard Medical School, 75 Francis St., Boston, MA 02115. Address reprint requests to J. E. Meyer.

Evaluation of a Dual-Screen, Dual-Emulsion Mammography System

Valerie P. Jackson¹
 Connie D. Harrill¹
 Susan J. White¹
 Kevin R. Gillespie^{1,2}
 John T. Mail¹
 Barry P. Katz³

We compared a new dual-screen, dual-emulsion film system for X-ray mammography with a widely used single-screen, single-emulsion combination for routine contact mammography in 100 patients with a variety of mammographic findings. By using a five-point rating scale (1 = poor, 5 = excellent), four blinded readers found the conventional combination superior in density (by 0.46 points on the rating scale), resolution (by 0.64 points), contrast (by 0.46 points), visibility of calcification (by 0.50 points), visibility of soft-tissue masses (by 0.37 points), and overall quality (by 0.47 points). No difference was seen in the graininess of the films.

In our study, the conventional system was consistently found to be slightly better than the dual-screen, dual-emulsion combination. The dual-emulsion mammograms required more careful scrutiny, particularly for detection of faint microcalcifications.

Current standard mammography screen-film systems, such as the Min R screen, Ortho M-1 film system (Eastman Kodak, Rochester, NY), are single-screen, single-emulsion combinations requiring radiation exposures of approximately 0.05 rad (0.05 cGy) average glandular dose without a grid [1]. When properly exposed and processed, they provide excellent contrast and resolution for mammography. Recently, a double-screen, double-emulsion system was developed that was designed to have minimal crossover and good contrast and resolution properties. The new system reportedly requires 2.5 times less radiation exposure and has slightly lower resolution, slightly higher noise, similar contrast, and decreased dust and dirt artifacts than the conventional combination does [1]. There have been only two studies of the efficacy of this system in the literature, and they predominantly involved the use of phantoms, rather than material from clinical cases [2, 3]. Our study is a blinded comparison of a conventional single-screen, single-emulsion system with the new dual-screen, dual-emulsion system for clinical X-ray mammography.

Subjects and Methods

One hundred symptomatic and asymptomatic women over age 35 were recruited for this study immediately after they had had a full conventional screen-film mammogram. The preliminary mammograms were obtained by using cassettes housing a single Kodak Min-R screen and Kodak Ortho M-1 single-emulsion film (OM-1). Most of the patients were chosen for the study because their preliminary mammograms revealed microcalcifications or small soft-tissue masses less than 2 cm in diameter. Five subjects had normal mammograms. Informed consent was obtained, and a single additional film was obtained by using the Kodak Min-R Fast dual-screen cassette and Kodak T-Mat M dual-emulsion film (T-Mat M). The mammogram was obtained in the view that depicted the abnormality optimally on the conventional study. The T-Mat M film was obtained by the technologist who performed the original study, on the same mammography unit, on the same day. Two dedicated mammography units were used: (1) Philips MammoDiagnost U-M unit (Philips Medical Systems, Shelton, CT) with 0.1- and 0.4-mm focal spots, molybdenum tube, and reciprocating grid,

Received September 19, 1988; accepted after revision November 14, 1988.

¹ Department of Radiology, Indiana University School of Medicine, Wishard Memorial Hospital, 1001 W. 10th St., Indianapolis, IN 46202. Address reprint requests to V. P. Jackson.

² Present address: Department of Radiology, St. Elizabeth's Hospital, 555 S. 70th St., Lincoln, NB 68510.

³ Department of Medicine, Indiana University School of Medicine, Wishard Memorial Hospital, and The Regenstrief Institute, Indianapolis, IN 46202.

AJR 152:483-486, March 1989
 0361-803X/89/1523-0483
 © American Roentgen Ray Society

Fig. 1.—Calcifications ranging from 1 mm (arrows) to <0.5 mm are seen equally well on single-emulsion (A) and double-emulsion (B) mammograms. Contrast and film density are similar in this case.

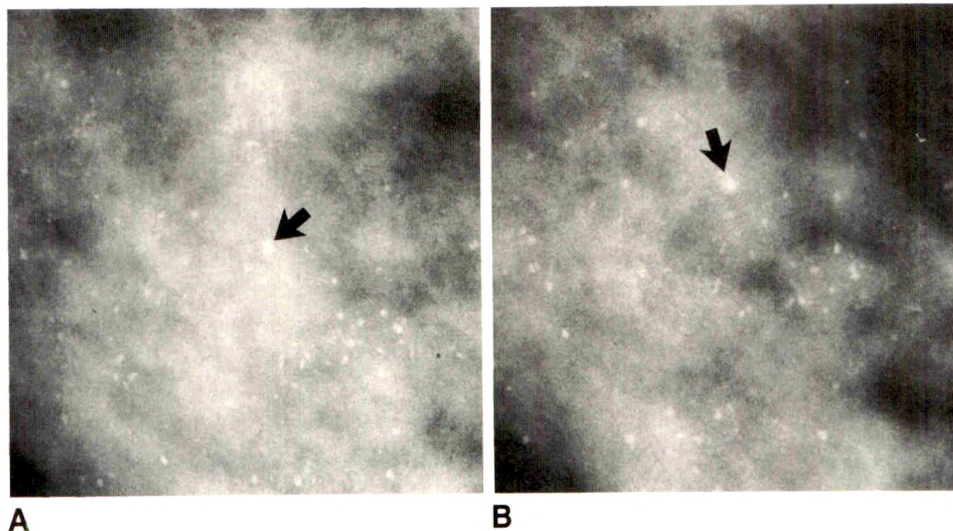


Fig. 2.—Multiple microcalcifications (arrows) <1 mm in size are seen much better on single-emulsion (A) than on double-emulsion (B) mammograms. Many particles less than 0.5 mm are not visible on double-emulsion film. Soft-tissue densities appear different because of slight change in patient's position between the two films.

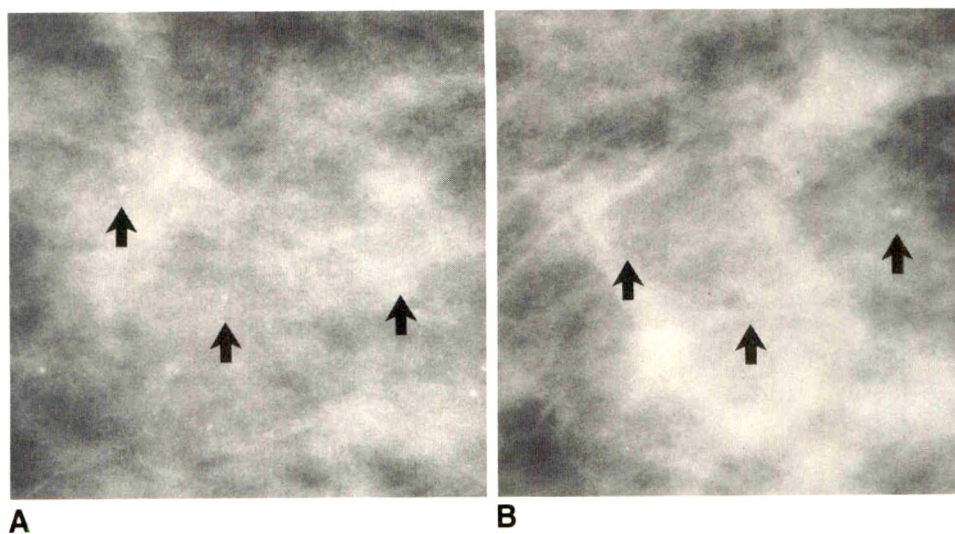
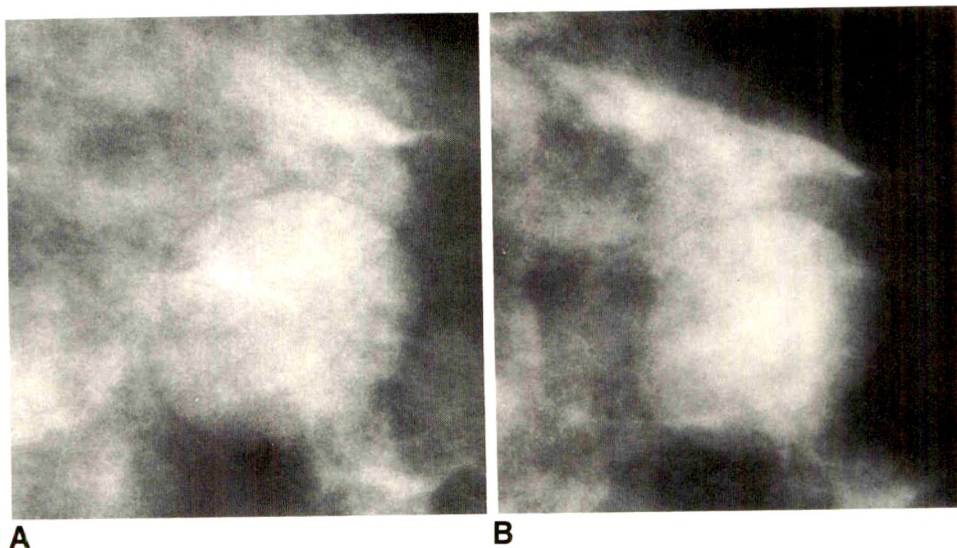


Fig. 3.—Well-circumscribed, 2-cm, low-density radiopaque soft-tissue mass on single-emulsion (A) and double-emulsion (B) mammograms. Border characteristics and internal density are better assessed on single-emulsion film.



Imaging of Pancreatic Neoplasms: Comparison of MR and CT

Edward Steiner^{1,2}
David D. Stark¹
Peter F. Hahn¹
Sanjay Saini¹
Joseph F. Simeone¹
Peter R. Mueller¹
Jack Wittenberg¹
Joseph T. Ferrucci¹

Thirty-two patients with pathologically proved pancreatic carcinomas or cystadenomas were evaluated with MR images obtained with T1-weighted spin echo (short TR/short TE), inversion recovery, and T2-weighted spin-echo (long TR/long TE) pulse sequences. CT was used as the reference standard to determine the ability of MR to delineate normal and abnormal pancreatic anatomy and thereby to exclude or detect pancreatic malignancy. Short TR/short TE spin-echo sequences were significantly better ($p < .05$) than inversion recovery or T2-weighted spin-echo sequences in resolution of both normal and abnormal anatomy. Resolution of pancreatic anatomy correlated ($r = .9$) with the image signal-to-noise ratio. In seven (22%) of 32 cases, MR visualized pancreatic tumors better than CT did because it showed a signal intensity difference between the tumor and normal pancreatic tissue. Overall, the slight superiority of MR over CT for tumor visualization tended to occur in larger tumors and was not statistically significant. On T1-weighted images, 63% (20 of 32) of pancreatic tumors studied had lower signal intensities than normal pancreatic tissue, whereas on T2-weighted sequences (TE = 60, 120, and 180 msec) only 41% (13 of 32) of tumors had increased signal intensities.

Currently available MR imaging techniques offer no significant advantages over CT for evaluating the pancreas for neoplasia.

Although CT has contributed significantly to pancreatic imaging, limitations in visualizing small tumors and retroperitoneal spread and in distinguishing inflammatory from neoplastic lesions require the development of improved imaging techniques [1]. MR imaging of the pancreas has been limited by image artifacts caused by respiratory motion, aortic pulsations, and bowel peristalsis, as well as by a lack of a suitable contrast material for the gut lumen [2-6]. One series described identification of the pancreatic head, body, and tail in only 60% of normal patients examined [7].

MR visualization of normal and diseased pancreas has been performed with T2-weighted, conventional, long TR/long TE, spin-echo (SE) pulse sequences (TR > 500 msec, TE > 28 msec). Recently, hepatic scanning with T1-weighted SE (short TR/short TE) pulse sequences was shown to reduce respiratory motion artifacts [6]. These pulse sequences are performed with extensive signal averaging during routine breathing and reduce all types of physiologic motion artifacts, in addition to producing higher signal-to-noise ratios (SNRs) [8].

In this study, we compared CT scans with MR images obtained with short TR/short TE, inversion recovery, and conventional long TR/long TE pulse sequences with respect to delineation of normal and abnormal pancreatic anatomy for detecting or excluding pancreatic neoplasms. Our principal goal was to determine whether motion-artifact suppression and increased SNR correlate with improved resolution of pancreatic anatomy.

Subjects and Methods

Patients

MR and CT examinations of the upper abdomen were performed in 32 patients with biopsy-proved tumors of the pancreas. Subjects were 38-75 years old. Tumors included

Received June 6, 1988; accepted after revision November 4, 1988.

D. D. Stark was supported in part by funds from the American Cancer Society JFRA-163 and PDT-326. S. Saini was supported in part by a Research and Education Fund Fellowship from the Radiological Society of North America.

¹Departments of Radiology, Massachusetts General Hospital and Harvard Medical School, Boston, MA 02114. Address reprint requests to D. D. Stark at Massachusetts General Hospital.

²Present address: Department of Radiology, Union Memorial Hospital, 201 E. University Pkwy., Baltimore, MD 21218.

AJR 152:487-491, March 1989

0361-803X/89/1523-0487

© American Roentgen Ray Society

anatomic resolution, resolution of MR images was consistently less than that of CT, never better than 1.7 on our grading scale. CT visualization of the normal pancreas was better than or equal to that of MR in 22 (69%) of 32 cases.

No significant differences were noted in MR visualization of the dorsal vs the ventral pancreatic margins. Specifically, flow void within the splenic vein only marginally improved resolution of the dorsal pancreatic margin, because of segmental appearance of the vein on adjacent transverse sections. Peripancreatic fat was helpful in ventral border delineation; however, evaluation of the pancreatic head was markedly limited by poor delineation of the second and third portions of the duodenum. A normal nondilated pancreatic duct could not be seen on any pulse sequence studied.

Pancreatic Neoplasms

The pancreatic tumors that we studied caused enough contour change to be seen readily with both CT and MR, and on MR they were best seen on the T1-weighted SE sequence (Fig. 1). Although the T1-weighted, short TR/short TE MR pulse sequence achieved an average grade of 2.2 compared with the 2.0 reference standard of CT (Table 2), this slight superiority of MR over CT was not statistically significant ($p > .05$). MR visualized the tumor better than CT did in seven (22%) of 32 cases.

Although anatomic detail is best seen on T1-weighted SE images, tumor inhomogeneities often were more conspicuous on the T2-weighted SE images, which showed increased

signal within the center of tumors, corresponding to low density zones on CT (Fig. 2).

Signal-intensity characteristics of the pancreatic neoplasms reveal that 20 (63%) of 32 tumors had a signal intensity less than that of normal pancreas on T1-weighted SE images. On the T2-weighted images, about 40% (12–13 tumors, depending on TE) of these tumors were of greater signal intensity than were normal regions of the pancreas. The different signal characteristics of tumor and normal pancreatic tissue aided tumor visualization by MR.

Extrapancreatic Disease

Retroperitoneal fat invasion (12 cases) and splenic vein patency were seen equally well with T1-weighted SE MR, inversion-recovery MR, and CT (difference not significant at $p = .05$). Of the MR pulse sequences studied, T1-weighted SE and inversion-recovery sequences were significantly more useful than the T2-weighted sequences for evaluating extrapancreatic spread of tumor ($p < .05$).

T1-weighted SE, inversion-recovery, and 60-msec T2-weighted SE sequences were significantly less useful ($p < .05$) than CT for assessing intrahepatic ductal dilatation (nine cases). Heavily T2-weighted SE sequences (120 and 180 msec) were able to detect subtle bile-duct dilatation as well as CT did (difference not significant at $p = .05$) (Table 2).

Correlation of SNR and Anatomic Resolution

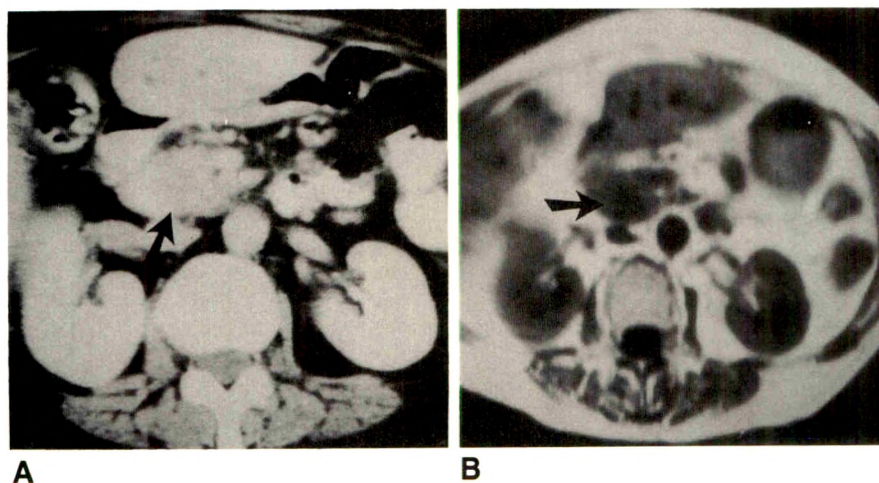
Time-normalized SNR measurements (Table 1) show that T1-weighted, short TR/short TE, SE pulse sequences have the greatest mean SNR of the pulse sequences studied ($p < .05$). The inversion-recovery sequences had the second best SNR, outperforming the long TR/long TE multiple SE sequences ($p < .05$).

A high degree of correlation was found between our quantitative SNR measurements and qualitative assessment of anatomic resolution, with $r = 0.9$ for resolution of normal anatomy, $r = 0.9$ for resolution of pancreatic mass, and $r = 0.8$ for detection of retroperitoneal spread. As predicted by our SNR data, the T1-weighted SE and inversion-recovery

TABLE 3: Relative Signal Intensities of Pancreatic Tumor vs Normal Pancreas

Pulse Sequence	Relative Signal (%)		
	Lower	Equal	Higher
T1-weighted spin echo	63	37	0
Inversion recovery	45	55	0
T2-weighted spin echo:			
60-msec TE	9	52	39
120-msec TE	13	47	40
180-msec TE	16	45	39

Fig. 1.—Carcinoma of pancreatic head. CT scan (A) and T1-weighted MR (SE 260/18) (B) show 2.3-cm mass (arrows) in head of pancreas. Pancreatic head is enlarged. MR image shows tumor as area of lower signal intensity than surrounding pancreatic tissue.



may also aid in decreasing motion artifact and thus in providing good anatomic resolution.

The MR technique evaluated in this study, including pulse sequences and 1.5-cm slice thickness, is the one employed at our institution for evaluating the liver and screening the entire upper abdomen [10]. As such, it is not a technique specifically adapted for pancreatic imaging. Indeed, thinner sections and techniques to reduce the field of view, such as surface coil imaging [3], might be used for a specific evaluation of the pancreas. Moreover, when gastrointestinal MR contrast agents become more widely available, they may be helpful in defining the boundaries of the pancreas.

In summary, large pancreatic carcinomas can be seen with MR, and the short TR/short TE, SE pulse sequence is an improvement over older pulse-sequence techniques. However, MR has no advantage over CT for evaluating the pancreas. We conclude that further work is needed to improve SNR, motion suppression, bowel opacification, and spatial resolution before MR can assume a major role in imaging pancreatic neoplasms.

REFERENCES

1. Van Dyke JA, Stanley RS, Berland LL. Pancreatic imaging. *Ann Intern Med* **1985**;102:212-217
2. Stark DD, Moss AA, Goldberg HI, Davis PL, Federle MP. Nuclear magnetic resonance imaging of the pancreas. *Radiology* **1984**;150:153-162
3. Simeone JF, Edelman RR, Stark DD, Wittenberg J, White EM, Butch RJ. Surface coil MR imaging of abdominal viscera: Part III. The pancreas. *Radiology* **1985**;157:437-441
4. Tscholakoff D, Hricak H, Thoeni R, Winkler ML, Margulis AR. MR imaging in the diagnosis of pancreatic disease. *AJR* **1987**;148:703-709
5. Hamm B, Wolf KJ, Felix R. Conventional and rapid MR imaging of the liver with Gd-DTPA. *Radiology* **1987**;164:313-320
6. Stark DD, Wittenberg J, Edelman R, et al. Detection of hepatic metastases: analysis of pulse sequence performance in MR imaging. *Radiology* **1986**;159:365-370
7. Stark DD, Moss AA. MRI of the pancreas. *Semin Ultrasound CT NMR* **1984**;5:428-438
8. Stark DD, Hendrick RE, Hahn PF, Ferrucci JT. Motion artifact suppression by fast spin-echo imaging. *Radiology* **1987**;164:183-191
9. *SAS user's guide: statistics*, 1982 ed. Cary, NC: SAS Institute, **1982**
10. Stark DD, Wittenberg J, Butch RJ, Ferrucci JT Jr. Hepatic metastases: randomized controlled comparison of detection with MR imaging and CT. *Radiology* **1987**;165:399-406

Pictorial Essay

MR Imaging of Liver Neoplasms

Ernst Rummeny,^{1,2} Sanjay Saini,¹ Jack Wittenberg,¹ Carolyn Compton,³ Peter F. Hahn,¹ Peter R. Mueller,¹ Joseph F. Simeone,¹ David D. Stark,¹ Ralph Weissleder,¹ Marc G. Dousset,¹ and Joseph T. Ferrucci, Jr.¹

Numerous clinical studies have suggested that MR imaging of the liver is most effective when performed on systems operating at low and intermediate (<1.0 T) magnetic field strengths [1]. In this pictorial essay, we illustrate our experience with more than 1000 MR examinations of hepatic neoplasms performed at 0.6 T (Teslacon, Technicare, Solon, OH).

Lesion Detection

Neoplastic tissues show abnormal signal intensity due to prolongation in their T1 and/or T2 relaxation times. MR images in which tissue signal intensity is based on T1 relaxation time (T1-weighted images) can be acquired with spin-echo (SE) and inversion-recovery (IR) pulse sequences. Selection of the shortest possible TE is essential for maximal T1 weighting [1]. With short TR/short TE, SE pulse sequences, signal averaging is used to reduce artifacts that arise due to physiologic motion. This combination improves image quality (higher signal-to-noise ratios) and increases lesion detectability (higher contrast-to-noise ratios) [1].

Our routine T1-weighted images are obtained with a spin-echo pulse sequence, 260–300/14–18 (TR/TE). This permits acquisition of 11 slices, and the entire liver can be covered with a single scan when a 15-mm slice thickness is used. With 10 acquisitions, the total scan time is about 7 min.

On T1-weighted images, liver neoplasms, both benign and malignant, appear hypointense relative to normal liver. Because of flow void, vascular structures also appear hypointense. Thus, on these images it may be difficult to distinguish small hepatic masses (whose size approaches that of blood vessels seen in cross section) from blood vessels (Fig. 1A).

T2-weighted images are used to confirm lesions identified or suspected on T1-weighted images because on T2-weighted pulse sequences hepatic masses appear hyperintense relative to normal liver and can be readily distinguished from vascular structures, which remain hypointense due to flow void (Fig. 1B). Another major use of T2-weighted pulse sequences is tissue characterization. To achieve both these goals, we use a triple-echo SE pulse sequence with TE times of 60, 120, and 180 msec. This provides mild, moderate, and heavy T2-dependent contrast, respectively. To acquire 11 slices in a single scan, the TR used is 2350 msec.

Tissue Characterization

Because benign hepatic masses, which include liver cysts and cavernous hemangiomas, are not uncommon, MR imaging may be useful in distinguishing them from malignant liver tumors. At MR imaging, cysts and hemangiomas are hypointense on T1-weighted images and extremely hyperintense on

Received October 3, 1988; accepted after revision November 9, 1988.

E. Rummeny is supported by the Deutsche Forschungsgemeinschaft, RU 374/1-2. S. Saini is supported by the Research and Education Fund of the Radiological Society of North America.

Presented as a scientific exhibit at the annual meeting of the American Roentgen Society, San Francisco, CA, May 1988. Recipient of ARRS Certificate of Merit.

¹ Department of Radiology, Massachusetts General Hospital and Harvard Medical School, 32 Fruit St., Boston, MA 02114. Address reprint requests to J. T. Ferrucci, Jr.

² Present address: Department of Radiology, Westfälische Wilhelms-Universität Münster, Albert-Schweitzer-Str. 33, D-4400 Münster, W. Germany.

³ Department of Pathology, Massachusetts General Hospital and Harvard Medical School, Boston, MA 02114.

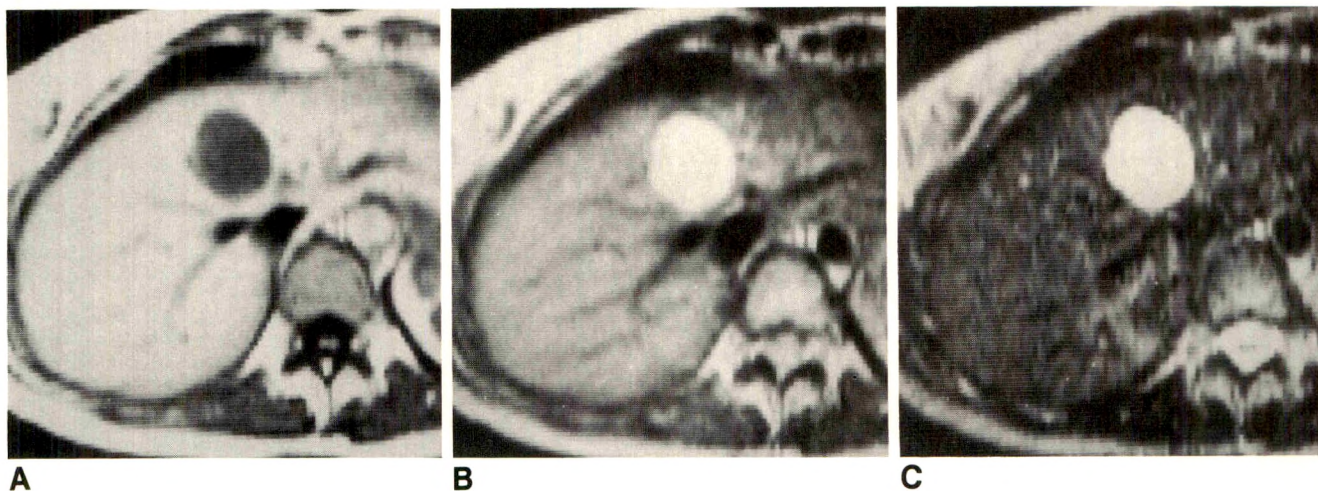


Fig. 3.—Typical cavernous hemangioma.

A, T1-weighted spin-echo image, 300/14. Hemangioma is hypointense relative to normal liver.

B, T2-weighted spin-echo image, 2350/60. Hemangioma is more intense than normal liver. Most hemangiomas have a homogeneous signal intensity and a sharp outer margin.

C, These features are seen also on heavily T2-weighted spin-echo image, 2350/180. Extremely high lesion-liver contrast is seen on these images because signal from normal liver diminishes while signal from hemangiomas remains relatively unchanged. Note that appearance of typical cavernous hemangioma is similar to that of simple hepatic cysts seen in Fig. 2.

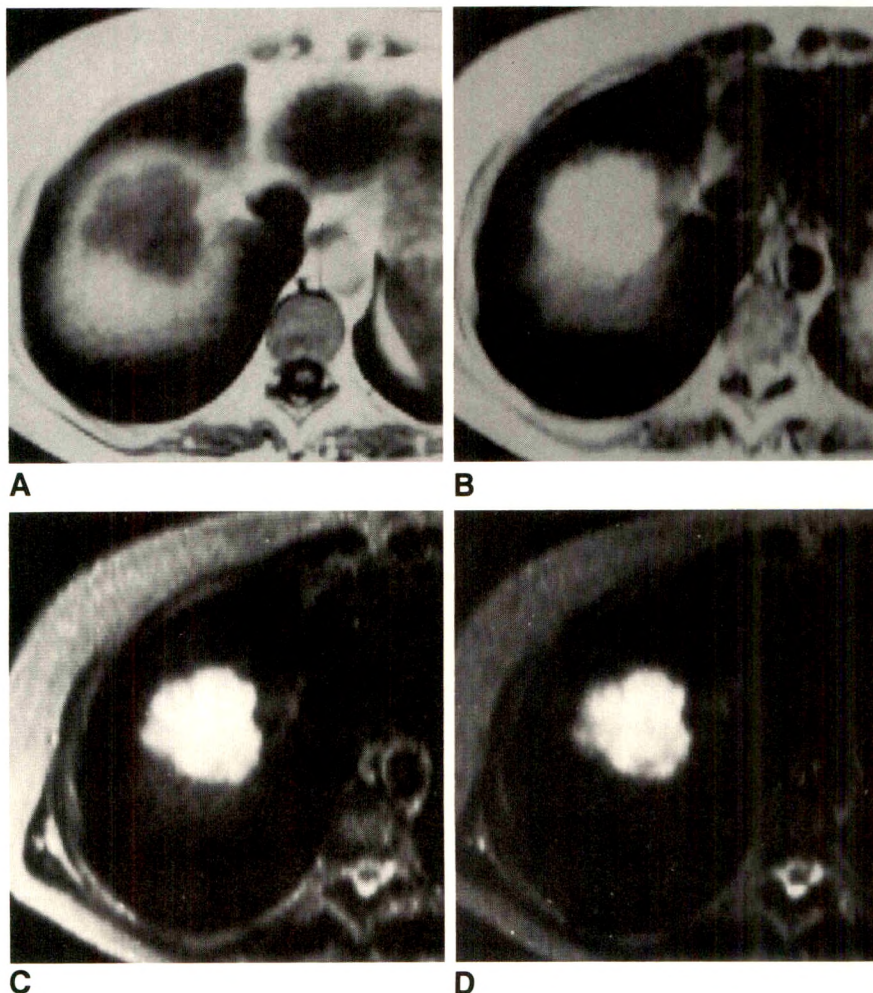


Fig. 4.—Atypical cavernous hemangioma.

A, Large (>5 cm) hemangiomas often show atypical features. This 6- to 7-cm hemangioma has a lobulated contour. Spin-echo image, 260/14.

B, Mildly T2-weighted spin-echo image, 2350/60. Lesion is markedly hyperintense with respect to normal liver.

C, Heavily T2-weighted spin-echo image, 2350/180. Lesion remains markedly hyperintense, indicative of benign cavernous hemangioma.

D, Wide window setting shows inhomogeneous signal intensity due to central scar (spin-echo image, 2350/180).

Fig. 7.—Atypical hyperintense liver metastases.

A, Hypointense solitary mass is seen posteriorly on T1-weighted spin-echo image, 300/14.

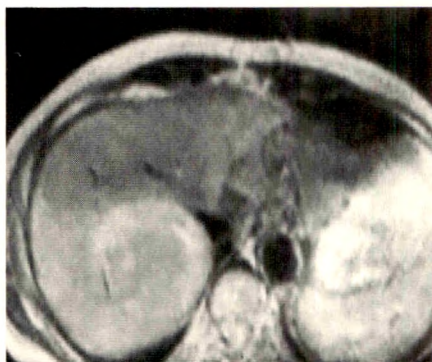
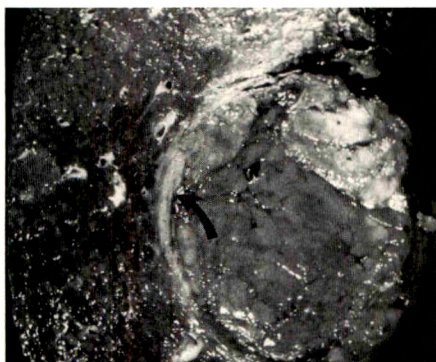
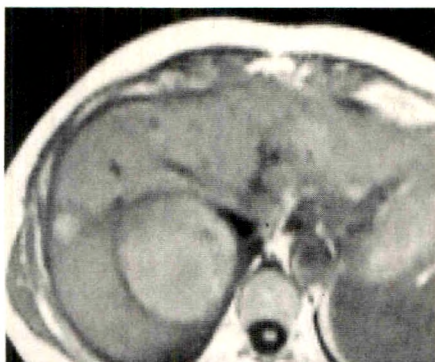
B, Heavily T2-weighted spin-echo image, 2350/180. Lesion appears markedly hyperintense. These features are commonly seen with hepatic cysts (Fig. 2B) and cavernous hemangiomas (Fig. 3C) but are rarely present in hypervascular metastases. This lesion was a metastasis from pancreatic islet cell carcinoma.



A



B



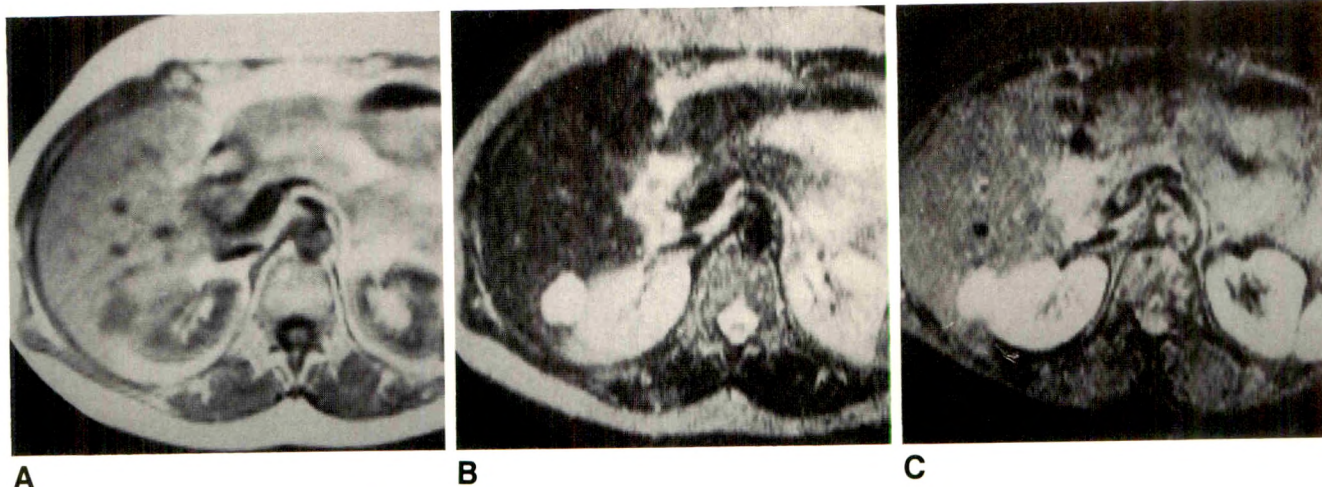


Fig. 11.—STIR image of cavernous hemangioma.
 A, T1-weighted spin-echo image, 300/14. A 2-cm hypointense mass is seen adjacent to right kidney in posterior segment of right hepatic lobe.
 B, Heavily T2-weighted spin-echo image, 2350/180. Lesion appears hyperintense and homogeneous with sharp outer margin, which typifies appearance of cavernous hemangioma.
 C, STIR image, 1500/100/30 (TR/TI/TE). Signal intensity from subcutaneous and retroperitoneal fat is absent. Hemangioma and spleen appear markedly hyperintense relative to normal liver, even on this T1-weighted pulse sequence.

Occasionally, metastases may appear hyperintense and mimic hemangiomas (Fig. 7). This has been seen with hypovascular metastases from pancreatic islet cell carcinoma and soft-tissue sarcomas.

MR features important for the characterization of hepatocellular carcinoma include a hypointense peripheral ring and isointensity on T1-weighted images (Fig. 8). These findings are due to fibrous capsules and fatty metamorphosis [3]. Tumor capsules, however, are not unique to hepatomas and can also be seen in benign primary hepatic tumors, such as hepatic adenomas (Fig. 9) [4].

Liver masses caused by focal nodular hyperplasia are characterized by near isointensity relative to normal liver on both T1- and T2-weighted pulse sequences and by a central radiating scar (Fig. 10) [5]. However, central scars are not specific for this tumor and can be seen in other benign and malignant hepatic tumors (Figs. 4B and 9B) [4].

Special Pulse Sequences

Phase-contrast pulse sequences exploit the presence of fatty deposition in diseased liver [7]. On T2-weighted phase-contrast images, there is reduction of signal from fatty liver while metastases show no change in signal intensity from in-phase images. This results in increased tumor-liver soft-tissue contrast (Fig. 5D).

Gradient-echo pulse sequences reduce scan times to approximately 20 sec (i.e., a single breath-hold), but they are associated with poor signal-to-noise and contrast-to-noise ratios (Fig. 2C).

REFERENCES

1. Ferrucci JT. MR imaging of the liver. *AJR* 1986;147:1103-1116
2. Wittenberg J, Stark DD, Forman BH, et al. Differentiation of hepatic metastases from hepatic hemangiomas and cysts by using MR imaging. *AJR* 1988;151:79-84
3. Itoh K, Nishimura K, Togashi K, et al. Hepatocellular carcinoma: MR imaging. *Radiology* 1987;164:21-25
4. Rummeny F, Weissleder B, Stark DD, et al. Primary liver tumors: diagnosis

Hepatic Lymphoma in Cyclosporine-Treated Transplant Recipients: Sonographic and CT Findings

Hiroshi Honda¹
 Edmund A. Franken, Jr.¹
 Thomas J. Barloon¹
 John L. Smith²

The purpose of this study was to determine the CT and sonographic features of hepatic lymphoma developing in organ transplant recipients taking cyclosporine. The four patients included in the study had non-Hodgkin lymphoma. Two of the cases were primary, with no associated lymphadenopathy or extrahepatic lesions. The hepatic lymphomas were characterized by multiple low-density areas on CT scans and hypoechoic areas on sonograms. In three of the four patients, the lesions regressed after the cyclosporine dosage was reduced.

We conclude that in cyclosporine-treated organ transplant recipients, hepatic lymphoma should be considered in the differential diagnosis of hepatic lesions with or without lymphadenopathy when multiple low-density lesions are shown by CT and hypoechoic lesions are shown by sonography.

Posttransplantation lymphomas in non-cyclosporine-treated recipients differ from the lymphomas of nontransplant patients in that they frequently affect extra-nodal sites, especially the CNS [1-3]. Histologically, these lymphomas are non-Hodgkin disease with B-cell proliferation. The Epstein-Barr virus has been implicated as the cause in patients with iatrogenic immunosuppression [1, 2, 4].

Cyclosporine-induced posttransplantation lymphomas are differentiated from the lymphomas of non-cyclosporine-treated transplant recipients by their sites of involvement, in particular whether or not they affect the CNS [5]. The purpose of this study was to determine the CT and sonographic features of the hepatic lesions seen in these patients.

Patients and Methods

From January 1980 through December 1987, 614 organ transplantations (530 kidney, 64 pancreas, 17 heart, and three liver) were performed on 572 recipients at our institution. During this period, lymphoma developed in 11 transplant recipients, seven of whom were treated with cyclosporine (in combination with steroids), which was first used in December 1983, as an immunosuppressive agent after organ transplantation. Four of the seven receiving cyclosporine (two kidney and two heart transplant recipients) had hepatic involvement. None of the non-cyclosporine-treated transplant recipients developed hepatic lesions. The hepatic lesions were histologically proved to be B-cell type non-Hodgkin lymphomas by biopsy. The four patients with hepatic involvement included three men and one woman, with an age range at the time of transplantation of 38 to 66 years (mean, 51 years). The interval from organ transplantation to diagnosis of lymphoma averaged 6.8 months (range, 4-14 months). CT and sonography were performed because the patients were febrile and complained of fatigue. CT was performed without IV contrast material in three transplant recipients because of their poor renal function. One transplant recipient had studies done with and without contrast enhancement. Liver biopsy was performed within 1 week of the imaging studies in all four transplant recipients.

Results

CT showed the hepatic lesions of posttransplantation lymphoma to be well-margined or poorly margined masses of various sizes. Diameters ranged from

Received June 17, 1988; accepted after revision October 28, 1988.

¹ Department of Radiology, The University of Iowa College of Medicine, Iowa City, IA 52242. Address reprint requests to H. Honda.

² Department of Surgery, The University of Iowa College of Medicine, Iowa City, IA 52242.

AJR 152:501-503, March 1989
 0361-803X/89/1523-0501
 © American Roentgen Ray Society

The striking feature of lymphoma in transplant recipients is the high frequency of CNS involvement [3, 7]. In addition to the CNS, the involvement of the gastrointestinal tract, intraperitoneal and retroperitoneal lymph nodes, and transplanted kidneys, lung, and liver has been noted in lymphoma [3]. Extranodal lymphoma, in particular, may grow in an infiltrative fashion throughout the parenchyma of the involved organ [11].

Cyclosporine is the principal immunosuppressive agent and is reported to have significantly improved longevity in transplant recipients [16, 17]. However, its use may result in various infections and neoplasms. The cyclosporine-induced posttransplantation lymphomas (lymphoproliferative disorders) are characterized by (1) early appearance after transplantation, (2) widespread involvement at the time of discovery, and (3) regression or complete resolution after reduction of the immunosuppressive agent, specifically the dose of cyclosporine [5].

In our cases, the time interval from transplantation to diagnosis of lymphoma averaged 6.8 months, whereas the interval in previous reports without cyclosporine therapy was 44–105 months [3, 10, 11]. There were no extrahepatic lesions in two of our four patients; however, the hepatic lesions in these patients were multiple, either diffusely spread or huge, mass lesions. The other two patients had extensive retroperitoneal lymphadenopathies, a mass in the iliopsoas muscle, and a splenic lesion; the hepatic lesions were homogeneous solid masses without the central low density that has been reported in non-cyclosporine-treated transplant recipients [3, 10]. The lack of central low-density areas, which have been correlated with tumor necrosis [3], and the homogeneous density may be attributed to cyclosporine therapy. CT showed two types of masses, well marginated and poorly marginated, in the same recipients. Sonography showed both types of masses as hypoechoic, solid masses. In three recipients, the hepatic lesion regressed after the cyclosporine dose was reduced.

REFERENCES

1. Hanto DW, Sakamoto K, Purtilo DT, Simmons RL, Najarian JS. The Epstein-Barr virus in the pathogenesis of posttransplant lymphoproliferative disorders. *Surgery* 1981;90:204–213
2. Hanto DW, Firzzer G, Purtilo DT, et al. Clinical spectrum of lymphoproliferative disorders in transplant recipients and evidence of the role of the Epstein-Barr virus. *Cancer Res* 1981;41:4253–4261
3. Tubman DE, Frick MP, Hanto DW. Lymphoma after organ transplantation: radiologic manifestations in the central nervous system, thorax, and abdomen. *Radiology* 1983;149:625–631
4. Hanto DW, Firzzer G, Gajl-Peczalska K, et al. The Epstein-Barr virus (EBV) in the pathogenesis of posttransplant lymphoma. *Transplant Proc* 1981;13:756–760
5. Harris KM, Schwartz ML, Slasky BS, Nalesnik M, Makowka L. Posttransplantation cyclosporine-induced lymphoproliferative disorders: clinical and radiologic manifestations. *Radiology* 1987;162:697–700
6. Hoover R, Fraumeni JFJ. Risk of cancer in renal transplant recipients. *Lancet* 1973;2:55–77
7. Penn I. Malignancies associated with immunosuppressive or cytotoxic therapy. *Surgery* 1978;83:492–502
8. Penn I. Tumor incidence in human allograft recipients. *Transplant Proc* 1979;11:1047–1051
9. Firzzer G, Hanto DW, Gajl-Peczalska KJ, et al. Polymorphic diffuse B-cell hyperplasias and lymphomas in renal transplant recipients. *Cancer Res* 1981;41:4262–4279
10. Frick MP, Salomonowitz E, Hanto DW, Gedgaudas-McClees K. CT of abdominal lymphoma after renal transplantation. *AJR* 1984;142:97–99
11. Frick MP, Salomonowitz E, Feinberg SB. Sonography of abdominal post-transplant lymphoma. *J Clin Ultrasound* 1984;12:383–385
12. Zornoza J, Ginaldi S. Computed tomography in hepatic lymphoma. *Radiology* 1981;138:405–410
13. Moss AA. Computed tomography of the hepatobiliary system. In: Moss AA, Gamsu G, Genant KH, eds. *Computed tomography of the body*. Philadelphia: Saunders, 1983:599–698
14. Strayer DS, Reppun TS, Levin M. Primary lymphoma of the liver. *Gastroenterology* 1980;78:1571–1576
15. Miller ST, Wollner N, Meyers PA. Primary hepatic or hepatosplenic non-Hodgkin's lymphoma in children. *Cancer* 1983;52:2285–2288
16. White DJG, Calne RY. The use of cyclosporine-A immunosuppression in organ grafting. *Immunol Rev* 1982;65:115–131
17. Hakala TR, Starzl TE, Rosenthal JT, Shaw BW, Iwatsuki S. Cadaveric renal transplantation with cyclosporine-A and steroids. *Transplant Proc* 1983;15:465–470

MR Differentiation of Hepatocellular Carcinoma from Cavernous Hemangioma: Complementary Roles of FLASH and T2 Values

Kuni Ohtomo¹
Yuji Itai
Hideo Yoshida
Takashi Kokubo
Kohki Yoshikawa
Masahiro Iio

Forty-two patients with hepatocellular carcinoma (hepatoma) and 18 patients with hemangioma were studied with MR imaging at 1.5 T to evaluate the efficacy of single-slice breath-hold FLASH (fast low-angle shot) images in distinguishing between the lesions and to compare with T2 differentiation using conventional spin-echo images. The difference between mean tumor-to-liver signal ratio on FLASH imaging of hepatocellular carcinoma (1.46 ± 1.06) and hemangioma (0.86 ± 0.45) was statistically significant ($p < .01$). Fifty-one (82%) of 62 lesions were classified correctly when the borderline of tumor-to-liver signal ratio between hepatoma and hemangioma was set at 0.9. The mean T2 values of hepatomas and hemangiomas were 48 ± 10 msec and 89 ± 20 msec, respectively. Fifty-seven (92%) of 62 lesions were correctly diagnosed with the T2 borderline of 80 msec. The five misdiagnosed lesions with the T2 borderline were hemangiomas smaller than 2 cm with tumor-to-liver signal ratios less than 0.9.

FLASH images appear promising for differentiating between hepatoma and hemangioma, and they complement T2 values in characterizing small lesions.

The value of rapid MR imaging with gradient-echo methods is currently being investigated for abdominal imaging of hepatic tumors [1, 2]. We evaluated the utility of single-slice breath-hold scans using the FLASH (fast low-angle shot) gradient-echo technique to differentiate hepatocellular carcinoma (hepatoma) from cavernous hemangioma (hemangioma). We then compared the results, characterizing tissue on the basis of T2 values calculated from conventional spin-echo (SE) pulse sequences [3, 4].

Materials and Methods

We performed MR scans in 42 patients with hepatoma and 18 patients with hemangioma at the University of Tokyo. The diagnosis of hepatoma was proved by pathologic examination in nine patients and angiography with clinical data (elevation of serum alpha-fetoprotein level and/or liver cirrhosis) in 33 patients [5]. The diagnosis of hemangioma was established by angiography in one patient, by contrast-enhanced CT in seven patients, and by sonography (with more than 6 months of follow-up) in 10 patients [6].

MR imaging was performed with a superconducting 2.0-T Magnetom unit (Siemens, Erlangen, W. Germany) operating at 1.5 T.

T2-weighted, multislice, SE images were obtained with 10-mm section thickness, two excitations, 5-mm interslice gap, and 17.1-min scanning time. In 46 patients, the time parameters used were 2000/28,75 (TR/first-echo TE, second-echo TE); in 14 patients, the time parameters were 2000/22,90. We obtained single-slice breath-hold FLASH scans at the center of the hepatic mass lesion, using 19/12, 90° flip angle, 10.2-sec scanning time, two excitations, a 256 × 256 matrix, and 10-mm section thickness. T2 values were calculated from a pair of images with different TEs [7]. Measurements of T2 and tumor-to-liver signal ratio (T/L) on FLASH images were obtained by using operator-defined regions of interest. When the tumor was inhomogeneous, the T2 or signal intensity of the widest homogeneous region was adopted as the value of the tumor. Statistical significance was calculated with the Student's *t* test for unpaired data.

Received September 21, 1988; accepted after revision November 14, 1988.

¹ All authors: Department of Radiology, University of Tokyo, 7-3-1 Hongo, Bunkyo-ku, Tokyo 113, Japan. Address reprint requests to K. Ohtomo.

AJR 152:505-507, March 1989
0361-803X/89/1523-0505
© American Roentgen Ray Society

was less than 0.9 in the five hemangiomas that had T2 values less than 80 msec.

Discussion

T2 shortening of small hemangiomas due to partial volume averaging with the surrounding hepatic parenchyma (which has a short T2) is the most important factor that limits the efficacy of T2 values for differentiating hepatoma from cavernous hemangioma [3, 4]. In this study, all lesions that were classified incorrectly with the borderline of T2 were hemangiomas smaller than 2 cm. The overall accuracy of T2 differentiation (92%) differed from that of our previous data (84%) [4] because this study included fewer small hemangiomas than our earlier study.

The breath-hold FLASH method can overcome partial volume averaging due to respiratory movement. Our results show that all eight hemangiomas smaller than 2 cm were correctly differentiated from hepatoma by using the borderline of T2 and T/L on FLASH with T2 priority.

In comparison with the surrounding liver parenchyma, hepatoma and hemangioma usually appear as areas of low signal intensity on T1-weighted, SE images and of high signal intensity on T2-weighted, SE images because of the prolonged relaxation times (T1 and T2). Hepatoma with fatty degeneration sometimes appears as an area of high signal intensity on T1-weighted images [8].

The contrast relationship on FLASH images has not been fully understood in clinical observations [2]. We cannot explain why the hepatomas usually appeared as areas of high signal intensity on theoretically T1-weighted FLASH images obtained with 19/12 and a 90° flip angle because no obvious fatty degeneration was seen within these tumors by other radiologic techniques, including sonography and CT. We obtained T1-weighted FLASH images because they are suitable for dynamic study in which a bolus injection of gadolinium-DTPA is used [9]. However, the usefulness of plain FLASH images may reduce the need for dynamic MR imaging.

In this series of cases, tumor-to-liver contrast on FLASH images was not sufficient to show tumors clearly because T/L values ranged from 0.9 to 1.1 in 18 (29%) of the 62 lesions. Additionally, overall accuracy of differentiation with T/L values on FLASH (82%) was inferior to that with T2 values (92%). Further study is necessary to establish optimal gradient-echo methods for detecting and differentiating hepatic tumors. The relative merits of T2 and T/L on FLASH in differential diagnosis also should be examined. Our experience is limited, but the single-slice, breath-hold FLASH technique appears promising for differentiating hepatoma from cavernous hemangioma. FLASH imaging and T2 play complementary roles in diagnosing small lesions.

REFERENCES

1. Edelman RR, Hahn P, Buxton R, et al. Rapid MR imaging with suspended respiration: clinical application in the liver. *Radiology* 1986;161:125-131
2. Unger EC, Cohen MS, Gatenby RA, et al. Single breath-holding scans of the abdomen using FISP and FLASH at 1.5T. *J Comput Assist Tomogr* 1988;12:575-583
3. Ohtomo K, Itai Y, Furui S, Yashiro N, Yoshikawa K, Iio M. Hepatic tumors: differentiation by transverse relaxation time (T2) of magnetic resonance imaging. *Radiology* 1985;155:421-423
4. Ohtomo K, Itai Y, Yoshikawa K, Kokubo T, Iio M. Hepatocellular carcinoma and cavernous hemangioma: differentiation with MR imaging. Efficacy of T2 values at 0.35 and 1.5 T. *Radiology* 1988;168:621-623
5. Okuda K, Obata H, Jinnouchi S, et al. Angiographic assessment of gross anatomy of hepatocellular carcinoma: comparison of celiac angiograms and liver pathology in 100 cases. *Radiology* 1977;123:21-29
6. Itai Y, Ohtomo K, Araki T, Furui S, Iio M, Atomi Y. Computed tomography and sonography of cavernous hemangioma of the liver. *AJR* 1983;141:315-320
7. Herfkens R, Davis P, Crooks L, et al. Nuclear magnetic resonance imaging of the abnormal live rat and correlations with tissue characteristics. *Radiology* 1981;141:211-218
8. Ebara M, Ohto M, Watanabe Y, et al. Diagnosis of small hepatocellular carcinoma: correlation of MR imaging and tumor histologic studies. *Radiology* 1986;159:371-377
9. Yoshida H, Itai Y, Ohtomo K, Kokubo T, Minami M, Yashiro N. Small hepatocellular carcinoma and cavernous hemangioma: differentiation on dynamic MRI by FLASH technique using Gd-DTPA. *Radiology* (in press)

Increased Prevalence of Cholelithiasis in Patients with Abdominal Aortic Aneurysm: Sonographic Evaluation

James J. Schuster¹
Vassilios Raptopoulos¹
Stephen P. Baker²

We performed a prospective study to determine the prevalence of cholelithiasis in patients with abdominal aortic aneurysm. Over an 18-month period, the gallbladder and the abdominal aorta were evaluated routinely in all consecutive patients referred to us for sonography of the abdomen and retroperitoneum. The patients were divided into two groups: those with an abdominal aortic aneurysm (aorta >3 cm in transverse diameter) ($n = 96$) and those whose aorta measured <3 cm in transverse diameter ($n = 538$), who served as control subjects. Cholelithiasis was found in 50% of patients with and 26% of patients without aneurysm ($p < .0001$). A stepwise logistic regression analysis found age alone to be predictive of cholelithiasis ($p = .030$). However, age was not predictive of cholelithiasis when included with abdominal aortic aneurysm in a multivariate model. Diabetes mellitus and gender were not predictive of cholelithiasis.

We found cholelithiasis in approximately half of the patients who had abdominal aortic aneurysms. This is almost double the prevalence in the general elderly population. A

surgical preference will be helpful for deciding whether concomitant evaluation of the gallbladder is indicated in all patients undergoing elective aneurysmectomy.

REFERENCES

1. Newman HF, Northup JD, Rosenblum M, Abrams H. Complications of cholelithiasis. *Am J Gastroenterol* **1968**;50:476-496
2. Melton LJ III, Bickerstaff LK, Hollier LH, et al. Changing incidence of abdominal aortic aneurysms: a population based study. *Am J Epidemiol* **1984**;120:379-386
3. Godwin JD, Korobkin M. Acute disease of the aorta. *Radiol Clin North Am* **1983**;21:551-574
4. Bernstein EF, Chan EL. Abdominal aortic aneurysm in high risk patients: outcome of selective management based on size and expansion rate. *Ann Surg* **1984**;200:255-263
5. Cooperberg PL, Gibney RG. Imaging of the gallbladder, 1987. *Radiology* **1987**;163:605-613
6. Raptopoulos V, Moss L, Reuter K, Kleinman P. Comparison of real-time and gray-scale static ultrasonic cholecystography. *Radiology* **1981**;140:153-154
7. Snedecor GW, Cochran WG. *Statistical methods*. Iowa City, IA: University of Iowa Press, **1980**:98-101
8. Dixon W, Brown M, Engelman L, et al. *BMDP statistical software*. Berkeley, CA: University of California Press, **1985**
9. String ST. Cholelithiasis and aortic reconstruction. *J Vasc Surg* **1984**;1:664-669
10. Ouriel K, Ricotta JJ, Adams JT, Deweese JA. Management of cholelithiasis in patients with abdominal aortic aneurysm. *Ann Surg* **1983**;198:717-719
11. Raptopoulos V, Goldberg RJ, Smith EH, Ellison RC. Clinicians' appraisal of sonography. *Radiology* **1987**;165:237-239
12. Bennion LJ, Grundy SM. Risk factors for the development of cholelithiasis in man (first of two parts). *N Engl J Med* **1978**;299:1161-1167
13. Fry RE, Fry WJ. Cholelithiasis and aortic reconstruction: the problem of simultaneous surgical therapy. Conclusions from a personal series. *J Vasc Surg* **1986**;4:345-350
14. Bickerstaff LK, Hollier LH, Van Peenen HJ, Melton LJ, Pairorero PC, Cherry KJ. Abdominal aortic aneurysm repair combined with a second surgical procedure—morbidity and mortality. *Surgery* **1984**;95:487-491
15. Thomas JH, McCroskey BL, Iliopoulos JI, Hardin CA, Hermreck AS, Pierce GE. Aortoiliac reconstruction combined with nonvascular operations. *Am J Surg* **1983**;146:784-787
16. Ottinger LW. Acute cholecystitis as a postoperative complication. *Ann Surg* **1976**;184:162-165

National Council on Radiation Protection and Measurements

60th Anniversary Meeting

(25th Annual Meeting of the Council)

Washington, DC, April 5-6, 1989

The forerunner organizations of the National Council on Radiation Protection and Measurements (NCRP) were first set up 60 years ago, and the Council itself, in its present form, is 25 years old this year. The annual meeting in this anniversary year will examine the status of radiation protection today—where we have come from, where we are, and where we are going—in a number of important basic and practical areas of radiation protection and measurement. The papers to be presented will concentrate on this theme and will exemplify the role of the NCRP in modern radiation protection as a field of importance to the radiation worker and to the public at large.

The speakers will include Dade W. Moeller, William J. Schull, R. J. Michael Fry, Seymour Abrahamson, Paul Slovic, John W. Baum, William R. Hendee, Marc Edwards, John E. Till, Fred A. Mettler, C. C. Lushbaugh, George M. Wilkening, Richard A. Tell, Paul L. Carson, Gail de Planque, Kenneth R. Kase, Manning Muntzing, and Warren K. Sinclair.

The meeting will be held in the Ballroom of the Vista International Hotel, 14th and M St. N.W., Washington, DC.

All interested are invited to attend. For further information, write to W. Roger Ney, Executive Director, NCRP, 7910 Woodmont Ave., Ste. 800, Bethesda, MD, 20814.

Large Colonic Neoplasms Missed by Endoscopy

Seth N. Glick¹
 Steven K. Teplick¹
 Dennis M. Balfe²
 Marc S. Levine³
 Arunas E. Gasparaitis⁴
 Dean D. T. Maglinte⁵
 Michael J. Shortsleeve⁶
 Jeffrey C. Brandon¹

Endoscopy is commonly accepted as the gold standard in the evaluation of neoplastic colonic disease. The procedure is used to confirm or exclude lesions detected on barium enemas, with the assumption that the endoscopist was successful in reaching the appropriate segment of the colon. We collected 18 cases, all with proved colonic neoplasm 2–8 cm in diameter that were detected by barium enema but overlooked on initial endoscopy. All of the lesions were relatively flat with little intraluminal protuberance. Histologic examination showed malignant foci in six of 11 tumors that were resected. In two of the other seven patients, unresected lesions progressed to advanced carcinomas.

This experience suggests that a repeat barium enema is indicated when endoscopy fails to detect a colonic tumor suspected on barium enema examination.

An increasing number of reports in the medical and surgical literature have concluded that the barium enema is unreliable in detecting both benign and malignant colonic neoplasms. Several investigators have suggested that colonoscopy should be the initial investigation in the detection of colonic neoplasms and, when complete, is sufficient to identify almost all malignant or potentially malignant colon lesions [1]. This is particularly true in high-risk groups such as patients with a strong family history or personal history of a previous colonic neoplasm [2]. In addition, there is a tendency to regard any lesion described on barium enema as falsely positive when it is not identified on endoscopy also. The possibility that the endoscopist may fail to detect large lesions is not widely recognized.

We encountered 18 patients with confirmed neoplastic lesions more than 2 cm in diameter that were identified on barium enema but were not detected on one or more endoscopic examinations although the level of the lesion was reached with the endoscope.

Materials and Methods

Eighteen patients, each with a colonic neoplasm having a minimum diameter of 2 cm that was not identified on endoscopy, were included in the study. Thirteen of the patients were from two institutions; the remaining five were from four other institutions.

The cases were collected randomly, because the analysis was not designed to compare the relative sensitivities of endoscopy and radiography for lesions in this size range. The intent was to describe the clinical and pathologic aspects of these lesions and emphasize the diagnostic difficulties encountered at endoscopy as a result of the morphologic features of the tumors. In each case, endoscopy was performed with a flexible instrument by experienced gastroenterologists, and the endoscopist was able to pass the endoscope up to or beyond the site of the lesion. All of the endoscopic procedures were performed within 3 months of the barium study with the majority (89%) taking place within 1 month. In 14 of 18 cases, the barium enema preceded endoscopy and the endoscopist had prior knowledge of the size, morphology, and location of the suspected abnormality. Six of the patients were at high risk for the development of a neoplasm (Fig. 1); five patients had a previous colonic carcinoma,

Received October 4, 1988; accepted after revision November 11, 1988.

¹ Department of Diagnostic Radiology, Hahnemann University Hospital, Broad and Vine Sts., Philadelphia, PA 19102. Address reprint requests to S. N. Glick.

² Mallinckrodt Institute of Radiology, Washington University School of Medicine, 510 S. Kingshighway, St. Louis, MO 63110.

³ Department of Radiology, Hospital of the University of Pennsylvania, 34th & Spruce Sts., Philadelphia, PA 19104.

⁴ Department of Radiology, University of Illinois Medical Center, 174 W. Taylor St., Chicago, IL 60601.

⁵ Department of Radiology, Methodist Hospital, 1701 N. Senate Blvd., Indianapolis, IN 46202.

⁶ Department of Radiology, Mt. Auburn Hospital, 330 Mt. Auburn St., Cambridge, MA 02130.

AJR 152:513–517, March 1989
 0361–803X/89/1523–0513
 © American Roentgen Ray Society

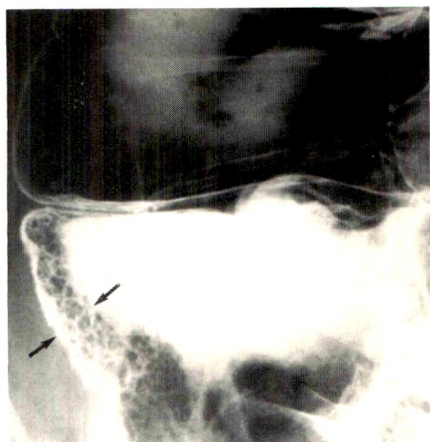
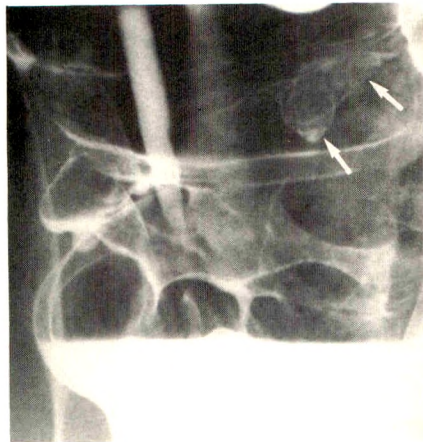
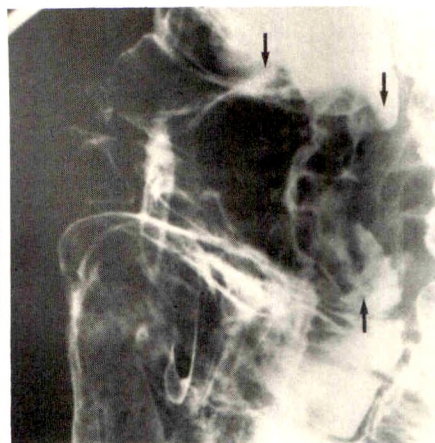


Fig. 3.—Air-contrast barium enema shows carpet lesion on lateral wall of cecum (arrows) that was missed at colonoscopy. Tumor was confirmed on repeat barium enema. No resection was performed because of recurrent colonic carcinoma in sigmoid colon.



A



B

Fig. 4.—A, Air-contrast barium enema shows 2½ by 2 cm sessile polypoid lesion on medial wall of cecum (arrows) that was not identified at colonoscopy. B, 3 years later, patient had anemia. Barium enema shows large, plaque-like advanced carcinoma (arrows) at site of previous polypoid lesion.

strated a sensitivity for barium enemas of 85–98% for polyps larger than 1 cm and a sensitivity of more than 90% with respect to invasive malignancy [9–18]. A few of these studies showed that a retrospective review of the films further improved the sensitivity, because the lesions not initially observed were present on the films [15, 17, 19]. Negative predictive values for colonic polyps larger than 1 cm was more than 95% [13, 20, 21]. The population in one study consisted of patients at high risk for neoplastic disease [21]. Lesion location also must be considered, because most of the lesions missed by radiography, regardless of size, were in the sigmoid colon. However, flexible sigmoidoscopy is adequate for detection of such missed lesions, and selective use of this technique in conjunction with the barium enema (often performed on the same day) is still less expensive than colonoscopy. The decrease in mortality from colonic cancer when these two techniques are combined in a screening protocol is greater than with periodic colonoscopy alone [22].

The issue that has not been adequately addressed in the literature concerns the diagnostic limitations of colonoscopy. In 10–30% of examinations, the entire colon is not totally evaluated [6, 7, 23]. Poor patient preparation, poor patient tolerance, too rapid withdrawal, inexperience, and “blind areas” on obscured haustral surfaces or in areas of angulation (e.g., flexures) also may account for diagnostic failures. In addition, the endoscopist may overestimate the extent of the colonoscopic evaluation or may misinterpret the anatomic location of a lesion within the colon, resulting in either a false-negative study or inadequate treatment [24]. Unfortunately, the concept of endoscopically missed lesions, particularly large ones, is not widely recognized, and the results of colonoscopy are usually accepted as unequivocal.

In the studies performed by Laufer et al. [25] and Thoeni and Menuck [9], endoscopy missed 11% and 2.7% of all polyps, respectively. In both series, all the missed polyps were smaller than 1 cm. Miller and Lehman [26] collected 54 endoscopically missed lesions from their own experience as well as from a literature review. Most were 0.5–1.5 cm, but at least three were larger than 3 cm. Fork et al. [16] found that endoscopy missed 9% of all polyps. Three lesions larger than 1.5 cm were missed by endoscopy. Thoeni and Petras [27, 28] found equal sensitivity for polyps that were larger than 2 cm in the sigmoid colon (93% endoscopy vs 95% radiography). In the right colon, endoscopy (not including incomplete studies) was significantly less successful (78% for endoscopy vs 88% for double contrast enema). Endoscopy missed three (19%) of 16 lesions that were larger than 2 cm, including a large invasive carcinoma. In the series by Evers et al. [29], 17% of rectal carcinomas were missed on rigid proctosigmoidoscopy, compared with only 6% missed by barium enema. In only two of nine endoscopic failures was the lesion not reached, and all were identified on reexamination prompted by the radiographic findings. Leinecke et al. [10] determined the false-negative rate for lesions larger than 1 cm as 15% for radiography and 12% for endoscopy. However, for lesions larger than 1.9 cm, the success rates shifted to 7% and 10%, respectively. In addition, several radiographically diagnosed polyps with negative endoscopy received no further follow-up, a frequent bias in many endoscopic series.

The endoscopist often has advanced knowledge of a lesion based on the radiographic findings, raising the question as to whether the sensitivity would be as high if endoscopy had been used exclusively. Unlike the barium enema, which may be subjected to repeat interpretation, the findings (or lack of) at endoscopy cannot be reviewed. Indeed, studies in which

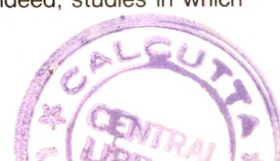
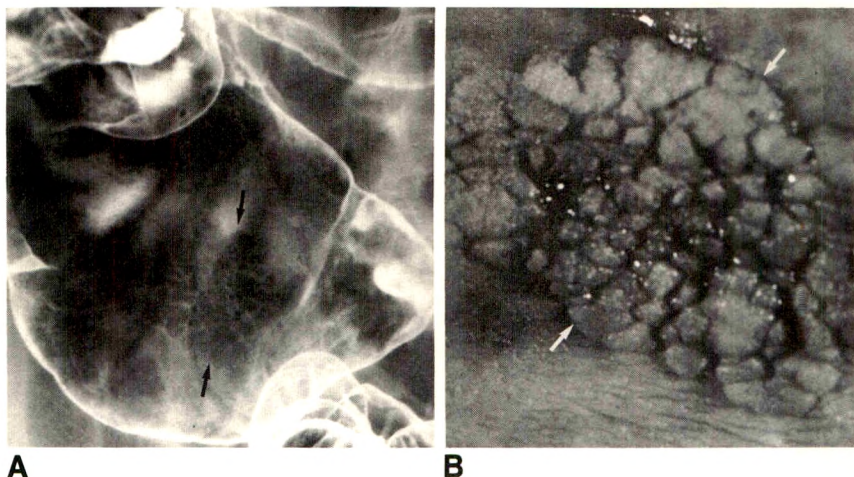


Fig. 7.—A, Barium enema shows 3 by 4 cm carpet lesion in cecum (arrows) proximal to annular carcinoma (not seen on this film). The pathologist could not identify the cecal lesion on the specimen.

B, After spraying cecum with blue dye, this flat, nodular lesion (arrows) became apparent. Tumor was adenomatous hyperplasia.



REFERENCES

- Neigut AI, Forde KA. Screening colonoscopy: has the time come? *Am J Gastroenterol* 1988;83:295-296
- Moore JRL, LaMont JT. Colorectal cancer: risk factors and screening strategies. *Arch Intern Med* 1984;144:1819-1823
- Reilly JC, Rusin LC, Theuerkauf FJ. Colonoscopy: its role in cancer of the colon and rectum. *Dis Colon Rectum* 1982;25:532-538
- Williams CB, Macrae FA, Bartram CI. A prospective study of diagnostic methods in adenoma follow-up. *Endoscopy* 1982;14:74-78
- Warden MJ, Petrelli NJ, Herrera L, Mittelman A. Endoscopy versus double-contrast barium enema in the evaluation of patients with symptoms suggestive of colorectal carcinoma. *Am J Surg* 1988;155:224-226
- Aldridge MC, Sim AJ. Colonoscopy findings in symptomatic patients without X-ray evidence of colonic neoplasms. *Lancet* 1986;2:833-834
- Durdey P, Weston PM, Williams NS. Colonoscopy or barium enema as initial investigation of colonic disease. *Lancet* 1987;2:549-551
- Chen YM, Ott DJ, Gelfand DW, Munitz HA. Impact of the barium enema on patient management. *Gastrointest Radiol* 1988;13:81-84
- Thoeni RF, Menuck L. Comparison of barium enema and colonoscopy in the detection of small colonic polyps. *Radiology* 1977;124:631-635
- Leinicke JL, Dodds WJ, Hogan WJ, Stewart ET. A comparison of colonoscopy and roentgenography for detecting polypoid lesions of the colon. *Gastrointest Radiol* 1977;2:125-128
- Fork F-T. Double contrast enema and colonoscopy in polyp detection. *Gut* 1981;22:971-977
- Ott DJ, Chen YM, Gelfand DW, Wu WC, Munitz HA. Single-contrast vs double-contrast barium enema in the detection of colonic polyps. *AJR* 1986;146:993-996
- Ott DJ, Chen YM, Gelfand DW, Wu WC, Kerr RM. Sensitivity of double-contrast barium enema: emphasis on polyp detection. *AJR* 1980;135:327-330
- Williams CB, Hunt RH, Loose H, Riddell RH, Sakai Y, Swarbrick ET. Colonoscopy in the management of colon polyps. *Br J Surg* 1974;61:673-682
- Kelvin FM, Gardiner R, Vas W, Stevenson GW. Colorectal carcinoma missed on double contrast barium enema study: a problem in perception. *AJR* 1981;137:307-313
- Fork F-T, Lindstrom C, Ekelund G. Double contrast examination in carcinoma of the colon and rectum: a prospective clinical series. *Acta Radiol [Diagn] (Stockh)* 1983;24:177-188
- Bolin S, Franzen L, Nilsson E, Sjobahl R. Carcinoma of the colon and rectum: tumors missed by radiologic examination in 61 patients. *Cancer* 1988;61:1999-2008
- Fork F-T. Radiographic findings in overlooked colon carcinomas. *Acta Radiol [Diagn] (Stockh)* 1988;29:331-336
- Kewenter J, Jensen J, Boijesen M, Lycke G, Tylan U. Perception errors with double-contrast enema after a positive guaiac test. *Gastrointest Radiol* 1987;12:79-82
- Fork F-T, Lindstrom C, Ekelund GR. Reliability of routine double-contrast examination (DCE) of the large bowel in polyp detection: a prospective clinical study. *Gastrointest Radiol* 1983;8:163-172
- Kjaergard H, Nordkild P, Hennild V, Pedersen VM, Geerdens J. Follow-up study after colorectal polypectomy: the predictive value of a negative double-contrast barium enema. *Scand J Gastroenterol* 1986;21:353-356
- Eddy DM, Nugent FW, Eddy JF, et al. Screening for colorectal cancer in a high-risk population: results of a mathematical model. *Gastroenterology* 1987;92:682-692
- Abrams JS. A second look at colonoscopy: indications, failures, and costs. *Arch Surg* 1982;117:913-917
- Frager DH, Frager JD, Wolf EL, Beneventano TC. Problems in the colonoscopic localization of tumors: continued values of the barium enema. *Gastrointest Radiol* 1987;12:343-346
- Lauffer I, Smith NC, Mullens JE. The radiological demonstration of colorectal polyps undetected by endoscopy. *Gastroenterology* 1976;70:167-170
- Miller RE, Lehman G. Polypoid colonic lesions undetected by endoscopy. *Radiology* 1978;129:295-297
- Thoeni RF, Petras A. Detection of rectal and rectosigmoid lesions by double-contrast barium enema examination and sigmoidoscopy. *Radiology* 1982;142:59-62
- Thoeni RF, Petras A. Double-contrast barium-enema examination and endoscopy in the detection of polypoid lesions in the cecum and ascending colon. *Radiology* 1982;144:257-260
- Evers K, Laufer I, Gordon RL, Kressel HY, Herlinger H, Gohel VK. Double-contrast enema examination for detection of rectal carcinoma. *Radiology* 1981;140:635-639
- Hoff G, Vatn M. Epidemiology of polyps in the rectum and sigmoid colon: endoscopic evaluation of size and localization of polyps. *Scand J Gastroenterol* 1985;20:356-360
- Waye JD, Brainfeld S. Surveillance intervals after colonoscopic polypectomy. *Endoscopy* 1982;14:79-81
- Eckardt VF, Fuchs M, Kanzler G, Remmele W, Stienen U. Follow-up of patients with colonic polyps containing severe atypia and invasive carcinoma. *Cancer* 1988;61:2552-2557
- Weyman PJ, Koehler RE, Zuckerman GR. Resolution of radiographic-endoscopic discrepancies in colon neoplasms. *J Clin Gastroenterol* 1981;3:89-93

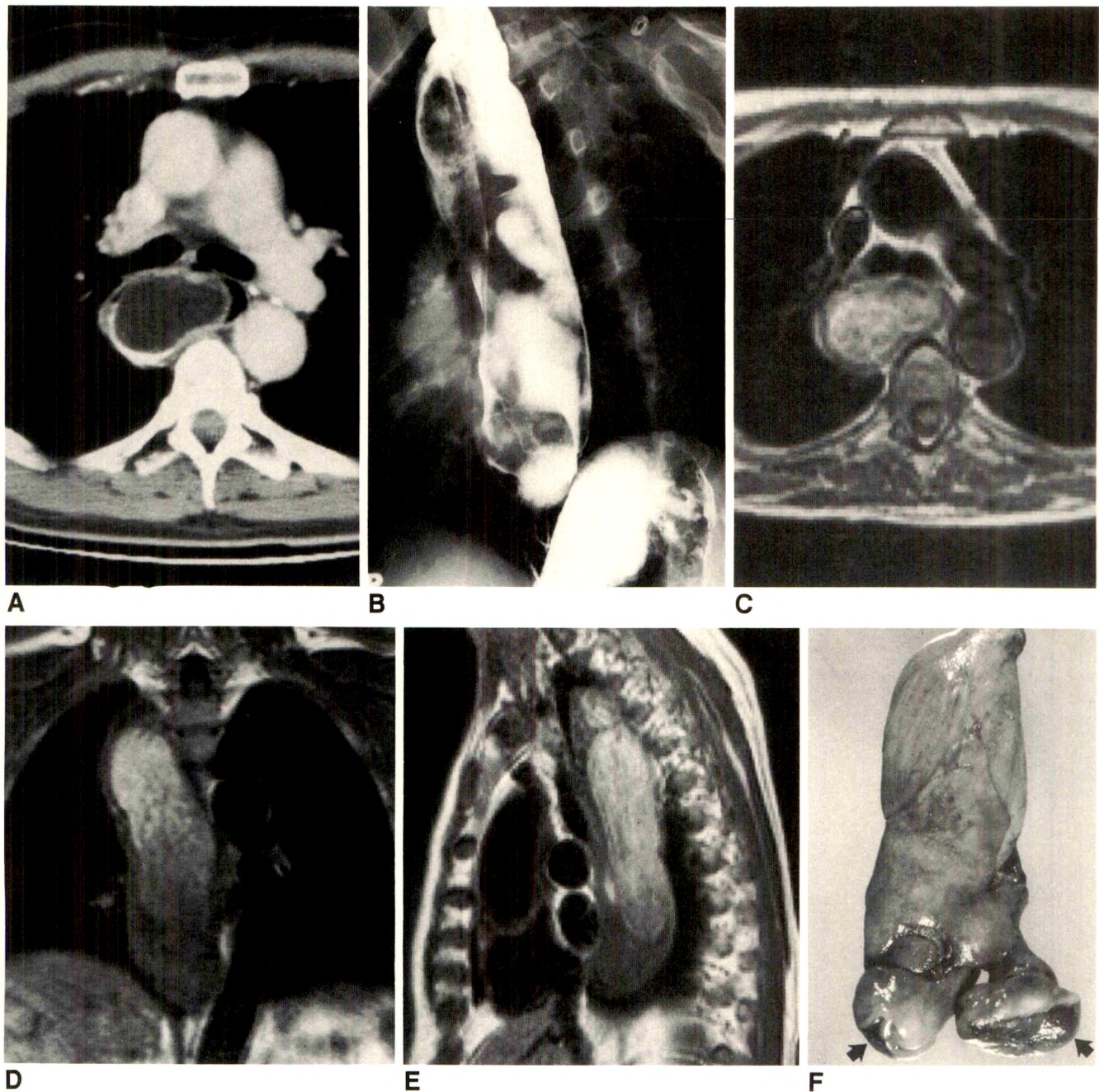


Fig. 1.—A, Contrast-enhanced CT scan at level of carina reveals posterior mediastinal mass with lipid attenuation. Oral contrast material outlines posterolateral aspect of mass.

B, Esophagram reveals polypoid filling defects in barium-filled esophagus.

C, Axial T1-weighted MR image, 700/24 (TR/TE), at level of carina shows posterior mediastinal mass with high signal intensity.

D, Coronal T1-weighted MR image, 500/32, shows cylindrical mediastinal mass with high signal intensity.

E, Sagittal T1-weighted MR image, 500/32, shows cylindrical posterior mediastinal mass with high signal intensity.

F, Gross pathologic specimen of giant fibrovascular polyp of esophagus. Ulcers are seen at distal bulbous ends of mass (arrows).

proportions. Seventy-two percent of the reported cases have occurred in adult men [4].

Giant fibrovascular polyps characteristically cause smooth, large, polypoid intraluminal filling defects on barium esophagrams. The point of attachment of the polypoid mass to the esophageal wall may be difficult to identify.

Esophagoscopy is of value, but the diagnosis cannot always be made endoscopically. Totten et al. [5] reported that 25% of solid intramural and intraluminal esophageal tumors were missed at endoscopy. Fibrovascular polyps may be overlooked because normal, intact esophageal mucosa covers the tumor. The endoscopist may think that the normal

Case Report

Direct Percutaneous Drainage of an Obstructed Afferent Loop

Charles W. Maile¹ and Philip D. Hanna²

Afferent loop obstruction is an uncommon complication of Billroth II gastroenterostomy. The treatment of afferent loop obstruction has traditionally been surgical. Recently, percutaneous drainage of obstructed afferent loops using a transhepatic approach was described [1]. In the case presented in this report, a direct percutaneous approach to afferent loop drainage was used successfully. To the best of our knowledge, this technique has not been reported before.

Case Report

A 68-year-old woman was admitted to the hospital with severe epigastric and chest pain. She had multiple medical problems including cardiovascular disease and chronic obstructive lung disease. She had suffered a myocardial infarction 2 months previously. Her medical history included a Billroth II gastroenterostomy for severe ulcer disease and a cholecystectomy, both performed more than 25 years earlier.

Serum amylase level was 1660 units/l, and a diagnosis of pancreatitis was made. Liver-function tests were normal. A CT examination confirmed severe pancreatitis with small peripancreatic fluid collections (Figs. 1A and 1B). In addition, marked afferent loop dilatation was shown, and a diagnosis of afferent loop obstruction was suggested. Endoscopy revealed a widely patent afferent loop orifice, but only a pinhole-sized afferent loop orifice.

The patient was a poor candidate for surgical decompression of her afferent loop because of her severe pancreatitis, chronic obstructive lung disease, and recent myocardial infarction. A transhepatic percutaneous approach was considered, but was declined because of concerns about her severe pancreatitis and potential associated

common-duct friability. A direct percutaneous approach via an anterior, transperitoneal path was selected. Under CT guidance, a sheathed 18-gauge needle was placed directly into the distal portion of the dilated afferent loop, passing between the left liver lobe and the gastric pouch and traversing only left-upper-quadrant fat. A 0.035-in. floppy-tipped guidewire was then introduced. The patient was transferred to a fluoroscopic room where an 8.5-French Cope-loop nephrostomy catheter (Cook, Bloomington, IL) was inserted and positioned with its tip within the distal afferent loop (Fig. 1C). The catheter initially was placed on closed dependent drainage, but subsequently was connected to low intermittent suction.

No abdominal complications relating to the catheter placement were identified. The pancreatitis gradually improved, with the serum and urine amylase levels falling to normal values by 18 days after drainage. The patient's respiratory status worsened shortly after drainage, but this was temporary and considered unrelated to the procedure. Elective surgical revision of her afferent loop was done 49 days after percutaneous drainage with a side-to-side duodenojunostomy. At surgery, the distal afferent loop orifice was found to be markedly narrowed by scar tissue. There was no evidence of intraperitoneal spillage of bowel content. No adhesions were identified between the distal afferent loop and the anterior abdominal wall.

Discussion

In their article describing transhepatic percutaneous afferent loop drainage, Lee et al. [1] discuss the theoretical possibility of direct percutaneous drainage. The direct approach was not used in their cases largely because of concerns regarding its safety.

Received July 11, 1988; accepted after revision August 30, 1988.

¹ Department of Radiology, North Memorial Medical Center, Minneapolis, MN 55422. Address reprint requests to C. W. Maile.

² South Denver Gastroenterology, P. C., 601 E. Hampden Ave., #260, Englewood, CO 80110.

Technical Note

An Internalized Double-J Catheter for Percutaneous Transgastric Cystogastrostomy

Barry A. Sacks,^{1,2} Jeffrey J. Greenberg,² David H. Porter,² Anthony Capobianco,³ Mark Painter,⁴ Robert Kim,³ Dan E. Orron,² and Ducksoo Kim²

The approach to management of pancreatic pseudocysts varies widely [1–8]. When pancreatic pseudocysts are associated with acute pancreatitis, the initial treatment is medical. Surgical intervention is reserved for pseudocysts that develop complications, persist beyond 6 weeks, are larger than 4 cm in size, or are associated with chronic pancreatitis. Surgically the aim is to create a large communication between the pseudocyst and a bowel loop (cystoenterostomy). The concepts of cystoenterostomy and percutaneous catheter drainage under CT and fluoroscopic guidance were combined to manage five retrogastric pseudocysts in four patients by placement of an internalized double-J stent.

Materials and Methods

A nasogastric tube is introduced, and the stomach insufflated with air. CT scans are obtained to select an appropriate path for catheter introduction. With the patient under local anesthesia, the 21-gauge needle of a Cope introducer set (Cook Inc., Bloomington, IN) is passed through the anterior abdominal wall and both walls of the stomach and into the pseudocyst (Fig. 1). Five to 10 ml of fluid are aspirated and sent for chemistry and culture. Depending on the individual radiologist's preference, the patient is carefully transferred to a fluoroscopy room, either after introduction of the 0.018-in. (0.46-mm) guidewire into the pseudocyst or after the tract is dilated with the 6.3-French Cope dilator and the 0.038-in. (0.97-mm) 3-mm J guidewire has been coiled in the cyst. The tract is then further dilated to 8 or 10 French.

A modified 8-French Percuflex ureteral double-J stent (Medi-tech, Watertown, MA) is introduced with its pusher catheter and positioned so that one end curls in the pseudocyst, the other in the stomach. Modification of the double-J stent involves shortening the length to 12 cm, measured with both pigtailed formed, from outer margin to outer margin. The presence of multiple side holes within the pigtailed and the absence of side holes along the shaft allow free drainage of the pseudocyst fluid directly into the stomach.

Two practical technical points warrant mentioning. The Cope dilator's tip, tapered to the 0.018-in. (0.46-mm) wire, is ideally designed so that it penetrates the anterior gastric wall easily without pushing it away. This creates an adequate initial tract for subsequent dilators. Secondly, it is worth overdilating the tract one or two French sizes, or using an introducer sheath, so that the double-J catheter will encounter little resistance during insertion. A heavy-duty guidewire may be necessary for dilatation through the muscular antrum.

Nasogastric suction and IV fluids are maintained for 24 hr to allow the anterior gastric wall puncture to seal. The patient can usually be discharged the following day, and follow-up CT is obtained in 2–4 weeks or as symptoms indicate. Other investigations including ERCP, sinography, and sonography were not needed in our patients.

Results

Between May 1985 and January 1988, five retrogastric pseudocysts in four patients were treated with this technique. The patients were 31–81 years old. All the pseudocysts fulfilled the basic requirement of being directly in contact with

Received July 11, 1988; accepted after revision September 13, 1988.

¹ Department of Radiology, Leonard Morse Hospital, 67 Union St., Natick, MA 01760. Address reprint requests to B. A. Sacks.

² Department of Radiology, Beth Israel Hospital, Boston, MA 02215.

³ Department of Surgery, Leonard Morse Hospital, Natick, MA 01760.

⁴ Department of Gastroenterology, Leonard Morse Hospital, Natick, MA 01760.

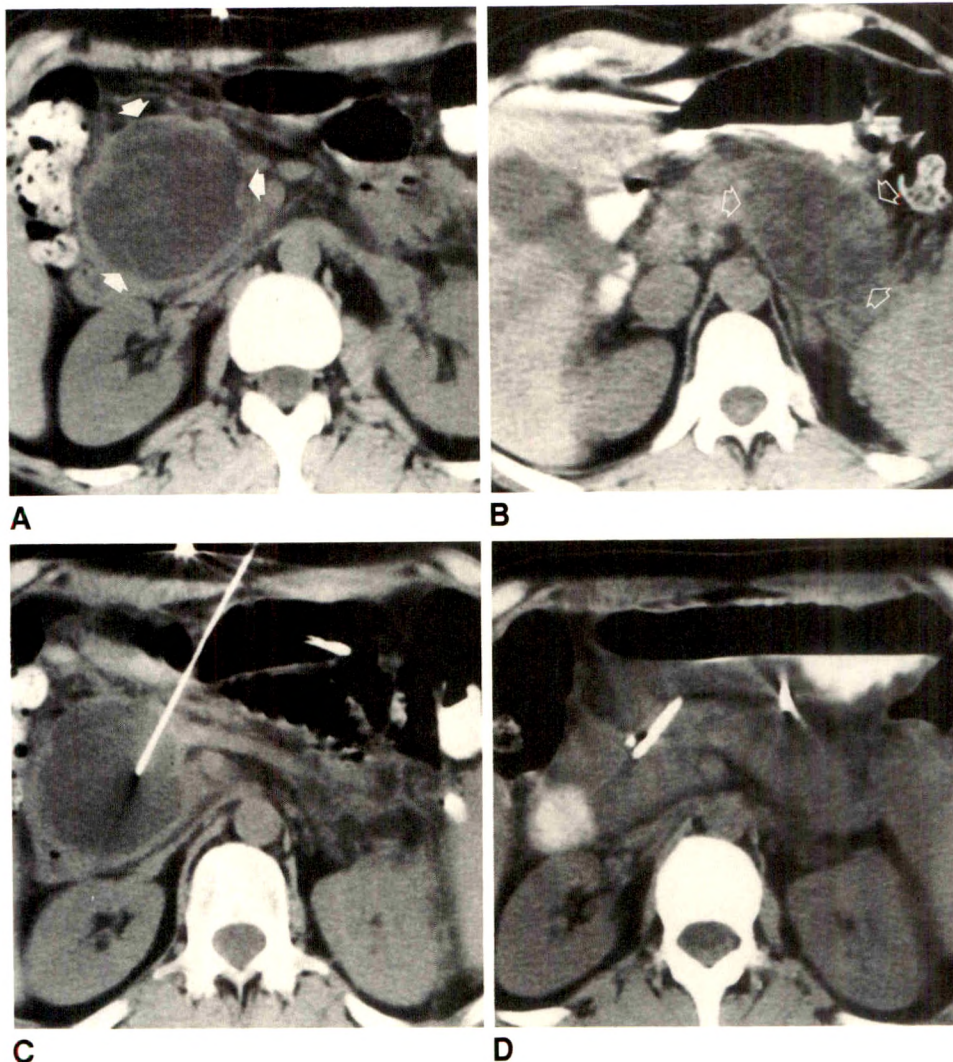
Fig. 2.—Patient in whom two pseudocysts were drained.

A, CT scan shows pseudocyst (arrows) arising from pancreatic head.

B, Second pseudocyst (arrows) in tail of pancreas.

C, Percutaneous transgastric puncture of pseudocyst in head of pancreas through proximal antrum.

D, CT scan 2 weeks after procedure shows marked reduction in size of both pseudocysts. Stents are still in place.



through the dilator. In a recent series [3], pseudocyst-ductal communication in four patients closed in two and persisted in two during external transgastric drainage. In the latter two patients, the drainage catheters were removed after 6 weeks anyway, without recurrence of the pseudocysts. Sinography in two patients in another series [5] showed direct communication of their pseudocysts with obstructed pancreatic ducts. The pseudocysts completely resolved in both patients, without recurrence. These outcomes and the results in our patients (as well as those reported by others [6, 7]) who were successfully drained internally without knowledge of associated fistulas support proceeding with internal drainage even if an initial sinogram shows ductal communication. The intention is that a long-term communication between the cyst and the stomach is created by the catheter and that it persists, as needed, even after the stent passes or is removed.

Another unresolved issue is whether internal drainage is appropriate when the initial pseudocyst aspirate returns viscous fluid. If the fluid is very thick or frankly purulent, we would opt for external transgastric drainage. However, there will be borderline cases, and in that situation a clinical decision

has to be made whether to proceed with a larger caliber stent or external drainage. One approach might be initial external drainage with subsequent conversion to internal drainage after the fluid has cleared and become less viscous.

Both complications occurring in our patients were technical. Manipulation of double-J catheters in the gastrointestinal tract is different from such manipulation in the genitourinary tract, and a definite learning curve exists. As physicians obtain more hands-on experience, these problems should not occur. Other potential problems include inadequate drainage of the pseudocyst due to premature spontaneous extrusion of the stent, obstruction of the catheter by debris, and required removal of stents endoscopically or fluoroscopically with a loop snare if they do not ultimately pass by themselves. From experience to date, the risks appear acceptable for the significant advantages gained by internalized drainage.

CT guidance offers superior control for the initial planning and puncture, with all aspects of the cross-sectional anatomy visible. However, once a guidewire is in a stable and satisfactory position, fluoroscopy control is advisable for the final tract dilatation and double-J stent positioning.

Technical Note

A New Technique for Removing Occluded Double Mushroom-Tipped Biliary Endoprostheses

Eugene Y-C Yeung,¹ Christopher O'Donnell,² Preston Carvalho,¹ and Andreas Adam¹

Percutaneous biliary endoprostheses are often used for internal drainage of malignant bile-duct obstructions [1–3]. Of the many different endoprostheses that are available, the double mushroom-tipped stent is one of the successful recent designs [3]. However, if the patient lives long enough, any type of stent will eventually become occluded.

We describe a technique by which we have removed the double mushroom-tipped stent successfully on seven occasions. We removed stents from six patients with hilar strictures (one patient had his stent changed twice); all six patients would otherwise have needed permanent external drainage.

Technique of Removal

The bile-duct system is punctured and opacified with contrast medium. A guidewire and catheter are inserted and negotiated alongside the stent and through the stricture to lie in the bile duct distal to the stricture. The catheter/guidewire combination is then manipulated into the distal mushroom, and the guidewire is advanced through the hole in the distal mushroom tip (Fig. 1A). We usually use a curved-tip catheter for biliary manipulations. The catheter is then advanced, pushing the stent distally. We usually use a 9-French catheter to push; if sufficient force cannot be generated, a stiffer catheter, a dilator, or a stiffer guidewire may be used. The stent can usually be pushed in this manner so that its distal tip rests in the duodenum and its proximal end is in or past the bile-duct stricture.

Advancement of the stent past this position is often impossible because the catheter/guidewire tends to loop in the duodenum (Fig. 1B). If this is the case, the catheter and wire are withdrawn from the distal mushroom and pulled back up the bile duct. The proximal lumen of the stent is then cannulated, either via the proximal end hole or the mushroom, and the catheter is readvanced to push the entire

stent into the duodenum (Fig. 1C). A sharp tug on the catheter usually withdraws it from the stent, leaving the stent entirely within the duodenum. A replacement endoprosthesis can then be inserted at the same session. Figures 2 and 3 are radiographs made during the procedure.

Results

We have employed our technique of removal on nine occasions in eight patients (one patient had his stent changed twice after reblockage some months later), all presenting with blocked stents and recurrent cholangitis (age range, 40–81 years; median, 64 years). All of the patients had hilar malignancies, and all had a single stent draining either the right or left duct into the common bile duct. Commercially available mushroom-tipped stents are not usually long enough to reach the duodenum from the liver hilum.

We removed the stents successfully on seven occasions. In one case, the guidewire could not be advanced through the distal mushroom tip because the tip was wedged against the side wall of the common bile duct. We solved this problem by using a second guidewire/catheter combination running alongside the stent and into the duodenum. Changing the patient's position and pushing this second guidewire distorted the bile duct sufficiently to allow the first guidewire to advance through the duct. The catheter/guidewire looped in the duodenum during advancement of the stent in five cases; this was easily overcome by catheterizing the proximal end hole or mushroom and then pushing the stent. We were unable to remove the stents in two patients because we could not

Received August 19, 1988; accepted after revision October 12, 1988.

¹ Department of Diagnostic Radiology, Royal Postgraduate Medical School, Hammersmith Hospital, Du Cane Road, London W12 0HS, U.K. Address reprint requests to E. Y-C Yeung.

² Department of Diagnostic Radiology, Royal Melbourne Hospital, Melbourne 3050, Australia.

AJR 152:527–528, March 1989 0361–803X/89/1523–0527 © American Roentgen Ray Society

Technical Note

Scrape Biopsy of Malignant Biliary Stricture Through Percutaneous Transhepatic Biliary Drainage Tracts

Conrad K. Y. Yip,¹ J. W. C. Leung,² M. K. M. Chan,³ and C. Metreweli¹

We describe a new technique for scrape biopsy of bile-duct strictures that can be done at the same time as percutaneous transhepatic biliary drainage.

Materials and Methods

Between July 1987 and May 1988, 15 patients with malignant bile-duct strictures diagnosed by sonography, CT, and ERCP/percutaneous transhepatic cholangiogram were included in the study. Their conditions were considered inoperable on the grounds of sonographic and CT findings, and endoscopic stent insertion was unsuccessful. The age range was 26–81 years (mean, 52 years). Male to female ratio was 7:8. The underlying diseases in the 15 cases were as follows: carcinoma of the pancreas (four), carcinoma of the gallbladder (three), cholangiocarcinoma (three), carcinoma of the common bile duct (one), secondary hilar tumors (three), and lymphoma (one).

Percutaneous transhepatic biliary drainage was performed by the standard technique: The stricture was negotiated with either a Lunderquist or Amplatz extra-stiff guidewire (Cook, Bloomington, IN) and then dilated up to 8 French by dilators (Judkins Coronary Dilator Series, William A. Cook, Melbourne, Australia). The scrape biopsy was then performed in the stricture by a modified "cutting dilator" (Fig. 1).

The modified "cutting dilator" was made from a 7-French, 20-cm-long dilator (Judkins Coronary Dilator Series, William A. Cook) by incising four forward-pointing flaps spaced 1 cm apart, in a spiral arrangement, over the distal shaft of the dilator. The incisions were made with a surgical blade at a 30° angle to the shaft of the dilator (Fig. 2A,B), stopping when the lumen of dilator was just reached so that its strength was not weakened. The flaps were erected by gentle rotation of the flat surface of the blade (Figs. 2 and 3). For distal strictures beyond the reach of the dilator, we used a 7-French angiocatheter with the flaps cut similarly.

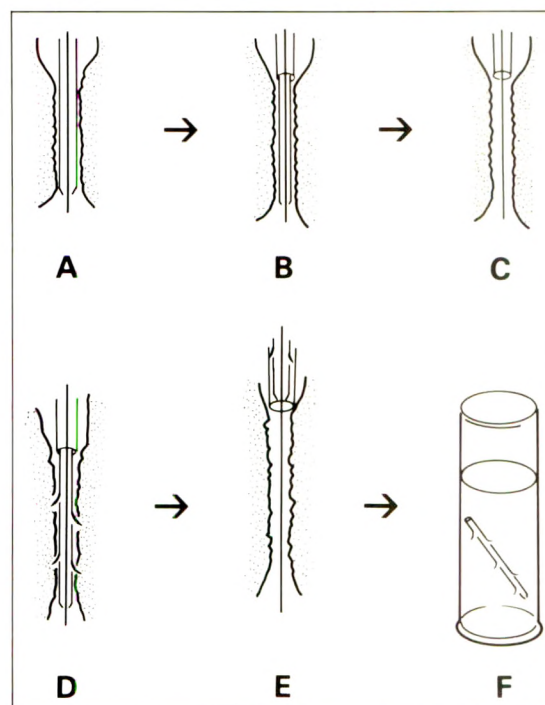


Fig. 1.—Diagram of procedure.

- A, Stricture is dilated to 8 French by dilators.
- B, 8-French dilator is removed and 8-French sheath with 8-French dilator reinserted (Sheath: 8 French, 13 cm, Desilets-Hoffmann set).
- C, 8-French dilator is removed leaving 8-French sheath above stricture.
- D, Modified 7-French dilator with forward flaps is inserted and three or four to-and-fro strokes are made through stricture.
- E, Modified 7-French dilator is retracted into sheath and then both are withdrawn together. Guidewire is left in situ for further procedures.
- F, Modified dilator is flushed with saline and its distal part containing the flaps is cut and collected in bottle along with saline. The sheath is also flushed with saline, which is collected in same bottle. Samples are sent for cytology and cell blocks.

Received August 3, 1988; accepted after revision October 7, 1988.

¹ Department of Radiology, Prince of Wales Hospital, Shatin, N.T., Hong Kong. Address reprint requests to C. K. Y. Yip.

² Department of Medicine, Prince of Wales Hospital, Shatin, N.T., Hong Kong.

³ Department of Pathology, Prince of Wales Hospital, Shatin, N.T., Hong Kong.

Changes in the Epididymis After Vasectomy: Sonographic Findings

Lionel J. Jarvis^{1,2}
Paul A. Dubbins¹

Scrotal sonograms were obtained in 31 men before vasectomy and at 2 and 12 months after vasectomy to determine the effect of the surgery on the sonographic appearance of the testis and epididymis. The sonographic appearance of the testis was unchanged after vasectomy. However, in 14 men (45%), there were persistent changes in the epididymis. These consisted of enlargement (14 patients), development of cysts (11 patients), and an inhomogeneous echo pattern (five patients). The presence of these sonographic changes was unrelated to symptoms.

The history of vasectomy in men referred for scrotal sonography should be noted so that the altered sonographic appearance of the epididymis may be interpreted properly.

Vasectomy is a popular method of male contraception, so that a significant proportion of men referred for scrotal sonography will have had a vasectomy. No study to date has evaluated the sonographic appearance of the testis and epididymis after vasectomy; therefore, we undertook a prospective study to assess the scrotum before and after vasectomy.

Subjects and Methods

Thirty-four men referred by general surgeons agreed to participate in the study. All were healthy with no history of trauma, surgery, or any disease involving the scrotum. Participation was voluntary, and informed consent was obtained. Of the 34 patients initially entering the study, two subsequently declined vasectomy and one refused further sonographic assessment. Of the remaining 31 patients, two were unavailable for follow-up at 1 year. The average age of the 31 men was 35 years.

Sonograms of the epididymis were obtained within 1 week before vasectomy by using real-time, direct-contact scanning with a 7.5-MHz mechanical-sector transducer. Both testes and epididymides were scanned in longitudinal and transverse planes, and the two sides were compared. Longitudinal and transverse dimensions of the testis were measured. The size of the epididymis was determined by measuring the largest diameter of the head of the epididymis and the diameter of the body of the epididymis posterior to the proximal third of the testis.

Sonography was repeated in a similar fashion 6–10 weeks after vasectomy and 1 year after vasectomy. All sonograms were obtained by the same radiologist, who had access to patient data. Subsequent interpretation of sonograms was done by consensus of two radiologists.

Results

Five patients had complications after vasectomy. Four experienced scrotal discomfort for several weeks, which subsequently resolved. Another had a post-operative scrotal infection requiring antibiotics. All were asymptomatic by 1 year. Sonograms showed no abnormality of the testis before vasectomy and no change after vasectomy.

Received June 16, 1988; accepted after revision October 28, 1988.

¹ Department of Diagnostic Ultrasound, Plymouth Group Hospitals, Freedom Fields Hospital, Greenbank Rd., Plymouth, Devon PL4 7JJ, United Kingdom. Address reprint requests to P. A. Dubbins.

² Present address: Department of Diagnostic Radiology, Royal Naval Hospital, Haslar, Gosport, Hampshire PL12 2AA, United Kingdom.

AJR 152:531–534, March 1989

0361–803X/89/1523–0531

© American Roentgen Ray Society

Fig. 1.—Longitudinal sonograms of left testis and epididymis before vasectomy (A) and 2 months after vasectomy (B) show increase in thickness of epididymis from 2 to 10 mm. Body of epididymis (arrows). T = testis.

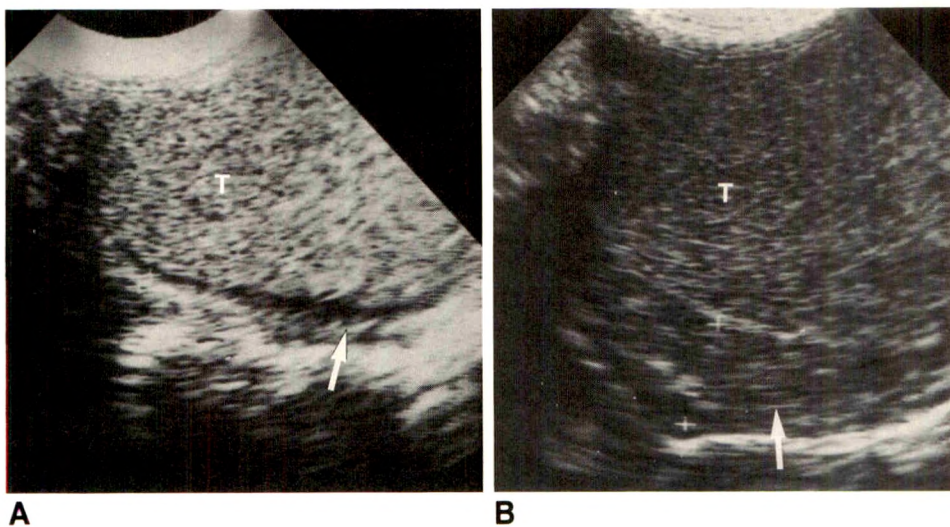


Fig. 2.—Longitudinal sonograms of



Duplex Doppler Sonography of Renal Transplants: Lack of Sensitivity and Specificity in Establishing Pathologic Diagnosis

Steven M. Genkins^{1,2}
 Fred P. Sanfilippo³
 Barbara A. Carroll¹

Recent reports have suggested the value of duplex Doppler sonography in the assessment of renal transplant function. Accurate diagnosis of acute rejection and its distinction from acute tubular necrosis and cyclosporine A toxicity have been claimed. We undertook a combined retrospective and prospective analysis of duplex Doppler examinations performed over a 2-year period to assess the value of such studies in evaluating renal allograft dysfunction. Seventy-seven sonographic examinations were performed on 77 renal transplants. A mean resistive index was calculated from Doppler measurements within main, segmental, and interlobar renal arteries by using the following ratio.

$$\frac{\text{peak systolic blood-flow velocity} - \text{minimum end-diastolic blood-flow velocity}}{\text{peak systolic blood-flow velocity}}$$

Forty-eight Doppler results were correlated with transplant biopsies and 29 with clinical course. Twenty-three episodes of acute allograft rejection were confirmed. When a resistive index of greater than or equal to 0.9 was used to indicate acute rejection, sonography had a sensitivity of only 9% and a specificity of 91% for this diagnosis. In one of eight cases of cyclosporine A toxicity and in three of six examples of acute tubular necrosis, the resistive index was greater than 0.9. In all six instances of chronic rejection, the resistive index was less than 0.84. None of eight patients with evidence of infection had a resistive index greater than 0.9. The resistive index range of 12 normally functioning allografts was 0.57–0.69. Correlation between the resistive index and the severity of arterial and arteriolar changes on biopsy was poor.

An increased resistive index of renal transplant blood flow, as measured by duplex Doppler sonography, usually signals pathologic changes in an allograft. However, our data indicate that this test is not as sensitive or specific in identifying the cause of transplant dysfunction as has been suggested previously.

Organ transplantation has become the preferred treatment for end-stage renal disease. In 1980, 4697 renal transplants were performed in the United States. Five years later, this number had increased to 7695 [1]. By 1985, there were over 25,000 functioning renal allografts in this country [1]. Transplant survival also has improved, largely because of more effective immunosuppression with cyclosporine A (CsA). One-year cadaveric allograft survival has increased from 53% in 1977 to 68% in 1984, while 1-year survival of living-related allografts has improved from 78% to 88% in the same time period [1].

In order to guide proper therapy in the large and growing renal transplant patient population, it has become increasingly important to develop noninvasive techniques that reliably detect and discriminate between such allograft complications as obstruction, rejection, CsA toxicity, acute tubular necrosis (ATN), and infection. Duplex Doppler sonography is one such technique, and several recent studies have suggested its value in assessing renal transplant dysfunction [2–13]. To determine the efficacy of this test, we undertook a combined retrospective and prospective study of sonographic examinations performed on renal allografts at our institution.

Received February 29, 1988; accepted after revision October 31, 1988.

¹ Department of Radiology, Box 3808, Duke University Medical Center, Durham, NC 27710.

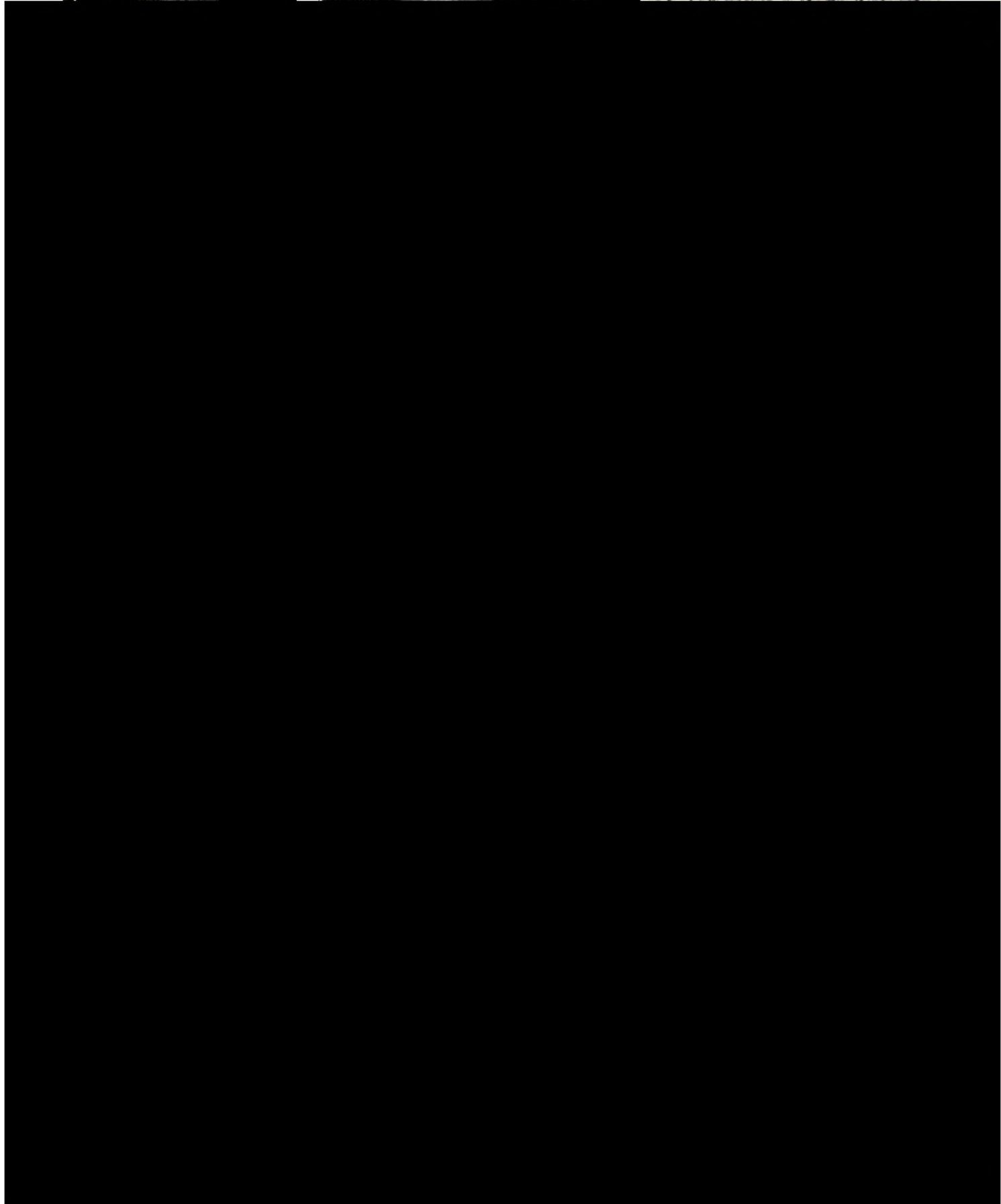
² Present address: Department of Radiology, Presbyterian Hospital, 200 Hawthorne Lane, P.O. Box 33549, Charlotte, NC 28233–3549. Address reprint requests to S. M. Genkins.

³ Department of Pathology, Box 3712, Duke University Medical Center, Durham, NC 27710.

AJR 152:535–539, March 1989

0361–803X/89/1523–0535

© American Roentgen Ray Society



produced the highest RIs. Surprisingly, three of six examinations that yielded an RI greater than 0.9 and that had an associated biopsy were of allografts that had no evidence of vascular or glomerular disease. One of six had only mild (grade 1) vascular and glomerular changes. Interestingly, all three of the transplants with an RI greater than 0.9 and no evidence of vascular or glomerular disease had severe tubular changes (grades 2 or 3). Thus, the pathologic basis for use of the RI in assessing malfunctioning renal allografts is uncertain.

A technical problem further limited the reliability of the duplex examination as performed on our sonographic systems. In those situations in which diastolic blood-flow velocity was significantly decreased, exactly those allografts in which precise measurements were most important, a 125- or 200-Hz wall filter, the minimum then available, limited accurate quantitation of end-diastolic blood-flow velocity and thus hindered calculation of a valid RI (Figs. 1, 2A, and 3A). Because of this problem, it is apparent that the pulsatility index, which incorporates mean blood-flow velocity over a cardiac cycle, may be a more accurate and useful measure of overall transplant perfusion. Moreover, other sonography systems that permit the use of lower-frequency wall filters when operated in the duplex Doppler mode and the recently introduced color-flow systems may allow more accurate quantitation of low-velocity blood flow. In addition, color-flow analysis may facilitate assessment of global allograft perfusion and localization of small intrarenal arteries for quantitative Doppler interrogation.

One case in our series indicated (Fig. 4) that an adult allograft in an infant or young child may be a special situation that poses additional problems for the diagnostic accuracy of the duplex Doppler examination. Others [7, 19] have alluded to these problems also. Although the cause remains uncertain, the RI may be elevated in such transplants in the absence of allograft disease. Therefore, duplex Doppler findings in young renal transplant patients should be interpreted with great caution.

Because duplex Doppler sonography has extremely low sensitivity and less-than-100% specificity in diagnosing pathologic changes in renal transplants (acute rejection in particular) and because it does not reflect the degree of vascular pathologic changes in an allograft, we believe that the quantitative results of this test should not determine initial decisions about the management of renal transplant cases in which evidence of allograft malfunction exists. Sonography still should be used (1) to evaluate possible obstruction and the presence of peritransplant fluid collections and (2) to confirm intact venous and arterial blood flow. However, when obstruction has been excluded, intact blood flow has been documented, serum CsA levels have been found not to be especially high, microbiologic studies have proved unrevealing, and clinical course is not compatible with ATN, sonographically guided renal-transplant biopsy should be performed unless there is overwhelming clinical evidence of rejection. This procedure has low morbidity, even in the early postoperative period, and usually provides a specific pathologic diagnosis, permitting prompt institution of therapy, which, it is hoped, leads to an improved allograft salvage rate.

Once the cause of transplant malfunction has been established and therapy instituted, serial duplex Doppler studies can be used to follow response to treatment.

ACKNOWLEDGMENTS

We thank James D. Bowie and H. Dirk Sostman for advice during this study, Louis Humphrey for technical assistance with image retrieval, Ed Flowers for technical assistance with data management, Annette Duncan for clerical assistance, and Debbie Prince and Patricia Graham for secretarial assistance in manuscript preparation.

REFERENCES

1. Eggers PW. Effect of transplantation on the Medicare end-stage renal disease program. *N Engl J Med* **1988**;318:223-229
2. Arima M, Ishibashi M, Usami M, et al. Analysis of the arterial blood flow patterns of normal and allografted kidneys by the directional ultrasonic Doppler technique. *J Urol* **1979**;122:587-591
3. Arima M, Takahara S, Ihara H, et al. Predictability of renal allograft prognosis during rejection crisis by ultrasonic Doppler flow technique. *Urology* **1982**;19(4):389-394
4. Berland LL, Lawson TL, Adams MB, Melrose BL, Foley WD. Evaluation of renal transplants with pulsed Doppler duplex sonography. *J Ultrasound Med* **1982**;1:215-222
5. Buckley AR, Cooperberg PL, Reeve CE, Magill AB. The distinction between acute renal transplant rejection and cyclosporine nephrotoxicity: value of duplex sonography. *AJR* **1987**;149:521-525
6. Malfi B, Ferretti G, Messina M, et al. Echo-Doppler velocimetry in the diagnosis of renal artery stenosis on transplanted kidney. *Clin Nephrol* **1986**;26(4):181-184
7. Murphy AM, Robertson RJ, Dubbins PA. Duplex ultrasound in the assessment of renal transplant complications. *Clin Radiol* **1987**;38:229-234
8. Reinitz ER, Goldman MH, Sais J, et al. Evaluation of transplant renal artery blood flow by Doppler sound-spectrum analysis. *Arch Surg* **1983**;118:415-419
9. Rifkin MD, Needleman L, Pasto ME, et al. Evaluation of renal transplant rejection by duplex Doppler examination: value of the resistive index. *AJR* **1987**;148:759-762
10. Rigsby CM, Taylor KJW, Weltin G, et al. Renal allografts in acute rejection: evaluation using duplex sonography. *Radiology* **1986**;158:375-378
11. Rigsby CM, Burns PN, Weltin GG, Chen B, Bia M, Taylor KJW. Doppler signal quantitation in renal allografts: comparison in normal and rejecting transplants, with pathologic correlation. *Radiology* **1987**;162:39-42
12. Steinberg HV, Nelson RC, Murphy FB, et al. Renal allograft rejection: evaluation by Doppler US and MR imaging. *Radiology* **1987**;162:337-342
13. Taylor KJW, Morse SS, Rigsby CM, Bia M, Schiff M. Vascular complications in renal allografts: detection with duplex Doppler US. *Radiology* **1987**;162:31-38
14. Imbasciati E, Banfi G, Egidi F, Tarantino A, Ponticelli C. Morphologic patterns of renal allograft rejection. *Contrib Nephrol* **1987**;55:105-122
15. Kolbeck PC, Wolfe JA, Burchette J, Sanfilippo F. Immunopathologic patterns of cyclosporine deposition associated with nephrotoxicity in renal allograft biopsies. *Transplantation* **1987**;43(2):218-224
16. Ruiz P, Kolbeck PC, Scroggs MW, Sanfilippo F. Associations between cyclosporine therapy and interstitial fibrosis in renal allograft biopsies. *Transplantation* **1988**;45(1):91-95
17. Sanfilippo F, Kolbeck PC, Vaughn WK, Bollinger RR. Renal allograft cell infiltrates associated with irreversible rejection. *Transplantation* **1985**;40(6):679-685
18. Norris CS, Barnes RW. Renal artery flow velocity analysis: a sensitive measure of experimental and clinical renovascular resistance. *J Surg Res* **1984**;36:230-236
19. Patriquin H, O'Regan S, Yasbek S, Robitaille P. Evaluation of childhood renal allografts by the duplex Doppler method. Presented at the meeting of the American Institute of Ultrasound in Medicine, New Orleans, LA, October **1987**

Digital Skeletal Radiography: Spatial Resolution Requirements for Detection of Subperiosteal Resorption

Mark D. Murphey¹

Forty direct-magnification (2:1 enlargement) radiographs showing various severities of subperiosteal resorption and 40 normal studies were selected and digitized. Images were processed to produce varying resolution, from 1.42 to 11.4 lp/mm, corresponding to pixel sizes ranging from 0.04 to 0.32 mm. The conventional and digitized images were evaluated by six radiologists giving their decision confidence on a graded scale. Receiver operating characteristic analyses were performed from these data to compare the digital images with the conventional films. The results show significant improvement in diagnostic accuracy as pixel size decreases to the level of 0.08 mm. Digital images with pixel sizes of 0.04 mm (11.4 lp/mm) were not significantly different from the magnification radiographs in terms of observer performance.

In conclusion, for high-resolution skeletal imaging as needed for detection of subperiosteal resorption, spatial resolution of 5.7 lp/mm or less resulted in a significant loss of diagnostic accuracy, as compared with conventional films.

The shift from film-screen radiography to digital technology offers several advantages, including improvement in image retrieval, decreased film cost, elimination of lost studies, and increased availability to clinicians [1, 2]. The parameters for digital radiography necessary to maintain diagnostic quality are being evaluated [3-12]. Few reported studies have examined these requirements quantitatively in skeletal radiology [13, 14].

Reports have been published recently concerning digital requirements in chest radiography [3-12]. Chest radiography is most often performed with medium-speed film-screen combinations, whereas skeletal imaging frequently uses slow-speed film-screen combinations. These different technical factors are necessary because of various requirements for resolution and diagnostic quality. This would suggest that demands for digital applications would also differ.

Pixel size has been emphasized in previous reports because of its correlation with spatial resolution in digital radiography [3, 4, 7-9, 12]. The necessary pixel size to maintain spatial resolution and diagnostic quality needs to be defined for different applications. Identification of fine-detail (high-frequency) information requiring small pixel size, such as septal lines in chest radiography and subtle mucosal abnormalities in double-contrast colon examinations, has been reported [4, 7, 8, 12]. To my knowledge, however, similar studies in skeletal radiography have not been performed.

Detection of subperiosteal resorption in the phalanges requires high-resolution skeletal radiography, similar to septal lines in chest imaging, which in many institutions requires magnification techniques [15-17]. Because subperiosteal resorption is one of the most demanding in terms of resolution in skeletal imaging, it was deemed highly suitable as a test for digital radiology systems. We digitized

direct-magnification hand radiographs of patients with secondary hyperparathyroidism due to chronic renal failure. A similar group of normal radiographs was also digitized. The digitized images were computer-processed to provide images of

Received August 31, 1988; accepted after revision November 10, 1988.

¹ Department of Diagnostic Radiology, University of Kansas Medical Center, 2-162 Bell Memorial Hospital, 39th St. and Rainbow Blvd., Kansas City, KS 66103. Address reprint requests to M. D. Murphey.

AJR 152:541-546, March 1989

0361-803X/89/1523-0541

© American Roentgen Ray Society

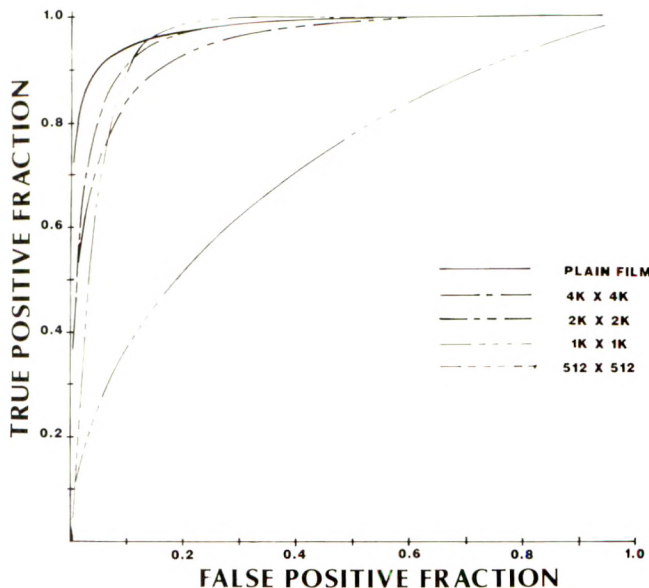


Fig. 2.—Receiver operating characteristic curves for detection of subperiosteal resorption in mild cases from original plain film and digitized images. 4K × 4K, 2K × 2K, 1K × 1K, and 512 × 512 images correspond to pixel sizes and spatial resolutions as described in Fig. 1.

TABLE 1: Chi-square Statistic from the Maximum Likelihood Estimate of the Receiver Operating Characteristic Curve Parameters

Plain Film vs Pixel Size of:	χ^2 (Probability ^a)	
	All Cases	Mild Cases
0.32 mm (1.42 lp/mm)	52.8 (.000)	55.0 (.000)
0.16 mm (2.85 lp/mm)	7.4 (.024)	7.7 (.021)
0.08 mm (5.7 lp/mm)	6.2 (.044)	6.1 (.047)
0.04 mm (11.4 lp/mm)	3.3 (.197)	3.4 (.187)

^a Probability that classes are the same.

TABLE 2: Area under Receiver Operating Characteristic Curves^a

Image	Area		
	All Cases	Mild Cases	Advanced Cases
Plain film	0.99	0.98	1.00
0.04 mm (11.4 lp/mm)	0.98	0.97	0.99
0.08 mm (5.7 lp/mm)	0.97	0.95	0.99
0.16 mm (2.85 lp/mm)	0.97	0.95	0.99
0.32 mm (1.42 lp/mm)	0.82	0.72	0.96

^a Curves are shown in Figures 1 and 2.

on the subset of examinations with only mild changes. The third ROC curve (not shown) compared the subset of advanced cases. Although certain areas of the curves overlap, in all groups of data there was a progressive increase in the area under the curves from the 0.32-mm pixel size image to the magnification plain film (Table 2).

The statistical estimates of probability of difference among the various ROC curves were computed (Table 1). For the ROC curves calculated from all cases as well as the mild subset, there was a statistically significant difference ($p < .05$) between the plain film vs images with pixel sizes of 0.32 mm, 0.16 mm, and 0.08 mm. The ROC curve evaluating the examinations with mild changes of subperiosteal resorption (Fig. 2) provides a clearer separation of the curves, which is on the basis of a more difficult visual task. The third ROC curve (not shown) evaluated the subset of more advanced cases and showed a difference only between the plain film and 0.32-mm pixel size image. Representative examples of mild and advanced cases of subperiosteal resorption on both the original plain film and digitized images are shown in Figures 3 and 4.

Discussion

The requirements of spatial resolution vary, depending on numerous factors including the system noise and the physical size, sharpness, and contrast of the object being examined. Both spatial and contrast resolution are important in diagnostic image quality. Only spatial resolution was varied in this study. Contrast resolution was held constant by use of the CLAHE algorithm. Contrast resolution is probably not as important in detecting subperiosteal resorption as in other tasks, such as breast microcalcification or evaluation of pulmonary nodules. This is at least partially due to the high contrast between bone and soft tissues.

In digital radiography, the issue of spatial resolution is related to questions of matrix and pixel size. Given the matrix size and physical dimensions of the field of view we can calculate that the pixel size is equal to the physical dimension divided by the matrix dimension size. Each line pair requires an ideal minimum sampling of at least two pixels. For example, a 1024 × 1024 matrix covering a field measuring 35 × 35 cm (~14 × 14 in.) would have a pixel size of 0.34 × 0.34 mm. In more familiar terms, the resolution is 1.4 lp/mm.

In our department, line-pair phantoms have a spatial resolution of 4 lp/mm for chest film-screen radiography, 8 lp/mm for typical nonmagnification film-screen skeletal images, and 12 lp/mm for direct-magnification (2:1 enlargement) hand radiographs. This increased spatial resolution necessary in skeletal radiography is accomplished by using slower speed systems, smaller focal spot sizes, and magnification techniques. If these differences in conventional film-screen spatial resolution for chest and bone radiography are considered, then digital radiology systems developed primarily for chest applications probably will be not suitable for skeletal imaging without modifications.

Digital systems must accommodate the increased spatial resolution in skeletal imaging to maintain similar diagnostic quality. If a digital system produces images that have less spatial resolution than their film-screen counterpart and that are statistically different in terms of diagnostic quality, then they are unlikely to be acceptable for a predefined diagnostic task. The digital system may still be acceptable for other diagnostic tasks. Before applications proceed, spatial-reso-

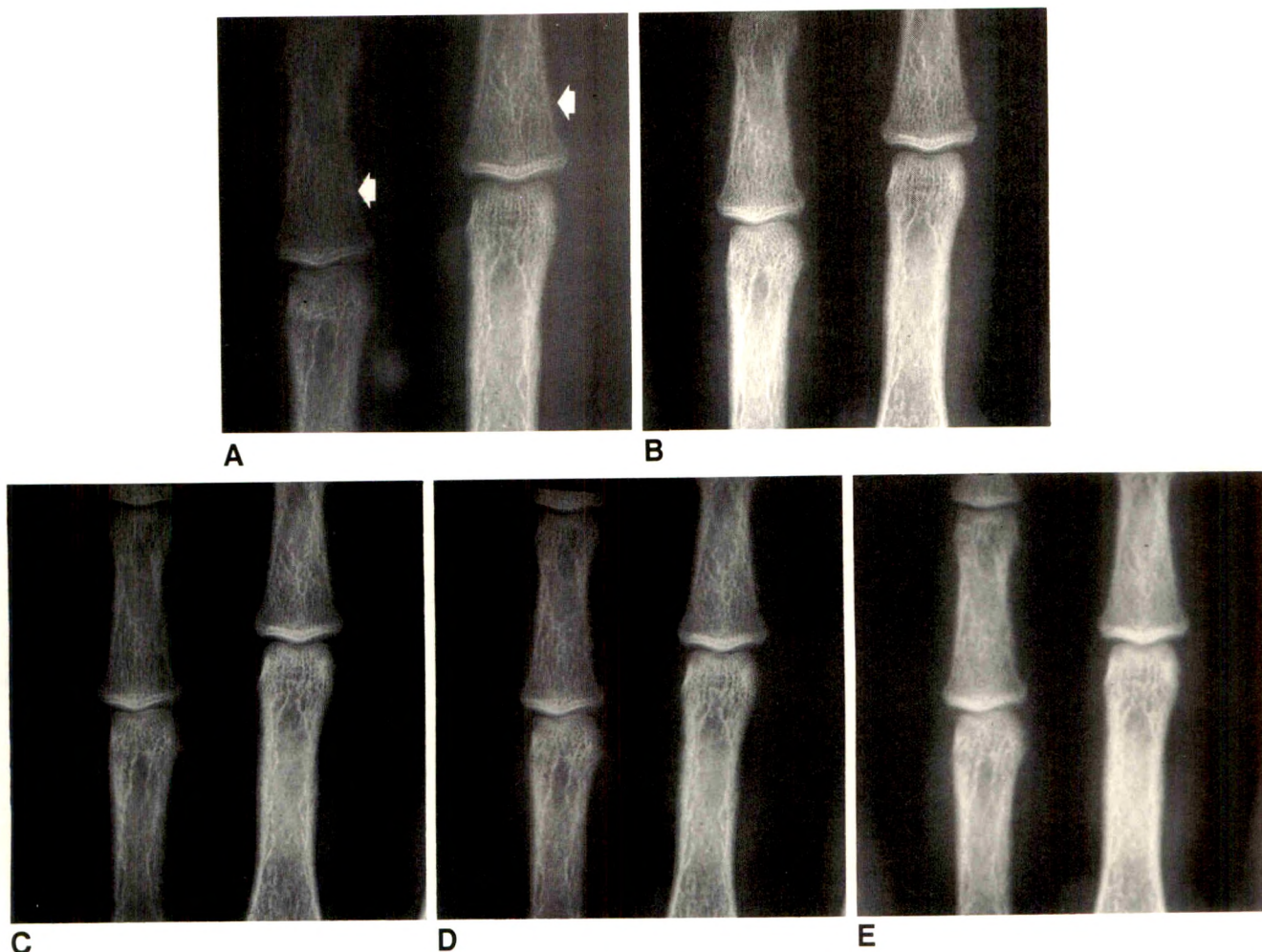


Fig. 4.—Representative example of advanced case of subperiosteal resorption mostly involving radial aspect of long and ring finger middle phalanges (arrows).

A, Original plain film.

B–E, Digital images with increasing pixel size (0.04, 0.08, 0.16, and 0.32 mm, respectively). Image quality progressively deteriorates with decreasing spatial resolution.

(ROC curve not shown), a difference was seen only at a pixel size of 0.32 mm (1.42 lp/mm), reflecting the relative ease of the diagnostic task.

Limitations of this study include the relatively small study size, which is unavoidable within practical constraints and is similar to other studies performed with chest radiography. Another limitation is that the gold standard is still a film-based system, and no direct pathologic data were available for the abnormal cases. However, parathyroid hormone levels were abnormal in all instances. Cases included in this series were only those considered abnormal by consensus opinion of two experienced observers. Finally, only the effects of spatial resolution were evaluated, with contrast resolution being held constant.

The implications of this study suggest that fine-detail skeletal applications will place increasing demands on spatial resolution in order to maintain diagnostic quality and accuracy. Although subperiosteal resorption is a good test of spatial

resolution, it cannot be compared with other diagnostic tasks. In terms of skeletal applications, work is in progress at this institution in an attempt to determine spatial-resolution requirements in evaluating nondisplaced fractures. This may be particularly important in relation to teleradiology.

We think that this study provides a relative gauge in terms of the most severe resolution demands that have been placed on digital systems. In many ways this is to be expected because higher spatial resolution is typical for skeletal film-screen systems. Although comparison of spatial-resolution requirements for differing diagnostic tasks is difficult, we know of no other studies showing a statistically significant difference in diagnostic quality at a higher spatial resolution (smaller pixel size) than that used in our evaluation.

Technical consideration such as image storage, retrieval, and processing (as well as monetary limitations) favor the use of smaller matrices, which implies larger pixel size. These constraints must be balanced with the known decrease in

Immature Bone Infarcts: Findings on Plain Radiographs and MR Scans

Peter L. Munk¹
Clyde A. Helms
R. Gary Holt

We studied the plain film findings in eight patients with immature bone-marrow infarction and correlated the findings with those of MR imaging in four of the cases. Seven patients had underlying systemic disease, including sickle cell disease (two), systemic lupus erythematosus (two), acute lymphocytic leukemia (one), non-Hodgkin lymphoma (one), and renal transplantation (one). In one patient, the bone infarct was

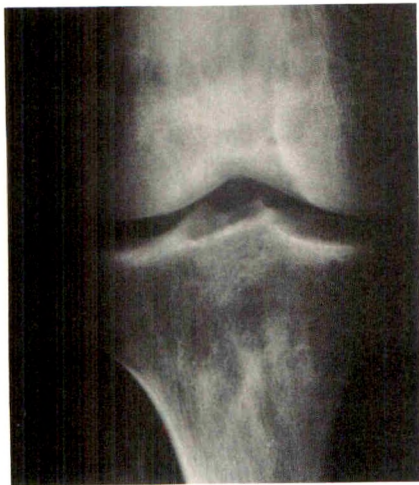


Fig. 4.—Immature bone infarct in a patient with sickle cell disease who had sudden onset of knee pain. Radiograph of knee shows patchy, mottled region of radiolucency with mild sclerosis of femur and tibia. Biopsy of tibia showed bone-marrow infarction.



Fig. 5.—Immature bone infarct in a patient with sickle cell disease. Radiograph of knee shows a patchy, mixed sclerotic and lytic lesion in distal diaphysis of femur. Biopsy, performed to exclude osteomyelitis, was consistent with early bone-marrow infarction.

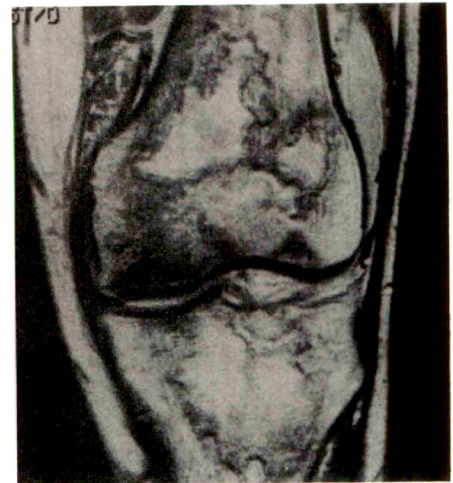


Fig. 6.—Immature bone infarct in a patient with acute lymphocytic lymphoma on chemotherapy, who presented with knee pain. Coronal MR image (2000/40) shows numerous lesions in both femur and tibia with high-signal centers and low-signal serpentine rims characteristic of bone infarcts. Only ill-defined, patchy lucencies were noted on conventional radiographs.

Discussion

Mature bone infarcts have a relatively typical appearance: a densely calcified area in the medullary cavity with serpentine borders surrounding a central radiolucent area [2]. In the early stages of bone infarcts, however, the plain film findings may be nonspecific and include only mottled bone rarefaction, sometimes with mild reactive sclerosis (Figs. 1A and 2–5). This was the appearance in all of our patients with immature infarcts, representing a combination of bone destruction, reactive new bone, and osteoporosis due to the concomitant hyperemia. Infection and malignancy often produce a similar radiographic appearance [5, 6]. The evolution of the more easily identified, chronic calcified state probably is due to a combination of calcific fat necrosis, bone apposition due to revascularization and repair, and osteoporosis of the surrounding bone as a result of the reactive hyperemia [7, 8].

Rao et al. [9] described the MR appearance of diaphyseal infarcts in patients with sickle cell disease. Chronic infarcts typically are of low signal (presumably due to fibrosis and/or calcification) on both T1- and T2-weighted sequences. Early infarcts, however, have intermediate to high signal on T1 sequences and high signal on T2, which is most likely a reflection of the edema associated with the infarct [7, 8]. The MR appearance of the early infarcts seen in our patients corresponded to the previous descriptions (Figs. 1B and 6). In our cases, the margins of the infarcted regions were delineated by a thin band of low signal relative to both the center of the lesion and the surrounding normal marrow [10]. This may be due to sclerosis and/or fibrosis at the infarct margin. The edges of the marrow infarcts had an appearance reminiscent of the serpentine margins seen on radiographs of chronic bone infarcts.

MR imaging was particularly useful in initially suggesting the diagnosis of infarction in all four of our patients in whom MR studies were available. Two of these patients had neoplastic disease, in whom the subtle plain film changes noted could have been due to tumor or infection. In both instances, the MR appearance of the lesions was thought to be sugges-

tive enough of bone marrow infarction (due to the similarity of previously reported MR images of bone infarct) that the patients should be followed clinically rather than undergo a bone biopsy [9, 10]. Follow-up on both patients (2 years and 1 year, respectively) shows no evidence of tumor or infection at the lesion sites.

Bone infarction is not routinely considered in immunocompromised patients. However, our observations suggest that when subtle radiographic changes are observed, particularly when several diaphyseal lesions are present, bone infarction should be added to the differential diagnosis. In patients presenting with subtle bone changes and a systemic process predisposing to bone-marrow infarction, MR imaging should be used.

REFERENCES

1. Greyson ND, Kassel EE. Serial bone-scan changes in recurrent bone infarction. *J Nucl Med* 1975;17(3):184–186
2. Koren A, Garty I, Katzuni E. Bone infarction in children with sickle cell disease: early diagnosis and differentiation from osteomyelitis. *Eur J Pediatr* 1984;142:93–97
3. Rao S, Solomon N, Miller S, Dunn E. Scintigraphic differentiation of bone infarction from osteomyelitis in children with sickle cell disease. *J Pediatr* 1985;107:685–688
4. Armas RR, Goldsmith SJ. Gallium scintigraphy in bone infarction: correlation with bone imaging. *Clin Nucl Med* 1984;9:1–3
5. Sweet DE, Madewell JE. Pathogenesis of osteonecrosis. In: Resnick D, Niwayama G, eds. *Diagnosis of bone and joint disorders*, 2nd ed. Philadelphia, Saunders, 1988:3188–3287
6. Robbins SL, Angell M. *Basic pathology*, 2nd ed. Philadelphia: Saunders, 1976:184
7. Beltran J, Herman LJ, Burk JM, et al. Femoral head avascular necrosis: MR imaging with clinical-pathologic and radionuclide correlation. *Radiology* 1988;166:215–220
8. Mitchell DG, Rao VM, Dalinka MK, et al. Femoral head avascular necrosis: correlation of MR imaging, radiographic staging, radionuclide imaging, and clinical findings. *Radiology* 1987;162:709–715
9. Rao VM, Fishman M, Mitchell DG, et al. Painful sickle cell crisis: bone marrow patterns observed with MR imaging. *Radiology* 1986;161:211–215
10. Vogler JB, Murphy WA. Bone marrow imaging. *Radiology* 1988;168:679–693

MR of Osteochondritis Dissecans and Avascular Necrosis of the Mandibular Condyle

Kurt P. Schellhas¹
 Clyde H. Wilkes²
 Hollis M. Fritts¹
 Mark R. Omlie³
 Lawrence B. Lagrotteria⁴

We studied 40 patients exhibiting radiologic changes of either osteochondritis dissecans (OCD) or avascular necrosis (AVN) involving the mandibular condyle to evaluate the structural changes associated with these lesions when using high-field-strength MR imaging. Various clinical indications for imaging each patient with routine radiography, tomography, and surface-coil MR included headache, temporomandibular joint (TMJ) and/or ipsilateral facial pain, joint crepitus, clicking, locking, and either recently acquired or changing (unstable) occlusal disorder. Radiologic findings included alterations in condyle morphology and MR signal characteristics compatible with either OCD or AVN or, in some cases, both. Previous nonsurgical mandibular trauma was temporally related to the onset of symptoms in eight patients. Five patients exhibiting either unilateral or bilateral AVN involving the condyles and condylar necks had undergone previous orthognathic surgery, including sagittal split mandibular osteotomies followed by intermaxillary fixation. One patient exhibiting condylar AVN with articular surface collapse and osseous destruction had undergone previous TMJ meniscectomy followed by insertion of a permanent Proplast implant. Thirty-one of 34 patients with no prior surgery and MR changes of condylar OCD/AVN had associated internal derangement of the TMJ meniscus. There was surgical confirmation of findings in 10 joints.

We assert that OCD and AVN are relatively common, clinically significant lesions of the mandibular condyle often associated with preexisting internal derangement of the temporomandibular joint.

Avascular (aseptic) necrosis (AVN) of the mandibular condyle is a relatively common disorder that is generally not recognized [1-5]. MR imaging is established as a highly sensitive and accurate procedure for the diagnosis of early osteochondritis dissecans (OCD) and AVN [6-17]. MR also has emerged as the procedure of choice for demonstration of internal derangements of the temporomandibular joint (TMJ) [3-5, 18-21]. Lesions with radiologic features of OCD and AVN involving the mandibular condyle and condylar neck are demonstrable with MR. Our intention is to demonstrate the appearance of these clinically significant but frequently unrecognized disorders with the use of high-field MR.

Materials and Methods

Forty patients (35 females and five males 14-61 years old, 45 joints) with MR findings compatible with either OCD or AVN were selected for study. All patients were evaluated with radiography, including submentovertex and anteroposterior, open-mouth, jaw-protruded radiographs; tightly collimated closed- and open-mouth lateral TMJ tomograms; and surface-coil MR. Indications for imaging included headache, TMJ and/or ipsilateral facial pain, joint crepitus, clicking and/or locking, and either acquired or changing malocclusion within 12 months of clinical evaluation (Table 1). Radiographic-tomographic findings considered suggestive of either AVN or OCD included alterations in condyle morphology, such as sharply defined articular surface defects (OCD) and either focal or generalized articular surface collapse (AVN). Associated findings such as hypertrophic spurs and articular sclerosis in either the temporal bone or condyle were noted. Selected patients with severe deformity on radiographs

This article appears in the January/February 1989 issue of *AJNR* and the March 1989 issue of *AJR*.

Received February 26, 1988; accepted after revision June 31, 1988.

Presented at the annual meeting of the American Society of Temporomandibular Joint Surgeons, Miami, FL, February 1988, and in part at the annual meeting of the American Association of Oral and Maxillofacial Surgeons, Boston, October 1988.

¹ Center for Diagnostic Imaging, 5775 Wayzata Blvd., Suite 190, St. Louis Park, MN 55416. Address reprint requests to K. P. Schellhas.

² Park Place Center, 5775 Wayzata Blvd., Suite 990, St. Louis Park, MN 55416.

³ 250 Central Ave. N., Wayzata, MN 55391.

⁴ 801 N. Plaza Dr., Suite 106, Schaumburg, IL 60195.

AJR 152:551-560, March 1989

0361-803X/89/1523-0551

© American Roentgen Ray Society

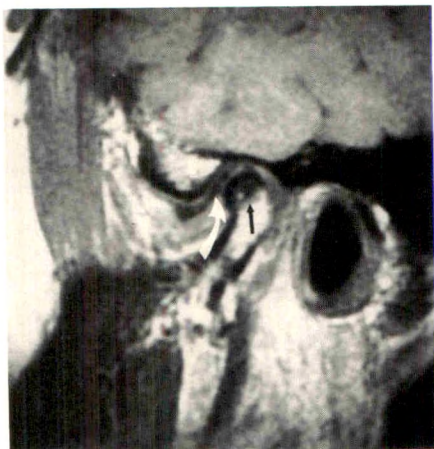
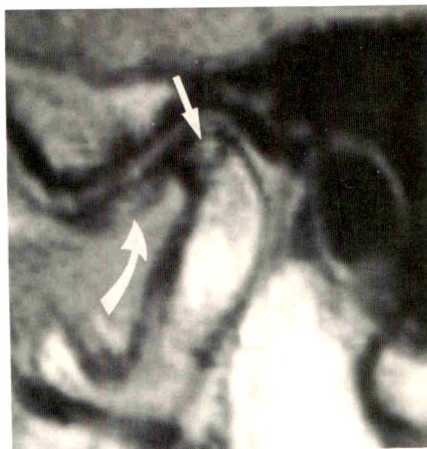
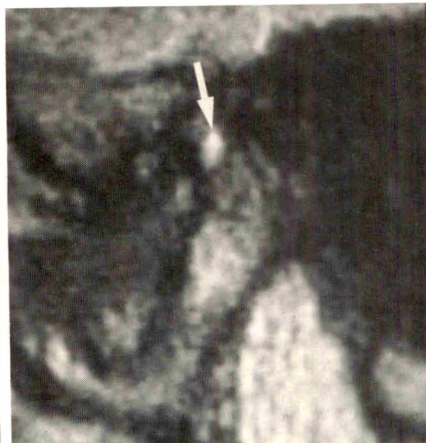


Fig. 5.—Subarticular avascular necrosis of mandibular condyle associated with internal derangement of temporomandibular joint meniscus in 34-year-old woman with 1 year history of temporomandibular joint clicking and crepitus and 3-month history of constant joint pain and acquired, fluctuating crossbite. MR image, 600/20, shows subarticular marrow hypointensity (straight arrow) beneath anteriorly displaced meniscus (curved arrow).



A



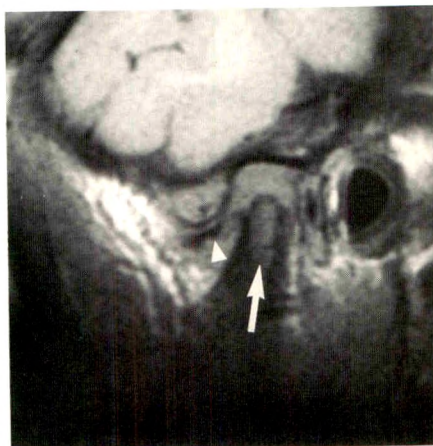
B

Fig. 6.—Subacute avascular necrosis with advanced internal derangement of temporomandibular joint in 61-year-old man with long history of temporomandibular joint clicking and recent onset of joint pain. Sagittal images, 2200/25 (A) and 2200/80 (B), show displaced and thickened meniscus (curved arrow) exhibiting high signal due to myxomatous degeneration. Subarticular condyle defect (straight arrows) exhibits intermediate (A) and high (B) signal.

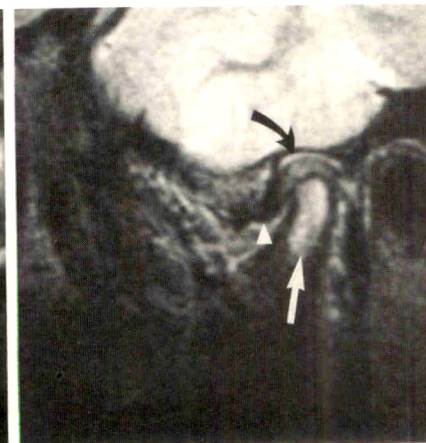
Fig. 7.—Subacute avascular necrosis with advanced internal derangement of temporomandibular joint associated with forward mandibular protrusion caused by intraoral splint and external head gear for attempted disk repositioning (no prior imaging procedures). This 14-year-old girl had malocclusion, 6-month history of temporomandibular joint locking, and 3-week history of intense joint pain after application of appliances.

A, Sagittal closed-mouth image, 600/20, shows condylar deformity with hypointense marrow signal (arrow). Meniscus (arrowhead) anteriorly displaced. Note widened joint space with absence of defined posterior meniscus attachment.

B, Sagittal image, 2200/100, reveals increased marrow signal (straight arrow) owing to medullary fluid. Superior compartment effusion (curved arrow) is present above swollen posterior attachment (above condyle). Arrowhead denotes displaced meniscus. Joint pain and tenderness promptly abated after removal of appliances.



A

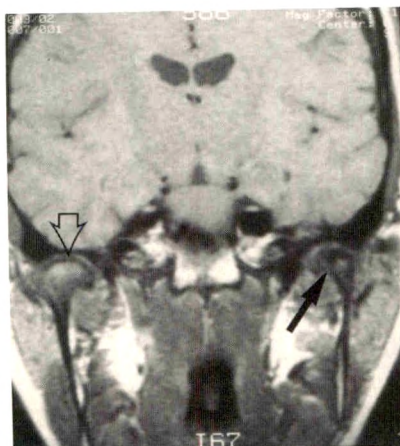


B

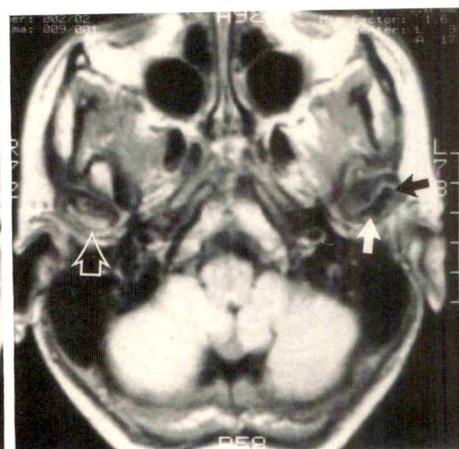
Fig. 8.—Old condylar avascular necrosis and deformity in 39-year-old woman with 3-month history of left-sided facial pain, temporomandibular joint locking, and malocclusion. (Study performed with head coil to evaluate "headache.")

A, Coronal image, 800/20, reveals hypointense and deformed left condyle (solid arrow) compared with normal right side (open arrow).

B, Axial image, 2000/20, shows condylar deformity and loss of marrow signal (solid arrows) compared with normal side (open arrow). Patient refused further investigation.



A

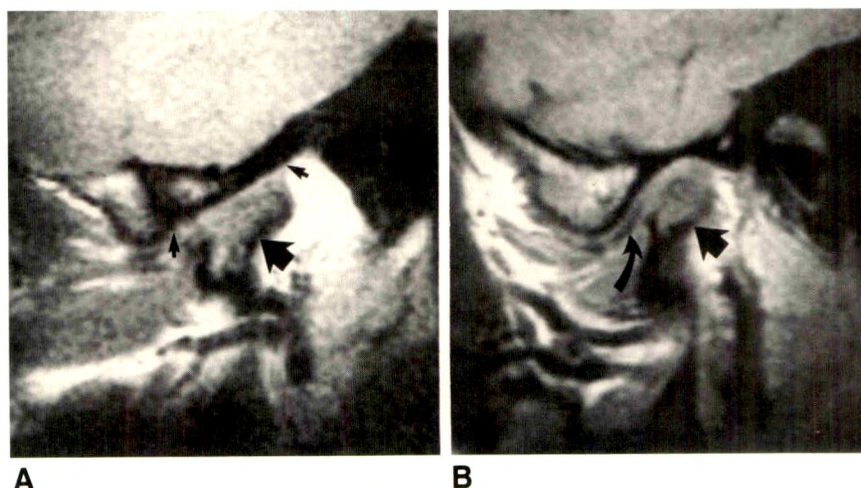


B

Fig. 13.—Old (A) and new (B) bilateral condylar avascular necrosis and meniscus derangements 3 months after failed orthognathic surgery in 15-year-old girl with painless openbite and retrognathia after unsuccessful initial orthodontics and subsequent sagittal split mandibular osteotomies, followed by 7½ weeks of intermaxillary fixation.

A, Sagittal image, 600/20, of left joint shows decreased signal from deformed condyle (large arrow). Note flattened articular surfaces of condyle and temporal bone (small arrows), suggesting long-standing disease. Tomograms revealed profound osseous sclerosis.

B, Decreased condylar signal (straight arrow) in opposite joint with displaced meniscus (curved arrow).



8–11, and 15) [14, 24–27]. We believe that many cases of acquired malocclusion, facial deformity, and condylar degeneration may be the consequence of AVN.

We found decreased marrow signal in cases of AVN on T1-weighted images (Table 3). Long TR/short TE images yielded variable signal characteristics with early AVN, healing, and OCD. Early AVN exhibited consistently high signal on T2-weighted images (Figs. 6, 7, 10, and 14) [14]. Acute OCD typically exhibited a hypointense central fragment surrounded by a zone of higher signal on both T1- and T2-weighted images (Figs. 2 and 3) [15]. We found GRASS images to be less reliable in evaluating these lesions than were either T1-weighted or long TR/short or long TE images due to the decreased spatial resolution and more variable signal characteristics associated with GRASS techniques [4, 21]. The MR findings associated with OCD and AVN in the mandibular condyle are similar to findings in the hips and major appendicular joints. The earliest detectable physiologic alteration in AVN appears to be vascular congestion with increased venous and capillary pressure, resulting in fluid transudation into the medullary space (Figs. 6, 7, 10, and 14) [14, 25]. MR is of particular value in detecting early lesions that may escape conventional radiographic detection. MR is also more accurate than scintigraphy in detecting early marrow changes prior to medullary infarction and structural collapse [9, 14, 16]. T2-weighted images are most helpful in demonstrating the early changes of marrow congestion and inflammation, both of which increase marrow fluid and result in increased signal. Simultaneous bone necrosis, inflammation, and healing may be observed on T2-weighted images (Figs. 6, 10, and 14). With late healing, there is replacement of normal, fat-containing hematopoietic marrow by hypointense fibrous tissue and sclerotic bone, resulting in loss of normal marrow signal (Figs. 8–12 and 14) [8, 12–14, 16]. Facial and joint pain; mechanical TMJ symptoms such as clicking, locking, and crepitus; and changing occlusion may be clinical hallmarks of ongoing necrosis, inflammation, and repair within the condyle and TMJ.

Radiologic changes of OCD and AVN are frequently observed in conjunction with joint effusion and internal derangement of the TMJ meniscus (Figs. 2, 3, and 5–16). This association suggests that meniscus derangement and joint

inflammation may initiate marrow inflammation. A high prevalence of pathologic hip effusion has been associated with acute and subacute AVN of the femoral head [10]. We have observed areas of subarticular decreased MR signal within the condyle after perforation of the disk or meniscus attachments, particularly when there is associated erosion of the overlying articular-bearing-surface cartilage (Figs. 2, 6, 9, and 10). Postmortem studies have shown that subcortical cystic change, marrow fibrosis, and osseous sclerosis frequently are found in degenerated or remodeled condyles beneath areas of cartilaginous erosion [28, 29]. These observations suggest that internal derangement of the TMJ, which often progresses to perforation, precedes and may initiate the development of either OCD or localized AVN and subsequent structural osseous changes.

Previous investigations have shown that blood supply to the condyle and condylar neck (proximal mandibular segment) may be significantly reduced after sagittal split mandibular osteotomy, especially if the split is proximal and associated with muscle stripping along the medial periosteal surface of the condylar neck [2, 30, 31]. AVN of the proximal mandibular segment may occur as a complication of orthognathic surgery and lead to malocclusion and facial deformity (Figs. 12 and 13) [2, 3, 31]. We believe that the postoperative altered condylar stress loading and joint immobilization during intermaxillary fixation may either initiate or aggravate meniscus derangement and lead to AVN (Figs. 12 and 13). We have observed both acute medullary congestion and internal derangement with nonsurgical condylar repositioning and altered stress loading (Fig. 7). The diagnosis of AVN and/or internal derangement of the TMJ meniscus before either nonsurgical occlusal adjustment or orthognathic surgery is of vital importance for treatment planning. We believe that a significant number of failed occlusal adjustment procedures, including orthognathic surgery, may be secondary to preexisting internal derangement of the TMJ and/or AVN. Condylar AVN and internal derangement of the TMJ should be considered in all cases of orthognathic surgical failure.

Because mandibular condyle OCD and AVN generally are not recognized, there are no accepted therapeutic measures. We suggest prompt “unloading” of the condyle once a diag-

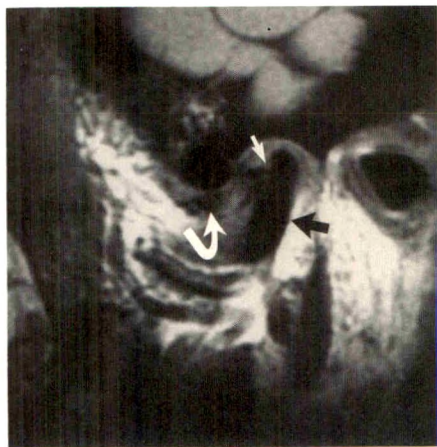


Fig. 15.—Extensive avascular necrosis, osseous deformity, condylar defect compatible with unstable osteochondritis dissecans, and advanced internal derangement of temporomandibular joint in 37-year-old woman with 10-month history of temporomandibular joint pain, locking, and acquired occlusal deficit. Sagittal MR image, 600/20, shows complete absence of marrow signal from both condyle and condylar neck (black arrow). Large articular surface defect (straight white arrow) is observed with late-stage meniscus (curved arrow) derangement. Surgery, 7 months after imaging, revealed depressed, pitted articular surface with partial resurfacing of condyle by fibrous tissue.

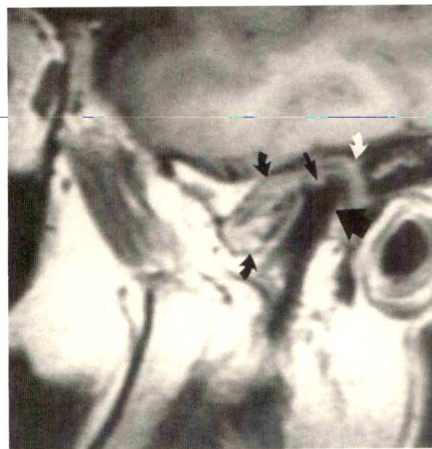


Fig. 17.—29-year-old woman with joint pain, dysfunction, crepitus, swelling, and worsening malocclusion 18 months after meniscectomy and permanent Proplast implant insertion. Destructive granuloma (curved arrows) fills joint capsule. Defect in articular surface of condyle (small straight arrow) secondary to direct granulomatous penetration through condylar surface. Absent marrow signal within condyle (large straight arrow) and condylar neck. (Reprinted from [3].)

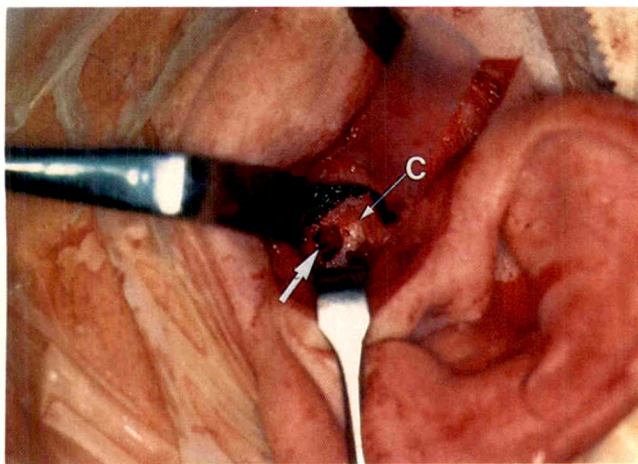


Fig. 16.—Unstable osteochondritis dissecans vs focal avascular necrosis in 52-year-old woman with long history of rheumatoid arthritis and

Norton, Jeffrey A. Jahn, the technical staff at the Center for Diagnostic Imaging, and Becky Borgerson for contributions. Special credit to Allan B. Reiskin for his earlier work and conclusions.

REFERENCES

1. Reiskin AB. Aseptic necrosis of the mandibular condyle: a common problem? *Quintessence Int* 1979;2:85-89
2. Behrman SJ. Complications of sagittal osteotomy of the mandibular ramus. *J Oral Surg* 1972;30:554
3. Schellhas KP, Wilkes CH, Fritts HM, Omlie MR, Heithoff KB, Jahn JA. Temporomandibular joint: MR imaging of internal derangements and post-operative changes. *AJNR* 1987;8:1093-1101, *AJR* 1988;150(2):381-389
4. Schellhas KP, Wilkes CH, Omlie MR, et al. The diagnosis of temporomandibular joint disease: two-compartment arthrography and MR. *AJNR* 1988;9:579-588, *AJR* 1988;151:341-350
5. Schellhas KP, Wilkes, CH, El Deeb M, Lagrotteria LB, Omlie MR. Permanent Proplast temporomandibular joint implants: MR imaging of destructive complications. *AJR* 1988;151:731-735
6. Totty WG, Murphy WA, Ganz WI, Kumar B, Daum WJ, Siegel MA. Magnetic resonance imaging of the normal and ischemic femoral head. *AJR* 1984;143:1273-1280
7. Ficat RP. Idiopathic bone necrosis of the femoral head: early diagnosis and treatment. *J Bone Joint Surg [Br]* 1985;67B:3-9

Pre- and Postoperative MR Imaging of the Cranio cervical Junction in Rheumatoid Arthritis

Elna-Marie Larsson¹
Stig Holtås¹
Stefan Zygmunt²

Ten patients with severe chronic rheumatoid arthritis with atlantoaxial subluxation were examined with conventional radiography and MR imaging of the cervical spine before and at an average of 6 months after posterior occipitocervical fusion. Periodontoid pannus formation was revealed by MR preoperatively in nine patients, all with mobile horizontal atlantoaxial subluxation. Compression of the medulla and/or upper cervical cord, due to subluxation and periodontoid pannus bulging into the spinal canal, was seen in seven patients. After the stabilizing surgery the periodontoid pannus had decreased in size in all patients with preoperative pannus. This reduction in the pannus seems to be the result of the atlantoaxial immobility achieved by the posterior fusion. Postoperatively, three patients had some remaining compression of the medulla and/or cord secondary to immobile subluxation, while the pannus posterior to the odontoid process had disappeared. Artifacts from the surgical stainless steel fixation material were confined to the posterior part of the neck on short TR/short TE MR images and did not interfere with the evaluation of the periodontoid region and the anterior part of the medulla/cervical cord.

We found that flexion and extension lateral radiographs, combined with sagittal short TR/short TE MR images in the neutral position, enable preoperative evaluation of patients with rheumatoid arthritis in the cervical spine. Postoperative MR should be performed only if there are residual or new symptoms.

MR imaging is useful in the evaluation of the cervical spine in patients with rheumatoid arthritis [1-5]. MR demonstrates narrowing of the spinal canal caused by vertebral dislocation and/or extradural granulation tissue, as well as the level(s) and degree of cord compression. Because the method is noninvasive and painless, it can be repeated easily and thus is suitable for the pre- and postoperative morphologic evaluation of these patients.

Compression of the medulla and upper cervical cord in patients with rheumatoid arthritis may be caused by atlantoaxial subluxation and mobility, as well as by periodontoid soft tissue; that is, pannus formation [6, 7]. The pannus consists of proliferative inflammatory granulation tissue derived from the synovia in the small joints and bursae adjacent to the odontoid process. After demonstrating significant spontaneous reduction of periodontoid pannus after posterior occipitocervical fusion in some of our patients [8] we undertook this prospective study. Our aim was to assess the extent of pannus and the degree of atlantoaxial subluxation and mobility and their effect on the medulla and cord before and after stabilizing surgery. The radiologic findings are described in this article; the clinical aspects of the patients with periodontoid pannus are discussed in another report [9].

Materials and Methods

From July 1986 through July 1987, 14 patients with chronic rheumatoid arthritis with atlantoaxial subluxation were surgically treated with posterior occipitocervical fusion. Ten of them, five men and five women 50-79 years old (mean age, 67 years), were examined with MR pre- and postoperatively and are described in this study.

This article appears in the January/February 1989 issue of *AJNR* and the March 1989 issue of *AJR*.

Received December 31, 1987; accepted after revision April 27, 1988.

This work was supported by a grant from the Swedish Medical Research Council, project no. K87-39X-08164-01A.

¹ Department of Diagnostic Radiology, University Hospital, S-221 85 Lund, Sweden. Address reprint requests to E.-M. Larsson.

² Department of Neurosurgery, University Hospital, S-221 85 Lund, Sweden.

AJR 152:561-566, March 1989
0361-803X/89/1523-0561
© American Roentgen Ray Society

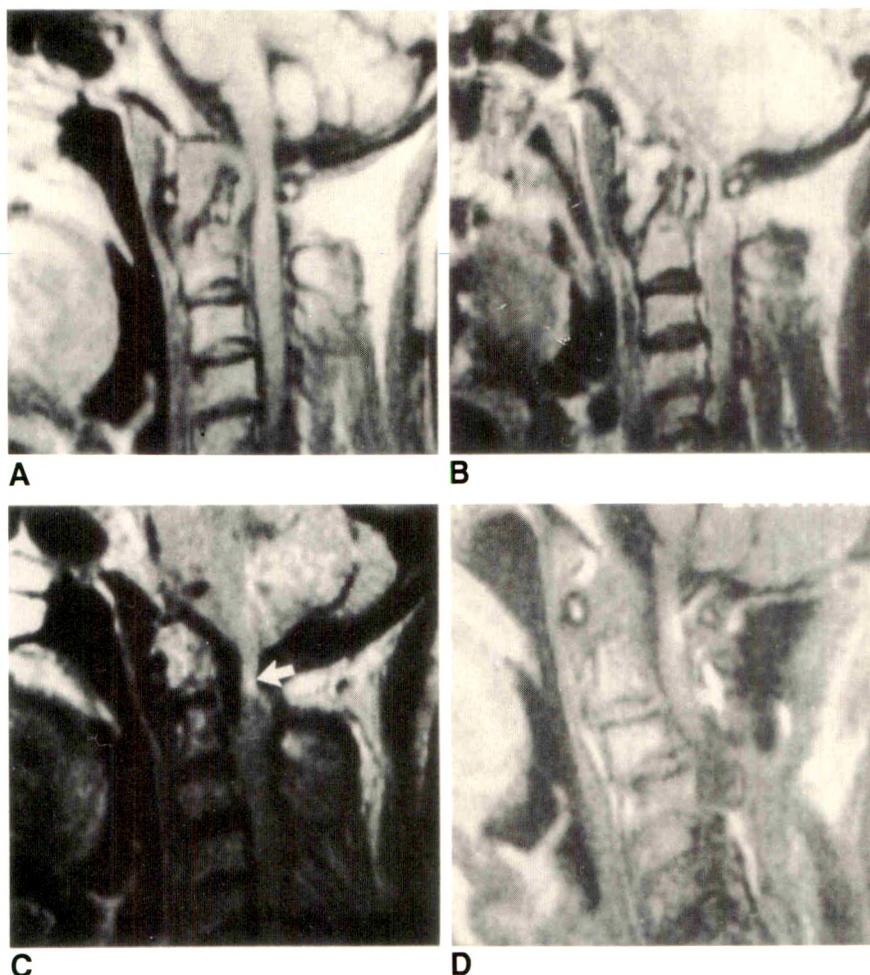
Fig. 2.—Case 3.

A, Preoperative short TR/TE sagittal MR image. Pannus with signal intensity equal to that of cord surrounds odontoid process. Compression of upper cervical cord is caused by horizontal atlantoaxial subluxation and pannus.

B, Preoperative long TR/TE sagittal MR image. Pannus exhibits high signal intensity.

C, MR slice adjacent to B. Increased signal intensity within cord at level of compression (arrow).

D, Postoperative short TR/TE sagittal MR image. Horizontal atlantoaxial subluxation and pannus have decreased. There is no remaining cord compression. (Odontoid process was better delineated on adjacent slice, which did not show spinal cord.)



patients (cases 4, 8, and 9) had no intraspinal pannus postoperatively; the compression was caused solely by the odontoid process (due to increased subluxation) (Fig. 4).

Preoperatively, five of the seven patients with symptoms and signs of myelopathy had compression of the medulla and/or cord, and one had isolated compression of the anterior subarachnoid space on MR. Postoperatively, three of these seven patients had recovered completely from their myelopathy, while four had improved. The neck pain had resolved or diminished after surgery in all eight patients with preoperative pain. The three patients with vertigo had improved postoperatively.

Increased signal intensity within the medulla or spinal cord at the level of compression was seen preoperatively on long TR/TE images in three patients (Fig. 2C), all with myelopathy, and could not be evaluated in two patients because of poor image quality. Postoperatively the upper cervical cord could not be evaluated on long TR/TE images because of artifacts from the fixation material (Fig. 5C).

Artifacts caused by the surgical fixation material (stainless steel wires and pins) were seen in the posterior part of the neck in all patients. The artifacts were smaller on short TR/TE images, usually extending to the posterior part of the cord, than on long TR/TE images, where they usually reached at

least the anterior border of the cord (Fig. 5). Thus, on postoperative short TR/TE images the odontoid process, the anterior subarachnoid space, and the ventral part of the medulla and upper cervical cord could be evaluated in all patients. The postoperative long TR/TE images could not be interpreted in this region because of artifacts.

Discussion

This study shows that compression of the medulla and upper cervical cord in patients with severe chronic rheumatoid arthritis is caused not only by atlantoaxial subluxation but frequently by periodontoid pannus also. Before the introduction of MR the intraspinal components of such pannus formation could be indirectly demonstrated by myelography, which may be very difficult to perform in patients with rheumatoid arthritis who have joint deformities and pain. CT myelography with sagittal reconstruction has recently been the preferred technique, as it depicts bony as well as soft-tissue abnormalities better than conventional radiography and myelography do [7]. However, CT myelography is invasive, does not allow direct sagittal imaging, and, postoperatively, may contain artifacts from the metallic fixation. MR provides

surrounded by pannus, erosion of the odontoid process may be overestimated on MR [5], as occurred in two of our patients (Figs. 3A and 3B).

In our investigation pannus was revealed preoperatively on MR in all nine patients with mobile atlantoaxial subluxation (Table 1). The increased signal intensity of the pannus on long TR/TE images in some patients could be consistent with an increased amount of water, as in inflammatory tissue (Fig. 2B). However, fibrous components probably are present within the pannus, since the signal intensity in pure inflammatory tissue should be higher than was noted in most patients in this study. Postmortem examinations support this assumption [6]. It has been suggested that mechanical dysfunction and instability in the craniocervical junction may cause formation of fibrous granulation tissue and hypertrophy of connective tissue elements as the abnormal response to chronic stresses and friction [14]. Thus, the rheumatoid per-

iodontoid inflammatory granulation tissue may increase due to hypertrophy of fibrous elements when instability has occurred. This is consistent with our findings in a previous report, where we noted that the periodontoid soft-tissue mass was largest in patients who had pronounced mobile horizontal atlantoaxial subluxation [5]. Incomplete reduction of horizontal atlantoaxial subluxation during surgery in some of the patients probably was due to fibrous pannus occupying the preodontoid space. Such pannus may also be partly responsible for incomplete reduction of horizontal subluxation on extension views on lateral radiographs (Table 1).

The reduction of pannus in our investigation seems to be the result of the atlantoaxial immobility achieved by the surgical posterior fusion. Only one of the patients exhibited atlantoaxial mobility on the 6-month postoperative examination. The pannus reduction in that patient could still have been caused by stabilization, since mobility did not recur until late in the postoperative period and was then smaller than before surgery.

In conclusion, our investigation has shown that compression of the medulla and upper cervical cord caused by atlantoaxial subluxation, as well as by periodontoid pannus, can be demonstrated by MR pre- and postoperatively. Further-

TABLE 1: Pre- and Postoperative Horizontal Atlantoaxial Mobility on Conventional Radiographs Compared with Size of Pannus on MR Images

Case No.	Sagittal Measurement (mm)			
	Atlantoaxial Mobility (Preodontoid Space in Flexion - Extension) on Conventional Radiographs		Odontoid Process + Posterior Pannus on MR Images	
	Preop	Postop	Preop	Postop
1	2 (18 - 16)	0 (12 - 12)	11	10
2	0 (2 - 2) ^a	0 (2 - 2)	-	-
3	7 (10 - 3)	0 (5 - 5)	12	10
4	5 (12 - 7)	0 (12 - 12)	11	9
5	12 (12 - 0)	4 (9 - 5)	16	10
6	7 (11 - 4)	0 (11 - 11)	10	7
7	5 (10 - 5)	0 (2 - 2)	11	9
8	3 (11 - 8)	0 (6 - 6)	13	9
9	5 (12 - 7)	0 (6 - 6)	16	10
10	9 (12 - 3)	0 (5 - 5)	16	9

Note.—Preop = preoperative; postop = postoperative.

^a This patient had severe vertical atlantoaxial subluxation; no pannus was present.

TABLE 2: Compression of Anterior Subarachnoid Space (SAS) and Medulla/Cervical Cord (MCC) on MR

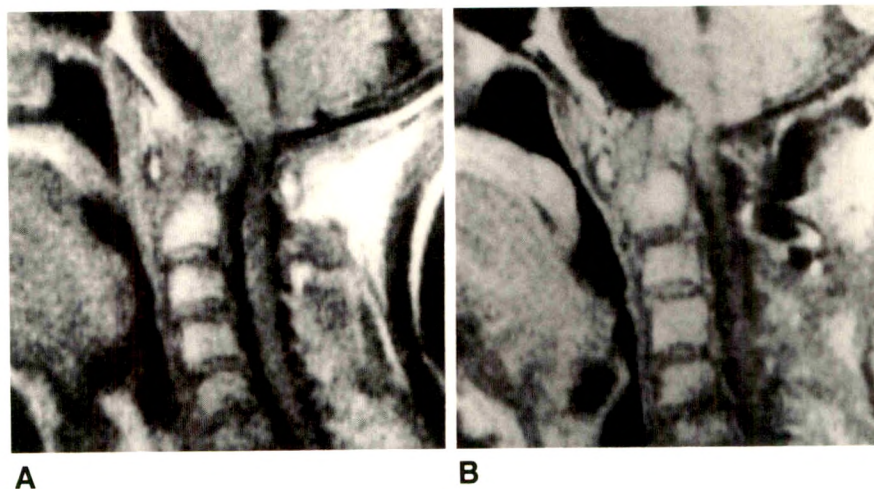
Case No.	Compression	
	Before Surgery	After Surgery
1	MCC	SAS
2	SAS ^a	SAS ^a
3	MCC	-
4	MCC	MCC ^a
5	MCC	SAS ^a
6	-	-
7	-	-
8	MCC	MCC ^a
9	MCC	MCC ^a
10	MCC	-

^a No pannus behind odontoid process; compression caused solely by odontoid process due to horizontal and/or vertical subluxation.

Fig. 4.—Case 9.

A. Preoperative short TR/TE sagittal MR image. Medulla and upper cervical cord are compressed by odontoid process (because of horizontal atlantoaxial subluxation) and pannus.

B. Postoperative short TR/TE sagittal MR image. Pannus behind odontoid process has disappeared. Horizontal subluxation is unchanged, but in addition there is vertical atlantoaxial subluxation. Because of this, the medulla and cord are still compressed.



Ectopic Ureterocele Without Ureteral and Calyceal Dilatation (Ureterocele Disproportion): Findings on Urography and Sonography

Jane C. Share¹
Robert L. Lebowitz

Eight infants and children (six girls) were seen over a 13-year period with duplex collecting systems and ectopic ureteroceles. In each, there was striking dissimilarity in size between the large ureterocele and its diminutive ureter and calyces. The upper moiety did not function and, except for the ureterocele, the indirect urographic and direct sonographic signs of duplication were absent or subtle. We call this entity ureterocele disproportion. Seven patients presented with urinary infection and one was found to have hydronephrosis of a dilated lower moiety in utero. Five had ipsilateral lower-pole reflux, which ranged in degree from 3 to 5 (on a scale of 1-5). Two had bilateral duplication; one of these had a typical contralateral ectopic ureterocele. The diagnosis of ureterocele disproportion was strongly suggested by urography and sonography and was confirmed at cystoscopy by direct puncture of the ureterocele and opacification of the upper moiety. All had surgery. The approach varied and depended on the status of the lower moiety and the contralateral kidney. One had incision of the ureterocele only. Five with lower-pole reflux had excision of the ureterocele and ipsilateral common-sheath reimplantation.

The term ectopic ureterocele has come to mean hydroureteronephrosis of the upper moiety of a duplex collecting system with the upper-pole ureter ending in a ureterocele (the dilated terminal or submucosal portion of the ureter). The affected upper moiety is obstructed, and often there is an element of dysplasia as well. Classic indirect urographic signs suggest the presence of the dilated, poorly functioning upper unit (Fig. 1A). In the usual case, the dilated upper-pole calyces, ureter, and ureterocele can be seen directly with sonography.

In some patients with ectopic ureteroceles, the upper moiety is severely dysplastic and does not function. Unlike the usual situation, the calyces and ureter are not dilated. Thus, the typical indirect urographic and direct sonographic signs (except for the presence of the ureterocele) may be subtle or absent (Fig. 1B). We have called this rare entity ureterocele disproportion, and only a few previous reports allude to it [1-3]. This report documents the presence of ureterocele disproportion, tells when to suspect it, and discusses the therapeutic implications. Occasionally an ectopic ureterocele is associated with a single (nonduplex) collecting system. That entity is not discussed here.

Materials and Methods

The records of the Department of Radiology for the 13-year period January 1975 to June 1988 were reviewed, and the medical records and radiographs of the children with ureterocele disproportion were analyzed.

Results

Eight children had ureterocele disproportion. They ranged in age from 2 weeks to 4 years at the time of diagnosis. Six were girls. Seven presented for their initial

Received September 22, 1988; accepted after revision November 21, 1988.

Presented at the annual meeting of the Society for Pediatric Radiology, San Diego, CA, April 1988.

¹ Both authors: Department of Radiology, The Children's Hospital, 300 Longwood Ave., Boston, MA 02115. Address reprint requests to R. L. Lebowitz.

AJR 152:567-571, March 1989
0361-803X/89/1523-0567
© American Roentgen Ray Society

Fig. 2.—4-year-old girl.

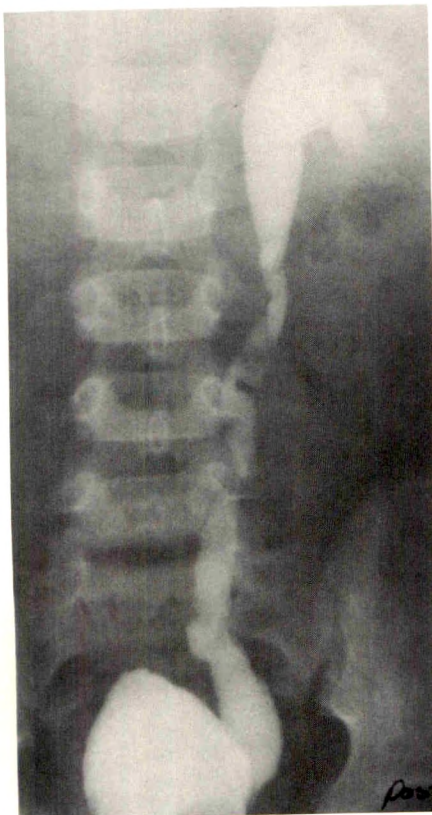
A and B, Voiding cystourethrogram shows large ureterocele on left and reflux into left lower moiety that resembles single (nonduplex) system.

C, Excretory urogram. Tomographic section shows small scarred lower moiety that resembles a single system.

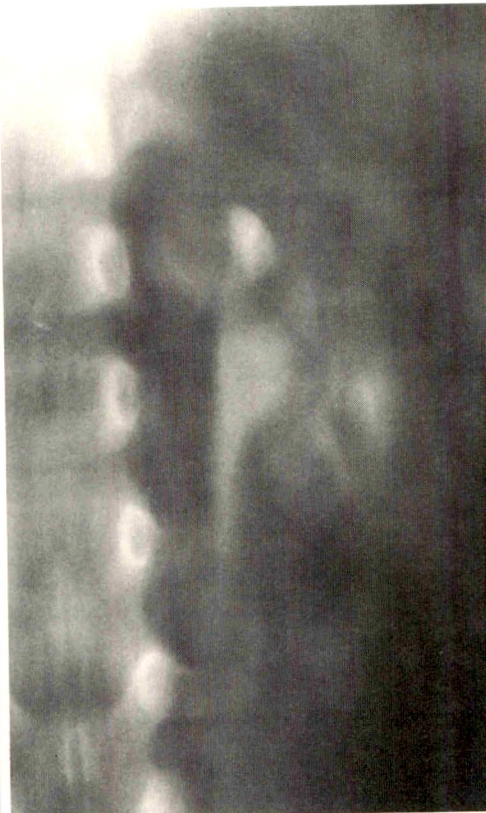
D, Retrograde ureterogram obtained by direct puncture and injection at time of surgery shows large ureterocele and its ureter, which is much smaller in caliber.



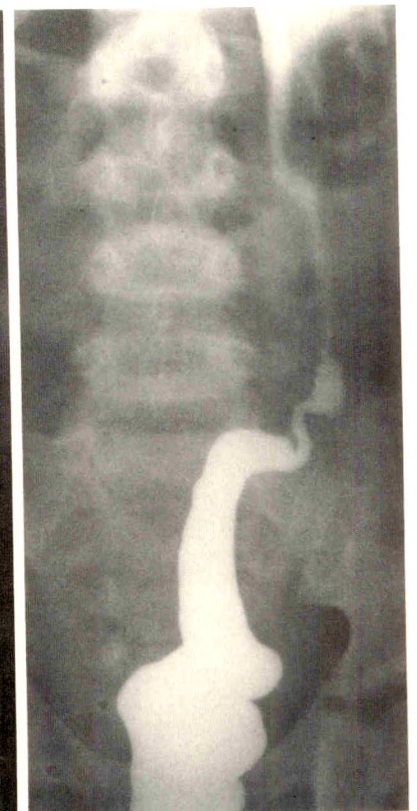
A



B



C



D

see directly, but again, the ease of recognition is directly proportional to the degree of dilatation.

We have called the situation "ureterocele disproportion" when there is a large ureterocele with a tiny dysplastic upper pole and a diminutive ureter. It has previously been called the nonobstructive ureterocele [1]. The indirect urographic and direct sonographic signs of duplication are absent or extremely subtle. The only clue to duplication may be the

presence of the ureterocele in the bladder. Thus, if an ectopic ureterocele is identified at urography or sonography without other signs of a duplex system, duplication with ectopic ureterocele is still the most likely diagnosis. Confirmation of the diagnosis, if necessary, is done by puncture of the ureterocele and injection of contrast material into the ureterocele.

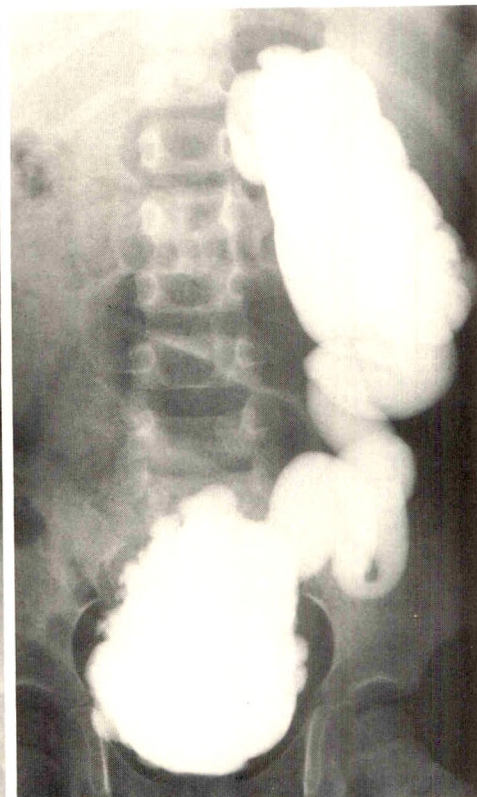
Surgical treatment in the typical case of ectopic ureterocele with a poorly or nonfunctioning, very dilated upper unit and a

Fig. 5.—4-year-old girl. Retrograde ureterogram. Direct puncture at time of surgery shows large left ureterocele (arrows) and its tiny left upper pole ureter.



5

Fig. 6.—3-year-old boy. Voiding cystourethrography revealed left ureterocele (not shown) and massive reflux into lower moiety of left duplex system that resembles a single system. Usual urographic clues to duplication are masked by distortion caused by reflux.



6

normal lower unit is on the kidney. It consists of removal of the dilated upper pole and a portion of its ureter through a flank incision. The ureterocele is decompressed from above and is left in place collapsed in the bladder [4]. In children with ureterocele disproportion, however, there is no dilatation of the diminutive upper pole and hence no stagnant urine. Thus if surgery is necessary, it is on the bladder, with either excision of the ureterocele plus reimplantation of the ureters or simply incision of the ureterocele.

REFERENCES

1. Bauer SB, Retik AB. The non-obstructive ectopic ureterocele. *J Urol* 1978;119:804-807
2. Lebowitz RL, Avni FE. Misleading appearances in pediatric urology. *Pediatr Radiol* 1980;10:15-31
3. Diamant MJ, Stanley P. Two unusual duplication anomalies of the urinary tract: use of percutaneous urography. *Urol Radiol* 1987;9:185-187
4. Lebowitz RL. *Postoperative pediatric urology*. New York: Appleton-Century-Crofts, 1981:59-77

Case Report

Diagnosis of Pulmonary Hemosiderosis by MR Imaging

Geoffrey D. Rubin,^{1,2} David K. Edwards, III,³ Murray A. Reicher,⁴ John M. Doemeny,⁴ and Stephen H. Carson¹

Idiopathic pulmonary hemosiderosis (IPH) is an uncommon but devastating disease in children [1]. The radiographic finding of a diffuse alveolar infiltrate [2], together with clinical findings of chronic, nonproductive cough, dyspnea, and iron-deficiency anemia, strongly suggest IPH, but open-lung biopsy is usually necessary for definitive diagnosis [1]. We present a case of IPH in which MR imaging of pulmonary parenchymal hemosiderin showed a preferential T2 shortening by paramagnetic ferric iron similar to that occurring in evolving intracranial hematomas. This noninvasive diagnosis allowed initiation of therapy and stabilization of the patient's cardiorespiratory status before lung biopsy. We suggest that in patients whose radiographic and clinical presentations suggest IPH, the MR findings permit sufficient diagnostic confidence to defer invasive maneuvers until the patient is clinically stable.

Case Report

A 2.5-year-old boy had recurrent vomiting, pallor, anorexia, and low fever for 1 week. On admission, his hematocrit was 14% (0.14), with red-cell indices and a smear suggesting iron deficiency; Coomb's test and a bone-marrow examination were negative. A chest radiograph revealed a faint, diffuse increase in interstitial markings. He was discharged on oral iron supplement.

He was readmitted 1 month later with marked pallor and vomiting. His arterial PO_2 was 39 mm Hg, and hematocrit was 9% (0.09). A chest radiograph showed a largely central, bilateral hazy infiltrate (Fig. 1). Gastric aspirate was negative for hemosiderin-laden macrophages. The patient was considered too unstable for lung biopsy or

even bronchial washings, so an MR study of the chest was obtained. The patient was premedicated with 700 mg of chloral hydrate and monitored with pulse oximetry during scanning. Transaxial thoracic scans (Fig. 2), obtained in a 1.5-T field, showed diffuse signal enhancement of the pulmonary parenchyma with T1 weighting (750/20 [TR/TE]) and a marked decrease in T2-weighted (1500/100) signal intensity relative to T1 weighting.

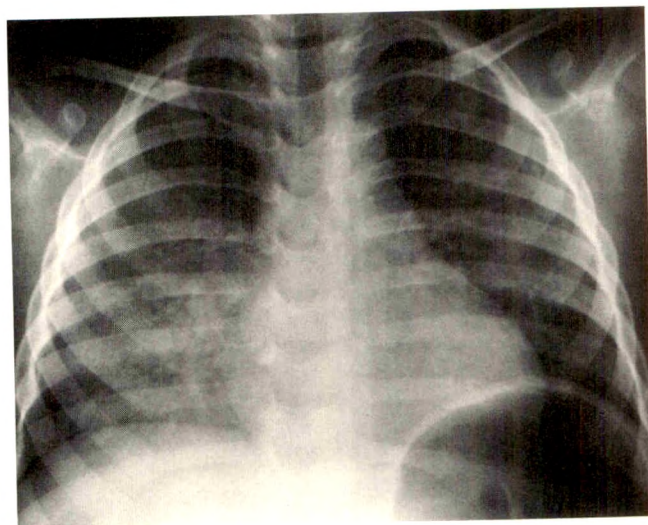


Fig. 1.—Idiopathic pulmonary hemosiderosis in a 2.5-year-old boy. Chest radiograph obtained on patient's second hospital admission shows bilateral, nonspecific infiltrates.

Received July 6, 1988; accepted after revision October 25, 1988.

¹ Department of Pediatrics, Mercy Hospital, 4077 Fifth Ave., San Diego, CA 92103.

² Present address: Department of Radiology, Stanford University Hospital, Stanford, CA 94395.

³ Departments of Radiology and Pediatrics (H-756), University of California Medical Center, 225 Dickinson Street, San Diego, CA 92103. Address reprint requests to D. K. Edwards, III.

⁴ Department of Radiology, Mercy Hospital, 4077 Fifth Ave., San Diego, CA 92103.

AJR 152:573-574, March 1989 0361-803X/89/1523-0573 © American Roentgen Ray Society

Efficacy of Chest Radiography in Pediatric Intensive Care

Carlos J. Sivit¹
 George A. Taylor¹⁻³
 Gabriel J. Hauser⁴
 Murray M. Pollack^{2, 4}
 Dorothy I. Bulas¹
 Christopher J. Guion¹
 Thomas Fearon^{1, 2}

We prospectively evaluated the efficacy and clinical usefulness of bedside chest radiography in a pediatric intensive-care unit. Seven hundred ninety-five radiographs were evaluated in 126 patients over a 10-week period. Eighty-one percent of all radiographs showed one or more cardiopulmonary abnormalities, and 25% of routine radiographs had findings that altered management of patients. Nineteen percent of radiographs, including 17% of routine radiographs, showed a malpositioned tube or catheter. Thirty-five percent of endotracheal tubes shown on postintubation radiographs and 41% of central venous catheters shown on post-catheter placement radiographs were malpositioned. Forty-five percent of radiographs with a previous reading showed a significant interval change. Radiographs in patients 1 year old or younger showed more cardiopulmonary abnormalities ($p < .04$), tube or catheter malpositions ($p < .03$), and significant interval changes ($p < .03$), and they elicited more changes in clinical management ($p < .01$) than did radiographs in patients over 1 year old. The frequency of management changes dictated by radiographs increased with increasing amounts of respiratory support ($p < .01$).

Our data indicate that bedside radiography in the pediatric intensive-care setting has a high efficacy and clinical utility.

Bedside portable chest radiography is time-consuming and costly. For example, 6000 portable chest radiographs, mostly routine, are obtained each year in our pediatric intensive-care unit, and this represents approximately 10% of the work done in our radiology department. Although chest radiography is frequently believed to be a valuable diagnostic aid in adult intensive-care patients, its clinical utility and diagnostic efficacy in children have not been evaluated. This study attempts to quantify the clinical utility of chest radiography in a pediatric intensive-care setting.

Materials and Methods

We collected clinical and radiographic data on every chest radiograph obtained in the pediatric intensive-care unit over a 10-week period. Radiographs were obtained daily on all patients with cardiopulmonary disease during the acute stage of the illness and every 3 days in chronic, stable, ventilated patients. These radiographs, obtained without specific clinical indications, were categorized as "routine." All radiographs were interpreted by a staff pediatric radiologist in conjunction with a pediatric radiology fellow. During a daily, weekday conference with the clinical intensive-care team, decisions to change management of patients after review of the daily routine radiographs were recorded. Tube or catheter malposition was determined on the basis of accepted institutional criteria for repositioning.

We classified cardiopulmonary findings as mild, moderate, or severe on the basis of radiographic appearance, using a modification of Henschke's classification [1]. Findings classified as mild were assessed as having no immediate impact on the clinical management of the patient. Moderate findings were those that could influence management of the patient and required close clinical and/or radiographic observation. Findings that would have an immediate impact on clinical management of patients were classified as severe. We compared all cardiopulmonary findings with those on the previous radiograph to assess the degree of

Received August 1, 1988; accepted after revision October 31, 1988.

¹ Department of Radiology, Children's Hospital National Medical Center, and The George Washington University School of Medicine and Health Sciences, 111 Michigan Ave. N. W., Washington, D. C. 20010.

² Department of Child Health and Development, Children's Hospital National Medical Center and The George Washington University School of Medicine and Health Sciences, 111 Michigan Ave. N. W., Washington, D. C. 20010.

³ Present address: Department of Radiology, The Johns Hopkins Hospital, 600 N. Wolfe St., Baltimore, MD 21205. Address reprint requests to G. A. Taylor.

⁴ Department of Critical Care Medicine, Children's Hospital National Medical Center and The George Washington University School of Medicine and Health Sciences, 111 Michigan Ave. N. W., Washington, D. C. 20010.

AJR 152:575-577, March 1989
 0361-803X/89/1523-0575

© American Roentgen Ray Society

routine examinations. One hundred ten (25%) daily routine radiographs had findings that altered management of patients. The most frequent management changes were repositioning of an in-dwelling device ($n = 75$, 68%), removal or placement of an in-dwelling device (11, 10%), change in drug therapy (11, 10%), performing further diagnostic procedures (four, 4%), and miscellaneous other changes (nine, 8%). Changes in management of patients were made more frequently in patients 1 year of age or younger than in those over 1 year of age (29% vs 20%, $p < .01$). In addition, management changes were made more frequently in patients receiving positive-pressure ventilation than in those receiving supplemental oxygen (29% vs 17%, $p < .01$). No management changes based on radiographic findings were made in patients who were not receiving respiratory support.

Discussion

The clinical utility of routine, portable chest radiographs in adult intensive-care units has been shown [1-4]. However, this utility must be reevaluated for children because age, size, and diagnostic differences could alter these results. On one hand, concerns over the cumulative radiation dose from multiple radiographs and the rising cost of medical care have led to increasing scrutiny of all "routine" examinations. On the other hand, as care becomes increasingly technological, the adequacy of physical examinations in detecting important clinical occurrences must be reassessed continuously. Studies of physical examinations in outpatient settings indicate that physical examinations may evaluate clinical status incom-

pathophysiologic impact is present may prevent considerable morbidity or mortality.

Abnormal findings were associated with radiographs of patients who were younger or required respiratory support therapies. Radiographs of patients less than 1 year old and patients receiving either supplemental oxygen or positive-pressure ventilation showed the highest frequency of abnormalities. Although our numbers are small ($n = 25$), routine radiographs of patients not receiving any respiratory support did not appear to affect clinical management.

The results from this evaluation of consecutive radiographs indicate that chest radiographs in pediatric intensive care detect a very high frequency of pulmonary abnormalities, significant interval changes, and tube and catheter malpositions. Most important, radiographs in this setting had a significant impact on decisions concerning management of patients. Omission of certain examinations and use of others on a more restricted basis have been recommended as cost-containment initiatives, and improvements are possible [7-10]. For example, the impact of chest radiography on patients not receiving respiratory support was low. Noninvasive assessment of endotracheal-tube position [11] may enable accurate evaluation of tube position without radiographs. Improved criteria for use of radiography in the pediatric intensive-care unit should be based on future innovations and current effectiveness as documented in this study.

REFERENCES

1. Henschke CI, Pasternack GS, Schroeder S, Hart KK, Herman PG. Bedside

Sonography of the Painful Hip in Children: 500 Consecutive Cases

María Miralles¹
 Gabino Gonzalez
 José R. Pulpeiro
 José M. Millán
 Isabel Gordillo
 Carmelo Serrano
 Francisco Olcoz
 Antonio Martinez

Five hundred children with a painful hip or a limp were evaluated prospectively by plain films and sonography. The clinical, radiographic, and sonographic findings were correlated with the final diagnoses. Sonography disclosed hip effusion in 235 patients, and plain films were abnormal in 58 of these 235 patients and in four others. Both sonography and plain films were normal in 261 patients. No sonographic signs served to differentiate sterile, purulent, or hemorrhagic effusion. Follow-up sonograms were performed in 202 patients. Sonography showed that 73% of patients with presumed transient synovitis had no effusion 2 weeks after diagnosis. Patients with hip disorders other than transient synovitis had persistent effusion for more than 2 weeks; however, that was also observed in 27% of patients with presumed transient synovitis.

Sonography was more sensitive than plain films for detecting hip effusion. However, sonographic detection of effusion changed the therapeutic approach in only six patients.

In the last few years, the use of sonography to evaluate painful hip in children has received much attention [1, 2]. Sonography has been reported to be useful for detecting intraarticular fluid [1, 3]. Sonography is more sensitive than plain films, showing effusion in many cases of radiographically normal transient synovitis of the hip [1, 2]. This paper reports the results of a prospective study of 500 patients who had clinical symptoms of hip disease and were evaluated by sonography and plain films.

Subjects and Methods

Between September 1984 and October 1987, 500 children (352 boys and 148 girls) who had clinical symptoms of hip disease (pain, limp) were evaluated prospectively. The age range was 10 months to 14 years (mean, 4 years 10 months). Anteroposterior plain films and sonograms of both hips were obtained in all patients. Plain films were considered positive if they showed bone abnormality or effusion. A difference of 1 mm or more between the two articular spaces was considered to represent hip effusion if the patient was not rotated. Sonograms were performed with a real-time sector scanner with high-frequency (5–7 MHz), short-focus transducers. Patients were examined supine with the hips in neutral position. The scans were oriented along the axis of the femoral neck showing the acetabular brim, femoral head and neck, and iliofemoral ligament (Fig. 1). The contralateral asymptomatic hip was examined in all cases, and was used as a normal reference. Sonography was considered positive if it showed an effusion. Hip effusion was diagnosed if an echo-free space between the femoral neck and the iliofemoral ligament was observed. Patients who had evidence of effusion underwent aspiration of the hip or follow-up sonograms, as dictated by the clinical setting. Needle aspiration of the hip was performed whenever septic arthritis was clinically suspected. Hip aspiration was done in 10 patients (seven with positive sonograms and three with normal sonograms). Follow-up sonograms were done every 2 weeks until the effusion disappeared. In all patients who had effusion at 2 weeks or had unusual findings (bilateral or recurrent effusion), diagnostic workup for arthritis (including serology for viruses and brucellosis) and plain films of the hip in frog-lateral view were performed. Selected patients had also nuclear imaging and CT studies or surgical confirmation.

Received June 30, 1988; accepted after revision November 14, 1988.

¹ All authors: Department of Radiology, Section of Pediatric Radiology, Hospital Primero de Octubre, Carretera de Andalucía, Km. 5.4, 28041 Madrid, Spain. Address reprint requests to J. R. Pulpeiro.

AJR 152:579–582, March 1989

0361–803X/89/1523–0579

© American Roentgen Ray Society

TABLE 2: Correlation Between Final Diagnoses and Radiographic and Sonographic Findings

Diagnosis	No.	Findings			
		PF+ SN+	PF+ SN-	PF- SN+	PF- SN-
Transient synovitis	471	42	0	173	256
Septic arthritis	7	3	1	1	2
Septic arthritis + osteomyelitis	2	2	0	0	0
Trauma	4	1	0	0	3
Brucellar arthritis	2	0	0	2	0
Rheumatoid arthritis	1	0	0	1	0
Perthes disease	10	7	3 ^a	0	0
Epiphysiolysis	1	1	0	0	0
Osteoid osteoma	2	2	0	0	0

Note.—PF+ SN+ = abnormal plain films and abnormal sonograms, PF+ SN- = abnormal plain films and normal sonograms, PF- SN+ = normal plain films and abnormal sonograms, and PF- SN- = normal plain films and normal sonograms.

^a Only bone abnormality on plain films, no effusion.

Fig. 3—Osteoid osteoma of the femur.

MR Imaging of Periventricular Leukomalacia in Childhood

Olof Flodmark¹
 Brian Lupton²
 David Li¹
 Gary K. Stimac³
 Elke H. Roland²
 Alan Hill²
 Michael F. Whitfield²
 Margaret G. Norman⁴

Eight children with clinical and radiologic abnormalities consistent with periventricular leukomalacia were investigated with MR imaging of the brain that employed both inversion-recovery and T2-weighted spin-echo imaging sequences. The more precise delineation of white and gray matter on inversion-recovery images as compared with CT allows a detailed demonstration of the anatomic features of periventricular leukomalacia; specifically, a reduced quantity of white matter in the periventricular region and centrum semiovale and, in more severe cases, cavitated infarcts that replace the immediate periventricular white matter. The T2-weighted spin-echo and short inversion time inversion-recovery images demonstrated abnormally increased signal in white matter that appeared normal on CT scans and only minimally abnormal on conventional inversion-recovery images. These abnormalities most probably represent white matter gliosis that extends beyond the immediate periventricular regions.

MR recognition of cerebral white matter abnormalities associated with periventricular leukomalacia may confirm the clinical suspicion of this diagnosis in children with spastic diplegia or quadriplegia.

Recent advances in perinatal care have improved the survival rate of premature infants, resulting in greater awareness of perinatal cerebral injury and neurologic sequelae. Cerebral injury may result from intraventricular hemorrhage, which occurs in 35–50% of premature infants [1, 2], and from hypoxic-ischemic cerebral insults [3–9]. Of these two principal mechanisms of injury, the hypoxic-ischemic parenchymal injury is considered to be most significant and is most commonly associated with long-term sequelae. In the preterm infant, hypoxic-ischemic insult often results in periventricular leukomalacia (PVL), a specific pattern of injury with infarctions in the periventricular brain tissue [10–12].

Although neurosonography may demonstrate lesions consistent with PVL during the first weeks of life [8, 13–18], the reliability of this technique in the diagnosis of PVL has recently been questioned [19]. The sensitivity and specificity of this imaging technique have yet to be established. No study exists in which findings on neonatal neurosonography have been correlated with clinical outcome in an unselected group of children who have been observed long enough to establish the true incidence of spastic diplegia/quadruplegia likely to have been caused by PVL. Although the clinical correlate between perinatal injury and subsequent motor handicap may be quite clear in prematurely born children with a severe motor handicap, it is not uncommon that mild or moderate forms of spastic diplegia remain undiagnosed during the first 6 to 8 months of life, thus making the perinatal cause of the handicap less obvious. This may be particularly true if neurosonography during the neonatal period was reported as normal or if the injury happened during fetal life. The availability of MR is increasing, and it is quite likely that MR will be the preferred imaging method in the investigation of such a child, thus making it important for the neuroradiologist to recognize the changes of PVL as they appear on MR, even in older children and in the absence of a typical history.

This article appears in the January/February 1989 issue of *AJNR* and the March 1989 issue of *AJR*.

Received January 27, 1988; accepted after revision May 24, 1988.

Presented in part at the annual meeting of the American Society of Neuroradiology, New York, May 1987.

¹ Department of Radiology, University of British Columbia Children's Hospital, 4480 Oak St., Vancouver, B.C., Canada V6H 3V4. Address reprint requests to O. Flodmark.

² Department of Pediatrics, University of British Columbia Children's Hospital, Vancouver, B.C., Canada V6H 3V4.

³ First Hill Diagnostic Center, Seattle, WA 98104.

⁴ Department of Pathology, University of British Columbia Children's Hospital, Vancouver, B.C., Canada V6H 3V4.

AJR 152:583–590, March 1989
 0361-803X/89/1523-0583
 © American Roentgen Ray Society

in the coronal planes but also in transaxial sections. Seven of the patients were scanned with conventional (long TI) IR sequences using the parameters of 1650/400/40/4 (TR/TI/TE/excitations) or 2450/400/40. Dual-echo coronal T2-weighted SE sequences, 2058/40, 120/2 (TR/first-echo TE, second-echo TE/excitations) or 2450/40, 120/2, were obtained in six patients, and one patient was examined with a multiple-echo long TR sequence (3000/26, 52, 104, 130, 156). Two patients were scanned with short TI IR (STIR) using 1183/100/40 or 1400/100/40. Single-echo T1-weighted SE sequences, 600/22, and T2-weighted SE sequences, 2000/60, were performed in an additional patient. Sedation was used as required (oral chloralhydrate 50 mg/kg). The MR examinations were approved by the Ethics Committee at the University of British Columbia and informed consent was obtained from the parents.

CT scans were performed with a GE CT/T 8800 scanner. Thin sections (5 mm) were obtained of the level of the lateral ventricles and viewed with a narrow window-width (60 H).

Results

Abnormalities on conventional IR scans were similar to those described previously on CT [20] and MR [21, 22]. The principal abnormality was reduction in the amount of periven-

tricular white matter. With mild radiologic abnormality (two cases), this reduction of white matter, seen on both axial and coronal IR scans, was limited to the peritrigonal region. These patients had no or limited reduction of white matter in the centrum semiovale and the ventricular size was normal. As a consequence of this white matter loss, prominent sulci were identified adjacent to the trigone of the lateral ventricles and were proved on coronal IR scans to represent dilatation of the most posterior aspect of the sylvian fissure. Small, well defined lesions of reduced signal on IR scans and high intensity on T2-weighted SE and STIR scans were observed in the white matter immediately adjacent to the dorsolateral aspects of the lateral ventricles. This finding, best seen on coronal images, was present in all patients irrespective of age or severity of damage (Fig. 1).

With more severe radiologic involvement (five cases), there was evidence of reduction in the quantity of white matter in the centrum semiovale, indicating damage to the corona radiata. In addition there was more marked reduction of periventricular white matter. The deep portions of the sylvian fissures were prominent, and there was ventriculomegaly involving principally the occipital horns. The gray matter deep

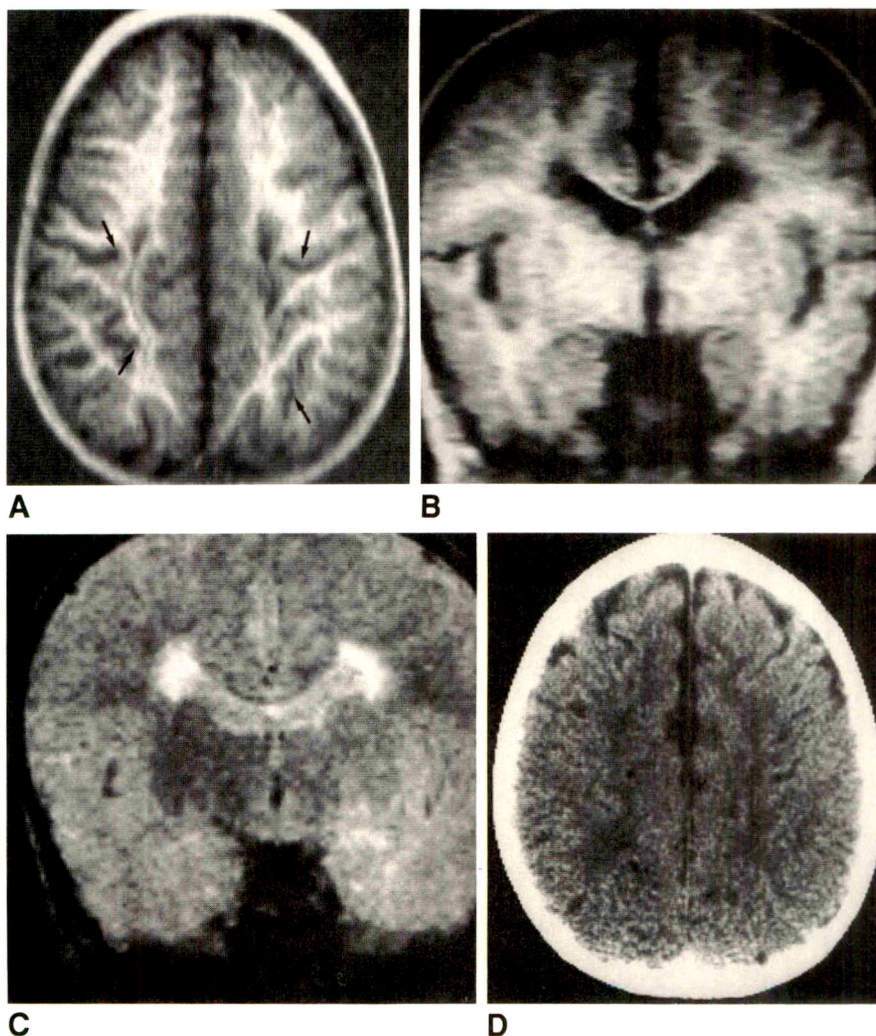


Fig. 2.—2½-year-old girl with moderately severe, symmetric spastic diplegia.

A, The end result from the periventricular infarction is demonstrated in this conventional IR image, 1650/400/40, in the axial plane, which shows a reduced amount of white matter in the centrum semiovale. Note the prominent, deep cortical sulci in close association with the ventricles (arrows).

B, Conventional IR image, 1650/400/40, in the coronal plane shows the same finding as in Fig. 1C but in a more anterior location.

C, Corresponding second-echo T2-weighted SE image, 2058/120, shows the high signal intensity within a more extensive area.

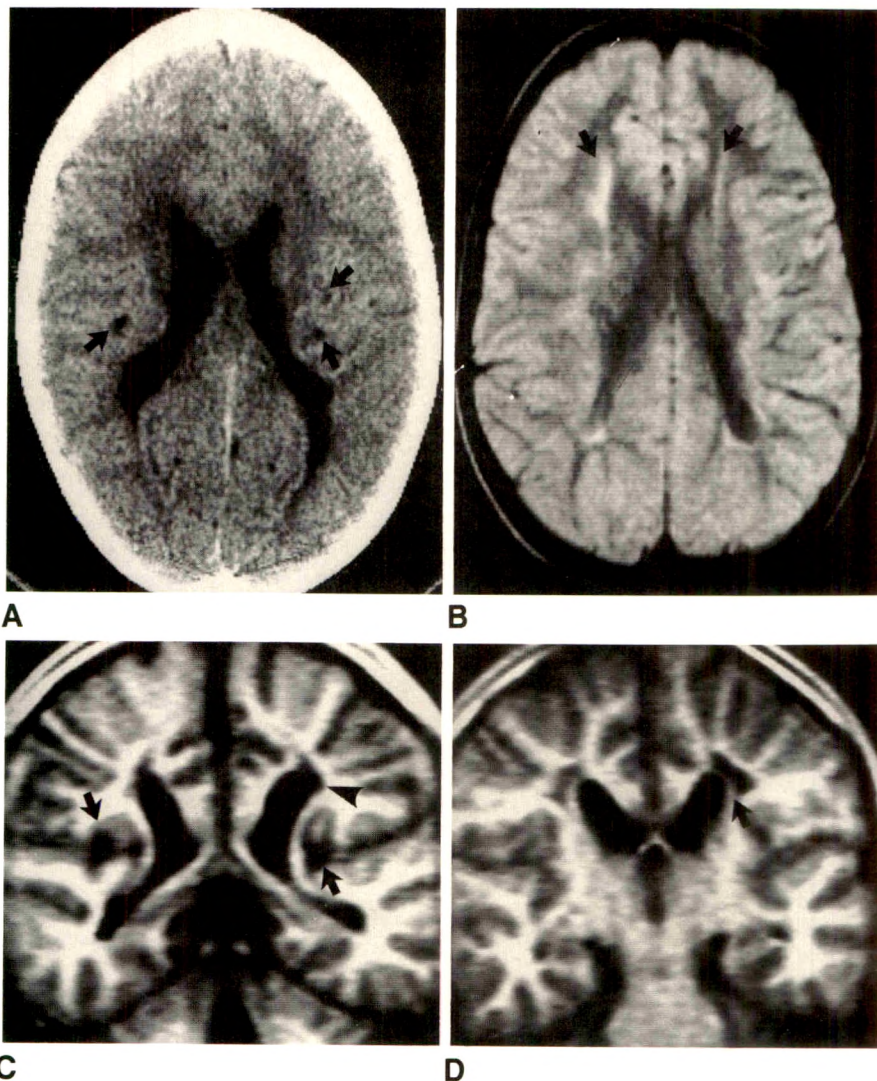
D, Axial CT slice in a plane comparable to A. Note reduced amount of white matter with prominence of some of the same sulci as in A.

Fig. 5.—A, CT scan of 9-year-old boy with moderate to severe quadriplegia shows virtually complete absence of peritrigonal white matter, with less severe loss of white matter anteriorly. The ventricles are moderately dilated. Note superficial "cystic" structures (arrows) in cortical tissue, and normal appearance of white matter deep in the frontal lobes.

B, Corresponding T2-weighted SE image, 2450/40, shows abnormal signal intensity in frontal white matter (arrows), tissue that had a normal CT appearance in A.

C, Conventional IR image, 1650/400/40, in the coronal plane demonstrates clearly that the "cystic" structures in the cortex represent widening of the deep parts of the sylvian fissure (arrows). Note the square shape of the dorsolateral aspects of the left ventricle (arrowhead), indicating that cavitated periventricular infarcts have become incorporated into the ventricle. The injury is less prominent on the right side, where the ventricle has maintained a more normal shape and more periventricular white matter with normal signal intensity remains. The child had an asymmetric quadriplegia, which was more severe in the right leg and arm.

D, A more anterior image in the same sequence shows a part of the periventricular cavitated infarct on the left side, which has maintained the thin wall separating it from the ventricle (arrow).



occipital lobes and extended into regions that appeared normal on CT and conventional IR images. The signal characteristics of these lesions differed from that of CSF by showing a high intensity on first-echo SE images. These lesions were also well shown by STIR because of the high tissue contrast with respect to normal white matter. White matter located more superficially (i.e., subcortically) and deep within the centrum semiovale demonstrated a normal appearance (Figs. 1 and 2).

In all cases, there was good correlation between clinical observations and the anatomic location of MR and CT abnormalities. In patients with asymmetric motor involvement, the MR and CT abnormalities corresponded to the clinical observations.

Discussion

Periventricular leukomalacia results from hypoxic-ischemic injury to watershed zones of arterial supply in the periventricular white matter of the immature brain [10–12, 23]. These

watershed zones are most prominent in the posterior periventricular white matter at the trigone of the lateral ventricles and in white matter adjacent to the foramina of Monro [10–12]. Additional injury may result from parenchymal hemorrhage in association with ischemic lesions, a finding that has been reported in approximately 25% of cases in an autopsy study. This likely represents spontaneous hemorrhage into reperused periventricular ischemic areas; that is, hemorrhagic infarction [23]. The anatomic location of PVL determines the characteristic neurologic sequelae observed in many survivors of low birth weight. Thus, lesions may affect either the geniculocalcarine tract and cause visual impairment or the corticospinal tracts in the corona radiata and damage the motor fibers, which control the function of lower limbs and trunk. Consequently, the classical neurologic sequelae of PVL include spastic diplegia or quadriplegia, and cortical blindness with relative preservation of cognitive functions, except in severe cases. In severe cases, the cerebral injury is more diffuse and results in multiple neurologic handicaps [10, 11].

Histopathologically, periventricular leukomalacia begins as coagulation necrosis with subsequent macrophage activity

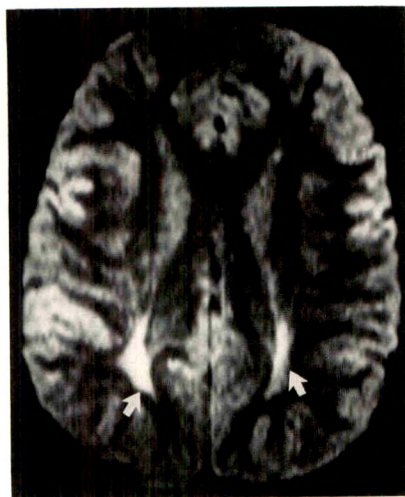
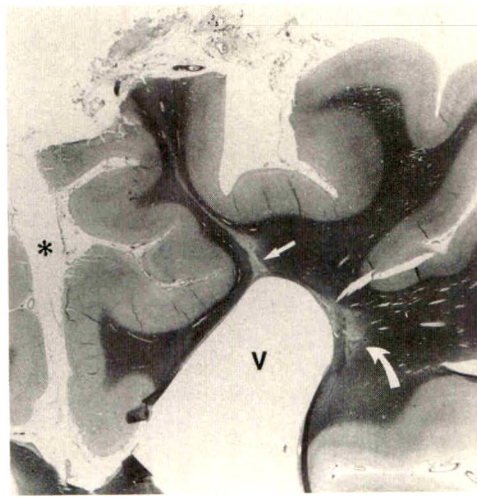


Fig. 6.—Axial STIR image, 1400/100/40, provides less anatomic detail than some T2-weighted SE images but shows well the abnormal signal (arrows) in the periventricular white matter.



A



B

Fig. 7.—Histologic sections of 19-year-old man, not part of this study, who was a first-born twin. Birth was at 30 weeks gestation with a difficult delivery. He had severe spastic quadriplegia, abnormal posture, and he was cortically blind. He could speak one or two words and could not respond to command. His brain weighed 1220 g (normal, 1500 g).

A, Whole tissue mount shows an unmyelinated scar (straight arrow) extending from enlarged ventricle (V) into the postcentral gyrus. Another scar (curved arrow) with focal calcification is seen in the paraventricular white matter. The interhemispheric fissure (asterisk) is identified. (Luxol fast blue/cresyl violet stain, $\times 4$)

B, This section shows another similar scar (arrows) stained for glial fibers. The lesion extends into the frontal lobe and represents gliosis. (V = ventricle.) (Holzer stain, $\times 50$)

proved essential for the CT diagnosis of PVL [20]. A similar technique able to show even minimal amounts of disease in the periventricular white matter may prove as important in MR imaging. However, the limited field strength of our MR systems prevented us from using this technique.

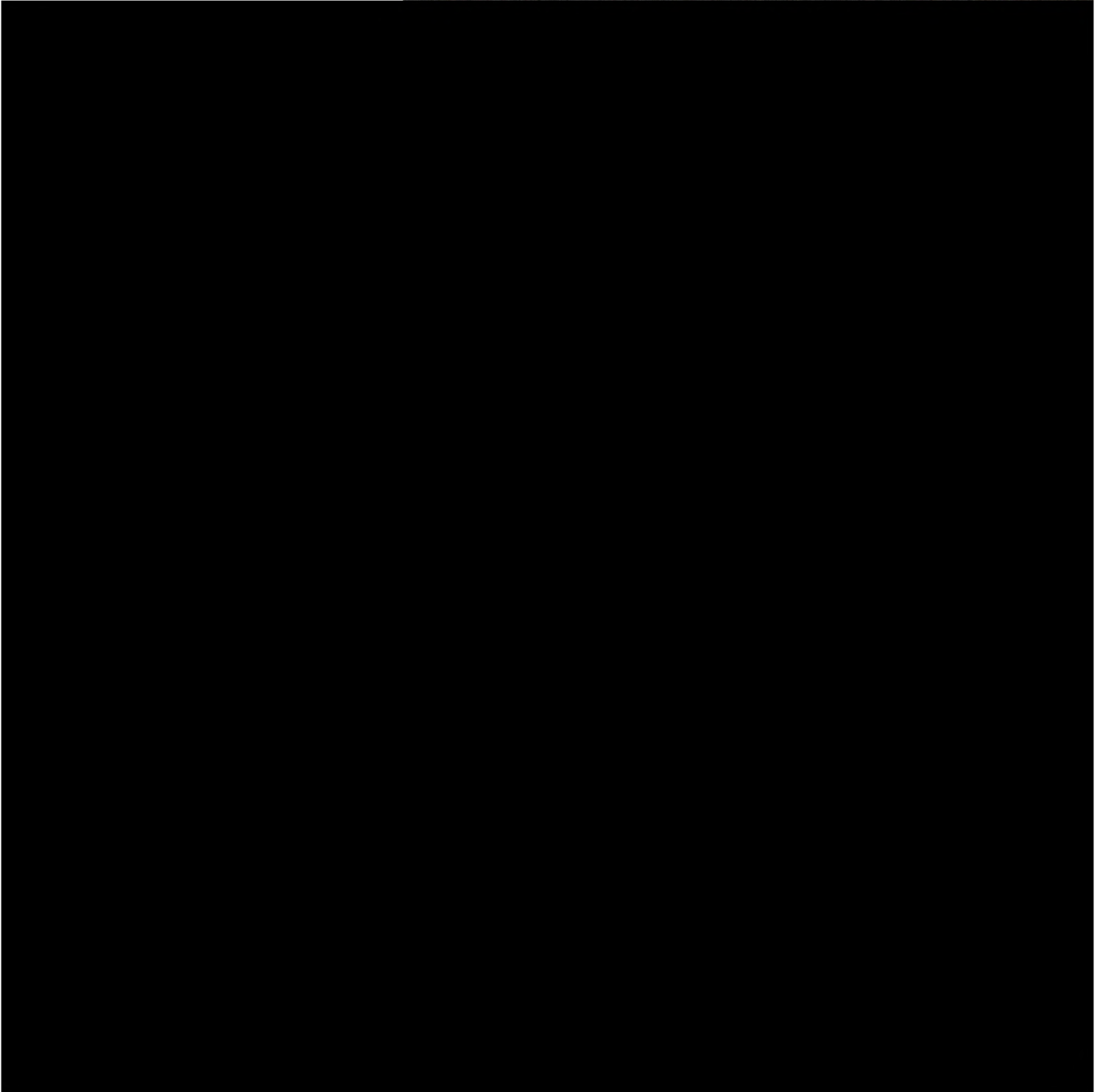
ACKNOWLEDGMENTS

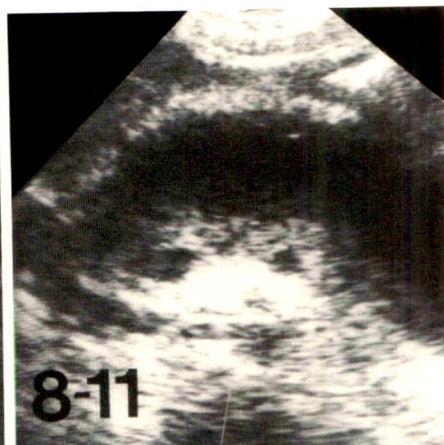
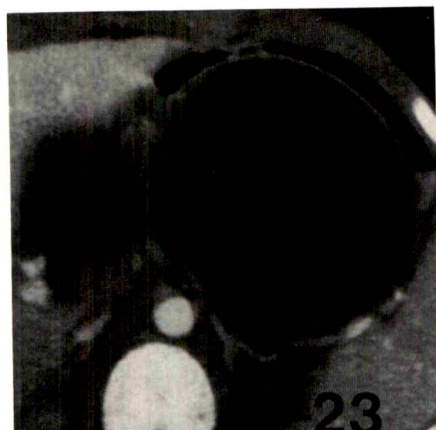
We thank J. Wada, J. E. Jan, and K. Farrell for allowing us to study their patients.

REFERENCES

- Papile LA, Munsick-Bruno G, Schaefer A. Relationship of cerebral intraventricular hemorrhage and early childhood neurologic handicap. *J Pediatr* 1983;103:273-277
- Flodmark O, Fitz CR, Harwood-Nash DC. CT diagnosis and short-term prognosis of intracranial hemorrhage and hypoxic ischemic brain damage in neonates. *J Comput Assist Tomogr* 1980;4:775-787
- Dubowitz LMS, Dubowitz V, Palmer PG, Miller G, Fawer CL, Levene MI. Correlation of neurologic assessment in the preterm newborn infant with outcome at 1 year. *J Pediatr* 1984;105:452-456
- Fitzhardinge PM, Flodmark O, Fitz CR, Ashby S. The prognostic value of computed tomography of the brain in asphyxiated premature infants. *J Pediatr* 1982;100:476-481
- Flodmark O. Diagnosis by computed tomography of intracranial hemorrhage and hypoxic/ischemic brain damage in neonates (thesis). Karolinska Institute, Stockholm, Sweden, 1981
- Fawer CL, Levene MI, Dubowitz LMS. Intraventricular haemorrhage in a preterm neonate: discordance between clinical course and ultrasound scan. *Neuropediatrics* 1983;14:242-244
- Shankaran S, Slovis TL, Bedard MP, Poland RL. Sonographic classification of intracranial hemorrhage. A prognostic indicator of mortality, morbidity, and short-term neurologic outcome. *J Pediatr* 1982;100:469-475
- Dubowitz LMS, Bydder GM, Mushin J. Developmental sequence of periventricular leukomalacia: correlation of ultrasound, clinical, and nuclear magnetic resonance functions. *Arch Dis Child* 1985;60:349-355
- Bozynski MEA, Nelson MN, Matalon TAS, et al. Cavitary periventricular leukomalacia: incidence and short-term outcome in infants weighing < 1200 grams at birth. *Dev Med Child Neurol* 1985;27:572-577
- DeReuck J, Chatta AS, Richardson EP Jr. Pathogenesis and evolution of periventricular leukomalacia in infancy. *Arch Neurol* 1972;27:229-236
- Banker BQ, Larroche JC. Periventricular leukomalacia of infancy. *Arch Neurol* 1962;7:386-410
- Shuman RM, Selednik LJ. Periventricular leukomalacia: a one-year autopsy study. *Arch Neurol* 1980;37:231-235
- Weindling AM, Rochefort MJ, Calvert SA, Fok T-F, Wilkinson A. Development of cerebral palsy after ultrasonographic detection of periventricular cysts in the newborn. *Dev Med Child Neurol* 1985;27:800-806
- Bowerman RA, Donn SM, DiPietro MA, D'Amato CJ, Hicks SP. Periventricular leukomalacia in the pre-term newborn infant: sonographic and clinical features. *Radiology* 1984;151:383-388
- Chow PP, Horgan JG, Taylor KJW. Neonatal periventricular leukomalacia: real-time sonographic diagnosis with CT correlation. *AJNR* 1985;6:383-388
- Nwaesei CG, Pape KE, Martin DJ, Becker LE, Fitz CR. Periventricular infarction diagnosed by ultrasound: a postmortem correlation. *J Pediatr* 1984;105:106-110
- Schellinger D, Grant EG, Richardson JD. Cystic periventricular leukomalacia: sonographic and CT findings. *AJNR* 1984;5:439-445
- Szymonowicz W, Schaefer K, Cussen LJ, Yu VYH. Ultrasound and necropsy study of periventricular haemorrhage in preterm infants. *Arch Dis Child* 1984;59:637-642
- Baarsma R, Laurini RN, Baerts W, Okken A. Reliability of sonography in non-hemorrhagic periventricular leukomalacia. *Pediatr Radiol* 1987;17:189-191
- Flodmark O, Roland EH, Hill A, Whitfield MF. Periventricular leukomalacia: radiologic diagnosis. *Radiology* 1987;162:119-124
- Wilson DA, Steiner RE. Periventricular leukomalacia: evaluation with MR imaging. *Radiology* 1986;160:507-511

Percutaneous Drainage of Traumatic Pancreatic Pseudocysts in Children





Before removing the catheter from a noninfected pseudocyst, a trial of oral feedings with the percutaneous drainage catheter clamped is recommended. This usually occurs around 3–4 weeks, when the patient is asymptomatic and drainage has nearly ceased. Fluid reaccumulation on sonography and increasing pancreatic drainage indicate that the catheter should remain in place, because there is persistent communication between the cyst and the pancreatic duct [7, 13]. Amylase values should remain stable, although a small rise in serum amylase not to exceed two and one-half times normal value is acceptable. Finally, the patient should remain asymptomatic. If all these criteria are fulfilled, the catheter may be withdrawn. Small residual pseudocysts still may be present and can be followed to resolution with serial sonograms.

Pseudocysts that communicate with the pancreatic duct (Fig. 6) take longer to completely resolve; however, percutaneous drainage can be used to treat these patients successfully [11].

Our experience suggests that percutaneous drainage is a safe and effective treatment for traumatic pancreatic pseudocysts in children. Surgical intervention usually can be avoided, but these children still require prolonged hospitalization for successful management. With more experience, percutaneous drainage may become the treatment technique of choice for this complicated problem.

REFERENCES

1. Cooney DR, Grosfeld JL. Operative management of pancreatic pseudocysts in infants and children: a review of 75 cases. *Ann Surg* 1975; 182:590–596
2. Slovis TL, VonBerg VJ, Mikelic V. Sonography in the diagnosis and management of pancreatic pseudocysts and effusions in childhood. *Radiology* 1980;135:153–155
3. Jeffrey RB Jr, Federle MP, Crass RA. Computed tomography of pancreatic trauma. *Radiology* 1983;147:491–494
4. Sarti DA. Rapid development and spontaneous regression of pancreatic pseudocysts documented by ultrasound. *Radiology* 1977;125:789–793
5. Bradley EL, Clements JL. Spontaneous resolution of pancreatic pseudocysts: implications for timing of operative intervention. *Am J Surg* 1975; 129:23–28
6. van Heerden JA, ReMine WH. Pseudocysts of the pancreas: review of 71 cases. *Arch Surg* 1975;110:500–505
7. vanSonnenberg E, Wittich GR, Casola G, et al. Complicated pancreatic inflammatory disease: diagnostic and therapeutic role of interventional radiology. *Radiology* 1985;155:335–340
8. Karlson KB, Martin EC, Fankuchen EI, et al. Percutaneous drainage of pancreatic pseudocysts and abscesses. *Radiology* 1982;142:619–624
9. Torres WE, Evert MB, Baumgartner BR, et al. Percutaneous aspiration and drainage of pancreatic pseudocysts. *AJR* 1986;147:1007–1009
10. Ho CS, Taylor B. Percutaneous transgastric drainage for pancreatic pseudocysts. *AJR* 1984;143:623–625
11. Nunez D Jr, Yrizarry JM, Russell E, et al. Transgastric drainage of pancreatic fluid collections. *AJR* 1985;145:815–818
12. Kugligowska E, Olsen WE. Pancreatic pseudocysts drained through a percutaneous transgastric approach. *Radiology* 1985;154:79–82
13. Darcy MD, Smith TP, Cragg AH, et al. Advantages of the left-duct approach for percutaneous biliary procedures. Presented at the annual meeting of the Radiological Society of North America, Chicago, November 1987

Herniation of the Suprasellar Visual System and Third Ventricle into Empty Sellae: Morphologic and Clinical Considerations

Benjamin Kaufman¹
 Robert L. Tomsak²
 Bruce A. Kaufman³
 Baha'Uddin Arafah⁴
 Errol M. Bellon⁵
 Warren R. Selman³
 Michael T. Modic¹

Intrasellar herniation of the optic nerve, optic chiasm, optic tract (suprasellar visual system, SVS), and antero-inferior third ventricle can occur into primary or secondary empty sellae. The anatomic part of this study evaluated the appearance of the SVS in subjects with normal sellae ($n = 52$), the patterns and prevalence of SVS herniation in enlarged primary empty sellae ($n = 24$), and the patterns of intrasellar herniation of the SVS in secondary empty sellae ($n = 8$). The clinical part of this study was to correlate the visual status with the anatomic patterns of the intrasellar herniated SVS. High-resolution MR and CT were used to define the anatomy. MR was superior to CT in all groups in defining accurately the SVS relationship to the sella turcica.

In the normal group, the SVS invariably had a straight-line appearance formed by the optic nerve, optic chiasm, and floor of the third ventricle and was above the sella. The SVS was herniated in three of 24 enlarged primary empty sellae. A difference in the appearance of the hypothalamic and infundibular recesses in the primary empty sella group with SVS herniation (dilated recesses and formation of an obtuse angle) and in the secondary empty sella group with SVS herniation (nondilated recesses and formation of an acute angle) was observed. Visual disturbances in primary empty sellae with SVS herniation were present in two of three subjects. Visual disturbances may be absent or minimal in primary empty sellae and secondary empty sellae with herniation of the SVS. Progression of the symptoms—visual field defects, optic atrophy, and loss of vision—is not inevitable. There was no correlation between the severity of visual symptoms and the degree of herniation of the SVS in either the primary or secondary sellae.

We found that intrasellar herniation of the SVS into a primary or secondary empty sella is well delineated with MR, and MR should facilitate decisions concerning surgery or therapy. Visual disturbances proved to be an unreliable indicator of herniation.

This article appears in the January/February 1989 issue of *AJNR* and the March 1989 issue of *AJR*.

Received January 27, 1988; accepted after revision June 2, 1988.

Presented at the annual meeting of the American Society of Neuroradiology, New York City, May 1987.

¹ Department of Radiology, University Hospitals of Cleveland, Case Western Reserve University, 2074 Abington Rd., Cleveland, OH 44106. Address reprint requests to B. Kaufman.

² Division of Ophthalmology, University Hospitals of Cleveland, Case Western Reserve University, Cleveland, OH 44106.

³ Division of Neurosurgery, University Hospitals of Cleveland, Case Western Reserve University, Cleveland, OH 44106.

⁴ Department of Medicine, University Hospitals of Cleveland, Case Western Reserve University, Cleveland, OH 44106.

⁵ Department of Radiology, Cleveland Metropolitan General Hospital, 3395 Scranton Rd., Cleveland, OH 44109.

AJR 152:597-608, March 1989

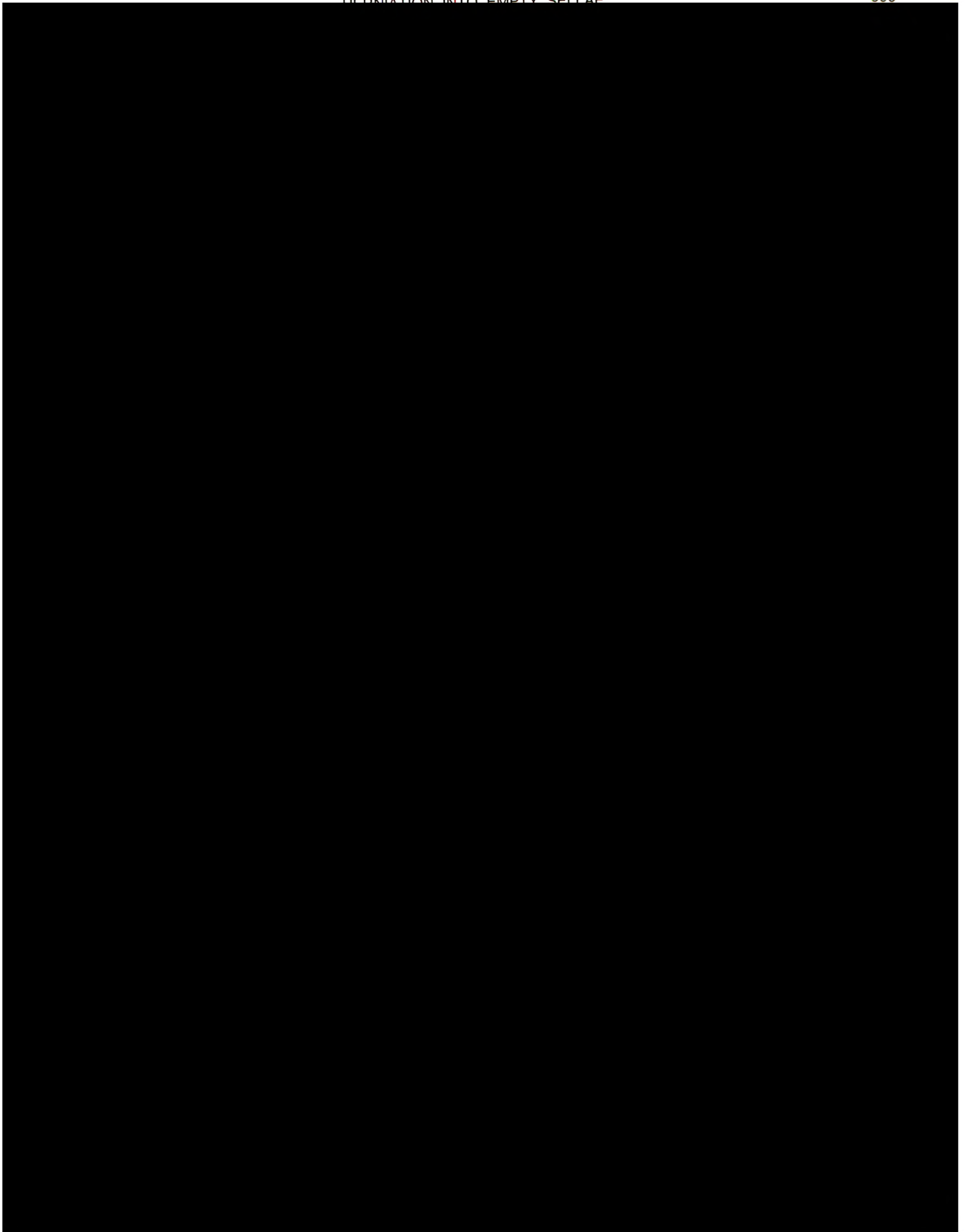
0361-803X/89/1523-0597

© American Roentgen Ray Society

Herniation of the suprasellar visual system (SVS) (i.e., suprasellar portions of the optic nerves, chiasm, and tracts and the antero-inferior third ventricle) into an empty sella can occur in the presence of either primary or secondary empty sellae [1-5].

The prevalence of herniation of the SVS and associated visual disturbances in primary empty sellae is not well established. A small number of cases suggesting herniation of the SVS have been reported [6-15], and only rarely has herniation been documented radiologically [1-4, 6, 10, 12, 15]. Herniation of the SVS into a secondary empty sella is more frequent and is associated with multiple causes resulting in inflammation and adhesions; associated visual symptoms are variable [1-3, 5, 9, 13, 16-18].

This study was undertaken (1) to determine the normal appearance of the SVS with normal sellae, (2) to determine the appearance and prevalence of SVS herniation into primary empty sellae, (3) to determine the appearance of the intrasellar herniation of the SVS in secondary sellae, and (4) to correlate visual disturbances with the observed patterns of herniation. Surgical procedures are available for therapy of visual disturbances associated with SVS herniation, and MR visualization of the SVS anatomy should be helpful in selecting and planning therapy.



Group 2

In the group of enlarged primary empty sellae, a normal SVS was defined in a way similar to that of group 1. The normal appearance of the SVS was present in 21 of 24 cases (Fig. 2). Any angulation downward of the SVS into the enlarged empty sella, as seen on sagittal and/or coronal sections, was considered to be herniation of the SVS. By using this definition, herniation of the SVS occurred in only three of the 24 cases of enlarged primary empty sellae found incidentally (Table 2; Figs. 3–5). One patient (Fig. 3) showed dilated lateral ventricles but no evidence of obstructive hydrocephalus. Another patient (Fig. 4) had enlarged lateral ventricles and the MR appearance of aqueductal stenosis of the distal aqueduct with dilatation of the proximal aqueduct. There were no clinical signs of hydrocephalus, but CSF pressures were not measured. The subject with minimal SVS herniation (Fig. 5) had a monocular upper temporal depression in the left visual field without any intraocular abnormalities.

The recess angle was acute in 21 subjects, slightly less than 90° in one subject (Fig. 3), nearly 90° in one subject (Fig. 5), and obtuse in one subject (Fig. 4).

Group 3

In all eight cases of secondary empty sellae with herniation of the SVS and anterior third ventricle, MR was unequivocally superior to CT in establishing the diagnosis (Figs. 6–10). Three patients with metal artifacts within the sella turcica showed the signal void and displaced signal artifact caused

by the intrasellar metal [19]. An abnormal orientation of the floor of the third ventricle was present in these three patients, and the appearance was the same as the abnormal orientation of the floor seen in patients with SVS without signal void artifacts from metal (Table 3). The recess angle was acute in five subjects and not identified in three subjects.

Visual findings included normal vision, visual field defects, optic atrophy, and loss of vision (Table 1).

Appearances of Herniation

The detailed anatomic features of intrasellar SVS herniation as seen on MR are given in Table 3 for primary (group 2) and secondary (group 3) empty sellae. Figure 2 is representative of the nonherniated SVS appearance in enlarged primary empty sellae and Figure 6 illustrates the features of intrasellar herniation of the SVS.

Discussion

The definition of intrasellar herniation of the SVS based solely on spatial relationships is the translocation of the anteroinferior third ventricle and the chiasm with optic nerves and optic tracts into the sella turcica. We found that MR was superior to CT in imaging the SVS, and our experience is consistent with a previous report [20].

The MR appearance of the SVS, optic and infundibular recesses, and anterior third ventricle and their relationships to the sella turcica in normal subjects (group 1) were consist-

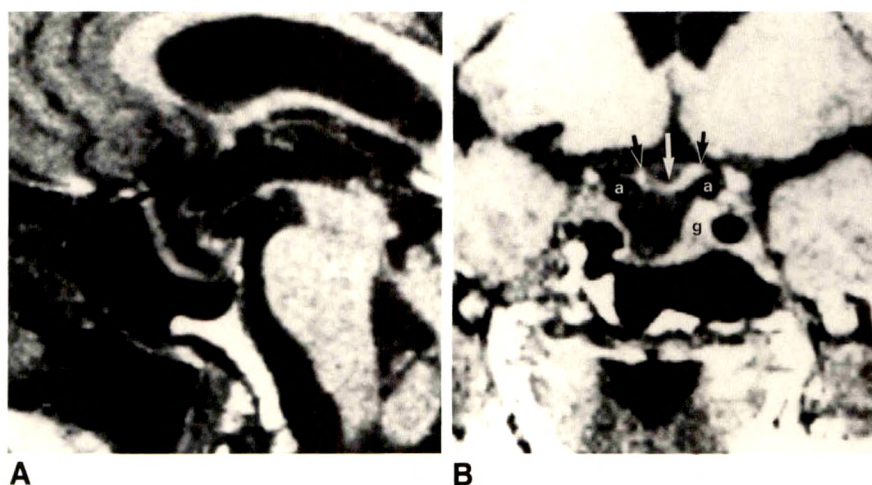


Fig. 3.—Case 9: 75-year-old man. Pronounced herniation of suprasellar visual system (SVS) and anteroinferior third ventricle into asymmetrically enlarged primary empty sella.

A, Sagittal T1-weighted section shows definite herniation of anteroinferior third ventricle and SVS into enlarged empty sella. Location of optic chiasm, as represented by posterior wall of optic recess (Fig. 1C), had a horizontal orientation. Dilatation of hypothalamic recess is present. Recess angle (formed by posterior wall of optic recess and anterior wall of hypothalamic recess) is slightly less than 90°.

B, Coronal T1-weighted section in plane of anterior clinoid processes shows optic nerves (short arrows) diverging upward from inferiorly bowed optic chiasm (long arrow) and going superiorly and laterally coursing normally over internal carotid arteries (a) as they are in contact with anterior clinoid processes. Pituitary gland (g) is to left and inferior; on other sections hypophyseal stalk was seen from hypothalamic region to displaced gland.

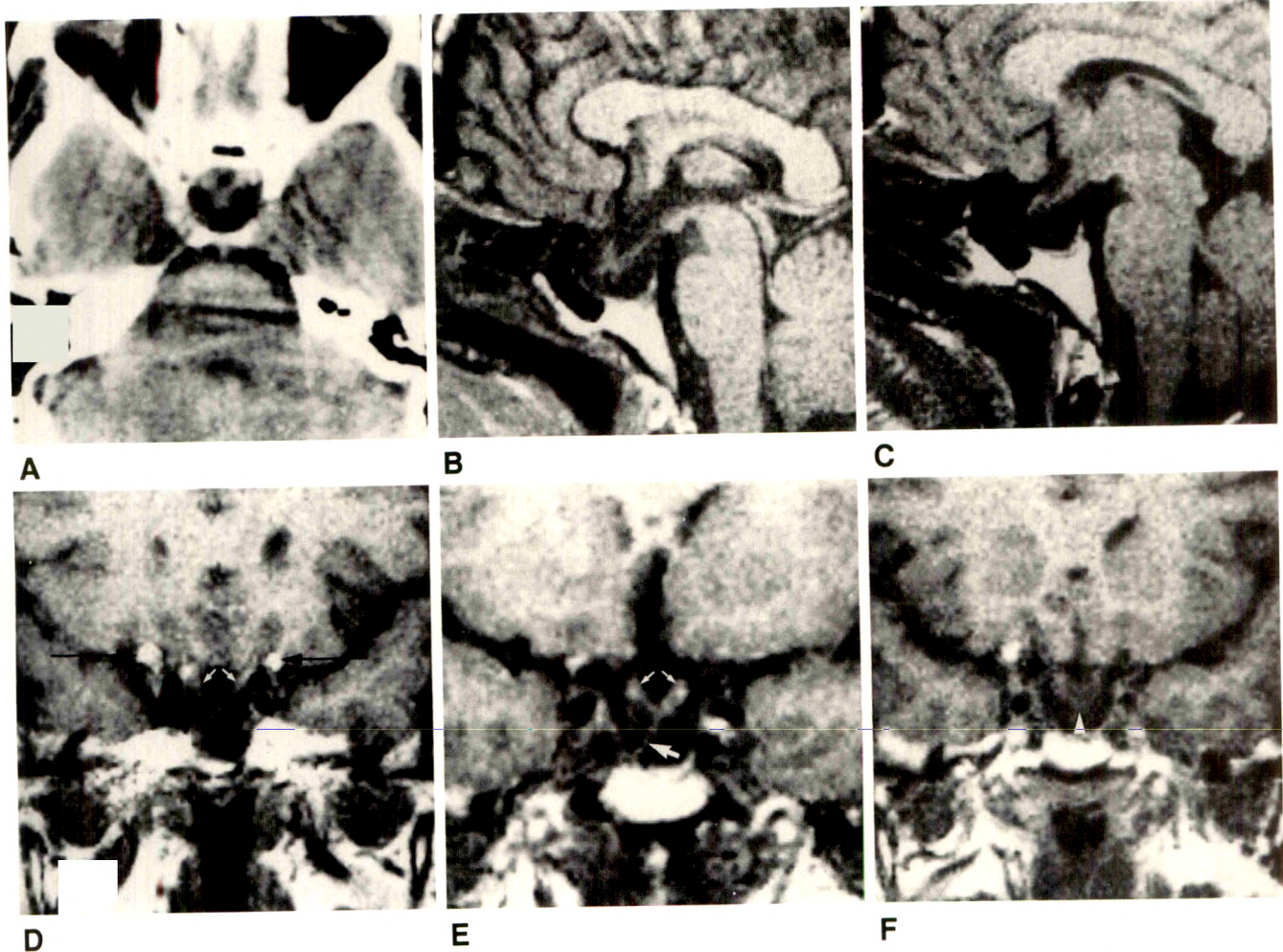


Fig. 6.—Case 1: 49-year-old woman. Multiple patterns of intrasellar herniation of suprasellar visual system (SVS) and anterior third ventricle into enlarged empty sella in a patient with coexisting prolactin-secreting adenoma.

A, Axial high-resolution nonenhanced CT scan shows enlarged sella with hypodense contrast and diverging tissue densities anteriorly; intrasellar SVS herniation. Original interpretation was "tissue anteriorly" surrounded by CSF or cystic tumor.

B, Sagittal T1-weighted image 1 year later shows herniation of anteroinferior third ventricle and chiasm into enlarged empty sella.

C, Parasagittal T1-weighted image shows composite image of optic tract and chiasm within empty sella.

D, Coronal T1-weighted image in plane of anterior clinoid processes (black arrows) shows optic nerves (white arrows) going from chiasm in center of sella to optic foramina. Optic nerves are contiguous with intraclinoid portion of internal carotid artery, a normal relationship.

E, Coronal T1-weighted image posteriorly to D shows marked angulation of optic nerves (small arrows) in plane of hypophyseal stalk (large arrow), which deviates to right toward floor of sella. Pituitary gland is presumed to be remodeled inferiorly with component on right side, as indicated by stalk. Pituitary function was normal.

F, Coronal T1-weighted image. Poorly defined density in center of sella is optic chiasm (arrowhead).

ent with the anatomic studies of Schaeffer [21] and with the radiologic appearances as reported by Bull [22] and Rosenbaum et al. [23].

Prevalence of SVS Intrasellar Herniation

Radiographically diagnosed herniation of the SVS in primary empty sellae has been reported rarely [1, 11]. In our cases, the CT demonstration of herniation was difficult, and initial interpretation did not readily identify the findings (Figs. 6 and 7). With secondary empty sellae, the circumstances were the same: Diagnosis of the herniated SVS was difficult to make with CT but could be made readily and accurately with MR.

Our experience suggests that intrasellar SVS herniation is more common than previous diagnostic techniques were capable of demonstrating.

Patterns of SVS Intrasellar Herniation

The patterns of herniation are the result of the varying degrees of herniation of the complex of the optic chiasm and anteroinferior third ventricle. The optic nerves and optic tracts have to extend from the herniated optic chiasm to their respective points of fixation, optic foramina and geniculate bodies, respectively, and the abnormal intrasellar course is readily appreciated. The altered orientation of the floor of the

Fig. 9.—Case 4: 42-year-old woman. Metrizamide-enhanced CT and MR comparison of intrasellar herniation of suprasellar visual system (SVS) into secondary empty sella. Pneumoencephalography with thin-section tomography 11 years earlier showed normal SVS and enlarged primary empty sella with coexisting microadenoma that was suspected to have infarcted spontaneously.

A, Axial metrizamide CT scan after metrizamide cisternography shows unequivocally optic chiasm (c), optic tract posteriorly (large arrow), and optic nerves (small arrows) diverging anteriorly.

B, Coronal T1-weighted section shows herniated optic chiasm (long arrow) and optic nerves (short arrows) within empty sella. Pituitary gland tissue is seen posteriorly.

C, Sagittal T1-weighted section shows slight herniation of antero-inferior third ventricle into superior portion of sella turcica and opticochiasmatic junction more inferiorly and centrally within empty sella. Thin rim of pituitary tissue is at bottom of sella.

D, Parasagittal T1-weighted section shows abnormal course of optic tract (arrow) directed from intrasellar position of chiasm.

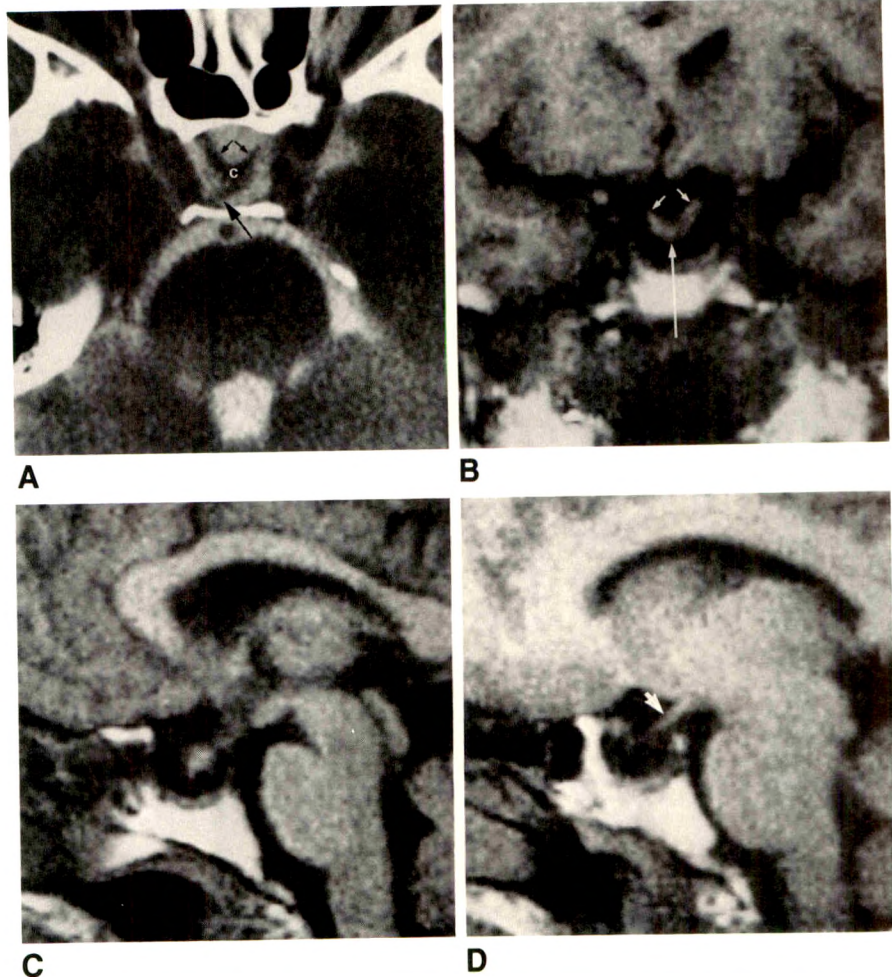


TABLE 3: Anatomic Features of Intrasellar Herniation of the Suprasellar Visual System

Feature	Primary Empty Sella	Secondary Empty Sella		
		Nonsurgical ^a	Surgical	
			With Metal ^b	Without Metal
Optic chiasm (coronal):				
Angled	1 (case 9)	4	0	1
Not angled	1 (case 10)	0	0	0
Minimally angled	1 (case 11)	0	0	0
Artifacts	0	0	3	0
Total	3	4	3	1
Optic nerves (coronal):				
Diverging	2 (cases 9 & 10)	4	2	1
Normal	1	0	0	0
Not seen	0	0	1	0
Total	3	4	3	1
Optic recess:				
Enlarged	3 (cases 9–11)	0	0	0
Not enlarged	0	4	0	1
Artifacts	0	0	3	0
Total	3	4	3	1
Hypothalamic recess:				
Enlarged	3 (cases 9–11)	0	0	0
Not enlarged	0	4	0	1
Artifacts	0	0	3	0
Total	3	4	3	1
Recess angle: ^c	1 (case 9)	0	0	0
Slightly less than 90°				
Almost 90°	1 (case 11)	0	0	0
Obtuse	1 (case 10)	0	0	0
Acute	0	4	0	1
Not identified	0	0	3	0
Total	3	4	3	1
Floor of third ventricle:				
Abnormal orientation	3	4	3	1
Sella:				
Intact, enlarged	3	3	0	0
Intact, not enlarged	0	1	0	1
Artifacts	0	0	3	0
Total	3	4	3	1

^a Example: case 1.^b Example: case 5. Signal void and displaced signal artifacts caused by metal obscured features in many instances.^c Angle formed by posterior wall of the optic recess and anterior wall of the infundibular recess.

Etiologic factors of SVS herniation in primary empty sellae ($n = 3$) have not been definitively defined, whereas multiple etiologic factors are involved in secondary empty sellae. The significance of the increased recess angle in SVS herniation in primary empty sella has yet to be determined.

REFERENCES

- Mortara R, Norrell H. Consequences of a deficient sellar diaphragm. *J Neurosurg* 1970;32:565–573
- Colby MY, Kearns TP. Radiation therapy of pituitary adenomas with associated visual impairment. *Mayo Clin Proc* 1962;37:15–24
- Lee WM, Adams JE. The empty sella syndrome. *J Neurosurg* 1968;28:351–356
- Kaufman B. Angiographic findings in non-tumorous enlargement of the sella turcica-enlarged "empty sella" (abstr). *Invest Radiol* 1970;5:201–202
- Olson DR, Guiot G, Derome P. The symptomatic empty sella. Prevention and correction via the transsphenoidal approach. *J Neurosurg* 1972;37:553–537
- Shinoda Y, Ohnishi Y, Abe M, et al. Empty sella syndrome with visual field disturbance. *Jpn J Ophthalmol* 1983;27:248–254
- Xistris E, Sweeney PJ, Gutman FA. Visual disturbances associated with primary empty sella syndrome. *Cleve Clin J Med* 1977;44(3):137–140
- Neelon FA, Goree JA, Lebovitz HE. The primary empty sella; clinical and radiographic characteristics and endocrine function. *Medicine (Baltimore)* 1973;52:73–92
- Foley KM, Posner B. Does pseudotumor cerebri cause the empty sella syndrome? *Neurology* 1975;25:565–569
- Berke JP, Buxton LF, Kokmen E. The "empty sella." *Neurology* 1975;25:1137–1143

MR and CT of Masses of the Anterosuperior Third Ventricle

Gerard A. Waggenpack¹
Faustino C. Guinto, Jr.

Six patients with masses of the anterosuperior portion of the third ventricle were imaged with MR and CT. Four patients had proved colloid cysts, one patient had a proved astrocytoma, and one patient had a presumed colloid cyst.

Multiplanar MR imaging provided accurate localization of the anterosuperior third-ventricle mass in all cases. The MR intensity characteristics of the colloid cysts varied and the astrocytoma could not be differentiated from the colloid cysts on MR. The astrocytoma contained a calcification that was clearly demonstrated on CT but was difficult to appreciate on MR. Neither MR nor CT was useful in predicting success of stereotactic aspiration of the colloid cysts in this small series, but the presence of thin, low-viscosity cyst contents could be suggested by both examinations.

Colloid cysts, meningiomas, choroid plexus papillomas, hamartomas, gliomas, vascular lesions, and granulomatous lesions are among the masses that may arise in the anterosuperior third ventricle (ASTV). A patient becomes symptomatic when the mass obstructs the flow of CSF at the foramina of Monro. Symptoms include headaches, vomiting, and mental and visual disturbances. Rarely, acute neurologic deterioration or sudden death may occur [1-3].

CT has proved useful for the diagnosis of masses of the ASTV [4-11]. More recently, MR imaging has added a new dimension to the characterization of masses of the ASTV [12-14]. A retrospective study was done to address two questions: (1) Can MR distinguish colloid cysts from other masses of the ASTV? (2) Can the MR appearance of a mass of the ASTV be used to predict whether or not stereotactic aspiration will be successful?

Materials and Methods

Six patients, three men and three women, ages 28 to 59, with a mass of the ASTV were examined with both MR and CT between April 1985 and November 1987. MR and CT studies were performed before any operative procedure except in one patient in whom MR was obtained after placement of an emergency ventriculoperitoneal shunt.

CT and MR studies of the ASTV yielded fluid

Fig. 2.—Case 2: Colloid cyst.

A, Coronal spin-echo MR image (500/32). Homogeneous mass with intensity similar to white matter is shown in anterosuperior third ventricle. Lateral ventricles are dilated.

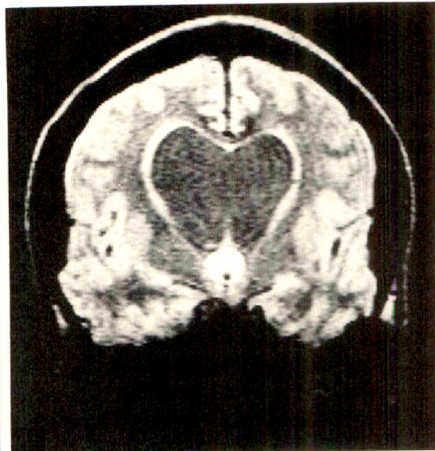
B, Coronal spin-echo MR image (2000/60). Mass has small internal area of hypointensity and peripheral hyperintensity.

C, Coronal spin-echo MR image (2000/120). Intensity of mass is now similar to intensity of CSF in lateral ventricles. Hypointensity is more pronounced.

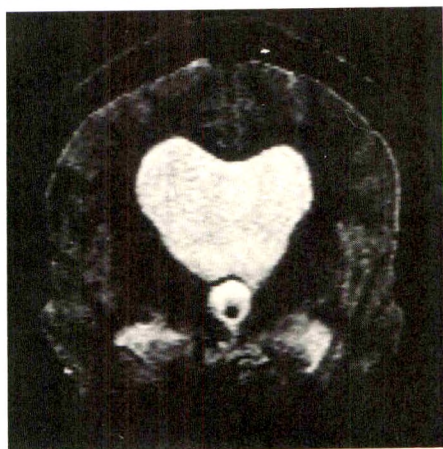
D, Noncontrast CT scan shows hyperdense mass in anterosuperior third ventricle. CT was obtained 4 days after the MR. No surgical procedure was done during the interim. Lateral ventricles are decompressed, indicating intermittent nature of the obstruction of the foramina of Monro.



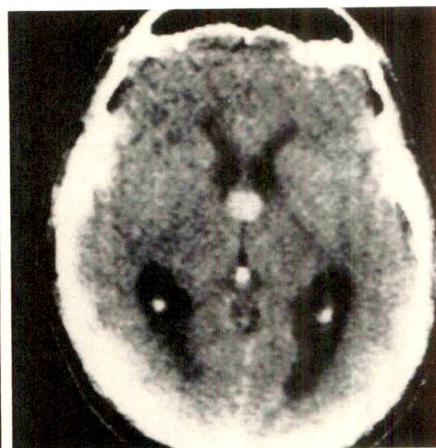
A



B



C



D



Discussion

The goal of therapy in the treatment of masses of the ASTV is to relieve the obstruction of the foramina of Monro. Open surgical resection of the mass may be performed with almost no risk of mortality [15]. However, significant morbidity may result because of injury to structures exposed in approaching the third ventricle. Memory disorders, convulsions, hemiplegia, impairment of consciousness, and visual field loss are among the deficits that may result [16]. Stereotactic aspiration may be performed if the mass is a colloid cyst. Excellent results with essentially no morbidity or mortality have been reported [5, 9, 10]. To date, most stereotactic aspirations have been performed by using CT guidance; however, guidance devices for use with MR imaging systems are currently under development [17].

Colloid cysts originate from folding of the primitive neuroepithelium, which gives rise to the choroid plexus and ependyma [18]. Shuangshoti et al. [18] have shown that the contents of the cysts are secretory and breakdown products of the epithelial lining of the cyst, including old blood, foamy cells, fat, hemosiderin-laden macrophages, cholesterol crystals, and CSF. Ions within the mucin of one third-ventricle colloid cyst included sodium, magnesium, calcium, copper, silicon, iron, and phosphorous [19]. Variations in the amount and distribution of these secretory and breakdown products and ions in colloid cysts would account for their varied appearances on CT and MR.

On CT, colloid cysts are usually hyperdense before IV contrast administration and often show mild enhancement after contrast is given, but the cyst may occasionally be isodense or hypodense [6–8, 13]. Dense contrast enhancement suggests a diagnosis other than colloid cyst, such as meningioma, choroid plexus papilloma, or craniopharyngioma. When MR contrast agents become more widely available the CT enhancement characteristics of masses of the ASTV will assume a less important role.

CT evidence of calcification in a colloid cyst is uncommon, with Ganti et al. [6] reporting calcification in one of 14 cases and Brooks and El Gammal [4] in one of six cases. CT is superior to MR for demonstration of intracranial calcifications [20]. In case 6, CT showed an unequivocal calcification in the astrocytoma; MR did not. There were no other MR, CT, or angiographic features to distinguish the astrocytoma from the colloid cyst.

On short TR MR images, the colloid cysts we studied were homogeneous and equal to or lower than white matter in intensity. This differs from the central hypointensity, peripheral hyperintensity reported by Roosen et al. [13] and Scotti et al. [14]. On long TR/long TE, one cyst in our study (case 2) showed internal hypointensity and peripheral hyperintensity, three others became uniformly hyperintense, and one appeared uniformly hypointense. The hypointense areas are due to structures with a short T2 relaxation time. A high concentration of paramagnetic ions causing a magnetic susceptibility effect could account for the low signal [14]. The high-signal-intensity areas of the cysts on the spin-density and long TR/long TE images are largely the result of the short T1 relaxation time of the cysts' contents [12]. If the T1 relaxation time is

very short, medium or high signal intensity may also be seen on the short TR images.

The wall of a colloid cyst consists of connective tissue containing sparse neutrophils, lymphocytes, plasma cells, and macrophages [18]. We were unable to identify the walls of the colloid cysts on the MR or CT images. The curving cyst walls may have been too thin to be resolved because of partial volume averaging.

We found the MR and CT appearance of the colloid cysts useful in predicting the presence of thin fluid, but this did not ensure complete aspiration of the contents of the cysts. Rivas and Lobato [10] found that low-density colloid cysts on CT images indicated the contents would be easier to aspirate than if the cysts were hyperdense, because the hyperdense cysts contained thicker colloid material than the hypodense or isodense cysts. Hall and Lunsford [7] did not find the CT appearance of colloid cysts helpful in predicting success of aspiration. The cyst in our case 1 contained thin fluid that was hypodense on CT. This cyst was slightly hypointense on the short TR MR image and uniformly hyperintense on spin-density and long TR/long TE sequences. This signal intensity behavior suggests the presence of relatively simple fluid containing little substance with minimal shortening of the T1 relaxation time of the fluid. The cysts with more viscous contents (cases 2, 3, and 4) were medium in intensity on the short TR images and hyperdense on CT. However, the cyst with thin fluid in case 1 was not as completely aspirated as one of the cysts with viscous contents (case 2). This was probably because, in addition to viscosity, success of aspiration can be influenced by position of the needle in the cyst and displacement of the cyst wall away from the aspiration needle.

Hydrocephalus of the lateral ventricles is usually seen with symptomatic masses of the ASTV [6–8]. CT may occasionally fail to show a mass of the ASTV in the presence of hydrocephalus [8, 21], but MR can show the mass when CT has not [21].

In summary, MR can localize accurately masses of the ASTV. Colloid cysts have varied appearances on MR images, reflecting differences in the contents of the cysts, and they cannot be reliably distinguished from other masses of the ASTV. Success of stereotactic aspiration of colloid cysts could not be predicted by either MR or CT.

REFERENCES

1. Chan RC, Thompson GB. Third ventricular colloid cysts presenting with acute neurological deterioration. *Surg Neurol* 1983;19:358–362
2. Leestma JE, Konakci Y. Sudden unexpected death caused by neuroepithelial (colloid) cyst of the third ventricle. *J Forensic Sci* 1981;26:486–491
3. McDonald JA. Colloid cyst of the third ventricle and sudden death. *Ann Emerg Med* 1982;11:365–367
4. Brooks BS, El Gammal T. Lesions at the foramen of Monro: evaluation by computed tomography, angiography and pneumoencephalography. *South Med J* 1983;76:1515–1523
5. Donauer E, Moringlane JR, Ostertag CB. Colloid cysts of the third ventricle. Open operative approach or stereotactic aspiration? *Acta Neurochir (Wien)* 1986;83:24–30
6. Ganti SR, Antunes JL, Louis KM, Hilal SK. Computed tomography in the diagnosis of colloid cysts of the third ventricle. *Radiology* 1981;138:385–391
7. Hall WA, Lunsford LD. Changing concepts in the treatment of colloid cysts.

Subdural and Epidural Empyemas: MR Imaging

Karen Weingarten¹
 Robert D. Zimmerman¹
 Richard D. Becker^{1,2}
 Linda A. Heier¹
 Alison B. Haimes¹
 Michael D. F. Deck¹

The MR images of six patients with extraaxial empyemas (five subdural and four epidural) were reviewed and compared with CT scans. MR demonstrated convexity and interhemispheric collections, which were mildly hyperintense relative to CSF and hypointense relative to white matter on short TR pulse sequences and hyperintense relative to CSF and white matter on long TR pulse sequences, allowing distinction from sterile effusions and most chronic hematomas. A hypointense rim, representing displaced dura, was depicted at the interface between the lesion and brain in epidural empyemas, a feature absent in subdural empyemas. Inflammation-induced parenchymal abnormalities, including edema, mass effect, and reversible cortical hyperintensity, were well depicted on MR imaging. MR was superior to CT in demonstrating the presence, nature, and extent of these lesions in all cases.

Because early and accurate diagnosis will significantly improve the prognosis of these serious infections, MR is preferred to CT for patients in whom an acute intracranial infection is suspected.

Subdural and epidural empyemas are uncommon extraaxial lesions, accounting for approximately 20–33% of all intracranial infections [1, 2]. The majority occur in the setting of sinusitis, have a fulminant clinical course, and require prompt diagnosis and emergent neurosurgical intervention [3–6]. Less often, they occur secondary to infection of a posttraumatic extraaxial hematoma or postcraniotomy cavity and have a prolonged, indolent course, but nonetheless require surgical drainage for proper management [7, 8]. Several authors have reported the failure of CT to reliably corroborate or exclude an acute extraaxial empyema [7, 9–11]; others have stressed that, while the empyema can be small and difficult, but not impossible, to visualize, the diagnosis should be suspected when, in the proper clinical setting, unexplained holohemispheric edema and mass effect are visualized on CT [12–15]. We present the MR features of six patients with extracerebral empyemas and evaluate the efficacy of MR imaging in comparison with that of CT for the initial diagnosis and follow-up of these lesions. The role of MR imaging in patients suspected of harboring an extraaxial empyema is discussed.

Materials and Methods

The CT and MR studies of six patients with surgically proved extraaxial empyemas were reviewed retrospectively. Two patients had subdural empyemas exclusively, one patient had an epidural empyema, and three patients had empyemas in both compartments. The study included four male and two female patients 9–32 years old (average age, 22 years).

Within 24 hr of presentation, all patients had both a CT and MR scan. In five patients, a contrast-enhanced CT scan was obtained. In one patient, only a nonenhanced CT scan was

This article appears in the January/February 1989 issue of *AJNR* and the March 1989 issue of *AJR*.

Received December 28, 1987; accepted after revision May 3, 1988.

Presented at the annual meeting of the American Society of Neuroradiology, New York City, May 1987.

¹ Department of Radiology, Division of Neuroradiology, The New York Hospital–Cornell Medical Center, 525 E. 68th St., New York, NY 10021. Address reprint requests to K. Weingarten.

² Present address: Department of Radiology, Temple Medical Center, 40–60 Temple St., New

planes in all patients. The routine short TR/short TE pulse sequence was 500–750/30 (TR range/TE). Long TR, multiecho pulse sequences, 2150/30–120 (TR/TE range), were done in five patients, and a long TR, single-echo sequence, 1500/90, was performed in one patient. The slice thickness was 7.5 mm and the interslice gap was 2.5 mm.

The extraaxial empyemas were analyzed with specific attention to the ability of MR, as compared with CT, to (1) detect the lesions and define their extraaxial location and extent, (2) distinguish extraaxial empyemas from sterile effusions and chronic hematomas, (3) distinguish subdural from epidural empyemas, and (4) detect parenchymal changes.

Representative Case Reports

Case 1

A 9-year-old boy had 2 days of fever, lethargy, and dull headache, which progressed to left hemiparesis, drowsiness, severe headache, and meningism. A nonenhanced CT study at another institution was interpreted as normal (Fig. 1A). However, on review, a hypodense interhemispheric subdural collection and sinusitis were seen. Contrast-enhanced CT and MR, performed on admission 12 hr later, demonstrated sinusitis, an interhemispheric subdural empyema, and a right frontal epidural empyema (Figs. 1B–1F). The underlying brain parenchyma was normal. The patient underwent a limited surgical procedure, consisting of an anterior right frontal craniotomy with evacuation of 50 ml of purulent material from the epidural and anterior portion of the subdural collections. Cultures grew *Hemophilus influenzae* and anaerobic *Streptococcus*. The patient worsened after surgery; a right posterior frontal craniotomy 2 days later revealed

cheesy purulence and meningovascularitis of the underlying brain. The patient improved initially, but deteriorated 2 weeks after the second craniotomy. Contrast-enhanced CT delineated large loculated subdural empyemas and right hemispheric cortical enhancement (Figs. 1G and 1H). MR the same day demonstrated enlargement of the interhemispheric collection (Figs. 1I and 1J), a right frontal convexity collection, retrospectively seen on CT (Fig. 1K), and hyperintensity on the long TR pulse sequences in the right parasagittal cortex, an area in which no parenchymal abnormalities were identified on CT. The patient underwent extensive right frontal and right subtemporal craniotomies with evacuation of large amounts of pus. Postoperative nonenhanced CT demonstrated no subdural collections or parenchymal abnormalities; MR demonstrated a small residual convexity collection and resolution of mass effect and cortical abnormalities (Fig. 1L). The patient was treated with IV antibiotics and recovered uneventfully.

Case 2

A 19-year-old woman, who had had several craniotomies 5 years earlier for sphenoid wing fibrous dysplasia, was seen with otitis media and meningitis. MR and contrast-enhanced CT demonstrated a dural-based mass contiguous with an eroded roof of the sphenoid sinus (Figs. 2B–2E). The ring-enhancing nature of the lesion on CT mimicked the appearance of a parenchymal abscess. On MR, the intensity of the lesion was typical of that seen in inflammatory fluid collections. A hypointense rim was absent. Craniotomy revealed a purulent subdural collection embedded in the inferior right frontal lobe with adjacent sphenoid sinusitis. Cultures grew *Hemophilus influenzae*. Follow-up MR demonstrated complete resolution of the lesion with minimal residual gliosis.

Fig. 2.—Case 2: 19-year-old woman with postoperative subdural empyema and multiple previous craniotomies, most recently 5 years earlier for sphenoid wing fibrous dysplasia.

A, Contrast-enhanced CT scan 6 months before presentation shows postoperative changes in inferior left frontal lobe.

B and C, Coronal MR images, 500/30 (B) and 2150/120 (C), on admission show sphenoid sinusitis and dural-based mass hyperintense relative to CSF. Note absence of hypointense rim and moderate amount of surrounding edema.

D and E, Axial nonenhanced (D) and enhanced (E) CT scans the same day show ring-enhancing lesion indistinguishable from parenchymal abscess.



A



B



C



D



E

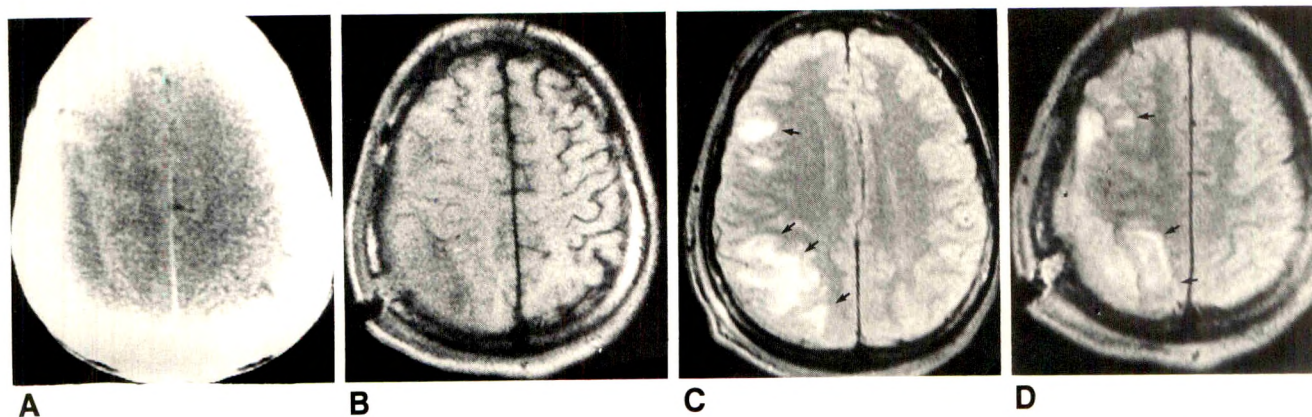


Fig. 4.—34-year-old man with subdural empyema secondary to infection of posttraumatic subdural hematoma.

A, Nonenhanced CT scan 2 weeks after injury shows right frontoparietal extraaxial fluid collection indistinguishable from subacute subdural hematoma.

B–D, Axial MR images, 500/30 (B) and 2150/60 (C and D), the same day show subdural empyema. Collection is hyperintense relative to CSF but hypointense relative to typical chronic hematoma; there is underlying cortical hyperintensity (arrows) and absence of hypointense medial rim.

E, Contrast-enhanced CT scan 2 weeks later shows irregular marginal enhancement suggestive of inflammatory nature of collection. Note lack of abnormal cortical enhancement.

F, Follow-up axial MR image, 2150/60, shows small residual collection and nearly complete resolution of parenchymal abnormalities.

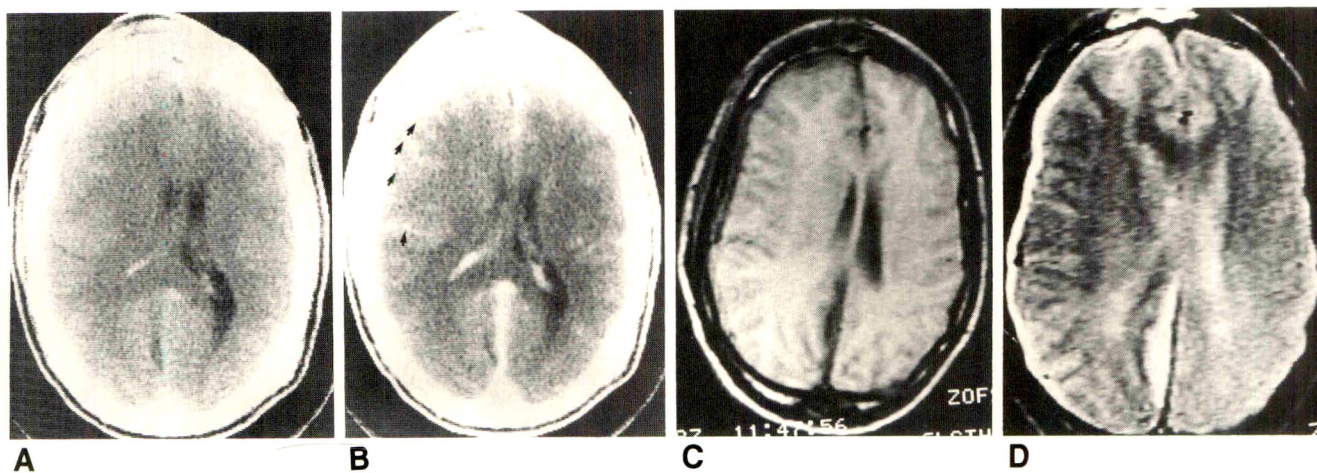
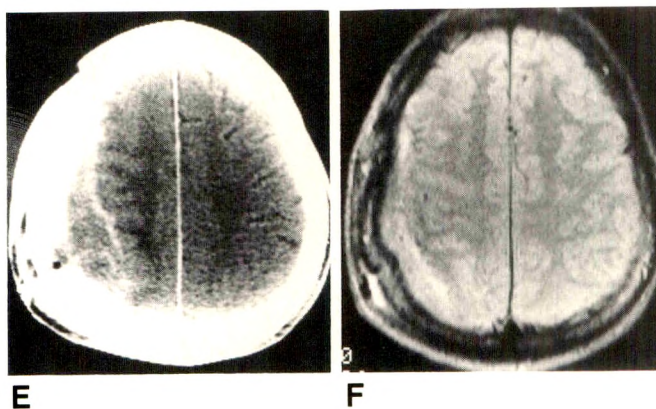


Fig. 5.—24-year-old man with otorhinologically induced subdural and epidural empyemas.

A and B, Nonenhanced (A) and enhanced (B) CT scans show right frontal sinusitis and poorly defined collection in interhemispheric fissure. Right hemispheric edema, mass effect, and right cortical (arrows) and falcine enhancement are present.

C and D, Axial 600/30 (C) and 2150/110 (D) MR images the same day show frontal sinusitis and right frontal, right convexity, and interhemispheric collections with intensity pattern typical of empyemas. Right frontal and convexity empyemas are visible only on MR. Note hypointense rim in former lesion and its absence in the latter, localizing these collections to epidural and subdural spaces, respectively.

space from paranasal sinus and otitic infections by way of retrograde thrombophlebitis of the bridging emissary veins [3, 5, 13]. Though the arachnoid acts initially as a barrier to the deeper spread of infection, unrestricted access in the supratentorial subdural space allows a thin layer of purulent material to be deposited diffusely over the cerebral convexity and/or in the parafalcine and paratentorial regions. An epidural empyema may occur in association with osteomyelitis of the

posterior paranasal sinus wall. However, an epidural empyema rarely occurs as an isolated event without the simultaneous presence or subsequent development of a subdural empyema (Figs. 1 and 5) [3, 13]. Progression of thrombophlebitis to involve the cortical veins and major dural sinuses ensues, with edema and ischemia of the subjacent cortex. Without prompt and aggressive therapy, irreversible dural sinus and venous thrombosis and secondary parenchymal

genic transformation of acute extraaxial empyemas into chronic extraaxial abscesses due to incomplete surgical drainage. Improvement in prognosis can be expected with the use of MR, due to its sensitivity and specificity for early and accurate diagnosis and its ability to monitor the response to therapy.

REFERENCES

1. Danziger A, Price H, Schechter MM. An analysis of 113 intracranial infections. *Neuroradiology* **1980**;19:31-34
2. Blaquiére RM. The computed tomographic appearances of intra- and extracerebral abscesses. *Br J Radiol* **1983**;56:171-181
3. Kaufman DM, Miller MH, Steigbigel NH. Subdural empyema: analysis of 17 recent cases and review of the literature. *Medicine (Baltimore)* **1975**;54(6):485-498
4. Joubert MJ, Stephanov S. Computerized tomography and surgical treatment of intracranial suppuration. *J Neurosurg* **1977**;47:73-78
5. Sharif HS, Ibrahim A. Intracranial epidural abscess. *Br J Radiol* **1982**;55:81-84
6. Kaufman DM, Litman N, Miller MH. Sinusitis: induced subdural empyema. *Neurology* **1983**;33:123-132
7. Luken MG, Whelan MA. Recent diagnostic experience with subdural empyema. *J Neurosurg* **1980**;52:764-771
8. Post EM, Modesti LM. "Subacute" postoperative subdural empyema. *J Neurosurg* **1981**;55:761-765
9. Bannister G, Williams B, Smith S. Treatment of subdural empyema. *J Neurosurg* **1981**;55:82-88
10. Sadhu VK, Handel SF, Pinto RS, Glass TF. Neuroradiologic diagnosis of subdural empyema and CT limitations. *AJNR* **1980**;1:39-44
11. Dunker RO, Khakoo RA. Failure of computed tomographic scanning to demonstrate subdural empyema. *JAMA* **1981**;246:1116-1118
12. Stephanov S, Joubert MJ, Welchman JM. Combined convexity and parafalx subdural empyema. *Surg Neurol* **1979**;11:147-151
13. Zimmerman RD, Leeds NE, Danziger A. Subdural empyema: CT findings. *Radiology* **1984**;150:417-422
14. Enzmann DR. Extracerebral infection. In: Enzmann DR, ed. *Imaging of infections and inflammations of the central nervous system: computed tomography, ultrasound, and nuclear magnetic resonance*. New York: Raven, **1984**:234-249
15. Weisberg L. Subdural empyema—clinical and computed tomographic correlations. *Arch Neurol* **1986**;43:497-500
16. Jacobson PL, Farmer TW. Subdural empyema complicating meningitis in infants: improved prognosis. *Neurology* **1981**;31:190-193
17. Borzone M, Capuzzo T, Rivano C, Tortori-Donati P. Subdural empyema: fourteen cases surgically treated. *Surg Neurol* **1980**;13:449-452
18. Smith HP, Hendrick EB. Subdural empyema and epidural abscess in children. *J Neurosurg* **1983**;58:392-397
19. Kjos BO, Brant-Zawadzki M, Kucharczyk W, Kelly WM, Norman D, Newton TH. Cystic intracranial lesions: magnetic resonance imaging. *Radiology* **1985**;155:363-369
20. Sze G, Zimmerman RD. The magnetic resonance imaging of infections and inflammatory diseases. *Radiol Clin North Am* **1988**;26:839-860
21. Macchi PJ, Grossman RI, Gomori JM, Goldberg HI, Zimmerman RA, Bilaniuk LT. High field MR imaging of cerebral venous thrombosis. *J Comput Assist Tomogr* **1986**;10:10-15
22. McMurdo SK, Brant-Zawadzki M, Bradley WG, Chang GY, Berg BO. Dural sinus thrombosis: study using intermediate field strength MR imaging. *Radiology* **1986**;161:83-86

³¹P Spectroscopy in Thrombolytic Treatment of Experimental Cerebral Infarct

Benjamin C. P. Lee^{1,2}
 John M. Brock³
 Teresa Fan³
 Anthony Seibert¹
 Chrit Moonen³
 Phillip Kissel⁴
 Bahram Chehrizi⁴
 E. Morton Bradbury³

Ischemic changes produced by autogenous clot embolization of intracranial arteries were monitored by continuous surface-coil ³¹P spectroscopy in 12 rabbits: six were used as controls and six were treated intravenously with tissue-type plasminogen activator. The animals were sacrificed and the brains were fixed with intravital stains.

The results indicate that spectral changes are reversible only when thrombolysis therapy is started within 30 min after ischemic changes are detected. The improvement of the ³¹P spectrum correlated with postmortem changes.

Tissue-type plasminogen activator (tPA)* is a thrombolytic agent recently approved by the FDA for the treatment of coronary occlusions [1, 2]. Since it is a naturally occurring agent that acts specifically on clots without inducing excessive bleeding in normal tissues, it may be potentially useful in the treatment of thrombotic disease of the cerebral arteries [3, 4]. It is known from experimental and clinical trials that thrombolysis is effective when tPA is administered intravenously within 3 hr of clot occlusion [5–7]. Arteries in the brain, unlike coronary vessels, are end arteries, unable to sustain prolonged ischemia because of the absence of collateral circulation [8–10]. Therefore, irreversible damage from arterial occlusions occurs much sooner in the brain than in the heart. Since conventional imaging techniques usually do not detect changes until several hours after they occur, other, nonimaging, methods must be used to monitor early ischemia [11–20]. The aim of this study is to develop an experimental model of cerebral ischemia in which the occlusions and effects of thrombolysis therapy may be evaluated by angiography, ³¹P spectroscopy, and postmortem intravital stains.

Materials and Methods

Twelve New Zealand white rabbits underwent carotid artery embolization with autogenous clots: six rabbits were used as controls and six were treated with tPA. ³¹P spectroscopy was performed on a 20-cm-bore 1.9-T Oxford TMR with Larmor frequency of 32.5 MHz. Magnetic field inhomogeneities were reduced by maximizing the root mean square of the H¹ with shim coils. We used a single-loop, double-tuned surface coil that measured 1 × 1.5 cm. The coil was placed in the center of the magnet and the heads of the animals were manipulated so that the hemisphere under evaluation was directly underneath. Spectral changes to a depth corresponding to the radius of the coil were detected. In addition to brain changes, spectra from the scalp and some from the contralateral hemisphere were also recorded.

To ascertain that a surface coil placed on the scalp recorded true brain spectra, a series of comparison experiments was performed: spectra were obtained by placing the coil (1) on the scalp, (2) on the skull after surgical removal of muscles, and (3) directly on the brain surface after a craniectomy was performed. There were no detectable differences in the appearance of the spectra from these locations. To optimize the sequences, different pulse widths were tried. A pulse width of 20 μsec was found to have adequate penetration through the brain surface and produced a spectrum with optimal signal/noise ratio. A repetition time of 2000 msec was selected, as it produced the best spectrum [16–18, 21]. At least 10 min

This article appears in the January/February 1989 issue of *AJNR* and the March 1989 issue of *AJR*.

Received December 31, 1987; accepted after revision June 19, 1988.

This work was supported by an NIH Regional

¹ Department of Radiology, University of California, Davis Medical Center, Sacramento, CA 95817.

² Department of Radiology, University of Minnesota Hospital and Clinic, Box 292, 420 Delaware St., S.E., Minneapolis, MN 55455. Address reprint requests to B. C. P. Lee.

³ Department of Biochemistry, University of California, Davis Medical Center, Sacramento, CA 95817.

⁴ Department of Neurological Surgery, University of California, Davis Medical Center, Sacramento, CA 95817.

AJR 152:623–628, March 1989

0361–803X/89/1523–0623

© American Roentgen Ray Society

* Tissue-type plasminogen activator (tPA) supplied by Genentech, Inc., South San Francisco, CA.

The degree of ischemia, as shown by the lack of brain parenchyma staining with TTC, was extremely variable, involving the entire hemisphere in one case (Fig. 3) and multiple areas in the middle cerebral artery region in four cases (with additional involvement of the posterior circulation in one other case) (Fig. 4).

Thrombolysis Group (³¹P Spectra)

Group 1.—There was no reversal of the ischemic changes (Fig. 5). The ischemic areas shown in the TTC-stained tissue sections were very similar to those seen in the control group.

Group 2.—The baseline PCr/Pi was approximately 2 (\pm 0.15). Total reversal of ³¹P spectra was achieved in one animal (Fig. 6); in the other two animals, there was partial reversal of

³¹P spectra (Fig. 7). Ischemic areas were demonstrated in all three animals in the TTC-stained brains, and were less extensive in distribution than in the control group (Fig. 8).

Discussion

Brain storage of high-energy PCr is interchangeable with ATP, which is required for cerebral metabolism. During normal aerobic activity, ATP is produced within the mitochondria by oxidative phosphorylation. When oxygen is unavailable during anoxia or ischemia, anaerobic metabolism is necessary. This mechanism is, however, inefficient and the ATP required for net metabolism has to be supplemented by depletion of the PCr pool. Metabolic by-products of this activity are Pi and lactic acid, which result in metabolic acidosis (Fig. 9) [23]. ³¹P

Fig. 2.—Anteroposterior view of common carotid injection.

A, After embolization there is occlusion of carotid bifurcation. Proximal portion of carotid artery is patent (arrowheads). Note occlusion of a number of external branches.

B, Right distal carotid (long arrow), middle (short arrows), and internal carotid (arrowheads) arteries have recanalized after tPA infusion.

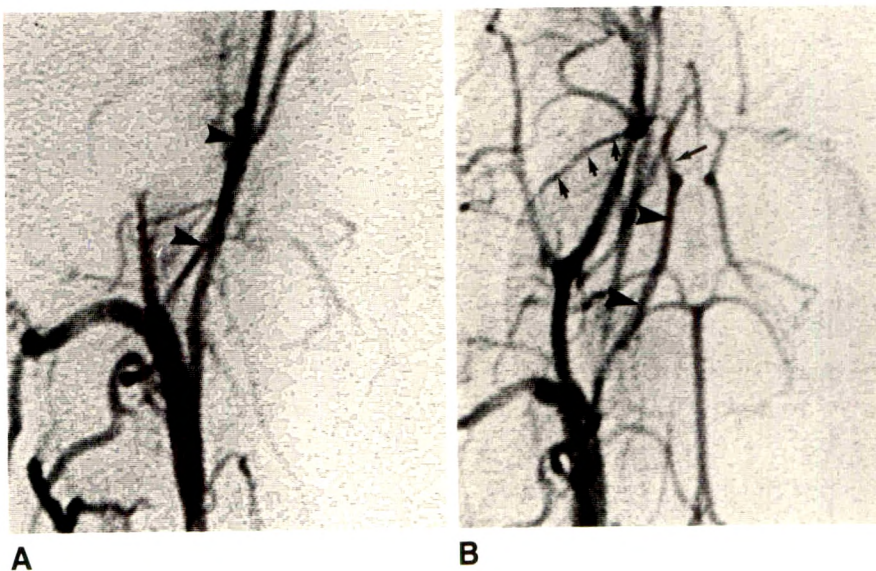


Fig. 3.—View of TTC-stained brain seen from top. Lack of staining of entire left hemisphere and portions of right hemisphere indicates infarcts in these regions (after embolization).

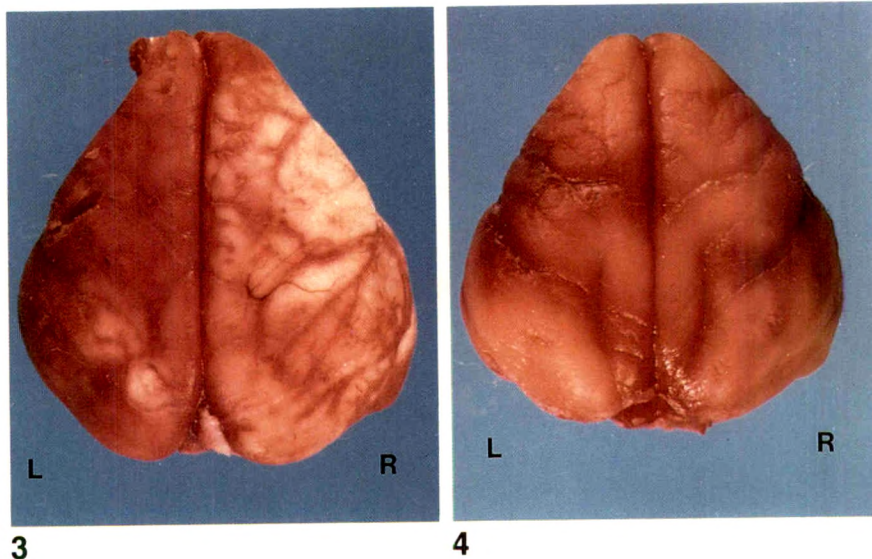


Fig. 8.—TTC-stained rabbit brain, top view (A) and left lateral view (B), shows only a small area of poor staining in distribution of middle cerebral artery. Right hemisphere is normal. (Thrombolysis, group 2.)

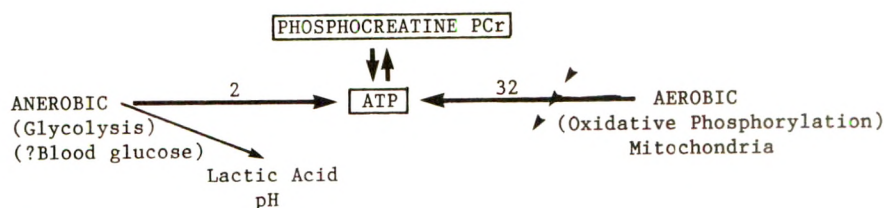
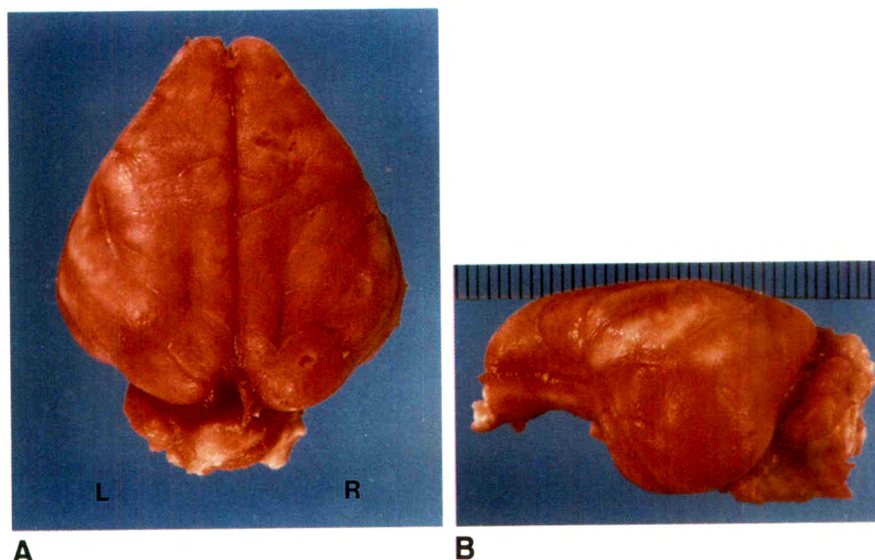
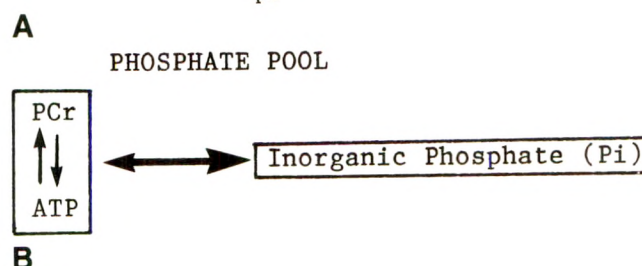


Fig. 9.—Metabolic pathway.

A, Normal aerobic metabolism produces 32 units of ATP, which is then stored as high-energy phosphocreatine. Anaerobic metabolism produces only 2 units of ATP but a considerable amount of lactic acid, causing acidosis.

B, During anaerobic metabolism, the phosphocreatine pool is depleted and inorganic phosphates (Pi) are produced.



only when the PCr pool begins to be depleted. At this stage, the changes are irreversible and death occurs.

Embolization

The rabbit was chosen because human tPA is 60% effective in this experimental animal [26]. The carotid circulation in the rabbit consists of an extensive network of external circulation and small internal carotid arteries [26–28]. The circle of Willis is prominent, however, and allows free communication between the carotid and vertebral basilar circulations. While a large embolus within the cervical portion of the internal carotid artery of a human patient often gives rise to severe infarcts of the cerebral hemispheres, a similarly located experimental embolus in the rabbit usually produces no detectable ischemic ³¹P spectral changes because of the effective cross flow within the circle of Willis. The infarcts that are produced by such proximal occlusions tend to be small and inconsistent in size and distribution. Because of the unpredictable nature of the infarcts produced by this technique, we chose to deliver

small emboli more selectively. Clots less than 400 μ m were injected through catheters selectively placed in the internal carotid arteries. Because of the small caliber of these vessels relative to the catheter, the arteries were invariably occluded and the air that accumulated within the catheter during the course of selective catheterization could not be purged prior to embolization, resulting in immediate death in several animals. This can be avoided by catheterization of the larger common carotid arteries and nonselective embolization. The cerebral flow carries the small emboli into the peripheral branches of the anterior and middle cerebral circulations and produces large infarcts, involving one or both hemispheres [29].

Sensitivity

The surface coil used in this study is designed so that it corresponds as closely as possible to the configuration and size of the cerebral hemispheres. In spite of this, a small amount of signal from the contralateral hemisphere is detect-

Pseudoaneurysm and Arteriovenous Fistula After Femoral Artery Catheterization: Association with Low Femoral Punctures

Robert S. Altin¹
Stephanie Flicker
Howard J. Naidech

We determined the location of arterial injury in 11 patients who had pseudoaneurysms with (six cases) or without (five cases) arteriovenous fistula as a complication of cardiac catheterization. Medical records and arteriograms were examined retrospectively. Ten of the 11 pseudoaneurysms identified were located below the level of the femoral head. Five of six patients with arteriovenous fistula had simultaneous catheterization of both the femoral artery and the femoral vein.

Although we did not determine the location of arterial puncture used in uncomplicated angiograms during the 5-year study period, our experience in 11 patients with pseudoaneurysms with or without arteriovenous fistula suggests that there is an association between a puncture site below the level of the femoral head and arterial injury. In addition, arteriovenous fistulas appear to be associated with simultaneous catheterization of the femoral artery and adjacent femoral vein.

Local complications of femoral artery catheterization are uncommon but occur in any institution where angiography and/or cardiac catheterization are performed on a regular basis. We think that they are becoming more frequent. This may result from an increase in interventional techniques, use of larger catheters, anticoagulation, and thrombolysis. Most local complications are in the following categories: hematoma, pseudoaneurysm, arteriovenous fistula, arterial obstruction, lymphocele, or abscess [1].

A pseudoaneurysm is a hematoma with a persistent communication to the artery. An arteriovenous fistula is an abnormal communication between an artery and vein. Femoral pseudoaneurysm has been related to puncture distal to the bifurcation of the common femoral artery [2]. Hemorrhage may be limited to the area surrounding the common femoral artery by the femoral sheath. Posterior bony support provided by the femoral head contributes to adequate arterial compression after catheter removal [2]. Most previous reports of local complications after angiography have not described the location of the arterial injury as it relates to either the femoral artery bifurcation or the femoral head [1, 3-5]. The purpose of this study is to determine the level of puncture in femoral arteries damaged during angiography relative to the femoral head and the bifurcation of the common femoral artery.

Materials and Methods

We reviewed the records of all patients in whom pseudoaneurysm and/or arteriovenous fistula of the femoral artery were diagnosed from 1983 to 1987 at our institution. During this period, there were 13,625 adult cardiac catheterizations and 1634 pediatric cardiac catheterizations, and 1300 arteriograms were performed in the radiology department. Sixteen patients had the diagnosis confirmed by angiography.

The arteriograms were reviewed to determine the level of the arterial puncture, which was assumed to be at the level of the pseudoaneurysm in 11 cases. Five additional cases had arteriovenous fistula without a localized collection of contrast material; reflux of contrast material distally in the femoral vein made localization of the fistula impossible. These patients

Received September 9, 1988; accepted after revision October 27, 1988.

¹ All authors: Department of Radiology, Deborah Heart and Lung Center, Browns Mills, NJ 08015. Address reprint requests to R. S. Altin.

AJR 152:629-631, March 1989
0361-803X/89/1523-0629
© American Roentgen Ray Society

4. Halpern M. Percutaneous transfemoral arteriography: an analysis of the complications in 1,000 consecutive cases. *AJR* 1964; 92:918-934
5. Ross RS. Arterial complications. *Circulation* 1968; 37:39-41
6. Helvie MA, Rubin JM, Silver TM, Kresowik TF. The distinction between femoral artery pseudoaneurysms and other causes of groin masses: value of duplex Doppler sonography. *AJR* 1988; 150:1177-1180
7. Fitzgerald EJ, Bowsher WG, Ruttley MST. False aneurysm of the femoral artery: computed tomographic and ultrasound appearance. *Clin Radiol* 1986; 37: 585-588
8. Mitchell DG, Needleman L, Bezzi M., et al. Femoral artery pseudoaneurysm: diagnosis with conventional duplex and color Doppler ultrasound. *Radiology* 1987; 165:687-690
9. Coughlin BF, Paushter DM. Peripheral pseudoaneurysms: evaluation with duplex ultrasound. *Radiology* 1988; 168:339-342



Scientific Program (200 papers)

Instructional Courses (60 hours)

Categorical Course on
Genitourinary Radiology

The Caldwell Lecture

Award Papers

Scientific Exhibits

Social, Golf, and Tennis Programs

Guest Programs



Come to the American Roentgen Ray Society 89th

ANNUAL MEETING



New Orleans Hilton May 7-12, 1989

Color Doppler Sonography of Hemodialysis Vascular Access: Comparison with Angiography

William D. Middleton¹
Daniel D. Picus
M. Victoria Marx
G. Leland Melson

This study was performed to define the color Doppler sonographic appearance of normal and abnormal hemodialysis vascular access and to compare color Doppler sonography with angiography. Twenty-eight patients (nine with Brescia-Cimino fistulas and 19 with synthetic grafts) were imaged with digital subtraction angiography and color Doppler sonography. The examinations were interpreted independently and then interpreted together to determine the accuracy of the two methods. With angiography as the gold standard, color Doppler sonography correctly identified 20 of 23 stenosed vessels, three of four occluded vessels, four of four thrombosed vessels, and 18 of 19 pseudoaneurysms. Overall, color Doppler sonography correctly identified all lesions that were seen angiographically in 16 of 19 patients with synthetic grafts and in four of nine patients with Brescia-Cimino fistulas. Five asymptomatic arterial steals were detected sonographically. One of these was identified with angiography.

Color Doppler sonography is an adequate means of imaging suspected complications of hemodialysis vascular access, and it should be used in selected patients. However, digital subtraction angiography is more sensitive and should be the initial imaging technique for most of these patients.

Adequate vascular access is essential for long-term hemodialysis. This is obtained through a variety of surgically created arteriovenous fistulas [1, 2]. Although these fistulas generally function well, all types of vascular access are prone to develop lesions that may interfere with hemodialysis [3]. In fact, malfunction of vascular access is the most frequent cause of hospitalization in patients who are on long-term hemodialysis [4].

Because potential sites for vascular access are limited, extending the life of an existing fistula or graft is of great benefit. Early detection, localization, and characterization of lesions that compromise hemodialysis are extremely important because they may allow correction before failure of the access. At our institution, radiologic evaluation of patients with suspected complications of vascular access relies on digital subtraction angiography (DSA) with direct injection of the synthetic graft or fistula [5].

Recent advances in Doppler imaging techniques have allowed for high-quality color Doppler sonography of superficial vessels. Initial results in the carotid bifurcation [6], femoral artery [7], and lower-extremity veins [8] suggest that color Doppler sonography will be a valuable noninvasive means of evaluating the peripheral vasculature. These reports have prompted us to investigate color Doppler sonography of vascular access. This study was undertaken to determine the color Doppler sonographic appearance of common vascular lesions associated with vascular access, to define its accuracy compared with angiographic methods, and to determine its role in evaluating suspected complications of vascular access with respect to angiography.

Subjects and Methods

The study group consisted of 28 patients referred to the radiology department for suspected complications of hemodialysis vascular access. There were 15 women and 13

Received September 19, 1988; accepted after revision October 31, 1988.

Presented at the annual meeting of the American Roentgen Ray Society, San Francisco, CA, May 1988.

¹ All authors: Washington University School of Medicine, Mallinckrodt Institute of Radiology, 510 S. Kingshighway Blvd., St. Louis, MO 63110. Address reprint requests to W. D. Middleton.

AJR 152:633-639, March 1989
0361-803X/89/1523-0633
© American Roentgen Ray Society

Fig. 2.—Morphologically normal arterial anastomosis with asymptomatic radial artery steal. Longitudinal color Doppler sonogram of end-to-side anastomosis between synthetic graft and radial artery shows blood flow in distal radial artery (DRA) is directed toward anastomosis, indicating arterial steal. Only distalmost portion of graft (G) is in plane of section. PRA = proximal radial artery.

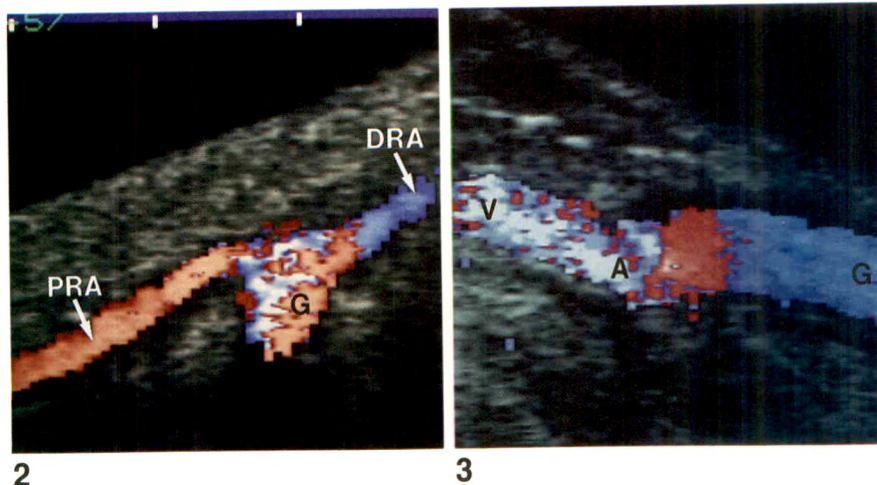


Fig. 3.—Normal venous anastomosis. Longitudinal color Doppler sonogram shows anastomosis (A) between synthetic graft (G) and draining vein (V).

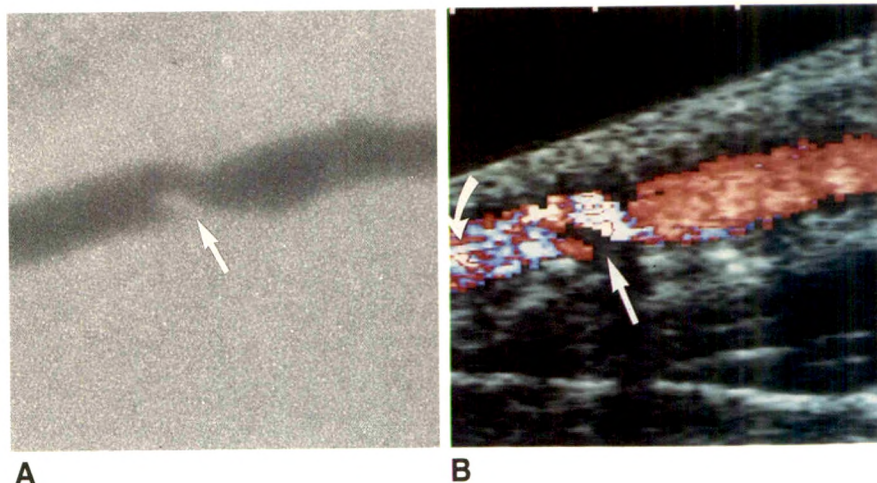


Fig. 4.—Graft stenosis.
A, Angiogram shows weblike stenosis (arrow) in venous limb of synthetic graft.
B, Longitudinal color Doppler sonogram shows morphologically similar weblike stenosis (straight arrow) and associated turbulent flow (curved arrow).

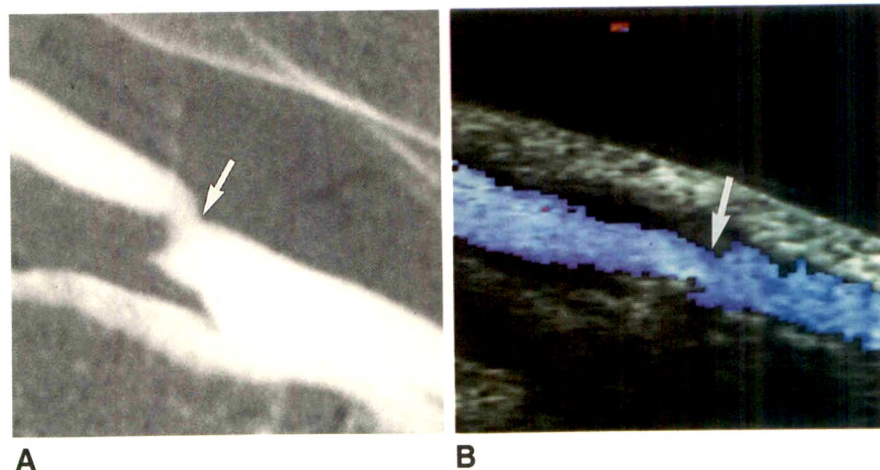


Fig. 5.—Venous anastomotic stenosis.
A, Angiogram shows focal stenosis at venous anastomosis of synthetic graft (arrow).
B, Longitudinal color Doppler sonogram shows morphologically similar focal stenosis (arrow) with normal associated flow.

ance of an occluded vessel was an abrupt termination of the vessel, with visualization of a collateral vessel oriented in a different plane (Fig. 6). Although color Doppler sonography detected the occlusions in these three cases, the pattern and full extent of collateral flow were not imaged as easily or as fully sonographically as they were angiographically. The one

false-negative color Doppler sonographic examination occurred in a patient with a direct arteriovenous fistula in whom the proximal radial artery was occluded.

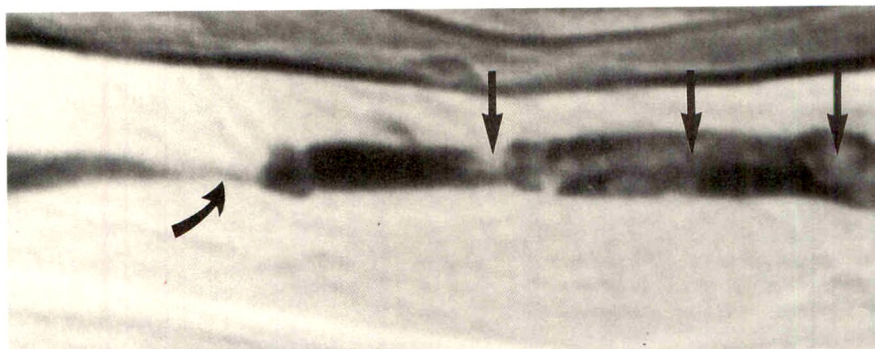
Four cases of thrombosis were detected angiographically, and all four also were seen with color Doppler sonography, for a sensitivity of 100%. In three cases, the thrombus totally

Fig. 7.—Nonocclusive venous thrombosis.

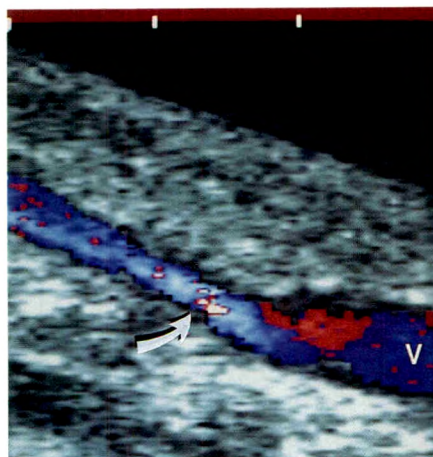
A, Angiogram of venous outflow shows tight stenosis (*curved arrow*) in vein and extensive distal filling defects before stenosis due to partial venous thrombosis (*straight arrows*).

B, Longitudinal color Doppler sonogram of venous outflow shows long tight stenosis (*arrow*) proximally and normal caliber vein distally (V).

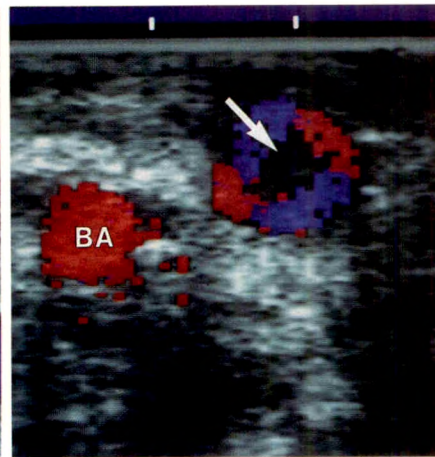
C, Transverse color Doppler sonogram through venous thrombosis shows central thrombus (*arrow*) with peripheral flow in vein. BA = adjacent brachial artery.



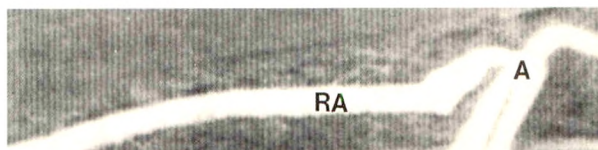
A



B



C



BA = adjacent brachial artery.

is slightly less accurate even though it is noninvasive. Therefore, we think that DSA should be the procedure of choice in the initial evaluation of most patients with suspected complications of hemodialysis vascular access. At the present time, color Doppler sonography should be used as the initial imaging examination in patients being evaluated for palpable masses or possible arterial steals and in patients with an allergy to contrast medium. Color Doppler sonography should also be used after angiography if the angiographic results are indefinite. Perhaps with further improvements in color Doppler sonography technology and/or increased experience in performing and interpreting the examinations, color Doppler sonography may have a greater role to play in patients with synthetic grafts.

ACKNOWLEDGMENTS

We thank Lynn Losse for manuscript preparation and Mary A. Middleton for manuscript review.

REFERENCES

1. Beven EG, Hertzner NR. Construction of arteriovenous fistulas for hemodialysis. *Surg Clin North Am* 1975;55:1125-1136
2. Giacchino JL, Geis WP, Buckingham JM, Ventuno LL, Bansal VK. Vascular access: long term results, new techniques. *Arch Surg* 1979;114:403-409
3. Mennes PA, Gilula LA, Anderson CB, Etheredge EE, Weerts C, Harter HR. Complications associated with arteriovenous fistulas in patients undergoing chronic hemodialysis. *Arch Intern Med* 1978;138:1117-1121
4. Hunter DW, So SK. Dialysis access: radiographic evaluation and management. *Radiol Clin North Am* 1987;25:249-260
5. Picus D, van Breda A, Katzen BT, Steinberg DL. Use of digital subtraction angiography for evaluation of vascular access for hemodialysis. *Cardiovasc Intervent Radiol* 1987;10:210-214
6. Middleton WD, Foley WD, Lawson TL. Pictorial essay. Color flow Doppler imaging of carotid artery abnormalities. *AJR* 1988;150:419-425
7. Mitchell DG, Needleman L, Rezzi M, et al. Femoral artery pseudoaneurysms: diagnosis with conventional duplex and color Doppler US. *Radiology* 1987;165:687-690
8. Foley WD, Middleton WD, Lawson TL, Hinson GW, Puller DR. Color flow Doppler imaging in suspected extremity venous thrombosis. Presented at the annual meeting of the Radiological Society of North America, Chicago, IL, November 1987
9. Middleton WD, Foley WD, Lawson TL. Flow reversal in the normal carotid bifurcation: color Doppler flow imaging analysis. *Radiology* 1988;167:202-210
10. Thomsen MB, Stenport G. Evaluation of clinical examination preceding surgical treatment of A-V fistula problems: is angiography necessary? *Acta Chir Scand* 1985;151:133-137
11. Gilula LA, Staple TW, Anderson CB, Anderson LS. Venous angiography of hemodialysis fistulas. *Radiology* 1975;115:555-562
12. Scheible W, Skram C, Leopold GR. High resolution real-time sonography of hemodialysis vascular access complications. *AJR* 1980;134:1173-1176
13. Weber M, Kuhn FP, Quintes W, Keidl E, Kohler H. Sonography of arteriovenous fistulae in hemodialysis patients. *Clin Nephrol* 1984;22:258-261
14. Kottle SD, Gonzalez AC, Macon EJ, Fellner SK. Ultrasonographic evaluation of vascular access complications. *Radiology* 1978;129:751-754

Insertion of Subclavian Hemodialysis Catheters in Difficult Cases: Value of Fluoroscopy and Angiographic Techniques

J. Bayne Selby¹
 Charles J. Tegtmeyer¹
 Celso Amodio^{2,3}
 Lori Bittner¹
 Nuzhet O. Atuk²

Double-lumen hemodialysis catheters designed to be placed via a subclavian vein approach have gained rapid acceptance over the past several years. Several studies have shown a significant rate of subclavian vein stenosis or occlusion after placement of these catheters. A large number of these patients require repeat placement of catheters with access often becoming increasingly difficult to obtain. Over the past 5 years, we have been asked to place 38 catheters in 34 patients that could not be placed at the bedside. Our procedure consists of obtaining a preliminary venogram to evaluate the reason for difficulty. The subclavian vein is then cannulated under direct fluoroscopic visualization while the peripheral venous line is injected with contrast material. Percutaneous angiographic techniques are then used to position the catheter. Satisfactory placement was obtained in all 38 cases. There were no complications, which is surprising considering the number of complications seen with the standard methods of insertion.

This represents a new role for the interventional radiologist, one that can be important in minimizing the number of new dialysis sites in any one patient.

The use of double-lumen subclavian catheters for temporary dialysis has gained rapid acceptance over the past 5 years [1-4]. This is a safe and relatively simple method to continue dialysis while the patient waits for a more permanent solution, such as recovery of renal function, construction of an arteriovenous fistula, or kidney transplant. These catheters are also being used more frequently for plasmapheresis [1]. Although most of these catheters are placed at bedside without difficulty, patients are referred to us for catheter placement when insertion is difficult.

These patients usually have had numerous unsuccessful attempts at catheter placement. Most often, the problems are inability to cannulate the vein or difficulty in passing the wire. Less often, patients are referred because of previous complications during placement such as large hematomas or pneumothorax.

We have developed a technique that uses fluoroscopic guidance and angiographic techniques that has allowed simple and rapid placement of 38 subclavian catheters in 34 patients. In addition to a 100% success rate, we have had no complications.

Materials and Methods

We reviewed the records from the radiology department at the University of Virginia Hospital of all patients in whom subclavian catheters were placed from January 1, 1983, to April 1, 1988. Preliminary arm venograms were obtained in all patients referred for catheter placement. Bilateral arm venograms were obtained when a specific side was not requested or when there was a question of patency of either subclavian vein (Fig. 1). A 19-gauge catheter placed in a medial antecubital vein was used whenever possible, and then 50 ml of contrast material were rapidly injected. Twelve radiographs were obtained after 30 ml of contrast material had been injected. After the first three films, the arm was lifted to obtain better filling of the superior vena cava [5]. The first three films were shot at one per second,

Received September 6, 1988; accepted after revision October 31, 1988.

Presented at the annual meeting of the American Roentgen Ray Society, San Francisco, CA, May 1988.

¹ Department of Radiology, Box 170, University of Virginia Medical Center, Charlottesville, VA 22908. Address reprint requests to J. B. Selby.

² Department of Internal Medicine, University of Virginia Medical Center, Charlottesville, VA 22908.

³ Present address: Instituto Dante Pazzanese de Cardiologie, Av. de Dante Pazzanese 500, Sao Paulo, Brazil 04012.

AJR 152:641-643, March 1989

0361-803X/89/1523-0641

© American Roentgen Ray Society

without fluoroscopic guidance, while physicians referred 30 cases (5.4%) to the radiology department.

Discussion

Insertion of central venous catheters has historically been performed at the bedside by the primary clinician. Patients with trauma or acute medical ailments usually require access for only a short period. Those requiring extended central venous access, such as cancer patients, often have a Hickman-type catheter placed in the operating room.

The growing acceptance of double-lumen subclavian catheters for hemodialysis or plasmapheresis has resulted in a new subset of patients who often require multiple temporary catheters, but for whom intraoperative placement is not warranted. At the University of Virginia Hospital, this has become the first choice of access for temporary indications. Most catheters are placed in the renal dialysis unit by a nephrologist.

As the popularity of this procedure has increased, so have referrals in cases of difficult placement. Over the past year, we have performed this technique at the rate of one every 3 weeks. A method for fluoroscopic guidance of antecubital venous puncture has been described [6], as has a percutaneous technique for repositioning of central venous catheters [7]. However, to our knowledge, this is the first description of a technique for placing subclavian catheters with fluoroscopic guidance.

A preliminary venogram is mandatory. The use of fluoroscopy allows selection of a more lateral site for the skin incision, where the vein maintains a large caliber and the risk of pneumothorax is less. Only 10–20 ml of contrast material are required to visualize the vein during the puncture. In obese patients, taping the breast down is helpful, because this more closely approximates the surface anatomy in the erect position. Failure to do this can result in kinking of the catheter when the patient stands up.

The major advantages of the technique are fourfold. The most obvious is direct visualization of the subclavian vein. Whereas multiple sticks are often required even in successful bedside placements, we have rarely needed more than one attempt. The second advantage is our ability to direct the wire when it does not naturally follow into the superior vena cava. We have encountered no difficulty in redirecting the wire into the inferior vena cava with a 5-French catheter. Third, we can use stiffer wires or a stiffener if threading the

catheter is difficult. This usually occurs when the patient is obese. Finally, we can immediately verify that position and function are satisfactory.

Compared with the lack of complications in catheter placement with our technique, complications associated with conventional placement are well documented [8, 9]. An immediate mechanical complication has been reported in 1–7% of cases [8]. These complications are pneumothorax, hemothorax, or hemomediastinum. Also 15 cases of life-threatening complications have been reported and have resulted in three deaths [9]. These have been related to malposition of the catheter tip, usually too low in the right atrium or tenting the superior vena cava. Visualization of the vein during puncture optimizes needle placement, thereby making pneumo- or hemothorax unlikely. The more serious complications are avoided by positioning the catheter tip just above the superior vena cava–right atrium junction while ensuring that it does not tent the wall.

Sepsis and subclavian vein thrombosis are also complications, usually related to the length of time the catheter is in the vein. Although we have not encountered these, it is less clear to what extent our technique is responsible. Certainly, our quicker, less traumatic procedure may decrease their likelihood.

REFERENCES

1. Uldall PR, Woods F, Bird M, Dyck R. Subclavian cannula for temporary hemodialysis. *Proc Clin Dial Transplant Forum* 1979;9:268–272
2. Fares LG II, Hsu TC, Leva R, Feldman SD, Fletcher HS, Seltzer MH. Subclavian cannulation. Valuable dialysis access alternative. *Am Surg* 1984;50(5):283–285
3. Nelson EW. Venous access techniques. *Urol Clin North Am* 1986;13(3):475–487
4. Anderson JT, Gammelgaard J, Nielsen LM, Clausen E. Subclavian vein catheterization for acute and chronic haemodialysis. A safe temporary vascular access. *Int Urol Nephrol* 1986;18(3):327–332
5. Natu SS, Sequeira JC, Weitzman AF. An improved technique for axillary phlebography. *Radiology* 1982;142:529–530
6. Richards MJ, Metcalf SA. Fluoroscopic guidance of intravenous puncture for catheter placement. *Radiology* 1983;146:226
7. Lois JF, Gomes AS, Pusey E. Nonsurgical repositioning of central venous catheters. *Radiology* 1987;165:329–333
8. Eisenhouer ED, Derveloy RJ, Hastings PR. Prospective evaluation of central venous pressure (CVP) catheters in a large city-county hospital. *Ann Surg* 1982;196:560–564
9. Vanherweghem JL, Cabolet P, Dhaene M, et al. Complications related to subclavian catheters for hemodialysis. Report and review. *Am J Nephrol* 1986;6(5):339–345

Perspective

On Journals: The Competition for Minds and Money

B. G. Brogdon¹

There is a growing perception that peer-reviewed scientific journals in our discipline are severely threatened by a competitive genre, of which Peter Ogle's *Diagnostic Imaging* is recognized as the best (worst?) and most successful example [1-4]. Various labeled as proprietary, disposable, newsmagazine-type, commercial, profit-oriented, or throwaway journals, these publications seduce advertising dollars away from traditional refereed journals because of huge circulation figures and (presumably) a wide readership seduced in turn by a glossy format, a *Readers Digest*-type approach to radiologic science and technology, and timely reportage of current events whether governmental, industrial, organizational, societal, or scientific.

Further, it is charged that these privately owned journals are seducing our young academicians/researchers to contribute by offering quick submission-production throughput and the broadest possible exposure.

But, do these journals really occupy the position of importance and prestige attributed to them? Are circulation numbers meaningful when subscriptions largely are free? Is the readership really large, loyal, attentive, retentive, and truly influenced? A limited survey of residents in radiology, the journal readers and industry customers of the next three or more decades, suggests otherwise.

Incorporated in a broader survey (to be reported later), a simple question, "What three medical newspapers, magazines, or journals do you most often read?" was asked of radiology residents at two meetings. One was the combined annual meeting of AUR/SCARD/A³CR² held in New Orleans in April 1988. The other, in Switzerland, was the International Diagnostic Course in Davos (IDKD), the largest annual gathering of radiologists in Europe with a March 1988 registration

of 772 physicians from 20 countries. These residents may not be typical. I think they are the cream of the crop. The AUR/SCARD/A³CR² attendees (mostly Chief Residents in academic programs) have special attributes leading to their selection. The European residents who get to the IDKD meeting by virtue of enlightened chairmen or personal determination are a special breed.

The questionnaire was offered also to postresidency radiologists (who identified themselves in the European fashion as "associate," "private practice," or "chairman") attending IDKD '88 to see if there is a substantial generation gap in journal-reading habits. The number and nationality of IDKD respondents is furnished in Table 1. There seemed to be no

TABLE 1: Numbers and Nationalities of European (IDKD) Respondents

Country	Resident	Postresident
Federal Republic of Germany	35	29
The Netherlands	15	15
Austria	15	12
Switzerland	10	15
Sweden	2	13
Belgium	7	2
Yugoslavia	0	4
Norway	0	3
France	2	1
Italy	1	1
Great Britain	0	1
Finland	0	1
Nationality unstated	0	1
Total	87	98

Note.—IDKD = International Diagnostic Course in Davos.

¹ Department of Radiology, University of South Alabama Medical Center, Mobile, AL 36617. Address reprint requests to B. G. Brogdon.

From the Editorial Office

Why We Edit

Elizabeth Whalen¹

The profession of editing is not popularly recognized or understood. Children dream of growing up to be doctors, lawyers, teachers, or firefighters—but some of them end up, quite happily, as editors. Many people outside the world of publishing do not even understand *what* an editor does. To add to the confusion, the word “editor,” even at our own journal, may refer to several different functions: we have an editor-in-chief and an associate editor (both of whom decide on the worthiness of articles for publication) and the manuscript editors (who prepare the accepted articles for publication). In this article, I focus on the job of the manuscript editor and explain our editing goals, reasons, and compulsions. I hope to make clear why we make the changes we do and why, after all, we edit.

Editing Goals

All our editing goals come from one source: the desire to produce a good journal. Because a good journal can only result from the publication of good articles, we strive to print articles that are scientifically correct and clear to the reader. If an article contains valid scientific information that is important to the reader and clearly communicates that information, that article makes a significant contribution to the quality of the journal.

By the time an article is accepted for publication, it should be scientifically correct, because it has been reviewed by specialists and by the editor-in-chief. If, however, inconsistencies in the data or flaws in logic have not been detected, it is the manuscript editor's job to catch them. So we check the information given; we verify that the tables, figures, and text all say the same thing and that the conclusion in the

abstract is the same as that at the end of the article. If any sentence is not logical, we question it. If, for example, it seems obvious from the context that the author meant “not” rather than “now,” we will change the word and ask the author to check it in the galley stage. We strive to catch all illogical sentences and inconsistencies in data before they get into print.

Even if the article is *perfect* scientifically, it will not make a contribution unless the message is clear to the readers. Clarity is certainly subjective, but often in technical journals such as ours, the author (who may be an expert in the subject matter) may assume that the readers know something that they do not. The manuscript editor watches for these “leaps in logic.” If a “therefore” makes no sense because no foundation has been laid for it, we will either try to fill in the gap or point out the problem to the author.

Another measure of quality for us is the correctness of references; the reader/researcher should be able to find the references cited. If an author's name is misspelled or if the year, volume number, or page numbers of a referenced article are wrong, then the person who wants to find the reference is faced with a difficult problem. Although we think it is ultimately the author's responsibility to ensure the correctness of references, we will ask about anything that seems to be wrong. If the page numbers for a journal article are cited as 356–787, we will ask, “Are page numbers OK? Was this article 431 pages long?” I remember one reference in which the first author's surname was spelled “Shpitz.” I had never seen a name spelled like that, and I assumed that a vowel was missing, so I wrote a query to the author who had cited the reference. The name was misspelled. He advised me that it should have been “Schpitz,” and I imagine that he wondered how I picked up such a “subtle” error!

¹ Publications Supervisor, *American Journal of Roentgenology*, 2223 Avenida de la Playa, Ste. 200, La Jolla, CA 92037. Address reprint requests to E. Whalen.

separate items: two substances + perfluorodecalin + perfluorotripropylamine.

Another reason for correcting wrong grammar is to eliminate sentences that the reader might find funny when they are not intended to be funny at all. Misplaced modifiers are the most common errors of this type. For example, we often find sentences that are structured like this one: "After turning the patient into the left posterior oblique position, multiple small stones separated along the gallbladder wall." Here the word "Turning" requires a subject (who is doing the turning?), and this sentence says that the little stones turned the patient to a new position. (Also, the use of "turning into" might bring to mind a phrase such as "turning into a pumpkin.") The editor should rephrase it ("After we turned the patient to the left posterior oblique position, multiple small stones separated along the gallbladder wall") and ask that the author verify the correctness of the change.

Correcting grammar is not a popular task. As Mawyer [4] pointed out: "The word 'grimoire,' meaning a wizard's book of black magic spells, has the same linguistic root as 'grammar.' As recently as the 16th century, the practice of 'gramarye' was a capital crime in Scotland, and people were burned or hung for it. Sometimes both. . . ." On one paper I edited, the author wrote, "Why in God's name did you change this?" He may have thought that burning or hanging would not be punishment enough.

Authors should know that we frequently do concede to jargon or popular usage, when that usage will be more clear to the reader than the strictly "correct" grammar. For example, I struggled with one paper that discussed "endothelial-like cells," an ungrammatical phrase meaning cells like endothelial cells. To make it proper, I would have had to use either that long phrase or two other unacceptable alternatives: "endothelium-like cells" (which is not what the author meant) or "endothelial-cell-like cells" (an editorial abomination). So, I left the phrase as the author had it, because I knew the readers would understand exactly what was meant.

Conclusion

I have been both a student and a teacher, and I know that sometimes when authors see their edited manuscripts they must feel as they did when they saw their essays marked up in elementary school. Grading or correcting (in the sense of a teacher grading or correcting papers) is not one of the purposes of manuscript editing. We seek (1) to improve the articles and thus improve the journal, (2) to make the articles

concise so that the *AJR* can give its readers as much current research as possible in each issue, (3) to clarify the typesetting and production instructions for the printer, and (4) to make the articles grammatically correct, within reason and with awareness that sometimes common usage is more clear than strict grammatical correctness.

I know that, at times, authors think that we have destroyed (or at least disrupted) their writing style. I remember a cartoon in which an editor sits at his desk reading the classic opening line of Dickens's *Tale of Two Cities*, "It was the best of times; it was the worst of times." The editor looks up from the manuscript and says thoughtfully, "Some things just cry out for editing." Although few *AJR* authors rank with Dickens in writing ability, we never deliberately tamper with an author's own style of expression. Overall, however, we are more concerned with the reader's understanding than with the author's attachment to a certain type of prose.

I hope that authors, when they look at a manuscript that seems to be "overedited," will feel as Bates does [5]: "Sometimes an editor stirs my ire, but often that same editor keeps me from making foolish errors. Even when I disagree with the suggestions, they make me take a second look, and that's good. So I must appreciate editorial advice and counsel even when I'm writing NO!!"

If there is still any doubt about why we edit, perhaps these words from the article by Scroggins [1] will explain more completely the editing passion: "We are obsessed with readers and their ability to understand printed words and thoughts as effortlessly as possible. We advocate clarity, consistency, correctness, and conciseness. . . . That obsession compels us to weed out wordy constructions, untangle convoluted sentences, unpack noun strings, and the like. . . . We search for words, phrases, and stylistic techniques that allow the reader to understand exactly, not partially, what the author intended." If, by our editing, we improve by one bit the communication between author and reader, then we have done our job well. The final satisfaction of editing is seeing the printed product and knowing that we have contributed to communicating important research to our readers.

REFERENCES

1. Scroggins MJ. In search of editorial absolutes. *STC Intercom* 1988;34(2):7
2. O'Connor M. *How to copyedit scientific books and journals*. Philadelphia: ISI Press, 1986:33-34
3. *Words into type*, 3rd ed. Englewood Cliffs, NJ: Prentice-Hall, 1974
4. Mawyer G. Investigative grammar. *J Urol* 1988;139:1128
5. Bates JD. How far should an editor go in changing a writer's work? *Editorial Eye* 1988;11:1-2

Letters

On the Value of Non-Contrast-Enhanced CT in Blunt Abdominal Trauma

Although an opposing view is always beneficial, in his commentary [1] Dr. Mindell reached several conclusions that may not be extracted from the paper by Kelly et al. [2] on the value of noncontrast CT in blunt abdominal trauma. I agree that some aspects in the data-gathering methodology are open to question, but they have been acknowledged by Kelly et al. in detail. Why repeat them? These limitations become particularly apparent when comparing the results of Kelly et al. with those of Wing et al. [3]. Wing et al. used contrast-enhanced scans, and Kelly et al. used combined noncontrast-contrast-enhanced scans as the gold standard for some of their patients. Wing et al. had a sensitivity and accuracy of 100% and 97.6% for contrast-enhanced CT, which compare favorably with the 92% and 91% values for the combined studies reported by Kelly et al. However, when the combined studies were considered as the gold standard, these values were significantly lower for contrast-only CT (74% and 84%, respectively). As expected, no significant difference in specificity occurred.

Dr. Mindell's objections are based on cost in both time and charges [1]. First, a patient who cannot tolerate an extra 5.5 min requires surgical intervention rather than CT [3]. Undoubtedly, physicians should be able to modify any protocol according to individual clinical circumstances. In practice, viewing the noncontrast images in an indiscriminate sequence helps both in detection and interpretation. Some of our residents even claim that this expedites decision making, which may have tempted some of them to peek at the noncontrast scans prematurely while the study of Kelly et al. was in progress.

Wing et al. showed that CT has played a substantial role in significantly decreasing the number of laparotomies, but the significance of CT in depicting lesions requiring surgical intervention in the absence of notable clinical suspicion is anecdotal. Is the information "no need for laparotomy" enough? Generally, patients are discharged after 24 hr of observation in the hospital when their CT study is normal and they have no other extraabdominal injuries. Although it has not been established whether conservative treatment of a patient with a "nonsurgical" injury should be any different, Kelly et al. showed a significantly higher sensitivity in detecting these injuries. But is the cost excessive? It seems that charging a patient having an additional limited (2-cm increment) sequence for a full combined noncontrast-contrast study (an extra \$81 at the University of Vermont) is extreme. The actual extra cost is no more than \$30. Are radiology departments so inflexible with their charges? Whatever the case, these calculations appear rather simplistic. They do not consider the money that is saved because use of CT results in fewer unnecessary exploratory

laparotomies [3] and fewer delayed complications from injuries originally missed. In the study of Kelly et al., three (9%) of the 34 injuries that required surgery were identified with the incorporation of a noncontrast sequence. The question of cost containment may be open to discussion, but nitpicking may be more costly.

Finally, I take a strong stand against the notion that the "larger goal" of CT is "the complete elimination of the need for diagnostic peritoneal lavage in blunt abdominal trauma" [1]. I disagree that this is or should be suggested as a goal for radiologists. Our goal at the University of Massachusetts has been better care and service for the patients by providing more accurate information. The study by Kelly et al. had the full support of our colleagues in surgery.

Vassilios Raptopoulos
University of Massachusetts Medical Center
Worcester, MA 01655

REFERENCES

1. Mindell HJ. Commentary. On the value of non-contrast-enhanced CT in blunt abdominal trauma. *AJR* 1989;152:47-48
2. Kelly J, Raptopoulos V, Davidoff A, Waite R, Norton P. The value of non-contrast-enhanced CT in blunt abdominal trauma. *AJR* 1989;152:41-46
3. Wing VW, Federle MP, Morris JA Jr, Jeffrey RB, Bluth R. The clinical impact of CT for blunt abdominal trauma. *AJR* 1985;145:1191-1194

Reply

Implementation of the recommendation of Kelly et al. [1] would have a significant impact on CT installations. Surely, it is appropriate to stress the potential bias in the data-gathering methodology. I am sorry if the authors think it is overdone; much praise is due Kelly et al. for conducting an ambitious project, under stressful emergency circumstances, to address a previously unanswered question. Dr. Raptopoulos's point about the results of Kelly et al. with contrast-only scanning is true: all previous studies lacked the gold standard of noncontrast scans. But, whatever the exact sensitivity of contrast-only CT in detecting small hematomas, in all major series to date, including those of Kelly et al. and involving hundreds of patients, clinically significant injuries have almost never been missed by the accepted contrast-only scanning protocols. It certainly was not clear to me from the article by Kelly et al. that the three patients requiring surgery, cited by Raptopoulos in his letter, were triaged only by additional noncontrast scanning. Raptopoulos argues that the small hematomas that may be detected by noncontrast scanning are clinically significant. However, it might be concluded from his own data that they are not. By themselves they do not indicate the need for surgical intervention, and in only one of 190 cases was the small

where tendons are angled about a bony surface and are separated from the underlying bone by a synovial bursa [1].

The interphalangeal sesamoid of the hallux is a type A sesamoid and together with its tendon of origin is incorporated into the joint capsule. Direct trauma in this case caused disruption of the joint capsule and forced the sesamoid into the joint, causing persistent dislocation.

We could find only a few reports [2, 3] of traumatic interposition of this sesamoid into the interphalangeal joint and, in these cases, the patients were treated with open reduction and surgical excision of the sesamoid. In our patient, after local anesthesia and traction, closed manipulation released the entrapped sesamoid from the joint and reduced the dislocation. Follow-up radiographs obtained 6 weeks later showed a normal-appearing joint and sesamoid bone.

This report describes successful management by closed reduction. Because closed manipulation can release the entrapped sesamoid, it should be attempted before resorting to surgery.

R. Szucs
J. Hurwitz

Medical College of Virginia
Virginia Commonwealth University
Richmond, VA 23298-0615

REFERENCES

1. Resnick D, Niwayama G, Feingold ML. The sesamoid bones of the hands and feet: participants in arthritis. *Radiology* 1977;123:57-62
2. Kohler A. *Borderlands the normal and early pathologic in skeletal radiology*. New York: Grune & Stratton, 1956:689-690.
3. Eibel P. Dislocation of the interphalangeal joint of the big toe with interposition of a sesamoid bone. *J Bone Joint Surg [Am]* 1954;36-A:880-882

MR Imaging as a Trigger for Persistent Claustrophobia

Because of its advantages, MR imaging is being used increasingly as a diagnostic tool. The imaging apparatus is a long, dark tube that causes transient claustrophobia in 1-5% of all patients [1]. We have recently described two patients who had no history of claustrophobia, tolerated MR imaging with great difficulty, and afterward noted persistent claustrophobia, which required psychiatric treatment [2].

At issue is whether claustrophobia would have developed in these patients without MR imaging and if the imaging served as the trigger for the claustrophobia. Although some current evidence [3] indicates that genetic factors play a role in the strength and content of phobic fears, there is disagreement about the nature of the trigger mechanism. Some authors think that the "conditioning experience" is a trigger, whereas others think that the "verbal or vicarious experience" is the trigger [4]. Our two patients did not fit into the typical age groups for the development of phobic fears [2]. This observation plus the sequence of events as outlined by these two patients appeared to implicate MR imaging as a possible trigger to the claustrophobia.

We think that our report should serve as a stimulus toward a systematic study of the possible occurrence of persistent claustrophobia after MR imaging. If such a study supports our observations, the acquisition of persistent claustrophobia via MR imaging may become a medicolegal problem. In this situation, MR stations may wish to do the following before patients are imaged: (1) ask if the patient has a history of phobia; (2) ask if anyone in the patient's family has a history of phobia; (3) warn the patient about the possible development of claustrophobia via MR imaging; and (4) perhaps, have the patient sign a release form.

D. Fishbain
M. Goldberg
E. Labbé
D. Zacher
R. Steele-Rosomoff
H. Rosomoff
University of Miami
South Shore Hospital and Medical Center
Miami Beach, FL 33139

REFERENCES

1. Hricak H, Amparo EG. Body MRI: alleviation of claustrophobia by prone positioning. *Radiology* 1984;152:819
2. Fishbain DA, Goldberg M, Labbé E, Zacher D, Steele-Rosomoff R, Rosomoff H. Long-term claustrophobia following magnetic resonance imaging. *Am J Psychiatry* 1988;145:1038-1039
3. Torgersen S. The nature and origin of common phobic fears. *Br J Psychiatry* 1979;134:343-351
4. McNally RJ, Steketee GS. *Behav Res Ther* 1985;28:431-435

Simpler Music/Audio System for Patients Having MR Imaging

Like Miyamoto and Kasson [1], I also have adapted an airplane pneumatic earphone headset for the delivery of music to patients within our MR scanner. However, I have been able to avoid all electronic interfacing by simply using a long length (approximately 20 ft [6.1 m]) of lightweight flexible tubing (originally intended for use with respirators) to carry in sound directly from a sound source (radio or tape player) located outside the RF-shielded room enclosing the scanner. The tubing enters the room through an unused space in the RF-penetration panel in the wall. At one end, the tubing is joined with tape to the end of the headphone tubing that normally would be plugged into the airplane seat armrest. At its other end, the tubing is coupled to the sound source by means of a funnel with its narrow end taped into the end of the tubing and its flared end taped over the speaker of the sound source. Despite the long length of the tubing and the simple mechanical acoustic coupling, the quality of the sound is adequate and has been found quite acceptable by patients. The system has been used for more than 1 year with no maintenance necessary. Thus, for essentially no direct cost (using scavenged materials) and with no effect on image quality or monitoring of patients, we have been able to provide patients with music to make their MR experience somewhat more pleasant.

Leon Axel
Hospital of the University of Pennsylvania
Philadelphia, PA 19104

REFERENCE

1. Miyamoto AT, Kasson RT. Simple music/audio system for patients having MR imaging. *AJR* 1988;151:1060

Combined ^{99m}Tc -Sulfide Colloid and ^{99m}Tc -RBC Studies for Localization of Gastrointestinal Bleeding Sites

An advantage of using ^{99m}Tc -RBC to detect sites of gastrointestinal bleeding is that the method permits recognition of intermittent bleeding. One major limitation is that localization of the bleeding site may be imprecise if abnormal activity is seen on delayed images only. Peristalsis can carry extravasated blood distally, and retrograde reflux

formed on admission and 6 months and 1 year later showed progressive periventricular hyperintensity of the right cerebral hemisphere (Fig. 1B). Cerebral angiography showed severe stenosis of the extracranial part of the right internal carotid artery on admission and progression to obstruction 1 year later.

To our knowledge, there have been no reports of progressive hyperintensity of the periventricular white matter on MR images. The cause of periventricular hyperintensity is thought to be hypoxia due to arteriosclerosis of long, penetrating arteries in the white matter. In our case, right-sided diffuse hypoperfusion was noted on SPECT before ipsilateral progressive hyperintensity was identified on MR images. The left periventricular region, to which blood flow was preserved, did not show the progression of hyperintensity. The cause of the periventricular hyperintensity noted on admission is uncertain. However, the possibility that chronic circulatory insufficiency is a cause of diffuse cerebral periventricular hyperintensity is suggested by the finding that the hyperintensity progressed on the hypoperfused side only.

Sung-eun Lee
Akio Terashi
Nippon Medical School
Tokyo, 102, Japan

REFERENCES

1. Zimmerman RD, Flemming CA, Lee BCP, Saint-Louis LA, Deck MDF. Periventricular hyperintensity as seen by magnetic resonance: prevalence and significance. *AJR* 1986;146:443-450
2. Gerard G, Weisberg LA. MRI periventricular lesions in adults. *Neurology* 1986;36:998-1001

The Left Hemidiaphragm and the Position of the Heart

It is generally accepted that the heart, which is positioned mainly on the left, causes the left hemidiaphragm to be lower than the right [1]. This is based on Wittenborg and Aviad's study [2] of 60 children with anomalous organ positions. Children with dextrocardia, regardless of the position of their liver, generally had a lower right hemidiaphragm.

However, the relationship between heart position and hemidiaphragm height has not been studied in normal adults. Therefore an analysis of normal radiographs was performed.

Posteroanterior and lateral chest radiographs of 37 patients (17 men and 20 women) who had no history of chest disease were reviewed. The average age of the patients was 40 years (range, 19-67). Measurements were made on the frontal radiograph as in Figure 1. The percentage of the heart to the left of midline was calculated as C divided by B. This was plotted against D, the hemidiaphragm height difference. The correlation coefficient and the significance level were calculated via standard methods.

The result was $r = .40$ ($p < .01$). The p -value is statistically significant, which supports the accepted concept of a relationship between the position of the heart and the height of the hemidiaphragm. The low correlation coefficient suggests that other factors independently influence the position of the heart and the height of the hemidiaphragm. The exact mechanism by which the heart affects the position of the diaphragm is unclear. Some authors [1] have referred to the role of heart mass. It has been suggested that the heart depresses the left hemidiaphragm [3]. Others have observed that when a patient is radiographed upside down, the relative position

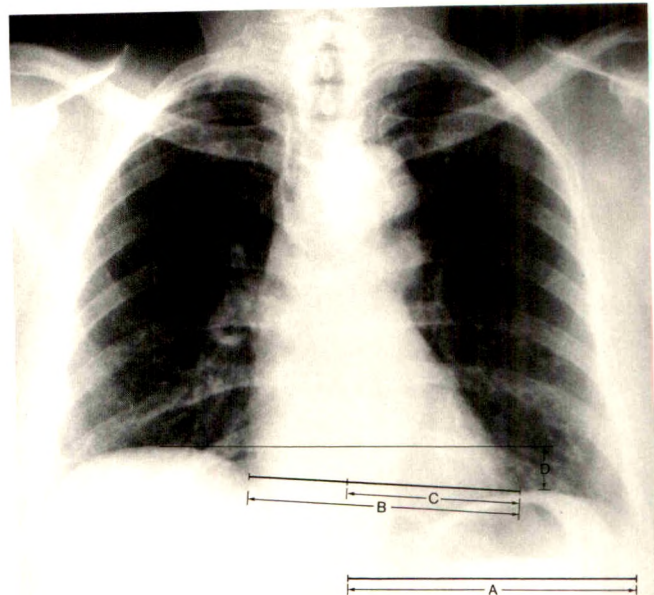


Fig. 1.—A = left hemidiaphragm width (measured from left costophrenic angle to midline). B = lower heart width (line between right and left borders of heart where each intersects diaphragm). C = lower heart to left of midline (distance along line B from midline to left border of heart). D = hemidiaphragm height difference (difference between peak heights measured perpendicular to midline; recorded as a negative number if left hemidiaphragm is highest).

of the hemidiaphragms does not change, implying that heart mass is not a factor [2].

In an attempt to test this proposition, I assumed that the mass of the heart correlated roughly with heart width adjacent to the diaphragms. Referring to Figure 1, B was divided by twice A to determine the width of the lower heart relative to the chest. When correlated with D, the hemidiaphragm height difference, $r = .04$ ($p < .75$). No relationship was demonstrated.

I was surprised by this result and considered what factors other than heart weight could influence the position of the diaphragm. One possibility is that the position of the diaphragm determines the position of the heart rather than vice-versa. Alternatively, a common structure, such as the pericardium, that invests the heart and attaches to the diaphragm might affect the relationship between the heart and the diaphragm. Lastly, the heart might shield the diaphragm from the negative pressure exerted by the elastic recoil of the lungs. The hemidiaphragms, asymmetrically covered by the heart, would assume asymmetrical domes of differing heights.

Eyal Barzel
SUNY Health Science Center at Brooklyn
Brooklyn, NY 11203

REFERENCES

1. Fraser RG, Paré JAP, Paré PD, Fraser RS, Genereux GP. *Diagnosis of diseases of the chest*. Philadelphia: Saunders, 1988:267-268
2. Wittenborg MH, Aviad I. Organ influence on the normal posture of the diaphragm: a radiological study of inversions and heterotaxies. *Br J Radiol* 1963;36:280-288
3. Felson B. *Chest roentgenology*. Philadelphia: Saunders, 1973:421

Balloon angioplasty in the treatment of pulmonary hypertension caused by pulmonary embolism. Voorburg JAI, Cats VM, Buis B, Bruschke AVG (JAIV, University Hospital-Leiden, Leiden, the Netherlands). *Chest* 94:1249-1253, Dec. 1988

We present a 30-year-old man with pulmonary hypertension after pulmonary embolism. Pulmonary angiography showed multiple stenoses in the pulmonary vascular tree. We treated four of these stenoses by balloon angioplasty in three sessions. Pulmonary artery pressure was reduced from 90/25 mm Hg (mean 46) to 78/13 mm Hg (mean 35) with concomitant increase of aortic pressure from 105/60 mm Hg (mean 75) to 134/68 mm Hg (mean 90). Pulmonary perfusion scintigraphy showed increase of perfusion in the treated segments. Two procedures were followed by transient segmental pulmonary edema, but no other complications were noted. We conclude that balloon angioplasty is a promising method of lowering pulmonary artery pressure and improving pulmonary perfusion in suitable cases of pulmonary hypertension secondary to pulmonary embolism.

Circulation

Comparison of simultaneously performed digital and film-based angiography in assessment of coronary artery disease. Gurley JC, Nissen SE, Booth DC, et al. (JCG, Rm. MN670, 800 Rose St., Lexington, KY 40536). *Circulation* 78:1411-1420, 1988

This study compared digital angiography (Digital) to conventional cineangiography (Cine) for the diagnosis and quantification of coronary artery disease. Digital and Cine were obtained simultaneously under identical radiographic conditions during routine coronary arteriography. Using visual inspection and manual calipers, four independent observers identified 131 stenoses in 18 patients with multivessel coronary disease. There was no difference in interobserver variability between Digital and Cine during multiple subgroup analyses. Overall, Digital yielded significantly greater estimates of stenosis severity than did either of two separate Cine observations ($p < 0.0001$; average difference, 6.25%), but the differences fell below the level of statistical significance when only the group of stenoses 50% or greater were considered. Digital and Cine correlated well for the assessment of stenosis severity ($r = 0.88$), but linear regression comparisons of multiple subgroups consistently indicated modest overestimation of Cine by Digital. Smaller vessels, branch vessels, and mild lesions increased the likelihood of overestimation by Digital. Digital was highly sensitive for identification of clinically relevant stenoses, but less specific and less predictive than a second observation of Cine. Our results indicate that Digital and Cine are not interchangeable imaging techniques and that potential differences must be considered when Digital is used for clinical decision making.

Gastroenterology

Aortic stenosis, idiopathic gastrointestinal bleeding, and angiodysplasia: is there an association? A methodologic critique of the literature. Imperiale TF, Ransohoff DF (TFI, Yale University School of Medicine, New Haven, CT). *Gastroenterology* 95:1670-1676, 1988

To assess the reported association between colonic angiodysplasia and aortic stenosis, we performed a quantitative and methodologic analysis of the literature. In four controlled studies that support an association between aortic stenosis and idiopathic gastrointestinal bleeding there are major methodologic deficiencies including the following: nonblinded data collection, noncomparable diagnostic examination, nonblinded ascertainment of exposure, and noncomparable demographic susceptibility. None of the studies directly assesses angiodysplasia. Additional case reports about aortic valve replacement used to treat bleeding from angiodysplasia are limited in number and in duration of follow-up. We conclude that the existing literature

does not demonstrate an association between aortic stenosis and angiodysplasia. Further controlled evaluation of this topic would be useful.

Reprinted with permission by the American Gastroenterological Association.

Peutz-Jeghers syndrome: a clinicopathologic survey of the "Harrisburg Family" with a 49-year follow-up. Foley TR, McGarrity TJ, Abt AB (TRF, The Milton S. Hershey Medical Center, The Pennsylvania State University, Hershey, PA). *Gastroenterology* 95:1535-1540, 1988

Of the original Peutz-Jeghers families reported by Jeghers, the "Harrisburg Family" has now been followed for 49 yr. Their 12 affected family members comprise the largest Peutz-Jeghers kindred reported. The course of this family illustrates that Peutz-Jeghers syndrome is not a benign disease. One family member developed a duodenal carcinoma in a hamartoma with adenomatous changes; this progression in the duodenum has not previously been reported. Ten patients underwent 75 polypectomies. One patient developed short bowel syndrome. Three patients died in young adulthood. The development of gastrointestinal malignancy in 2 of the 12 affected patients suggests that Peutz-Jeghers syndrome may be a premalignant condition. Consequently, even asymptomatic gastric, duodenal, and colonic polyps should be removed endoscopically. If surgical intervention is necessary, intraoperative endoscopy with polypectomy may prevent the development of a short bowel syndrome. Colonoscopic screening of patients and their family members may be beneficial and surveillance for extraintestinal malignancy appears to be warranted.

Reprinted with permission by the American Gastroenterological Association.

Digestive Diseases and Sciences

Diffuse excess mucosal collagen in rectal biopsies facilitates differential diagnosis of solitary rectal ulcer syndrome from other inflammatory bowel diseases. Levine DS, Surawicz CM, Ajer TN, Dean PJ, Rubin CE (DSL, University of Washington, Division of Gastroenterology RG-24, Seattle, WA 98195). *Dig Dis Sci* 33(11):1345-1352, Nov. 1988

Solitary rectal ulcer syndrome (SRUS) is sufficiently uncommon that the clinician or general pathologist may lack familiarity with the disorder and may confuse it with other inflammatory bowel diseases. To evaluate the role of collagen staining in facilitating the differential diagnosis of SRUS, an initial open review was undertaken on 1672 consecutive patients whose 4780 colorectal biopsies were stained with H&E with added saffron to demonstrate collagen. Excess mucosal collagen was present in 39 (2.3%) of these patients. Twenty patients with a diffuse excess of mucosal collagen in biopsies from rectal ulcer margins or from otherwise abnormal rectal mucosa had SRUS; in the remaining 19 patients, excess mucosal collagen was focal (seven ischemic colitis, five collagenous colitis, three adenocarcinoma, and four chronic idiopathic ulcerative colitis). Diffuse excess mucosal collagen never was seen in idiopathic inflammatory bowel disease (128 Crohn's colitis and 446 ulcerative colitis). Blinded reviews then were performed on rectal biopsies from 33 patients with a variety of diagnoses (14 SRUS and 19 controls). Diffuse excess collagen by saffron staining was consistently observed in SRUS but was absent in all 19 controls. Additional blinded reviews were carried out because the collagen staining pattern in ischemic colitis, although focal, could potentially be confused with SRUS. It was possible to differentiate these two diseases blindly from one another by using additional histologic criteria (14 SRUS and 12 ischemic colitis). We conclude that the demonstration of a diffuse excess of mucosal collagen in rectal biopsies facilitates the diagnosis of SRUS and differentiates it from idiopathic ulcerative colitis and Crohn's disease, with which SRUS is often confused, and other inflammatory bowel diseases.

of Radiology, Hospital of the University of Pennsylvania, 3400 Spruce St., Philadelphia, PA 19104). *J Thorac Imaging* 3(4):11-28, 1988

This article reviews the chest radiographic manifestations of asbestos exposure. While the chest radiograph (CXR) is a highly valuable tool in the evaluation of asbestos-related disease, there are ongoing controversies regarding the sensitivity and specificity of the plain film in diagnosing asbestos-related disorders. Autopsy series indicate that at least 60% of pleural plaques may be overlooked. Conversely, such series indicate that up to 20% of plaques are falsely diagnosed. The significance of visceral pleural thickening and the definition and positive predictive value of diffuse pleural thickening as they relate to asbestos exposure are unresolved issues. Data suggest that the CXR may fail to reflect significant asbestosis in 10% to 20% of cases. On the other hand, the presence of overlying pleural abnormalities as well as technical factors may contribute to overreading of interstitial disease. Data on the rate of false positive readings for asbestosis are limited. Considered alone, the CXR can support but not specifically establish nor exclude the diagnosis of asbestosis. In practice, an ILO grade of less than 1/0 implies that the diagnosis is unlikely. A constellation of positive CXR findings may increase specificity, although the diagnosis rests on a combination of multiple clinical criteria.

Journal of Ultrasound in Medicine

Doppler criteria for intrauterine growth retardation: predictive values. Benson CB, Doubilet PM (CBB, Dept. of Radiology, Brigham and Women's Hospital, 75 Francis St., Boston, MA 02115). *J Ultrasound Med* 7:655-659, Dec. 1988

Published data concerning proposed antenatal Doppler criteria for intrauterine growth retardation (IUGR) was critically analyzed using the same technique that has been previously applied to conventional (non-Doppler) sonographic criteria for IUGR. Fifteen studies of Doppler criteria, each conducted in such a way that sensitivity and specificity could be determined, were identified through a literature review. These studies encompassed a variety of arterial waveform and volume blood flow criteria. Bayes' theorem was then used to determine the positive predictive value of each criterion if used as a screening test for IUGR. Criteria involving vessels that have been studied by at least two groups, including those involving umbilical artery waveform, uterine arcuate artery waveform, and umbilical vein

volume blood flow, had positive predictive values that fell in a low range (17-57%) similar to that previously found for conventional criteria. Two criteria, using fetal internal carotid artery and thoracic aortic waveforms, had higher positive predictive values (66 and 100%, respectively) in initial studies, but the data have yet to be replicated by other groups. It is concluded that no Doppler criterion has yet been established as a clinically useful method to screen for IUGR antenatally.

Reprinted with permission by the American Institute of Ultrasound in Medicine.

Journal of Computer Assisted Tomography

MR characteristics of prostatic carcinoma and benign prostatic hyperplasia at 1.5 T. Griebel J, Hess CF, Schmiedl U, Koelbel G (CFH, Radiologische Klinik der Universitaet Tuebingen, Roentgenweg 11, D-7400 Tuebingen, FRG). *J Comput Assist Tomogr* 12(6):988-994, Nov./Dec. 1988

Sixty-one patients with histologically proven disorders of the prostate [prostatic carcinoma (PC), 41; benign prostatic hyperplasia (BPH), 9; PC and BPH, 11] underwent magnetic resonance imaging at 1.5 T. Using single [spin echo (SE) 400/30] and dual (SE 1,600/30, 90) SE sequences, multislice contiguous scans were obtained in transverse, sagittal, and coronal planes through the prostate. In 27 patients (PC 14, BPH 6, PC and BPH 7) multiecho sequences with eight echoes (SE 1,600/30, 60, 90, 120, 150, 180, 210, 240) were acquired and T2 images were calculated in the planes with best depiction of circumscribed prostatic pathology. In these patients the Bhattacharyya coefficient, a quantitative criterion for the discrimination between normal and pathological tissue, derived by means of mathematical decision theory, was applied. This analysis showed the best discrimination between PC and normal prostate with echo time (TE) 90 and 120 ms [error rate (ER) for confusing these tissues 20-30%]. There was no significant difference between the signal intensities of PC and BPH at any parameter setting, but PC could be discriminated from the compressed peripheral glandular regions that often accompany BPH [minimal ER (20-30%) at TE 90 and 120 ms]. This distinction is of clinical value, since PC usually arises in the periphery of the prostate. Calculated T2 images did not show advantages for the detection of PC.

in MR imaging. The advanced practicum will be offered April 17–21 and Sept. 11–15. The basic practicum will be given June 19–23 and Oct. 23–27. Category 1 credit: 40 hr. Fee: \$1250; if a participant attends two practicums, the fee for the second week will be reduced to \$800. Information: Ms. Peggy Williams, The Johns Hopkins Medical Institutions, Office of Continuing Education, Turner Bldg., 720 Rutland Ave., Baltimore, MD 21205; (301) 955-3169.

1989 Neuroradiology Review Course

The Depts. of Radiology and Continuing Medical Education, Loyola University of Chicago, are sponsoring 1989 Neuroradiology Review Course, April 29–30, at the Oak Brook Hills Hotel and Conference Center, Oak Brook, IL. The course is designed to provide a better understanding of neuroradiology and new techniques. It is intended for neuroradiologists, neurosurgeons, and residents. Program director: Behrooz Azar-Kia. Category 1 credit: 16 hr. Fee: physicians, \$170; residents, \$100. Information: Linda K. Gunzburger, Ph.D., Director of Educational Research and Development, Loyola University Stritch School of Medicine, 2160 S. 1st Ave., Maywood, IL 60153; (312) 531-3237.

Correction: The Leading Edge in Diagnostic Ultrasound

The correct dates for The Leading Edge in Diagnostic Ultrasound, sponsored by the Dept. of Radiology, Division of Diagnostic Ultrasound, Thomas Jefferson University Hospital, are May 10–12. The preconference tutorials on prostate and vascular ultrasound will be held May 10. For more details, see the February 1989 issue of the *AJR*.

Radiology Review Course

The Depts. of Radiology, Mount Sinai Medical Center, Miami Beach, FL, and the University of Miami School of Medicine, Miami, FL, are sponsoring a radiology review course, May 14–19, at the Sheraton Bal Harbour, Bal Harbour, FL. The program is planned and structured for residents completing their training and physicians in practice who desire an up-to-date review of imaging of all the major organ systems, including the chest, cardiovascular system, abdomen, retroperitoneum, pelvis, musculoskeletal system, and CNS. Didactic presentations will be augmented with audiovisuals, and informal case presentations will conclude each session. The Self-Study Center is an integral part of the program. Registrants will be able to review approximately 180 cases that use the spectrum of imaging techniques to determine the definitive diagnosis and stress the differential diagnosis of each case. Category 1 credit: 39.5 hr. Fee: \$390. Information: Lucy R. Kelley, Radiology Seminars, P. O. Box 143762, Coral Gables, FL 33114–3762; (305) 674-2810.

Emission Tomography of the Heart

Emission Tomography of the Heart will be held May 20 at the Westin Hotel, Seattle, WA. This postgraduate course is offered by the North American Society for Cardiac Radiology and Harvard Medical School and is cosponsored by the Council on Cardiovascular Radiology, the American Heart Association. Program director: Heinrich R. Schelbert. Category 1 credit: 6 hr. Fee: \$150. Information: Harvard Med-CME, P. O. Box 825, Boston, MA 02117; (617) 732-6265.

Challenge 89: Decisions in Imaging

Challenge 89: Decisions in Imaging will be held in London, England, June 24–30. This multimodality correlative course will present topics in MR imaging, CT, and sonography. The emphasis will be on the indications for and the results obtained with each technique individually and in combination. Program Coordinator: Ronald Friedman. Faculty: W. D. Boswell, Jr., Graeme Bydder, P. M. Colletti, David Cosgrove, J. M. Halls, Christine Heron, Andrew Hine, Janet Husband, Rod Mohiaddin, Donald Longmore, P. W. Ralls, Simon Rees, Richard Underwood, Brian Worthington, I. R. Young, and C.-S. Zee. Category 1 credits will be awarded. Fee: physicians, \$450 before March 31, \$495 after March 31; fellows, residents, interns, technicians, and nurses (letter required), \$350 before March 31, \$395 after March 31. Information: University Imaging Associates, LAC/USC Medical Center, Box 66, 1200 N. State St., Los Angeles, CA 90033; (213) 226-7245.

Symposium on Breast Disease

The Dept. of Radiology and the Office of Continuing Medical Education, The University of Michigan Medical School, are sponsoring the 3rd Annual Symposium on Breast Disease: Diagnostic Imaging and Current Management, July 23–26, at the Grand Hotel, Mackinac Island, MI. Highlights of the course will include presentation of the newest developments in breast imaging and diagnostic techniques, including mammography, other breast imaging techniques, and fine-needle aspiration biopsy; an update on the role and implications of breast cancer screening; and a summary of the latest pathologic, surgical, and radiation oncology approaches to breast cancer. Course director: Dorit D. Adler. Program chairman: William Martel. Guest faculty: Ingvar Andersson, J. E. Meyer, and D. D. Paulus. Category 1 credit: 13 hr. Information: Debbie DeSmyther, Program Assistant, Office of Continuing Medical Education, Towsley Center, Box 0201; University of Michigan Medical School, Ann Arbor, MI 48109–0201; (313) 763-1400.

Royal Australasian College of Radiologists Annual Meeting

The 40th annual meeting of the Royal Australasian College of Radiologists will be held Oct. 19–23 in Melbourne, Australia. The program will include state-of-the-art lectures by guest and local faculty, original papers, and scientific exhibits. The Nisbet Symposium will focus on the imaging and treatment of liver tumors, and a symposium on the management of gastrointestinal malignancy will feature selected speakers who will address aspects of surgery, radiation oncology, and medical oncology. The deadline for registration information is March 1989. Program director: Frank Burke. Information: Louise Read or Mary Moyano, Conference Secretariat, 1st Floor, 387 Malvern Rd., S. Yarra, 3141, Melbourne, Australia; telephone: (03) 824-0022; fax: (03) 240-0771.

Advances in Chest, Interventional, and Ultrasound

The Dept. of Radiology, University of California, Irvine, and the Great Teachers Foundation will present Advances in Chest, Interventional, and Ultrasound, Nov. 25–Dec. 10, in South America (Caracas, Isla Margarita, Manaus, Recife, Rio de Janeiro, Buenos Aires, and Bariloche). The course is designed to provide interaction with leading physicians in South America and discussions of the latest concepts in chest, interventional, and ultrasound radiology. Program director:

Florence, (Jan)

Magnetic Resonance Imaging 1989: National Symposium, April 30–May 5, Orlando, FL (Feb)

Surgical Neuroangiography, May 1–5, New York (Dec)

Annual Mid-Pacific Diagnostic Ultrasound Conference, May 2–6, Big Island of Hawaii (Jan)

International Congress of Peer Review in Biomedical Publication, May 10–12, Chicago (Sept)

Sonography Symposium, May 26–27, Nashville, TN (Jan)

Radiology in Scandinavia and the Soviet Union, June 17–July 11, Copenhagen, Stockholm, and Leningrad (Jan)

CAR '89, June 25–28, Berlin (Jan)

1989 International Congress of Radiology, July 1–8, Paris (May)

Third World Medicine—Tropical Radiology and the Problem of AIDS, July 19–Aug. 5, East Africa (Nairobi, Maasa-Mara, Lake Baringo, Lake Turkana, Mombasa, and Lamu) (Jan)

Imaging, Intervention, Ireland—1989, Sept. 2–10, Dublin, Cong, and New Market, Ireland (Feb)

Update in Chest Radiology, Sept. 10–23, England and Scotland (Feb)

Society of Uroradiology Postgraduate Course, Sept. 25–28, Hilton Head, SC (Dec)

World Congress for Bronchology, Oct. 18–20, 1989, Tokyo, and Oct. 21–22, 1989, Kyoto, Japan (Nov)

AJR carries announcements of courses, symposia, and meetings of interest to its readers if received a minimum of 5 months before the event. There is no charge; receipt of items by the *AJR* Editorial Office is not acknowledged. Submit items for publication typed double-spaced. Provide title, date, location, brief description, sponsor, course directors, fees, category I credit, and address and telephone number for additional information. Faculty from the host institution will not be listed. Guest faculty names will appear **only** if initials are provided. Mail news items to *AJR* Editorial Office, 2223 Avenida de la Playa, Suite 200, La Jolla, CA 92037-3218.

MEETING REGISTRATION FORM
THE SOCIETY FOR PEDIATRIC RADIOLOGY
APRIL 5-9, 1989

Enclosed is my registration for the 32nd annual meeting of The Society for Pediatric Radiology, April 5-9, 1989. Mail this registration form and check before **March 1, 1989** to Mary J. Ryals, Ryals & Associates, P. O. Box 1925, Roswell, GA 30077-1925; (404) 641-9773.

Name _____

Address _____

City, State, & Zip _____

Office Telephone () _____

Hotel Reservation at _____

Name of Guest(s) _____

SPR Member, \$100; Accompanying Person of SPR Member, \$40; Nonmember of SPR, \$250; Accompanying Person of Nonmember of SPR, \$175; Resident in Diagnostic Radiology, No charge (Letter of verification required); Fellow in Pediatric Radiology or Diagnostic Imaging, No charge (Letter of verification required); Accompanying Person or Resident or Fellow, No charge.

HOTEL RESERVATION REQUEST FORM
THE SOCIETY FOR PEDIATRIC RADIOLOGY
APRIL 5-9, 1989

Mail this form directly to the Plaza San Antonio Hotel, 555 S. Alamo at Durango St., San Antonio, TX 78205; (512) 229-1000. Group rates are \$115 for single or double. Reservation form must be received by **March 12, 1989**. After that date, rooms may be secured on a space-available basis.

Name _____

Address _____

City, State, & Zip _____

Office Telephone () _____

Arrive _____ Depart _____

Credit Card (type & exp. date) _____

Card Number _____

Name on Card _____

Invitation to the 1989 American Roentgen Ray Society Meeting in New Orleans, LA, May 7-12, 1989

I am pleased to extend an invitation to all radiologists to attend the 89th annual meeting of the American Roentgen Ray Society in New Orleans, LA, May 7-12, 1989. In keeping with the ARRS tradition, outstanding scientific and social programs will be provided.

The excitement of a meeting set in New Orleans requires no further description. The opportunity for busy radiologists to attend a major national meeting while enjoying all that New Orleans has to offer is ideal.

The scientific program, instructional courses, and categorical course are certain to be interesting and informative (see Table 1 for schedule).

Scientific Program

Two hundred scientific papers have been selected from more than 400 abstracts. Scientific sessions will be devoted to all major body systems, angiography, interventional techniques, sonography, and mammography, as well as technologies. Special emphasis has been placed on discussion of new developments.

The innovative and extremely well-received Friday morning minisymposium is entitled "Gastrointestinal Radiology Update 1989." An outstanding faculty has been assembled for what I am sure will be a very stimulating program.

Instructional Courses

Joseph T. Ferrucci, Chairman of the Instructional Course Committee, has put together 60 instructional courses. Faculty members have been drawn from across the entire country, with emphasis on luminaries from the South. A superlative educational experience is anticipated, and advance registration is recommended.

Categorical Course

An extraordinary categorical course on genitourinary imaging (uroradiology) has been fashioned. The course covers all aspects of the field, including equipment and principles of diagnosis. This course is certain to be popular, and advance registration is advised.

TABLE 1: Summary of 1989 American Roentgen Ray Society Meeting

Sunday May 7	Monday May 8	Tuesday May 9	Wednesday May 10	Thursday May 11	Friday May 12
	8-9:30 Instructional courses	8-9:30 Instructional courses	8-9:30 Instructional courses	8-9:30 Instructional courses	8-10 Symposium: gastrointestinal imaging update
9-noon Categorical course: genitourinary imaging	10-10:30 Opening cere- monies				
	10:30-12:30 Scientific programs	10-12:30 Scientific programs	10-12:30 Scientific programs	10-12:30 Scientific programs	10:30-12:30 Symposium: gastrointestinal imaging update
1:30-3 Categorical course: genitourinary imaging	1:30-3:30 Categorical course: genitourinary imaging	1:30-3:30 Scientific programs	1:30-3:30 Scientific programs	1:30-3:30 Scientific programs	
3:30-5:30 Categorical course: genitourinary imaging	4-5:30 Instructional courses and cate- gorical course: genitourinary imaging	4-5:30 Instructional courses and cate- gorical course: genitourinary imaging	4-5:30 Instructional courses and cate- gorical course: genitourinary imaging	4-5:30 Instructional courses and cate- gorical course: genitourinary imaging	

Categorical Course on Uroradiology

American Roentgen Ray Society 89th Annual Meeting

May 7-11, 1989, New Orleans Hilton, New Orleans, LA

Sunday, May 7

10:00-10:10 a.m.

10:10-10:50 a.m.

10:50-11:30 a.m.

11:30-Noon

Break

1:30-2:15 p.m.

2:15-3:00 p.m.

Break

3:30-4:15 p.m.

4:15-5:00 p.m.

Contrast Media/Infection/Renal Masses (Moderators: Pollack [a.m.] and Mellins [p.m.])

Welcome and Introduction

Contrast media. Comparison of ionic and nonionic agents: pharmacology, physiology, and guidelines for practical usage (*Katzberg*)

Toxicity and reactions to contrast media (*Pfister*)

Evaluation of the azotemic patient (*Talner*)

Acute renal infections (*McClennan*)

Chronic renal infections (*Kenny*)

Cystic diseases of the kidney (*Hartman*)

Neoplasms of the kidney (*Stanley*)

Monday, May 8

1:30-2:15 p.m.

2:15-2:45 p.m.

2:45-3:15 p.m.

Break

3:45-4:15 p.m.

4:15-5:00 p.m.

Prostate/Bladder/Scrotum (Moderator: Davidson)

Imaging of the urinary bladder (*Hattery*)

Epidemiology and natural history of carcinoma of the prostate (*Amis*)

Ultrasonography of the prostate (*Rifkin*)

CT and MRI of the prostate (*Hricak*)

Imaging of the scrotum (*Rosenfield*)

Tuesday, May 9

3:30-4:05 p.m.

4:05-4:40 p.m.

4:40-5:15 p.m.

Stone Disease (Moderator: Newhouse)

Radiological aspects of urolithiasis (*Bush*)

Extracorporeal stone therapy (ESWL) (*LeRoy*)

Interventional procedures in urolithiasis (*Banner*)

Wednesday, May 10

3:30-4:00 p.m.

4:00-4:45 p.m.

4:45-5:15 p.m.

Impotence and Erectile Insufficiency (Moderator: Lang)

Pathology and physiology of impotence (*Goldstein*)

Radiology of impotence (*Bookstein*)

Radiology of penile prostheses (*Cohan*)

Thursday, May 11

3:30-4:05 p.m.

4:05-4:40 p.m.

4:40-5:15 p.m.

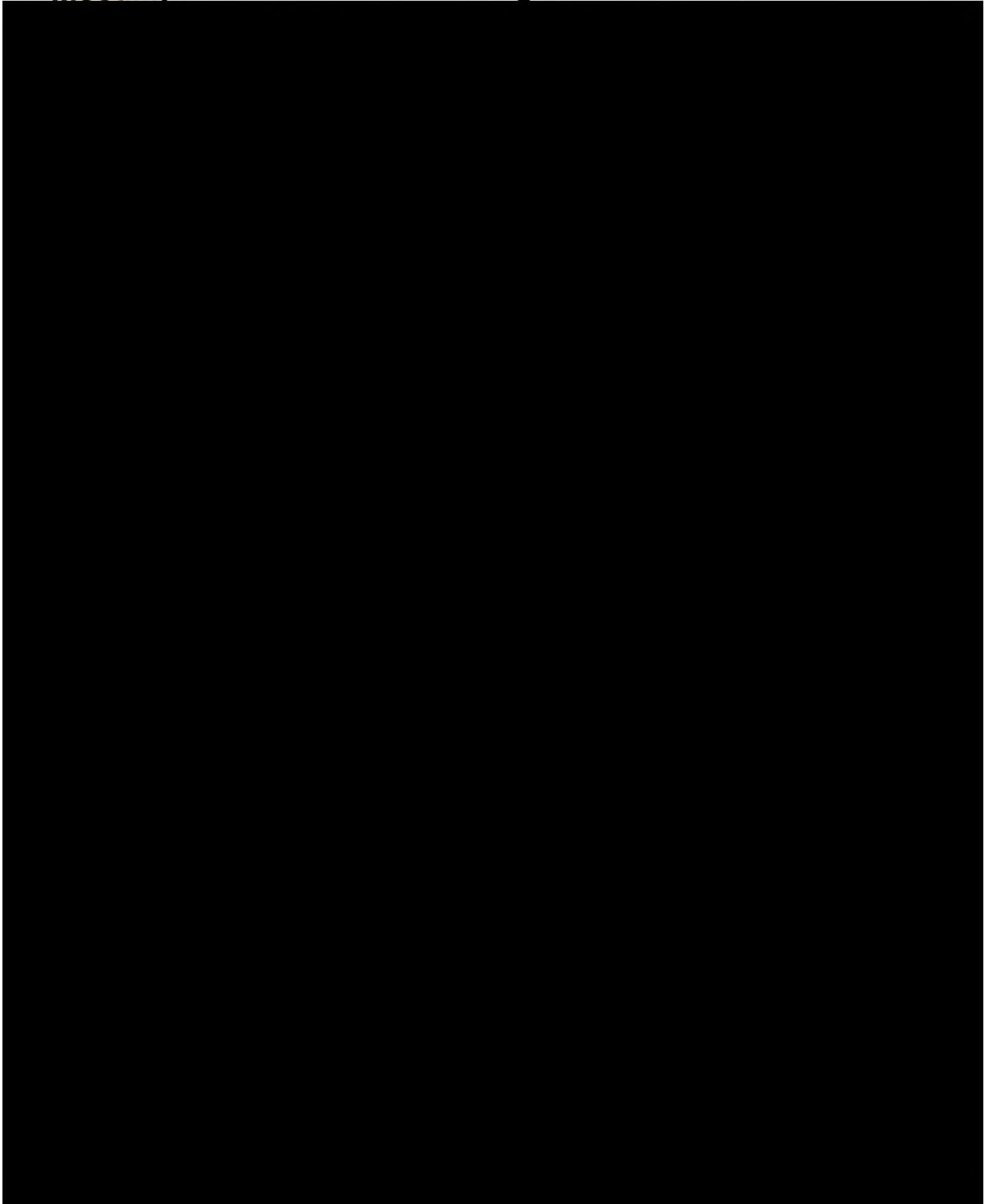
Retroperitoneum (Moderator: Hartman)

Adrenal imaging (*Dunnick*)

Perinephric disease (*Levine*)

Retroperitoneal disease (*Lee*)

Meeting and Local Activities Registration Form:



Hotel Registration Form: ARRS 89th Annual Meeting

May 7-12, 1989, New Orleans Hilton Riverside and Towers

New Orleans, LA

Mail to:

ARRS Housing Bureau

New Orleans Hilton Riverside and Towers

Attention: Reservations Office

Poydras at the Mississippi

New Orleans, LA 70140

(PLEASE MAKE CHECKS PAYABLE TO THE NEW ORLEANS HILTON RIVERSIDE AND TOWERS—NOT TO THE ARRS)

Individual guest name _____

Address _____

City & State _____ ZIP _____

Arrival date/time _____ Departure date/time _____

Individual requesting reservation _____

Address _____

City & State _____ ZIP _____

Please forward with your reservation a deposit of one night's room rate to be applied to the last night of your scheduled stay, or provide credit card information to guarantee your reservation. The hotel accepts American Express, Diners Club, Carte Blanche, Visa, Master Card, and Hilton credit cards. The deposit will hold your room until 6 a.m. of the morning following your scheduled arrival date. In the event of an early departure, the deposit is nonrefundable unless the hotel is notified prior to or at the time of check-in. Cancellation notice of 14 days is required for a deposit refund.

Check accommodations desired

Room Category	Rate
Singles	
Main	_____ \$108
Riverside	_____ \$118
Towers	_____ \$132
Doubles	
Main	_____ \$124
Riverside	_____ \$134
Towers	_____ \$148
1-bedroom suite	_____ \$290/390
2-bedroom suite	_____ \$375/475

Deposit amount (1 night's rate) \$ _____

☐ Check enclosed
☐ Credit card: _____
 Type of card _____ Exp. date _____

Card number _____

Signature _____

Important Information:

- Reservations must be received by the New Orleans Hilton Riverside and Towers/ARRS Housing Bureau no later than April 7 to be assured of written confirmed accommodation. Reservations after that time are subject to availability. We urge you to make your reservations promptly.
- Written confirmation of your reservation will be sent to you by the hotel.
- To change or cancel reservations, please call either Hilton Reservations Service at 1-800-HILTONS or the hotel directly at (504) 561-0500.
- If you plan to share a room, please send in only one housing form. Be sure to list all names of occupants of rooms. Assignment is delayed until complete information is received.
- Check-in is after 3 p.m., or earlier if the room is available. Check-out time is 1 p.m.
- Parking is available at the hotel.



1989 ARRS Meeting Summary, May 9-12, 1989 New Orleans, LA

A comprehensive description of the meeting, including the scientific program, Categorical Course in Genitourinary Imaging, and instructional courses, appears in this issue of the *AJR*. A special loose insert on the meeting also accompanies this issue. Meeting and registration forms will be found in the February and March issues. These may be photocopied.

Accreditation

All courses and scientific sessions carry AMA Category I credit on an hour-for-hour basis.

Meeting Format

Scientific Program. Sessions will be grouped in parallel sessions, Monday–Thursday. A total of 189 scientific papers will be presented. In addition, on Wednesday, May 10, the afternoon session will feature award papers and the Caldwell Lecture, which will be delivered by Senator Bill Bradley (D-NJ). On Friday, there will be a special symposium on gastrointestinal imaging.

Categorical Course in Genitourinary Imaging. This 15.5-hr course will be Sunday–Thursday.

Luncheon Sessions. Registrants may enroll in special luncheon sessions, Monday–Thursday. A box lunch will be provided.

Exhibits

Scientific and Technical Exhibits and Case of the Day Presentations will be presented in the Grand Salon of the New Orleans Hilton Riverside and Towers, Monday–Thursday, May 8–11. The Case of the Day will be presented by Marilyn Siegel of Washington University and Mallinckrodt Institute, St. Louis, MO.

Local Activities

General Reception. Tuesday evening, May 9, for all registrants.

Golf Tournament. Monday, May 8, English Turn Country Club. Transportation leaves the hotel at 11 a.m.; shotgun start is at 12:30 p.m.

Men's and Women's Tennis Tournaments. Monday, May 8, at the New Orleans Hilton Riverside and Towers, New Orleans, LA.

Local Tours. Sunday, May 7, 1–4 p.m., Overview of New Orleans; 7:30–10 p.m., Evening on the Mississippi; Monday, May 8, 9 a.m.–4 p.m., Plantations of Old Louisiana; 8–10:30 p.m., Dinner at Gallier Hall; Tuesday, May 9, 9:30 a.m.–3:30 p.m., Elegant Homes of New Orleans; Wednesday, May 10, 9–11:30 a.m., Creole Connection; 12:30–5 p.m., Audubon Zoo/River Cruise; 7–10 p.m., Evening Overlooking the Mississippi; Thursday, May 11, 11 a.m.–2:30 p.m., Cajun Swamp Tour. No refunds after April 20.

Meeting Registration

Preregistration will be accepted until April 7. There will be on-site registration. Official badges and program books will be available at the registration desk, New Orleans Hilton Riverside and Towers. No confirmations will be mailed.

Course Registration

Register early—enrollment is limited. List first, second, and third choices for each period. Also, indicate whether you wish to take the categorical course. Deadline for mail registrations is April 7. All ticket orders will be filled by postmark. Course tickets will not be mailed. Tickets will be available on and after Sunday, May 6 (after 1 p.m.), at the ARRS registration desk in the New Orleans Hilton Riverside and Towers. There will be on-site registration for courses not already filled.

Hotel Registration

Reservations are handled by the ARRS Housing Bureau, New Orleans Hilton Riverside and Towers, Attn: Reservations Office, Poydras at the Mississippi River, New Orleans, LA 70140. These must be received by April 7. Make check payable to New Orleans Hilton Riverside and Towers.

Fees

Meeting:	
ARRS members and resident members	No fee
Nonmembers	\$250
Nonmember physicians in training (with verification)	25
Categorical course (all who attend)	75
Luncheon sessions/each	12
Golf tournament	75
Tennis tournaments	50
Local tours	20–75

Cancellations and Fee Refunds

Fees will be refunded only if cancellation is received by April 20, 1989. Send to American Roentgen Ray Society, 1891 Preston White Drive, Reston, VA 22091.

Transportation Discounts

United and Delta airlines are offering discounts, up to 40%, on airfares. For United, call (800) 521-4041 and mention ARRS account number 9099D. For Delta, call (800) 241-6760 and reference account number M-0045.

Budget Rent A Car is offering special rates on car rentals. Call (800) 772-3773 and mention that you are attending the American Roentgen Ray Society annual meeting.

For ARRS
Office Use

Date Rec'd _____

I.D.# _____

AMERICAN ROENTGEN RAY SOCIETY APPLICATION FOR MEMBERSHIP

Date: _____

Category of Membership: ☐ Active
(Check One) ☐ Corresponding
☐ In-Training

Name (Please Print) _____ Degree(s) _____
First Initial Last

Mailing Address _____ Date of Birth _____
Street/Box

City/State/Country _____ Zip Code _____ Telephone () _____

A. Education: (List name of institution, years attended, and degree and type received.)

Undergraduate: _____

Graduate (Medical School, Graduate School, etc.):

Postgraduate (Internship, Residency, Fellowship, etc.):

B. Licensure:

Licensed to practice _____ in _____ since _____
(Type) (State, Province, etc.)

C. Appointments/Memberships: (In-Training applicants: skip to Section F on reverse.)

Present Appointments: Academic _____

Hospitals _____

Memberships in Scientific Societies: _____

Offices or Committee Assignments: _____

Government Service (Military or Civilian) _____ (Position) _____ (Years)

Continued on Reverse Side

DETACH HERE

DETACH HERE

Classified Advertisements

Positions Available

WANTED—Aggressive radiologist to head a new, free-standing, diagnostic center in Orlando, FL. Partnership opportunity. Malpractice paid. Attractive compensation package. Reply to Central Diagnostic Services, 79 W. Underwood St., Orlando, FL; (407) 648-4051. 3ap

MRI RADIOLOGIST—The Dept. of Radiology at Northwestern University Medical School in Chicago is seeking a radiologist with experience in MRI to serve as Director of the MRI facility at Northwestern Memorial Hospital, a 750-bed university hospital. This is an academic position, requiring a strong interest in clinical teaching and research, as well as patient care. Academic rank depends on qualifications. Send inquiries with a CV to Lee F. Rogers, M.D., Chairman, Dept. of Radiology, Northwestern University Medical School, 710 N. Fairbanks, Chicago, IL 60611. An affirmative action, equal opportunity employer. 3-5ap

DIAGNOSTIC RADIOLOGIST, DALLAS METROPLEX—Position available immediately for BC/BE radiologist to join 3-person group. Our practice includes 2 hospitals and an outpatient clinic. Fellowship training in MRI desired. Reply to Box 072, AJR (see address this section). 3-5ap

BC/BE DIAGNOSTIC RADIOLOGIST to join 4 radiologists at a large, multispecialty, staff model HMO. Practice includes general radiology, mammography, CT, nuclear medicine, and ultrasound. The dept. recently has been outfitted with 2 new GE R&F rooms and a new GE Pace CT scanner. The position offers a competitive salary with a comprehensive benefits program. Medical West Community Health Plan is located in western Massachusetts, approximately 60 min from the Berkshires and 90 min from Boston. Please send CV to Robert P. Newman, M.D., Chief, Dept. of Radiology, MWCHP, Inc., 444 Montgomery St., Chicopee, MA 01020. We are an equal opportunity/affirmative action employer. 3-5a

SOUTHERN INDIANA—Radiologist to join 5-member group in hospital and office practice. Some interest and experience in interventional studies desirable, but all areas of expertise will be considered. All imaging modalities, including MRI, available in 400-bed hospital. 80,000 exams annually. Competitive salary for 2 yr leading to partnership. T. Cook, M.D., P. O. Box 5249, Evansville, IN 47716-5249. 3-5ap

FRAMINGHAM, MA—BC/BE diagnostic radiologist to join 6-member group at 311-bed teaching hospital. Experience in angiography and interventional radiology necessary. Send CV to Herbert D. Weintraub, M.D., c/o Framingham Union Hospital, 115 Lincoln St., Framingham, MA 01701; (508) 626-3525. 3-6ap

DIAGNOSTIC RADIOLOGIST—Yale New Haven Medical Center is seeking a board-certified or eligible radiologist with additional experience or training in CT and diagnostic ultrasound for a full-time faculty position. Candidates should be able to interpret cross-sectional images and do cross-sectional interventional procedures. This appointment will include work about half time in the Dept. of Diagnostic Radiology at Yale and about half time at the affiliated West Haven VA Medical Center. Academic rank commensurate with experience. Candidates must be U.S. citizens or must qualify as permanent residents in the U.S. Please send CV and bibliography to Arthur T. Rosenfield, M.D., Dept. of Diagnostic Radiology, Yale University School of Medicine, 333 Cedar St., New Haven, CT 06510. Yale University is an equal opportunity/affirmative action employer; applications from women and minority groups are encouraged. Applications should be submitted no later than May 1, 1989. 3-4a

UNEXPECTED OPENING JULY 1989 FOR BE/BC DIAGNOSTIC RADIOLOGIST to join 5-man group in Missoula, MT, a university city of 50,000, located in mountainous, western Montana. Looking for a general radiologist with proficiency in MRI, ultrasound, CT, angiography, etc. Administrative skills preferable. Our group of 6 full-time radiologists covers both of Missoula's hospitals (210 and 130 beds). Progressive medical environment with 100+ physicians. One yr to full partner income and 2 yr to partnership. Abundant, nearby recreational opportunities include skiing, fishing, backpacking, hunting, etc. Send CV to Missoula Radiology, Inc., P. O. Box 2039, Missoula, MT 59806; (406) 721-4906. 3-4ap

DIAGNOSTIC RADIOLOGIST—Immediate opening to join 2 other radiologists in a large, multi-specialty group practice serving 4 outpatient offices in Rochester, NY. State-of-the-art Toshiba fluoroscopy, ATL ultrasound, and LoRad mammography equipment. Ultrasound, mammography, and CT experience preferable. 32,000 exams/yr. Please contact Dennis S. Moss, M.D., Rochester Medical Group Associates, P.C., Radiology Dept., 800 Carter St., Rochester, NY 14621; (716) 338-1400 x4096. EOE/MF. 3-6a

CHIEF, RADIOLOGY SERVICE—VA Medical Center, Augusta, GA, is seeking a qualified radiologist for Chief, Radiology Service. Board certification required. Subspecialty interest in chest, skeletal, GI, or interventional radiology is desirable, but not essential. Faculty appointment commensurate with qualifications and experience. This 1142-bed, tertiary-care medical center is affiliated with the Medical College of Georgia (MCG). Augusta enjoys a moderate climate, reasonable cost of living, numerous recreational facilities, and institutions of higher learning. Augusta is known as the Garden City of the South and home of the Masters Gold Tournament. An equal opportunity employer. For additional information, contact Henry M. Altharis, Sr., M.D., Chief of Staff; (404) 823-2224. 3a

IMAGING RADIOLOGIST—If lifestyle is an important consideration in your choice of an employment opportunity, read on. Do you want to hone your skills and become an "expert" in a limited area of radiologic diagnosis instead of being a generalist? Would you like to escape the hassles and bureaucratic entanglements of a hospital environment and also avoid night and weekend call? If you answered "yes" to these questions, you may be interested in joining our 2-man group in an office-based practice that concentrates on diagnostic ultrasound and mammography, with a little general radiology for diversion. This is a full-time position leading to partnership after 3 yr. Salary is competitive and the position is available now. Send resume to AVMAR, 3003 N. Central, #121-249, Phoenix, AZ 85012. 3-4ap

DIAGNOSTIC RADIOLOGIST—The San Francisco VA Medical Center is recruiting a board-certified radiologist with expertise in cross-sectional imaging including ultrasound (primarily), CT, and MRI. Position available July 1, 1989. The SFVA has a fully integrated teaching affiliation with the University of California, San Francisco. Minimum 1 yr of teaching and research experience is essential. Equal opportunity/affirmative action employer. Search continues until position is filled. Submit CV to Susan D. Wall, M.D., Assistant Chief, Radiology (114), VA Medical Center, 4150 Clement St., San Francisco, CA 94121. 3-4a

IMMEDIATE OPENING—BC/BE radiologist, full- or part-time, to join 2 radiologists in outpatient imaging center. General diagnostics includes MRI. Flexible hrs, weekdays only, no weekends or call. Generous salary and vacation leading to early partnership. Send CV to L. Carr, M.D., 342 22nd Ave. N., Nashville, TN 37203. 2-3ap

GENERAL RADIOLOGIST with special interest and expertise in pediatric radiology needed for hospital-based practice in 350-bed community hospital. Candidate also should be familiar with CT, ultrasound, nuclear medicine, and angiography. Reply c/o Petronio T. LeRona, M.D., Maricopa Medical Center, Dept. of Radiology, P. O. Box 5099, Phoenix, AZ 85010; (602) 267-5361. EOE. 3-4a

DIAGNOSTIC RADIOLOGIST—Radiologists seek board-certified radiologist with experience in CT, nuclear medicine, general radiology, and ultrasound including Doppler, for a hospital-based, private practice in 225-bed general hospital in Forest Hills, NY. Immediate opening leading to partnership. Contact M. Tartell, M.D.; (718) 544-5858. 2-4ap

DIAGNOSTIC RADIOLOGIST—Ten-man, private practice group seeks BC/BE diagnostic radiologist. Candidate must have at least 1-yr fellowship in CT/ultrasound, MRI, angio/interventional, or nuclear medicine. Practice covers 2 hospitals and an outpatient office with a total of 120,000 exams/yr. Beautiful midwestern university town. Excellent salary/fringes with early partnership arrangement. Send CV or call Joe McColley, M.D., 909 E. University St., Bloomington, IN 47401; (812) 336-9446. 2-4ap

DIAGNOSTIC RADIOLOGIST—The UCLA Dept. of Radiological Sciences is seeking a board-certified radiologist for its Primary Care/Family Practice Section. Position requires strong interests in teaching, patient care, and knowledge of abdominal CT for evaluation of trauma. Send application, including CV and names and addresses of 3 references, or inquiries to Hooshang Kangaroo, M.D., Chairman, Dept. of Radiological Sciences, UCLA Medical Center, Los Angeles, CA 90024-1721, an EO/AA employer that encourages applications from members of minority groups and women. 2-7a

SKELETAL RADIOLOGIST—The UCLA Dept. of Radiological Sciences has a full- or half-time faculty position available in skeletal radiology. Candidate must be board-certified, have a clinical background in skeletal radiology, and have a strong interest in teaching. Send application, including CV and names and addresses of 3 references, or inquiries to Hooshang Kangaroo, M.D., Chairman, Dept. of Radiological Sciences, UCLA Medical Center, Los Angeles, CA 90024-1721, an EO/AA employer that encourages applications from members of minority groups and women. 2-7a

WILMINGTON, NORTH CAROLINA—Group of 8 radiologists seeking fellowship-trained neuroradiologist and general diagnostic imaging radiologist with staff-level experience. This 400-bed, university-affiliated, regional-referral hospital has all diagnostic imaging capabilities including GE Signa 1.5-T MRI, 2 GE 9800 CT scanners, Toshiba SPECT system, and complete angio/interventional suites. Busy private outpatient office. Progressive growing community in Cape Fear area of coastal North Carolina. Address CV to John Remington, M.D., 2212 Delaney Ave., Wilmington, NC 28403. 2-4ap

RADIOLOGIST—Board-certified/eligible radiologist wanted to join 3 board-certified radiologists in busy, university-affiliated, community hospital near Boston. Area offers many educational and recreational opportunities. We seek a general radiologist with demonstrated ability in mammography, angio/interventional, ultrasound, and CT. MR experience a plus. Liberal benefits, vacation, and educational leave. Competitive salary leading to full partnership in professional corporation. Address inquiries to Steven Sitzman, M.D., The Malden Hospital, One Hospital Rd., Malden, MA 02148; (617) 322-7560 x5164. 2-3ap

COASTAL CALIFORNIA—Immediate opening for board-certified radiologist to provide day-off/vacation relief. Hospital, private office, group. Sunny northern California. Ultrasound, CT, and mammography. No angiography or MRI. CA license required, malpractice insurance provided. No weekends or call. Minimum 1/2 yr coverage. Reply Box N61, *AJR* (see address this section). 1-3ap

IMAGING RADIOLOGIST—THE CAROLINAS—Progressive, 12-man group seeking an exceptional individual with fellowship training or junior staff experience in body imaging. Must be board-certified and competent in a wide range of general diagnostic skills including mammography. Prosperous and reputable 650-bed community hospital planning major expansion. One hospital, 1 office practice with state-of-the-art equipment; 4 CT scanners (2 Picker, 2 GE 9800), MRI (GE Signa), and 7 ultrasound units (3 Acuson). A choice practice and excellent location in the heart of the Carolinas. Contact Box 221249, Charlotte, NC 28222. 1-3ap

THE DEPT. OF RADIOLOGY AT TRIPLER ARMY MEDICAL CENTER, HONOLULU, HI, is recruiting academically oriented radiologists for several divisions of the dept.: ultrasound, imaging (CT and/or MRI), interventional, chest, genitourinary, mammography, pediatric, neuro-radiology, and general diagnostic radiology. We are particularly interested in radiologists with ultrasound training or extensive experience. Our dept. offers a fully-accredited residency program with 18 residents and 15 attending full-time staff. Numerous consultants from across the country lecture on a continuing and regular basis. The hospital is a modern tertiary-care center serving the state and the entire Pacific Basin. A strong residency program, a diverse and interesting patient population, excellent equipment, and a tropical lifestyle are positive aspects of the practice. Academic credentials and/or experience are necessary. Recently graduated fellows are encouraged to apply. Board certification is mandatory. Candidates should be particularly interested in patient care, teaching, and research. Salary and benefits are competitive and generous. Tripler is an EO/EEOE employer. Please contact Dr. Mark F. Hansen, Col., MC, Chief, Dept. of Radiology, TAMC, HI 96859-5000; (808) 433-6393. Dr. Hansen will be present at the RSNA meeting. 3a

EMORY UNIVERSITY, DEPT. OF RADIOLOGY seeks a Ph.D. or M.D. with either NMR spectroscopy or imaging experience for a full-time faculty position. The candidate must be able to originate fundable research projects using NMR and collaborate with other faculty members (in or out of radiology) on NMR research. Knowledge of spin behavior is essential. Medicine, biology, or biochemistry, analog electronics, and computer science are useful skills. Two 1-m clinical imagers operating at 0.5 T and 1.5 T and a 30-cm 200-MHz instrument, all fully-programmable, will be available. The dept. is part of an 800-bed, tertiary-care complex giving ample opportunity for collaborations requiring clinical material. Seven full-time Ph.D. scientists, in the radiology dept., are currently involved in NMR. Qualified candidates please contact Thomas Dixon, M.D., Director, Frits Philips Magnetic Resonance Research Center, 419 Woodruff Memorial Bldg., Emory University, Atlanta, GA 30322. Emory University is an equal opportunity/affirmative action employer. 12-3a

DIAGNOSTIC RADIOLOGY—Fellowship-trained radiologist desired to join 23-person expanding, established practice. Pediatric experience desirable, but not mandatory. Contact Lester Goldberg, M.D., Memorial Hospital, 3501 Johnson St., Hollywood, FL 33021; (305) 985-5886. 12-3ap

DIAGNOSTIC ONCORADIOLOGIST—The Division of Oncoradiology at the Dana-Farber Cancer Institute, a Harvard University affiliate, has an opening at the instructor/assistant professor level for a general radiologist with an interest in oncology beginning July 1989 or sooner. Patient care responsibilities with a close working relationship with the clinical staff, teaching, and research opportunities abound. There are 52 beds with a large outpatient service. All new equipment is available including a GE-9800 CT scanner. Please send CV to Maxine Jochelson, M.D., Director, Division of Oncoradiology, Dana-Farber Cancer Institute, 44 Binney St., Boston, MA 02115. 11-4a

GU RADIOLOGIST, BRIGHAM & WOMEN'S HOSPITAL—The Dept. of Radiology at Brigham & Women's Hospital/Harvard Medical School is seeking a radiologist to direct its GU Section. The position combines clinical activities with teaching and research. Candidates must be board-certified and have experience in all aspects of GU radiology, as well as an interest/commitment to academic work. Please send CV to B. Leonard Holman, M.D., Chairman, Dept. of Radiology, Brigham & Women's Hospital, 75 Francis St., Boston, MA 02115. Harvard Medical School is an affirmative action/equal opportunity educator and employer. 11-4a

ULTRASOUND STAFF RADIOLOGIST, BRIGHAM & WOMEN'S HOSPITAL—The Dept. of Radiology at the Brigham & Women's Hospital/Harvard Medical School is seeking a radiologist for a full-time, academic position in ultrasound. We perform 60-85 scans per day, including OB-GYN, abdominal, Doppler, small parts, neonatal, and interventional. Research and teaching opportunities are available. Candidate must be BC/BE with fellowship training in ultrasound. Please send CV to B. Leonard Holman, M.D., Chairman, Dept. of Radiology, Brigham & Women's Hospital, 75 Francis St., Boston, MA 02115. Harvard Medical School is an affirmative action/equal opportunity educator and employer. 11-4a

DIAGNOSTIC RADIOLOGIST competent in interventional and MR to join growing 3-man practice in northern Arkansas. Modern hospital-based practice includes CT, ultrasound (including duplex vascular), angiography, DSA, interventional, lo-dose mammography, and computerized nuclear medicine. Mobile MR and on-site Radiation Center being added. Located in beautiful resort area of Ozark Mountains, 110 mi from Springfield, MO, 150 mi from Little Rock, and 190 mi from Memphis, and serves 100,000 area population. Excellent recreational activities in family-oriented rural environment. Competitive starting salary with full-partnership in 1 yr. Contact Marc Trager, M.D., P.O. Box 1137, Mountain Home, AR 72653; (501) 425-1760. 11-4a

HARTFORD, CT—Position available for a board-certified radiologist to join an established group of 7. Practice includes hospital and 3 private offices, all fully equipped, including CT, MRI and CT experience is an essential requirement. Competitive starting salary and benefits. Please enclose CV with initial correspondence to Jeffrey Blau, M.D., 40 Hart St., New Britain, CT 06052; (203) 229-2059. 3xa

HARTFORD, CT—Actively growing practice has position available for board-certified radiologist to join an established group of 7. Practice includes hospital and private offices, performing approximately 70,000 exams per yr. Training and/or experience in CT and MRI necessary. Please send CV with correspondence to M. Lee Wallace, M.D., 40 Hart St., New Britain, CT 06052; (203) 229-2059. 3xa

BOARD-CERTIFIED OR ELIGIBLE RADIOLOGIST sought to join staff covering 4 hospitals and an outpatient clinic in S.E. Georgia. Skills must include general diagnostic, ultrasound, nuclear medicine, mammography, CT, and special procedures. Salary negotiable. Send letters of inquiry with CV and letters of reference to Director, Regional Diagnostics, P.O. Box 147, Vicalia, GA 30474; (912) 537-1150. 3xa

CROSS-SECTIONAL RADIOLOGIST, INTERVENTIONALIST—Board-certified diagnostic radiologist with fellowship training wanted to join 5-member dept. in 214-bed community hospital. Group also active in busy outpatient facilities and free-standing Magnetic Resonance Center. Primary responsibility will be ultrasound, CT, and nonangiography interventional, with back-up for primary angiographer. Competence in Doppler studies desired. Call and/or send CV attention Jon Robins, M.D., or Edward Janon, M.D., 6699 Alvarado Rd., Ste. 2100, San Diego, CA 92120; (619) 583-4214. 3xa

PEDIATRIC RADIOLOGIST—Yale New Haven Medical Center, Yale University School of Medicine, is seeking a pediatric radiologist for full-time faculty appointment. Academic rank is at the level of assistant or associate professor, dependent on qualifications. A strong interest in patient care, research, and teaching is required. Please send inquiries along with CV to Marc Keller, M.D., Diagnostic Radiology, Yale University School of Medicine, 333 Cedar St., New Haven, CT 06510. Yale University is an equal opportunity/affirmative action employer; applications from women and minority groups are encouraged. 3-4a

DIAGNOSTIC RADIOLOGIST—Yale University School of Medicine is seeking a radiologist with special interest in body MRI including a focus in cardiac MRI for a full-time faculty appointment. Equipment includes 2 GE 1.5-T scanners, a 2-T advanced NMR fast scanner, a 0.4-T superkinetics, a 2-T CSI, and 300- and 20-MHz spectrometers. Academic rank is at the level of assistant professor. A strong interest in patient care, research, and teaching is required. Please send inquiries along with CV to Shirley McCarthy, M.D., Ph.D., Diagnostic Radiology, Yale University School of Medicine, 333 Cedar St., New Haven, CT 06510. Yale University is an equal opportunity/affirmative action employer; applications from women and minority groups are encouraged. 3-4a

INTERVENTIONAL RADIOLOGIST—Board-certified radiologist with fellowship training in vascular/interventional radiology for position starting July 1, 1989. Academic rank is at the level of assistant professor. This active clinical service performs the entire range of diagnostic and interventional procedures including embolization, angioplasty, infusion therapy, IVC filter placement, atherectomy, and laser angioplasty. A program in biliary lithotripsy is the responsibility of the section. The interventional inpatient service admits 100 patients/yr, primarily for embolization and angioplasty. The interventional clinic evaluates referred patients and patients seen in follow-up. Please send applications with CV to Donald F. Denny, Jr., M.D., Chief, Vascular and Interventional Radiology, Yale University School of Medicine, P.O. Box 3333, New Haven, CT 06510. Yale University is an equal opportunity/affirmative action employer. Applications from women and minority group members are encouraged. Application deadline is March 1, 1989. 3a

NEURORADIOLOGIST—Immediate opening for recently trained neuroradiologist in busy suburban practice in Southwest. Current CT, MRI, and arteriography skills required. Highly competitive salary/benefits. Send CV to Box K49, *AJR* (see address this section). 3xa

THE DEPT. OF RADIOLOGY AT THE TORONTO GENERAL HOSPITAL

invites applications for the following 1-yr fellowships beginning July 1, 1989: **FELLOWSHIP IN THORACIC IMAGING**—This program offers extensive, in-depth exposure to all aspects of thoracic imaging, including plain film radiography, chest tomography (approximately 250 studies/yr), ICU radiology (56-bed ICU), thoracic CT (650 studies/yr), nuclear lung scanning (700 studies/yr), and transthoracic needle biopsy (500/yr). There is close liaison with the Divisions of Pulmonary Pathology, Cytopathology, Pulmonary Medicine (6 full-time chest physicians), and Thoracic Surgery (5 full-time non-cardiac thoracic surgeons). **FELLOWSHIP IN MUSCULOSKELETAL RADIOLOGY**—This position offers extensive clinical experience in arthrography, CT, MRI, and trauma radiology. There are opportunities for participation in research and teaching. The Toronto General Hospital is a 1000-bed, tertiary- to quaternary-care institution and is a primary teaching affiliate of the Faculty of Medicine at the University of Toronto. The fellowships are open to individuals who have completed an accredited residency in radiology. Application, including CV and references, should be sent to C.S. Ho, M.B., Acting Radiologist-in-Chief, Dept. of Radiology, Toronto General Hospital, 200 Elizabeth St., Toronto, Ontario, M5G 2C4. 2-3cp

CARDIOVASCULAR/INTERVENTIONAL RADIOLOGY FELLOWSHIP AT THOMAS JEFFERSON UNIVERSITY HOSPITAL

—A 1-yr fellowship position is available starting 7/1/89. This fellowship includes experience in a wide range of diagnostic angiography and both vascular and nonvascular interventional procedures. These include balloon angioplasty, laser thermal angioplasty, thrombolytic therapy, atherectomy, intravascular stent placement, IVC filter placements, renal and biliary drainage procedures, abscess drainages, and stone retrievals. Optional training also available in coronary angiography. Facilities include state-of-the-art angiographic and digital subtraction equipment. Contact either Geoffrey A. Gardiner, Jr., M.D. or David C. Levin, M.D., Dept. of Radiology, Thomas Jefferson University Hospital, 111 S. 11th St., Philadelphia, PA 19107. Thomas Jefferson University is an equal opportunity/affirmative action employer. 1-6cp

FELLOWSHIP IN PEDIATRIC RADIOLOGY

—Dept. of Radiology, Children's Hospital Medical Center, Cincinnati, OH, offers a 1- or 2-yr fellowship in pediatric radiology beginning July 1, 1989. Children's Hospital Medical Center is a 344-bed institution where approximately 85,000 radiologic exams are done per yr by 10 attending radiologists. Training includes all aspects of pediatric imaging including conventional radiology, neuro-radiology, abdominal imaging, ultrasound, nuclear medicine, CT, MRI, and vascular/interventional techniques. Equipment includes digital fluoroscopy, Acuson and ATL ultrasound units with Doppler and color-flow Doppler capabilities, Gamma and SPECT tomographic nuclear cameras, GE 9800 Quick CT Scanner, 1.5-T GE MRI, and angiographic suite with digital vascular imaging. Requirements for the fellowship include completion of a radiology residency with training in the various subspecialties of diagnostic imaging. Contact Donald R. Kirks, M.D., Director, Dept. of Radiology, Children's Hospital Medical Center, Elland & Bethesda Aves., Cincinnati, OH 45229-2899; (513) 559-8058. 12-8cp

NUCLEAR MEDICINE RESIDENCY, JULY 1, 1989—San Francisco General Hospital Medical Center, University of California, San Francisco, has a Program B, 2-yr, ACGME-approved program satisfying the American Board of Nuclear Medicine training requirements both in basic science and performance/interpretation of imaging and nonimaging in vivo procedures, radioimmunoassay, and radionuclide therapy. Emphasis is on SPECT, nuclear cardiology, and use of computers. Prerequisite is 2-yr, ACGME-approved residency in internal medicine, pathology, pediatrics, or radiology. Send CV to Myron Pollycove, M.D., Chief, Nuclear Medicine Dept., San Francisco General Hospital Medical Center, San Francisco, CA 94110. Equal opportunity/affirmative action employer. 3-4c

Tutorials/Courses

FIFTH ANNUAL LONDON-PARIS FALL ULTRASOUND—Sept. 17-23, 1989. Category I accreditation, international faculty. For information, contact Medical Seminars International, 9800 D Topanga Canyon Blvd., Ste. 232, Chatsworth, CA 91311; (818) 700-9821. 3-9d

PRACTICUM IN SWALLOWING: VIDEO ASSESSMENT OF DYSFUNCTION—April 8-9, 1989, Washington, DC. For further information, contact John Vargo at the Office of Continuing Medical Education, The George Washington University Medical Center; (202) 994-4285. 3d

MARCH 31-APRIL 1, 1989—Urologic Ultrasound Imaging: A Practical Approach to Prostate, Kidney, Bladder, and Scrotal Scanning with Matthew Rifkin and Peter Scardino, Hilton Head, SC. Fee: \$250. Contact Ruth Harker, Teknar, Inc., 267 Wolfner Dr., Fenton, MO 63026; (800) 233-3605. 2-3d

ALASKA 89—CRUISE THE INLAND PASSAGE—July 8-15, 1989, CME I accreditation, Professor Lawrence Bassett, M.D., Breast Imaging. For information, contact Medical Seminars International, 9800 D Topanga Canyon Blvd., #232, Chatsworth, CA 91311; (818) 700-9821. 1-6d

AJR Classified Advertisements Information**Box Responses and Address for Ad Placement**

Write Box _____, AJR, 2223 Avenida de la Playa, Suite 200, La Jolla, CA 92037-3218 (619) 459-2229; FAX: (619) 459-8814.

How to Place an Ad

AJR accepts classified advertising for Positions Available, Positions Desired, Fellowships and Residencies, and Tutorials/Courses. Ads are accepted by mail or FAX.

Rates: \$6.00/line with a \$30 minimum charge. Box service is \$10 additional for each month the ad appears. There are discounts for multiple insertions: 10% for 2-3 insertions; 20% for 4 or more. To estimate lines, count all words and divide by 7.

Billing: Ads must be prepaid, or advertisers will be billed after the ad appears providing a purchase order number is submitted with the advertising copy. Terms are net 30 days.

Deadlines: 6 weeks prior to issue date. For specific deadlines, telephone the AJR editorial office.

Estimating Ad Charges

Line charge: divide total words by 7 and multiply by \$6.00 \$
Multiple insertions? If so, multiply by number x
Subtotal \$
Discount applies to two or more insertions. Subtract 10% if ad appears 2-3 months, 20% if 4 months or more -
Subtotal \$
Box response requested? If so, multiply number of months by \$10.00 +
Approximate advertising charge \$

GET THE MOST OUT OF IMAGING PROCEDURES

NEW!

Fetal Sectional Anatomy and Ultrasonography

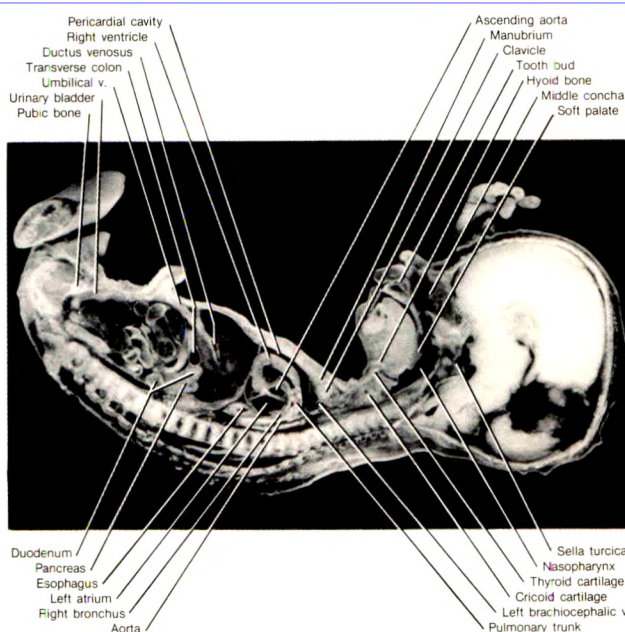
Lewis H. Nelson III, MD and
Walter J. Bo., PhD

Enhance your interpretive skills with the one text that helps you translate the two-dimensional images on paper to the three-dimensional image you actually see.

Combining images and drawings, this text-free atlas provides the facts you need to get the most out of ultrasonographic procedures. Anatomical sections that feature both sagittal and transverse orientation make this book easy to use during scanning, while the clearly-labeled illustrations eliminate the need for cross-referencing to tables.

Drs. Nelson and Bo have created an atlas which employs not only ultrasonography, but also magnetic resonance imaging and computer tomography as imaging modalities to present a complete reference of fetal anatomy. Serial transverse sections of a mid-pregnancy male fetus and sagittal sections of a term, anencephalic female fetus are labeled on the actual image for easy identification at a glance.

1988/224 pages/365 illustrations/6400-2/\$65.00/\$78.00 outside the US and Canada



NEW!

Computed Cranial and Spinal Imaging A Practical Introduction

John M. Stevens

Superb illustrations and eminent authors distinguish this new work on optimal imaging of neurological disorders.

From initial choice of imaging modality through interpretation of results, this text spells out exactly how to approach investigation and management decisions, with the strengths, limitations, and uses of CT and MRI examined clearly and in detail. Both normal and pathological appearances of the brain, spine, paranasal sinuses, and orbits are examined with extensive accompanying illustrations. You'll also find essential information on when to administer intravenous or intrathecal contrast enhancement.

1988/224 pages/illustrated/
7931-X/\$44.95 (available only in
North America)



Williams & Wilkins

428 East Preston Street
Baltimore, Maryland 21202

Broadway House
2-6 Fulham Broadway
London SW6 1AA England

Ordering is as easy as picking up your phone:

In the US just dial, toll-free
1-800-638-0672.

30 day FREE trial for all books! (US only)

